Dicle Üniversitesi 1973

National Hydrogen Association Türkiye

International Association for Hydrogen Energy

International Journal of Hydrogen Energy

IHTEC 2024

www.ihtec2024.org

8th International HYDROGEN TECHNOLOGIES Congress

12-15 May 2024

Dicle University, Diyarbakır, Türkiye



PROCEEDINGS

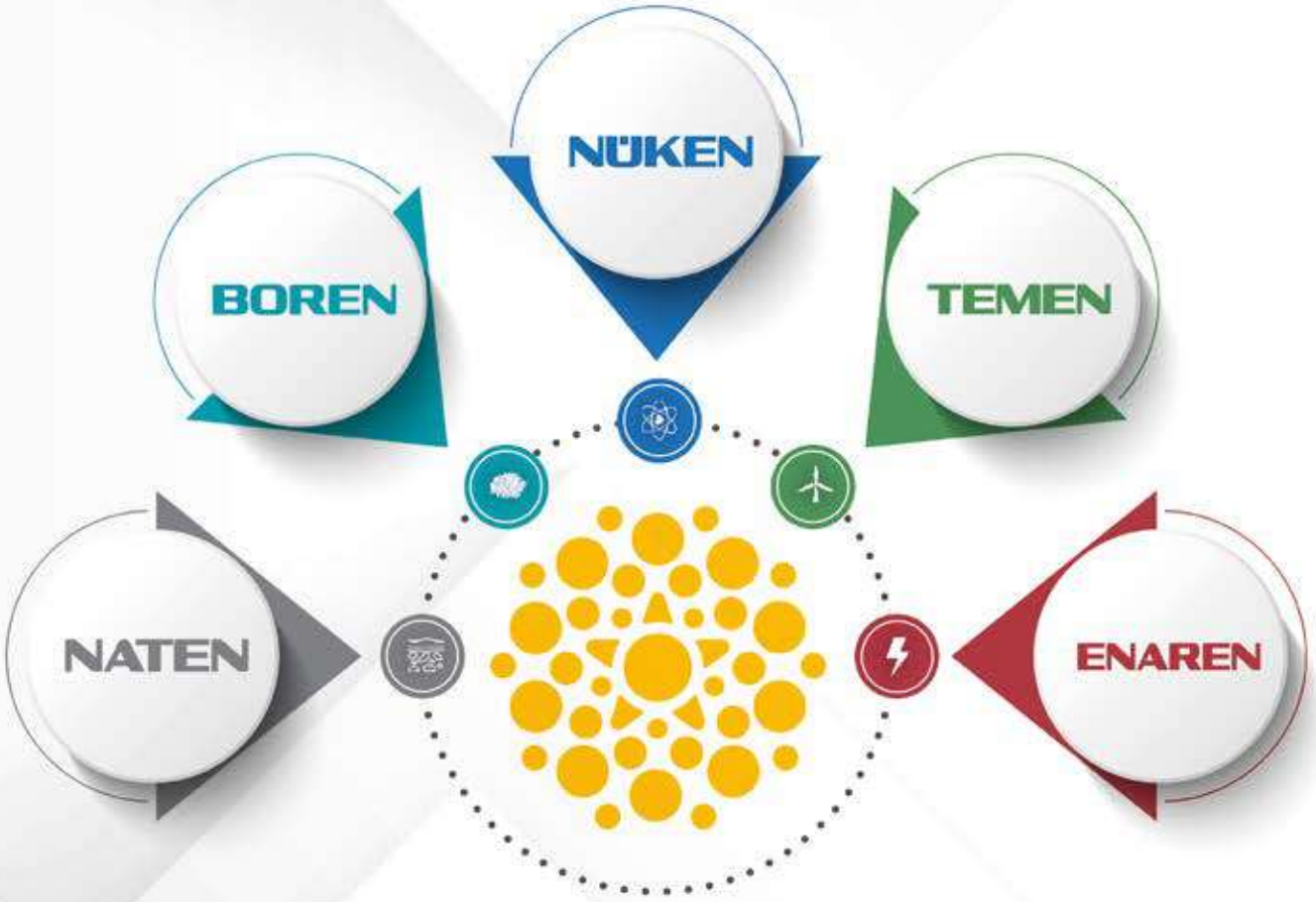
EDITORS

İbrahim Dinçer
Mahmut Temel Özdemir
Heybet Kılıç
Mehmet Emin Asker
Cem Haydaroğlu

ISBN: 978-605-70717-8-1

TENMAK
TURKISH ENERGY, NUCLEAR AND MINERAL RESEARCH AGENCY

ENERJİ, NÜKLEER VE MADEN TEKNOLOJİLERİNİN **AR-GE KURUMU**



TENMAK

TÜRKİYE ENERJİ, NÜKLEER VE MADEN ARAŞTIRMA KURUMU

T.C. ENERJİ VE TABİİ KAYNAKLAR BAKANLIĞI

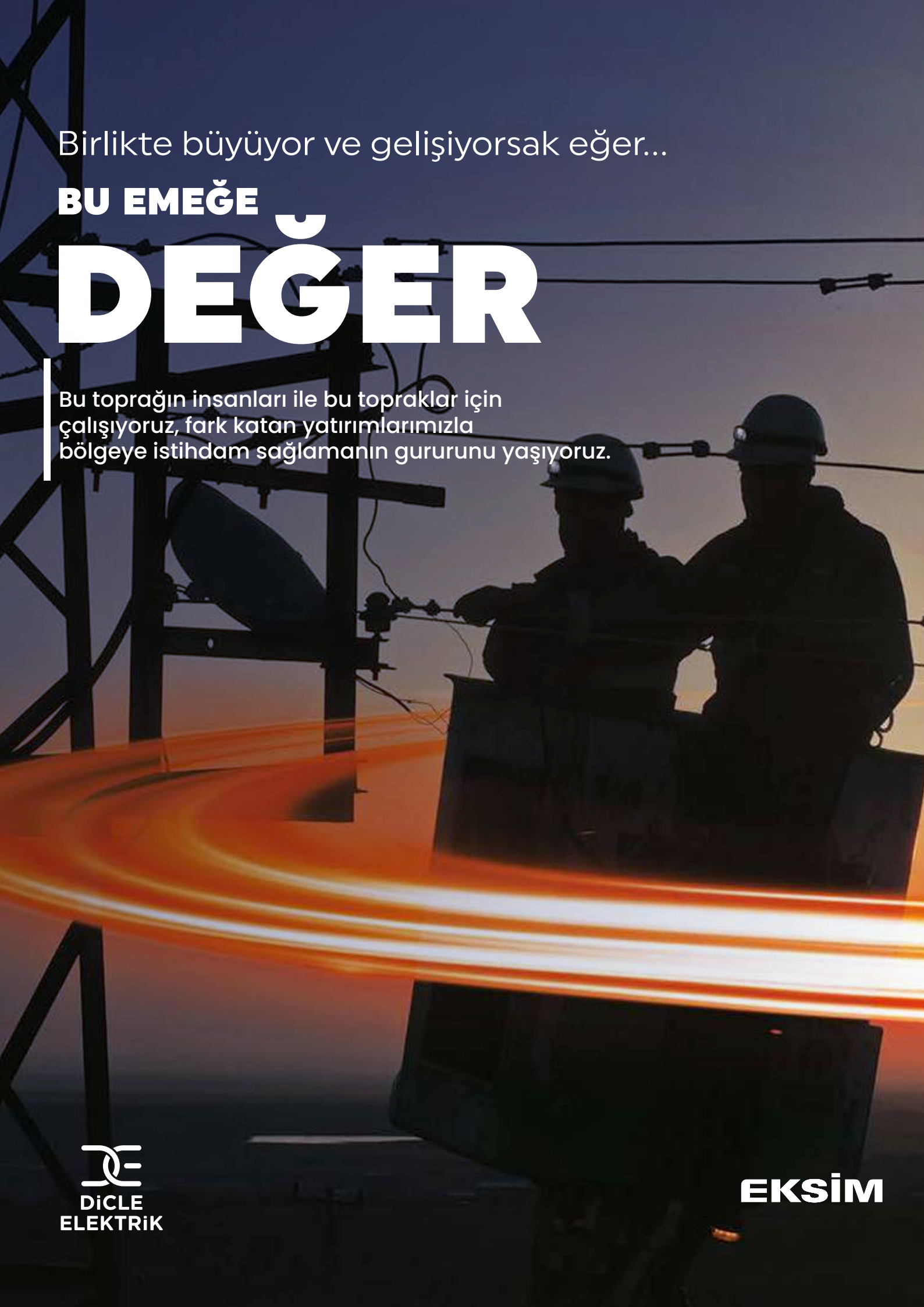
tenmakbaskanlik

PROCEEDINGS

EDITORS

İbrahim Dinçer
Mahmut Temel Özdemir
Heybet Kılıç
Mehmet Emin Asker
Cem Haydaroğlu

ISBN: 978-605-70717-8-1


Birlikte büyüyor ve gelişiyorsak eğer...
BU EMEĞE
DEĞER
Bu toprağın insanları ile bu topraklar için
çalışıyoruz, fark katan yatırımlarımızla
bölgeye istihdam sağlamanın gururunu yaşıyoruz.
DİCLE
ELEKTRİK
EKSİM

INDEX

Forewords	4
Committees	6
Scientific Program	10
Oral Proceedings	26
Posters	693

FOREWORDS

MESSAGE FROM THE PRESIDENT

The Hydrogen Technologies Association has been committed to advancing hydrogen energy technologies and knowledge since 2014. To achieve this objective, we have formed partnerships with academic institutions, government agencies, corporations, and individuals. We have organized numerous local and international conferences, seminars, panel discussions, and meetings to promote innovation and progress in this industry. These activities have highlighted the Association's significant role and established it as a prestigious entity on a global scale. Over the years, we have published e-bulletins, hosted the Hydrogen Technologies Association Awards, and conducted thorough analyses of the transportation, industrial, chemical, and power and heat sectors. Additionally, we have produced a variety of reports.

The 8th International Hydrogen Technologies Congress (IHTEC-2024) was effectively organized from May 12-15, 2024, at Dicle University in Diyarbakır, Türkiye. The Dicle University organizing committee, with the administration's unwavering support, successfully executed this event, which included a plethora of technical and social activities that left an enduring impression on the attendees. The committee communicated with more than 1,273 researchers from 96 countries who were interested in learning about the congress. Consequently, we received 237 paper submissions from 15 countries, of which 206 were accepted for presentation. The papers were the subject of discussion in four simultaneous sessions over three days. The topics covered were diverse, including hydrogen energy production, storage, distribution, transportation, utilization, fuel cells, and renewable energy. Additionally, the congress included eight keynote and invited speakers who provided distinctive perspectives on hydrogen technologies, challenges, opportunities, and future orientations.

Professor Abdulkadir Balıkçı, president of the Turkish Energy, Nuclear and Minerals Research Agency (TENMAK), delivered a noteworthy presentation entitled "Energizing Türkiye's Future: The Green Hydrogen Revolution." Furthermore, Prof. Adnan Midilli of Istanbul Technical University moderated a panel discussion titled "Challenges and Opportunities for The Region in the New Hydrogen Economy," which included speakers Hüseyin Devrim (TEK-SİS), Can Erkey (Koç University), Ali Rıza Arslan (Hydrogenix), and Ragıp Kızıltaş (TENMAK – Clean Energy Research Institute). A special session was also included in the congress, during which company executives and representatives showcased their technologies, products, and services that were associated with hydrogen technologies.

The perpetual honorary president of the Hydrogen Technologies Association, Prof. Turhan Nejat VEZİROĞLU, is one of the first names that comes to mind when discussing hydrogen energy in the global context. Consequently, the congress bestowed five awards: Nejat Veziroğlu Special Award, Service Award, Technology Award, Young Researcher Award, and Student Researcher Award.

The Turkish Energy, Nuclear, and Mineral Research Agency (TENMAK) served as the main sponsor of the congress, with Dicle Elektrik, ETİ KROM A.Ş., and HydrogenX providing additional gold sponsorship. The Diyarbakır Governor, Diyarbakır Municipality, GAP, KARACADAĞ Development Agency, Diyarbakır OIZ, AK-DAL, Anton Paar, Otostore, Behiye Pala Mühendislik, Mitras Enerji, SPCA, Solino, Jiper, Ünteks, Eksim Enerji, TRL Instrument, EFG, and Turuncu Şarj were additional supporters. We are profoundly appreciative of their contributions.

Our congress was extensively covered by local and national media, such as TRT, Anadolu Agency, and Uzay TV, thereby guaranteeing that our activities and results were communicated to a wide audience.

I am deeply grateful to Professor Mehmet KARAKOÇ, the Rector of Dicle University, for his unwavering support. Special recognition is also due to Professor M. Siraç ÖZERDEM (Dean of the Faculty of Engineering), Professor Ahmet YARDIMEDEN, Assoc. Professor Cafer BUDAK, Assoc. Professor Mahmut Temel ÖZDEMİR, Assist. Professor Heybet KILIÇ (Congress Chair), Assist. Professor Cem HAYDAROĞLU (Congress Co-Chair), Assist. Professor M. Emin ASKER, and Lecturer Yahya AKIL (Technical Chair of the Congress), as well as the faculty and staff of the Electrical and Electronics Engineering Department and Technical Schools, for their substantial contributions to the congress's success.

Lastly, I would like to express my gratitude to the BROS congress team and the Association's board members for their unwavering commitment and hard work.

Prof. Dr. İbrahim Dinçer
President, National Hydrogen Association

FOREWORDS

MESSAGE FROM THE CHAIRS

It is with great pleasure and honor that we welcome you to the 8th International Hydrogen Technologies Congress (IHTEC-2024), hosted by Dicle University in Diyarbakır, Türkiye. This event is particularly special as it coincides with our university's 50th anniversary celebrations, marking half a century of academic excellence and innovation.

This year's congress represents a significant milestone in our collective efforts to propel hydrogen energy technologies to the forefront of sustainable development. The diverse range of topics, from hydrogen production and storage to fuel cells and renewable energy, underscores the broad scope and dynamic nature of our field.

The success of IHTEC-2024 is a testament to the collaborative spirit and dedication of many individuals and organizations. We extend our deepest gratitude to our Rector, Professor Mehmet KARAKOÇ, whose steadfast support has been pivotal. We also acknowledge the invaluable contributions of the senior management team of Dicle University, who have provided unwavering encouragement throughout the planning and execution of this event.

We are particularly grateful to the leadership within the Faculty of Engineering. Special thanks are due to Professor M. Siraç ÖZERDEM, Professor Ahmet YARDIMEDEN, Assoc. Professor Cafer BUDAK, Assoc. Professor Mahmut Temel ÖZDEMİR, Assist. Professor M. Emin ASKER, and Lecturer Yahya AKIL. Their dedication and tireless efforts have been crucial in bringing this congress to fruition. We also appreciate the hard work and support of the academic and administrative staff of the Dicle University.

We owe a special debt of gratitude to Professor İbrahim DİNÇER, whose visionary leadership as General Chair has been instrumental in shaping the direction and success of this congress. His guidance and collaboration with the Hydrogen Technologies Association have set a high standard for excellence, making IHTEC-2024 a beacon of innovation and knowledge sharing. We deeply value his contributions and are honored to continue building on the strong foundation he has established.

We are confident that the rich discussions, innovative presentations, and collaborative interactions at IHTEC-2024 will drive forward the advancement of hydrogen technologies. This congress is not just an academic gathering but a convergence of minds committed to shaping a sustainable future.

We sincerely hope that IHTEC-2024 will be a memorable and beneficial experience for all participants, fostering new ideas and partnerships that will benefit our country and humanity at large.

Assist. Prof. Dr. Heybet KILIÇ
Congress Chair, IHTEC-2024

Assist. Prof. Dr. Cem HAYDAROĞLU
Congress Co-Chair, IHTEC-2024

COMMITTEES

Honorary Chairs

Karakoç, Mehmet / *Rector, Dicle University, Türkiye*
Veziroglu, Turhan Nejat / *Founder, International Association for Hydrogen Energy (IAHE), International Journal of Hydrogen Energy (IJHE), USA*

General Chair

Dincer, Ibrahim / *National Hydrogen Association, Türkiye*

Congress Chair

Kılıç, Heybet / *Dicle University, Türkiye*

Congress Co-chair

Haydaroğlu, Cem / *Dicle University, Türkiye*

Technical Chairs

Yardımeden, Ahmet / *Dicle University, Türkiye*
Asker, Mehmet Emin / *Dicle University, Türkiye*

Organizing Committee

Akil, Yahya / *Dicle University, Türkiye*
Akbulut, Ruken / *Mitras Enerji, Türkiye*
Arpa, Orhan / *Dicle University, Türkiye*
Arserim, M. Ali / *Dicle University, Türkiye*
Arvas, Yaşar / *General Manager, DİCLE EDAŞ, Türkiye*
Asker, Mehmet Emin / *Dicle University, Türkiye*
Asubay, Sezai / *Dicle University, Türkiye*
Benteşen Yakut, Yurdagül / *Dicle University, Türkiye*
Budak, Cafer / *Dicle University, Türkiye*
Cansız, Mustafa / *Dicle University, Türkiye*
Fırat, Hüseyin / *Dicle University, Türkiye*
Gençoğlu, Muhsin Tunay / *Fırat University, Türkiye*
Gümüş, Bilal / *Dicle University, Türkiye*
Haydaroğlu, Cem / *Dicle University, Türkiye*
Kılıç, Eylem / *Van Yüzüncü Yıl University, Türkiye*
Kılıç, Heybet / *Dicle University, Türkiye*
Kızıltaş, Ragıp / *TENMAK, Türkiye*
Nergiz, Mehmet / *Dicle University, Türkiye*
Poyraz, İlhami / *Dicle University, Türkiye*
Özcan, Ömer Faruk / *Dicle University, Türkiye*
Özerdem, Mehmet Siraç / *Dicle University, Türkiye*
Turan, Kadir / *Dicle University, Türkiye*
Tüzün, Nedim / *Vice General Manager, DİCLE EDAŞ, Türkiye*
Yardımeden, Ahmet / *Dicle University, Türkiye*
Yıldırım, Burak / *Bingöl University, Türkiye*
Yıldız, A. Nasır / *Dicle University, Türkiye*
Yılmaz, Musa / *University of California Riverside, USA*

Conference Planning Coordinators

Arat, Hüseyin Turan / *Sinop University, Türkiye*
Haydaroğlu, Cem / *Dicle University, Türkiye*
Kılıç, Heybet / *Dicle University, Türkiye*

Executive Committee

Colpan, Can Özgür / *Dokuz Eylül University, Türkiye*
Dincer, Ibrahim / *National Hydrogen Association, Türkiye / University of Ontario Institute of Technology, Canada*
Eroğlu, İnci / *Middle East Technical University, Türkiye*
Kantürk Figen, Aysel / *Yıldız Technical University, Türkiye*
Karakılçık, Mehmet / *Cukurova University, Türkiye*
Karaosmanoglu, Filiz / *İstanbul Technical University, Türkiye*
Midilli, Adnan / *İstanbul Technical University, Türkiye*
Özkaya, Bestami / *Yıldız Technical University, Türkiye*
Özdemir, Mahmut Temel / *Fırat University, Türkiye*
Solmaz, Ramazan / *Bingöl University, Türkiye*

COMMITTEES

International Scientific Board

Veziroglu, T.N. / *USA*
Amani, Y. / *USA*
Avaca, L.A. / *Brazil*
Azbar, N. / *Türkiye*
Baker, R. / *UK*
Barbir, F. / *USA*
Baykara, S. / *Türkiye*
Bolcich, J.C. / *Argentina*
Chen, W.H. / *Taiwan*
Dincer, I. / *Canada*
Eroglu, I. / *Türkiye*
Goltsov, V.A. / *Ukraine*
Hamdullahpur, F. / *Canada*
Hepbasli, A. / *Türkiye*
Hirohisa, U. / *Japan*
Kakac, S. / *Türkiye*
Karakoc, H. / *Türkiye*
Karaosmanoglu, F. / *Türkiye*
Kargı, F. / *Türkiye*
Kendall, K. / *UK*
Koca, A. / *Türkiye*
Kumbur, E.C. / *USA*
Li, X. / *Canada*
Mench, M.M. / *USA*
Midilli, A. / *Türkiye*
Min, Z. / *China*
Miranda, P.E. / *Brazil*
Mohammadi, A.H. / *South Africa*
Muradov, N. / *USA*
Naterer, G.F / *Canada*
Ozkar, S. / *Türkiye*
Ozturk, T. / *Türkiye*
Ramenskiy, A.Y. / *Russia*
Rosen, M.A. / *Canada*
Sahin, O./ *Türkiye*
Sahin, S./ *Türkiye*
Sattler, C./ *Germany*
Sheffield, J.W. / *USA*
Spazzafumo, G. / *Italy*
Stanislaw, S. / *Poland*
Stolten, D. / *Germany*
Vasudevan, S. / *India*
Veziroglu, E.A. / *USA*
Veziroglu, A. / *USA*

Teknoloji neredeyse BİZ ORADAYIZ!

Dünyanın bakırdan beklentisini daha ileriye taşımak için madenden son ürüne kadar tüm üretim sürecini gerçekleştirmekle kalmıyor, üretim potansiyelimizi AR-GE çalışmalarımızla güçlendiriyoruz; sayısız sektöre yepyeni çözümler sunuyoruz.



ETİ BAKIR



HYDROGENIX

HYDROGEN AND ENERGY STORAGE TECHNOLOGIES INC.

HYDROGEN TIME
ONE STOP SHOP
for
NET ZERO CARBON

01 **DECARBONIZATION and EFFICIENCY**

Decarbonization and energy efficiency roadmap for industrial and residental facilities

02 **HYDROGEN TRANSMISSION**

Hydrogen transmission and consultancy, feasibility studies and project design

03 **GREEN HYDROGEN PRODUCTIONS**

Hydrogen production based on renewable energy sources

04 **R&D and SYSTEM INTEGRATION**

Hydrogen systems integration (EPC) and maintenance

Turgut Özal Bulvarı No:143
Sahilyolu İdealtepe 34841
Maltepe/İstanbul/TURKEY

+90 216 417 00 82
info@hydrogenix.com.tr
www.hydrogenix.com.tr

SCIENTIFIC PROGRAM

SCIENTIFIC PROGRAM

Day 1- Sunday May 12, 2024

	Registration Desk
13:00-17:00	**Registration**

Day 2 - Monday May 13, 2024

	HALL A
09:15-10:00	**Opening Talks** **Heybet KILIÇ** (Congress Chair) **İbrahim DİNÇER** (President, National Hydrogen Association) **Nedim TÜZÜN** (Deputy General Manager, DEDAŞ) **Gökhan Kürşat DEMİR** (Deputy Production Manager, ETİ Bakır) **Mehmet KARAKOÇ** (Rector, Dicle University) **Ali İhsan SU** (Governor of Diyarbakir, to be confirmed)
10:00-10:35	**Theme Speaker / Abdulkadir BALIKÇI** (Energizing Türkiye's future:The Green Hydrogen Revolution)
10:35-10:55	**Coffee Break**
	Chair: Wei-Hsin Chen
10:55-11:35	**Keynote Speaker / İbrahim Dincer** (Hydrogen Energy Technologies: New Perspectives)
11:35-12:15	**Keynote Speaker / Seeram Ramakrishna** (Electrospun Nanomaterials for the Hydrogen Economy)
12:15-13:45	**Lunch** **Board Meeting of Hydrogen Technologies Association** (Invite only)

SCIENTIFIC PROGRAM

Day 2 - Monday May 13, 2024

	PARALLEL SESSIONS		PARALLEL SESSIONS	
	HALL A	**HALL B**	**HALL C**	**HALL D**
13:45-15:30	**Session 1A: TENMAK Session**	**Session 1B: Green Hydrogen-I**	**Session 1C: Fuel Cells-I**	**Session 1D: Modeling, simulation and optimization-I**
	Chair: Adnan Midilli	**Chair: Ramazan Solmaz**	**Chair: Bestami Özkaya**	**Chair: M. Siraç Özerdem**
	Turkish Energy, Nuclear and Research Agency (TENMAK) **Bahadır SAYGI** **Energy and Technology Policies of TENMAK** **Celal ERBAY** **Funding Programmes of TENMAK** **Gülten ÖZÇAYAN**	**(Invited Talk)** Potential of membrane engineering in the field of hydrogen generation and purification: strategies to meet the targets of the European Clean Hydrogen Alliance in the framework of the European Green Deal **/ Adolfo Lulianelli**	**#31** Prediction of Short-Term Voltage Loss of PEM with Single-Step and Multi-Step LSTM Networks / **Yurdagül Benteşen Yakut**	**#6** 0-D Mathematical Modeling of Anion Exchange Membrane Water Electrolyzer / **Ceren Celebi**, Can Ozgur Colpan and Yılser Devrim
			#16 Investigation of a Sacrificial Template Material Suitable for Fabrication of Anode Support Microtubes in Microtubular Solid Oxide Fuel Cells / **Ahmet Alp Sunecli**, Cigdem Timurkutluk, Tolga Altan, Sezer Onbilgin and Bora Timurkutluk	**#135** Analyzing Energy Efficiency in Hydrogen Energy from Agriculture: A Bibliometric Approach / **Masud Kabir** and Sami Ekici
		#212 Evaluation of Hydrogen Energy Concept from Elementary School to University: Opinions of Energy Systems Engineers on Hydrogen Energy Concept **/ Eylem Kılıç**	**#79** PEMFC Performance of Pt Catalyst Decorated on Heat-Treated Carbon Black / **Ayşenur Öztürk Aydın** and Ayşe Bayrakçeken	**#55** Exploring the Impact of Channel Geometry and Temperature on Solid Oxide Electrolyzer Cell Performance / **Berre Kumuk**
		#37 Biohydrogen Production in a Biofilm Photobioreactor with Functionalized Microfiber Flock / **Emrah Sagır**, Harun Koku Tuba Bayramoğlu et.al.	**#32** Investigation of the Current Effect on Electrochemically Deposited Pt Catalyst Properties for PEMFCs / **Jülide Hazal Özdemir** and Aysel Kantürk Figen	**#21** Development of Electrolytic Cation Exchange Integrated Reactor for H_2 Generation and CO_2 Extraction / **Hilal Sayhan Akci Turgut** and Ibrahim Dincer
		#47 Fabrication of Graphene Oxide Based Composite Membranes for Anion Exchange Membrane Water Electrolyzers / Yılser Devrim and **Nisa Gökçen Önel**	**#41** Integration of an SOFC with Closed Brayton and Rankine Cycles for Hydrogen Production: Thermodynamic Analysis and Heat Recovery Considerations / Mohammad Ali Sabbaghi, Ehsan Baniasadi and **Hadi Genceli**	**#139** Evaluation of Exergy Efficiency of a PEM Fuel Cell System / Sinan Kapan, **Zehra Ural Bayrak** and Nevin Çelik
		#48 A Novel Bi/W/Cd Photocatalyst for Hydrogen Production Via Water Splitting / Ceren Sakallı and **Halit Eren Figen**	**#201** 2D Transition Metal Carbide (MXene) as Promising Catalyst for Fuel Cells / **Emre Oguz Koroglu**	**#104** Estimating the Remaining Useful Life of PEM Fuel Cell with LSTM Method / **Mehmet İsmail Gürsoy**
		#187 Hydrogen andHydrogen TechnologiesinHealthcare Institutions / **Duygu Yıldırım**, CemHaydaroğlu, Burak Yıldırım, Mahmut TemelÖzdemir andOzan Erdinc	**#12** Parametric Evaluation of a Hydrogen-driven Lightweight Vehicle with Thermally Coupled FC/MH tank system / **Sera Ayten Çetinkaya**, Mehmet Akif Ezan, Mustafa Umut Karaoğlan and Can Ozgur Colpan	**#203** Energy Management in Microgrids with Hybrid Energy Storage Systems Utilizing Batteries and Proton Exchange Membrane/Fuel Cells / **ÖmerFaruk Özcan**, Heybet Kilic and Ömer Faruk Özgüven

SCIENTIFIC PROGRAM

Day 2 - Monday May 13, 2024

15:30-15:50	**Coffee Break**			
	PARALLEL SESSIONS		**PARALLEL SESSIONS**	
	HALL A	**HALL B**	**HALL C**	**HALL D**
15:50-18:05	**Session 2A: Fuel Cells-II**	**Session 2B: Green Hydrogen-II**	**Session 2C: Modeling, simulation and optimization-II**	**Session 2D: Renewable Hydrogen Technologies and Application-I**
	Chair: İnci Eroğlu	**Chair: Nevin Çelik**	**Chair: Muhsin Tunay Gençoğlu**	**Chair: İbrahim Kaya**
	#45 Boron-Based Hydrogen Storage Materials as a Hydrogen Source in Synthetic Fuel Production / **Berfin Ekin Ülgen**, Bilge Coşkuner Filiz, Korkut Açıkalın, Hülya Civelek Yörüklü and Aysel Kantürk Figen	**#132** Synthesis of Titanium Dioxide (TiO_2) Based Photocatalyst and Investigation of Hydrogen Production Activity / **Beyza Yıldırım**, Muhammed Iberia Aydin and Aysel Kantürk Figen	**#138** Catalyst Selection for Microplastic Photodegradation Via MCDM Analysis / **Hulya Civelek Yörüklü**	**#185** Investigation of Hydrogen Production Potential by Using the Concentrated Multi-Junction Photovoltaic Solar Cell / **Cihangir Kale** and Hikmet Esen
	#119 Enabling Interactive G2V and V2G Integration Through Smart Fault Protection and Bi-Directional Power Flow Control in EV Charging Stations / Samet Öner and **Gokay Bayrak**	**#220** Second-Life Battery Utilization in Solar Power Plants: Economic Analysis, Revenue Optimization, and Profit Increase / Feyza Turan, **Ali Rıfat Boynueğri,** Ali Furkan Tetik, Ozan Erdincand Yavuz Ates	**#120** CFD Combustion Model Optimization for Hydrogen Blended Combustion in Furnace Experimental System / **Onur Salcı** and Semiha Öztuna	**#51** Journey to a Sustainable Future: The Importance of Renewable Hydrogen in Industrial and Domestic Applications / **Nesrin İlgin Beyazit**
	#90 Proton Exchange Membrane Fuel Cell Applications of Multirotor UAV / **Merve Yıldırım**, Harun Koku and İnci Eroğlu	**#123** Optimization of Electrospinning Parameters to Get Nano Hematite Fibers as a Photo Anode for Hydrogen Production Through Water-Splitting / **Şükrü Kaya** and Cevat Sarıoglu	**#128** Design of a New MPPT Controller in PEM Fuel Cell System / **Servan Marşil**, Cem Haydaroğlu and Heybet Kilic	**#53** Machine Learning Analysis of Biogas Tri-reforming for Syngas Production / Ahmet Coşgun, M. Erdem Günay and **Ramazan Yıldırım**
	#69 Oxygen Mobility Behavior of Calcium Doped $BaZrO_3$ Perovskite Electrocatalysts / Enes Emre Yılmaz, **Elvan Burcu Koşma** and Meltem Karaismailoğlu Elibol	**#116** Fault Diagnosis Method for Polymer Electrolyte Membrane Fuel Cells Using Deep Learning Technologies / **Meltem Yavuz Çelikdemir**	**#130** A new controller design based on Fuel Cells / **Serhat Doğan**, Cem Haydaroğlu and Bilal Gümüş	**#68** Synthesis and Characterization of La and Ga Promoted Copper-Containing Catalysts for Methanol Steam Reforming Reaction / **Orhan Özcan** and Ayşe Nilgün Akın
	#27 De-noising of a Fuel Cell Hybrid Microgrid, Including Energy Generation, Consumption, and Storage Units / Sıtkı Akkaya, **Mehmet Güçyetmez**, Murat Uyar and Şekip Esat Hayber	**#33** Investigation of Hydrogen Production Performance of KBH_4 Hydrolysis with Thin Film TiO_2 Catalyst / **Ayşenur Şeşe** and Meryem Sena Akkus	**#186** Thermodynamic Performance Assessment of PEMFCPowered Air to Water Heat Pump / **Anil Erdogan**, Ozge Ozcan Bilgilioglu, Oguz Yildirim, Suleyman Aykut Korkmaz, Omer Can Inci and Can Ozgur Colpan	**#71** Operation modes and hup mutation determine H2 and PHB production in Rhodobacter capsulatus / **Ertan Hoşafçı**, Etkin Tarlan, Tuba Hande Ergüder Bayramoğlu and Harun Koku

SCIENTIFIC PROGRAM

Day 2 - Monday May 13, 2024

...	PARALLEL SESSIONS / Continued..		PARALLEL SESSIONS / Continued..	
	HALL A	**HALL B**	**HALL C**	**HALL D**
	Session 2A: Fuel Cells-II	**Session 2B: Green Hydrogen-II**	**Session 2C: Modeling, simulation and optimization-II**	**Session 2D: Renewable Hydrogen Technologies and Application-I**
	#106 Fuel Cell and Battery Powered Brushless Direct Current Motor Control for Light Electric Vehicle Applications / **Habip Şahin**, Muhammed Sefa Çetin, Muhsin Tunay Gençoğlu and Ozan Erdinç	**#178** Electrochemical Hydrogen Production Activity of Self-Assembled Monolayer Film Prepared from Bingöl Walnut Leaf Extract on Copper Surface / **Yeşim Aydın Dursun** and Ramazan Solmaz	**#166** Renewable Energy Supported and Hydrogen Energy Storing Off-Grid Smart City Design / **Emrullah Kocaman**, Hüseyin Yağlı, Recep Yumrutaş, Ali Koç and Yıldız Koç	**#77** A Study on Geothermal-Based H_2S-FeCl Hybrid Process for Hydrogen Production and H_2S Removal / **Sulenur Asal**, Adem Acır and Ibrahim Dincer
	#28 The Detection of Power Quality Change During Multiple Disturbances for Microgrid Protection and Fuel Cell Health / Sıtkı Akkaya, **Mehmet Güçyetmez**, Murat Uyar and Şekip Esat Hayber	**#192** Power to Hydrogen: Assessing the Transition of Electric Charging Stations to Green Hydrogen / **Meltem Yavuz Çelikdemir** and Hasan Gunduz	**#167** Development of Optimization-Based Energy Management System in Hybrid Charging Stations / Abuzer Çalışkan and **Hasan Bektaş Perçin**	**#221** Enhanced Battery State-of-Health Estimation Using Artificial Intelligence and Multiple Charge/Discharge Features / **Cafer Budak**
	#46 Optimum Design and Techno-economic Evaluation of PV Integrated On-Site Hydrogen Refueling Stations / Reyhan Atabay and **Yılser Devrim**	**#5** Design and Thecno-Economic Analysis of a Combined Heat and Power System with Hydrogen Storage / **Mehmet Ali Köprü**, Dursun Öztürk and Burak Yıldırım	**#179** Advancing Power System Reliability with AI-Driven Monte Carlo Simulations for Hydrogen Fuel Cell Integration / Dogan Urgun and **Gokhan Gungor**	**#174** Cooperative Games to Support the Development of the Hydrogen Economy / **Sofía De-León Almaraz**, Andrea Gelei and Tamás Solymosi
	#113 Optimal Design of a Solar Powered On-Grid Hybrid Charging Station for Electric-Hydrogen Vehicles / **Habip Şahin**, Cihangir Kale and Hikmet Esen		**#95** A New Approach to Determine Model Parameters of Proton Exchange Membrane Fuel Cells Using Convolutional Neural Network / **Mustafa Tan** and Cem Emeksiz	**#129** Hydrogenation of Safflower Oil for Sustainable Biocomposite Production: Process Optimization and Characterization / **Ercan Aydoğmuş** and Cenk Yanen
19:00-21:00	**Gala Dinner ( )**			

SCIENTIFIC PROGRAM

Day 3 - Tuesday May 14, 2024

	HALL A			
	Chair: Fariborz Haghighat			
09:00-09:40	**Keynote Speaker / Zhe Chen** (Hydrogen- A Carrier in Future Clean and Sustainable Energy Systems)			
09:40-10:20	**Keynote Speaker / Wei-Hsin Chen** (Hydrogen Production and Separation Optimization for Decarbonization and Net Zero)			
10:20-10:40	**Coffee Break**		**Coffee Break**	
	PARALLEL SESSIONS		**PARALLEL SESSIONS**	
	HALL A	**HALL B**	**HALL C**	**HALL D**
10:40-12:35	**Session 3A: Company Overview Presentations-I**	**Session 3B: Renewable Hydrogen Technologies and Application-II**	**Session 3C: Energy, exergy and economic analyses-I**	**Session 3D: Conventional hydrogen technologies and applications**
	Chair: Adnan Midilli	**Chair: Mehmet Nergiz**	**Chair: HüseyinTuran Arat**	**Chair: Aysel Kantürk Figen**
	Anton Paar Seda GİRAY ÖZEN Application and Sales Specialist **TEK-SİS** Hüseyin DEVRIM General Manager **Bataryasan Enerji** Mehmet Fatih KAYA General Manager **Aspilsan** Emre ATA Hydrogen and Fuel Cell Development Center Manager **YEO Teknoloji** Ali KELEŞ	**#121** Hydrogen Blended NG Fuelled a Process Heating Application / **Onur Salcı**, Semiha Öztuna and Mustafa İlbaş	**#10** A Comprehensive 4E Analysis and Multi-Objective Optimization of a Hybrid Trigeneration System Powered by a Solar Tower and Wind Turbine for Producing Green Hydrogen, Electricity, and Cooling / Faizan Khalid and **Syed Abuzar Suhail**	**#58** Colorless Distributed Combustion (CDC) Effects on Hydrogen – Methane Composite Fuel Mixture Combustion Characteristics / **Osman Kumuk** and Serhat Karyeyen
		#217 Assessing the Environmental Footprint of Catalysts in Photoelectrochemical Hydrogen Production Through Life Cycle Analysis / **Muhammed Iberia Aydin** and Ibrahim Dincer	**#49** Experimental Studies and Comprehensive Analysis of Energy, Exergy, Environmental, and Enviroeconomic Aspects of Diesel Fuel, Waste Tyre Pyrolitic Oil, and Oxy-Hydrogen Gas Mixture Used for Diesel Engine / **Salih Özer**, Halil Erdi Gülcan, Samet Çelebi and Usame Demir	**#102** Thermodynamic Assessment of an Improved Solar Powered Multi-Generation System Using a Thermoelectric Generator / Mohammad Ali Sabbaghi, Ehsan Baniasadi and **Hadi Genceli**
		#109 Supervised Learning Based PEM Fuel Cell Model / Soner Çelikdemir, **Burak Özdemir** and Mahmut Temel Özdemir	**#54** Catalytic Activity of W-O and Fe-O in H_2S Decomposition / **Yaren Ataseven**, Mert Yekta Doğan, Sena Yaşyerli, H. Mehmet Taşdemir, Hüseyin Arbağ and Nail Yaşyerli	**#110** Preparation and Performance Investigation of Self-supported CoB Catalysts for Sodium Borohydride Hydrolysis Reaction / Jülide Hazal Özdemir, Hüseyin Elçiçek, Görkem Kökkülünk and **Oğuz Kaan Ozdemir**

SCIENTIFIC PROGRAM

Day 3 - Tuesday May 14, 2024

...	PARALLEL SESSIONS / Continued..		PARALLEL SESSIONS / Continued..	
	HALL A	**HALL B**	**HALL C**	**HALL D**
	Session 3A: Company Overview Presentations-I	**Session 3B: Renewable Hydrogen Technologies and Application-II**	**Session 3C: Energy, exergy and economic analyses-I**	**Session 3D: Conventional hydrogen technologies and applications**
		#140 Heterojunction Cr_2O_3/Cuo Photocathode for Photoelectrochemical Hydrogen Production / **Ender Faki**, Fatih Tezcan, Gökmen Sığırcık and Gülfeza Kardaş	**#237** Impact of Green H2 on Global Warming and Production: Transportation Challenges **/ Zaheer Abbas**	**#155** Novel Bi_2S_3 and $NiBiS_3$ Electrocatalysts for Alkaline Hydrogen Evolution Reactions / **Goncagül Aksaray**, Mehmet Erman Mert, Başak Doğru Mert and Gülfeza Kardaş
		#152 Enhancing Operation Reliability of PV/PEMFC/Battery-Based Distributed Generation via Deep Supervised Learning Approach / **Alper Nabi Akpolat**	**#14** Hydrogen Fuel Quality, Testing, Reference Materials Production, Proficiency Testing Scheme / **Erinc Engin**, Thomas Bacquart, Abigail Morris and Pierpaolo Modugno	**#157** NiP Cathode Catalyst for Alkaline Water Electrolyser / **Goncagül Aksaray**, Ender Faki, Yakubu Sawadogo Adam, Patrick Marcel Seumo Tchekwagep, Murat Farsak and Gülfeza Kardaş
		#154 Multi-optimization of Hydrogen Production of a Solar-based S-I Thermochemical Cycle / Ramazan Çakıroğlu, Gamze Şener, **Oğuz Kaan Çinici** and Adem Acır	**#4** Assessing the Thermodynamic Examination of Solar Heliostat-based Multigeneration Plant Integrated with LNG Regasification Cycle for Hydrogen Generation / **Fatih Yılmaz**, Murat Ozturk and Resat Selbas	**#163** Design, Data Analysis and Prototype Manufacturing of Off-Grid Domestic Refrigerator Systems / Burak Halis Güneş, Bahattin Sevinçli, Ufukhan Acar, Tahsin Altuğ Özden, Olgun Konur, Suleyman Aykut Korkmaz, **Anıl Erdoğan** and Rüstem Aşık
		#164 Modeling and Control of the PEMFC Energized Mobile Robot / **Tevfik Yiğit**	**#161** Thermodynamic Analysis of the Integration of Reverse Osmosis Desalination, Reverse Electrodialysis and Photo-Chloralkaline System Using Renewable Energy for Enhanced Brine Management and Hydrogen Production / **Nadira Salsabila**, Muhammad Usman Sajid and Yusuf Bicer	**#162** The Effect of TiO_2 Coating on PEC Efficiency of Hematite Photoanode Produced by Thermal Oxidation of Electrodeposited Fe Thin Films / **Uğur Oktay** and Cevat Sarıoglu
		#171 Hydrogen-based Mobile Fast Charging Station for Disasters and Emergencies / **Tevfik Yiğit,** Hakan Celik and Zehra Ural Bayrak	**#9** A Sustainable Geothermal Based Multigeneration Plant for Green Hydrogen Generation; Energy and Exergy Analysis / **Fatih Yılmaz**, Murat Ozturk and Resat Selbas	**#175** Nano Iron Powder Usage in HHO Dry Cell Electrolyte Solution / Mustafa Kaan Baltacıoğlu and **Onur Bulut**
12:35-14:30	**Lunch** **Meeting Between Hydrogen Technologies Association and Companies** (Invite only)		**Lunch** **Meeting Between Hydrogen Technologies Association and Companies** (Invite only)	

SCIENTIFIC PROGRAM

Day 3 - Tuesday May 14, 2024

	PARALLEL SESSIONS		PARALLEL SESSIONS	
	HALL A	**HALL B**	**HALL C**	**HALL D**
14:30-16:15	**Session 4A:Company Overview Presentations-II**	**Session 4B: Hydrogen vehicles-I**	**Session 4C: Hydrogen storage and materials**	**Session 4D: Hydrogen thermodynamics**
	Chair: Can Özgür Colpan	**Chair: Bilal Gümüş**	**Chair: Sedat Bingöl**	**Chair: Mehmet Karakılçık**
	Dicle Elektrik Ahmet KIRAT Deputy General Manager, DEDAŞ **Filament Technology** Yusuf Can UZ-CEO **Hydrogenix** Ali Rıza ARSLAN General Manager **TRL Instruments** Bülent ATAMER Consultant **TÜPRAŞ** Ela AYRAL R&D Researcher |Project & incentives Management- Clean Hydrogen Team	**#44** Emission Analyses of Hydrogen Fuels Obtained From Different Sources for Various Vehicles / **Sumeyya Ayca** and Ibrahim Dincer	**#13** Characterisation of a Graphite Electrode Coated with a Nickel-Modified Nickel-Iron Alloy and Catalytic Effect in an Alkaline Medium / Ali Topak and **Serap Toprak Döşlü**	**#26** A Solar Integrated System with a New Hydrogen Generator / **Mehmet Gursoy** and Ibrahim Dincer
		#225 Thermal Performance of a Biogas-Fed Multi-generation Plant for Power, Cooling, and Hydrogen Generation with LNG Cold Energy Recovery / Shoaib Khanmohammadi, **Gamze Soyturk** and Onder Kizilkan	**#50** Hydrogen Storage and Metal Hydride Storage / **Nesrin İlgin Beyazit**	**#82** The Investigation of Hydrogen Production by Using Proton Exchange Membrane Electrolysis Cell Technology / Hacı Soğukpınar, İsmail Bozkurt, Serkan Cag, Mustafa Yavaş, Ayhan Atız and **Mehmet Karakılçık**
		#63 Accelerating Towards Hydrogen: A Qatar Scenario-Based Life Cycle Cost Comparison between Conventional, Electric, and Hydrogen Fuel Cell Vehicles / **Yusuf Bicer**, Carlos Mendez, Brenno Castrillon Menezes, Marcello Contestabile	**#66** Retrofitting Analysis of LNG FSRU with On-Board Ammonia and Hydrogen Storage Tanks / **Dindha Andriani**, Omer Abedrabboh and Yusuf Bicer	**#83** A Superadiabatic Hydrogen Sulfide Combustion System for Clean Hydrogen Production / **Muhammad Ishaq** and Ibrahim Dincer
		#224 A novel SOFC based multi-generation system with recompression sCO2-BC, reheat tCO2-RC, HDH unit and H2 production / **Gamze Soyturk** and Onder Kızılkan	**#70** Effect of different Solvents on Hydrogen Production from Hydrolysis of Potassium Borhydride with a New and Active Ni-Based Catalyst Synthesized by Green Synthesis / Ömer Şahin, **Selma Ekinci**, Mehmet Sait İzgi and Erhan Onat	**#99** Developing Exergetic Sustainability Indicators of Anion Exchange Membrane Electrolyzer / **Furkan Şengüler** and Adnan Midilli
		#80 Simulational Anaylses of Hybrid Fuel Cell Locomotive / Mustafa Tunahan Başar, **Mustafa Kaan Baltacıoğlu** and Hüseyin Turan Arat	**#89** Well-Integrity Issues in the Underground Hydrogen Storage Sites / **Sukru Merey** and Hakkı Aydın	**#108** Investigation of the Effects of Hydrogen and Water Vapor Addition on Compression Engine Performance and Exhaust Emissions / Zafer Akbalık and **Orhan Arpa**
		#114 Comparative Environmental Impact Evaluation of Diesel Fuels and Liquid Hydrogen in Transportation / **Assem Abdurakhmanova** and Ibrahim Dincer	**#100** Optimizing Underwater Hydrogen PEMFC Applications: A 2-D Mathematical Modeling Framework for Metal Hydride-Based Hydrogen Storage Systems / **Berna Sezgin**, Tayfur Öztürk and İnci Eroğlu	**#158** The Effect of Using Nanofluid in a Parabolic Trough Collector on Its Thermodynamic Performance and Hydrogen Production / **Orhan Şahmerdan**, Canan Cimşit and Müslüm Arıcı
		#169 Fuel Cell Powered Visible Light Communication System Design / **Yavuz Erol**	**#141** Hydrogen Generation from Ethylenediamine Bisborane Solution with Metal Catalyst Coated on Metal Oxide / Reduced Graphene Oxide / **Burak Uygar Mert Yorgun**, Gülay Özkan and Göksel Özkan	**#159** The Performance Comparison of a Hydrogen Production System Utilizing Solar Energy with Nanofluid in Its Parabolic Trough Collector for Antalya and Kocaeli / **Orhan Şahmerdan**, Canan Cimşit and Müslüm Arıcı

SCIENTIFIC PROGRAM

Day 3 - Tuesday May 14, 2024

16:15-16:35	**Coffee Break**		**Coffee Break**	
	PARALLEL SESSIONS		**PARALLEL SESSIONS**	
	HALL A	**HALL B**	**HALL C**	**HALL D**
16:35-18:35	**Session 5A: Hydrogen in smart grids**	**Session 5B: Green Hydrogen-III**	**Session 5C: Fuel Cells-III**	**Session 5D: Hydrogen separation and purification**
	Chair: Mesut Şeker	**Chair: Habip Şahin**	**Chair: Zehra Ural Bayrak**	**Chair: Can Özgür Colpan**
	(Invited Talk) Energy Ships for Hydrogen Production / **Wolfram Reiners**	**#42** Development of Electro-biomembrane Integrated Renewable-based System to Produce Fresh Water and Biohydrogen for Sustainable Communities / **A. Yagmur Goren**, Ibrahim Dincer and Ali Khalvati	**#118** The Effective Parameter Estimation for a PEMFC Based on Archimedes Optimization Algorithm / Abuzer Çalışkan and **Hasan Bektaş Perçin**	**#40** Development of Polybenzimidazole Containing MOF Membranes for Anion Exchange Membrane Water Electrolysis / **Hasan Altınışık** and Yılser Devrim
		#93 Investigation of Methane Catalytic Decomposition over Mesoporous Carbon Supported Ni/La Based Catalysts / **Hazal Pınar Köse** and Dilek Varışlı	**#131** Control Parameters Optimization of HHO Dry Cell by Metaheuristic Algorithms / Çağlar Conker and **Mustafa Kaan Baltacıoğlu**	**#75** Sonic Hydrogen Production: An Experimental Investigation / **Moslem Sharifishourabi**, Ibrahim Dincer and Atef Mohany
	#133 Impacts of Hydrogen Fuel Stations on Distribution Networks / **Halil İbrahim Tekin** and Bilal Gümüş	**#94** Development of Bimetallic Catalysts for CO_x-free Hydrogen Production by Microwave-Assisted Catalytic Methane Decomposition / **Ceren Acar** and Dilek Varışlı	**#136** Use of Rotor Wound Synchronous Motor in Fuel Cell Electric Vehicles / **Kıvanç Doğan**, Ahmet Orhan and Abuzer Çalışkan	**#205** Activated Carbon from Sugar Beet Pulp for CO_2 Capture / Fahriye Dönmez Dayı, **Salahaldeen Aljafreh**, Damla Dumlu and Nezihe Ayaşşablona
	#145 Analysis of Real Grid Voltage Fluctuation Problem with Nickel Hydrogen Batteries Using DIGSILENT Program / **Hulusi Faik Orhan** and Abuzer Çalışkan	**#111** Synthesis of $Cd_{0.7}Zn_{0.3}S$/ MoS_2 Catalysts and Investigation of Their Activities in Photocatalytic H_2 Production / **İbrahim Kaba** and Özge Kerkez Kuyumcu	**#146** Identifying the Battery Status and Battery Capacity in Discharge based on Battery Current by Machine Learning Methods / **Yasin Sönmez**	**#56** Evaluation of Hydrogen Production by Cobalt Chloride Thermochemical Method in a Fusion Reactor / **Medine Özkaya** and Adem Acır
	#226 Applications and Challenges in High Pressure Gas Sorption / **Seda Giray Özen**	**#97** Leveraging Renewable Energy for Türkiye's Future Hydrogen Supply Chain: A Stochastic Programming Model / **Busenur Türkali Özbek**, Ahmet Erdoğan and Mehmet Güray Güler	**#148** Comparative Analysis of YSZ and SCSZ Electrolytes in Solid Oxide Fuel Cells (SOFCs) with Novel PrCeMn Electrocatalyst / **Esra Balkanli Unlu**, Meltem Karaismailoglu and Halit Eren Figen	

SCIENTIFIC PROGRAM

Day 3 - Tuesday May 14, 2024

...	PARALLEL SESSIONS / Continued..		PARALLEL SESSIONS / Continued..	
	HALL A	**HALL B**	**HALL C**	**HALL D**
	Session 5A: Hydrogen in smart grids	**Session 5B: Green Hydrogen-III**	**Session 5C: Fuel Cells-III**	**Session 5D: Hydrogen separation and purification**
	#107 Evaluation of a Decarbonized Combined Heat and Power (CHP) Plant, Incorporating Photovoltaic Panels and Hydrogen Re-electrification / Maryam Karami, Parsa Fathi and **Parisa Heidarnejad**	**#168** Some Policies About Green Hydrogen Use for Decarbonization of Steel Industry / **Ali Eren Aluç** and Adnan Midilli	**#149** Circle-Inspired Optimization Algorithm for Parameter Estimation in Photovoltaic and Fuel Cell Systems / **Süleyman Yıldız**	**#147** Hydrogen Production with Cu-Cl Thermochemical Cycle Integrated into Next-Generation Nuclear Power Plant for Sustainable Cities / **Muhammet Mert Dincer** and Merve Ozturk.
	#115 Exploring Novel Sustainable Energy Management Techniques: Unlocking the Potential of Black Sea Hydrogen Sulfide into Usable Energy / **Elifnaz Unay**, Bestami Özkaya, Doğukan Tunay and Oğuz Kaan Özdemir	**#34** Hydrogen Transport Using Ammonia / **Miray Deşer Karip** and Mustafa Kaan Baltacıoğlu	**#29** Silicotungstic Acid-Incorporated Waste Tire-Derived Activated Carbon Catalysts for DME Production / Altay Usta, Barıs Tekce, **Ogun Tastan** and Birce Pekmezci Karaman	**#189** HOPat: A New Feature Extraction Function Based on the Atomic Orbitals of the Hydrogen Atom / **Habip Şahin**, Şengül Doğan and Türker Tuncer
	#127 Analysis of a Microgrid with Hydrogen Storage from a Technoeconomic Perspective / **Elifnur Bayraktar**, Cem Haydaroğlu, Yahya Akıl, Faruk Barlaz, and Heybet Kilic	**#137** Thermodynamic Analysis of Hydrogen Production with Different Solar Collectors / **Arif Karabuga**	**#15** Effects of Volume Fraction and Particle Size on Triple-Phase Boundaries in Solid Oxide Fuel Cell Anodes / **Emre Ucar** and Bora Timurkutluk	**#61** Hydrogen Detection and Electrical Properties of Perovskite $TiSiO_4$ Schottky Diode / **Lütfi Bilal Taşyürek** and Necmettin Kilinc
	#150 Utilization of Modular Floating Offshore Energy Islands with High Green Hydrogen Penetration: A P2X example **/ Alper Nabi Akpolat**	**#191** Assessment of Sensitivity to Temperature and Feedstock Characteristics in Biomass Pyrolysis using Aspen Plus / **Kaan Erdem**, Duygu Gündüz Han and Adnan Midilli	**#105** Investigation of Hydrogen Production from Brine by Using Membrane Cell Process Technology / Hacı Soğukpınar, İsmail Bozkurt, **Serkan Cag**, Mehmet İsmail Gürsoy, Ayhan Atiz and Mehmet Karakılçık	**#73** Gas Leakage from Hydrogen Car Stored Tanks: A Bow-Tie Risk Analysis / **Mehmet Tunç** and Ramazan Solmaz
18:35-19:40	**Board Meeting of Hydrogen Technologies Association (Invite only)**			

SCIENTIFIC PROGRAM

Day 4 - Wednesday May 15, 2024

	PARALLEL SESSIONS		PARALLEL SESSIONS	
	HALL A	**HALL B**	**HALL C**	**HALL D**
09:00-10:25	**Session 6A: Sustainable hydrogen technologies**	**Session 6B: Renewable hydrogen technologies and applications-III**	**Session 6C: Hydrogen vehicles-II**	**Session 6D: Syngas technologies**
	Chair: Ramazan Solmaz	**Chair: Mehmet Karakılçık**	**Chair: Hüseyin Turan Arat**	**Chair: Fatih Sorgulu**
	(Invited Talk) Past, Present and Future of Polymer Electrolyte Membrane Electrolyzers for Green Hydrogen Production / **Can Erkey**	**#173** Off-grid cities with an Environmental Analysis Approach for Sustainability: A Review Considering Alternative Fuels, Renewable Energy Sources and Energy Storing / **Emrullah Kocaman**, İbrahim Furkan Korkmaz, Hüseyin Yağlı and Özkan Köse	**#124** Energy Management Strategy for Improving Flight Performance of Fuel Cell Hybrid Quadrotor UAV / Sencer Ünal and **Murat Kayaoğlu**	**#7** Syngas Reforming on Microwave Cracking Bed Following Bubling Coal and Biomass Pyrolysis Tar Mix / **Yildirim İsmail Tosun** and Fethullah Chichek
		#176 Exergetic Sustainability Indicators of E-methanol Production depending on green hydrogen / **Selçuk İnaç** and Adnan Midilli	**#134** A Review of Performance, Combustion, and Emissions of Diesel Engines Fuelled with Hydrogen / **Mert Gülüm**	**#22** Reactivity of Nickel Based Monolithic Catalyst in the Oxidative Steam Reforming of Biogas with H_2S / **Merve Doğan Özcan**, Orhan Özcan and Ayşe Nilgün Akın
	#188 Fabrication of 3D Ordered Mesoporous 1T-phase MoS_2/C for Electrochemical Hydrogen Evolution / **Derya Öncel Özgür** and Filiz Aktı	**#17** Developing a Visible Light Communication System for Grid Protection in a Green Hydrogen Powered EV Charging Station / Murat Daş and **Gokay Bayrak**	**#153** Comparison of Diesel and Fuel Cell Powered Locomotives in terms of Environmental and Technological Change / Kenan Doğan and **Zehra Ural Bayrak**	**#25** $CeCoO_3$ as an Effective Catalyst Support for Ni in Methane Reforming Reactions / **Atalay Calisan** and Deniz Üner
			#122 Performance Evaluation for an Hybrid E-scooter Worked with FC/Battery Integration / Sencer Ünal and **Hilal Bıyık**	**#35** Heating Tubes Design for Parametric Study of Steam Reformer at Small Scale / **Muhammed Murat Aksoy** and Onder Kaska

SCIENTIFIC PROGRAM

Day 4 - Wednesday May 15, 2024

...	PARALLEL SESSIONS / Continued..		PARALLEL SESSIONS / Continued..	
	HALL A	**HALL B**	**HALL C**	**HALL D**
	Session 6A: Sustainable hydrogen technologies	**Session 6B: Renewable hydrogen technologies and applications-III**	**Session 6C: Hydrogen vehicles-II**	**Session 6D: Syngas technologies**
	#67 Enhancing Photocatalytic Partial Oxidation of Methane to Methanol: Experimental Investigation of 2D and Oxide Catalysts / **Amira Chebbi**, Alessandro Sinopoli, Ahmed Abotaleb and Yusuf Bicer	**#198** Development of a High-Performance Fully Automatic PEM Water Electrolyser Control System for Solar Energy-Assisted Hydrogen Production / **Eda Nur Çakıraslan**, Emre Özdoğan, Eren Batuhan Orhan, Ahmet Altun, Murat Kıstı and Mehmet Fatih Kaya	**#170** Securing the Future a Comprehensive Study on the Implications of Cyber Intrusions on Battery Management in Fuel Cell Electric Vehicles / **Hasan Gunduz**	**#52** Development of SBA-15/Cordierite Monolith Supported Catalysts and Their Use in Hydrogen Production by Partial Oxidation of Methane / **İlke Ilıcak Bayraktar** and Halit Eren Fige
	#160 Effects of Chemical Machining Characteristics of Aluminum as Metallic Bipolar Material / **Deniz Okka** and Orhan Çakır	**#204** Steam Reforming of Sugar Beet Pulp in the Presence of Ni/Dolomite Catalyst for the Synthesis of Hydrogen-Rich Gas / **Tolga Kaan Kanatlı**, Nasrin Pourmoghaddam, Serkan Karadeniz and Nezihe Ayas	**#24** Hetero-junction Catalysts for H_2-N_2 Cyclic Energy Storage with Artificial Solar N_2 Fixation / **Bilge Coskuner Filiz**, Korkut Açıkalın, Hulya Civelek Yoruklu, Murat Çalışkan and Serço Sekis Yeşilkaya	**#59** Numerical Study for Low-Emission Coke Oven System Using Combustion of Coke Oven Gas under CDC Conditions / **Osman Kumuk**
	#78 A Floating SMR and Ocean-Based Community Energy System with Hydrogen and Molten Salt Storage / **Mert Temiz** and Ibrahim Dincer	**#103** The Closed Loop Control for Enhanced Performance of Quasi-Switched Boost Inverters in PEM Fuel Cell-Based Residential Applicationss / **Melike Esen Güngör**, Ozan Gülbudak, Mustafa Gökdağ, Mehmet Özdemir and Ahmet Orhan	**#76** Catalytic Ammonia Decomposition Over Nickel and Ruthenium Supported on Al2O3 Pellets for Hydrogen Production / Ali Turgay Şan, Mehmet Çakır and **Halit Eren Figen**	**#193** Experimental Investigation of Distinct Surface Geometries of Nickel Coated 3D Printed Electrodes / **Ibrahim Eren Dincer** and Martin Agelin-Chaab
	#81 Hydrogen Gas Production from Agropyron repens by Dark Fermentation / **Nurten Dilara Kaplan** and Hidayet Argun	**#96** An Integrated Solution to Overcome Salt Lake Droughts with Hydrogen Production and Storage / **Dogan Erdemir** and Ibrahim Dincer	**#218** Electroplating of Copper- Based Materials and Investigation of Their HER Performance / **Zeynep Kuyumcu**, Hurmus Gursu, Muhammed Iberia Aydin and Ibrahim Dincer	**#202** A Strategy Study on Green Hydrogen Valleys / **Adnan Midilli**
10:25-10:40	**Coffee Break**		**Coffee Break**	

SCIENTIFIC PROGRAM

Day 4 - Wednesday May 15, 2024

	PARALLEL SESSIONS		PARALLEL SESSIONS	
	HALL A	**HALL B**	**HALL C**	**HALL D**
10:40-12:15	**Session 7A: Fuel Cells-IV**	**Session 7B: Modeling, simulation and optimization-III**	**Session 7C: Energy, exergy and economic analyses-II**	**Panel Session**
	Chair: Hüseyin Turan Arat	**Chair: Anıl Erdoğan**	**Chair: M. Ali Arserim**	
	#172 Comperative Evaluation of Non-Precious Material Catalysts for PEM Fuel Cells in Terms of Cost, Stability and Activity / **Erman Çelik**	**#182** Integrating RLS and FCS-MPC for Enhanced Control in Hydrogen Fuel Cell and Grid Inverter Systems / **Sulman Shahzad** and Muhammad Abbas Abbasi	**#199** Solar Tracking Systems Applications in Planar Solar Panels / **Gizem Gül Katırcıoğlu**, Mehmet Daş and Ebru Akpınar	**Challenges and Opportunities for The Region in the New Hydrogen Economy (This panel will be held in Turkish)** **Moderator:** **Adnan MİDİLLİ** İstanbul Technical University **Panelists:** **Hüseyin DEVRİM** TEK-SİS, Türkiye **Can ERKEY** Koç University, Türkiye **Ali Rıza ARSLAN** Hydrogenix, Türkiye **Ragıp KIZILTAŞ** TENMAK – Clean Energy Research Inst. (TEMEN)
	#177 Ni-Modified Self-Assembled Monolayer Films of Bingöl Pollen on Copper Substrate as a Novel Anode Catalyst for Methanol Electrooxidation Reaction / **Yeşim Aydın Dursun** and Ramazan Solmaz	**#60** Numerical Simulation of Methane Dry Reforming over Supported Nickel Catalyst / Ahmed Aheed Ali Mohammed, Mohammed Al-Marri and **Anand Kumar**	**#208** Analysis and Assessment of a Biomass-Based Cogeneration System with Hydrogen-Fueled Gas Turbine / **Fatih Sorgulu** and Ibrahim Dincer	
	#38 Maximizing Power Efficiency: The FC+PV+WT Hybrid Renewable Energy System / **Ayse Kocalmis Bilhan**	**#210** Current Sharing and Voltage Regulation Based on Dynamic Consensus Algorithm in PV-Fuel Cell-Battery Sourced DC Microgrid / **İlhami Poyraz** and Mehmet Emin Askerşablona	**#142** Investigation of the Use of Carbon-Based Supports in the Catalytic Hydrolysis of Ethylenediamine Bisborane / **Bensu Naz Örs**, Gülay Özkan and Göksel Özkan	
	#206 Performance of Nanometric Ti/TiN Bilayer Cathodic Arc Evaporated Coating on 304SS as Bipolar Plate for PEMFC / **Enis Furkan Uçar**, Erkut Yılmaz and Özden Kısacık	**#112** Synthesis of $CuS/CuInS_2/TiO_2$ Catalysts and Investigation of Their Activities in Photocatalytic H_2 Production / Elif Tuğba Yılmaz, **İbrahim Kaba** and Özge Kerkez Kuyumcu	**#197** Economic and Strategic Evaluation of Underground Hydrogen Storage Areas / **Hatice Karakilcik**	
	#211 Enhanced Performance Prediction for Proton Exchange Membrane Fuel Cells: A Comparative Study of LSTM and Conventional Methods / **Masud Kabir** and Sami Ekici	**#165** Use of Hydrogen as Secondary Fuel in Internal Combustion Engines: A Approach on Combustion, Performance and Emissions / Süleyman Şimşek and **Muhammed Uçum**	**#228** Assessing the Environmental Footprint of Catalysts in Photoelectrochemical Hydrogen Production Through Life Cycle Analysis **/ Ayse Kocalmis Bilhan**	
	# 219 Proton Exchange Membrane Water Electrolysis System: Steady-State Modeling and Assessment / **Nurettin Sezer** and Sertac Bayhan	**#190** Alternative Fuel Mixtures and Sustainable Development: An Energy and Environmental Perspective Evaluation of Diesel, Biodiesel, and Alcohol Blends / **Halis Deviren**	**#57** One Step Towards a Green Future: Retrofitting of the Internal Combustion Engines for the Utilization of the Hydrogen Fuel / **Hilmi Ersin Oktar**, İbrahim Hakkı Tonyalı and Ahmet Hamit Apaydın	
	#216 Modeling and Simulation Photovoltaic-Electrolyzer-Fuel Cell in Microgrids **/ Musa Yilmaz**	**#235** Green Hydrogen The Innovation of Green Energy / **Syed Muhammad Ahmer Ali**	**#101** Hydrogen Quality Effect to Generator Performance / **Kerim Kenan Kiremit**	

SCIENTIFIC PROGRAM

Day 4 - Wednesday May 15, 2024

12:15-12:35	**Awards and Closing Ceremony**			
14:00-19:00	**Sur İçi Cultural Trip**			

SCIENTIFIC PROGRAM

Poster Session (Online)

#8 Syngas Desulfurization following Microwave Cycled Gas Bubbling on Coal and Biomass Pyrolysis / Yildirim İ. Tosun and Fethullah Chichek

#11 A System Design for Co_2 Capture with Hydrogen and Methanol Production in a Cement Plant / Ibrahim Akgun and Ibrahim Dincer

#23 Biohydrogen and Biomethane Production Using An Integrated Bioelectrochemical and Anaerobic Digestion Reactor From Poplar and Cow Manure Wastes / Ahmet Faruk Kilicaslan, Aysegul Kara, Ibrahim Dincer and Ali Khalvati

#36 Design of a Novel Solar-Based Sustainable Energy System with Energy Storage / Ayse Sinem Meke and Ibrahim Dincer

#39 Electric Airplane Energy Storage and PEM Fuel Cell Island Airport Microgrid Load Frequency Control / Cem Haydaroglu

#43 Design and Simulation ofa Novel Copper-Chlorine Thermochemical Cycle for Hydrogen Production / Sibel Uygun Batgi and Ibrahim Dincer

#62 Design of an Integrated Multigenerational Energy System for Oleic Acid and Hydrogen Production / Kubilay Karayel and Ibrahim Dincer

#64 Electrolytic Hydrogen Production with Coaxial Cylinder Electrolyzers: A CFD Study / Mohamed M. Ismail and Ibrahim Dincer

#65 Design and Analysis of a New Multigeneration System for a Hospital / Andre Bolt, Ibrahim Dincer and Martin Agelin-Chaab

#74 An Integrated Plant for Urea and Ammonium Acetate Production Designed with Renewables / Zunayed Zakir Arnab and Ibrahim Dincer

#91 Green Hydrogen Production System for A Village / Inci Eroglu, Harun Koku and Esra Gül Sendesen

#92 Techno-Economic Analysis of Green Hydrogen Integration in Smart Grids: Pathways to Sustainable Energy Systems / Muhammad Raza Zaffar, Mohsin Raza Zaffar, Sulman Shahzad and Heybet Kilic

#98 Case Study of a Self-Powered Building Using Hydrogen as an Energy Carrier / Inci Eroglu, Harun Koku and Mine Keles

#117 Green Hydrogen: A Keystone in Pathways to Decarbonized Offshore Power Transmission - Technologies, Policies, and Future Directions / Yusuf Yurtsever, Jalal Sahebkar Farkhani and Heybet Kilic

#125 Design and Theoretical-Economic Analysis of Hydrogen Storage Power System : The Case of Dicle University / Faruk Barlaz, Cem Haydaroğlu, Yahya Akıl and Heybet Kilic

#143 Determining the Hybrid Energy Potential of Türkiye's Blue Homeland in the Aegean Sea / Soner Çelikdemir and Mahmut Temel Özdemir

#144 Strategic Importance of Hydrogen within the Scope of Turkey's New Century Vision / Mehmet Fırat Doğan

#180 A Recurrent Neural Network Model Predictive Control (RNN-MPC) Strategy for Efficient Energy Management in Hybrid Battery-Hydrogen Systems / Sulman Shahzad and Heybet Kilic

#181 Model-Free Predictive Control of a Hydrogen Energy Nano Grid System / Sulman Shahzad and Heybet Kilic

#183 Green Hydrogen: Innovations, Challenges, and Opportunities in a Low-Carbon World / Sulman Shahzad and Heybet Kilic

#209 Investigation of the Photocatalytic Activity of Pd(0) NPs-Decorated Benzene Ring Doped Nanosheet g-C_3N4 (Pd@BD-g-C_3N_4) in the Hydrolysis Reaction of Ammonia Borane / Halil İbrahim Önal and Feyyaz Durap

SCIENTIFIC PROGRAM

Poster Session (Online)

#213 Power Flow Control for Renewable Energy Hydrogen based Dual Active Bridge used DC Microgrids / Heybet Kilic and Mehmet Emin Aske

#214 Utilizing Battery-Super Capacitor Energy Storage for Hybrid Photovoltaic, Wind, and Fuel Cell Systems / Mehmet Emin Asker

#215 Improving Power Quality in Microgrids with PEM Electrolyzer/Fuel Cell System / Heybet Kilic

#222 Evaluation of Hydrogen Transportation by Trucks in terms of Occupational Health and Safety: A Preliminary Hazard Analysis / Mehmet Tunç and Ramazan Solmaz

#223 Safety Risks in Solar-Hydrogen Energy System: Fine Kinney Risk Analysis / Mustafa Doğrubaş, Mehmet Tunç, İbrahim Yasin Erdoğan and Ramazan Solmaz

#227 The Energy Trilemma Approach Assessment of Hydrogen Production Potential in Türkiye /Kadir Akgün, Bestami Özkaya and Fatma Zehra Küçük

#229 Production of Black Phosphorus Doped Metal Chalcogen Hybrid Materials and Their Use in Photocatalytic Hydrogen Production / Ecem Nur Demirel, Bahadır Keskin and Atıf Koca

#230 Smale-Scale Electricity Generation with Biohydrogen using PEM Fuel Cell / Bugra Yilmaz, Barbaros Durmus and Muhsin Tunay Gencoglu

#231 Integrated System Design that Produces Electricity with Solar, Wind, Hydrogen and Biomass Energy / Bugra Yilmaz and Muhsin Tunay Gencoglu

#194 Classification of Organic and Recyclable Waste used in Green Hydrogen Production with Deep Learning Models / Hüseyin Fırat

ORAL PROCEEDINGS

Assessing the thermodynamic examination of solar heliostat-based multigeneration plant integrated with LNG regasification cycle for hydrogen generation

[1]Fatih Yilmaz, [1]Murat Ozturk, [2]Resat Selbas
[1] Isparta University of Applied Sciences, Mechatronics Engineering, Isparta/Türkiye
[2] Isparta University of Applied Sciences, Mechanical Engineering, Isparta/Türkiye

Abstract
This developed paper addresses a comprehensive thermodynamic analysis evaluation of hydrogen and power production with the integration of solar heliostat-assisted supercritical and transcritical CO_2 power generation cycles and LNG regasification systems**.** The system comprises a supercritical Brayton cycle, a transcritical Rankine cycle, a PEM unit, and LNG regasification unit for the production of clean power and hydrogen. The developed plant is motivated by a solar tower circuit. Complete thermodynamic mathematical investigation is performed to determine system performance. According to the analysis findings, the proposed plant is capable of 11381 kW of net power generation. Moreover, the energetic efficiency of the entire plant is determined as 42.94% and 45.13%, respectively.

Keywords: Energy, solar, LNG, hydrogen, CO_2 cycles

I. Introduction

As the need for energy increases step by step, the tendency towards fossil fuels increases, and carbon dioxide emissions increase accordingly. At this point, humanity needs to reduce or eliminate the use of fossil fuels and meet its energy requirements from renewable energy sources. Renewable energy sources are environmentally friendly energy types, which are mainly solar, biomass, wind, geothermal, and hydro, and are in a critical position for the future. Another important issue is the energy efficiency method, for this method, the combined plants for example, -cogeneration, trigeneration, and multigeneration- have gained importance, especially in terms of higher performance ratio. Combined systems offer possible answers to address global energy, environmental, and economic worries in a clean, efficient, and cost-effective manner (Dincer and Acar, 2015). Solar energy has wide application possibilities in the "Carbon neutrality" process due to its compensations of being renewable, and pollution-free (Hao et al. 2023). At this point, the combination of solar energy and multigeneration plants has many advantages, and these combined systems are at an important point in moving to net zero emissions. For this reason, there are many studies in the literature on hydrogen production with the integration of these systems, and are ongoing.

Sharifishourabi et al. (2023) developed a performance evaluation of a solar-based combined plant that combined a Steam Rankine cycle, thermal energy storage, organic Rankine cycle, absorption refrigeration system, and hydrogen generation unit. Gursoy and Dincer, (2023) proposed a new integrated model that produces beneficial products. The energy efficiency of this system is found as 22.64%. Yhan et al. (2023) suggested a solar heliostat-based integrated plant that combined with the Helium Brayton cycle and transcritical CO2 cycle. This system has 34.68% efficiency. Again, Yhan and Caliskan (2023) developed a solar united model in terms of energy and exergy efficiency. Yilmaz et al. (2023) examined a solar-assisted combined plant that generates beneficial products. The system has been investigated for energy and exergy efficiency and found as 43.77% energy efficiency.

The newly developed paper deals with the thermodynamic investigation of the solar energy-based combined energy convention plant for generating power and green hydrogen. Detailed energy, exergy efficiency, and exergetic destruction rates of the overall plant are used to determine the system performance variations.

II. System design and thermodynamic analysis

In this study, the design of a combined supercritical Brayton, transcritical Rankine cycles, and LNG regasification unit, as shown in Figure 1, is discussed. Here, the system is supported by solar heliostat mirrors and CO_2 is preferred as the working fluid. Additionally, it is aimed to produce hydrogen by PEM electrolysis.

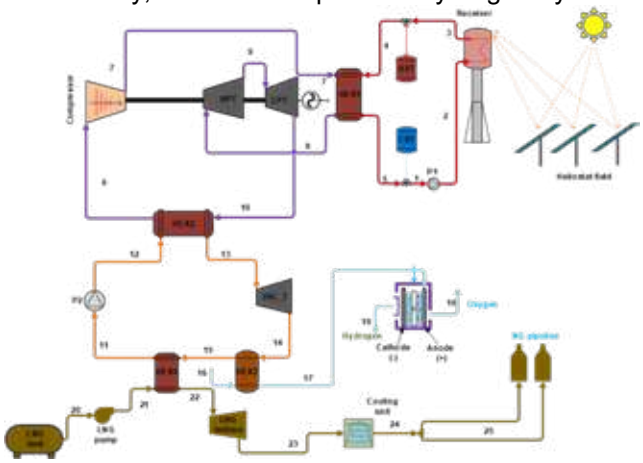


Fig.1. Representative diagram of the modeled combined solar power

For thermodynamic modeling of the system, mass, energy, and exergy balance equations are applied as follows (Cengel et al. 2011; Dincer 2020);

$$\dot{m}_i = \dot{m}_e \quad (1)$$

$$\dot{Q}_i + \dot{W}_i + \sum \dot{m}_i h_i = \dot{Q}_e + \dot{W}_e + \sum \dot{m}_e h_e \quad (2)$$

$$\dot{E}x^{\dot{Q}_i} + \dot{E}x^{\dot{W}_i} + \sum \dot{m}_i ex_i = \dot{E}x^{\dot{Q}_e} + \dot{E}x^{\dot{W}_e} + \sum \dot{m}_e ex_e + \dot{E}x_{des} \quad (3)$$

The Brayton and Rankine cycles performance ratio can be modeled as;

$$\eta_{BC} = \frac{\dot{W}_{HPT} + \dot{W}_{LPT} - (\dot{W}_{HC})}{\dot{m}_7(h_8 - h_7)} \quad (4)$$

$$\psi_{BC} = \frac{\dot{W}_{HPT} + \dot{W}_{LPT} - (\dot{W}_C)}{\dot{m}_7(ex_8 - ex_7)} \quad (5)$$

$$\eta_{tRC} = \frac{\dot{W}_{tRC} - (\dot{W}_{P2})}{\dot{m}_{12}(h_{13} - h_{12})} \quad (6)$$

$$\psi_{tRC} = \frac{\dot{W}_{tRC} - (\dot{W}_{P2}}{\dot{m}_{12}(ex_{13} - ex_{12})} \quad (7)$$

Overall system;

$$\eta_{sys} = \frac{\dot{W}_{net} + (\dot{m}_{H_2} LHV_{H_2})}{\dot{Q}_{solar}} \quad (8)$$

$$\psi_{sys} = \frac{\dot{W}_{net} + (\dot{m}_{H_2} ex_{H_2})}{\dot{E}x_{Q,solar}} \quad (9)$$

III. Results and discussion

The assumptions made in the model design are presented in Table 1. Accompanied by these assumptions in Table 1, thermodynamic analysis is carried out according to the energy and exergy efficiencies method, and the analysis findings are depicted in Table 2.

Table 1. Parameters study design indicators for thermodynamic analysis

Parameters	Unit	Value
Solar radiation	W/m^2	650
Heliostat efficiency	%	75
Heliostat inlet temperature	℃	100
Wind speed	m/s	4.5
Supercritical Brayton cycle		
Compressor inlet temperature	℃	35
Compressor inlet pressure	kPa	7500
HPT turbine inlet temperature	℃	700.1
HPT turbine inlet pressure	kPa	18750
Transcritical Rankine cycle		
Pump input temperature	℃	25.44
Pump input pressure	kPa	6500
Pump outlet pressure	kPa	9750
LNG tank outlet temperature	℃	-161.5
Reference temperature	℃	25
Reference pressure	kPa	101.3

Table 2. Thermodynamic analysis results of the modeled plant

Indicators	Value	Unit
$\dot{W}_{net,BC}$	4916	kW
$\dot{W}_{net,tRC}$	2010	kW
$\dot{W}_{LNG}$	7176	kW
$\dot{W}_{net,sys}$	11381	kW
$\dot{m}_{Hydrogen}$	0.005643	kg/s
η_{sys}	42.94	%
ψ_{sys}	45.13	%
SI	1.822	-

To examine the system performance change, a parametric evaluation is employed on the impact of solar radiation and compressor compression rate. Fig. 2, Fig. 3, and Fig.4 present the influence of solar radiation on the system performance, net power, and hydrogen generation load, energetic and exergetic efficiency of subsystems the overall system, respectively. It is noted that the enhancement of the solar radiation rate from 500 to 750 W/m^2, power and hydrogen ğproduction rates increase, and also overall system's energy and exergy efficiency increase.

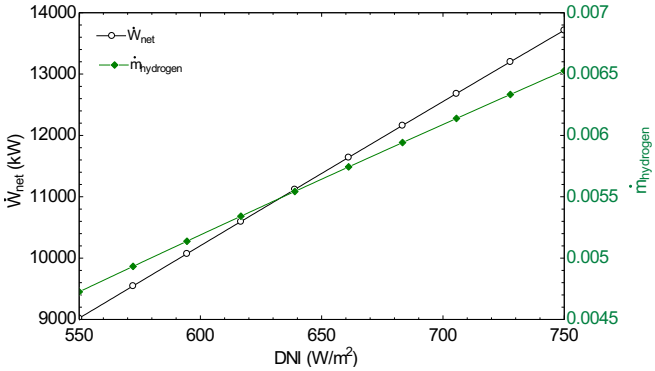


Fig. 2. Impact of the solar radiation on the net power and hydrogen capacity

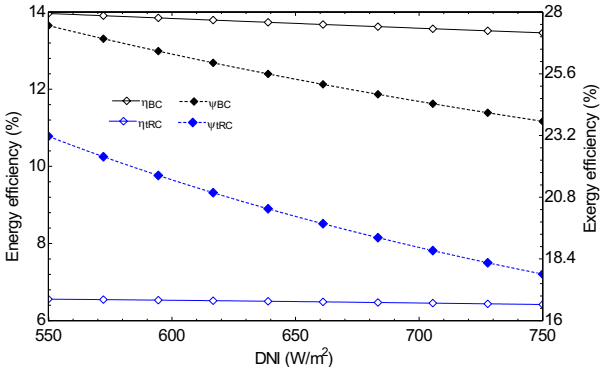


Fig. 3. Effect of solar radiation on the performance rate of the subsystems

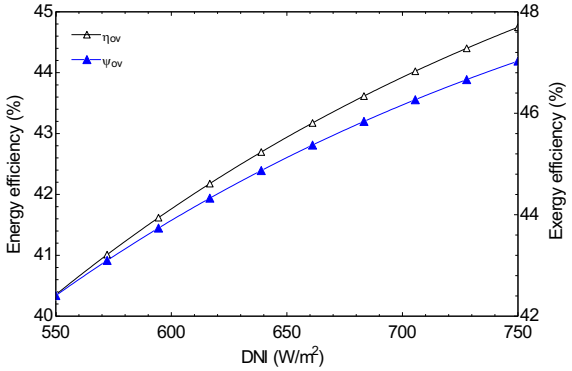


Fig. 4. Overall system efficiency vs different solar radiations

Another important parameter is the effect of changing the BC compressor compression ratio. As the compressor compression ratio increases from 1.5 to 4.5, both the power and the amount of hydrogen increase as revealed in Fig. 5, the thermodynamic efficiency of the subsystems increases as seen in Fig.6, and finally, the energy and exergy efficiency of the whole system also increases as exposed in Fig. 7.

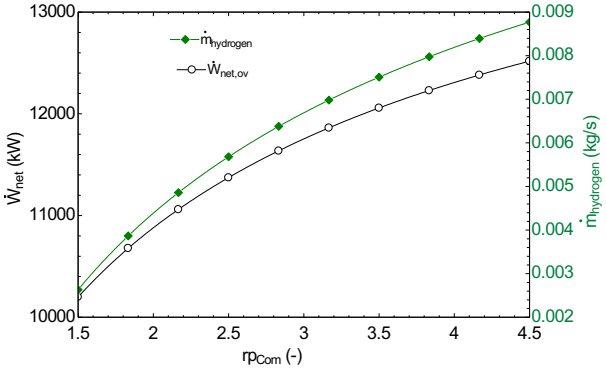


Fig.5. Interpretation of the net power and hydrogen rate vs different compressor compression ratio

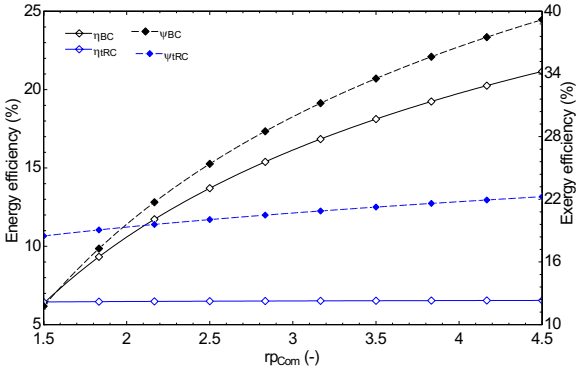


Fig.6. The relationship between the performance ratio of the subsystems and various compressor compression ratio

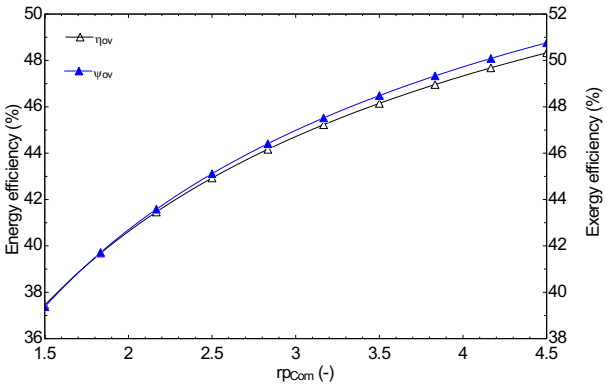


Fig. 7. The relationship between the performance ratio of the entire model and various compressor compression ratio

IV. Conclusion

In the newly developed current research, the proposal of the solar tower-based combined plant integrated with the CO2 cycle, LNG regasification, and PEM unit is examined for clean power and hydrogen generation. To determine the system efficiency, a parametric examination is also accomplished on the influence of solar radiation and the compression ratio of the compressor on the developed model efficiency. The system can generate 11381 kW of net power and 0.005643 kg/s of green hydrogen. The energy and exergy efficiency of the entire configuration are computed at 42.94% and 45.13%, respectively. The developed solar-based plant has a 1.822 sustainability index value. Moreover, an increment in the solar radiation value has a encouraging consequence on the entire system's efficiency.

References

Cengel, Y. A., Boles, M. A., & Kanoğlu, M. (2011). *Thermodynamics: an engineering approach* (Vol. 5, p. 445). New York: McGraw-hill.

Dincer, İ. (2020). *Thermodynamics: a smart approach*. John Wiley & Sons.

Dincer, I., & Acar, C. (2015). A review on clean energy solutions for better sustainability. *International Journal of Energy Research*, *39*(5), 585-606.

Gursoy, M., & Dincer, I. (2023). A solar based system for integrated production of power, heat, hot water and cooling. *Energy*, 128943.

Hao, X., Shan, S., Gao, N., Chen, G., Wang, Q., & Gu, T. (2023). Performance analysis of a novel combined cooling, heating and power system with solar energy spectral beam splitting. *Energy Conversion and Management*, *276*, 116500.

Khan, Y., Caliskan, H., & Hong, H. (2023). A comparative study of combined cycles for concentrated solar power for efficient power generation using low Global Warming Potential (GWP) fluids to reduce environmental effects. *IET Renewable Power Generation*.

Khan, Y., Singh, D., Caliskan, H., & Hong, H. (2023). Exergoeconomic and Thermodynamic Analyses of Solar Power Tower Based Novel Combined Helium Brayton Cycle-Transcritical CO2 Cycle for Carbon Free Power Generation. *Global Challenges*, 2300191.

Sharifishourabi, M., Dincer, I., & Mohany, A. (2023). Performance assessment of a novel solar heliostat and digester-based multigeneration system with hydrogen production. *Applied Thermal Engineering*, *232*, 121094.

Yilmaz, F., Ozturk, M., & Selbas, R. (2023). Development and assessment of a solar-driven multigeneration plant with compressed hydrogen storage for multiple useful products. *International Journal of Hydrogen Energy*, *48*(99), 39043-39063.

Design and Thecno-Economic Analysis of a Combined Heat and Power System with Hydrogen Storage

[1*] Mehmet Ali Köprü [2]Dursun Öztürk, [1]Burak Yildirim
[1] Bingol University, Engineering and ArchitectureFaculty, Departman of Electrical-Electronics Engineering, Bingöl, 12000, Türkiye
[2] Bingol University, Vocational and Tech. High School, Bingöl, 12000, Türkiye

* makopru@bingol.edu.tr

Abstract

This study conducts an analysis of a renewable energy-based system addressing the energy needs of independent rural households engaged in livestock farming, a fundamental component of rural development. The system incorporates photovoltaic panels (PV), wind turbines (WT), biogas, aqua electrolyzer (AE), fuel cells (FC), a boiler, battery storage system (BSS), and hydrogen storage tanks (HST). The primary objective of this study is to produce green hydrogen using renewable sources while evaluating animal waste with a zero-waste approach. The generated and stored hydrogen provides power to fuel cells. The system is simulated using HOMER software. The obtained biogas and stored hydrogen fulfill the electrical requirements of the system, while the resulting heat meets a significant portion of the thermal demand. According to the analysis results, the optimal configuration includes 5 kW PV, 3 kW WT, 2 kW FC, 3 kW AE, 3 kW biogas, 30 kg HST, 2 kW converter, and 2 kWh BSS.

Keywords: Hydrogen, fuel cell, biogas, energy management, HOMER

I. Introduction

The rapid growth of the world population and industrial development is causing a continuous increase in energy demand. Issues such as the depletion of fossil fuels, insufficient energy production, and the generation of environmentally harmful greenhouse gases pose significant threats to the world (Gökçek & Kale, 2018). Therefore, considering environmental, social, and economic factors, the use and development of renewable energy sources (RES) as alternatives to fossil fuels are of great importance.

While RES are abundant and sustainable, the continuous variability of energy derived from sources such as solar and wind necessitates the use of energy storage systems. However, for a community not connected to the electrical grid, ensuring stable power from a single renewable energy source can be challenging (Das et al., 2021). To overcome this challenge and reduce storage capacity, stable power can be provided by creating microgrids using hybrid renewable energy systems (HRES) (Islam et al., 2021). Microgrids and HRES are increasingly utilized to enhance the energy production potential of sources like solar, wind, biogas, and to reduce energy storage capacity. BSS are commonly used for storing electrical energy. However, there is a growing interest in converting excess energy produced by HRES into hydrogen and storing it in hydrogen tanks for energy storage.

For the production of green hydrogen, AE are combined with power supplied by RES (Abdolmaleki & Berardi, 2021). Hydrogen can function as an energy carrier used for energy storage and transportation. This characteristic makes it a crucial component of a clean and reliable energy system (Dinçer & Aydın, 2023). Hydrogen can be easily stored in pressurized tanks and later utilized by FC to convert chemical energy into electricity when needed.

The main objective of this study is to examine the feasibility of an independent combined heat and power (CHP) system for a family engaged in livestock farming in a remote area away from the city center. Specifically, the study integrates a biogas system by harnessing the potential of gas found in animal manure. The configuration of an HRES with hydrogen-battery storage is designed and analyzed. The techno-economic analysis of the system, optimized simultaneously for electrical and thermal loads based on the actual consumption values of a rural family in Bingöl province and the region's meteorological conditions, is conducted in this study.

II. Experimental Set-up and Procedure

A microgrid design has been implemented to meet the heating and electricity needs of a family residing in a rural area. The region's solar, wind, and temperature data were obtained from NASA data available in the HOMER Pro software. HOMER Pro is a program developed by the National Renewable Energy Laboratory (NREL) for the techno-economic analysis of grid-connected or off-grid power systems and the optimal design, sizing, and planning of Hybrid Renewable Energy Systems (HRES) (Shahzad et al., 2017; Akan, 2023). The analysis of the hybrid energy system designed with HOMER Pro software was conducted. In this study, the designed HRES consists of a combination of PV, WT, FC, BSS, HST, boiler, and biogas conversion systems. The unit cost values of the components comprising the HRES are provided in Table 1, and a schematic representation is shown in Figure 1.

Tablo 1. Unit cost values of system components

Components	Installation Cost ($/kW)	Replacement Cost ($/kW)	Op. - Maint. Cost ($/kW-yr)	Lifespan (Yr)
PV System	700	700	10	25
Wind Turbine	1500	1500	10	20
Biogas Gen.	1000	1000	0.1/h	20000 h
Electrolyzer	1000	1000	10	15
Hyd. Tank	400/kg	400/Kg	0/Kg	25
Fuel Cell	1000	1000	0.01/h	50000h
Battery	300/battery	300/ battery	10/ battery	10
Converter	300	300	0	15

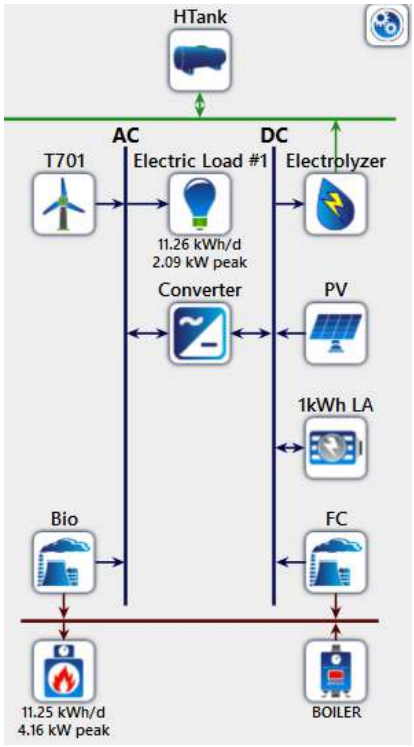


Fig. 1. Configuration of hybrid renewable system meeting electrical and thermal load demands

The characteristics of the system components used in the scenario are as follows: a Generic Flat Plate PV module (0-6 kW), a T701 wind turbine with a 3m rotor diameter (0-3 kW), and a small farmstead with a total of 20 large and 200 small livestock animals. The assumed daily manure production is 10 kg for a cow and 1 kg for a goat or sheep (Bhatt et al., 2016; Tiam Kapen et al., 2022). A recovery factor of 0.7 is considered, and it is assumed that 0.036 m3 of biogas is produced per 1 kg of wet manure, requiring 0.73 m3 of biogas for 1 kWh (Yimen et al., 2018). The biogas generator (0-3 kW), FC (0-3 kW), a generic 1 kWh lead-acid battery with a 12V nominal voltage and a capacity of 83.4Ah, and AE (0-5 kW) values were input for optimization. The optimization results suggest the following configuration: 5 kW PV panels, 3 kW wind turbine, 2 kW biogas generator, 2 kW FC, 2 kWh battery storage system (BSS), 3 kW electrolyzer (AE), and a 30 kg hydrogen storage tank (HST) for electricity production from solar energy. To store the system's electrical energy and meet the load demand, a 0.995 kW converter is recommended.

III. Results and Discussions

The recommended HRES is designed to meet a daily energy production of 31 kWh and fulfill an energy demand with a peak value of 4,160 kW. The system's capital cost is calculated as $26,398, with operating costs at $3,915 and maintenance costs at $3,432. The Net Present Cost (NPC) for the system is $32,757, and the Levelized Cost of Energy (COE) is $0.605/kWh. The energy demand is met as follows: 61.8% from PV panels, 25.7% from the WT, 6.45% from FC, and 6.02% from biogas. Figure 2.a illustrates the monthly energy production from each energy source. A daily thermal energy demand of 11 kWh is required for heating, with a peak value of 4,156 kW for the thermal load. In this system, 46.7% of the thermal load is met by FC, 39.2% by the boiler, and 14.1% by biogas. A significant portion of the house's thermal energy is generated by FC. In addition to converting stored hydrogen into

electrical energy, FC is used to meet a portion of the community's thermal load demands. Figure 2.b displays the production sources fulfilling the thermal load.

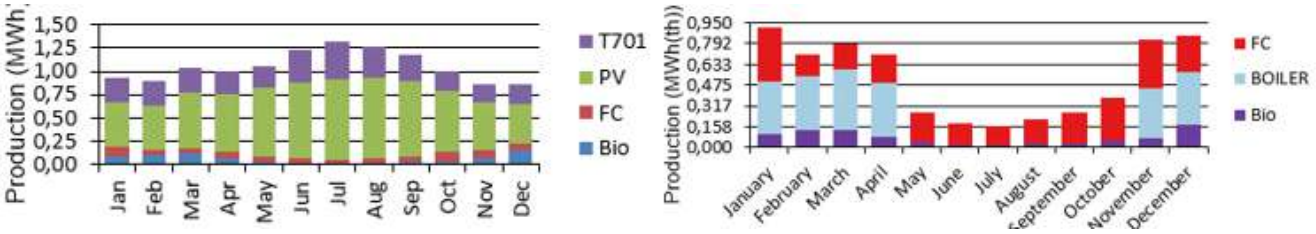


Fig. 2: a) Amount of electrical energy produced by month b) Amount of thermal load produced by month

The excess energy generated by PV, WT, and biogas energy sources to meet the load demand is initially stored in batteries; subsequently, the remaining energy is stored in a HST via an AE. The monthly production of hydrogen by the microgrid is illustrated in Figure 3. Particularly during the summer months, an increase in hydrogen production is observed, attributed to the longer daylight hours.



Fig. 3: Amount of hydrogen produced by month

The majority of electricity production is achieved by PV panels. The power output graph of the PV panel is shown in Figure 4.a, with a noticeable increase in production, especially during the summer months. Gaps in the power output graph indicate weak production on cloudy days. The annual contribution of the PV panel to electricity production is 7812 kWh/yr. The power output graph for the wind turbine is provided in Figure 4.b. Despite intermittent periods, the WT has generated almost continuous electricity throughout the year, contributing a total of 3243 kWh/yr. The power output graph for the biogas generator is illustrated in Figure 4.c. The small-capacity generator comes into operation only when the generated energy is insufficient. The generator has contributed to a total of 815 kWh/yr of electricity production and 2933 kWh/yr of heat production.

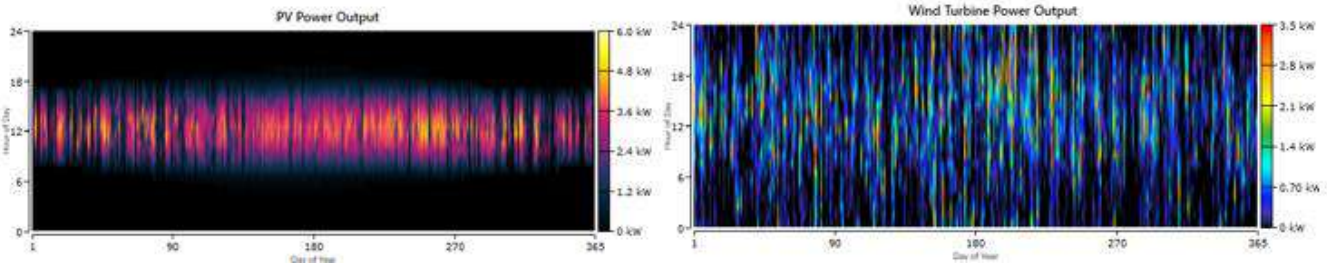
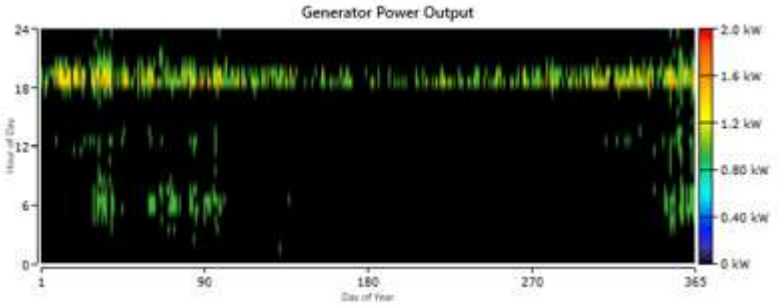


Fig. 4: a) Power output graph of PV panel b) Power output graph of wind turbine



c) Power output graph of the biogas generator

It is observed that the AE typically operates at full capacity, especially during daylight hours, producing hydrogen. The power output graph of the AE is shown in Figure 5.a, while the FC's power output graph is depicted in Figure 5.b. Excess energy generated by the microgrid is stored in the HST, totaling 7,244 kWh/year of energy input over the AE's operational period of 4,910 hours/year, resulting in the conversion of 156 kg of hydrogen. The stored hydrogen is utilized by the FC to meet the system's demand during periods when the sun is not shining, and energy

production is insufficient. The FC comes into operation specifically during these times, contributing to 815 kWh/year of electricity production and 2,933 kWh/year of thermal energy production over its operational period of 2,203 hours/year.

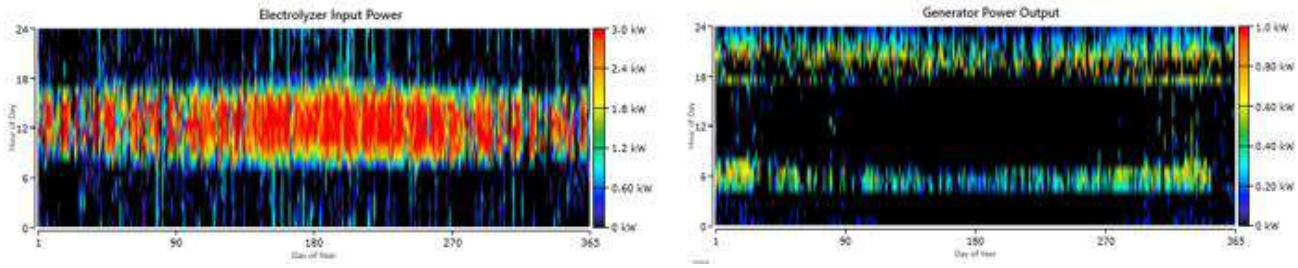


Fig. 5: a) Power output graph of electrolyzer b) Power output graph of fuel cell

V. Conclusions

Providing electricity to individual homes or communities located away from the grid is a challenging and costly process, especially in challenging terrains. Therefore, generating energy on-site with HRES is a more environmentally friendly and cost-effective option. Since the energy produced by HRES is not constant throughout the day, storage is essential. Consequently, storing excess energy as hydrogen can be advantageous. A CHP system has been designed to meet the electricity and heating needs of a family engaged in livestock farming in Bingöl province. The designed system utilizes PV, WT, FC, and biogas energy to produce power and directs excess energy to BSS and HST. Hydrogen storage is facilitated through an AE and the stored hydrogen is used by the FC when the microgrid's energy demand cannot be met. The system's net present cost is $32,757, with a levelized energy cost of $0.605/kWh. The PV panel generates 7,812 kWh, the wind turbine produces 3,243 kWh, and biogas contributes 815 kWh of electricity annually. Additionally, the FC produces 2,933 kWh of thermal energy. Excess energy is efficiently stored through battery and hydrogen storage systems. Using a high-capacity HST for storing excess energy during the summer months may be more advantageous than relying on batteries.

References

Abdolmaleki, L. and U. Berardi, Comparative analysis among three solar energy-based systems with hydrogen and electrical battery storage in single houses. 2021.
Akan, A.E.J.E.J.o.M., Engineering, Natural and M. Sciences, Techno-Economic Analysis of a Farm's Hybrid Energy System: The Case of Konya Rural. 2023. 10(29): p. 1-27.
Arévalo, P., et al., Energy control and size optimization of a hybrid system (photovoltaic-hidrokinetic) using various storage technologies. Sustainable Cities and Society, 2020. 52: p. 101773.
Arzu Coskun Avci, Ethem Toklu, A new analysis of two phase flow on hydrogen production from water electrolysis, International Journal of Hydrogen Energy, Volume 47, Issue 11, 2022, Pages 6986-6995, ISSN 0360-3199, https://doi.org/10.1016/j.ijhydene.2021.03.180.
Bhatt, A., et al., Feasibility and sensitivity analysis of an off-grid micro hydro–photovoltaic–biomass and biogas–diesel–battery hybrid energy system for a remote area in Uttarakhand state, India. 2016. 61: p. 53-69.
Das, B.K., M.S.H.K. Tushar, and R. Hassan, Techno-economic optimisation of stand-alone hybrid renewable energy systems for concurrently meeting electric and heating demand. Sustainable Cities and Society, 2021. 68: p. 102763.
Ibrahim Dincer, Muhammed Iberia Aydin, New paradigms in sustainable energy systems with hydrogen, Energy Conversion and Management, Volume 283, 2023, 116950, ISSN 0196-8904, https://doi.org/10.1016/j.enconman.2023.116950.
Gökçek, M. and C. Kale, Techno-economical evaluation of a hydrogen refuelling station powered by Wind-PV hybrid power system: A case study for İzmir-Çeşme. International Journal of Hydrogen Energy, 2018. 43(23): p. 10615-10625.
Islam, M.S., et al., Techno-economic optimization of a zero emission energy system for a coastal community in Newfoundland, Canada. Energy, 2021. 220: p. 119709.
Shahzad, M.K., et al., Techno-economic feasibility analysis of a solar-biomass off grid system for the electrification of remote rural areas in Pakistan using HOMER software. 2017. 106: p. 264-273.
Tiam Kapen, P., et al., Techno-economic feasibility of a PV/battery/fuel cell/electrolyzer/biogas hybrid system for energy and hydrogen production in the far north region of cameroon by using HOMER pro. Energy Strategy Reviews, 2022. 44: p. 100988.
Yimen, N., et al., Analyzing of a photovoltaic/wind/biogas/pumped-hydro off-grid hybrid system for rural electrification in Sub-Saharan Africa—Case study of Djoundé in Northern Cameroon. 2018. 11(10): p. 2644.

0-D Mathematical Modeling of Anion Exchange Membrane Water Electrolyze

[1,2*]Ceren Celebi, [3]C. Ozgur Colpan, [4]Yilser Devrim

[1] Dokuz Eylul University, Maritime Faculty, Department of Marine Engineering, Tınaztepe, Buca, Izmir, 35390, Türkiye
[2] Dokuz Eylul University, The Graduate School of Natural and Applied Sciences, Mechanical Engineering Department, Tinaztepe, Buca, Izmir, 35397, Türkiye
[3] Dokuz Eylul University, Faculty of Engineering, Mechanical Engineering Department, Tinaztepe, Buca, Izmir, 35397, Türkiye
[4] Atilim University, Faculty of Engineering, Department of Energy Systems Engineering, Incek, Ankara, 06836, Türkiye

* E-mail: ceren.celebi@deu.edu.tr

Abstract

Anion exchange membrane (AEM) water electrolysis emerges as a promising method for hydrogen production through electricity. A pivotal advantage of AEM water electrolysis is its capacity to substitute conventional noble metal electrocatalysts with cost-effective transition metal catalysts. The focus of ongoing research into the development of AEM is to achieve optimal value by striking a balance between low cost and high performance. For this purpose, this study delves into the mathematical modeling of an anion-exchange membrane, encompassing electrochemical reactions and mass transfer phenomena. The mathematical equations of the zero-dimensional, steady-state model were solved in the MATLAB environment. A comprehensive parametric study was conducted to investigate the effect of various parameters such as activation potential coefficients, membrane thickness, and molarity of KOH solution on the performance of the AEM water electrolyzer. The performance metric considered is the efficiency of the AEM electrolyzer. The results show that molarity and exchange current density are proportional to efficiency. This research aims to provide valuable information and guidance to researchers working in the AEM water electrolysis field.

Keywords: AEM water electrolyzer, Mathematical modeling, MATLAB, Performance assessment

Introduction

Hydrogen plays a crucial role in sustainable energy solutions, but there are still obstacles to overcome regarding its widespread industrial use, particularly in production and storage. Developing efficient, cost-effective technologies for these processes is crucial. Electrolyzers have emerged as vital tools, converting renewable electricity into storable hydrogen. Two commercially available technologies for this purpose are alkaline water electrolysis (AWE) and proton exchange membrane water electrolysis (PEMWE). Anion exchange membrane water electrolysis (AEMWE) aims to have the advantages of both technologies while avoiding their disadvantages. This technology offers improved efficiency compared to AWE, due to the employment of a membrane as a substitute for a separator. Additionally, the electrodes are conveniently accessible, eliminating the requirement for costly electrolytes typically employed in PEMWE.

To develop electrolyzer systems that will direct technological developments, it is essential to understand the basic processes of anion exchange membranes and conduct studies to increase their efficiency. Models simulating complex electrochemical reactions, mass transfer phenomena, and membrane behavior within AEMWE provide valuable data for design optimization, performance prediction, and investigation of new materials and operating conditions. This article examines the main factors affecting its operation characteristics and explores the challenges in modeling these.

Modeling

An Anion Exchange Membrane Water Electrolyzer (AEMWE) involves complex transport processes and electrochemical reactions. A 0D model has been developed to simplify the process of establishing a relationship between the cell voltage and current. The primary objective of this model is to identify the factors responsible for the deviation between the actual and ideal cell voltages.

$$V_{cell} = V_{Rev} + \eta_{act,a} + \eta_{act,c} + (\eta_{ohm} + \eta_{KOH}) \quad (1)$$

Reversible Cell Voltage

Reversible cell voltage is the theoretical maximum voltage achievable by the cell under ideal conditions, where all overpotentials are eliminated, and the cell operates at its equilibrium potential. This voltage is calculated based on the Nernst equation, as described in Eq. 2 [1].

$$V_{Rev} = -\frac{\Delta G}{nF} + \frac{RT}{nF}\log\frac{(P-P_{H_2O})^{1.5}}{a} \quad (2)$$

R, n, and F represents the universal gas constant ($\mathrm{J/mol \cdot K}$), the number of moles, and Faraday's constant (96485.3 $\mathrm{C/mol}$), respectively. ΔG, The standard Gibbs free energy change was calculated using Eq. 3. Enthalpy (H) and entropy (S) values in the equation were obtained using the variable C_p approach. Terms P_{H_2O} and a refers partial

pressure of water vapor in the electrolyzer and the activity of water, which are calculated in terms of molarity (M) and temperature (T) using Eqs. 4 and 5, respectively.

$$\Delta G = \Delta H - T\Delta S \tag{3}$$

$$\log P_{H_2O} = -0.01508M - 0.0016788M^2 + 2.25887 \times 10^{-5}M^3 + (1 - 0.0012062M + 5.6024 \times 10^{-4}M^2 - 7.8228 \times 10^{-6}M^3) \times (35.4462 - \frac{3343.93}{T} - 10.9 \log T + 0.004165T) \tag{4}$$

$$\log a = -0.0225M + 0.001434M^2 + (\frac{1.38M - 0.9254M^2}{T}) \tag{5}$$

Activation Overpotential

Activation Overpotential refers to the voltage required to initiate electrochemical reactions at the electrodes by overcoming energy barriers. It is calculated as shown in Eqs. 6 and 7 for the anode and cathode electrodes, respectively [1,2].

$$j_a = i_{0,a}\,(1-\Theta)\,\{\exp(\frac{\alpha_a\, n\, F}{\mathrm{RT}}\eta_{\mathrm{act},a}) - \exp(\frac{-(1-\alpha_a)\, n\, F}{\mathrm{RT}}\eta_{\mathrm{act},a})\} \tag{6}$$

$$j_c = i_{0,c}\,(1-\Theta)\,\{\exp(\frac{\alpha_c\, n\, F}{\mathrm{RT}}\eta_{\mathrm{act},c}) - \exp(\frac{-(1-\alpha_c)\, n\, F}{\mathrm{RT}}\eta_{\mathrm{act},c})\} \tag{7}$$

i_0 is the exchange current density $(\mathrm{A/m^2})$ and η is the overpotential (V), and α stands for transfer coefficient.

The formation of bubbles at the electrode can block the electrocatalyst surface and ion-conducting pathways in the electrolyte. This may result in energy loss, reducing overall system performance [3]. Eq. 8 [4], describes the bubble coverage, which relates the bubble effect to the applied current, and has been integrated into activation and ohmic losses.

$$\Theta = 0.023 j^{\,0.3\left(\frac{P_{ref}}{P}\times\frac{T}{T_{ref}}\right)^{1.5}} \tag{8}$$

Ohmic Overpotential

Ohmic overpotential is caused by ion resistance and increases linearly with the applied current. This voltage was calculated as shown in Eq. 9 and values of ohmic resistance, R $(\mathrm{m\Omega.\,cm^2})$, extracted from the literature [5].

$$\eta_{\mathrm{ohmic}} = \frac{R\,I}{A} \tag{9}$$

A $(\mathrm{cm^2})$ signifies the active surface area of the membrane, whereas I (A) represents the applied current. The resistance of the electrolyte was calculated depending on its molarity and temperature using Eq. 10 and Eq. 11 [1]. This term added into ohmic overpotential for better fitting.

$$\sigma_{\mathrm{KOH}} = -2.041M - 0.0028M^2 + 0.005332M.T + 207.2\,(\frac{M}{T}) + 0.001043M^3 - 0.0000003(M^2.T^2) \tag{10}$$

where σ_{KOH} presents the specific conductivity in S/cm, M represents the molarity in mol/L, and T represents the temperature in Kelvin.

$$R_{KOH} = \frac{1}{\sigma_{KOH}\left(1-\left(\frac{2}{3}\Theta\right)\right)^{1.5}}\left(\frac{d_{am}}{S_a} + \frac{d_{cm}}{S_c}\right) \tag{11}$$

d_{am}, d_m, and S_a, S_c values represent the distance between the anode or cathode and the membrane and the anode and cathode cross-sectional surface areas respectively, in $\mathrm{m^2}$.

Finally, the efficiency of the electrolyzer is calculated as shown in Eq. 12 [2].

$$\eta_{eff} = 1 - (\frac{V_{Loss}}{V_{cell}}) \tag{12}$$

The values used in the calculations are represented in Table 1.

Table 1. Coefficient values for different conditions

		1 M-50 µm	1 M-25 µm	0.1 M-50 µm	0.1 M-25 µm
Anode exchange current density ($i_{0,a}$)	(A/m^2)	0.129	0.129	0.100 [assumed]	0.100 [assumed]
Cathode exchange current density ($i_{0,c}$)	(A/m^2)	8.885 [6]	8.885 [6]	6.067 [6]	6.067 [6]
Resistance (R_Ω)	$(m\Omega.\,cm^2)$	300 [5]	196 [5]	460 [assumed]	320 [assumed]

It should be noted that the operating temperature is 50°C and the transfer coefficients α_a, α_c are taken as 0.69 [7] and 0.51 [8] for each calculation, respectively.

Results and Discussion

The comparison of the experimental data taken from Ref. [5] and the result of the modeling in this paper is shown in Fig.1a. It should be noted that experimental data obtained from the literature depend on the membrane type, and the voltage values are also affected by the specific ionomer used as a binder in the catalyst layer. It is known that as molarity increases, exchange current density increases, also reducing the ohmic resistance, thus the increase in molarity increases the efficiency by reducing overpotential. Fig.1b shows how the efficiency is affected depending on the thickness and molarity of the AEMION HNN-5 model membrane. As expected, efficiency was observed to be inversely proportional to thickness and directly proportional to molarity.

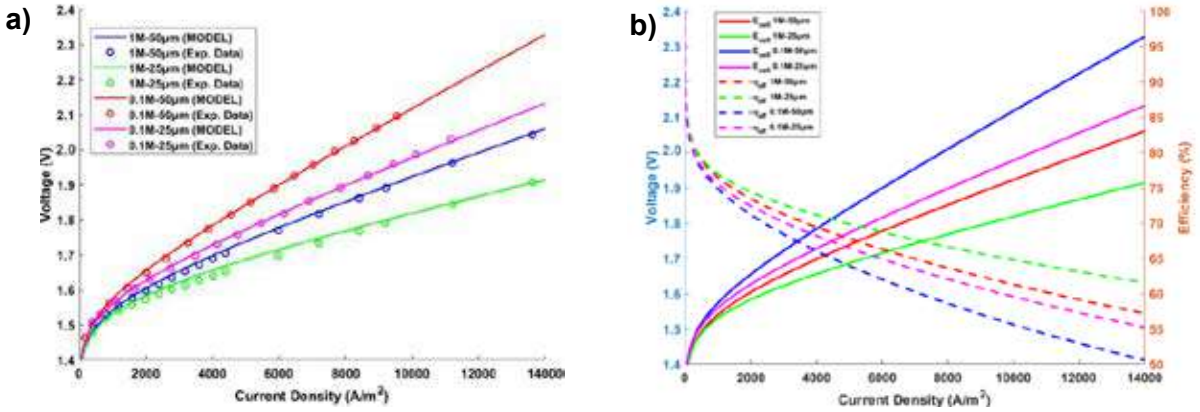


Fig. 1 a) Comparison between model results and experimental data [5] **b)** Voltage-Electrolyzer efficiency relationship

Fig.2a and Fig.2b summarize the effects of the cathode transfer coefficient and exchange current density values on voltage, respectively. As can be seen, as α_c and i_0 increase, there is a decrease in overpotential values. It is noteworthy that these values vary depending on several factors such as temperature, molarity, electrode type, and solution type.

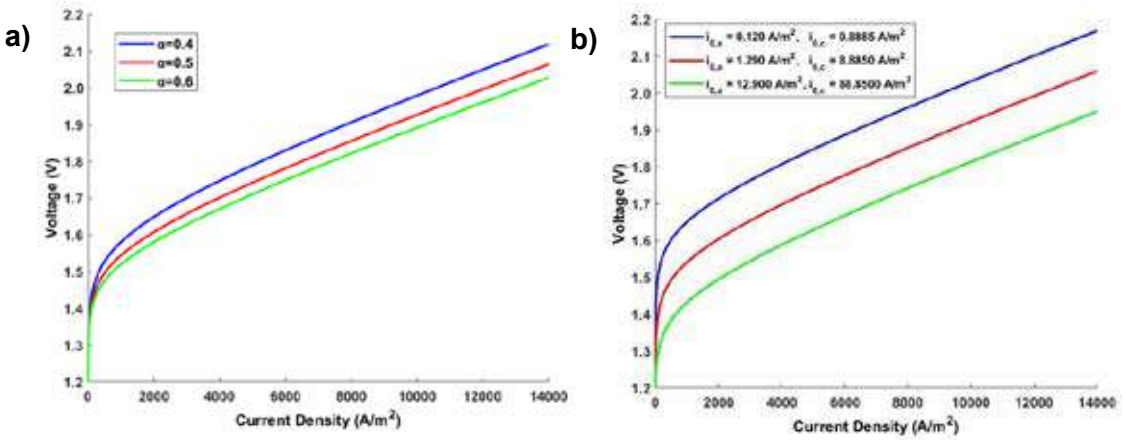


Fig. 2 Effects of **a)** Cathode Transfer coefficient values **b)** Exchange current density values on the AEMWE voltage

Conclusions

The study compared the model results with experimental data and observed the effect of the modeling parameters. In AEMWE, compared the PEM, the type of membrane, as well as the relationship of the type of electrode and electrolyte with the membrane and its response to temperature, pressure and molarity changes, should be examined in detail. Exchange current density and membrane resistivity values should not be evaluated independently of each other, the relationship between the two should be observed in detail. In addition to molarity, the effect of the type of solution must also be taken into account.

In summary, the model shows that increasing the molarity of the solution and exchange current density reduces overpotential values, leading to higher efficiency. As a result of this modeling, the highest efficiency observed was 61% at 1.4 $\mathrm{A/cm^2}$, using a 25 μm membrane in a 1 M solution. Additionally, a thicker membrane in a 1 M solution exhibited higher efficiency than a thinner membrane in a 0.1 M solution. Moreover, it is observed that efficiency increases with the rise in exchange current density, a pivotal factor influencing voltage values. The literature

highlights the dependence of this factor on various parameters such as electrode and electrolyte type, molarity, and operating temperature.

Acknowledgements

The authors would like to thank The Scientific and Technological Research Council of Türkiye (TÜBİTAK) (Grant Number: 123M878) for their support and funding of the project.

References

Ding, S., Guo, B., Hu, S., Gu, J., Yang, F., Li, Y., Dang, J., Liu, B., & Ma, J. (2022). Analysis of the effect of characteristic parameters and operating conditions on exergy efficiency of alkaline water electrolyzer. Journal of Power Sources, 537, 231532.

An, L., Zhao, T. S., Chai, Z. H., Tan, P., & Zeng, L. (2014). Mathematical modeling of an anion-exchange membrane water electrolyzer for hydrogen production. International Journal of Hydrogen Energy, 39(35), 19869–19876.

Vogt, H., & Balzer, R. J. (2005). The bubble coverage of gas-evolving electrodes in stagnant electrolytes. Electrochimica Acta, 50(10), 2073–2079.

Jang, D., Cho, H.-S., & Kang, S. (2021). Numerical modeling and analysis of the effect of pressure on the performance of an alkaline water electrolysis system. Applied Energy, 287, 116554.

Fortin, P., Khoza, T., Cao, X., Martinsen, S. Y., Oyarce Barnett, A., & Holdcroft, S. (2020). High-performance alkaline water electrolysis using AemionTM anion exchange membranes. Journal of Power Sources, 451, 227814.

Liu, J., Kang, Z., Li, D., Pak, M., Alia, S. M., Fujimoto, C., Bender, G., Kim, Y. S., & Weber, A. Z. (2021). Elucidating the Role of Hydroxide Electrolyte on Anion-Exchange-Membrane Water Electrolyzer Performance. Journal of The Electrochemical Society, 168(5), 054522.

H. Xu, Y. S.-H. V. K. R. P. J. K. (2016). Hydrogen and Oxygen Evolution Catalysis for Water Electrolysis 2.

Narayanamoorthy, B., Datta, K. K. R., & Balaji, S. (2012). Kinetics and mechanism of electrochemical oxygen reduction using Platinum/clay/Nafion catalyst layer for polymer electrolyte membrane fuel cells. Journal of Colloid and Interface Science, 387(1), 213–220.

Syngas Reforming on Microwave Cracking Bed following Bubling Coal and Biomass Pyrolysis Tar Mix

[1**]Yıldırım İsmail Tosun, [2]Fethullah Chichek,
[1*] Şırnak University, Engineering Faculty, Mining Engineering Department, Şırnak, 73000, Türkiye
[2] *Azerbaijan Science Academy , Department of Radiation Problems, Baku, Azerbaijan*
fcicek49@gmail.com

Abstract
In this study, the significant reforming tests for pyrolysis coal and wood tar mix have been made on low iron poor zinc ores containing PbO, ZnO, Fe2O3 inclusions as granules controlled with coal and biomass char/tar feed in order to reach catalytic reforming at 700 C providing heat transfer in microwave radiated cell to sequent column reactor. However, the results of filled bed poor iron slime yielded high heat transfer to coal and biomass char and tar. Due to the complex chemistry of coal, and porosity, heat conduction decreased in the microwave radiated cell system by granule size decrease. The iron slime conductivity distribution was raised temperature in the microwave activation dependent on the microwave heating power.
Heated iron slime granules in microwave radiation cell provided high heat conduction solid tar mixing gas flows. The gas flowed through sequent column are cycled for reforming hydrogen rich gas. one of the most promising technologies for advanced thermal energy conduction and radiation managed by microwave irony slime heating under microwave radiation favorable economic potential and intrinsic parameters. The development of catalytic granule pellet technology for column is a key issue in the catalytic hydrogen rich gas processing. As for coal pyrolysis tar and biomass and coal char with gas, catalysis poor zinc ore, granule pellets in the sequent column were mixed in and partially refornmed at approximately around 700°C. We have already reported the successful results of reforming using auger and injected coal gas. However, cycled biochar carbon/ tar gas and heat carrier irony slime dust/ biomass tar vapors with copper, lead and zinc oxide fines sorped in porous catalytic pellet basket. High rich hydrogen gas reforming is provided from coal and biomass tar products, such as Pb, Zn, Cu catalyzing hydrogen enrichment in column tube gasifier at about 5-7 % extraction yields. In this study, there was a few cycling steps studied in reforming column with solid packed catalyst flow by the low iron poor zinc ores of Hakkari and Şırnak (FeO and Fe2O3 oxide metal fines influenced the cracking reforming tar gas, even zinc salt mixture.

Keywords Syngas reforming, microwave column, bubbling bed, Coal Tar, Biomass Tar”

I. Introduction

There are various objectives to make the necessary arrangements to increase the use of biomass and solar energy as the other device. Considering the known biomass area of the potential high forest fields in northern Anatolia and located in central and eastern Anatolia.(Karayilmazlar et al.2015) it is seen as having low to medium heat resources. As we have seen in our country there is a significant potential for biomass resources will be invested. The low heat waste will be great source for waste heat and in comparison the electricity production may reach on 60-70 % thermal performances by microwave co-combustion.(Gürel 2020)
In conventional thermal processing, energy is transferred to the material through convection, conduction, and radiation of heat from the surfaces of the material. In contrast, microwave energy is delivered directly to materials through molecular interaction with the electromagnetic field. (Jian 2015) In conventional methods, energy is transferred due to thermal gradients, but microwave heating is the conversion transfer of electromagnetic energy to thermal energy through direct interaction of the incident radiation with the molecules of the target material.(Anietie et al.,2022)
In conventional thermal processing, energy is transferred to the material through convection, conduction, and radiation of heat from the surfaces of the material. In contrast, microwave energy is delivered directly to materials through molecular interaction with the electromagnetic field. In conventional methods, energy is transferred due to thermal gradients, but microwave heating is the conversion transfer of electromagnetic energy to thermal energy through direct interaction of the incident radiation with the molecules of the target material.(Jacob et al.,1995)
Enthalpy efficiency especially indirectly heated coal in microwave radiation is highly depended on the porosity of coal, ash amount of coal and amount of susceptor put in the microwave system. However the heat conductivity of susceptor to coal was also effects energy change (Andrew and Metaxas, 1991).
The kinetics of the combustion, spontaneous combustion and ignition temperature and volatile matter of coal is also critical under microwave combustion. The equilibrium constant of exothermic reaction and reaction kinetics can be related to the standard Gibbs free energy change for the reaction by the equation (Lu et al.,2007, Wu etal. 2002)
The ability for high extract yield of molten salts during biomass tar pyrolysis was investigated in this study. The thermo gravimetric analysis at bubbling bed reactor was recorded to study the thermal melting characteristics and bubbling affect of molten salt as the pyrolysis extracts. The NaCl-KCl-MgCl2 is appropriate for the preparation of H2-rich gas and the char with semi molten melts during hot gas passage and microporous form due to bubbling activation effect. NaCl-KCl-MgCl2 was efficient salt mixture for tar pyrolysis.

II. Materials and Methods

A type K thermocouple (wire diameter of 0.20 mm) was employed and the temperature was measured immediately after turning the power off. The variables studied were: incident microwave power, processing time and sample mass. For the microwave combustion tests, coal and biomass mixed tar samples weighing about 15–20 g as given in Table 1, were placed in fireclay combustion boats and heated. (Figure 1 and Figure 2) The catalytic cracking was managed in the experimentation by Fe2O3 PbO and ZnO ore pellets as given in Table 2.

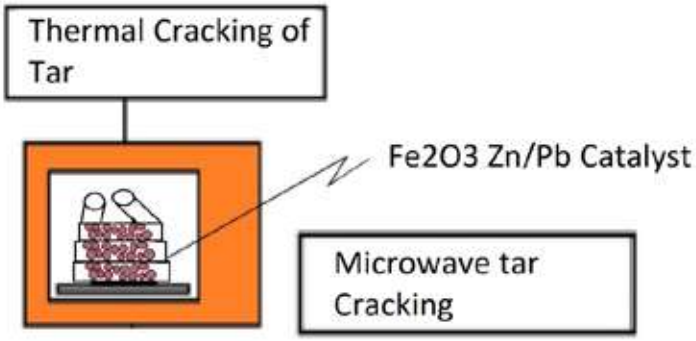


Fig. 1 Thermolysis Tar Cracking through Fe2O3 Zn/Pb catalyst.

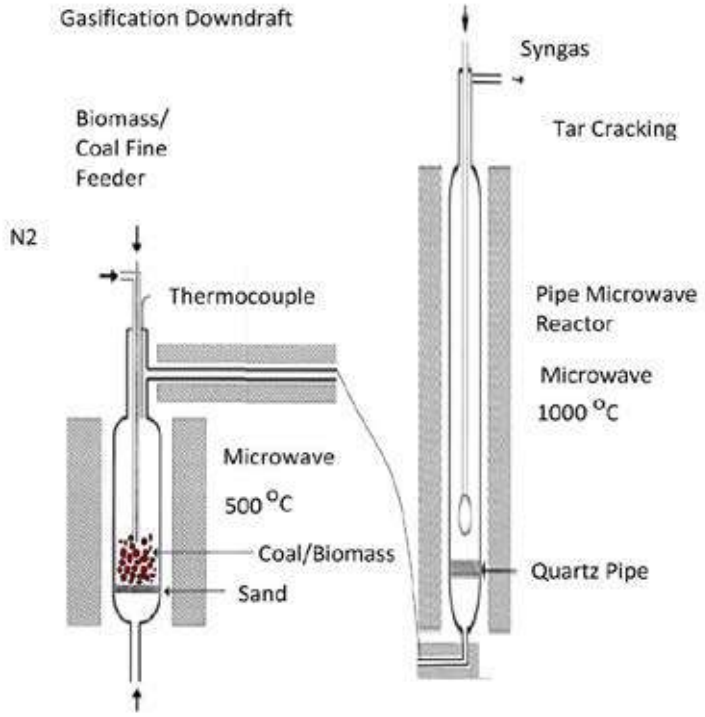


Fig. 2 Gasification and Thermolysis Tar Cracking through Fe2O3 Zn/Pb catalyst.

Table 1. Proximate Analysis of coal and biomass samples

Materials	C	H	O	S	N	Ash
Coal, Şırnak Asphaltite	22	5	15	7	2	42
Biomass, Oak wood straw	30	19	45	0,5	4	0,2
75%Biomass Tar	75	7	12	1		5
50%Biomass Tar	65	7	10	2		13

Table 2. Analysis of catalysts samples

Catalysts	ZnO	PbO	Fe2O3	FeO	Fe3O4	Silicate
Hakkari Calcined iron ore	12	5	41	2	4	32

Şırnak Calcined zinc ore/iron	39	11	15	5	4	22

2.1. Susceptor Fe2O3 and Catalyst Zn/Pb ZnO/PbO Effect

Such metal oxides require oxidation to break down the matrix of the tar condensed and oxidize or passivate the stuck matter following pyrolysis. The microwave treatment methods include combustion, chlorination, pressure oxidation, drying, torrefaction, pyrolysis digestion and gasification of waste materials. Microwaves could be utilized as an alternative source of energy for the treatment of ferrite materials by oxidation in some of the unit operations such as drying, calcining and smelting of massive texture by decreasing surface area of catalyst. Carbon and metal oxides are known to be very good microwave absorbers and they can be rapidly and selectively heated. Some researhers may improve heat it was indirectly heated by microwaves, therefore using hematite as a susceptor. Catalytic bed heat is adsorbed by conductive heat passage to tar melting on metal oxide pores as given below equation. (Aznar et al.,1997),

$$\theta = (T - T_a)/(T_i - T_a) \quad (1)$$

2.2. Tar Cracking Performance

There are excellent microwave heating conduction to gasified cracking of tar over hematite and Zn/Pb catalyst, which is used at higher temperature crackings even more than in high presurrized gasification. The exergy of microwave pyrolysis and thermolysis tar cracking is geatly depended on heat content of catalytic bed. The bubbling flow of gasification and porosity of catalyst in the microwave pipe reaction bed in the reactor as illustrated in Figure 2 and this high exergy was resulted at 30 minutes time as leads to lower power rates in the microwave syngas reforming.(Nørskov et al 2014, Rustamov et al.,1998, Dayton 2002, Devi et al 2003)

Table 3. Summary of catalyst details for tar cracking

Type	Performance % for reformed H2	references
Ni	22 H2-35 CH4	Dayton 2002
Pd/Pt	32 H2-35 CH4	Devi etal. 2003
Pt/Rd	32 H2-35 CH4	Han and Kim, 2008
Zeolite/Mo	27 H2-25 CH4	Dayton 2002
Clay/Co	29 H2-25 CH4	Devi etal. 2003
Fe2O3	22 H2-35 CH4	Han and Kim, 2008
Pb/Zn-Al2O3	21 H2-25 CH4	Dayton 2002

3. Results and Discussion

The kinetics of the cracking following pyrolysis and cracking temperature and partial pressure of volatile matter of biomass/ coal tar are also critical under microwave tar cracking. It can be seen that the solid content of tar oil increases significantly faster in the microwave cracking rates than in conventional control tests. More than 75% of the tar was removed within 10 minutes with microwave heated gasification of biomass/coal, while in conventional combustion the same degree of tar removal would require several hours.(Elliot, 1987) metal oxide and carbonate reactions may be performed as given below equations through gasifier;

M2CO3 +H2O(g) 2MOH+CO2(g) (1)
M2CO3+C M2O+2CO(g) (2)
H2(g)+CO2(g) CO(g)+H2O(g) (3)
M2CO3+H2(g)›2M(g)CO2(g)H2O(g) (4)
M2CO3›M2O+CO2(g) (5)

The influence of sulfates NaCl-KCl-MgCl2 and Na2SO4-K2SO4-MgSO4 on the pyrolysis process of biomass is shown in Eq. 7 and 8. It can be found that the pyrolysis process of biomass changes abnormally after the addition of sulfates. The char and methane were rapidly consumed from 300 °C and completely disappeared at about 450 °C. Almost all char derived from biomass tar pyrolysis was converted into CO2(g), and the reactions involved were mainly (5) and (6). As the temperature increased, sulfates went through a more complex conversion process with possible reactions (7) to (11).

M2SO4+2C ›M2S+2CO2(g) (6)
M2SO4+CH4 ›M2S+CO2(g)2H2O(g) (7)
M2S+3CO2(g) ›M2O+SO2(g)+3CO(g) (8)
M2O+H2O(g) ›2MOH (9)
M2SO4+H2(g) ›2MOH+ SO2(g) (10)
Li2S+M2SO4 ›M2S+Li2SO4 (11)

4. Conclusions

In modified pipe microwave reactor, where the average concentration of solids amounts to 10 - 50 g/m^3, i.e. the conditions for residence time are long enough for the thermal cracking of biomass tar and coal tar and extensive gas mixing with 60-70% N2 and air so enhancing biomass pyrolysis and tar feeding inlet in order to take the down draft gas, heat transfers to the microwave cracking section. It is necessary to create conditions of internal circulation without the transported coal and waste in modified pipe and downdraft gasified, 90-95% tar yield were observed at the end of combustion. Total heat values of biochars are of approximately 17.8 kJ/ kg for corn stalk and 16.2 kJ/ kg for forest oak wood waste for tar cracking by microwave.

At 750^{o}C, the pyrolysis gas obtained from Hakkari iron ore catalysts contained 30,42 vol% H2 with the H2/CO ratio reaching 1,41. The carbonates demonstrated excellent improvement for the gas composition of biomass char pyrolysis products, with 62,7 vol% and 57,2 vol% syngas (H2/CO) collected from the Hakkari iron ore catalysts and PbO content was effective in cracking pyrolysis systems at 750 ^{o}C, respectively. Silicates, oxides, the bio-oil and char prepared by biomass char pyrolysis also achieved better quality. The thermodynamic equilibrium resulted of the high extract gas formation of H2and CO from biomass and coal tar in metal oxide composition of Şırnak zinc ore/iron during biomass tar pyrolysis. The sulfur reaction between MgCl2 and char tar char under high temperature 750^{o}C determined the high gas H2 yield and CO in pyrolysis gas products with the low consumption of magnesium salts in the ores and deterioating the biomass tar pyrolysis system.

References

Adjaye, J.D., N.N. Bakhshi, Catalytic conversion of a biomass-derived oil to fuels and chemicals. 2. Chemical kinetics parameter estimation and model predictions, Biomass Bioenergy, 8 (1995), pp. 265-277

Andrew C Metaxas,1991, Microwave Heating, Power Engineering Journal 5(5):237 - 247,IEEE Xplore,DOI: 10.1049/pe:19910047

Anietie O. E., C F Jisieike, T H Ibrahim, E Betiku, Chapter 2 - Biodiesel and its properties, Editor(s): A. Arumugam, Production of Biodiesel from Non-Edible Sources, Elsevier, 2022, Pages 39-79, ISBN 9780128242957,

Aznar, M.P. , M.A. Caballero, J. Gil, A. Olivares, J. Corella, Hydrogen by biomass gasification with steam-O_2 mixtures and steam reforming and CO-shift catalytic beds downstream of the gasifier R.P. Overend, E. Chornet (Eds.), Making a business from biomass. Proceedings of the third biomass conference of the Americans, Elsevier Science, Oxford, UK (1997), pp. 859-860

Bridgwater, A.V. , Production of high grade fuels and chemicals from catalytic pyrolysis of biomass, Catal. Today, 29 (1996), pp. 285-295

Dayton D., 2002, A review of the literature on catalytic biomass tar destruction, National Renewable Energy Laboratory, Golden, Colorado, USA. .(2002)

Delgado, J. , M.P. Aznar, J. Corella, Biomass gasification with steam in steam in fluidised bed: effectiveness of CaO, MgO, and CaO–MgO for hot raw gas cleaning, Ind. Eng. Chem. Res., 36 (1997), pp. 1535-1543

Demirbas, A. i Hydrogen production from biomass by the gasification process, Energy Sources, 24 (2002), pp. 59-68

Devi L., Ptasinski K.J., Janssen F.J.J., 2003, A review of the primary measures for tar in biomass gasification processes, Biomass Bioenergy 24, 125-140. .(2003)

Elliot. D.C. ,1987, "Relation of Reaction Time and Temperature to Chemical Composition of Pyrolysis Oils", ACS Symposion Series 376, Pyrolysis Oils from Biomass". Edited by E.J. Soltes and T.A. Milne. Denver, CO. April 1987. .(1987)

Grange, P. , E. Laurent, R. Maggi, A. Centeno, B. Delmon, Hydrotreatment of pyrolysis oils from biomass: reactivity of the various categories of oxygenated compounds and preliminary techno-economical study, Catal. Today, 29 (1996), pp. 297-301

Gürel, B., 2020, Türkiye'deki güncel biyokütle potansiyelinin belirlenmesi ve yakilmasıyla enerji üretimi iyi bir alternatif olan biyokütle atiklar için sektörel açidan ve toplam yanma enerji değerlerinin hesaplanmasi, Mühendislik Bilimleri ve Tasarım Dergisi, 8(2), 407 – 416, 2020, e-ISSN: 1308-6693

Han J., Kim H., 2008, The reduction and control technology of tar during biomass/pyrolysis: an overview. Renewable and Sustainable Energy Reviews 12, 397-416.(2008)

https://doi.org/10.1016/B978-0-12-824295-7.00004-8.

Jacob J, Chia LHL, FYC Boey. Review-thermal and non-thermal interaction of microwave radiation with materials. Journal of Materials Science 1995; 30 (21): 5321-7.

Jian Xu, Chapter 9 - Microwave Pretreatment, Editor(s): Ashok Pandey, Sangeeta Negi, Parameswaran Binod, Christian Larroche, Pretreatment of Biomass, Elsevier, (2015), Pages 157-172, ISBN 9780128000809, https://doi.org/10.1016/B978-0-12-800080-9.00009-8.

Karayilmazlar, S., Saraçoğlu, N., Çabuk, Y., & Rıfat, K. U. R. T. (2011). Biyokütlenin Türkiye'de enerji üretiminde değerlendirilmesi. Bartın Orman Fakültesi Dergisi, 13(19), 63-75.

Marquevich, M. , S. Czernik, E. Chornet, D. Montane, Hydrogen from biomass: steam reforming of model compounds of fast-pyrolysis oils, Energy Fuels, 13 (1999), pp. 1160-1166

Nørskov, J K. , F Studt, F. Abild-Pedersen, T. Bligaard, Fundamental Concepts in Heterogeneous Catalysis, 2014 by John Wiley & Sons, Inc, ISBN 978-1-118-88895-7

Raveendran, K., A. Ganesh, K.C. Khilar, Pyrolysis characteristics of biomass and biomass components, Fuel, 75 (1996), pp. 987-998

Rustamov, V.R. , K.M. Abdullayev, E.A. Samedov, Biomass conversion to liquid fuel by two-stage thermochemical cycle, Energy Conv. Manage., 39 (1998), pp. 869-875

Sutton D., B. Kelleher, J.R.H. Ross,Review of literature on catalysts for biomass gasification, Fuel Process. Technol., 73 (2001), pp. 155-173

Wang, D., S. Czernik, D. Montane, M. Mann, E. Chornet, Biomass to hydrogen via fast pyrolysis and catalytic steam reforming of the pyrolysis oil or its fractions, Ind. Eng. Chem. Res., 36 (1997), pp. 1507-1518

Yin XL, Wu CZ, Zheng SP, Chen Y. Design and operation of a CFB gasification and power generation system for rice husk. Biomass Bioenergy (2002);V23:181–7.

A sustainable geothermal based multigeneration plant for green hydrogen generation; Energy and exergy analysis

[1]Fatih Yilmaz, [1]Murat Ozturk, [2]Resat Selbas
[1] Isparta University of Applied Sciences, Mechatronics Engineering, Isparta/Türkiye
[2] Isparta University of Applied Sciences, Mechanical Engineering, Isparta/Türkiye

Abstract

The developed research deals with the thermodynamic performance analysis of a sustainable geothermal based multigenerational plant for green power, hydrogen, and heating loads. For this aim, the system basically consists of a double flash-Binary geothermal power plant consisting of two separators and two steam turbines, two organic Rankine cycles with ammonia fluid, a PEM electrolyzer, and a domestic hot water preparation unit. The analysis results indicate that the proposed system's net power generation capacity is 1104 kW. In addition, the system can produce a 3997kW heating load with hot water, and finally, it can also generate 0.002421 kg/s of green hydrogen.

Keywords: energy, exergy, hydrogen, sustainability, power, geothermal

I. Introduction

Global energy demand has been increasing trend as of the industrial revolution. In the global energy mix, which a large portion of global energy demands still come from fossil fuels and give rise to many problems. Looking at the data for 2020, fossil fuels constitute 83.7% of global energy, nuclear 4.3% and renewable energy sources 12% (Razi and Dincer, 2022). The use of fossil fuels causes environmental problems such as global warming, and this is one of the most important issues that directly affects humanity today. One of the most effective ways to solve this problem is the effective use of renewable energy resources. Additionally, at this point, the concept of green hydrogen is a prominent issue in recent years. Green hydrogen offers the most important sustainable solution to decarbonise key sectors, reducing dependence on fossil fuels. In short, green hydrogen is a method of decomposing water into hydrogen and oxygen by electrolysis using renewable energy sources (Hassan et al. 2024). Renewable energy-supported hydropower production methods are an indispensable technology to overcome global environmental problems. Among these, geothermal energy offers many advantages and has a mature technology for production of power, hydrogen, heating, and other beneficial products.

In the literature, there are several papers about on the geothermally driven multigeneration plant for production of hydrogen. Tekkanat et. (2023) proposed a new study that is combined with geothermal energy for beneficial products. The analysis show that overall system has 59.53% of energy efficiency and also can be generate the 0.0015 kg/s hydrogen. Furthermore, Bozgeyik et al. (2023) developed a geothermal-biomass assisted multigeneration plant. Their system can be generated 3.52 kg/h hydrogen and overall energy efficiency is computed as 65.55%. Yilmaz and Ozturk (2023) investigated a multigeneration plant that driven by geothermally which is computed as overall energy and exergy efficiencies are 42.48% and 38.26%. Moreover, some studies in the literature in 2023 and 2024 can be summarized and presented here (Sharifishourabi et al. 2023; Turgut and Dincer, 2023; Temiz and Dincer, 2024; Aslan and Yilmaz, 2024; Yilmaz et al. 2024).

The main purpose of this study is to design, analyze and present a geothermal supported combined system, which is a sustainable method. With this system, we examine the changes in performance criteria by performing thermodynamic analysis of clean and sustainable power, heating and green hydrogen production.

II. Model definition and Mathematical modeling

The developed paper embraces a double Flash-binary geothermal power plant as illustrated in Fig. 1. This system comprises two separators, two steam turbines, two ORCs, a PEM electrolyzer, and a domestic hot water generation unit. At 200 ℃geothermal water enters the expansion valve, decreasing the pressure and temperature. After that, it arrives at separator 1, and then it splits into the saturated vapor and liquid phases. HEX1 connects the ORC system, and geothermal water and thermal energy transfer occur here. Finally, the designed plant can generate power with four turbines, hydrogen with a PEM unit, and heating loads with a domestic hot water generation unit.

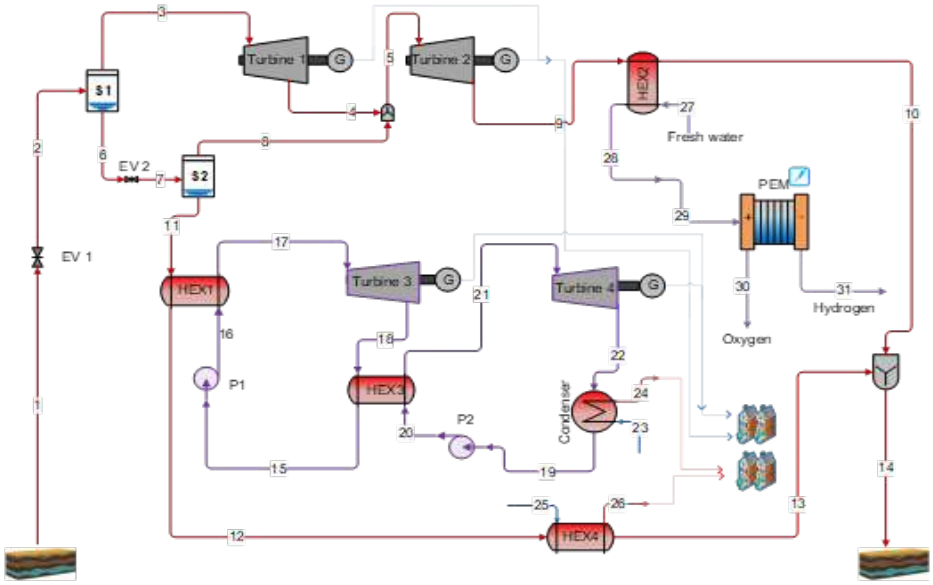


Fig.1. A schematic flow chart of the developed plant

For thermodynamic modeling of the system, mass, energy, and exergy balance equations are applied as follows (Cengel et al. 2011; Dincer 2020);

$$\dot{m}_{in} = \dot{m}_{out} \quad (1)$$

$$\dot{Q}_{in} + \dot{W}_{in} + \sum \dot{m}_{in} h_{in} = \dot{Q}_{out} + \dot{W}_{out} + \sum \dot{m}_{out} h_{out} \quad (2)$$

$$\dot{E}x^{\dot{Q}_{in}} + \dot{E}x^{\dot{W}_{in}} + \sum \dot{m}_{in} ex_{in} = \dot{E}x^{\dot{Q}_{out}} + \dot{E}x^{\dot{W}_{out}} + \sum \dot{m}_{out} ex_{out} + \dot{E}x_D \quad (3)$$

Overall system efficiency;

$$\eta_{sys} = \frac{\dot{W}_{net} + (\dot{m}_{H_2} LHV_{H_2}) + \dot{Q}_{heating}}{(\dot{m}_1 h_1 - \dot{m}_{14} h_{14})} \quad (4)$$

$$\psi_{sys} = \frac{\dot{W}_{net} + (\dot{m}_{H_2} ex_{H_2}) + \dot{E}x_{Q,heating}}{(\dot{m}_1 ex_1 - \dot{m}_{14} ex_{14})} \quad (5)$$

III. Results and discussion

Considering the system for thermodynamic programming, some assumptions are presented in Table 1. Accompanied by these assumptions, analysis is made with the EES program and the case study results are depicted in Table 2.

Table 1. Parameters study design indicators for thermodynamic analysis

Parameters	Unit	Value
Geothermal unit		
T_1	℃	200
$\dot{m}_{geo}$	$kg/_s$	50
rp1	-	2.5
$\eta_{isT1-T2}$	%	92
ORC-1 and ORC 2		
Working fluid	Ammonia	
T_{15}	℃	49.36
P_{15}	kPa	2000
P_{16}	kPa	3000
T_{19}	℃	24.89
P_{19}	kPa	1000
P_{20}	kPa	3000
PEM		
PEM inlet temperature	℃	78
PEM inlet pressure	kPa	101.3
Reference		
Reference temperature	℃	25
Reference pressure	kPa	101.3

Table 2. Thermodynamic analysis results of the modeled plant

	η (%)	ψ (%)
Overall system	19.63	23.73
System products		
$\dot{W}_{T1}$	780.3 kW	
$\dot{W}_{T2}$	64.2 kW	
$\dot{W}_{T3}$	250.1 kW	
$\dot{W}_{T4}$	518.8 kW	
$\dot{W}_{net}$	1104 kW	
$\dot{W}_{heating}$	3997 kW	
$\dot{m}_{hydrogen}$	0.002421 $kg/_s$	

As the geothermal water temperature increases, the beneficial outputs obtained from the system and the increase in system performance are shown in Figures 2, 3, and 4. The increase in source temperature means that the quality of the geothermal fluid increases and it operates at a higher enthalpy, thus it has a positive effect on the system.

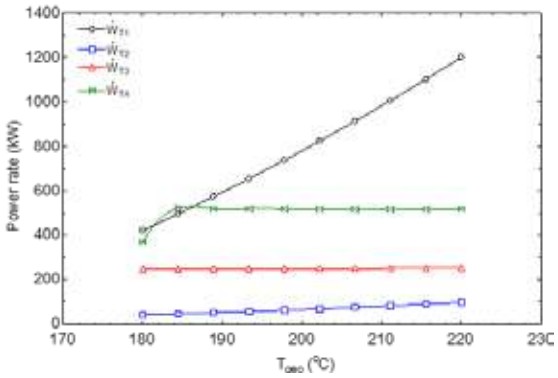


Fig.2. Effect of T_1 on the power generation rates of Turbines

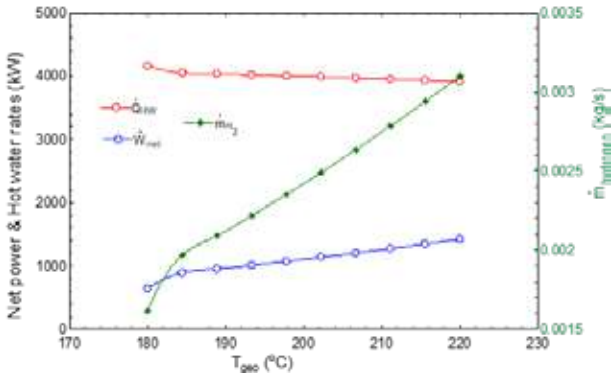


Fig.3. Effect of T_1 on the beneficial products

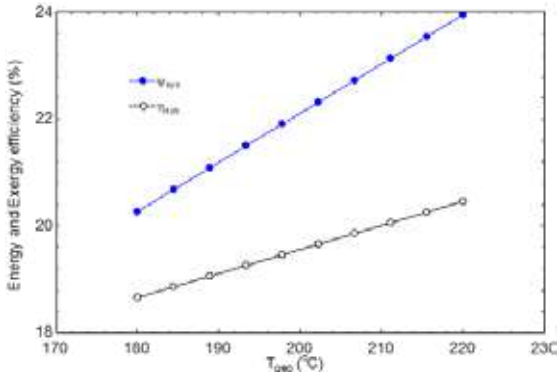


Fig.4. Effect of T_1 on the energy and exergy efficiency

While Figure 5 shows the increase in the amount of net power and hydrogen produced from the system due to the increase in geothermal mass, Figure 6 shows the increase in system performance due to this increasing mass flow rate of geothermal.

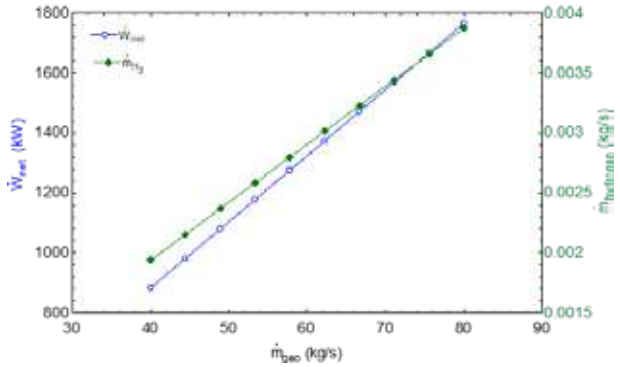


Fig.5 Change of the power and hydrogen rate vs $\dot{m}_{geo}$

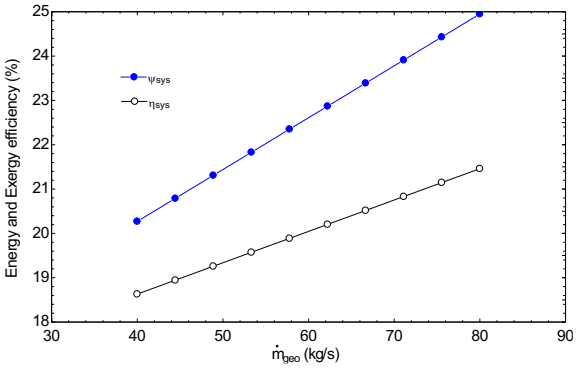


Fig.6 Change of the overall system performance ratio vs $\dot{m}_{geo}$

The effect in the separator inlet pressure (P_2) designed system performance is important. Figure 7 shows the change in net electricity production and hydrogen exchange with the change of P_2 pressure from 450 kPa to 1050 kPa. In other general terms, Figure 8 shows the system performance changes in this pressure range. Up to approximately 750 kPa pressure, the system's products and system performance increase and then decrease.

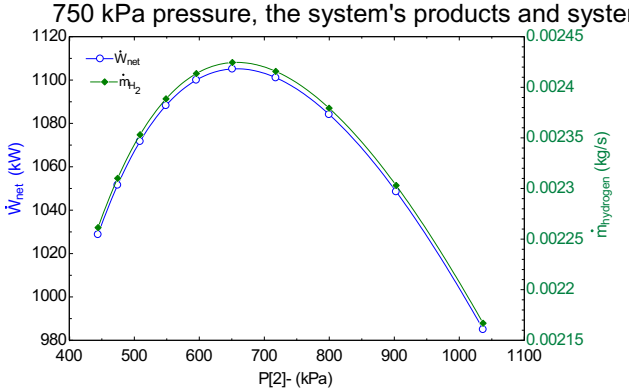


Fig.7 The effect of P_2 on the net power and hydrogen generation rate

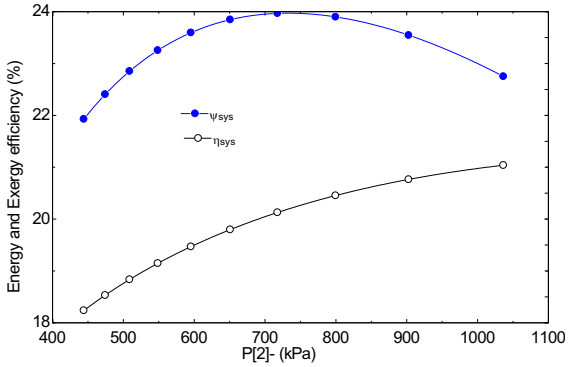


Fig.8 The effect of P_2 on the system performance ratio

IV. Conclusion

In this study, a comprehensive thermodynamic analysis of a geothermal supported combined system was analyzed and presented according to its energy and exergy efficiencies. The aim of the system is the production of clean and sustainable hydrogen, power and heating. Some of the main results obtained can be summarized as follows;

- The system net electricity production capacity is determined as 1104 kW. This system also. It has the capacity to produce 0.002421 kg/s of green hydrogen.
- The energy and exergy efficiency of the entire system was calculated as 19.63% and 23.73%.

References

Arslan, M., & Yilmaz, C. (2024). Development of models for green hydrogen production of Turkey geothermal Resources: A case study demonstration of thermodynamics and thermoeconomics analyses. *Fuel*, *359*, 130430.

Bozgeyik, A., Altay, L., & Hepbasli, A. (2023). Energetic, exergetic, exergoeconomic, environmental and sustainability analyses of a solar, geothermal and biomass based novel multi-generation system for production of power, hydrogen, heating, cooling and fresh water. *Process Safety and Environmental Protection*, *177*, 400-415.

Cengel, Y. A., Boles, M. A., & Kanoğlu, M. (2011). *Thermodynamics: an engineering approach* (Vol. 5, p. 445). New York: McGraw-hill.

Dincer, İ. (2020). *Thermodynamics: a smart approach*. John Wiley & Sons.

Hassan, Q., Algburi, S., Sameen, A. Z., Salman, H. M., & Jaszczur, M. (2024). Green hydrogen: A pathway to a sustainable energy future. *International Journal of Hydrogen Energy*, *50*, 310-333.

Razi, F., & Dincer, I. (2022). Renewable energy development and hydrogen economy in MENA region: A review. *Renewable and Sustainable Energy Reviews*, *168*, 112763.

Sharifishourabi, M., Dincer, I., & Mohany, A. (2023). Development and assessment of a new solar-geothermal based integrated energy system with sonic hydrogen generation for buildings. *Journal of Building Engineering*, *80*, 107944.

Tekkanat, B., Yuksel, Y. E., & Ozturk, M. (2023). The evaluation of hydrogen production via a geothermal-based multigeneration system with 3E analysis and multi-objective optimization. *International Journal of Hydrogen Energy*, *48*(22), 8002-8021.

Temiz, M., & Dincer, I. (2024). Development of a hybridized small modular reactor and solar-based energy system for useful commodities required for sustainable cities. *Energy*, *286*, 129562.

Turgut, H. S. A., & Dincer, I. (2023). Assessment of a new binary geothermal based methanol synthesis plant with power, hydrogen and freshwater. *Energy Conversion and Management*, *294*, 117576.

Yilmaz, F., & Ozturk, M. (2023). Modeling and parametric analysis of a new combined geothermal plant with hydrogen generation and compression for multigeneration. *International Journal of Hydrogen Energy*.

Yilmaz, F., Ozturk, M., & Selbas, R. (2024). Development and assessment of a newly developed renewable energy-based hybrid system with liquid hydrogen storage for sustainable development. *International Journal of Hydrogen Energy*, *56*, 406-417.

A Comprehensive 4E Analysis and Multi-Objective Optimization of a Hybrid Trigeneration system powered by a Solar Tower and Wind Turbine for producing Green Hydrogen, Electricity, and Cooling

[1]Faizan Khalid, [1*]Syed Abuzar Suhail, [1]Mohd Rihan
[1]Aligarh Muslim University, Centre for Integrated Green and Renewable Energy, Zakir Husain College of Engineering and Technology, Aligarh, 202001, India

* E-mail: syedabuzar10@gmail.com , fkhalid.igre@amu.ac.in

Abstract
In the pursuit of advancing global efforts towards sustainable energy solutions, this research delves into the dynamic landscape of innovative energy systems. Amid the escalating race to harness diverse energy sources for various applications, the study focuses on the design and analysis of a cutting-edge trigeneration system. This system, poised at the forefront of technological evolution, concurrently generates green hydrogen, electricity, and cooling. Harnessing the synergies of a hybrid source, comprising a solar tower and wind turbines, the research investigates the energetic, exergetic, ecological efficiency, and environmental impact, coupled with the Levelized Cost of Electricity (LCOE). Functionally, the trigeneration system allocates its components to powering the grid, producing green hydrogen through electrolysis, and driving a vapor compression cycle for cooling load generation. Employing the TOPSIS method for optimization, the research also endeavours to elevate the system's overall performance and results.

Keywords: 4E Analysis, green hydrogen, TOPSIS optimization, solar-wind hybrid, trigeneration

I. Introduction

The ever-increasing global energy demand (Dawood, Anda, and Shafiullah 2020), coupled with environmental concerns, necessitates a shift towards clean and sustainable energy sources. Green hydrogen, a flexible energy carrier crafted through the process of water electrolysis driven by sustainable energy sources, presents a compelling strategy for the decarbonization of multiple sectors, spanning transportation, industrial activities, and power generation (Staffell et al. 2019). However, the intermittent nature of renewable sources like solar and wind poses challenges to meeting consistent hydrogen production demands (Li, Liu, and Li 2022).

Hybrid renewable energy systems, combining solar and wind resources, offer a potential solution by exploiting the complementary nature of these sources and addressing intermittency issues (Babaremu et al. 2022). Notably, solar towers, concentrating solar power (CSP) plants with a central receiver tower, have been gaining traction due to their ability to achieve high heat concentrations and potentially higher efficiency compared to conventional photovoltaic (PV) systems (Awan, Zubair, and Chandra Mouli 2020).

This study presents the exploration of a novel hybrid system combining a solar tower and a wind turbine for trigeneration production of green hydrogen, electricity, and cooling. This approach aims to leverage the strengths of both technologies: the high energy density and dispatchability of the solar tower and the cost-effectiveness and ambient-dependent nature of wind energy. The system will be evaluated through a comprehensive 4E analysis, encompassing energetic, exergetic, ecological, and environmental, to assess it's overall feasibility. Additionally, a multi-objective optimisation, TOPSIS method, is conducted to identify the optimal system configuration that balances the competing objectives of maximising hydrogen production, minimising electricity costs, and providing the required cooling load.

This research contributes to the growing body of research focused on innovative renewable energy systems for clean and sustainable hydrogen production. By investigating the potential of a hybrid solar tower and wind turbine system for multi-generation, this study aims to inform the development and deployment of future sustainable energy solutions.

II. Experimental Set-up and Procedure

The Trigeneration system, as depicted in **Fig. 1**, operates on the synergistic utilization of two renewable energy sources. The primary source is a Concentrated Solar Tower, designed to harness solar energy efficiently. The generated heat from the solar tower serves as the driving force for a Heat Recovery Steam Generator (HRSG), a pivotal component in the Rankine cycle.

Within the Rankine cycle, the HRSG bifurcates its energy output into two distinct channels: the first, channeled through a steam turbine and thermo-electric generator (TEG), constitutes the initial segment of electricity generation. Simultaneously, the system incorporates a second segment powered by wind turbines, introducing a hybrid dimension to the overall energy framework. Both segments converge at the centralized Control Panel.

The consolidated electrical output undergoes further delineation at the Control Panel, segregating into three distinct pathways. The first stream, designated as $W_{ELECTRIC}$, seamlessly integrates into the electrical grid, contributing to the communal power supply. The second stream, denoted as $W_{ELECTROLYZER}$, directs its energy towards an electrolyzer, facilitating the production of green hydrogen. This hydrogen serves as a valuable resource, transitioning to fuel applications at a dedicated fuel station, thereby supporting vehicular needs within the community.

The third and final stream of electricity drives a Vapor Compression Refrigeration (VCR) cycle. This cycle, featuring an electrically powered compressor, generates $Q_{COOLING}$, a cooling load directed to the community for

various refrigeration purposes.

In summation, the Trigeneration system presents a meticulously designed framework where renewable energy sources harmoniously converge, providing diversified outputs for community welfare. This systematic approach encompasses electricity generation, green hydrogen production, and refrigeration, showcasing a multifaceted and sustainable energy solution for contemporary needs.

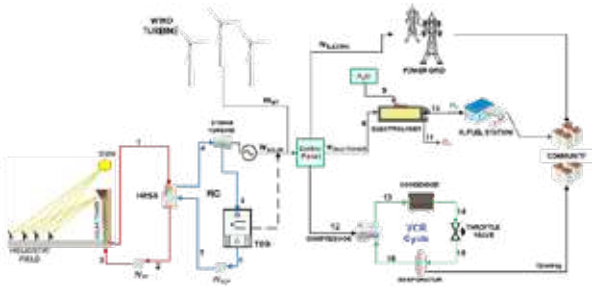


Fig. 1: Schematic Overview detailing the Functional Components of the Hybrid Trigeneration System

III. Analysis

The formulas for conducting the 4E analysis (Ahamad et al. 2023) are listed below:

Energy Efficiency: It may be expressed as follows, represents the system's total usable energy produced divided by the fuel input energy

$$\eta_{energy} = \frac{W_{ELECTRIC} + W_{TEG} + Q_{COOLING} + HHV \times \dot{m}_{10} - W_{HTF,SP} - W_{RCP}}{Q_{C.R} + W_{wind\ speed}} \quad (1)$$

Exergy Efficiency: The exergy input divided into the entire system is referred to as the product exergy output, and it may be calculated using the following formula:

$$\eta_{exergy} = \frac{W_{ELECTRIC} + W_{TEG} + E_{x_{COOLING}} + HHV \times \dot{m}_{10} - W_{HTF,SP} - W_{RCP}}{E_{x,CR} + W_{wind\ speed}} \quad (2)$$

$$\dot{E}x^{Q}_{evaporator} = \dot{Q}_{evaporator}\left(\frac{T_0+273}{T_{evaporator}+273} - 1\right) \quad (3)$$

Environmental Analysis: Examining the setup's overall environmental impact while operating in various climatic conditions is crucial for any analysis to be thorough. Even if the modern plant generates energy solely from green sources like solar and wind, certain exhaust effluents are still emitted into the environment, which could be harmful to the planet's ecology. The current study examines the environmental competency of the setup in order to better illustrate and identify the relationship between the environment and the power producing mechanism, or ecological efficiency (EE) (Alibaba et al. 2020).

$$EE = \left[\frac{0.206\eta_e \ln(135-IP)}{\eta_e + IP}\right]^{0.5} \quad (4)$$

And f_{CO_2e} is the Carbon dioxide equivalent emission coefficient, which is given by:

$$f_{CO_2e} = f_{CO_2} + 80\ f_{SO_2} + 50\ f_{NO_x} + 67\ f_{PM} \quad (5)$$

$$f^{CO}_{CO_2} = 985 \times 10^{-3}\frac{LHV}{10466} \quad (6)$$

$$f_{CO_2e} = f_{CO_2} + 80\ f_{SO_2} + 50\ f_{NO_x} + 67\ f_{PM} \quad (7)$$

$$f_{PM} = (C_{PM} \times 10^{-6})V_{vg}\ /m_{steam} \quad (8)$$

$$f_{NO_x} = (C_{NO_x} \times 10^{-6})V_{vg}\ /m_{steam} \quad (9)$$

$$f_{SO_2} = (C_{SO_2} \times 10^{-6})V_{vg}\ /m_{steam} \quad (10)$$

$$C_{PM} = 1\ \left(\frac{mg}{Nm^2}\right), C_{NO_x} = 149\ \left(\frac{mg}{Nm^2}\right), C_{SO_2} = 5.48\ \left(\frac{mg}{Nm^2}\right) \quad (11)$$

Where, V_{vg} is exhaust gas' volume flow rate (in Nm^3/s)

Economic Analysis: Levelized cost of energy (LCOE), a useful method for characterising the average cost of each unit of electricity (Thirugnana et al. 2023), is utilised to measure the economic performance of any plant from a lifetime standpoint. The metric is often stated in terms of $/kW. In general, the universal formula of LCOE is assessed as,

$$LCOE = C_{total}/(W_{net} \times \tau) \quad (12)$$

TOPSIS Analysis: Evaluation of system performance is dependent on several results, some of which are more important to users than others. To deal with this, TOPSIS analysis is used to calculate a priority score from several operational parameters. After that, the TOPSIS-AHP method is utilised to prioritise performance outcomes by including weights from the Analytic Hierarchy Process (AHP). To address element divergence in performance attributes, standardisation is applied. The evaluation of ideal scenarios yields the performance scores for outcomes. Values for Euclidean distance at each step are also given. Table 10 provides a summary of the final rankings and significance of the hybrid system's outcomes.

IV. Results and discussions

This study utilizes a trigeneration system powered by solar and wind energy. The hybrid system combines a solar tower and wind turbine. However, the system's performance is influenced by variables such as demographics and weather conditions, particularly Direct Normal Irradiation (DNI), a key factor in solar energy utilization.

Fig. 2 depicts the variation of four crucial parameters on which the system's performance is evaluated, namely energy efficiency, exergy efficiency, ecological efficiency (EE), and levalized cost of electricity (LCOE), and how they change with respect to the change in the value of DNI. For calculation purposes, the value of the DNI is varied from 600 W/m^2 to 1100 W/m^2. The values of three parameters, namely energy efficiency, exergy efficiency, and ecology efficiency (EE), maintain similar values despite the substantial increase in the value of DNI. On the other hand, the levelized cost of electricity (LCOE) sharply decreases with an increase in the DNI. With an incremental DNI value, the cost of electricity that it will be sold at shows an approximately 44% decrease in its cost over the project's lifetime.

Similarly, the variation in the same four parameters is studied with respect to the change in the wind speed value. As in the case of DNI, there isn't any substantial change with an increase in wind speed in the same three efficiencies, but surprisingly, the value of LCOE also remains nearly constant. For the project timeline, DNI has a major impact on the end cost of electricity, but with increasing wind speed, no similar trend is observed.

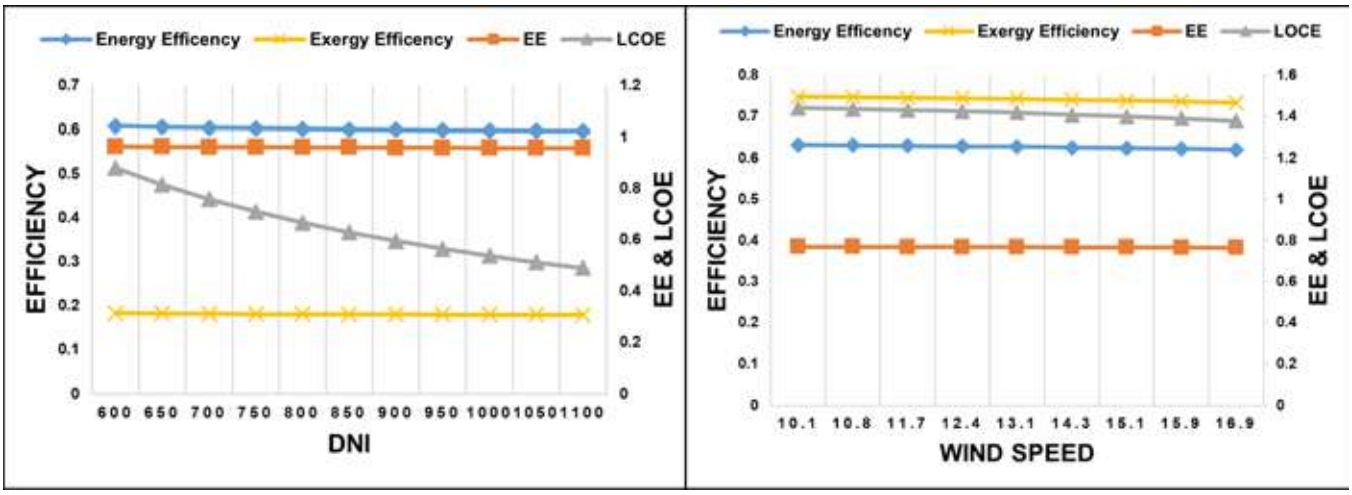


Fig. 2: Variation of energy, exergy, ecological efficiency and LCOE with DNI and Wind Speed

As explained above in the TOPSIS analysis, to address element divergence in performance attributes, standardisation is applied. The evaluation of ideal scenarios yields the performance scores for outcomes. Values for Euclidean distance at each step are also given in Tab. 1. Tab. 2 provides a summary of the final rankings and significance of the hybrid system's outcomes.

Tab. 1: Matrix depicting both optimal and suboptimal solutions, accompanied by the corresponding performance scores

S.No.	Outcomes	DNI	Wind Speed	Power Ratio	Turbine Inlet Temperature (TIT)	P_i score
Weightages		0.35	0.25	0.25	0.15	
1	Exergy Efficiency	0.043931988	0.023897115	0.035449759	0.013560091	0.458589
2	Energy	0.146540639	0.131048833	0.118221914	0.078429404	0.571045

	Efficiency					
3	Ecological Efficiency	0.232459654	0.159488306	0.189696913	0.099367331	0.541411
4	Environmental Efficiency	0.212269477	0.138991409	0.106216642	0.079316367	0.443716

Tab. 2: Outcomes ranked in the descending order

Outcomes	P_i Score	Ranking
Energy Efficiency	0.571045	1
Ecological Efficiency	0.541411	2
Exergy Efficiency	0.458589	3
Environmental Efficiency	0.443716	4

V. Conclusions

This study employed a solar and wind-powered trigeneration system, combining a solar tower and wind turbine. Varied Direct Normal Irradiation (DNI) values (600 W/m^2 to 1100 W/m^2) minimally affect energy, exergy, and ecological efficiency (EE). Conversely, the levelized cost of electricity (LCOE) significantly decreases with rising DNI, indicating a ~44% lifetime cost reduction. Wind speed variations exhibit negligible impact on efficiencies, with LCOE remaining nearly constant. DNI notably influences end electricity costs over the project timeline, unlike wind speed, as the W_{net} of solar is large. Optimization ranks energy efficiency highest and environmental efficiency lowest, with prioritization of and within system constraints.

References

Ahamad, Taufique, Mohd Parvez, Shiv Lal, Osama Khan, and Mohammad Javed Idrisi. 2023. “4-E Analysis and Multiple Objective Optimizations of a Novel Solar-Powered Cogeneration Energy System for the Simultaneous Production of Electrical Power and Heating.” *Scientific Reports* 13 (1): 1–23. https://doi.org/10.1038/s41598-023-49344-2.

Alibaba, Massomeh, Razieh Pourdarbani, Mohammad Hasan Khoshgoftar Manesh, Israel Herrera-Miranda, Iván Gallardo-Bernal, and José Luis Hernández-Hernández. 2020. “Conventional and Advanced Exergy-Based Analysis of Hybrid Geothermal–Solar Power Plant Based on ORC Cycle.” *Applied Sciences* 10 (15): 5206. https://doi.org/10.3390/app10155206.

Awan, Ahmed Bilal, Muhammad Zubair, and Kotturu V.V. Chandra Mouli. 2020. “Design, Optimization and Performance Comparison of Solar Tower and Photovoltaic Power Plants.” *Energy* 199 (May): 117450. https://doi.org/10.1016/j.energy.2020.117450.

Babaremu, Kunle, Nmesoma Olumba, Ikenna Chris-Okoro, Konyegwachie Chuckwuma, Tien-Chien Jen, Oluseyi Oladijo, and Esther Akinlabi. 2022. “Overview of Solar–Wind Hybrid Products: Prominent Challenges and Possible Solutions.” *Energies* 15 (16): 6014. https://doi.org/10.3390/en15166014.

Dawood, Furat, Martin Anda, and G.M. Shafiullah. 2020. “Hydrogen Production for Energy: An Overview.” *International Journal of Hydrogen Energy* 45 (7): 3847–69. https://doi.org/10.1016/j.ijhydene.2019.12.059.

Li, Jinze, Pei Liu, and Zheng Li. 2022. “Optimal Design and Techno-Economic Analysis of a Hybrid Renewable Energy System for off-Grid Power Supply and Hydrogen Production: A Case Study of West China.” *Chemical Engineering Research and Design* 177 (January): 604–14. https://doi.org/10.1016/j.cherd.2021.11.014.

Staffell, Iain, Daniel Scamman, Anthony Velazquez Abad, Paul Balcombe, Paul E. Dodds, Paul Ekins, Nilay Shah, and Kate R. Ward. 2019. “The Role of Hydrogen and Fuel Cells in the Global Energy System.” *Energy & Environmental Science* 12 (2): 463–91. https://doi.org/10.1039/C8EE01157E.

Thirugnana, Sathiabama T., Abu Bakar Jaafar, Srithar Rajoo, Ahmad Aiman Azmi, Hariharan Jai Karthikeyan, Takeshi Yasunaga, Tsutomu Nakaoka, Hesam Kamyab, Shreeshivadasan Chelliapan, and Yasuyuki Ikegami. 2023. “Performance Analysis of a 10 MW Ocean Thermal Energy Conversion Plant Using Rankine Cycle in Malaysia.” *Sustainability* 15 (4): 3777. https://doi.org/10.3390/su15043777.

Parametric Evaluation of a Hydrogen-driven Lightweight Vehicle with Thermally Coupled FC/MH tank system

[1*]Sera Ayten Çetinkaya, [2]Mehmet Akif Ezan, [2]Mustafa Umut Karaoğlan [2]C. Ozgur Colpan
[1]The Graduate School of Natural and Applied Sciences, Dokuz Eylul University, Izmir, Türkiye
[2]Department of Mechanical Engineering, Faculty of Engineering, Dokuz Eylul University, Izmir, Türkiye

*E-mail: sera.acetinkaya@gmail.com

Abstract

In recent years, the pursuit of low-emission or emission-free technologies in the automotive sector has led to an increased focus on the utilization of hydrogen technologies. Fuel cell technology, which generates power through chemical reactions involving hydrogen, is employed to meet propulsion needs in vehicles. Proton Exchange Membrane (PEM) fuel cells, favored for their ease of use and power density, utilize hydrogen in its pure form. Metal Hydride (MH) tanks can be used for storing pure hydrogen in technologies where fuel cells are employed. MH tanks chemically store hydrogen, thus causing fluctuations in tank temperature during charging and discharging. Effective operation necessitates the implementation of thermal management for MH tanks. In this study, different thermal management strategies of MH tank with and without thermal coupling with the fuel cell are examined numerically. A 1D mathematical model is developed in MATLAB/Simulink environment by resolving mass balance, kinetic balance, and energy balance equations for the MH tank. The performance of fuel cell/MH tank thermal coupling scenarios are comparatively evaluated for a specific driving cycle.

Keywords: Hydrogen Storage, Fuel Cell, Thermal Management, Metal Hydride, Fuel Cell Vehicles

I. Introduction

Numerous studies in the literature have investigated the thermal behaviour between proton exchange membrane fuel cells (PEMFC) and metal hydride (MH) hydrogen storage systems, employing a variety of cooling methods, both through experimental and theoretical approaches. Cano et al. (2014) developed a thermal model for a free air-breathing fuel cell selected for an automotive application. They have controlled the blowers, which are vital for airflow and thermal regulation, to optimize system efficiency. Zhu et al. (2019) integrated a PEM fuel cell and an MH hydrogen storage tank thermally by utilizing a heat exchanger and control system. They used the heat produced by the fuel cell to heat the coolant in the cooling system and heated the MH tanks. Following this, they developed a mathematical model to investigate the system's dynamic behavior, corroborating their findings through experimental validation. Omrani et al. (2019) theoretically explored the thermal connection within a system comprising an open-cathode PEMFC and an MH tank, developing a mathematical model to simulate the heat transfer between PEMFC waste heat and MH storage. Rahimi and Mahmoodi (2019) utilized heat pipes to convey heat from the fuel cell to the MH tank and conducted analyses utilizing Computational Fluid Dynamics (CFD) simulations. Zhang et al. (2020) introduced a thermal management system for an open-cathode PEM fuel cell, employing a novel MPC (Model predictive control) approach to control blowers. By creating a thermal model, linearizing it, and applying closed-loop MPC, they validated the effectiveness of the system through various load tests to outperform conventional PI controllers. Chabane et al. (2021) outlined the thermal interaction topology between an MH tank and PEMFC for vehicle applications. They developed the system utilizing MATLAB/Simulink and conducted analyses to assess its performance.

Current work uses the finite volume method to develop a 1D mathematical MH tank desorption model in Matlab/Simulink. The model was validated using data obtained from the literature. The FC-MH model was created by combining the MH model with the fuel cell's power output. In the previous study [7], the operating conditions of the FC-MH system were examined under two different scenarios to determine the most suitable system regarding the driving range of the vehicle. Current work extends the model developed in the previous study to integrate the MH tank with the fuel cell. A waste heat profile for the fuel cell was generated based on its power output, and a model was developed to supply heat to the MH tank using an auxiliary heater via a PID controller. Additionally, the profile of the heat transfer coefficient depending on the airflow was correlated and defined in the model.

II. System Description and Mathematical Model

The integrated FC-MH system considered in this study is intentionally designed for lightweight vehicles. The schematic of the system and the specifications of the vehicle, fuel cell, and metal hydride tank are explained in the previous study by the authors [7]. To examine the effect of tank geometry on operational performance, three different cases have been identified where the stored hydrogen amount remains constant (94 g), but the aspect ratio varies, as depicted in Fig. 1. A specific driving cycle has been utilized to calculate the power requirement to be provided by the fuel cell. The cycle range is approximately 8 km, and the amount of hydrogen required to complete one cycle is estimated to be 15 g.

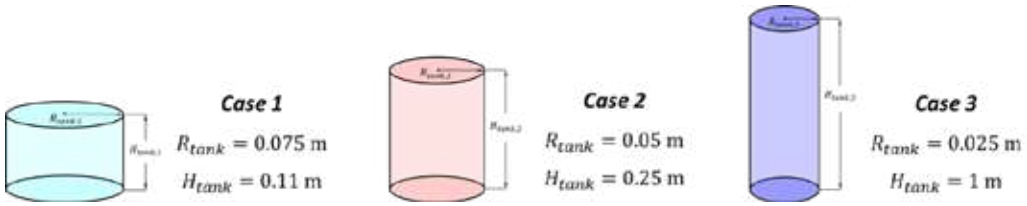


Fig. 1: MH tank dimensions for the selected configurations

The 1D mathematical model has been developed in the Matlab/Simulink environment. In the model, the hydrogen flow rate is determined based on the power requirement of the fuel cell and is defined in the demand block subsystem. In Figure 2, an overview of the Simulink model is represented, and detailed information on the modeling of the MH hydrogen storage system can be found in Ref. [10]. Waste heat from the fuel cell is transferred to the metal hydride tanks to maintain the hydrogen desorption rate at the required range by controlling the temperature of the MH tank. It is assumed that in cases where the waste heat is insufficient to provide the necessary flow rate, an additional heater will be activated with adjustable heating power. A PID controller is employed to adjust the auxiliary heater's power dynamically.

Apart from heat losses related to natural convection, water evaporation, and radiation, 36% of the generated heat within the fuel could be recovered by the cooling system of the fuel cell [5]. The temperature rise of the working fluid through the fuel cell due to the extracted heat was calculated using two different models at different currents, and the results are compared with those of the reference study [4]. The specifications of the fuel cell used to validate the model are given in Table 1. In the first method, temperatures were calculated using thermal voltage (Eq. (1)), while in the second method, temperatures were calculated using efficiency (Eq. (2)).

$$\dot{Q}_{waste,volt} = I \cdot (V_{th} - V_{cell}) \tag{1}$$

$$\dot{Q}_{waste,eff} = \dot{Q}_{max} \cdot \left(1 - \frac{\eta_{FC}}{100}\right) \tag{2}$$

$$\dot{Q}_{waste} = \dot{n}_{H_2O} \cdot \bar{c}_{p,water}(T_{out} - T_{amb}) + \dot{n}_{O_2,out} \cdot \bar{c}_{p,O_2}(T_{out} - T_{amb}) + \dot{n}_{N_2,out} \cdot \bar{c}_{p,N_2}(T_{out} - T_{amb}) \tag{3}$$

where $\dot{Q}_{waste}$ is the waste heat from the fuel cell, V_{th} is the thermal voltage (water is assumed as vapor), V_{cell} is the cell voltage of the fuel cell, $\dot{n}_{H_2O}$, $\dot{n}_{O_2,out}$, $\dot{n}_{N_2,out}$ are the molar flow rates of water, oxygen, and nitrogen, respectively. $\bar{c}_{p,water}$, $\bar{c}_{p,O_2}$, and $\bar{c}_{p,N_2}$ are the specific heats of water, oxygen, and nitrogen, respectively. T_{out} is the outlet temperature of the fuel cell, T_{amb} is the ambient temperature, $\dot{Q}_{max}$ is the maximum heat of the fuel cell, and η_{FC} is the efficiency of the fuel cell.

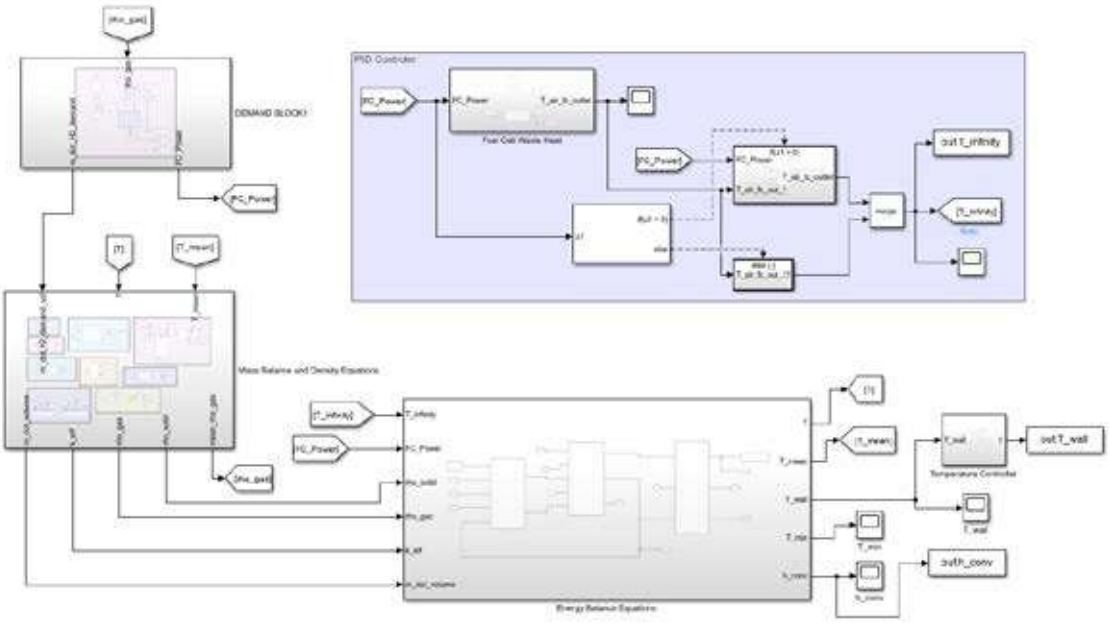


Fig. 2: Matlab/Simulink Model for FC-MH system

Table 1. Specifications of the PEM Fuel Cell [8]

H1000XP Fuel Cell	Type of Fuel Cell	PEM
	Number of Stack	50
	Dimensions	26.4 cm × 20.3 cm × 10.4 cm
	Rated Power	1000 W
	H_2 Pressure at the Inlet	0.45 – 0.55 bar
	Reactants	Hydrogen and Air
	Maximum Stack Temperature	65 °C

III. Results and Discussion

The temperature characteristic of the fuel cell has been validated against the results given in the study by Cano et al. [4]. Two models developed were compared with the simulation and experimental results of the reference study, and the results are presented in Fig. 3. According to the comparison, the results calculated using thermal voltage exhibited a more consistent characteristic compared to those obtained using fuel cell efficiency. Therefore, in the model, the temperature characteristic of the fuel cell was calculated using the thermal voltage method.

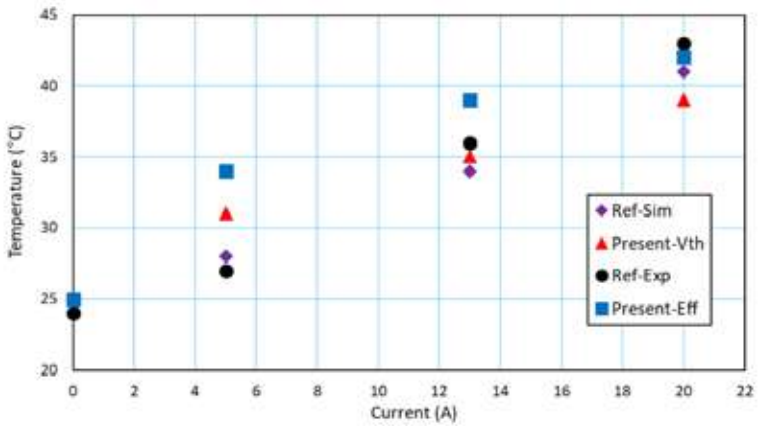
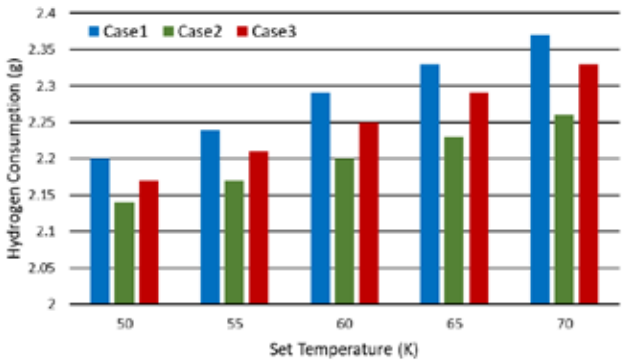


Fig.3: Validation results for fuel cell characterization with [4]

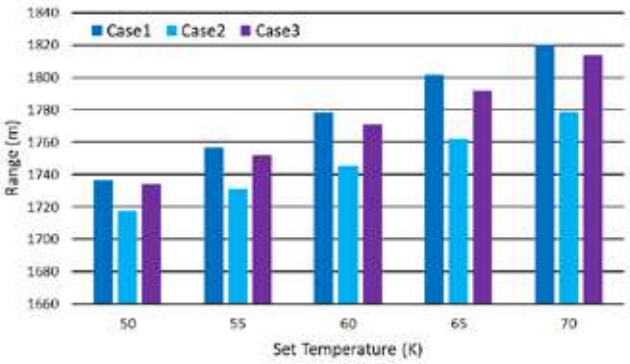
Parametric analyses for the fuel cell integrated MH tank are conducted for five different air set temperatures and the detailed results are provided in Table 2. Major results are also comparatively represented as column graph in Fig. 4. It is concluded that Case-1 demonstrates the best performance under different set temperatures.

Table 2. Hydrogen consumption, duration, and range in different set temperatures

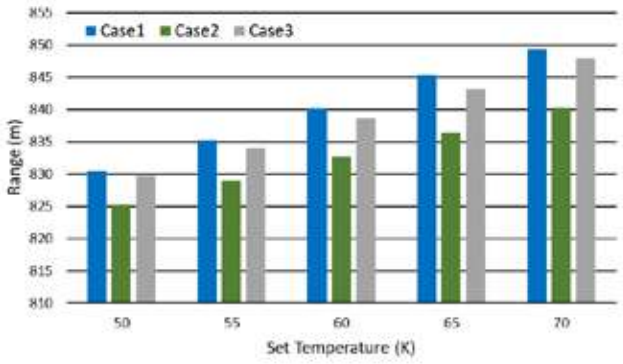
Set Temperature [°C]	**Hydrogen Consumption [g] / Duration [s] / Range [m]**		
	Case 1	**Case 2**	**Case3**
50	2.20 / 830.4 / 1736.71	2.14 / 825.33 / 1717.32	2.17 / 829.76 / 1734.16
55	2.24 / 835.2 / 1756.68	2.17 / 828.96 / 1731.01	2.21 / 834.11 / 1752.04
60	2.29 / 840.16 / 1778.24	2.2 / 832.64 / 1745.86	2.25 / 838.58 / 1771.31
65	2.33 / 845.3 / 1801.44	2.23 / 836.42 / 1761.93	2.29 / 843.19 / 1791.75
70	2.37 / 849.32 / 1820.42	2.26 / 840.31 / 1778.9	2.33 / 847.95 / 1813.9



(a)



(b)



(c)

Fig. 4. Effects of set temperature and tank configuration on (a) hydrogen consumption, (b) duration, and (c) range

IV. Conclusion

The aim of this study is to design a temperature controller for a fuel cell thermally connected system to metal hydride hydrogen storage tanks to keep the temperature of the MH tanks at the optimum level. To ensure the model's validity, the temperature characteristic of the fuel cell is compared with a reference study from the literature and integrated into the model. A PID controller is designed to control the power consumption of the axuliary heater in cases where the waste heat from the fuel cell is insufficient. It is observed that Case-1 yields the best results. While the scenario with the lowest aspect ratio would be expected to perform the worst, its better performance compared to the other scenarios is attributed to the variations in the heat transfer coefficient under different geometries.

Acknowledgements

This work has been supported by Dokuz Eylül University Scientific Research Projects Coordination Unit under grant number FBA-2023-2996.

References

Zhu, D., Ait-Amirat, Y., N'Diaye, A., & Djerdir, A. (2019). Active thermal management between proton exchange membrane fuel cell and metal hydride hydrogen storage tank considering long-term operation. Energy Conversion and Management, 202, 112187.

Omrani, R., Nguyen, H. Q., & Shabani, B. (2019). Open-cathode PEMFC heat utilisation to enhance hydrogen supply rate of metal hydride canisters. Energy Procedia, 160, 542-549.

Rahimi, R., & Mahmoodi, F. (2019). Transient three-dimensional simulation of a metal hydride hydrogen storage tank interconnected to a PEM fuel cell by heat pipes. Iranian Journal of Hydrogen & Fuel Cell, 6(2), 117-132.

Cano, M. H., Kelouwani, S., Agbossou, K., & Dubé, Y. (2014). Free air breathing proton exchange membrane fuel cell: Thermal behavior characterization near freezing temperature. Journal of Power Sources, 246, 650-658.

Cetinkaya, S. A., Disli, T., Soyturk, G., Kizilkan, O., & Colpan, C. O. (2022). A review on thermal coupling of metal hydride storage tanks with fuel cells and electrolyzers. Energies, 16(1), 341.

Chabane, D., Iqbal, M., Harel, F., Djerdir, A., Candusso, D., Elkedim, O., & Fenineche, N. E. (2021). Coupling a metal hydride tank with a PEMFC for vehicular applications: A simulations framework. International Journal of Energy Research, 45(11), 16511-16523.

Cetinkaya S.A., Ezan M.A., Karaoglan M.U., and Çolpan, C. O. (2023). Analysis of Thermally Coupled Fuel Cell and Metal Hydride Hydrogen Storage Tank System for Lightweight Vehicles. Conference: 14th International Exergy, Energy and Environment Symposium (IEEES-2023), Istanbul, Türkiye.

H-1000 XP Fuel Cell Stack, 2024. https://www.horizoneducational.com/h-1000-xp-fuel-cell-stack/p1407 (Date of Access: 20.04.2023)

Busqué, R., Torres, R., Grau, J., Roda, V., & Husar, A. (2017). Effect of metal hydride properties in hydrogen absorption through 2D-axisymmetric modeling and experimental testing in storage canisters. International journal of hydrogen energy, 42(30), 19114-19125.

Disli, T., Çetinkaya, S. A., Ezan, M. A., & Colpan, C. O. (2023). Numerical investigations on the absorption of a metal hydride hydrogen storage tank based on various thermal management strategies. International Journal of Hydrogen Energy.

Zhang, B., Lin, F., Zhang, C., Liao, R., & Wang, Y. X. (2020). Design and implementation of model predictive control for an open-cathode fuel cell thermal management system. Renewable Energy, 154, 1014-1024.

Characterisation of a graphite electrode coated with a nickel-modified nickel-iron alloy and catalytic effect in an alkaline medium

[1*]Ali Topak, [2,3]Serap Toprak Döşlü
[1] Mardin Artuklu University, Institute for Graduate Education, Department of Chemistry, Mardin, 47200, Türkiye
[2] Mardin Artuklu University, Faculty of Health Sciences, Department of Nutrition and Dietetics, Mardin, 47200, Türkiye
[3] Mardin Artuklu University, Central Research Laboratory, Mardin, 47200, Türkiye

*E-mail:a.topak@hotmail.com, seraptoprak@artuklu.edu.tr

Abstract

In this study, a binary NiFe coating ($Ni^{2+}Fe^{2+}$ in the coating bath) with different composition was deposited on a graphite surface (G) by an electrochemical method to increase the catalytic activity and hydrogen gas production in an alkaline medium. The catalytic efficiency of the new composite coating (G/$N_{i\%}$95$Fe_{\%5}$–Ni) obtained by the modification of nickel (Ni^{2+}) at different durations (30, 60 and 75 s) on a G/$Ni_{\%95}Fe_{5\%}$ electrode selected for its quality in 1 M KOH solution was investigated by impedance spectroscopy (EIS), linear scanning voltammetry (LSV) and cyclic voltammetry (CV). Hydrogen gas measurements were performed by electrolysis of the electrodes in 1 M KOH solution and these measurements were compared. The prepared electrodes were also characterised by scanning electron microscopy (SEM), X-ray diffraction (XRD) and energy dispersive X-ray spectroscopy (EDX). The main objective was to determine a suitable composition for the deposition of NiFe on a graphite electrode and to determine the optimal time for Ni deposition in order to improve the electrical quality of the coating.

Keywords: NiFe coatings, Ni modified, electrocatalyst, HER, alkaline electrolysis.

I. Introduction

Hydrogen, which can be synthesised and used electrochemically without carbon emissions, is a promising clean energy source of the future due to its high efficiency (Tariq et al., 2023). The electrocatalytic performance in the hydrogen evolution reaction (HER) is mainly related to the material of the electrocatalyst (Döşlü et al., 2021). The desired properties of the carrier material are that it is inexpensive, available in large quantities, corrosion-resistant and has high electrical conductivity. Thanks to these properties, graphite has been used as a carrier material for years (Telli et al., 2013, Nazlıgül et al., 2022). According to the volcanic curve, metals such as Ni and Fe with effective electrocatalyst behaviour and strong hydrogen bonds can be selected as catalysts (Montemore et al., 2023, Çil and Tarhan., 2021). Chemical environment, structure and morphological adaptations are the key point for the catalytic efficiency of Ni alloy electrodes (Gong et al.2016, Döşlü ve Döner.2024). The crystal structure, chemical composition, porosity, size distribution, electrical conductivity and surface chemistry of the alloy determine the performance of the electrocatalyst (Vij et al., 2017).

Our aim in this study is to alloy metals such as nickel and iron, which have high catalytic capabilities and are relatively inexpensive and readily available, on the surface of graphite and alloy them in different compositions; to produce a new, highly catalytically effective, low-overvoltage, structurally long-term stable electrode material (G/NiFe-Ni) and to use this electrode as a cathode in the production of hydrogen by electrolysis. In this way, the cost-effectively produced G/NiFe-Ni alloy can be used on an industrial scale instead of expensive metals and/or coatings. The analyses showed that the Ni-modified NiFe-coated graphite electrode has a higher catalytic activity for HER.

II Experimental setup and procedure

NiFe alloys with different chemical compositions are deposited by electrodeposition on a graphite surface (0.283 cm^2). The NiFe bath consists of the chemicals $NiSO_4.6H_2O$ and $FeSO_4.7H_2O$. The percentage of NiFe in the bath solution ranged from 99% to 1% in six different ratios, the current density was 14.15 mA, the temperature was 25°C and the deposition times were calculated according to Faraday's law for each composition. Before deposition, the graphite electrode is polished with emery paper. Working; graphite, reference; Ag/AgCl- (3 M KCl) and counter; Pt- (2 cm^2) electrodes. G/$Ni_{\%99}Fe_{\%1}$, G/$Ni_{\%98}Fe_{\%2}$, G/$Ni_{\%97}Fe_{\%3}$, G/$Ni_{\%96}Fe_{\%4}$, G/$Ni_{\%95}Fe_{\%5}$ and G/$Ni_{\%97}Fe_{\%3}$ electrodes are analysed by EIS, LSV and CV techniques in 1 M KOH solution at room temperature using the three-electrode method. The G/$Ni_{\%95}Fe_{\%5}$ electrode showed better catalytic performance than the others. To develop this electrode, Ni on the electrode surface is modified by applying a bath solution containing 15 g $NiSO_4.6H_2O$ and 0.625 g H_3BO_3 in a total volume of 50 mL to the electrode surface for 30, 60 and 75 seconds at a current density of 14.15 mA and temperature conditions of 25°C. Working electrode; G/$Ni^{\%95}Fe^{\%5}$, reference electrode; Ag/AgCl and counter electrode; Pt (2 cm^2). The prepared electrodes are analysed using EIS, LSV and CV techniques under the same conditions. EIS, LSV and CV techniques; Pt plate, Ag/AgCl and prepared electrocatalysts are used in three electrode arrangements as counter, reference and working electrodes, respectively. EIS; was performed at an amplitude of 5 mV and a frequency range of 10^5 to 10^{-1} Hz. LSV; were performed between-1.80 V and-1.00 V with a sampling rate of 1.0 mVs^{-1} and CV curves were obtained with a sampling rate of 50 mVs^{-1} (using Gamry Instruments Reference 3000). G, G/$Ni^{\%95}Fe^{\%5}$ and G/$Ni^{\%95}Fe^{\%5}$-Ni(60s) electrodes placed at the bottom of an inverted burette in 1 M KOH are electrolysed at a constant potential of 3 V for

1 h and the amounts of hydrogen gas released are measured. The electrocatalysts are the cathode and the platinum plate is the anode. These electrodes were analysed by SEM for the surface morphology, EDX (JEOL JSM 6510) for the chemical composition and XRD (RIGAKU ULTIMA IV) for the phase.

III. Results and discussions

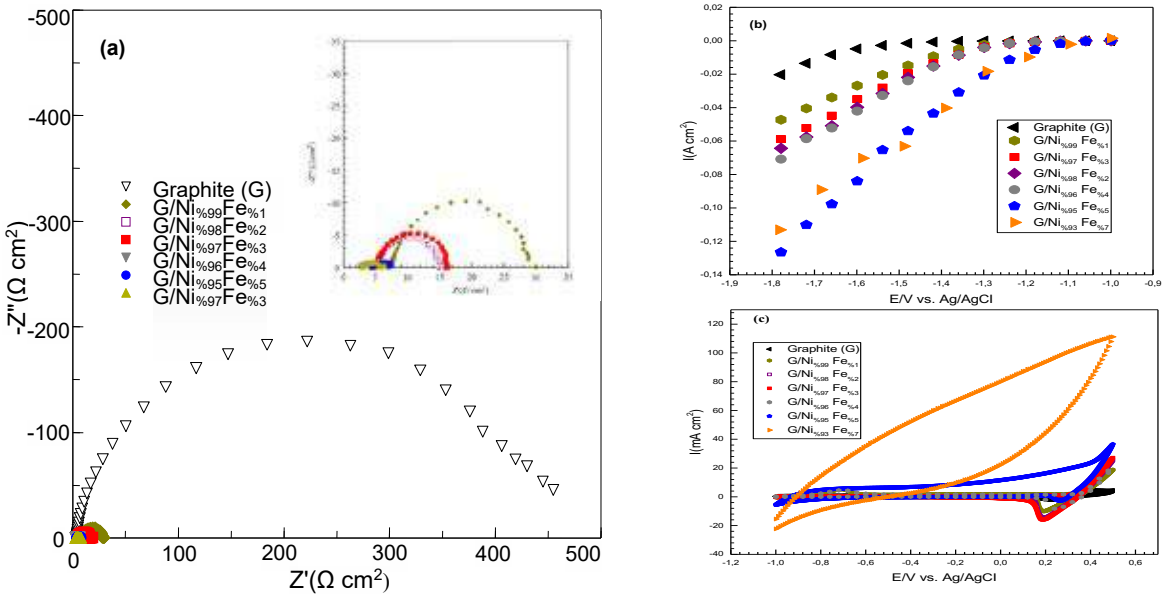


Fig.1: Nyquist curves (a), the current-potential curves (b) and the cyclic voltammograms (c) for graphite (G), (G), G/Ni%99Fe%1, G/Ni%98Fe%2, G/Ni%97Fe%3, G/Ni%96Fe%4, G/Ni%95Fe%5 and G/Ni%93Fe%7 in 1 M KOH solution at 298 K.

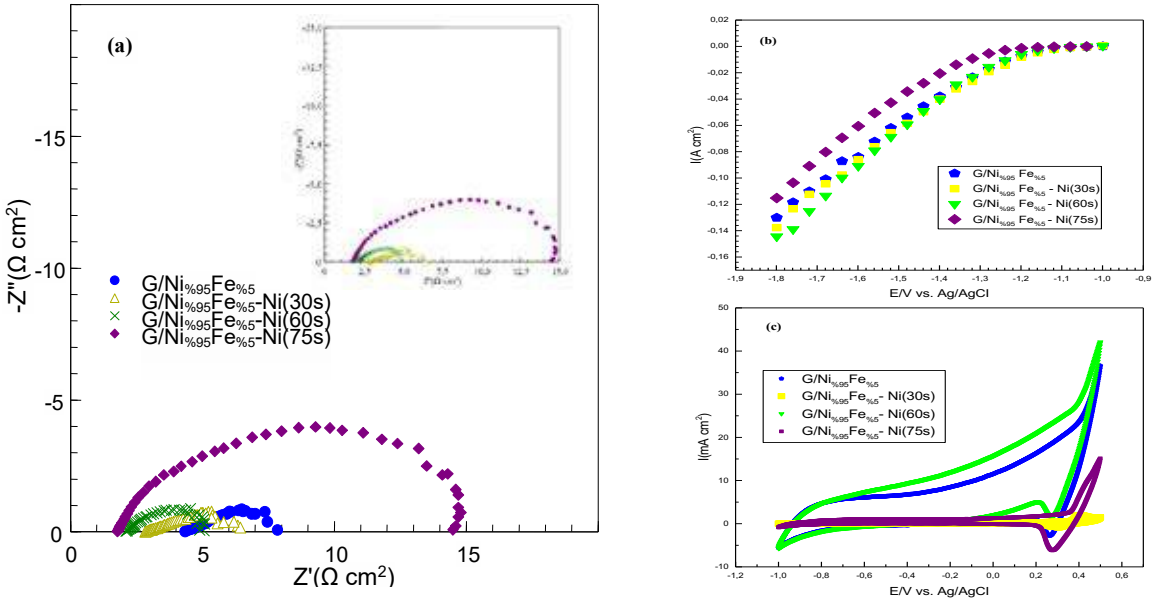


Fig.2: Nyquist curves (a), the current potential curves (b) and the cyclic voltammograms (c) for G/Ni%95Fe%5, G/Ni%95Fe%5-Ni(30s), G/Ni%95Fe%5-Ni(60s) and G/Ni%95Fe%5-Ni(75s) in 1 M KOH solution at 298 K.

In general, it can be seen from the Nyquist curve (Fig. 1a) that the deposition of the NiFe alloy reduces the resistance and increases the electrical conductivity compared to the bare electrode (graphite), and from the current potential curve (Fig. 1b) that the current density increases. Resistance and current density vary with different compositions of the NiFe alloy. The performance of Ni%95Fe5% composition with low resistance, low overvoltage and high current density is better (Table1). As can be seen in Fig.2, the best time for the modified Ni is set to 60 seconds. When the deposition time was longer than 60 seconds, the thickness formed on the electrode surface affected the ion diffusion at the interface between the electrodeand solution, and the resistance increased with the closure of the active centres (Farsak et al., 2022). The electrocatalyst G/Ni%95Fe%5-Ni(60s) has the lowest initial potential, higher current density and low resistance for the HER (Table 1).

The volumes of hydrogen gas released at the graphite(G), G/Ni%95Fe%5 and G/Ni%95Fe%5-Ni(60s) electrodes are 23.20, 33.90 and 72.70 mL, respectively (Fig. 3). Most of the hydrogen is obtained from Ni-modified G/Ni%95Fe%5-Ni(60s) electrocatalysts.

Tab.1: Polarization resistances of electrodes.

Electrode	RΩ
Graphite(G)	*452.0*
G/Ni%99Fe%1	*23.1*
G/Ni%98Fe%2	*11.2*
G/Ni%97Fe%3	*12.6*
G/Ni%96Fe%4	*4.1*
G/Ni%95Fe%5	*3.7*
G/Ni%93Fe%7	*3.9*
G/Ni%95Fe%5-Ni(30s)	*3.4*
G/Ni%95Fe%5-Ni(60s)	*2.9*
G/Ni%95Fe%5-Ni(75s)	*12.6*

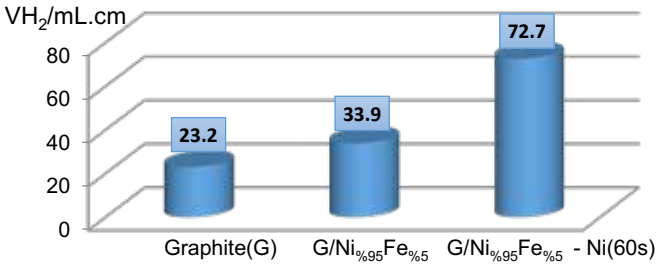


Fig.3: Released hydrogen gas in 1 hour at a potential of 3 V for graphite(G), G/Ni%95Fe%5 and G/Ni%95Fe%5-Ni(60s) in a 1 M KOH solution at 298 K.

Fig.4(a, b) shows the graphite surface and traces of emery on the surface. In Fig.4(c, d) the graphite surface is no longer visible except for a few irregular nano-cavities. It can be seen that the NiFe alloy is homogeneously distributed on the surface in a densely stacked spherical structure and has a porous structure. The average size of the spheres is about 1.10 µm. Fig.4(e, f) shows that the morphology of the Ni-modified G/Ni%95Fe%5 electrode is smooth except for small irregular grains and micro-lines on the surface. A similar morphology has also been reported in the literature (Omanovic et al., 2005).

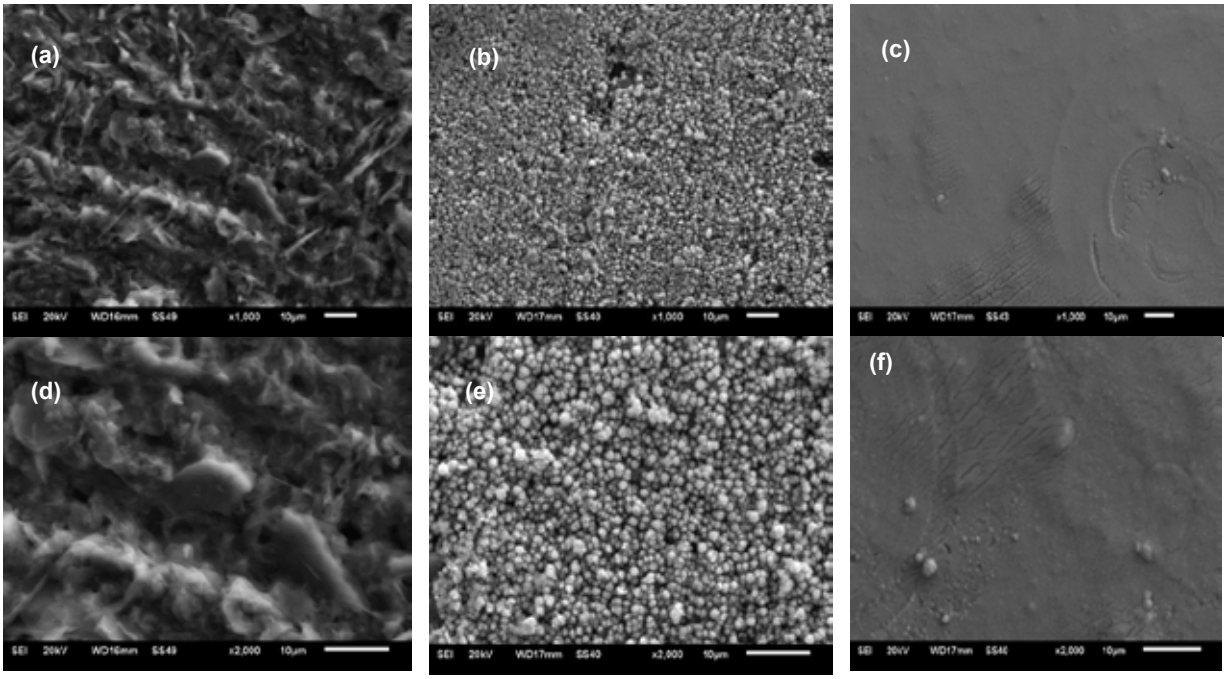


Fig.4: SEM images of the electrodes graphite (G)(a,b), G/Ni%95Fe%5(c,d) and G/Ni%95Fe%5-Ni(60s)(e,f) (20 kV, 10 µm and 2000x-1000x).

The graphite electrode (G) is trigonal and the main phase of G/Ni%95Fe%5, G/Ni%95Fe%5-Ni(60s) electrodes has an amorphous structure with a surface-centred cubic Ni structure (Fig. 5). Due to their closely spaced atomic radii, Ni and Fe form an alloyed and indistinguishable solid solution in which no Fe peak is observed (Ghaffarinejad et.al., 2023).

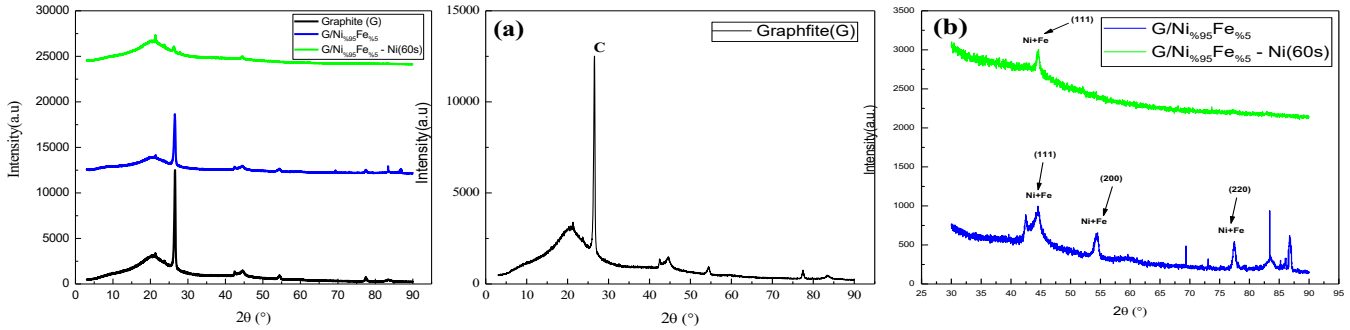


Fig.5: XRD pattern of graphite(G) (a) and G/Ni%95Fe%5 (b), G/Ni%95Fe%5–Ni(60s) electrodes (b)(3° to 90°diffraction).

IV. Conclusions

To summarise, the coating activities depend on changes in chemical composition. The most synergistic combination was the G/Ni%95Fe%5 electrode with 60 seconds Ni modification. CV showed the distribution of the modified Ni atoms G/Ni%95Fe%5 on the electrode surface. EIS and LSV analyses showed that the performance of the G/Ni%95Fe%5-Ni(60s) electrocatalyst was better. The greater production of hydrogen gas by this electrocatalyst with less energy was consistent with the analysis. SEM, EDX and XRD showed the positive effect of increasing the surface area and crystalline structure for HER. Therefore, the G/Ni%95Fe%5-Ni(60s) electrocatalyst may be preferable as a cathode.

Acknowledgements

The authors are very grateful to the Mardin Artuklu University Research Fund Office for financial support (project number: MAÜ.BAP.23.SBF.012). We are very grateful to Assoc.Prof Murat FARSAK for his advice.

References

Çil, M. A., Tarhan, C. (2021). A study on hydrogen, the clean energy of the future: Hydrogen storage methods. Journal of Energy Storage, 40, 102676.

Döşlü Toprak, S., Döner, A., Yıldız, R. (2021). Electrocatalysis property of CuZn electrode with Pt and Ru decoration. International Journal of Hydrogen Energy, 46, 22409-22421.

Döşlü Toprak, S., Döner, A. (2024). Electrochemical behavior of Pt nano-particles dispersed on Cu/Ni electrode in alkaline environment. International Journal of Hydrogen Energy, In Press, Corrected Proof.

Farsak, M., Telli, E., Hançer, H. (2022). The catalytic effect of trimetallic alloy modified C-felt electrodes on hydrogen evolution reaction. International Journal of Hydrogen Energy, 47, 25145-25154.

Ghaffarinejad, A., Abdollahi, A., Arabi, M. (2023). Electrodeposition of Ni - Fe on graphite rod as an efficient and binder-free electrocatalyst for oxygen and hydrogen evolution reactions. Journal of Alloys and Compounds, 937, 168400.

Gong, M., Wang, D. Y., Chen, C. C., Hwang, B. J., Dai, H. (2016). A mini review on nickel-based electrocatalysts for alkaline hydrogen evolution reaction. Nano Research, 9, 28-46.

Montemore, M. M., Stratton, M., Zhang, S. (2023). Addressing complexity in catalyst design: From volcanos and scaling to more sophisticated design strategies. Surface Science Reports, 78, 100597.

Nazlıgül, H., Ergen, E., Doğru Mert, B. (2022). Electrochemical Production of Transition Metal-Based Electrocatalysts for Hydrogen Production. Osmaniye Korkut Ata University Journal of the Institute of Science and Technology, 5, 206-215.

Omanovic, S., Navarro-Flores, E., Chong, Z. (2005). Characterization of Ni, NiMo, NiW and NiFe electroactive coatings as electrocatalysts for hydrogen evolution in an acidic medium. Journal of Molecular Catalysis A: Chemical, 226, 179-197.

Tariq, S., Ahmad, A., Luque, R., M. Asiri, A. (2023). Nanomaterial-based MOF-derived single-atom catalysts for electrolytic conversion of energy. Micro and Nano Technologies, 289-309.

Telli, E., Döner, A., Kardaş, G. (2013). Electrocatalytic oxidation of methanol on Ru deposited NiZn catalyst at graphite in alkaline medium. Electrochimica Acta, 107, 216-224.

Vij, V., Sultan, S., M. Harzandi, A., Meena, A., N. Tiwari, J., Lee, W. G., Yoon, T., S. Kim, K. (2017). Nickel-Based Electrocatalysts for Energy-Related Applications: Oxygen Reduction, Oxygen Evolution, and Hydrogen Evolution Reactions. ACS Catalysis, 7, 7196-7225.

Hydrogen Fuel Quality, Testing, Reference Materials Production, Proficiency Testing Scheme

[1*] Erinc Engin, Thomas Bacquart, Abigail Morris, Pierpaolo Modugno
[1] National Physical Laboratory, Hampton Rd, Teddington TW11 0LW, UK

* E-mail: erinc.engin@npl.co.uk

Abstract
The enforcement of regulation on hydrogen fuel quality is a need supported by car manufacturer, policy makers and end users. Several laboratories in Europe and worldwide are becoming able to measure hydrogen fuel quality according to ISO 14687. However, it is currently difficult to evaluate the quality of these laboratories. Lack of analytical methods, gas calibrants, reference material and inter-laboratory comparison is a barrier for European commercial laboratory to prove their competences and obtain ISO 17025 accreditation. NPL has ISO 17025 accreditation and developed reference materials for hydrogen fuel quality. NPL will present new results on stability of contaminant in sampling container including type IV vessel and advice for hydrogen fuel sampling. The presentation will provide advanced results and good practices to ensure reliability and accuracy of hydrogen quality analytical laboratory.

Keywords: Hydrogen quality, fuel cell hydrogen vehicles, ISO14687, gas analysis, proficiency testing.

I. Introduction

The foreseen use of fuel cell electric vehicles (FCEV) is quickly moving from light duty such as cars to heavy duty applications such as buses or trucks (ISO 14687 (2019)). Hydrogen could represent 32% of the European fuel mix in 2050 and supply 17% of the heavy-duty vehicles by 2030 (Samsun, Rex, Antoni and Stolten (2022)). Following these drivers, the hydrogen infrastructure is expected to significantly increase over the next few years with a target of 4500 hydrogen refueling stations (HRS) in Europe by 2030 (https://commission.europa.eu/strategy-and-policy/priorities-2019-2024/european-green-deal/delivering-european-green-deal_en (2024)) and a target of 13 million FCEVs (HCHO (2021)).
FCEVs require hydrogen fuel with a composition specification to avoid any improper performance of the FCEV. The enforcement of regulation on hydrogen fuel quality (European Directive 2014/94/EU IEA (2023)) become a societal need supported by car manufacturer, policy makers and end users. Hydrogen fuel quality need to comply with international standards (EN 17124 (2022)) to ensure fuel quality at the nozzle of the HRS. Therefore, EU laboratories are developing capability to measure the contaminants specified in EN 17124. New challenges arise to ensure results accuracy and laboratories agreement. Overcoming these challenges require that the metrological tools be available and recognized: reference materials, calibrants, proficiency testing schemes, accreditation.
The National Physical Laboratory (NPL) has successfully developed analytical methods and obtained ISO 17025 (2017) accreditation for testing to measure accurately hydrogen contaminants according to EN17124. This involved development of new reference materials for hydrogen fuel contaminants where NPL is accredited according to ISO 17034 (2016) for majority of the impurities existed in hydrogen (ISO 14687:2019). NPL will present new insights on proficiency testing scheme guidance for hydrogen fuel quality (HyQuality and MetroHyVe 2). An overview on different new sampling systems will be provided with emphasis around their validation (EU project MethyTruck). Finally, the behavior of hydrogen fuel contaminants in type IV tank will be presented with emphasis on the methodology and the perspective of the results.

II. Experimental Set-up and Procedure

New hydrogen fuel reference materials and proficiency scheme

NPL developed new sets of binary and multi contaminants in hydrogen gas mixture gravimetrically (ISO 6142-1 (2015)) in different cylinders (aluminum, aluminum with passivation). Mixtures containing 7 to 12 contaminants were studied over 1 year. Based on this knowledge, MetroHyVe 2 and HyQuality proficiency testing were realized. Results will be presented with a review of the different good and bad practices involving the reference materials used (cylinder type, composition), the length of the proficiency testing (i.e., 3 months to 2 years), the scheme (shared cylinder versus batch). Following the state-of-the-art review, NPL will present a new proficiency scheme for 2024.

III. Analysis

New sampling system

NPL has developed several sampling systems to achieve sampling of hydrogen gas from various production facility, fuel cell electrical vehicles or heavy-duty application. The systems developed have been applied in real situation and hydrogen gas quality according to ISO 14687 (2019) was achieved. Based on the challenges to develop and validate sampling system, NPL is developing test to evaluate the ability of sampling system to sample accurately reactive compounds such as sulphur compounds. The presentation will highlight the recovery rate for sulphur compounds at nmol/mol for some of the sampling system recently developed. The 1st sampling intercomparison was realized in 2023 and a new project MethyTruck is progressing sampling standardization especially for heavy duty HRS. The results will highlight the requirements for validation and standardization to

ensure the representativity of the results.

IV. Results and discussions

New container

Recent NPL studies investigated the behavior of contaminant in type IV tank vessel. These types of tanks are often used in transport application however little is known about the interaction of contaminants within the containers. NPL developed a system to accurately contaminate a type IV vessel with non-reactive (nitrogen), low reactivity (CO) and reactive (hydrogen sulphide) compounds. The studies investigated the behavior of these compounds in the type IV tank cylinder over time and at varying pressure and at level close to ISO 14687 threshold. The results are the first evaluation of the impact of the type IV vessel onto the hydrogen fuel composition.

V. Conclusions

The National Physical Laboratory has been developing hydrogen fuel quality measurement and standards for the past 8 years. New reference materials for a large part of the hydrogen fuel contaminants are now available with stabilities monitored. Novel analytical methods have been applied to measure hydrogen chloride, sulphur and hydrocarbons extending the ability to monitor outside of ISO 14687 scope.

Sustainable proficiency testing scheme to assess analytical laboratory performance has been developed and were optimized based on new hydrogen fuel reference materials. The stability of hydrogen contaminants was realized in novel type of cylinders and type IV vessel highlighting the difference in behaviour depending on the internal surface of the vessel.

Finally, the validation of hydrogen fuel sampling will be highlighted and perspectives to support these new requirements will enhance new research needs on material passivation, intercomparison and contaminants behaviour study.

The results presented by NPL will highlight new critical issues to ensure adherence to regulation and international standard (ISO 14687) which seems highly challenging today.

References

ISO 14687:2019 Hydrogen fuel quality Product specification.
Samsun R.C., Rex M., Antoni L., Stolten D. Deployment of Fuel Cell Vehicles and Hydrogen Refueling Station Infrastructure: A Global Overview and Perspectives. Energies, 2022, 15, 4975. https:// doi.org/10.3390/en15144975.
https://commission.europa.eu/strategy-and-policy/priorities-2019-2024/european-green-deal/delivering-european-green-deal_en Accessed on March 12, 2024.
HCHO, Fuel Cells and Hydrogen Observatory, 2021 Technology & Market Report, Chapter 1, July 2021.
IEA (2023), Global EV Outlook 2023, IEA, Paris, 2023. https://www.iea.org/reports/global-ev-outlook-2023, License: CC BY 4.0.
EN 17124, Hydrogen fuel. Product specification and quality assurance. Proton exchange membrane (PEM) fuel cell applications for road vehicles.
ISO/IEC 17025:2017 General requirements for the competence of testing and calibration laboratories.
ISO 17034:2016 General requirements for the competence of reference material producers.
ISO 6142-1, Gas analysis - Preparation of calibration gas mixtures - Gravimetric method for Class I mixtures. 2015.
ISO 14687 Hydrogen fuel quality—product specification. International Organization for Standardization, Geneva, Switzerland, 2019.

Effects of Volume Fraction and Particle Size on Triple-Phase Boundaries in Solid Oxide Fuel Cell Anodes

[1,2*] Emre Ucar, [1,2] Bora Timurkutluk
[1] Niğde Ömer Halisdemir University Prof. Dr. T. Nejat Veziroglu Clean Energy Research Center, 51240, Niğde, Türkiye
[2] Niğde Ömer Halisdemir University, Mechanical Engineering Department, 51240, Niğde, Türkiye

* E-mail: emreucar@ohu.edu.tr

Abstract
The particle size distributions of commercial NiO and YSZ powders are measured to determine microstructural properties required for the virtual reconstruction of possible solid oxide fuel cell (SOFC) anode microstructures with different volume fractions. Triple phase boundary (TPB) length measurements are then carried out numerically to evaluate the effects of microstructural properties on the performance of anodes having 30 % porosity. Among the cases considered, the results reveal that the volume fraction and particle size of the catalyst phase are very effective parameters on TPB density. The highest active TPB density value is calculated as 10.16 $\mu m \cdot \mu m^{-3}$ at the volume fraction of 35 % catalyst, 35 % electrolyte, and 30 % pore phase when the average particle size of the catalyst phase is the smallest (~0.18 μm).

Keywords: Solid Oxide Fuel Cell Anode, Synthetic Microstructure Generation, Triple-Phase Boundary

I. Introduction

Membrane electrode assembly of SOFCs are manufactured by coating electrode layers on opposite sides of a dense electrolyte layer. The most commonly used SOFC anode material is Ni-YSZ composite. This composite has a great thermal and mechanical compatibility with the YSZ-based electrolyte layers, as well as significant electrochemical activity and chemical stability under high operating temperatures and reducing conditions. Electrochemical reactions in the anode electrode occur at anode triple-phase boundaries (TPBs), where anode catalyst, electrolyte and pore phases come into contact, allowing hydrogen and oxygen ions to react electrochemically to generate electrons. Therefore, increasing the quantity and density of TPBs plays an important role in improving the anode thereby the cell electrochemical performance.

The literature utilizes two experimental techniques for investigating the electrode microstructures of SOFCs: focused ion beam scanning electron microscopy (FIB-SEM) (Xiang et al., 2022, Hoffrogge et al., 2023) and X-ray nanotomography (Heenan et al., 2017). Microstructural data collected from real SOFC anode electrodes are used to reconstruct realistic 3D anode microstructures to link the microstructural properties to anode performance. In contrast to these experimental-based techniques, numerical reconstruction can be considered time- and cost-effective approach since manufacturing, imaging and image processing steps can be avoided. Most numerical studies are based on randomly distributing spherical particles of each phase into a representative cubic volume (Janardhanan et al., 2008, Zheng and Ni, 2017). Nonetheless, experimental and numerical reconstruction studies have revealed that the parameters forming the microstructure must be well designed and developed in order to provide a large number of active TPBs. In this respect, electrode microstructures have been reconstructed, and TPB measurements have been performed in general.

In this study, the structural parameters required for reconstructing the microstructure commercially available NiO and YSZ powders are determined to reconstruct various SOFC anode microstructures synthetically by varying volume fractions and particle sizes. The resultant TPB densities are computed to evaluate the anode microstructural properties on its performance.

II. Materials and method

Synthetic anode microstructures were generated via Dream.3D software based on powder particle size distributions. Dream.3D is open-source software that simulates the desired microstructure by randomly dispersing multiple phases with varying volume fractions and/or particle sizes into a representative control volume. The software also allows to control the particle size distribution with μ and σ values, representing the mean value of a lognormal particle size distribution and the standard deviation, respectively. The software generates the particle size distribution using the lognormal distribution. In addition, it also includes minimum and maximum σ cutoff values, by which the minimum and maximum particle size ranges for each phase can be set. On the other hand, the proper control volume dimension and resolution must be precisely determined. While resolution represents the edge length of each voxel dividing the representative cubic control volume, dimension determines how many voxels should be used. The multiplication of dimension and resolution values represents the length of one edge of the cubic control volume. For constructing a representative cubic control volume, it's necessary to know the volume fraction of each phase, the μ and σ values that give the particle size distribution of each phase, the minimum and maximum σ cut-off values, and dimension and resolution values. As a result, the same values were set in all three directions (x, y, and z axes), resulting in a representative cubic control volume, or microstructure. The method we used in the generation of synthetic microstructure was confirmed in the previous study by Timurkutluk et al. (2021). Synthetic anode microstructures generated are also given in Figure 1 as an example.

TPB lengths of the generated synthetic microstructures are calculated with COMSOL Multiphysics. The total TPB length is calculated by adding up all voxel edges where the three phases intersect. Active TPB lengths were also calculated, taking into account that each phase should be in a related percolation network. Measurements were performed and averaged from six different directions (± x, ± y, and ± z) to minimize the multidimensional effect of each 3D synthetic microstructure generated. Table 1 illustrates the catalyst and electrolyte materials employed to generate the anode synthetic microstructure, along with the parameter values set in Dream.3D.



(a) (b)

Fig. 1: Synthetic anode microstructures with different volume fractions consisting of Ni (green), YSZ (yellow) and Pore (black) phases: volume fraction for catalyst-electrolyte-pore with 15-55-30 (a) and 35-35-30 (b) synthetic microstructures

Tab. 1: Catalyst and electrolyte materials used and parameter values set in Dream.3D

Materials	Powder No	Powder Name and Trademark	μ	σ	Minimum σ Cutoff Value	Maximum σ Cutoff Value
Catalyst	1	NiO-F (Novamet)	-0.37681	0.46229	5	3
	2	NiO (J. T. Baker)	0.11549	0.41007	5	3
	3	NiO-F (Fuel Cell Materials)	-2.05726	0.81041	5	3
Electrolyte	4	YSZ8-TC (Fuel Cell Materials)	-0.89822	0.29298	5	3

III. Analysis

Three phases were defined in the Dream.3D software: catalyst (Ni), electrolyte (YSZ), and pore. Various solid volume fractions were defined in the software with μ and σ values according to the particle size distributions experimentally obtained. After that, dimension and resolution values were decided to generate a representative cubic control volume. The length of one edge of the representative cubic control volume is the multiplication of these two parameters. Dimension, which is the number of elements dividing the total volume in each direction, was determined by selecting the biggest average particle size among all phases. Similarly, resolution value was decided according to the smallest average particle size. The details can be found elsewhere (Timurkutluk et al., 2021). After these parameters were defined in the Dream.3D software, cubic synthetic microstructures were generated. Anode electrode microstructures with three main designs were generated using three different commercial Ni catalysts and one YSZ electrolyte material. To investigate the influence of the solid volume fraction, nine different cases were established, while the volume fraction of the pore phase was fixed at 30% and the average pore size was set to 0.5 μm in all cases. Therefore, 27 different anode microstructures were reconstructed and investigated in this study. Moreover, 15 different microstructures were generated for each case to eliminate randomness of the software, and all necessary measurements were carried out (i.e., 405 microstructures in total). Table 2 summarizes all of the anode electrode designs considered.

Tab. 2: All of the anode electrode design cases

Design	Case No	Powder Mixture	Dimension	Resolution (μm)	L (μm)	Average Particle Size (μm)			Volume Fraction (%)		
						Catalyst	Electrolyte	Pore	Catalyst	Electrolyte	Pore
A	1-9	1 and 4	90	0.085	7.65	0.763415	0.425155	0.5	15-55	55-15	30
B	10-18	2 and 4	144	0.085	12.24	1.22088	0.425155	0.5	15-55	55-15	30
C	19-27	3 and 4	141	0.0355	5.0055	0.177483	0.425155	0.5	15-55	55-15	30

COMSOL Multiphysics was used to calculate the TPB lengths. Measurements were carried out to clarify total, active, and inactive TPB length in all cases. Additionally, six different directions of the representative cubic control volume were also considered to reduce the multidimensional effect. On the other hand, since 15 different microstructures were generated for each case, the results obtained for each case are essentially based on the average of 90 data. Finally, for each case, TPB densities were determined by dividing the TPB length values by the volume of the corresponding cubic control element.

IV. Results and discussions

The effect of the volume fraction of the electrolyte and catalyst phases on the active TPB density is depicted in Figure 2. It is observed in all cases that the active TPB density tends to increase with the volume fraction of the catalyst phase up to some point and then shows a decreasing trend. However, the point of maximum TPB density

is found to be dependent on the average particle size of the catalyst phase, indicating that both the particle size and volume fraction are of great significance. In this regard, A7, B16 and C23 exhibits the highest active TPB density in the cases with design A, B and C, respectively. The highest active TPB density value among all designs, on the other hand, is obtained from C23, where the volume fractions of the catalyst and electrolyte phase are equal to 35%. The increase in active TPB density can be explained by the decrease in inactive TPBs due to the isolated catalyst and the improvement of the percolation network of the catalyst phase. It is clearly seen that the use of a low amount of catalyst leads to lower TPB density values. On the other hand, despite increasing catalyst phase volume fraction above a certain limit negatively affects both the active and the total TPB density due to increase in inactive TPB formation originated from the isolated electrolyte. Therefore, above a certain catalyst phase volume fraction value, it becomes difficult for the electrolyte phase to maintain continuity in a percolation network. Especially, increasing the catalyst phase volume fraction above 50 % significantly decreases the active TPB density. As a result, it appears that the catalyst phase volume fraction is an important parameter for TPB density, however it should be decided by considering its particle size as well.

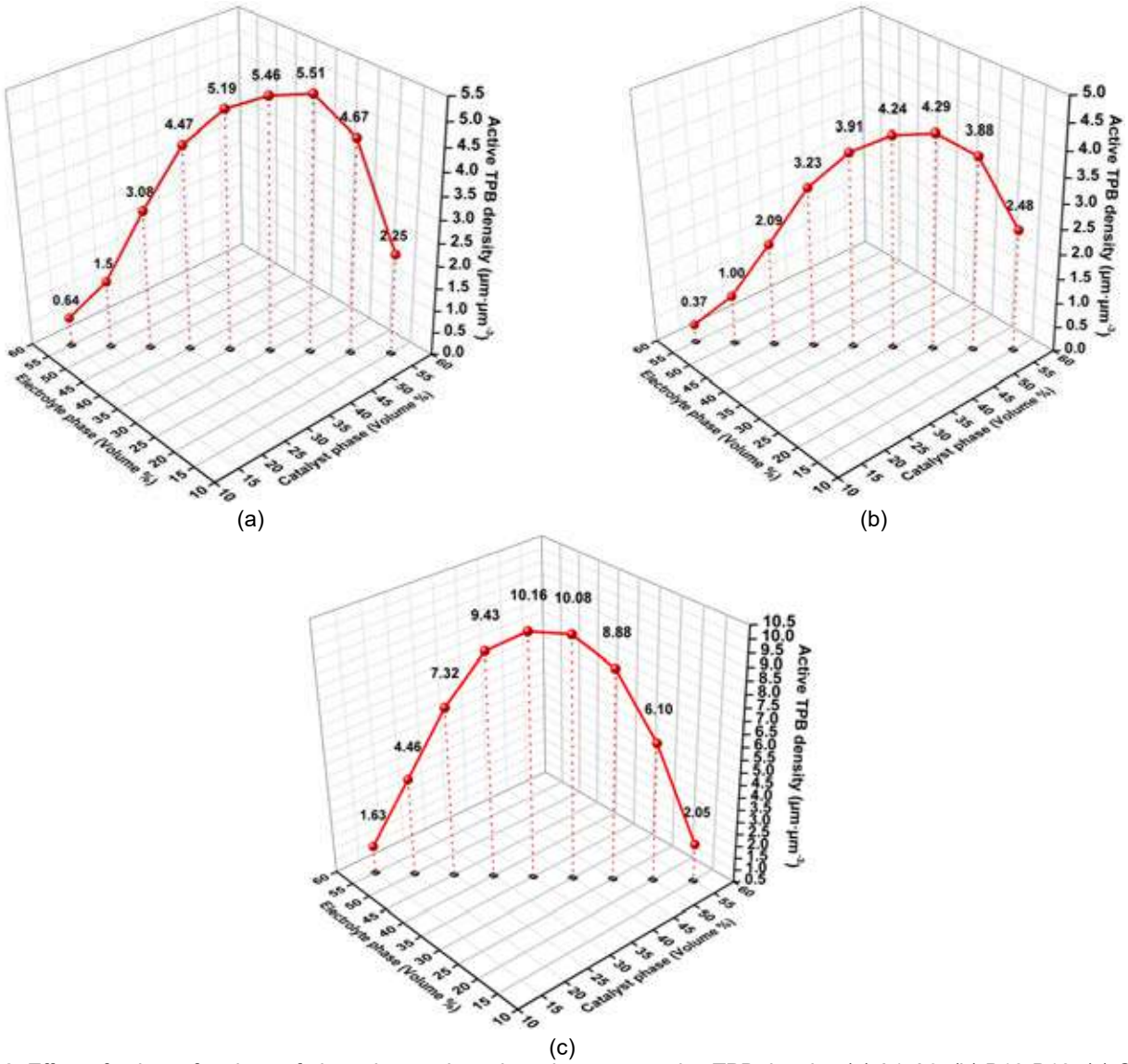


Fig. 2: Effect of volume fractions of electrolyte and catalyst phases on active TPB density: (a) A1-A9, (b) B10-B18, (c) C19-C27

This is more obvious in Table 3. Since the surface area is adversely related to the particle size, TPBs can be expected to increase with the particle size. That is why the anodes having C design (i.e., with the finest catalyst) show relatively higher active TPB density for a certain solid volume fraction. On the other hand, the improvement in TPB density with decreasing the catalyst particle size tends to decrease with increasing its volume fraction. It is found reasonable since inactive electrolyte phase covered by the catalyst phase is expected to increase due to reduced amount of the electrolyte phase with increasing catalyst content. It is also determined that the volume fraction at the percolation threshold tends to decrease with decreasing the particle size.

Tab. 3: Effect of catalyst phase average particle size on active TPB density

Cases	Volume Fraction (%)			Active TPB Density (μm·μm^{-3})
	Catalyst	Electrolyte	Pore	
A1	*15*	*55*	*30*	*0.64*
A2	*20*	*50*	*30*	*1.50*
A3	*25*	*45*	*30*	*3.08*
A4	*30*	*40*	*30*	*4.47*
A5	*35*	*35*	*30*	*5.19*
A6	*40*	*30*	*30*	*5.46*
A7	*45*	*25*	*30*	*5.51*
A8	*50*	*20*	*30*	*4.67*
A9	*55*	*15*	*30*	*2.25*
B10	*15*	*55*	*30*	*0.37*
B11	*20*	*50*	*30*	*1.00*
B12	*25*	*45*	*30*	*2.09*
B13	*30*	*40*	*30*	*3.23*
B14	*35*	*35*	*30*	*3.91*
B15	*40*	*30*	*30*	*4.24*
B16	*45*	*25*	*30*	*4.29*
B17	*50*	*20*	*30*	*3.88*
B18	*55*	*15*	*30*	*2.48*
C19	*15*	*55*	*30*	*1.63*
C20	*20*	*50*	*30*	*4.46*
C21	*25*	*45*	*30*	*7.32*
C22	*30*	*40*	*30*	*9.43*
C23	*35*	*35*	*30*	*10.16*
C24	*40*	*30*	*30*	*10.08*
C25	*45*	*25*	*30*	*8.88*
C26	*50*	*20*	*30*	*6.10*
C27	*55*	*15*	*30*	*2.05*

V. Conclusions

In this study, various SOFC anode electrode microstructures with different solid volume fractions and particle sizes are virtually generated by using particle size data experimentally obtained from commercial NiO and YSZ powders. The electrochemical performances of the anodes are then evaluated by measuring active TPB density. Among the cases considered, the highest active TPB density value of 10.16 μm·μm^{-3} is obtained from the anode microstructure having the smallest average catalyst phase particle size (~0.18 μm) and containing equal volumes of catalyst and electrolyte phases.

References

Heenan T.M.M., Bailey J.J., Lu X., Robinson J.B., Iacoviello F., Finegan D.P., Brett D.J.L., Shearing P.R., Three-phase segmentation of solid oxide fuel cell anode materials using lab based X-ray nano-computed tomography, Fuel Cells, 17(1), 75-82, (2017).

Hoffrogge P.W., Schneider D., Wankmüller F., Meffert M., Gerthsen D., Weber A., Nestler B., Wieler M., Performance estimation by multiphase-field simulations and transmission-line modeling of nickel coarsening in FIB-SEM reconstructed Ni-YSZ SOFC anodes I: Influence of wetting angle, Journal of Power Sources, 570, 233031, (2023).

Janardhanan V.M., Heuveline V., Deutschmann O., Three-phase boundary length in solid-oxide fuel cells: A mathematical model, Journal of Power Sources, 178(1), 368-372, (2008).

Timurkutluk B., Altan T., Toros S., Genc O., Celik S. and Korkmaz H. G., Engineering solid oxide fuel cell electrode microstructure by a micro-modeling tool based on estimation of TPB length, International Journal of Hydrogen Energy, 46(24), 13298-13317, (2021).

Xiang Y., Dong Z., Zhong Z., Jiao Z., Simulation of fracture formation in solid oxide fuel cell anode using peridynamic modeling method, Journal of Peridynamics and Nonlocal Modeling, 4(2), 201-214, (2022).

Zheng K.Q., Ni M., Reconstruction of solid oxide fuel cell electrode microstructure and analysis of its effective conductivity, Science Bulletin, 61(1), 78-85, (2016).

Investigation of a Sacrificial Template Material Suitable for Fabrication of Anode Support Microtubes in Microtubular Solid Oxide Fuel Cells

[1,2*] Ahmet Alp Sunecli, [1,2] Cigdem Timurkutluk, [1,2] Tolga Altan, [1,2] Sezer Onbilgin, [1,2] Bora Timurkutluk
[1] Niğde Ömer Halisdemir University, Prof. Dr. T. Nejat Veziroglu Clean Energy Research Center, Niğde, 51240, Türkiye
[2] Niğde Ömer Halisdemir University, Department of Mechanical Engineering, Niğde, 51240, Türkiye

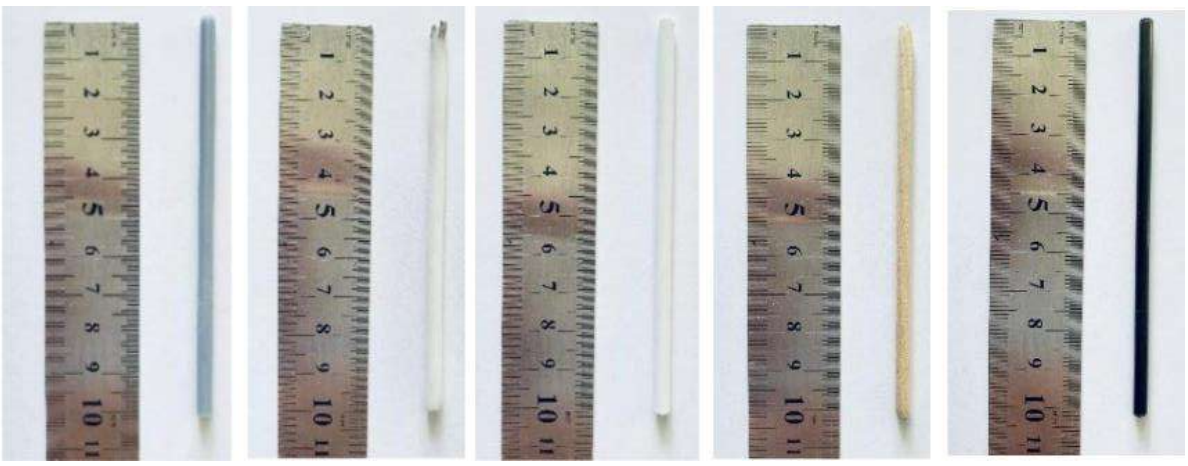
* E-mail: ahmetalp_sunecli@mail.ohu.edu.tr

Abstract
Unlike the conventional extrusion method, microtubular anode supports for solid oxide fuel cells (SOFCs) are fabricated using tape casting and isostatic pressing in this study. In this method, a continuous anode support film manufactured by tape casting is wrapped around a pin that acts as a mold. Since they are co-sintered after lamination through isostatic pressing, the pin material is of great significance in obtaining anode support microtubes without any mechanical damage. In this regard, pins are produced using five different materials: resin, polyamide, PLA, wood, and carbon fibre. The mold made of PLA material yields promising results regarding manufacturability of microtubular anode supports. These anode supports are also coated with electrolyte and cathode layers by the dip coating to produce microtubular cells. The cells are tested at 800 °C under hydrogen flow and open cathode environment.

Keywords: Solid Oxide Fuel Cell, Microtubular, Tape Casting, Wrapping

I. Introduction
Tape casting is a conventional technique used in the fabrication of planar SOFCs due to its low cost and simplicity (Moon at al., 2006). The method is based on preparing a slurry containing the relevant powders and other necessary additives. After homogenization and acquiring a suitable viscosity, the slurry is tape cast in thin layers. These tapes are then stacked on top of each other according to the desired thickness and the lamination process is usually completed with an isostatic press. Alternative, we have suggested tape casting for the fabrication of microtubular anode supports as well by winding the anode support tape on metallic rod followed by isostatic lamination process (Altan et al., 2022). Moreover, we have recently succeeded to fabricate microtubular SOFCs with thread-like surface patterns by winding the anode support tape on a threaded metallic rod (Timurkutluk et al., 2023). On the other hand, using metallic rod limits the surface patterning since the rod needs to be removed prior to sintering for a successful support fabrication. Therefore, in this study, we focus on the identification of a rod material that can be sintered together with the anode support and burned out during this process without damaging the anode support. In this regard, five different materials (i.e., resin, polyamide, PLA, wood, and carbon fibre) are considered and tested as a sacrificial template.

II. Experimental
Nickel oxide (NiO, NiO-A, Novamet, New Jersey, USA) and yttria stabilized zirconia (YSZ, 8 mol% yttria stabilized zirconia, Tosoh, Tokyo, Japan) powders were mixed with a certain proportion of dispersant, binder, plasticizer and solvent. Then, the mixture was ball milled for 24 hours. After magnetic stirring for ~4 hours to obtain the desired viscosity for the tape casting, the slurry was tape cast onto a silicone-coated Mylar strip with a doctor blade height of 300 µm and a tape width of 8 cm. Following the drying process under the ambient conditions for around 30 min, the film was cut into small pieces with a length of 15 cm. These tapes were wrapped around pre-prepared resin, polyamide, PLA, wood and carbon fibre molds of 4mm diameter (Fig. 1).



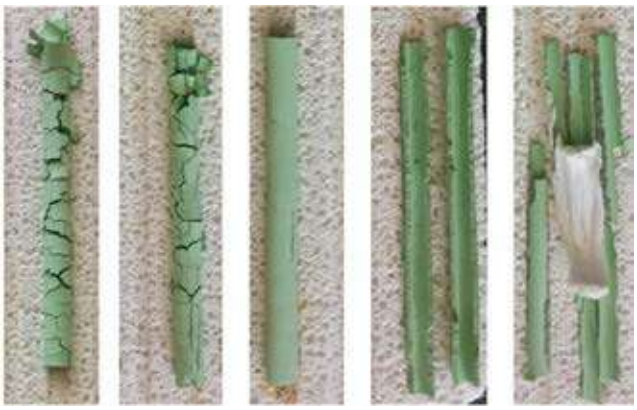
(a) (b) (c) (d) (e)

Fig. 1: Photo of the rods: (a) resin, (b) polyamide, (c) PLA, (d) wood, (e) carbon fibre rods

The lamination was carried out under 70 MPa pressure for 4 minutes with an isostatic pressing device. The laminates were then cut into 7 cm length microtubes by a laser cutter and subjected to a pre-sintering at 1100 ºC for 2 h. NiO (NiO-F, Novamet)-YSZ anode functional, YSZ electrolyte, LSM ($(La_{0.80}Sr_{0.20})_{0.95}MnO_{3-x}$: LSM20-HP, Nexceris, Ohio, USA)-YSZ cathode functional and LSM (LSM20-P, Nexceris)-YSZ cathode current collecting layers were fabricated by dip coating in the given order. The sintering of anode functional layer was performed at 1200 ºC for 2 h and the electrolyte layer was sintered at 1400 ºC for 4 h, while both cathode layer was fired at 1000 ºC for 2 h. The electrochemical performances of the cells were measured under 0.3 NL/min hydrogen flow by a fuel cell test station (Arbin Instruments, FCTS, Texas, USA) at 700-800 ºC. Microstructures of all cells were also investigated by SEM (Carl Zeiss, Evo 40, Oberkochen, Germany).

III. Results and Discussions

It is observed that the molds made of carbon fibre, wood, polyamide and resin significantly damage the anode support layer during pre-sintering step, while PLA mold causes relatively less damage (Fig. 2). Due to this potential, PLA molds in the form of a pipe with 4 mm inner diameter and 0.5 mm wall thickness were produced using a 3D printer to reduce the amount of material during burn out step. To further improve the mechanical strength of the anode support layer, the anode support tapes of 22 cm and 30 cm length were then wrapped on these pipes. A steel pin as a support was placed inside the PLA pipes to prevent the anode support from any damage during the isostatic pressing process. The pin was then removed from the structure. Two new microtubular cells were fabricated similarly, i.e., C22 and C30, named according to the tape length used (Fig. 3.).



(a) (b) (c) (d) (e)

Fig. 2: Anode supports wrapped on various (a) resin, (b) polyamide, (c) PLA, (d) wood, (e) carbon fiber molds supported anode views after sintering process



(a) (b)

Fig. 3: Photo of C22 (a) and C30 (b)

The electrochemical performances of C22 and C30 at 800 °C are compared in Fig.4. It is seen that C22 produced using 22 cm long anode support tape exhibits a maximum power density of 290 mW/cm^2, while that of C30 prepared by 30 cm long anode tape is measured as 365 mW/cm^2 at 800 °C. SEM micrographs of the anode supports are given Fig. 5. It is observed that the relatively low performance measured from C22 is originated from its relatively lower anode support porosity that may lead to increased gas diffusion resistance. This is found reasonable since the relatively shorter tape length used in the fabrication of C22 may yield a denser structure under the same laminating conditions. Nevertheless, this needs to be confirmed through further analyses such as impedance spectroscopy.

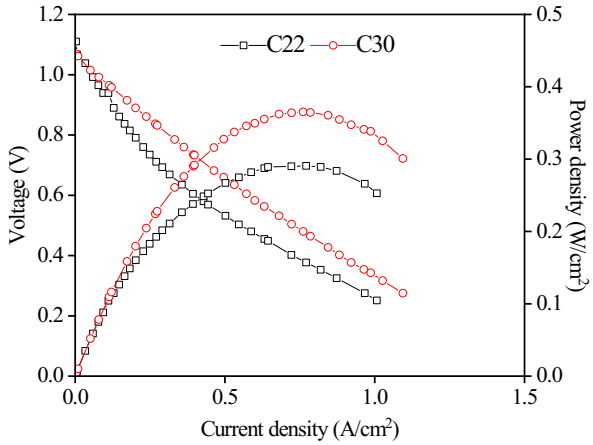
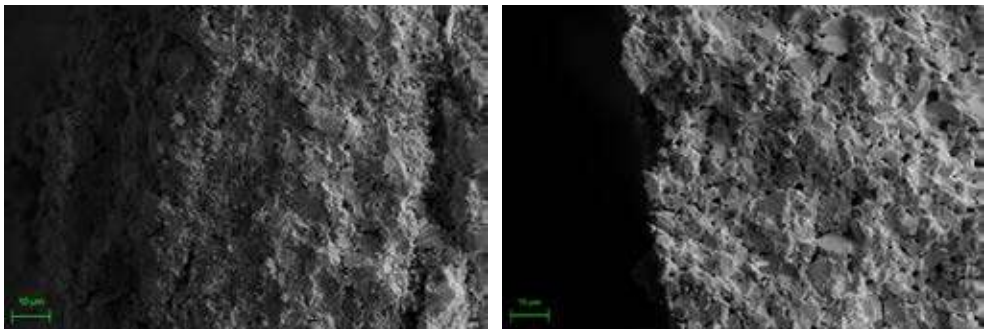


Fig. 4: Electrochemical performances of C22 and C30



(a) (b)

Fig. 5: SEM images of anode support in C22 (a) and C30 (b)

IV. Conclusions

In this study, microtubular anode supports are fabricated by wrapping the corresponding tape on a rod followed by lamination and co-sintering. To reveal a suitable material for the rod that can burn out without damaging the anode support, rods made of five different materials are considered. After initial observations and some improvements in the design, the rod fabricated by a 3D printer from PLA is found to be promising for this purpose. Furthermore, with the suggested fabrication method, pins with various forms of surface patterns can be easily 3D printed from PLA and these molds can be employed in the production of surface patterned microtubular solid oxide fuel cells with improved electrolyte-electrode interfaces thereby high performance.

References

Altan T., Timurkutluk C., Timurkutluk B., Celik S., Tape casting coupled with isostatic pressing as an alternative fabrication method for microtubular solid oxide fuel cells, International Journal of Hydrogen Energy, 47(16), 9735-9743, (2022).

Moon H., Kim S.D., Hyun S.H., Kim H.S., Development of IT-SOFC unit cells with anode-supported thin electrolytes via tape casting and co-firing, International Journal of Hydrogen Energy, 33, 1758-1768, (2008).

Timurkutluk B., Onbilgin S., Altan T., Timurkutluk C., Manufacturability of bolt-microtubular anode supports for solid oxide fuel cells, Journal of Power Sources, 592, 233971, (2024).

Developing a Visible Light Communication System for Grid Protection in a Green Hydrogen Powered EV Charging Station

[1]Murat Das, [2*]Gökay Bayrak
[1]Bursa Technical University, Graduate School, Master of Electrical and Electronics Engineering, Bursa, 16310, Türkiye
[2]Bursa Technical University, Smart Grids Lab., Electrical and Electronics Engineering, Bursa, 16310, Türkiye

E-mail: gokay.bayrak@btu.edu.tr ([*]Corresponding Author)

Abstract
In this study, a Visible Light Communication (VLC) System is proposed for grid protection in a green hydrogen-powered EV charging station (EVCS). An innovative structure has been studied in which the excess energy generated by the photovoltaic (PV) system during the day is stored as hydrogen and in which EVCSs are fed with a fuel cell system from hydrogen during the hours when the sun is not shining. VLC is recommended to integrate this system into the grid and improve its required protection functions. The developed VLC-based monitoring and protection system was tested in the laboratory in real time under different grid conditions such as frequency and voltage changes. An FPGA-based protection algorithm is also implemented by using LabVIEW software. The obtained experimental results show that VLC responds quickly to frequency and voltage changes and can be used as an alternative, effective, and innovative protection method in green hydrogen-powered EVCS.

Keywords: EV charging station, Visible Light Communication (VLC), Smart Grid Protection, Green Hydrogen

I. Introduction

The surge in electric vehicle (EV) interest has spurred the need for charging infrastructure. Researchers have explored various charging methods, including battery swapping, wireless, and wired charging. However, EVs still face the challenge of longer charging times than conventional vehicles. Battery swapping stations allow for quick swaps but require an extensive inventory of fully charged batteries, posing supply chain issues. Wireless charging offers convenience but is slower than other methods (Baum et al., 2022). Wired charging, particularly utilizing AC and DC modes, remains the most prevalent. These stations involve a direct connection between the vehicle and the power source via charging cables equipped with control circuits. Despite their popularity, wired charging technologies have safety concerns, notably with MOD 1 charging (Johnson et al., 2022).

Visible Light Communication (VLC) technology has emerged as a promising solution for efficient and secure data transmission in charging systems. Leveraging high data rates and low power consumption, VLC offers potential benefits for EV charging stations (Çakmak, R., et al., 2024).

Furthermore, hydrogen fuel cell technology presents an alternative to EV power. Hydrogen fuel cells provide fast refueling times and longer driving ranges, addressing some EV limitations. However, challenges such as infrastructure and production hinder widespread adoption (Song, C. 2022). As EV demand rises, integrating innovative technologies like VLC and hydrogen fuel cells into charging infrastructure becomes crucial. These advancements contribute to sustainable transportation ecosystems by improving charging efficiency and addressing EV range concerns. In addition, the integration of green energy systems such as solar and wind power for EV charging is gaining momentum. These renewable energy sources not only reduce carbon emissions but also contribute to the sustainability of the transportation ecosystem by providing clean energy for charging EVs (Shrivastava, A. et al., 2023).

II. Experimental Set-up and Procedure

The system depicted in Figure 1a focuses on the output of a sinusoidal signal from the developed system. Visible Light Communication (VLC) was employed using a LabVIEW interface to ensure the considered system's stable operation. VLC is viewed as a significant complement to next-generation communication systems, offering high data transfer speeds, non-harmful effects on health, secure signal isolation properties, and a compact structure with a significantly wide bandwidth, thereby consuming less power in data transmission. Moreover, the output signal of the sinusoidal signal will feed an EV charging station using a green hydrogen energy system, further enhancing the sustainability of the charging process.

In this study, real-time voltage and frequency data will be acquired via a LabVIEW software interface developed on an FPGA platform. Subsequently, the acquired data will be experimentally processed using a VLC-based modulator/demodulator design. The system will then be tested to enable the transmission of signals to a breaker for disconnection in case of voltage or frequency imbalances in a grid-connected power system. This innovative approach, facilitating communication via light to mitigate switching and data losses, aims to propose a practical technological solution for innovative protection methods crucial in smart grid applications. Experimental setups for the VLC communication system for green hydrogen-powered EVCS are showcased in Figure 1b, providing insight into ongoing laboratory investigations.

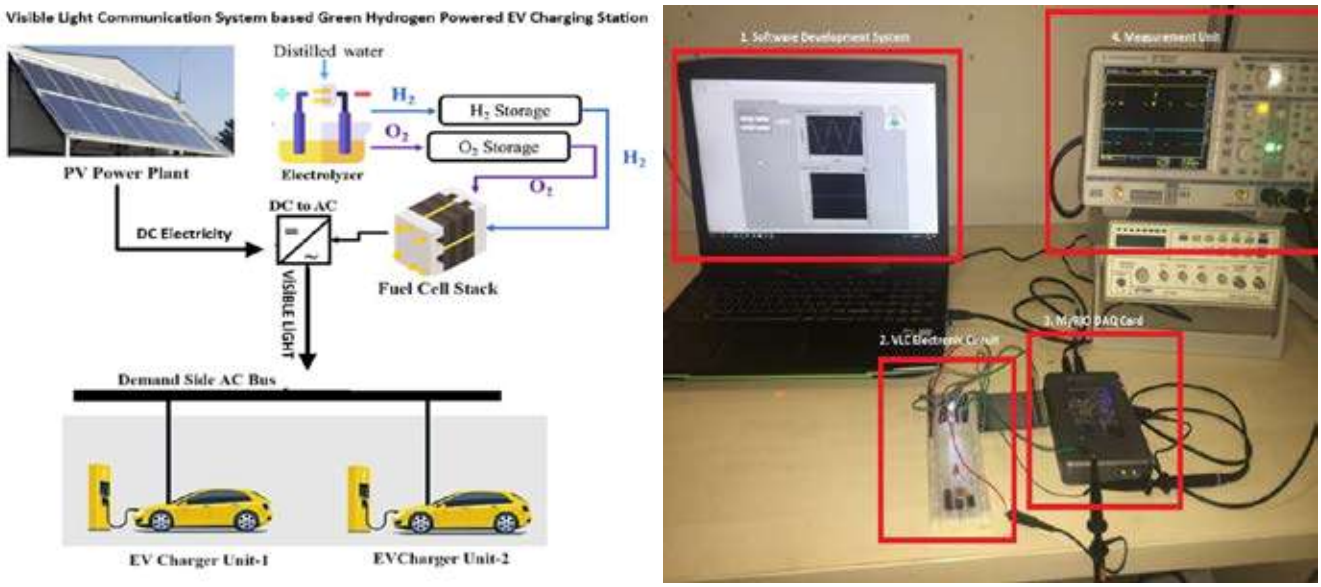


Fig. 1: a) Studied green hydrogen-powered EVCS system block diagram, b) Proposed VLC system for green hydrogen-powered EVCS

The visible light spectrum ranges from 400 nm (800 THz) to 700 nm (400 THz), with transmission bandwidths limited to the MHz range due to constraints in LED materials and photodetectors. In recent years, visible light communication (VLC) systems have leveraged LEDs as transmitters and photodiodes as receivers, capitalizing on their longevity, low power consumption, and eye-safety advantages over conventional light sources. This dual functionality of illumination and communication has expanded the utility of VLC systems, with applications ranging from office lighting to wireless data transmission.

The emergence of VLC, particularly amidst advancements in smart grid technologies, offers secure, high-speed data transmission with minimal bandwidth requirements. Moreover, evolving smart grid systems underscore the need for novel protection mechanisms, prompting the development of new safeguarding systems. Preliminary work on a VLC communication system, as depicted in Figure 2, has commenced, aiming to detail the design of a transmitter-receiver communication system for the implementation of grid protection for EVCSs.

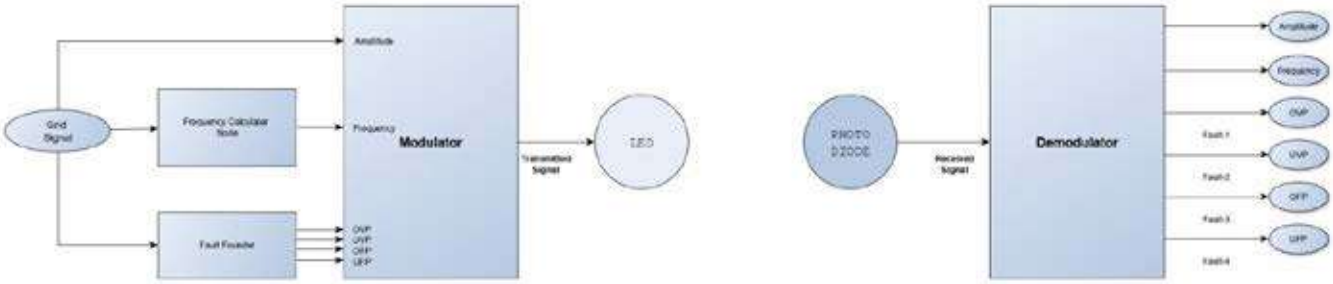


Fig. 2: General block diagram of proposed VLC system for the implementation of grid protection for EVCSs

III. Analysis

In this study, an embedded electronic protection system has been realized to safeguard the electrical power system against four different fault parameters. In the proposed VLC system, where the sinusoidal signal from the grid is read through the analog input of the MyRIO processor and directed to the modulator block via the LabVIEW interface. The modulation and demodulation of the signal were achieved using VHDL code lines. This FPGA code (VHDL) was compiled using Xilinx's VIVADO IDE to generate a file type compatible with LabVIEW content and debugged; it was then simulated. The addition of the generated code to the interface and loading it onto the myRIO card was facilitated using the IP Generator block in LabVIEW FPGA.

Figure 3 presents oscilloscope images of the modulator (LED) input and demodulator (OPT 101 Photodiode) output of the VLC system. The yellow and blue signals depicted in the oscilloscope screen represent the received and transmitted messages, respectively. The crucial aspect here is the points where the signal rises and falls. The absence of differences in rise and fall times is among the greatest advantages of this system. Additionally, the signals always follow each other, and there is no phase difference observed on the analog signal. If required, phase differences can be added in the software section.

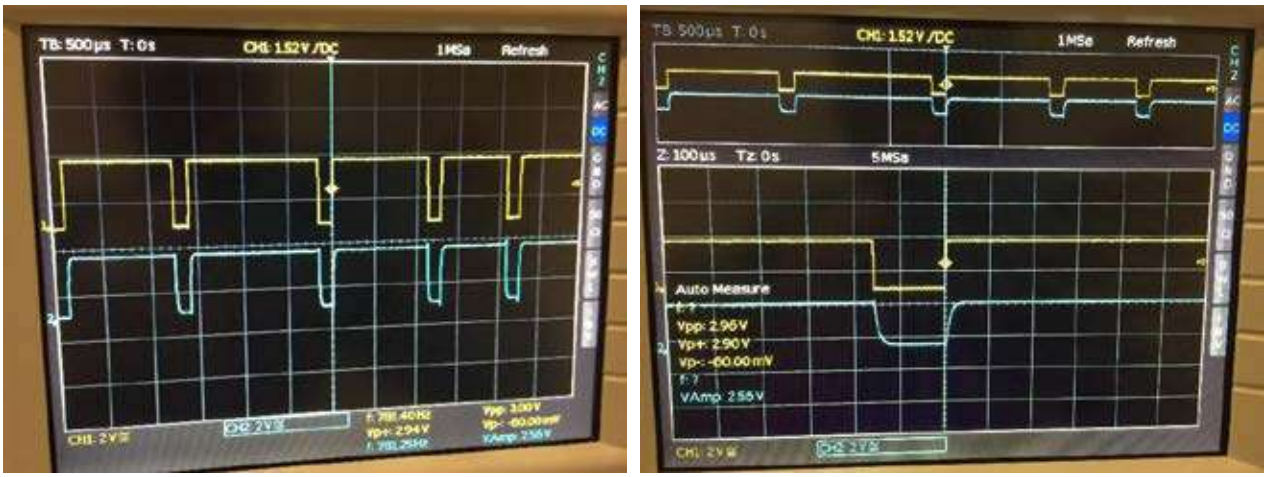


Fig. 3: Experimental results for proposed VLC protection schema

The definition of energy quality in electrical power systems is used to indicate variations in voltage and frequency in the grid and waveform distortions in the current drawn from the grid. Many electrical devices are not sensitive to changes in grid voltage and frequency. However, devices controlled by electronic circuits, which have become increasingly common in recent years, are highly sensitive to energy quality.

This study aims to mitigate waveform distortions in grid current and voltage caused by significant load changes in electrical power systems, particularly in response to the growing number and applications of power electronic circuits in recent years, using Solid State Relays (SSRs).

In the general block diagram of the VLC system, the modulation of the frequency and amplitude of the sinusoidal signal read from the grid using a fault detector block. These values will be modulated and transmitted to the myRIO DAQ card.

IV. Results and discussions

Based on the described experimental setup and procedures outlined in the study, several significant observations and results were obtained, which are discussed below.

The system's response to various fault conditions, such as overvoltage, under voltage, over frequency, and under frequency, was assessed with circuit breaker activation thresholds set at a ±10% tolerance level for voltage and frequency deviations. Tables were used to record logical state transitions indicating the circuit breaker's intervention. For instance, Table 1 demonstrates the circuit breaker's response to overvoltage situations, where logical state transitions signify its activation when grid parameters exceed defined thresholds. These findings highlight the system's ability to promptly detect and address grid anomalies, thereby enhancing operational safety and stability.

Table 1. *Tested over voltage grid condition*

Time (s)	0	1	2	3	4	5	6	7	8	9
Grid Amplitude (V)	65	152	215	268	308	337	342	331	304	250
Grid Frequency (Hz)	50	50	50	50	50	50	50	50	50	50
Circuit Breaker (Logical)	0	0	0	0	0	1	1	1	1	1

Moreover, the LabVIEW interface enabled the real-time supervision and management of the system. Through a graphical user interface (GUI), users can conveniently access vital system parameters, such as sinusoidal signal attributes, fault detection status, and control configurations. The interface's modular structure facilitated smooth incorporation with FPGA technology, facilitating concurrent processing of data and commands. The system accurately identified deviations in voltage and frequency from reference values and promptly activated the appropriate corrective measures as shown in Figure 4. The fault detection module effectively distinguished between different fault types and engaged the circuit breaker as necessary.

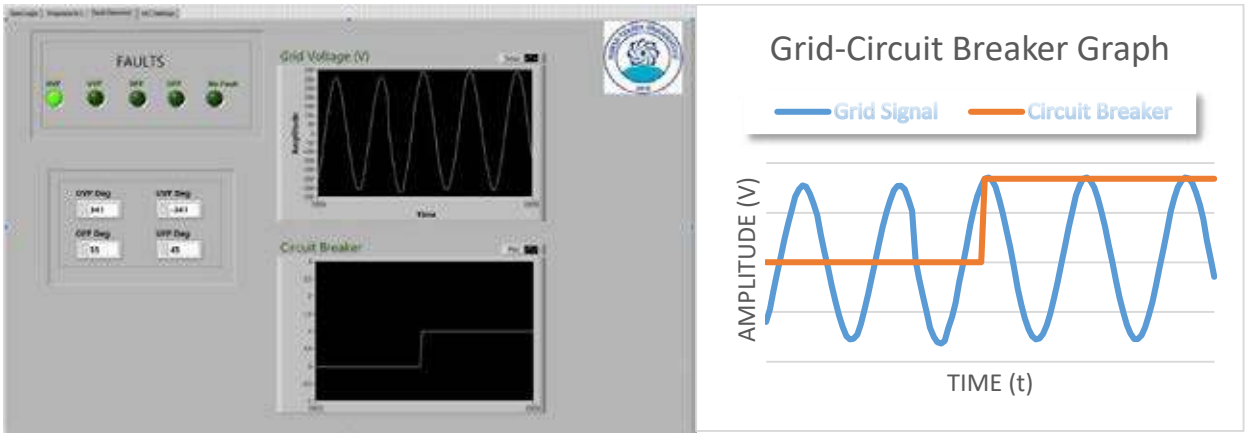


Fig. 4: Real-time monitoring system and triggered protection signal for SSR circuit breaker

Additionally, the proposed VLC system successfully demonstrated its capability to transmit and receive sinusoidal signals with minimal distortion. The GUI provided comprehensive visualization of transmitted and received signals, facilitating real-time monitoring and assessment of system performance. Overall, the experimental results indicate the efficacy and reliability of the developed system in detecting and mitigating grid anomalies. The seamless integration of LabVIEW with FPGA technology enabled efficient control and monitoring of the system, highlighting its potential for application in smart grid and power management systems. Further research could focus on enhancing the system's robustness and scalability to accommodate larger-scale grid networks and more complex fault scenarios.

V. Conclusions

In conclusion, the study underscores the effectiveness of integrating Visible Light Communication (VLC) technology and LabVIEW-based interfaces in addressing challenges within EVCS infrastructure and green hydrogen-powered smart grid systems. The experimental results demonstrate the system's robust performance in detecting and responding to grid anomalies promptly, thereby enhancing operational safety and stability. The seamless integration of LabVIEW with FPGA technology enables efficient control and monitoring, highlighting its potential for widespread application in sustainable transportation ecosystems and power management systems. Future research endeavors could focus on further enhancing the system's scalability and robustness to accommodate evolving grid networks and complex fault scenarios.

Acknowledgements

This study was conducted within the scope of a master's thesis project at Bursa Technical University Graduate School.

References

A. Fişne ve C. Toket, «Görünür Işık Haberleşmesi'nde Kanal Yapısının İncelenmesi,» IEEE, no. 22, pp. 1646-1649, 2014.

Baum, L., Darvish, S., & Schulz, D. (2022). Mobile AC/DC test device for electric vehicle charging infrastructure communication. e & i Elektrotechnik und Informationstechnik, 139(2), 149-154

ÇAKMAK, Recep; MERAL, Hasan; BAYRAK, Gökay. A new intelligent charging strategy in a stationary hydrogen energy-based power plant for optimal demand side management of plug-in EVs. International Journal of Hydrogen Energy, 2024.

Grasel, B., Baptista, J., & Tragner, M. (2022). Supraharmonic and Harmonic Emissions of a Bi-Directional V2G Electric Vehicle Charging Station and Their Impact on the Grid Impedance. Energies, 15(8), 2920.

Johnson, J., Berg, T., Anderson, B., & Wright, B. (2022). Review of Electric Vehicle Charger Cybersecurity Vulnerabilities, Potential Impacts, and Defenses. Energies, 15(11), 3931

Łuczak, W. K. (2022). Development of an EVSE charging station and an onboard charger control system for a prototype electric vehicle (Doctoral dissertation, Instytut Maszyn Roboczych Ciężkich).

M. Akanegawa et all. «Basic study on traffic information system using LED traffic lights,» IEEE Transactions, vol. 2, no. 4, pp. 197-203, 2001.

Paul Sathiyan, S., Jensen, S., & Abirami, J. (2022). Electric Vehicle Charging Technology: Recent Developments. Innovations in Electronics and Communication Engineering, 487-493.

Shrivastava, A., Ranga, J., Narayana, V. N. S. L., & Borole, Y. D. (2021, September). Green Energy Powered Charging Infrastructure for Hybrid EVs. In 2021 9th International Conference on Cyber and IT Service Management (CITSM) (pp. 1-7). IEEE.

Song, C. (2022). Research on Power Line Carrier Communication between Electric Vehicle and Electric Vehicle Supply Equipment. International Core Journal of Engineering, 8(1), 556-566

Soponoudomsit, P., et all. (2022, May). Safety Function Designs in Mode 3 EVSE. In 2022 19th International Conference on Electrical Engineering/Electronics, Computer, Telecommunications and Information Technology (ECTI-CON) (pp. 1-4). IEEE.

Development of Electrolytic Cation Exchange Integrated Reactor for H_2 Generation and CO_2 Extraction

*Hilal Sayhan Akci Turgut and Ibrahim Dincer
Clean Energy Research Laboratory (CERL), FEAS, Ontario Tech University, Oshawa, Ontario, L1H 7K4, Canada

*E-mail: Hilal.Akci@ontariotechu.ca

Abstract
Carbon dioxide (CO_2) is extracted from naturally existing seawater, mostly in the form of bicarbonate and carbonate, using a sophisticated electrolytic cation exchange process. The method also produces hydrogen gas (H_2). The influence of various factors, such as voltage electrolyte amount and pH, on the efficiency of CO_2 synthesis is examined. Optimization studies were conducted to enhance the CO_2 and H_2 production rates. The results demonstrate maximum CO_2 production rate of 1479.73 mg/min.

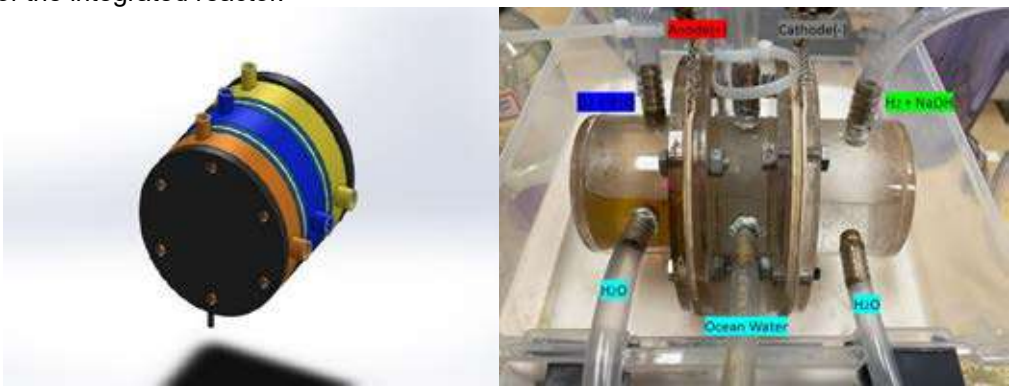
Keywords: Hydrogen, Ocean water, Electrolysis, Carbon capture.

I. Introduction

Carbon capture and storage (CCS) technology research has made great progress in combating the worldwide rise in human CO_2 levels in the Earth's atmosphere. Seawater has an estimated total carbon dioxide (CO_2) content of 100 mg/L, with around 2-3% in dissolved form (Takahashi et al., 1981). Willauer et al. (2017) presented a unique E-CEM module with three configurations that reduced seawater pH by 65% during testing. This pH decrease enabled the conversion of carbonate and bicarbonate ions back into CO_2 gas, which aided in water recovery. In another work, Xu et al. (2022) used electrodeionization to recover ammonia from wastewater for fuel use. The study studied NH_3 recovery, NH_4^+ penetration, and the interaction of NH_4^+ and Na^+ with functional groups within a cation exchange membrane (CEM) using both theoretical computations and experimental trials. Na_2SO_4 was used as the supporting electrolyte in this investigation. The approach presented in this study uses protons produced at the anode during electrolysis to acidify seawater. At the same time, electrons devour protons at the cathode, producing hydrogen gas.

II.System Description

Figure 1 demonsrates the E-CEM integrated reactor that consists of three compartments: an anode, a central oceanwater chamber, and a cathode compartment. This design employs continuous electrodeionization (CEDI) to remove ionizable compounds from liquids by modifying their ionic transport properties via an electrical potential. It makes this process easier by employing electrically active media, such as semipermeable ion exchange membranes. The continuous flow mechanism moves ocean water through the E-CEM's central compartment, while water flows through the anode and cathode compartments. When the module receives direct current, the anode oxidizes, producing H^+ ions and O_2 gas. When the pH of seawater falls below or equal to 6, bicarbonate and carbonate re-equilibrate to generate carbonic acid. This reaction involves the conversion of hydrogen ions and sodium bicarbonate to carbonic acid and sodium ions. The CO2 from the carbonic acid is obtained from the center compartment of the integrated reactor.



a) b)

Fig. 1: The Integrated E-CEM Reactor
a) Novel structure of the Integrated E-CEM; b) The present Integrated E-CEM

According to equation 1, a mole of hydroxide ions (OH^-) is chemically replaced for every mole of bicarbonate ions ($HCO3^-$) in oceanwater, as per the complete reaction. Overall chemical reaction:

$$2H_2O + 2HCO_3^- \rightarrow 2OH^- + O_2 + 2H_2 + 2CO_2 \quad (1)$$

III. Results and discussion

Figure 2 shows a comparison of CO_2 production numbers derived using the Box-Behnken approach with the comparable experimental results. While there are minor differences between the actual and projected numbers, there is a strong overall connection. The alignment of the greatest and lowest CO_2 production figures with the average values implies that the anticipated values are accurate. The tight connection between planned and actual results within the range of average CO_2 production levels, which are generally between 900 and 1400 mg/min, is especially notable. This shows that the suggested method is appropriate for the experimental scenario. These data demonstrate the predictive model's accuracy in calculating CO_2 production inside the experimental system. Significant progress has been made in improving the module's re-equilibration time by evaluating four E-CEM configurations. However, examining these early "proof of concept" devices was critical for determining the fundamental principles driving ion transport in this specific application.

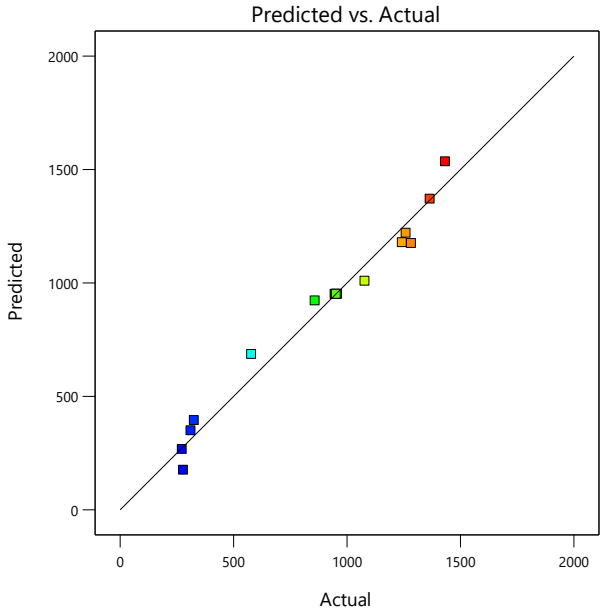


Fig. 2: Predicted and Actual Values of Carbon Dioxide Extraction

IV. Conclusions

In summary, the utilization of the CO_2 content of seawater to simultaneously produce hydrogen and CO_2 was successfully demonstrated. Comprehensive research was conducted to assess hydrogen production across various system parameters, indicating a maximum generation rate of 2.2 mg/min. The highest efficiency, 7.82%, was consistent with predictions, with hydrogen generation correlated directly with both voltage and electrolyte content. Different factors, including as voltage, electrolyte amount, and pH, were explored for their effect on CO_2 synthesis efficiency. Optimization studies have been implemented to increase both CO_2 and H_2 production rates. The results showed a maximum CO_2 generation rate of 1479.73 mg/min. These findings emphasize ocean water's potential as a source of sustainable hydrogen generation while also addressing CO_2 emissions.

References

Takahashi, T., Broecker, W. S., & Bainbridge, A. E. (1981). The alkalinity and total carbon dioxide concentration in the world oceans. *Carbon cycle modelling, SCOPE*, *16*(3078), 271-286.

Willauer, H. D., DiMascio, F., Hardy, D. R., & Williams, F. W. (2017). Development of an electrolytic cation exchange module for the simultaneous extraction of carbon dioxide and hydrogen gas from natural seawater. *Energy & Fuels*, *31*(2), 1723-1730.

Xu, L., Liu, D., Liu, W., Yang, J., Huang, J., Wang, X., & He, Q. (2022). Ammonia Recovery from Wastewater as a Fuel: Effects of Supporting Electrolyte on Ammonium Permeation through a Cation-Exchange Membrane. *ACS omega*, *7*(24), 20634-20643.

Reactivity of Nickel Based Monolithic Catalyst in the Oxidative Steam Reforming of Biogas with H_2S

[1*]Merve Doğan Özcan, [1]Orhan Özcan, [1]Ayşe Nilgün Akın
[1]Kocaeli University, Faculty of Engineering, Department of Chemical Engineering, Kocaeli, 41001, Türkiye

* E-mail: mervedoganozcan@gmail.com

Abstract
In this study, particulate and monolith NiCe/MgAl catalysts for syngas production by oxy-steam reforming (OSR) of biogas were prepared using the sol-gel method followed by incipient wetness impregnation. Activity tests were conducted in a once-through flow reactor at temperatures of 600, 700, and 800 ℃ with a fixed GHSV of 45000 mL/g_{cat}.h and molar feed ratio of $CH_4/CO_2/O_2/H_2O$ = 1/0.67/0.1/0.3. The catalysts were characterized using N_2-physisorption, XRD, SEM, TGA, and ICP-OES techniques. The monolith NiCe/MgAl (NCMA) catalyst exhibited lower carbon accumulation compared to the particulate catalyst at all reaction temperatures. However, the particulate NCMA catalyst achieved the highest CH_4 (94%) and CO_2 (80%) conversions at 800 ℃. When exposed to 12 ppm H_2S, the particulate NCMA catalyst only experienced a 10% decrease in CH_4 conversion after 180 min.

Keywords: Biogas, H_2S, Oxidative steam reforming, Syngas, Ni-based catalyst

I. Introduction

Syngas, which is composed of hydrogen (H_2) and carbon monoxide (CO), is considered an alternative clean fuel due to its ease of transport and low cost. However, its applicability depends on the H_2/CO ratio (Paladino Lino et al., 2019). Depending on this ratio, the syngas can be converted to methanol, diesel through Fischer-Tropsch synthesis (Kumar and Pant, 2020).

Syngas is commonly produced from methane through various reforming reactions (López-Ortiz et al., 2017). In recent years, significant efforts have been made towards using biogas as an alternative to methane to produce synthesis gas. Biogas is produced from the anaerobic fermentation of substances and is composed of 50-75% CH_4, 25-50% CO_2, 0-10 N_2, and 0-3% H_2S (Appari et al., 2014). Therefore, biogas is an alternative and renewable fuel that helps reduce greenhouse gas emissions. Oxidative steam reforming of biogas (OSR) can overcome several challenges, such as high energy requirements, sintering of the support and metal phase, and carbon accumulation (Vita et al., 2019).

Ni-based catalysts on various supports have been extensively studied due to the availability and low cost of the metal. However, the use of Ni catalysts is often accompanied by the formation of carbon, which leads to catalyst deactivation (Damyanova et al., 2011). Oxides such as Al_2O_3, ZrO_2, CeO_2, and MgO, as well as mixed oxides, are excellent support materials for Ni-based catalysts. Hydrotalcite-derived mixed oxide catalyst supports have been extensively studied due to their highly active metal dispersion, resistance to carbon formation and sintering, and high surface area. They also have advantages such as adjustable acid-base properties. However, sulfur impurities are inevitable in the biogas production process. Nickel catalysts can lead to deactivation even in the presence of low levels of sulfur (Chen et al., 2017). Therefore, ongoing studies focus on the development of sulfur and carbon-resistant catalysts.

In this study, particulate and monolith NiCe/MgAl catalysts were prepared for syngas production through OSR using the sol-gel method followed by incipient wetness impregnation. The catalysts were characterized by N_2-physisorption, XRD, SEM, HRTEM, TGA, Raman, and ICP-OES. Activity tests were conducted to determine the sulfur resistance of the catalysts in the presence of 12 ppm and 50 ppm H_2S.

II. Experimental Set-up and Procedure

The MgAl support was prepared using the sol-gel method. To prepare the support, specific quantities of magnesium ethoxide and aluminum triisopropylate were taken in a four-neck flask and 150 mL of ethanol was added. Next, 5 mL of HNO_3 was added dropwise to the solution. The solution was stirred at 450 rpm and heated to 70 °C. While heating, 50 mL of ammonia (25%) was added to the solution to stabilize the pH at 10. When the temperature reached 70 °C, 3 mL of deionized water was added dropwise for the hydrolysis under reflux for 18 hours. The solution was then cooled to room temperature, filtered, and washed three times with ethanol. The resulting material was dried in an oven at 40 °C. The support was designated as MA. Subsequently, calcination was performed in a muffle furnace at 900 °C for 5 hours, heated at a rate of 1 °C per minute. The support material was sieved (60-80 mesh) and mixed with Ludox in a specific ratio. It was then shaped into a monolith using a 2-cc syringe. After preparing the support material, Ni (10 wt.%) and Ce (2.5 wt.%) were loaded onto the supports using incipient wetness impregnation. The resulting catalyst was denoted as NCMA.

The catalytic activity tests were performed in a quartz packed-bed reactor at temperatures of 600 °C, 700 °C, and 800 °C. Prior to the activity test, the catalysts were reduced in situ with a 40 mL/min H_2 flow for 1 hour at 900 °C. The space velocity was set at 45000 mL/g_{cat}.h with a constant feed ratio of $CH_4/CO_2/O_2/H_2O$ = 1/0.67/0.1/0.3. The effluent gases were analyzed using Agilent 7890B gas chromatography equipped with FID and TCD detectors.

III. Results and discussions

Fig. 1 shows the XRD patterns of the support (monolith MA) and catalysts (monolith and particulate NCMA) after calcination and reduction. The patterns reveal the presence of SiO_2 phase at 2θ = 22.1°, 31.2°, 36.0°, 56.7° (COD 9006306), Mg(Al)O periclase phase at 2θ = 37.1°, 43. 0°, 62.8°, 74.8°, 79.3° (COD 9006789), and $MgAl_2O_4$ phase at 2θ = 31.4°, 44.9°, 59.6°, 65.4° (COD 9005809). The NCMA catalysts exhibited the presence of the CeO_2 and NiO phases at 2θ = 28.2°, 47.4°, 56.7° (COD 4343161) and 2θ = 37.1°, 43.0°, 62.5° (COD 4320493), respectively.

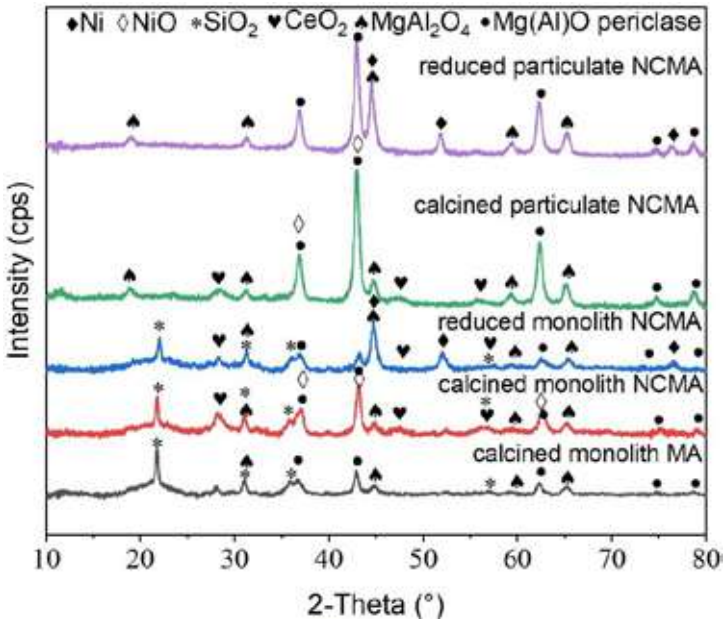


Fig.1: XRD patterns of the support and catalysts.

Tab. 1 presents the BET surface area, pore volume, and mean pore diameter of the reduced catalysts. The particulate NCMA exhibits a higher BET surface area (64.26 m^2/g) compared to the monolith NCMA (21.87 m^2/g). Similarly, the pore volume of NCMA (0.29 cm^3/g) is higher than that of the monolith NCMA (0.10 cm^3/g). The Ni and Ce contents of the catalysts, as determined by ICP-OES, are close to the desired theoretical values (10 wt.% for Ni and 2.5 wt.% for Ce). Additionally, the calculated Mg/Al molar ratios are close to the theoretical values of 3/1.

Tab.1: N_2-physisorption and ICP-OES results of reduced catalysts

Catalyst	BET surface area (m^2/g)	BJH desorption pore volume (cm^3/g)	BJH desorption average pore diameter (nm)	Mg/Al	Si (wt.%)	Ni (wt.%)	Ce (wt.%)
Monolith NCMA	21.9	0.10	12.9	2.4	28	9.8	2.3
Particulate NCMA	64.3	0.29	11.1	2.4	-	10.0	2.5

The performance of monolith and particulate NCMA catalysts for oxidative steam reforming of biogas was evaluated at 600, 700, and 800 °C using a $CO_2/CH_4/O_2/H_2O$ ratio of 1/0.67/0.1/0.1/0.3. The results are presented in Fig. 2, which shows that the CH_4 conversion rate increases with temperature for both catalysts. At 800 °C, the monolith NCMA catalyst achieved 83.5% conversion, while the particulate NCMA catalyst achieved 93.9% conversion. Furthermore, the particulate NCMA exhibited higher CH_4 conversion rates compared to the monolith at all reaction temperatures. Similarly, the CO_2 conversion values increased with temperature, and the particulate NCMA yielded higher conversion rates. Additionally, the H_2 yield of NCMA was higher than that of monolith NCMA. The H_2/CO molar ratio was similar for both catalysts, with values ranging from 1.8 to 1.5 depending on the reaction temperature.

The TGA results of the spent catalysts indicate that the monolith NCMA is more resistant to carbon than the particulate NCMA. SEM images of spent particulate and monolith NCMA catalysts revealed the presence of filament carbon at a reaction temperature of 600 °C. However, no detectable carbon was observed at 800 °C. This finding was confirmed by XRD analysis, which detected a carbon peak in the used catalysts at 600 °C for both types of catalysts.

When 12 ppm H_2S was present, the particulate NCMA showed a 10% decrease in methane conversion after 180 minutes of reaction, while the monolith catalyst showed a 25% decrease. When 50 ppm H_2S was present, both catalysts experienced a loss of activity of approximately 50% after 180 minutes.

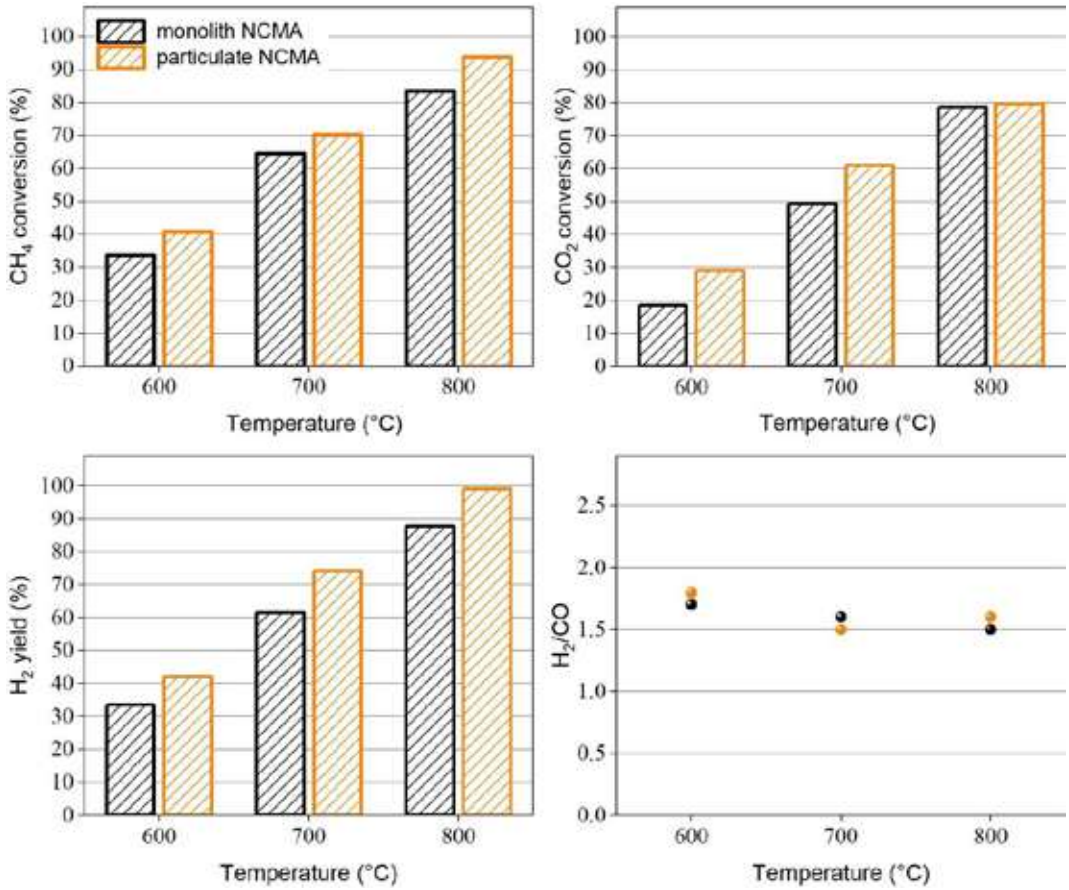


Fig.2: Reactivity results of catalysts: Time = 90 min., T = 800 °C, $CH_4/CO_2/O_2/H_2O$ = 1/0.67/0.1/0.3, GHSV = 45000 mL/g_{cat}.h.

IV. Conclusion

Herein, monolith and particulate NiCe/MgAl catalysts (NCMA) were prepared using the sol-gel method followed by incipient wetness impregnation for syngas production by oxy-steam reforming (OSR) of biogas. The characterization results indicate that the particulate NCMA has a higher BET surface area (64.3 m^2/g) compared to the monolith NCMA (21.9 m^2/g). Additionally, the TGA results show that the monolith NCMA has a lower carbon deposition rate than the particulate NCMA at 600, 700, and 800 °C. The particulate NCMA catalyst achieved the highest conversions of CH_4 (94%) and CO_2 (80%) at 800 °C.

Acknowledgments

This work was funded by Kocaeli University Research Fund with project numbers 2019/069 and FDK-2020-2068.

References

Appari S., Janardhanan V. M., Bauri R., Jayanti S., Deutschmann O., A detailed kinetic model for biogas steam reforming on Ni and catalyst deactivation due to sulfur poisoning, Applied Catalysis A: General, 471, 118–125 (2014).

Chen X., Jiang J., Yan F., Li K., Tian S., Gao Y., Zhou H., Dry Reforming of Model Biogas on a Ni/SiO_2 Catalyst: Overall Performance and Mechanisms of Sulfur Poisoning and Regeneration, ACS Sustainable Chemistry and Engineering, 5(11), 10248–10257 (2017).

Damyanova S., Pawelec B., Arishtirova K., Fierro J. L. G., Biogas reforming over bimetallic PdNi catalysts supported on phosphorus-modified alumina, International Journal of Hydrogen Energy, 36(17), 10635–10647 (2011).

Kumar R., Pant K. K., Promotional effects of Cu and Zn in hydrotalcite-derived methane tri-reforming catalyst, Applied Surface Science, 515, 146010 (2020).

López-Ortiz A., González-Vargas P. E., Meléndez-Zaragoza M. J., Collins-Martínez V., Thermodynamic analysis and process simulation of syngas production from methane using $CoWO_4$ as oxygen carrier, International Journal of Hydrogen Energy, 42(51), 30223–30236 (2017).

Paladino Lino A. V., Assaf E. M., Assaf J. M., X-ZrO_2 addition (X= Ce, La, y and Sm) on $Ni/MgAl_2O_4$ applied to methane tri-reforming for syngas production, Journal of CO_2 Utilization, 33, 273–283 (2019).

Vita A., Italiano C., Ashraf M. A., Pino L., Specchia S., Syngas production by steam and oxy-steam reforming of biogas on monolith-supported CeO2-based catalysts, International Journal of Hydrogen Energy, 43(26), 11731–11744 (2018).

Hetero-junction Catalysts for H_2-N_2 Cyclic Energy Storage with Artificial Solar N_2 Fixation

[1*]Bilge Coşkuner Filiz, [2]Korkut Açıkalın, [3]Hülya Civelek Yörüklü, [4]Murat Çalişkan, [5]Serço Serkis Yeşilkaya

[1]Department of Metallurgy and Materials Engineering, Yildiz Technical University, İstanbul, Türkiye
[2]Department of Energy Systems Engineering, Yalova University, Yalova, Türkiye
[3] Department of Environmental Engineering, Yildiz Technical University, İstanbul, Türkiye
[4] Department of Physics, Yildiz Technical University, İstanbul, Türkiye

*e-mail:coskuner@yildiz.edu.tr

Abstract

The ammonia (NH_3) with its capability of storing 19.65% of its mass in hydrogen (H_2) is prominent liquied medium to store H_2. The investigation of conversion atmospheric N_2 gas, comprising the majority of the atmosphere, into NH_3 compound via photocatalytic approaches using hetero-junction catalysts in solar simulated system forms the basis of our study, aimed at sustainable production of chemical energy storage environments based on green chemistry principles. NH_3 compound is capable of storing 19.65% of its mass in H_2 and its ability to be stored in liquid form under much milder conditions compared to H_2 emphasizes NH_3 as forefront energy storage agent. Rutile, when compared to various phases, demonstrates higher efficiency in converting N_2 to NH_3. The carbon nitride-(C_3N_4) structure, with N-sized voids similar to dinitrogen, is anticipated to exhibit high N_2 chemical sorption capability, potentially leading to elevate N_2 chemisorption from atmospheric mixtures and increased NH_3 selectivity.

Keywords: Hetero-junction, Catalyst, N_2 fixation, Artificial Solar

I. Introduction

In accordance with the Twelfth Development Plan, the significance of energy technologies has increased with the aim of meeting the growing energy demand through changing needs and sustainable sources to reduce the diverse global impacts of climate change and elevate the levels of alignment with global goals by developed and developing countries under the Paris Agreement. The "2030 Sustainable Development" agenda, unanimously adopted by the 193 member states of the United Nations, including Turkey, in 2015, has become a top priority for our country in the international arena, particularly in the aftermath of the crises caused by the COVID-19 pandemic in 2020 and the Russia-Ukraine war that started in 2022, for the construction of a sustainable and inclusive global economy based on effective and national energy systems. The European Green Deal, along with the goal of becoming the first climate-neutral continent by 2050, has necessitated the use of green and sustainable sources to meet energy needs. In light of these developments and expectations, the development of nature-based and eco-friendly technologies for the carbon-zero and self-reliant operation of energy production, storage, and consumption systems has gained importance. Particularly, to effectively meet the increasing energy demand, it is essential to develop technologies related to chemical energy storage environments for renewable and sustainable approaches, as indicated by references [1-3]. Nitrogen (N), one of the fundamental elements, constitutes 78% of the atmosphere in the form of nitrogen molecules (N_2) containing a triple covalent bond (N≡N). Upon examining the nitrogen cycle, atmospheric N_2 can be transformed into nitrogen oxides (NO, NO_2, N_2O) through natural processes such as lightning, radiation, and nitrogen-fixing bacteria converting it to ammonia (NH_3). Additionally, ammonia (NH_3) stands out as one of the most extensively produced chemicals due to its significance as a nitrogen source for fertilizers, a clean energy carrier, and a potential transportation fuel (owing to its high energy density and lack of CO_2 emissions) (Baltrusaitis, 2017; Dybkjaer, 1995; Ghavam et al., 2021). The investigation of the conversion of atmospheric N_2 gas, comprising the majority of the atmosphere, into NH_3 compound via photocatalytic approaches using floating hetero-junction catalysts in a solar simulated system forms the basis of our study, aimed at the sustainable production of chemical energy storage environments based on green chemistry principles. NH_3 compound is capable of storing 19.65% of its mass in H_2 and its ability to be stored in liquid form under much milder conditions compared to hydrogen emphasizes NH_3 as a forefront energy storage agent (Chatterjee et al., 2021).

II. Solar N_2 Fixation

NH_3, considered one of the most important green energy storage carriers, is primarily produced through the Haber-Bosch process, which operates at high temperature (300–500 °C) and pressure (150–300 atm) and results in the production of over 400 Mt of CO_2. Therefore, there is a necessity to produce NH_3 through environmentally friendly alternative methods for its use in power fuel cells in the energy sector in the near future, as highlighted by Zhang et.al.(2020) and Nguyen et.al.(2021). In nature, NH_3 can be produced through the photosynthesis process by microorganisms that perform photosynthesis under ambient temperature and atmospheric pressure conditions, phenomenon known as biological N_2 fixation (Zuburer, 2021; Chehade and Dincer, 2021). Developing photocatalytic processes for N_2 fixation and NH_3 production inspired by nature, specifically using artificial solar-energy, as

alternative to the Haber-Bosch process, aligns with European Union Green Deal action plan for transition to green and circular economy to be completed by 2050 without contributing CO_2 emissions (Zhang et al., 2020; Shi et al., 2020). From chemical reaction perspective, N_2 fixation is typical oxidation reaction with increasing nitrogen valence. Therefore, photo-generated holes in valence band of semiconductor are required to conduct photosynthesis of nitrate (Liu et al., 2019). Recently, it has been discovered that TiO_2-based white paint can produce nitrate from atmospheric-nitrogen under long sunlight exposure due to its photocatalytic reaction. To achieve this, semiconductor-like photocatalyst can be used to activate N≡N bond for direct nitrate synthesis and its breakdown (Yuan et al., 2013). The low solubility of N_2 in aqueous media restricts the fixation rate by limiting contact of N_2 with the catalyst. Using porous materials can significantly enhance diffusion kinetics of N_2 by providing active regions, adjusting surface hydrophilicity, and accelerating the photocatalytic reaction through mass transfer processes. Employing porous materials with a high specific surface area enhances adsorption process of N_2, promoting catalytic N_2 fixation ($N_2 + H_2O \rightarrow NH_3/(NH)^{+4}$) (Chen et al., 2018; Shi et al., 2019;). However, practical application of catalytic systems in homogeneous systems is challenging for recovery and may lead to secondary contamination. To address these issues, a proven method is to immobilize powder photocatalysts on different substrates such as glass plates, synthetic fabrics, or ceramic membranes. Nevertheless, traditional immobilization methods still experience shortcomings such as reduced surface area and weak adhesion to the photocatalyst (Dang et al., 2019).

III. Catalysts for Photocatalytic N_2 fixation

Upon reviewing the literature, it is evident that type-1 (Rong et al., 2018; Deythade et al., 2018;), type-2 (Wang et al., 2013; Hu et al., 2016; Vesali-Kermani et al., 2020), and z-scheme (Cao et al., 2017; Ai et al., 2020; Wu et al., 2019) heterostructured catalysts are employed for N_2 fixation. For the successful execution of photocatalytic N2 fixation, the catalyst to be utilized needs to consist of at least two catalytic structures with distinct oxidation and reduction capabilities (Lee et al., 2021). Following the photocatalytic N_2 fixation reaction, products such as NH_3, NH_2, NO_2, and NO_3 can be obtained, and the composition of heterostructured catalysts influences the products and efficiency obtained (Lee et al., 2021; Liv et al., 2019). A review of published studies on this topic indicates a general focus on powdered forms of catalyzers with photocatalytic properties, including g-C_3N_4, TiO_2 (Yuan et al., 2013;; Liu et al., 2018; Liu et al., 2019; Liang et al., 2017), and catalysts containing Fe found in the structure of biomolecules performing photosynthesis (Zeng et al., 2021; Li et al., 2018).

Although solar energy-based photocatalytic N_2 fixation is highlighted in the literature, the process efficiency remains below the targeted level due to factors such as low efficiency, limited light absorption, and the inability to determine suitable active compositions. Therefore, the development of photocatalysts capable of economically producing NH_3 from N_2 using solar radiation becomes crucial (Liu et al., 2019). To achieve high photocatalytic performance, proper design of the photocatalyst and the photoreaction system is essential to optimize proton/electron transfer, light absorption, charge separation, mass transport, adsorption, and activation. The N_2 fixation reaction involves reduction (NRR, N_2+3H2O → 1/4 2NH_3+ 3/2 O_2) and elevation (NOR, $2N_2 + 5O_2 + 2H_2O \rightarrow$ ¼ $4HNO_3$) redox reactions (Chen et al., 2021).

V. Conclusions

Research on photocatalytic N_2 fixation, particularly highlighted as a green and alternative process for NH_3 production, reveals several key findings. Various strategies have been developed to enhance the photocatalytic N_2 fixation properties of catalysts, including the introduction of defects, precision engineering, doping, co-catalytic, and hetero-junction structures. Notably, TiO_2, Fe_2O_3, and ZnO are recognized as leading catalysts for N_2 photofixation, attributed to their ability to increase N_2 solubility and enhance the endothermic reaction efficiency. However, a gap in research is identified concerning predominantly powder-based catalysts developed for N_2 fixation, with limited investigations on nanofiber-based heterojunction catalysts using solar simulation systems.

Acknowledgements

The authors gratefully acknowledge the financial support of TÜBİTAK for the following project; Grant no: 123M783

References

Ai, M., Zhang, J. W., Wu, Y. W., Pan, L., Shi, C., & Zou, J. J. 2020. “Role of vacancies in photocatalysis: a review of recent progress”, Chemistry–An Asian Journal, 15(22), 3599-3619.

Baltrusaitis, J. 2017. “Sustainable ammonia production”, ACS Sustainable Chemistry & Engineering, 5(11), 9527-9527.

Cao, Q., Kumru, B., Antonietti, M. and Schmidt, B.V. 2020. “Graphitic carbon nitride and polymers: a mutual combination for advanced properties”, Materials Horizons, 7(3), 762-786.

Chatterjee, S., Parsapur, R.K. and Huang, K.W. 2021. “Limitations of ammonia as a hydrogen energy carrier for the transportation sector.”, ACS Energy Letters, 6(12), 4390-4394.

Chehade, G. and Dincer, I., 2021. “Progress in green ammonia production as potential carbon-free fuel”, Fuel, 299, 120845.

Chen, G., Wong, N.H., Sunarso, J., Wang, Y., Huang, X., Xiong, X. and Wang, F., 2021. Characterization of BiOBr/g-C3N4 heterostructures immobilized on flexible electrospun polyacrylonitrile nanofibers for photocatalytic applications. Applied Surface Science, 569, p.151011.

Chen, S., Dong, L., Tianyou, P.. 2021. “Fundamentals and Recent Progress of Photocatalytic Nitrogen-Fixation Reaction over Semiconductors." Solar Rrl 5, 2, 2000487.

Dang, W., Wang, B., Xu, Z., Zhang, X., Li, F., Zhao, K., Hu, X. and Tang, Y., 2023. Pore structure, thermal insulation and compressive property of ZrO2 nanofiber aerogels with carbon junction fabricated by freeze drying. *Journal of Non-Crystalline Solids*, *600*, p.122031.

Deythade, V., Gupta, A., & Umare, S. S. 2018. “Graphitic carbon nitride− γ-gallium oxide (GCN-γ-Ga2O3) nanohybrid photocatalyst for dinitrogen fixation and pollutant decomposition”, ACS Applied Nano Materials, 1(10), 5581-5588.

Dong, G., Sun, G., Tian, G., Qi, S. and Wu, D., 2019. “Robust Polyimide Nanofibrous Membrane with Bonding Microstructures Fabricated via Dipping Process for Lithium-Ion Battery Separators”, Energy Technology, 7(7), 1801072.

Dybkjaer, I. 1995. “Ammonia production processes”, In Ammonia., Berlin, Heidelberg: Springer.

Ghavam, S., Vahdati, M., Wilson, I.A. and Styring, P. 2021. “Sustainable ammonia production processes”, Frontiers in Energy Research, 34.

J. Li, M. Zhang, X. Li, Q. Li, J. Yang, Effect of the calcination temperature on the visible light photocatalytic activity of direct contact Z-scheme g-C3 N4 -TiO2 heterojunction, Appl. Catal. B: Environ. 212 (2017) 106–114.

J. Liu, R. Li, X. Zu, X. Zhang, Y. Wang, Y. Wang and C. Fan, Chem. Eng. J., 2019, 371, 796–803.

Li, M., Huang, H., Low, J., Gao, C., Long, R., & Xiong, Y. 2019. “Recent progress on electrocatalyst and photocatalyst design for nitrogen reduction”, Small Methods, 3(6), 1800388.

Li, T., Xia, J., Chen, Q., Xu, K., Gu, Y., Liu, Q., Luo, Y., Guo, H. and Traversa, E., 2021. “Monodisperse Cu Cluster-Loaded Defective ZrO2 Nanofibers for Ambient N2 Fixation to NH3”, ACS Applied Materials & Interfaces, 13(34), 40724-40730.

Liang, Z., Ba, G., Li, H., Du, N. and Hou, W., 2020. Facile synthesis of silicon-doped polymeric carbon nitride with enhanced photocatalytic performance. *Journal of Alloys and Compounds*, *815*, p.152488.

Liu, Y., Cheng, M., He, Z., Gu, B., Xiao, C., Zhou, T., Guo, Z., Liu, J., He, H., Ye, B. and Pan, B. 2019. “Pothole-rich ultrathin WO3 nanosheets that trigger N≡ N bond activation of nitrogen for direct nitrate photosynthesis.”, Angewandte Chemie International Edition, 58(3), 731-735.

Nguyen, D.L.T., Tekalgne, M.A., Nguyen, T.H.C., Dinh, M.T.N., Sana, S.S., Grace, A.N., Shokouhimehr, M., Vo, D.V.N., Cheng, C.K., Nguyen, C.C. and Kim. S.Y. 2021. “Recent development of high-performance photocatalysts for N2 fixation: A review.”, Journal of Environmental Chemical Engineering, 9(1), 104997.

Rong, X., Mao, Y., Xu, J., Zhang, X., Zhang, L., Zhou, X., ... & Wu, Z. 2018. “Bi2Te3 sheet contributing to the formation of flower-like BiOCl composite and its N2 photofixation ability enhancement”, Catalysis Communications, 116, 16-19.

Shi, R., Zhang, X., Waterhouse, G.I., Zhao, Y. and Zhang, T. 2020. “The journey toward low temperature, low pressure catalytic nitrogen fixation.”, Advanced Energy Materials, 10(19), 2000659.

Vesali-Kermani, E., Habibi-Yangjeh, A., Diarmand-Khalilabad, H., & Ghosh, S. 2020. “Nitrogen photofixation ability of g-C3N4 nanosheets/Bi2MoO6 heterojunction photocatalyst under visible-light illumination”, Journal of colloid and interface science, 563, 81-91.

Wu, G., Yu, L., Liu, Y., Zhao, J., Han, Z., & Geng, G. 2019. “One step synthesis of N vacancy-doped g-C3N4/Ag2CO3 heterojunction catalyst with outstanding “two-path” photocatalytic N2 fixation ability via in-situ self-sacrificial method”, Applied Surface Science, 481, 649-660.

Yuan, S. J., Chen, J. J., Lin, Z. Q., Li, W. W., Sheng, G. P., & Yu, H. Q. 2013. “Nitrate formation from atmospheric nitrogen and oxygen photocatalysed by nano-sized titanium dioxide”, Nature Communications, 4(1), 1-7.

Zhang, G., Sewell, C.D., Zhang, P., Mi, H. and Lin, Z., 2020. “Nanostructured photocatalysts for nitrogen fixation”, Nano Energy, 71, 104645.

Zhang, Suyun, et al. Synthesis of boron-doped g-C_3N_4 with enhanced electro-catalytic activity and stability. Chemical Physics Letters, 2017, 672: 26-30.

Zhang, Y., Mao, F., Yan, H., Liu, K., Cao, H., Wu, J., & Xiao, D. 2015. “A polymer–metal–polymer–metal heterostructure for enhanced photocatalytic hydrogen production”, Journal of Materials Chemistry A, 3(1), 109-115.

Zheng, J., Lu, L., Lebedev, K., Wu, S., Zhao, P., McPherson, I.J., Wu, T.S., Kato, R., Li, Y., Ho, P.L. and Li, G. 2021. “Fe on molecular-layer MoS2 as inorganic Fe-S2-Mo motifs for light-driven nitrogen fixation to ammonia at elevated temperatures”, Chem Catalysis, 1(1), 162-182.

Zheng, X., Zhang, Z., Li, X. and Ding, C., 2019. “MnO–carbon nanofiber composite material toward electro-chemical N 2 fixation under ambient conditions”, New Journal of Chemistry, 43(21), 7932-7935.

Zheng, Z., Wu, L., Han, Y., Chen, J., Zhu, S., Yao, Y., ... & Li, L. 2022. “Gut microbiota-controlled tryptophan metabolism improves D-Gal/LPS-induced acute liver failure in C57BL/6 mice”, Engineering, 14, 134-146.

Zuberer, D.A. 2021. “Biological dinitrogen (N2) fixation: introduction and nonsymbiotic”, In Principles and applications of soil microbiology, 423-453.

Electronic References

[1] Türkiye Cumhuriyeti Cumhurbaşkanlığı Strateji ve Bütçe Başkanlığı 11. Kalkınma Planı, https://www.sbb.gov.tr/wp-content/uploads/2022/07/On_Birinci_Kalkinma_Plani-2019-2023.pdf

[2] Birleşmiş milletler Raporu, https://www.un.org/annualreport/index.html

[3] Avrupa Birliği Yeşil Mütabakatı, https://climate.ec.europa.eu/eu-action/european-green-deal_en

$CeCoO_3$ as an effective catalyst support for Ni in methane reforming reactions

Atalay Calisan, Deniz Uner*
Chemical Engineering Department, Middle East Technical University, 06800 Ankara, Türkiye

* e-mail: uner@metu.edu.tr

Abstract
A perovskite catalyst support with oxygen pumping capacity, $CoCeO_3$, is developed to compensate for the deficiency in oxygen chemical potential of the reactants in steam reforming and dry reforming of methane reactions. Our results indicated that it is possible to provide sufficient amount of oxygen through the catalytic material such that carbon growth is inhibited. Furthermore, it was demonstrated that intermittent and very short excursions of steam or carbon dioxide can compensate for the needed oxygen chemical potential, further assisting to protect the stability of the catalyst against coke deposition.

Keywords: methane steam reforming, methane dry reforming, perovskite, coke management

I. Introduction

Methane reforming is a major industrial process for hydrogen production. Although reforming is a well-established technology, the overall process still suffers from problems such as heat and mass transfer limitations as well as coke deposition (Luisetto et. Al, 2017; Arora and Prasad, 2016). The thermochemical information for main reforming reactions reveal clearly that these reactions are nonspontaneous under ambient conditions. Elevated temperatures (>891 K for steam methane reforming (SMR) and >915 K for dry reforming of methane (DRM)) are needed for these reactions to become thermodynamically favorable. Due to the constraints imposed by thermodynamics, steam (SMR) and dry (DRM) reforming reactions are energy intensive reactions (Mueller-Langer et al 2007). High temperatures are needed to operate under thermodynamically favorable conditions (Nikkoo and Amin, 2011; Carapelluci and Giordano, 2020). The industrial reactors operate at temperatures between 800 °C to 1000 °C at 20-30 bars (Rostrup-Nielsen and Rostrup-Nielsen, 2016) . Higher conversions are reachable at lower temperatures for high steam to carbon ratios (Figure 1b). However, using excess steam has certain drawbacks such as reactor size and low hydrogen concentration. Steam to carbon ratios lower than 2.5 are generally desired for economically viable hydrogen production (Rostrup-Nielsen et al., 2002). CO/H_2 ratio is controlled by the contribution of water-gas shift reaction. Furthermore, higher CO selectivity is achieved at high temperatures by suppressing Boudouard reaction, $2CO \rightleftharpoons CO_2+C$. Carbon deposition is an important side reaction in reforming process since metals used for catalytic activity of reforming also enhances the carbon formation (Rostrup-Nielsen, 1997; Leung et al., 2020; Ay and Uner, 2015).

II. Experimental Set-up and Procedure

$CeCoO_3$ perovskites are synthesized by using Pechini sol-gel method. Appropriate amounts of precursors $Co(NO_3)_2.6H_2O$ and $Ce(NO_3)_3.6H_2O$ were dissolved in deionized water. The aqueous solutions of metal nitrates were mixed under continuous stirring. Citric acid solution was prepared in a separate beaker to achieve a molar ratio of total metal ions to citric acid 1:2. After complete dissolution of precursors, citric acid was added to the solution slowly at constant stirring. The final solution was mixed to give complexation for about 1h at room conditions. Thereafter, the temperature of solution was set to 50 °C for gelation process. The gel was further treated at 110 °C for 8 h. The formed cake was ground in an agate mortar. $CeCoO_3$ was obtained by calcination at 350 °C for 3h followed by 650 °C for 5 h. The full characterization of the catalysts was performed through temperature programmed analysis by using Micromeritics Chemisorp 2720. The reactive gases were 10% H2 in Ar (Linde) for TPR, 2% O2 in He (Linde) for TPO, and 99.999% He (Linde) for TPTD. Philips model PW1840 (1729) X-ray diffractometer was used to measure XRD patterns using Ni filtered Cu-Kα 945 radiation at a scan rate of 0.05 degrees/s . XRD, Phenom ProX Desktop SEM with integrated EDS was used for morphology analysis. Gold coated samples were analyzed by high sensitivity multi-mode back scattering detector (15kV).
The reaction test were proformed in a home built system. Catalysts in powder form was loaded into a 6mm OD quartz reactor and supported by quartz wool from both sides. The packing zone was 3 cm long in the middle of a 60cm long tube. The experimental setup was previously described inCalisan et al. (2019). Balzers Prisma QME 200 mass spectrometer (MS) from Pfeiffer Vacuum was used for product gas analysis during dynamic experiments. This electric quadrupole (24V, 2A) MS is able to scan the mass to charge ratios within the range of 1-100amu. Tungsten filament was used as an ion source. Sample chamber pressure was monitored with vacuum gauge (Pfeiffer Inficon PKR 251) transmitter which is connected to Inficon Single Gauge readout. The required vacuum was sustained $<10^{-5}$ torr throughout all experiments.

III. Analysis

A Gibbs free energy minimization method was used to estimate the effect of temperature and oxidizer/methane ratios on equilibrium conversion of methane. The results presented in Figure 1 clearly reveal the favorable effect on the oxidizer amounts on the equilbirum conversions. At higher oxidizer to methane ratios, the reaction is favorable at lower temperatures. Steam is a better oxidizer under both 30 and 3 oxidizer to methane ratios. The compensation for higher oxidizer methane ratios can be provided by another oxygen source. In order to compensate for the local oxygen fluctuations, a catalyst is proposed that can provide oxygen flux to the intrmediates can aid the suppression of undesired coke build-up during the reforming reactions. This catalyst benefits from the facile oxygen excahnage charaxcteristics of oxides of both Co and Ce. The perovskite structure enables a structural stability with facile oxygen transfers. The reduction and oxidation characteristics of these materials were fully characterized by temperature programmed reduvtion and temperature programmed oxidation measurements. Their reducibility were calculated and are given in Table 1.

Table 1 Degree of reducibility of studied catalysts up to 850 °C

Catalysts	Atomic Oxygen Balance (per g catalyst)		Reduction Extent
	Expected H_2 Consumption amount (mmol)	Measured Consumption by TPR (mmol)	
13 wt. % Ni-Al_2O_3	27.8*	3.5	100% (Ni only)
$CeCoO_3$	12.1	7.5	62.1%
5 wt. % Ni-$CeCoO_3$	12.4	10.4	83.6%
Co_3O_4	16.6	16.6	100.0%
CeO_2	11.6	1.9	16.0%

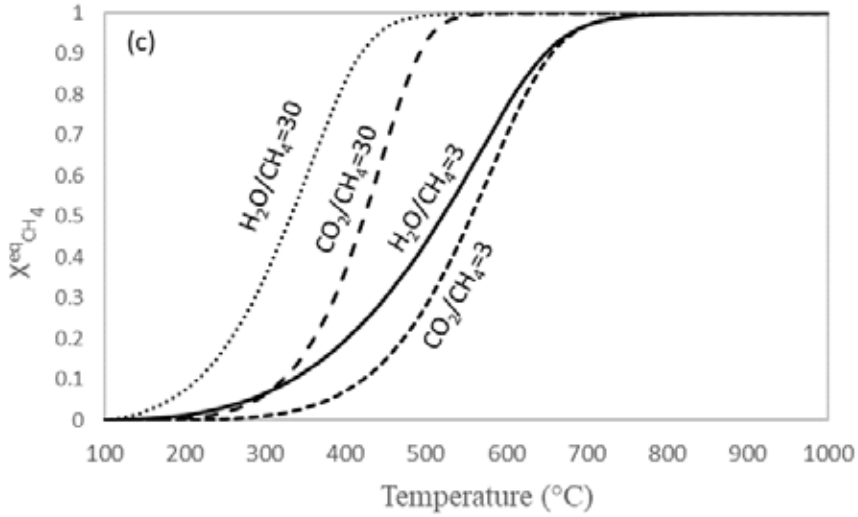


Fig.1: The effect of temperature, H_2O/CH_4 and CO_2/CH_4 ratios on methane equilibrium conversion during SMR and DRM

The dry reforming performance of $CeCoO_3$,13 wt. % Ni-Al_2O_3 and 5 wt. % Ni-$CeCoO_3$ are shown in Figure 2. All catalysts were reduced under 10%H_2-Ar up to 700 °C (10 °C/min). Following to the reduction, the reactor was swept up to 800 °C. The composition of reactants was kept constant at 10% CH_4, 10% CO_2 balanced with Argon. After the activation step, CO and H_2 amounts dropped around 14mins and gradually increased as reaction proceeds for Ni-$CeCoO_3$. However, syngas composition gradually decreased as the reaction proceeds. A low reforming activity was observed for $CeCoO_3$ unlike the superior activity for Ni-Al_2O_3.

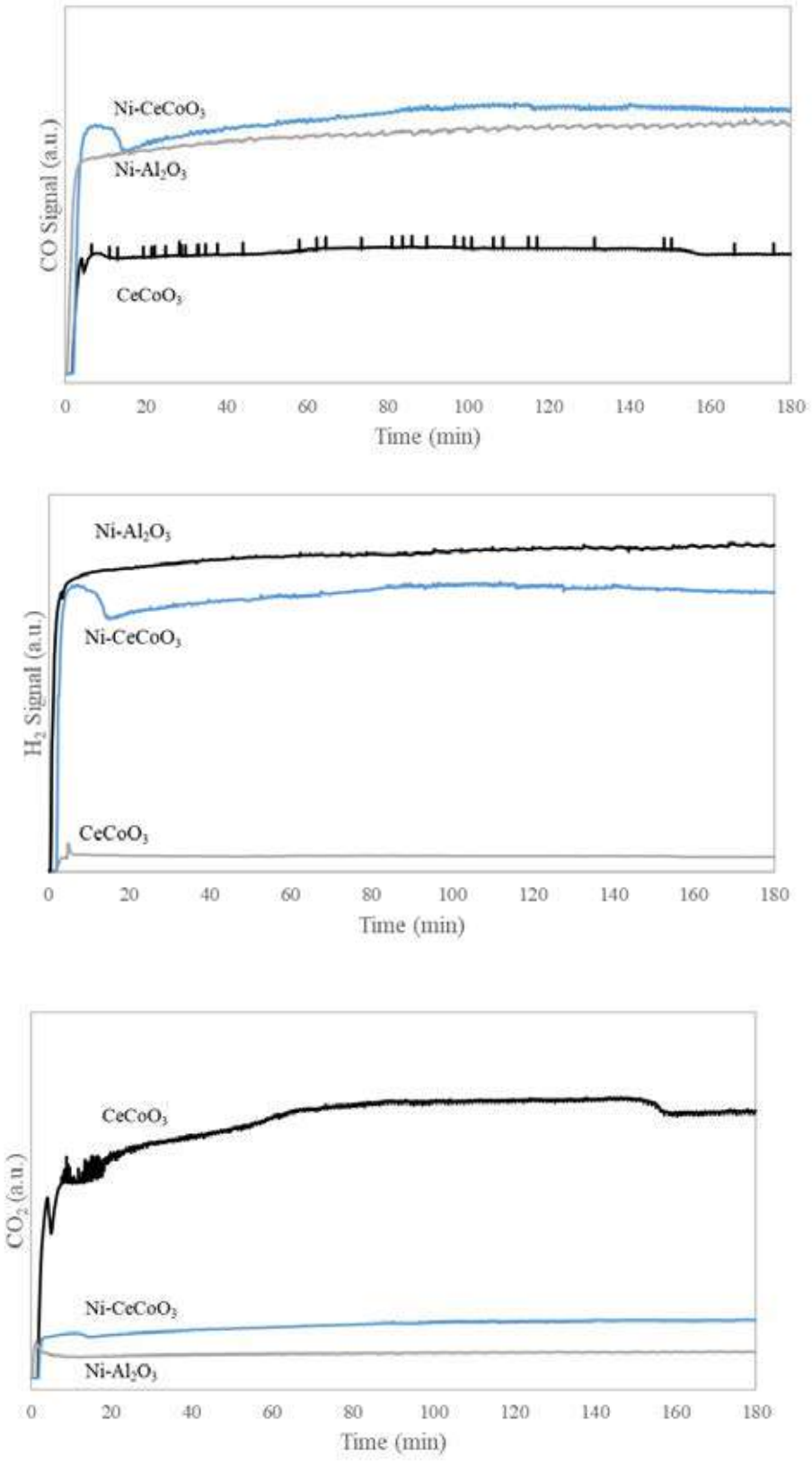


Fig. 2: Carbon monoxide, hydrogen, and carbon dioxide profiles during DRM reaction over $CeCoO_3$ and Al_2O_3 supported Ni catalysts. The activity of Ni free $CeCoO_3$ is also reported.

V. Conclusions

The advantage of the proposed process lies in the following facts. In order to maintain a favorable oxygen chemical potential, steam reformers are operated at high steam to methane ratio. Since steam is a condensable material, it is possible to separate unreacted steam from syngas at the exit of the reactors. However, the same strategy cannot be applied to CO_2, the excess CO_2 needed to maintain sufficient oxygen chemical potential to inhibit carbon build up will remain in syngas. Here we propose that a reducible oxide support can maintain oxygen chemical potentials needed for sufficient CO formation rates and can inhibit coke build up. The oxygen depleted from the support, however, needs to be periodically replenished by periodic pulses of oxidizers, such as CO_2 or H_2O.

Acknowledgements
The authors acknowledge partial financial support from TUBITAK 1003 program under grant no 213M006. A.Ç., acknowledges partial financial support through TUBITAK 2211 program.

References

Arora, S. and Prasad, R An overview on dry reforming of methane: Strategies to reduce carbonaceous deactivation of catalysts, *RSC Adv.*, vol. 6, no. 110, pp. 108668–108688, (2016), doi: 10.1039/c6ra20450c.

Ay, H.; and D. Üner, "Dry reforming of methane over CeO2 supported Ni, Co and Ni–Co catalysts," *Appl. Catal. B Environ.*, vol. 179, pp. 128–138, Dec. 2015, doi: 10.1016/j.apcatb.2015.05.013.

Calisan, A. ; C. G. Ogulgonen, A. Yilmaz, D. Uner, and S. Kincal, "Steam Methane Reforming Over Structured Reactors Under Concentrated Solar Irradiation (Accepted Manuscript)," *Int. J. Hydrogen Energy*, vol 44, 18682-18693 (2019), 10.1016/j.ijhydene.2019.04.033

Carapellucci, R. and L. Giordano, Steam, dry and autothermal methane reforming for hydrogen production: A thermodynamic equilibrium analysis *J. Power Sources*, vol. 469, no. May, p. 228391, (2020), doi: 10.1016/j.jpowsour.2020.228391.

Leung, S. L.; S. L., J. Wei, W. L. Holstein, M. Avalos-Borja, and E. Iglesia, "Dynamics and Mechanism of Carbon Filament Formation during Methane Reforming on Supported Nickel Clusters," *J. Phys. Chem. C*, 2020, doi: 10.1021/acs.jpcc.0c05590.

Luisetto I. *et al.*, Ni supported on γ-Al2O3promoted by Ru for the dry reforming of methane in packed and monolithic reactors, *Fuel Process. Technol.*, vol. 158, pp. 130–140, (2017), doi: 10.1016/j.fuproc.2016.12.015.

Mueller-Langer, F.; E. Tzimas, M. Kaltschmitt, and S. Peteves, Techno-economic assessment of hydrogen production processes for the hydrogen economy for the short and medium term, *Int. J. Hydrogen Energy*, vol. 32, no. 16, pp. 3797–3810, Nov. (2007), doi: 10.1016/J.IJHYDENE.2007.05.027.

Nikoo, M. K. ; and N. A. S. Amin, "Thermodynamic analysis of carbon dioxide reforming of methane in view of solid carbon formation," *Fuel Process. Technol.*, vol. 92, no. 3, pp. 678–691, (2011), doi: 10.1016/j.fuproc.2010.11.027.

Rostrup-Nielsen, J. R. and T. Rostrup-Nielsen, "Large-scale hydrogen production," *Cattech*, vol. 6, no. 4, pp. 150–159, (2002) Accessed: Jul. 05, 2016. [Online]. Available: http://link.springer.com/article/10.1023/A:1020163012266.

Rostrup-Nielsen, J. R. ; J. Sehested, and J. K. Nørskov, "Hydrogen and synthesis gas by steam- and C02 reforming," *Adv. Catal.*, vol. 47, pp. 65–139, (2002), doi: 10.1016/S0360-0564(02)47006-X.

Rostrup-Nielsen, J. R. Industrial relevance of coking *Catal. Today*, vol. 37, no. 3, pp. 225–232, (1997), doi: 10.1016/S0920-5861(97)00016-3.

A Solar Integrated System with a New Hydrogen Generator

[1*] Mehmet Gursoy and Ibrahim Dincer.
[1]Clean Energy Research Laboratory (CERL), FEAS, Ontario Tech University, Oshawa, Ontario, L1H 7K4, Canada

E-mail: mehmet.gursoy@ontariotechu.net

Abstract
The primary objective of this research is to examine the integrated power process that harnesses solar power for several purposes, including electricity generation, freshwater production, and hydrogen synthesis. The proposed research entails the incorporation of various elements, such as a solar through collector system, a combination of power cycles (steam and organic Rankine cycle), a multi-effect desalination (MED) unit, a distinctive hybrid electrolyzer system, a wave energy system, and a hydrogen storage and refuelling station. The generated electricity served some purposes, functioning as both a power source for hydrogen synthesis and meeting the electrical needs of the surrounding population. Thermodynamic assessment is used to evaluate the effectiveness of the system being studied. The annual power amount was found to be 166,818,848 kWh by the power cycles. The energy efficiency of solar-driven power cycles is 12.71%, whereas the exergy efficiency is 13.39%. The hybrid hydrogen reactor produces 1953 mL/h.

Keywords: Solar energy, renewable energy, wave energy, hydrogen production, hybridized water electrolysis

I. Introduction

Hydrogen is a feasible and environmentally friendly energy substitute that holds promise for a more environmentally conscious future. The fact that it is readily accessible and produces less pollution when burned makes it a very promising alternative to traditional fossil fuels. Nevertheless, the process of generating hydrogen in a manner that is both environmentally friendly and efficient has significant challenges. Electrolysis systems have historically been used for hydrogen production, but their energy consumption has limited their widespread adoption. Photochemical-conventional hybrid electrolysis is going to alter the process of hydrogen production. A photochemical-conventional hybridized hydrogen generator is a procedure that combines solar technology with traditional electrolysis to enhance the efficiency of hydrogen production.

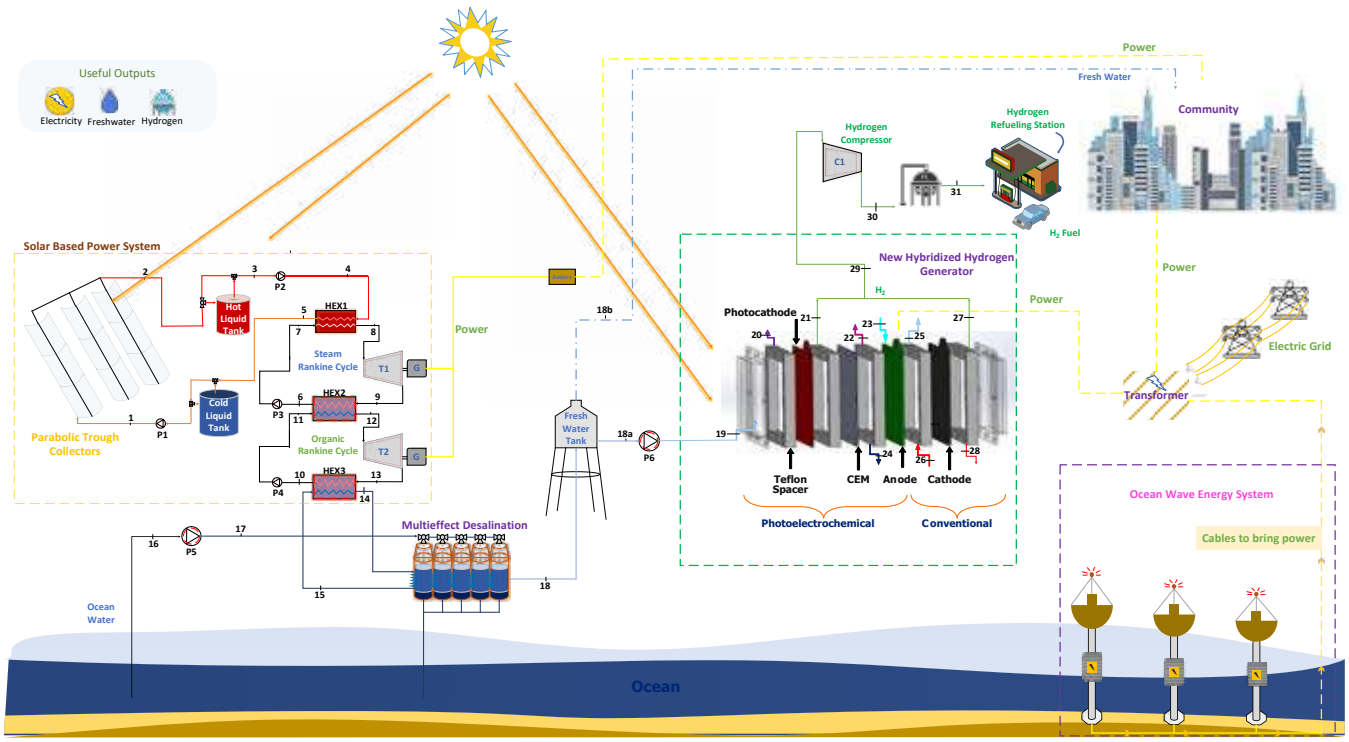


Fig.1: A schematic of the proposed system's layout

Karaca and Dincer (2023) developed a novel photoelectrochemical reactor that utilizes a distinct mesh conic photoelectrode shape for the purpose of solar-assisted hydrogen generation. The reactor undergoes electrochemical experiments under many situations, including both illuminated and non-illuminated conditions, to accurately assess its performance. In another study, a photoelectrochemical reactor was constructed by Aydin, Selcuk, and Dincer (2022) to investigate its efficacy in treating textile wastewater and recovering sodium hydroxide. The reactor is a combination of some features found in photoelectrochemical cells and the electrodialysis process.

The fundamental concept behind photoelectrochemical-conventional hybrid electrolysis is to employ photovoltaic cells, which harness solar energy, to provide the necessary electrical current for the process of electrolyzing water. An area that shows promise for the sustainable production of hydrogen over an extended period is the investigation of photoelectrochemical processes. The field of photoelectrochemical (PEC) technology exhibits the potential to expedite the transition towards a more environmentally friendly and enduring energy infrastructure, owing to continuous research and development endeavours. To accomplish this, numerous issues may be addressed, and the characteristics of the materials used in the technology can be enhanced. The primary objective of the project is to develop a hybrid electrolyzer that fulfils certain criteria to enhance the efficiency of hydrogen generation. Additionally, the objective encompasses ensuring the system's continuous operation even in the absence of solar power.

II. System Description

Figure 1 depicts the schematic structure of the proposed system. The energy and exergy analyses of the proposed system were conducted using the EES (Engineering Equation Solver) software program, while the solar system and wave energy system were analyzed using System Advisor Model (SAM) software. The study is on the design of hydrogen production with a particular emphasis on achieving high efficiency across many scenarios. Furthermore, the solar system supplies the designated community with both power and fresh water. The electricity is generated using wave energy and is used to meet the energy demands for hydrogen production. Utilizing the photoelectrochemical-conventional hydrogen production system offers a great prospect for sustainable and eco-friendly generation of hydrogen. Furthermore, it facilitates the production of hydrogen from water by harnessing the electricity supplied by the combined cycle. Afterwards, the produced hydrogen is transferred to a storage tank, while the hydrogen refuelling station enables the delivery of services to the community.

The reactor consists of two separate electrolysis cells: the photoelectrochemical cell and the conventional cell. The PEC consists of three main components: an anode, a cation exchange membrane, and a photocathode. The essential aspect of the research is the shared anode for both cells. The anode electrode type was determined to be a bipolar plate because of the two active surfaces in the electrolysis. Three distinct electrolytes ($NaCl_{sat}$, fresh water from the MED unit, KOH) are used. In addition, the membrane functions to neutralize the presence of OH^- ions in the cathode compartment by selectively allowing the flow of Na^+ ions from the anode to the cathode partition. The reactor is fitted with clear windows to enable the irradiation of the photocathode. The following equation may describe the chemical process of hydrogen production in the hybrid electrolyzer:

For the PEC cell:

$$Overall\ reaction = 2H_2O + 2NaCl \rightarrow H_2 + Cl_2 + 2NaOH \quad (1)$$

$$Anode = 2Cl^- \rightarrow Cl_2 + 2e^- \quad (2)$$

$$Photocathode = 2H_2O + 2e^- \rightarrow H_2 + 2OH^- \quad (3)$$

For the conventional cell:

$$Overall\ reaction = 2H_2O \rightarrow 2H_2 + O_2 \quad (4)$$

$$Anode = 2H_2O \rightarrow O_2 + 4OH^-_{aq} + 4e^- \quad (5)$$

$$Cathode = 4OH^-_{aq} + 4e^- \rightarrow 2H_2 + 2H_2O \quad (6)$$

The equations given below are used to calculate the comprehensive energy and exergy efficiencies of the system respectively:

$$\eta_{overall} = \frac{\dot{m}_{18b}h_{18b} + \dot{m}_{29}LHV_{H_2} + W_{net}}{\dot{Q}_{in PT} + W_{in wave}} \quad (7)$$

and

$$\psi_{overall} = \frac{\dot{m}_{18b}ex_{18b} + \dot{m}_{29}(ex_{29} + ex^{ch}_{H_2}) + W_{net}}{Ex^{\dot{Q}_{in PT}} + W_{in wave}} \quad (8)$$

III. Results and Discussion

The solar trough plant and wave energy plant that make up the planned system each have a power output capacity of 19 MW and 6.7 MW, respectively. Eureka, California, USA, is the subject of a case study involving 26,489 inhabitants. Considering the geographic characteristics, climatic circumstances, community support, and energy needs, Eureka is a suitable location for hosting a wave energy and solar trough system. During an average climatic year, a total of 290 gigawatt-hours (GWh) of electricity is required. The solar trough collectors have access to an annual solar radiation of 1478.25 kWh/m^2. Conversely, the town of Eureka in the USA experiences an average wind speed of 4.2 m/s at a height of 100 m. Figure 2 depicts the total amount of power generated during a standard meteorological year. The annual power amount was found to be 166,818,848 kWh. The energy and exergy efficiencies of solar-driven power cycles are determined to be 12.71% and 13.39%, respectively. The intensity of

solar radiation rises during the summer months and fluctuates throughout the day. Consequently, solar power systems are able to absorb a greater amount of solar energy.

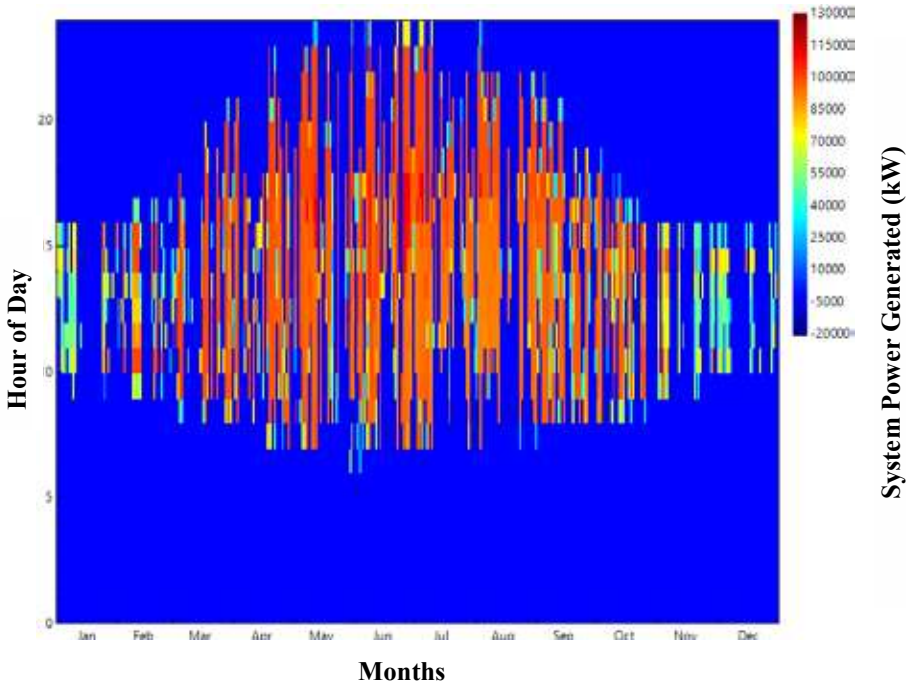


Fig. 2: System power produced over a year (kW)

By implementing integrated systems with power cycles, it is possible to effectively absorb and store energy, resulting in a significant increase in electricity output. Maximizing solar power generation requires optimizing system design and leveraging storage technology. A hybridized hydrogen reactor can produce 1953 mL/h of hydrogen.

IV. Conclusions

The suggested system optimizes the use of renewable sources by combining solar and wave resources and incorporating solar-powered cycles with a unique hydrogen generator. Maintaining a consistent energy supply is crucial, necessitating the use of several backup systems. On an annual basis, a total of 290 GWh of power is needed during a typical climatic year. The solar trough collectors get a yearly solar radiation of 1478.25 kWh/m^2. The yearly power quantity was determined to be 166,818,848 kWh. Solar-driven power cycles exhibit energy and exergy efficiencies of 12.71% and 13.39%, respectively. The sun's radiation strength increases throughout the summer months and varies throughout the day. As a result, solar power systems have the capacity to capture a larger quantity of solar energy. The hybrid hydrogen reactor generates 1953 mL/h.

References

Aydin, Muhammed Iberia, Huseyin Selcuk, and Ibrahim Dincer. 2022. “A Photoelectrochemical Reactor for Ion Separation and Hydrogen Production.” *Energy* 256 (October): 124641. https://doi.org/10.1016/j.energy.2022.124641.

Karaca, Ali Erdogan, and Ibrahim Dincer. 2023. “Design and Experimental Investigation of a New Photoelectrochemical Reactor for Green Hydrogen Production.” *Chemical Engineering Science* 265 (January): 118181. https://doi.org/10.1016/j.ces.2022.118181.

De-noising of a Fuel Cell Hybrid Microgrid, including Energy Generation, Consumption, and Storage Units

[1]Sıtkı Akkaya, [1]Mehmet Güçyetmez, [2]Murat Uyar, [2*]Şekip Esat Hayber
[1] Sivas University of Science and Technology, Department of Electrical-Electronic Engineering, Sivas, 58140, Türkiye
[2] Bursa Uludağ University, Department of Electrical-Electronic Engineering, Bursa, 16059, Türkiye

*sehayber@uludag.edu.tr

Abstract
Microgrids containing hybrid energy sources are rapidly becoming widespread. On the other hand, innovative energy components such as fuel cells are also integrated into microgrid structures. However, these energy systems are affected by various environmental noises called white noise. In this study, a de-noising process was carried out for a microgrid where solar energy and a battery management system, including fuel cells, were used in addition to traditional synchronous generator generation. In addition to the structural noises produced by the system, noises occurring in the external environment were modeled, and noise reduction was carried out and evaluated statistically.

Keywords: Microgrid, fuel cell, de-noising

I. Introduction

Developing and diversifying electrical energy production techniques, especially in the last ten years, has led to producing energy on-site, consuming it on-site, storing the remaining energy, and using it later (Kyriakopoulos and Arabatzis, 2016). Thus, whenever there is any technological development regarding energy, it is tried to be adapted to the current energy system so that energy can be used optimally in different places with different geographical features (Yeo and Yee, 2014). Considering the sources from which hydrogen is obtained, it is one of the most potential resources on earth. Therefore, it is inevitable that fuel cells that use hydrogen energy will take part in future energy systems, just like PV panels do today (Winter, 2009). Studies involving fuel cells are being developed and continue to be developed (Behling, 2012). In this context, the development of fuel cells within microgrid structures is also essential because most geographies of the earth are far from the main grid or technically do not have the opportunity to connect to the main grid.

Additionally, working independently from the main grid is recommended to put less load on the grid (Vandoors et al., 2010). On the other hand, microgrids containing various energy sources, including fuel cells, are exposed to various disruptive external effects (Akinyele, 2020). One of these is white noise effects, manifesting with variables such as rain, temperature, and machine noise. These disruptive components are structurally present in the energy system. If not intervened, they will harm the economic life of the devices in the energy system and the switching patterns of the system (Demir and Sangiovanni-Vincentelli, 2012). The main contributions of this paper are summarized as follows:

- A complete microgrid structure with production, consumption, storage, and control units was considered,
- White noise was added to the structural noise of this structure, and noise filtering was performed for the situation where the noise occurred.
- By applying the continuous wavelet transform (CWT) to the noised and de-noised signals, it can be seen that the white noise-induced anomalies occurring in microgrid switching were reduced.

II. Experimental Set-up and Procedure

The microgrid system shown in Fig. 1a, developed by (Dudgeon G., 2024) and published in Mathworks (Mathworks, 2022), abbreviated as FC-MG in this study, was examined. In the microgrid, two fuel cells, PV Array and Battery, form the DC system, and two AC Generators and active and reactive loads constitute the AC part. While converters make the DC/AC connection, the load flow in the system is operated predominantly on the DC side and is controlled by the Power Transfer Management System. It is stated that the system has the components in Fig. 1b and is based on renewable energy, hydrogen technology, microgrid, storage, and power conversion. MPPT method was used to control PV panels.

The power management is designed to facilitate DC power transfer when AC active power demand or PV power exceeds 8 MW, limit power transfer to 1.5 MW, and direct power to the battery when the power provided from PV arrays and fuel cells exceeds 500 kW.

More detailed information about Simulink blocks in the system can be obtained from (Mathworks, 2022). In this study, since it is a hybrid energy system that includes production, consumption, energy conversion, and fuel cell, such a comprehensive power system was preferred for noise analysis and de-nosing process. The study examined all the components that make up the energy system, and then the system-related degradations were focused on. Although some disturbances are mentioned in the model, modeled white noise is not addressed. As another step, 20 dB white noise was added to the system. The system's responses to noise were examined. Then, de-noising was performed, and finally, statistical values were obtained for the signals obtained due to the noisy and de-noising process.

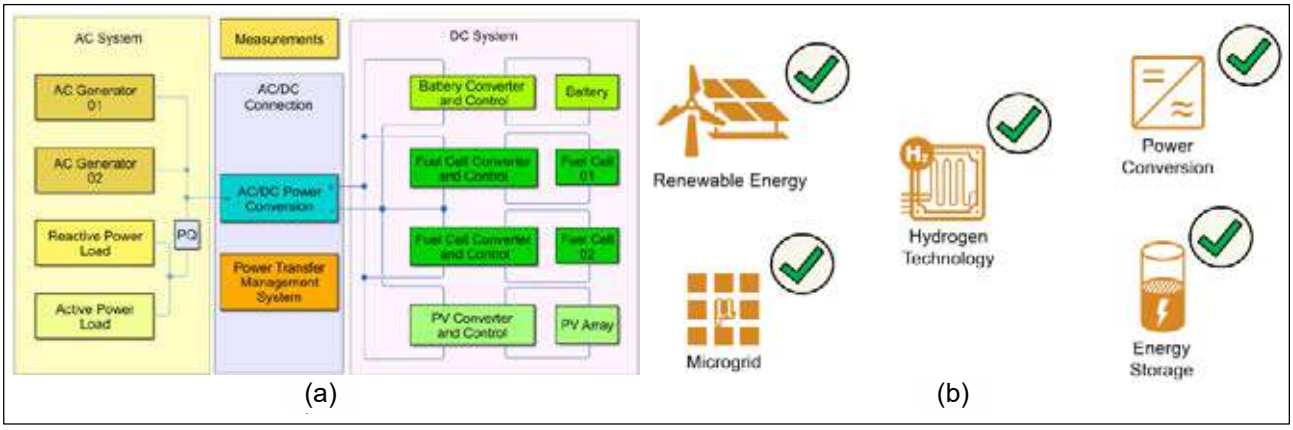


Fig. 1: (a) Experimental Fuel Cell Microgrid Simulink schematic of the proposed study, (b) Components consisting of the FC-MG system (Dudgeon G., 2024)

III. Analysis

The fundamental model describing the noisy signal can be expressed as follows:

$$s(n) = f(n) + \sigma e(n) \tag{1}$$

where time *n* is evenly distributed, in a basic scenario, assume *e*(*n*) follows a Gaussian white noise distribution *N*(0,1), with noise level *σ* set to 1. The primary objective of de-noising is attenuating the noise component within the signal s(n) and recovering the underlying function *f*. The de-noising process encompasses three main stages:

a. Decomposition

Select a wavelet and a level N, then compute the wavelet decomposition of the signal $s(n)$ at level N. Common wavelet types include Daubechies, symlets, coiflets, and biorthogonal wavelets.

b. Detail Coefficients Thresholding

For each level from 1 to *N*, determine a threshold and apply soft thresholding to the detail coefficients. Most coefficients contribute noise with variance σ^2, while only a few contribute to the signal. Estimating σ^2 involves calculating a robust estimator from the median of wavelet coefficients. This median (*M*) is independent of the magnitude of large-magnitude coefficients related to the signal, unlike the mean value. In the case of zero mean and variance σ_0^2, Eq. 2 can be seen,

$$E\{M\} = 0.6745\sigma_0 \tag{2}$$

The estimated noise variance $\tilde{\sigma}$ is obtained from the median M_x of absolute wavelet coefficients as the following.

$$\tilde{\sigma} = \frac{M_X}{0.6745} \tag{3}$$

Despite the influence of piecewise smooth signal *f* on M_x being negligible, the soft threshold estimator $\widetilde{F}$ remains at least as regular as the original signal *f*, albeit with slightly differing magnitudes due to smaller wavelet coefficients. Contrastingly, hard thresholding preserves coefficients with amplitudes above a threshold *T*, inducing errors manifesting as oscillations or ripples near irregular points. The initial data comprises a pulse signal and a sinusoidal component, encompassing both piecewise smooth and irregular segments. Coiflet 2 wavelets are utilized for coefficient calculation.

The variance σ^2 of white noise is determined using $\tilde{\sigma}$ and the threshold is set to $T = \sqrt{2log_e N}$.

c. Reconstruction

Perform wavelet reconstruction using the original approximation coefficients of level *N* and the modified detail coefficients from levels 1 to *N* (Luo et al., 2012).

IV. Results and discussions

In Fig. 2 and 3, real-time signal, noise power spectrum, and continuous wavelet transform (CWT) graphs showing the weight of signal and noise power as changing from yellow to turquoise for noisy and de-noising signals are given, respectively. The yellow color in CWT charts indicates the required fundamental component. The power

increases from turquoise to yellow. A noisy signal with a basic amplitude of 6000 V was applied to the data received from the FC-MG, and its power is around 75 dB in 0.02 s, as seen in Fig. 2b. After 0.02 s, a 20 dB noise continues throughout the signal. From the CWT graph of the signal in Fig. 2c, it can be easily detected from the yellow and green color distribution that the signal contains noise. In the CWT graph, the power increases from turquoise to yellow. It can be seen that the power increases in places where noise occurs, but it also causes the fundamental component to spread in frequency. If the values in the de-noising applied graphs in Fig. 3a, b, and c are evaluated against these values in Fig. 3a, b, and c, it can be seen in Fig. 3a that the signal is significantly free of noise at the 50 Hz fundamental frequency.

On the other hand, in Fig. 3b, the amplitude of the noise power for 0.02 s was obtained almost precisely as the original signal, which was 60 dB. The noise signal strength completely lost its effect after 0.05 s. From the CWT graph of the de-noised signal in Fig. 3c, the yellow color gains weight, the original signal strength increases, and a much more regular color scale is obtained.

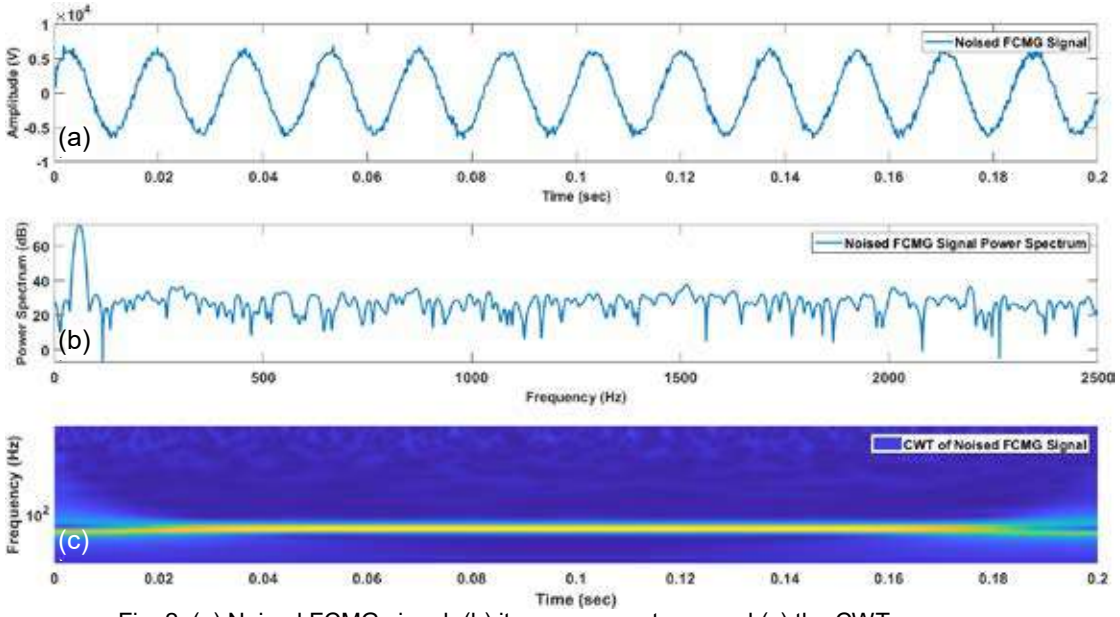


Fig. 2: (a) Noised FCMG signal, (b) its power spectrum, and (c) the CWT response

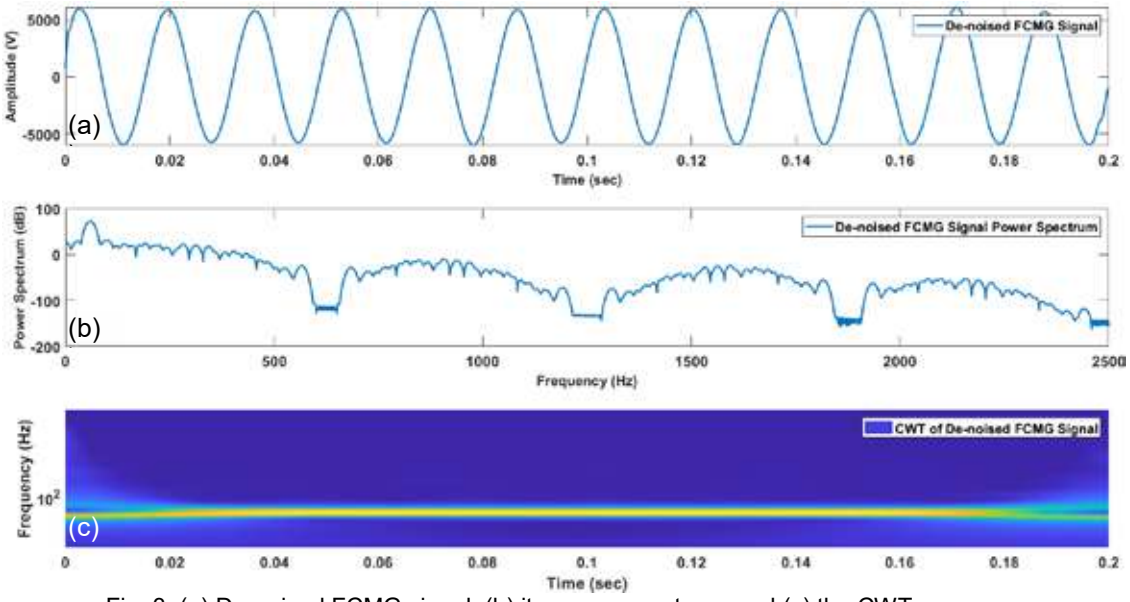


Fig. 3: (a) De-noised FCMG signal, (b) its power spectrum, and (c) the CWT response

In Fig. 4, the peak values of three signals are zoomed in. From Fig. 4, while the signal amplitude of the original MG-FC system was 6000 V, the peak value of the noisy signal increased to 6800 V because of the addition of noise. The de-noising signal was obtained as 5927 V. From Table 1, with the de-noising process, the noise amount of the noise signal was reduced by 12.8% from the value of (6800 V/6000 V)×100 and almost the same signal as the original FC-MG signal was obtained.

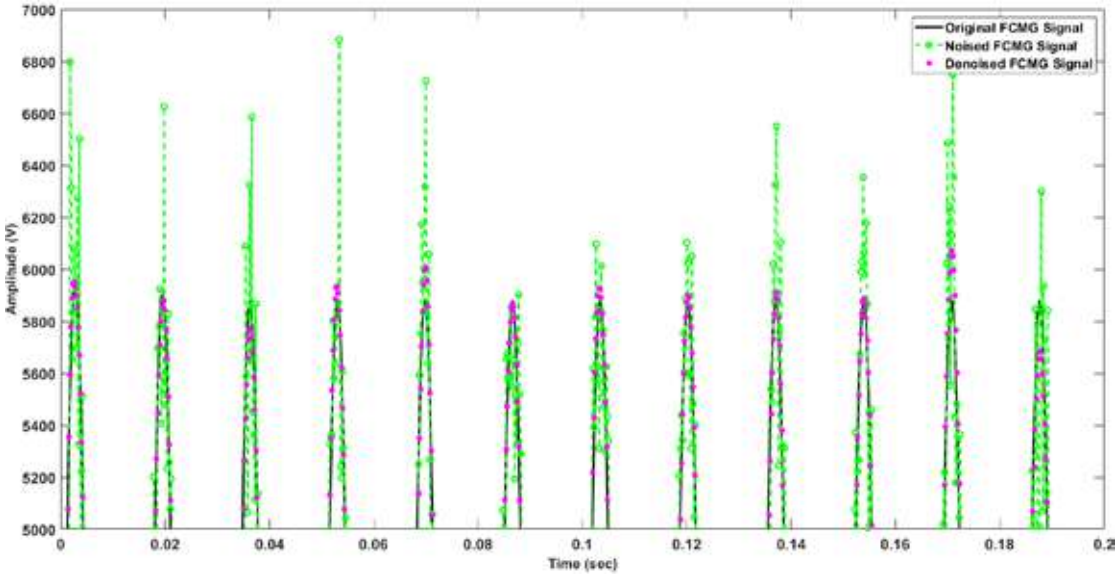


Fig. 4: Zoomed-in view of the peak values of three signals

Tab. 1: Statistical values of original FC-MG, Noised FC-MG, and De-noised FC-MG systems

	Min. Value	Max. Value
Original FC-MG	-5920 V	5950 V
FC-MG Noised	-6780 V	6880 V
FC-MG De-Noised	-6010 V	6070 V
Decrease in Noise (FC-MG Noised/ FC-MG De-Noised)	**12.8%**	**13.3%**
Accuracy (FC-MG De-Noised/ Original FC-MG)	1.5%	2%

V. Conclusions

Suppression of the disturbing white noise source has become crucial in the functioning of expanding microgrids since the noise source cannot be detected precisely. In this study, with the statistical evaluation of noised and de-noised situations in the FC-MG system, it was observed that the noise dB values in the signal's power spectrum decreased significantly, and the noise reduction was obtained up to 13.3%. Based on this, it can be said that such microgrid structures with de-noising will have a healthier tripping process and stable frequency response. Further study shows that noise levels at different dB values can be analyzed.

References

Akinyele, D., Olabode, E., Amole, A., Review of fuel cell technologies and applications for sustainable microgrid systems. Inventions, 5(3), 42, (2020).

Behling, N. H., Fuel cells: current technology challenges and future research needs, Newnes, (2012).

Demir, A., & Sangiovanni-Vincentelli, A., Analysis and simulation of noise in nonlinear electronic circuits and systems Springer Science & Business Media, 425, (2012).

Dudgeon G., Hybrid AC/DC Microgrid with PV, Battery and Fuel Cells (https://github.com/mathworks/Modeling_a_Hybrid_Microgrid/releases/tag/v1.0.0), GitHub. Retrieved February 7, (2024).

Kyriakopoulos, G. L., Arabatzis, G., Electrical energy storage systems in electricity generation: Energy policies, innovative technologies, and regulatory regimes, Renewable and Sustainable Energy Reviews, 56, 1044-1067, (2016).

Luo, G., Zhang, D., & Baleanu, D. D., Wavelet de-noising, Advances in wavelet theory and their applications in engineering, physics and technology, 634, 6-13, (2012).

Mathworks Inc. https://www.mathworks.com/matlabcentral/fileexchange/114945-hybrid-ac-dc-microgrid-with-pv-battery-and-fuel-cells, (2022).

Vandoorn, T. L., Renders, B., Degroote, L., Meersman, B., & Vandevelde, L., Active load control in islanded microgrids based on the grid voltage, IEEE Transactions on Smart Grid, 2(1), 139-151, (2010).

Winter, C. J., Hydrogen energy—Abundant, efficient, clean: A debate over the energy-system-of-change. International journal of hydrogen energy, 34(14), S1-S52, (2009).

Yeo, I. A., & Yee, J. J., A proposal for a site location planning model of environmentally friendly urban energy supply plants using an environment and energy geographical information system (E-GIS) database (DB) and an artificial neural network (ANN), Applied Energy, 119, 99-117, (2014).

The Detection of Power Quality Change During Multiple Disturbances for Microgrid Protection and Fuel Cell Health

[1]Sıtkı Akkaya, [1]Mehmet Güçyetmez, [2]Murat Uyar, [2*]Şekip Esat Hayber
[1] Sivas University of Science and Technology, Department of Electrical-Electronic Engineering, Sivas, 58140, Türkiye
[2] Bursa Uludağ University, Department of Electrical-Electronic Engineering, Bursa, 16059, Türkiye

*E-mail: sehayber@uludag.edu.tr

Abstract
In recent years, the use of hydrogen energy and, therefore, fuel cells in power systems has been increasing. However, as with every unit added to the microgrid, fuel cells are required so that the power quality of the electrical grid does not deteriorate. On the other hand, in addition to fuel cells, many devices negatively affecting power quality are also in the microgrid structure. In this study, fuel cell-induced power quality degradations are detected to prevent the fuel cell from being completely damaged. In the case of multiple simultaneous degradations, the degradation source is determined. Thus, microgrid and fuel cell protection can be provided by making the relevant relay switch on time.

Keywords: Fuel cell, power quality, microgrid, multiple degradations

I. Introduction

In the last decade, the electric power system has included many small and medium-sized production, consumption, and storage units (Lovins, 2020). In addition, thousands of circuit breakers have begun to be used in the power system to intervene in malfunctions that may occur due to overload and short-circuit situations caused by these units (Smeets et al., 2014). These protection devices added to the system are themselves a source of degradation. As a result, with the expansion of microgrids in the electrical power system, power quality disturbances such as transients, flickers, or harmonics, which can manifest themselves at different times or simultaneously, have begun to occur more frequently (Sepasi et al., 2023). These degradations negatively affect the basic parameters of the power system, such as frequency, current, voltage, and power, causing a decrease in energy efficiency, a decrease in the economic life of machines, and product losses. While fuel cells, control malfunctions, CB tripping, equipment failures, and power system faults are the sources of transients, industrial furnaces, on-linear loads, transformers, generators, and battery chargers are the general sources of harmonics. AC motor drives, arc furnaces, and motor starting are the most common causes of flickering (Akkaya, 2023). Detecting simultaneous disturbances is very important to determine which device in the system is malfunctioning, to intervene before this device completely breaks down, and to prevent the balance of the entire system caused by this device. The main contributions of this paper are summarized as follows:

- Transient analysis of the composed signal was carried out; although the transient analysis is too hard to detect,
- Three disturbance components with transient were analyzed simultaneously,
- Continuous Wavelet Transform (CWT) as a signal processing method was applied to the composed signal with transient.
- As a result of power quality analysis, each disturbance was detected separately; therefore, fuel cell health or protection of the fuel cell was carried out without a filter.
- In addition, the cost can be reduced, and fuel cell-specific preventive protection can be provided.

II. Experimental Set-up and Procedure

Some experimental set-ups for the harmonic, flicker, or transient disturbances can be used, as in Fig.1.

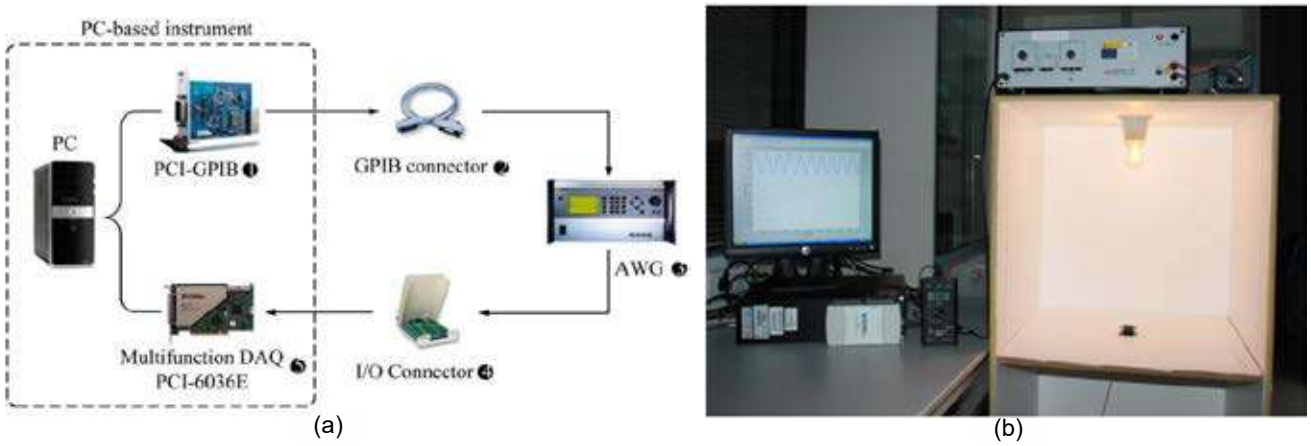


Fig. 1: Sample Experimental Set-ups (a) for Harmonics and interharmonics Measurement (Chang et al., 2009), (b) for Flicker Effect (Lodetti et al., 2019)

Three different signals, including flicker, harmonic, and transient disturbances, were initially obtained synthetically. Signals are at 5 kHz, 0.2 ms wide, and are processed using the Continuous Wavelet Transform (CWT) technique as a signal processing method. Each separately generated signal was then simultaneously combined into a single time interval. It was visualized with CWT to monitor each signal's formation characteristics and time. Then, three signals were created simultaneously and plotted on the time axis. Finally, the CWT of the combined signal was also taken, and the total signal was obtained visually. Thus, an operator can understand the disturbance and its severity from the visualized signal and intervene.

III. Analysis

This section will explain harmonics, flicker, and transient disturbances analytically. These disturbances are stated in terms of fundamental frequency and voltage amplitude changes. The fundamental frequency and voltage amplitude can be defined in Eq. 1.

$$v(t) = A\sin(2\pi f_0 t) \tag{1}$$

Where f_0, 50 Hz, is the fundamental frequency and A, 220 V_{rms}, is the voltage amplitude.

Harmonics are the most known and common disturbance type, and the highest-level harmonics are seen in the 3rd, 5th, and 7th signal components. The harmonic signal is given by the Eq. 2.

$$v_1(t) = \sin(2\pi f_0 t) + \alpha_3 \sin(2\pi 3 f_0 t) + \alpha_5 \sin(2\pi 5 f_0 t) + \alpha_7 \sin(2\pi 7 f_0 t) \tag{2}$$

Where α_3, α_5, and α_7 are the third, fifth, and seventh components' coefficients of the harmonics signal, respectively. These coefficients must satisfy the $0.05 \leq \alpha_3, \alpha_5, \alpha_7 \leq 0.5$ condition.

Fig. 2 shows a typical harmonic distortion signal of 0.2 s.

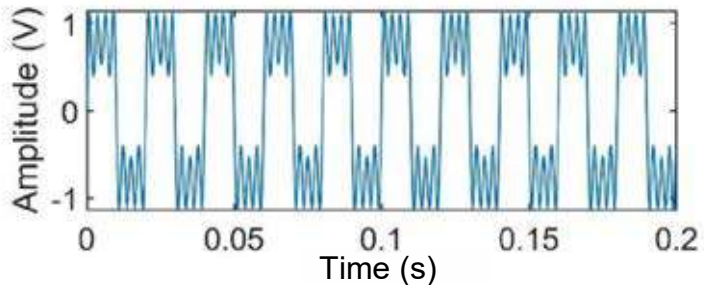


Fig. 2: Harmonics

Another disturbance signal is flicker. It is widely seen from the frequency deviation in light bulbs. Flicker can be formalized as in Eq. 3. The typical flicker signal based on inter-harmonics can be seen in Fig. 3.

$$v_2(t) = [1 + \alpha_{\text{flicker}} \sin(2\pi f_{\text{flicker}} t)]\ \sin(2\pi f_0 t) \tag{3}$$

Where α_{flicker} is the coefficient of the flicker signal, f_{flicker} is the frequency of the flicker signal. α_{flicker}, f_{flicker} must satisfy the $0.05 \leq \alpha_{\text{flicker}} \leq 0.2794,\ 1\ \text{Hz} \leq f_{\text{flicker}} \leq 25\ \text{Hz}$ conditions, respectively.

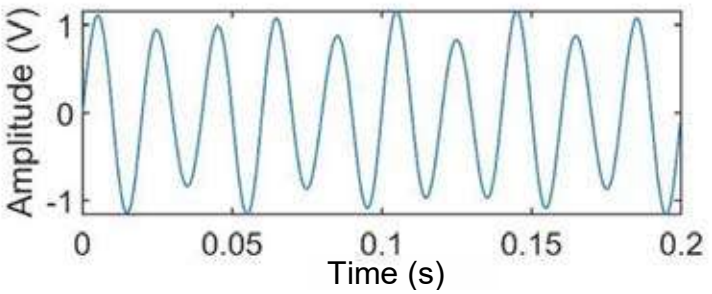


Fig. 3: Flicker based on interharmonics

The last type of disturbance is transient. It is terminative for the power systems. The mathematical model of the transient (interruption) is given in Eq. 4 according to the IEEE1459 standard. In Fig. 4, the typical interruption signal can be seen.

$$v_3(t) = [1 - \alpha_{\text{interruption}}(u(t - t_1) - u(t - t_2))]\ \sin(2\pi f_0 t) \tag{4}$$

Where $\alpha_{interruption}$ is the coefficient of the interruption signal, t_1 and t_2 are the transient times. $\alpha_{interruption}$, t_1 and t_2 must satisfy the $0.9 \leq \alpha_{\text{interruption}} \leq 1,\ T_0 \leq t_2 - t_1 \leq 9T_0$ conditions, respectively.

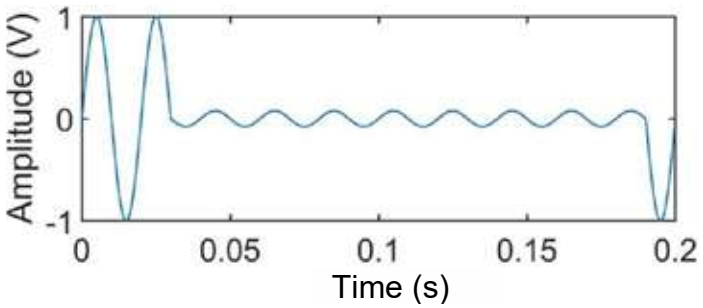


Fig. 4: Typical interruption disturbance signal

As the number of devices or equipment in the power system increases, there is a greater possibility of simultaneous disturbances. Fig. 5 shows a combined harmonic, flicker, and transient disturbance for 0.2 s.

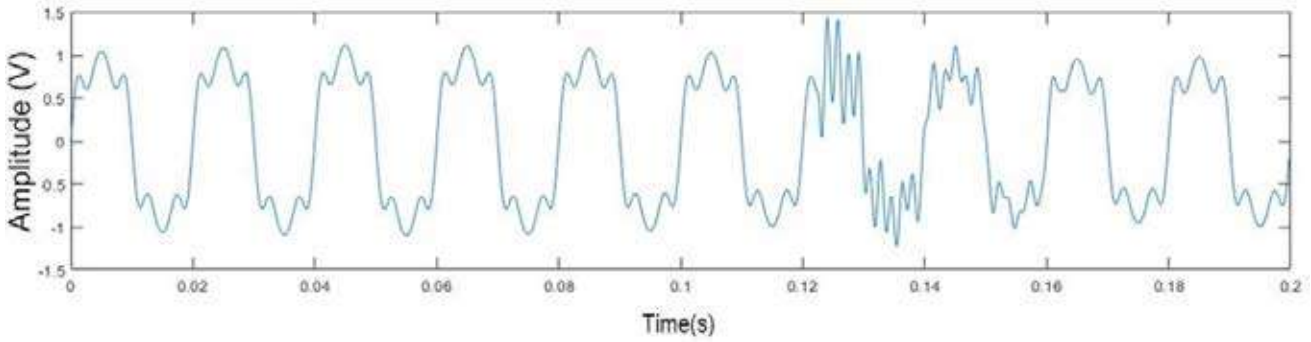


Fig. 5: A combined disturbance consisting of harmonics, flickers, and transients

Continuous Wavelet Transform (CWT) is a signal transformation technique suitable for visualizing the disturbance signals.

Continuous Wavelet Transform (CWT) is applied to time series signal as follows Eq. (5).

$$W_s(a,b) = \int v(t) a^{-\frac{1}{2}} \overline{\psi(\frac{t-b}{a})} \mathrm{dt} \quad (5)$$

In this equation, ψ: wavelet window, $\overline{\psi}$: conjugate of ψ, *b* is time-shifting, and a is the coefficient of scaling (Lilly, 2017).

IV. Results and discussions

The obtained signals are given in Fig. 6. The combined signal was obtained in Fig. 6a. Fig. 6b. shows the CWT-transformed visual form of the combined signal in Fig. 6a., which is the main purpose of this study. The pure signal is visualized as in Fig. 6c. Harmonic, flicker, and transient signals are visualized in Fig. 7d, e, and f, respectively.

In particular, the transient feature is directly related to the fuel cell and can be easily detected when a malfunction occurs in the fuel cell's operation. When the disturbances in power systems come together, it is unclear from the time-axis signal in Fig. 6a. which sources or devices these disturbances originate. However, the disturbances can be easily detected with the CWT conversion of this signal, as in Fig. 6b. With this conversion method, an operator can detect transient-producing fuel cells individually, while the combined signal can also determine whether there is any degradation in the fuel cell or the amount of degradation. Thus, preventive maintenance or fault detection can be carried out for power systems containing fuel cells.

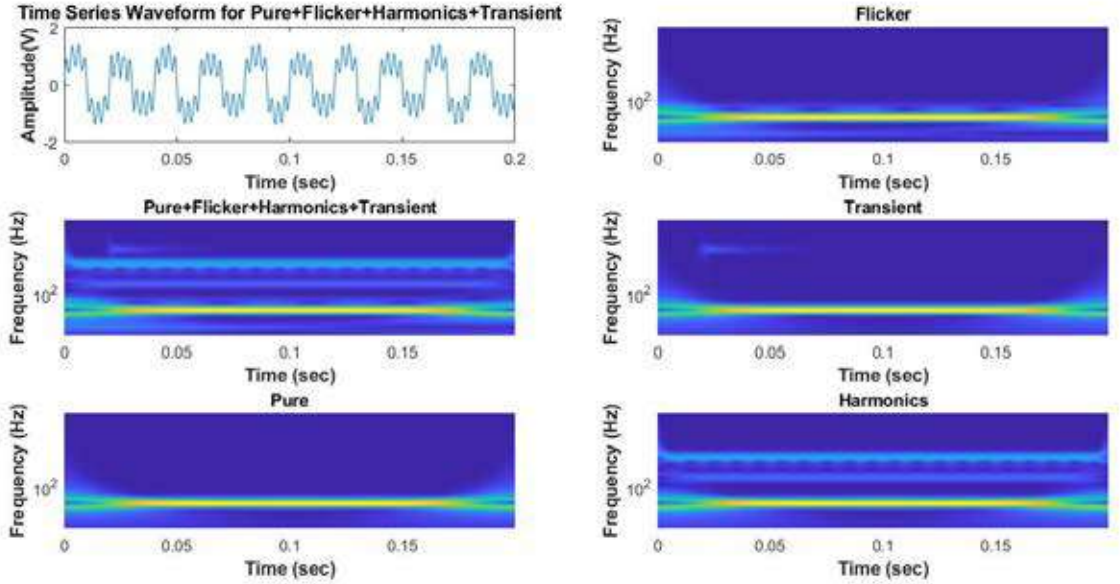


Fig. 5: (a) The combined Time Series Signal consisting of three disturbance types, (b) The visualized type of combined signal by CWT technique, (c) CWT response of Pure Signal, (d) CWT response of Signal with Harmonics, (e) CWT response of Signal with flicker, (f) CWT response of Signal with Transient

V. Conclusions

As with every element in the power system, fuel cells also add degradation. When the components come together, simultaneous degradation occurs, and the health of the fuel cell cannot be understood with traditional signal processing methods. With the visualized method applied in this study, preventive interventions become possible by distinguishing the current state of the fuel cell from the transient signal originating from the fuel cell and the total degradation in the power system. In future studies, more degradation types can be applied with hybrid CWT methods, and their effects can be examined.

References

Akkaya, S., A Review of the Experimental Studies on Analysis of Power Quality Disturbances, Book Chapter, Pioneer and Contemporary Studies in Engineering, Duvar Publishing, 453-477, (2023). https://doi.org/10.59287/pcse.361

Chang, G. W., Chen, C. I., & Liang, Q. W. (2009). A two-stage ADALINE for harmonics and interharmonics measurement. *IEEE Transactions on Industrial Electronics*, *56*(6), 2220-2228.

Lilly, J. M., Element analysis: A wavelet-based method for analysing time- localized events in noisy time series, *Proceedings of the Royal Society A: Mathematical, Physical and Engineering Sciences*, 473, 2200, (2017).

Lodetti, S., Azcarate, I., Gutiérrez, J. J., Leturiondo, L. A., Redondo, K., Sáiz, P., & Bruna, J. (2019). Flicker of modern lighting technologies due to rapid voltage changes. *Energies*, *12*(5), 865.

Lovins, A. B., *Small is profitable: the hidden economic benefits of making electrical resources the right size*. Routledge., (2020).

Sepasi, S., Talichet, C., & Pramanik, A. S., Power Quality in Microgrids: A Critical Review of Fundamentals, Standards, and Case Studies. *IEEE Access*, (2023).

Smeets, R., Van der Sluis, L., Kapetanovic, M., Peelo, D. F., & Janssen, A., *Switching in electrical transmission and distribution systems*. John Wiley & Sons, (2014).

Silicotungstic Acid-Incorporated Waste Tire-Derived Activated Carbon Catalysts for DME Production

[1*]Altay Usta, [1]Barış Tekçe, [1]Ogün Taştan, [1]Birce Pekmezci Karaman
[1] Gazi University, Engineering Faculty, Chemical Engineering Department, Ankara, 06510, Türkiye

* E-mail:bircepekmezci@gazi.edu.tr

Abstract
Alternative fuels are imperative due to the greenhouse gas emissions resulting from fossil fuel consumption. Rising costs of crude oil-derived transportation fuels have also prompted research into alternative fuels. Dimethyl ether (DME) has garnered attention for its eco-friendly properties. This study focuses on synthesizing novel catalysts for DME production and evaluating their activity in the methanol dehydration reaction. Silicotungstic acid-incorporated carbon-based materials are used as solid acid catalysts. Activated carbons have been synthesized from waste tires, and silicotungstic acid is impregnated into the activated carbon. Optimal synthesis parameters for high surface area and mesoporous structure have been determined. The effects of activating agents, impregnation ratios, and carbonization temperatures on their properties have been examined. The activity tests of the catalysts were evaluated alongside their characterization studies (including XRD, EDS, SEM, N_2 physical adsorption, and DRIFTS. KOH-activated and STA incorporated acitaved carbon exhibited the highest DME selectivity and methanol conversion.

Keywords: dimethyl ether, activated carbon, waste tires, methanol

I. Introduction

Activated carbon is a porous material that can be derived from inorganic sources such as waste tires through pyrolysis. Due to its porous structure and environmentally friendly, cost-effective nature, it finds extensive applications in various industries. The surface areas of commercially available activated carbons generally 400-1000 m^2/g. There are two main methods for producing activated carbon from waste tires: physical activation and chemical activation. Physical activation involves a two-step process. In this method, the raw material to be used in activated carbon production is converted into a solid substance called "char" in an inert gas environment at a reaction temperature of 500 - 600 ºC. Then, the chars are transformed into activated carbon using partial gasification with carbon dioxide, steam, air, or their mixture at temperatures of 800 - 1000 ºC. On the other hand, chemical activation occurs in a single step. In this process, the raw material is impregnated with a chemical called an activating agent, and then activated carbon production is carried out by carbonizing it in an inert atmosphere at temperatures ranging from 200 to 800 ºC. Activated carbons obtained through chemical activation have higher surface areas and generally possess mesoporous structures (Dogan etc., 2024). Additionally, while physical activation yields low activated carbon efficiency and requires high energy consumption due to its operation at high temperatures, chemical activation is preferred in this study to produce activated carbon from waste tires.

Dimethyl ether is regarded as an exceptional clean-burning option for transportation fuel in compression-ignition engines, suitable for household use as an alternative to LPG, and even for power generation (Karaman vd., 2020). With its notable cetane rating of 55-60, elevated oxygen content, and clean combustion features resulting in minimal NOx and soot emissions, along with zero SO_2 emissions, DME emerges as a sustainable fuel alternative for the future. Solid acid catalysts are used for the dehydration of methanol (Ozcan vd., 2022). This study evaluated the effectiveness of activated carbon as a supported material and silicotunctic acid incorporation to the activated carbon on DME selectivity and methanol selectivity. The study is particularly notable for the evaluation of waste tires and for conducting research on alternative fuel production. The study adopts an environmentally friendly approach, emphasizing both fuel production and catalyst synthesis.

II. Experimental Set-up and Procedure

In the study, activated carbon was synthesized from waste tires, which had been processed to obtain particles of 10 mm in size by separating the steel and fibers. Activated carbon production was carried out through chemical activation, with KOH and $ZnCl_2$ utilized as activators. The activating agent-to-waste tire impregnation ratio was chosen as 1:4 (weight of raw materials to weight of chemicals). The heterogeneous solution was mixed under room conditions for 24 hours, and then dried at 100°C for 1 day. Carbonization experiments were conducted in a fixed-bed glass reactor at 800°C for 1 hour. The carbons were removed from the reactor and washed with concentrated HCl solution under reflux for 2 hours to remove ash.

Activity test studies were conducted within a continuous flow-packed bed reaction system. Helium was used as the carrier gas flowing at a rate of 30 mL/min, while methanol was pumped into the system at a rate of 5 mL/min. The reactor was maintained at a reaction temperature of 150-350°C. All pipelines were heated to 200°C via variacs. The

resultant gas product was directly routed to the gas chromatography device. These experimental procedures were conducted over a total duration of 3 hours.

III. Analysis

To determine the surface area, pore size, and pore volume of the catalysts, N_2 adsorption-desorption analysis was performed. The crystal structure of the catalysts was determined by X-ray diffractogram (XRD) analysis. Additionally, DRIFTS analysis was performed to determine the acid sites of the catalysts and SEM-EDS analysis was conducted to determine the surface morphology and composition.

The activity test results were evaluated in terms of methanol conversions (Eq. 1) and DME (Eq. 2), Formaldehyde (Eq. 3) selectivity values:

$$\text{Methanol conversion} = \frac{F_{MeOH,in} - F_{MeOH,out}}{F_{MeOH,in}} \quad (1)$$

$$\text{DME selectivity} = \frac{F_{DME}}{F_{MeOH,in} - F_{MeOH,out}} \quad (2)$$

$$\text{Formaldehyde selectivity} = \frac{F_{FA}}{F_{MeOH,in} - F_{MeOH,out}} \quad (3)$$

IV. Results and discussions

The activated carbon (AC) exhibited a well-developed porous structure. The type of activating agents highly influenced the surface area. The maximum surface area was obtained with the KOH treatment, reaching 773 m^2/g surface area with a high contribution of mesoporosity. After STA loading, a maximum decrease of 20% was observed in all structural parameters of the AC. The 8STA@AC catalysts had a surface area of 625 m^2/g with a 2.2 nm average pore diameter. The metal contents of the catalysts were determined by ICP-OES analysis, which indicated that the desired amount of STA was successfully incorporated into the AC.

The activity test results showed that STA incorporation enhanced the catalytic activity of the activated carbon. Pure activated carbon exhibited a very low methanol conversion (8%) and high formaldehyde selectivity (60%). However, STA-impregnated support material (by mass 8%) demonstrated a 60% methanol conversion and high DME selectivity under the same reaction conditions (200°C and atmospheric pressure). Increasing the reaction temperature enhanced methanol conversion. At a temperature of 350°C, high selectivity to DME (~100%) and high methanol conversion (60%) were achieved.

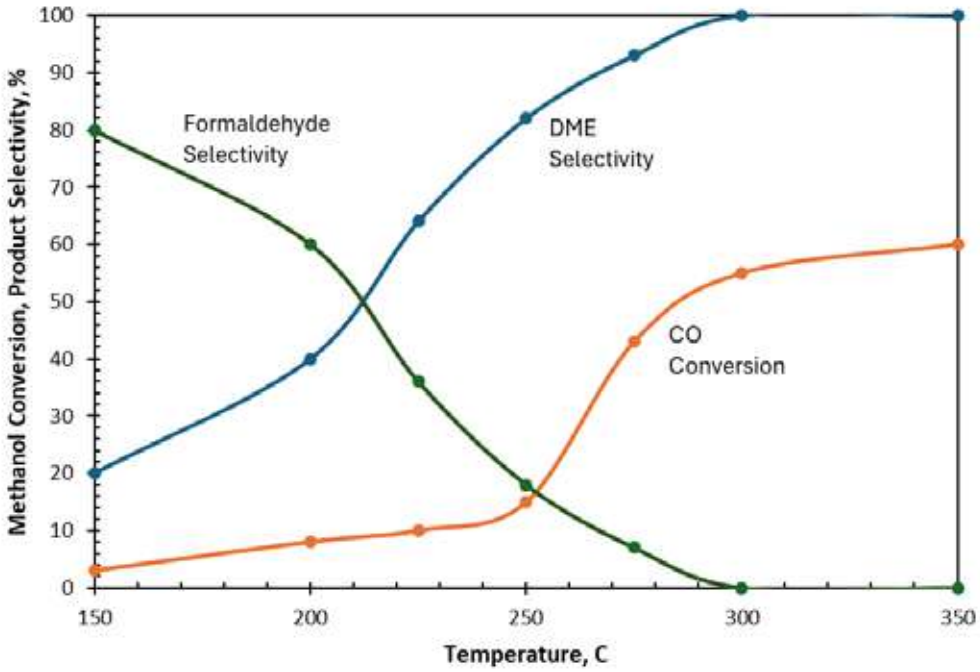


Fig 1. Metanol Conversion and Selectivity of DME and formaldehyde over 8STA@AC

V. Conclusions

The catalytic activity of activated carbons synthesized from waste tires, which possessed high surface area and mesoporous structure, was determined in this study. Carbon-based materials impregnated with silicotungstic acid were successfully utilized as solid acid catalysts. The activated carbons were synthesized from waste tires in an environmentally friendly and cost-effective manner, with silicotungstic acid impregnation. It was demonstrated that the addition of silicotungstic acid enhanced catalytic activity, particularly increasing the high selectivity of dimethyl ether and methanol conversion. This study made a significant contribution to the synthesis and performance of solid acid catalysts used in alternative fuel production.

Acknowledgements

TUBITAK 2209A are gratefully acknowledged for their financial support. The authors also thank the Central Laboratory of METU for the characterization results of the synthesized materials.

References

Dogan, M. Y., Tasdemir, H. M., Arbag, H., Yasyerli, N., & Yasyerli, S. H_2 production via H2S decomposition over activated carbon supported Fe-and W-catalysts. International Journal of Hydrogen Energy. 2024 https://doi.org/10.1016/j.ijhydene.2024.02.316

Karaman, B., Oktar, N., Doğu, G., & Doğu, T. Bifunctional silicotungstic acid and tungstophosphoric acid impregnated Cu–Zn–Al & Cu–Zn–Zr catalysts for dimethyl ether synthesis from syngas. Catalysis Letters, *2020; 150*, 2744-2761.

Karaman B, Oktar N. Tungstophosphoric acid incorporated hierarchical HZSM-5 catalysts for direct synthesis of dimethyl ether. Int J Hydr Energy 2020;45(60):34793–34804. https://doi.org/10.1016/j.ijhydene.2020.07.044

Ozcan MC, Karaman BP, Oktar N, Dogu T. Dimethyl ether from syngas and effect of CO_2 sorption on product distribution over a new bifunctional catalyst pair containing STA@SBA-15. Fuel. 2022;330:125607. https://doi.org/10.1016/j.fuel.2022.125607

Prediction of short-term voltage loss of PEM with single-step and multi-step LSTM Networks

[1*]Yurdagül Benteşen Yakut
[1] Dicle University, Faculty of Engineering, Electrical and Electronics Engineering Department, Diyarbakır, 21280, Türkiye

* E-mail: bentesen@dicle.edu.tr

Abstract
The aim of this paper is to predict the short-term voltage loss of PEMFC with single-step and multi-step LSTM network. The data set was filtered, normalized, respectively, and then training and test sets were created according to single-step and multi-step modes. Finally, 650h and 850h were taken as the starting point of the testing stage. It has been observed that the voltage decreasing over time can be determined with a high success performance. The most notable observations were: (i) It has been observed that the success rates of the proposed models are high according to the R2 criterion, and the success rate has been determined in the [0.999933, 0.796337] range. (ii) The desired prediction values were obtained with few epoches such as 10, (iii) a system in which the predictions can follow the actual values has been modelled. The reasons of the getting high performance with few epochs are related with proposed deep recurrent neural network based on LSTM, data preprocessing and the predicted values are not used for the next prediction step.

Keywords: Hydrogen energy, fuel cell, voltage loss, predicting, LSTM

I. Introduction

Fossil fuels-based energy systems, having unique importance, have been using extremely high levels with growing world population and energy demands of the population. Fossil fuels causes air pollution and damage to the world. This situation has pushed us to look for alternative new energy sources. Among the development of new energy technologies, fuel cells with sufficient efficiency and low emissions are considered as one of the most promising vehicular power sources (Kheirandish etal, 2016). Proton exchange membrane fuel cells (PEMFCs) are regarded as one of the most promising power technologies bacause of advantages of low operating temperature, high power conversion efficiency, and zero pollution (Liu etal, 2017). It can be seen that a wide variety of research has been done on the design, performance and durability of PEMFC systems (Liu etal 2016, Sutharssan etal 2017). Prognostics is an important tool in the life and cost management of the PEMFCs (Jardine etal, 2006). Because, even if this technology is close to being competitive, it is not yet ready to be considered for large scale industrial deployment. For example, PEMFC still must be optimized, particularly by increasing their limited lifespan. Enhancing PEMFCs durability involves not only developing a better understanding of ageing phenomena but also requires the ability to emulate the behavior of the whole system to support the development of improvements to those systems. With this motivation; the aim of this paper is to predict the short-term voltage loss of PEMFC with single-step and multi-step LSTM (long-short-term memory) network.

LSTM network is a type of recurrent neural network (RNN) capable of learning order dependence in sequence prediction problems. RNN in which the outputs from neurons are used as feedback to the neurons of the previous layer. However, almost all RNNs are nowadays replaced with LSTM to solve major shortcomings in the RNNs: vanishing and exploding gradients (Hamad and Abdulrahman, 2022). The proposed approach was employed in the IEEE PHM 2014 Data Challenge. Different time scales were used to increase the prediction performance.

II. Experimental Set-up and Procedure

Data Description: The data sets used in development and evaluation of the proposed method were provided by FCLAB Research Federation (Gouriveau etal, 2014) in which the test bench is adapted for Fuel Cells with a power up to 1 kW (electrical power). The data was drawn from 5 seperated cell PEMFC stacks, each of which has an area of 100 cm^2, and each cell is composed of diffusion layers, machined flow distribution plates and commercial membranes. The nominal current density of the cells is 0.70 A/cm^2 and their maximal current density is 1 A/cm^2. More than 20 parameters (stack voltage, current, current density, inlet and outlet temperature of H2 (Air), inlet and outlet pressure of H2 (Air), etc.) in the PEM system were measured. Two data sets were provided from two different regimes;

a) Stationary regime: fuel cell 1 (FC1) was operated under constant current of 70 A,

b) Dynamic regime: fuel cell 2 (FC2) was operated under a ripple current of 70 A with a 7A oscillations at a frequency of 5 kHz.

It is necessary to determine the indicator that can characterize the health status of fuel cells. The stack voltage directly reflecting output performance is widely used (Sun etal, 2023). So in this study, the parameter of stack voltage was selected for prediction the short-term voltage degradation.

Data Preprocessing: The selected data, stack voltage parameter, is the battery data within 1150h sampled under stationary regime. From Fig. 1, it is evident that the stack voltage drops with time, indicating degradation phenomena. After the preliminary screening of the data, it is necessary to remove the invalid noise in the data. Hence, moving average filter proposed by (Long etal. 2022) was employed in this paper (Fig.1). After noise processing, the filtered voltage data is then normalized to the interval [-1,1] for improving the training speed and accuracy of the model.

spited into two parts such as learning and testing sets.

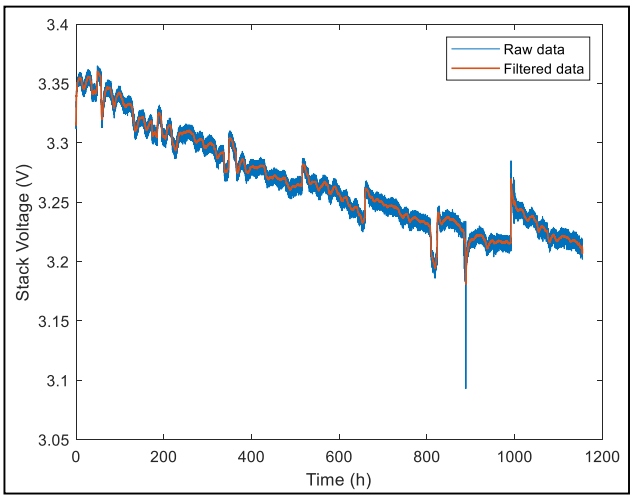


Fig.1 The stack voltage drops with time, indicating degradation phenomena.

Evaluation Index: MAPE (Mean Absolute Percentage Error), RMSE (Root Mean Square Error) and R^2 (Coefficient of Determination) are emplyed to evaluate the prediction accuracy of the proposed model. The formulas are given below:

$$MAPE = \frac{1}{m}\sum_{i=1}^{m}\left|\frac{\hat{x}_i - x_i}{x_i}\right| \times 100\% \quad (1)$$

$$RMSE = \sqrt{\frac{1}{m}\sum_{i=1}^{m}(x_i - \hat{x}_i)^2} \quad (2)$$

$$R^2 = 1 - \frac{\sum_{i=1}^{m}(x_i - \hat{x}_i)^2}{\sum_{i=1}^{m}(x_i - \bar{x}_i)^2} \quad (3)$$

where x_i, $\hat{x}_i$ and $\bar{x}_i$ are the actual value of the original data, predicted value and mean value of the measured voltage, respectively.

III. Analysis

Prediction Mode: The aim of this paper is to predict the short-term voltage loss of PEMFC with single-step and multi-step LSTM network. The stack voltage prediction was performed on the basis of both the single-step and multi-step operations. In the single-step prediction shown in Fig.2(a), the current time series is applied to predict the value at the next time, and the actual observed value is also used for the prediction at the subsequent time since the stack voltage can be collected as the forecast goes on. The multi-step prediction shown in Fig.2(b) where the current measured time series to predict future values at multiple time points, and the observed values are fed into the model after each prediction. Then the proposed model is updated to predict the next few steps (Sun etal, 2023).

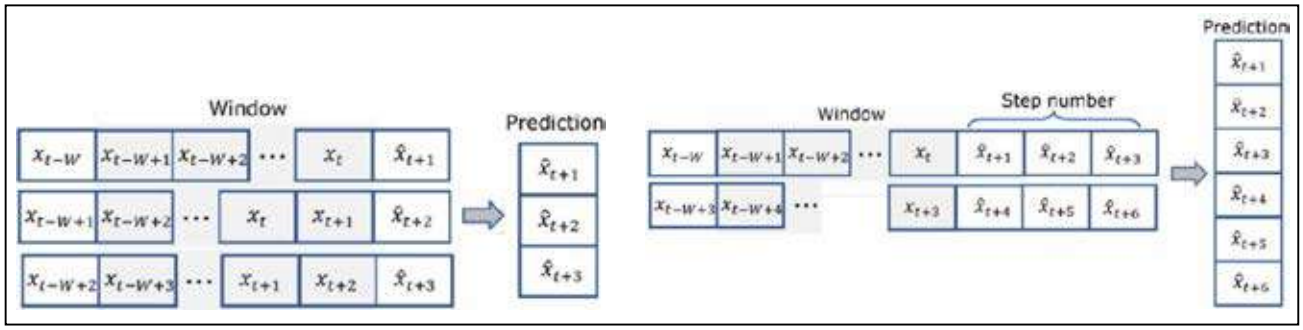


Fig.2 (a) The process of single-step prediction mode and (b) the process of multi-step prediction mode (Sun etal, 2023).

x $actual\ value$, $\hat{x}$ $predicted\ value$

Proposed LSTM Network:

LSTM is a special network having three “gate” structures (Fig.3). As shown in figure, the state of an LSTM unit is mainly controlled by three gates: the forgetting gate, input gate, and output gate. First, the forgetting gate determines what information should be forgotten from the cellular state. Second, the input gate determines how much new information is added to the neuron state. Finally, the output gate is used to control how many current neural unites state are filtered and how many controlling units state are filtered. More details of LSTM can be referred to (Xie etal, 2020).

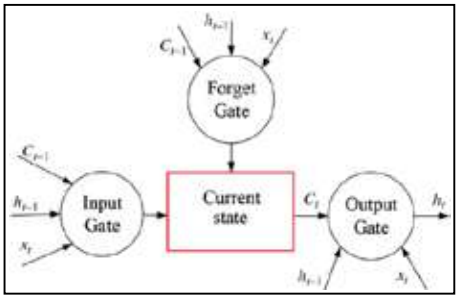


Fig.3 LSTM unit structure with three gates. x_t is the input of the current step, h_t is the output of the current network, C_t is the cell state of the current LSTM unit, x_{t-1}, h_{t-1}, C_{t-1} are the input, output, and cell state for the previous unit, respectively.

During the process of constructing the task model, the dropout method was used in the network. Dropout refers to the temporary discarding of the neural network unit from the network according to a certain probability during the training of the deep learning network, which is a means to prevent over-fitting. The proposed Deep recurrent neural network based on LSTM is shown in Table 1.

Tab. 1: Configuration of the proposed deep recurrent neural network based on LSTM

Layer	Layer name	Detailed information
1	Sequence Input	Sequence input with 5/25/1000 dimensions (for different applications)
2	LSTM	LSTM with 200 hidden units
3	Dropout	10% dropout
4	Fully Connected	300 fully connected layer
5	Fully Connected	1/5/50 fully connected layer (for different applications)
6	Regression Output	mean-squared-error

As for related training parameters for proposed network; the maximum epoch is assigned to 10 depending on the actual convergence trend. Besides, the minimum batch size of each training epoch is 60. The dynamic learning rate is set to 0.005 initially and decreases in the form of piecewise every 5 epochs to avoid training loss oscillation and overfitting. The gradient threshold is set to be 1 to prevent gradient explosion, and the Adam algorithm demanding only first-order gradients is applied for model training.

IV. Results and discussions

After parameter identification and splitting the data for learning and testing stages, the models were applied to the training and test data sets for predicting the short-term voltage loss of PEMFC. Training and test data were splited in two different forms such as (a) starting point for testing is 650h (data was splited as 1h-649h period for the training set, 650h-1150h period for the testing set), (b) starting point of testing is 850h (data was splited as 1h-849h perod for the training set, 850h-1150h period for the testing set). Then the splited data with different input and output dimensions are applied to the models. The data sizes evaluated in this study are 5/1, 25/1, 25/5 and 1000/50. In the learning stages of the models, it is found that the mean square errors gradually decreased with the increase of training times. As an example, the loss and RMSE change obtained during the training process are given in Fig. 4(a) and the prediction result is shown in Fig.4(b).

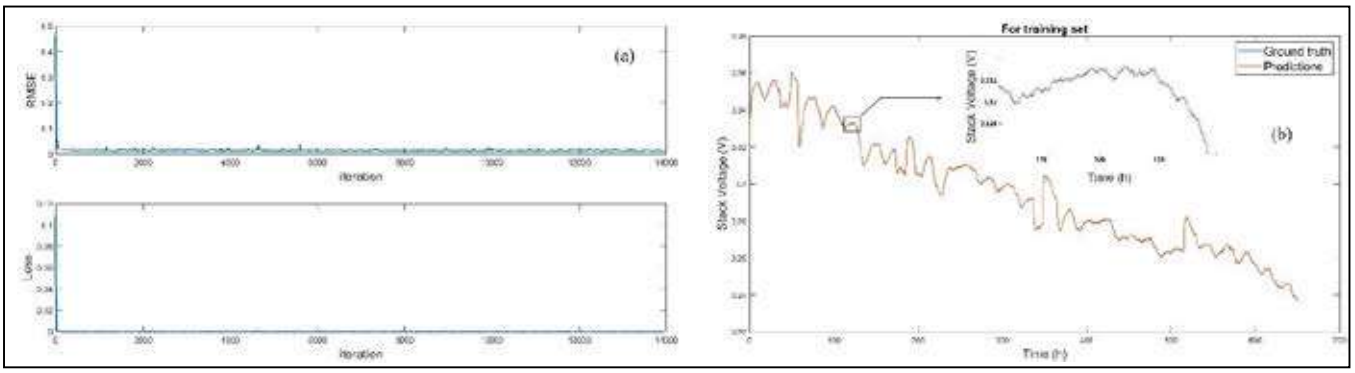


Fig.4 The training performance of the model having the data size of 5/1 and testing starting point for 650h
(a) Training loss and RMSE changes of model (b) prediction result of proposed LSTM for training set.

With testing stages, the observed values for different starting values with different prediction mode are given in Table 2. It can be seen from the table that the success rates of the proposed models are high according to all criteria. However, it is seen that the best prediction performance among the models is achieved with the 5/1 model with testing starting point of 650h. The test performance graph of this model is shown in figure 5.

Tab. 2: Comparison of prediction with different starting points for single-step and multi-step datasets.

Starting point	Prediction Mode	input / output dimensions	RMSE	MAPE	R^2
650 h	Single-step	5 / 1	0.000798426	0.0247684	0.999933
850 h	Single-step	5 / 1	0.00218588	0.0678447	0.999914
650 h	Single-step	25 / 1	0.00264506	0.082081	0.999212
850 h	Single-step	25 / 1	0.00143243	0.0444792	0.998926
650 h	Multi-step	25 / 5	0.00292781	0.0908684	0.998848
850 h	Multi-step	25 / 5	0.000452879	0.0140313	0.998677
650 h	Multi-step	1000 / 50	0.00934704	0.288867	0.796337
850 h	Multi-step	1000 / 50	0.0058717	0.18222	0.896191

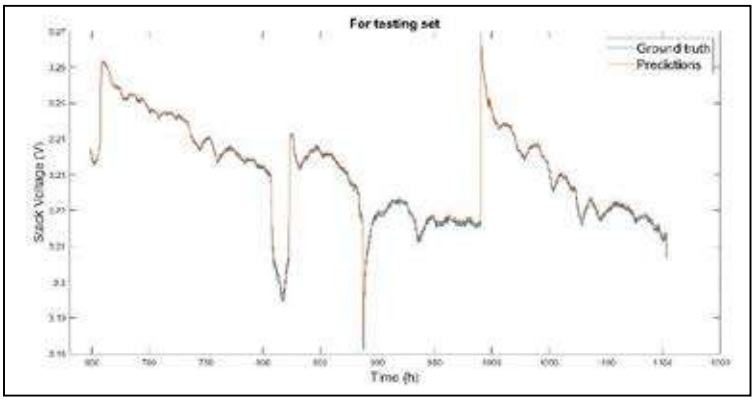


Fig.5 The prediction performance of testing set for the model having the data size of 5/1 with starting point for 650h

V. Conclusions

The aim of this paper is to predict the short-term voltage loss of PEMFC with single-step and multi-step LSTM network. The most notable observations were: (i) It has been observed that the success rates of the proposed models are high according to the R2 criterion, and the success rate has been determined in the [0.999933, 0.796337] range. (ii) The desired prediction values were obtained with few epoches such as 10, (iii) a system in which the predictions can follow the actual values has been modelled. The reasons of the getting high performance with few epochs are related with proposed deep recurrent neural network based on LSTM, data preprocessing and the predicted values are not used for the next prediction step.

References

Kheirandish A., Motlagh F., Shafiabady N., Dahari M., Dynamic modelling of PEM fuel cell of power electric bicycle system, International Journal of Hydrogen Energy, 41(22), 9585-9594 (2016).

Liu H., Chen J., Hou M., Shao Z., Su H., Data-based short-term prognostics for proton exchange membrane fuel cells, International Journal of Hydrogen Energy, 42(32), 20791-20808, (2017).

Jardine AKS., Lin D., Banjevic D., A review on machinery diagnostics and prognostics implementing condition-based maintenance, Mechanical Systems and Signal Processing, 20(7), 1483-1510, (2006).

Liu H., Chen J., Ouyang Q., Su H., A review on prognostics of proton exchange membrane fuel cells, The proceedings of the 13th IEEE vehicle power and propulsion conference, 1-6, (2016).

Sutharssan T., Montalvao D., Chen YK., Wang WC., Pisac C., Elemara H., A review on prognostics and health monitoring of proton exchange membrane fuel cell. Renew Sustain Energy, 75, 440-450, (2017).

Hamad Z., Abdulrahman I., Deep learning-based load forecasting considering data reshaping using MATLAB Simulink. Int J Energy Environ Eng, 13, 853–869 (2022).

Gouriveau, R., Hilairet, M., Hissel, D., Jemei, S., Jouin, M., Lechartier, E., Morando, S., Pahon, E., Pera, M.C., Zerhouni, N., IEEE PHM 2014 Data Challenge: Outline, Experiments, Scoring of Results, Winners. Tech. Rep., IEEE 2014 PHM Challenge. (2014).

Sun B., Liu X., Wang J., Wei X., Yuan H., Dai H., Short-term performance degradation prediction of a commercial vehicle fuel cell system based on CNN and LSTM hybrid neural network, International Journal of Hydrogen Energy, 48(23), 8613-8628 (2023).

Long B., Wu K., Li P., Li M., A Novel Remaining Useful Life Prediction Method for Hydrogen Fuel Cells Based on the Gated Recurrent Unit Neural Network. Applied Sciences. 12(1):432 (2022).

Xie R., Ma R., Pu S., Xu L., Zhao D., Huangfu Y., Prognostic for fuel cell based on particle filter and recurrent neural network fusion structure, Energy and AI, 2, 100017, (2020).

Investigation of the Current Effect on Electrochemically Deposited Pt Catalyst Properties for PEMFCs

[1*]Jülide Hazal Özdemir, [2,3]Aysel Kantürk Figen
[1] Yildiz Technical University, Metallurgical and Materials Engineering, Istanbul 34220, Türkiye
[2] Yildiz Technical University, Chemical Engineering, Istanbul 34220, Türkiye
[3]Yıldız Technical University, Clean Energy Technologies Institute, Istanbul, 34220, Türkiye

E-Mail: jhazal@yildiz.edu.tr

Abstract

Catalyst materials, among the components of Proton Exchange Membrane Fuel Cells (PEMFCs), play a crucial role in determining the system's performance, offering a clean alternative for meeting energy demand. Platinum's (Pt) high electrocatalytic activity enhances cell performance by facilitating rapid and efficient reactions. Additionally, Pt's high surface area and chemical stability are essential for prolonged use and high efficiency. In this context, the production method of Pt and the parameters used are determinant in catalyst properties. In this study, galvanostatic generic pulse method was employed to investigate the electro-deposition parameters in PEMFCs, and their impact on catalyst properties was evaluated through electrochemical characterization. The identified parameters in this study provide valuable insights for subsequent surface modification strategies aimed at enhancing electrocatalytic performance, thus offering a potential roadmap for improving electrochemical performance.

Keywords

Proton-Exchange Membrane Fuel Cell, Catalyst, Platinum, Electrochemical Deposition

I. Introduction

The escalating global demand for energy mirrors the trajectory of socio-economic advancement and the relentless pursuit of elevated quality standards. This situation underscores the urgent need for a diversified energy landscape to meet the multifaceted demands of contemporary society. Currently, primary energy sources predominantly rely on fossil fuels, including coal, natural gas, and oil, with coal-based power generation comprising 70% of global electricity production [1], [2]. Nonetheless, the utilization of these non-renewable reservoirs exacts significant tolls on ecological integrity, notably through the emission of detrimental gases, catalyzing climate variations, and aggravating global warming. Consequently, there is a compelling driving force to investigate alternative renewable energy pathways [3].

Fuel cells represent a promising way within the realm of electrochemical systems, offering efficiency and cleanliness by directly converting the chemical energy of fuels into electric energy. Furthermore, their inherent compatibility with renewable energy sources, such as hydrogen and hydrocarbons, positions them as key players in the transition towards a sustainable energy future [4]. Therefore, fuel cell utilization holds the potential to mitigate the drawbacks associated with fossil fuels, such as their finite nature and the emission of greenhouse gases resulting from combustion. Among these systems, proton exchange membrane fuel cells (PEMFCs) emerge as a beneficial alternative. Their virtues include minimal emissions, operational versatility across a range of temperatures, robust power density, and impressive energy conversion efficiencies [5]. However, despite these merits, impediments to widespread commercial adoption persist. These challenges include limited operational lifetimes, the management of water utilization, sluggish kinetics of the oxygen reduction reaction (ORR), and reliance on precious metals like platinum (Pt). Addressing these limitations, especially considering the high-priced Pt-based catalysts, is crucial for facilitating the global commercialization of PEMFC technology [6], [7]. Various synthesis methods such as wet impregnation, microwave-assisted deposition, physical precipitation, sputtering techniques, electroless deposition, hydrothermal synthesis, chemical reduction, and electrochemical deposition may be used to develop a Pt-based catalyst [8], [9]. The electrochemical deposition method, with its advantages of enabling easy single-step synthesis, allowing for alloying and doping flexibility, being an environmentally friendly process, and ensuring homogeneous Pt dispersion on the substrate material, is intriguing for the development of highly efficient and cost-effective catalyst materials [10]. The electrodeposition method relies on electrochemically depositing porous Pt nanomaterials onto substrate material (e.g. carbon substrates) through the application of varying current or potential values. If the coating with the application of current is elected various parameters such as applied current/current densities, deposition solution concentration, current application-standby durations (T_{on}-T_{off}), and cycle numbers significantly influence the deposition amount and the electrochemical active surface area (EASA) of the final product [11], [12], [13].

In pursuit of a deeper understanding of electrochemical deposition's efficacy in catalyst synthesis, this study aims to determine the effect of varying current values on the deposition, keeping the Ton-Toff times (second) and the amount of load (Q) applied to each electrodeposition constant. In this context, electrodeposition was carried out by applying four different current (A) values, and the resulting catalysts were subjected to electrochemical characterization.

II. Experimental Set-Up and Procedure

For the deposition process, preparation of the coating solution was performed, ensuring precise composition and reagent concentrations. Hence, the desired quantity of Pt solution (Chloroplatinic acid hegza hydrate Sigma Aldrich, 37%, 0,05 M) and 150 ml of 0,5 M H_2SO_4 was mixed via a magnetic stirrer. Subsequently, the carbon paper which was used as a substrate material underwent a preparation by utilizing a 31 mm punch and cautiously cutted. After that, the carbon papers were placed in Teflon sample holders guaranteeing optimal positioning for the electrodeposition process. The electrical conductivity was controlled by using a multimeter (Tt Technic, 9808). This step ensured that the presence of conductivity of the substrate materials which is necessary for successful electrodeposition. The electrodeposition process was performed employing a range of distinct current values via the galvanostatic generic pulse method as given in Table 1.

Table 1. Parameters of experimental studies for galvanostatic generic pulse method

Sample Code	Current (mA)	T_{on} (s)	T_{off} (s)	Cycles
ELK100	100	0,1	0,5	2000
ELK300	300	0,1	0,5	2800
ELK500	500	0,1	0,5	4600
ELK700	700	0,1	0,5	14000

Each current value was meticulously selected to explore its specific impact on the deposition process, facilitating a comprehensive understanding. The number of cycles required to keep the load value constant for each coating under different applied currents were calculated separately. Although the applied T_{on} and T_{off} values were kept constant for each sample, the number of cycles varied according to these calculations. Finally, the Pt deposited carbon papers were subjected to drying process at 50°C for 12 h.

III. Analysis

After the synthesis stage, the deposition amount (g) in the deposited samples post-coating was determined. Gamry Instruments, Interface 1010B Potentiostat/Galvanostat and Pine Research Instruments Rotating Systems were used for electrochemical characterizations. Cyclic voltammetry testing, allowing for the examination of electrochemical reactions by cyclically increasing and decreasing electrode potential over time, was conducted at different scan rates (mV/s). Linear sweep voltammetry tests, employed to understand the kinetics of the oxygen reduction reaction (ORR), involved the gradual reduction of electrode potential over time. This technique enables the measurement of reaction rate at a specific potential.

IV. Results and Discussion

(a) The deposition amount (g) and (b) the change in electrochemical active surface area (EASA, m^2/g_{Pt}) of the coated samples were demonstrated in Figure 1 as a function of applied current (mA) values. As illustrated in the graphs, while an increase in the applied current results in a decrease in the coating amount (g), an increase in the EASA (m^2/g_{Pt}) values was observed.

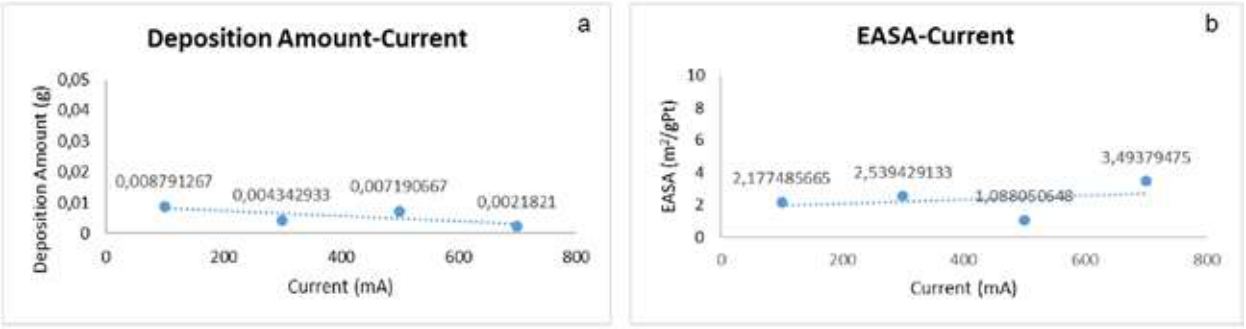


Figure 1. (a) The deposition amount (g) and (b) the change in electrochemical active surface area (EASA, m^2/g_{Pt}) of the coated samples as a function of different currents

The electrochemical deposition process conducted under low currents entails the transmission of less electrical charge to the electrode surface. Consequently, the completion of the coating process may take longer as the diminished electrical charge provides the transfer of coating material to the electrode surface at a slower pace. Hence, an extended duration is required due to the slower deposition of coating material. When low current values are preferred, while maintaining a constant applied charge, additional cycles need to be performed, necessitating more time spent on the electrode surface. As a result, a higher deposition of Pt occurs. Furthermore, electrochemical deposition conducted at low currents typically ensures a more uniform coating, thereby promoting the deposition of a greater amount of Pt onto the substrate surface. Therefore, electrochemical coating conducted under low currents generally leads to a higher deposition amount. When a high current is applied, the electrochemical deposition process progresses faster due to the increased transmission of electrical charge to the electrode surface. Consequently, the coating material is transported and accumulated onto the electrode surface more rapidly, resulting in a shorter completion time for the coating process [14], [15], [16].

In the cases where coating is performed with direct current (DC), the high current application typically leads to a more irregular and heterogeneous coating. Moreover, excessive use of high currents may result in undesirable side effects such as overheating, which can adversely affect the quality of the coating. Therefore, the homogeneity and quality of coatings obtained through high current application may decrease. On the other hand, when coating is carried out with alternating current (AC), the current is applied at certain intervals and constantly changing direction. During these waiting periods, the metal ion concentration at the interface of the substrate material and the coating solution can be restored. Moreover, with the constantly changing flow direction, the coating material can be transported to different regions in every direction. This allows for a more homogeneous distribution and a more equal coating thickness on the electrode surface. Therefore, it is possible to obtain smaller particle sizes with homogeneous distribution on the substrate surface [17].

In the relevant study, electrochemical coatings were carried out using the galvanostatic generic pulse method, preferring AC. In this context, it is observed that the amount of deposition decreases with increasing current values. It is seen that the increase in EASA (m^2/g_{Pt}) is achieved with increasing current values due to the decreasing amount of coating and the effect of the homogeneous distribution made possible by applying AC.

V. Conclusion

With the increasing focus on clean energy technologies becoming a fundamental necessity of our modern times, one way to enhance Proton Exchange Membrane Fuel Cells (PEMFCs), which stand out for their advantages, is through the development of catalyst materials with high efficiency. In this study, the effects of applied current deposition amount and particle size on catalyst materials developed via electrodeposition method were investigated using electrochemical characterization techniques. The determined optimal parameters, based on the obtained data, serve as pioneering work for future studies aiming to develop catalyst materials via the electrodeposition method.

References

1. Mohtasham, J., *Renewable energies.* Energy Procedia, 2015. 74: p. 1289-1297.
2. Manju, S. and N. Sagar, *Progressing towards the development of sustainable energy: A critical review on the current status, applications, developmental barriers and prospects of solar photovoltaic systems in India.* Renewable and Sustainable Energy Reviews, 2017. 70: p. 298-313.

3. Moriarty, P. and D. Honnery, *Sustainable energy resources: Prospects and policy*, in *Clean energy for sustainable development*. 2017, Elsevier. p. 3-27.
4. Basu, S., *Future directions of fuel cell science and technology*, in *Recent Trends in Fuel Cell Science and Technology*. 2007, Springer. p. 356-365.
5. Wang, C., et al., *Recent progress on the key materials and components for proton exchange membrane fuel cells in vehicle applications.* Energies, 2016. 9(8): p. 603.
6. Pavel, C.C., et al., *Highly efficient platinum group metal free based membrane-electrode assembly for anion exchange membrane water electrolysis.* Angewandte Chemie International Edition, 2014. 53(5): p. 1378-1381.
7. Ayers, K.E., et al., *Research advances towards low cost, high efficiency PEM electrolysis.* ECS transactions, 2010. 33(1): p. 3.
8. Do, C.L., et al., *Properties of Pt/C nanoparticle catalysts synthesized by electroless deposition for proton exchange membrane fuel cell.* Advances in Natural Sciences: Nanoscience and Nanotechnology, 2013. 4(3): p. 035011.
9. Sharma, R., et al., *Particle size-controlled growth of carbon-supported platinum nanoparticles (Pt/C) through water-assisted polyol synthesis.* Acs Omega, 2019. 4(13): p. 15711-15720.
10. Zhang, W., et al., *Electrodeposited platinum with various morphologies on carbon paper as efficient and durable self-supporting electrode for methanol and ammonia oxidation reactions.* International Journal of Hydrogen Energy, 2023. 48(7): p. 2617-2627.
11. Ganesan, A. and M. Narayanasamy, *Ultra-low loading of platinum in proton exchange membrane-based fuel cells: a brief review.* Materials for Renewable and Sustainable Energy, 2019. 8(4): p. 18.
12. Paul, M.T. and B.D. Gates, *Mesoporous platinum prepared by electrodeposition for ultralow loading proton exchange membrane fuel cells.* Scientific reports, 2019. 9(1): p. 4161.
13. Gautam, S., A.M. Hadley, and B.D. Gates, *Controlled Growth of Platinum Nanoparticles during Electrodeposition Using Halide Ion Containing Additives.* Journal of The Electrochemical Society, 2022. 169(11): p. 112508.
14. Rahayu, Y., S. Budi, and V. Fauzia. *Electrodeposition of Platinum (Pt) Particles as a Catalyst of Hydrogenation of Acetone*. in *IOP Conference Series: Materials Science and Engineering*. 2019. IOP Publishing.
15. Ahn, S.H., et al., *One-step co-electrodeposition of Pt–Ru electrocatalysts on carbon paper for direct methanol fuel cell.* Chemical engineering journal, 2012. 181: p. 276-280.
16. Medrano-Banda, A., et al., *Galvanostatically Deposited PtNi Thin-Films as Electrocatalysts for the Hydrogen Evolution Reaction.* ChemistryOpen, 2022. 11(2): p. e202100241.
17. Liu, Y., et al., *Self-terminating electrodeposition of Pt on WC electrocatalysts.* Applied Surface Science, 2020. 504: p. 144472.

Investigation Of Hydrogen Production Performance of KBH_4 Hydrolysis with Thin Film TiO_2 Catalyst

[1*] Ayşenur Şeşe, Meryem Sena Akkuş
[1] Ankara Yıldırım Beyazıt University, Engineering and Natural Science Faculty, Energy System Engineering Department, Keçiören, Ankara, 06010, Türkiye

* E-mail: msakkus@aybu.edu.tr aysenursese@yaani.com

Abstract
Hydrogen, a clean and versatile energy carrier, requires efficient storage solutions for widespread adoption. This study tackles this challenge by exploring the use of potassium borohydride (KBH4) for its high hydrogen content and favorable dehydrogenation properties. However, practical applications require effective catalysts to facilitate hydrogen release, with TiO_2 thin films emerging as promising candidates due to their chemical stability, oxidation power, and cost-effectiveness. This project aims to coat nanoporous TiO_2 films on lamellae using magnetron sputtering and utilize them for KBH_4 hydrolysis to generate hydrogen. The study will characterize the prepared catalysts, analyze reaction products, and optimize conditions for maximum hydrogen production. By successfully demonstrating this sustainable hydrogen generation method, the project promises significant advancements in science, technology, and the economy, positioning researchers and Turkey as pioneers in this crucial field.

Keywords: Hydrolysis, Photocatalysis, Hydrogen Production, Titanium dioxide, Potassium Borohydride

I. Introduction

Potassium Borohydride can be used as a high-density hydrogen supplier in portable fuel cells due to its attractive features such as being non-toxic, cost-effective, stable in many solvents, and transporting the hydrogen in its structure with high efficiency and safety. The hydrogen in its structure is generally released by catalytic hydrolysis or thermolysis methods [Kilinc, D., & Sahin, O. (2020)]. It is possible to produce hydrogen with high purity and efficiency, provided that an appropriate catalyst is used to accelerate the reaction kinetics of the hydrolysis of KBH_4 (Equation (1)) [Kilinc, D., & Sahin, O. (2020)].

$$KBH_4 + 2\ H_2O \rightarrow KBO_2 + 4\ H_2 \quad (1)$$

As can be seen from the equation given in Equation 1, two moles of the produced hydrogen met from KBH_4, and the remaining two moles are from the water. To extend the shelf life of metal borohydride solutions and to prevent the hydrogen released when kept waiting, basic solutions such as sodium hydroxide (NaOH), and potassium hydroxide (KOH) can be added to the solution and stored as alkali solutions [L. Damjanović, S. Bennici and A. Auroux (2010)].
TiO_2 is the most suitable semiconductor for photocatalytic applications due to its advantages such as high efficiency, low cost, high chemical stability, and biocompatibility under ultraviolet light. Electron-hole pairs are formed when TiO_2 is excited with ultraviolet light. These electron-hole pairs formed produce *OH radicals and O2* superoxides oxidize the impurities in the environment and ensure their removal over time [Mills, A., & Le Hunte, S. (1997)]. TiO_2 photocatalyst is used for many applications in powder form; however, TiO_2 thin films come to the forefront due to their various advantages such as reusability, easier separation from the system, and large- and small-scale production compared to powders. Since TiO_2 is not a strong optical absorber, it allows transparent materials such as glass to be coated without compromising their optical properties [Lettieri, S., Pavone, M., Fioravanti, A., Santamaria Amato, L., & Maddalena, P. (2021)].

The incorporation of TiO_2 in the hydrolysis of KBH_4 represents a novel application not documented in existing literature. This study aims to contribute by shedding light on this unexplored aspect, thereby enriching the academic discourse on catalysis and hydrogen production processes.

II. Experimental Set-up and Procedure

Our project work will consist of two phases. The first is the preparation and characterization of the catalyst. In the experimental setup to be developed in the second part, the conditions under which hydrogen production is best will be determined.

II.I Catalyst Preparation

During this phase, the TiO2 catalyst preparation involves selecting flat glass lamellae as a substrate for ease of cutting and coating. Cleaning the substrate is crucial to ensure a homogeneous film formation. The slides undergo sequential ultrasonic baths at 50°C in acetone, isopropyl alcohol, and ethanol for 10 minutes each, followed by rinsing with deionized water and drying at 80°C. After cleaning, slides are cut to the desired dimensions and coated with TiO2 using magnetron sputtering. The Optosense Magnetron Sputtering device in AYBU Central Research Laboratory (MERLAB) facilitates this process, resulting in a thin film coating on the TiO_2 substrate.

II.II Catalyst Characterization
The surface properties of the synthesized catalysts will be examined in the SEM device, and their structural properties will be examined using XRD.

II.III Hydrolysis Experiment Setup
KBH_4 catalytic hydrolysis experiments will be using a heating stirrer plate, a water bath to keep the reaction temperature constant, a 3-necked glass reactor, and a pressure-compensating liquid feed burette. Supported TiO2 prepared for obtaining hydrogen by the KBH_4 catalytic hydrolysis method will be weighed on a precision scale and added to the three-pending feeding burette containing KBH_4 solution will be connected. The volume of hydrogen produced in the gas burette system against time will be recorded.

II.IV Determination of optimum conditions in the hydrolysis of KBH4
In hydrolysis experiments, the effects of initial KBH_4 concentration, NaOH concentration, catalyst amount, and temperature parameters on the hydrogen production rate will be examined. Hydrolysis experiments will be carried out between 24-50 °C. As a result of the experiments, the hydrogen amounts will be recorded against the measured time. In the study, experimental design methods will be used to determine the optimum conditions. According to the data, the observed velocity expression will be determined, and the activation energy will be calculated. In addition, the maximum hydrogen production rate will be calculated [Damjanović, L., Bennici, S., & Auroux, A. (2010)].

III. Analysis
The hydrolysis experiment was conducted to investigate the effectiveness of the TiO_2 catalyst. During the catalyst coating stage, the catalyst surface was prepared using the thin film TiO_2 deposition method. The TiO_2 coating aimed to enhance the surface properties of the catalyst, thereby improving the reaction rate and optimizing the hydrogen production performance. In the hydrolysis experiment, appropriate amounts of KBH_4 compound were added to the experimental environment and interacted with the TiO_2 catalyst. This interaction enhanced the hydrolysis reaction rate and efficiency. Additionally, HCl acid was introduced into the experimental environment further to accelerate the reaction and support hydrogen gas production. Throughout the experimental stages, the performance of the TiO_2 -coated catalyst was carefully monitored, and relevant data were recorded. Hydrogen gas production was measured to evaluate the catalyst's activity and hydrolysis reaction kinetics. The obtained data were analyzed, considering parameters such as hydrogen production rate, total gas quantity, and other relevant factors.

The results demonstrated the catalytic capability of the TiO_2 -coated catalyst in the hydrolysis reaction and revealed a significant improvement in hydrogen production performance. The high surface area of TiO_2 facilitated the formation of active sites that enhanced catalytic activity and increased the reaction rate. This hydrolysis experiment conducted with the TiO_2 catalyst represents an important step towards understanding the role of TiO_2 in KBH_4 hydrolysis, enhancing efficiency in hydrogen production processes, and contributing to sustainable energy sources.

To calculate the efficiency of hydrogen production, it is determined by comparing the experimental hydrogen volume to the theoretical hydrogen volume and multiplying the result by one hundred.

IV. Results and discussions

In this study, a TiO_2 -coated thin film catalyst was successfully prepared using the sputter magnetron device through the physical vapor deposition (PVD) technique. The sputter magnetron device is a vacuum-based system and consists of fundamental components used in the coating process.

For the preparation of the thin-film catalyst coated with TiO_2, the sputter magnetron device was tuned with various parameters. The pressure setting was set at 3.11x10-6 torr, 10 mtorr was preferred for gas flow, and the rotation speed was set to 5 rpm. For RF power, the value was determined as 120W. The fast ramp setting was 1W/s. The total processing time was 160 minutes, and the substrate temperature was fixed at room temperature. These meticulous adjustments ensure that the TiO_2 -coated thin-film catalyst is successfully created with the desired quality and properties.

You can examine a table that shows the different parameters used in the experiments and the efficiency results obtained. The table contains the conditions applied for each experiment and the resulting hydrogen production efficiencies.

Temperature (K)	Amount of Catalyst (g)	Volume of HCl (ml)	Percentage of NaOH	Efficiency (%)
313	1.25	1	2	85
313	0.86	2	2	90
297	1	4	5	70
321	1	0.5	5	45
317	1	1.5	5	55
321	1.3	3	2	88
312.5	1.18	3.25	3.5	76
328	1.5	6	2	98
328	1.3	3	3	84

V. Conclusions

The experiment reached a remarkable 98% efficiency in KBH4 hydrolysis at 328K temperature, with 1.5g catalyst and 6 ml HCl volume, alongside a 2% NaOH concentration. This outcome underscores the substantial impact of temperature, acid concentration, and catalyst composition on efficiency. TiO2 exhibited robust resistance to acidic environments, enhancing hydrogen production. Notably, escalating NaOH concentrations negatively impacted reaction kinetics, while HCl had a positive effect. These findings underscore TiO2's pivotal role in hydrogen generation, promising advancements in sustainable energy solutions. In conclusion, the successful process validates TiO2's efficient utilization in KBH4 hydrolysis, offering prospects for enhanced hydrogen production technologies.

Acknowledgments

This research was supported by the TÜBİTAK, Turkey under the project number 2209-A.

References

Kilinc, D., & Sahin, O. (2020). High volume hydrogen evolution from KBH_4 hydrolysis with palladium complex catalyst. Renewable Energy, 161, 257–264. https://doi.org/10.1016/j.renene.2020.06.035

c. A review on the current progress of metal hydrides material for solid-state hydrogen storage applications. International Journal of Hydrogen Energy, 41(28), 12108–12126. https://doi.org/10.1016/j.ijhydene.2016.05.244

L. Damjanović, S. Bennici and A. Auroux, A direct measurement of the heat evolved during the sodium and potassium borohydride catalytic hydrolysis. Journal of Power Sources, 195, 3284-3292, 2010. https://doi.org/10.1016/j.jpowsour.2009.11.105

Mills, A., & Le Hunte, S. (1997). An overview of semiconductor photocatalysis. Journal of Photochemistry and Photobiology A: Chemistry, 108(1), 1–35. https://doi.org/10.1016/s1010-6030(97)00118-4

Lettieri, S., Pavone, M., Fioravanti, A., Santamaria Amato, L., & Maddalena, P. (2021). Charge Carrier Processes and Optical Properties in TiO_2 and TiO_2-Based Heterojunction Photocatalysts: A Review. Materials, 14(7), 1645. https://doi.org/10.3390/ma14071645

Yaşar, S. (2012). Titanyum Oksit Yarıiletken Filminin Elde Edilmesi, Optik ve Kristal Özelliklerinin Incelenmesi (Order No. 28635355). Available from ProQuest Dissertations & Theses Global. (2637398386). https://www.proquest.com/dissertations-theses/titanyum-oksit-yarıiletken-filminin-elde-edilmesi/docview/2637398386/se-2

Kelly, P., & Arnell, R. (2000). Magnetron sputtering: a review of recent developments and applications. Vacuum, 56(3), 159–172. https://doi.org/10.1016/s0042-207x(99)00189-x

Shaginyan, L. R., Mišina, M., Kadlec, S., Jastrabík, L., Macková, A., & Peřina, V. (2001). Mechanism of the film composition formation during magnetron sputtering of WTi. Journal of Vacuum Science &Amp; Technology A: Vacuum, Surfaces, and Films, 19(5), 2554–2566. https://doi.org/10.1116/1.1392401

Damjanović, L., Bennici, S., & Auroux, A. (2010). A direct measurement of the heat evolved during the sodium and potassium borohydride catalytic hydrolysis. Journal of Power Sources, 195(10), 3284–3292. https://doi.org/10.1016/j.jpowsour.2009.11.105

Hydrogen Transport Using Ammonia

[1]Miray Deşer Karip, [2]Kaan Baltacıoğlu
[1] İskenderun Technic Universty, Mechanical Engineering Faculty, İskenderun, Hatay, Türkiye

* E-mail: mirayydeser@hotmail.com

Abstract
The energy crisis and climate change that have taken effect in recent years affect the whole world. Green hydrogen is at the forefront of combative policies due to the energy crisis and climate change. The world is researching and testing new technologies in the production, distribution and transportation of green hydrogen, which acts as multiple energy providers. It has been determined that this type of energy will play a role in large projects in the near world, and countries, companies, universities are collaborating in the field of green hydrogen and even countries are seen making geopolitical agreements.

Keywords: Green Hydrogen, Energy Crisis, Climate Change, Green Hydrogen Transport, Green Hydrogen Production

I. Introduction

Hydrogen is an element that consists of one proton and one electron, doesnt exist in free form and is included in other compounds. For example, in water, two hydrogen atoms consist of one oxygen atom. Hydrogen; It is found combined in hydrocarbons, water, etc. Additionally, hydrogen can be produced from various energy sources such as nuclear energy, natural gas, solar and wind.

Green hydrogen is the most encouraged and researched energy source in the projects that emerge within the 2030-2050 zero CO2 and green energy framework of all countries, especially the European Union. With the investments, incentives and collaborations made by the whole world in green hydrogen, the world can achieve a carbon-free life and fight against climate change. They have shown how serious they are in their policies. Green hydrogen continues to reach a market value of 60.6 billion dollars, with approximately a thousand projects and investments of approximately 320 billion dollars by 2030, based on the 2023 'Hydrogen Insights' report. Half of the more than a thousand projects are in industrial applications, the other part is in industrial applications. The estimated capacity of electrifiers to produce green hydrogen is approximately 230 GW in 2030 production.

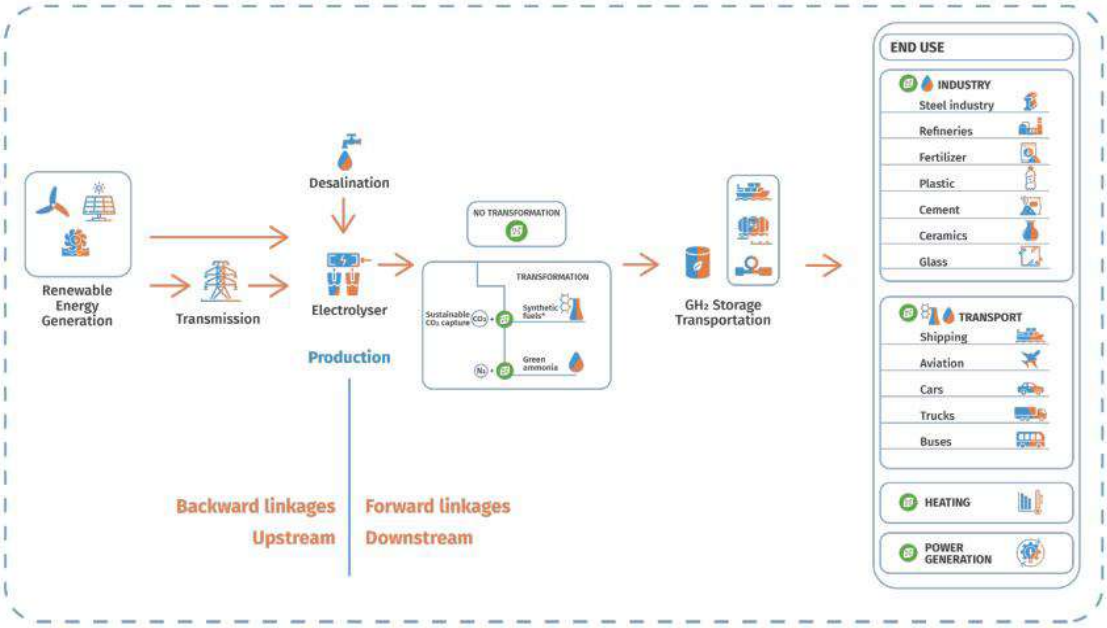


Fig. 1: Hydrogen Production and End Use

Green hydrogen is produced through electrolysis, splitting water into hydrogen and oxygen. Electrolyzers are divided into four groups according to the electrolyte and operating temperature: alkaline, polymer electrolyte membrane (PEM), anion exchange membrane (AEM) and solid oxide (SOEC). While alkaline and polymer electrolyte membrane electrolyzers are produced commercially, anion exchange membrane and solid oxide

electrolyzers are still on laboratory scale. Although alkaline electrolyzers are more widely used than PEM in water electrolyzers, it is expected that PEM type electrolyzers will surpass alkaline systems in the near future. Today, the efficiency of electrolyzers varies between 60-85%, depending on their technology.

Type	Commercial Status	Considerations
Alkaline	Mature	• Simple system design. • Have other applications with existing supply chain that can be scaled up. • Slower dynamic response; less suited for variable renewable energy (VRE) support.
Proton exchange membrane (PEM)	Commercial, fast growth	• Platinum and iridium are required. Current global iridium production could support annual deployment of up to 3-7.5 GW a year. • Faster dynamic response; well suited to VRE and voltage regulation.
Solid oxide electrolyser cells (SOEC)	Demonstration plants	• No cycling (ramp up or down); well suited for constant base load hydrogen production.
Anion exchange membrane (AEM)	Limited deployment	• Does not use any precious metals. • Membrane is less expensive than that used for PEM.

Fig. 2: Main Electrolyser Technology Comprison

Transportation and transmission issues are as important as the production of green hydrogen, and many new projects are trying to facilitate its transportation. Hydrogen transportation methods are carried by pipelines, high-pressure cylinders on the road, tube trailers and cryogenic tanks. As the distance to be transported increases, the volumes it will enter become safer.

The method of transporting ammonia by ship, which allows it to be transported to the farthest distances and is currently used, is via the ammonia transport method. Hydrogen can be converted into ammonia and transported over long distances by ship, and fuel savings can be achieved by using ammonia as ship fuel.

II. Transmission of Green Hydrogen by Shipping

Transporting hydrogen to where it will be used is a challenging task, as it has the lowest density of all gases and is also flammable when mixed with the least amount of air. Due to the low volumetric energy density of hydrogen, its transportation, storage and final delivery to the point of use can create a significant cost. There may also be security issues.
Today, almost all hydrogen is transported from the point of production to the point of use by pipeline and road by liquid tanker trucks or gas cylinder trailers.

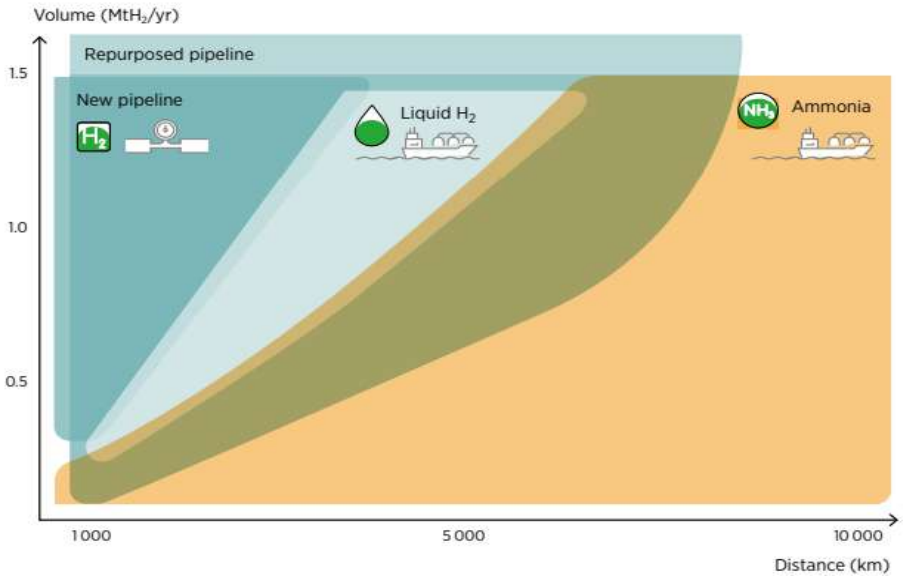


Fig. 3: Hydrogen Transportation Type

In the absence of pipelines, for longer distances hydrogen is mostly transported and delivered as a liquid in super-insulated tanker trucks called liquid tankers. To liquefy hydrogen, it must be cooled to cryogenic temperatures (-253°C /-423°F) through the liquefaction process. Once hydrogen is liquefied, it can be stored at very low temperatures in large, insulated tanks in a liquefaction plant. Liquid hydrogen can be stored as a liquid when delivered, but ultimately must be vaporized into a high-pressure gas for distribution.

Liquefying hydrogen requires energy; liquefaction currently consumes more than 30% of the energy content of hydrogen and is expensive. In addition, some of the stored liquid hydrogen will be lost through evaporation or “boiling off,” especially when small tanks with large surface-to-volume ratios are used. Fundamentally, hydrogen liquefaction is an energy-intensive process, and maintaining the low temperature required for long-distance transportation and storage purposes results in additional energy losses and associated costs. This also adds to the overall cost of using hydrogen as an energy source.

Transport gaseous hydrogen, it must be compressed to 180 bar or higher and pumped into long cylinders stacked on a trailer. This gives the appearance of long tubes; hence the name tube trailer.

There is also another transportation alternative being tested. Hydrogen could be converted into multiple carriers with higher energy density and higher carrying capacity, and could potentially be cheaper to transport over long distances. This is called material-based storage, where solids and liquids that can chemically absorb or react with hydrogen are used to bind it. Substances currently identified as potential hydrogen carriers include liquid ammonia and methanol.

Using ammonia as a carrier for hydrogen is probably the option with the most potential. Its energy density by volume is almost twice that of liquefied hydrogen, making it much easier to store and transport.
Under this approach. Ammonia, the energy carrier for hydrogen, is produced through ammonia synthesis. This chemical process allows hydrogen and nitrogen to react and turn into liquid ammonia.
The ammonia is then transported to its destination and "cracked" to release hydrogen at the point of use. It is currently estimated that cracking will result in 13-34% energy loss, but developments to reduce this are ongoing.

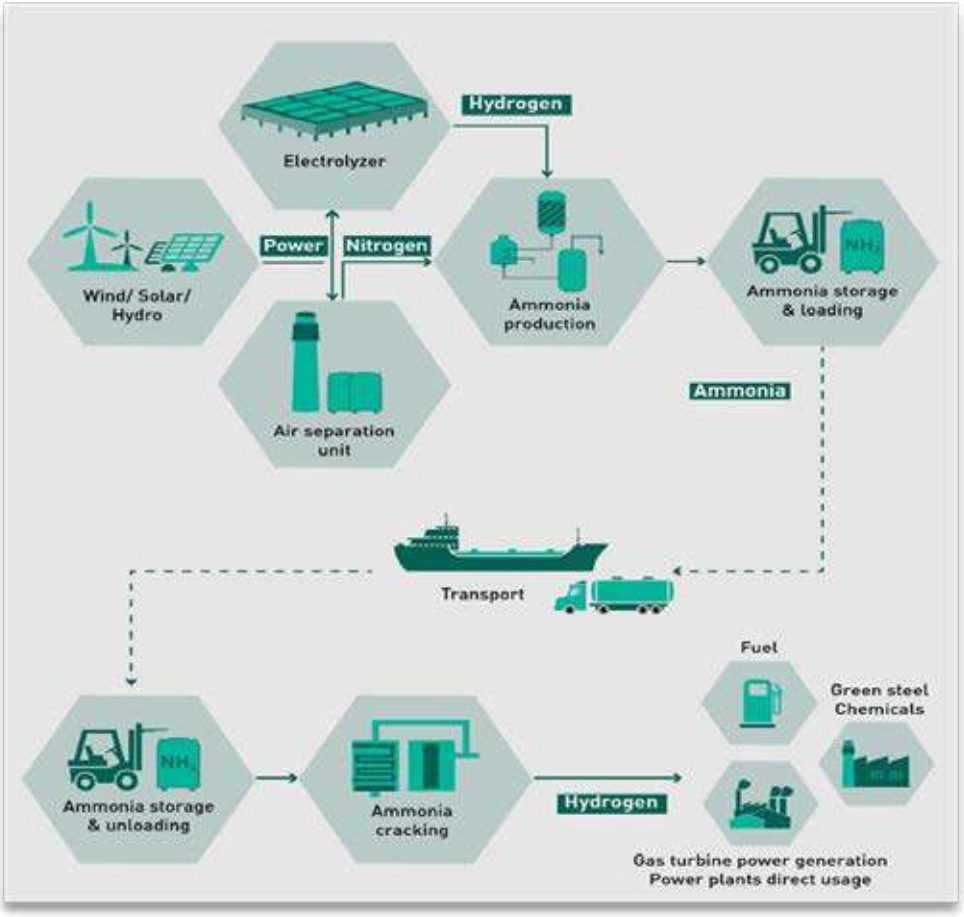


Fig. 4: Ammonia Cracking System

Transporting hydrogen using ammonia has many advantages. For example, ammonia has long been used in various industries and there is widespread infrastructure for ammonia synthesis. Additionally, ammonia can be stored in slightly refrigerated tanks at -33 °C or at ambient temperatures under pressure of 8-10 bar. This makes the storage and transportation of ammonia relatively simple and affordable.

There are also disadvantages to using ammonia. Although the infrastructure for producing ammonia exists as mentioned above, the process of breaking it down is still relatively new and not energy efficient. Additionally, after cracking, additional steps are required to purify the hydrogen for use. Additionally, some concerns have been expressed that ammonia is a toxic substance and, in the event of a leak, could have a negative impact on air, soil and water quality, as well as on the health of people living nearby.

IV. Results

The potentially critical role of hydrogen is increasing worldwide. Directing the future of hydrogen work on strategy documents and regulations to provide the necessary information continues to increase. of hydrogen from production to final use in the value chain, which includes all processes that existing gaps are being worked on.especially important in achieving net zero emissions one of the arguments is that hydrogen has entered our lives.It is known that it will add great value.

Sea transportation is not the ideal solution for pure hydrogen due to its low energy density. It is therefore usually transported in a derivative form, i.e. in combination with another substance. Ammonia has proven to be a suitable derivative here for several reasons: firstly, the energy density of ammonia is much greater than the energy density of hydrogen, and secondly, several million tons are already transported by ships every year. After transportation, ammonia is separated into water and nitrogen by cracking.

References

https://thinktech.stm.com.tr/tr/enerji-krizinin-cozumunde-yesil-hidrojen-devrimi-ii-dunyada-yesil-hidrojen-endustrisi-ve-politikalari

https://hydrogencouncil.com/wp-content/uploads/2023/05/Hydrogen-Insights-2023.pdf

https://media.licdn.com/dms/document/media/D4D1FAQEI67OWvTidSg/feedshare-document-pdf-analyzed/0/1691505679234?e=1711584000&v=beta&t=KVBg_9XprOrQi9jsO6agWbZKk_Ph0fQDKcqvOCybGaY

https://www.ideaport.org.tr/img/blog/6242f838ab621.pdf

https://www.irena.org/-/media/Files/IRENA/Agency/Publication/2022/Jan/IRENA_Geopolitics_Hydrogen_2022.pdf?rev=1cfe49eee979409686f101ce24ffd71a

https://www.irena.org/-/media/Files/IRENA/Agency/Publication/2022/Apr/IRENA_Global_Trade_Hydrogen_2022.pdf?rev=3d707c37462842ac89246f48add670ba

Heating Tubes Design for Parametric Study of Steam Reformer at Small Scale

[1*]Muhammed Murat Aksoy, [2]Onder Kaska
[1] Osmaniye Korkut Ata University, Faculty of Engineering and Natural Science, Department of Energy Systems Engineering, Osmaniye, 80000, Türkiye
[2] Osmaniye Korkut Ata University, Faculty of Engineering and Natural Science, Department of Mechanical Engineering, Osmaniye, 80000, Türkiye

* E-mail: muhammedmurataksoy@osmaniye.edu.tr

Abstract
In this study, we aim to investigate and optimize steam reformers for hydrogen (H_2) production using propane (C_3H_8) as the hydrocarbon fuel to generate syngas. The primary objective is to assess the impact of varying heating tube geometries, including circular, rectangular, and triangular designs, on the performance of the steam reformer at small-scale. Additionally, we are exploring the generation of carbon monoxide (CO) resulting from the reverse water gas shift (WGS) reaction, which has the potential to affect reactor operation. The novelty of our study lies in the comprehensive analysis of different heating tube configurations and their implications for hydrogen production. Our findings could contribute to the development of more efficient and reliable steam reformer systems for fuel cell applications, addressing challenges related to CO generation. For the same amount of propane inlet, we have observed that the circular or rectangular heating tube configurations yields better performance, with hydrogen production reaching 2.27 x 10^{-2} kg/m^3 at the exit of the steam reformer for square heating tube design.

Keywords: Steam Reformer, Propane, Hydrogen, Heating tubes, Syngas

I. Introduction

Steam reformer is mostly used to produce hydrogen (Dincer and Acar 2015). For this case, the reaction of hydrocarbon fuel and water is needed to obtain H_2 production. For fuel cells, the need for hydrogen could also be met from steam reforming of hydrocarbons. From the thermochemical perspective, products of endothermic process (i.e., syngas) during the steam reforming from hydrocarbon fuels are thoroughly explained in the literature (Pashchenko 2022). Hence, we investigated steam reformers at small scale varying heating tubes geometry to produce hydrogen for fuel cell applications. The thermochemical process starts through the porous catalytic bed with the help of the energy from the heating tubes. The important parameters to suppress the carbon formation are steam to carbon ratio and the temperature at the outlet of the steam reformer. Therefore, steam to carbon ratio should be between 2.5 and 4.5 mol/mol in practice and the carbon formation could be possible under 580°C at the outlet of steam reformer (Gateau 2007; Moulijn et al. 2013).
In this numerical study, we have employed different heating tubes to investigate the heat transfer through the catalytic bed. For the parametric study, we have defined several small-scale reactors that hot air gases would pass through base model (circular), circular tubes with channels, rectangular tubes, and triangular tubes. We investigate the hydrogen concentration, mass fractions, and temperature changes along the reactor for each simulated case.

II. Material and Method

We have numerically investigated multiple steam reformer reactors at small-scale. We have used COMSOL program to simulate the systems. A schematic steam reformer reactor is shown in Fig. 1, including the view of the designed heating tubes. Basically, we employed transport phenomena into the catalytic bed to calculate the mass transport in porous media applying Maxwell-Stefan diffusion, and we used Darcy's Law for the fluid flow. For the heating tubes, we conducted laminar fully developed flow for the non-isothermal conditions. Also, we assumed that the homogeneous porous medium is isotropic for the heat transfer, and the simulations were created for the temperature of 700K of the steam reformer inlet of the catalytic bed. The temperature of hot air at the inlet of the heating tubes were taken as 900K and 1000K. The calculations of outlet of both heating tubes and bed were performed assuming to have a dominant convective heat transport.

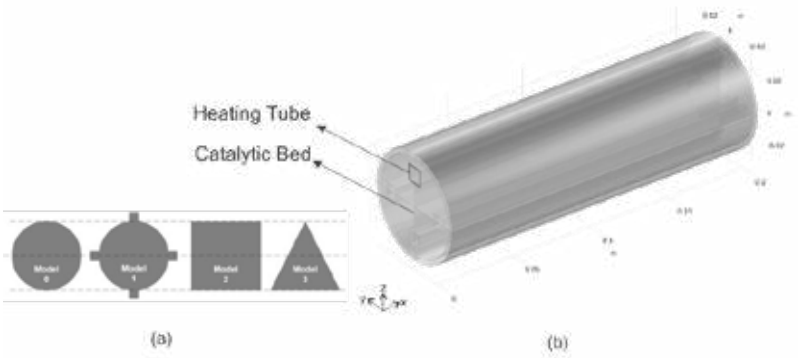


Fig. 1: Schematic view of setup and reactor (a) heating tubes design (b) steam reformer

In steam reformer, propane and water reactions occurs as follows:

$$C_3H_8 + H_2O \rightarrow H_2 + CO_2$$

The endothermic process of the propane with an enthalpy of 410 kJ/mol occurs in the steam reformer. The production of hydrogen and water can cause to produce small amount of carbon monoxide as well. Hence, the reverse water gas shift reaction (WGS) occurs as follows(Kanoğlu et al. 2020):

$$CO + H_2O \leftrightarrow CO_2 + H_2$$

The Arrhenius activation energy method was applied for the calculation of these reactions in which the activation energies were taken as 83.14 kJ/mol and 112 kJ/mol for steam reformation of C_3H_8 and CO through WGS, respectively.

We have used 4 heating tubes geometry for each reformer: Model 0 is the base circular tubes, Model 1 is the circular tubes having rectangular channels, Model 2 is the square tubes, and Model 3 is the triangular tubes. Bed diameter is 60 mm, and its length is 0.2 m. There is an insulation jacket around the bed. Diameter of circle in Model 0 is 8 mm, and other models are based on this model as can be seen in Fig. 1a. A similar problem to Model 0 can be found in COMSOL application manual (Comsol 2022). Even though the whole drawing of the reactor can be seen in Fig. 1b., we have only simulated one quarter of the reactor for computational efficiency.

III. Results and Discussions

Our aim is to investigate the effect of different heating tubes and compare its results with the base case (i.e., Model 0). Therefore, we have presented hydrogen concentrations, temperature profiles, and mass fractions of species.

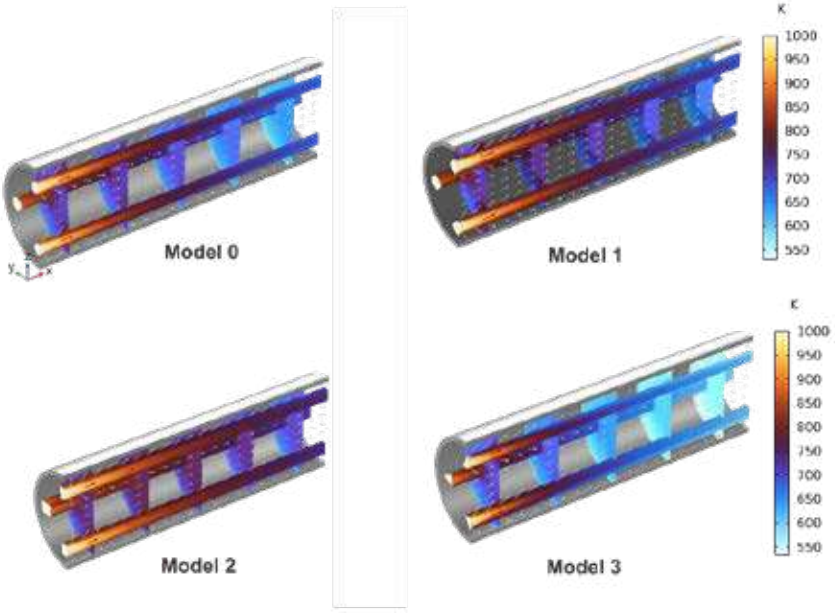


Fig. 2: Temperature variations in heating tubes and bed

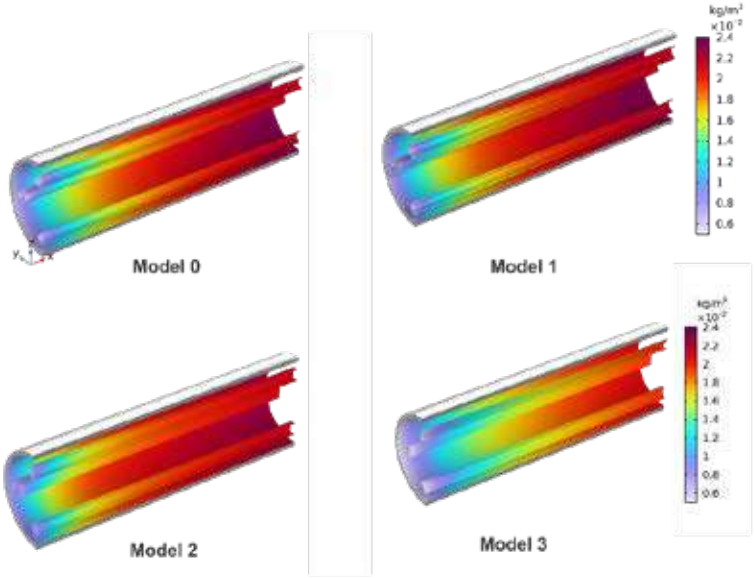


Fig. 3: Hydrogen production in steam reformer

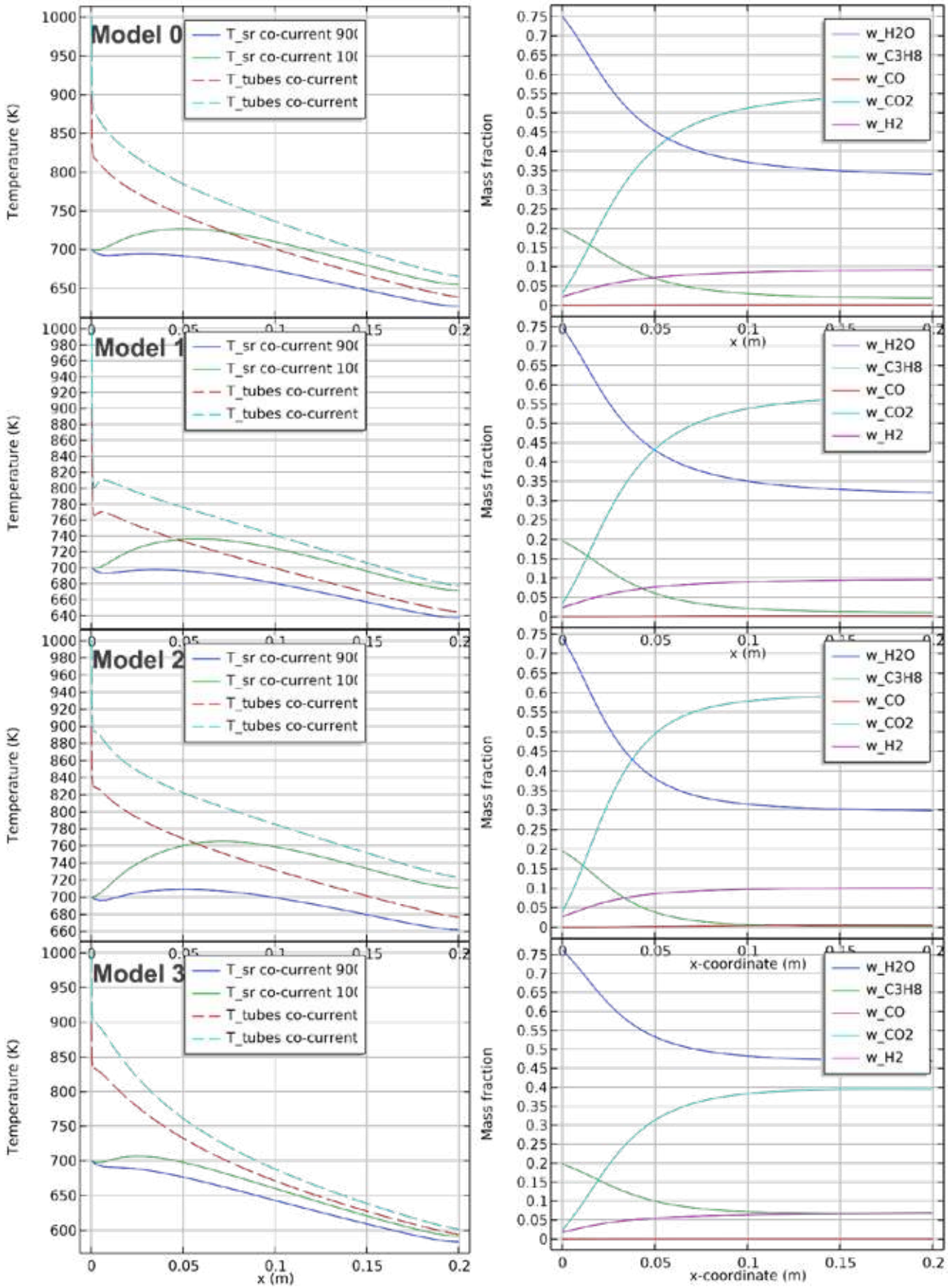


Fig. 4: Temperature profiles along the bed and mass fractions of species

All simulations were conducted under co-current flow conditions between the heating tubes and the reformer bed. Fig. 2 shows the temperature distribution across the heating tubes and the bed in five distinct slices, with an inlet temperature of 1000K for the tubes. The heat transfer from tubes to the reformer bed can be clearly depicted in this figure. The energy exchange between tubes and bed is accomplished better for Model 2 and 3 in comparison with other models as indicated by the darker blue color. The arrows representing the total heat flux on the symmetry

surfaces confirm the co-current flow setup. Regarding heat transfer efficiency, Model 3 exhibits the less effective heating tubes due to its lower temperature distribution within the reformer. The temperature distribution is directly related with the hydrogen production. Therefore, hydrogen concentration ratios are reflected in Fig. 3. Similar to temperature profiles, Model 3 has the lowest of hydrogen ratio through the flow. Model 1 and 2 seems to be efficient reactor compared to the base model (i.e., Model 0). For instance, in Model 2, the minimum hydrogen production is 0.63×10^{-2} kg/m^3 (3.58 mol/m^3), which is higher than the minimum values observed in other models, and its maximum H_2 production reaches 2.27×10^{-2} kg/m^3 (11.2 mol/m^3) through the bed.

Fig. 4 represents the temperature profiles (left column) and mass fractions (right column) with respect to x-coordinate of the bed. The data of steam reformer temperatures (T_sr) and mass fractions of species were taken from the centerline of the catalytic bed. The data of tubes temperatures (T_tubes) were taken from one of the tube walls. The inlet temperature of tubes is designated for two simulations, and it is 900K or 1000K, but the reformer temperature is 700K at the inlet for all cases. The outlet temperatures of reformer for Model 2 are higher than the other models as a sign of higher quantity of reformed propane. Also, for Model 2, the average temperatures are 693K and 729K in bed and in tube outflows, respectively. In Fig. 4, right column shows the mass fractions for all models. Additionally, the mass fraction data reveal small amounts of CO formation due to the WGS reaction, with Model 2 showing a maximum CO mass fraction of 0.005. However, even small amounts of CO can be harmful due to catalyst poisoning. The inlet mass fraction of propane remains relatively constant across all cases, with most of it being reformed in the middle of the reactor, leading to a nearly constant H2 production after a certain distance (i.e., x=0.1m) along the bed. Therefore, it can be inferred that reducing the length of the current setup by half would still yield the same concentration of H_2. Overall, these findings highlight the importance of heat transfer efficiency and temperature distribution in steam reformer performance, with implications for hydrogen production rates and potential catalyst-related challenges such as CO formation.

IV. Conclusions

We have numerically investigated hydrogen production potential in a small-scale reactor by reforming propane. Various steam reformers were designed by altering the geometry of heating tubes across four different cases. Our analysis focused on understanding the effect of energy transfer into the catalytic bed, with consistent input parameters except for the heating tube geometry. The results showed that obtained syngas including H_2 and CO can also be useful for fuel cell stack design Specifically, we found that circular or rectangular (square tube for this study) tube structures outperformed triangular tubes in terms of performance metrics such as heat transfer efficiency and hydrogen production rates. Furthermore, our findings suggest implications for small-scale fuel cell stacks, indicating that while the reactor length may be shorter than studied, increasing the number of tubes could enhance both heat transfer and hydrogen production. This underscores the importance of optimizing tube configurations and exploring additional operating parameters for future research aimed at improving overall system performance and efficiency.

References

Comsol (2022) Steam Reformer. In: COMSOL. https://www.comsol.com/model/steam-reformer-3861. Accessed 19 Mar 2024

Dincer I, Acar C (2015) Review and evaluation of hydrogen production methods for better sustainability. Int J Hydrog Energy 40:11094–11111. https://doi.org/10.1016/j.ijhydene.2014.12.035

Gateau P (2007) Design of Reactors and Heat Exchange Systems to Optimize a Fuel Cell Reformer. In: Proceedings of the COMSOL User's Conference. Grenoble, France

Kanoğlu M, Çengel YA, Cimbala JM (2020) Fundamentals and Applications of Renewable Energy. McGraw-Hill Education

Moulijn JA, Makkee M, van Diepen AE (2013) Chemical Process Technology, 2nd edn. John Wiley & Sons

Pashchenko D (2022) Natural gas reforming in thermochemical waste-heat recuperation systems: A review. Energy 251:123854. https://doi.org/10.1016/j.energy.2022.123854

Biohydrogen production in a biofilm photobioreactor with functionalized microfiber flock

Emrah Sagir[1*], Ezgi Melis Dogan-Guner[2], Harun Koku[2], Erhan Bat[2], Bora Mavis[3], Tuba Hande Erguder[4], Buket Kocaman[4], Simal Cam[4], Berfin Bagatarhan[5], Yaren Yagmur Acioglu[1], Murat San[2], Mustafa Utku Yıldırım[3], Cansen Sirin Ozbudak[2], Asya Kibar[2]

[1]Department of Biology, Osmaniye Korkut Ata University, 80000, Osmaniye, Türkiye.
[2]Department of Chemical Engineering, Middle East Technical University, 06800, Ankara, Türkiye
[3]Department of Mechanical Engineering, Hacettepe University, Ankara 06800, Türkiye
[4]Department of Environmental Engineering, Middle East Technical University, 06800, Ankara, Türkiye
[5]Department of Biology, Middle East Technical University, 06800, Ankara, Türkiye

* E-mail:emrahsagir@osmaniye.edu.tr

Abstract

Biological hydrogen production (biohydrogen) is promising due to its renewable nature. Photofermentative biological hydrogen is realized by purple non-sulfur bacteria (PNSB), using various organic substrates such as volatile fatty acids. PNSB can be immobilized to increase their concentrations and enhance their stability. Under appropriate conditions, biofilms may appear as a special and effective form of bacteria immobilization. In the present study, the PNSB species *Rhodobacter capsulatus* was used for hydrogen production in a biofilm photobioreactor. In the study, an electrostatic flocking technique was used to produce polyamide flock microfibers and the flocks were attached to support to create immobilization matrices. Results revealed that it was possible to immobilize *R. capsulatus* cells both on functionalized and non-functional microfiber flocks. *R. capsulatus* biofilm development was followed by the production of biohydrogen for 14 days.

Keywords: Biofilm, biohydrogen, electrostatic flocking, Rhodobacter capsulatus

I. Introduction

Hydrogen is a clean, sustainable, and alternative energy source that shows promise for meeting future energy demands. Biological production of hydrogen, i.e. biohydrogen has attracted interest due to its renewable and sustainable production potential.

One promising photosynthetic group for biological hydrogen production is purple non-sulfur bacteria (PNSB). One of the biological processes known as photofermentation is primarily fueled by PNSB, which uses organic substrates as electron donors and produces molecular hydrogen in an anaerobic environment with minimal nitrogen and light.

Since photofermentation works under light with a wide range of wavelengths (400–1000 nm), mild pressure and temperatures, it is thought to be a viable technique for using solar energy and other carbon sources across a wide range of light spectrums (Koku et al. 2002). However, the process should be improved to achieve economic feasibility (Genc and Koku, 2024).

Bacterial cell immobilization is an application where bacteria become stationary within a specific support material/matrix by attaching to its surface. Some microorganisms can form a special structure referred to as biofilm by adhering to a surface or to each other (Sagir and Alipour, 2021).

Electrostatic flocking is one way to achieve both attractive and useful surfaces. Using this technique, chopped fibers or desired natural or synthetic particles can be adhered to the surface while an electric field is present (McCarthy et al. 2021).

Electrostatic flocking is a quick and affordable way to cover big surfaces (McCarthy et al. 2021). In contrast to other surface treatment techniques like knitting, weaving, and electrospinning, it offers the flexibility to modify the flocked fibers' orientation perpendicular to the surface, enabling the creation of three-dimensional structures (Tonndorf et al. 2018).

There are relatively few studies on biofilm formation of *R. capsulatus* in the literature. This study aims to demonstrate immobilization of *R. capsulatus* on the polyamide microfiber surfaces produced via electrostatic flocking. Polyamide flocks were amine silanated and positively charged to enhance the attachment of negatively charged *R. capsulatus* onto the surface. We examined the influence of aminosilane functionalized fibers on the attachment of *R. capsulatus* and hydrogen production.

II. Experimental Set-up and Procedure

The bacterial culture was grown on modified BP medium (BP, 1981), containing 20 mM acetate and 10 mM glutamate (20/10, A/G). Growth of bacteria and biofilm assay were carried out by a UV-Spectrophotometer (Shimadzu UV-1800). Polyamide 6,6 (PA 6,6) flocks were used for the electrostatic flocking of fibers. Glass surfaces were used for flocked surfaces to be used in growth medium studies and commercial epoxy adhesive was used for the substrate of electrostatic flocking. APTMS and ethanol were utilized for aminosilane functionalization of flock fibers. The 350 mL Roux culture glass reactor containing flock slides was filled with the growing bacteria.

Following that, the reactors were sealed and loaded with growth (20/10 A/G) or hydrogen production (30/2 A/G) media, as appropriate. To ensure an anaerobic atmosphere, they were flushed with argon for five minutes. The reactors were continuously illuminated with a tungsten lamp producing 2500 Lux of light at 30 °C of incubation. The set-up of the experiment is shown in Fig. 1.



Fig. 1: Experimental set-up of hydrogen production

III. Analysis

A scanning electron microscope (SEM) (Tescan Vega3) was used to analyze the microorganisms on the microfiber flocks. Prior to the SEM investigation, Au/Pd coating was applied to the flock slide samples. The bacteria-biofilm on the flock fibers was also observed using a metallurgical optical microscope (Motic BA310-Met). A modified spectrophotometric crystal violet biofilm assay was used to quantify the amount of biofilm that formed (Kamimura et al. 2022).

The generation of organic acid and the consumption of acetic acid were analyzed using HPLC. Gas chromatography was used to evaluate the composition of the generated gas (GC). Using a spectrophotometer (Shimadzu UV-1800) set at 660 nm, the bacteria's growth was measured. A gas chromatograph (Agilent 6890 N) fitted with a SupelcoCarboxen 1010 column (150 mm x 4.1 mm) and a Thermal Conductivity Detector (TCD) was used to examine the composition of evolved biogas. The carrier gas was argon with a 25 mL/min flow rate. On average, 90% of the evolved gas was hydrogen. By using water displacement, the evolved gas was gathered in graded tubes. Samples of 2 mL were extracted from the photobioreactors every 24 hours for analysis of organic acids. The pH change was measured by a pH meter (Mettler Toledo 3311). Using High-Performance Liquid Chromatography (HPLC) (Shimadzu 20A series, Japan) with a UV detector (Shimadzu FCV-10AT) the organic acid content of the samples was determined by an the Alltech I0A-1000 ion-exchange column.

IV. Results and discussions

Biohydrogen production was achieved after bacteria was grown and immobilized on 20/10 A/G for a week. The following week, hydrogen was produced using a biofilm photobioreactor that was supplied with 30/2 A/G hydrogen production media. Polyamide flocks were amine silanated for enhanced attachment of the bacteria. Biofilm formation has been observed under optic microscope both in functional and non-functional microfiber containing photobioreactors (Fig. 2).

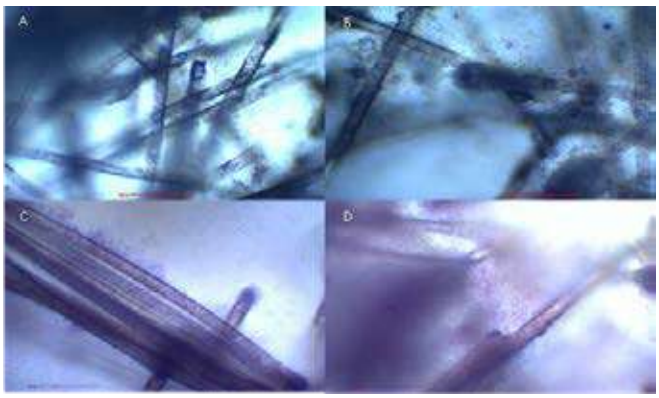
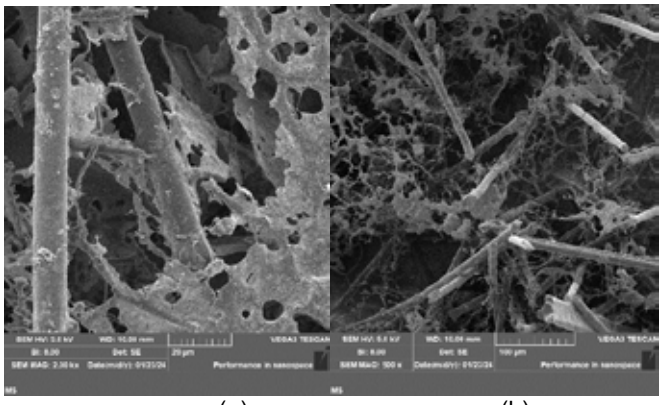


Fig. 2: Microscopic biofilm images of non-functional (A,C) and functional (B,D) microfiber flocks grown on 20/10 A/G and 30/2 A/G media (Motic) (50X)

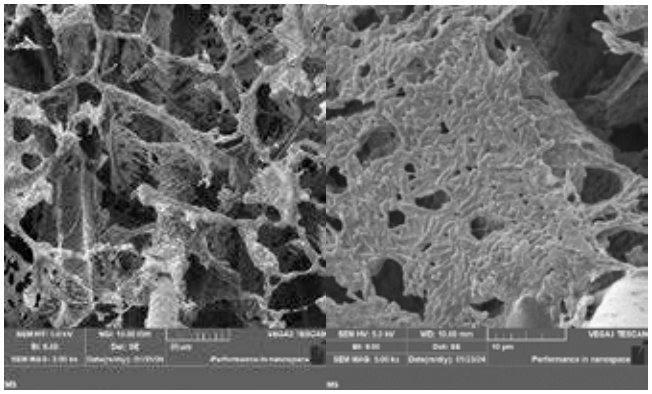
SEM images of functionalized and non-functionalized microfiber flocks in PBRs were also shown (Fig. 3-4). There has been a web-like matrix structure between microfibers. It can be signs of biofilm which is observed on the Scanning Electron Microscope. Hydrogen production rates of biofilm with functional and non-functional microfibers were 0.34 mmol/L/h and 0.33 mmol/L/h, respectively.



(a) (b)

Fig. 3: SEM images of functional microfibers on 20/10 A/G growth medium (a), and 30/2 A/G hydrogen production medium (b).

Functionalized flocks had somewhat higher (Abs:0.62) biofilm production than non-functional flocks (Abs:0.51), according to the spectroscopic analysis of the modified crystal violet biofilm assay.



(a) (b)

Fig. 4: SEM images of non-functional microfibers on 20/10 A/G growth medium (a) and 30/2 A/G hydrogen production medium (b).

Biological hydrogen production was achieved for subsequent two run of operation through 168 h (Fig. 5). Biohydrogen was produced both with functionalized and non-functionalized flocks in PBRs.

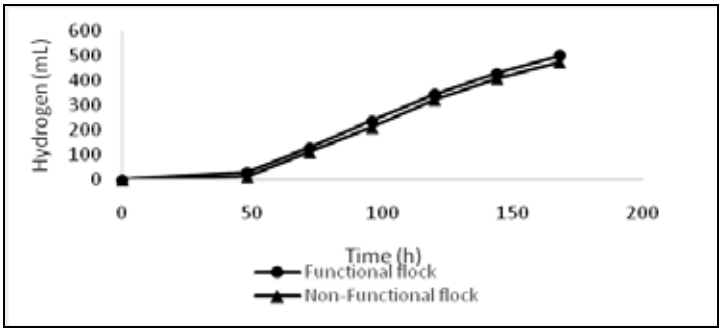


Fig.5: Cumulative hydrogen production of biofilm PBR with functional and non-functional flocks.

V. Conclusions

Optical microscope and SEM images showed that the bacteria had adhered to the microfiber flocks through adsorption. Biohydrogen production has been carried out by the biofilm either with functionalized and non-functionalized polyamide flocks. Similar results in biofilm growth and hydrogen production have been obtained in the microfiber flocks. Functionalized microfibers had a slightly higher impact on biofilm formation and hydrogen production. With functional and non-functional microfibers, the rates of hydrogen production in biofilm PBR were 0.34 mmol/L/h and 0.33 mmol/L/h, respectively. Further research is going on to optimize the hydrogen production.

Acknowledgements

This research has received funding from TÜBİTAK (The Scientific and Technological Research Council of Turkey) TUBITAK Project Number: 222M104 (TÜBİTAK 1001 project).

References

Biebl H., Pfennig N., Isolation of members of the family Rhodospirillaceae. Editor: Starr M.P., Stolp H., Truper H.G., Balows A., Schlegel H.G., The Prokaryotes, 1, 267-273, (1981). Springer: New York.

Genc S, Koku H., A preliminary techno-economic analysis of photofermentative hydrogen production, International Journal of Hydrogen Energy, 52, 212-222, (2024).

McCarthy A., John J. V., Saldana L., Wang H., Lagerstrom M., Chen S., Su Y., Kuss M., Duan B., Carlson M. A., Xie J., Electrostatic Flocking of Insulative and Biodegradable Polymer Microfibers for Biomedical Applications, Advanced Healthcare Materials, 10, 2100766, (2021).

Kamimura, R., Kanematsu, H., Ogawa, A., Kogo, T., Miura, H., Kawai, R., Hirai N, Kato, T., Yoshitake, M, Barry, DM., Quantitative Analyses of Biofilm by Using Crystal Violet Staining and Optical Reflection, Materials (Basel). 15(19), 6727, (2022).

Kumari U.M., Das S., Bacterial biofilm and extracellular polymeric substances in the moving bed biofilm reactor for wastewater treatment: A review, Bioresource Technology, 345,126476, (2022).

Sagir E., Alipour S., Photofermentative hydrogen production by immobilized photosynthetic bacteria: Current perspectives and challenges, Renewable and Sustainable Energy Reviews, 14, 110796, (2021).

Tonndorf R., Gossla E., Kocaman R. T., Kirsten M., Hund R.D., Hoffmann G., Aibibu D., Gelinsky M., Cherif C., Factors affecting the mechanical and geometrical properties of electrostatically flocked pure chitosan fiber scaffolds., Textile Research Journal, 88, 1965–1978, (2018).

Maximizing Power Efficiency: The FC+PV+WT Hybrid Renewable Energy System

[1*]Ayse Kocalmis Bilhan
[1]Nevşehir Haci Bektas Veli University, Electrical Electronic Eng. Dept., Nevşehir, 50200, Türkiye

* E-mail: akbilhan@gmail.com

Abstract
The present research presents a proposal for a Hybrid Renewable Energy System (HRES) that incorporates a fuel cell (FC) stack, a solar photovoltaic (PV) module, and a wind turbine (WT). This paper discusses the modeling of the HRES PV array, wind turbines, and FC, and proposes an integrated Perturb and Observe (IPO) approach to maximize the power output. Additionally, it is analyzed various system configurations to determine the most effective configuration for power generation. Using MATLAB/SIMULINK, it is designed a grid-connected HRES with FC stack, PV, and wind with a battery bank. It is analyzed the output power and voltage performance of the proposed HRES with and without using the IPO-MPPT algorithm. The empirical results indicate that FC+PV+W is the optimum combination to meet the load demand against intermittent PV and wind energy systems.

Keywords: Fuel cell, pv array, renewable energy, wind turbine

I. Introduction

The utilization of various renewable energy sources has gained significant attention in recent years due to their environmental and economic benefits. Harnessing the kinetic energy of wind through wind turbines, converting solar radiation into electrical energy via photovoltaic panels, converting the potential energy of water in rivers or dams into electrical energy through water turbines, and tapping into the thermal energy stored in the ground through geothermal energy are some of the methods currently employed for generating renewable energy. Moreover, fuel cells have emerged as a promising technology for producing electrical energy via electrochemical reactions. Despite the lucrative and eco-friendly nature of solar arrays and wind farms as alternatives to fossil fuel, their usage still faces limitations due to inadequate structure and methods to manage the intermittency of on-site (decentralized or distributed) energy generation. An Hybrid Renewable Energy Systems (HRES), whether off-grid (isolated) or grid-tied, can address this issue. In grid-connected operation, when the energy produced by the HRES exceeds the current load demand, surplus power is supplied to the grid. Conversely, whenever the HRES is insufficient to meet the load requirements, it obtains power from the grid to fulfill the local load demand (Ammari et al., 2022; Kamel et al., 2021; Khalil and Dincer, 2024; Thirunavukkarasu et al., 2023). The employment of hybrid renewable energy generation is a more viable option for modern microgrid design, offering several environmental and socio-economic benefits

Wind and photovoltaic (PV) power-generating systems are subject to various stochastic and discontinuous parameters such as temperature, time, seasons, and weather conditions. Therefore, these energy sources alone cannot meet the load demand reliably. For this reason, fuel cells, which have become very popular with the studies carried out today, are used together with photovoltaic and wind energy systems to form HRES. The most cost-effective method to increase the efficiency of hybrid renewable energy systems is the application of the maximum power point tracking (MPPT) algorithm. Numerous approaches have been proposed in the literature to extract the maximum power point (MPP), varying depending on the type of sensing elements, cost, efficiency, load, and accurate monitoring ranges caused by sudden temperature changes, shading, or fluctuations. wind speed (Hossain et al., 2024; Khan and Mathew, 2019; Thaler et al., 2023).

In this study, a grid-connected HRES with converters is studied and analyzed in MATLAB/Simulink environment. The objective of this approach is to control the operational state of the entire system by finely adjusting the mppt in response to varying conditions. This research aims to compare the effectiveness of these different system configurations such as FC, FC+PV, FC+WT, FC+PV+WT, and provide insight into efficiency assessments of alternative HRES.

II. System Component and Modelling

The combination of FC, WT, and PV array power generation systems with dedicated converters creates the conventional HRES. The fundamental architecture of the envisioned HRES is illustrated in Figure 1.While FC and PV are directly connected to the DC-DC converter, WT is connected to the DC-DC converter circuit after rectifying the voltage with a generator and rectifier circuit. These energy sources are combined at the shared DC link to form an HRES. The proposed HRES is subsequently attached to Maximum Power Point Tracking MPPT system. The suggested FC+WT+PV energy generation system involves an IPO-MPPT controller. The accomplishment of maximum energy output from the HRES is facilitated by implementing a maximum power tracking algorithm concurrently. The next sections will clarify the mathematical model for the Fuel Cell (FC), Photovoltaic (PV) array, and Wind, providing a comprehensive understanding of the system's functionality.

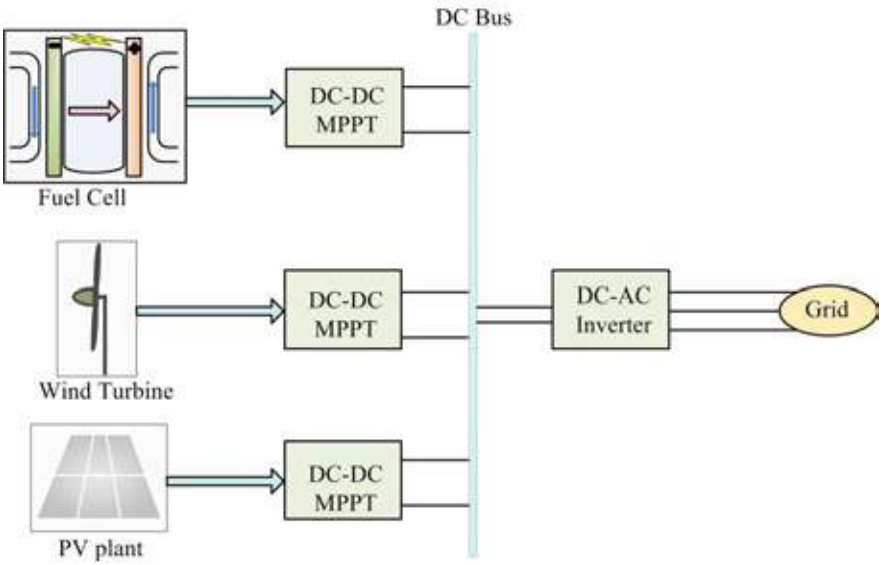


Fig. 1: The schematic diagram of the proposed HRES

II. I. Fuel Cell (FC)

Fuel Cells (FCs) are electrochemical devices that transform chemical energy into electrical energy and provide several benefits such as modularity, high scalability, good transient response, low emissions, and safety (Dincer and Ishaq, 2022). While fuel cells can be classified in various ways depending on the type of electrolyte used in the fuel cell system, Proton Exchange Membrane Fuel Cells (PEMFCs) were used in this study. The circuit diagram is given in Figure 2. The electrochemical reactions and the output voltage of FC are given in Equation1 and Equation 2.

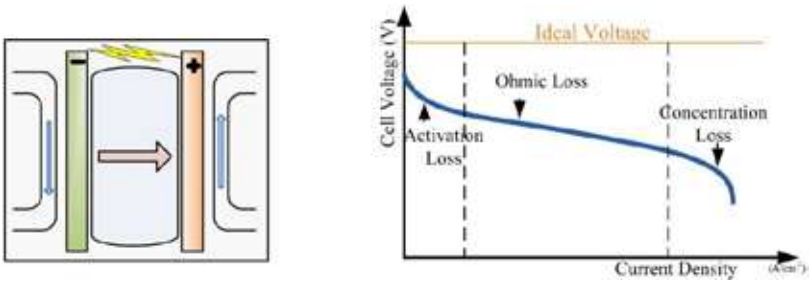


Fig. 2. The circuit diagram and V-I polarization curve of PEMFC

$$\left.\begin{aligned} &Anode\ Reaction:\ H_2 \rightarrow 2H^+ + 2e^- \\ &Cathode\ Reaction:\ \tfrac{1}{2}O_2 + 2H^+ + 2e^- \rightarrow H_2O \\ &Overall\ Reaction:\ H_2 + \tfrac{1}{2}O_2 \rightarrow H_2O + electrical_energy + heat_energy \end{aligned}\right\} \quad (1)$$

$$V_{FC} = E - V_{act} - V_{\Omega} - V_C \quad (2)$$

where, V_{FC}, E, V_{act}, V_C, and V_{Ω} represent the output voltage value, the electrochemical thermodynamic voltage, the voltage drop due to activation, the voltage drop due to density or mass, the voltage drop on the electrodes and membrane, respectively.

II. II. PV Array

The photovoltaic (PV) cell directly converts solar radiation into DC power. However, the energy supplied by a single PV cell is limited to around 1V. As a solution, PV panels, arrays, and systems are created by connecting PV cells in parallel, series, or both. Modeling PV cells is a challenging task due to their non-linear characteristics. As a result, various photovoltaic cell models have been proposed, including the single diode model, two diode model, and others. In this study, the single diode model, known for its high accuracy and simplicity, was used (as shown in Figure 3).

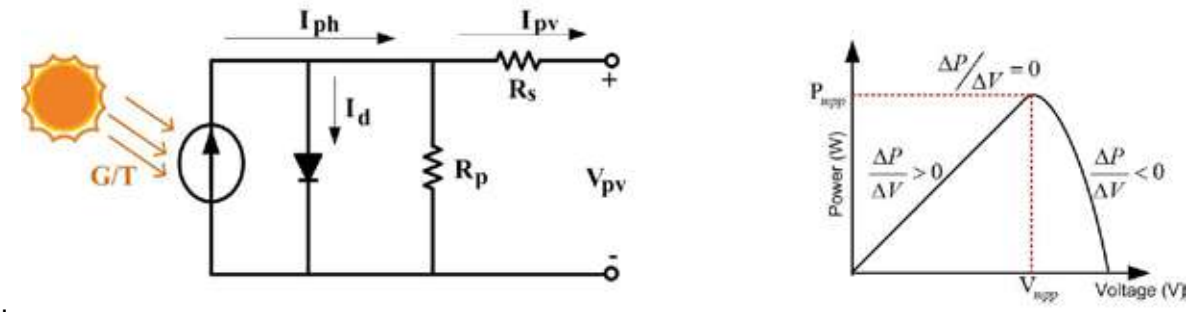


Fig. 3. Single diode model of PV cell and P-V polarization curve.

As it is seen Figure 3, it is consist of a current source, a diode, a series resistance and parallel resistance which represent metal contacts (R_s) and leakage of the PN junction (R_p). G/T is solar radiation and temperature.

In the Equation 3 and 4, the output current and voltage of a PV cell were derived by using Kirchhoff`s current law;

$$I_{pv} = I_{pv} - I_s\left[\exp\left(\frac{q\left(V_{pv}+I_{pv}R_s\right)}{nKT}\right)\right] - \frac{V_{pv}+I_{pv}R_s}{R_{sh}} \quad (3)$$

$$V_{pv} = \frac{nKT}{q}\left[\frac{I_{ph}+I_d-I_{pv}}{I_{pv}}\right] - R_s I_{pv} \quad (4)$$

where; I_{pv}; and V_{pv} represent PV cell output current (A) and PV cell output voltage (V), respectively. I_{ph} is the photocurrent or light-generated current, I_s is the saturation current, q is electron charge ($1.6x10^{-19}$C), k is Boltzmann constant ($1.38064x10^{-23}$ j/k), T is cell temperature in Kelvin degrees (273.15 +°C), n is ideality factor of the diode. All these parameters are calculated under standard test conditions such as *G* = 1000W/m², *T* = 25°C, and *AM* = 1.5 (Ruban et al., 2023).

II.III Wind Turbine

Wind energy conversion systems (WECSs) convert the kinetic energy in the wind first into mechanical energy and then into electrical energy. The wind turbine system is composed of several components, including a generator, blade, electronic converters, filter, and control system. The generator plays a crucial role in converting mechanical power into electrical power, while the wind turbine harnesses wind power and converts it into electrical energy. However, the electrical energy generated by the generator cannot be directly connected to the electrical grid system due to its unsuitability. Therefore, converters are employed to connect wind turbines to the electrical grid system, and the voltage generated by the generator is regulated by control systems.

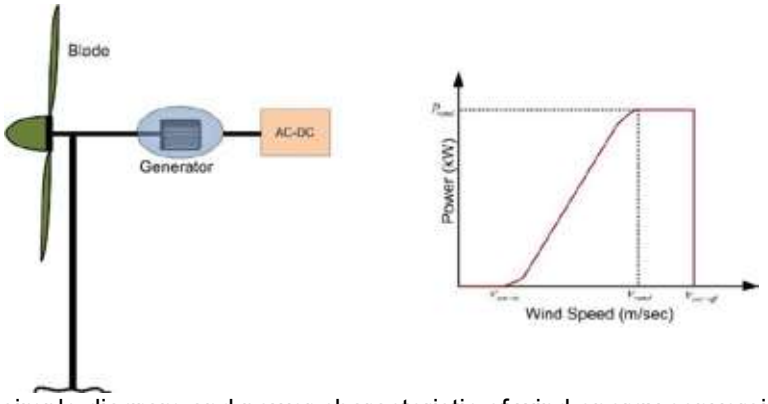


Fig. 4. The simple diagram and power characteristic of wind energy conversion system.

To determine the mechanical power obtained from the wind turbine, Eq.5 is utilized, which takes into account the swept area of the rotor blades (A), air density (ρ), power conversion coefficient (C_p), and wind speed (v). If the swept area, air density, and wind speed are assumed to be constant, the aerodynamic power can be obtained via the power factor of the wind turbine. Additionally, the ratio between the angular velocity of the wind turbine and wind speed, known as the type speed ratio, can be expressed as λ, which is given in Eq. 6 (Silva et al., 2023).

$$P_m = \frac{1}{2}\rho A C_p(\lambda,\beta)v^3 \quad (5)$$

$$\lambda = \frac{\omega_m R}{v} \quad (6)$$

III. Results and discussions

In the context of renewable energy systems, such as fuel cell, solar, and wind power systems, the implementation of Maximum Power Point Tracking (MPPT) serves as a crucial mechanism aimed at optimizing power output despite variations in hydrogen availability, solar irradiance, and wind speed. Conventionally, the integration of dedicated controllers for individual components within hybrid renewable energy systems (HRES), such as fuel cell, solar, and wind generation units, has been a common practice, resulting in increased expenses and system complexity. The pseudocode summary for this control algorithm is presented in below.

```
Input V=[Vfc Vpv Vw]; I=[ Ifc Ipv Iw];
Output= Power
1: Computes the generating powers of FC, PV, WT such as Pfc=Vfc*Ifc, Ppv=Vpv*Ipv, and Pw=Vw*Iw stores in P=[Pfc Ppv Pw]
2: Computes ΔP and ΔV
3: for I=k
4:   if ΔP>0;
5:      if ΔV>0;
6:         d=d-Δd
7:      elseif ΔV<0;
8:         d=d+Δd
9:      end
10:     else ΔV>0;
11:        d=d+Δd
12:     elseif ΔV<0;
13:        d=d-Δd
14:     end
15: apprise V(k-1)=V(k);
16:      I(k-1)=I(k);
17: end
```

V. Conclusions

In this study, it is proposed a grid-tied HRES with FC, solar, and wind using converters. A novel fast and highly accurate MPPT controlling algorithm has been implemented to excerpt the highest energy of FC, solar, and wind energy systems. It is investigated various system configurations that incorporate fuel cell, photovoltaic, and wind turbine elements to identify the most effective configuration for the Maximum Power Point Tracking (MPPT) control algorithm. It is conducted a rigorous analysis of the output power and voltage performance of the proposed Hybrid Renewable Energy System (HRES) utilizing the control algorithm. It is observed that the combination of fuel cell, photovoltaic, and wind turbine labeled as FC+PV+WT emerges as the optimal configuration for fulfilling the energy demand load.

References

Ammari, C., Belatrache, D., Touhami, B., Makhloufi, S., 2022. Sizing, optimization, control and energy management of hybrid renewable energy system—A review. Energy and Built Environment 3, 399–411. https://doi.org/10.1016/j.enbenv.2021.04.002

Dincer, İ., Ishaq, H., 2022. Renewable Hydrogen Production. Elsevier.

Hossain, M.B., Islam, M.R., Muttaqi, K.M., Sutanto, D., Agalgaonkar, A.P., 2024. A power dispatch allocation strategy to produce green hydrogen in a grid-integrated offshore hybrid energy system. International Journal of Hydrogen Energy 62, 1103–1112. https://doi.org/10.1016/j.ijhydene.2024.03.051

Kamel, A.A., Rezk, H., Abdelkareem, M.A., 2021. Enhancing the operation of fuel cell-photovoltaic-battery-supercapacitor renewable system through a hybrid energy management strategy. International Journal of Hydrogen Energy, Developments of Hydrogen Fuel Cell Technologies 46, 6061–6075. https://doi.org/10.1016/j.ijhydene.2020.06.052

Khalil, M., Dincer, I., 2024. Investigation of a community-based clean energy system holistically with renewable and hydrogen energy options for better sustainable development. Journal of Cleaner Production 440, 140895. https://doi.org/10.1016/j.jclepro.2024.140895

Khan, M.J., Mathew, L., 2019. Comparative study of maximum power point tracking techniques for hybrid renewable energy system. International Journal of Electronics 106, 1216–1228. https://doi.org/10.1080/00207217.2019.1584917

Ruban, N., Rudnik, V., Askarov, A., Maliuta, B., 2023. Frequency control by the PV station in electric power systems with hydrogen energy storage. International Journal of Hydrogen Energy 48, 28262–28276. https://doi.org/10.1016/j.ijhydene.2023.04.048

Silva, R.N., Nunes, M.M., Mendes, R.C.F., Brasil, A.C.P., Oliveira, T.F., 2023. A novel mechanism of turbulent kinetic energy harvesting by horizontal-axis wind and hydrokinetic turbines. Energy 283, 128985. https://doi.org/10.1016/j.energy.2023.128985

Thaler, B., Posch, S., Wimmer, A., Pirker, G., 2023. Hybrid model predictive control of renewable microgrids and seasonal hydrogen storage. International Journal of Hydrogen Energy 48, 38125–38142. https://doi.org/10.1016/j.ijhydene.2023.06.067

Thirunavukkarasu, M., Sawle, Y., Lala, H., 2023. A comprehensive review on optimization of hybrid renewable energy systems using various optimization techniques. Renewable and Sustainable Energy Reviews 176, 113192. https://doi.org/10.1016/j.rser.2023.113192

Development of Polybenzimidazole Containing MOF Membranes for Anion Exchange Membrane Water Electrolysis

[1,2]Hasan Altınışık, [2]Yılser Devrim
[1] Atılım University, Department of Energy Systems Engineering, Incek Golbasi Ankara, 06830, Türkiye
[2] Atılım University, Graduate School of Natural and Applied Sciences, Department of Mechanical Engineering, Incek Golbasi Ankara, 06830, Türkiye

* E-mail: yilser.devrim@atilim.edu.tr

Abstract
Anion exchange membrane water electrolysis (AEMWE) is promising for large-scale green hydrogen (H_2) production. However, water electrolysis via anion exchange membrane in alkaline media has some limitations, such as low ionic conductivity and membrane stability. This work presents experimental results of polybenzimidazole (PBI)/zeolitic imidazolate framework (ZIF-8) composite anion exchange membranes with high ionic conductivity, porosity, and durability for green hydrogen production. The structural and electrochemical characteristics of the PBI/MOF composite membranes were examined by the TGA, XRD, XPS, and electrochemical techniques. Synergistic effects between polymer and MOF structures combined the advantages of the materials and enabled the development of an anion exchange composite membrane (PBI/modified-ZIF8) with high H_2 production potential.

Keywords: Anion exchange membrane water electrolysis, anion exchange membrane, composite membrane, Metal-organic frameworks, hydrogen production

I. Introduction

Today, the need for alternative energy sources has increased due to the increasing global warming problem. Hydrogen energy has high energy density and zero emissions and has been seen as a sustainable and renewable energy source that can replace fossil fuels. There are various methods to produce hydrogen, such as hydrocarbon reforming, pyrolysis, biomass processes, and water electrolysis. Among these, hydrogen production by water electrolysis is of great interest due to its advantages of high efficiency, zero emissions and high purity production. Moreover, using energy generated from renewable sources in electrolyzers increases the sustainability of hydrogen production by water electrolysis. Four main water electrolysis systems are used: alkaline water electrolysis (AWE), proton exchange membrane water electrolysis (PEMWE), solid oxide water electrolysis (SOWE) and anion exchange membrane water electrolysis (AEMWE) (Park et al., 2019). Among them, AWEs work with liquid alkaline electrolytes and are low-cost (David et al., 2019). PEMWEs can produce high-purity hydrogen with high efficiency. However, the acidic electrolyte causes corrosion of catalysts and other components (Feng et al., 2021). SOWEs allow the use of high-temperature electrolyzers with high efficiency and good stability, but have limitations in large-scale applications, such as bulky system design, safety issues with electrodes and sealing (Sebbahi et al., 2022).

AEMWEs have been developed in recent years as an alternative water electrolysis system. They utilize an anion exchange membrane (AEM), alkaline electrolyte, and low-cost PGM-free electrocatalysts. The presence of a solid electrolyte in AEMWE reduces gas migration and allows for high-purity hydrogen production like PEMWE. However, due to the harsh alkaline environment, AEMWEs show poor performance and stability (Li et al., 2020). To overcome these challenges, research and development of new membranes are ongoing.

Polybenzimidazole polymers (PBI) have a tight chain structure based on strong hydrogen bonds and π-π interactions between polymer chains. Their high thermal stability and gas separation properties make them good membrane candidates for AEMWE systems (Cong et al., 2021). PBI shows low ionic conductivity in pure form for AEMWE applications, poor alkalinity in aqueous solutions, and mechanical stability decreases with heavy alkali doping (>8M). Composite membranes are being produced to overcome these limiting factors. MOF structures are interesting as polymer fillers due to their large surface area, porosity, high ionic conductivity and easy processability. In this study, the PBI/ZIF-8 composite membranes were prepared and hydrogen production performance was investigated in the AEMWE system.

II. Experimental Procedure

a. **PBI Polymer Preparation:** In the synthesis of pPBI, 3,3-Diaminobenzidine (DAB) is dissolved in a certain amount of polyphosphoric acid (PPA) at 140 °C. Then, terephthalic acid (TPA) is added to the solution, and the temperature is increased to 180 °C. The solution is reacted for 18 hours in a Nitrogen atmosphere with the help of a mechanical stirrer. The polymer obtained at the end of the reaction is washed with DI water and dried at 80 °C.
b. **ZIF-8 and Modified ZIF-8 Preparation:** In the synthesis of ZIF-8, firstly, the solution of $Zn(NO_3)_2.6H_2O$ and methanol was added to the solution of 2-methyl imidazole and methanol and stirred at room temperature for 1 hour (Fig. 2.a). The white crystals formed were separated by centrifugation with methanol and dried. In the synthesis of modified ZIF-8, ZIF-8 crystals and NBu_4OH (tetrabutylammonium hydroxide) solution were prepared and stirred at 70 °C for 24 hours (Fig. 2.b). At the end of the reaction, modified ZIF-8 was separated from the solution and dried.
c. **Composite Membrane Preparation:** PBI based composite membranes were prepared by solution casting

method with 2.5% MOF doping.

III. Analysis

The structural characterization of the polymer, MOF, and composite membranes was performed by Nuclear Magnetic Resonance (NMR), Fourier transform infrared spectroscopy (FTIR), Thermogravimetric Analysis (TGA), X-ray Diffraction (XRD), X-ray Photoelectron Spectroscopy (XPS) methods. The morphological properties of the materials were investigated with field-emission scanning electron microscopy (SEM), and the electrochemical characterization was conducted by electrochemical measurements. AEMWE performance tests were conducted at Atılım University Hydrogen Energy and Fuel Cells Research Laboratory.

IV. Results and Discussions

Fig. 1 shows the FTIR spectra of the PBI polymer. The polymer exhibited characteristic adsorption bands at approximately 3250 and 1624 cm-1 due to the stretching vibration of N-H and C=H groups. A strong adsorption band around 2000-3500 cm-1 shows that the polymer may contain residual PPA (Malinowski et al., 2014). -8 particles have four characteristic peaks at 2926, 1600, 1145, and 995 cm−1, assigned to vibrations of C−H, C=N, and C−N in the imidazole ring, respectively (C. Wu et al., 2017).

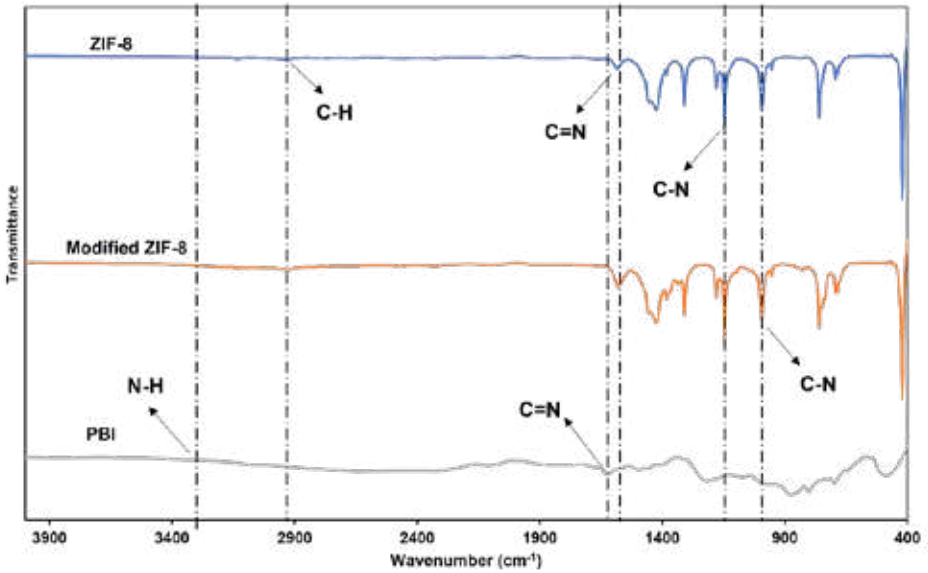


Fig 1. FTIR of PBI polymer, ZIF-8 and modified ZIF-8 particles

The XRD analysis was done to determine the crystal structure of ZIF-8 and modified ZIF-8 (Fig 2.). The strong peaks of ZIF-8 show good agreement with the literature. The peaks at 2θ= 7.3°, 10.35°, 12.70°, 14.80°, 16.40° and 18.00° correspond to the planes (110), (200), (211), (220), (310), and (222) respectively (Teknologi et al., 2017). The diffraction patterns of the modified ZIF-8 structure do not show a significant difference from the unmodified sample. This proves that the MOF structure does not decompose in a highly alkaline environment (pH > 14) and shows high chemical stability. The decrease in the intensities of the peaks indicates that the atomic arrangement of ZIF-8 was modified by tetrabutylammonium hydroxide, but the crystal structure was preserved during the process (Sadakiyo et al., 2014).

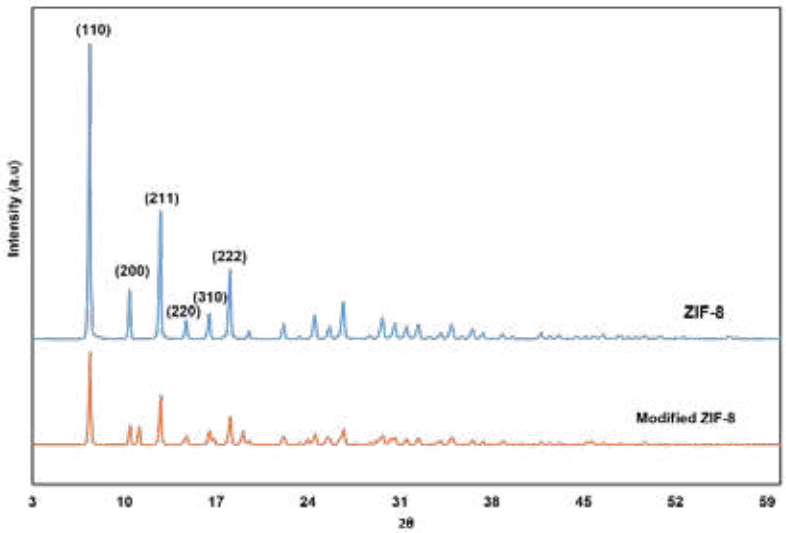


Fig 2. XRD patterns of ZIF-8 and modified ZIF-8 particles

TGA analysis results of ZIF-8 and Modified ZIF-8 structures are given in Fig.3. 27.95% and 33.4% of the weights of ZIF-8 and Modified ZIF-8 were preserved, respectively. These data prove that the synthesized MOF structures show higher thermal stability compared to literature studies (S. Wang et al., 2020; Yin et al., 2015).

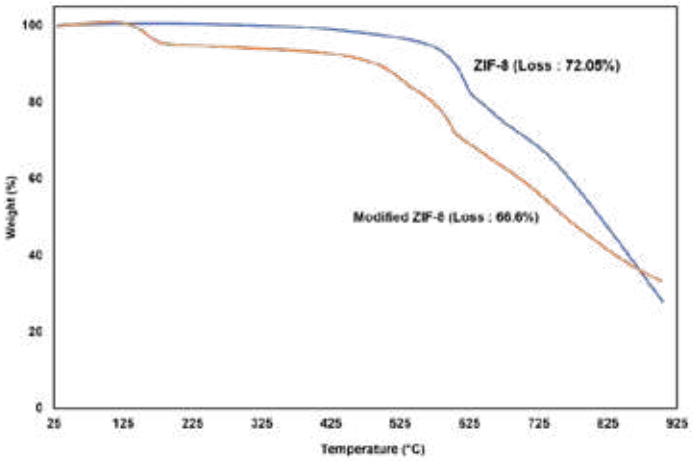


Fig 3. TGA curves of ZIF-8 and modified ZIF-8

The KOH and water uptake abilities of membranes used in alkaline environments are determining factors in electrochemical performance. In this study, "KOH uptake" experiments of the synthesized PBI and PBI-MOF composite membranes were carried out in 2 M KOH, and "water uptake" experiments were carried out in deionized water. As shown in Fig. 4, the PBI-MOF-1 composite membrane has better KOH and water uptake values than the base PBI membrane.

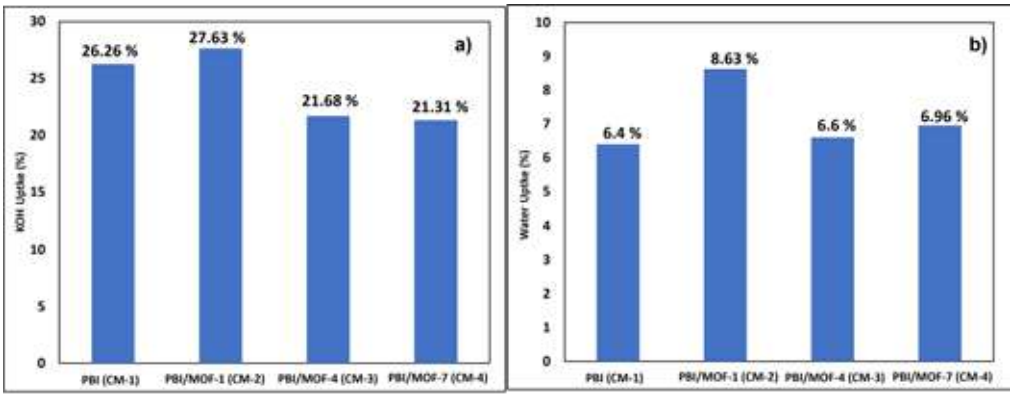


Fig 4. a) KOH and b) water uptake experiment results of PBI and PBI-MOF composite membranes

V. Conclusions

In this study, PBI/MOF composite membranes were successfully prepared and physically and electrochemically characterized for AEMWE application. The obtained characterization results showed that the PBI/ZIF-8 composite membranes were suitable for the AEMWE system for H_2 production.

Acknowledgments

The Scientific and Technological Research Council of Turkey (TUBITAK) supported this study under grant number 123M878.

References

Cong, S., Wang, J., Wang, Z., & Liu, X.. Polybenzimidazole (PBI) and benzimidazole-linked polymer (BILP) membranes. In *Green Chemical Engineering* (Vol. 2, Issue 1, pp. 44–56). KeAi Communications Co. (2021)

David, M., Ocampo-Martínez, C., & Sánchez-Peña, R.. Advances in alkaline water electrolyzers: A review. In *Journal of Energy Storage* (Vol. 23, pp. 392–403). Elsevier Ltd. (2019)

Feng, Z., Esteban, P. O., Gupta, G., Fulton, D. A., & Mamlouk, M. Highly conductive partially cross-linked poly(2,6-dimethyl-1,4-phenylene oxide) as anion exchange membrane and ionomer for water electrolysis. *International Journal of Hydrogen Energy*, *46*(75), 37137–37151. (2021)

Li, D., Park, E. J., Zhu, W., Shi, Q., Zhou, Y., Tian, H., Lin, Y., Serov, A., Zulevi, B., Baca, E. D., Fujimoto, C., Chung, H. T., & Kim, Y. S.. Highly quaternized polystyrene ionomers for high performance anion exchange membrane water electrolysers. *Nature Energy*, *5*(5), 378–385. (2020)

Malinowski, M., Iwan, A., Paściak, G., Parafiniuk, K., & Gorecki, L.. Synthesis and characterization of para- and meta-polybenzimidazoles for high-temperature proton exchange membrane fuel cells. *High Performance Polymers*, *26*(4), 436–444. (2014)

Park, J. E., Kang, S. Y., Oh, S. H., Kim, J. K., Lim, M. S., Ahn, C. Y., Cho, Y. H., & Sung, Y. E.. High-performance anion-exchange membrane water electrolysis. *Electrochimica Acta*, *295*, 99–106. (2019)

Sebbahi, S., Nabil, N., Alaoui-Belghiti, A., Laasri, S., Rachidi, S., & Hajjaji, A. Assessment of the three most developed water electrolysis technologies: Alkaline Water Electrolysis, Proton Exchange Membrane and Solid-Oxide Electrolysis. *Materials Today: Proceedings*, *66*, 140–145. (2022).

Teknologi, J., Hadi, N. A., Nordin, M., Fauzi Ismail, A., Yahya, N., & Bahru, J.. *Zeolitic Imidazole Framework 8 Decorated Graphene Oxide (Zif-8/Go) Mixed Matrix Membrane (Mmm) For Co2/Ch4 Separation* (Vol. 79) (2017)

Integration of an SOFC with Closed Brayton and Rankine Cycles for Hydrogen Production: Thermodynamic Analysis and Heat Recovery Considerations

[1]Mohammad Ali Sabbaghi, [2]Ehsan Baniasadi, [3] Hadi Genceli
[1] Department of Mechanical Engineering, Yazd University, Yazd, Iran
[2] Department of Mechanical Engineering, University of Isfahan, Isfahan, Iran
[3] Faculty of Mechanical Engineering, Yildiz Technical University, Besiktas, Istanbul, 34349, Türkiye

* E-mail: hgenceli@yildiz.edu.tr

Abstract

This research introduces an innovative system designed for cogeneration of power, heat, and hydrogen, capitalizing on solid oxide fuel cell (SOFC) technology. The surplus heat produced by the SOFC is effectively utilized to drive both a closed Brayton and a steam Rankine cycle, thereby maximizing energy utilization. To gain a comprehensive understanding of the system's performance, the study investigates the impact of varying design parameters on system efficiency. The findings demonstrate that increasing the current density from 5500 A/m^2 to 9500 A/m^2 leads to a notable enhancement in power output, albeit at the expense of a slight reduction in overall efficiency. Moreover, the research identifies optimal values for system efficiencies concerning the SOFC temperature and fuel utilization factor, providing valuable insights for system optimization. At a temperature of 556K, the system achieves impressive energy and exergy efficiencies of 82.48% and 80.1%, respectively.

Keywords: Fuel cell, Thermodynamic analysis, Hydrogen, Closed Brayton cycle, Rankine cycle

I. Introduction

The growing population, escalating energy consumption, and technological advancements have directed researchers towards the utilization of high-efficiency technologies. Among the emerging energy production technologies, fuel cells have been recognized as a highly practical and significant tool. This technology has attracted much attention due to numerous advantages, including high efficiency, environmental pollution reduction, and noise reduction Mirbagheri (2023). In fuel cells, electrochemical reactions occur to generate direct current. In their study, Wang (2012) conducted thermodynamic assessment of a hybrid system using an SOFC. Their investigation revealed that the energy and exergy efficiencies reached 70% and 60%, respectively. Al-Sulaiman (2010) investigated a combined system consisting of a SOFC and an Organic Rankine Cycle (ORC). They improved this system using a single-stage absorption cycle. They demonstrated that the integration of these two technologies led to a remarkable increase in the tri-generation system's efficiency, approximately 22% higher than similar systems. Furthermore, Choudhary (2017) conducted a comprehensive examination of a system involving an SOFC integrated with a gas turbine to create a hybrid system. Remarkably, the overall system efficiency was determined to be approximately 62%, a substantial improvement compared to conventional systems. Tan (2017) evaluated the thermodynamic performance of a combined system consisting of an SOFC, a gas turbine (GE), and a Kalina cycle (KC) in their study. In this research, they concluded that if the KC cycle utilizes the heat generated by the gasoline engine, it can lead to an increase of up to 10.3% in the overall energy efficiency. Ozcan (2015) examined the performance of tri-generation system based on SOFC with various types of fuels.
Literature review suggests that the utilization of hybrid systems in simultaneous energy production can significantly improve efficiency and enhance system performance. Therefore, considering this matter, this study investigates the thermodynamic analysis of a novel hybrid energy production system that utilizes the energy derived from SOFC to operate two sub-systems: a gas turbine and a steam Rankine cycle. The impact of main cycle variables on the energy and exergy efficiencies of the system has been examined. The findings of this study provide valuable insights for energy designers and specialists.

II. System Description

In Figure 1, the proposed hybrid system is illustrated. In this system, methane and air are separately fed into the compressor and after vaporization; Water is blended with methane within the heat exchanger. At this stage, the anode inputs undergo reforming and shifting reactions, resulting in the production of hydrogen required for the electrochemical reaction. A portion of the heat generated in this electrochemical reaction is used to supply the energy needed for the endothermic reforming reaction. Additionally, another part of this heat is used to heat the fuel cell products. Subsequently, the cathode exhaust air and unutilized anode fuel are fully combusted to generate combustion gases in the afterburner. Then, the afterburner exhaust gases, after traversing the heaters, enter two sub-systems of the Closed Brayton Cycle (CBC) and the Rankine Cycle (RC) for the purpose of recovering heat, and finally are released to the atmosphere. The following assumptions are incorporated for modelling the system tan (2017):

- The entire system operates under steady-state conditions, with negligible changes in kinetic and potential energies.
- All gases are assumed to follow ideal gas behaviour.

- The equipment is fully insulated, thereby preventing any heat removal into the surrounding environment.
- Any unreacted gases are entirely combusted in the afterburner.
- The compressors, turbines, and pumps exhibit isentropic efficiencies.

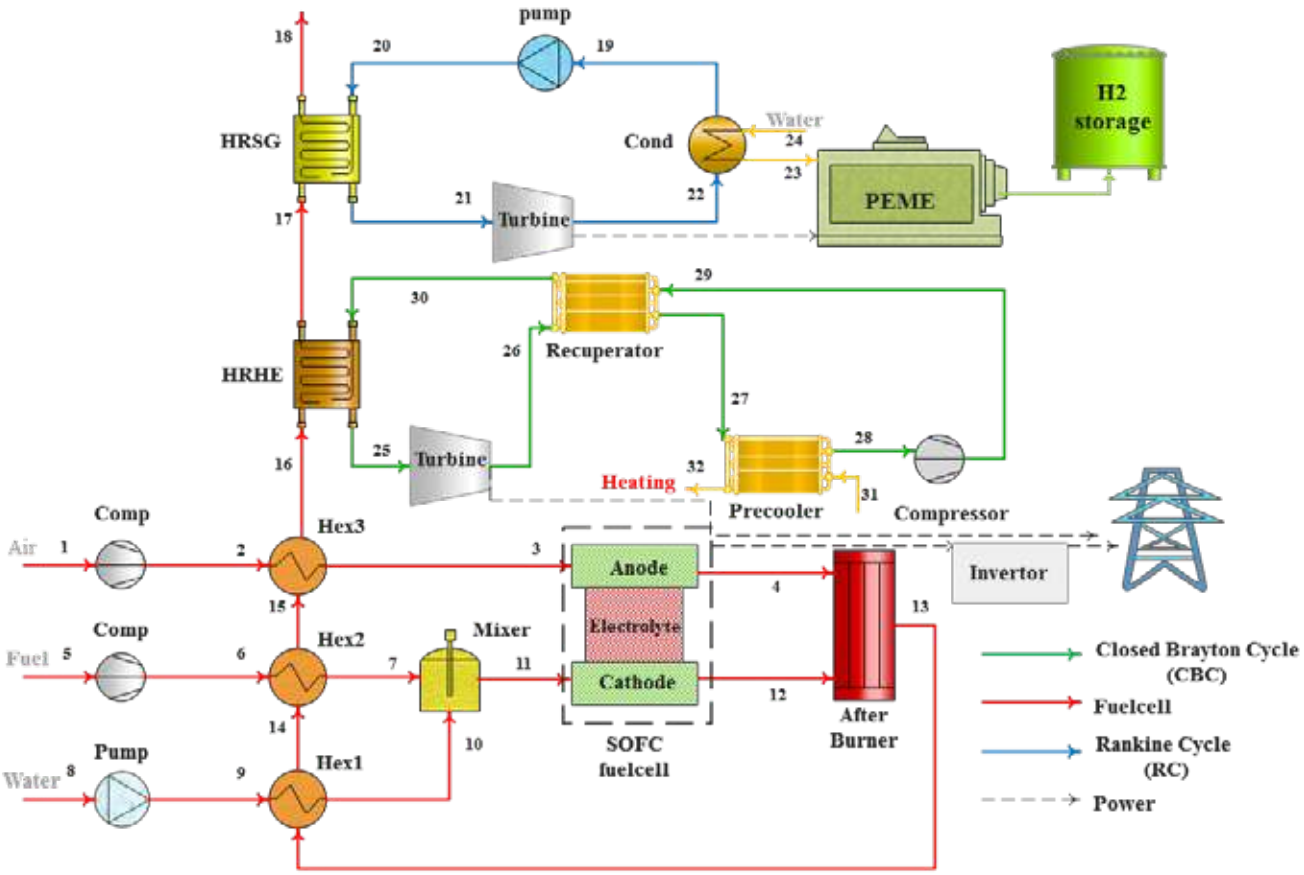


Figure 1. Schematic diagram of the studied system

III. System modelling

The formulation of the system model, in accordance with the first and second laws of thermodynamics, is carried out using control volumes for all system components to elucidate their performance. In this approach, the first and second laws of thermodynamics are utilized to examine and analyze each of the system components, in the form of equations 1-2 Sabbaghi (2024).

$$\dot{Q}_{cv} + \sum_{in} \dot{m}_i h_i = \dot{W}_{cv} + \sum_{out} \dot{m}_e h_e \quad (1)$$

$$\dot{E}x_Q + \sum_i \dot{m}_i e x_i = \sum_e \dot{m}_e e x_e + \dot{E}x_W + \dot{E}x_D \quad (2)$$

There are various types of exergy, among which, in this study, physical and chemical exergies are considered. The values of these two are determined from equations 3-4 Sabbaghi (2024).

$$e x_{ph} = (h - h_0) - T_0(s - s_0) \quad (3)$$

$$e x_{ch} = \sum x_i e_{0,i}^{ch} + \bar{R}T_0 \sum x_i \ln(x_i) \quad (4)$$

The energy and exergy efficiencies of the investigated system are determined based on equations 5-6.

$$\eta_{en} = \frac{\dot{W}_{net,SOFC} + \dot{W}_{net,CBC} + (m_{H2} \times LHV_{H2})}{\dot{m}_{fuel} \times LHV_{fuel}} \quad (5)$$

$$\eta_{ex} = \frac{\dot{W}_{net,SOFC} + \dot{W}_{net,CBC} + \dot{E}x_{H2}}{\dot{E}x_{fuel}} \quad (6)$$

The equations employed to model the SOFC and PEME are taken from references Baniasadi (2023), and Sabbaghi (2023).

III. I. Validation

Simulated data are compared with existing data to validate the accuracy of the modelling outcomes. Specifically, the methane-consuming SOFC model is verified by contrasting the results with those reported by Tan [6] in Table 1. The study's results show a strong agreement with the outcomes from the referenced studies.

Table 1. Comparing the outcomes of this study with the experimental findings reported by Tan et al [6]

Current Density (A/m^2)	Cell Voltage (V) (Present study)	Cell Voltage (V) Tao et al	Power Density (W/m^2) (Present study)	Power Density (W/m^2) Tao et al
2000	0.724	0.76	0.144	0.15
3000	0.709	0.68	0.197	0.21
4000	0.664	0.62	0.235	0.26
5000	0.635	0.57	0.271	0.295
6000	0.608	0.52	0.278	0.315

IV. Results and discussion

Table 2 includes the generated and consumed electricity for each section of the system. These data facilitate comparisons of power generation capacities and energy and exergy efficiencies by integrating different cycles into the SOFC. The table shows that adding the CBC and steam RC cycles to the base cycle results in an extra electrical power output of around 358.04 kW compared to the fuel cell alone.

Table 2. System performance results

Parameter	Value
Power consumption of the AC (kW)	210.9
Power consumption of the FC (kW)	2.255
Power generation of the SOFC (kW)	442.5
Power generation of the CBC turbine (kW)	204.6
Power generation of the RC turbine (kW)	190.4
Power consumption of the CBC compressor (kW)	32.21
Power consumption of the RC pump (kW)	4.748
Power consumption of the SOFC Pump (kW)	5.546
Energy efficiency	0.87
Exergy efficiency	0.845

The variations in the temperature of the SOFC are shown to affect the system efficiencies in Figure 2. In this figure, the temperature of the SOFC ranges from 500K to 1000K. An increase in the temperature results in a decrease in the output power. In other words, as the temperature increases, the electrical power of the SOFC decreases due to a reduction in fuel cell voltage. Conversely, since the mass flow rate of the afterburner and the inlet energy to the subsystems increase. The interaction between these two factors results in the curve illustrated in Figure 2. The output power of a fuel cell increases linearly with the increase in current density and fuel molar flow rate. The reason for this is that more chemical energy is converted into electrical energy, leading to an increase in the power output. However, it should be noted that the rate of increase in input energy and exergy is much higher than that of the output products, which can result in a reduction in energy and exergy efficiencies. These variations are illustrated in Figure 3.

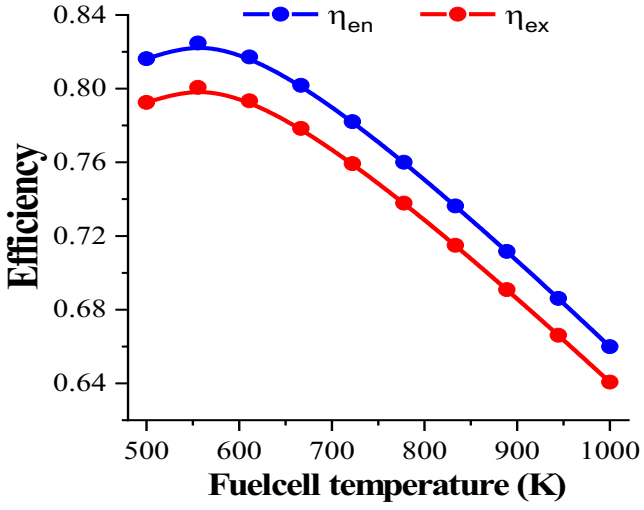


Fig 2. System efficiencies changes with fuel cell temperature

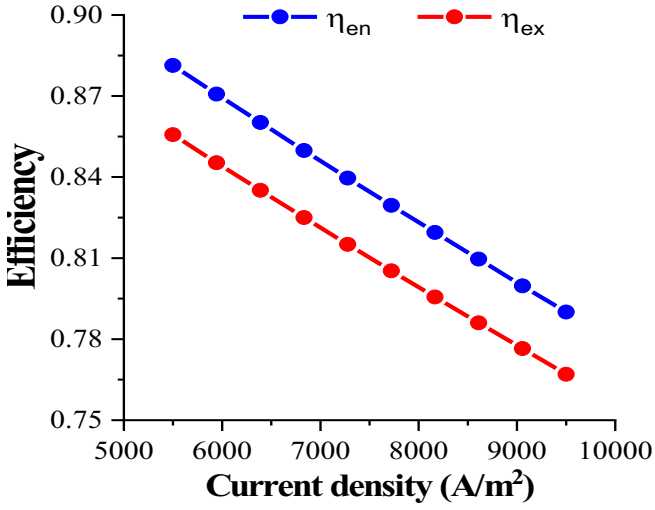


Fig 3. System efficiencies changes with fuel cell current density

Figure 4 depicts the effect of the fuel utilization coefficient (U_f) on the system efficiencies. The value of U_f ranges from 0.8 to 0.9. The results that the system efficiencies initially experience a slight increase up to a certain point and then gradually decrease. The maximum energy and exergy efficiencies, occurring at a fuel utilization coefficient of approximately 0.79, are 82.77% and 80.35%, respectively. As the U_f increases, the net output power of the system decreases. Concurrently, the molar flow rate of inlet air to the SOFC increases while both the fuel flow rate and the cell voltage decrease.

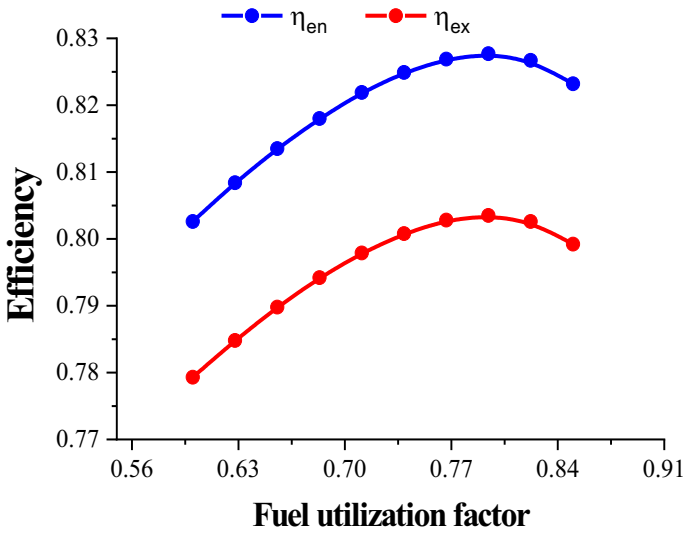


Figure 4. System efficiencies changes with fuel utilization factor

V. Conclusion

In the proposed hybrid system, a SOFC is utilized to generate electricity, heat, and hydrogen simultaneously. Extensive analysis of this system's performance is conducted, employing thermodynamic analysis. The results demonstrated that the efficiency of this system is heavily influenced by the temperature of the fuel cell, the current density, and the fuel utilization factor. Furthermore, the energy and exergy efficiencies of the system are optimized for specific values of the fuel utilization factor and the temperature of the fuel cell. The efficiencies of the system experience a decreasing trend with increasing current density; however, the output power increases.

References

Al-Sulaiman FA, Dincer I, Hamdullahpur F. Energy analysis of a trigeneration plant based on solid oxide fuel cell and organic Rankine cycle. Int J Hydrogen Energy, 35(10): 5104e13, (2010).

Baniasadi et al., Exergy-economic analysis of a solar-geothermal combined cooling, heating, power and water generation system for a zero-energy building, International Journal of Hydrogen Energy, 48 (99); 39064-39083, (2023).

Choudhary T, Sahu M, Krishna S. Thermodynamic analysis of solid oxide fuel cell gas turbine hybrid system for aircraft power generation. SAE Technical Paper; (2017).

Mirbagheri MH, Baniasadi E, Genceli H. Exploring the performance of an innovative integrated solar tower power plant with hydrogen generation and storage. Int J Hydrogen Energy, 48(99), 39271-39285 ,(2023).

Ozcan H, Dincer I. Performance evaluation of an SOFC based trigeneration system using various gaseous fuels from biomass gasification. Int J Hydrogen Energy; 40(24):7796e807, (2015).

Sabbaghi M A, & Sefid M. Risk, sensitive analysis, and optimization of a new multi-generation system activated by solar and biomass energies. Energy Report, 11, 1006-1018, (2024).

Sabbaghi MA., Sefid, M. Evaluation of a Modified Organic Rankine Cycle to Produce Power, Hydrogen and Desalinated Water by Combining Geothermal and Biomass Energies from 4E viewpoints. Journal of Mechanical Engineering of Tabriz University, 52(4), 301-310, (2022).

Sabbaghi Ma, Sefid M. Exergy-environmental analysis and optimisation of the modified organic Rankine cycle driven by geothermal and biomass energies, Int J of exergy, 40(2): 144-161, (2023).

Tan L, Dong X, Gong Z, Wang M. Investigation on performance of an integrated SOFC-GE-KC power generation system using gaseous fuel from biomass gasification. Renew Energy, 107:448–61, (2017).

Wang J, Yan Z, Ma S, Dai Y. Thermodynamic analysis of an integrated power generation system driven by solid oxide fuel cell. Int J Hydrogen Energy; 37:2535–45, (2012).

Development of Electro-biomembrane Integrated Renewable-based System to Produce Fresh Water and Biohydrogen for Sustainable Communities

[1*]A. Yagmur Goren, [1]Ibrahim Dincer, [2]Ali Khalvati
[1] Clean Energy Research Laboratory (CERL), Faculty of Engineering and Applied Science, Ontario Tech. University, 2000 Simcoe Street North, Oshawa, Ontario L1G 0C5, Canada
[2] Viona Consulting INC., Agro-Environmental Innovation and Technology, Research and Development Company, Thornhill, Ontario L3T 0C6, Canada

* E-mail: Aysegul.Kara@ontariotechu.ca

Abstract
As the consequences of global warming become more severe, it is more crucial than ever to capitalize on all locally accessible potential renewable energy sources and produce sufficient useable energy outputs to meet community demands while causing the least damage to the ecosystem. Therefore, in this study, an innovative integrated system with a unique electro-biomembrane unit that uses biomass energy from poplar leaves was performed and evaluated with thermodynamic modeling. The proposed system was particularly developed to produce concurrent electricity, biohydrogen, freshwater, and irrigation water. The Engineering Equation Solver program was used to analyze and evaluate the energy and exergy efficiency, exergy destruction levels for particular system elements, thermophysical parameters, and subsystem characteristics. The findings indicate that using solar power and biomass as renewable energy sources, the proposed integrated system provided 2924.42 kW of power, 59,616 kg of fresh water, and 328.56 kg of biohydrogen per day.

Keywords: Electro-biomembrane reactor, hydrogen, desalination, energy efficiency, exergy, sustainability

I. Introduction

A growing interest in global initiatives to lower carbon emissions has sharply increased demand for renewable energy sources and sustainable energy solutions. Until 2050, significant effort must be made to attain net-zero carbon emissions. Renewable alternatives are needed to fulfill the present energy needs for heating, power, and fuel for transportation. Interestingly, there has been a noticeable change in favor of using renewable resources to generate energy and power for transportation in the previous few years. Using leftover electricity from renewable sources to produce hydrogen, which may be utilized as an alternative fuel, is a novel strategy for energy storage. Nevertheless, despite some advances, there are significant drawbacks, such as almost 660 million people still lacking access to electricity. Thus, reaching SDG 7 objectives is essential for sustainable cities and societies worldwide. Moreover, the growing global energy demand has deemed it essential to use renewable energy sources like biomass, solar, and wind (Alqahtani, 2023).

In this regard, certain studies have been conducted on energy systems that utilize integrated renewable energy sources to provide several valuable outputs like electricity and hydrogen. Green hydrogen is frequently produced by electrolysis, which splits water using extra renewable energy. On the other hand, there have been challenges for effective and simultaneous fresh water, energy production, wastewater treatment, and their effects on necessities, considering them from a renewable energy-based perspective. Therefore, the potential of lab-scale electro-biomembrane systems for concurrent energy and biohydrogen production, wastewater treatment, and desalination was considered in this study, combining renewable resources (Goren et al., 2024). Overall, the goal of this research is to advance the state-of-the-art in the manners that follow, each with its novelties: (ı) constructing a sustainable energy system that combines renewable energy sources with the production of biohydrogen for energy storage to meet the energy demand, (ii) combining concentrated photovoltaic solar systems to produce multiple valuable outputs to cover the requirements for sustainable agriculture, desalination, and biohydrogen production as a new concept, and (iii) using real data to model subsystems using realistic simulation software packages, evaluate the system using energy and exergy methodologies of thermodynamics.

II. System description

The proposed renewable energy system is presented in Fig. 1, and it combines various components to maximize resource utilization and energy production. The concentrated photovoltaic (PV) cells were used in the solar system to generate high-temperature steam (HTS), which is utilized to produce electricity. This HTS may also be directed toward the electro-biomembrane system to accelerate the electrochemical conversion for biohydrogen production. Other important parts of the system are producing fresh water, desalination, and minimizing waste sludge obtained from a wastewater treatment plant (WTP), seawater, and domestic wastes, respectively, using an electro-biomembrane system. Moreover, extra water is kept in reserve in the communal and irrigation storage tanks to ensure a continuous water supply to communities and agricultural fields. The WTP and sludge also supply water and microorganisms to the electro-biomembrane system, assisting in biohydrogen production. The solar plant also provides electricity and freshwater owing to the utilization of a multi-stage flash desalination process with the help of excess heat from the solar system that is distributed to the community and homes to provide household electrical and freshwater requirements.

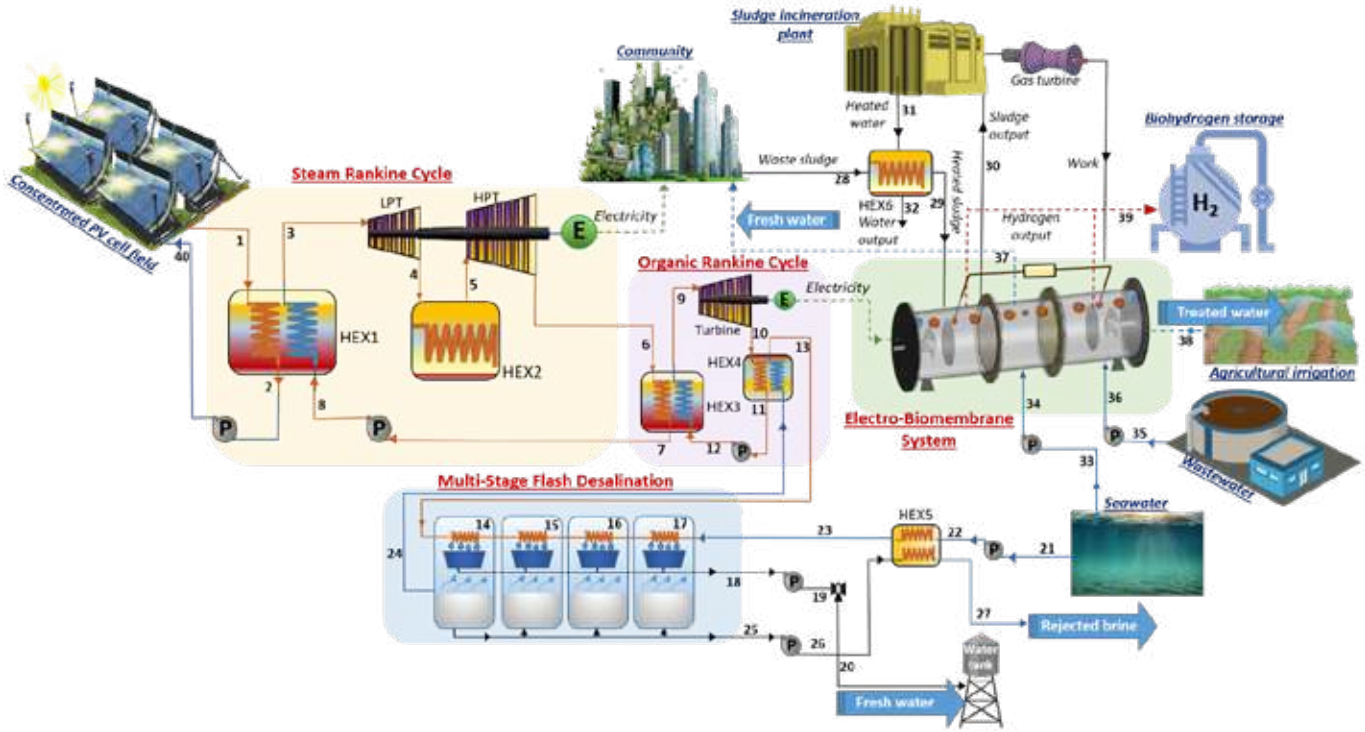


Fig. 1: The suggested biohydrogen production and renewable-based integrated system.

III. Analysis

The first and second laws of thermodynamics are investigated from the perspectives of energy and exertion to gain insight into the system (Dincer, 2020). Each system component and the points at which the components are connected are examined. Thermophysical characteristics are determined for each state point to determine the energy and energy inputs for each component. Subsystems and the integrated system are also examined to determine total energy and energy inputs.

IV. Results and discussion

The EES software calculated the values for each state point for the proposed system. The specific exergy values for state points in steam and organic Rankine cycles are presented in Fig. 2. The highest specific exergy values were 3287 kJ/kg for state point 3 in steam Rankine cycle and 412.2 kJ/kg for state point 9 in organic Rankine cycle. Overall, the result revealed that the freshwater production was 2484 kg/h and biohydrogen production was 13.69 kg/h. Furthermore, solar energy and biomass were used as the main drivers of a proposed integrated system. The overall net work output of the integrated system was found as 2924.42 kW. Consequently, the daily biohydrogen and freshwater capacities were 328.56 kg/day and 59,616 kg/day, respectively.

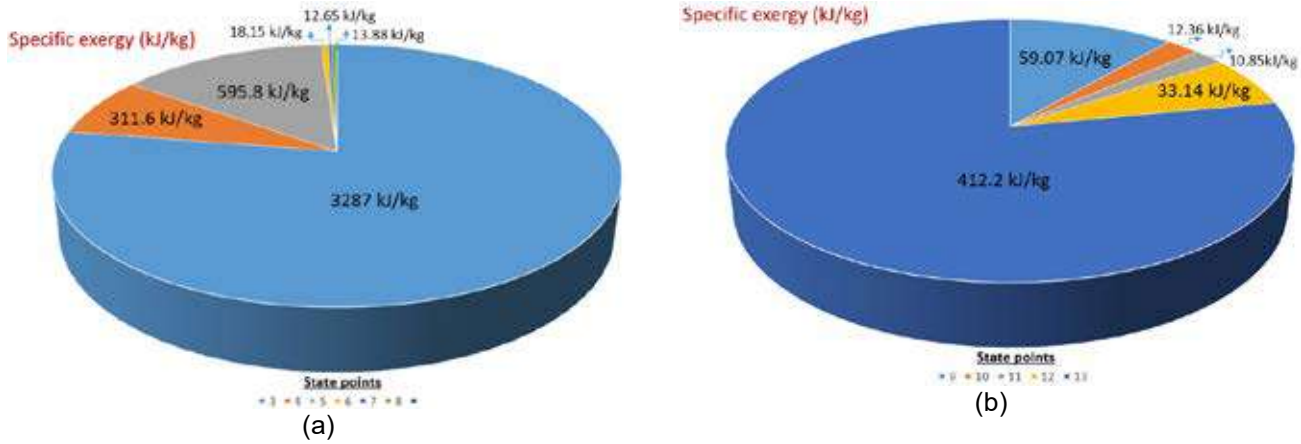


Fig. 2: The specific exergy values of each state point for (a) the Steam Rankine cycle and (b) the Organic Rankine cycle.

V. Conclusions

The energy, biohydrogen, and freshwater production performance of the proposed renewable-based powered electro-biomembrane integrated system was significantly promising, considering its considerably high biohydrogen and freshwater production yields. The total biohydrogen and freshwater production values were 13.69 kg/h and 2484 kg/h, respectively. In addition, the total work yield of the integrated system was 2924.42 kW. Consequently, these results proved that the novel electro-biomembrane reactor could be a promising candidate for real-scale

application to provide energy, freshwater, and irrigation water for communities when it is combined with renewable energy resources.

References

Alqahtani, T., Performance evaluation of a solar thermal storage system proposed for concentrated solar power plants. Applied Thermal Engineering, 229, 120665 (2023).

Goren, A.Y., Dincer, I., Khalvati, A., Development of a unique integrated bioreactor for simultaneous desalination and bioenergy and biohydrogen production. Chemical Engineering Journal, 486,150312 (2024).

Dincer, I., Thermodynamics: A Smart Approach, (2020), 1st ed., John Wiley & Sons, London

Emission Analyses of Hydrogen Fuels Obtained from Different Sources for Various Vehicles

*[1,2]Sumeyya Ayca,[1,3]Ibrahim Dincer

[1]Yildiz Technical University, Department of Mechanical Engineering, Istanbul, Türkiye
[2]Istanbul Aydin University, Faculty of Engineering, Department of Aerospace Engineering, Kucukcekmece, Istanbul, Türkiye
[3]Ontario Tech University, Clean Energy Research Laboratory, Oshawa, Ontario, Canada

*Corresponding author's e-mail: sumeyya.ayca@std.yildiz.edu.tr

Abstract

In this investigation, the comparative analysis focused on the emissions emanating from various vehicle categories fueled by hydrogen derived through diverse hydrogen production methodologies. The study scrutinized the CO_2, CH_4, NO_x, and SO_x emissions associated with hydrogen generated from 8 distinct sources, encompassing both renewable and non-renewable origins, across 3 distinct vehicle classifications. The evaluation utilized the Greenhouse Gases, Regulated Emissions, and Energy Use in Transport (GREET) software, renowned for its Life Cycle Assessment (LCA) capabilities. Noteworthy observations revealed that among Car, Heavy Duty Vehicles (HDV) and Sport Utility Vehicle (SUV) classifications, HDV vehicles exhibited the highest emission rates. The emission rates of the HDV vehicle type were obtained as follows: CO_2 emissions at 211.3 kg/h km in Pathway8, CH_4 emissions at 0.3 kg/h km in Pathway3, NO_x emissions at 0.08 kg/hkm in Pathway4, and SO_x emissions at 0.04 kg/h km in Pathway3.

I. Introduction

Hydrogen fuel, recognized as a clean and dependable energy carrier, presents a viable option for use in vehicular applications. The methodologies employed in obtaining hydrogen play a crucial role in emission analyses. Candelaresi et al. (2021) conducted an investigation utilizing the Life Cycle Assessment (LCA) method to analyze emissions from hydrogen-fueled vehicles. Their study revealed that hybrid hydrogen vehicles equipped with internal combustion engines exhibit lower emissions. Valente et al. (2020) explored the emission impacts of different hydrogen fuel production methods in fuel cell electric vehicles. Their research demonstrated that the utilization of renewable hydrogen, as opposed to conventional hydrogen derived from steam methane reforming, yields notably positive effects on emission levels. In this study, eigh distinct hydrogen production methodologies were scrutinized using the GREET program, an LCA software. The investigation delves into the repercussions of altering hydrogen production methods on various categories of hydrogen-powered vehicles, with a focus on the emissions of carbon dioxide (CO_2), methane (CH_4), sulfur oxides (SO_x), and nitrogen oxides (NO_x) gases. The findings of these analyses are presented graphically and elaborated upon in Section II and Section III of this study.

II. Methodology

In this investigation, emission analyses of hydrogen fuel applicable to three distinct vehicle categories were conducted using the Life Cycle Assessment (LCA) methodology. The analyses were executed utilizing the GREET program, a software specializing in LCA. The study examined eight different pathways representing the sources from which hydrogen fuel is procured, listed as follows:

- Pathway1: Central Plants: Compressed G.H_2 production from Biomass
- Pathway2: Central Plants: Compressed G. H_2 production from Chlorine plants
- Pathway3: Central Plants: Compressed G. H_2 production from Coal
- Pathway4: Central Plants: Compressed G. H_2 production from Coke Oven Gas
- Pathway5: Central Plants: Compressed G. H_2 production from Natural Gas
- Pathway6: Central Plants: Compressed G. H_2 production from Nuclear Energy (Thermo Chemical Cracking of Water)
- Pathway7: Central Plants: Compressed G. H_2 production from PEM Electrolysis - Solar (or Wind)
- Pathway8: Central Plants: Compressed G. H_2 production from Pet Coke

Throughout the analyses, variations in the pathway of hydrogen fuel were introduced across three diverse vehicle classifications, and the corresponding emission values were scrutinized. The vehicle types under investigation are delineated as follows:

- Car: FCV - Gaseous H_2 (Type 1 Ni-MH Conventional Material)
- HDV (Heavy Duty Vehicles): Combination Long-Haul Truck FCV - Gaseous H_2
- SUV (Sport Utility Vehicle): FCV - Gaseous (Type 1 Ni-MH Conventional Material)

The study involved the analysis of emission levels pertaining to CO_2, CH_4, SO_x, and NO_x gases. The data resulting from these analyses were visually represented through graphical displays.

III. Results and Discussion

The graphical depiction of the data acquired within the study is presented in Figures 1-4. Figure 1 presents an analysis of the impact of varying hydrogen sources on CO_2 emissions across three distinct vehicle types. The highest emission value was observed in the HDV category utilizing hydrogen fuel sourced from Pathway 8. In Figure 2, the

investigation delves into the influence of hydrogen source variations on CH_4 emissions across different vehicle types. Notably, the HDV vehicle type exhibited the greatest impact when supplied with hydrogen from Pathway 3, with Pathways 4 and 5 also showing comparably high emission values. Moving on to Figure 3, the examination focuses on the effect of hydrogen source alterations on NO_x emissions among various vehicle types. The HDV vehicle type demonstrated the highest emission level when fueled by hydrogen obtained from Pathway 4. Finally, in Figure 4, the analysis of SO_x emissions across different vehicle types reveals that the HDV category supplied with hydrogen from Pathway 3 exhibited the highest emission value.

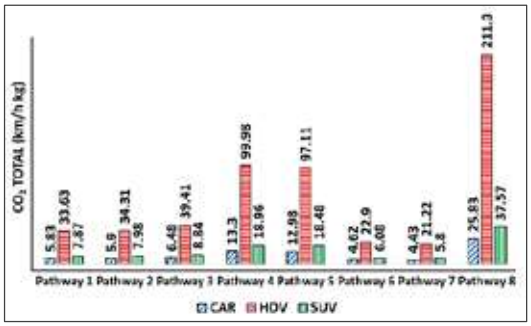


Fig.1: The impact of altering hydrogen sources on CO_2 emissions with respect to distinct vehicle classifications.

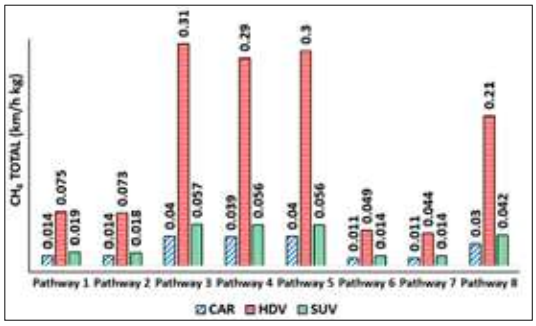


Fig.2: The impact of altering hydrogen sources on CH_4 emissions with respect to distinct vehicle classifications.

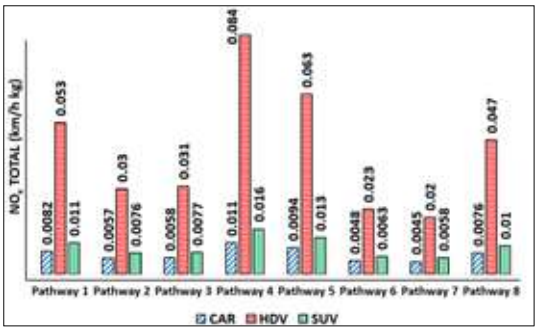


Fig.3: The impact of altering hydrogen sources on NOx emissions with respect to distinct vehicle classifications.

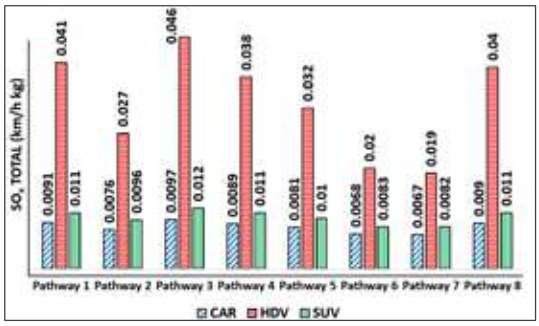


Fig. 4: The impact of altering hydrogen sources on SOx emissions with respect to distinct vehicle classifications.

IV. Conclusion

The analyses revealed that the highest emission values were observed when hydrogen fuel obtained through specific hydrogen production methods—Pet Coke from Pathway 8, Coal from Pathway 3, and Coke Oven Gas from Pathway 4—was utilized in HDV types. The emission rates for HDV vehicles were as follows: CO_2 emissions of 211.3 kg/h km in Pathway 8, CH_4 emissions of 0.3 kg/h km in Pathway 3, NO_x emissions of 0.08 kg/h km in Pathway 4, and SO_x emissions of 0.04 kg/h km in Pathway 3.

References

Candelaresi D., Valente A., Iribarren D., Dufour J., Spazzafumo G. 2021. Comparative life cycle assessment of hydrogen-fuelled passenger cars. International Journal of Hydrogen Energy, 46 (72), pp. 35961-35973.

Valente A., Iribarren D., Candelaresi D., Spazzafumo G., Dufour J. 2020. Using harmonised life-cycle indicators to explore the role of hydrogen in the environmental performance of fuel cell electric vehicles. International Journal of Hydrogen Energy, 45 (47), pp. 25758-25765.

Boron-Based Hydrogen Storage Materials as a Hydrogen Source in Synthetic Fuel Production

[1]Berfin Ekin Ülgen, [2,5]Bilge Coşkuner Filiz, [4]Korkut Açıkalın, [3,5]Hülya Civelek Yörüklü, [1,5*]Aysel Kantürk Figen
[1]Yıldız Technical University, Faculty of Chemistry-Metallurgy, Department of Chemical Engineering, Istanbul, 34220, Türkiye
[2]Yıldız Technical University, Faculty of Chemistry-Metallurgy, Department of Metallurgy and Materials Engineering, Istanbul, 34220, Türkiye
[3]Yıldız Technical University, Faculty of Civil Engineering, Department of Environmental Engineering, Istanbul, 34220, Türkiye
[4]Yalova University, Faculty of Engineering, Department of Energy Systems Engineering, Yalova, 77200, Türkiye
[5]Yıldız Technical University, Clean Energy Technologies Institute, Istanbul, 34220, Türkiye

*E-mail: akanturk@yildiz.edu.tr

Abstract

The utilizing synthetic fuel as a hydrogen (H_2) carrier looks promising strategy in the H_2 economy and allows the integration of H_2 carrying-production with carbon dioxide (CO_2) conversion. In our concept, boron-based H_2 storage materials ($NaBH_4$, KBH_4, and NH_3BH_3) are used as H_2 and heat source for conversion of CO_2 to synthetic fuel. Firstly, hydrogenation capacities of boron-based H_2 storage materials were investigated under different pH conditions. synthetic fuel production was carried out in a batch type and temperature-controlled reactor equipped with mass flow controller (MFC) for supplying CO_2. The effects of temperature, $NaBH_4$ amount and CO_2 flow rate on the hydrogenation efficiency were examined and Central Composite Experimental Design methodology was used for parametric optimization. After the hydrogenation was completed, solid and liquid products were isolated and identified. The environmental impact of the hydrogenation process was evaluated by examining the carbon mass balance.

Keywords: LOHC, hydrogen storage, formic acid, CO_2 hydrogenation, boron-based materials, sodium borohydride, synthetic fuel

I. Introduction

H_2, has the ability to form compounds with most elements in nature, that has the potential to replace fossil fuels. However, the H_2 economy, storage and production challenges avert the applications of this alternative energy carrier (Chen et al., 2017). In particular, the decrease in H_2 storage efficiency and production yield limits the applications to be carried out an industrial scale (Orimo et al., 2007). The Paris Agreement outlines the requirement to limit the rise in global mean temperature to less than 2 °C over pre-industrial levels by end of the century. The control of total CO_2 emissions to be below 20 Gt CO_2 year by 2050 is mandated to achieve this [1]. Consequently, there has been an increase of interest in the use of CO_2 and its conversion into valuable chemicals recently (Jepsen at al., 2014).

Boron-based materials have the potential to be used as H_2 sources for the CO_2 hydrogenation of valuable chemicals such as HCOOH due to their specific characteristics and variation in reduction efficiencies (Eq.1) (Minkina at al., 2008; Jepsen at al., 2014).

$$CO_2 + H_2 \rightarrow HCOOH \qquad Eq.1$$

Sodium borohydride ($NaBH_4$) is an excellent storage medium for H_2 due to its approximately 10.8 wt.% H_2 content, inflammability, affordability, and high safety rating (Özkan at al., 2019). Even though ammonia borane (NH_3BH_3) is more stable at room conditions and the hydrolysis reaction occurs in the presence of appropriate catalysts, $NaBH_4$ and KBH_4 in solid forms are susceptible to moisture in the atmosphere. There is a KBH_4> $NaBH_4$ > NH_3BH_3 relationship between the rates of H_2 production from aqueous solutions prepared at neutral pH value of these compounds (Minkina et al., 2008; Jepsen et al., 2014).

This study includes hydrogenation capacity due to the altering of the boron-based H_2 storage materials and pH values of reaction medium, with a focus on the influence of H_2 generation properties on synthetic fuel production and optimization of reaction parameters. $NaBH_4$, KBH_4, and NH_3BH_3 which were used as a H_2 source for the hydrogenation reactions exhibit controlled H_2 release through the hydrolysis reaction accelerated in presence of suitable catalysts (Jepsen et al., 2014). In order to assess an effect of hydrogenating agents and pH on the boron-based CO_2 hydrogenation, the experiments were performed.

II. Experimental Set-up and Procedure

Boron-based hydrogen storage (B-H) compounds such as $NaBH_4$ (SBH, Merck, 97% purity), KBH_4 (KBH, Alfa Aesar, 98% purity) and NH_3BH_3 (AB, Sigma Aldrich, 97% purity) were used as H_2 and heat source. Hydrogenation reactions were carried out in a batch type glass reactor under ambient conditions (25 °C, 1 atm) under different pH values (4,7, and 10). B-H compound and solvent were loaded inside the reactor and saturating it with CO_2 gas (99.99999% purity) for 10 min and establishing an internal reactor pressure of 1 atm. Hydrogenation reactions were conducted under varied reaction conditions (temperature, $NaBH_4$ amount, CO_2 flow rate) and Central Composite Experimental Design methodology was applied for parameter optimization. After the hydrogenation reaction, solid, liquid and gas products were analyzed.

III. Analysis

The exhaust gaseous products from the reactor were analyzed online with infrared detector-equipped gas analyzer (IGA, TESTO). Measurements were continued until stability was reached, and hydrogenation efficiencies were calculated based on the obtained steady-state data, providing insights into the effectiveness of the hydrogenation reactions under the specified conditions. Based on the gas analysis results, the conversion efficiency of CO_2 gas was calculated. The efficiency yield was calculated based on the CO_2 concentration in the gas input stream, determining the amount and composition of the gaseous products remaining after hydrogenation and based on the percentage conversion.

Post-reaction, the resulting liquid and solid products were separated through centrifugation, and the liquid phase was subjected to comprehensive analysis using Fourier-transform infrared spectroscopy (FT-IR), nuclear magnetic resonance (NMR), gas chromatography with flame ionization detection (GC-FID), and high-performance liquid chromatography (HPLC). The solid products obtained after crystallization were further processed for characterization. Characterizations of the solid product obtained after the drying step (under vacuum at 80 °C) were carried out by XRD and FTIR analysis.

IV. Results and discussions

Within the scope of this study, firstly, B-H compound experiments were carried out and the CO_2 hydrogenation efficiency (%) in aqueous media was examined (Fig 2). Due to the stable nature of the aqueous solutions of AB compound, H_2 production and CO_2 hydrogenation did not occur (Minkina et al., 2008; Jepsen et al., 2014). The FTIR and NMR analysis of the liquid and solid products obtained after the hydrogenation confirmed that there is no CO_2 hydrogenation reaction occurred with AB. SBH and KBH compounds showed H_2 production followed by CO_2 hydrogenation. Based on the IGA results were determined that the CO_2 hydrogenation values of SBH and KBH were 53±2% and 19±2%, respectively (Fig 2a). Similarly, CO_2 hydrogenation efficiency of SBH was determined as 49% by MS analysis. Results shows that SBH is the most suitable B-H compound for CO_2 hydrogenation, has been used in pH screening.

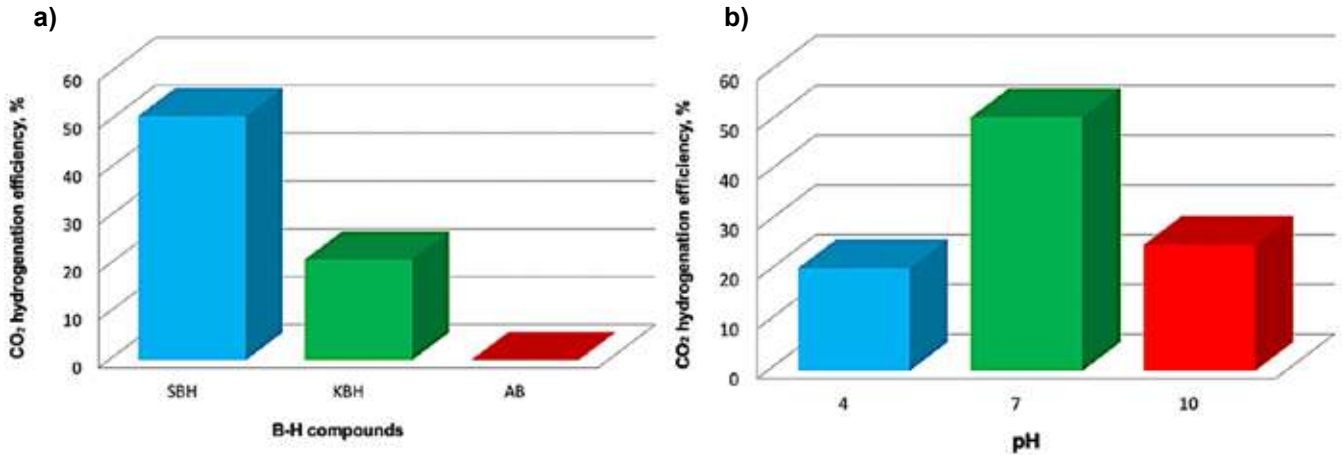


Fig. 2: CO_2 hydrogenation efficiency of B-H compounds (25°C and pH:7) and pH screening (25°C)

CO_2 hydrogenation via SBH hydrolysis reactions at different pH values (4, 7 and 10)) under ambient conditions (1 atm, 25°C) were investigated as given in Fig.2b. Since the change in solution pH affects H_2 output rate from SBH, the pH changes indirectly affect the CO_2 hydrogenation efficiency. The hydrogenation of CO_2 resulted in low efficiency due to rapid hydrolysis under acidic conditions (pH:4, H_2 production rate: 3.02 mL/min). The highest hydrogenation efficiency (53±2%) was achieved under neutral condition (pH:7). Low efficiency (29±2%) was obtained due to the decrease in the hydrolysis activity of the SBH compound at high pH (10) value.

Within the scope of parametric optimization examinations based on Central Composite Experimental Design methodology, it was determined that the most effective parameter on efficiency was SBH amount, the second effective parameter was temperature, and the parameter with a very low effect was CO_2 flow rate. As a result, 0.6 M SBH, 45°C, pH:7 and 50 mL/min CO_2 flow rate were determined as optimum conditions for the CO_2 hydrogenation for synthetic fuel production. Additionally, HCOOH and methanol (CH_3OH) content were determined following CO_2 hydrogenation when the results of FTIR, NMR, GC-FID, and HPLC were assessed.

V. Conclusions

Consequently, CO_2 hydrogenation reactions were carried out in the batch reactor in presence of SBH, KBH and AB, which are hydrogen sources, under ambient conditions. It was found that the highest performance belongs to SBH compound in a neutral environment (pH:7). This comparison was important for understanding both the chemical behavior of B-H compounds under ambient conditions and their pH-dependent CO_2 hydrogenation efficiency. It was concluded that pH change significantly affects CO_2 hydrogenation performance of SBH and the successful realization of HCOOH and CH_3OH synthesis achieved. The hydrogenation of CO_2 with SBH compound under ambient conditions with efficiency of approximately 50% with production of HCOOH is a promising result for H_2 storage applications.

Acknowledgements
This research was supported by the TUBITAK (Project No: 221M293). Authors would like to thank to Assoc. Prof. Dr. Halit Eren FİGEN for MFC system and GC-MS analysis.

References

Beiron, J., Normann, F., Kristoferson, L., Stromberg, L., Gardarsdottir, S.O. and Johnsson, F., 2019. Enhancement of CO_2 absorption in water through pH control and carbonic anhydrase–a technical assessment. Industrial & Engineering Chemistry Research, 58(31), pp.14275-14283.

Chen, W., Ouyang, L. Z., Liu, J. W., Yao, X. D., Wang, H., Liu, Z. W., & Zhu, M. (2017). Hydrolysis and regeneration of sodium borohydride ($NaBH_4$)–A combination of hydrogen production and storage. Journal of Power Sources, 359, 400-407.

Dovgaliuk, I., Hagemann, H., Leyssens, T., Devillers, M. and Filinchuk, Y., 2014. CO_2-promoted hydrolysis of KBH_4 for efficient hydrogen co-generation. international journal of hydrogen energy, 39(34), pp.19603-19608.

Jepsen, L.H., Ley, M.B., Lee, Y.S., Cho, Y.W., Dornheim, M., Jensen, J.O., Filinchuk, Y., Jørgensen, J.E., Besenbacher, F. and Jensen, T.R., 2014. Boron–nitrogen based hydrides and reactive composites for hydrogen storage. Materials Today, 17(3), pp.129-135.

Li, J., Hong, X., Wang, Y., Luo, Y., Huang, P., Li, B., ... & Pimerzin, A. A. (2020). Encapsulated cobalt nanoparticles as a recoverable catalyst for the hydrolysis of sodium borohydride. Energy Storage Materials, 27, 187-197.

Minkina, V.G., Shabunya, S.I., Kalinin, V.I., Martynenko, V.V. and Smirnova, A.L., 2008. Long-term stability of sodium borohydrides for hydrogen generation. international journal of hydrogen energy, 33(20), pp.5629-5635.

Orimo, S. I., Nakamori, Y., Eliseo, J. R., Züttel, A., & Jensen, C. M. (2007). Complex hydrides for hydrogen storage. Chemical reviews, 107(10), 4111-4132.

Özkan, G., Akkuş, M. S., & Özkan, G. (2019). The effects of operating conditions on hydrogen production from sodium borohydride using Box-Wilson optimization technique. International Journal of Hydrogen Energy, 44(20), 9811-9816.

Zhang, W., Zhang, X., Huang, Z., Li, H. W., Gao, M., Pan, H., & Liu, Y. (2021). Recent Development of Lithium Borohydride-Based Materials for Hydrogen Storage. Advanced Energy and Sustainability Research, 2(10), 2100073.

UNFCCC. Key aspects of the Paris Agreement. UNFCCC. https://unfccc.int/most-requested/key-aspects-of-the-paris-agreement

Optimum Design and Techno-economic Evaluation of PV Integrated On-Site Hydrogen Refueling Stations

[1]Reyhan Atabay, [2]Yılser Devrim
[1]Atılım University, Graduate School of Natural and Applied Sciences, Department of Mechanical Engineering, Incek Gölbaşı Ankara, 06830, Türkiye
[2]Atılım University, Department of Energy Systems Engineering, Incek Gölbaşı Ankara, 06830, Türkiye

* E-mail: yilser.devrim@atilim.edu.tr

Abstract
A crucial aspect of photovoltaic panel (PV)-integrated hydrogen refueling station (HRS) design is the sizing of system components. HRS design depends on the target amount of hydrogen to be produced daily and the availability of solar energy in the study area. In this study, we have meticulously sized different components for a PV-HRS producing 170 kg hydrogen/day. Our economic assessments have thoroughly evaluated the feasibility and cost-effectiveness of adopting a PV-integrated HRS, considering initial investment expenditures, operational expenses, and future revenue streams.

Keywords: Hydrogen refueling station, renewable energy, photovoltaic panel, anion exchange membrane electrolyzer, on-site hydrogen production

I. Introduction

Problems such as global warming, climate change, and the depletion of fossil fuels have been the main motivations behind the search for precise solutions to alternative fossil fuels. Therefore, renewable energy sources are needed worldwide (Abe et al., 2019). Among renewable energy sources, hydrogen is recognized as the most crucial source of clean, carbon-free fuel. The main issues in the hydrogen supply system include inadequate development of hydrogen production, transportation, equipment storage, and insufficient hydrogen supply in structures such as hydrogenation and distribution. Hydrogen is a versatile energy carrier that may be created from various sources, including water, biomass, and fossil fuels. Steam-methane reforming is the most frequent manufacturing method, accounting for around 65% of global hydrogen generation (Baykara, 2018). Other typical methods include water electrolysis. Water electrolysis may produce hydrogen at a few cubic centimeters per minute to thousands of cubic meters per hour. Hydrogen created with electricity supplied from renewable energy sources has numerous environmental advantages. Renewable energy sources provide significant benefits for hydrogen production at these stations since they are both environmentally friendly and cost-effective (Holladay et al., 2009).

The utilization of hydrogen energy, particularly in vehicles, is one of the critical answers to the global warming challenge. However, for hydrogen to become widely used in automobiles, a hydrogen infrastructure that supports sustainable mobility based on fuel cell vehicles is required. They function as hubs, facilitating hydrogen supply to FCVs. Optimizing the hydrogen supply system, expanding the hydrogen supply infrastructure, and lowering users' hydrogen costs are critical to enabling a broader range of FCV applications. One of the primary impediments to adopting fuel cell vehicles (FCEVs) is the scarcity of hydrogen refueling stations (HRSs). The availability of these stations is critical for fuel supply for FCEVs that use hydrogen as a source of energy generation (Minutillo et al., 2021).

In this study, a PV-based renewable energy generating system is modeled to deliver hydrogen to the HRS, and the best configurations are determined through a techno-economic analysis of the system under various scenarios (Gökçek & Kale, 2018). To the best of our knowledge, no previous studies in the literature have reported on the design and techno-economic analysis of an on-site hydrogen refueling station powered by a grid-connected photovoltaic solar PV system in Ankara, Turkey's capital city. Despite advancements in understanding the potential of HRS, there is still a lack of research on public perception and acceptance of these facilities and their potential impact on local communities.

II. Experimental Set-up and Procedure

This study describes the design and techno-economic evaluation of an on-site hydrogen refueling station based on an AEMWE unit coupled with a grid-connected PV plant for 1, 3, and 5 MW of installed power. The designed HRS has a hydrogen production capacity of 170 kg H_2/day. The hydrogen production capacity is estimated based on meeting the daily hydrogen needs of ten vehicles and three buses, with cars having 5 kg hydrogen tanks and buses having 40 kg hydrogen tanks. The hydrogen filling pressure of fuel cell vehicles is typically 350 bar for heavy-duty vehicles and 700 bar for automobiles. AEMWE was chosen for hydrogen production in the study due to its significant benefits in cost-effectiveness, energy efficiency, scalability and operational flexibility. Fig. 1 depicts an HRS integrated with a grid-connected PV system schematic diagram. The proposed HRS system includes an on-grid PV system for electricity generation, an anion exchange membrane water electrolyzer for hydrogen synthesis, a storage compressor, high-pressure storage via a cascade system, a pre-cooling unit, and a dispenser.

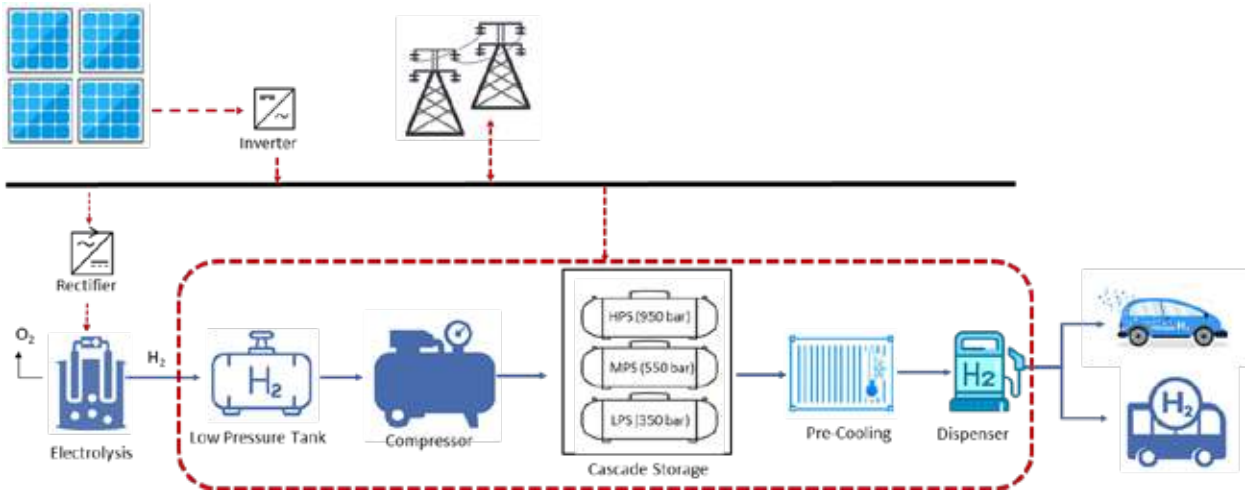


Fig. 1. Schematics of the on-grid PV integrated HRS

IV. Results and discussions

In the HRS system, the electricity generated by PV is the primary energy source. However, if the generated electricity is not sufficient, the energy deficit is met by grid electricity. Figure 2 shows the daily electricity balance for a PV installation capacity of 5 MW. Based on the proposed HRS's hydrogen demand of 170 kg H2/day, the power consumed by the electrolyzer is 9500 kWh/day. It is determined that the HRS system fully meets the electricity demand of the electrolyzer in April-October, when solar radiation is high throughout the year, and the surplus electricity can be sold to the grid.

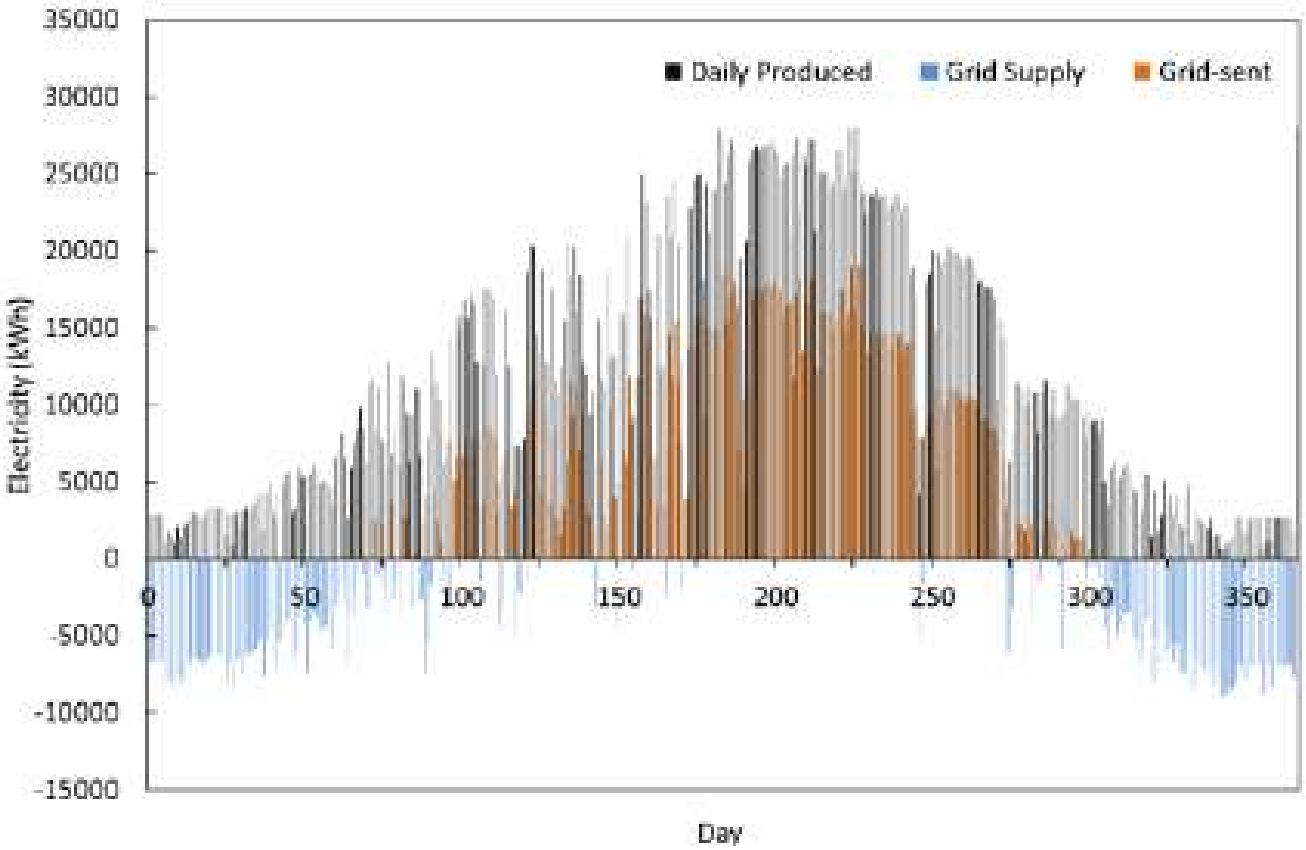


Fig. 2. Daily electricity production and grid balance of PV system with 5 MW installed power

Fig. 3 shows the ratio of HRS components to total cost for 5 MV PV installed capacity and 20 years of operating time. In the proposed HRS system, the most cost arises from PV. The levelized cost of hydrogen (LCOH) is an essential economic evaluation index (Micena et al., 2020). The LCOH, determined by assessing investment, operational, maintenance, and replacement costs, is one of the most critical indicators in economic assessment indices. The LCOH, calculated by estimating the investment, operational, maintenance, and replacement costs, is one of the most relevant indicators among the economic assessment indexes (Eq. 1).

$$LCOH = \frac{C_{total} - C_{Electrical\ Revenue}}{Annual\ H_2\ production} \quad (1)$$

The total annualized cost of the energy system ($, €/year$) includes installation, operation and maintenance costs. As the PV-integrated HRS examined in this study is grid-connected, the excess electricity generated from the PV system is sold to the grid ($C_{Electrical\ Revenue}$, €/year). To show the effect of time on LCOH in short-, medium-, and long-term investment cases, LCOH values were determined by assuming technical and financial lives of 10, 15, and 20 years. Fig. 4 illustrates the LCOH values of HRS with different PV installed power and system lifetime. According to techno-economic analyses, a decrease in LCOH values was determined with increasing system lifetime.

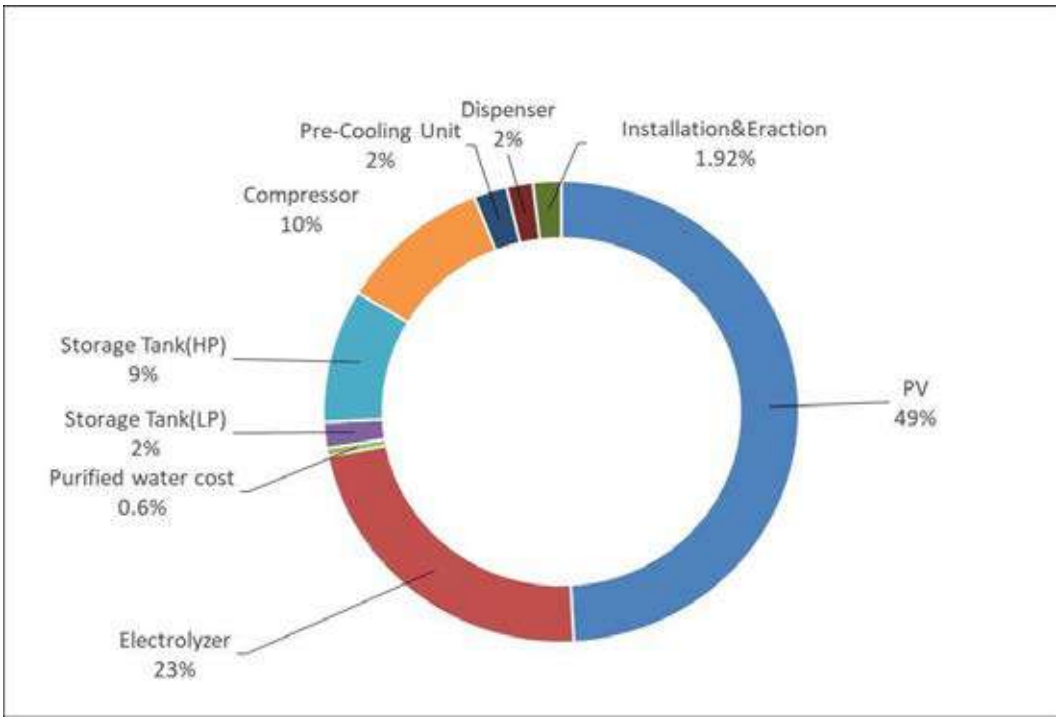


Fig. 3. The ratio of HRS components to total cost for 5 MV PV installed capacity and 20 years operating time.

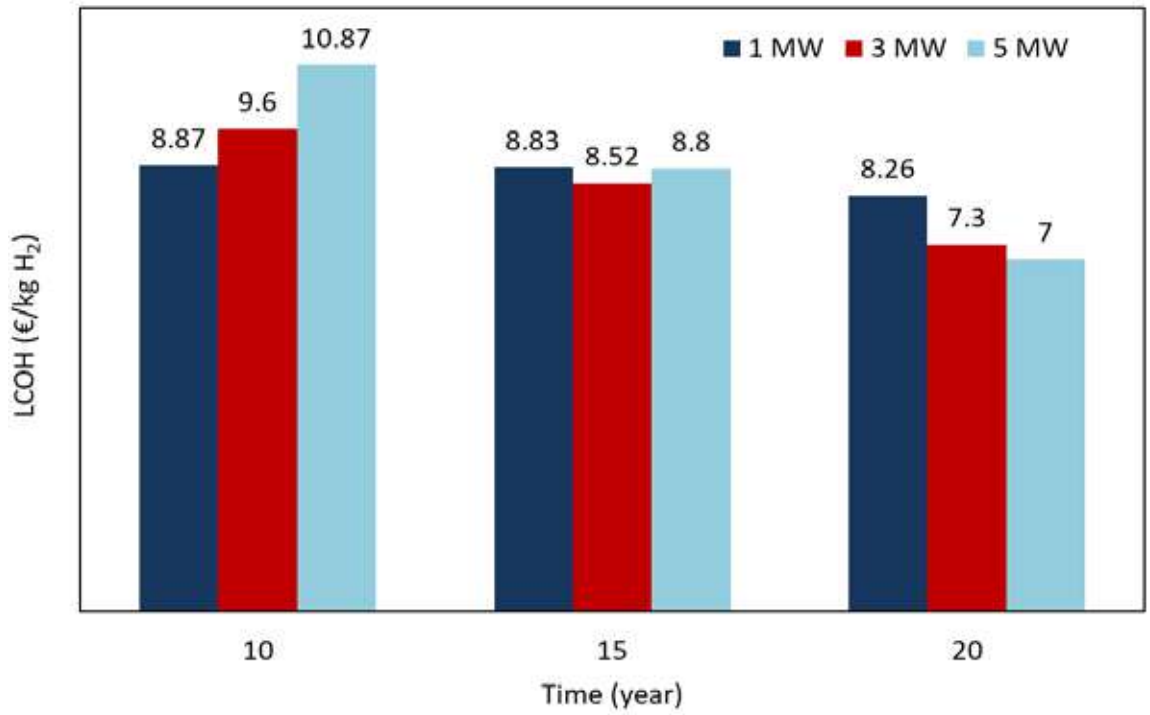


Fig. 4. LCOH values of HRS with different PV installed power and system lifetime.

V. Conclusions

We investigate the sizing and optimization of on-grid PV renewable energy systems with integrated HRS. Three alternative PV capacities were tested to determine the best cost for the HRS system. This study shows that building a renewable energy-based hydrogen refueling station is technically and economically feasible. HRS powered by renewable energy are better regarding environmental factors than conventional hydrogen production routes. Using renewable energy for hydrogen production will help countries achieve zero emissions and reduce their dependence on imported fossil fuels for transportation. Renewable energy technologies are getting better and cheaper day by day, and accordingly, the cost of renewable energy-based hydrogen production is expected to decrease in the near future.

References

Abe, J. O., Popoola, A. P. I., Ajenifuja, E., & Popoola, O. M. (2019). Hydrogen energy, economy and storage: Review and recommendation. *International Journal of Hydrogen Energy*, *44*(29), 15072–15086. https://doi.org/10.1016/j.ijhydene.2019.04.068

Baykara, S. Z. (2018). Hydrogen: A brief overview on its sources, production and environmental impact. *International Journal of Hydrogen Energy*, *43*(23). https://doi.org/10.1016/j.ijhydene.2018.02.022

Gökçek, M., & Kale, C. (2018). Optimal design of a Hydrogen Refuelling Station (HRFS) powered by Hybrid Power System. *Energy Conversion and Management*, *161*(December 2017), 215–224. https://doi.org/10.1016/j.enconman.2018.02.007

Holladay, J. D., Hu, J., King, D. L., & Wang, Y. (2009). An overview of hydrogen production technologies. In *Catalysis Today* (Vol. 139, Issue 4, pp. 244–260). https://doi.org/10.1016/j.cattod.2008.08.039

Micena, R. P., Llerena-Pizarro, O. R., de Souza, T. M., & Silveira, J. L. (2020). Solar-powered Hydrogen Refueling Stations: A techno-economic analysis. *International Journal of Hydrogen Energy*, *45*(3). https://doi.org/10.1016/j.ijhydene.2019.11.092

Minutillo, M., Perna, A., Forcina, A., Di Micco, S., & Jannelli, E. (2021). Analyzing the levelized cost of hydrogen in refueling stations with on-site hydrogen production via water electrolysis in the Italian scenario. *International Journal of Hydrogen Energy*, *46*(26). https://doi.org/10.1016/j.ijhydene.2020.11.110

Fabrication of Graphene Oxide Based Composite Membranes for Anion Exchange Membrane Water Electrolyzers

[1*]Yılser Devrim [2]Nisa Gökçen Önel
[1] Atılım University, Engineering Faculty, Energy System Engineering Department, Incek, Ankara, 06830, Türkiye
[2] Atılım University, Engineering Faculty, Chemical Engineering Department, Incek, Ankara, 06830, Türkiye

* E-mail: yilser.devrim@atilim.edu.tr

Abstract
Due to climate change concerns, the interest in hydrogen energy and technologies has brought clean hydrogen production technologies to the forefront, especially by water electrolysis. This paper investigates the use of graphene oxide (GO), phosphanated graphene oxide (PGO) and sulfated graphene oxide (SGO) as fillers to improve the performance of anAEMs used in water electrolysis. The unique qualities of these fillers were investigated through a synthesis and characterization study focusing on their structural, thermal and conductivity properties. Synthesis methods, including the Hummer method and composite material development, are discussed and their impact on membrane properties. PGO enhances water retention and conductivity, while SGO exhibits exceptional gas permeability, proton conductivity and membrane stability. This research sheds light on the potential applications of these fillers in advancing AEM technology and provides insights into their role in mitigating climate change and facilitating sustainable energy solutions.

Keywords: Graphene, graphene oxide, sulfonated graphene oxide, phosphonated graphene oxide

I. Introduction

Hydrogen is one of the best alternative energy carriers to solve today's growing energy security and environmental challenges. Hydrogen can be produced using natural gas reforming, water electrolysis, direct solar water splitting, etc. In energy conversion, water electrolysis is a promising technology as it can utilize intermittent clean energy sources such as wind, tides and solar energy to produce hydrogen from water sources. Water electrolyzers can accept high current inputs per surface area, operate in dynamic modes and respond quickly, all of which are requirements for storing intermittent energy sources (Chisholm ve Cronin, 2016).

Besides the most widely used commercial alkaline electrolyzers (AEL) and proton exchange membrane electrolyzers (PEMEL), anion exchange membrane water electrolyzers (AEMWEL) have the combined advantages of AEL and PEMEL. Similar to PEMELs, ADMWEL systems can be realized with a compact and improved system design. Transition metals can be used in ADMWEL systems instead of noble metals used in PEMEL systems. Unlike AEL systems, distilled water or low-concentration alkaline solution can be used as an electrolyte instead of concentrated KOH. Membranes containing anion exchange groups used in AEMWEL are cheaper than Nafion-based membranes. In addition, due to the absence of metal ions in AEMWELs, the interaction between CO_2 and the membrane is low. This technology also has the advantages of no corrosive liquid electrolyte, no leakage, volumetric stability, ease of use and reduced size and weight of the electrolyzer (Du vd., 2022; Vinodh vd., 2023).

Anion exchange membrane (AEM), one of the key components in AEMWELs systems, transfers OH^- ions from the cathode to the anode and prevents gas migration and electron transfer during the electrochemical process. In electrolysis applications, AEMs should exhibit high permeability, good ionic conductivity, robust thermal and mechanical stability and superior chemical stability. However, due to the poor chemical stability and low ionic conductivity caused by the basic working environment, the membranes used in AEMEL systems show decreased performance. Therefore, both the cationic parent group and the stability of the main polymer parent structure play a key role in making the AEM durable. Enhancing the mechanical properties of AEMs necessitates incorporating various filler materials. In the past decade, different approaches have been attempted to mitigate the degradation of AEMs at elevated temperatures and to enhance their ionic conductivity (Ion-Ebrasu vd., 2020). Graphene oxide (GO) has garnered substantial interest in nanomaterial fillers due to its commendable thermal stability and high specific surface area. The production of GO typically involves using Hummer's method, which was primarily chosen for its superior efficiency and satisfactory safety profile. Furthermore, composite GO materials incorporating phosphates and sulfates have been developed to augment the properties of GO, thereby enhancing the membrane's performance [4, 5]. For this purpose, synthesis methods have been researched and developed. Sulphanated graphene oxide (SGO) stands out for its exceptional gas permeability, proton conductivity, and membrane stability(Basso Peressut vd., 2021). Additionally, phosphate graphene oxide (PGO) enhances water retention capacity and conductivity within the membrane structure (Etesami vd., 2018).

This study focuses on preparing AEM with GO, pGO, and sGO fillers and detailed characterization of the prepared membranes. The results show that the targeted GO structures were successfully prepared, and the KOH retention, which significantly affects the membranes' AEM performance, was increased.

II. Experimental Set-up and Procedure

GO and Modified GO Preparation: The synthesis of GO was conducted using the Hummer method. Initially, 3.0 grams of graphite powder and 70 ml of sulfuric acid were mixed in a Teflon beaker, placed in an ice bath, and stirred. Subsequently, 9.0 grams of potassium permanganate were slowly added while stirring continued. The mixture's

temperature was raised to 40 °C and stirred for 30 min. Then,150 ml of distilled water was gradually added while stirring continued, and the temperature was increased to 95 °C. After 15 minutes of stirring, another 500 ml of distilled water was added, followed by 15 ml of 30% hydrogen peroxide. At this point, the color of the mixture transitioned from dark brown to yellow. It was allowed to settle for 24 hours. In the final stage, the mixture was washed in a centrifuge three times with 250 ml of a 1:10 HCl solution and distilled water, then dried in an oven at 60 (J. Chen vd., 2013). Within the scope of the study, sulfonated (Xu vd., 2011) and phosphonated GOs (Abouzari-Lotf vd., 2019) were prepared for AEMWE application according to literature (Figure 1).

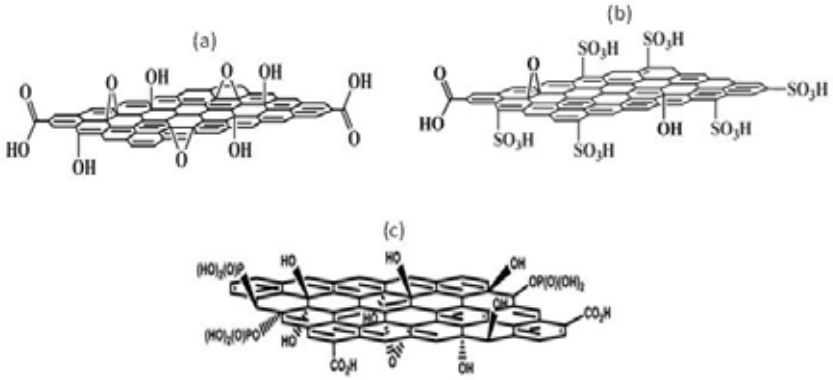


Figure 1. a) GO, b) sulfonated GO and c) phosphonated GO

Composite AEM Preparation: In this study, composite membranes were prepared using Fumion® solution. GO and modified GOs were added to the Fumion® solution according to the designed additive addition. The prepared solution was stirred until homogeneous solutions were formed and poured onto the glass surface. Finally, the membranes are heated in a vacuum oven at 80°C for 12 hours.

III. Analysis

X-ray diffraction identified the GO and modified GOs' crystalline nature (Rigaku Ultima-IV, Cu Kα radiation, 1.54056 Å). X-ray photoelectron spectroscopy (XPS) was examined by PHI 5000 VersaProbe Al Kα instrument under vacuum (0–900 eV, and X-ray spot size of 100 μm). IR spectra were obtained with a Bruker IFS 66/S FT-IR spectrometer. Mechanical properties were determined with the Instron 3367 universal test machine. KOH and water uptake, ion conductivity and mechanical analysis were executed to determine AEM application capability.

IV. Results and Discussions

Figure 2 shows the XRD patterns of GO and modified GOs. The sharp peak with a center of 12.57° in the GO diffraction pattern indicates the GO layers' planar reflection (002) structure. At the same time, this characteristic peak of the GO structure shows that the distance (d-spacing) between the graphene layers is 0.703 nm (7.03 Å). After the phosphating process of graphene oxide, a new peak at 2θ=23° indicates that the modification was partially successful and the presence of oxygenated functional groups in the structure (Shiva Kumar vd., 2018). With the sulfation process, the pure graphene oxide peak shifted to the left and another peak appeared at 2θ=20.8°. The replacement of covalent groups in the graphene oxide structure with sulfate groups can be shown as the reason for this situation.

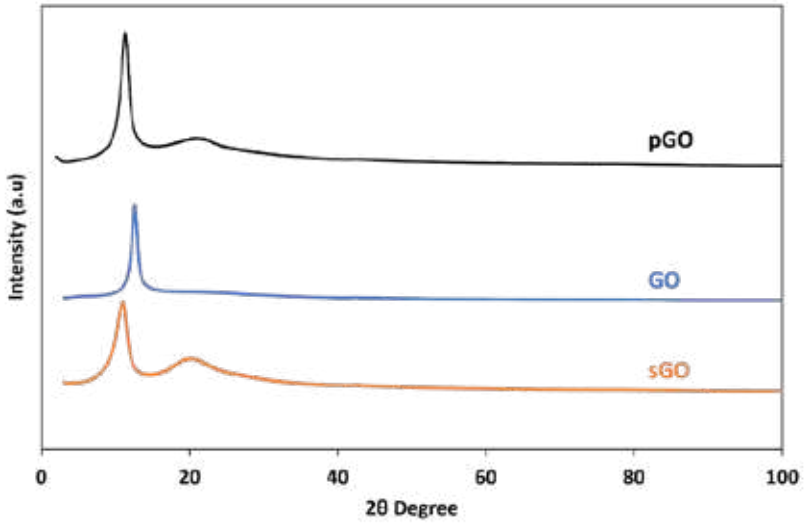


Fig. 2: XRD Patterns of GO, SGO and PGO, and PGO-2

Fig. 3 displays the FTIR spectra of GO and modified GOs, highlighting characteristic peaks corresponding to different chemical bonds. These include C-O-C (~1033 cm^{-1}), C-O (~1227 cm^{-1}), C=C (~1617 cm^{-1}), and C=O (1710 – 1720 cm^{-1}). The FTIR analysis indicates successful synthesis of graphene oxide, with deviations ranging from 5 cm^{-1} to 28 cm^{-1}. Distinct peaks are expected between 3103-3535 cm^{-1} for O-H bonds and 1040 -1100 cm^{-1} for P-O, C-P, and P=O bonds for pGO sample. These peaks are observed with greater clarity and in the expected positions in the revised pGO synthesis. For sGO, a notable peak at 1081 cm^{-1} corresponding to -SO_3- bonds distinguishes it. The FTIR results for sulfonated graphene oxide exhibit this peak prominently.

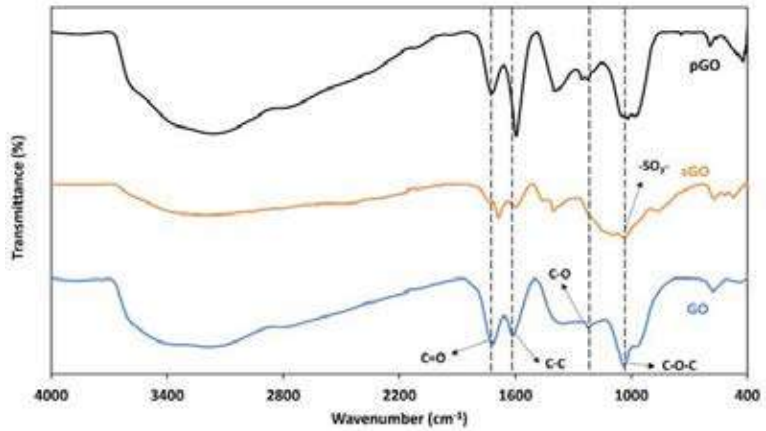


Fig. 3: FTIR Patterns of GO, sGO and pGO

Fig. 4 illustrates the XPS survey and C1s spectra of GO. High-intensity O1s peaks indicate oxygenated functional groups on the GO surface. Analysis reveals 67.8% carbon and 31.4% oxygen. C1s deconvolution shows peaks for C - C, C-O, C-O-C, and C=O (X. Chen vd., 2020).

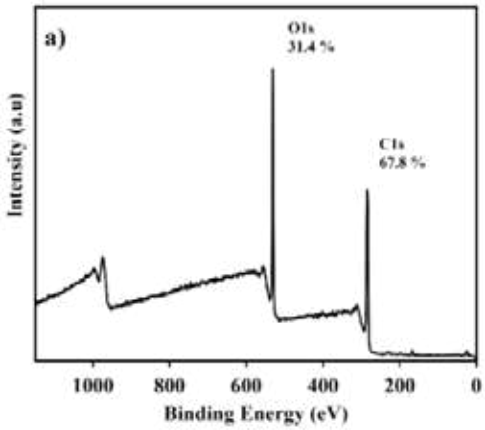


Fig. 4: XPS Patterns of GO

Fig. 5 shows the C1s spectra of GO, sGO, and pGO. C1s of GO was deconvoluted into C-C at 283.9 eV, C-O at 285.8 eV, C-O-C at 287.4 eV, and C=O at 288.3 eV. C1s of sGO deconvoluted into C-C at 283.13 eV and C-O at 285.12 eV (Cao vd., 2018). C1s of pGO deconvoluted into C=C at 283.81 eV, C-C at 283.86 eV and C-P at 286.0 eV (Liu vd., 2015).

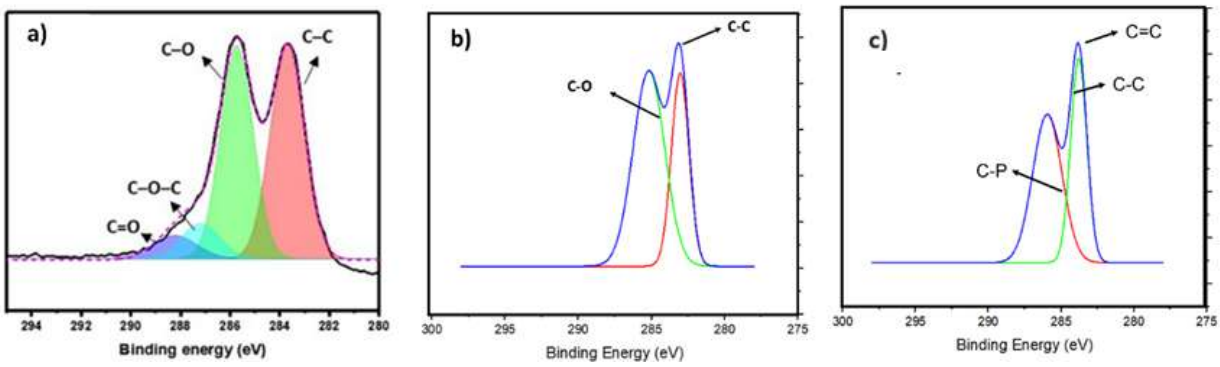


Fig. 5: XPS Patterns of a) GO, b) sGO and c) pGO

In AEMWE applications, membranes' KOH uptake ability is a determining factor in electrochemical performance. In this study, "KOH uptake" experiments of the synthesized composite membranes were carried out in 2 M KOH. The KOH uptake rates for Fumasep, F/GO, F/sGO and F/pGO membranes were determined as 52%, 78%, 69% and 76%, respectively. Compared to the reference Fumasep membrane, the KOH retention degrees of F/GO, F/sGO and F/pGO membranes showed an increase.

V. Conclusions

In this study, GO and modified GO-doped composite AEMs were developed for AEMWE application, and their structural properties and performances were investigated. The results show that the prepared GO-based composite membranes have improved properties for AEMWE application. This research provides insights into the potential applications of these synthesized fillers in AEM technology, highlighting their role in facilitating sustainable energy solutions and contributing to efforts to mitigate climate change. Further research and development in this field holds promise to ensure continued progress in the hydrogen economy and promote environmental sustainability.

References

Abouzari-Lotf, E., Zakeri, M., Nasef, M. M., Miyake, M., Mozarmnia, P., Bazilah, N. A., … Ahmad, A. 2019. "Highly durable polybenzimidazole composite membranes with phosphonated graphene oxide for high temperature polymer electrolyte membrane fuel cells". Journal of Power Sources, *412*, 238-245.

Basso Peressut, A., Latorrata, S., Gallo Stampino, P., Dotelli, G. 2021. "Development of self-assembling sulfonated graphene oxide membranes as a potential proton conductor". Materials Chemistry and Physics, *257*, 123768.

Cao, N., Zhou, C., Wang, Y., Ju, H., Tan, D., Li, J. 2018. "Synthesis and characterization of sulfonated graphene oxide reinforced sulfonated poly (ether ether ketone) (SPEEK) composites for proton exchange membrane materials". Materials, *11*(4).

Chen, J., Yao, B., Li, C., Shi, G. 2013. "An improved Hummers method for eco-friendly synthesis of graphene oxide". Carbon.

Chen, X., Wang, X., Fang, D. 2020. "A review on C1s XPS-spectra for some kinds of carbon materials". Fullerenes Nanotubes and Carbon Nanostructures.

Chisholm, G., Cronin, L. 2016. "Hydrogen From Water Electrolysis". Içinde *Storing Energy: With Special Reference to Renewable Energy Sources* (ss. 315-343). Elsevier Inc.

Du, N., Roy, C., Peach, R., Turnbull, M., Thiele, S., Bock, C. 2022. "Anion-Exchange Membrane Water Electrolyzers". Chemical Reviews, *122*(13), 11830-11895.

Etesami, M., Abouzari-Lotf, E., Ripin, A., Mahmoud Nasef, M., Ting, T. M., Saharkhiz, A., Ahmad, A. 2018. "Phosphonated graphene oxide with high electrocatalytic performance for vanadium redox flow battery". International Journal of Hydrogen Energy, *43*(1), 189-197.

Ion-Ebrasu, D., Pollet, B. G., Caprarescu, S., Chitu, A., Trusca, R., Niculescu, V., … Vasile, B. S. 2020. "Graphene inclusion effect on anion-exchange membranes properties for alkaline water electrolyzers". International Journal of Hydrogen Energy, *45*(35).

Liu, X., Li, J., Wang, X., Chen, C., Wang, X. 2015. "High performance of phosphate-functionalized graphene oxide for the selective adsorption of U(VI) from acidic solution". Journal of Nuclear Materials, *466*.

Luo, Z., Gong, Y., Liao, X., Pan, Y., Zhang, H. 2016. "Nanocomposite membranes modified by graphene-based materials for anion exchange membrane fuel cells". RSC Advances, *6*(17).

Shiva Kumar, S., Ramakrishna, S. U. B., Rama Devi, B., Himabindu, V. 2018. "Phosphorus-doped graphene supported palladium (Pd/PG) electrocatalyst for the hydrogen evolution reaction in PEM water electrolysis". International Journal of Green Energy, *15*(10), 558-567.

Vinodh, R., Kalanur, S. S., Natarajan, S. K., Pollet, B. G. 2023. "Recent Advancements of Polymeric Membranes in Anion Exchange Membrane Water Electrolyzer (AEMWE): A Critical Review". Polymers.

Xu, C., Cao, Y., Kumar, R., Wu, X., Wang, X., Scott, K. 2011. "A polybenzimidazole/sulfonated graphite oxide composite membrane for high temperature polymer electrolyte membrane fuel cells". Journal of Materials Chemistry, *21*(30), 11359-11364.

A Novel Bi/W/Cd Photocatalyst for Hydrogen Production Via Water Splitting

[1]Ceren Sakalli, [1,2]*Halit Eren Figen
[1] Yildiz Technical University, Faculty of Chemical and Metallurgical Engineering, Department of Chemical Engineering, Esenler, Istanbul, 34220, Türkiye
[2] Yildiz Technical University, Clean Energy Technologies Institute, Istanbul, 34220, Türkiye

* E-mail:hfigen@yildiz.edu.tr

Abstract

This study focuses on sustainable photocatalytic hydrogen production to meet the increasing energy demand alongside the growing global population. Photocatalytic hydrogen production relies on a reduction process facilitated by light absorption. The research emphasizes photocatalytic water splitting, investigating various catalyst preparation methods, with a preference for the hydrothermal method. Catalysts used for photocatalytic water splitting in the literature were examined, and tungsten was chosen considering band gap and heterojunction compatibility. Bismuth was selected for its ability to form a single-step heterojunction structure in developing tungsten oxide. Experimental investigation of cadmium for Bi-W doping in a solar simulator, revealed the superior performance of Bi-WO_3-CdO catalyst compared to others. Consequently, comparisons were made among WO_3-CdO, Bi-WO_3, and Bi-WO_3-CdO. This study aims to enhance renewable energy use, reduce fossil fuel consumption, and promote sustainable hydrogen production methods.

Keywords: Renewable energy sources, photocatalytic hydrogen production, hydrothermal method, water splitting, photocatalyst, bismuth, tungsten, cadmium.

I. Introduction

The global rise in population and industrial activities has pushed the capacities of traditional fossil fuels to their limits, leading to an urgent need for renewable and eco-friendly energy solutions. Among these, hydrogen energy stands out as a promising alternative, celebrated for its cleanliness and sustainability (Dincer and Joshi, 2013).

Constituting a significant portion of the universe's mass, Hydrogen does not exist freely on the Earth's surface due to its high density. Its emission of water vapor, which does not pollute the environment or create any harmful gases or chemicals causing a greenhouse effect, is a factor that makes hydrogen energy valuable. (Dixon, 2006).

Recent research has particularly focused on hydrogen production through photocatalytic processes, a promising avenue due to its straightforward system configuration and utilization of solar energy. In this process, leverages light energy to water splitting into hydrogen and oxygen in the presence of a semiconductor photocatalyst. (Herrmann, 2017). Among the materials studied, tungsten trioxide (WO_3) is notable for its indirect band gap and specific band gap energy. In this study, efforts to boost of WO_3 photocatalytic performance have focused on strategies like doping and heterojunction formation, with bismuth doping notable for enhancing material properties. Doping with metals including Ti, Zn, Dy, and research on less-explored CdO doping of WO_3-Bi, aim to optimize its narrow band gap and sunlight absorption capabilities (Dutta et al., 2021).

The production of hydrogen via photocatalytic methods involves three principal stages: the absorption of photons to generate electron-hole pairs within the semiconductor; the migration of these charges to the catalyst surface; and the catalytic reduction of water to produce hydrogen. (Mutlubas and Ozdemir, 2019) This synthesis of photocatalysts, leveraging techniques such as hydrothermal, sol-gel, and calcination, is pivotal for the effective production of hydrogen. The environmentally benign and economically viable nature of these processes, especially the hydrothermal method, underscores the potential of photocatalytic hydrogen production as a clean, sustainable energy source. (Dutta etal., 2021). Research in this field is vital for future energy needs and environmental challenges, emphasizing hydrogen energy's role in moving towards renewable sources.

II. Experimental Set-up and Procedure

This study focused on enhancing of WO_3 photocatalytic activity for water splitting through bismuth modification and CdO doping, utilizing the hydrothermal method to create heterojunctions. The performance of the synthesized Bi-WO_3 and Bi-WO_3-CdO catalysts was evaluated, in photocatalytic water splitting.

In the study, analytical grade chemicals including HNO_3, $Bi(NO_3)_3 \cdot 5H_2O$, $(NH_4)_6W_{12}O_{39} \cdot xH_2O$, $CdCl_2 \cdot H_2O$, NaOH, distilled water, and ethanol were used for synthesis of catalysts and reaction studies.

Tab. 1: Experimental codes and their contents

Code/Content	Bi	W	CdO

CS11	+	+	-
CS13	-	+	+
CS14	+	+	+
CS15	+	+	+

In this study, synthesized Bi- WO_3, CdO, and Bi- WO_3-CdO composites aimed at enhancing photocatalytic water splitting efficiency.

- **Bi-WO_3 Synthesis (CS11):**

Utilizing the hydrothermal method, $Bi(NO_3)_3 \cdot 5H_2O$ and $(NH_4)_6W_{12}O_{39} \cdot xH_2O$ were dissolved in distilled water, keeping a Bi:W ratio of 2:1 (Gui etal., 2012). The solution underwent hydrothermal treatment at 180°C for 24 hours, followed by centrifugation, drying at 75°C for 12 hours, and calcination at 500°C for 4 hours.

- **CdO Preparation:**

For the CdO component, $CdCl_2 \cdot H2O$ was dissolved in deionized water, treated with NaOH to precipitate CdO, which was then dried at 150°C for 20 hours and calcined at 500°C for 2 hours to achieve purity. (Salem, 2014).

- **WO_3 -CdO Composite (CS13)**:

The WO_3-CdO composite was prepared by mixing ethanol solutions of WO_3 and CdO, drying at 75°C for 12 hours, and calcinating at 500°C for 4 hours. This process aimed to harness a 4% CdO-WO_3 ratio, selected for optimal hydrogen production due to the synergistic effects. (Tahir etal., 2019).

- **Bi- WO_3 -CdO Composite (CS14 & CS15):**

For both composites, $Bi(NO_3)_3 \cdot 5H_2O$ was dissolved in distilled water, with HNO3 added to the solution. For CS14, a pre-prepared WO3-CdO (CS13) mixture was then integrated, whereas, for CS15, both $(NH_4)_6W_{12}O_{39} \cdot xH_2O$ and CdO were dissolved alongside. Following mixing, each solution was transferred to a Teflon-coated autoclave for hydrothermal reaction, adhering to the CS11 procedure.

III. Analysis

To evaluate the performance of the produced catalysts, comparative tests were conducted on the results obtained using the water displacement method in solar simulation. In order to find the appropriate amount of catalyst, firstly, different combinations of catalyst amounts (10mg/20mg/40mg) and 5 ml DI water were tried, 20 mg catalyst and 5 ml deionized water combination was selected, and experiments were carried out.

The catalyst and DI water were placed in a 10 ml volumetric flask, sealed with airtight tape, and observed for gas flow using the water displacement method under solar simulation. During the experiments, a solar simulator (Fytronix) with 400-1000nm wavelength range was used. The reactor system is shown schematically below (Fig.1)

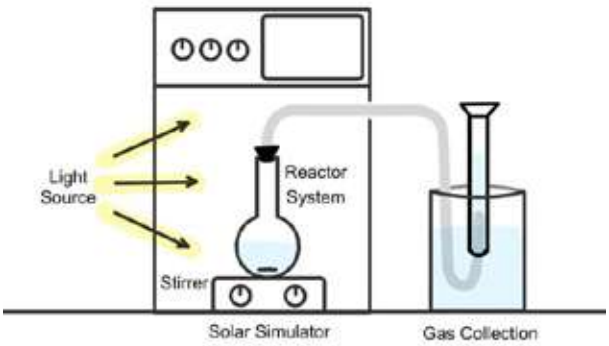


Fig. 1: Solar simulator and reactor system

Photocatalytic hydrogen production reaction from water splitting takes place in the photoreactor system, as in the following equation (Dincer and Joshi, 2013):

$$H_2O \rightarrow H_2 + \frac{1}{2}O_2 \quad (1)$$

Using the water displacement method, the product gas (hydrogen and oxygen; stoichiometrically 2:1) released as

a result of reactions in the photoreactor exposed to 400–1000 nm wavelength was collected. The volume versus time data was then obtained and illustrated to compare the catalysts' performance versus time (Fig 2).

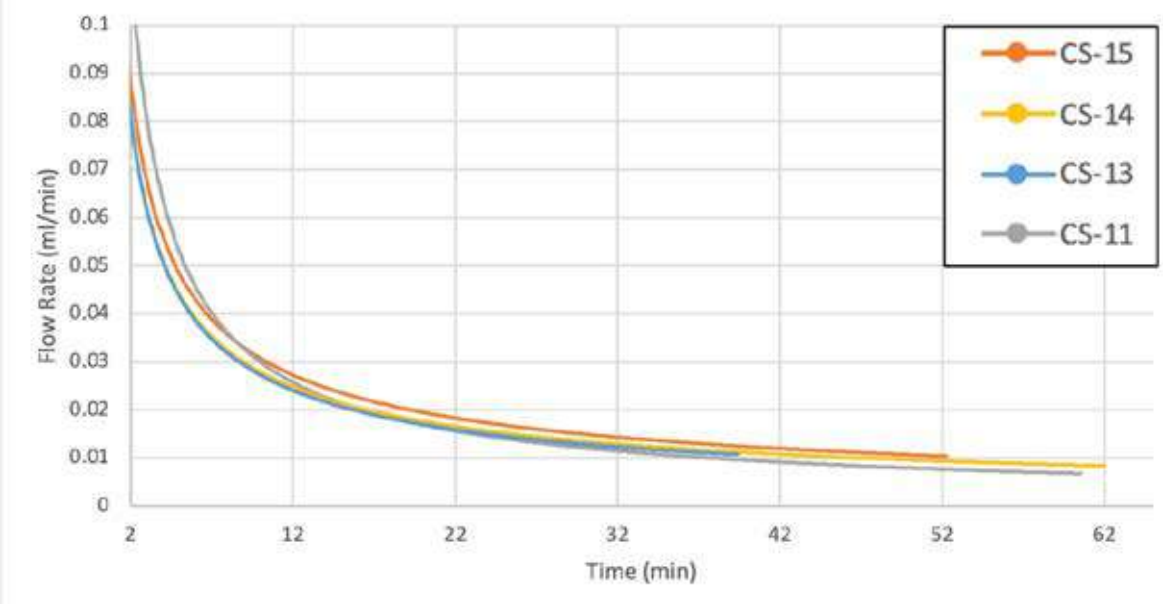


Fig. 2: Product gas stream flow rates

IV. Results and discussions

Photocatalytic water splitting reaction was investigated in a 10 ml batch reactor. The reactor was placed into a solar simulator (Figure 1). The Solar simulator provide sunlight effect between 400-1000 nm. The photocatalytic hydrogen formation performance of the catalysts prepared for the water splitting reaction was tested under sunlight irradiation.

For Equation 1, 33.3% of the flow rate represents oxygen and 66.6% represents hydrogen flow rate. When interpret the experimental results accordingly, the average flow rate for hydrogen is 1280 µmol/h.gr cat for CS15. The graph in Figure 2 shows the photocatalytic hydrogen production activity of CS11(Bi-W), CS13(W-Cd), CS14(Bi-W-Cd) and CS15(Bi-W-Cd) catalysts. CS14 and CS15 showed photocatalytic hydrogen production activity at the flow rate and exhibited a higher H2 production activity than CS13. (Hao etal., 2022) When the time interval is divided into first-middle-end as 0-10, 10-25 and 25-60, respectively; It can be seen that CS15 had a strong start in the first period and its performance was quite high compared to the others, showed a more stable performance in the middle period and increased its performance in the last period and again exhibited the strongest performance. On the other hand, CS14, had a more stable start in the first interval, then improved its performance in the middle interval and performed at the top of the list in the last interval, and performed equal to CS15 in the last period. CS13 was below the others in the first period, when the overall flow performance was evaluated it started with a high flow rate, then decreased and stabilized over time. For CS11, it can be observed that the first and middle time intervals are fluctuating and performing, but in the last time period it becomes stable and falls below the others.

V. Conclusions

It is concluded that Cd-doped catalysts Bi-W-Cd (CS14, CS15) exhibited better performance than the W-Cd (CS13) catalyst alone and Bi-W (CS11) in terms of H2 production activity and the CS15 had the best performance among the synthesized catalysts. Additionally, it is observed that CS14 and CS15 exhibit better reaction activity than CS13 in some time intervals. While the flow performance of the catalysts is evaluated, it is seen that cadmium exhibits positive effects on the catalysts for each period and cadmium doping contributes to the effectiveness of the catalyst in longer time intervals.

Acknowledgements

The authors are gratefully acknowledged for financial support of solar simulator system (Yildiz Technical University Research Foundation, Project No: FBA-2023-5648).

References

Dincer, I., Joshi, A. S., Solar Based Hydrogen Production Systems, Springer, 1-141 (2013).

Dutta, V., Sharma, S., Raizada, P., Thakur, V. K., Khan, A. A. P., Saini, V., Singh, P., An overview on WO3 based photocatalyst for environmental remediation, Journal of Environmental Chemical Engineering, 9(1), 105018 (2021).

Gui, M. S., Zhang, W. D., Chang, Y. Q., Yu, Y. X., One-step hydrothermal preparation strategy for nanostructured WO3/Bi2WO6 heterojunction with high visible light photocatalytic activity. Chemical Engineering Journal, 197, 283-288 (2012).

Hao, X., Shao, Y., Xiang, D., Jin, Z, Photocatalytic overall water splitting hydrogen production over ZnCdS by spatially separated WP and Co3O4 cocatalysts. Solar Energy Materials and Solar Cells, 248, 111970 (2022).

Herrmann, J.M., Photocatalysis, Kirk-Othmer Encyclopedia of Chemical Technology, 1–44 (2017).

Mutlubaş, H., Özdemir, Z. Ö., Hydrogen as an energy carrier and hydrogen production methods, Bartın University International Journal of Natural and Applied Sciences, 2(1), 16-34 (2019).

Dixon, R. K., Advancing Towards A, Hydrogen Energy Economy: Status, Oppurtunities and Barriers, Mitigation and Adaptation Strategies for Global Change, Springer, p.1 (2006).

Salem, A., Silver-doped cadmium oxide nanoparticles: Synthesis, structural and optical properties, The European Physical Journal Plus, 129, 1-12 (2014).

Tahir, M. B., Sagir, M., Abas, N., Enhanced photocatalytic performance of CdO-WO3 composite for hydrogen production, International Journal of Hydrogen Energy, 44(45), 24690-24697 (2019).

Experimental studies and Comprehensive Analysis of Energy, Exergy, Environmental, and Enviroeconomic Aspects of Diesel Fuel, Waste Tyre Pyrolitic Oil, and Oxy-Hydrogen Gas Mixture Used For Diesel Engine

[1] Salih Özer, [2,*]Halil Erdi Gülcan, [3,4]Samet Çelebi, [5]Usame Demir ,
[1] Department of Mechanical Engineering, Muş Alparslan University, Muş, Türkiye
[2]Department of Mechanical Engineering, Faculty of Technology, Selçuk University, Konya, Türkiye
[3] Department of Arifiye Voc. Scholl, Motor Vehicles and Transportation Tech., Sakarya University of Applied Science, Sakarya, Türkiye
[4] Department of Automotive Technologies Application and Research Center, Sakarya University of Applied Sciences, Sakarya, Türkiye
[5]Department of Mechanical Engineering, Bilecik Şeyh Edebali University, Bilecik, Türkiye

* E-mail: halil.gulcan@selcuk.edu.tr

Abstract

This study investigates the performance and emissions characteristics of diesel, waste tire pyrolysis oil, and oxy-hydrogen (HHO) gas fuel blends. Experiments were carried out at constant 3000 RPM with torque values of 1.6 Nm, 1.6 Nm, 3.2 Nm, 6.4 Nm, 7.9 Nm, and 12.8 Nm. As a result of the experiments, fuel consumption and emissions (CO, CO_2, HC, NO_x, and smoke opacity) measurements were carried out. Energy, exergy, environmental, and enviroeconomic analyses were carried out using experimental results. Energy and exergy analyses show that waste tire pyrolysis oil increases fuel energy and exergy but also increases exergy destruction, whereas HHO addition decreases exergy destruction. Sustainability analysis indicates that HHO addition enhances sustainability indices, particularly when combined with waste tire pyrolysis oil blends. Furthermore, using waste tire pyrolysis oil contributes to reducing annual CO_2 emissions and costs, thus offering potential environmental benefits. While waste tire pyrolysis oil negatively impacts performance and emissions, HHO addition improves both, promising avenues for improving engine efficiency and reducing environmental impact in the future.

Keywords: Diesel fuel,Waste tire pyrolysis oil, Oxy-hydrogen gas, Exergy and Enviroeconomic analyses

I. Introduction

The global energy landscape is undergoing significant transformation Gielen D. (2019) due to technological advancements Hassan Q. (2024), environmental concerns Koirala BP. (2016), and economic imperatives Blondeel M. (2021), highlighting the need for alternative fuel options. Diesel fuel, despite its efficiency and availability Kalghatgi G. (2019), poses environmental challenges such as air pollution and greenhouse gas emissions. This necessitates exploring cleaner, sustainable alternatives.

Reutilizing waste oil as diesel fuel offers a dual benefit: reducing reliance on fossil fuels and addressing waste management issues Bezergianni S. (2017). Millions of liters of used lubricating oil discarded annually represent a significant opportunity for creating cost-effective, environmentally friendly fuel options Phetyim N. (2018), Arpa O. (2010). However, transforming waste oil into diesel-compatible fuel requires meticulous processing to remove impurities and adjust properties to meet diesel engine standards Owusu PA. (2018), Zandi-Atashbar N. (2017).

Another promising avenue is using waste tyre oil (WTO) as diesel fuel, addressing waste management and sustainable energy production challenges. Tyres, at the end of their life, contribute to environmental waste due to their non-biodegradable nature. Pyrolysis of tyres produces WTO, which can be a sustainable alternative to conventional diesel, albeit with necessary engine or fuel modifications Oni BA. (2021). This not only aids in waste reduction but also offers economic benefits by transforming waste into a valuable commodity.

Additionally, integrating oxy-hydrogen (HHO) gas, generated through water electrolysis, as a supplemental fuel in diesel engines has emerged as a potential solution for enhancing engine efficiency and reducing pollutants Paparao J. (2022). HHO gas's unique properties promise more complete fuel combustion, leading to improved fuel economy and reduced emissions.This study aims to explore the energy, exergy, environmental, and enviroeconomic aspects of diesel fuel, waste tyre oil, and oxy-hydrogen gas in diesel engines.

By reviewing existing literature and industry insights, it seeks to provide a comprehensive understanding of these alternative fuels, highlighting their benefits, challenges, and potential for future research. The goal is to contribute to the development of sustainable fuel options that balance energy security, environmental sustainability, and economic growth.

II. Experimental Set-up and Procedure

This study investigated the combustion characteristics of diesel, waste tyre pyrolytic oil, and HHO fuel blends in a single-cylinder diesel engine. Diesel fuel and waste tyre oil were sourced commercially, with the waste oil undergoing filtration and heating (at 70°C, followed by 110°C for 3 hours) to remove impurities. Based on preliminary tests, fuel mixtures were determined as 100% Diesel (D), and blends containing 20% (DW20), 40% (DW40), and

60% (DW60) waste tyre oil by volume, with their properties detailed in a table.

A UCR-branded hydrogen generator, part of a commercial vehicle hydrogen kit, produced HHO gas. The HHO production was adjustable via current levels, with safety ensured through a natural gas valve, a flow meter for precise gas flow towards the engine, and a spark check valve.

The experimental setup (Fig.1) involved a single-cylinder, air-cooled, naturally aspirated engine with specific technical specifications provided. A mixing chamber facilitated optimal mixing of HHO and air before the engine intake. Exhaust gas emissions (CO, CO_2, HC, smoke, and NO_x) and fuel consumption were precisely measured, with device specifications and measurement precision detailed.

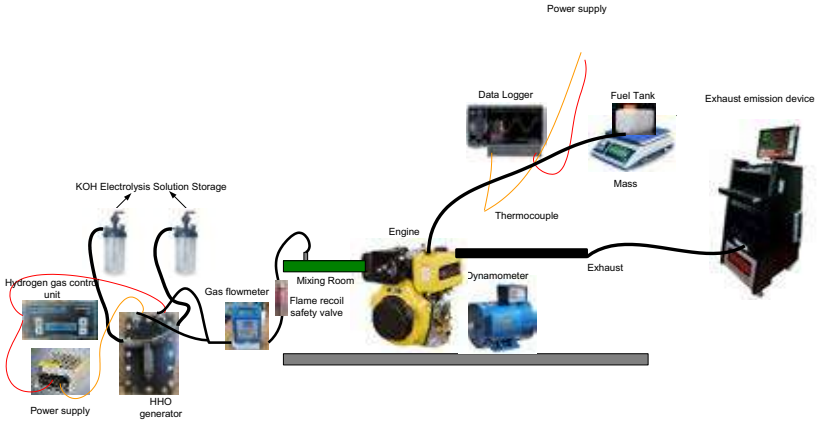


Fig. 1. Schematic view of the experimental setup.

Data uncertainties were calculated using the Kline McClintock method Karagöz Y. (2016), Deb M. (2015), with accuracies of measurement tools and uncertainties summarized. Engine tests were conducted at a constant speed of 3000 RPM under various loads, with the engine initially warmed up using diesel fuel. The transition to test fuels involved gradually reducing liquid fuel supply while introducing HHO gas to achieve desired power output. Measurements were recorded for analysis once steady-state conditions were attained.

III. Theoretical methodology

This study assesses the energy, exergy, sustainability, environmental, and enviroeconomic impacts of diesel, waste tire pyrolysis oil, and HHO fuel blends through comprehensive analyses. Assumptions for the analyses include steady engine operation, combustion products reaching chemical equilibrium, ideal gas behavior of inflow and outflow gases, and constant flow properties within the analysis control volume. The ambient temperature and pressure are set at 301 K and 101 kPa, respectively.

The energy analysis follows the first law of thermodynamics, equating the system's energy gain to the energy output, including the engine's fuel energy, net power, exhaust energy, and lost energy. The exergy analysis, indicating the potential for useful work and quantifying energy degradation, calculates the system's exergy input, output, destruction, and lost exergy, considering fuel's chemical exergy factor.

The environmental analysis evaluates the CO_2 emissions from engine operation using the fuel blends across different engine loads, calculating the annual CO_2 emission amount and its environmental-economic cost based on the operational period and CO_2 price per ton.

Key equations include the energy balance (Eq. 1), the detailed calculation of fuel energy, net engine power, exhaust energy, and lost energy (Eqs. 2-5), thermal efficiency (Eq. 6), exergy balance (Eq. 7), and detailed exergy calculations (Eqs. 8-15). Entropy production is derived from exergy destruction (Eq. 16), and the sustainability index is calculated to evaluate the blends' sustainability (Eq. 17). Finally, the annual CO_2 emissions and their cost are determined (Eqs. 18-19), providing a holistic view of the fuels' environmental and economic impacts.

IV. Results and discussions

Increasing engine load decreases HC and CO emissions but increases CO_2 emissions across diesel, waste tire pyrolysis oil, and HHO blends. The DHHO10 blend significantly reduces HC emissions, demonstrating improved combustion efficiency with HHO addition. Waste tire oil's higher density leads to incomplete combustion, but HHO's oxygen and hydrogen content aids in reducing HC emissions.

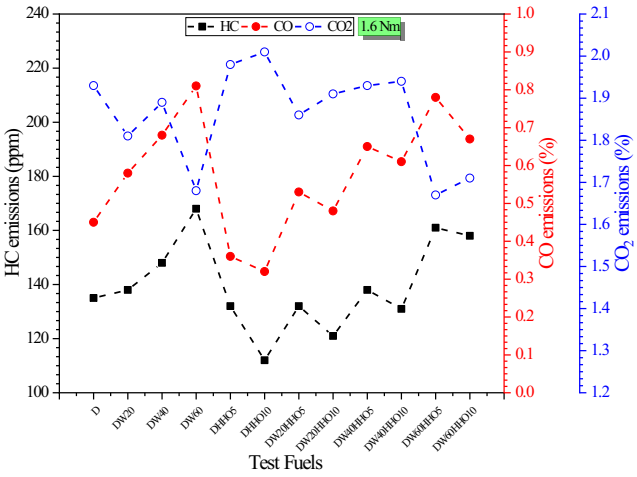


Fig. 2 Variations of HC, CO, and CO2 emissions for diesel, waste tire pyrolysis oil, and HHO test fuels.

Increasing engine load enhances fuel energy, brake power, exhaust energy, and loss energy for all fuel blends at Fig. 3. DW60 shows the highest fuel energy; DHHO10, with HHO, demonstrates the lowest, improving combustion efficiency. Exhaust energy loss increases with load but varies minimally across blends. HHO addition consistently reduces fuel consumption and lost energy across all conditions.

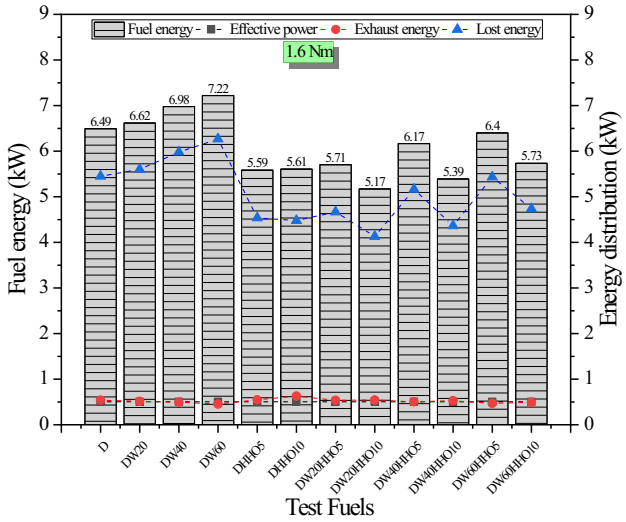


Fig. 3. Variations of fuel energy, exhaust energy, and lost energy parameters of energy analysis for diesel, waste tire pyrolysis oil, and HHO test fuels.

Adding waste tire pyrolysis oil to diesel reduces first-law efficiency due to higher fuel consumption. However, incorporating HHO into these blends enhances efficiency, with DHHO10 achieving the highest values under most conditions. The improvement is attributed to better combustion and reduced fuel consumption, with HHO notably increasing efficiency, especially at higher loads.

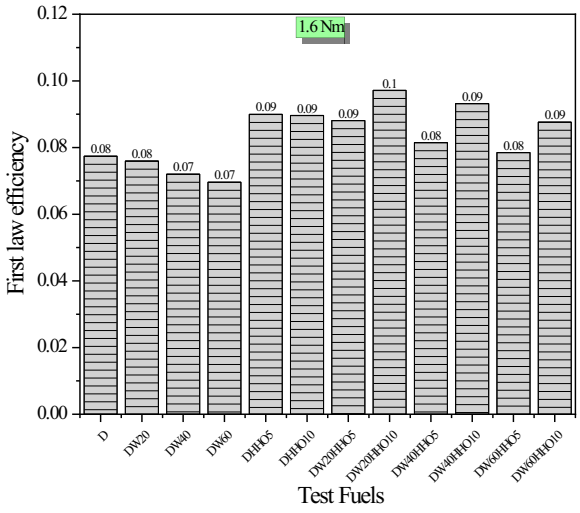


Fig. 4. Variations of first law efficiency for diesel, waste tire pyrolysis oil, and HHO test fuels.

Adding waste tire pyrolysis oil to diesel increases fuel exergy due to higher fuel consumption, while integrating HHO reduces it by enhancing combustion efficiency. The highest and lowest fuel exergies were observed with DW60 and DHHO10 blends, respectively. Exhaust exergy and exergy destruction also vary, with HHO addition generally leading to lower values across all loads.

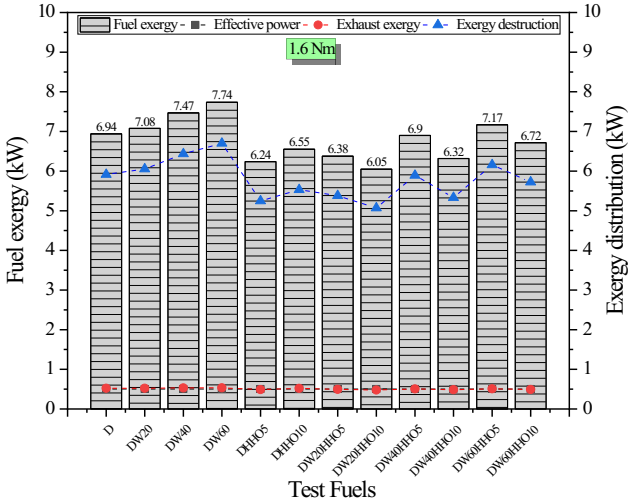


Fig. 5. Variations of fuel exergy, exhaust exergy, and exergy destruction parameters of exergy analysis for diesel, waste tire pyrolysis oil, and HHO test fuels.

V. Conclusions

This study finds that blending waste tire pyrolysis oil with diesel increases HC and CO emissions but decreases CO_2 emissions, improving with HHO addition due to enhanced combustion efficiency. Waste tire oil blends exhibit trade-offs between NO_x emissions and smoke opacity, with HHO reducing smoke opacity but slightly increasing NO_x. The best fuel energy, exergy, and sustainability outcomes are achieved with a diesel-HHO blend (DHHO10), showing high first law efficiency and low exergy destruction. While waste tire oil reduces CO_2 emissions and costs, its performance and emissions are optimized by adding HHO, suggesting future research into nanoparticle-enhanced blends for better combustion and environmental outcomes.

References

Gielen D, Gorini R, Wagner N, Leme R, Gutierrez L, Prakash G, et al. Global Energy Transformation: A Roadmap to 2050 (2019).
Hassan Q, Viktor P, J. Al-Musawi T, Mahmood Ali B, Algburi S, Alzoubi HM, et al. The renewable energy role in the global energy Transformations. Renew Energy Focus 2024;48:100545. https://doi.org/10.1016/J.REF.2024.100545 (2024).
Koirala BP, Koliou E, Friege J, Hakvoort RA, Herder PM. Energetic communities for community energy: A review of key issues and trends shaping integrated community energy systems. Renew Sustain Energy Rev 2016;56:722–44. https://doi.org/10.1016/J.RSER.2015.11.080 (2016).
Blondeel M, Bradshaw MJ, Bridge G, Kuzemko C. The geopolitics of energy system transformation: A review. Geogr Compass 2021;15:e12580. https://doi.org/10.1111/GEC3.12580 (2021).
Kalghatgi G. Development of Fuel/Engine Systems—The Way Forward to Sustainable Transport. Engineering 2019;5:510–8. https://doi.org/10.1016/J.ENG.2019.01.009 (2019).
Bezergianni S, Dimitriadis A, Faussone GC, Karonis D. Alternative Diesel from Waste Plastics. Energies 2017, Vol 10, Page 1750 2017;10:1750. https://doi.org/10.3390/EN10111750 (2017).
Phetyim N, Pivsa-Art S. Prototype Co-Pyrolysis of Used Lubricant Oil and Mixed Plastic Waste to Produce a Diesel-Like Fuel. Energies 2018, Vol 11, Page 2973 2018;11:2973. https://doi.org/10.3390/EN11112973 (2018).
Arpa O, Yumrutaş R, Argunhan Z. Experimental investigation of the effects of diesel-like fuel obtained from waste lubrication oil on engine performance and exhaust emission. Fuel Process Technol 2010;91:1241–9. https://doi.org/10.1016/J.FUPROC.2010.04.004 (2010).
Owusu PA, Banadda N, Zziwa A, Seay J, Kiggundu N. Reverse engineering of plastic waste into useful fuel products. J Anal Appl Pyrolysis 2018;130:285–93. https://doi.org/10.1016/J.JAAP.2017.12.020 (2018).
Zandi-Atashbar N, Ensafi AA, Ahoor AH. Nano-CeO2/SiO2 as an efficient catalytic conversion of waste engine oil into liquid fuel. J Clean Prod 2017;166:1010–9. https://doi.org/10.1016/J.JCLEPRO.2017.08.103 (2017).
Oni BA, Sanni SE, Olabode OS. Production of fuel-blends from waste tyre and plastic by catalytic and integrated pyrolysis for use in compression ignition (CI) engines. Fuel 2021;297:120801. https://doi.org/10.1016/J.FUEL.2021.120801 (2021).
Paparao J, Murugan S. Dual-fuel diesel engine run with injected pilot biodiesel-diesel fuel blend with inducted oxy-hydrogen (HHO) gas. Int J Hydrogen Energy 2022;47:17788–807. https://doi.org/10.1016/J.IJHYDENE.2022.03.235 (2022).
Karagöz Y, Sandalci T, Koylu UO, Dalkiliç AS, Wongwises S. Effect of the use of natural gas-diesel fuel mixture on performance, emissions, and combustion characteristics of a compression ignition engine. Adv Mech Eng 2016;8:1–13. https://doi.org/10.1177/1687814016643228/ASSET/IMAGES/LARGE/10.1177_1687814016643228-FIG13.JPEG (2016).
Deb M, Sastry GRK, Bose PK, Banerjee R. An experimental study on combustion, performance and emission analysis of a single cylinder, 4-stroke DI-diesel engine using hydrogen in dual fuel mode of operation. Int J Hydrogen Energy 2015;40:8586–98. https://doi.org/10.1016/J.IJHYDENE.2015.04.125 (2015).

Hydrogen Storage and Metal Hydride Storage

[1*] Nesrin İlgin Beyazit
[1] Dicle University, Department of Mechanical Engineering, Diyarbakır, Türkiye

* E-mail:nesrinilgin@gmail.com

Abstract
Metal hydride storage is a storage method that stands out with high storage capacity, fast storage sizes and reliable performance. Reviews show superior models of some metal hydride products. Metal hydride storage technology has a wide range of applications, from replacing solar and wind energy in portable storage systems. The development and dissemination of this technology can play a key role in the transition to sustainable energy.

Keywords: Metal hydride storage, hydrogen storage, sustainable energy, renewable energy, energy storage systems

I. Introduction

Hydrogen storage means storing hydrogen gas for the purpose of transmitting energy. Hydrogen storage methods are of great importance in terms of safety and efficiency. Storage tanks are used to store hydrogen gas in special containers (Dinçer & Ezan, 2020). Hydrogen has properties such as being light, having high energy density and a wide combustion range. Since hydrogen gas is explosive, safety precautions are of great importance. Compressed hydrogen gas, liquid hydrogen and metal hydride storage are commonly used storage methods. (Celep, 2023).

Hydrogen storage represents a critical area for the effective use of renewable energy sources. In this section, the basic principles of hydrogen storage and various storage methods will be discussed in detail. In particular, the importance and advantages of metal hydride storage will be examined..(Vural et al.2022) ,(EMEKSİZ and Burak2022) Hydrogen storage is generally based on the processes of absorption and release of hydrogen. Storage materials absorb and chemically bind hydrogen and then release hydrogen when needed, contributing to energy production. This process takes place in line with the characteristics of the storage materials and storage conditions. (Pehlivan, 2020),(Aydin, 2023).

Different storage methods include physical storage, chemical storage and physicochemical storage. The physical storage method is achieved by compressing hydrogen gas under pressure or liquefying it at low temperatures and is often used for industrial applications (Dinçer & Ezan, 2020).
The chemical storage method allows hydrogen to be stored by reacting with chemical compounds, and this is usually achieved using metal hydrides or chemical hydrogen carriers (Sorgulu et al.2022).
Physicochemical storage method is a method that combines physical and chemical storage principles, and materials such as metal organic frameworks offer the potential for physicochemical storage in hydrogen storage. (Akbulut Uludağ, 2021).

Metal hydride storage plays an important role in the field of hydrogen storage. Metal hydrides form metal-hydrogen compounds by absorbing hydrogen and have high storage capacity. (Hirscher et al.2020). Thanks to these properties, metal hydrides are preferred as safe, effective and high-capacity hydrogen storage materials. The metal hydride storage process is based on the processes of absorption and release of hydrogen. Metal hydrides absorb hydrogen, store it in their crystal structures, and release it when the hydrogen needs to be released. This process plays an important role in hydrogen storage and energy conversion systems.

Consequently, hydrogen storage is a critical area and contributes to the effective use of renewable energy sources. In the development of energy storage technologies, basic principles and various storage methods play an important role. Metal hydride storage is an important element in creating sustainable energy systems thanks to its high capacity and effective storage features.

II. Metods

Details such as the methods used in the application of metal hydride storage technology and the working principles of these methods, their effects on the hydrogen storage process, storage capacity and efficiency are very important. Metal hydride storage technology stands out as an effective and reliable method for hydrogen storage. This technology chemically binds and stores hydrogen by absorbing it into the crystal structures of metal materials. In the hydrogen storage process, metal hydrides absorb hydrogen to form metal-hydrogen compounds. This process relies on a reversible chemical reaction between the storage and release of hydrogen (Hynes et al.2021).

In metal hydride storage technology, hydrogen gas is absorbed and incorporated into the crystal structure of the metal material. During this process, hydrogen atoms are trapped between metal atoms (Güler, 2022).

Storage capacity varies depending on the structure and composition of the metal hydride (Yolun, 2021).

The absorption and release of hydrogen generally depends on temperature and pressure conditions. In certain temperature and pressure ranges, metal hydrides absorb or release hydrogen (Dal, 2020). Therefore, temperature and pressure control are important during the storage process
The storage capacity of metal hydrides depends on their capacity to absorb and release hydrogen. Metal hydrides with high storage capacity have the potential to store more hydrogen. Moreover, the efficiency of the storage process is directly related to the rate of absorption and release of hydrogen (Sayım, 2023).

Metal hydride storage technology plays an important role in the hydrogen storage process. Metal hydride storage technology increases hydrogen storage capacity and improves the efficiency of energy storage systems. The storage capacity of metal hydrides varies depending on temperature and pressure conditions, and the efficiency of the storage process is important. (Kocaman, 2021). Therefore, metal hydride storage technology makes significant contributions to the development of sustainable energy storage systems.

III. Results and discussions

Findings regarding the performance of metal hydride storage technology provide important information regarding storage capacity, speed, reliability and application areas. Metal hydrides attract attention with their high hydrogen storage capacity (KOŞAR, 2021). Storage capacity is directly related to the capacity to absorb and release hydrogen. Studies show that certain metal hydride compositions have high storage capacity. In particular, it is stated that titanium-based metal hydrides have high hydrogen storage capacity (Dikmen, 2022)(Aldemir, 2020) (Türkyılmaz, 2021) (Tan, 2022) (Caner, 2021).

The performance of metal hydride storage technology is also evaluated in terms of storage speed. Storage rate refers to the rate of absorption and release of hydrogen. Experimental studies show that certain metal hydrides have rapid hydrogen absorption and release properties (Alshhab, 2022) (Devrim, 2020) (Bolat, 2021) (Aldemir, 2020) (SAYIM, 2023). This feature is an important factor in energy storage and recycling processes.

The reliability of metal hydride storage technology is important for the stable and safe hydrogen storage process. It is stated that metal hydrides exhibit stable performance in hydrogen storage and release processes. This highlights the reliability of metal hydride storage technology.(Bannenberg et al.2020) (Malleswararao & Dutta, 2022) (Luo et al.2020).

Metal hydride storage technology has a wide range of applications in energy storage, transportation and conversion systems. In particular, the use of metal hydride storage technology is becoming widespread in areas such as portable hydrogen storage systems, solar and wind energy integration, electric vehicles and energy storage facilities (Dinçer & Ezan, 2020) (Bolat, 2021).

Findings regarding the performance, storage capacity, speed, reliability and application areas of metal hydride storage technology play a key role in the development of sustainable energy storage systems. Experiments reveal that certain metal hydride compounds have high storage capacity, fast storage processes, reliable performance and wide application areas (SAYIM, 2023) (Bolat, 2021) (Uzun, 2021) (Akbulut Uludağ, 2021) (Köse, 2021) (Dursun, 2024) (Süleymanoğlu, 2023) (Güler, 2022) (Yolun, 2021).

V. Conclusions

Hydrogen storage technologies are extremely important for the efficient use of renewable energy resources and the development of energy storage systems. In particular, the metal hydride storage method stands out with its high storage capacity, fast storage processes and reliable performance. Research has proven that some metal hydride compounds have these superior properties. Therefore, metal hydride storage technology plays a vital role in the development of sustainable energy storage systems.

Metal hydride storage technology has a wide range of applications in various fields, from portable hydrogen storage systems to solar and wind energy integration. This wide range of uses enables hydrogen to be further strengthened as a clean and sustainable energy source. Information about the performance, storage capacity, speed, reliability and application areas of metal hydride storage technology is an important guide and source of motivation in the development of sustainable energy storage systems in the future. The advancement of this technology will make significant contributions to the spread of renewable energy and reducing our dependence on fossil fuels.

For metal hydride storage technology to be more widely adopted, reducing its cost is of great importance. Additionally, the safety and durability of metal hydride storage systems are critical for the widespread use of this technology. Therefore, further research and development is needed.

In conclusion, metal hydride storage technology is a technology that may have a key role in the transition to

sustainable energy. The development and dissemination of this technology will be a guide for a cleaner and sustainable future. Therefore, the development and dissemination of this technology is of critical importance for a sustainable energy future.

References

Dinçer, İ. & Ezan, M. A. (2020). Tüba Enerji Depolama Teknolojileri Raporu. Ankara: Türkiye Bilimler Akademisi Yayınları.researchgate.net

Celep, F. (2023). Uçucu yanıcı gazların birikme davranışının hesaplamalı akışkanlar dinamiği simülasyonu yöntemiyle incelenmesi= Inestigation of the accumulating behaviors of ….sakarya.edu.tr

Vural, A., URAL, M. N., & ÇİFTÇİ, A. (2022). Yenilenebilir ve Nükleer Enerji Kaynaklarının Retrospektif Değerlendirilmesi. Journal of Investigations on Engineering and Technology, 5(2), 115-134.dergipark.org.tr

EMEKSİZ, C., & Burak, K. A. R. A. (2022). Enerji Depolama Teknolojilerinin İncelenmesi ve Karşılaştırmalı Analizi. International Journal of Multidisciplinary Studies and Innovative Technologies, 6(2), 134-142.dergipark.org.tr

Pehlivan, F. (2020). Çok duvarlı karbon nanotüplerin modifikasyonu, karakterizasyonu ve hidrojen depolama kapasitesinin belirlenmesi.balikesir.edu.tr

Aydin, S. Ö. (2023). Türkiye'nin enerji arz güvenliğinde yeşil hidrojen potansiyeli.mef.edu.tr

Sorgulu, F., Öztürk, M., Javani, N., & Dinçer, İ. (2022). Hidrojen ve Doğal Gaz Karışımının Evsel Cihazlarda Kullanımının Deneysel ve Teorik Olarak İncelenmesi. Cihannüma Teknoloji Fen ve Mühendislik Bilimleri Akademi Dergisi, 1(1).cihannumaakademi.org

Akbulut Uludağ, A. (2021). Lityum Hava Pillerde Enerji Depolama ve Yaşam Döngüsü Analizi.sakarya.edu.tr
Hirscher, M., Yartys, V. A., Baricco, M., von Colbe, J. B., Blanchard, D., Bowman Jr, R. C., ... & Zlotea, C. (2020). Materials for hydrogen-based energy storage–past, recent progress and future outlook. Journal of Alloys and Compounds, 827, 153548.sciencedirect.com

Hynes, N. R. J., Sankaranarayanan, R., Kannan, P. S., Khan, A., Khan, A. A. P., Asiri, A. M., & Dzudzevic-Cancar, H. (2021). Solid-state hydrides for hydrogen storage. In Nanomaterials for hydrogen storage applications (pp. 249-264). Elsevier.researchgate.net

Yolun, A. (2021). Olivin bazlı şarj edilebilir pillerin üretimi ve elektrokimyasal performanslarının geliştirilmesi.inonu.edu.tr

Dal, İ. (2020). Yüksek performanslı stabil faz değişim malzemesinin geliştirilmesi.bilecik.edu.tr

Güler, A. (2022). Li iyon piller için grafen takviyeli spinel LiMn2O4 nanoçubuk katot materyallerinin sentezi ve elektrokimyasal özelliklerinin geliştirilmesi= Synthesis and development ….sakarya.edu.tr

Sayım, A. (2023). Sodyumborhidrür (NaBH4) bileşiğinin insansız hava araçlarında (İHA) yakıt olarak kullanılabilirliğinin araştırılması.iste.edu.tr

Kocaman, B. (2021). Enerji depolama teknolojileri.iksadyayinevi.com

KOŞAR, C. (2021). Hidrojen Depolama Yöntemleri. Open Journal of Nano.dergipark.org.tr

Dikmen, İ. C. (2022). Elektrikli araçlar için akıllı batarya yönetim sisteminin tasarımı ve uygulaması.inonu.edu.tr

Aldemir, M. (2020). Jet motorlarında hidrojenin alternatif yakıt olarak kullanımının araştırılması.yok.gov.tr

Türkyılmaz, M. (2021). Türkiye'de yakıt pillerinin gelişimi.amasya.edu.tr

Tan, S. (2022). Ultrasonik destekli akımlı kaplama tekniği ile üretilen ni-w-tio2 kaplamaların tribolojik davranışlarının incelenmesi= Pulse electrodeposition of ni–w–tio2 composite ….sakarya.edu.tr

Caner, C. (2021). Manyetik Katı Faz Ekstraksiyonu Metodu ile Bazı Ağır Metal İyonlarının Önderiştirilmesi ve USN-ICP-OES ile Tayini.sakarya.edu.tr

Alshhab, A. (2022). KLİK KİMYASI KULLANILARAK YENİ BORONAT ESTERLERİN SENTEZİ: SPEKTROSKOPİK ÖZELLİKLER VE BİYOLOJİK UYGULAMALARI.HTML

Devrim, S. (2020). Vİskoelastik jel dolgulu koruge çekirdekli sandviç plakların ok yükü performansının sonlu elemanlar yöntemi ile incelenmesi.uludag.edu.tr

Bolat, M. (2021). Dağıtık enerji üretim sistemleri için enerji depolama sistem tasarımı, planlanması ve uygulaması.sakarya.edu.tr

Bannenberg, L. J., Heere, M., Benzidi, H., Montero, J., Dematteis, E. M., Suwarno, S., ... & El Kharbachi, A. (2020). Metal (boro-) hydrides for high energy density storage and relevant emerging technologies. International Journal of Hydrogen Energy, 45(58), 33687-33730.arxiv.org

Malleswararao, K. & Dutta, P. (2022). Applications of metal hydride based thermal systems: a review. Applied Thermal Engineering.HTML

Luo, Y., Wang, Q., Li, J., Xu, F., Sun, L., Zou, Y., ... & Zhang, K. (2020). Enhanced hydrogen storage/sensing of metal hydrides by nanomodification. Materials Today Nano, 9, 100071.HTML

Uzun, E. (2021). NCA tabanlı katot elektrotlarının çamur bileşiminin elektrokimyasal özelliklere etkisi.sakarya.edu.tr

Köse, C. (2021). Grafen takviyeli CuO anot elektrotlarının tasarımı ve Li-iyon pil uygulamaları.sakarya.edu.tr

Dursun, H. (2024). Elektrikli taşıtlarda kullanılan batarya modülünün ısıl performansının sayısal ve deneysel araştırılması.uludag.edu.tr

Süleymanoğlu, T. (2023). LaxSr1-xFeyM1-y (M: Mn, Co, Ni, Cu) O3 gözenekli perovskitin incelenmesi ve süper kapasitör uygulama yaklaşımı ile kristal yapı, elektrik ve iyon taşıma özelliklerinin ….sakarya.edu.tr

Journey to a Sustainable Future: The Importance of Renewable Hydrogen in Industrial and Domestic Applications

[1*] Nesrin İlgin Beyazit
[1] Dicle University, Department of Mechanical Engineering, Diyarbakır, Türkiye

* E-mail:nesrinilgin@gmail.com

Abstract
In recent years, challenges such as climate change and the depletion of fossil fuels have increased due to the increasing growth of changing energy. This durable, renewable energy attracts attention as an energy source obtained by breaking down water molecules through electrolysis. Offering a clean and sustainable alternative for residential and industrial use, the energy source offers various advantages. First of all, being a carbon-free energy source, meaning no greenhouse gas emissions, it offers an environmentally friendly option and helps reduce carbon. In addition, the topics that can be used and stored as fuels in various areas such as replaceable energy, heating, electricity production, transportation and industrial processes are mentioned.

Keywords: Renewable Hydrogen, Sustainable Energy, Carbon Emissions Reduction

I. Introduction

Among the resources used in the energy production process, there are renewable energy sources that are naturally renewable(Tanriöver, 2020). These resources offer important advantages such as reducing the risk of depletion and environmental impacts of fossil fuels (Arslan, 2022). However, the rapid increase in energy need and global problems such as climate change support the search for more sustainable energy sources. (Genç, 2022).

Renewable energy sources are energy obtained from natural sources such as solar, wind, hydroelectric, biomass and geothermal. These resources are sustainable and environmentally friendly compared to fossil fuels because they are infinitely renewable (ARSLAN, 2023).

There are different energy sources such as solar energy converted directly into electricity through solar panels, wind energy used to produce electricity with wind turbines, and hydroelectric energy obtained from water resources. In addition, resources such as biomass energy obtained from the combustion of organic substances or biochemical processes and geothermal energy obtained from temperature differences under the ground can also be used (Emeksiz & FINDIK, 2021). We can ensure energy security by reducing dependence on fossil fuels, and we can do this by using renewable energy sources. Hydrogen energy obtained by using hydrogen gas, which is the most abundant in nature, can be obtained from various sources. (ERSOY, 2022).

Hydrogen energy can be used by converting it into electrical energy through fuel cells or hydrogen-powered engines. While only water is produced as a result of the combustion process of hydrogen, one of the advantages of hydrogen is that its energy density is high. Hydrogen energy is widely used in domestic and industrial applications depending on the purpose or area of use (SAYIM & MERT, 2023).

II. Evsel Uygulamalar

Domestic applications constitute an important area of renewable hydrogen energy. Various advantages are obtained with the use of hydrogen energy in homes. (Değirmenci, 2023).
Home appliances powered by hydrogen energy provide energy efficiency by using hydrogen gas obtained from renewable energy sources. (Acaray, 2023). These home appliances produce electrical energy through hydrogen fuel cells. In this way, while the electrical energy needs used in homes are met, harmful emissions to the environment are also significantly reduced (ALAHMAD et al., 2023). Örneğin, suyu hidrojenle ısıtarak evlerin ısınma ihtiyacını karşılayan hidrojenle çalışan kombi sistemleri mevcuttur. Ayrıca elektrik enerjisi sağlamak için kullanılan hidrojen yakıt hücreli ev jeneratörleri de bulunmaktadır (Mechmet, 2023).
Hydrogen fuel cell vehicles are one of the domestic applications of hydrogen energy and offer an environmentally friendly transportation option (Yeniay, 2022). These vehicles produce electrical energy as a result of chemical reactions in hydrogen fuel cells and enable the vehicle to move with this energy. (Bakış, 2023). The advantages of hydrogen fuel cell vehicles include zero emissions and high energy efficiency. These vehicles offer a clean transportation option by reducing air pollution caused by fossil fuels. (Özbay et al.2020).
Hydrogen energy storage methods used to increase energy savings and ensure energy security in homes are very important. These methods include hydrogen tanks, hydrogen batteries and hydrogen storage tanks. Hydrogen tanks store hydrogen gas to meet homes' energy demands (Sayım, 2023). Hydrogen batteries, on the other hand, store hydrogen by converting it into electrical energy. Hydrogen storage tanks, on the other hand, store hydrogen gas used in homes for a long time and ensure its safe use. These storage methods provide energy stability in homes as well as an alternative option to meet power demands (Kaş, 2022).
Since it is a clean energy source, the environmental effects of hydrogen energy have very positive effects. When hydrogen energy is used, it produces only water vapor and heat and does not cause harmful emissions into the

atmosphere (Sağır, 2021). Thanks to this feature, hydrogen energy plays an effective role in reducing environmental pollution and combating climate change. In addition, thanks to vehicles running on hydrogen energy, air pollution due to fossil fuels is also significantly reduced. These environmental impacts highlight the importance of future domestic and industrial uses of hydrogen energy (Demirkan, 2023).

III. Endüstriyel Uygulamalar

Industrial applications are an area where hydrogen energy is widely used. Factories operating with hydrogen energy are environmentally friendly in their production processes. In these factories, hydrogen is used as energy sources, replacing other traditional energy sources used as fuel in various production processes. Factories powered by hydrogen energy increase energy efficiency in industry, reduce environmental impact and represent an important step on the journey to the future as a sustainable energy source (Salcı, 2023).

The use of hydrogen in industrial processes has spread over a wide area. Particularly in the chemical industry, hydrogen is used in the production processes of many different products. Hydrogen energy is used effectively in the production of important chemicals such as hydrochloric acid, ammonia and methanol. In addition, hydrogen serves as a fuel used in petrochemical production processes in refineries and metallurgy. The use of hydrogen in industrial processes both increases energy efficiency and reduces negative effects on the environment. (TOKATLI et al.2022).

Industrial hydrogen production and storage methods enable the use of hydrogen energy in industrial applications. Hydrogen is produced by splitting water, usually by electrolysis. In this process, water molecules are separated into hydrogen and oxygen gases by using electrical energy. After its production, hydrogen is stored using various storage methods. These methods include different technologies such as compressed hydrogen gas storage, liquefied hydrogen storage and metal hydride storage. (MUTLUBAŞ & ÖZDEMİR, 2023).

The economic and social benefits of industrial applications are very important. Renewable hydrogen energy stimulates economic growth when used in industrial applications. Factories that produce based on renewable energy resources reduce energy costs and create job opportunities. The use of industrial hydrogen also minimizes environmental impacts and is an important step towards sustainability. Thus, the aim is to leave a clean environment to future generations. In addition, the positive impact of industrial practices on the environment increases the general health of society and provides social benefits. (Arslan, 2022).

IV. Results and discussions

In this study, the importance and future of domestic and industrial applications are examined in the context of renewable hydrogen energy. Renewable hydrogen energy is of great importance for a sustainable future. Hydrogen can be used as an alternative to traditional fossil fuels and can minimize environmental impacts. In addition, the fact that hydrogen energy is storable and portable ensures that it has the potential to transform the energy sector. Renewable hydrogen energy contributes to diversifying energy sources and increasing energy security, while also helping to reduce greenhouse gas emissions.Therefore, renewable hydrogen energy is an important step towards energy transition and a sustainable future. (ATEŞ et al.2023).

Evsel ve endüstriyel uygulamalar, yenilenebilir hidrojen enerjisinin geleceğini belirlemektedir. Evsel uygulamalarda, hidrojen enerjisiyle çalışan ev aletlerinin kullanımının yaygınlaşması gerekmektedir. Örneğin, gelecekteki ulaşımın önemli bir parçası olabilecek hidrojenli yakıt hücreli araçların kullanımı artmalıdır. Ayrıca, evlerde hidrojen enerjisinin depolanmasıyla ilgili araştırmalar hızlanmalı ve güvenli depolama yöntemleri geliştirilmelidir. Endüstriyel uygulamalarda ise hidrojen enerjisiyle çalışan fabrikaların sayısının artması beklenmektedir.

Hidrojenin endüstriyel süreçlerde kullanılması, enerji verimliliğini artırır ve çevre dostu bir üretim sağlar. Ayrıca, endüstriyel hidrojen üretimi ve depolama yöntemlerinin geliştirilmesi, daha sürdürülebilir bir endüstriyel sektörün ortaya çıkmasına katkı sağlar. Bu nedenle, evsel ve endüstriyel uygulamaların geleceği, yenilenebilir hidrojen enerjisinin yaygınlaşmasıyla şekillenecektir. Yenilenebilir hidrojen enerjisinin evsel ve endüstriyel uygulamalarının geliştirilmesi için teknolojik araştırmaların ve yenilikçi projelerin desteklenmesi gerekmektedir. Bu sayede, hidrojen enerjisiyle çalışan ev aletleri ve araçlar gibi yeni uygulamaların geliştirilmesi mümkün olabilir. Ayrıca, enerji altyapısının yenilenmesi ve hidrojen enerjisi depolama yöntemlerine odaklanılması gerekmektedir. Güvenli ve etkili depolama yöntemleri geliştirilerek enerji verimliliği artırılabilir. Ekonomik teşviklerle birlikte, yenilenebilir hidrojen enerjisinin kullanımının yaygınlaştırılması sağlanabilir. Bu önerilerin dikkate alınmasıyla, yenilenebilir hidrojen enerjisinin evsel ve endüstriyel uygulamalarının önemi artar ve sürdürülebilir bir geleceğe doğru ilerlenmesi hız kazanır.

V. Conclusions

It is a sustainable energy source. Its use in domestic areas needs to increase and become widespread in industrial processes. It should be aimed to increase the domestic and industrial use of hydrogen energy by supporting technological research, updating the energy infrastructure and providing economic incentives. These steps will accelerate progress towards a sustainable future.

References

Tanriöver, M. (2020). Yenilenebilir enerjinin Türkiye ekonomisine yansımaları.yok.gov.tr

Genç, G. (2022). Türkiye ve dünyada yenilenebilir enerji kaynaklarının kullanım alanlarının karşılaştırılması.cankaya.edu.tr

ARSLAN, H. (2023). YENİLENEBİLİR ENERJİ YATIRIMLARININ FİNANSMAN MODELLERİ. Avrasya Sosyal ve Ekonomi Araştırmaları Dergisi.dergipark.org.tr

Arslan, Z. F. (2022). Yenilenebilir enerjinin Türkiye ekonomisine ve işletmelerde üretim stratejilerine etkisi.uludag.edu.tr

Emeksiz, C. & FINDIK, M. M. (2021). Sürdürülebilir kalkınma için yenilenebilir enerji kaynaklarının Türkiye ölçeğinde değerlendirilmesi. Avrupa Bilim ve Teknoloji Dergisi.dergipark.org.tr

ERSOY, G. (2022). GELECEĞİN ENERJİ KAYNAĞI: YEŞİL HİDROJEN EKONOMİSİ. KAYES-2022.asead.org.tr

SAYIM, A. & MERT, S. O. (2023). Sodyumborhidrür Bileşiğinin İnsansız Hava Araçlarında Yakıt Depolayıcısı Olarak Kullanılabilirliğinin Araştırılması. MAS Journal of Applied Sciences.masjaps.com

Acaray, S. C. (2023). Enerji etkin peyzaj tasarımı için bir model önerisi.uludag.edu.tr

ALAHMAD, H., TAŞKESEN, E., & BİLEN, E. N. (2023). Uzay Tabanlı Güneş Enerjisine Genel Bakış. Researcher.dergipark.org.tr

Mechmet, A. (2023). Yapılarda ısı pompasının kullanımının enerji etkinliği bağlamında incelenmesi-Edirne örneği.trakya.edu.tr

Yeniay, G. M. (2022). Yeşil binalarda yangın güvenliği ve risk analizi.msgsu.edu.tr

Bakış, A. N. (2023). Yakıt hücrelerinde kullanılan da-da güç dönüştürücü devrelerinde yapay sinir ağı tabanlı parametre tahmini.kmu.edu.tr

Özbay, H., Közkurt, C., DALCALI, A., & Tektaş, M. (2020). Geleceğin ulaşım tercihi: Elektrikli araçlar. Akıllı Ulaşım Sistemleri ve Uygulamaları Dergisi, 3(1), 34-50.dergipark.org.tr

Sayım, A. (2023). Sodyumborhidrür (NaBH4) bileşiğinin insansız hava araçlarında (İHA) yakıt olarak kullanılabilirliğinin araştırılması.iste.edu.tr

Kaş, R. (2022). Yenilenebilir enerji sistemlerinin bulunduğu bir mikroşebekede enerji depolama sistemlerinin maliyet optimizasyonu.ktun.edu.tr

Sağır, İ. H. (2021). Türkiye'de enerji üretiminde yenilenebilir enerji kaynaklarının yeri.erbakan.edu.tr

Demirkan, L. (2023). İklim değişikliği ile mücadele sürecinde kömürden çıkış için alternatif mali politikalar.balikesir.edu.tr

Salcı, O. (2023). Fırın sisteminde hidrojen gazı katkılı doğal gaz yakıtlı proses brülörü yanma analizleri ve optimizasyonu.trakya.edu.tr

TOKATLI, M., SAYDAM, F., Murat, H. A. L., KOŞATEPE, A., ÇOLAK, M., & YÜKSEL, Ç. (2022). Alüminyum Alaşımlarının Dökümünde Yaygınca Kullanılan Sıvı Metal Temizleme Yöntemlerinin İncelenmesi. Journal of the Institute of Science and Technology, 12(1), 423-434.dergipark.org.tr

MUTLUBAŞ, H. & ÖZDEMİR, Z. Ö. (2023). Hidrojenin Kullanım Alanları ve Hidrojen Ekonomisi. Yekarum.dergipark.org.tr

ATEŞ, M. H., ÇAKAN, C. D., & KURTOĞLU, S. (2023). YENİLENEBİLİR ENERJİ VE CARİ İŞLEMLER DENGESİ ANALİZİ: ARDL SINIR TESTİ YAKLAŞIMI. Nişantaşı Üniversitesi Sosyal Bilimler Dergisi, 11(3), 346-365.dergipark.org.tr

Development Of SBA-15/Cordierite Monolith Supported Catalysts And Their Use In Hydrogen Production By Partial Oxidation Of Methane

[1*]İlke Ilıcak Bayraktar, [1,2]Halit Eren Figen
[1] Yildiz Technical University, Faculty of Chemical and Metallurgical Engineering, Department of Chemical Engineering, Esenler, Istanbul, 34220, Türkiye
[2] Yildiz Technical University, Clean Energy Technologies Institute, Istanbul, 34220, Türkiye

* E-mail:ilkeilicak7@gmail.com, hfigen@yildiz.edu.tr

Abstract
In this study, catalysts were obtained by coating Al_2O_3/SBA-15/Ni and SBA/CeO_2/Ni on the cordierite monolith surface with the wash coating method. CH_4 conversions and H_2 selectivities were examined by the partial oxidation reaction of methane. Activity tests of the catalysts were carried out in a tubular reactor at 800°C, at different flow rates and CH_4 feed volumes (%). The incorporation of CeO_2 played an important role in the activity of the catalyst. Particularly noteworthy, 93.5% methane conversion and 94.8% hydrogen selectivity were achieved by feeding 2 vol% CH_4 at 400 ml/min flow of the SBA/CeO_2/Ni monolith catalyst.

Keywords: Hydrogen production, Partial oxidation of methane, Monolith support

I. Introduction

Climate changes have begun to occur with the increase in greenhouse gas emissions that threaten human and natural life. For this reason, the Paris agreement signed by many countries in 2015 aimed to keep the global average temperature increase well below 2 degrees and not exceed 1.5 degrees until 2050 (IEA, 2023). In line with the targets, interest in renewable energy technology has increased in order to meet the energy needs of the world. Hydrogen can be obtained from fossil fuels such as natural gas and coal or from renewable energy sources such as biogas by applying heat through the reforming process of hydrogen (Momirlan and Veziroglu 2005). There were different methods to obtain hydrogen from fossil fuels. The most preferred of these is steam reforming (Dincer, 2008). The partial oxidation of methane attracts attention because it is an exothermic reaction and requires lower energy requirements (Figen and Baykara, 2015). Hickman et al. They stated that with the ideal H_2/CO ratio being 2:1, synthesis gas can be obtained through partial catalytic oxidation of methane (Hickman and Schmidt, 1993). The main reaction of catalytic partial oxidation of methane (CPOM) provides 2 mol H_2 and ~36 kJ/mol energy as expressed below (1) (Figen and Baykara, 2015).

$$CH_4 + {}^1/_2\,O_2 \rightarrow CO + 2H_2 \qquad \Delta H_r^\circ = -36\ kJ\ mol^{-1} \tag{1}$$

Many transition metals are used for the catalytic partial oxidation reaction, but among them, Ni-based catalysts are mostly preferred due to their high activity and low cost. However, Ni-based catalysts cause sintering and carbon accumulation at high temperatures (Enger and Lødeng, 2008). For this reason, Ni metal supporting metal oxides are used. Cerium dioxide (CeO_2) helps reduce carbon buildup. It is also one of the important reducible oxide supports used in catalysts because it has a remarkable oxygen storage/exchange capacity. SBA-15 structures have high pore diameters and have the potential to contain charged metal particles in their pores. For this reason, it is frequently used as a supporting material in catalysts (Kiani and Meshksar, 2023).
In this study, monolith catalysts were used because they have high mechanical strength, low coefficient of thermal expansion, and are resistant to high temperatures and temperature shocks (Nijhuis and Beers, 2001). It has been reported that aluminum coating on cordierite monolith increases the surface area and improves metal dispersion. In this study, studies were carried out on the production of hydrogen from methane by partial oxidation reaction by coating Al_2O_3/SBA-15/Ni and SBA/CeO_2/Ni on cordierite monoliths.

II. Experimental Set-up and Procedure

Preparation of monolith catalysts

The catalytic partial oxidation reaction was carried out in a tube-type reactor. Cordierite monoliths were prepared in the form of cylinders with a diameter of 13 mm and a length of 20 mm before being coated with catalysts in accordance with the reactor dimensions. In order to ensure easy adhesion of metals to ceramic monolith surfaces, 5 M alumina nitrate solution was prepared and coated by the wash coating method. It was then calcined at 900°C for 5 hours. During the calcination process, aluminum nitrate decomposed into nitrates and cubic crystalline gamma-alumina (γ-Al_2O_3) phase was formed [9]. During the synthesis of SBA-15, 2.4 g F127 and 0.027 g NH_4F were mixed in 84 ml 1.3 M HCl at room temperature until clear. Then, it was kept in a water bath at 10°C for 1 hour. Meanwhile, 2 g of PVA was dissolved in 10 ml of H_2O at 80°C. The cooled Pluronic solution was placed in the mixer and PVA solution was added. Then, 3.7 ml TEOS and 1.2 ml n-hexane were added to the solution and stirred overnight. The resulting solution was subjected to hydrothermal treatment at 100 °C for 24 h in a closed Teflon container (Thahir

and Wahab, 2019).
At the same time, CeO_2 solutions were prepared. The pH was adjusted to 6 with 1 M ammonium hydroxide (NH_4OH) solution. Finally, the catalysts coated with alumina, SBA-15 and metal oxides were coated by the wash coating method on $Ni(NO_3)_2{\cdot}6H_2O$ aqueous solution prepared by the sol-gel method. After each coating process, the catalysts were dried at 110°C for 1 hour. After the desired accumulation was achieved, calcination was applied at 900°C for 5 hours.

III. Analysis

Performance tests of the prepared catalysts were carried out under atmospheric pressure in a stainless steel tubular reactor with an inner diameter of 14 mm and a length of 1 m. In order to reach high temperatures, a tube furnace (Protherm, PTF 14/50/450), mass flow controller (Teledyne Hastings, HFC 202), mass flow control station (TRL Instruments) and mass spectrometer (Hiden Analytical QGA) were used.

Hydrogen temperature programmed reduction (TPR) measurements were performed with a 5% H_2/N_2 gas mixture by volume introduced into the reactor at a rate of 200 ml/min. During analysis, the temperature was increased at 5 °C/min up to 1000 °C. According to the amount of H_2 released, the amount of H_2 consumed during the reduction reaction was calculated and the reduction temperatures of the catalysts were determined. Before starting the partial oxidation reaction, the catalysts were reduced with H_2 at a rate of 3°C/min according to the reduction temperatures obtained as a result of TPR.

Methane conversions and hydrogen selectivities of monolithic catalysts were calculated at 800°C temperatures. The volume ratio of CH_4/O_2 feed gases was studied to be 2:1.Total flow rates of the feed were studied at 400 ml/min and 800 ml/min. The CH_4 conversions and H_2 selectivities of the catalysts are explained by the following equation 2 and 3 respectively (Peng and Jin, 2022):

$$X_{CH4}(\%) = \frac{CH4,in - CH4,out}{CH4,in} \times 100 \quad (2)$$

$$S_{H2}(\%) = \frac{H2,out}{H2,out+CH4,out} \times 100 \quad (3)$$

IV. Results and discussions

As seen in Figure 1, the reducibility of monolith catalysts was characterized by the H_2 TPR method. The main peaks shown by monolith catalysts with Ni contents at 500°C in Al_2O_3/SBA-15/Ni catalyst and 520°C in SBA-15/CeO_2/Ni can be assigned to NiO particles. The inclusion of cerium oxide in the catalyst can cause a shift in the reduction peaks towards higher temperatures, which can be attributed to an increase in nickel dispersion. It can be said that the cerium oxide content leads to an increase in catalytic reducibility. The peaks at approximately 720°C can be attributed to the strong interaction between Ni^{2+} and the SBA-15 support.

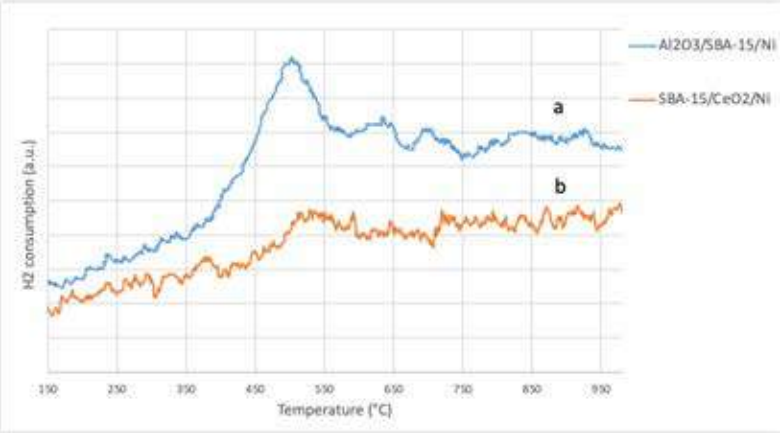


Fig. 1: H_2-TPR profiles of (a) Al_2O_3/SBA-15/Ni; (b) SBA-15/CeO_2/Ni.

The catalytic behavior of SBA-15 supported Ni and CeO_2 catalysts by partial oxidation reaction of methane on cordierite monolith was investigated at 800 °C. Methane conversions and hydrogen selectivities of the catalysts according to the flow rate and the volume of CH_4 (%) fed are calculated in Table 1 and Table 2. According to the results obtained, it was seen that there was an inverse relationship between flow rate and contact time. As the contact time decreased, CH_4 conversion and H_2 selectivity decreased. In addition, it has been proven that the volume of methane fed also affects the reaction conversion. It can be said that the increase in the activity of the

catalysts with the addition of CeO_2 causes the strong interaction between CeO_2 and NiO to increase oxygen mobility on the surface and provide suitable conditions for carbon removal.

Tab. 1: CH_4 conversion (%) and H_2 selectivity (%) by methane partial oxidation reaction of Al_2O_3/SBA-15/Ni catalyst coated on monolith

Catalyst	Temperature (°C)	Flow rate (ml/min)	Vol. (%) CH_4 in feed	CH_4 conv. (%)	H_2 Selectivity(%)	H_2/CO
Al_2O_3/SBA-15/Ni monolith	*800*	*800*	*2*	*76,0*	*81,0*	*2*
Al_2O_3/SBA-15/Ni monolith	*800*	*800*	*5*	*75,4*	*80,4*	*2*
Al_2O_3/SBA-15/Ni monolith	*800*	*800*	*10*	*74,7*	*78,6*	*2*
Al_2O_3/SBA-15/Ni monolith	*800*	*400*	*2*	*88,0*	*89,9*	*2*
Al_2O_3/SBA-15/Ni monolith	*800*	*400*	*5*	*87,8*	*91,2*	*2*
Al_2O_3/SBA-15/Ni monolith	*800*	*400*	*10*	*87,1*	*89,9*	*2*

Tab. 2: CH_4 conversion (%) and H_2 selectivity (%) by methane partial oxidation reaction of SBA-15/CeO_2/Ni catalyst coated on monolith

Catalyst	Temperature (°C)	Flow rate (ml/min)	Vol. (%) CH_4 in feed	CH_4 conv. (%)	H_2 Selectivity(%)	H_2/CO
SBA-15/CeO_2/Ni monolith	*800*	*800*	*2*	*88,5*	*91,8*	*2*
SBA-15/CeO_2/Ni monolith	*800*	*800*	*5*	*86,0*	*89,6*	*2*
SBA-15/CeO_2/Ni monolith	*800*	*800*	*10*	*83,4*	*86,6*	*2*
SBA-15/CeO_2/Ni monolith	*800*	*400*	*2*	*93,5*	*94,8*	*2*
SBA-15/CeO_2/Ni monolith	*800*	*400*	*5*	*92,6*	*94,8*	*2*
SBA-15/CeO_2/Ni monolith	*800*	*400*	*10*	*92,4*	*94,2*	*2*

V. Conclusions

Ni and mesoporous SBA-15 based catalyst samples supported on cordierite monolith were prepared by the wash coating method, and the effect of metal oxide supports such as cerium oxide and alumina on the catalytic activity was investigated. CH_4 conversions and H_2 selectivities were examined in the partial oxidation reaction of catalysts at different flow rates and CH_4 feed volumes. It has been proven that SBA-15/CeO_2/Ni catalyst achieves 93.5% CH_4 conversion and 94.8% H_2 selectivity at 2% methane feed at 800°C and 400 ml/min flow. Adding different proportions of CeO_2 can improve the activity of the catalyst.

Acknowledgements

References

Enger BB, Lødeng R, Holmen A, A review of catalytic partial oxidation of methane to synthesis gas with emphasis on reaction mechanisms over transition metal catalysts. Appl Catal A Gen 346:1–27 (2008).

Dincer I., Hydrogen and fuel cell technologies for sustainable future, Journal of Mechanical and Industrial Engineering, 2.1 (2008).

International Energy Agency (IEA), Net Zero Roadmap: A Global Pathway to Keep the 1.5 °C Goal in Reach - 2023 Update, (2023).

Figen HE, Baykara SZ, Hydrogen production by partial oxidation of methane over Co based, Ni and Ru monolithic catalysts. Int J Hydrogen Energy 40:7439–7451 (2015).

Hickman DA, Schmidt LD, Production of Syngas by Direct Catalytic Oxidation of Methane. Science, 259:343–346 (1993).

Kiani P, Meshksar M, Rahimpour MR, Biogas reforming over La-promoted Ni/SBA-16 catalyst for syngas production: Catalytic structure and process activity investigation. Int J Hydrogen Energy 48:6262–6274 (2023).

Momirlan M, Veziroglu TN, The properties of hydrogen as fuel tomorrow in sustainable energy system for a cleaner planet. Int J Hydrogen Energy 30, 795–802 (2005).

Nijhuis TA, Beers AEW, Vergunst T, et al, Preparation of monolithic catalysts. Catal Rev Sci Eng 43 (2001).

Peng X, Jin Q, Molecular simulation of methane steam reforming reaction for hydrogen production. Int J Hydrogen Energy 47:7569–7585 (2022).

Thahir R, Wahab AW, Nafie N La, Raya I, Synthesis of high surface area mesoporous silica SBA-15 by adjusting hydrothermal treatment time and the amount of polyvinyl alcohol. Open Chem 17:963–971 (2019).

Machine Learning Analysis of Biogas Tri-reforming for Syngas Production

[1]Ahmet Coşgun, [2]M. Erdem Günay [1*]Ramazan Yıldırım,
[1] Boğaziçi University, Department of Chemical Engineering, Istanbul, 34342, Türkiye
[2]Istanbul Bilgi University, Department of Energy Systems Engineering, Istanbul, 34060, Türkiye

* E-mail:yildirra@boun.edu.tr

Abstract
In this study a dataset containing 951 data points (116 experiments across 29 experimental articles) for biogas tri-reforming was analyzed using machine learning techniques. CH_4 and CO_2 conversion with produced H_2/CO ratio were predicted by random forest and decision tree algorithms by using 33 descriptors including type of catalyst, catalyst preparation conditions and method, reaction conditions and feed gas compositions used. Predictive models for CH_4 conversion (training and testing R2s of 0.99 and 0.80 respectively) and CO_2 conversion (training and testing R2s of 0.98 and 0.88 respectively) were quite succesfull while the classification tree algorithm provided heuristic rules for CH_4 conversion with 80% efficiency.

Keywords: biogas reforming, tri-reforming, machine learning, CH4 conversion

I. Introduction

Tri-reforming of methane (TRM) has emerged as an attractive path for synthesis gas (syngas) production; it combines steam reforming (SRM), dry reforming (DRM), and partial oxidation (POX) reactions in a single process (Alli 2023, Osat 2022). Adding O_2, H_2O, and CO_2 together with CH_4 to a reforming reactor offers several advantages as first introduced by Song and Pan (2004). TRM constitutes a viable alternative for syngas production, by leveraging endothermic and exothermic reactions within a single reactor and utilizing waste flue gas (Chen 2018, Diez-Ramirez 2016).

CO_2 and CH_4 with small amounts of impurities are the main components of the biogas while their ratio varies depending on its source. Biogas is mainly produced from anaerobic digestion of sewage sludge or manure (typically contains 60–80% CH_4 and 20–40% CO_2) or bacteria decomposion of organic waste (landfill gas; typically, 40–60% CH_4 and 40–60% CO_2) (Han 2020). The syngas produced from TRM process can have a variety of (H_2/CO) ratios, which can be controlled by adjusting the feed composition and reaction conditions (Diez-Ramirez 2016).

Syngas is important to produce valuable chemicals and fuels (Chen 2018), and can be produced through SRM produces syngas with a H_2/CO ratio of about 3, (suitable for for ammonia synthesis) while DRM produces H_2/CO ratios around 1, which is highly suitable for dimethyl ether production. POX, as the sole exothermic reforming reaction, on the other hand, produces syngas with the H_2/CO ratio of around 2, (ideal for methanol production and Fisher-Tropsch proces) (Yin 2020, Han 2020, Osat 2022). TRM combines the advantages of all three processes with an H_2/CO molar ratio of about 2. (Diez-Ramirez 2016). While POX decreases the energy needs of process, the presence of H_2O and O_2 serve as oxidizing agents, and mitigates coke formation and enhance catalyst stability (Diez-Ramirez 2016, Han 2020).

Due to the complexity of the TRM process, numerous studies have been conducted to understand its behavior. Machine learning, can be employed to analyse these studies as we did for on DRM (Şener 2017), and SRM (Baysal 2017) before.

II. Method

A comprehensive dataset was constructed by reviewing scientific papers on biogas tri-reforming published between 2004 and 2024, sourced from “Web of Science” database. Following a detailed preprocessing step, a total of 951 data points were included in the dataset, originating from 116 experiments across 29 experimental articles. Input variables (descriptors) are chosen as the type of catalyst, catalyst preparation conditions and method, reaction conditions and feed gas compositions, while CH_4, CO_2 conversion (%) and H_2/CO ratio were designated as output (target) variables. For CH_4 conversion classification, data were divided into three equal parts, denoted as high, medium, and low classes, with the delineation for the medium class set at 40% and 80%.

Random forest (RF) algorithm was employed for predicting CH_4, CO_2 conversion (%) and H_2/CO ratio. The *RandomForestRegressor* from *sklearn.ensemble* package in Pyhton (scikit-learn 1.4.1) was utilized for implementing RF. 5-fold cross-validation was applied in the model construction. The instances with unknown value of time on stream (TOS) were imputed with median values. The model is optimized by scanning a wide range of the parameters of *n_estimators* (number of trees in forest) and *min_samples_leaf* (number of instances in a terminal node of a tree) and the results were evaluated to find the model with minimum complexity and highest prediction accuracy. Subsequently, the best model was achieved by using a test set of unseen data comprising 30% of the overall dataset. Evaluation criteria for the RF algorithm were selected as the mean squared error (MSE), mean absolute error (MAE), root mean squared error (RMSE) and R-squared (R^2). Decision tree (DT) analysis was conducted to extract heuristic rules guiding high to CH_4 conversion (%). *DecisionTreeClassifier* from sklearn.tree package in Pyhton (scikit-learn 1.4.1) was utilized for DT modeling and *graphviz* package is used for visualization of the rules. *Gini index* was chosen as the optimization criteria in DT algorithm, and the model was once again

tested using unseen data comprising 30% of the overall dataset.

III. Analysis

The dataset has 33 input variables with different number of instances for different output variables (951 for CH_4, 916 for CO_2, 684 for H_2/CO ratio). Active metal, support, promoter materials of the catalysts and their amounts, catalyst preparation method, calcination and reduction temperatures and times, together with reaction conditions (pressure, temperature, TOS, W/F ratio) and feed compositions are taken as descriptor variables. The structures of dataset are summarized in Figure 1, as the first layer is the active metal, the second layer is the active promoter, the third layer is the support, and the fourth layer is the textural promoter of the experimented catalyst. The size of area is propotional with the frequency of material apparence in the dataset.

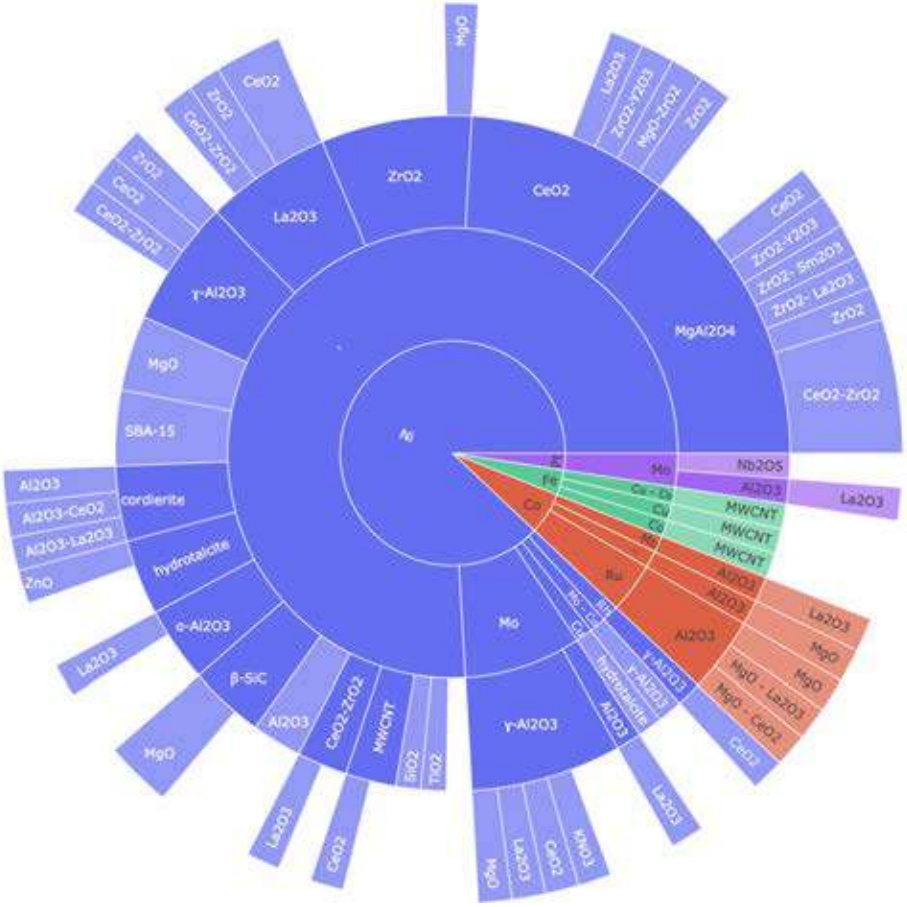


Fig. 1: Hierarchical structure of catalyst in the dataset; active metal constituting the first layer, active promoter in the second layer, support material in the third layer, the textural promoter in the fourth layer.

Before applying the Random Forest (RF) algorithm, instances with missing values other than Time on Stream (TOS) were removed. The dataset consisting of 116 experiments was then split into two subsets: a training set (comprising 81 experiments) and a testing set (consisting of 35 out of the total 116 experiments). A 5-fold cross-validation procedure was employed to identify the optimal model parameters, which were determined to be *n_estimators*=100 and *min_samples_split*=2. Subsequently, the RF model was evaluated using the testing subset.

Decision Tree (DT) models were utilized for classification purposes, particularly focusing on CH_4 conversion (%). This model generates generalized rules for three classes: low, medium, and high conversion. Achieving high conversion and accurately predicting the pathways for attaining such results are selected as most important objectives in this study. To address this, the modeling process involved customizing the weights of different classes, with the highest weight assigned to the high conversion class.

IV. Results and discussions

In Figure 2, the results of the optimal random forest model are presented, showing the experimental versus predicted values for CH_4 conversion (%), CO_2 conversion (%), and H_2/CO molar ratio. Data points from the training set are depicted in blue, while those from the test set are shown in red.

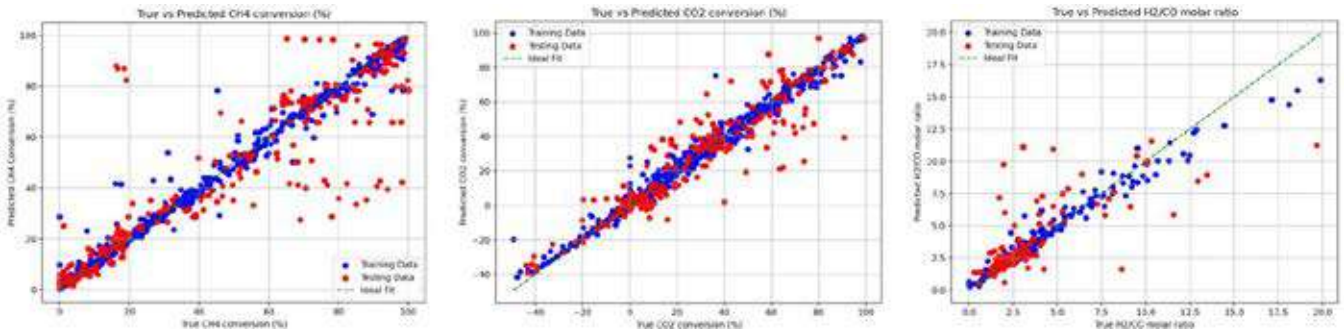


Fig. 2: RF model results for biogas tri-reforming: (a) CH_4 conversion (%), (b) CO_2 conversion, (c) H_2/CO molar ratio.

Table 1 provides statistical metrics for the RF model of the biogas tri-reforming process. By analyzing the R^2 values, it is evident that powerful models were developed for CH_4 and CO_2 conversion. The prediction accuracy for the H_2/CO molar ratio was lower as expected due to smaller number of data ponts and higher sensitivity against the changing feed composition.

Tab. 1 Results of RF model metrics for biogas tri-reforming process.

		CH4 conversion (%)	CO2 conversion (%)	H2/CO molar ratio
Train	Mean Squared Error (MSE)	13.69	18.42	0.24
	Root mean squared error (RMSE)	3.70	4.29	0.49
	Mean Absolute Error (MAE)	1.81	2.45	0.21
	R-squared (R^2)	0.987	0.983	0.966
Test	Mean Squared Error (MSE)	230.42	126.92	2.44
	Root mean squared error (RMSE)	15.18	11.27	1.56
	Mean Absolute Error (MAE)	8.38	7.34	0.73
	R-squared (R^2)	0.795	0.876	0.574

The optimized DT model and its corresponding rules are presented in Figure 3. Notably, a robust rule for high conversion class is deduced, particularly emphasizing the influence of high reaction temperature (>743.5 °C), high normalized W/F ratio (>1870.3 mgcat*min/ml), and the presence of Ni catalyst. This finding aligns with the literature, suggesting that elevated reaction temperatures are typically associated with higher conversion rates. This is because carbon formation via the Boudouard reaction from CO and CH_4 cracking becomes less significant at higher temperatures (Han 2020). According to Wang et al. (1996), CH_4 cracking, occurs above 557°C, whereas the Boudouard reaction, which generates carbon from CO, occurs below 700°C (Han 2020). Additionally, the flow rate plays a significant role, as reversely related to W/F, which is also stated in the literature, TRM performance tends to improve as pressure and feed flow rates decrease (Osat 2020).

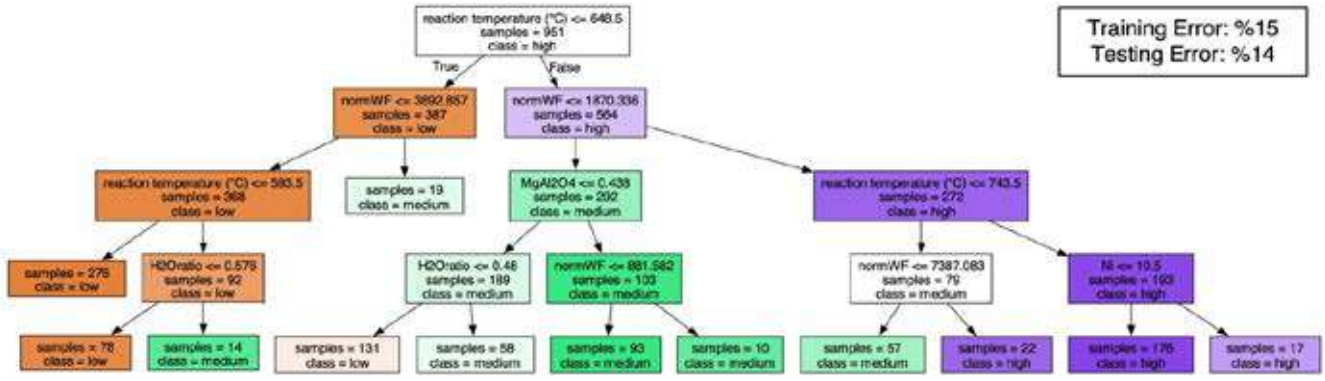


Fig. 3: DT model results for biogas tri-reforming: (a) CH_4 conversion (%), (b) CO_2 conversion, (c) H_2/CO molar ratio.

V. Conclusions

In summary, a database comprising information from 29 scientific articles on biogas tri-reforming was compiled and analyzed. The aim was to utilize the Random Forest algorithm to predict CH_4 and CO_2 conversion rates and H_2/CO ratio. Additionally, the Decision Tree algorithm was employed to understand the relationship between input and output variables for CH_4 conversion. RF algorithm successfully predicted CH_4 and CO_2 conversion rates, along with the produced H_2/CO ratio, yielding satisfactory R^2 values of 0.795, 0.876, and 0.574, respectively. DT algorithm provided heuristic rules with an accuracy exceeding 80% for CH_4 conversion. These findings suggest that both RF and DT algorithms hold promise in determining optimal reaction conditions and feed compositions for biogas tri-reforming, particularly regarding the utilization of the resulting syngas.

Acknowledgements
There are no acknowledgements to declare.

References

Alli R.D., de Souza P.A.L., Mohamedali M., Virla L.D., Mahinpey N., Tri-reforming of methane for syngas production using Ni catalysts: Current status and future outlook, Catalysis Today, 407, 107–124 (2023).

Baysal M., Günay M.E., Yıldırım R., Decision tree analysis of past publications on catalytic steam reforming to develop heuristics for high performance: A statistical review, International journal of hydrogen energy, 42, 1, 243-254 (2017).

Chen L., Gangadharan P., Lou H.H., Sustainability assessment of combined steam and dry reforming versus tri-reforming of methane for syngas production, Asia-Pac J Chem Eng., Vol:13, e2168 (2018).

Diez-Ramirez J., Dorado F., Martinez-Valiente A., Garcia-Vargas J.M., Sanchez P., Kinetic, energetic and exergetic approach to the methane tri-reforming process, International journal of hydrogen energy, 41, 19339-19348 (2016).

Han D., Kim Y., Cho W., Baek Y., Effect of Oxidants on Syngas Synthesis from Biogas over 3 wt % Ni-Ce-MgO-ZrO2/Al2O3 Catalyst, Energies, 13, 297 (2020).

Osat M., Shojaati F., Development of a Trireforming Fluidized- Bed Reactor with a Hydrogen Permselective Membrane, Chem. Eng. Technol., 45, No. 5, 824–833 (2022).

Sener N., Günay M.E., Leba A., Yıldırım R., Statistical review of dry reforming of methane literature using decision tree and artificial neural network analysis, Catalysis Today, 299, 289-302 (2018).

Song C., Pan W., Tri-reforming of methane: a novel concept for catalytic production of industrially useful synthesis gas with desired H2/CO ratios, Catalysis Today, 98, 463–484 (2004).

Yin W., Guilhaume N., Schuurman Y., Model biogas reforming over Ni-Rh/MgAl2O4 catalyst. Effect of gas impurities, Chemical Engineering Journal, 398, 125534 (2020).

Wang S., Lu G.Q., Millar G.J., Carbon Dioxide Reforming of Methane to produce synthesis gas over Metal-supported catalysts: State of the Art., Energy Fuels, 10, 896–904 (1996).

Catalytic Activity of W-O and Fe-O in H_2S Decomposition

[1*] Yaren Ataseven, [1] Mert Yekta Doğan, [1] Sena Yaşyerli, [1] H. Mehmet Taşdemir, [1] Hüseyin Arbağ, [1] Nail Yaşyerli
[1] Gazi University, Engineering Faculty, Chemical Engineering Department, Maltepe, Ankara, 06570, Türkiye

* E-mail: yaren.ataseven@gazi.edu.tr

Abstract

The catalytic thermal H_2S decomposition reaction has recently attracted intense attention from researchers for the production of CO_x-free H_2. In this study, tungsten oxide (W-O) and iron oxide (Fe-O) catalysts were prepared by the complexation method. Catalytic activity tests of single metal oxides were performed in a continuously flow packed-bed reactor system at 800 °C using a conventional heating system and 1% H_2S-N_2 mixture. Catalysts properties were determined using XRD, EDS and N_2-Adsorption-desorption technique. As a result of activity tests, 12% H_2S and 4% H_2S conversions were obtained with W-O catalyst and Fe-O catalyst, respectively. At the same temperature and gas composition, the thermodynamic equilibrium H_2S conversion is 28%. Activity test results performed in 60 minutes showed that the W-O catalyst was more stable and had higher activity in obtaining H_2 through H_2S decomposition. Synthesis and characterization studies continue within the scope of this study.

Keywords: Tungsten, Iron, H_2 Production, H_2S decomposition

I. Introduction

With the increasing energy demand, studies on obtaining H_2 as a zero-carbon and highly efficient energy carrier have been intensifying recently. It is stated in the literature that it has the highest combustion heat per unit mass among known conventional fuels. However, since H_2 typically does not exist freely in nature, its production techniques should be developed. H_2S gas is released in very high amounts in many fossil fuel-based industrial processes. It is also known that it is dramatically present This gas, which is toxic, corrosive and causes acid rain, must be safely removed from the process. In terms of both environmental sustainability and economic viability, the use of H_2S gas as a raw material in CO_x-free H_2 production is important. While the Claus process remains the primary method for converting H_2S into elemental sulfur, ongoing research aims to develop alternative approaches for utilizing H_2S as a carbon-free source for hydrogen production (Chen et al., 2020).

There are many methods investigated in obtaining H_2 from H_2S: catalytic/non-catalytic decomposition at high temperatures, electrolysis, plasma, biological processes, oxidative catalytic/non-catalytic decomposition, photocatalytic. The efficiency of obtaining H_2 through catalytic H_2S decomposition depends significantly on the effectiveness of the catalyst, and catalyst development studies continue. This reaction (R1; Guldal et al., 2018) has garnered attention due to its potential to convert H_2S into CO_x-free H_2 and elemental sulfur.

$$H_2S(g) \leftrightarrow H_2(g) + 1/n\ S_n(g) \quad \Delta H^o_{298} = 21\ kJ/mol;\ \Delta G^o_{298} = 33\ kJ/mol \qquad (R1)$$

H_2S decomposition reaction is reversible and highly endothermic reaction limited by thermodynamic equilibrium (Barin,1989). Due to its highly endothermic nature, achieving significant conversions of H_2S requires high energy. The efficiency of obtaining H_2 through catalytic H_2S decomposition depends significantly on the effectiveness of the catalyst, and catalyst, such as metal-oxide/metal-sulfide/metal-carbide, development studies continue. Among these metals, Mo, Ni, Cu, and Cr are frequently investigated, with alumina and SiC emerging as noteworthy support materials (Chen et al., 2019, 2020; Chivers et al., 1980; Reshetenko et al., 2002).

Reshetenko et al. (2002) examined the activities of metal oxide catalysts (γ-Al_2O_3, α-Fe_2O_3, V_2O_5) in the H_2S decomposition reaction at high temperatures (500-900°C). They mentioned the reduction of transition metal oxides at the beginning of the reaction and the subsequent formation of sulfides (R2) under the influence of reaction media proceed. They stated that the formed sulfide has an active role in H_2S decomposition reaction. The proposed reaction mechanism to obtain H_2 by H_2S decomposition reaction on metal sulfide structures is two-step. In the first step (R1), the lowest metal-sulfides react with H_2S to obtain the highest metal-sulfides and H_2. In the Second Step (R2), the lowest metal-sulfides and elemental sulfur are obtained again by regeneration of the highest metal-sulfides (Reshetenko, 2002).

$$M_xO_y + yH_2S \rightarrow M_xS_y + yH_2O \qquad (R2)$$
$$M_xS_y + zH_2S \rightarrow M_xS_{y+z} + zH_2 \qquad (R3)$$
$$M_xS_{y+z} \rightarrow M_xS_y + zS^o \qquad (R4)$$

In this study, W-O and Fe-O catalysts were prepared by complexation method to obtain CO_x-free H_2 by H_2S decomposition reaction. The behavior of W-O and Fe-O catalysts in the H_2S decomposition reaction was investigated with catalytic activity tests. This study is carried out and continues within the scope of the TÜBİTAK project.

In this ongoing study, tungsten oxide and iron oxide catalysts were synthesized using the complexation method. The activity of synthesized catalysts was examined for hydrogen (H_2) production through the decomposition of hydrogen sulfide (H_2S) in a conventional heating system at 800 °C to compare the activity of the activated carbon (AC) supported Fe- and W- catalysts.

II. Experimental

Preparation of Metal-Oxide Catalysts

W-O and Fe-O catalysts were prepared by using the complexation method. The complexation method is based on the complex formation of metal salts with a polyfunctional organic acid containing at least one hydroxyl or carboxyl group in its structure. Catalysts that are highly porous and have uniform metal distribution can be prepared by the complexation method. Ammonium metatungstate hydrate (Merck, $H_{26}N_6O_{40}W_{12}$) and iron (III) nitrate nanohydrate (Merck, $Fe(NO_3)_3.9H_2O$) were used as tungsten and iron sources, respectively. Ethanol (Merck, 99.9%) is used as a solvent. Solutions of metal salts and citric acid (Merck, $C_6H_8O_7$) are prepared in an equimolar ratio. The citric acid solution is slowly added to the metal salt solution and are mixed in a magnetic stirrer with a heater kept at a temperature of 60°C. At this stage, organo-metallic complexes are expected to form. The mixing process is continued until the solution becomes highly viscous. The viscous solution is poured into glasses as thin layer. Fe and W containing solutions were kept in the oven at 80°C and 60°C, respectively. Solutions are held until solid foam is formed. The resulting solid foams are carefully crushed and ground into powder. Then, the powders are calcined for 6 hours in a muffle furnace at a temperature of 800°C (10°C/min) in an air environment. and metal oxide catalyst is obtained.

Catalytic Activity Test

Catalytic activity test of the catalysts was carried out in a conventional continuous flow packed bed reactor system. Quartz glass with an inner diameter of 6 mm was used as the reactor. This system utilized 1% hydrogen sulfide (H_2S) diluted in high-purity nitrogen (N_2 balance), with a total flow rate of 100 mL/min, operating at 800°C and atmospheric pressure. 0.1 g of catalyst was used in activity tests. In order to fix the catalyst bed, both sides are supported with glass wool. Analysis of the effluent gas stream was conducted using an SRI-8610C gas chromatography apparatus equipped with a Chromosil-310 capillary column, employing high-purity nitrogen as the carrier gas. Hydrogen sulfide conversion values were determined using the equation (E1).

$$H_2S\ conversi\ on\ (\%) = 100 * \frac{F_{H_2,out}}{F_{H_2S,in}} \quad (E1)$$

where F is the molar flow rate in mole/min.

III. Results and discussions

In this study, iron oxide and tungsten oxide catalysts were synthesized using the complexation method and were tested at 800°C for H_2 production from H_2S decomposition reaction. Figure 1 shows the XRD patterns of Fe-O and W-O catalysts prepared by the complexation method. XRD patterns show that both catalysts are in oxide forms as expected (α-Fe_2O_3, WO_3). Fig. 2 shows the H_2S conversion values obtained with these catalysts with respect to time. At the end of the 60-minute reaction period, approximately 12% and 4% H_2S conversion were obtained with the W-O and Fe-O, respectively. It was observed that W-O catalyst was more stable and had higher activity in production H_2 through H_2S decomposition. Low conversions were obtained at the beginning of the activity test with both catalysts. Over time, H_2S conversions began to increase. This may be an indication of the transformation of the metal oxide into a metal-sulfide, as stated in the literature. Peaks belonging to Fe-S (such as FeS, $Fe_{1-x}S$) in the XRD patterns of the Fe-O catalyst after the activity test confirm this situation. W-O catalyst showed higher conversion than Fe-O catalyst. In a recent study carried out by our Research Group, 2% H_2S conversion was reported without a catalyst at 800°C. The 4% H_2S obtained after 60 minutes with the Fe-O catalyst showed that the catalytic activity of Fe-O was very low under these conditions. However, AC supported Fe- and W- catalysts showed 25% and 24% H_2S conversions which are very close to equilibrium (28%) conversion value (Dogan, 2024).

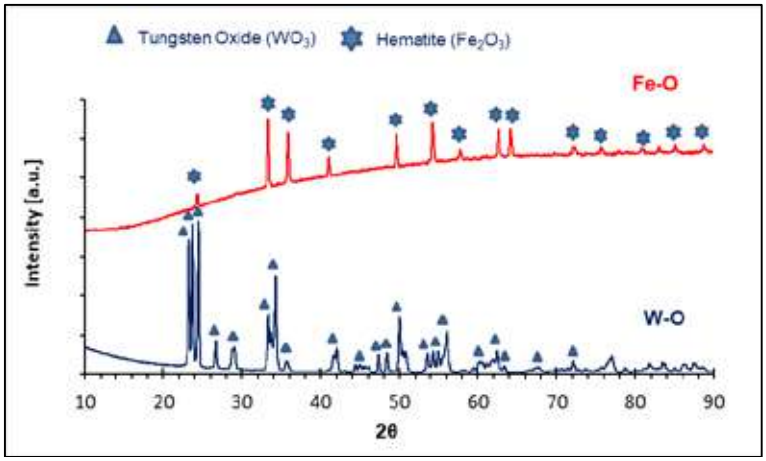


Fig 1. XRD patterns of Fe-O and W-O catalysts

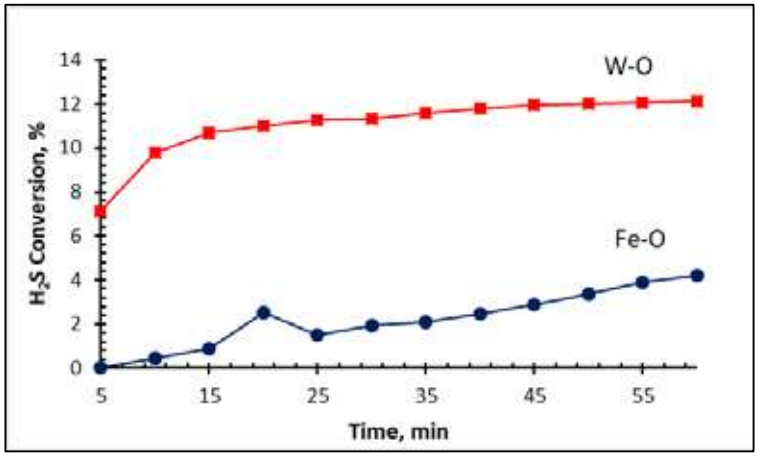


Fig 2. Catalytic actvity of W-O and Fe-O catalysts in H_2S decomposition at 800°C (%1H_2S-N_2, Catalyst: 0.1 g; Total gas flow rate: 100 mL/min)

V. Conclusions

In this ongoing study, Fe-O and W-O catalysts were prepared using complexation method. It was determined by XRD analysis that the prepared catalysts were in oxide forms (α-Fe_2O_3, WO_3). The catalytic activity of the Fe-O and W-O catalysts were investigated for H_2S decomposition reaction at 800 °C. As a result of the activity tests, an 12% H_2S conversion value was obtained for the W-O catalyst and 4% for the Fe-O catalyst. It has been observed that the tungsten-containing catalyst is more promising in the H_2S decomposition reaction compared to the iron-containing catalyst. Our studies on carbon-free H_2 production by the decomposition reaction of H_2S using Fe-O and W-O catalysts continue.

Acknowledgements

The Scientific and Technological Research Council of Turkey Research Fund (Grant TUBITAK-122M400) is gratefully acknowledged. The Authors would like to acknowledge Prof. Dr. Gülşen Doğu of Gazi University for valuable comments.

References

Barin İ., Thermochemical Data of Pure Substances, VCH Verlagsgesellschaft, Weinheim, Germany (1989).

Chen, J., Xu, W., Zhu, J., Wang, X., Wang X., Zhou J., Highly Effective Microwave Catalytic Direct Decomposition of H_2S Over Carbon Encapsulated Mo_2C-CoC@SiC Composite, International Journal of Hydrogen Energy, 44, 25680-25634 (2019).

Chen, J., Xu, W., Zhu, J., Wang, X., Wang X., Highly Effective Direct Composition of H_2S by Microwave Catalysis

on Core-Shell Mo_2N-MoC@SiO_2 Microwave Catalyst, Applied Catalysis B: Environmental, 268, 118454 (2020).

Chivers, T., Hyne, J.B., Lau, C., The Thermal Decomposition of Hydrogen Sulfide Over Transition Metal Sulfides, International Journal of Hydrogen Energy, 5, 499-506, (1980).

Dogan, M.Y., Tasdemir, H.M., Arbag, H.M., Yasyerli, N., Yasyerli, S., H_2 Production via H_2S Decomposition over Activated Carbon Supported Fe- and W- Catalysts, International Journal of Hydrogen Energy, Article in press, (2024).

Guldal, N.O., Figen, H.E., Baykara, S.Z., Perovskite catalysts for hydrogen production from hydrogen sulfide, International Journal of Hydrogen Energy, 43, 1038-1046, (2018).

Reshetenko T.V., Khairulun S.R., Ismagilov Z.R., Kuznetsov V.V., Study of the Reaction of High-Temperature H_2S Decomposition on Metal Oxides (γ-Al_2O_3, α-Fe_2O_3, V_2O_5), International journal of Hydrogen Energy, 27, 387-394 (2002).

Exploring the Impact of Channel Geometry and Temperature on Solid Oxide Electrolyzer Cell Performance

[1*]Berre Kumuk
[1] Iskenderun Technical University, Iskenderun Vocational School of Higher Education, Department of Motor Vehicles and Transportation Technologies, 31200, Iskenderun, Hatay, Türkiye

* E-mail:berre.kumuk@iste.edu.tr

Abstract
Solid Oxide Electrolyzer Cells (SOECs) show promise for eco-friendly hydrogen production, focusing on efficiency. This study explores channel geometry and temperature effects on SOEC performance, analyzing cell design and operating conditions. Computational simulations and experiments assess rectangular, triangular, and semicircular geometries. Interdigitated channels enhance mass transport, serpentine designs extend residence times, and planar configurations simplify manufacturing. Rectangular channels outperform others by 10%. Higher temperatures improve kinetics, with a 15% performance increase from 1073 K to 1273 K. Tailoring channel geometry and temperature is crucial for specific hydrogen production goals.

Keywords: Solid oxide electrolyzer cell, channel geometry, temperature effect.

I. Introduction

Solid oxide electrolyzers (SOECs) have increasingly gained attention as a vital component of energy conversion technologies. These electrolyzers employ high-temperature, solid oxide electrolytes to drive electrochemical reactions, offering a promising avenue for efficient and sustainable hydrogen production and other electrochemical processes (Hu et al, 2022). The unique characteristics of SOECs, such as their high efficiency, fast response times, and versatility in various applications, make them a subject of significant research and development efforts in the field of electrochemical engineering.

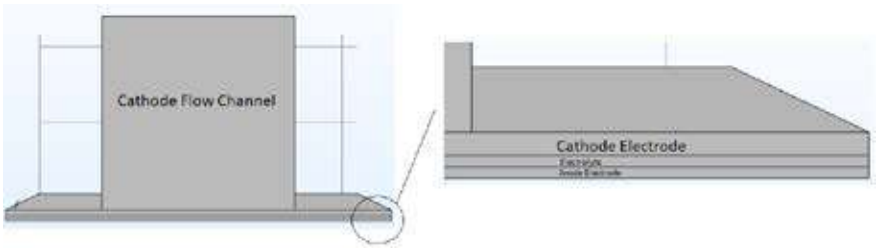
There are numerical and experimental studies in the literature that examine the performance of solid oxide electrolyzers under different parameters. Ni et al. (2007) was identified the component thickness effect on the anode-supported solid oxide electrolysis configuration. The findings revealed that increasing electrode porosity and pore size can reduce voltage loss. In terms of operation, both temperature and steam molar fraction elevated to enhance solid oxide electrolysis electrical efficiency. Wang et al. (2010) evaluated at 650°C the performance of an intermediate-temperature solid oxide electrolysis cell for steam electrolysis, considering various steam concentrations. As the steam concentration increased, the cell voltage exhibited a decrease, primarily attributed to reduced steam electrode polarization. Srinivas et al. (2023) aimed to model the impact of different electrolytes, namely scandium-doped zirconia (SCGZ), yttrium-stabilized zirconia (YSZ), and gadolinium-doped ceria (GDC), under varying temperature and pressure conditions. Biswas et al. (2023) delved into the electrochemical performance of three distinct cathode configurations, composed of copper and gadolinia doped ceria (Cu-GDC) cermets, for steam electrolysis conducted at 800°C in a tubular SOEC.

In this study, the numerical impact of flow channel geometry on solid oxide electrolyzer performance has been examined. Additionally, the influence of temperature on these geometries' performance has also been investigated numerically. It is well recognized that numerical studies serve as a crucial initial step for experimental research [32]. This study is expected to fill an important gap for researchers intending to conduct experimental studies on flow channel geometry.

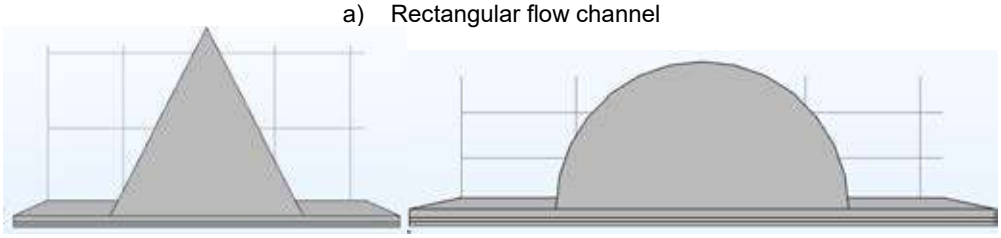
II. Analysis

Solid oxide electrolyzers (SOECs) are a class of electrochemical devices that play a crucial role in the field of energy conversion and storage. These devices are primarily used for the production of hydrogen and syngas through the electrolysis of water and carbon dioxide. Developing an accurate mathematical model of SOEs is essential for optimizing their performance and understanding the underlying physical and chemical processes involved.

In this study, we employ COMSOL Multiphysics to develop a comprehensive numerical model for the simulation of SOEC operation. This model aims to provide valuable insights into the complex electrochemical and transport phenomena occurring within the SOEC, enabling the design and improvement of these vital components in various energy conversion applications. The (a) rectangular flow channel, (b) triangular flow channel and (c) semicurcilar flow channel geometry used in the SOEC analyses are shown in Fig. 1 and the model parameters are given in Table 1.



a) Rectangular flow channel



b)Triangular flow channel c)Semicurcilar flow channel

Fig.1: SOECs geometry.

The main assumptions made in this study were as follows (İlbas et al. (2020)):

•The distribution of temperature within each subsystem is assumed to be constant due to its very small size.

•The velocities of the fluid and partial pressures are assumed to be uniformly uniform in each subsystem and in every direction.

•The viscosity of the fluid in each subsystem is the same.

Tab:1. Model Parameters (Chen et al. (2023))

Cell Structure Parameters		
Anode thickness	$15x10^{-6}$	[m]
Electrolyte thickness	$15x10^{-6}$	[m]
Cathode thickness	$31x10^{-6}$	[m]
Cell length	40	[mm]
Channel height	1.05	[mm]
Channel weight	1.05	[mm]

Tab.2: Governing Equations

Description	Governing equaiton
Mass	$\frac{\partial \rho}{\partial t} + \nabla \cdot (\rho \vec{u}) = Q_{mass}$
Momentum	$\nabla\left\{-pI + \frac{\mu}{\varepsilon}[\nabla\vec{u} + (\nabla\vec{u})^T] - \frac{2\mu}{3\varepsilon}\nabla\vec{u}\right\} - \left(\frac{\mu}{B_0} + Q_{mom}\right)\vec{u} = \frac{\rho}{\varepsilon}\left(\frac{\partial\vec{u}}{\partial t} + \frac{\vec{u}}{\varepsilon}\nabla\vec{u}\right)$
Conservation of species	$\varepsilon\rho\frac{\partial \omega_i}{\partial t} + \nabla \cdot \vec{j_i} + \rho(\vec{u} \cdot \nabla)\omega_i = R_i$
Conservation of charge	$\nabla \cdot (-\sigma_{ion}\varphi_{ion}) = Q_{ion}; \nabla \cdot (-\sigma_e\varphi_e) = Q_e$
Energy	$\rho C_P\frac{\partial T}{\partial t} + \rho C_P\vec{u} \cdot \nabla T = \nabla \cdot \left(\kappa^{eff}\nabla T\right) + Q$

Table 2 shows that the governing equations for SOEC model[12].

III. Results and discussions

The utilization of COMSOL Multiphysics, equipped with a dedicated Fuel Cell & Electrolyzer Module for numerical modeling, enabled a comprehensive examination of cathode supported, and rectangular flow channel SOEC, allowing for in-depth analyses of various operating conditions, ultimately contributing to a better understanding of SOEC behavior and performance optimization. As depicted in Fig. 2, the results from both numerical simulations and experimental data exhibited a striking alignment, affirming the accuracy and reliability of our computational models.

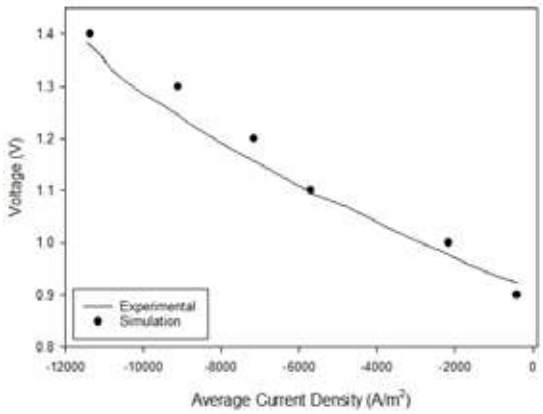
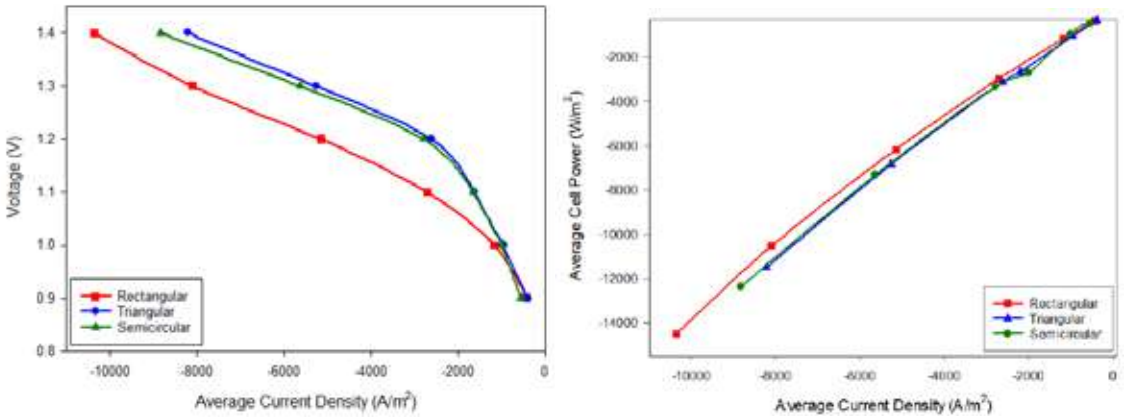


Fig. 2 Model validation with experimental results (Chen et al. (2023))

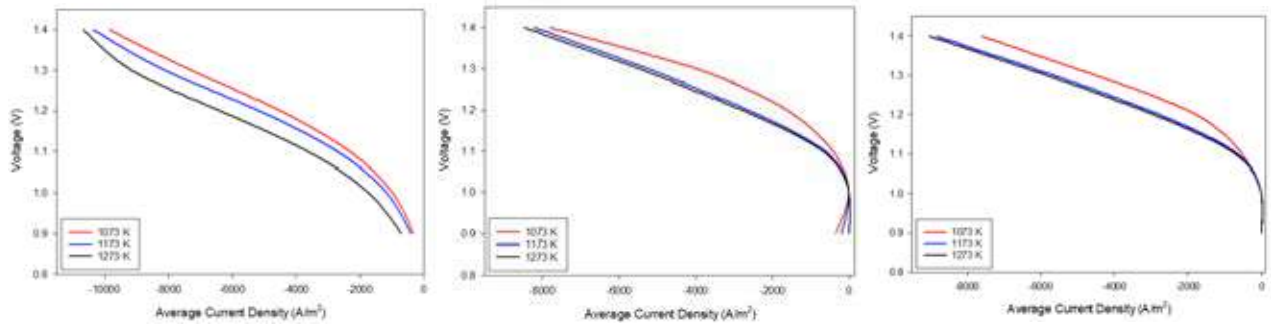
In this study, we conducted a comprehensive comparison of polarization and performance results within rectangular, triangular, and semicircular flow channels at an operating temperature of 1073 K. The outcomes of this investigation are visually presented in Fig.3. Through this comparative analysis, we were able to discern the distinct advantages and trade-offs associated with each channel geometry in terms of its impact on polarization and overall performance. These findings provide valuable insights into the optimization of flow channel designs for high-temperature applications and underscore the significance of selecting the most suitable geometry to enhance the efficiency and effectiveness of the system.



(a) Polarization curve (b) Performance curve

Fig. 3 Flow channel geometry effect on (a) polarization curve, and (b) performance curve

As seen Fig. 3, rectangular flow channel SOEC exhibited the best performance, based on the analysis conducted. Rectangular flow channels offer a larger internal surface area compared to other geometries of similar dimensions, owing to their four equal sides. This increased surface area allows for a greater placement of electrocatalysts, facilitating a higher number of electrochemical reactions to occur simultaneously. This, in turn, enhances the overall performance of the system by promoting more efficient conversion of reactants. Rectangular flow channels generally provide a more uniform distribution of reactants across the electrode surfaces. The even flow of gases and electrolytes reduces the likelihood of localized concentration gradients and associated polarization losses. This contributes to improved mass transport and, consequently, enhanced cell performance. Rectangular flow channels tend to exhibit lower pressure drop characteristics compared to triangular or semicircular counterparts. Lower pressure drops mean that the system requires less energy to maintain the desired flow rates, resulting in improved overall energy efficiency. The rectangular flow channel geometry also lends itself well to efficient heat transfer. Heat generated during electrochemical reactions can be more effectively dissipated in square channels, helping to maintain a consistent temperature throughout the cell.



a) Rectangular flow channel b) Triangular flow channel c) Semicurcilar flow channel

Fig.4: The effect of temperature on polarization curve (a) rectangular (b) triangular, and (c) semicircular flow channel.

As can be seen in Fig.4., in rectangular flow channels, higher temperatures generally promote faster electrochemical reactions at the electrodes due to increased kinetic energy, resulting in lower activation overpotentials and reduced resistive losses. In triangular flow channels, temperature impacts the flow patterns, affecting mass transport and local temperature distribution. Elevated temperatures can enhance convective heat and mass transfer, potentially reducing overpotentials and improving overall efficiency. In semicircular flow channels, temperature can similarly affect flow patterns and thermal gradients, impacting mass transfer and electrochemical kinetics.

IV. Conclusions

In this study, the utilization of COMSOL Multiphysics with a dedicated Fuel Cell & Electrolyzer Module enabled a comprehensive analysis of cathode-supported SOECs. The results were rigorously validated through experimental investigations, demonstrating a strong alignment between numerical simulations and experimental data. Rectangular flow channels exhibited superior performance due to enhanced electrochemical reactions, and efficient heat transfer. Temperature had a significant impact on the mole fraction of water and hydrogen in these channels. Overall, this research underscores the effectiveness of rectangular flow channels for SOEC applications and highlights the importance of temperature control in optimizing performance across various flow channel geometries.

In conclusion, the study provides valuable insights into the behavior and performance optimization of SOECs, particularly in the context of rectangular flow channels. The robust correlation between numerical simulations and experiments enhances confidence in the predictive capabilities of the model for future research and applications. This work underscores the advantages of rectangular flow channels in terms of reactant distribution and performance and highlights the influence of temperature on mole fraction profiles. Apart from these specified parameters, an impactful observation has been made regarding the significance of non-uniform temperature operating conditions, a common occurrence in experimental studies, on the overall performance of the cell. It contributes to our understanding of SOECs and provides a foundation for further research and development in this field.

References

Biswas S., Kaur G., Giddey S., Steam electrolysis in solid oxide electrolytic cells using a cermet of copper and gadolinia doped ceria cathode, Electrochimica Acta, 468, 143150 (2023).

Chen H., Wang J., Xu X., Parametric Study of Operating Conditions on Performances of a Solid Oxide Electrolysis Cell, Journal of Thermal Science, 32, 1973-1988 (2023).

Hu K., Fang J., Ai X., Huang D., Zhong Z., Yang X., Wang L., Comparative study of alkaline water electrolysis, proton exchange membrane water electrolysis and solid oxide electrolysis through multiphysics modelling, Applied Energy, 312, 118788 (2022).

Ilbas M., Kumuk B., Alemu MA., Arslan B., Numerical investigation of a direct ammonia tubular solid oxide fuel cell in comparison with hydrogen, International Journal of Hydrogen Energy, 45 (60), 35108-35117 (2020).

Ni M., Leung MKH., Leung DYC., Parametric study of solid oxide steam electrolyzer for hydrogen production, International Journal of Hydrogen Energy, 32 (13), 2305-2313 (2007).

Srinivas S., Dhanushkodi SR., Chidambaram RK., Skrzyniowska D., Korzen A., Taler J., Benchmarking Electrolytes for the Solid Oxide Electrolyzer Using a Finite Element Model, Energies, 16 (18), 6419 (2023).

Wang Z., Mori M., Araki T., Steam electrolysis performance of intermediate-temperature solid oxide electrolysis cell and efficiency of hydrogen production system at 300Nm^3h^{-1}, International Journal of Hydrogen Energy, 35 (10) 4451-4458 (2010).

Evaluation of Hydrogen Production by Cobalt Chloride Thermochemical Method in a Fusion Reactor

[1,] *Medine Özkaya, [2]Adem Acir,
[1]Gazi University, Vocational School of Technical Sciences, Department of Machinery and Metal Technologies, Ankara/Türkiye
[2]Gazi University, Faculty of Technology, Department of Energy Systems Engineering, Ankara, 06000, Türkiye

* E-mail: medineozkaya@gazi.edu.tr

Abstract
The aim of this study is to examine the hydrogen production amount of the Co-Cl thermochemical cycle integrated into the PACER fusion reactor. First, two different coolants were preferred, these are FLiNaBe and FLiBe. In addition, PuF_4 nuclear fuel was mixed into these two coolants at the rate of 0.25%, 0.50%, 0.75% and 1%. The tritium breeding ratio (TBR) value was calculated by performing neutronic analysis under these conditions. Then, energy multiplication factor (M), total thermal power (P_{hpf}), and hydrogen production amount ($\dot{m}$) values were calculated depending on the tritium breeding ratio (TBR) value. As a result, the highest hydrogen production amount was obtained as 9.66 kg / s from the nuclear fuel mixture of 99% FLiNaBe + 1% PuF_4.

I. Introduction

Hydrogen, which is considered the cleanest energy source of the future, is abundant in the universe, but has bonded with other elements in nature. Therefore, a primary energy source is needed to use hydrogen as fuel. Nuclear power plants, which are an important energy source, have also been preferred for hydrogen production as both electricity and heat sources. There are many studies in the literature on the use of nuclear power plants as energy sources. Xixin and Kaoru (2005) show that the high-temperature gas-cooled reactor (HTGR) can be used to produce hydrogen via the S-I thermochemical cycle. For this purpose, they showed that the S-I thermochemical cycle, which is in the experimental stage, was carried out in a laboratory environment. They also confirmed the feasibility of recycling all reactants used in the S-I cycle in a closed loop. Özkaya et al. (2023) integrated the hydrogen production test into the PACER fusion reactor to calculate hydrogen production by the Fe-Cl thermochemical cycle. Three different nuclear fuels were mixed into the coolant used in the reactor in three different proportions. Additionally, the energy production of the reactor was calculated by enriching ^6Li at all refrigerant and nuclear fuel ratios. As a result, it was stated that ^6Li enrichment increased hydrogen production under all conditions. In this study, the hydrogen production amount of the cobalt chloride (Co-Cl) thermochemical cycle hydrogen production facility modified to the PACER fusion reactor was calculated. Additionally, the effect of two different coolants used in the reactor on hydrogen production was examined.

II. Problem Description

The fusion reaction part with a radius of 3000 cm is located in a rock zone. The PACER fusion reactor consists of two void zones, a coolant zone and SS-304 stainless steel. Nuclear fusion takes place at its very center (Özkaya et al. 2023; Acır, 2004). In this study, a Cobalt chloride (Co-Cl) thermochemical cycle hydrogen production facility was integrated into the PACER fusion reactor. The volume of the Pacer fusion reactor coolant zone is determined as 25% molten salt + 75% void. Two different coolants have been identified: FLiBe and FLiNaBe. The coolant and PuF_4 ratios are; It is 0.25% PuF_4 + 99.75% Molten salt, 0.50% PuF_4 + 99.50% Molten salt, 0.75% PuF_4 + 99.25% Molten salt, 1% PuF_4 + 99% Molten salt.

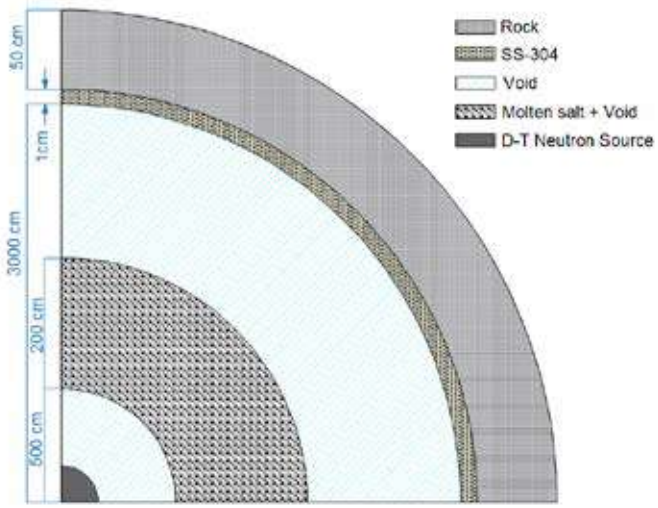


Fig. 1: PACER fusion reactor cross-sectional view

III. Hydrogen Production and methodology

PACER fusion reactor is a good energy source that can meet both the electricity and heat needs of the systems. The heat energy required by the cobalt chloride (Co-Cl) thermochemical cycle, which is a pure cycle, is also obtained

from the PACER fusion reactor.

The required total thermal power required (P_{hpf}) by the Co-Cl thermochemical cycle hydrogen production facility is calculated with eq. (1) given below (Özkaya et al. 2023):

$$P_{hpf} = (1-\psi) * \eta_{ihx} * \frac{P_f}{Q} * [Q * (x_a + x_n * M) + 1] \quad (1)$$

The (1-ψ) given in eq. (1) expresses the thermal power rate required by the hydrogen production test, and this rate is calculated with eq. (2). Again, M given in equation (1) is expressed as the energy multiplication factor and is given in eq. 3 (Özkaya et al. 2023):

$$(1-\psi) = 1 - \frac{1}{\eta_{IHX} * \eta_{ds} * [Q*(X_a + X_n * M)+1]\eta_{gt}} + \frac{X_{aux} + X_{isp}}{\eta_{IHX} * \eta_{gt}} \quad (2)$$

$$\mathrm{M} = \frac{200\ \mathrm{MeV} * \langle \Phi * \Sigma_f \rangle + 4{,}7484\ \mathrm{MeV} * T_6 - 2{,}467\ \mathrm{MeV} * T_7}{14{,}1\ \mathrm{MeV}} + 1 \quad (3)$$

In order to calculate the hydrogen production amount of the system, the q_{tot} value must be calculated. In order to calculate the q_{tot} value, the principle of conservation of energy and shomate equations are used (Çengel ve Boles 2013).

$$\dot{E}_{in} = \dot{E}_{out} \quad (4)$$

$$\dot{Q}_{in} + \dot{W}_{in} + \sum n_{in} H_{in} = \dot{Q}_{out} + \dot{W}_{out} + \sum n_{out} H_{out} \quad (5)$$

$$Q = \sum n_{out} (\bar{h}_f^o + \bar{h} - \bar{h}_0)_{out} - \sum n_{in} (\bar{h}_f^o + \bar{h} - \bar{h}_0)_{in} \quad (6)$$

$$\bar{h}(T) - \bar{h}_0 = AT + B\frac{T^2}{2} + C\frac{T^3}{3} + D\frac{T^4}{4} - \frac{E}{T} + F - H \quad (7)$$

The $\bar{h}_f^o$ given here refers to the enthalpy of formation. T is 1/1000 of the temperature and its unit is K. The values A, B, C, D, E, F, H, known as shomate coefficients and given in Table 1, are fixed.

Compound	Temperature K	$\bar{h}_f^o$ kJ/mol	A	B	C	D	E	F	H
CoCl2(s)	973.15	-312.55	79.30939	14.28782	-6.29370	1.31786	-0.40281	-338.1274	-312.5452
H_2O (g)	973.15	-241.83	30.092	6.832514	6.793435	-2.53448	0.082139	-250.881	-241.8264
Co3O4 (s)	973.15	-910.02	177.09530	-100.43610	185.77920	-49.04861	-3.48395	-971.54150	-910.02000
HCl (g)	973.15	-92.310	32.123920	-13.458050	19.868520	-6.853936	-0.04967	-101.62060	-92.31201
H_2(g)	973.15	0.0000	33.06618	-11.36342	11.43282	-2.77287	-0.15856	-9.98080	0.0
CoO (s)	973.15	-237.74	43.65000	22.38373	-16.89386	6.55616	0.532263	-249.8643	-237.7353
O_2 (g)	973.15	0.0000	30.03235	8.77297	-3.98813	0.78831	-0.7416	-11.32468	0.0
Co (s)	973.15	0.0000	-204.57600	515.58200	-421.55000	129.55800	17.92670	94.61550	0.0

Table 1. Enthalpy values of compounds and constants of the Co-Cl thermochemical cycle required for Shomate calculations (NIST Chemistry WebBook).

The following equation (8,9) is used to calculate the hydrogen production amount of the Co-Cl thermochemical cycle (Özkaya et al. 2023).

$$\dot{m}_x = \frac{P_{hpf}}{q_{tot}} \quad (8)$$

$$\dot{m}_y = \dot{m}_x . \frac{u_y}{u_x} . \eta \quad (9)$$

III. I. Hydrogen production of Co-Cl termochemical cycle

Co-Cl thermochemical cycle, which is a four-step cycle; It consists of thermal decomposition, hydrochlorination, reduction and hydrolysis reactions. First, in the hydrolysis step, water (H_2O) and Cobalt chloride ($CoCl_2$) react and form Cobalt dioxide (Co_3O_4), hydrochloride (HCl) and hydrogen (H_2). In the second step, Cobalt dioxide (Co_3O_4) forms Cobalt oxide (CoO) and oxygen (O_2) by thermal decomposition method. In the third step, known as the reduction step, Cobalt dioxide (Co_3O_4) and hydrogen (H_2) react to form Cobalt (Co) and water (H_2O). The last step is called the hydrochlorination step, and in this step, Cobalt (Co) and hydrochloride (HCl) react to form cobalt

chloride ($CoCl_2$) and hydrogen (H_2). Only water and heat are input into the cycle, and hydrogen and oxygen are output from the system. The temperature required in the entire phase of the cycle is 973.15 K.

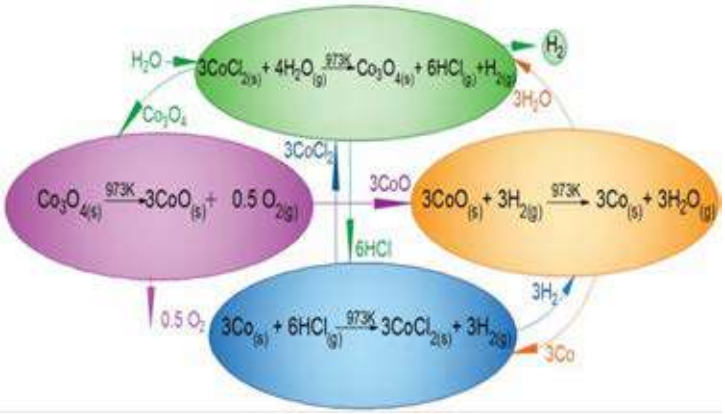


Fig. 2: Schematic representation of the cobalt chloride (Co-Cl) thermochemical cycle

IV. Results and discussions

The thermal energy required by the Co-Cl thermochemical cycle is provided by the PACER fusion reactor. In order to calculate thermal energy, the energy multiplication factor (M) value is needed. The M value is important for the continuity of the energy produced in the facility. Its exact value is determined by the value of the tritium breeding ratio (TBR) calculated by neutronic analysis. The TBR value is a value that determines whether the reaction is continuous or not, and for the reaction to be continuous, the TBR value must be greater than 1.05 (TBR>1.05). The effect of nuclear fuel PuF4 mixed into FLiBe and FLiNaBe coolants on TBR and M values is given in fig. 3 and fig. 4.

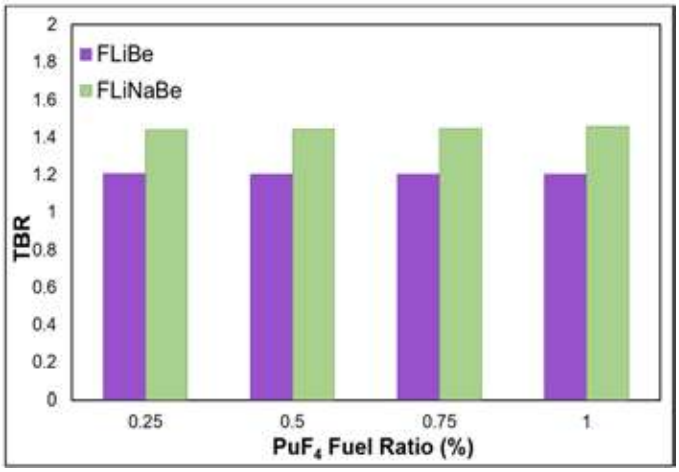


Fig. 3: TBR change graph for coolant FLiBe and FLiNaBe

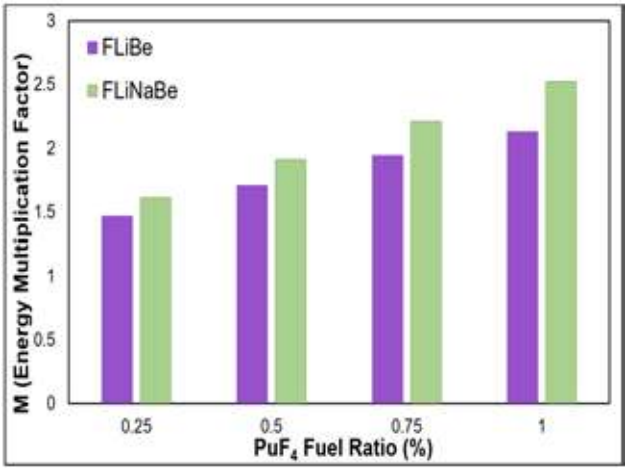


Fig. 4: M change graph for coolant FLiBe and FLiNaBe

As seen in fig. 3, the TBR value of coolant FLiNaBe is higher than that of coolant FLiBe. In addition, it is seen that the nuclear fuel PuF_4 mixed in both coolants increases the TBR value, albeit in a very small amount. When the M value is examined in Figure 4, it is seen that the energy multiplication factor of FLiNaBe is more than the energy multiplication factor of FLiBe, depending on the TBR value. Increasing the ratio of PuF_4 nuclear fuel mixed into the refrigerants increased the M value. The highest M value was obtained from the PuF_4 mixture mixed with 1% FLiNaBe coolant and this value is approximately 2.52.

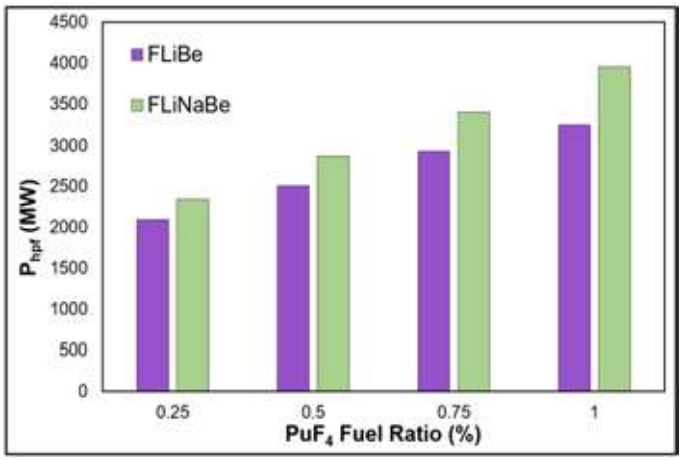


Fig. 5: P_{hpf} (MW) change graph for coolant FLiBe and FLiNaBe

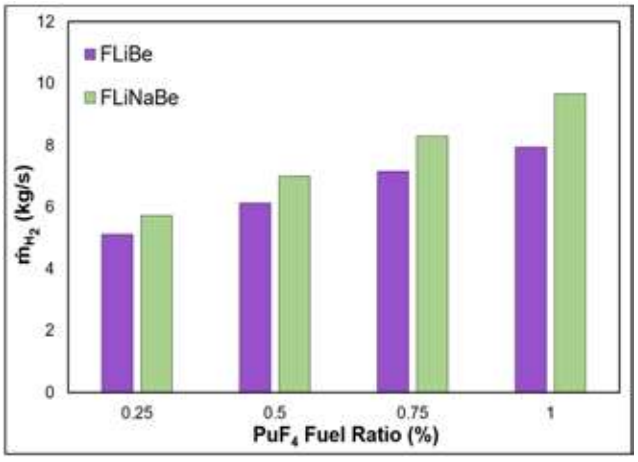


Fig. 6: $\dot{m}_{H_2}$(kg/s) change graph for coolant FLiBe and FLiNaBe

When Fig.5 and Fig. 6 are examined, it is seen that the amount of total thermal energy (P_{hpf}) required by the facility and the amount of hydrogen produced (ṁ) increase depending on the M value. P_{hpf} and $\dot{m}_{H_2}$ values of FLiNaBe used as coolant are higher than FLiBe coolant. Additionally, increasing the amount of nuclear fuel PuF_4 mixed into the refrigerant increased the P_{hpf} and $\dot{m}_{H_2}$ values. The lowest amount of total thermal energy (P_{hpf}) and hydrogen production amount ($\dot{m}_{H_2}$) were obtained from the coolant 99.75% FLiBe and 0.25% PuF_4 and were calculated as approximately 2089.5 MW and 5.10 kg/s, respectively. The highest amount of total thermal energy (P_{hpf}) and hydrogen production amount ($\dot{m}_{H_2}$) were obtained from the coolant 99% FLiNaBe and 1% PuF_4 and were calculated as approximately 3950.1 MW and 9.66 kg/s, respectively.

V. Conclusions

The following results were obtained by calculating the hydrogen production of the cobalt chloride (Co-Cl) thermochemical cycle integrated into the PACER fusion reactor.

- ✓ The TBR, P_{hpf}, M and ṁ values of the coolant FLiBe used in the PACER fusion reactor are higher than the TBR, P_{hpf}, M and ṁ values of the coolant FLiBe (FLiNaBe>FLiBe).
- ✓ Increasing the amount of nuclear fuel PuF_4 mixed into the coolants increased the amount of hydrogen produced.
- ✓ The lowest hydrogen production amount was calculated as approximately 5.10 kg/s from a mixture of 99.75% FLiBe and 0.25% PuF4 nuclear fuel.
- ✓ PACER fusion reactor can be used as an energy source in the production of hydrogen by the Co-Cl thermochemical method.

References

Acır A., PACER füzyon reaktöründe yakıt ve enerji üretiminin incelenmesi, PhD. Thesis, Gazi University, Türkiye (2004).

Çengel, Y., A. and Boles, M., A., Mühendislik Yaklaşımıyla Termodinamik, Editor Pınarbaşı, A., Seventh Edition, Palme Publishing, Ankara, 2013.

NIST Chemistry WebBook. Http://Webbook.Nist.Gov/Chemistry/; (2018).

Özkaya M., Acır A., Yalçın Ş., Investigation of the hydrogen production of the PACER fusion blanket integrated with Fe–Cl thermochemical water splitting cycle, Nuclear Engineering and Technology, 55(11), 4287-4294, 2023.

Xinxin W., Kaoru O., Thermochemical Water Splitting for Hydrogen Production Utilizing Nuclear Heat from an HTGR, Tsinghua Science & Technology, 10(2), 270-276, 2005.

One Step Towards a Green Future: Retrofitting of the Internal Combustion Engines for the Utilization of the Hydrogen Fuel

[1*] Hilmi Ersin Oktar, [2]İbrahim Hakkı Tonyalı, [3]Ahmet Hamit Apaydin
[1] TÜBİTAK Rail Transport Technologies Institute (RUTE), Engine and Transmission Systems Group, Kocaeli, 41470, Türkiye

* E-mail: oktarhilmi@gmail.com

Abstract
As a part of the ongoing efforts globally to prevent global warming and reduce carbon footprint, the utilization of the green hydrogen is seen as a crucial tool to achieve the targets determined by "Green Deal Action Plan" of the Türkiye. In this study, evaluations were made regarding the utilization of the hydrogen, which is considered as the fuel of the future, and the modifications were made for the utilization of the hydrogen in the existing test infrastructure and engine were explained in detail. The aim of the study was to promote the widespread usage of the hydrogen in conventional engines and test infrastructure, in line with Turkiye's green hydrogen strategy. As a result, a research engine and test infrastructure capable of performing experimental studies with hydrogen fuel have been transformed. In the initial experiments, it was evaluated that the utilization of hydrogen in the engines holds significant potential.

Keywords: Hydrogen, Green energy, Internal combustion engine, Test cell

I. Introduction

The Paris climate agreement, aims to prevent global warming and return to pre-industrial conditions, signed by 197 countries. The agreement aims to limit global temperature rise through emission reduction measures and achieve carbon neutrality worldwide by 2050. Additionally, the European Union (EU) has committed to being a pioneer in this effort, setting the goal of becoming the first carbon-neutral continent through the Green Deal agreement.

Hydrogen, a carbon-free molecule with many advantageous properties, is considered a key alternative energy source and dubbed the future fuel. Consequently, hydrogen is seen as a significant tool for reducing the global carbon footprint, with strategic goals set for its utilization. Countries aim to design transformative policies and contribute to these goals through research, and development projects.

In Turkiye, the Green Deal Action Plan was established on July 16, 2021 by Republic of Turkiye Ministry of Trade (2021), and a working group was formed accordingly. Subsequently, in accordance with the legally binding decisions of the agreement dated October 7, 2021, Turkiye aims to reduce its current carbon emissions by 21% by 2030 and achieve carbon neutrality by 2053. The Turkiye Hydrogen Technologies Strategy and Roadmap, developed by Republic of Turkiye Ministry of Energy and Natural Resources (2023), aims to create an efficient value chain from the production to the end-use of green hydrogen, based on domestic and national technologies.

Conventional internal combustion engines, which are widely used in the energy and transportation sectors and contribute to a significant amount of global emissions, present a challenge due to their widespread usage. Due to the potential for near-zero pollutant emissions compared to fossil fuels and significant contributions to global emission reductions, global companies are shifting towards hydrogen-fueled engine projects, rather than fossil fuel-based engine projects, and sharing various plans and projections. These projections anticipate a rapid increase in usage rates alongside development efforts.

This study aims to provide guidance for development efforts in Turkiye within this emerging global market, where hydrogen-fueled internal combustion engines are predicted to replace conventional engines. It seeks to outline a roadmap for the transformation of existing test infrastructures and conventional engines.

II. Experimental Set-up and Procedure

To perform experimental studies with hydrogen in conventional test cells, it is necessary to adapt the storage and distribution infrastructure and undertake various efforts to ensure the safety of the facility and equipment.

In the present study, hydrogen (99.999% purity) was stored using a single bundle consisting of 12 tubes at 200 bar pressure. The first-stage pressure regulation was located in an open area at outside, while the second-stage pressure regulator was positioned where the fuel line enters the test room. Additionally, a thermal mass flow meter (Vögtlin GSM-D9KA / flow rate <500 ln/min) was installed in the fuel line, followed by a buffer tank to dampen measurement fluctuations caused by injector pulses.

In order to cut off the fuel supply in case of emergency, a solenoid-actuated shut-off valve has been installed, creating a fuel supply line using two flame arresters to prevent flame backflow and fuel injectors.

The precautions to be taken in hydrogen-fueled operations are detailed in the ISO/TR 15916 (2015). According to the standard, the concentration range of between 1% and 2% is considered the first alarm zone where ventilation is performed, and the area where it exceeds 2% is considered the second alarm zone, requiring the fuel supply to be cut off.

In the specified scenarios, a safety panel has been installed along with 4 hydrogen gas detectors (Prosense P-3535), an explosion-proof fan and a hood, enabling the fuel supply to be cut off and ventilation to be controlled from the control room.

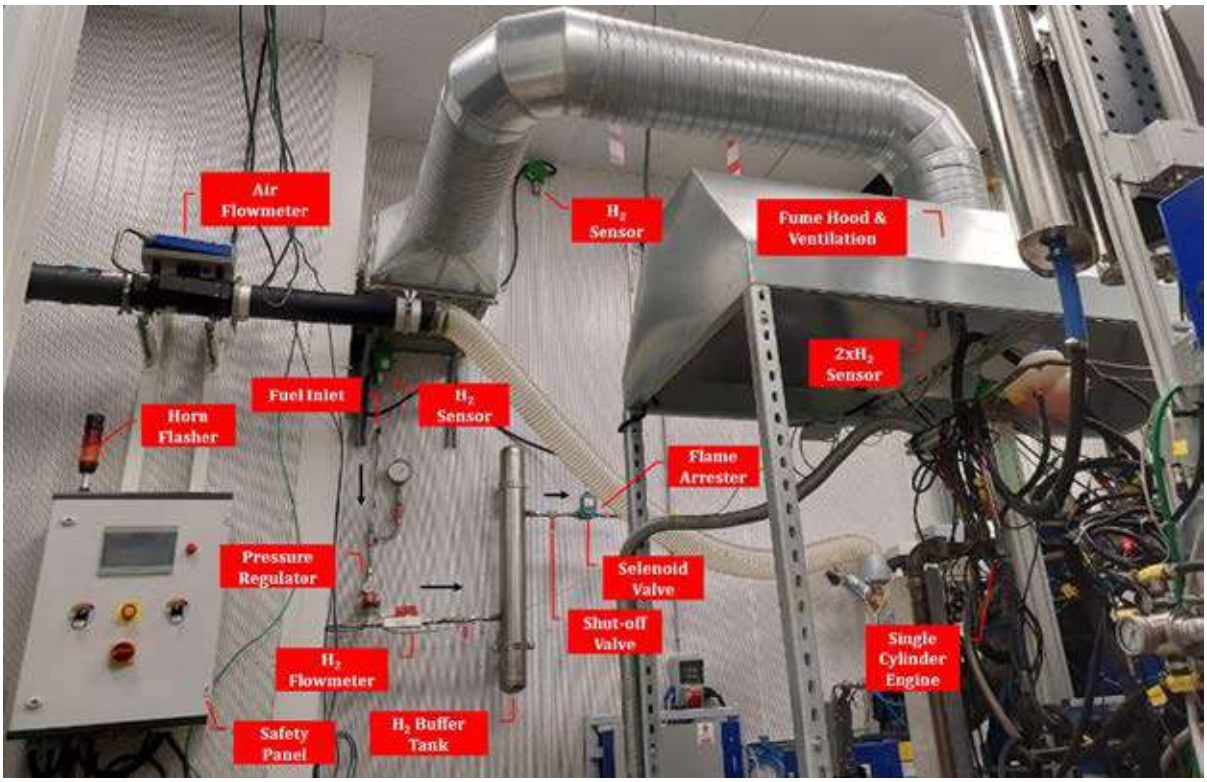


Fig. 1: The overall view of the experimental installation

Furthermore, various revisions have been made for the usage of hydrogen in the single-cylinder spark-ignited research engine:

• A cold rated spark plug with an iridium tip (Denso IXU27), which does not contain platinum (as it accelerates the reaction with hydrogen), has been used. Additionally, the spark gap, which was initially 0.8 mm, has been reduced to 0.3 mm to break down the voltage.

• For the injection of hydrogen into the intake manifold, a Bosch NGI2 injector designed for the usage of gas fuels deemed more suitable in terms of sealing function has been employed. (Konrad Reif, 2015)

III. Analysis

In the present study, the fuel consumption quantities for the engines with 20-200 kW maximum power was calculated based on the maximum power and average power values derived from ISO 8178-4 (International Standard Organization, 2017) test cycles (Type C1-C2-E-F), and the required number of bundles was determined and shared in the Figure 2 (30% average thermal efficiency is assumed).

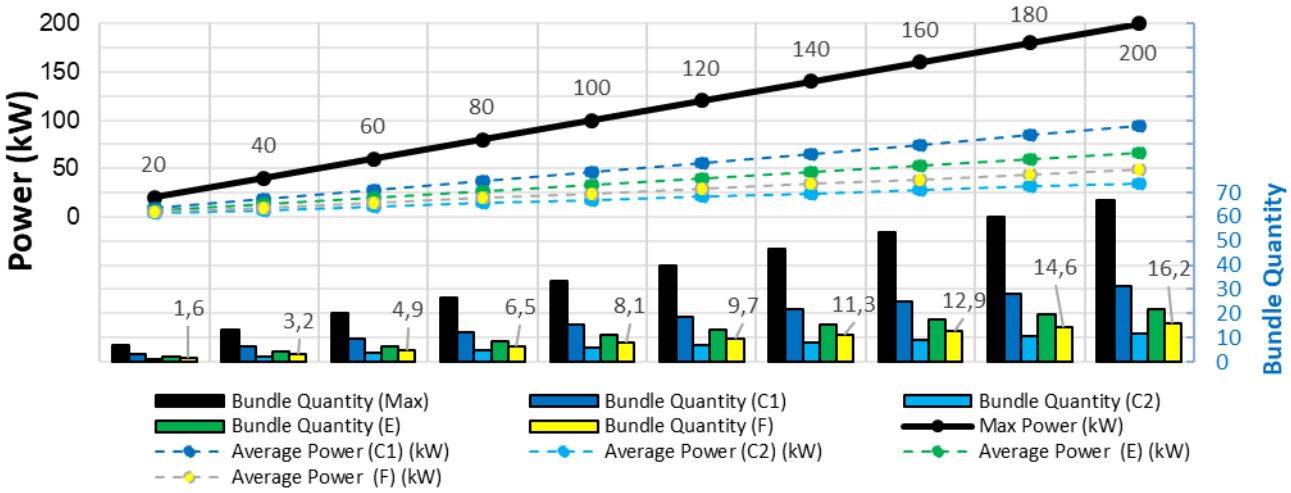


Fig.2: Average power values and the corresponding bundle quantities

Additionally, measurements were taken at 1 ms intervals up to 15 ms injection time for the Bosch NGI2 injector used for hydrogen injection, and the hydrogen mass depending on the injection time graph was obtained (Figure 3).

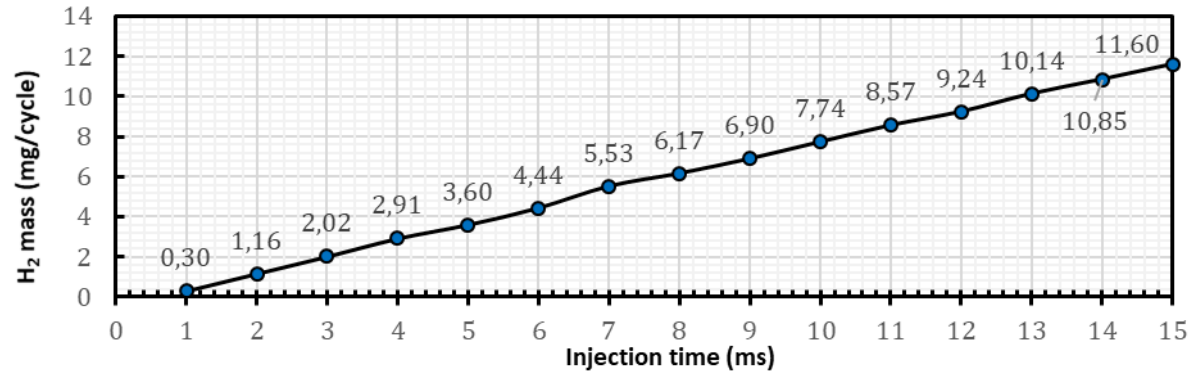


Fig.3: Hydrogen mass depending on the injection time for Bosch NGI2 injector

The stoichiometric volumetric ratio for the hydrogen/air mixture is defined as 29.53% in the ISO/TR 15916 (International Standard Organization, 2015). The amount of fuel required per cycle for a naturally aspirated engine was calculated using the equation below:

$$m_{H_2} = 0{,}2953 \times V_{cyl} \times \rho_{H_2} \quad (1)$$

Where, m_{H_2} defines H_2 mass (mg/cycle); V_{cyl}, cylinder volume (454 cm^3); ρ_{H_2}, H_2 density (kg/m^3@ 101,325 kPa, 293,15°K)

Injector flow rate evaluation was made to ensure fuel supply at a stoichiometric rate. According to this:

• the safe injection window for injection into the intake port starts at 5°CA (crank angle) after the exhaust valve is closed (to ensure the evacuation of hot residual gas that may cause pre-ignition), and ends at before the bottom dead center (it is planned to end to prevent backflow) (Figure 4).

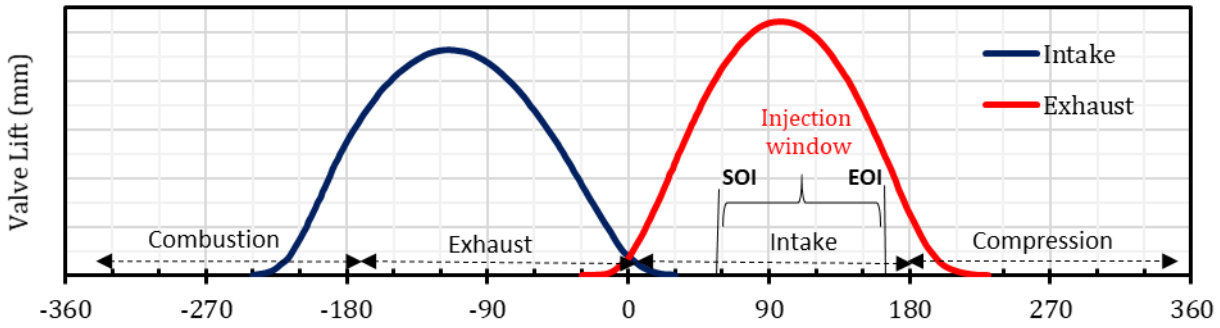


Fig.4: Hydrogen mass depending on injection time

• It has been determined that the amount of fuel calculated as approximately 11.23 mg in stoichiometric condition can only be taken at 1000 rpm with the Bosch NGI2 injector in the widest injection window range, and that the stoichiometric ratio cannot be reached at higher speeds because there is not enough injection time. In future studies, it was evaluated that the usage of multiple injectors was necessary to perform stoichiometric studies at higher speeds.

IV. Results and discussions

On trasformed experimental setup, test studies were carried out on the naturally aspirated internal combustion engine at 1000 rpm, full throttle opening and within safe injection time. Figures 5 and 6, in-cylinder pressure graphs obtained under test conditions of 1000 rpm engine speed, 6.75°CA spark advance and injection time for 10 ms are shared.

As can be seen from the test results, the burn rate of the hydrogen is significantly high. Compared to conventional fuels, it is known that hydrogen has the highest flame speed (H2 flame speed: 2.7 m/s @25 °C and 101.3 kPa). For example, hydrogen has an almost 90 times higher flame speed compared to gasoline fuel (Gasoline laminar flame speed: 0.3 m/s @25 °C and 101.3 kPa). These results show that hydrogen could burn at almost constant volume. Also, results show that hydrogen combustion can come very close to the ideal Otto cycle and that combustion can occur at high efficiency. In addition, it is considered that hydrogen, which has a wide volumetric flammability range, can provide ease of load control by providing high burn rate and the ability to operate even under very poor operating conditions.

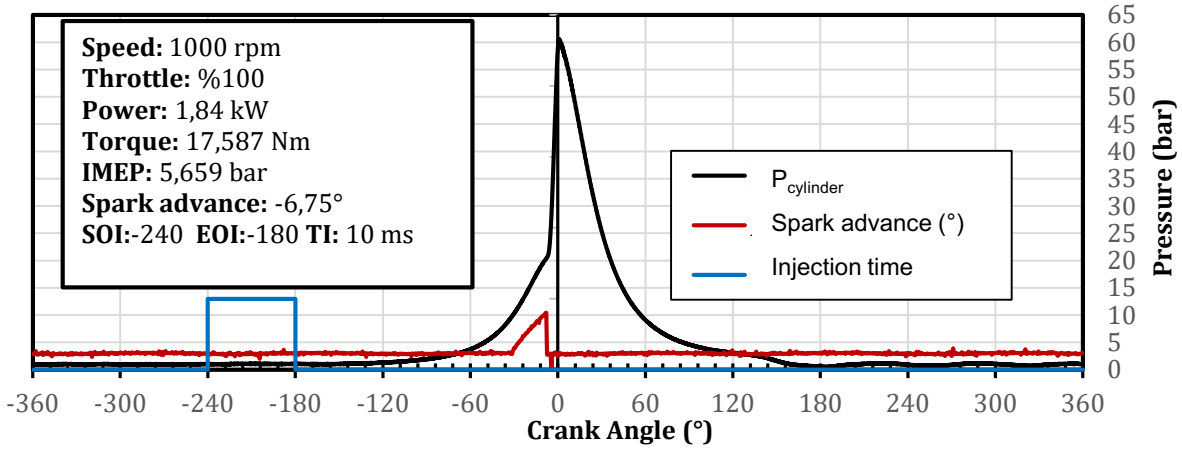


Fig. 5: In-cylinder pressure depending on crank angle for 10 ms injection time

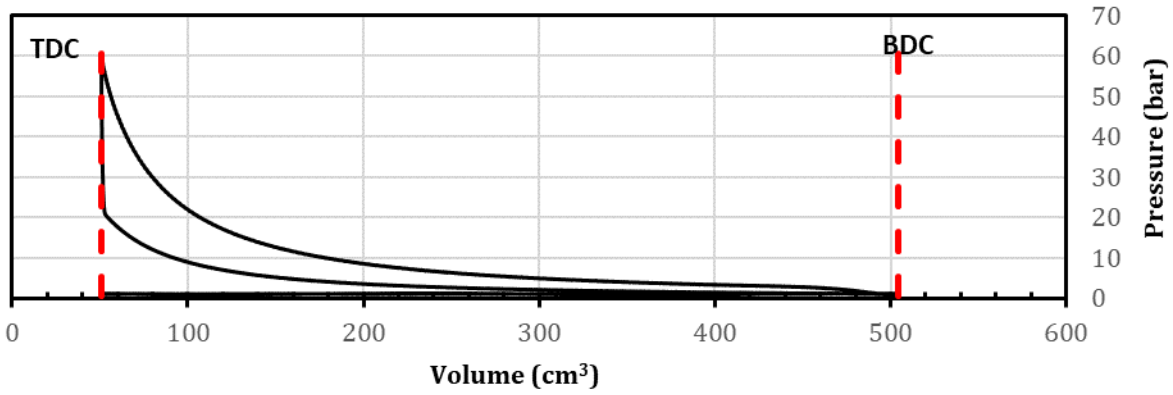


Fig. 6: In-cylinder pressure based on in-cylinder volume for 10 ms injection time

V. Conclusions

In the present study, the feasibility of studies to be carried out with hydrogen fuel in conventional internal combustion engines and existing test infrastructures was experienced at low costs, and the advantages of hydrogen fuel having the highest energy per unit weight, high burn rate and wide volumetric flammability range were observed in the first tests.

According to the test results, it is thought that further expanding studies on hydrogen, which is thought to play a critical role in the fight against climate change and energy transformation, can fully reveal the potential of hydrogen and accelerate a green energy transformation.

Acknowledgements

This research was supported by the TÜBİTAK Rail Transportation Technologies Institute (RUTE)

References

Republic of Turkiye Ministry of Trade, Green Deal Action Plan (2021). [Online]: https://ticaret.gov.tr/data/60f1200013b876eb28421b23/MUTABAKAT%20YE%C5%9E%C4%B0L.pdf

Republic of Turkiye Ministry of Energy and Natural Resources, The Turkiye Hydrogen Technologies Strategy and Roadmap (2023). [Online]: https://enerji.gov.tr/Media/Dizin/SGB/tr/Kurumsal_Politikalar/HSP/ETKB_Hidrojen_Stratejik_Plan2023.pdf

International Standard Organization. (2015). ISO/TR 15916:2015 - Basic considerations for the safety of hydrogen systems. In *ISO Online Catalog*.

International Standard Organization. (2017). ISO 8178-4 Reciprocating internal combustion engines — Exhaust emission measurement. In *ISO 8178-4*.

Konrad Reif. (2015). Gasoline Engine Management - Systems and Components. In *Springer Vieweg*.

Colorless Distributed Combustion (CDC) Effects on Hydrogen – Methane Composite Fuel Mixture Combustion Characteristics

[1,2*]Osman Kumuk, [2]Serhat Karyeyen
[1] Iskenderun Technical University, Iskenderun Vocational School of Higher Education, Department of Electronical and Automation, 31200, Hatay, Türkiye
[2] Gazi University, Faculty of Technology, Department of Energy Systems Engineering, Teknikokullar 06560, Ankara, Türkiye

* E-mail:osman.kumuk@iste.edu.tr

Abstract
Although hydrogen and methane mixtures have the potential to reduce carbon-based emissions, the high levels of NO_X pollutant emissions during hydrogen combustion necessitate the development of new combustion methods. One such method is Colorless Distributed Combustion (CDC), which enables achieving ultra-low pollutant emissions by providing advantages such as decreased flame instability, reduced combustion noise, and increased combustion efficiency. Therefore, analyses were conducted to evaluate the performance of methane enriched with hydrogen under CDC regime at an equivalence ratio of 0.83 and 5 kW power. During the analyses, the k-e turbulence model and the P-1 radiation model were used. To achieve CDC, the oxygen concentration in the oxidizer was changed from 21% O_2 to 19% and 17% using CO_2 as diluent. The temperatures of both the air and fuel were maintained at a constant level and the results indicated that as the oxygen concentration decreased, the temperature distribution became more homogeneous. The utilization of CO_2 as a diluent proved effective in reducing both temperature and NO_X levels, attributed to its higher heat capacity.

Keywords: H_2-CH_4 Combustion, CDC, Ultra-Low NO_X

I. Introduction
In conjunction with tightening regulations on emissions from various power generation systems, the increasing demand for low-emission technologies has encouraged scientific research into new combustion techniques aimed at reducing emission levels in combustion chambers Khalil and Gupta (2011). The inadequacy of the current thermal field in combustion chambers leads to issues of homogeneous combustion and an increase in emissions such as NO_X. Colorless Distributed Combustion (CDC), similar to the principles of High-Temperature Air Combustion (HiTAC), offers the potential to achieve stable combustion in combustion chambers, thereby reducing NO_X and CO emissions. An advantage of colorless distributed combustion is its ability to not generate visible flame appearances, hence being referred to as colorless. This results in negligible visible appearances compared to traditional flames. The technique of Colorless Distributed Combustion enables less pollutant combustion products through the recirculation of hot combustion products into the oxidizer. This leads to a slowing down of the combustion reaction rate, and the flame propagates effectively such as reported in Kekec and Karyeyen (2022). In another study, Karyeyen et al. (2019) examined hydrogen-rich gas fuels under colorless distributed combustion conditions at an inlet temperature of 300 K. In their experimental study, they investigated emissions of pollutants known as NO_X and CO, as well as OH^* images. They concluded that the addition of diluents to the mixture significantly reduced the brightness of OH^*, and the levels of NO_X and CO emissions. In another experimental study, Khalil and Gupta (2013) found a significant decrease in CO emissions as a result of hydrogen enrichment, and expanded the combustion limits by adding hydrogen to the mixture. While there are numerous studies in the literature, acceptable methods within the scope of CDC include MILD, FLOX, and HiTAC combustion techniques Ahmadi and Hosseini (2018); Ilbas etal. (2022); Khalil and Gupta (2013, 2014, 2016); Tsuji etal. (2002); Wang etal. (2020).

II. Materials and Methots
An existing combustion chamber and a methane burner mounted on it (Fig. 1) were used for all modelling cases as there has still been experimental results Karyeyen etal. (2017). After validation of three-dimensional modeling along with the experimental study results is performed (as seen in Fig.2), numerical investigations were conducted for further analysis. The burner power was set at 5 kW, with an equivalence ratio of 0.83 for all cases. The inlet air and fuel temperatures were consistently maintained at 300 K throughout the experiment. Before transition to colorless distributed combustion process was started, initially, the fuels was burned at 21% O_2 concentration, followed by reducing the O_2 concentration in the oxidizer to 19% and 17%. Pure methane and its fuel mixtures with hydrogen (10% $\mathbf{H_2}$ - 90% $\mathbf{CH_4}$ and 20% $\mathbf{H_2}$ - 80% $\mathbf{CH_4}$) were investigated under conventionl and CDC situtation. Combustion characteristics were obtained under these conditions.

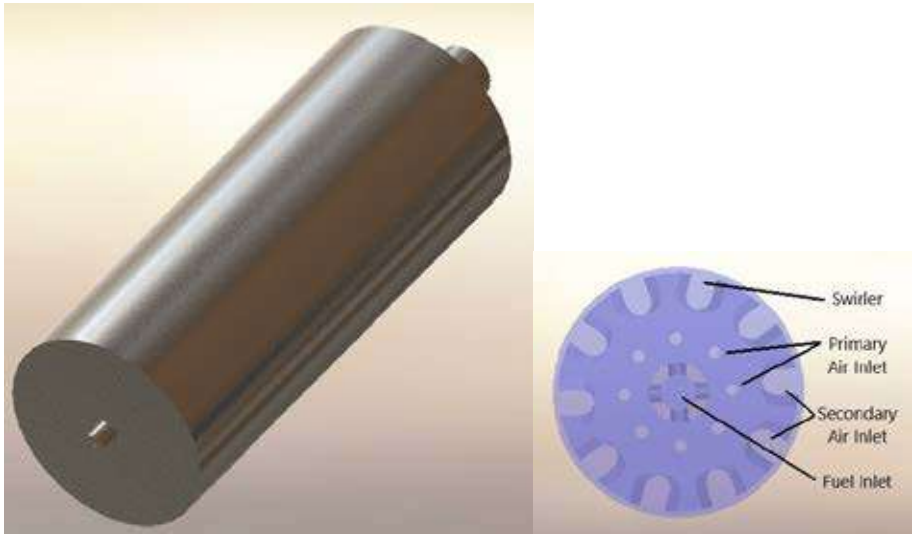


Fig. 1. Combustion chamber and burner model Karyeyen (2016)

Transport equations for all species are continuity, energy, and momentum, and they were employed in computational fluid dynamics studies. The general form of the transport equation is shown in Equation 1 Ilbas etal. (2022). However, the flow is considered as steady-state (so, the first term of the equation is not included).

$$\frac{\partial(\rho\Phi)}{\partial t} + div \quad (\rho\Phi u) = \mathrm{div}(\Gamma grad \quad \Phi) + S_{\Phi} \tag{1}$$

As previously noted, numerical prediction results must be validation through experimental measurements to ensure the validity of the current study and any subsequent modeling cases. Consequently, the present study was compared with existing experimental data Karyeyen etal. (2017) conducted under identical combustion conditions. This comparison is shown in Fig. 2. The predicted temperature profiles in the combustor on the axial distance are represented as shown in Fig. 2, which corresponds to the reported in Karyeyen etal. (2017). Despite slight differences between the measurements and the predictions, it was concluded that the model showed a satisfactory fit with values or trends.

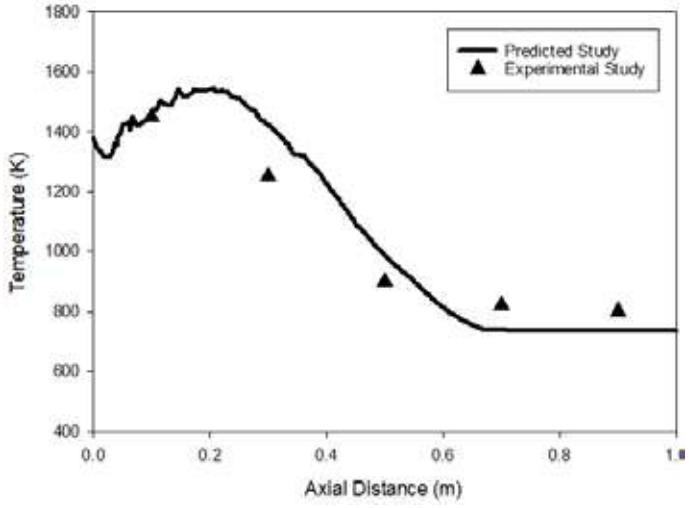
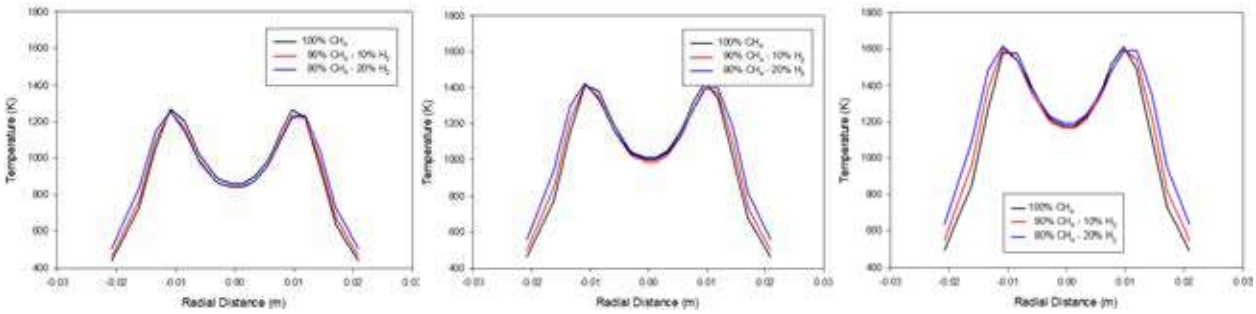


Fig. 2. Comparison of measured and predicted axial temperature distributions Karyeyen etal. (2017)

III. Results and Discussions

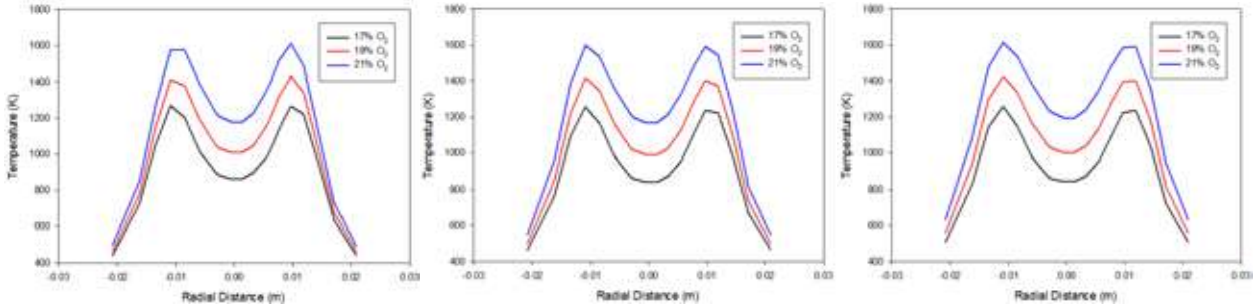
Detailed radial temperature profiles are presented here for all conditions. Analyses were conducted to clarify the effects of fuels and oxygen concentration on the thermal field and NO_X pollutant emissions. Fig. 3 illustrates the effects of hydrogen addition into the methane. As hydrogen is added into the methane, slight increase in temperature levels have been observed. This increase can be attributed to maintaining the total heat load constant. In this way, the same thermal power is met by less methane and more hydrogen, resulting in a slight increase on the temperature levels. Fig. 4 shows CO_2 dilution effects on the temperature profile. The oxidizer is diluted at different levels which results in oxygen concentrations of 21%, 19%, and 17% in the oxidizer.



a) 17% O_2 b) 19% O_2 c) 21% O_2

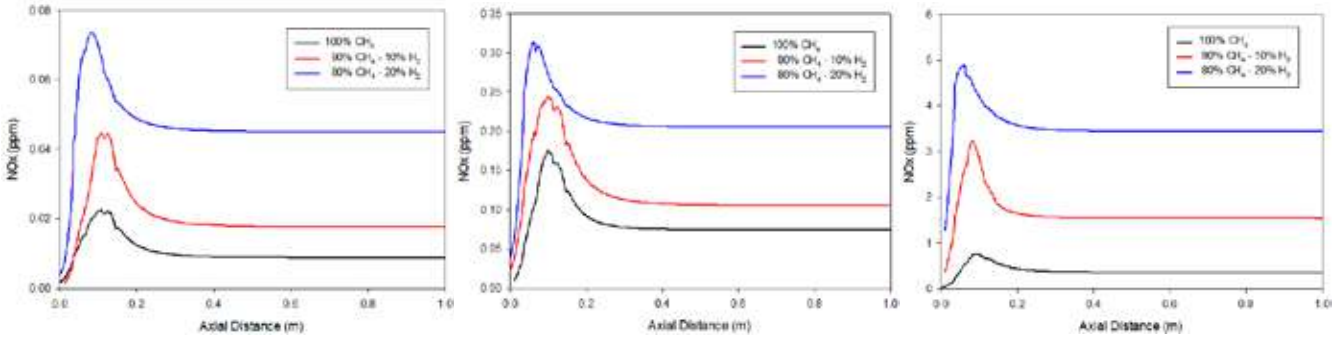
Fig. 3. Temperature graph of different hydrogen fuel additions

A significant drop in temperature levels is observed with decreasing oxygen concentration. For instance, methane fuel combustion reached a highest temperature of approximately 1600 K at 21% oxygen, but dropped to around 1300 K at 17% oxygen. Similar patterns were noted with hydrogen-containing fuels, though temperatures remained relatively stable at 17% O_2. This suggests that hydrogen enrichment is feasible even with lower oxygen concentrations. Such an approach offers potential for countries reliant on natural gas imports and other technologically advanced nations to decrease imports and enhance combustion efficiency through the use of hydrogen-enriched natural gas.



a) 100% CH_4 b) 90% CH_4 – 10% H_2 c) 80% CH_4 – 20% H_2

Fig. 4. Temperature graph of different oxygen concentrations with CO_2 dilution



a) 17% O_2 b) 19% O_2 c) 21% O_2

Fig. 5. NO_X pollutant emissions

Minimizing pollutant emissions is essential in combustion processes, aligning with environmental regulations. Previous research has highlighted the capacity of CDC (Combustion Dynamics Control) to achieve ultra-low NO_X emission. Consequently, this section of the current study focuses on presenting and analyzing the prediction results for NOX pollutant emissions, as depicted in detail in Figure 5. Under conventional circumstances, it is predicted that the NO_X level at the outlet would be approximately 3.8 ppm. However, a reduction in oxygen concentration led to less NO_X levels, which suggests that ultra-low NO_X was achieved (below 1 ppm). This demonstrates that reducing oxygen concentration (with CO_2 dilution) is an effective way to achieve ultra-low NO_X targets. In addition to the examination of oxygen concentration effects, hydrogen enrichment is examined along with dilution effects. It is observed that hydrogen enrichment resulted in a comparative increase in NO_X emissions in all examined scenarios. This increase can be associated with higher temperature regions, which are attributed to mass-based heating values. Nevertheless, transition to CDC resulted in achieving ultra-low NO_X levels.

Conclusion

The combustion characteristics of methane and hydrogen mixture fuels have been investigated at varying oxygen levels through CO_2 dilution. With an increase in hydrogen content, a significant rise in temperature levels in thermal zones has been observed. Enrichment of hydrogen has shifted the position of the flame closer to the fuel inlets, attributed to hydrogen having a higher flame velocity than methane. Upon analysis of pollutant emissions, a notable

reduction in NO_X levels has been observed with decrease in oxygen percentage. This reduction is expected to keep NO_X levels below 1 ppm in all less oxygen concentration cases, which can be considered as a significant conclusion contributing to a cleaner atmospheric conditions.

Acknowledgements
The authours gratefully aclnowledge Gazi University for Ansys Fluent usage. Dr. Osman Kumuk gratefully acknowledge TUBITAK (The Scientific and Technological Research Council of Turkey) for TUBITAK 2218 Programme scholarship as a post-doctoral associate.

References

Ahmadi R., Hosseini S. M., Numerical investigation on adding/substituting hydrogen in the CDC and RCCI combustion in a heavy duty engine, Applied Energy, 213, 450–468, (2018).

Ilbas M., Kumuk O., Karyeyen S., Modelling of the gas-turbine colorless distributed combustion: An application to hydrogen enriched – kerosene fuel, International Journal of Hydrogen Energy, 47(24), 12354–12364, (2022).

Ilbas M., Karyeyen S., Experimental analysis of premixed and non-premixed methane flames by using a new combustion system, Res. Eng. Struct. Mat., 4(1), 1-14, (2018).

Karyeyen S., Experimental and numerical investigations of combustion characteristics of coal gases in a developed combustor, Gazi University, Graduate School of Natural and Applied Science, (2016).

Karyeyen S., Feser J. S., Gupta A. K., Swirl assisted distributed combustion behavior using hydrogen-rich gaseous fuels, Applied Energy, 251, 113354, (2019).

Kekec K. B., Karyeyen S., H2 – CH4 blending fuels combustion using a cyclonic burner on colorless distributed combustion, International Journal of Hydrogen Energy, 47(24), 12393–12409, (2022).

Khalil A. E. E., Gupta A. K., Distributed swirl combustion for gas turbine application, Applied Energy, 88(12), 4898–4907, (2011).

Khalil A. E. E., Gupta A. K., Hydrogen addition effects on high intensity distributed combustion, Applied Energy, 104, 71–78, (2013).

Khalil A. E. E., Gupta, A. K., Velocity and turbulence effects on high intensity distributed combustion, Applied Energy, 125, 1–9, (2014).

Khalil A. E. E., Gupta A. K., Fuel property effects on distributed combustion, Fuel, 171, 116–124, (2016).

Tsuji H., Gupta A. K., Hasegawa T., Katsuki M., Kishimoto K., Morita, M., High Temperature Air Combustion : From Energy Conservation to Pollution Reduction, High Temperature Air Combustion, (2002).

Wang Z., Feser J. S., Lei T., Gupta A. K., Performance and emissions of camelina oil derived jet fuel blends under distributed combustion condition, Fuel, 271, 117685, (2020).

Numerical Study for Low-Emission Coke Oven System Using Combustion of Coke Oven Gas under CDC Conditions

[1,2*]Osman Kumuk
[1] Iskenderun Technical University, Iskenderun Vocational School of Higher Education, Department of Electronical and Automation, 31200, Hatay, Türkiye
[2] Gazi University, Faculty of Technology, Department of Energy Systems Engineering, Teknikokullar 06560, Ankara, Türkiye

* E-mail:osman.kumuk@iste.edu.tr

Abstract
Researchers have developed a three-dimensional mathematical model specifically tailored for the integrated staged combustion chambers found in high-capacity coke ovens. Using Computational Fluid Dynamics (CFD) software like Ansys Fluent, they meticulously solved the model numerically and cross-checked its accuracy against existing literature, particularly focusing on the central temperature. Their analysis factored in variables such as the temperature variance within the coke bed and the levels of NOx concentration in the exhaust gases. The findings underscore the pivotal role of staged combustion in enhancing temperature uniformity across the coke bed and curbing NOx emissions in the exhaust, particularly beneficial for larger coke oven setups. This research anticipates that the model developed and the data gathered will significantly contribute to the realization of large-scale coke ovens boasting superior energy efficiency and reduced emissions.

Keywords: COG Combustion, CDC, Ultra-Low NO_X

I. Introduction

The coke produced from mixtures of coking coal and bituminous coal has a wide range of applications. 90% of this coke is used for iron production in blast furnaces. Regenerative coke ovens are widely used worldwide and contribute to over 90% of the total coke production. Guo and Tang Guo and Tang (2005) established a computational fluid dynamic model using the PHOENICS CFD package to analyze the coking process in a coke oven. Their model simultaneously predicts the transient composition and temperatures of gas and solid phases, gas phase velocity, and porosity and density of the semi-coke phase. Jin etal. Jin et al. (2012) developed and numerically solved a three-dimensional transient mathematical model with coupled coking and combustion chambers to describe thermal processes in the coke oven. They demonstrated the suitability of the proposed model for enhancing production efficiency through measures such as preheating, adjusting moisture content, and densification of charging coke gas. Zhao etal. Zhao et al. (2021) conducted an energy balance analysis to determine the importance of suitable heat storage and appropriate exhaust gas outlet temperature for selective non-catalytic reduction (SNCR) denitrification in flue gas desulfurization systems. Additionally, they developed a new thermal storage assessment index called Total Thermal Storage Temperature (TTST) by adjusting thermal storage parameters in ten different scenarios to examine their effects on SNCR denitrification temperature suitability. The model was validated against experimental data, demonstrating that staged combustion in large-scale ovens could enhance temperature homogeneity and reduce exhaust NO concentration, while also showing that preheating coke gas, controlling moisture, or compressing it could increase coke production efficiency. Although there are many studies in the literature, there are acceptable methods within the scope of NOx reducing combustion techniques Gamrat et al. (2016); Ilbas and Karyeyen (2017); Karyeyen et al. (2019); Karyeyen and Ilbas (2020); Xiao et al. (2023); Xiaohe et al. (2021).

II. Materials and Methots

The experimental results of Karyeyen et al. Karyeyen et al. (2019) and numerical studies by Li et al. Li et al. (2020) are depicted in Figure 1 for the combustion chamber modeling under all operating conditions. Following the validation of three-dimensional modeling with experimental results, numerical investigations were conducted for further analysis as shown in Figure 2. The burner power was set at an equivalence ratio of 0.8 for all cases. Prior to transitioning to colorless distributed combustion, fuels were initially burned at a 21% O_2 concentration, then the O_2 concentration in the oxidizer was reduced to 19%, 17%, and 15%. Conditions of nitrogen and carbon dioxide dilution were explored under CDC conditions, yielding combustion characteristics.

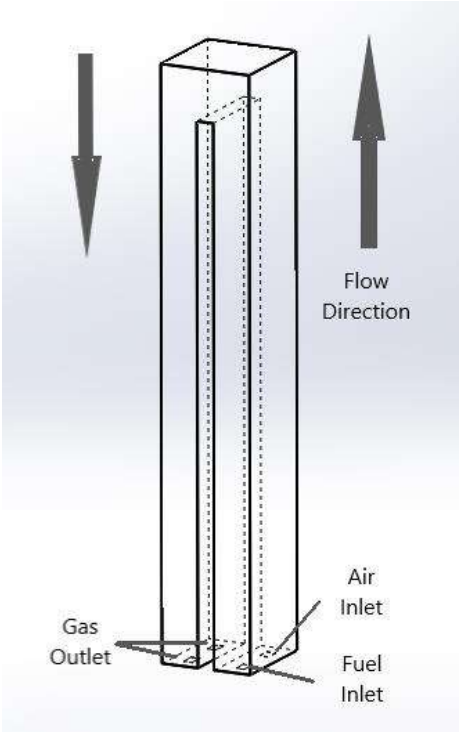


Fig. 1. Combustion chamber and burner model (Li et al. 2020)

The predicted emission (NOx) profiles at the gas outlet of the combustion chamber are presented in Figure 2, corresponding to those reported by Karyeyen et al. Karyeyen et al. (2019) and Li et al. Li et al. (2020). Despite minor discrepancies between measurements and predictions, it was concluded that the model exhibited satisfactory agreement with the values or trends.

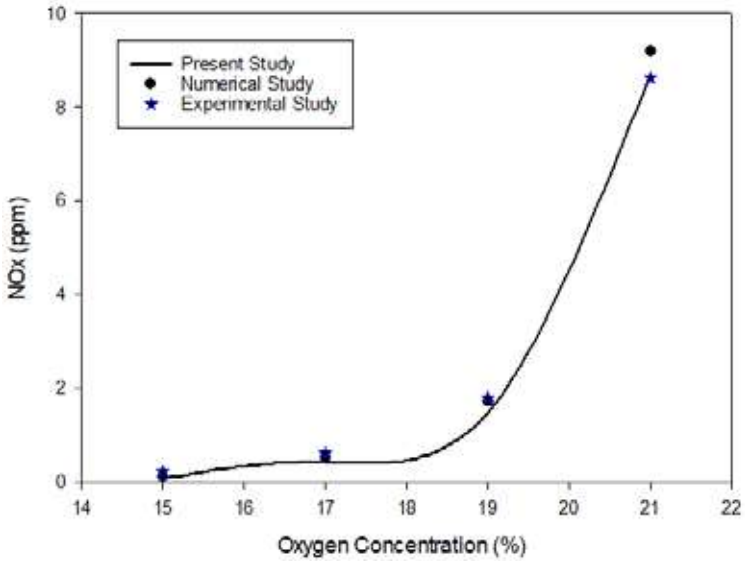
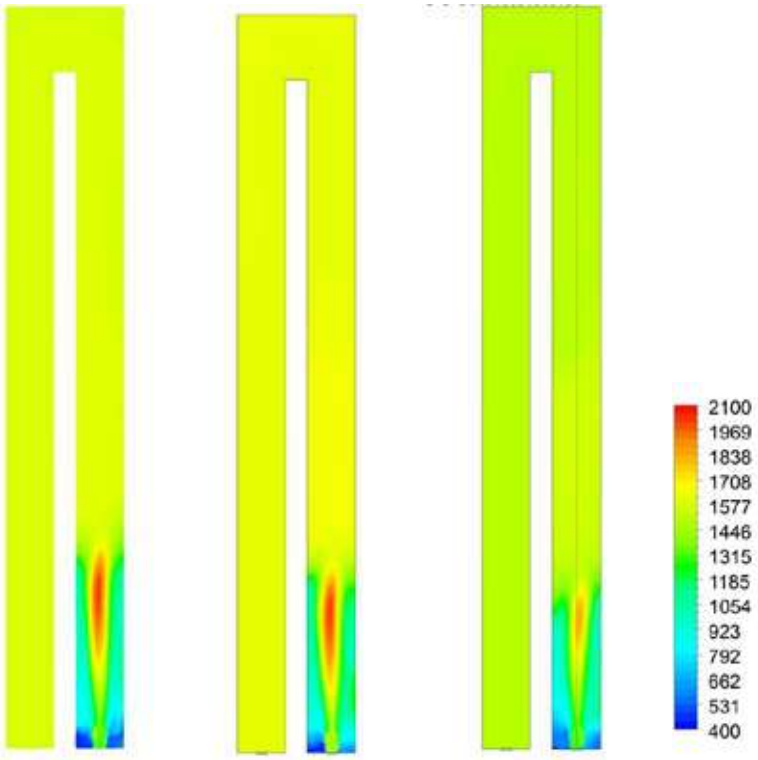


Fig. 2. Comparison of measured and predicted gas outlet NOx distributions

III. Results and Discussions

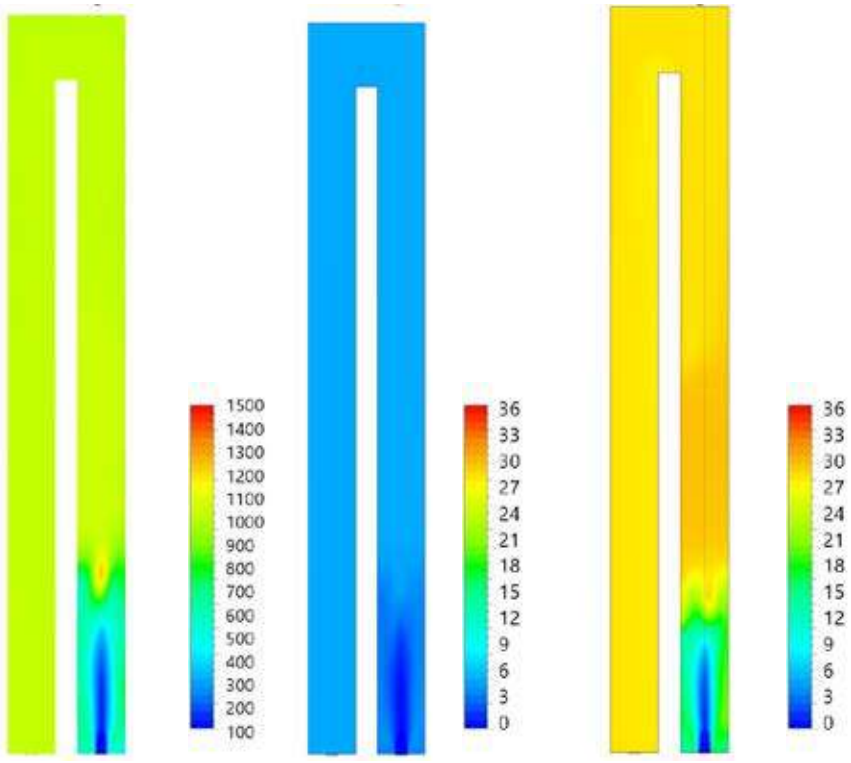
Detailed temperature profiles for various CO_2 and N_2 conditions are presented in this section. Analyses have been carried out to elucidate the impact of fuel and oxygen concentration on the thermal field and NO_X pollutant emissions. Figure 3 illustrates the effects of 21% O_2, 15% O_2/ CO_2, and 15% O_2/N_2 dilutions. When coke gas fuel is considered, a slight decrease in temperature levels is observed due to the dilution effects of oxygen concentration. This decrease can be attributed to maintaining the total heat load constant.



a) 21% O_2 b) 15% O_2 (CO_2 Dilition) c) 15% O_2 (N_2 Dilition)

Fig. 3. Temperature contour of different dilition ratio

A significant reduction in temperature levels is noted with decreasing oxygen concentration. For example, combustion of coke oven gas fuel reached exhaust temperatures of approximately 1560 K at 21% oxygen, but decreased to around 1434 K for 15% CO_2 in oxygen and approximately 1490 K for 15% N_2 in oxygen. Here, dilution demonstrates a more homogeneous combustion and diluent effect.



a) 21% O_2 b) 15% O_2 (CO_2 Dilition) c) 15% O_2 (N_2 Dilition)

Fig. 4. NO_X pollutant emissions of different dilition ratio

Reducing pollutant emissions in combustion processes is vital to comply with environmental regulations. Previous research has highlighted the capability of CDC to achieve low NO_X emissions. Consequently, this section of the current study focuses on presenting and analyzing the predicted results of NO_X pollutant emissions, as detailed in Figure 4. Under conventional conditions, it is estimated that the NO_X level at the outlet for 21% O_2 would be

approximately 869 ppm. For 15% O_2/CO_2, this value is 5.42 ppm, and for 15% O_2/ N_2, it is 24.22 ppm. However, a decrease in oxygen concentration has resulted in lower NO_X levels, indicating the achievement of low NO_X. This demonstrates that reducing oxygen concentration is an effective way to achieve low NO_X targets.

Conclusion

The decrease in oxygen level significantly affects the thermal zones in the combustion chamber. For instance, at a concentration of 21% O_2, the maximum temperature for coke oven gas combustion was approximately 1560 K. However, with the reduction in oxygen level, the distribution of the thermal zone becomes more homogeneous, and the position of the flame changes. These changes are the initial indicators of reaching CDC conditions. The flame position shifts closer to the inlets because the flame speed of diluent gases is lower than that of oxygen. It has been observed that the decrease in oxygen level reduces the temperature difference between the wall and the center, indicating the transition to CDC. The reduction in the percentage of oxygen results in a significant decrease in the predicted NO_X levels. For example, after a concentration of 19% O_2, NO_X levels are expected to be below 2 ppm in all cases. This is a significant indication of the transition to CDC.

Acknowledgements

The authours gratefully aclnowledge Gazi University for Ansys Fluent usage. Dr. Osman Kumuk gratefully acknowledge TUBITAK (The Scientific and Technological Research Council of Turkey) for TUBITAK 2218 Programme scholarship as a post-doctoral associate.

References

Gamrat S., Poraj J., Bodys J., Smolka J., Adamczyk W., Influence of external flue gas recirculation on gas combustion in a coke oven heating system, Fuel Processing Technology, 152, 430–437, (2016).

Guo Z., Tang H., Numerical simulation for a process analysis of a coke oven, China Particuology, 3(6), 373–378, (2005).

Ilbas M., Karyeyen S., An experimental and numerical study on turbulent combustion of hydrogen-rich coal gases in a generated non-premixed burner, Fuel, 194, 274–290, (2017).

Jin K., Feng Y., Zhang X., Lin W., Zhang C., Yang J., Ma X., Numerical analysis on thermal processes in coupled coking and combustion chambers of coke oven, Huagong Xuebao/CIESC Journal, 63(3), 788–795, (2012).

Karyeyen S., Feser J. S., Gupta A. K., Swirl assisted distributed combustion behavior using hydrogen-rich gaseous fuels, Applied Energy, 251, 113354, (2019).

Karyeyen S., Ilbas M., Application of distributed combustion technique to hydrogen-rich coal gases: A numerical investigation, International Journal of Hydrogen Energy, 45(5), 3641–3650, (2020).

Li Z., Yi Q., Zhang Y., Zhou H., Zhao Y., Huang Y., et al., Numerical study and design strategy for a low emission coke oven system using oxy-fuel combustion of coke oven gas, Journal of Cleaner Production, 252, 119656, (2020).

Xiao K., Wang Y., Hu H., Wen Z., Lou G., Su F., et al., Numerical analysis on heat transfer process in the coke oven with the multi-chamber coupling mathematical model, Case Studies in Thermal Engineering, 44, 102858, (2023).

Xiaohe X., Zhaomin L., Shilin Y., Houzhang T., Baixiang X., Jun H., Coke preheating combustion study on NOx and SO2 emission, Journal of the Energy Institute, 97, 131–137, (2021).

Zhao Y. J., Feng J. X., Huang S. P., Hu S. Y., Analysis and evaluation of the influence of heat storage material on coke oven flue gas exothermic process, Thermal Science, 25(2 Part A), 1095–1108, (2021).

Numerical Simulation of Methane Dry Reforming over Supported Nickel Catalyst

[1]Ahmed Aheed Ali Mohammed, [1,2*]Dr. Mohammed Al-Marri, [1*]Dr. Anand Kumar,
Department of Chemical Engineering department, Qatar University, Doha, P O Box 2713, Qatar
Gas Processing Center, Qatar University, Doha, P O Box 2713, Qatar

[*]E-mail: m.almarri@qu.edu.qa; akumar@qu.edu.qa

Abstract
Herein, simulation of the dry reforming of methane over nickel-based catalysts supported on alumina in a laboratory reactor is presented. The reactor system was simulated using COMSOL 6.2 at isothermal conditions of 650°C, containing an equimolar ratio of CH_4 to CO_2 in the feed. The results indicate that, under the simulated conditions, carbon deposition is nearly negligible, with an order of magnitude of approximately 10^{-16}. With approximately 0.026 grams of catalyst, the H_2/CO molar ratio reaches (as evaluated) 0.6331. When the feed enters with a mean velocity of 3 cm/s, the steady state is believed to be approximately reached after 150 seconds. Overall methane conversion is found to be around 20%.

Keywords: Methane dry reforming, Numerical simulation, Hydrogen production, COMSOL 6.2

I. Introduction

The rapid growth of the global population (projected to be more than 9 billion by 2050 (Johnson et al., 2023)), accompanied by consistently increasing energy demand (expected to increase by more than 40% from 2024 to 2040 (Ahmad & Zhang, 2020)) imposes a great challenge on energy generation sector. Up to date, fossil fuels remain the primary energy source (more than 81% of total world energy generation is coming from them (In Partnership with Statistical Review of World Energy 2023 | 72 Nd Edition, n.d.)). However, it is a fact that (and intuitively known) energy generation from fossil fuels is associated with huge amount of CO_2 being produced and emitted into the atmosphere. In 2022, about 37.15 billion tons of CO_2 have been emitted into the atmosphere as a result of using fossil fuels (Friedlingstein et al., 2023). Along with the already emitted and accumulated through the previous years, atmospheric CO_2 concentration is being sky-rocketed, and projected to be exponentially increasing. Such a concentration is highly recommended to be severely reduced, if not completely curtailed, as CO_2 is considered a greenhouse gas which contributes to the global warming and creates a serious threat to the eco-system.

One potential way to reduce CO_2 emission while covering the energy demand is to transfer to an alternative “cleaner and eco-friendly” energy source. In this regard, hydrogen gas production has received enormous attention and effort. On the other hand, in order to lower down already emitted CO_2 atmospheric concentration, CO_2 conversion into other value-added chemicals is of great importance. Thus, dry reforming of methane has received huge investigations and research efforts as being considered promising technology for hydrogen “clean energy source” production as well as carbon conversion at the same time. Nevertheless, the research scope is wide open in such a process, as there are numerous challenges associated with it.

In this paper, we provide the results of COMSOL 6.2 numerical simulation study of DRM over 10% Ni over alumina catalyst that is widely investigated and used for such a reaction.

II. Model Development

We consider here six chemical reactions (from 1 to 6) as they are considerably dominant in DRM, especially under high temperatures (Alli et al., 2023; Jun et al., 2024a; Osat et al., 2023; Soleimani & Lehner, 2022).

$$CH_4 + CO_2 \leftrightarrow 2CO + 2H_2 \qquad \Delta H^o_{298K} = 247.3 \ \frac{kJ}{mol} \qquad (1)$$

$$CO_2 + H_2 \leftrightarrow CO + H_2O \qquad \Delta H^o_{298K} = 41.2 \ \frac{kJ}{mol} \qquad (2)$$

$$CH_4 \leftrightarrow C + 2H_2 \qquad \Delta H^o_{298K} = 75 \ \frac{kJ}{mol} \qquad (3)$$

$$H_2O + C \leftrightarrow CO + H_2 \qquad \Delta H^o_{298K} = 131.4 \ \frac{kJ}{mol} \qquad (4)$$

$$CO_2 + C \leftrightarrow 2CO \qquad \Delta H^o_{298K} = 172.2 \ \frac{kJ}{mol} \qquad (5)$$

$$CH_4 + H_2O \leftrightarrow CO + 3H_2 \qquad \Delta H^o_{298K} = 206 \ \frac{kJ}{mol} \qquad (6)$$

The associated catalytic reaction rates over Ni/Al_2O_3 catalyst are extracted from literature (Benguerba et al., 2015; Jun et al., 2024a, 2024b; Palma et al., 2016). Typical parametric values were utilized in the simulation, which are planned to presented during the conference.

Reactor Configuration:
The reactor consists of three main sections, the inlet, catalyst bed (middle, blue colored), and the outlet. Of course, all three sections are assumed to be perfectly cylindrical in shape with straight line section separation from inlet and the catalyst bed, and catalyst bed and outlet. The diagram below shows the half-cross section view of the reactor. One has to notice that, dimensions appear for the inlet, outlet and catalyst bed are in fact the height and the radius (not the diameter) of the reactor tube. The quartz tube (reactor) is assumed to be 0.003 m in thickness in this study.

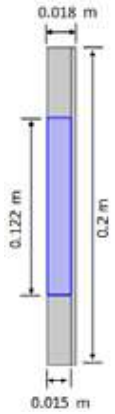


Figure 1: Reactor half cross-sectional view (configuration)

Model Assumptions
The assumptions postulated in this study can be listed as:

1. No catalyst deactivation: since the reaction temperature is relatively high, and the carbon deposition is expected to be very little because of the presence of remarkable (stoichiometric amounts needed for total reforming) amounts of the gasification agents.
2. Fully developed Laminar flow in inlet and outlet sections: since the average gas velocity through these two sections is not that high, and the residence time of the fluid phase is kind of enough, this assumption could be considered suitable.
3. The carbon deposition is affecting the porosity of the bed but not the catalytic activity of the solid material.
4. Uniform porosity distribution through the cross-sectional area of the bed (only changes with bed length as time goes on).
5. Uniform chemical species distribution (concentration) through the inlet
6. Constant some physical properties (such as heat capacity, enthalpy, entropy, thermal conductivity and binary diffusivities).

Model Parameters:
Standard chemical and physical properties of different materials were utilized in the simulation. Due to lack of space here, their values along with the reaction parameters will be presented during the conference.

III. Results and discussion:

As methane passes through the reactor, its concentration decreases as it reacts. When it reaches the catalyst bed, the flow characteristics change, primarily due to flow through porous media (Darcian flow). In this region, the concentration profile exhibits a slight increase, indicating that the bed provides some resistance to the flow. The nearly straight-line profiles at the inlet and outlet suggest the absence of reaction in these sections, as no catalyst is present there. Conversely, there isn't much change observed between 150 seconds and 30,000 seconds. Therefore, it could be inferred that a steady state is being reached after 150 seconds, as depicted in Figure 2. Furthermore, methane conversion is not particularly high, attributed to the relatively low reaction temperature of 650 °C (considered low for DRM) and the amount of catalyst used in this study, or in other words, the catalyst packing density.

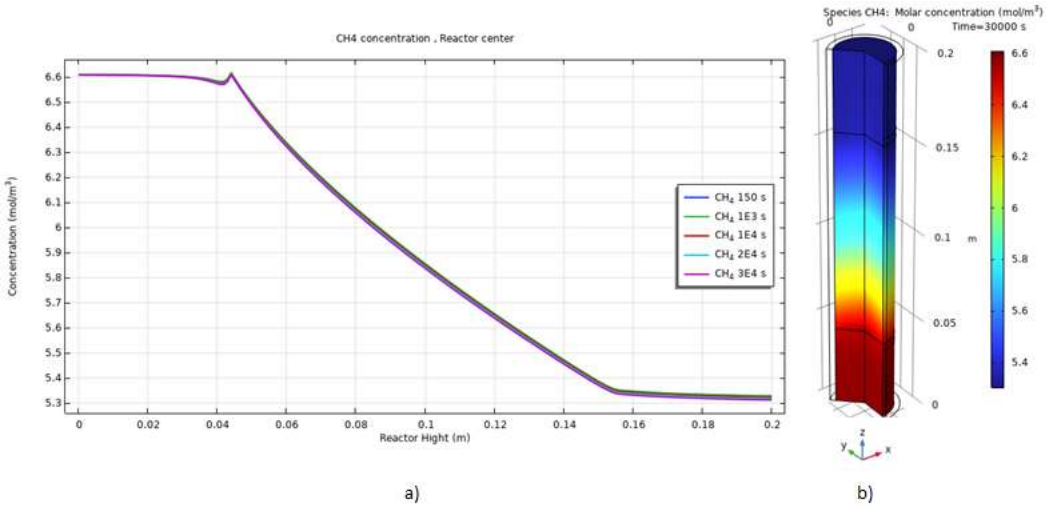


Figure 2: a) Methane concentration at the bed center at different times at 650 °C, b) Methane concentration throughout the reactor at steady state at 650 °C.

Despite the small amount of catalyst (approximately 0.026 grams) and the relatively low temperature, the hydrogen-to-carbon monoxide molar ratio is found to be promising, reaching a value of 0.6331. It is anticipated to increase significantly at higher temperatures and with a greater amount of catalyst. Figure 3 illustrates the H_2/CO molar ratio at the center of the reactor. It should be noted that the H_2/CO ratio may exhibit a maximum value at a certain point within the bed (slightly shown in figure 3 below) due to the involvement of various chemical reactions with complex rates in this process. This behavior is contingent upon the operating conditions, including the concentrations and flow rates of the inlet reactants, temperature, pressure and the catalyst amount.

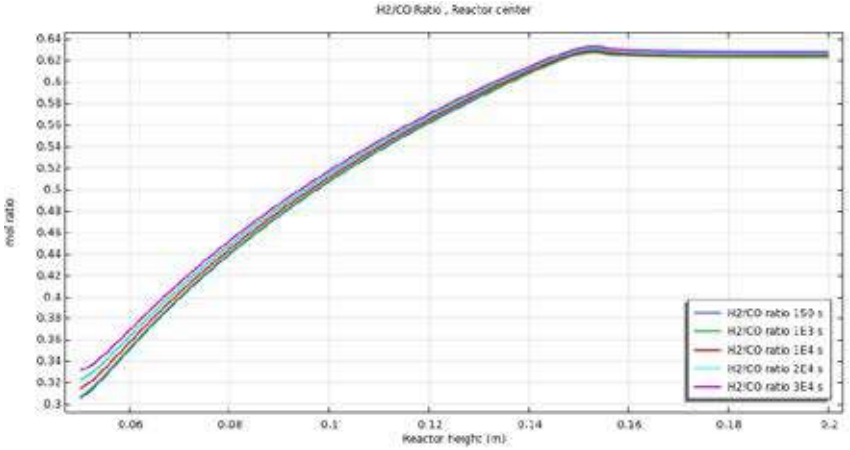


Figure 3: H_2/CO molar ratio at the bed center at 650 °C at different times.

A promising finding from this study is the very low magnitude of expected carbon deposition (in the range of 10^{-16} order of magnitude), as evaluated by the program. This opens the door to comparing the performance and durability of various catalysts for DRM. Moreover, it allows for optimizing the operating conditions to extend the catalyst lifetime significantly, especially if there are no other means of deactivation, or they are negligible. As indicated by the nature of the chemical reactions described above, all are endothermic. Therefore, it is intuitively expected that the temperature of the bed would be lower than its surroundings, as the reactions absorb energy. This expectation is further confirmed by the temperature distribution evaluated through simulation (not shown). As the reactants pass through the reactor, the temperature begins to increase again due to the continuous energy transfer from the tube surface, which is maintained at 650 °C, to the reactive fluid.

IV. Conclusion

Methane dry reforming holds promise as a technology for both hydrogen production and CO_2 conversion simultaneously. However, due to the numerous chemical reactions involved, each with its own complex reaction rates, analyzing reactor performance is highly challenging and requires sophisticated computer software. One significant challenge lies in understanding the kinetics and the impact of carbon deposition on catalyst activity, which directly influences the overall efficiency of the dry reforming process. Numerical simulation provides profound insights into the transient behavior of both the reactor and the catalyst. It aids in analyzing catalyst performance, guiding the development of suitable catalysts, and optimizing reactor configurations to achieve the desired goals of methane dry reforming.

Acknowledgements
This publication was made possible by NPRP grant (NPRP14S–0302–210011) from the Qatar National Research Fund (a member of Qatar Foundation). The statements made herein are solely the responsibility of the author(s).

References

Ahmad, T., & Zhang, D. (2020). A critical review of comparative global historical energy consumption and future demand: The story told so far. In *Energy Reports* (Vol. 6, pp. 1973–1991). Elsevier Ltd. https://doi.org/10.1016/j.egyr.2020.07.020

Alli, R. D., de Souza, P. A. L., Mohamedali, M., Virla, L. D., & Mahinpey, N. (2023). Tri-reforming of methane for syngas production using Ni catalysts: Current status and future outlook. *Catalysis Today*, *407*, 107–124. https://doi.org/10.1016/j.cattod.2022.02.006

Benguerba, Y., Dehimi, L., Virginie, M., Dumas, C., & Ernst, B. (2015). Modelling of methane dry reforming over Ni/Al2O3 catalyst in a fixed-bed catalytic reactor. *Reaction Kinetics, Mechanisms and Catalysis*, *114*(1), 109–119. https://doi.org/10.1007/s11144-014-0772-5

Friedlingstein, P., O'Sullivan, M., Jones, M. W., Andrew, R. M., Bakker, D. C. E., Hauck, J., Landschützer, P., Le Quéré, C., Luijkx, I. T., Peters, G. P., Peters, W., Pongratz, J., Schwingshackl, C., Sitch, S., Canadell, J. G., Ciais, P., Jackson, R. B., Alin, S. R., Anthoni, P., … Zheng, B. (2023). Global Carbon Budget 2023. *Earth System Science Data*, *15*(12), 5301–5369. https://doi.org/10.5194/essd-15-5301-2023

Johnson, D. R., Geldner, N. B., Liu, J., Baldos, U. L., & Hertel, T. (2023). Reducing US biofuels requirements mitigates short-term impacts of global population and income growth on agricultural environmental outcomes. *Energy Policy*, *175*. https://doi.org/10.1016/j.enpol.2023.113497

Jun, Y. B., Park, J. H., Kim, H. S., Jung, K. S., Yoon, S. P., & Lee, C. W. (2024a). A simulation model for ruthenium-catalyzed dry reforming of methane (DRM) at different temperatures and gas compositions. *International Journal of Hydrogen Energy*, *49*, 786–797. https://doi.org/10.1016/j.ijhydene.2023.07.199

Jun, Y. B., Park, J. H., Kim, H. S., Jung, K. S., Yoon, S. P., & Lee, C. W. (2024b). A simulation model for ruthenium-catalyzed dry reforming of methane (DRM) at different temperatures and gas compositions. *International Journal of Hydrogen Energy*, *49*, 786–797. https://doi.org/10.1016/j.ijhydene.2023.07.199

Osat, M., Shojaati, F., & Hafizi, A. (2023). A multi-objective optimization of three conflicting criteria in a methane tri-reforming reactor. *International Journal of Hydrogen Energy*, *48*(16), 6275–6287. https://doi.org/10.1016/j.ijhydene.2022.06.221

Palma, V., Ricca, A., Meloni, E., Martino, M., Miccio, M., & Ciambelli, P. (2016). Experimental and numerical investigations on structured catalysts for methane steam reforming intensification. *Journal of Cleaner Production*, *111*, 217–230. https://doi.org/10.1016/j.jclepro.2015.09.004

Soleimani, S., & Lehner, M. (2022). Tri-Reforming of Methane: Thermodynamics, Operating Conditions, Reactor Technology and Efficiency Evaluation—A Review. In *Energies* (Vol. 15, Issue 19). MDPI. https://doi.org/10.3390/en15197159

Accelerating Towards Hydrogen: A Qatar Scenario-Based Life Cycle Cost Comparison between Conventional, Electric, and Hydrogen Fuel Cell Vehicles

[1,2*]Carlos Méndez, [3]Brenno Castrillon Menezes, [2]Marcello Contestabile, [1]Yusuf Biçer,
[1]Division of Sustainable Development, College of Science and Engineering, Hamad Bin Khalifa University, Qatar Foundation, Education City, Doha, Qatar
[2]Qatar Environment and Energy Research Institute, Doha, Qatar
[3]Division of Engineering Management and Decision Sciences, College of Science and Engineering, Hamad Bin Khalifa University, Qatar Foundation, Education City, Doha, Qatar

*E-mail: CDelgado@hbku.edu.qa

Abstract

Qatar's primary mode of transportation are private cars, which represents a negative environmental impact. To mitigate this circumstance, the country has established electric vehicle goals to reduce fossil-fuels' exhausted gases while depending on hydrocarbon-based electricity. Hence, the present study analyzes the incorporation of hydrogen fuel cell vehicles (HFCVs) powered by clean hydrogen. For this approach, a life cycle cost (LCC) analysis compares conventional, electric, and hydrogen fuel cell vehicles. To do so, emissions are taken after tailoring a GREET model integrated to economic aspects to resemble Qatar's context. Results indicate that HFCVs' LCC starts as the least viable and gradually decreases the gap with conventional and electric vehicles along the decades. Moreover, applying a 20% purchase incentive and an 80% H_2 subsidy converts HFCVs into the most appealing option. Furthermore, ICEV taxation makes it less appealing than EVs and accelerates non-incentivized HFCVs parity by over a decade.

Keywords: Life Cycle Cost, Sustainable Transport, Hydrogen Fuel Cell Vehicle

I. Introduction

Today's conventional technologies for motor engine transportation currently meet the transport sector's growing demand despite their significant environmental footprint. Globally, in 2022, road transport represented 74% of the total emissions generated by the transport sector (International Energy Agency, 2023). Private cars, specifically, represent a substantial share of road transport in several regions and countries, like Qatar and the GCC, where it represents 67% of road transportation (UITP, 2021). To mitigate, Qatar launched the green car initiative, aiming to have an electric vehicle (EV) share of 4% by 2022 and 10% by 2030. Although this approach will reduce tailpipe emissions, the environmental impact of natural gas power plants for electricity production will remain. Hence, deploying other technologies, such as hydrogen fuel cell vehicles (HFCVs), must be considered.

Studies have been carried out to compare diverse vehicle technologies, including EVs with HFCVs. From a lifecycle assessment (LCA) perspective, it evidences that EVs present a higher environmental impact than HFCVs, mainly due to the battery manufacturing and disposal process (Bicer & Dincer, 2018). A lifecycle cost (LCC) analysis concluded that Plug-in Hybrid Electric Vehicle (PHEV) is the most adaptable option, given its fuel duality, followed by battery electric vehicles (BEVs). However, while considering the running cost, HFCVs present a better result (1 US$ lower) than BEVs, converting the former into a viable option in a near future (Offer et al., 2010). Complementary, while considering a future decline in hydrogen costs, HFCVs are projected to yield a better lifecycle economics outcome than conventional vehicles by 2035 (Wang et al., 2023).

The present study aims to account for both environmental and economic aspects to cover an LCC comparison analysis between HFCVs, BEVS, and internal combustion engine vehicles (ICEVs) within Qatar. It addresses existent literature gaps such a single parameter change comparison (e.g., environmental impact) or the non-inclusion of HFCVs in previous national studies. Moreover, policy instruments for HFCV adoption (e.g., purchase price incentive) are also considered to analyze their impacts on the LCC profile.

II. Methodology

LCC evaluates product's lifecycle cost while accounting for its environmental costs. To develop such an approach, diverse economic variables are considered; also, environmental parameters are variated inside the Greenhouse Gases, Regulated Emissions, and Energy Use in Transportation (GREET) model to calculate the outcomes. This grouping is used to carry out an ICEV-BEV-HFCV comparison of current and projected LCC profile. The approach is further used

to determine the main aspects that may be addressed to enable or accelerate HFCV adoption from end-users. To carry out this comparison the following LCC governing equation is used:

$$LCC = \frac{\left(PC_i - RV_{ij}\right)}{(1+r)^{j-1}} + \sum_{j=1}^{n}\left(\frac{FC_{ij} + MC_{ij} + EC_{ij} + WT_{ij}}{(1+r)^{j-1}}\right) \Big/ n.ADT_i \quad (1)$$

Where, PC is the vehicle purchase cost; RV, salvage price; FC, fuel cost; MC, maintenance and repair cost; EC, environmental cost; WT, water cost; n, maximum service life; ADT, annual distance traveled; r, discount rate; I, individual vehicle; j, particular year of service.

To execute the calculations, fuel, hydrogen, and electricity prices are assumed as indicated in Tab. 1. This is based on the national gasoline distribution company (WOQOD) data base, the middle east's hydrogen production (plus distribution) cost, and Kahramaa's (Qatar General Electricity & Water Corporation) listed electricity prices (Hydrogen Council, 2020; Massarweh et al., 2023; Nyangon et al., 2016; Rashid et al., 2019). By varying economic aspects ranging from HFCVs incentives (e.g., purchase price incentive and H_2 subsidy), to ICEVs purchase tax to disincentivize opting for conventional vehicles, potentially, a total of 648 scenarios are considered,

Tab. 1 Fuel Prices

Year	H_2 (US$/kg)		Traditional Fuels (US$/l)	Electricity (US$/kWh)
	Blue	Green	NG Power Plant	Solar Power Plant
2023	*8.60*	*8.73*	*0.030*	*0.049*
2030	*3.70*	*3.83*	*0.053*	*0.052*
2040	*2.90*	*3.00*	*0.079*	*0.077*
2050	*1.21*	*1.25*	*0.110*	*0.068*

For the environmental parameters, GREET is adjusted to resemble Qatar's context, considering combine-cycle natural gas turbine plants and centralized solar power plants for electricity production, steam methane reforming for H_2 production, a fuel distribution distance equivalent to the length between the Ras Laffan and the WOQOD fuel depot location, and a water production cost of 1.135 US$/m^3 (Saleem et al., 2023).

III. Results and discussions

Analyzing the scenarios that consider blue H2 and electricity from NG power plants, initial results in which no incentive or tax are considered indicate that ICEVs present the best LCC value, as showcased in Fig. 1. On the other hand, HFCVs present the least favorable outcome in the initial years; however, this technology gets positive since the gap with the other ICEVs and BEVs decreases. Eventually, HFCVs become more competitive, from an LCC perspective, that ICEVs and BEVs within a five-year stretch, between 2046 and 2050. Moreover, the simulation branch associated with green H_2 and renewable energy resembles Fig. 1 trend, with HFCVs closing the gap in a slower rate given the increase in green hydrogen production costs.

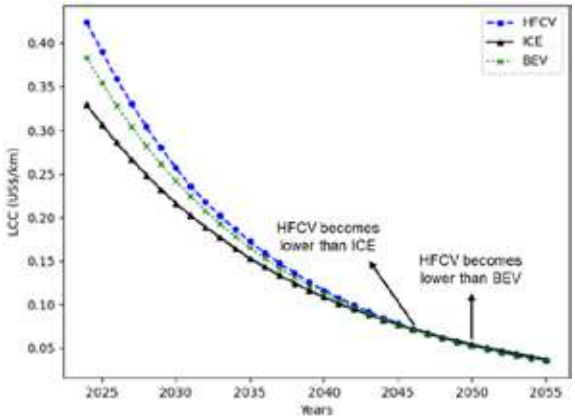


Fig. 1 LCC Comparison, Scenario Tree Lower branch (without incentives or taxes)

The implementation of incentives can accelerate the HFCV adoption process, Fig. 2(a) shows how several approaches influence the HFCV's LCC value, being the combination of the most aggressive fuel subsidy and purchase price incentive the most influential. Fig. 2(b) illustrates how the implementation of the combination approach immediately converts HFCV LCC's into the lowest value.

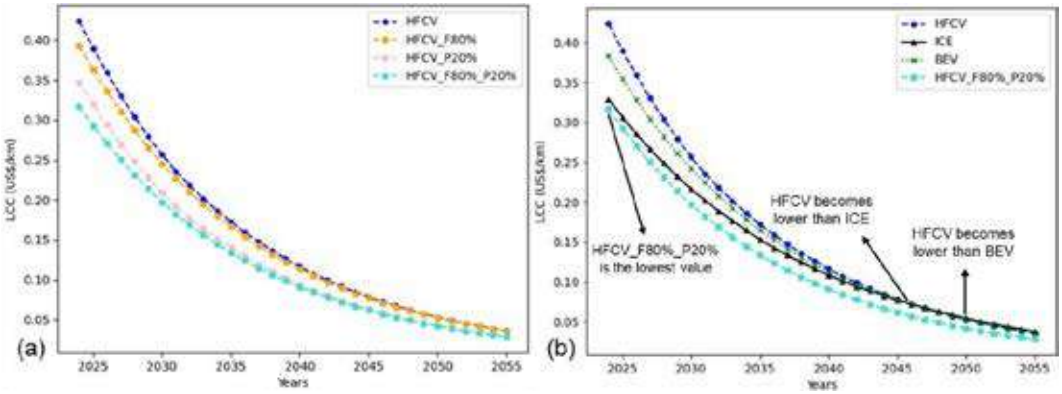


Fig. 2 Incentives Influence: (a) Diverse incentives impact on HFCVs; (b) Base case vs HFCV with 80% fuel discount and 20% Purchase Price

While aiming to disincentivize ICEVs use, Fig. 3 shows how the implementation of a 40% purchase and 30% emission taxes, increases ICEV's LCC, making it less appealing than EVs and acerating the intersection with HFCVs by over a decade.

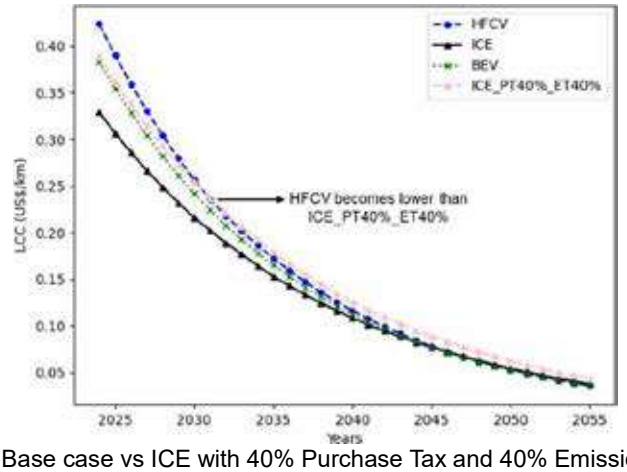


Fig. 3 Base case vs ICE with 40% Purchase Tax and 40% Emission Tax

IV. Conclusions

This study incorporates environmental and economic aspects into an LCC analysis. The approach highlights how, without applying any policy instrument, HFCVs powered by blue H_2 starts out as the least viable option, and, with time, closes the gap with the other technologies. While incorporating a 20% purchase price incentive, 80% H_2 subsidy, HFCVs LCC immediately becomes the lowest value. Moreover, while only addressing ICEVs via a 40% and 30% purchase and emission tax, its LCC value is immediately higher than the EV's result, while HFCVs parity is gained over a decade faster than in the original case.

Acknowledgements

The authors acknowledge the support provided by the Hamad Bin Khalifa University, Qatar Foundation, Qatar (210008390)

References

Bicer, Y., & Dincer, I. (2018). Life cycle environmental impact assessments and comparisons of alternative fuels for clean vehicles. Resources, Conservation and Recycling, 132, 141–157. https://doi.org/10.1016/J.RESCONREC.2018.01.036

Hydrogen Council. (2020). Path to hydrogen competitiveness A cost perspective. www.hydrogencouncil.com.

International Energy Agency. (2023). Transport - Energy System. https://www.iea.org/energy-system/transport

Massarweh, O., Al-khuzaei, M., Al-Shafi, M., Bicer, Y., & Abushaikha, A. S. (2023). Blue hydrogen production from natural gas reservoirs: A review of application and feasibility. Journal of CO2 Utilization, 70, 102438. https://doi.org/10.1016/J.JCOU.2023.102438

Nyangon, J., Byrne, J., & Taminiau, J. (2016). An assessment of price convergence between natural gas and solar photovoltaic in the U.S. electricity market. https://doi.org/10.1002/wene.238

Offer, G. J., Howey, D., Contestabile, M., Clague, R., & Brandon, N. P. (2010). Comparative analysis of battery electric, hydrogen fuel cell and hybrid vehicles in a future sustainable road transport system. Energy Policy, 38(1), 24–29. https://doi.org/10.1016/J.ENPOL.2009.08.040

Rashid, K., Safdarnejad, S. M., Ellingwood, K., & Powell, K. M. (2019). Techno-economic evaluation of different hybridization schemes for a solar thermal/gas power plant. Energy, 181, 91–106. https://doi.org/10.1016/J.ENERGY.2019.05.130

Saleem, H., Abounahia, N., Siddiqui, H. R., & Zaidi, S. J. (2023). Qatar desalination research: An overview. Desalination, 564, 116802. https://doi.org/10.1016/J.DESAL.2023.116802

UITP. (2021). MENA TRANSPORT REPORT 2020/2021.

Wang, B., Li, Z., Zhou, J. X., Cong, Y., & Li, Z. (2023). Technological-economic assessment and optimization of hydrogen-based transportation systems in China: A life cycle perspective. International Journal of Hydrogen Energy, 48(33), 12155–12167. https://doi.org/10.1016/J.IJHYDENE.2022.12.189

Retrofitting Analysis of LNG FSRU with On-Board Ammonia and Hydrogen Storage Tanks

Dindha Andriani*, Omer Abedrabboh, Yusuf Bicer
Division of Sustainable Development, College of Science and Engineering,
Hamad Bin Khalifa University, Qatar Foundation, Education City, Doha, Qatar

Emails: dian17620@hbku.edu.qa*, omab33742@hbku.edu.qa, ybicer@hbku.edu.qa

Abstract
Natural gas, a versatile and extensively utilized fossil fuel, has been influential in meeting global energy demands for many years. It is renowned for its efficiency, relatively lower carbon emissions than other fossil fuels, and its role in ensuring energy security. However, as concerns about climate change and environmental sustainability intensify, a growing imperative exists to transition towards more renewable and low-carbon energy carriers. This study conducts a comprehensive retrofitting analysis of Liquefied Natural Gas (LNG) Floating Storage and Regasification Units (FSRUs) for on-board storage of emerging renewable energy carriers—ammonia and hydrogen. The primary focus lies in assessing the viability of modifying the existing LNG storage tank to suit these carriers by examining the storage tank materials, heat ingress within layers, and the Boil-Off Gas (BOG) from LNG, ammonia, and hydrogen. Results indicate that hydrogen exhibits the highest total daily BOG (1.03%), followed by LNG (0.57%) and ammonia (0.17%). Essential parameters such as thermodynamic conditions, storage tank design, and BOG management are examined to evaluate the feasibility of this innovative approach.

Keywords: Alternative Fuels, Boil-Off Gas, Heat Analysis, Maritime Sustainability, Storage Design.

I. Introduction

Initially designed for LNG handling, FSRUs present as a viable alternative. It has witnessed significant growth, with 34 vessels operational, serving as terminals or tankers. These vessels' total storage capacities and daily consumption volumes range from 125,000 to 170,000 m^3 and 240 to 750 million standard $feet^3$ per day, respectively (Hays, 2021). However, the carbon footprint associated with LNG transport underscores the need for more sustainable energy carriers. Transitioning existing LNG terminals to accommodate climate-neutral energy carriers such as liquid hydrogen (LH_2) or liquid ammonia (LNH_3) presents logistical and technical challenges. While LH_2 offers superior energy density, its extremely low boiling point necessitates substantial thermal insulation modifications. Conversely, LNH_3 boasts better physical characteristics in terms of boiling temperature but presents handling and safety challenges due to its toxicity. Material compatibility remains a critical consideration in terminal conversion projects, with a significant portion of the investment cost tied to storage tank construction. Steel material selection plays a pivotal role, with certain alloys suitable for ammonia or hydrogen applications. If LH_2-compatible steel is utilized in the storage tank's construction and a greater boil-off rate is acceptable, around half of the LNG investment cost might be reused with LH_2 (Riemer et al., 2022). As of now, there is no previous research on regasification and storage vessels in this area which covers retrofication storage tank for renewable energy carriers.

II. System Design Integration and Analysis

Key considerations entail assessing compatibility between existing FSRU infrastructure and the requirements for ammonia and hydrogen storage, addressing material compatibility, heat transfer analysis, and implementing a robust Boil-Off Gas (BOG) recovery system. As shown in *Fig 1,* the retrofit design encompasses tank materials, insulation systems, heat transfer methods, and optimal operating conditions to ensure compatibility, structural integrity, and efficiency. The three energy carries require well-insulated storage tanks to sustain low-temperature storage in tanks before loading.

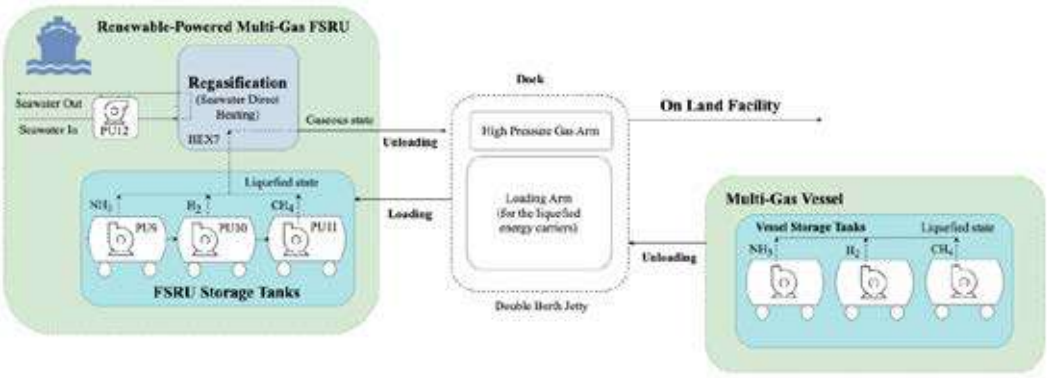


Fig 1. Schematic diagram of the storage tanks inside FSRU

The European Maritime Safety Agency (EMSA)'s case study on integrating ammonia fuel tanks into large ships explored general type C cylindrical while the first ship to successfully transport hydrogen from Japan to Australia,

Suiso Frontier, employed the spherical shape for storing liquid hydrogen during voyage. *Fig 2* illustares the typical shape of ammonia and hydrogen storage tank using COMSOL Multiphysics simulator. (Al-Breiki & Bicer, 2020)'s study indicates ammonia's lower BOG than LNG, thus requiring less insulation for ammonia tanks, especially in long-distance transportation. Furthermore, recent research by (Machaj et al., 2022) examined the compatibility of LNG Type C cryogenic tanks with ammonia, finding that LNG tanks likely support ammonia storage due to their chromium-rich austenitic stainless-steel composition (such as SS316L and SS304). On the other hand, due to its extremely lower temperature, hydrogen tank requires more insulation layers. Cross-section area of the storage tanks and their properties are shown in *Fig 3* and *Tab 1*, respectively.

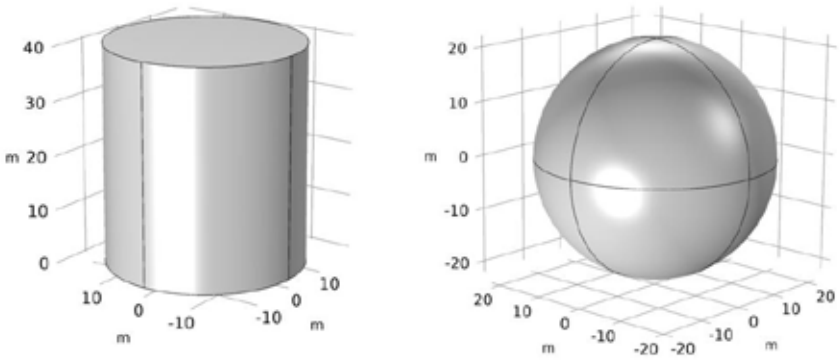


Fig 2. Storage tank shapes for (left) liquid ammonia and (right) liquid hydrogen of volume 40,000 m3

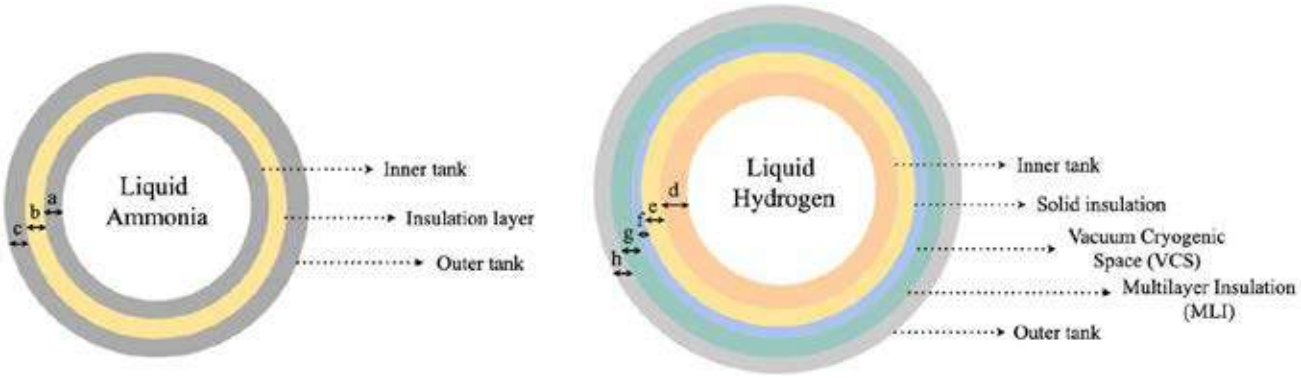


Fig 3. Structure diagram of a conventional cryogenic storage tank for (left) ammonia and (right) hydrogen

Tab 1. Materials and thermophysical properties of each layer in ammonia and hydrogen storage tank. λ is thermal conducticity, ρ is density, Cp is specific heat capacity at constant pressure, and Th is layer thickness.

Tank layers	**Ammonia storage tank**		**Hydrogen storage tank**	
	Material	**Thermophysical properties**	**Material**	**Thermophysical properties**
Inner tank	(a) Carbon-steel	λ = 23 W/(m·K) ρ = 7850 kg/m3 Cp = 0.47 kJ/(kg·K) Th = 0.12 m	(d) Carbon fiber reinforced polymers	λ = 0.2 W/(m·K) ρ = 2000 kg/m3 Cp = 1.0 kJ/(kg·K) Th = 0.5 m
Insulation layer	(b) Polyurethane foam	λ = 0.02 W/(m·K) ρ = 40 kg/m3 Cp = 1.3 kJ/(kg·K) Th = 0.1 m	(e) Polyurethane foam	λ = 0.02 W/(m·K) ρ = 40 kg/m3 Cp = 1.3 kJ/(kg·K) Th = 0.1 m
			(f) VCS (air)	λ = 0.03 W/(m·K) ρ = 60 kg/m3 Cp = 2.0 kJ/(kg·K) Th = 0.02 m

			(g) MLI (alluminium)	λ = 0.01 W/(m·K) ρ = 45 kg/m3 Cp = 0.3 kJ/(kg·K) Th = 0.1 m
Outer tank	(c) Carbon-steel	λ = 23 W/(m·K) ρ = 7850 kg/m3 Cp = 0.47 kJ/(kg·K) Th = 0.007 m	(h) Stainless steel	λ = 20 W/(m·K) ρ = 7850 kg/m3 Cp = 0.47 kJ/(kg·K) Th = 0.07 m
Tank dimensions	Volume: 40,000 m^3 (vertical cylinder) Radius: 17.84 m Height: 40 m		Volume: 40,000 m^3 (spherical) Diameter: 42.44 m	

In addition, a particular emphasis is placed on strategies to harness the latent energy within BOG, further aligning the retrofit with sustainable energy practices. BOG during the storage phase calculation is shown in *Equation (1).* Whereas during un/loading is evaluated by the formula in *Equation (2)*. These formulas were used to examine the corresponding BOG generation due to heat transfer within the tank layers using the Engineering Equation Solver (EES) software (Klein & Alvarado, 2024).

$$BOG_{Storage(onboard)} = \frac{\text{Evaporated Energy}}{\text{Stored Energy}} = \frac{\frac{Q}{\Delta H_{vap}}}{\frac{\rho \cdot V \cdot \text{No. tanker}}{t_S \cdot 3600}} \quad (1)$$

Where Q is the energy content of the energy carrier, ΔH_{vap} is the vaporization rate, ρ is the density, V is the tanker volume, and t_s is storage time in hour.

$$BOG_{Loading/Unloading} = \frac{(t_l \cdot Hc_t) + (c_p \cdot M_h)(T_h - T_c)}{\Delta H_{vap}} \quad (2)$$

Where t_l is loading/unloading time in hour, Hc_t is the tanker heat capacity, c_p is the specific heat at constant pressure, M_h is the heel mass, T_h is the heel temperature, and T_c is the energy carrier temperature.

III. Results and Discussion

This section examines the effect of heat transfer due to the temperature difference within layers between the ambient and the cryogenic temperature of the liquid containment. Examining the tank temperature gradient at the 72-hour mark (assuming a max of 3-day storage time) in the XZ cut plane, as shown in *Fig 4* is essential for evaluating the thermal distribution within the tank. This gradient serves as a pivotal indicator of heat dispersion influencing the generation of BOG.

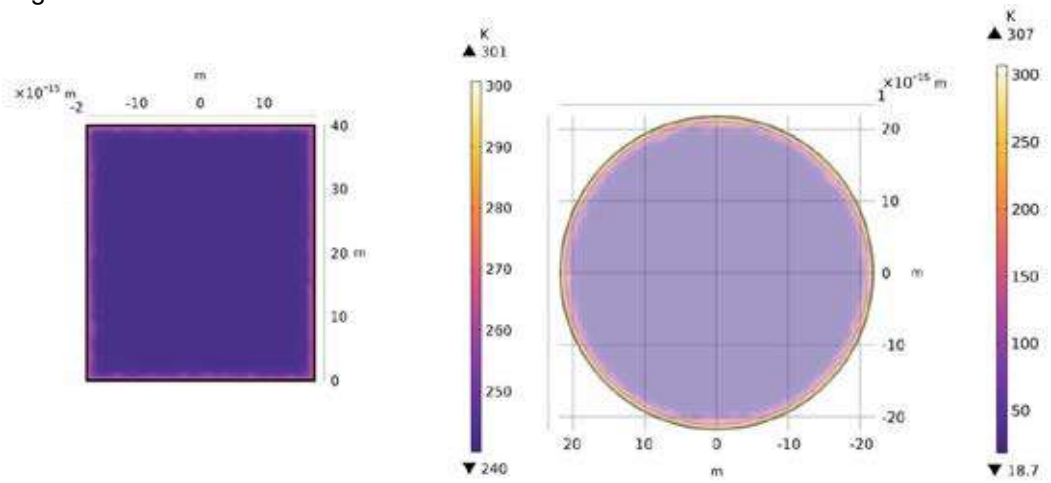


Figure 4. Tank temperature gradient at 72h in XZ cut plane for (left) ammonia and (right) hydrogen

Simultaneously, analyzing the heat ingress and temperature fluctuations over time, as shown in *Fig 5* allows for a deeper understanding of thermal behavior within the storage system. Thermal conductivity and insulation properties of the tank material play a critical role in determining the extent of heat ingress and, consequently, BOG generation.

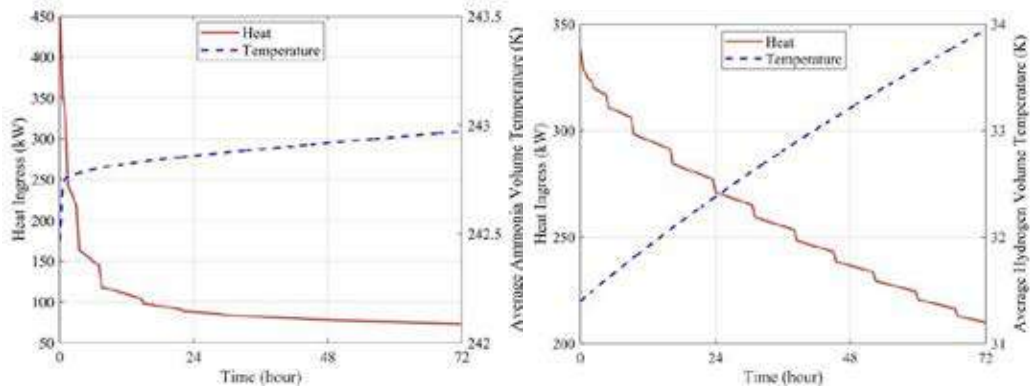


Figure 5. Heat ingress and temperature of (left) ammonia and (right) hydrogen with time

A sensitivity analysis evaluated various parameters' impact on BOG rates for energy carriers. With longer on-board storage times, total BOG rises as shown in *Fig. 6*. Increased temperature within the storage tank, caused by surrounding heat ingress over time, leads to higher BOG rates due to greater heat availability for vaporization. This results in reduced liquid mass in the tank, as BOG generation is inversely proportional to the final mass.

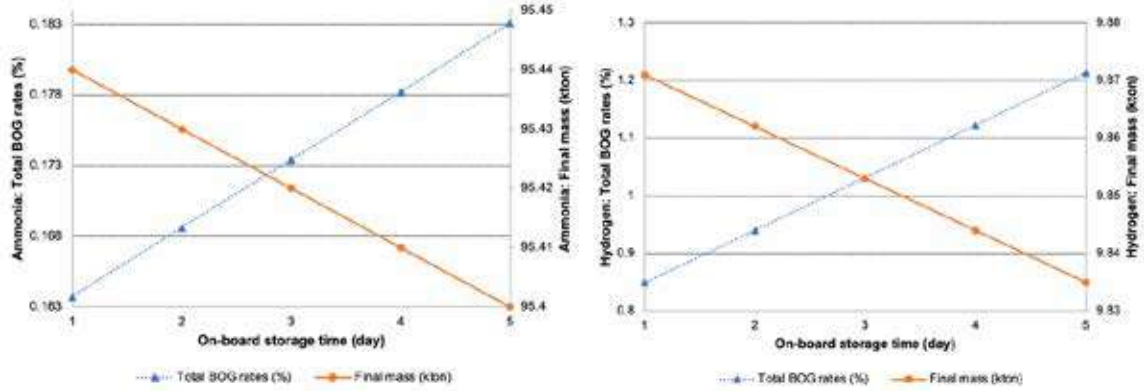


Figure 6. Effect on storage time on total BOG generated and final mass before offloading for (left) ammonia and (right) hydrogen

IV. Conclusions

The integration of ammonia and hydrogen as renewable energy sources within the LNG FSRU framework signals a significant step toward a decarbonized energy future. Essential parameters such as the specific heat capacity, thermal conductivity, and heat transfer coefficients possess a significance in determining the efficiency of storage systems. Sensitivity analysis, particularly focusing on ammonia and hydrogen, underscores the profound impact of onboard storage duration on BOG generation. Prolonged storage duration results in a gradual increase in total BOG and a decrease in offloading mass due to rising temperatures within the storage tank, induced by external heat ingress. Thermodynamic analysis extracted from EES software reveals hydrogen's highest daily BOG rate, requiring further exploration into heat transfer analysis within storage tanks, enhancing retrofit efficiency and environmental sustainability.

Acknowledgments

This publication was made possible by the Graduate Sponsorship Research Award (GSRA9-L-1-0530-22062) from the Qatar National Research Fund (a member of Qatar Foundation) and Hamad Bin Khalifa University (210017620). The findings herein reflect the work and are solely the authors' responsibility.

References

Al-Breiki, M., & Bicer, Y. (2020). Investigating the technical feasibility of various energy carriers for alternative and sustainable overseas energy transport scenarios. *Energy Conversion and Management*, *209*(February), 112652. https://doi.org/10.1016/j.enconman.2020.112652

Hays. (2021). *Navigating the new world of work*. Annual Report and Accounts. https://www.aa.com.tr/en/energy/analysis/navigating-the-new-world-of-fsru/13942

Klein, S. A., & Alvarado, F. (2024). *Engineering Equation Solver, version 10.792, F-Chart Software*.

Machaj, K., Kupecki, J., Malecha, Z., Morawski, A. W., Skrzypkiewicz, M., Stanclik, M., & Chorowski, M. (2022). Ammonia as a potential marine fuel: A review. *Energy Strategy Reviews*, *44*(September), 100926. https://doi.org/10.1016/j.esr.2022.100926

Riemer, M., Schreiner, F., & Wachsmuth, J. (2022). Conversion of LNG Terminals for Liquid Hydrogen or Ammonia - Analysis of Technical Feasibility under Economic Considerations. *Fraunhofer Institute for Systems and Innovation Research ISI, Karlsruhe, Germany*.

Enhancing Photocatalytic Partial Oxidation of Methane to Methanol: Experimental Investigation of 2D and Oxide Catalysts

[1*]Amira Chebbi, [2]Alessandro Sinopoli, [2]Ahmed Abotaleb,[1]Yusuf Bicer
[1]Division of Sustainable Development, College of Science and Engineering, Hamad Bin Khalifa University, Qatar Foundation, Doha, Qatar
[2]Qatar Environment and Energy Research Institute, Hamad Bin Khalifa University, P.O. Box 34410, Qatar Foundation, Doha, Qatar

* E-mail: amch51864@hbku.edu.qa

Abstract
As the global population expands, so does the need for energy, posing a growing challenge. Reliance on fossil fuels, which release greenhouse gases such as carbon dioxide (CO_2) and methane (CH_4) during combustion, intensifies environmental concerns, underscoring the urgency for sustainable energy solutions. Converting photocatalytic methane to methanol at high yields remains a significant challenge. This study investigates the photoactivity and selectivity of photocatalysts toward the desired product methanol. Two pristine photocatalysts, $W_{18}O_{49}$ and g-C_3N_4, along with two of their respective composites ($W_{18}O_{49}$ (0.3)/g-C_3N_4 and $W_{18}O_{49}$ (0.6)/g-C_3N_4), were synthesized and analyzed using SEM technique. The photocatalytic test was conducted to assess their performance. The reaction products are analyzed using gas chromatography. When $W_{18}O_{49}$ was coupled with g-C_3N_4, the yield of methanol increased. Among the four catalysts tested, $W_{18}O_{49}$(0.3)/g-C_3N_4 demonstrated the highest methanol yield (62.3 μmol g^{-1} h^{-1}) under visible light and 100% selectivity towards methanol. These findings highlight the potential of catalyst composites in enhancing the selectivity and efficiency of methane conversion to methanol.

Keywords: Methane photo-conversion, green energy carrier, tungsten oxide, graphitic carbon nitride, solar energy

I. Introduction

The emission of greenhouse gases like carbon dioxide (CO_2) and methane (CH_4) contributes to global warming and climate change. Human activities such as burning fossil fuels and deforestation have escalated CO_2 levels in the atmosphere, leading to more frequent and prolonged natural disasters like droughts, heat waves, floods, wildfires, and acid rain. Statistics reveal a global land and ocean surface temperature rise of 0.85°C from 1880 to 2012, along with an average global sea level increase of 0.19 meters (Hansen et al., 2013). CH_4 represents the predominant constituent of natural gas and has gained considerable traction as a fuel source due to its superior mass heat relative to other hydrocarbons. CH_4 is also a potent greenhouse gas, with a global warming potential (GWP) about 28-36 times higher than CO_2 over a 100-year timeframe, making it a significant contributor to climate change. Methanol (CH_3OH) is a widely used chemical in several industrial applications and processes. It is a valuable alternative fuel to LPG, gasoline, and gas oil (Spadaro et al., 2018). Its ease of handling, storage, and transportation makes it a more advantageous energy carrier compared to hydrogen (H_2). Additionally, CH_3OH has several chemical derivatives.

The photocatalytic partial oxidation (P-POM) of CH_4 involves using CH_4 as a raw material and an additional oxygen source, such as oxygen or hydrogen peroxide. Through a series of steps facilitated by light, this process converts CH_4 into CH_3OH (Chebbi et al., 2023). This innovative approach offers an alternative method for producing CH_3OH at ambient temperatures and pressures, potentially utilizing solar light and significantly reducing energy requirements. Consequently, it helps mitigate greenhouse gas emissions released into the atmosphere. Photocatalytic reactions are comprised of three steps: Light absorption, charge separation, and product formation. During light absorption, photons are absorbed, and the subsequent charge separation results in the excitation of electrons from the valence band to the conduction band, creating positively charged holes. In the final step, product formation occurs through a redox reaction (Ran et al., 2018). Several studies are exploring the utilization of Graphitic carbon nitride (g-C_3N_4) and tungsten oxide ($W_{18}O_{49}$) in photocatalysis due to their unique properties. g-C_3N_4 is the most stable carbon nitride allotrope, capable of absorbing visible light and maintaining stability even under high temperatures and chemical exposure. Additionally, it is non-toxic, abundantly available, and easily prepared (Han et al., 2021). On the other hand, $W_{18}O_{49}$'s high photocatalytic performance can be attributed significantly to two key factors: the localized surface plasmon resonance (LSPR) effect and the presence of oxygen vacancies (Zhou et al., 2023).

This work examines the photoactivity and selectivity of catalysts for photocatalytic partial oxidation of CH_4 to CH_3OH, focusing on four synthesized and analyzed catalysts.

II. Experimental Setup and Procedure

The synthesis of $W_{18}O_{49}$/g-C_3N_4 involved several steps to prepare high-quality materials for photocatalytic applications. Firstly, to prepare pristine $W_{18}O_{49}$, a 15 mM solution of tungsten hexachloride (WCl_6) was prepared by dissolving 2.9 g of WCl_6 in 50 mL of ethanol, followed by thorough mixing to achieve homogeneity. This solution was then transferred to a Teflon-lined autoclave and heated at 200°C for 24 hours to facilitate the reaction. The

resulting solid product was washed with ethanol through centrifugation and dried at 80°C to obtain the desired product.

Simultaneously, 4.0 g of melamine was subjected to controlled heating at 550°C in a tubular furnace to initiate thermal treatment. To synthesize $W_{18}O_{49}$/g-C_3N_4, a solution was prepared by dissolving 2 g of melamine in 20 mL of deionized water, followed by adding 0.6 g of $W_{18}O_{49}$. The mixture was stirred for 30 minutes to ensure homogeneity and then heated to remove excess water content. The resulting solid was dried at 80°C and annealed at 550°C for 4 hours to enhance material properties.

An alternative method for $W_{18}O_{49}$/g-C_3N_4 preparation involved grinding 500 mg of melamine and 300 mg of $W_{18}O_{49}$ together until achieving a homogeneous blue color. The mixture was then heated in a tubular furnace at a gradual temperature increase until reaching 450°C.

For photocatalytic testing, the synthesized material was dispersed in a stainless-steel reactor containing 60 mL of deionized water and 40 mL of diluted hydrogen peroxide. The reactor was purged with CH_4 for 30 minutes to remove residual oxygen and other contaminants before being sealed and saturated with CH_4 (purity 99.999%) for 15 minutes. The photoreaction was conducted under visible light for 2 hours (400-700 nm), and the resulting liquid solution was processed through Gas Chromatography (GC) analysis for evaluation.

Scanning electron microscopy (SEM) was performed by (FEI Quanta650FEG SEM) for imaging to investigate surface morphology. Additionally, the liquid Samples were analyzed for the quantification of CH_3OH by Agilent 7890B GC system equipped with a flame ionization detector (FID) and headspace sampling system.

III. Results and discussion

The SEM analysis was utilized to investigate the morphology of pristine $W_{18}O_{49}$ and g-C_3N_4 and their composites. g-C_3N_4 exhibits a smooth layered structure with flakes reminiscent of graphite. In contrast, $W_{18}O_{49}$ displays a spherical nanoparticle morphology, as illustrated in Fig.1b. The combined composite, $W_{18}O_{49}$ (0.3)/g-C_3N_4, exhibits a new distinct morphology, as shown in Fig.1c. The morphology cannot be assigned to either the layered structure of g-C_3N_4 or the spherical structure of $W_{18}O_{49}$. The composite SEM image of $W_{18}O_{49}$ (0.6)/g-C_3N_4, as depicted in Fig. 1d, reveals distinct regions predominantly occupied by $W_{18}O_{49}$ and g-C_3N_4 while maintaining the original morphology of the pristine materials.

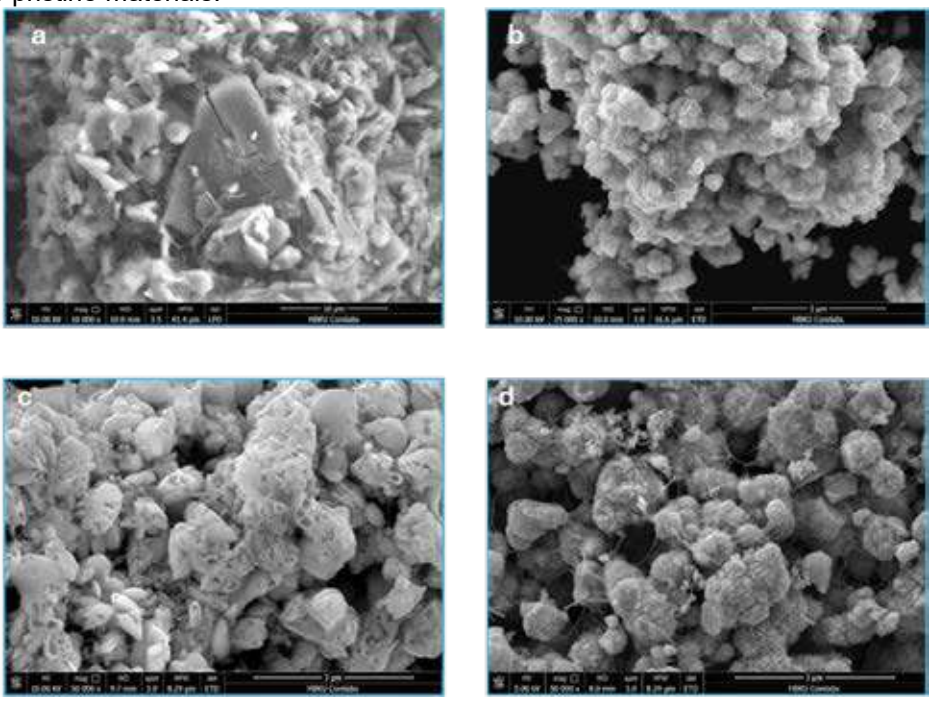


Fig. 1: SEM images of (a) g-C_3N_4, (b) $W_{18}O_{49}$, (c) $W_{18}O_{49}$ (0.3)/g-C_3N_4, (d) $W_{18}O_{49}$ (0.6)/g-C_3N_4

Tab. 1: catalytic activity of synthesized catalysts.

Catalyst	Light Source	Methanol yield (μmol/g*h)	Methanol selectivity %
g-C_3N_4	Visible	13.130	82.018
$W_{18}O_{49}$	Visible	16.066	42.129
$W_{18}O_{49}$(0.6)/g-C_3N_4	Visible	62.294	100.000
g-C_3N_4(0.3)/$W_{18}O_{49}$	Visible	5.476	31.007

In the catalytic evaluation presented in Tab. 1, the pristine catalysts $W_{18}O_{49}$ and g-C_3N_4 demonstrated significant catalytic activity, with values of 16.1 μmol g^{-1} h^{-1} and 13.1 μmol g^{-1} h^{-1} emphasizing its remarkable sensitivity to visible light. Several studies have revealed that g-C_3N_4 exhibits inefficient absorption of visible light (below 460 nm), and a limited specific surface area (approximately 10 m^2g^{-1}) contribute to a low photocatalytic efficiency when exposed to visible light (Cao et al., 2022; Zeng et al., 2022). The composite $W_{18}O_{49}$(0.3)/g-C_3N_4 demonstrated a catalytic activity of 62.3 μmol g^{-1} h^{-1}, emphasizing collaborative interactions between the components for enhanced visible light utilization and increased catalytic performance. g-C_3N_4(0.3)/$W_{18}O_{49}$ exhibited a catalytic activity of 5.5 μmol g^{-1} h^{-1} under visible light, suggesting the influence of varying synthetic protocols on the composite catalyst's performance. This divergence in catalytic behavior can be attributed to variations in catalyst morphologies and differences in the distribution of elements. The research examined the selectivity for the formation of the reaction product CH_3OH under visible light exposure. Composite $W_{18}O_{49}$(0.6)/g-C_3N_4 exhibited absolute selectivity towards CH_3OH, showing a 100% preference, whereas g-C_3N_4(0.3)/$W_{18}O_{49}$ displayed a selectivity value of 30%. The diverse catalytic activities observed among the individual catalysts and their composite counterparts highlight the importance of catalyst selection and synthesis methods in optimizing the performance of the photocatalytic process.

IV. Conclusions

Photocatalytic partial oxidation of CH_4 to CH_3OH is a sustainable process that converts CH_4, a potent greenhouse gas, to produce CH_3OH, a H_2 carrier. To implement this process, an experimental setup and protocol must be established. Additionally, the development of catalysts with high activity and stability is required. g-C_3N_4 is non-toxic, readily available, easy to prepare, and holds significant promise for composite materials. $W_{18}O_{49}$ reaction sites enhance the separation of photogenerated carriers and improve light absorption compared to WO_3 due to the LSPR effect and oxygen vacancies The following primary outcomes are obtained from the experimental study: Two pristine photocatalysts, $W_{18}O_{49}$ and g-C_3N_4, along with two of their respective composites ($W_{18}O_{49}$ (0.3)/g-C_3N_4, $W_{18}O_{49}$ (0.6)/g-C_3N_4), were synthesized and analyzed using SEM. In the catalytic evaluation, pristine $W_{18}O_{49}$ and g-C_3N_4 yielded CH_3OH with 16.1 μmol g^{-1} h^{-1} and 13.1 μmol g^{-1} h^{-1} under visible light, respectively. Furthermore, the highest CH_3OH yield among the four catalysts was achieved by $W_{18}O_{49}$(0.3)/g-C_3N_4 (62.3 μmol g^{-1} h^{-1}). The study investigated the selectivity towards the reaction product CH_3OH under visible light exposure, where $W_{18}O_{49}$(0.6)/g-C_3N_4 demonstrates absolute selectivity towards CH_3OH, displaying a 100% preference.

Acknowledgment

The authors acknowledge the support provided by Hamad Bin Khalifa and the Qatar Environment and Energy Research Institute for their assistance, as well as Core Labs' support in characterization studies. Additionally, we extend our appreciation to Dr. Muhammed Anwar for his valuable contributions to GC analysis and results.

References

Cao, A., Zhang, M., Su, X., Romanovski, V., & Chu, S. (2022). In Situ Fabrication of NiS2-Decorated Graphitic Carbon Nitride/Metal-Organic Framework Nanostructures for Photocatalytic H2Evolution. *ACS Applied Nano Materials*, *5*(4), 5416–5424. https://doi.org/10.1021/acsanm.2c00417

Chebbi, A., Sinopoli, A., Abotaleb, A., & Bicer, Y. (2023). Photocatalytic conversion of carbon dioxide, methane, and air for green fuels synthesis. *Catalysis Science & Technology*. https://doi.org/10.1039/D3CY00675A

Han, C., Su, P., Tan, B., Ma, X., Lv, H., Huang, C., Wang, P., Tong, Z., Li, G., Huang, Y., & Liu, Z. (2021). Defective ultra-thin two-dimensional g-C3N4 photocatalyst for enhanced photocatalytic H2 evolution activity. *Journal of Colloid and Interface Science*, *581*, 159–166. https://doi.org/10.1016/J.JCIS.2020.07.119

Hansen, J., Sato, M., Russell, G., & Kharecha, P. (2013). Climate sensitivity, sea level and atmospheric carbon dioxide.

Philosophical Transactions of the Royal Society A: Mathematical, Physical and Engineering Sciences, *371*(2001). https://doi.org/10.1098/RSTA.2012.0294

Ran, J., Jaroniec, M., & Qiao, S. Z. (2018). Cocatalysts in Semiconductor-based Photocatalytic CO2 Reduction: Achievements, Challenges, and Opportunities. *Advanced Materials*, *30*(7), 1704649. https://doi.org/10.1002/ADMA.201704649

Spadaro, L., Arena, F., & Palella, A. (2018). Which Future Route in the Methanol Synthesis? Photocatalytic Reduction of CO2, the New Challenge in the Solar Energy Exploitation. In *Methanol: Science and Engineering*. Elsevier B.V. https://doi.org/10.1016/B978-0-444-63903-5.00016-9

Zeng, G., Duan, M., He, J., Ge, F., & Wang, W. (2022). Sulfate doped graphitic carbon nitride with enhanced photocatalytic activity towards degradation of methylene blue. *Materials Letters*, *309*, 131310. https://doi.org/10.1016/j.matlet.2021.131310

Zhou, Z., Tang, R., Li, L., Xiong, S., Zeng, H., Zheng, J., Gong, D., Huang, Y., & Deng, Y. (2023). W18O49-based photocatalyst: Enhanced strategies for photocatalysis employment. *Separation and Purification Technology*, *319*, 124028. https://doi.org/10.1016/J.SEPPUR.2023.124028

Synthesis and Characterization of La and Ga Promoted Copper-Containing Catalysts for Methanol Steam Reforming Reaction

[1*]Orhan Özcan, [1]Ayşe Nilgün Akın
[1] Kocaeli University, Faculty of Engineering, Department of Chemical Engineering, Kocaeli, 41001, Türkiye

* E-mail: orhan.ozcan@kocaeli.edu.tr

Abstract
In this study, La and Ga-doped Cu/Zr/La/Al and Cu/Zr/Ga/Al catalysts were prepared using one-pot sonochemical co-precipitation method and tested for methanol steam reforming (MSR) to produce H_2 with low CO. Reactivity of the catalysts was investigated at 246 and 200 °C with a reactant ratio (H_2O/CH_3OH) of 1.5 and a space-time ratio (W/F_{A0}) of 100 kg.sec.mol^{-1} in a flow reactor. Physicochemical properties were characterized by N_2 adsorption, XRD, and ICP-OES. The X-ray diffraction patterns of the calcined samples revealed the presence of crystalline CuO, as well as highly dispersed Zr, La, and Ga phases. Mesoporous structures were observed in all catalysts, with BET surface areas ranging from 79.9 to 97.3 m^2/g. No strong correlation between CH_3OH conversion, H_2, CO_2, CO selectivities, and the composition of all catalysts was observed. However, these catalysts are notable for their low CO selectivities. Additionally, no detectable formation of CO was observed at 200 °C.

Keywords: Methanol steam reforming, hydrogen production, sonochemical co-precipitation

I. Introduction

The production of hydrogen is essential for the development of sustainable energy systems. It can help reduce greenhouse gas emissions and mitigate climate change. Additionally, hydrogen can be utilized in fuel cells to generate electricity with high efficiency and zero emissions, making it a promising alternative to conventional technologies. Thus, research focuses on developing efficient and sustainable methods for hydrogen production from renewable sources (Ajanovic et al., 2022).

Methanol steam reforming (MSR) is a promising technology for hydrogen production in various industrial processes. It involves the conversion of methanol into H_2 and CO_2. MSR operates at lower temperatures (200-300 °C) compared to other reforming reactions, such as methane reforming. Methanol is in the liquid phase, which makes it easier to handle and transport. It has no sulfur and a high H/C ratio which makes the MSR reaction important (Cai et al., 2020). Also, methanol can be produced from renewable sources such as biomass or captured carbon dioxide (Pérez-Fortes et al., 2016). Fuel cell technologies, such as high-temperature proton exchange membrane fuel cells (HT-PEMFC), can use hydrogen produced through MSR. Therefore, improving the performance and efficiency of MSR systems integrated with fuel cell technologies, including reformer and catalyst design, is necessary to explore their potential (Li et al., 2023).

Various catalyst types have been studied in the literature, including copper-based and noble metal-based catalysts. Copper-based catalysts are commonly used in MSR due to their high activity and selectivity towards CO_2 over CO. However, these catalysts can be easily deactivated and have low stability (Kappis et al., 2021). Different methods can be used to improve copper-based catalysts. One approach is to add modifying additives such as rare earth oxides (CeO_2 and La_2O_3), nickel oxide, magnesium oxide, and gallium oxide. Another method is to incorporate different metals like zinc, zirconia, ceria, and chromium. Lanthanum has been reported to enhance catalytic activity and stability. Lanthanum oxide reduces the acidity of the support, suppressing the coke formation (Kapran and Orlyk, 2017), while gallium promotes the conversion of carbon intermediates, leading to increased conversion (Yang et al., 2023).

In the present study, CuZrAl catalysts promoted by La and Ga were prepared using one-pot ultrasound-assisted co-precipitation method and investigated in MSR. The physicochemical properties were characterized using N_2 physisorption, XRD, and ICP-OES.

II. Experimental Set-up and Procedure

Catalysts with varying percentages of La (4.3 - 12.8 wt.%) and Ga (3.7 - 11.2 wt.%) were prepared using one-pot ultrasound-assisted co-precipitation. In addition, a Cu/Zr/Al catalyst without La or Ga was also prepared for comparison. The solution of metal salts was added dropwise to the previously prepared aqueous solution of Na_2CO_3 under ultrasound (90W) irradiation at 70 °C. After the aging process at 70 °C for 20 h, the precipitates were filtered and washed with deionized water at room temperature. Drying was carried out in an oven at 110 °C for 18 h prior to calcination in a muffle furnace at 500 °C (5°C/min) for 4 h.

Tab. 1 presents all catalysts with their theoretical compositions and designations. The calcined catalysts were crushed and sieved to a particle size of 250-500 µm and placed in the microreactor. Prior to each experiment, the fresh catalysts were reduced at 330 °C for 1 h. The performances of all catalysts were measured at reaction temperatures of 246 °C and 200 °C with a space-time ratio of 100 kg.s.mol^{-1} and a feed molar ratio (H_2O/CH_3OH) of 1.5 throughout the experiments. The reaction products of H_2, CO, and CO_2 were analyzed using a customized 7890B GC system equipped with TCD and FID.

Tab. 1: Target metal contents and designations of copper-based catalysts

Catalyst	Cu (wt.%)	Zr (wt.%)	La (wt.%)	Ga (wt.%)	Al (wt.%)	Designation	Zr/Al molar ratio
Cu/Zr/Al	39.9	22.2			10.6	CZA-1	0.6
Cu/Zr/La/Al	39.9	22.2	4.3		7.9	CZLA-2	0.8
Cu/Zr/La/Al	39.9	22.2	12.8		2.6	CZLA-4	2.4
Cu/Zr/Ga/Al	39.9	22.2		3.7	7.9	CZGA-2	0.8
Cu/Zr/Ga/Al	39.9	22.2		11.2	2.6	CZGA-4	2.4

III. Results and discussions

Fig. 1 shows the X-ray diffraction patterns of all samples after calcination. The peaks at 30.54, 50.95, and 60.58 2θ angles, which are attributed to the ZrO_2 phase (Crystallography Open Database (COD) Card no: 1538970), were not observed indicating the absence of crystalline Zr species. Similarly, the crystalline phases of La_2O_3 (Card no: 1010278, 2θ: 26.16, 29.16, 48.62) and Ga_2O_3 (Card no: 2004987, 2θ: 35.22, 38.51, 66.36) were not observed, indicating a high distribution of these structures in the catalyst. In addition, the X-ray diffraction analysis revealed the presence of crystalline CuO with peaks at 2θ angles of 35.61, 38.93, and 49.06, corresponding to the (0,0,2), (1,1,1), and (2,0,-2) lattice structures, respectively (Card no: 1011148). These peaks were identified due to the high copper content in the catalyst composition.

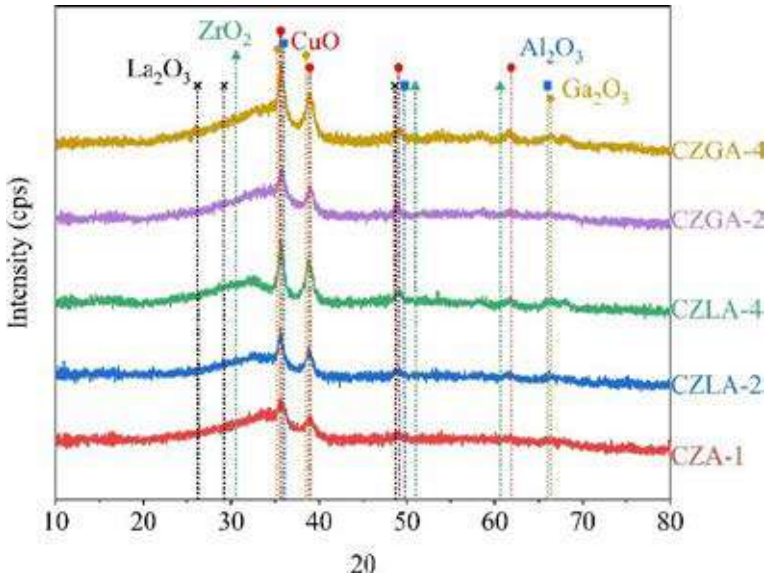


Fig. 1: XRD patterns of Cu/Zr/Al catalysts with different La and Ga loadings

Tab. 2 reports the compositions of all catalysts as determined by ICP-OES. Also reported in Tab. 2 are the BET surface area, BJH desorption pore volume, and BJH desorption average pore width obtained from measurements of N_2 adsorption. The results indicate that the targeted loadings were successfully achieved using the one-pot ultrasound-assisted coprecipitation method.

Tab. 2: Catalyst characterization results

Catalyst	Cu (wt.%)	Zr (wt.%)	La (wt.%)	Ga (wt.%)	Al (wt.%)	S_{BET} (m^2/g)	Pore vol. (cm^3/g)	Pore width (nm)
CZA-1	37	21			10.3	95.9	0.34	8.6
CZLA-2	38	21	4.0		7.9	97.3	0.38	9.7
CZLA-4	39	21	11.2		2.6	83.6	0.38	11.7
CZGA-2	38	22		2.8	7.9	86.7	0.29	8.4
CZGA-4	40	22		8.3	2.7	79.9	0.19	6.0

Fig. 2a displays the MSR activities of all catalysts at 246 °C in comparison to equilibria. No strong correlation between CH_3OH conversion and H_2, CO_2, and CO selectivities with catalyst composition was observed for any of the prepared catalysts. However, these catalysts are noteworthy for their low CO selectivities when compared to a commercial catalyst reported in our previous study (Özcan and Akın, 2022). The behavior of the catalysts at a lower reaction temperature of 200 °C was also investigated and is presented in Fig. 2b. Due to the endothermic nature of the MSR reaction, methanol conversions decreased as the temperature decreased. However, detectable CO formation was not observed for all the in-house catalysts.

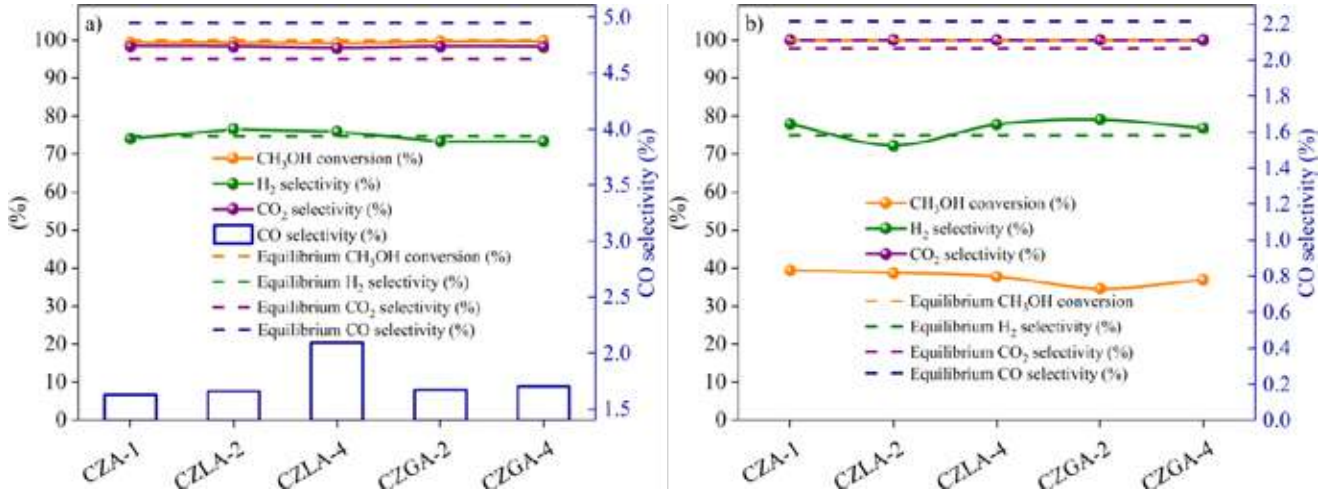


Fig. 2: Activity results of the catalysts. Experimental conditions: W/F_{A0} = 100 kg.sec.mol^{-1}, H_2O/CH_3OH = 1.5 at 246 °C (a) and 200 °C (b)

IV. Conclusions

This study presents the preparation and reactivity measurements of Cu/Zr/Al catalysts doped with La and Ga in the MSR. The XRD patterns showed crystalline CuO peaks corresponding to (0,0,2), (1,1,1), and (2,0,-2) lattice structures. The absence of crystalline Zr, La, and Ga peaks suggests that they are highly dispersed in the structure. BET surface area measurements ranged from 79.9 m^2/g to 97.3 m^2/g, and the pore volume distributions indicated the mesoporosity. Also, no strong correlation between the catalyst composition and activity was observed. However, these catalysts have lower CO selectivity compared to the commercial catalyst presented in our previous study (Özcan and Akın, 2022).

Acknowledgments

This work was supported by Kocaeli University Research Fund with Project Numbers: 2018/091 and FMP-2021-2775.

References

Ajanovic A., Sayer M., Haas R., The economics and the environmental benignity of different colors of hydrogen, International Journal of Hydrogen Energy, 47, 24136-24154, (2022).

Cai F., Ibrahim J.J., Fu Y., Kong W., Zhang J., Sun Y., Low-temperature hydrogen production from methanol steam reforming on Zn-modified Pt/MoC catalysts, Applied Catalysis B: Environmental, 264, 118500, (2020).

Kappis K., Papavasiliou J., Avgouropoulos G., Methanol Reforming Processes for Fuel Cell Applications, Energies, 14, 8442, (2021).

Kapran A.Y., Orlyk S.M., Hydrogen Production in Methanol Reforming on Modified Copper-Zinc Catalysts: A Review, Theoretical and Experimental Chemistry, 53, 1-16, (2017).

Li N., Cui X., Zhu J., Zhou M., Liso V., Cinti G., Sahlin S.L., Araya S.S., A review of reformed methanol-high temperature proton exchange membrane fuel cell systems, Renewable and Sustainable Energy Reviews, 182, 113395, (2023).

Özcan O., Akın A.N., Comparison of a commercial water-gas shift catalyst and La modified Cu-based catalysts prepared by deposition-precipitation in methanol steam reforming, Turkish Journal of Chemistry, 46, 1069-1080, (2022).

Pérez-Fortes M., Schöneberger J.C., Boulamanti A., Tzimas E., Methanol synthesis using captured CO_2 as raw material: Techno-economic and environmental assessment, Applied Energy, 161, 718-732, (2016).

Yang W.W., Ma X., Tang X.Y., Dou P.Y., Yang Y.J., He Y.L., Review on developments of catalytic system for methanol steam reforming from the perspective of energy-mass conversion, Fuel, 345, 128234, (2023).

Oxygen mobility behavior of calcium doped $BaZrO_3$ perovskite electrocatalysts

[1*]Enes Emre Yilmaz, [2]Elvan Burcu Koşma, [2]Meltem Karaismailoğlu Elibol
[1] Turkish-German University, Department of Material Science and Technology, Istanbul, 34820, Türkiye
[2] Turkish-German University, Department of Energy Science and Technology, Istanbul, 34820, Türkiye

* E-mail: e190101017@stud.tau.edu.tr

Abstract
Perovskite oxides, specifically those produced from $BaZrO_3$, have attracted significant attention due to their diverse range of applications in several fields, such as their use as electrolytes or electrocatalysts in fuel cell technologies. This paper presents an overview of the sol-gel method used to produce $BaZrO_3$ perovskite powders and the impact of calcium cation addition on the perovskite structure.

Keywords: sol-gel, perovskite, oxygen vacancies, oxygen mobility

I. Introduction

The perovskite structure is commonly described by the chemical formula ABO_3, wherein A and B denote distinct cations. Perovskite oxides comprise extensive families within the realm of oxide compounds. These structures typically feature 12-coordinated cations occupying the larger A site, alongside 6-coordinated cations at the smaller B site (Karuppiah and Ashok, 2019). Perovskite oxides have been extensively studied in the field of solid-state physics as they contain various cations and anions. Due to their distinctive characteristics, which include catalytic reactions, ferroelectricity, thermoelectricity, magnetism, oxide ion conduction, and proton conduction, materials possessing a perovskite structure are highly favored (Manju et al., 2019). Moreover, perovskites demonstrate suitability as electrodes in Solid Oxide Fuel Cell (SOFC) applications, as they can have the capacity to contain a significant amount of oxygen vacancy (Irvine, 2009). These vacancies arise within the structure depending on the nature of the cations present. The ionic conduction facilitated by the movement of oxygen vacancies through the lattice is a crucial aspect of their functionality (Hanif et al., 2022).
There are many synthesis methods available to produce perovskite oxide ceramics. Sol gel method, co-precipitation technique, hydrothermal synthesis, solid state reactions, Pechini process and low temperature solution combustion are some examples of these (Assirrey, 2019). In this study, the sol-gel method was used due to such reasons as the precise control of the characteristics of the materials (such as size, shape, and texture) size and simplicity of implementation low cost, production of high-quality materials (Danks et al., 2016), (Navas et al., 2021).

II. Experimental Set-up and Procedure

Synthesis procedure

Stoichiometric quantities of $BaZr_{(1-x)}Ca_xO_3$ (x= 0.1, 0.2, 0.3, 0.4) prepared with $Ba(NO_3)_2$ (ThermoScientific) $ZrO(NO_3)_2$ (ABCR), and $Ca(NO_3)_24H_2O$ (Carlo Erba) and dissolved in distilled water. Following that, an 1M aqueous solution of citric acid monohydrate ($C_6H_8O_7H_2O$, Carlo Erba) was added dropwise to the precursor solution, serving as a chelating agent. The mixture was stirred overnight, then ammonium hydroxide was slowly added until the solution reached pH 7. Then, the precursor solution was stirred on a heating plate and heated at 100 °C until gel formation was obtained. Subsequently, the resulting gel was dried in the oven at 230 °C. Ultimately, the dried black powder was transferred to a box furnace (Protherm, Eurotherm 3208) to yield perovskite powder. The calcination process was carried out at 1300°C for a duration of 8 hours, with a heating rate of 1 °C/min.

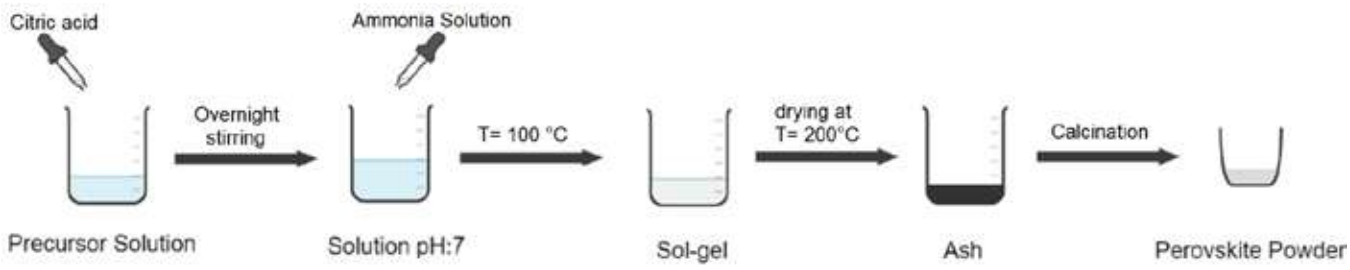


Fig. 1: Synthesis procedure of the perovskite materials

Characterization

The crystal structure of the synthesized perovskite powders was examined utilizing X-ray diffraction (XRD)

techniques. The samples' XRD data were collected using a PANanalytical Empyrean powder X-ray diffractometer, employing CuKa radiation at 45 kV and 40 mA. The scanning procedure contains a step size of 0.01 and a scanning angle range from 10° to 90°. Analysis of the diffraction patterns for phase identification was performed using the X'Pert Highscore Plus software.
To assess the redox characteristics and oxygen-active species of each perovskite samples, H_2 temperature-programmed reduction (H_2-TPR) experiments were carried out using a stainless-steel reactor. In H_2-TPR measurement, 0.2 g of each sample was loaded into the stainless-steel reactor. The reactor was heated by an electrical furnace to 1000°C at a rate of 3°C /min, within a reducing gas environment composed of 5% H_2/N_2 flowing at a rate of 200 mL /min.

III. Results and discussions

Figure 2 shows the X-ray diffraction (XRD) patterns of the produced $BaZrO_3$, $Ba_{0.9}Ca_{0.1}ZrO_3$, $Ba_{0.8}Ca_{0.2}$ ZrO_3 , $Ba_{0.7}Ca_{0.3}ZrO_3$, and $Ba_{0.6}Ca_{0.4}ZrO_3$ perovskite powders for analyzing their phase compositions and structural features. All samples exhibit distinct diffraction patterns with strong peaks at 2θ angles of 30.15, 37.11, 43.17, 53.56, 62.67, 71.10, 79.11, and 86.89. All synthesized calcium doped perovskite powders were formed in $Ba_{0.8}Ca_{0.2}$ ZrO_3 phase. It has also been observed that impurity occurs in $BaCa(CO_3)_2$ phase. In $BaZrO_3$, strong peaks occurred in the $BaZrO_3$ phase, while impurity was observed in the ZrO_2 phase.
The crystal planes corresponding to these peaks are (110), (111), (200), (211), (220), (310), (222), (321). It should also be noted that the intensities of peaks increase as the calcium ratio increases.

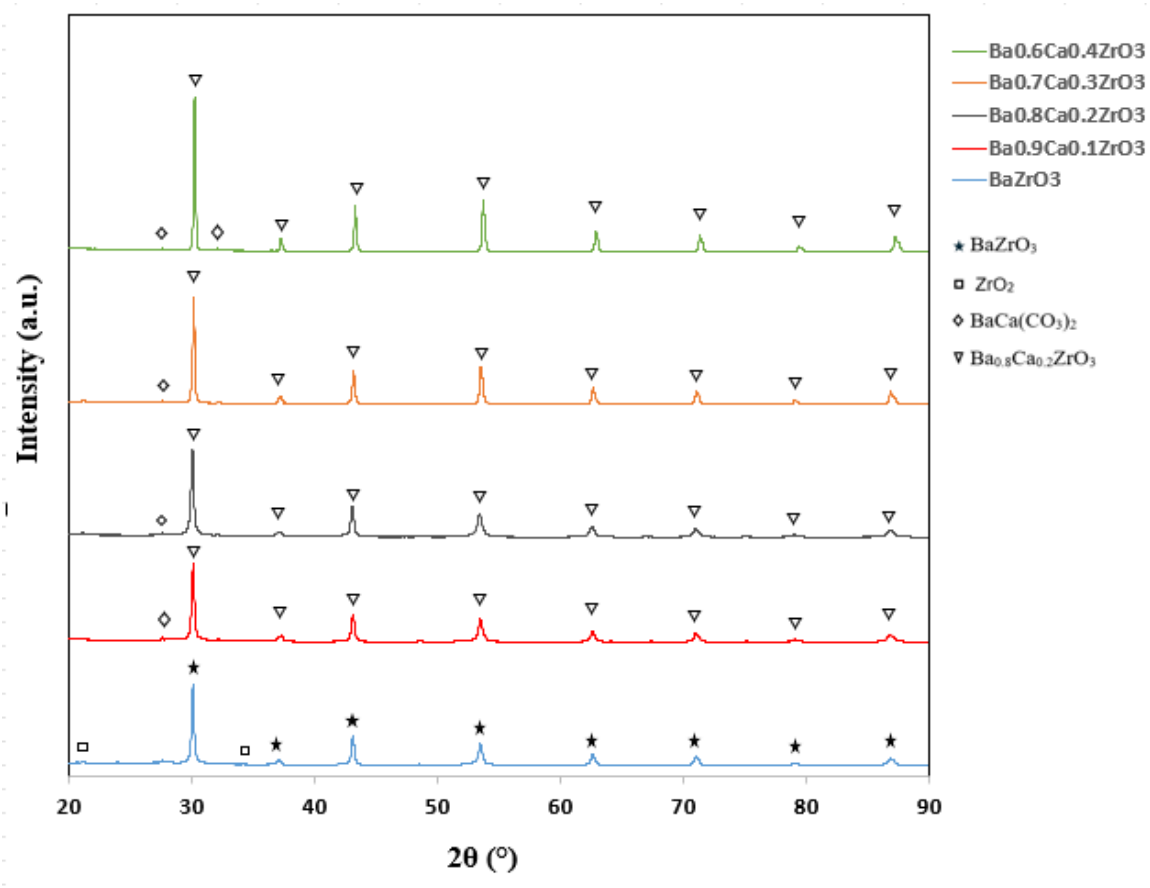


Fig. 2: XRD patterns of the samples $BaZrO_3$(blue), $Ba_{0.9}Ca_{0.1}ZrO_3$(red), $Ba_{0.8}Ca_{0.2}ZrO_3$ (orange) $Ba_{0.7}Ca_{0.3}ZrO_3$(black), $Ba_{0.6}Ca_{0.4}ZrO_3$ (green).

In Figure 3, the increase in hydrogen consumption with temperature in the H_2-TPR profiles is demonstrated. The reducibility of the produced perovskites is linked to their capacity to free oxygen from their structure. The $BaZrO_3$ perovskite material exhibits three reduction peaks around 525 °C, 620 °C and 790 °C. These reduction peaks can be assigned to the reduction of the oxygen species in the bulk lattice structure. (Wang et al., 2013).
Observations of two peaks at 346 °C and 447 °C were made in the presence of $Ba_{0.9}Ca_{0.1}ZrO_3$ sample. The profile of the $Ba_{0.8}Ca_{0.2}ZrO_3$ sample was similar, with peaks at 356 and 462.Two peaks have been noticed at 585 °C as well as 352 °C, respectively, for the $Ba_{0.7}Ca_{0.3}ZrO_3$ sample. A distinct peak appears in the presence of $Ba_{0.6}Ca_{0.4}ZrO_3$ sample at 445 °C.
The $Ba_{0.6}Ca_{0.4}ZrO_3$ sample exhibits the most noticeable peak in comparison to all other calcium-doped perovskites. An analysis of the phase intensities in the XRD data of the samples may provide an explanation for this behavior.

The sample $Ba_{0.6}Ca_{0.4}ZrO_3$ contains the most intense $Ba_{0.8}Ca_{0.2}ZrO_3$ phase. The production of the perovskite phase leads to an increase in lattice oxygen, potentially resulting in increased hydrogen consumption. Additionally, it appears that calcium-doped samples have lower temperature peaks than $BaZrO_3$ samples. Introducing Ca results in the formation of the $Ba_{0.8}Ca_{0.2}ZrO_3$ crystal phase, which may enhance the production of additional lattice oxygen species and facilitates the movement of oxygen.

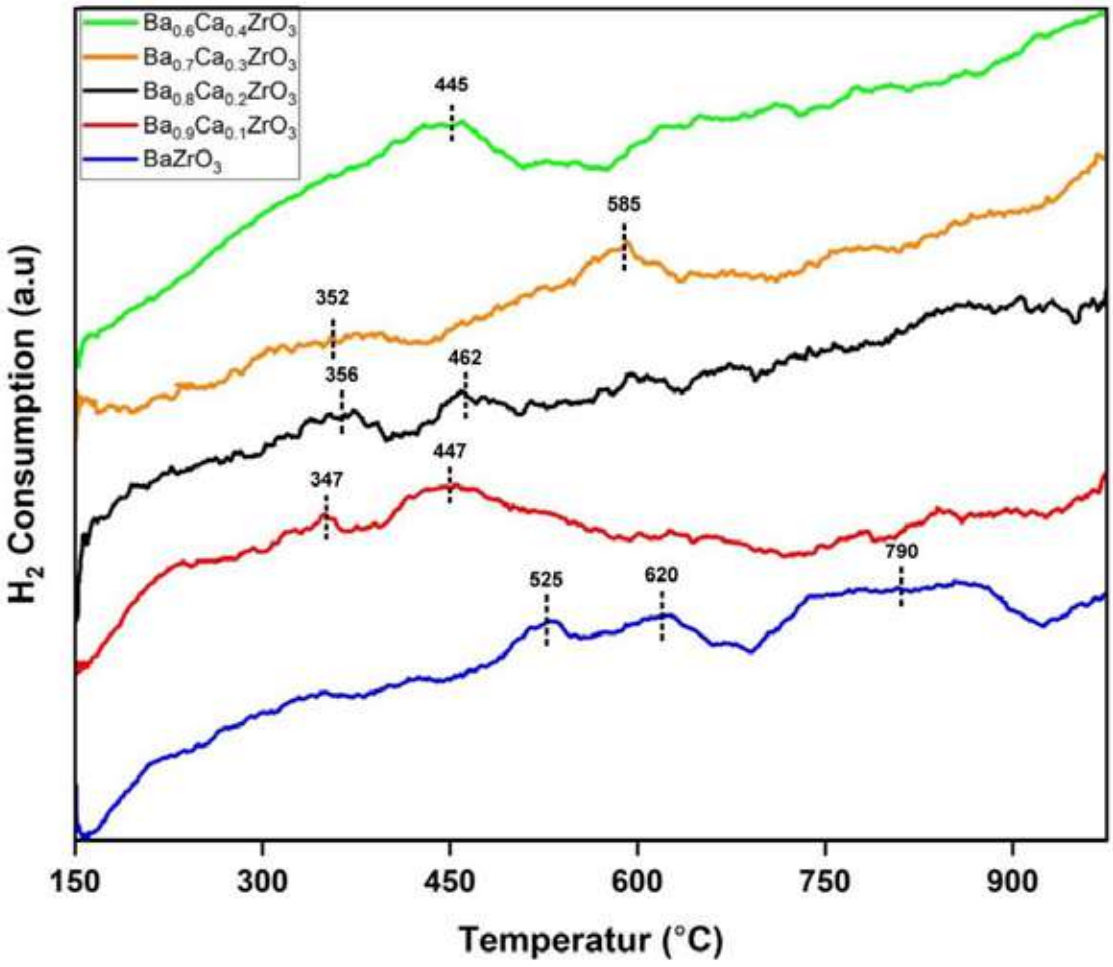


Fig. 3: H_2-TPR profiles of $BaZrO_3$(blue), $Ba_{0.9}Ca_{0.1}ZrO_3$(red), $Ba_{0.8}Ca_{0.2}ZrO_3$ (orange) $Ba_{0.7}Ca_{0.3}ZrO_3$(black), $Ba_{0.6}Ca_{0.4}ZrO_3$ (green).

V. Conclusions

It is well established that oxygen vacancies within the perovskite structure have a beneficial impact on the movement of protons and oxygen ions, thereby enhancing the ability to reduce oxygen and conduct protons. An effort was made in this research attempt to generate oxygen vacancies in the $BaZrO_3$ perovskite structure by generating lattice oxygen species. In order to accomplish this, Ca ions were incorporated into the $BaZrO_3$ perovskite structure, and their distinct characteristics were investigated. It was proven by XRD analysis that the desired Ca doped perovskite phase was successfully obtained. Additionally, H_2-TPR peaks were observed in calcium added perovskites at lower temperatures. Considering the enhanced electrocatalytic performance of the materials with increased oxygen mobility, this type of perovskites can be utilized in electrocatalytic applications.

Acknowledgements

This study was supported by Turkish–German University Scientific Research Projects Commission under the grant no: 2022BF06.

References

Assirey E., Perovskite synthesis, properties and their related biochemical and industrial application. Saudi Pharmaceutical Journal, 27(6), 817–829, (2019).

Danks A.E., Hall S.R., Schnepp Z., The evolution of 'sol–gel' chemistry as a technique for materials synthesis. Materials Horizons, 3(2), 91–112. (2016).

Hanif M.B., Rauf S., Motola M., Babar Z.U.D., Li C., Recent progress of perovskite-based electrolyte materials for solid oxide fuel cells and performance optimizing strategies for energy storage applications. Materials Research Bulletin, 146, 1-20, (2022).

Irvine J.T.S., Perovskite Oxide Anodes for SOFCs. Fuel cells and hydrogen energy, 167–182. (2009).

Karuppiah K., Ashok A.M., Review of proton- and oxide-ion-conducting perovskite materials for SOFC applications. Nanomaterials and Energy, 8(1), 51–58, (2019).

Manju P., Ajith M., Jaiswal-Nagar D., Synthesis and characterization of $BaZrO_3$ nanoparticles by citrate-nitrate sol-gel auto-combustion technique: Systematic study for the formation of dense $BaZrO_3$ ceramics. Journal of the European Ceramic Society, 39(13), 3756–3767, (2019).

Navas D., Fuentes S., Castro-Alvarez A., Chávez-Ángel E., Review on Sol-Gel Synthesis of perovskite and oxide nanomaterials. Gels, 7(4), 275, (2021).

Wang Z., Liu B.Y., Li J. Highly effective perovskite-type $BaZrO_3$ supported Ru catalyst for ammonia synthesis. Applied Catalysis A: General, 458,130-136, (2013).

Effect of different Solvents on Hydrogen Production from Hydrolysis of Potassium Borhydride with a New and Active Ni-Based Catalyst Synthesized by Green Synthesis

Ömer Şahin[1], Selma Ekinci[2] , Mehmet Sait İzgi[3], Erhan Onat[4*]
[1] Istanbul Technical University, Department of Chemical Engineering, Faculty of Chemical and Metallurgical Engineering, , 34469, Istanbul, Türkiye
[2] Batman University, Vocational School of Technical Sciences, Department of Chemistry and Chemical Process Technology, Batman, 72070, Türkiye
[3]Siirt University, Engineering and Architecture Faculty, Siirt, 56100 , Türkiye
[4]Bitlis Eren University, Vocational School of Organized Industrial Zone, Department of Electrical and Energy, Bitlis,13100, Türkiye

* e-mail: eonat@beu.edu.tr

Abstract
In this study, hydrogen production studies were carried out through the hydrolysis of potassium borohydride (KBH4), a highly suitable hydrogen storage material for a clean environment, in the presence of caffeine-based carbon quantum dot (CQD) supported Ni (0) nanoparticle catalyst. The hydrolysis of potassium borohydride in the presence of the newly synthesized Ni@CQD catalyst was tested both in pure water and in ethanol solvent environment. It was determined that the Ni@CQD catalyst showed excellent activity in the ethanol environment (TOF = 1696.8 h^{-1}) and reusability (99% retained at the end of the 6th cycle). Analyzes of the Ni@CQD catalyst synthesized for the first time were performed using advanced analytical methods (XRD, ICP-OES, XPS, BET, TEM-EDS). The results showed that Ni(0) nanoparticles were homogeneously distributed on the CQD surface and the average particle size was 1.2 ± 0.1 nm. Kinetic data were obtained by performing the catalytic hydrolysis reaction of KBH4 at temperatures between (303-333 K) in the presence of Ni@CQD catalyst. Ea, ΔH and ΔS values were calculated from the kinetic data. Additionally, the rate equation of the catalytic hydrolysis reaction was determined.

Keywords: Potassium borohydride, Carbon quantum dots, Hydrogen, Green synthesis.

I. Introduction

In response to the increasing need for energy, environmentally friendly energies need to be researched and produced in order for energy to be environmentally sensitive and sustainable (E. Onat, Sahin, Izgi, & Horoz, 2021). Therefore, considering the negative effects of fossil fuels on global warming and the environment, cheap and reusable energy is needed. In this respect, especially hydrogen stands out as an alternative to fossil fuels(Marbán & Valdés-Solís, 2007). As is known, hydrogen is obtained from electrolysis of water, solar energy and metal hydrides. Of these, boron hydrides with high hydrogen content such as $NaBH_4$, KBH_4, $LiBH_4$ and NH_3BH_3 provide advantages in both transportation and storage of hydrogen. Although much work has been done with sodium borohydride (NaBH4), not much work has been done with potassium borohydride (KBH4) (Balbay, Şahin, & Saka, 2017; Erhan Onat, Izgi, Şahin, & Saka, 2024; Salih Keskin, Şahin, & Horoz, 2022; Şahin, Dolaş, & Özdemir, 2007). The hydrolysis of KBH4 in water is as follows.

$$KBH_4 + 2H_2O \rightarrow KBO_2 + 4H_2O \quad (1)$$

Since hydrolysis reactions are slow, catalysts are required to increase hydrogen production. Expensive catalysts such as Ru, Pd usually perform very well in hydrolysis reactions. However, since they are rare elements, they are not very useful. Instead, recently, support materials; CeO_2, CNT, MOF, Al_2O_3 and GO (Akbayrak, Tonbul, & Özkar, 2016; Izgi, Sahin, & Saka, 2019; Sait Izgi, Şahin, & Saka, 2019) are used to dope the metal on these support materials, causing both homogeneous dispersion and increased catalytic activity of the catalyst.
The aim of our study here is to develop a cheaper, useful and better catalyst compared to expensive catalysts; we synthesized caffeine-based carbon quantum dots (CQD) and doped Ni metal on it and examined the effect of Ni@CQD catalyst on hydrogen production in KBH^4 hydrolysis both in pure water and ethanol medium. It was observed that the catalyst we synthesized performed better than expensive catalysts and the hydrogen production rate was 12262 $mL*gcat^{-1}*min^{-1}$ at 303 K in ethanol medium.

II. Experimental Set-up and Procedure

Within the scope of the study, CQD synthesis was achieved from caffeine under hydrothermal conditions. CQD synthesis was carried out by hydrothermal method (İzgi et. al., 2024). NI@CQD supported catalyst was synthesized by loading Ni metal atoms into the synthesized CQD. The structure of the synthesized material was elucidated using UV, XRD, ICP-OES, XPS, BET, TEM-EDS analysis methods.
The synthesis was carried out in pure water and ethanol. The synthesized material structure was used in hydrolysis after drying and comminution in nitrogen atmosphere. The parameters of pure water and ethanol media were analyzed separately for comparison. The parameters examined were solution medium, amount of catalyst,

hydrogen source concentration, temperature and reproducibility. The experimental setup used in hydrolysis is given in Figure 1.

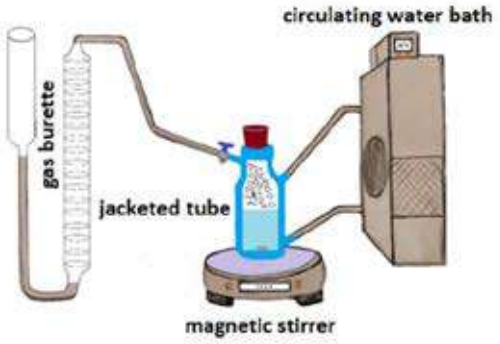


Fig. 1: Hydrolysis reaction setup

III. Analysis

The fluorescence property of the synthesized CQDs was investigated under UV light (Figure 2). As a result of the investigation, it was determined that CQDs synthesized from caffeine showed fluorescence.



Fig. 2: CQD appearance under 360 nm UV light

After CQD synthesis, Ni@CQD structure with Ni metal loading was analyzed by XRD, ICP-OES, XPS, BET, TEM-EDS techniques. EDX, XPS and TEM analyses are given in Figure 3. When the figures are examined, it is seen that Ni metal atoms are successfully attached to CQDs. Again, it was seen that a homogeneous particle-sized material structure with high surface area was synthesized.

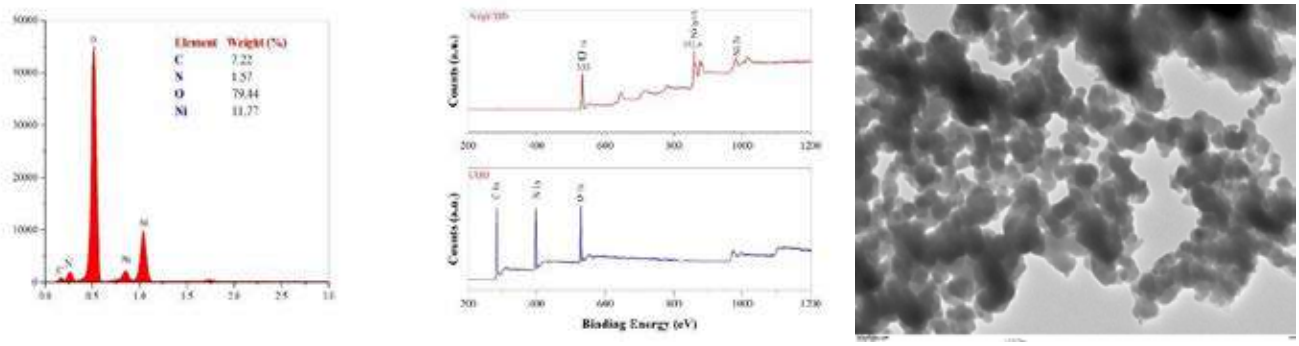


Fig. 3: Ni@CQD EDX, XPS and TEM analysis

IV. Results and discussions

After the successful synthesis of CQD and Ni@CQD, hydrolysis was carried out in accordance with the experimental setup given in Figure 4' 4e. As a result of hydrolysis with different solvents, it was determined that the best hydrogen yield was obtained using ethanol. As a result of the hydrolysis reaction carried out at 303 K with KBH_4 hydrogen source and catalyst containing 4.8 mg Ni, a hydrogen yield of over 12000 mL/g.min was obtained.

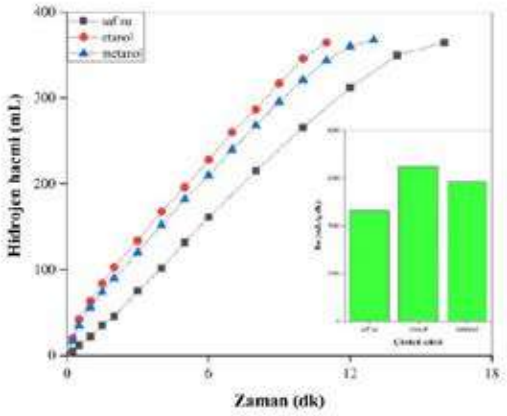


Fig. 4: H_2 yields of Ni@CQD catalysts synthesized in different solvents

As a result of hydrolysis processes, the best cycle frequency values of the catalysts under the best conditions were calculated and the data obtained as a result of these calculations are given in Table 1.

Table 1: Some experimental data

KBH_4 Concentration (%)	Temperature (K)	TOF (h^{-1})
% 1	303	1046,8
% 2	303	1536,9
% 4	303	1696,8
% 8	303	1140,6

After determining the optimum conditions for hydrolysis, temperature parameters were examined for the interpretation of kinetic data (Figure 5). It is understood from the figure that the hydrogen yield increases rapidly parallel to the temperature increase. When the figure is analyzed, it will be clearly seen that hydrogen production increases with increasing temperature.

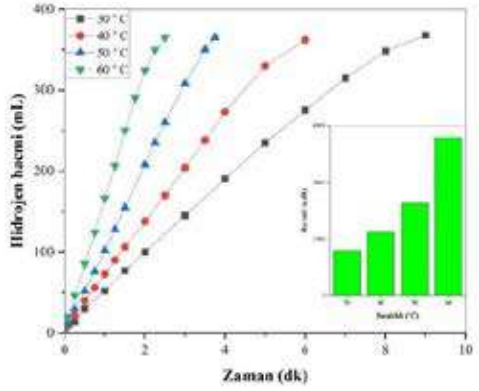


Fig. 5: Hydrolysis data at different temperatures

V. Conclusions

Hydrogen production from ethanolysis of KBH4 in the presence of Ni@CQD catalyst was performed for the first time in this study. The hydrogen production rate (HPR) of the synthesized catalyst caffeine-based carbon quantum dots supported Ni catalyst at optimum experimental conditions (10 mL solution, 303 K, 10% KOH, 4% KBH4) was determined as 12262 mL*gcat-1 *min-1. The high catalytic activity of the catalyst synthesized here is due to the homogeneous distribution of Ni(0) metal on the CQD and the porous structure of the catalyst. The chemical compositions and morphology structures of this caffeine carbon dot-supported Ni catalysts were carefully characterized by XRD, TEM, BET, EDS, , XPS, and ICP/OES analyses.

Acknowledgements
"The Scientific Research Projects Coordinatorship of Siirt University has supported a part of this study with the project numbered 2022-SİÜFEB-010.

References

Akbayrak, S., Tonbul, Y., & Özkar, S. (2016). Ceria-supported ruthenium nanoparticles as highly active and long-lived catalysts in hydrogen generation from the hydrolysis of ammonia borane. *Dalton Transactions, 45*(27), 10969-10978.

Balbay, A., Şahin, Ö., & Saka, C. (2017). Effect of acid addition on hydrogen production from potassium borohydride hydrolysis. *Energy Sources, Part A: Recovery, Utilization, and Environmental Effects, 39*(13), 1383-1389.

Izgi, M. S., Sahin, O., & Saka, C. (2019). gamma-Al2O3 supported/Co-Cr-B catalyst for hydrogen evolution via NH3BH3 hydrolysis. *Materials and Manufacturing Processes, 34*(14), 1620-1626. doi:10.1080/10426914.2019.1594280

Marbán, G., & Valdés-Solís, T. (2007). Towards the hydrogen economy? *International Journal of Hydrogen Energy, 32*(12), 1625-1637.

Onat, E., Izgi, M. S., Şahin, Ö., & Saka, C. (2024). Highly active hydrogen production from hydrolysis of potassium borohydride by caffeine carbon quantum dot-supported cobalt catalyst in ethanol solvent by hydrothermal treatment. *International Journal of Hydrogen Energy, 51*, 362-375.

Onat, E., Sahin, O., Izgi, M. S., & Horoz, S. (2021). An efficient synergistic Co@CQDs catalyst for hydrogen production from the hydrolysis of NH3BH3. *Journal of Materials Science-Materials in Electronics, 32*(23), 27251-27259. doi:10.1007/s10854-021-07094-9

Sait Izgi, M., Şahin, Ö., & Saka, C. (2019). γ-Al2O3 supported/Co-Cr-B catalyst for hydrogen evolution via NH3BH3 hydrolysis. *Materials and Manufacturing Processes, 34*(14), 1620-1626.

Salih Keskin, M., Şahin, Ö., & Horoz, S. (2022). Efficiency of TiO2-supported Ni-Mo-Ru–B catalyst for hydrogen production from potassium borohydride hydrolysis. *Journal of the Australian Ceramic Society, 58*(3), 973-979.

Şahin, Ö., Dolaş, H., & Özdemir, M. (2007). The effect of various factors on the hydrogen generation by hydrolysis reaction of potassium borohydride. *International Journal of Hydrogen Energy, 32*(13), 2330-2336.

İzgi, M. S., Onat, E., Şahin, Ö., & Saka, C. (2024). Green and active hydrogen production from hydrolysis of ammonia borane by using caffeine carbon quantum dot-supported ruthenium catalyst in methanol solvent by hydrothermal treatment. International Journal of Hydrogen Energy, 51, 180-192.

Comparison of Wild Type and Uptake Hydrogenase-Deficient Strains of *Rhodobacter capsulatus* on H_2 and PHB Production

[1]Ertan Hoşafcı, [2]Etkin Tarlan, [1]Tuba Hande Erguder, [2*]Harun Koku
[1] Middle East Technical University, Faculty of Engineering, Environmental Engineering Department, Üniversiteler Mah. Dumlupınar Blv. No.1, Ankara, 06800, Türkiye
[2] Middle East Technical University, Faculty of Engineering, Chemical Engineering Department, Üniversiteler Mah. Dumlupınar Blv. No.1, Ankara, 06800, Türkiye

* E-mail:harunk@metu.edu.tr

Abstract
Hydrogen (H_2), a clean and renewable source of energy, is widely accepted to have the potential to address the increasing global energy demand and reduce carbon emissions. One pathway of production is via photoheterotrophic microorganisms that convert organic substrates into H_2 and by-products, one of which is poly-hydroxybutyrate (PHB). One such microorganism that show great promise in biohydrogen production is *Rhodobacter capsulatus*. In this study, two strains of *R. capsulatus*, namely a Wild-Type and the uptake hydrogenase-deficient YO3, were compared in their H_2 production and PHB accumulation. Highest H_2 productivity was observed as 0.41 mmol/L·h in YO3 while highest PHB accumulation was observed as 40.1 % of cell dry weight (cdw) with YO3 strain. The strains were also compared with respect to their substrate utilization rate, growth and by-product formation, and it was concluded that YO3 strain is more advantageous in terms of all investigated aspects.

Keywords: *Rhodobacter capsulatus*, hydrogen, poly-hydroxybutyric acid, bioreactor operation

I. Introduction

Purple non-sulfur bacteria (PNSB) are a class of facultative anaerobes. Containing species capable of photoautotrophy, chemoautotrophy and photofermentation, PNSB are a diverse class. Among various PNSB, *R. capsulatus* is a species that has demonstrated exceptional capabilities in biohydrogen production, while also having the ability to produce poly-hydroxybutyrate (PHB), a biodegradable polymer with wide range of applications (Boran *et.al.,* 2012). PHB is synthesized by most species of bacteria as an intracellular storage compound in response to stress conditions, mostly applied in the form of nutrient limitation or environmental factors such as temperature, light and pH. This biopolymer can be extracted from the cells and processed into various forms, such as films, fibers and bioplastics (Keshavarz and Roy, 2010). Production of PHB by *R. capsulatus* offers a sustainable alternative to petroleum-based plastics, contributing to the reduction of plastic waste and environmental pollution. *R. capsulatus* is potentially a viable species for co-production of H_2 and PHB, since it requires high carbon to nitrogen ratio to produce both products contrary to other microbial species which typically excel on the production of single product. *R. capsulatus* can adapt to wide range of environmental conditions and substrates, making it highly versatile for biohydrogen and PHB production. Combined with the high C/N requirement of H_2 and PHB biosynthesis may lead to potential use of waste material as bioreactor feed, that is otherwise a significant economical burden on the industry (Uyar *et.al.,* 2015). Further, *R. capsulatus* YO3 is a mutant strain that is synthesized by deleting the gene responsible from the biosynthesis of enzyme uptake hydrogenase (hup). The enzyme is responsible from the utilization of H_2 as an alternative electron donor. It was seen in previous studies that YO3 strain capable of achieving higher H_2 productivities, but no studies investigate the relation between H_2 and PHB for YO3 strain (Androga *et.al.*, 2011). This study aims to investigate biohydrogen and PHB production by wild type (WT) and a mutant (YO3) strain of *R. capsulatus*. To this purpose, photobioreactors were set up under controlled conditions to compare the performance of WT and YO3 strain with respect to high H_2 and PHB production with minimal by-product formation.

II. Experimental Set-up and Procedure

Wild-type strain of *Rhodobacter capsulatus* (*R. capsulatus* WT (DSM1710)) was acquired from DSMZ German Collection of Microorganisms and Cell Cultures GmbH. Dr. Yavuz Öztürk, Ph.D., cultured the mutant strain of Rhodobacter *capsulatus* (*R. capsulatus* YO3) (Ozturk *et.al.,* 2006).

Mineral-peptone yeast extract (MPYE) medium was employed for the initial activation and growth of the cultures. Modified version of Biebl and Pfennig's (BP) medium was utilized for the adaptation media and experimental sets. 20 mM of acetate and 10 mM of glutamate was used as carbon and nitrogen sources, respectively, in the adaptation media. In the experimental sets, BP medium with 65 mM of acetate as carbon source and 2 mM of glutamate were employed (Boran *et.al.,* 2010).

Photobioreactors were set up either with a working volume of 350 mL and 10 mL of headspace flat clear glass bottles (Dimensions 90mm*40mm*140mm) or with clear glass serum bottles with a working volume of 100 mL and 10 mL headspace. Inoculation ratio was 10 % (v/v). Reactors were sealed with silicone stoppers, and the headspace was purged with argon to establish anaerobic conditions. Throughout the operation, reactors were maintained in cooled incubators at a constant temperature of 30°C under 2500 lux continuous illumination (Boran *et.al.,* 2010).

Sets 1 and 2 were operated to investigate the PHB accumulation over time, and the impact of feeding on the bioreactors, while Set 3 investigated the relation between H_2 production and PHB accumulation. Daily samples were

taken from Sets 1, 2 and 3 while Set 4 was analyzed only during initial and final days of bioreactor operation. Volume withdrawn for sampling was replaced with sterile BP medium without any carbon or nitrogen content to maintain a constant working volume during operation. For fed-batch reactors, feeding was done by injecting BP medium with high C and N concentrations once the initial C source concentration had reached zero. A summary of operated bioreactor sets can be seen in Table 1 below.

Tab. 1: Experimental setup used in the study

Experimental set	Effective volume (mL)	Mode of operation
Set 1	*350*	*Batch and Fed-batch*
Set 2	*350*	
Set 3	*350*	*Batch*
Set 4	*100*	

III. Analysis

Produced biogas was quantified by fitting 100 mL sterile syringes to the reactor stoppers. Composition of the biogas was analyzed by injecting 100 µL of headspace gas into a gas chromatograph (GC), following the methodology outlined in the reference Özsoy Demiriz *et.al.* (2019). pH was measured using a pH meter (Mettler Toledo MP220). Growth was determined using an absorbance spectrophotometer (Shimadzu UV-1800) at a wavelength of 660 nm and expressed as cell dry weight (cdw, mg/mL) as described by Boran *et.al.* (2010). Samples intended for high-performance liquid chromatography (HPLC), Na^+ content, and conductivity measurements were centrifuged (Eppendorf MiniSpin Plus Centrifuge) and the supernatant was filtered through 0.22 µm sterile cellulose-acetate filters. Organic acids content was determined via high-performance liquid chromatography (HPLC) (Shimadzu LC 20AT) following Oflaz and Koku (2021). Sodium content was measured using a flame photometer (Jenway PFP7) at 589 nm. Conductivity was determined using a conductivity meter (Hach Sension 378). For PHB anlayses, biomass samples were subjected to acidic methanolysis as described by Braunegg *et.al.* (1978). Prepared samples were then injected into a GC for quantification, following the methodology outlined by Özsoy Demiriz *et.al.* (2019). PHB content of the cells is expressed as a percentage of the cell dry weight.

IV. Results and discussions

Observed PHB accumulations can be seen in Fig. 1 for Set 1 and 2. Fig. 2 shows the observed PHB accumulation and H_2 productivity of Set 3.

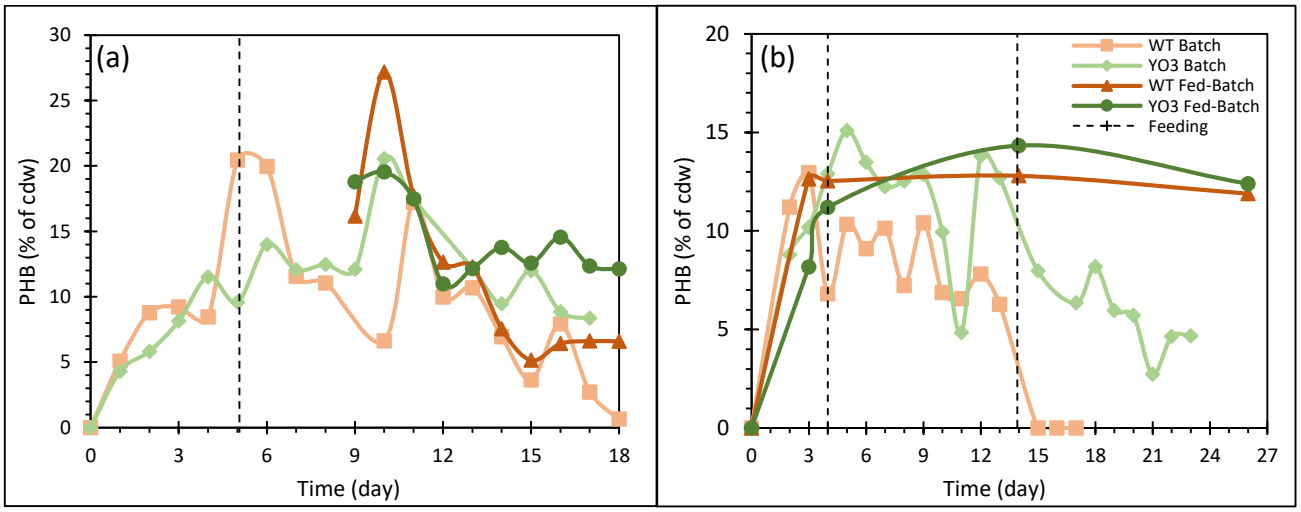


Fig. 1: Observed PHB accumulation in (a) Set 1 and (b) Set 2 for *R. capsulatus* WT and YO3.

It was observed from Set 1, 2 and 3, in batch mode of operation YO3 strain accumulated slightly more PHB than WT. PHB accumulation continued until Day 10 (Sets 1 and 2, Fig.1) and Day 6 (Set 3, Fig. 2a), where rate of degradation of PHB exceeded rate of accumulation afterwards, most likely due to depletion of the substrate in the bioreactors. In fed-batch mode of operation, it was observed that YO3 strain was more stable in terms of PHB accumulation and although WT strain accumulated more PHB (27.8 % of cdw, Day 10), it degraded rapidly (Fig.1a). Fed-batch reactors of Set 2 confirmed the stability of YO3 strain in terms of PHB accumulation further, where PHB had been kept accumulated around ~ 14 % of cdw (Fig. 1b) as long as reactors were supplied with feed.

Maximum H_2 productivity was observed to be higher in YO3 strain (Fig.2), however cumulative H_2 production was higher in WT strain (data not shown). Combining with PHB accumulation observed in Set 3, it might be speculated that YO3 is a strain that degrade substrate earlier (Fig.3), accumulating high amount of PHB and achieving higher H_2 productivities in the earlier stage of bioreactor operation, suggesting that providing constant substrate concentration (i.e., feeding) would potentially result in higher cumulative H_2 production via YO3 strain.

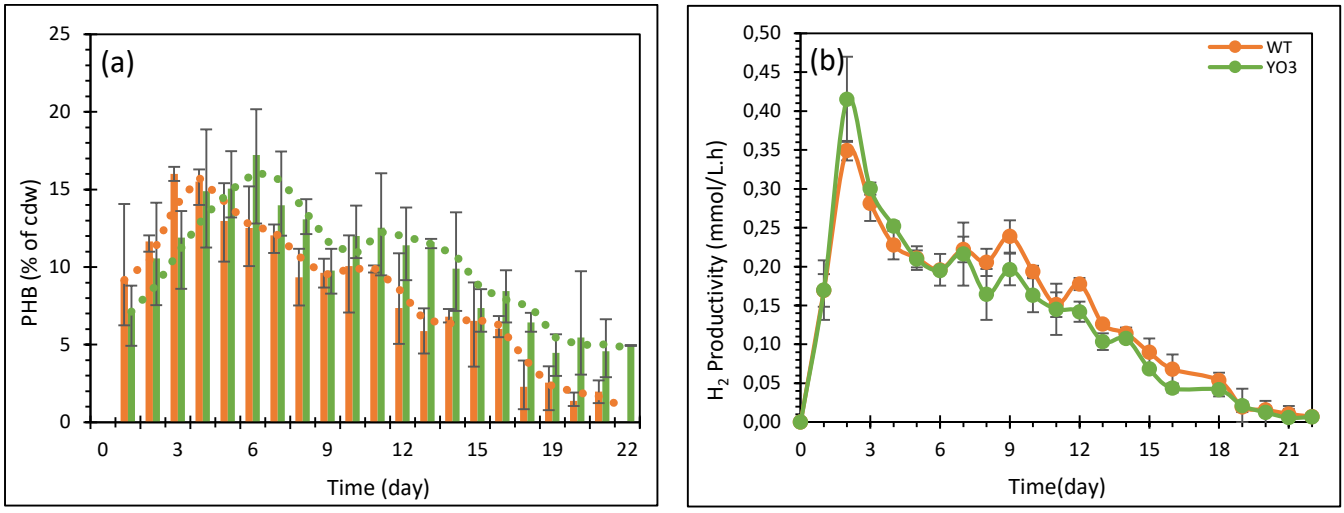


Fig. 2 Observed (a) PHB accumulations and (b) H_2 productivities in Set 3 for *R. capsulatus* WT and YO3. Dotted line shows the average of triplicate reactors.

Based on the information obtained in Sets 1, 2, and 3, a final Set 4 was operated to eliminate the effect of sampling on the performance of bioreactors and select the best suited strain to be potentially used in continuous production of H_2 and PHB. Observing higher substrate consumption (WT: 40.03 ± 2.99 mM, YO3: 50.92 ± 11.26 mM acetic acid), higher cumulative H_2 production (WT: 69.93 ± 8.00 mL, YO3: 81.50 ± 7.02 mL), less growth (WT: 1.04 ± 0.01 gcdw/L, YO3: 0.93 ± 0.01 gcdw/L), less by-product formation (WT: 24.68 ± 0.32 mM, YO3: 21.19 ± 1.62 mM formic acid) and more PHB accumulation (WT: 28.47 ± 2.30 %, YO3: 40.05 ± 1.61 %), *R. capsulatus* YO3 strain was concluded to be superior than WT strain in every investigated aspect (Fig. 3).

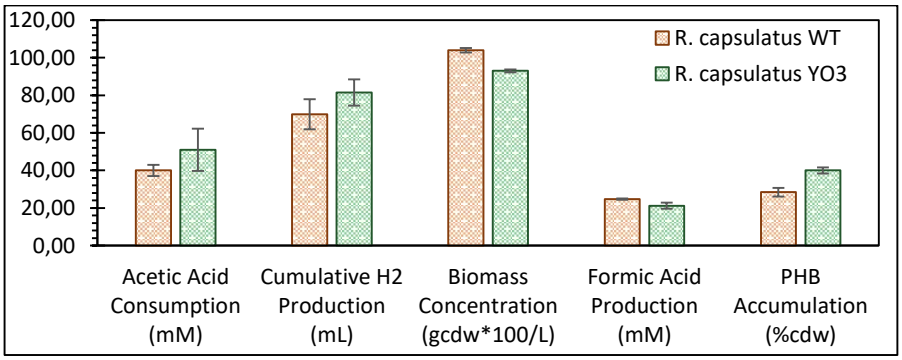


Fig. 3 Summary of performance of strains in Set 4 with respect to substrate utilization, H_2 and PHB production, growth and by-product formation.

V. Conclusions

In this study, *R. capsulatus* WT and YO3 strains were compared in their H_2 production and PHB accumulation. WT strain accumulated higher amounts of PHB, however the concentration was not sustained and decreased rapidly. YO3 strain also responded more positively to feeding. When substrate concentration was not allowed to decrease, YO3 strain accumulated more PHB. YO3 was observed to reach higher H_2 productivity, but decreased rapidly as the substrate consumed, while WT produced more H_2.

Overall, it was seen that YO3 was superior to WT having a higher substrate degradation, H_2 production, PHB accumulation and less by-product formation.

References

Androga, D. D., Ozgur, E., Gunduz, U., Yucel, M., & Eroglu, I. (2011). Factors affecting the longterm stability of biomass and hydrogen productivity in outdoor photofermentation. International Journal of Hydrogen Energy, 36(17), 11369–11378. https://doi.org/10.1016/j.ijhydene.2010.12.054

Biebl, H., & Pfennig, N. (1981). Isolation of Members of the Family Rhodospirillaceae.

Boran, E., Özgür, E., Van Der Burg, J., Yücel, M., Gündüz, U., & Eroglu, I. (2010). Biological hydrogen production by Rhodobacter capsulatus in solar tubular photo bioreactor. Journal of Cleaner Production, 18(SUPPL. 1). https://doi.org/10.1016/j.jclepro.2010.03.018

Boran, E., Özgür, E., Yücel, M., Gündüz, U., & Eroglu, I. (2012). Biohydrogen production by Rhodobacter capsulatus Hup - mutant in pilot solar tubular photobioreactor. International Journal of Hydrogen Energy, 37(21), 16437–16445. https://doi.org/10.1016/j.ijhydene.2012.02.171

Braunegg, G., Sonnleimer, B., & Lafferty, R. M. (1978). A Rapid Gas Chromatographic Method for the Determination of Poly-~-hydroxybutyric Acid in Microbial Biomass. In European J. Appl. Microbiol. Biotechnol (Vol. 6).

Keshavarz, T., & Roy, I. (2010). Polyhydroxyalkanoates: bioplastics with a green agenda. In Current Opinion in Microbiology

(Vol. 13, Issue 3, pp. 321–326). https://doi.org/10.1016/j.mib.2010.02.006
Oflaz, F. B., & Koku, H. (2021). Pilot-scale outdoor photofermentative hydrogen production from molasses using pH control. International Journal of Hydrogen Energy, 46(57), 29160–29172. https://doi.org/10.1016/j.ijhydene.2020.10.086
Özsoy Demiriz, B., Kars, G., Yücel, M., Eroğlu, İ., & Gündüz, U. (2019). Hydrogen and poly-B-hydroxybutyric acid production at various acetate concentrations using Rhodobacter capsulatus DSM 1710. International Journal of Hydrogen Energy, 44(32), 17269–17277. https://doi.org/10.1016/j.ijhydene.2019.02.036
Öztürk, Y., Yücel, M., Daldal, F., Mandaci, S., Gündüz, U., Türker, L., & Eroğlu, I. (2006). Hydrogen production by using Rhodobacter capsulatus mutants with genetically modified electron transfer chains. International Journal of Hydrogen Energy, 31(11), 1545–1552. https://doi.org/10.1016/j.ijhydene.2006.06.042
Uyar, B., Gürgan, M., Özgür, E., Gündüz, U., Yücel, M., & Eroglu, I. (2015). Hydrogen production by hup- mutant and wild-type strains of Rhodobacter capsulatus from dark fermentation effluent of sugar beet thick juice in batch and continuous photobioreactors. Bioprocess and Biosystems Engineering, 38(10), 1935–1942. https://doi.org/10.1007/s00449-015-1435-2

Gas Leakage from Hydrogen Car Stored Tanks: A Bow-Tie Risk Analysis

Mehmet Tunç, Ramazan Solmaz
Bingöl University, Health Sciences Faculty, Occupational Health and Safety Department, 12000, Bingöl, Türkiye

E-mail: mtunc@bingol.edu.tr; rsolmaz@bingol.edu.tr; rsolmaz01@gmail.com

Abstract
In this study, safety evaluations are conducted on hydrogen storage tanks in hydrogen cars using the bow-tie method. The method mainly involves identifying a hazard, top event, causes, preventive barriers, mitigative barriers, and consequences. The hazard element identified is the hydrogen storage tank, and the top event is gas leakage. Six causes (gas characteristics, high temperature, traffic accidents, object impact/collision, unstable tank installation, and human error) and three consequences (asphyxiation, explosion, and fire) are identified. The recommendations are then provided along with preventive and mitigative barriers.

Keywords: Hydogen, gas leakage, safety, bow-tie method, occupational health, occupational safety

I. Introduction

Hydrogen gas, the most common element in the universe, is odorless and colorless. It rises rapidly to the upper atmosphere due to its low density (0.08999 g/L) (Subramani, 2015). As its demand has significantly increased in recent decades (IRENA, 2019), occupational safety is crucial in areas where hydrogen is used, much like in every new technology embraced by humanity. Hydrogen tanks in cars are also among the priority systems that require careful consideration. Given hydrogen's high volatility, flammability, and explosiveness, this study evaluates gas leakage in hydrogen tanks used in cars from a safety perspective.

The rapid depletion of fossil fuels, the continuous increase in their prices and their negative effects on human and environmental health have led people to alternative energy sources. One of the areas where fossil fuels are widely used is vehicle fuel. Battery and hydrogen vehicles are among the most promising technologies of the future and studies in this field continue intensively. However, the safety precautions in these vehicles, especially due to hydrogen, are also extremely important. In this study, a risk analysis of accidental gas leakage from hydrogen car stored tanks has been conducted using the bow-tie method.

II. Experimental Set-up and Procedure

Before commencing the study, the hydrogen car system pictured by Barilo (Fig. 1) was analysed, followed by an evaluation of gas leakage from hydrogen tanks in used cars from a safety perspective.

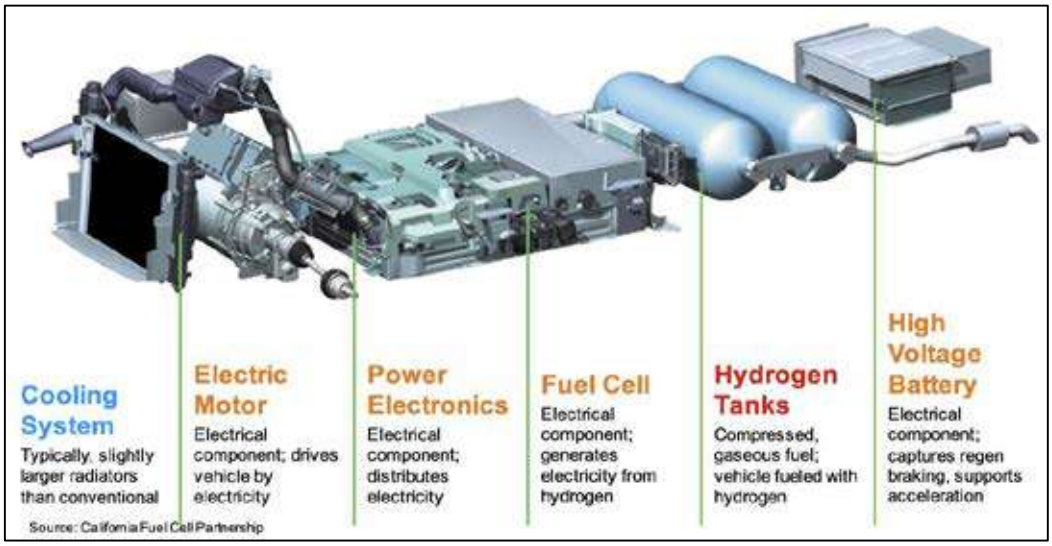


Fig. 1. Typical hydrogen car system design (Barilo, 2015; LaFleur, 2021)

Bow-tie risk analysis method is used to assess hydrogen stored tank (HST). In bow-tie method there are eight main elements (Fig. 2); hazard, top event, consequences (impacts), threats (causes), prevention barriers, mitigation barriers, degradation factor, and degradation control. To apply the bow-tie method, the hazard element is first determined at the middle top of the diagram. Subsequently, the top event element, which derives from the hazard element, is identified in the middle of the diagram. The consequences (impacts) resulting from the top event are placed on the right side of the diagram, while the threats (causes) that lead to the top event are placed on the left side of the diagram. Prevention barriers are employed to prevent the causes that lead to the occurrence of the top event. Mitigation barriers are used after the occurrence of the top event to reduce or mitigate the negative consequences of the event. The detailed diagram is shown below:

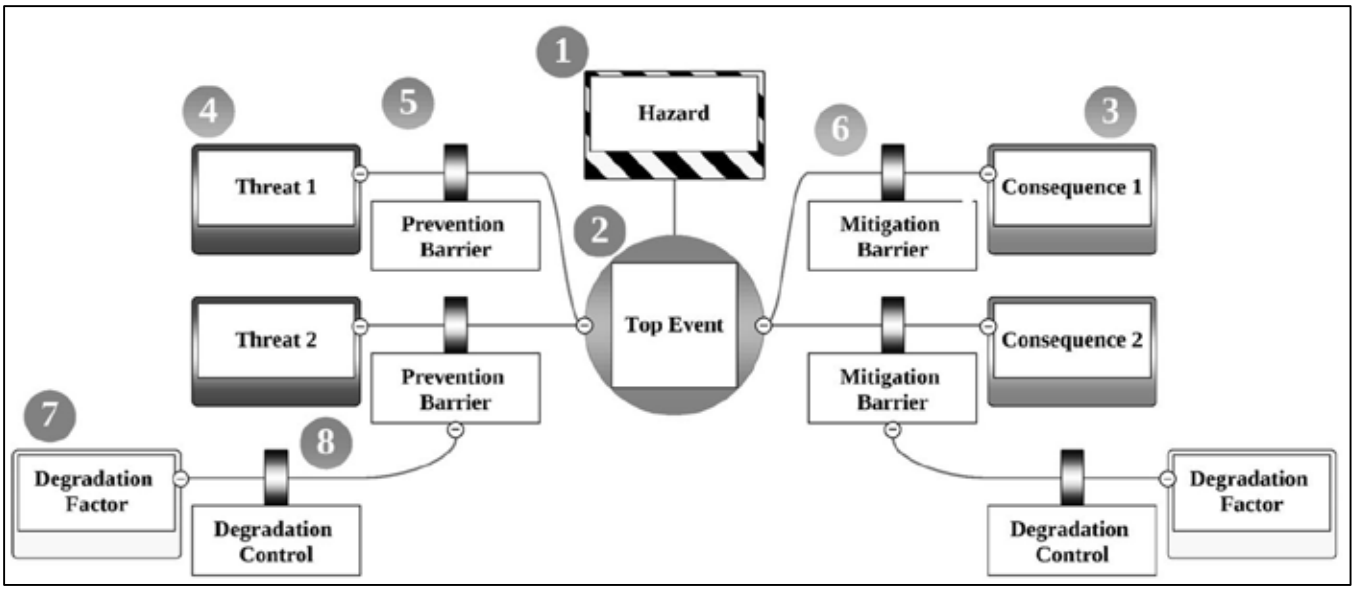


Fig. 2. Standard bow tie elements (CCPS, 2018)

In the study, the analyzed hazard was HST. Since gas leakage caused from the HST, it is selected as the top event. Six causes and three consequences of the gas leakage (top event) are identified (Fig. 3). All elements, including preventive and mitigative barriers are discussed and analyzed.

III. Results and discussions

Once the bow-tie diagram for the HST (hazard element) and gas leakage (top event element) is created, the other elements of the diagram are then discussed.

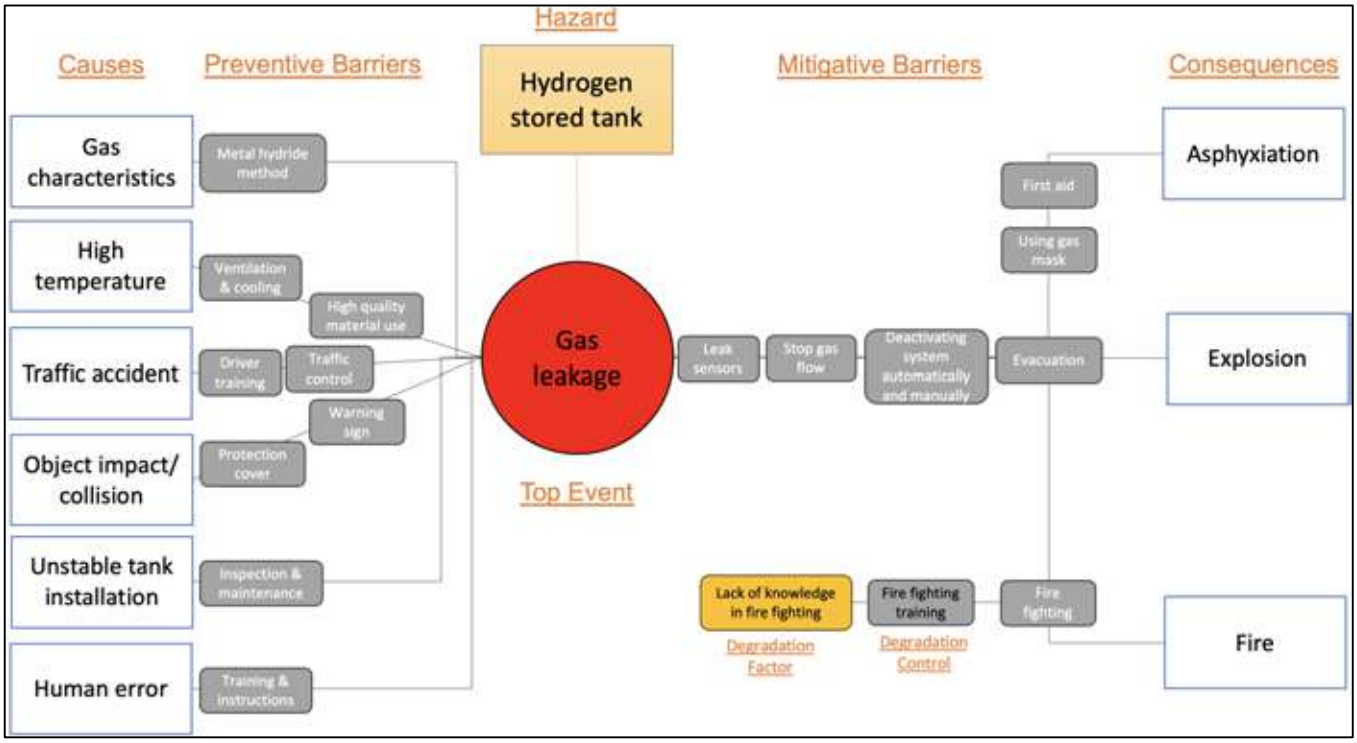


Fig. 3. Bow-tie analysis for gas leakage in hydrogen stored tank

Causes and preventive barriers

While *gas characteristics* may not directly cause hydrogen leakage, they can accelerate the leakage speed. Two main difficulties of hydrogen gas are its low volumetric energy density necessitates high-pressure compression for transportation, and its small molecules increase the risk of leaks. One approach to addressing these issues is converting hydrogen into a liquid state, yet this is expensive and complex due to the very low liquefaction temperature of hydrogen at approximately 20 Kelvin (-253.15^{o} C). For preventing this situation, metal hydride storage technology is suggested as a preventive barrier (Subramani, 2015). Besides that, odorizing and colorizing may not prevent gas leakage, but they can be helpful in early recognition. However, odorizing should not be relied

upon as a trusted barrier, given that hydrogen is highly volatile and odorants may not disperse uniformly.

High temperatures present an additional challenge for HTS. Ventilation and cooling system would be beneficial to avoid HTS from high temperature. To address this issue effectively, it is advisable to install a ventilation and cooling system. These systems help regulate the temperature in hydrogen cars, ensuring HTS do not exceed safe operating limits. Proper ventilation allows for the dissipation of any excess heat generated inside the hydrogen car, while the cooling system actively maintains a suitable temperature to prevent overheating. By implementing these preventive barriers, the risk of HST experiencing high temperatures and potential hazards associated with them can be significantly reduced. High-quality materials for tanks can be crucial for safety, as they have the ability to withstand higher temperatures. This is particularly important in ensuring the survival and integrity of tanks under challenging thermal conditions.

Traffic accidents can lead to impacts on HST, resulting in the leakage of hydrogen gas. While it may not be possible to completely prevent this cause, driver training programs and enhanced traffic controls can help prevent the risks. Specialized training on car safety should be provided to drivers who opt for hydrogen cars to ensure safe handling and operation.

As preventive barriers, using protection covers for HST and installing warning signs on the tanks are recommended to prevent the risk of gas leakage from *object impacts or collisions*.

Unstable installation of tank can also lead to gas leakage. Therefore, it is imperative to conduct continuous inspections and maintenance to ensure stable installation and prevent potential leaks.

Human error, such as improper handling of equipment or failure to follow safety protocols, can also contribute to gas leakage incidents. Therefore, comprehensive training programs, strict adherence to safety procedures, and regular monitoring of tank performance are essential to minimize the consequences of human-related gas leaks.

Consequences and mitigative barriers

Hydrogen is not a toxic gas but similar to other gases, it has the potential to cause oxygen deficiency, resulting in asphyxiation (Rigas, 2012). However, due to hydrogen's buoyancy and diffusivity, it is unlikely to stay confined in situations where asphyxiation could occur. (EERE, 2024). If gas leakage does not occur inside the car, the likelihood of asphyxiation in hydrogen cars is very low. However, if such a situation arises, the use of gas masks and immediate application of first aid procedures are crucial. Gas masks provide protection against inhaling hazardous gases, while prompt first aid can help alleviate the effects of oxygen deficiency or other gas-related risks. Additionally, emergency response protocols should be in place to swiftly address any gas-related incidents and ensure the safety of individuals in the affected area.

Hydrogen becomes explosive within the concentration range of 15% to 59% in the atmosphere. Even a tiny spark can cause an explosion if there is a hydrogen gas leak (Lanz, 2001). Therefore, in the event of a potential explosion, evacuation must be carried out, and nobody should remain in the vicinity.

The wide range of hydrogen's flammability, from 4% to 75%, makes it potentially dangerous. While smaller fires caused by hydrogen are best managed using a dry powder retardant, carbon dioxide, or halon extinguisher, large fires can be extinguished by stopping the fuel source. If driver does not know how to extinguish fire (degradation factor), a degradation control measure must be identified, such as providing fire fighting training in this context. Hydrogen fires can be persistent, and if not stopped at the source, they will continue to burn. If extinguishing the fire is not possible, the area around the fire should be evacuated, and the fire should be allowed to burn out on its own (Lanz, 2001).

Apart from the mentioned mitigative barriers, there are common barriers against asphyxiation, explosion, and fire, as shown in the diagram (Fig. 3): leak sensors, stopping gas flow, automatic and manual system deactivation.

Leak sensors play a crucial role in detecting gas leakages early, enabling prompt action to be taken. The most critical mitigative barrier is cutting off gas flow, which significantly reduces or removes the risk of asphyxiation, explosion, or fire. Stopping or cutting off the gas flow is likely the most effective method to prevent adverse consequences since hydrogen fires cannot be extinguished. The automatic deactivation system further enhances safety measures by swiftly shutting down operations during emergencies or gas leaks. In the event of any issues with the automatic system, it is recommended to install a manual deactivation system near the driver for an immediate response.

IV. Conclusions

In this study, gas leakages stemming from HTS are analyzed using the bow-tie method. Various causes and consequences of gas leakage are identified, along with their preventive and mitigative barriers. The primary focus is on implementing measures to prevent fire, explosion, and asphyxiation.

Acknowledgements

The authors are greatly thankful to Bingöl University, Health Sciences Faculty, Occupational Health and Safety Department for supporting this study.

References

Barilo N., Safety Considerations for Hydrogen and fuel cell applications. Hydrogen Safety Panel, ICC Annual Business Meeting, Long Beach, CA, September 29 (2015).

CCPS, Energy Institute, Bow ties in risk management, a concept book for process safety. DOI: 10.1002/9781119490357 (2018).

EERE (The Office of Energy Efficiency and Renewable Energy), Hydrogen safety, Fact sheet series. https://www1.eere.energy.gov/hydrogenandfuelcells/pdfs/h2_safety_fsheet.pdf (Acessed: March 20, 2024).

LaFleur, C., Global Hydrogen Safety Codes and Standards, July 21, 2021.

IRENA (International Renewable Energy Agency), Hydrogen: a renewable energy perspective. Report prepared for the 2nd Hydrogen Energy Ministerial Meeting in Tokyo, Japan (2019).

Lanz, A., Heffel, J., Messer, C., Hydrogen Fuel Cell Engines and Related Technologies. Energy Technology Training Center, College of the Desert, Palm Desert, CA, USA (2001).

Rigas, F., Amyotte, P., Hydrogen safety. CRC Press, https://doi.org/10.1201/b12267 (2012).

Subramani V., Basile A., Veziroglu T.N., Compendium of hydrogen energy, volume 1: hydrogen production and purification. Woodhead Publishing (2015).

Sonic Hydrogen Production: An Experimental Investigation

Moslem Sharifishourabi*, Ibrahim Dincer and Atef Mohany
Clean Energy Research Laboratory, Faculty of Engineering and Applied Science, Ontario Tech. University, 2000 Simcoe Street North, Oshawa, Ontario, L1G 0C5, Canada

*Corresponding author Email: moslem.sharifishourabi@ontariotechu.ca

Abstract
This study introduces an innovative hydrogen production technique utilizing ultrasounds. Specifically, it experiments with 40 kHz ultrasonic transducers, with distilled water as the primary medium. The research focuses on understanding how the temperature of the sonoreactor's solution impacts hydrogen generation rates and explores the effects of incorporating alcohol and CO_2 into the solution. Initial findings reveal that increasing the solution temperature from 40°C to 60°C enhances hydrogen production, increasing the yield from 0.15 µmol/min to 0.19 µmol/min. Furthermore, the addition of alcohol and CO_2 solution further boosts the production rate, showcasing a promising avenue for enhancing the efficiency of sonic hydrogen production. This exploration not only contributes to the advancement of hydrogen generation technologies but also highlights the potential for more sustainable and efficient energy sources.

Keywords: Sonic Hydrogen Production, Sonohydrogen, Ultrasound, Ultrasonic.

I. Introduction

The increasing demand for energy across the globe is intensifying our reliance on fossil fuels. This uptick in consumption underscores the urgent necessity for a paradigm shift towards inventive and ecologically benign energy generation methods that avoid the emission of deleterious pollutants. In this context, hydrogen emerges as an alternative fuel source, particularly in the transportation sector, thanks to its high energy density. Moreover, hydrogen's potential extends beyond terrestrial transportation, offering promising prospects for aviation and maritime sectors, where its high energy density could significantly reduce carbon emissions and dependence on oil-derived fuels. The versatility of hydrogen also shines in its application within fuel cell technologies, which convert chemical energy directly into electrical energy with water vapor as the only byproduct. However, the shift toward hydrogen as a cornerstone of our future energy system also necessitates advancements in production, storage, and distribution infrastructures.

Hydrogen can be produced through various methods, including thermoelectrochemical, thermochemical, chemical, and photonic processes, each offering its own benefits and challenges. The sonic method, which uses ultrasound technology, stands out as a promising area in hydrogen generation. Ultrasounds are sound waves with frequencies beyond the range of human hearing, usually above 20kHz, and are used in numerous fields such as medical diagnostics and industrial cleaning.

In the realm of hydrogen production, using ultrasound technology leads to a process known as sonohydrogen, where water molecules are split into hydrogen and oxygen by ultrasonic waves [1]. This approach presents an innovative and potentially more environmentally friendly method compared to conventional fossil fuel-based processes [2]. The objectives of this study are to first, introduce and explore an innovative technique for hydrogen production using ultrasound technology; second, examine the impact of solution temperature on hydrogen generation rates and third, investigate the effects of adding alcohol and CO_2 to the water solution on hydrogen production.

II. Methodology and Experimental Setup

The sonohydrogen production experiment employs a setup that harnesses ultrasonic cavitation to generate hydrogen gas (see Fig.1). The system consists of a power supply that delivers electrical energy to an ultrasonic generator. This generator is tasked with converting electrical energy into high-frequency sound wave, specifically designed to operate piezoelectric transducers at frequencies of 40 kHz. The transducers, submerged in a water tank, convert the electrical signals from the ultrasonic generator into mechanical vibrations, thus emitting ultrasonic waves. These waves induce the formation of cavitation bubbles within the liquid environment. As these bubbles collapse, the intense local conditions of temperature and pressure break the molecular bonds of water, leading to the production of hydrogen and oxygen gases.

Positioned at the peak of the water tank, a hydrogen sensor monitors the concentration of hydrogen gas produced, providing real-time data on the experiment’s efficacy. The hydrogen gas is directed to a hydrogen storage unit, where it is kept for potential applications. An Arduino board serves as the control interface for the experiment, facilitating the monitoring of hydrogen levels and the adjustment of the ultrasonic generator's settings. This board represents the critical connection between the physical experiment and the digital monitoring, ensuring accurate control and data collection throughout the hydrogen production process.

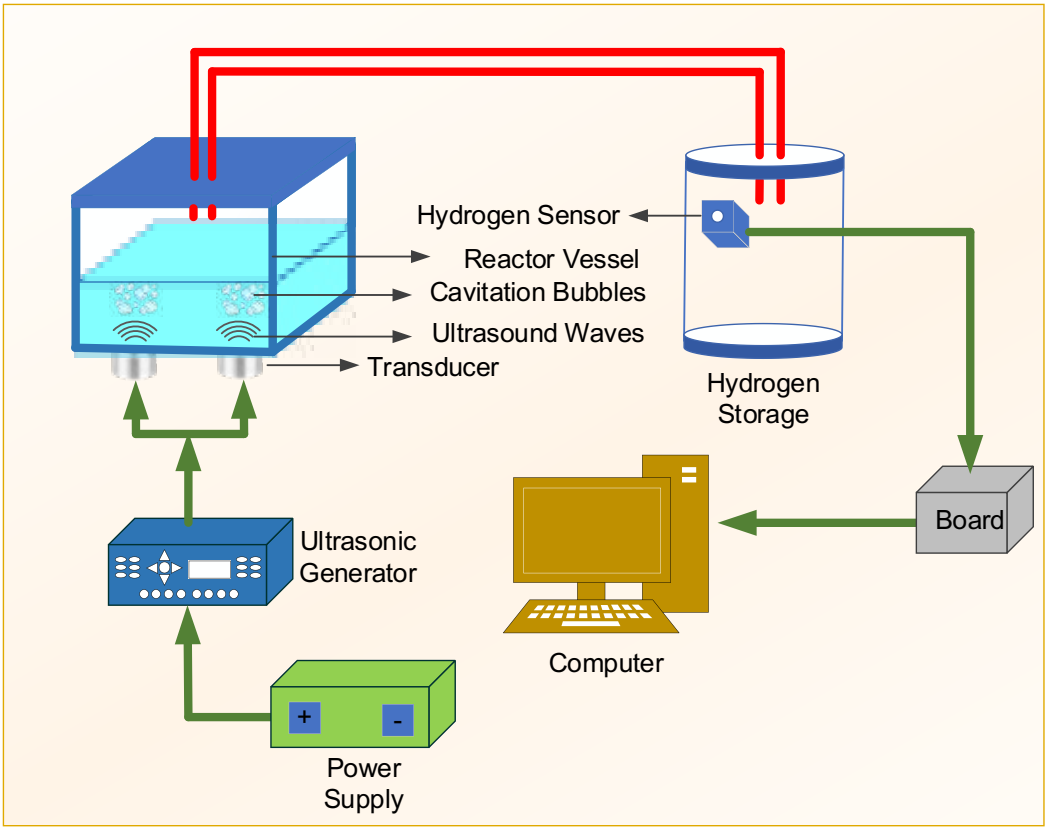


Fig. 1: Schematic showing experimental setup of the study.

III. Results and Discussion

Fig.2 presents the effects of varying temperatures on the rate of hydrogen production. It is evident that an increase in temperature from 40°C to 60°C enhances the production rate of hydrogen, escalating from 0.15 micromoles to 0.19 micromoles. This observation suggests a positive correlation between temperature and hydrogen production efficiency, indicating that higher temperatures may facilitate the chemical reactions involved, thereby accelerating the generation of hydrogen. Further analysis and experimentation could provide deeper insights into the thermal dynamics of the process and help optimize conditions for maximum hydrogen yield.

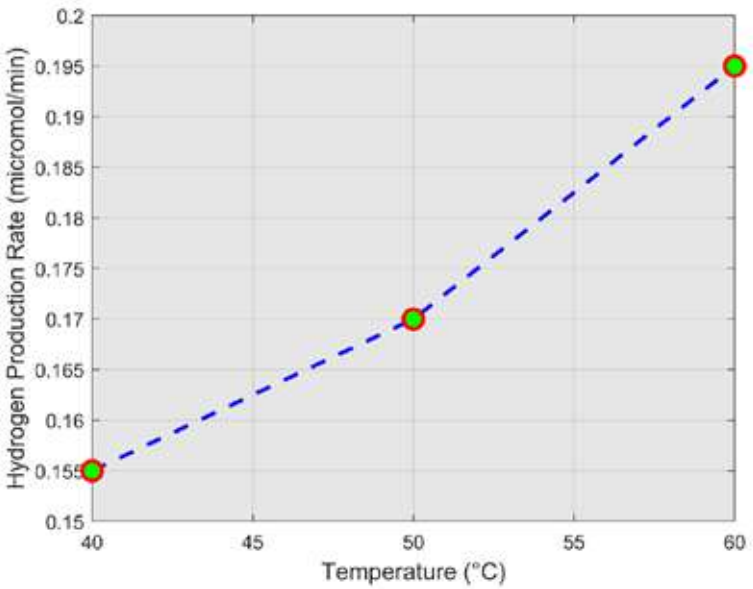
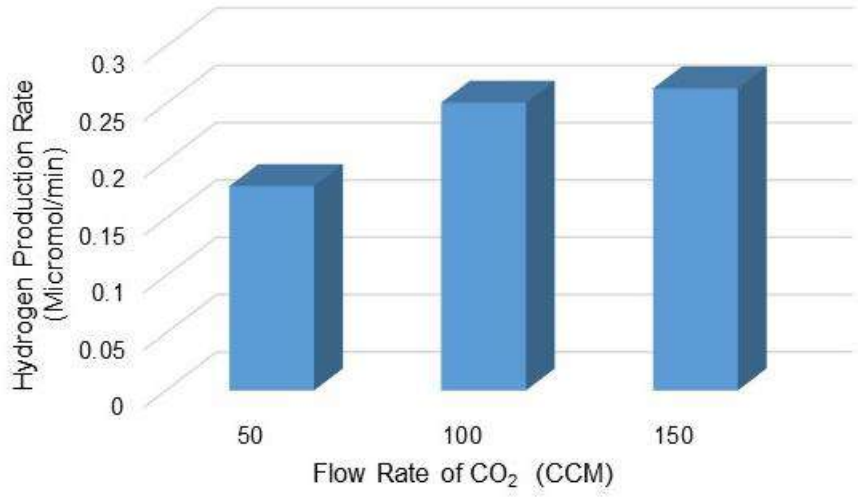


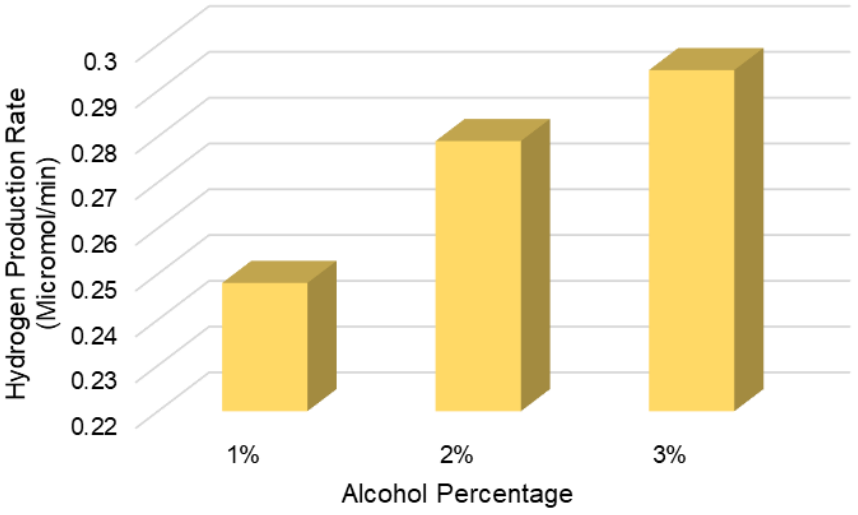
Fig. 2. Effect of temperature on the hydrogen production rate.

Fig. 3 illustrates the effects of introducing CO_2 and alcohol into water on hydrogen production rates at 40 °C. Fig. 3a details the impact of CO_2 addition, revealing a general increase in hydrogen production. Specifically, when the CO_2 injection flow rates are 50, 100, and 150 CCM, the corresponding hydrogen production rates are observed to be 0.17, 0.25, and 0.26 micromoles per minute, respectively. This indicates a positive relationship between the CO_2 injection rate and the efficiency of hydrogen production. Fig. 3b examines the influence of adding alcohol to

the water within the reactor. The introduction of alcohol also results in an enhanced production rate of hydrogen. Notably, the data suggest that varying the alcohol concentration may lead to different outcomes in hydrogen generation. For alcohol concentrations of 1%, 2%, and 3%, the hydrogen production rates are recorded at 0.24, 0.27, and 0.29 micromoles per minute, respectively. This trend underscores the potential of alcohol concentration as a critical factor in optimizing hydrogen production, suggesting the need for further investigation into the effects of different alcohol percentages on the process.



(a)



(b)

Fig. 3. Effect of some parameters on the hydrogen production rate: (a) Flow rate of injected CO_2 in CCM and (b) percentage of injected alcohol to the water

IV. Conclusions

This article aims to experimentally investigate hydrogen production using ultrasound technology. Through the experimental use of ultrasound technology, specifically 40 kHz ultrasonic transducers, it demonstrates a novel approach to generating hydrogen. The findings indicate that the temperature of the sonoreactor's solution plays a critical role in the efficiency of hydrogen production. An increase in hydrogen yield occurs when the temperature of the solution rises from 40°C to 60°C, increasing the production rate from 0.15 micromoles per minute to 0.19 micromoles per minute. Additionally, the introduction of alcohol and CO_2 to the water further enhances the hydrogen production rate, suggesting that the composition of the solution significantly impacts the effectiveness of the sonic hydrogen production process.

References

M. Sharifishourabi, I. Dincer, and A. Mohany, “Implementation of experimental techniques in ultrasound-driven hydrogen production: A comprehensive review,” *International Journal of Hydrogen Energy*, vol. 62, pp. 1183–1204, Apr. 2024, doi: 10.1016/j.ijhydene.2024.03.013.

S. S. Rashwan, I. Dincer, and A. Mohany, “A review on the importance of operating conditions and process parameters in sonic hydrogen production,” *International Journal of Hydrogen Energy*, vol. 46, no. 56, pp. 28418–28434, Aug. 2021, doi: 10.1016/j.ijhydene.2021.06.086.

Catalytic ammonia decomposition over nickel and ruthenium supported on Al_2O_3 pellets for hydrogen production

[1]Ali Turgay Şan, [2]Mehmet Çakır, [1,3]Halit Eren Figen
[1] Yildiz Technical University, Faculty of Chemical and Metallurgical Engineering, Department of Chemical Engineering, Esenler, Istanbul, 34220, Türkiye
[2] Yildiz Technical University, Naval Architecture and Maritime Faculty, Department of Marine Engineering, Beşiktaş, Istanbul, 34349, Türkiye
[3] Yildiz Technical University, Clean Energy Technologies Institute, Istanbul, 34220, Türkiye

* E-mail: sanaliturgay@gmail.com

Abstract
The moment numerous hazardous gases get released into the environment to meet the need for energy, environmental disasters happen. When hydrogen energy is burned, both with and without oxygen, all that is released are water molecules, making it an ecologically friendly fuel. The technologies used today for hydrogen production are not clean. Thermochemical ammonia decomposition, electrochemical water hydrolysis, and biochemical methods take precedence over these. Hydrogen storage and transportation are, however, intrinsically challenging. There is a high diffusion coefficient. There is little energy density. Because of this, hydrogen energy need a carrier in order to go to its intended destination. Ammonia (NH_3) is utilized extensively across the world as a hydrogen transporter. It is simple to store and transport. NH_3 has got a high hydrogen content. In this study, nickel and ruthenium metals were coated on alumina pellet. Various analysis methods have been examined. Ammonia decomposition reaction was carried out in a fixed bed gas reactor.

Keywords: Hydrogen production, ammonia decomposition, supported catalyst

I. Introduction

The demand for energy has increased due to rapid population expansion and the associated increase in human activity, leading to excessive greenhouse gas emissions from fossil fuels. The Kyoto Protocol and the Paris Agreement aim to prevent negative effects and meet global energy demand sustainably by UNFCC 2015.

Renewable energy sources like solar, wind, and hydropower are crucial for sustainability but have limitations due to location, weather, and climate change by Dincer 2000.

Energy can be stored by mechanical, chemical, electrical, or electrochemical processes and transported to where it is needed by Le vd., 2023. Hydrogen molecules can be stored in compressed gas, liquefied, liquid organic frameworks, alanates and chemical methods by Hassan et al 2021. However, these methods present low energy density. Difficulties causes hydrogen to be expensive for the end user up to $15 @700bar, 2,9MJ/l by Scovell, 2022.

Carbon-free chemical carriers and a renewable energy source are needed for green hydrogen production. These molecules include water and ammonia by Ma et al., 2024.

Ammonia, composed of 17.8% hydrogen by weight, is commercially produced globally and can be transported via various ways by Kass et al., 2023. Despite its colorless, caustic, and toxic nature, it has a flash point of 650 °C and can self-ignite in open air at concentrations between 15-28% by Yang et al., 2021.

Ammonia decomposition (Eq:1.) by Muroyama et al 2012 requires a temperature above 400 °C, and catalysts are necessary for high conversion rates at low temperatures. Nickel and ruthenium are active metals for ammonia decomposition, with ruthenium being the most active. The activity order of metals can be listed as Ru>Rh>Ni>Co>Ir>Fe>>Pt>Cr>Pd>Cu>>Pb. Aluminum oxide (Al_2O_3) has a large pore capacity and excellent chemical and physical stability. This characteristic has led to a great deal of research on heterogeneous catalysts by McCullough et al., 2020.

$$2NH_{3(g)} \rightarrow N_{2(g)} + 3H_{2(g)} \quad (1)$$

II. Experimental Set-up and Procedure

In this study, hydrogen synthesis by catalytic decomposition of ammonia was studied. It was carried out using nickel, ruthenium transferring solution via a pump on aluminum pellets. Chemicals used in the studies; nickel (II) nitrate hexahydrate, urea, citric acid, aluminum oxide pellet, pure water, hydrogen, nitrogen and ammonia gas. In experimental studies, Fluka® $RuAl_2O_3$ commercial powder catalyst was used for comparison study. Nickel solution was prepared as 1 molar, and 1:3 urea was used as the reducing agent. Ruthenium solution was prepared at 0.05 molar. The prepared solutions were left to mix for overnight. After all coating steps, the catalysts were washed by passing pure water. The drying process was carried out at 120°C for 2 hours. The calcination was processed in a muffle furnace at 700°C for 5 hours at a rate of 3°C/min. The prepared catalyst are given in Table 1.

Tab. 1: Ammonia decomposition rates of prepared catalysts at various temperatures

Catalyst	Code	Metal: support ratio
$NiAl_2O_3$	*R1*	*1:20*
$RuAl_2O_3$	*R2*	*1:20*
$RuNiAl_2O_3$	*R3*	*2:3:20*
$RuNiAl_2O_3$	*R4*	*1:3:20*
Fluka	*comercial*	*5:19*

The catalyst coating setup consists of a solution beaker, perilastic pump, fixed bed tank and tubing. After the washed and dried Al_2O_3 pellets were placed in the tank, the solution (Ni and or Ru) was passed through the pump at a constant rate. After the washing, drying and calcination steps, the catalysts were placed in a fixed bed tube type gas reactor and temperature programmed reduction (TPR) analysis was performed. The catalysts, whose reduction temperature was determined, were tested using a mass spectrometer in a 2% ammonia-nitrogen gas mixture environment.

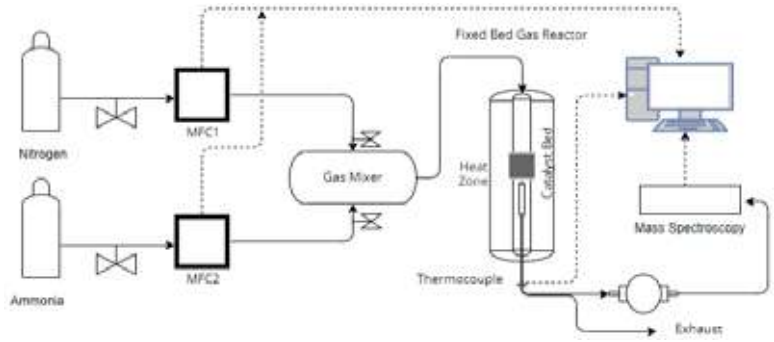


Fig. 1: Experimental ammonia decomposition process set-up

III. Analysis

The reduction behaviour of supported nickel and ruthenium species, as well as their interactions with supports, were studied using the H_2-TPR approach. The results were obtained using the Hidden Analytical QGA (Mass Spectroscopy) device for reducing gases. TPR Analysis results for sample catalysts (R1, R2, R3, com..) are shown in Figure 1. TPR analyses were carried out in a 5% hydrogen-nitrogen environment at 3°C/min. 1 gram of each sample was placed in the catalyst chamber. Analysis showed that the coating structure was multilayered and metal oxides interacted with the aluminium oxide layer. In structures containing nickel, it appears that nickel forms a bulk structure ($NiAl_2O_4$) with support around 800°C.

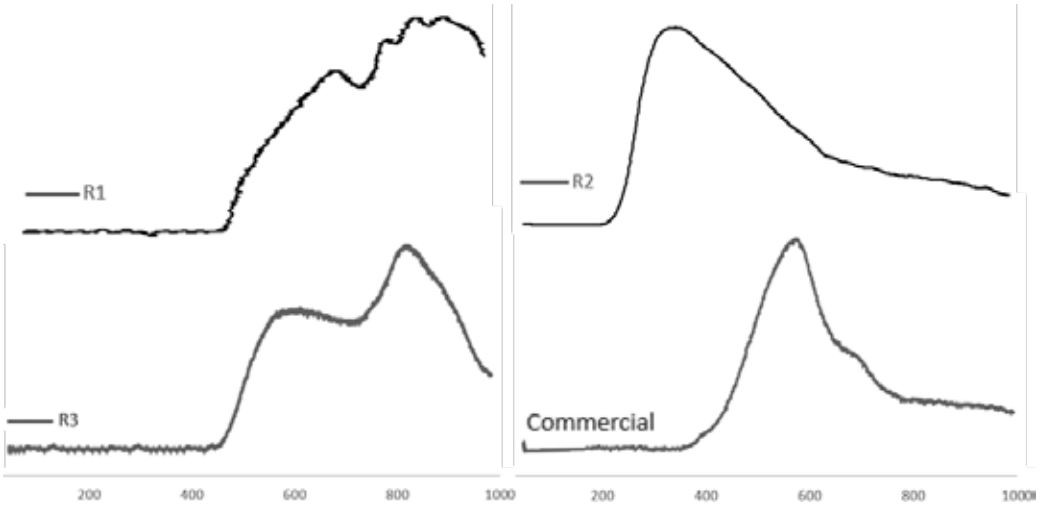


Fig. 2: TPR analysis results of R1, R2, R3, com.

IV. Results and discussions

The synthesised catalysts were tested for ammonia decomposition which is described in equation 1. using the catalyst test system illustrated in Figure 1. Between 400-550 °C temperature range, remarkable conversion rates were observed for the catalysts.

The ammonia decomposition reaction was carried out in the catalyst bed for 5 hours. According to these findings shown in Table 2, the R3 catalyst achieved the maximum ammonia conversion at operating temperatures. By coating an additional layer of Ruthenium metal between the R3 ($RuNiAl_2O_3$) and R4 ($RuNiAl_2O_3$) catalysts, the ammonia conversion rate was more than doubled at 450 °C. The noticeable improvement in the R3 catalyst also

showed better performance at higher temperatures. As a result of this result, it was observed that the two-layer ruthenium oxide on nickel oxide was of critical importance.
According to the results obtained (Table 2.), it was determined that the conversion rates increased at the same temperatures as more catalyst was coated on the alumina pellets catalyst support.

The R2 ($RuAl_2O_3$) catalyst, provided by adding relatively less quantities of Ruthenium metal to the ammonia conversion, has reasonably high conversions at temperatures up to 500 °C when compared to the catalyst R1 having just Nickel; a considerable rise 46% was seen at higher temperatures (550 °C). R3 ($RuNiAl_2O_3$) catalyst 8% compared to R2 ($RuAl_2O_3$) at 550 °C; It showed 58% more ammonia conversion compared to R1.

Tab. 2: Ammonia decomposition rates of prepared catalysts at various temperatures

Catalyst	NH_3% conversion @400 °C	NH_3% conversion @450 °C	NH_3% conversion @500 °C	NH_3% conversion @550 °C	GHSV ($mL/g_{cat}.h$)
R1	*5.5*	*23.1*	*38.6*	*53.1*	*30000*
R2	*12.3*	*28.9*	*49.5*	*77.8*	*30000*
R3	*42.9*	*58.1*	*66.2*	*83.9*	*30000*
R4	*10.3*	*23.2*	*37.9*	*50.5*	*30000*
Fluka	*11.6*	*20.2*	*30.3*	*44.5*	*30000*

V. Conclusions

In this work, ammonia decomposition was investigated using supported catalysts in a fixed bed reactor. Ruthenium-doped catalysts outperformed catalysts rather than without noble metal. However, when ruthenium metal was coated alone (R2 - $RuAl_2O_3$), the conversion rates remained lower than the bimetallic R3 ($RuNiAl_2O_3$).

The bulk structure generated by nickel oxide with aluminum oxide support during the calcination step prevented the catalyst from sintering at temperatures above the reduction temperature. Ruthenium oxide is reduced at a lower temperature than nickel oxide according to TPR results. When comparing R2 and R3, it is reasonable to predict that the catalyst life will be extended at high temperatures, and the conversion rate will be comparable. As a result, it was determined that the presence of nickel and ruthenium enhanced the coating process.

Acknowledgements

This research was supported by the TUBITAK 1507 Research Projects Funding Program (Project No: 7220095).

References

United Nations. Framework Convention on Climate Change. *Adoption of the Paris agreement*. 2015

Dincer, I. Renewable Energy and Sustainable Development: A Crucial Review. Renewable and Sustainable Energy Reviews, 4, 157-175, (2000).

Hassan, I. A., Ramadan, H. S., Saleh, M. A., & Hissel, D., Hydrogen storage technologies for stationary and mobile applications: Review, analysis and perspectives. *Renewable and Sustainable Energy Reviews*, *149*, 111311-111311, (2021).

H. Muroyama, C. Saburi, T. Matsui, ve K. Eguchi, “Ammonia decomposition over Ni/La2O3 catalyst for on-site generation of hydrogen”, *Applied Catalysis A: General*, c. 443-444, ss. 119-124., 2012.

Kass, M. D., Keiser, J. R., Liu, Y., Moore, A., & Polsky, Y., Assessing Compatibility of Natural Gas Pipeline Materials with Hydrogen, CO2, and Ammonia. *Journal of Pipeline Systems Engineering and Practice*, *14*(2), 1177-1192, (2023).

Katherine M., P.-H., Pei-Hua C., Juan J., ve Jochen L., Material Discovery and High Throughput Exploration of Ru Based Catalysts for Low Temperature Ammonia Decomposition”, *Materials*, 13,8, 1869-1888, (2020).

Le, T. T., Sharma, P., Bora, B. J., Tran, V. D., Truong, T. H., Le, H. C., & Nguyen, P. Q. P. Fueling the future: A comprehensive review of hydrogen energy systems and their challenges. *International Journal of Hydrogen Energy*, 54, 791-816, (2023).

Ma, N., Zhao, W., Wang, W., Li, X., & Zhou, H., Large scale of green hydrogen storage: Opportunities and challenges. *International Journal of Hydrogen Energy*, *50*, 379-396, (2024).

Scovell, M. D., Explaining hydrogen energy technology acceptance: A critical review. *International Journal of Hydrogen Energy*, *47*(19), 10441-10459, (2022).

Yang, B., Ding, W., Zhang, H., & Zhang, S., Recent progress in electrochemical synthesis of ammonia from nitrogen: Strategies to improve the catalytic activity and selectivity. *Energy & Environmental Science*, *14*(2), 672-687, (2021)..

Yang, G., & Park, S.-J. Conventional and Microwave Hydrothermal Synthesis and Application of Functional Materials: A Review. *Materials*, *12*(7), 1177-1195, (2019).

A Study on Geothermal-Based H_2S-FeCl Hybrid Process for Hydrogen Production and H_2S Removal

[1,2*] Sulenur Asal, [2] Adem Acır, [1] Ibrahim Dincer
[1] Clean Energy Research Laboratory, FEAS, Ontario Tech. University, Oshawa, ON, Canada
[2] Gazi University, Faculty of Technology, Department of Energy Systems Engineering, Ankara, Türkiye
* E-mail: sulenurasal@gazi.edu.tr

Abstract
This study presents a new integrated system to produce H_2 and remove H_2S. The integrated system uses geothermal energy as a heat source for the Rankine cycle. Moreover, H_2S, which is one of the byproducts of geothermal, is utilized with Fe-Cl to produce hydrogen. The required heat and electrical power to produce hydrogen via the H_2S-FeCl hybrid process is met from the Rankine cycle. The presented system is analyzed using the first and second laws of thermodynamics. Both hydrogen production and the energy and exergy efficiencies of the overall system are investigated with numerous source temperatures. As a consequence of the calculations, H_2 production increases as the source temperature rises. Furthermore, the energy efficiency of the overall system increases slightly with rising source temperature, while there is a remarkable decrease in the exergy efficiency of the overall system.
Keywords: Integrated systems, H_2S-FeCl hybrid process, hydrogen production, energy, exergy

I. Introduction
Hydrogen, a promising solution to meet the increasing energy demand, requires heat or electrical power to be produced via various methods. Geothermal energy can be one of the clean options for generating hydrogen. Additionally, geothermal power plants release a high amount of H_2S as a byproduct. When the literature studies are examined, it is seen that there are lots of studies on geothermal-based hydrogen production. Ghazvini et al. [1] reviewed hydrogen production methods based on geothermal energy, and they investigated geothermal-based hydrogen production systems technically, economically, and environmentally. Mahmoud et al. [2] presented a study on geothermal energy based hydrogen production systems. In the study, various types of geothermal power plants were investigated, including flash, binary, recuperative, organic Rankine cycle, etc. They calculated produced hydrogen between 5.44 kg/h and 13958 kg/h. Balta et al. [3] used geothermal energy as a source to produce hydrogen via a four-step copper-chlorine cycle. Studies were carried out from the perspective of energy and exergy. At the end of the study, the energy and exergy efficiencies of the proposed system were calculated as 21.67% and 19.35%, respectively. Cao et al. [4] modeled a system that comprises geothermal flash, Kalina cycle, electrolyser, and ammonia-water absorption refrigeration system. They calculated the highest energy efficiency of the proposed system, approximately 26.25% for 170°C geothermal water temperature.

Differing from the literature, this study aims to remove H_2S and produce H_2 using the H_2S-FeCl hybrid process. Geothermal energy is a clean energy source to produce hydrogen, and also H_2S can be removed via the H_2S-FeCl hybrid process. The analysis is carried out using energy and exergy approaches. The Rankine cycle and H_2S-FeCl hybrid process are integrated, and also the energy and exergy efficiencies of the Rankine cycle and the overall system are examined according to the various geothermal source temperatures.

II. System Description
This proposed system integrates the H_2S-FeCl hybrid process and the Rankine cycle to produce hydrogen and to remove H_2S, which is one of the byproducts of geothermal. Fig. 1 illustrates the proposed system layout.

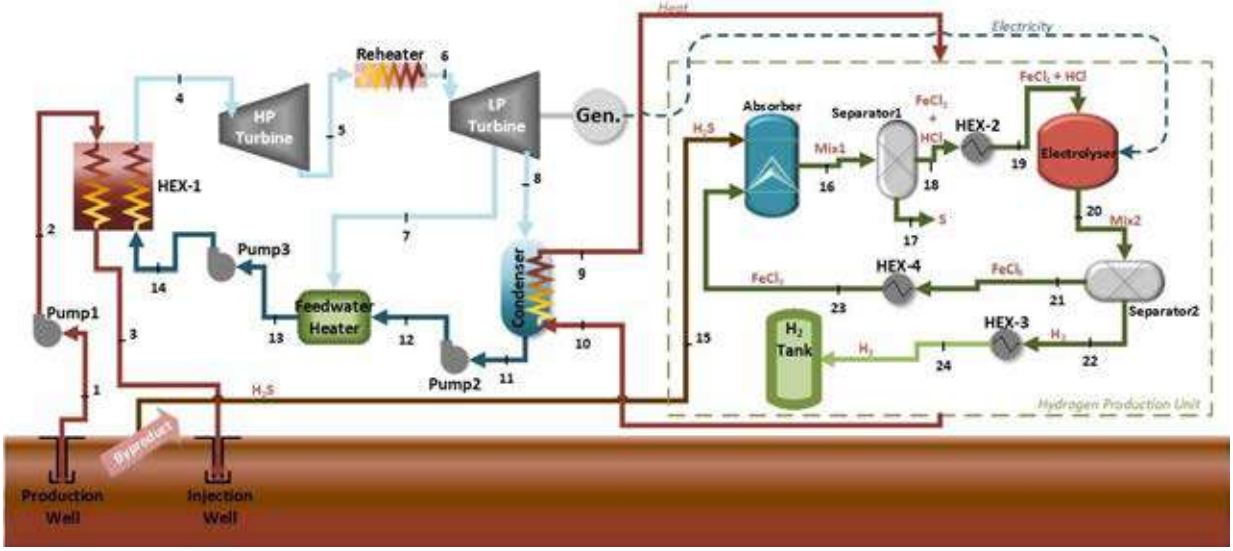


Fig. 1: System layout of the proposed system

The heat from the geothermal source at 250°C is used to turn the Rankine cycle. Heat exchanger 1 absorbs heat and turns the turbine wheels. The efficiency of heat exchanger 1 is assumed as 100%. Electrical power is generated via generator, which has 98% efficiency. Efficiencies of high- and low-pressure turbines and pumps are considered as to be 85%. The H_2S-FeCl hybrid process uses heat and electrical power to produce hydrogen. These requirements are met by the Rankine cycle's condenser and generator.

III. Analysis

Geothermal-based H_2S-FeCl hybrid process system is investigated using the first and second laws of thermodynamics. While the analysis is carried out, all processes take place in a steady state. The kinetic and potential energy and exergy changes are ignored. The mass, energy, entropy, and exergy balance equations are given with Eqs. (1-4) [6].

$$\sum \dot{m}_{in} = \sum \dot{m}_{out} \tag{1}$$

$$\sum \dot{Q}_{in} + \sum \dot{W}_{in} + \sum \dot{m}_{in}\left(h_{in} + \frac{V_{in}^2}{2} + gZ_{in}\right) = \sum \dot{Q}_{out} + \sum \dot{W}_{out} + \sum \dot{m}_{out}\left(h_{out} + \frac{V_{out}^2}{2} + gZ_{out}\right) \tag{2}$$

$$\sum \dot{S}_{in} + \sum \frac{\dot{Q}_{in}}{T_s} + \dot{S}_{gen} = \sum \dot{S}_{out} + \sum \frac{\dot{Q}_{out}}{T_s} \tag{3}$$

$$\sum \dot{E}x_{in} + \sum \dot{E}x_{in}^{Q} + \sum \dot{W}_{in} = \sum \dot{E}x_{out} + \sum \dot{E}x_{out}^{Q} + \sum \dot{W}_{out} + \dot{E}x_d \tag{4}$$

where, $\dot{S} = \dot{m}\ s$, $\dot{E}x = \dot{m}\ ex$ and $ex = (h - h_0) - T_0(s - s_0)$.

The H_2S-FeCl hybrid process consists two reactions; one of them is absorption and the other is electrolysis. Reactions are given in Eqs. (5-7). In the first step, sour gas mixture, which comes from geothermal source as a byproduct, reacts with aqueous phased $FeCl_3$ at between 60°C and 80°C. Sour gas composition comprises 15% H_2S and 85% N_2 gases. At the end of the absorption reaction, 2 moles $FeCl_2$, 2 moles HCl and 1 mole S occur. Products of the first reaction is sent to the separator 1. Here, sulfur is separated from the solution. The solution enters electrolysis cell and gas phased H_2 and aqueous phased $FeCl_3$ occur under 0.74-0.76 V. Mixture enters separator 2 and H_2 is obtained as a product, whereas $FeCl_3$ goes to the first reaction to be reused [7,8].

$$2FeCl_{3(aq)} + H_2S_{(g)} \rightarrow 2FeCl_{2(aq)} + 2HCl_{(aq)} + S \tag{5}$$

$$2FeCl_{2(aq)} + 2HCl_{(aq)} \rightarrow H_{2(g)} + 2FeCl_{3(aq)} \tag{6}$$

$$H_2S_{(g)} \rightarrow H_{2(g)} + S \quad \text{(net reaction)} \tag{7}$$

The energy and exergy efficiencies of the overall system are calculated using Eq. (8) and (9), respectively.

$$\eta_{en,overall} = \frac{\dot{m}_{H_2}\ LHV_{H_2}}{\dot{Q}_{in}} \tag{8}$$

$$\eta_{ex,overall} = \frac{\dot{m}_{H_2}\ ex_{H_2}}{\dot{E}x_{in}^{Q}} \tag{9}$$

IV. Result and Discussion

The system performance is examined through energy and exergy approaches. According to the geothermal source temperature, the performance of the Rankine cycle is investigated. Fig. 2 shows variations in the energy and exergy efficiencies of the Rankine cycle. It is observed that the energy efficiency increases slightly as the source temperature goes up from 225°C to 300°C. Regarding the exergy efficiency, there is a considerable diminish depending on the rising source temperature. The energy and exergy efficiencies of the Rankine cycle are calculated 21.1% and 49.1%, respectively, at 250°C source temperature.

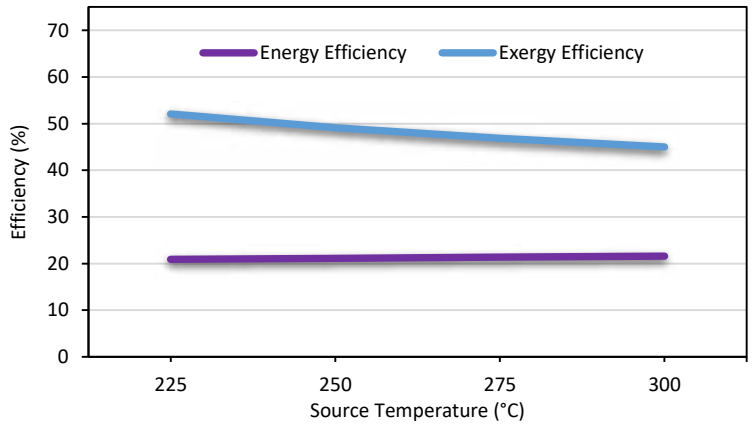


Fig. 2: Energy and exergy efficiency change of the Rankine cycle depending on source temperature

In Fig. 3, both the energy and exergy efficiencies of the overall system and hydrogen production amounts are given according to the geothermal source temperature. With the increasing source temperature, the amount of hydrogen

production increases slowly. While the 1.99 kg/s of hydrogen is produced at 225°C source temperature, it rises to 2.06 kg/s under the 300°C. With respect to the energy efficiency of the overall system, there is a slight improvement. While it is calculated as 34.4% at 225°C, it rises to 35.6% at 300°C source temperature. In contrast, as for the exergy efficiency of the overall system, there is a remarkable decline as the source temperature increases. The exergy efficiency changes between 83.8% and 72.4%. Consequently, with this designed system, H_2 is produced with high efficiency and at the same time, H_2S, a byproduct of geothermal power plant, is eliminated.

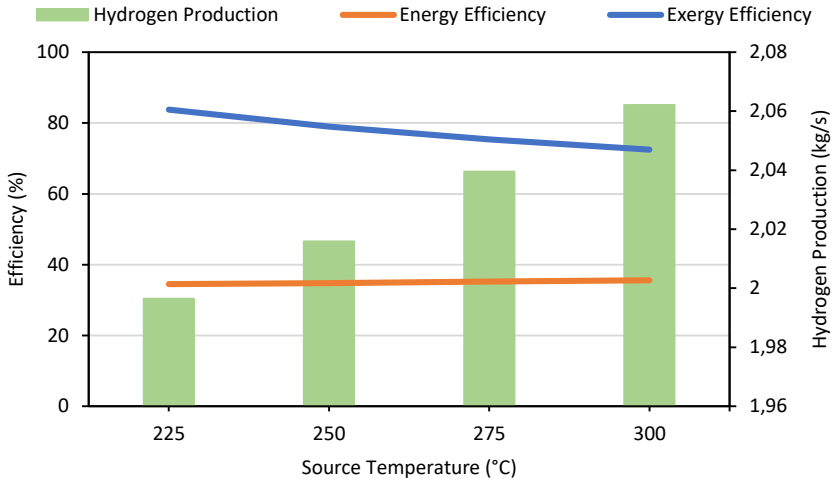


Fig. 3: Variations of the energy and exergy efficiencies for the overall system and hydrogen production amounts by geothermal source temperature

V. Conclusions

As a result of this study, the following are obtained: (a) The energy efficiency of the Rankine cycle increases as the source temperature rises, while the exergy efficiency decreases. (b) Hydrogen production goes up with increasing source temperature. (c) The energy and exergy efficiencies are calculated 43.8% and 79.0% for the overall system according to the 250°C source temperature, respectively.

Acknowledgement

Sulenur Asal would like to thank The Scientific and Technological Research Council of Turkiye (TUBITAK) for the financial support within the scope of the 2214-A International Doctoral Research Fellowship Program for Turkish Citizens.

References

[1] Ghazvini M, Sadeghzadeh M, Ahmadi MH, Moosavi S, Pourfayaz F. Geothermal energy use in hydrogen production: A review. Int J Energy Res 2019;43:7823–51.
[2] Mahmoud M, Ramadan M, Naher S, Pullen K, Ali Abdelkareem M, Olabi AG. A review of geothermal energy-driven hydrogen production systems. Therm Sci Eng Prog 2021;22:100854.
[3] Tolga Balta M, Dincer I, Hepbasli A. Energy and exergy analyses of a new four-step copper-chlorine cycle for geothermal-based hydrogen production. Energy 2010;35:3263–72.
[4] Cao L, Lou J, Wang J, Dai Y. Exergy analysis and optimization of a combined cooling and power system driven by geothermal energy for ice-making and hydrogen production. Energy Convers Manag 2018;174:886–96.
[5] Karapekmez A, Dincer I. Modelling of hydrogen production from hydrogen sulfide in geothermal power plants. Int J Hydrogen Energy 2018;43:10569–79.
[6] Dincer I (2021) Thermoydnamics: A Smart Approach, 1st ed., John Wiley & Sons, London n.d.
[7] Mizuta S, Kondo W, Fujii K, Iida H, Isshiki S, Noguchi H, et al. Hydrogen Production from Hydrogen Sulfide by the Fe-Cl Hybrid Process. Ind Eng Chem Res 1991;30:1601–8.
[8] Adewale RA, Berrouk AS, Dara S. A process simulation study of hydrogen and sulfur production from hydrogen sulfide using the Fe-Cl hybrid process. J Taiwan Inst Chem Eng 2015;54:20–7.

A Floating SMR and Ocean-Based Community Energy System with Hydrogen and Molten Salt Storage

Mert Temiz*, Ibrahim Dincer
Clean Energy Research Laboratory (CERL), Faculty of Engineering and Applied Science,
Ontario Tech. University, 2000 Simcoe Street North, Oshawa, Ontario L1G 0C5, Canada

E-mails: Mert.Temiz@OntarioTechU.ca, Ibrahim.Dincer@OntarioTechU.ca

Abstract
The current study investigates the hybridization of floating small modular nuclear reactor with ocean energy in order to maximize the source utilization for multiple useful outputs. A molten salt energy storage system is incorporated with a three-stage power generation cycle where steam Rankine, organic Rankine and ammonia Trilateral cycles are combined. The energy and exergy points of views are considered to design and analyze the proposed system. Hydrogen energy system is used as the energy storage alternative, as well as to meet community's hydrogen demand. Time dependent analysis with changing parameters showed that the average energy and exergy efficiencies in a typical year are 34.71% and 38.10%, respectively.

Keywords: Floating SMR, ocean energy, hydrogen, sustainable community

I. Introduction
In order to address net zero targets, it is crucial to replace fossil fuel-based energy infrastructure with sustainable alternatives, such as with nuclear or renewables (Ruth et al., 2014). The intermittency of renewables effects the reliability of alternative energy systems. From this aspect, continuous energy supplies such as nuclear, and energy storage options are very critical to have a complete energy solution for net zero (Dincer, 2023). Current study investigates an hybridized energy system with small modular nuclear reactor (SMR) and ocean-based integrated system, in order to generate power, hydrogen and heat for communities in a sustainable manner. The proposed system is investigated from energy and exergy aspects of thermodynamics.

II. System description and analysis
The proposed system consists of a floating SMR, where it is connected with a land-based molten salt energy storage tank. A direct-contact molten salt carbon dioxide heat exchanger unit is used to transfer heat from nuclear fuel to the molten salt via helium and carbon dioxide. The connection between land and floating SMR is considered to be made via a molten salt thermofluid line. In the land-based system, a steam Rankine cycle, organic Rankine cycle, and ammonia trilateral cycle are combined in order to work in an operational strategy according to the available heat at molten salt tanks. Hydrogen is used as the alternative energy storage option which is generated by anion exchange membrane electrolyzer and consumed by the proton exchange membrane fuel cell. The proposed system generated district heating, hydrogen, domestic hot water, and power for a sustainable community as shown in Fig. 1.

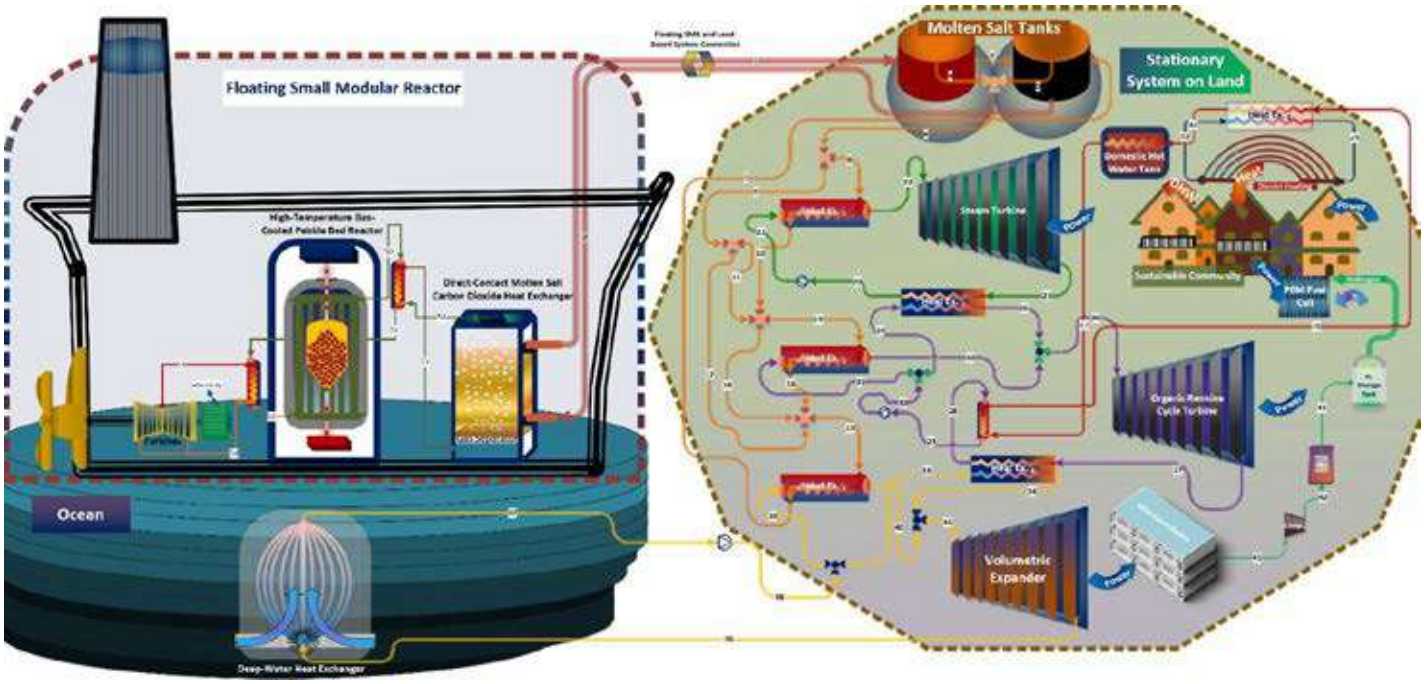


Fig. 1: A layout of the proposed system

The integrated system and its subsystems with components are analyzed through the energy, entropy and exergy

balance equations introduced by Dincer (Dincer, 2020). The general balance equations can be expressed as

$$\sum_i \dot{Q}_i + \sum_i \dot{W}_i + \sum_i \dot{m}_i \left(h_i + \frac{V_i^2}{2} + gZ_i\right) = \sum_o \dot{Q}_o + \sum_o \dot{W}_o + \sum_o \dot{m}_o \left(h_o + \frac{V_o^2}{2} + gZ_o\right) \quad (1)$$

$$\sum_i \dot{m}_i s_i + \sum_{net} \frac{\dot{Q}_{net}}{T_S} + \dot{S}_{gen} = + \sum_o \dot{m}_o s_o \quad (2)$$

$$\sum_i \dot{E}x_{\dot{Q}_i} + \sum_i \dot{W}_i + \sum_i \dot{m}_i ex_i = \sum_o \dot{E}x_{\dot{Q}_o} + \sum_o \dot{W}_o + \sum_o \dot{m}_o ex_o + \dot{E}x_d \quad (3)$$

The overall energy and exergy efficiencies are calculated as follows:

$$\eta_{en,ov} = \frac{\dot{W}_{El,net} + \dot{m}_{H_2} LHV_{H_2} + \dot{Q}_{District\ Heating} + \dot{Q}_{DHW}}{\dot{Q}_{SMR}} \quad (4)$$

$$\eta_{ex,ov} = \frac{\dot{W}_{El,net} + \dot{m}_{H_2} LHV_{H_2} + \dot{E}x_{Q_{District\ Heating}} + \dot{E}x_{Q_{DHW}}}{\dot{E}x_{Q_{SMR}}} \quad (5)$$

where ocean energy is not considered since it is used to create a room for low temperature condensation process for the ammonia trilateral cycle.

III. Results and discussion

The proposed system is analyzed from energy and exergy aspects for a typical year with changing parameters for the load and ambient weather conditions. The obtained results showed that the overall energy efficiency is changed between 20.13% and 62.56% in a typical year, according to the changing parameters in the hourly resolution. The winter months typically lead to lower energy efficiencies. When one looks at the exergy efficiency, the difference between the energy and exergy efficiency is higher during the cold ambient temperatures as shown in Fig. 2. This is typically due to the fact that the district heating and domestic hot water consists lower exergy content compared to the energy content. The overall exergy efficiency in a typical year is found to be 38.10%, which is changed between 8.78% and 80.07% according to the hourly calculations and changed between 27.40% and 63.33% according to the daily calculations.

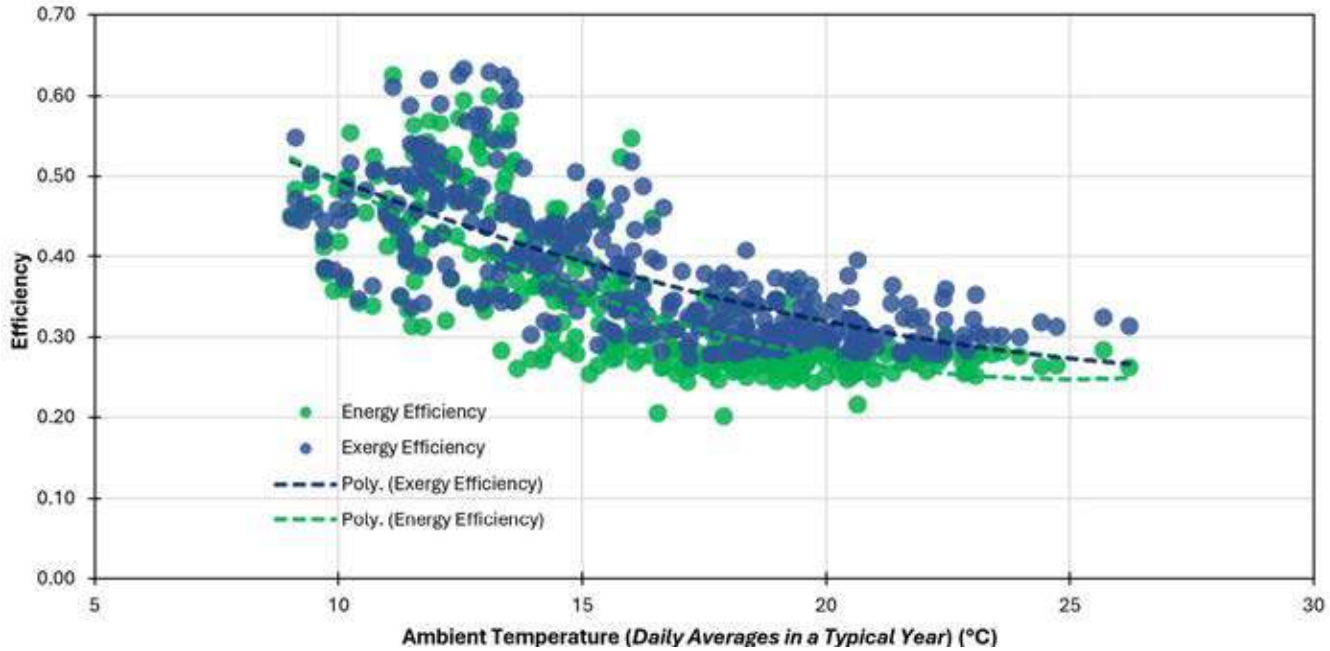


Fig. 2: The overall energy and exergy efficiencies by changing ambient temperatures in a typical year

IV. Conclusions

A nuclear renewable hybrid energy system is designed for resilient communities. According to the obtained results, time dependent analysis with changing parameters showed that the average energy and exergy efficiencies in a typical year are 34.71% and 38.10%, respectively. For more resilient communities, it is crucial to supply continuous energy, which is less dependent on changes of renewable sources. Nuclear renewable hybrid energy systems can ensure energy security in an environmentally friendly manner.

References

Dincer, I., Thermodynamics: A Smart Approach. John Wiley & Sons (2020).
Dincer, I., Hydrogen 1.0: A new age. International Journal of Hydrogen Energy, 48(43), 16143–16147, (2023).
Ruth, M. F., Zinaman, O. R., Antkowiak, M., Boardman, R. D., Cherry, R. S., & Bazilian, M. D., Nuclear-renewable hybrid energy systems: Opportunities, interconnections, and needs. Energy Conversion and Management, 78, 684–694, (2014).

PEMFC Performance of Pt Catalyst Decorated on Heat-Treated Carbon Black

[1]Ayşenur Öztürk Aydın, [2*]Ayşe Bayrakçeken
[1] Atatürk University, Faculty of Engineering, Chemical Engineering Department, Erzurum, 25240, Türkiye
[2] Atatürk University, Nanoscience and Nanoengineering Research and Application Center, Erzurum, 25240, Türkiye

* E-mail:ayse.bayrakceken@gmail.com

Abstract
Pt nanoparticles (NPs), a key catalyst for electrochemical reactions in polymer electrolyte membrane fuel cells (PEMFCs), tend to agglomerate when they come into contact, reducing the catalyst's active surface area. Pt NPs are typically supported by low-cost carbon-based materials. Carbon materials with appropriate surface area provide a homogeneous distribution of Pt NPs. The disadvantage of these materials is their electrochemical oxidation and corrosion under harsh operating conditions (high potential, high humidity, etc.) of PEMFCs. Heat treatment at high temperatures to make carbon materials resistant to corrosion is one of the applications in the literature. In this work, carbon black (Vulcan XC 72R) was heat treated in a nitrogen atmosphere at 1000, 1200, 1400, and 1500 °C before being evaluated in PEMFC as a Pt catalyst support. Pt/Vulcan XC 72R-1000 was the best catalyst, with PEMFC performance values measured as 649.2 mA/cm^2 and 388.2 mW/cm^2 at 0.6 V.

Keywords: Vulcan XC 72R, carbon black, heat treatment, catalyst support, oxygen reduction reaction, PEMFC

I. Introduction

Polymer electrolyte membrane fuel cells (PEMFCs) are the most popular form of FCs because of their high power efficiency. It is critical to develop materials with high performance and durability to achieve the desired targets in fuel cell electric vehicles (FCEVs), which are a fundamental application area of PEMFCs. Pt metal is the primary catalyst in PEMFCs due to its high catalytic activity for the oxygen reduction reaction (ORR). Carbon-based materials often serve as supports to enable uniform dispersion of Pt nanoparticles (NPs), which range in size from 2 to 4 nm. Carbon materials can be available in different morphologies, are inexpensive, and have good electrical conductivity. The disadvantage of these materials is that the corrosion of carbon at high potentials (≥ 1.2 V) weakens its interactions with the Pt catalyst, resulting in considerable resistance to oxygen transfer (Borup et al. (2020)).

Heat treatment of carbon materials in an inert environment at high temperatures is one method for increasing their corrosion resistance. It aims to increase the graphitization degree of the carbon material, improving its chemical and thermal stability. At high temperatures, the disordered structure in carbon dissolves, sp^2 hybridization increases, and a graphitic crystal structure forms. Studies wherein heat-treated carbon materials are catalyst support in PEMFCs yielded favorable ORR activity, membrane electrode assembly (MEA) performance, and durability. Li et al. (2022) applied heat treatment to BP-2000 carbon blacks at 1800, 2000, 2200, and 2400 °C. The Pt/GBP-2200 catalyst exhibited the highest ORR activity; the Pt/GBP-2200 and Pt/C catalysts showed a voltage drop of 4% and 10.3%, respectively, at 1000 mA/cm^2, following the accelerated stress test (AST) at 1.5 V. With a different approach, Kim et al. (2024) prepared the PtNi alloy catalysts on Vulcan XC 72R and applied them to heat treatment at 500, 700, and 900 °C in a hydrogen atmosphere. They recorded the highest ORR activity with the Pt_7Ni_3/C-700 catalyst.

In this study, Vulcan XC 72R carbon blacks were heat treated at 1000, 1200, 1400, and 1500 °C and employed as Pt catalyst support in PEMFCs. The prepared catalysts are expected to have improved performance and durability.

II. Experimental Set-up and Procedure

Catalyst supports were commercial carbon black (Vulcan XC 72R, Cabot). This material was placed in the oven in horizontal ceramic crucibles and kept in a nitrogen atmosphere at 1000, 1200, 1400, and 1500 °C for one hour. After the heat treatment period, nitrogen flow continued until the oven temperature dropped below 100 °C, and then the samples were taken out of the oven.

The microwave-assisted polyol method was used to prepare the Pt catalyst (20% wt.) on original and heat-treated carbon blacks. Carbon blacks (100 mg) dissolved in 50 mL of ethylene glycol were mixed with 5.2 mL of a 0.05 M Pt precursor ($H_2PtCl_6.6H_2O$) solution and stirred for an hour. The mixture was then microwaved at 800 W for 1 min before being suddenly cooled. Centrifugation was used to remove the solid material from the solution, which was then washed with acetone and distilled water. The resulting solid was dried at 100 °C for 12 hours.

The electrochemical study of Pt catalysts was first performed using a three-electrode setup. For this purpose, a film layer of catalyst solutions (28 $\mu g_{Pt}/cm^2$) was produced on glassy carbon (GC, 0.1963 cm^2). The required catalyst was dissolved in 1,2-propanediol and distilled water, as well as Nafion solution (Ion Power, 15% wt.), and stirred for 24 hours. 5 µL of the prepared solution was dropped onto the GC and allowed to dry at room temperature overnight.

The second phase of the electrochemical analysis was the PEM fuel cell test station. For this reason, the first MEA was prepared. A commercial Pt/C (Tanaka) catalyst was used in the anode electrode, whereas the Pt/Vulcan XC 72R catalyst was used in the cathode electrode of MEA at a loading rate of 0.4 mg/cm^2. Catalyst inks were prepared by collecting the relevant catalyst with Nafion solution, 2-propanol, and distilled water, and these inks were

applied by spraying on gas diffusion layers (GDLs, Sigracet 34 BC). After reaching the desired loading on the GDL, the anode and cathode electrodes were combined in a hot press device with the commercial Nafion membrane (Nafion-212) to form the MEA structure.

III. Analysis

Brunauer Emmett Teller (BET, Micromeritics 3Flex) analysis was performed to understand how the surface areas and pore sizes of heat-treated Vulcan XC 72R carbon blacks changed. Surface morphologies that underwent structural changes due to heat treatment were visualized using a scanning electron microscope (SEM, Zeiss Sigma 300). X-ray diffraction (XRD, PANalytical Empyrean) analysis was performed to elucidate the crystal structures of the prepared Pt catalysts. Inductively coupled plasma mass spectrometry (ICP-MS, Agilent 7800) analysis was used to determine Pt loadings on the support materials. The hydrophobicity of the produced catalysts was evaluated using a contact angle measurement instrument.

For electrochemical analysis, a three-electrode cell system connected to the potentiostat was used. The three-electrode system consists of an Ag/AgCl electrode as the reference electrode, Pt wire as the counter electrode, a catalyst film layer formed on GC as the working electrode, and perchloric acid (0.1 M) as the electrolyte. By taking cycling voltammetry (CV) measurements (-0.28-0.92 V, 50 mV/s) in a nitrogen-fed electrolyte environment, the peak areas of hydrogen adsorbed and desorbed on the Pt surface were calculated, and the electrochemical surface area (ECSA) values of the catalysts were found by using these peak areas. Fuel cell performance was measured using a test station (Henatech, 600 W). Fig. 1 shows the single FC at this station. The prepared MEAs were placed in the active area (4.41 cm^2) where the gas flow channels are located in the single FC, and the cell was closed by compressing. Subsequently, nitrogen gas was sent to the system, causing the temperature of the humidification tanks, gas line, and FC to rise to 70 °C. Afterward, hydrogen and oxygen gases (0.25 slpm) were delivered to the anode and cathode electrodes, respectively, and current values were measured at a relative voltage with certain periods.



Fig. 1: Single FC in the test station

IV. Results and discussions

Fig. 2 gives the nitrogen adsorption-desorption isotherms of the Vulcan XC 72R carbon blacks. The formation of a hysteresis loop in the relative pressure range of 0.8-1.0 indicates the type-IV isotherm in which meso and micropores coexist. The BET surface areas of Vulcan XC 72R, Vulcan XC 72R-1000, Vulcan XC 72R-1200, Vulcan XC 72R-1400, and Vulcan XC 72R-1500 were determined as 241.0, 185.6, 174.5, 153.2, and 133.9 m^2/g, respectively. The heat treatment caused the BET surface areas to gradually decrease (Inoue et al. (2012)).

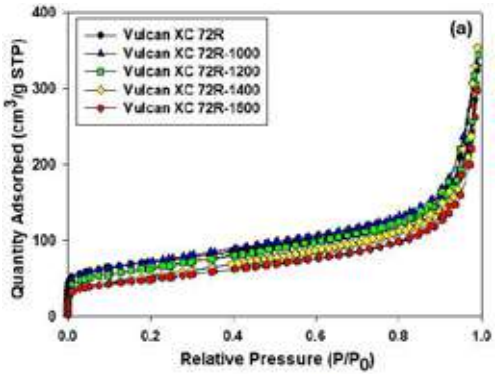


Fig. 2: BET isotherms of the Vulcan XC 72R carbon blacks

The SEM images in Fig. 3 show that the Vulcan XC 72R carbon blacks have a morphology consisting of bushy clusters formed by the irregular aggregation of spherical NPs (Gu et al. (2019)). As the heat treatment increases, the clusters dissolve and decrease. Fig. 4 exhibits the XRD pattern of Pt/Vulcan XC 72R catalysts. The peaks at 39º, 46º, 67º, 81º, and 86º are (111), (200), (220), (311), (222) crystal planes assigned to the face-centered cubic (fcc) structure of Pt (Öztürk et al. (2018)). ICP-MS analysis determines the % wt. Pt of the Vulcan XC 72R, Vulcan XC 72R-1000, Vulcan XC 72R-1200, Vulcan XC 72R-1400, and Vulcan XC 72R-1500 as 14.7, 15.2, 14.9, 13.1, and 14.0, respectively.

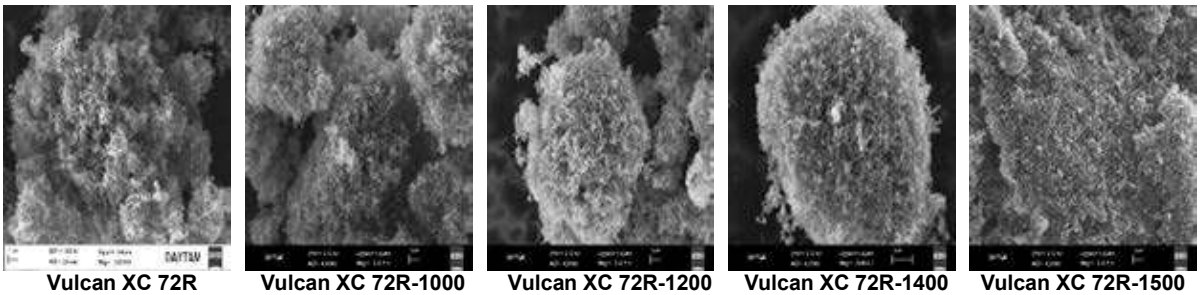


Fig. 3: SEM images of the Vulcan XC 72R carbon blacks

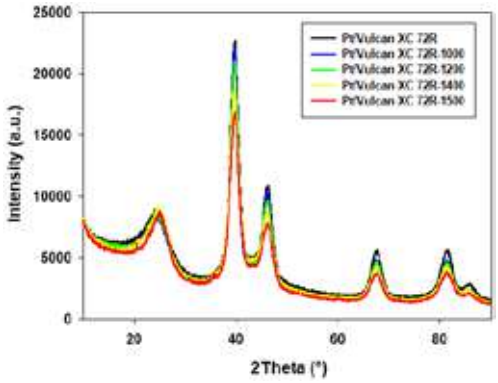


Fig. 4: XRD analysis of the Pt/Vulcan XC 72R catalysts

Tab. 1 shows the contact angle values at 70 °C on the surface of the Pt/Vulcan XC 72R catalysts. Pt/Vulcan XC 72R-1200 has the most hydrophobic surface (146.52 ± 0.97).

Tab. 1: Contact angle values of the surfaces covered with Pt/Vulcan XC 72R catalyst inks

Catalyst	Contact Angle
Vulcan XC 72R	145.64 ± 2.97
Vulcan XC 72R-1000	145.99 ± 2.91
Vulcan XC 72R-1200	146.52 ± 0.97
Vulcan XC 72R-1400	132.51 ± 1.57
Vulcan XC 72R-1500	126.02 ± 2.15

Fig. 5 demonstrates the CV diagrams of Pt/Vulcan XC 72R catalysts. The peaks of the hydrogen adsorbed (cathodic way) and desorbed (anodic way) in the range of -0.1-0.2 V are evident. ECSA values of Vulcan XC 72R, Vulcan XC 72R-1000, Vulcan XC 72R-1200, Vulcan XC 72R-1400, and Vulcan XC 72R-1500 were 33.7, 40.1, 28.1, 21.7, and 18.3 m^2/g, respectively.

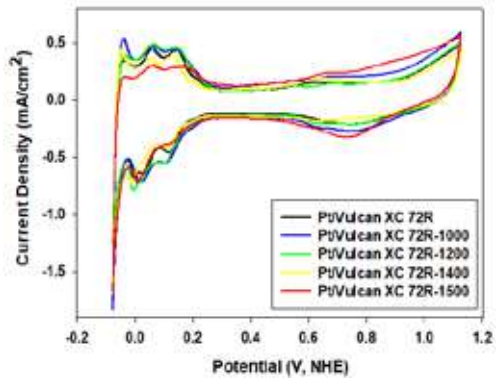


Fig. 5: CV analysis of the Pt/Vulcan XC 72R catalysts

In Fig. 6, the Vulcan XC 72R-1000 catalyst provided better performance results than other catalysts at 0.6 V. Vulcan XC 72R, Vulcan XC 72R-1000, Vulcan XC 72R-1200, Vulcan XC 72R-1400, Vulcan XC 72R-1500, and Tanaka catalysts gave 483.4, 649.2, 297.7, 556.2, 406.1, and 633.8 mA/cm^2 current densities, respectively. The Pt/Vulcan XC 72R-1000 catalyst also reached 388.2 mW/cm^2 at 0.6 V.

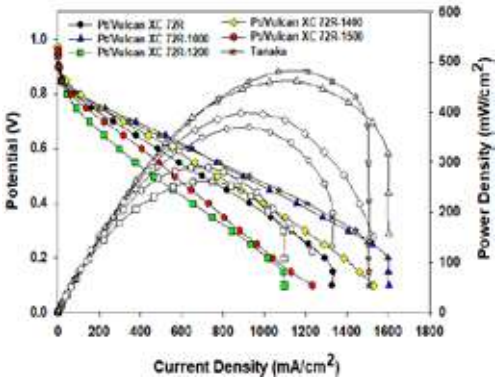


Fig. 6: Polarization curves of the Pt/Vulcan XC 72R catalysts and Tanaka catalyst

V. Conclusions

It was aimed at creating catalyst support materials that will increase the performance of Pt catalysts by applying heat treatment (1000, 1200, 1400, and 1500 ºC) to Vulcan XC 72R carbon black. In heat-treated carbon blacks, BET surface areas decreased, and the morphological structures began to dissolve as the temperature increased. Pt/Vulcan XC 72R-1000 has the second-most hydrophobic catalyst surface. The Pt/Vulcan XC 72R-1000 provided the highest ECSA value (40.1 m^2/g) and the current and power density (649.2 mA/cm^2 and 388.2 mW/cm^2) values. Heat treatment at 1000 °C has improved the performance of Vulcan XC 72R carbon black.

Acknowledgments

The authors gratefully acknowledge the Atatürk University Scientific Research Projects Coordination Unit for financial support with the project number of FDK-2021-9284.

References

Borup, R. L., Kusoğlu, A., Neyerlin, K. C., Mukundan, R., Ahluwalia, R. K., Cullen, D. A., Recent developments in catalyst-related PEM fuel cell durability, Current Opinion in Electrochemistry, 21, 192-200, (2020).

Inoue, H., Hosoya, K., Kannari, N., Ozaki, J., Influence of heat-treatment of Ketjen Black on the oxygen reduction reaction of Pt/C catalysts, Journal of Power Sources, 220, 173-179, (2012).

Gu, L., Chu, Y., Du, H. M., Zhang, Y., Zhao, J. S., Xie, Y., Supramolecular Iron Complex Formed Between Nitrogen Riched Phenanthroline Derivative and Iron With Improved Oxygen Reduction Activity in Alkaline Electrolyte, Frontiers in Chemistry, 7, 1-12, (2019).

Kim, S-I., Lim, S-Y., Son, M., Kim, T., Highly Active and Stable Bimetallic Ordered Catalysts for Oxygen Reduction Reaction Improvement in Polymer Exchange Membrane Fuel Cells, Applied Surface Science, 656, 1-7, (2024).

Li, B., Xie, M., Wan, K. C., Wang, X. L., Yang, D. J., Liu, Z. K., A High-Durability Graphitic Black Pearl Supported Pt Catalyst for a Proton Exchange Membrane Fuel Cell Stack, Membranes, 12, 1-19, (2022).

Öztürk, A., Bayrakçeken Yurtcan, A., Synthesis of polypyrrole (PPy) based porous N-doped carbon nanotubes (N-CNTs) as catalyst support for PEM fuel cells, International Journal of Hydrogen Energy, 43, 18559-18571, (2018).

Simulational Anaylses of Hybrid Fuel Cell Locomotive

[1]Mustafa Tunahan Başar, [2]Mustafa Kaan Baltacioğlu, [3*]Hüseyin Turan Arat
[1] Department of Motor Vehicles and Transportation Technologies, Vocational School of Taşova Yüksel Akın, Amasya University, Amasya,05800, Türkiye
[2] Department of Mechatronics Engineering, Iskenderun Technical University, Iskenderun, Hatay, 31200, Türkiye
[3] Department of Mechanical Engineering, Sinop University, Sinop, 57000, Tükiye

* E-mail: htarat@sinop.edu.tr

Abstract
Hybrid electric and propulsion systems have been widely used in locomotive/rail applications in the last decade. In this simulational study, a hybrid locomotive (fuel cell and battery) was modeled and analyzed with the AVL Cruise M program. The selected route was 488 km in length between Ankara and İstanbul. The analyses were done for the modeled locomotive under a hybrid propulsion system via a fuel cell pack and high voltage battery couple. Battery parameters such as SOC, energy, power; and Fuel Cell parameters such as temperature, energy, hydrogen consumption were simulated under specified conditions. As a result, a fuel cell-powered locomotive's energy and route results were investigated and presented by graphs.

Keywords: Hydrail, Locomotive, Fuel cell, Hydrogen, Efficiency.

I. Introduction

Railway transportation, which has a very important place in the transportation sector; has started to equip itself with electric/hydrogen propulsion systems for increasing emissions and a more green society (Al-Hamed and Dincer, 2021). The sector, which has been experiencing technological developments for the last 50 years with batteries and basic electric transmission, and with hydrogen engines/fuel cells for the last 15 years, currently accounts for 1 percent of the world's total emissions (even this figure was 95 million tons in 2022) (Statista, 2023). The diversity and development of fuel cells are increasing day by day, and thus their efficiency and power/weight ratios are also increasing (Mekhilef et al., 2012). Compact and modular fuel cells that can be used in industrial, marine and railway vehicles are slowly starting to be produced in the market (Sürer and Arat, 2022, Stobnicki and Gallas, 2022).

Especially in Germany and other EU countries, powering locomotives with hydrogen is among the important project topics (Gjerdingen, 2020). The global railway network has reached circa 1.3 million km, which of those 275 thousand km are in EU countries. The USA and China also have a railway network of 250 thousand km and 156 thousand km, respectively. The compound annual growth rate (CAGR) is increasing by 6.73%, with expected to nearly 583 billion dollars market sharing reaching in 2024 (Railway Technology, 2014, Rail Transport Global Market Report, 2024). In this study, we focus on the issue of alternative fuel transportation, which has become widespread in our country; The hybrid fuel cell locomotive, which uses a fuel cell and high voltage battery together, was modeled with AVL Cruise M and the results were presented, indeed.

II. Materials and Method

In this study, the locomotive whose features are given in Table 1 was inspired by the AVL Cruise M model. The main propulsion system that drives the modeled locomotive is a semi-hybrid propulsion system and consists of a fuel cell and HV (high voltage) battery. After vehicle modeling was completed, the route determination process started. A route, which can be seen in Figure 1, was created between two important and crowded (>25% of the total population of Turkiye) provinces of Turkey (Ankara-Istanbul). The 90-tonne locomotive was simulated through a 488 km route. There are 2 tunnels in this route and the total length is determined as 7 km. It is assumed that the train has 4 stops in total and the load carried at each stop is 2 tons. 1st stop; is Ankara Polatlı; the 2nd is Polatlı-Eskişehir, the 3rd Eskişehir-Sakarya and the 4th stop is; Sakarya-Istanbul.

Tab. 1. Specification of modeled Locomotive

Locomotive and parts	***Specification***
Propulsion	Fuel Cell Locomotive (FC) Fuel Cell: 5000 cell, 2720 cm^2, max current: 2500 A HV battery:262 cell, 2000 V max voltage, connection eff:0.94, SOC:55-70%
Length/ Weight	25 m/ 90 tons
Frontal Area	13.5 m
Wheel Rolling R	546 mm (static), 550mm (Dynamic)
Rote and stop lengths.	488 km Total; Ankara-Polatlı: 82 km, Polatlı-Eksişehir: 142 km, Eskişehir-Sakarya: 143 km (consists of 2 tunnels; 5 km) Sakarya- İstanbul: 121 km (consist of 1 tunel 2 km)

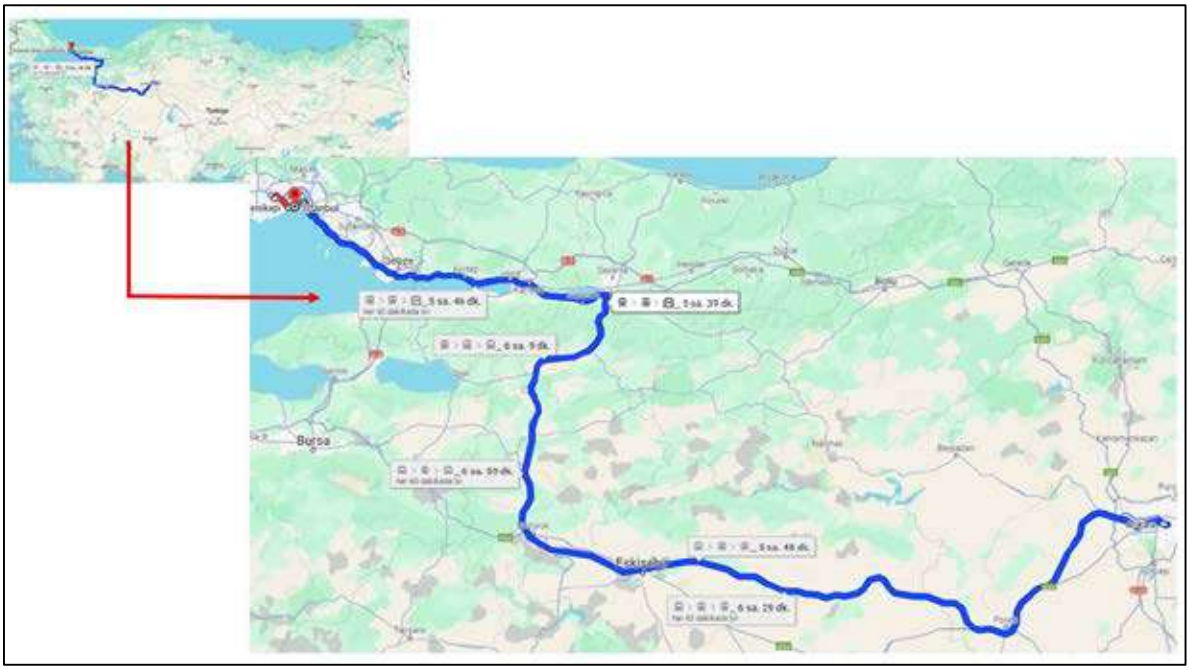


Fig. 1. Route of FC locomotive.

Figure 1 shows the route of the rail transportation vehicle. There is also an existing high-speed train line with similar location information on the current route. However, the electricity supply is provided by a catenary line. In this study, the development of fuel cell systems as an alternative to this high-speed train application is evaluated. Structures such as tunnels have also been defined in the system in order to observe the differences in the energy analysis of the locomotive designed on the new route. The vehicle, which operates between Ankara and Istanbul, completes the journey with a short stop in Eskişehir and Sakarya.

III. Result and Discussion

Figure 2 shows the power requirements of the electric motor graphically. It can be stated that the first observed phenomenon is that the power is provided from the battery at very low levels (1400 kW) between Ankara and Polatlı. It is considered that a secondary energy source (Fuel cell) is used due to the short distance. As the distance between Polatlı and Eskişehir increases, the amount of power consumed also increases. Between Eskişehir and Sakarya, especially in locations where tunnels are located, power requirements from the battery increase by 85%. It is expected that fuel cells will be put into operation at high rates in this range. Between Sakarya and Istanbul, this situation tends to decrease significantly with the support of the fuel cell. It can be stated that a more balanced fuel consumption is achieved.

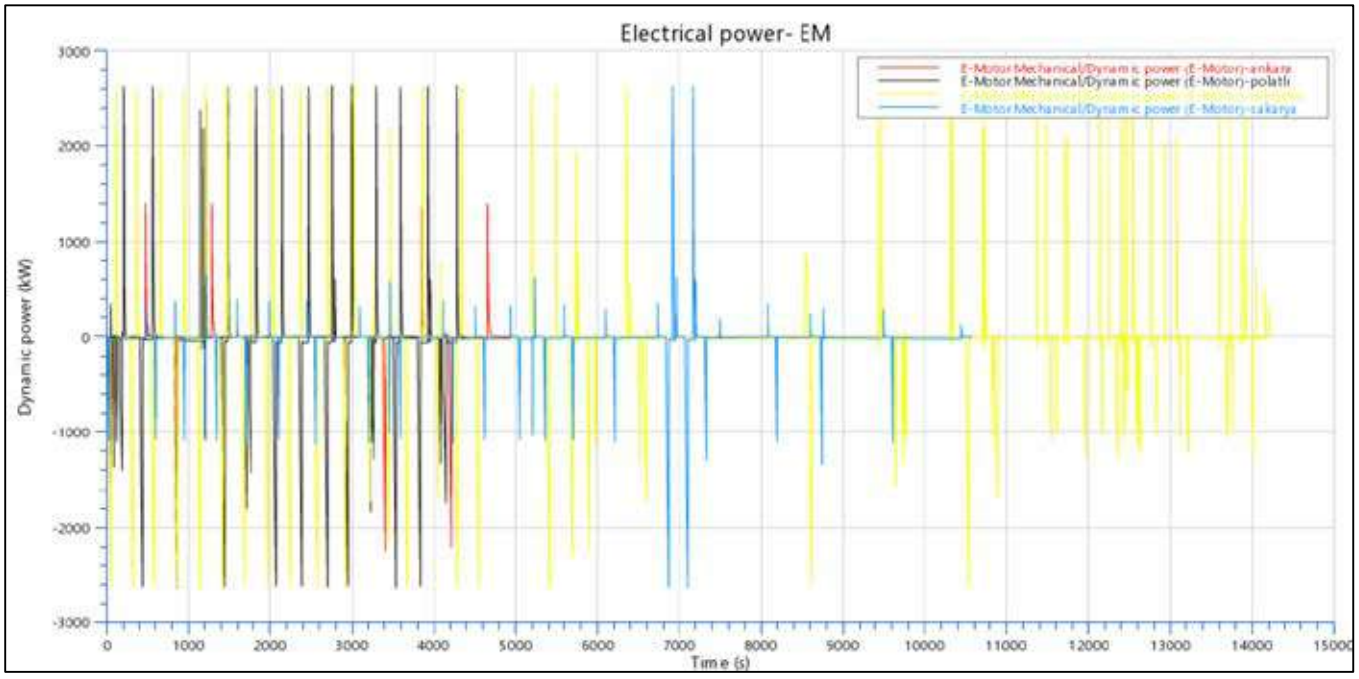


Fig. 2. Electric Motor Power of Locomotive (AVL Cruise M, 2021)

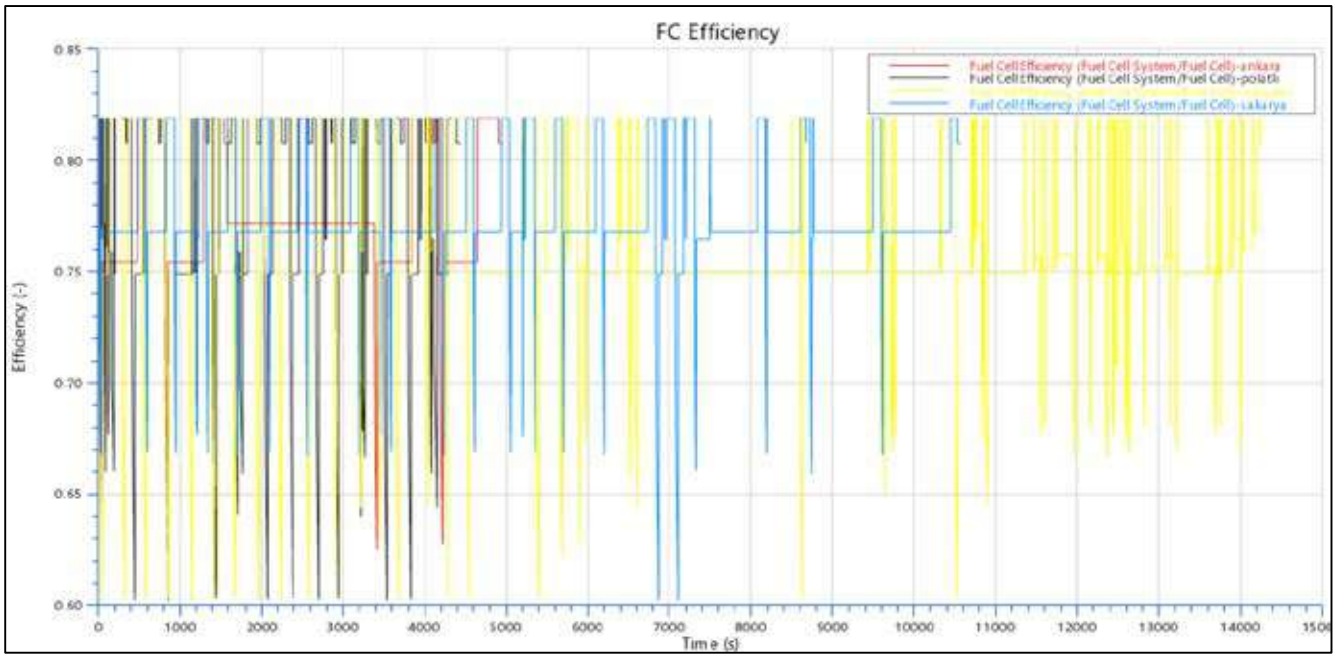


Fig. 3. Fuel Cell efficiency (AVL Cruise M, 2021)

When the efficiency values are examined, it is seen that although the fuel cell is used as an energy trigger throughout the journey, it is performed effectively between Eskişehir and Sakarya, which is the most critical region of the line. While it is observed that the fuel cell supports sudden consumption in short distances, it can be stated that it operates at a stable efficiency between Sakarya and Istanbul. While critical situations such as slopes and tunnels that occur in geographical conditions during the journey increase the use of the battery system, it can be stated that fuel cell energy supply works with more efficiency under constant travel conditions (figure 3).

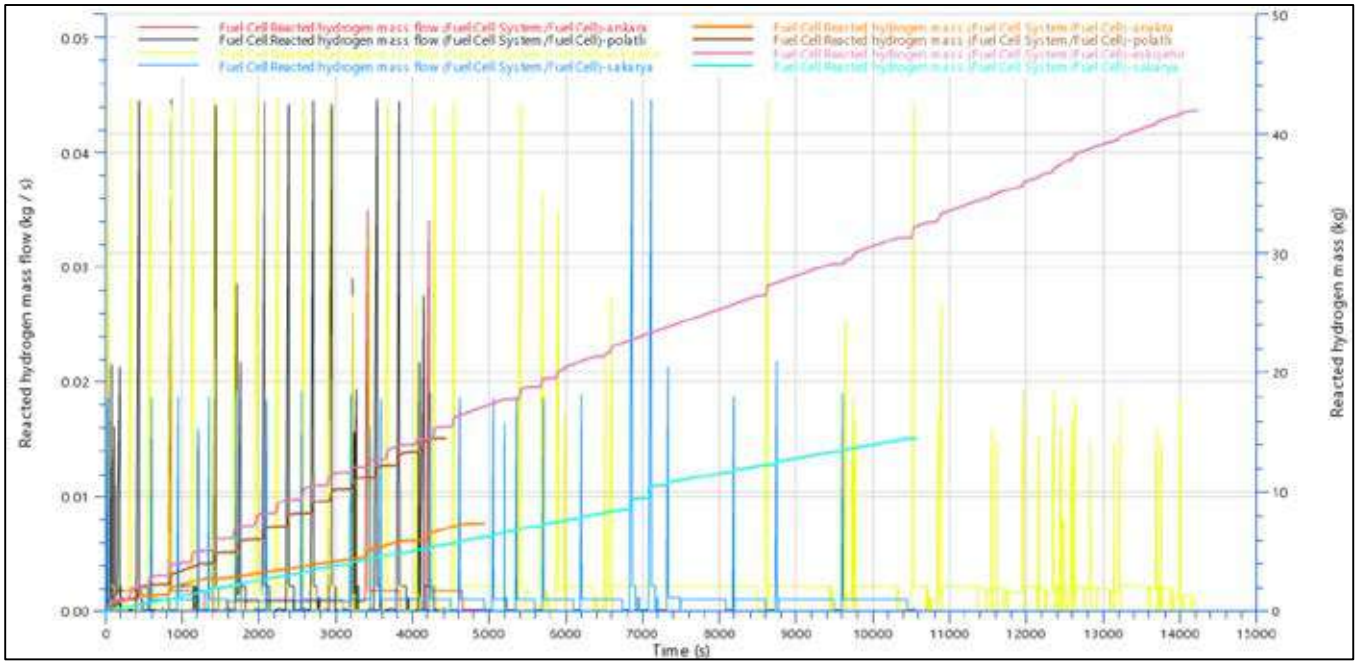


Fig. 4. Hydrogen mass and mass flow of Fuel Cell Locomotive for all routes (AVL Cruise M, 2021)

When the hydrogen masses consumed during the journey are evaluated, it is seen that the maximum increases are experienced between Eskişehir and Sakarya, which is the most critical region of the journey. However, it is considered that there is a direct relationship between the increase in sudden consumption in short-distance regions and the low power requirements of the electric motor. It is noteworthy that the hydrogen produced between Sakarya and Istanbul is used especially in tunnels and in difficult geographical conditions. It is seen that the system is supported by high usage of the fuel cell, especially in cases where the battery is weak and sudden power needs must be met (between Eskişehir and Istanbul). In addition, the battery system and fuel cell work in full harmony throughout the journey (figure 4).

IV. Conclusions

In this simulational study; a 25-meter 90-tonne locomotive was modeled for prediction of powered by FCEV. For this purpose, a railway route is designed between Ankara and İstanbul. Totally 488 km route with assumed 4 stops and 7 km tunnel indeed. FC system was coupled with a high voltage battery and a total 15000 sec simulations was run under these conditions. In route, the Ankara – Polatlı path is shorter than the others and needs less energy requirement. FC efficiencies were varying between 0.6 and 0.85. Maximum hydrogen consumption was generated in the third part of the route.Totally 74.5 kg H2 is used for 488 km (15.2 kg/100km). Electric Machine (EM) has run under a maximum of 2600kW. These results showed the possibility of FCEV locomotive usage in railways has advantages from the view of non-emissions expectations for the near future. Additionally, it is concluded that AVL Cruise M platform is very successful and favorable software for vehicle simulations with in consists railways.

Acknowledgment

This study was conducted with AVL CRUISE M. Authors acknowledge to AVL-AST, Graz, Austria to provide these simulation tools under the University Partnership Program (UPP).

References

Al-Hamed, K. H., & Dincer, I. (2021). Comparative evaluation of fuel cell-based powering systems for cleaner locomotives. Thermal Science and Engineering Progress, 23, 100912.

AVL, Users Guide Book. AVL Cruise M examples, Version 2021.

Carbon dioxide (CO_2) emissions from rail worldwide from 2010 to 2022 https://www.statista.com/statistics/1414708/carbon-dioxide-emissions-rail-worldwide/ (Accesed;27.03.2024)

Gjerdingen, I. K. (2020). Hydrogen technology experimentation for sustainable mobility-A case study of hydrogen fuel cell experimentation in Lower Saxony in Germany (Master's thesis).

Mekhilef, S., Saidur, R., & Safari, A. (2012). Comparative study of different fuel cell technologies. Renewable and Sustainable Energy Reviews, 16(1), 981-989.

Rail Transport Global Market https://www.researchandmarkets.com/report/rail#:~:text=The%20rail%20transport%20market%20size,(CAGR)%20of%206.7%25. (Accesed;27.03.2024)

Railway Technology https://www.railway-technology.com/features/featurethe-worlds-longest-railway-networks-4180878/?cf-view (Accesed;27.03.2024)

Stobnicki, P., & Gallas, D. (2022). Adoption of modern hydrogen technologies in rail transport. Journal of Ecological Engineering, 23(3).

Sürer, M. G., & Arat, H. T. (2022). Advancements and current technologies on hydrogen fuel cell applications for marine vehicles. International Journal of Hydrogen Energy, 47(45), 19865-19875.

Hydrogen Gas Production from *Agropyron repens* by Dark Fermentation

[1]Nurten Dilara Kaplan, [1*]Hidayet Argun
[1] Pamukkale University, Engineering Faculty, Department of Environmental Engineering, Kınıklı Campus Pamukkale, Denizli, 20070, Türkiye

* E-mail: hargun@pau.edu.tr

Abstract

In this study, *Agropyron repens* (AGR) was evaluated for hydrogen gas production by dark fermentation using compost consortia as inoculum. AGR is a fast-growing, invasive weed able to spread on agricultural lands and farming plants. However, its rhizome and leaves are rich in carbohydrates and nitrogen offering a potential substrate. In this context, a Box-Wilson statistical experiment design was used to determine the proper blend of rhizome and leaves resulting in the most convenient hydrogen production. The highest hydrogen yield and rate of 28.31 mmolH_2/100 mL and 0.26 mLH_2/min was obtained by blending 12.5 g rhizome with 1.5 g leaf in 100 mL working volume. According to the analysis of variance (ANOVA) the quadratic model explaining the effect of rhizome and leaf concentration on hydrogen production was found to be significant. Rhizome did have a more significant effect on hydrogen production than leaf. In this study, the experimental conditions were kept as basic as possible to keep the process economically viable. The compost inoculum was effective in the conversion of the biomass to hydrogen with a short lag phase. Hydrogen production from AGR by dark fermentation offers a potential and renewable approach to be applied to many countries.

Keywords: *Agropyron repens*, weed, bio-hydrogen

I. Introduction

Environmentally friendly and sustainable hydrogen production technologies are emerging rapidly as an alternative to fossil-based (Sekoai et al. 2020). Dark fermentative hydrogen from biomass is one of those carbon-neutral alternative methods (Ndayisenga et al. 2021). However, not all types of biomasses can be used as substrates (Argun et al. 2017). Non-edible, fermentable carbohydrate-rich biomass can be considered as a potential source. Moreover, it should be readily available with minimum pre-treatment requirements (Reginatto and Antônio 2015). Weeds can grow on almost all types of arable land, and some are harmful to crops due to their invasive growth (Kubiak et al. 2022). However, their high adaptability and massive growth offer the formation of a renewable biomass to be considered as substrate. Not all weeds are suitable for this purpose, but AGR is a potential one. In this study, we present how hydrogen can be produced from AGR rhizomes and leaves in bench-scale batch-operated experiments for the first time.

II. Experimental Set-up and Procedure

Batch dark fermentation experiments were carried out in gas-tight and sealed boro silicate glass bottles of 310 mL at 37 ^oC for about 5 days. AGR rhizome and leaves were collected from the campus field of Pamukkale University, dried at 50 ^oC, ground to mesh size less than 1 mm, and stored in closed glass bottles in a refrigerator. The inoculum was collected from a compost heap of wood and grass clippings near the campus. It was then subjected to heat treatment to inactivate any methanogens and enrich spores forming hydrogen-producing bacteria. The experimental conditions were adjusted according to the Box-Wilson statistical experiment design consisting of 11 experiments in total. Rhizome and leaf concentrations were chosen as the independent variables while hydrogen yield, hydrogen rate, and TVFA yield were set as the responses.

III. Analysis

Gas and liquid samples were regularly analyzed to track the fermentation performance. The hydrogen concentration in gas samples was determined using a gas chromatograph of Agilent Co (7820A). Analyses performed on liquid samples comprised of total volatile fatty acid (TVFA) and chemical oxygen demand (COD) concentration, total organic carbon (TOC), total phosphorus, and total nitrogen content as described earlier (Argun and Dao 2016). The pH was monitored regularly and kept manually neutral. Calculations of hydrogen yield and rate were done after all data was collected and experimental results were correlated to the quadratic model of the Box-Wilson design and the related constants of the function were derived using the non-linear regression analysis tool of the software statistica (trial version). The significance of the model and parameters were assessed according to the analysis of variance (ANOVA).

IV. Results and discussions

According to the Anova, the quadratic model was found to be significant with a p-value less than 0,05. Rhizome concentration alone did have a significant effect on hydrogen production while leaf concentration did not. Hydrogen

yield and rate increase apparently by increasing rhizome concentration. Probably due to higher fermentable sugar input into the fermentation media. 15 g/L leaf concentration did have an increasing effect on hydrogen rate when blended with 125 g/L rhizome. TVFA yield on the other hand increased with increasing the rhizome concentration since volatile fatty acids are produced in the broth during fermentation along with hydrogen. Triplicate verification experiments proved the accuracy of the model with a high precision regression coefficient of >95%.

V. Conclusions

Agropyron repens an invasive weed was found to be a potential renewable, carbon-neutral biomass for dark fermentative hydrogen production. The rhizome is rich in carbohydrates and leaves in nitrogen. Therefore, a suitable blend of rhizome and leaves can welcome the carbon and nitrogen demand of the microbial consortia as proven in this study. The inoculum source showed that compost can contain potential hydrogen producers and biomass hydrolyzing microorganisms since the lag phase from hydrogen production was low. A quadratic model function was derived efficiently describing the effects of rhizome and leaf concentrations on hydrogen yield/rate and TVFA yield. The process was kept as simple as possible to develop an economical approach. Higher productivity is possible to be obtained using vitamin and trace element supplements. The repeatability of the model with high precision at different times showed that the derived model was reliable. Our studies are ongoing on the subject matter

Acknowledgments

This study was supported by Pamukkale Üniversitesi Bilimsel Araştırmalar ve Projeler Koordinasyon Birimi with a grant number 2021FEBE072.

References

Argun H., Dao S., Hydrogen gas production from waste peach pulp by dark fermentation and electrohydrolysis. Int J Hydrogen Energy 41:11568–11576. (2016)

Argun H., Pelin G., Kapdan I.K., Biohydrogen Production Potential of Different Biomass Sources. In: Singh A, Rathore D (eds) Biohydrogen Production: Sustainability of Current Technology and Future Perspective. Springer India, New Delhi, pp 11–48. (2017).

Kubiak A., Wolna-Maruwka A., Niewiadomska A., Pilarska A.A., The Problem of Weed Infestation of Agricultural Plantations vs. the Assumptions of the European Biodiversity Strategy. Agronomy 12, (2022).

Ndayisenga F., Yu Z., Zheng J., et al., Microbial electrohydrogenesis cell and dark fermentation integrated system enhances biohydrogen production from lignocellulosic agricultural wastes: Substrate pretreatment towards optimization. Renewable and Sustainable Energy Reviews 145:111078. (2021).

Reginatto V., Antônio R.V., Fermentative hydrogen production from agroindustrial lignocellulosic substrates. Brazilian Journal of Microbiology 46:323–335. (2015).

Sekoai P.T., Daramola M.O., Mogwase B., et al., Revising the dark fermentative H2 research and development scenario – An overview of the recent advances and emerging technological approaches. Biomass Bioenergy 140:105673. (2020).

The Investigation of Hydrogen Production by Using Proton Exchange Membrane Electrolysis Cell Technology

[1,*]Haci Sogukpinar, [2]Ismail Bozkurt, [3]Serkan Cag, Mustafa Yavas, [4]Ayhan Atiz, [5]Mehmet Karakilcik

[1]Department of Electric and Energy, Vocational School, University of Adiyaman, 02040, Türkiye
[2]Department of Mechanical Engineering, Faculty of Engineering, University of Adiyaman, 02040, Türkiye
[3]Department of Machinery and Metal Technology Vocational School, University of Adiyaman, 02040, Türkiye
[4]Department of Computer Technologies, Vocational School, University of Adiyaman, 02040, Türkiye
[5]Department of Physics, Faculty of Sciences and Letters, University of Cukurova, Adana 01330, Türkiye

* E-mail: hsogukpinar@adiyaman.edu.tr

Abstract
In this study, hydrogen production was investigated numerically by using Proton Electrolyte Membrane (PEM) technology by using commercial COMSOL software. For this, a cell was modeled and a numerical calculation was performed to explain the current and potential distribution in an electrochemical cell by taking into account the separate transport of ions and uncharged species in the electrolyte due to diffusion, migration, and convection, using the Nernst-Planck equations. Charge transfer reactions were described using electrode kinetics or predefined Butler-Volmer and Tafel expressions. Ohm's law was used in conjunction with charge balance to describe the flow of current in electrodes, as we are familiar with in normal electricity. Electrolyte potential, electrolyte current density vector, and H_2 and O_2 production concentration in the cell were calculated and discussed. Under 3V potential and 77 °C temperature, A maximum 180 mol/m^3 H_2 concentration at the cathode, and 50 mol/m^3 O_2 was calculated at the anode.

Keywords: PEM, Hydrogen Production, COMSOL, Nernst-Planck equations

I. Introduction

The most promising technique for environmentally friendly and high purity hydrogen production appears to be Proton Electrolyte Membrane (PEM). Hydrogen and oxygen obtained with this technique can be used directly in the fuel cell. However, due to economic problems, only 4% of hydrogen production is produced by electrolysis of water. With the development of low-cost electrocatalysts for water electrolysis with PEM and the increasing demand for green hydrogen production, it is expected that interest in hydrogen production by water electrolysis with PEM will increase in the near future (Kumar and Himabindu, 2019). Benghanem et al. (2024) investigated the efficiency of two different electrolyzers (proton exchange membrane and alkaline water electrolyzer) integrated with the photovoltaic panel. Two different solutions (KOH and brine) were used for the alkaline electrolyzer. It has been experimentally determined that the best hydrogen production is achieved when KOH is used as the electrolyte in the alkaline electrolyzer. At the same time, it has been observed that the integrated system consisting of photovoltaic panel and proton exchange membrane has higher efficiency than the alkaline water electrolyzer. Atiz and Karakilcik (2024) examined hydrogen production at different voltage, current density and ambient temperature configurations using PEM electrolyzer integrated with PV and PV-T. At the same time, the effect of cooling the PV-T system at different flow rates on the energy and exergy efficiency of the system was determined. It has been observed that higher voltage and current are obtained in the cooled panels, therefore it has a minimal negative impact on the efficiency of the PEM, furthermore more hydrogen is produced in the cooled system. Aghakhani et al. (2023) investigated current CO_2 emissions of hydrogen production with PEM and alkaline technologies for three different scenarios. Sensitivity analysis based on cell properties and energy sources was performed using empirical equations. Gu et al. (2023) proposed an energy management strategy to increase hydrogen production and energy efficiency throughout the day by designing a PV-Battery-PEM water electrolysis system. The energy efficiency of the system has been tested under different operating conditions with and without battery, and it has been seen that the proposed system will provide stable hydrogen production throughout the day. In this study, a mathematical model was developed to investigate electrochemical events such as voltage-current distribution, mass transfer, hydrogen, and oxygen production occurring in the cell using proton exchange membrane technology, and the model was solved with COMSOL Multiphysics commercial software.

II. Materials and methods

Hydrogen To perform this numerical calculation, Nernst-Planck equations were used to describe the current and potential distribution in an electrochemical cell, taking into account the separate transport of charged and uncharged species in the electrolyte due to diffusion, migration, and convection. The physical module interface used supports different definitions of combined charge and mass transfer in the electrolyte, and the electrode kinetics for charge transfer reactions were described using arbitrary expressions or predefined Butler-Volmer and Tafel expressions. The current density in the electrolyte medium is defined as (COMSOL, 2024):

$$i_s = -\sigma_{s,\text{eff}} \nabla \Phi_s \quad (1)$$

Where, $\sigma_{s,eff}$ is the effective electrical conductivity (S/m) and the charge balance equation in the phase is defined as:

$$\nabla . i_s = -i_{v,tot} \quad (2)$$

Where, $i_{v,tot}$ is the sum of the volumetric current density contributions of the electrode reactions occurring in the gas diffusion electrode areas. Darcy's law states that the velocity field is determined by the pressure gradient, fluid viscosity, and the structure of the porous medium. If we combine Darcy's law with the continuity equation:

$$\frac{\partial}{\partial t}(\rho \varepsilon_p) + \nabla . (\rho \mathbf{u}) = \theta_m \quad (3)$$

where ρ is the fluid density, ε_p is the porosity, and θ_m is a mass source term. Porosity can be defined as the portion of the control volume occupied by pores. Therefore, porosity can vary from zero for pure solid objects to one for free-flowing medium. The overall mass balance of diluted species in an electrolyte is defined for each species i by the following equations:

$$\frac{\partial c_i}{\partial t} + \nabla . N_i = R_{i,tot} \quad (4)$$

where N_i is the total flux of species i. Flow in an electrolyte is described by the Nernst-Planck equations and describes the flow of charged solute ions through diffusion, migration, and convection, which are the first, second, and third terms on the right side of the equation below, respectively.

$$N_i = -D_i \nabla c_i - z_i u_{m,i} F c_i \nabla \Phi_l + c_i \mathbf{u} = \boldsymbol{J_i} + \boldsymbol{c_i} \mathbf{u} \quad (5)$$

where c_i is the ion concentration, z_i is the valence, D_i is the diffusion coefficient, u_m is the mobility, F is the Faraday constant, Φ_l electrolyte potential, u is the velocity vector and J_i is the molar flux according to convective transport. The anode and cathode cell size were determined as 2x1 mm, and the membrane thickness was determined as 0.15 mm. Tertiary Current Distribution, Nernst-Planck Interface in the electrochemistry module was applied for the modeling. The electrochemical reaction is defined at the anode and cathode, and the free electrons and hydrogen ions formed at the anode pass to the anode and form H2 gas. The cell temperature was determined as 77 °C. Nernst Einstein equation was introduced to simulate the migration of charged ions in the electrolyte. Electrolyte conductivity was determined as 50 S/m, and electrolyte volume fraction was set 0.5. COMSOL mesh module was used physics-controlled mesh types were chosen and an extremely fine mesh type was implemented for this model. 9540 triangular mesh elements were created. Mesh distribution is given in Fig. 1. Mesh quality was examined in terms of skewness and the lowest mesh quality was calculated as 0.49, the average mesh quality was 0.89 and the highest value was 1. Therefore, the mesh quality was found to be quite good.

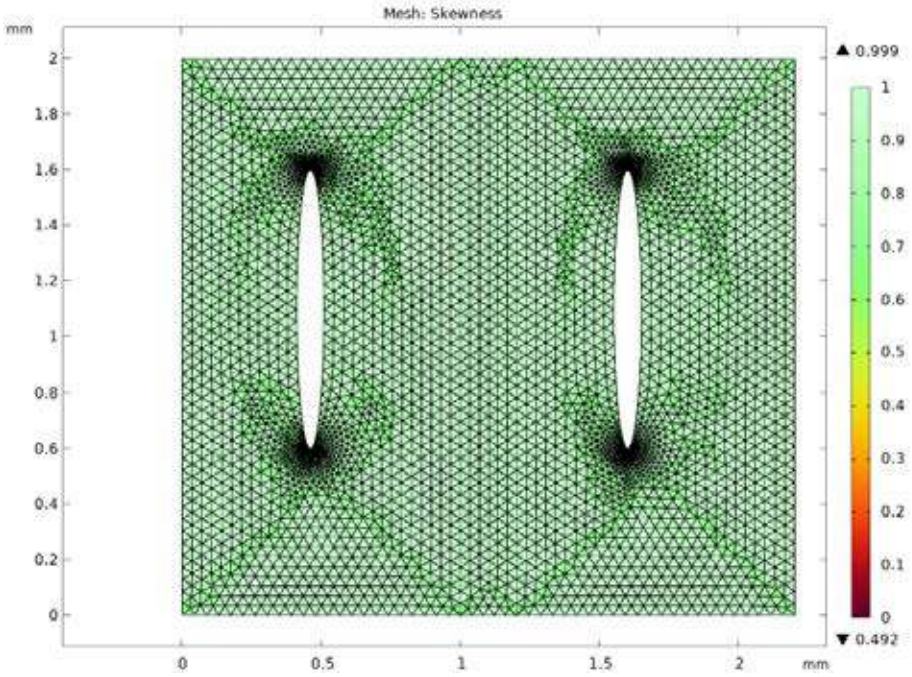


Fig.1 Mesh distribution

III. Results and discussion

In this study, hydrogen production using proton exchange membrane technology was investigated numerically. Electrolyte potential and Electrolyte current density vector were calculated and presented in Fig.2. It is seen that the electric current density vectors become tighter at the anode and cathode spikes, and it is expected that the reaction products will concentrate in these areas.

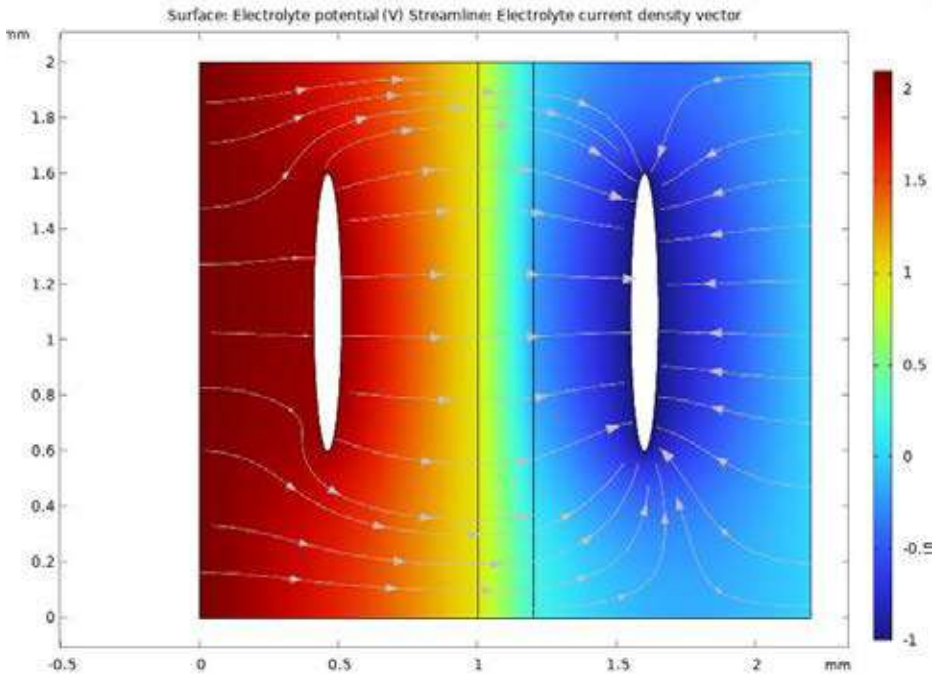


Fig.2 Electrolyte potential and Electrolyte current density vector

H_2 concentration along the cell with surface and line graph is given Fig. 3. As we mentioned before, water moves from bottom to top at a very low speed and the reaction products also migrate upward. Fig 3 indicates that the hydrogen gas density is quite high on the electrode surface facing the anode side inside the cathode. Because, while H^+ ions migrate from the anode to the cathode, they first react on the anode surface of the electrode and the line graph shows that the hydrogen density is concentrated around the electrode surface.

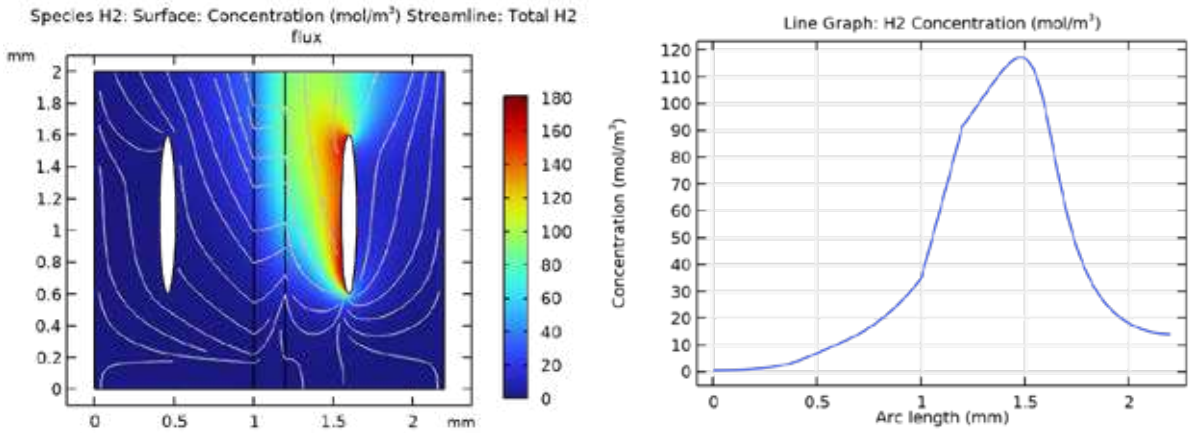


Fig.3 H_2 concentration (a) surface, (b) line graph

Oxygen concentration along the cell is calculated and presented in Fig. 4 with a surface and line graph. Oxygen gas is densely formed around the electrode in the anode region and almost no oxygen is formed in the cathode. Because oxygen is formed at the anode by a direct reaction and leaves the cell by moving upwards due to the density difference.

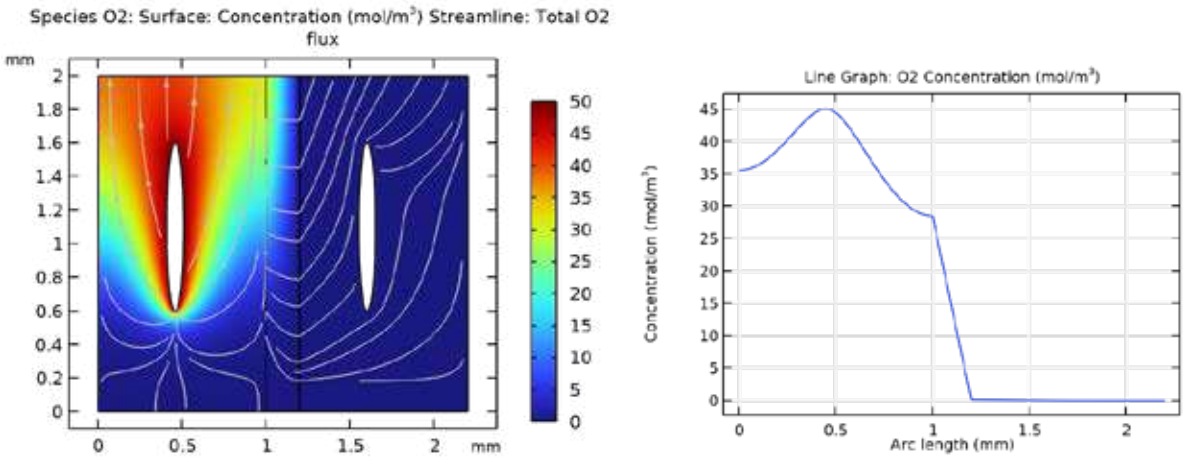


Fig.4 O_2 concentration (a) surface, (b) line graph

IV. Conclusions

In this study, a mathematical model was developed to investigate electrochemical events such as voltage-current distribution, mass transfer, hydrogen, and oxygen production occurring in the cell using proton exchange membrane technology, and the model was solved with COMSOL Multiphysics commercial software. Numerical values depending on hydrogen and oxygen formation were calculated and plotted in graphs. Hydrogen is seen as the inexhaustible energy source of the future with its renewable structure. Therefore, it is important to investigate hydrogen production processes without carbon emissions. Only H_2 and O_2 come out of electrolyzed water as products, and when H_2 burns, it combines with O_2 and turns into water again. Nowadays, while hydrogen-powered cars, buses, and even planes have started to make test runs, it is important to develop multiple serial hydrogen production processes without emissions.

Acknowledgements

Many thanks to Middle East Technical University and Adiyaman University for technical support

References

Aghakhani A., Haque N., Saccani C., Pellegrini M., Guzzini A., Direct carbon footprint of hydrogen generation via PEM and alkaline electrolysers using various electrical energy sources and considering cell characteristics, International Journal of Hydrogen Energy, 48, 30170-30190 (2023).

Atiz A., Karakilcik M., Assessment of hydrogen generation and thermodynamic efficiencies of PEM coupled with PV and PV-T under diverse circumstances, International Journal of Hydrogen Energy Available online 19 January 2024 In Press, Corrected Proof.

Benghanem M., Almohamadi H., Haddad S., Mellit A., Chettibi N., The effect of voltage and electrode types on hydrogen production powered by photovoltaic system using alkaline and PEM electrolyzers, International Journal of Hydrogen Energy, 57, 625-636 (2024).

COMSOL Electrochemistry Module Users Guide. http://www.comsol.com. 2024.

Gu X., Ying Z., Zheng X., Dou B., Cui G., Photovoltaic-based energy system coupled with energy storage for all-day stable PEM electrolytic hydrogen production, Renewable Energy, 209, 53-62 (2023).

Kumar SS., Himabindu V., Hydrogen production by PEM water electrolysis – A review, Materials Science for Energy Technologies, 2, 442-454 (2019).

A superadiabatic hydrogen sulfide combustion system for clean hydrogen production

Muhammad Ishaq* and Ibrahim Dincer
CERL, FEAS, Ontario Tech. University, 2000 Simcoe St, Oshawa, ON L1G 0C5, Canada

*Corresponding author e-mail: Muhammad.ishaq@ontariotechu.net

Abstract
The present work aims to develop a thermodynamic equilibrium model for the partial oxidation of hydrogen sulfide (H_2S) at superadiabatic conditions to study its respective thermodynamic product distribution attainable within the superadiabatic zone. Superadiabatic partial oxidation allows the flame temperature to be in excess of the adiabatic temperature attained in free air. The process is critically studied by varying different operating variables (input H_2S temperature, SAC REAC pressure, input oxidant temperature, H_2S recirculation split fraction, and air to H_2S molar ratio) with an overall goal of optimizing the H_2S conversion into hydrogen. The developed model predicts satisfactory H_2 and low SO_2 production flow rate within a superadiabatic partial oxidation regime at an operating pressure below 0.5 bar. At 0.25 bar, H_2S conversion into H_2 is found to be 23.48%. Additionally, higher SAC operating pressure leads to higher proportions of unreacted H_2S and lower conversion in H_2 in the outlet stream. The overall energy and exergy efficiencies of the integrated energy system are found to be 87.51% and 70.08% respectively. The dissociation of H_2S in the presence of stoichiometric air results in an elemental sulfur and hydrogen production rate of 0.0019 kg/s and 0.0012 kg/s respectively.

Keywords: Hydrogen, Hydrogen sulfide, Power generation, Hydrogen production, Energy, Exergy, Efficiency.

1. Introduction

Hydrogen sulfide (H_2S) is a colorless, flammable gas with a characteristic rotten egg odor. Hydrogen sulfide is removed during the purification of natural gas. In chemical plants, it is considered one of the unwanted byproducts because of its negative impacts on human health and the environment. The Claus process is well-known for producing elemental sulfur in a purified form, but these processes generate low-quality steam, waste the hydrogen in the form of water, and do not entirely utilize H_2S as a potential source of hydrogen. Furthermore, the Claus process is not well suited for small-scale plants having low concentrations of H_2S in the flu gaseous stream. Clean hydrogen technology is promising because of its positive impact on the environment and in meeting the increasing energy requests in different sectors. There is a plethora of different technologies for hydrogen production that are reported in existing literature (Ishaq and Dincer, 2024).

The present study is part of research activities ongoing in the Clean Energy Research Laboratory of Ontario Tech University (University of Ontario Institute of Technology) on the topic of hydrogen production using hydrogen sulfide from Lake Ontario, Canada. In this study, a thermodynamic model of superadiabatic combustion of H_2S is developed for the first time in the Aspen Plus simulation environment. Various sensitivity analyses are computed to assess the thermodynamic product composition, hydrogen sulfide conversion, and hydrogen production rate within the superadiabatic zone. The major objectives of the present study are (1). To develop a novel design of hydrogen and power co-production system based on partial oxidation of H_2S rich stream. (2). To simulate the concept of superadiabatic combustion of hydrogen sulfide in the Aspen Plus simulation environment. (3). To investigate the system thermodynamically in terms of energy and exergy efficiencies.

2. System and analysis

The integrated energy system (SACIES) for clean hydrogen and power production is analyzed thermodynamically in terms of mass, energy, and exergy balances including the determination of energy and exergy efficiencies. Aspen Plus process simulator is used for the mass and energy balance and the simulation schematic of the system is presented in Fig 1. For simulating the plant in Aspen Plus, the Soave-Redlich-Kwong equation of state (SRK-EOS) is employed as a base thermodynamic method because it is the updated form of the conventional Redlich and Kwong (RK-EOS). Several assumptions are respected before starting the simulation in Aspen Plus. (1). The developed plant design is supposed to achieve quasi-state equilibrium. (2). A steady-state simulation model is developed for the plant. (3). Thermal and pressure losses across different components are neglected. (4). A superadiabatic combustion reactor is simulated adiabatically, and it achieves thermal and chemical equilibrium in the Gibbs reactor. The process of superadiabatic combustion is initiated by premixing the H_2S waste gas stream with air or enriched air. By manipulating the conditions of these input reactants, the above exothermic process (1) can satisfy the exothermicity of process (2). Every single molecule of H_2S that undergoes the partial oxidation reaction can provide enough energy to drive the thermal decomposition of up to 10 additional H_2S molecules.

3. Results and discussion

The operating and design conditions of the superadiabatic reactor substantially affect hydrogen production and the overall performance of the system. Specifically, superadiabatic reactor operating pressure influences the rate of partial oxidation reaction and overall efficiency of the process regarding the elemental sulfur and hydrogen production. However, the inlet oxidant temperature decides the reaction conditions inside the reactor during the combustion process. Accurate control of both parameters is essential for a better hydrogen production rate.

Consequently, Fig. 2 depicts the sensitivity results of changing pressure in the superadiabatic reactor and input oxidant temperature, and their effect is examined in terms of hydrogen production rate.
It is found that at the ambient temperature of the inlet oxidant, the hydrogen production rate drops from 1.44 kmol/h at 0.25 bar to 0.76 kmol/h at 4 bar causing an overall decreasing percentage of 30.79%. At greater inlet oxidant temperatures of 300°C, 500°C, and 700°C of the oxidant, this decreasing trend reduces further down to 27.90%, 25.83%, and 23.91% respectively. It is further found that lower pressure values exhibit higher hydrogen production. It is devoted to the fact that at lower pressure, the reaction rates are typically faster, leading to a more rapid conversion of hydrogen sulfide to hydrogen. Additionally, lower pressures can favor the shift of the equilibrium toward higher hydrogen production. Finally, by maintaining SAC REAC pressure of 0.25 bar and inlet oxidant temperature of 700°C, the overall hydrogen production rate can reach up to 2.50 kmol/h.

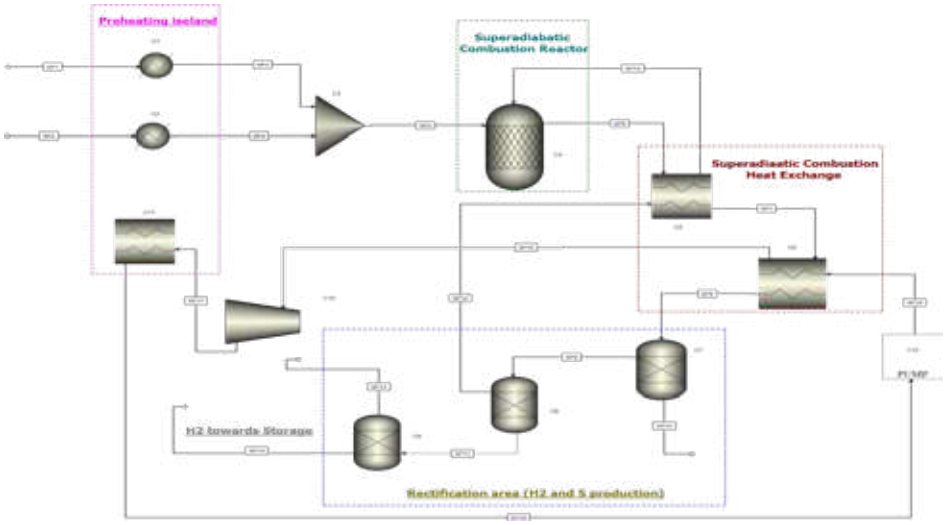


Fig.1: A complete design of the proposed system based on H_2S superadiabatic combustion simulated in the Aspen Plus simulation environment.

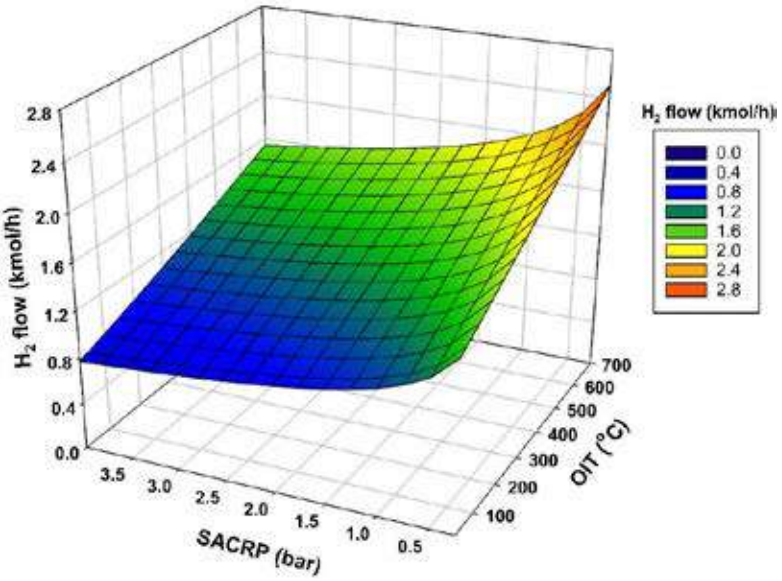


Fig. 2: Hydrogen production rate obtained from the sensitivity results of varying SAC REAC operating pressure and input oxidant temperature.

4. Conclusion

The present hydrogen and power co-production system is investigated thermodynamically in terms of energy and exergy efficiencies. For hydrogen production, superadiabatic combustion of H_2S is developed and simulated for the first time in the Aspen Plus industrial process simulator. The simulation of superadiabatic combustion is computed to identify the key process parameters, optimize the entire process, and assess their quantitative and qualitative influence on the overall hydrogen production performance. The study recapitulates the following findings: (i) The overall energy and exergy efficiencies of the present plant are 87.51% and 70.08% respectively. The combustion of H_2S in the presence of stoichiometric air generates elemental sulfur and hydrogen production rates of 0.0019 kg/s and 0.0012 kg/s, and (ii) the overall hydrogen production rate towards the storage tank is found to be 100. 14kg/day.

Reference

Ishaq, M., & Dincer, I. (2024). Performance evaluation of a renewable source integrated power generation system coupled with heat storage. Journal of Energy Storage, 85, 111066.

Well-Integrity Issues in the Underground Hydrogen Storage Sites

[1*]Şükrü Merey, [2]Hakkı Aydın
[1] Batman University, Department of Petroleum and Natural Gas Engineering, Batman, 72100, Türkiye
[2] Middle East Technical University, Department of Petroleum and Natural Gas Engineering, Ankara, 6800, Türkiye

* E-mail: sukru.merey@batman.edu.tr

Abstract

This study analyzes the cement quality of several wells in the Caspian Sea and Western Anatolia Region using cement bond logs. Wells in depleted oil and gas reservoirs are particularly susceptible to hydrogen leakage behind production casings during underground hydrogen storage projects. A detailed analysis of well conditions in depleted oil and gas reservoirs is crucial for assessing the feasibility of underground hydrogen storage (UHS) projects. Additionally, various sensing technologies can monitor hydrogen migration behind production casings. Detecting temperature changes caused by hydrogen adsorption in overburden formations is crucial for ensuring well integrity. This study investigates these temperature changes due to hydrogen adsorption in the selected case well by non-isothermal numerical simulations.

Keywords: Hydrogen, casing cement, gas leakage, underground hydrogen storage, well completion, well integrity

I. Introduction

According to the Paris Agreement, carbon emissions should be decreased to net zero by 2050 (IPCC, 2018). This has led to a trend of decreasing consumption of hydrocarbon energy sources and reducing carbon footprint. Hydrogen (H_2) is not considered a primary energy source, but it has the potential to be a valuable energy carrier.

Underground hydrogen storage (UHS) offers a cost-effective solution for storing excess energy from renewable sources and utilizing it during periods of seasonal decline in renewable energy production. Therefore, existing underground natural gas storage sites, depleted natural gas & oilfields, aquifers, and salt caverns are considered potential sites for UHS (Panfilov, 2016; Kurz et al., 2022). Several field-scale UHS applications (primarily in salt caverns) exist worldwide in countries like Germany, UK, USA, France, Czech Republic, and Argentina, with hydrogen concentrations ranging from 10% to 95%, storage depths between 200 m and 1330 m, and operating pressures from 10 bar to 150 bar since the 1970s (Panfilov, 2016; Kurz et al., 2022). According to Hassanpouryouzband et al. (2020), over 1 million m^3 of hydrogen is stored in salt caverns. Depleted gas and oil reservoirs are particularly attractive for UHS projects due to their existing wells, pipeline systems, and production facilities. However, well integrity problems (i.e., unintended leaks along the wellbore from the reservoir) pose a risk to storing hydrogen safely (Aftab et al., 2023). Moreover, there are many other uncertainties (i.e., caprock sealing risk, hydrogen-rock interaction, cushion gas necessity, fault leakage, etc.) in UHS (Heinemann et al., 2021). Casing cement quality is essential for the well integrity in UHS sites. In several experimental studies (Aftab et al., 2023), the geochemical interaction of hydrogen and casing cements in API standards was found negligible. However, due to the smaller sizes of hydrogen molecules compared to methane (the diffusion coefficient of hydrogen in air is $6.1x10^{-5}$ m^2/sec; that of natural gas is $1.6x10^{-5}$ m^2/sec) (Sharma et al., 2024).), hydrogen leakage along the microfractures in cement, the intersection between casing-cement or intersection between cement-formation is a possible risk. Therefore, especially in existing wells, investigating well integrity is crucial, which is the focus of this study.

II. Materials and Methods

The density of methane is 0.65 kg/m^3 at 0°C (Kurz et al., 2022). Hydrogen has a very low density (nearly 0.09 kg/m^3 at 0°C) compared to methane (CH_4). This is because hydrogen molecules are much smaller, resulting in a diffusion coefficient in the air nearly four times higher than that of natural gas (hydrogen: $6.1x10^{-5}$ m^2/sec; natural gas: $1.6x10^{-5}$ m^2/sec) Sharma et al., 2024). Hydrogen is a highly flammable gas (Hydrogen flammability range: 4-74 % vol.; Natural gas flammability range: 5-15 % vol.) (Sharma et al., 2024). In the Darcy flow equation (Eq. 1), viscosity is an important property that governs the flow rate. Lower viscosity means higher flow rates. By using the Peng-Robinson Equation of States (EOS) approximation and other related equations (Wei et al., 2023), this study estimated the viscosity of methane and hydrogen at various pressure and temperature conditions. As illustrated in Fig.1, hydrogen has a higher flow tendency than that of methane. While this characteristic can be advantageous for UHS applications, it also presents potential challenges for well integrity due to increased ease of leakage.

The depleted oil & gas reservoirs are considered a potential location for UHS. Especially available wells and surface facilities make these fields economical for UHS. However, without evaluating the current status of available wells, the feasibility of UHS in depleted oil & gas reservoirs should not be made. The well integrity status of these available wells is questionable. In this study, cement bond logs (CBL) of several wells in the Caspian Sea Region of Azerbaijan and the Western Anatolian Region of Turkiye (Fig. 2) were analysed to recognize potential leakage behind the production casing. The evaluation reveals sections with good cement bonds between casing and formations, but also sections with poor bonding - these latter sections pose potential risks for hydrogen leakage during UHS applications.

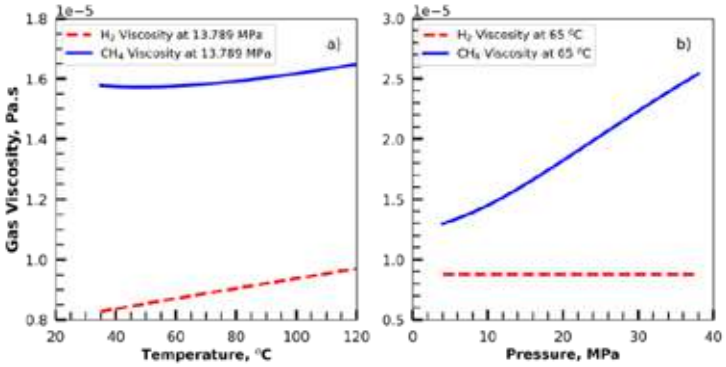


Fig. 1: Viscosity of H_2 and CH_4 a) at different temperatures and 13.789 MPa b) at different pressures and 65 °C

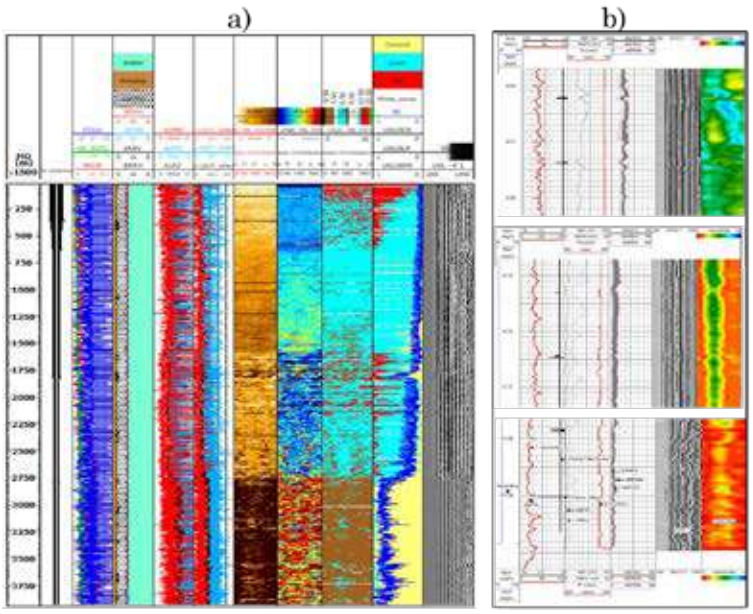


Fig. 2: CBL of a) a well in the Caspian Sea and b) several wells in the Western Anatolia Region

UHS wells should utilize sensor technology to monitor for potential hydrogen leakage behind the casing. Preventing hydrogen leakage is critical for both health, safety, and environmental (HSE) reasons, as well as economic considerations. Recent applications of Distributed Temperature Sensing (DTS) technology have demonstrated its effectiveness in monitoring well integrity for gas hydrate, geothermal, and carbon capture and storage (CCS) wells (Garcia-Ceballos et al., 2023). The adsorption is exothermic so temperature increases in several overburden formations (i.e., shales, clays, coals, etc) due to hydrogen adsorption might be detected with DTS. This study aims to investigate the temperature increases due to hydrogen adsorption for the selected reservoir conditions in case of hydrogen leakage in the upward direction.

III. Analysis

Darcy flow equation (Eq. 1) is used to predict the flow of hydrogen behind the production casing in this study. For the adsorption of hydrogen on the formation (i.e., shale, clays, coals, etc.), the Langmuir isotherm model (Eq. 2) was used.

$$q = \frac{kA}{\mu}\frac{\Delta P}{L} \quad (1)$$

and

$$m_{ads} = \frac{Pm_L}{P_L+P} \quad (2)$$

Where q defines the flow rate; k, permeability; A, cross-sectional area; μ, viscosity; ΔP, pressure change, L, length; m_{ads}, adsorption amount at a pressure of P; m_L, half of this mass is adsorbed; P_L, the pressure at which half of this mass is adsorbed.

Fig. 3 shows the case study showing the hydrogen leakage from the UHS reservoir at 1350 m (65°C and 5.5 MPa) through Formation A (shaly formation at 65°C and 13.8 MPa) at 600 m.

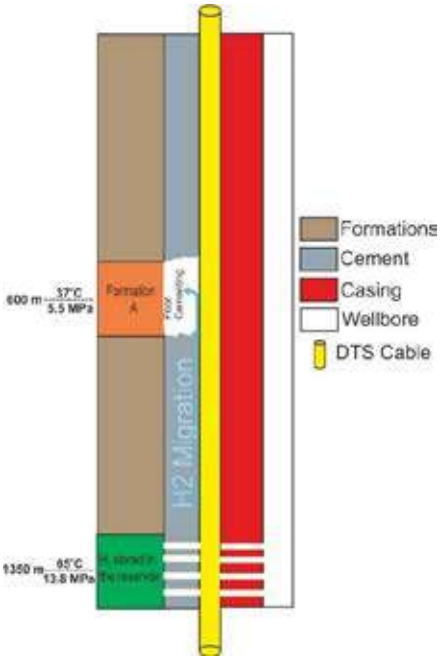


Fig. 3: Case study showing H_2 migration behind the production casing

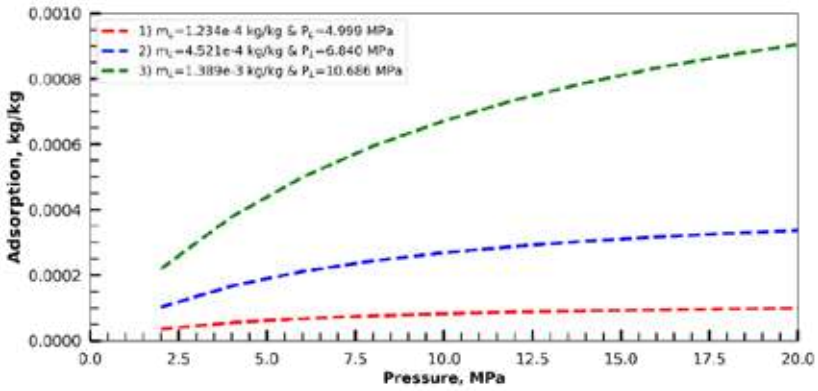


Fig. 4: Selected Langmuir hydrogen adsorption isotherms in Formation A in Fig. 3

Overall, the potential hydrogen leakage from the H_2 stored reservoir at 1350 m to Formation A at 600 m and temperature increases due to hydrogen (physical) adsorption were tracked by non-isothermal numerical simulations. This temperature spike might be useful to be detected by DTS technology, which is important for good integrity.

IV. Results and discussions

Following an evaluation of cement bond logs (CBL) for production casings in several wells located within the Caspian Sea (Azerbaijan) and the Western Anatolian Region, findings suggest the necessity for re-logging wells designated for UHS in depleted oil and gas reservoirs. This re-evaluation using CBL technology is crucial to identify potential leakage pathways. If such concerns are identified, corrective actions, including well completion procedures and cementing repairs, become essential to ensure well integrity for UHS applications.

After non-isothermal numerical simulations of hydrogen migration from the reservoir at 1350 m to Formation A at 600 m, the temperature changes near the wellbore were tracked. The simulations revealed that exothermic hydrogen adsorption induces small temperature spikes near the wellbore. As listed in Tab. 1, higher heat releases if the adsorption capacity is high in Formation A. The DTS resolution is in the range of 0.01 to 0.1°C so the temperature increase with hydrogen adsorption might be detected if the hydrogen adsorption capacity of the formation is high enough. Thus, it is important to know the adsorption capacities of overburden formations in UHS sites and this information might be useful for tracking well integrity in UHS sites.

Tab. 1: Temperature increase in Formation A after hydrogen leakage (Fig. 3) for different Langmuir hydrogen adsorption isotherms (Fig. 4)

Adsorption Case	m_L, kg/kg	P_L, MPa	Temperature Increase, °C
1	*$1.234x10^{-4}$*	*4.999*	*0.395*
2	*$4.521x10^{-4}$*	*6.840*	*0.434*
3	*$1.389x10^{-3}$*	*10.686*	*0.541*

V. Conclusions

Overall, the following concluding remarks and suggestions were obtained in this study for UHS projects in the depleted oil & gas reservoirs:

- Prior to initiating a UHS feasibility project, a thorough evaluation of the depleted reservoir's hydrogen storage potential, existing well integrity, and the condition of production facilities is essential.
- CBL analysis of all wells is necessary to assess potential leakage pathways behind the production casings.
- If CBL analysis identifies leakage risks, a repair cement job may be required.
- An evaluation of hydrogen embrittlement risks in existing production casings, pipes, and surface facilities is crucial to ensure their safe operation during UHS operations.
- The overburden formations should also be characterized in order to understand their interactions with hydrogen.
- New monitoring wells (equipped with pressure sensors, temperature sensors, and other geophysical sensing technology) should be drilled in UHS fields.

References

Aftab, A., Hassanpouryouzband, A., Martin, A., Kendrick, J. E., Thaysen, E. M., Heinemann, N., Utley, J., Wilkinson, M., Haszeldine, R. S., Edlmann, K. Geochemical Integrity of Wellbore Cements during Geological Hydrogen Storage. Environmental Science & Technology Letters, 10(7), 551–556 (2023).

Garcia-Ceballos, A. Jin, G., Collett, T.S., Haines, S., Merey, S. Monitoring a gas hydrate field with DTS for long-term well integrity. Annual International Meeting for Applied Geoscience and Energy (IMAGE), 28 August–1 September 2023 in Houston, Texas.

Hassanpouryouzband, A., Joonaki, E., Edlmann, K., Heinemann, N., Yang, J. Thermodynamic and transport properties of hydrogen containing streams. Scientific Data, 7(1), 222 (2020).

Heinemann, N., Alcalde, J., Miocic, J. M., Hangx, S. J. T., Kallmeyer, J., Ostertag-Henning, C., Hassanpouryouzband, A., Thaysen, E. M., Strobel, G. J., Schmidt-Hattenberger, C., Edlmann, K., Wilkinson, M., Bentham, M., Stuart Haszeldine, R., Carbonell, R., Rudloff, A. Enabling large-scale hydrogen storage in porous media – the scientific challenges. Energy & Environmental Science, 14(2), 853–864 (2021).

IPCC. *IPCC report Global Warming of 1.5 C: Summary for Policymakers*. (2018).

Kurz, R., Winkelmann, B., Freund, S., McBain, M., Keith, M., Zhang, D., Cich, S., Renzi, P., Schmitt, J. Transport and storage. In Brun, K. & T. Allison (Eds.), Machinery and Energy Systems for the Hydrogen Economy. Elsevier, ISBN: 978-0-323-90394, pp. 215-249 (2022).

Panfilov, M. Underground and pipeline hydrogen storage. In R. B. Gupta, A. Basile, & T. N. Veziroğlu (Eds.), Compendium of Hydrogen Energy. Elsevier, ISBN: 978-1-78242-362-1, 91-115 (2016).

Sharma, P., Burolia, A. K., Mandal, A., Neogi, S. Commercially available resources for physical hydrogen storage and distribution. In D. Jaiswal-Nagar, V. Dixit, & S. Devasahayam (Eds.), Towards Hydrogen Infrastructure (pp. 225–256). Elsevier, ISBN: 978-0-323-95553-9, 225-256 (2024).

Wei, C., Raad, S.M.J., Leonenko, Y., Hassanzadeh, H. Correlations for prediction of hydrogen gas viscosity and density for production, transportation, storage, and utilization applications. International Journal of Hydrogen Energy, 48 (89), 34930-34944 (2023).

Proton Exchange Membrane Fuel Cell Applications of Multirotor UAV

*Merve Yıldırım, Harun Koku, *İnci Eroğlu,
[1] Middle East Technical University, Engineering Faculty, Chemical Engineering Department, Dumlupınar Bulvarı, Çankaya Ankara, 06800,Türkiye

*E-mail:merve.yildirim_03@metu.edu.tr; ieroglu@metu.edu.tr

Abstract

This research centered around the commercial usage of UAVs and primarily focuses on applications in agriculture. With the usage of UAVs in agriculture, precision agriculture has become a significantly important area that is constantly evolving and growing. This study discusses the requirements of UAVs used in agriculture, and the specifications of conventional UAVs used in agricultural applications are examined. It is concluded that traditional UAVs with battery systems are insufficient for endurance in crop monitoring applications. Thus, a fuel cell and battery hybrid system was proposed as the alternative power method for UAVs. The fuel cell and battery hybrid system were designed for a battery-powered commercial agricultural drone DJI Matrice 30, and endurance was increased to 4 hours from 41 minutes.

Keywords: UAV, PEM Fuel Cell, precision agriculture, multirotor UAV

I. Introduction

Sustainable agriculture, crucial in the face of our rapidly growing human population, has encountered challenges such as climate change, a lack of arable land, and inefficient resource utilization. However, the advent of precision agriculture applications, harnessed through remote sensing technology, offers a beacon of hope. These applications are designed to eradicate these problems and enhance agricultural yield. With the aid of remote sensing technology, farmers can now monitor fields and conduct crop analysis with unprecedented precision. In the future of precision agriculture, the development of UAVs for agricultural applications should be championed (Tsouros et al., 2019).

UAV technology is used for several applications, such as crop monitoring, aerial photography, and spraying. The requirements of UAVs used in agriculture and deficiencies of commercial UAVs with batteries used in agricultural applications were discussed. It was concluded that the stability, hovering, and VTOL (vertical takeoff and landing) attributes of multirotors benefit agriculture applications. However, crop monitoring applications are generally conducted via small multirotor UAVs (1-5kg), which have relatively less endurance because of the limited battery capacity. Due to the portability and low-cost requirements of small UAVs, increasing battery size is not an appropriate solution to increase endurance.

II. Experimental Set-up and Procedure

The voltage and maximum power are essential when considering crop monitoring applications' mission profiles. A PEMFC is being attempted to provide the same power and voltage values as a battery-powered crop monitoring conventional drone. The reference drone is selected as DJI-Matrice 30. Specifications are given in Table 1. The reference drone's voltage and maximum power values are 26.1 V and 525 W, respectively. The PEMFC stack should perform these values, as specified in Table 2. The voltage output of each cell is based on its operating parameters and conditions, including temperature, pressure, and stoichiometric ratio of air and hydrogen. In this study, the minimum operation temperature of PEMFC is targeted and selected as 60 (Devrim et al., 2015).

The pressure is selected as 1 atm, considering the UAV's 100 m altitude. The stoichiometry of the hydrogen and air is determined as 1.5. The cell's active area is another critical design criterion that is directly correlated with the fuel cell stack's power output. The active electrode area is 100 cm2. To achieve 26.1 V, 77 individual cells are used.

The fuel cell stack was tested at the test station. Performance data were received after 20 minutes. Voltage values were changed continuously while corresponding current data were read by a Programmable DC Electronic Load. The polarization curve was plotted by using current against voltage data.

Table 1. Technical Specifications of DJI Matrice 30 (*DJI - Official Website*, n.d.)

Flight Battery Name	TB30
Voltage (V)	26.1
Battery Type	LiPo 12 S
Maximum Input Power (W)	525
Endurance (min)	41
Takeoff mass (g)	3998

Table 2. Parameters and specifications of the tested fuel cell stack and the hydrogen storage tank.

Active Area (cm^2)	100
Membrane type	Naflon XL 27.5 micrometer
Cathode type	Sigraraced 34BC
Hydrogen stoichiometry	1.5
Air stoichiometry	1.5
Membrane Electrode Assembly (MEA) (mm)	58.21
Thickness (mm)	173
Hydrogen tank volume (L)	7
Hydrogen tank pressure (bar)	350
Hydrogen tank mass (g)	3750
Stored hydrogen mass (g)	268.93

III. Results and discussions

Figure 1 shows the tested stack's performance. 583.44 W maximum power was achieved at 26.52 A and 22.33 stack voltage, corresponding to 0.29 cell voltage as seen in the polarization curve. The current density was 0.22 A/(cm2) at 0.34 V by considering the voltage input of DJI Matrice 30. Operating voltage and output power were obtained as 26 V and 580.84 W, respectively.

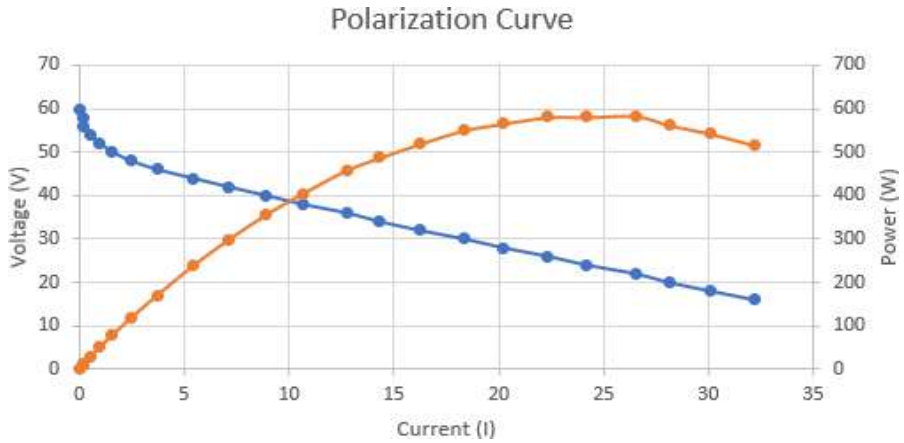


Figure 1. Polarization curve of the PEM fuel cell stack.

LHV of consumed hydrogen flow is determined by considering propulsion system losses for the PEM fuel cell system (Gong, 2014), as seen in Figure 2.

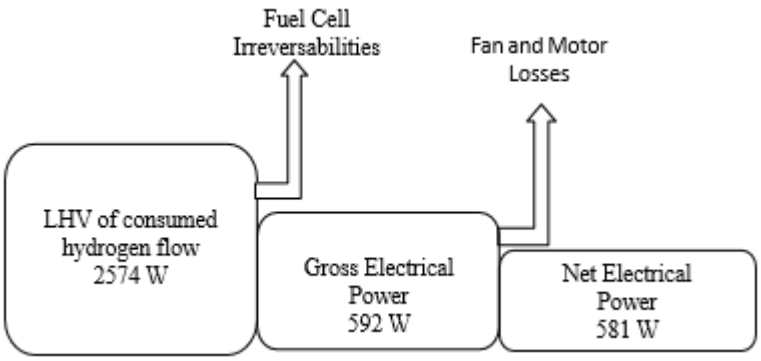


Fig. 2: The propulsion system loses for the PEM fuel cell system.

The amount of released heat energy was calculated as 1981.98 Wh. An air-cooled fuel cell stack with a cooling channel design was proposed as a cooling method for the destructive effect of increasing temperature on the

membrane and contamination of the membrane electrode assembly. It was validated that pure fuel cell systems were not feasible regarding response time to sudden power requirements in several studies and flight tests (Verstraete et al., 2012).

Thus, this study uses two additional batteries with the fuel cell system. The technical specifications of these batteries are given in Table 3.

Table 3. Technical specifications of the battery

Name	Lithium Polymer
Nominal Pack Voltage (V)	22.2
Weight (g)	114

The limited flight time of multirotor drones used for crop monitoring in precision agriculture applications is a significant disadvantage. Since conventional lithium battery technologies may not be adequate for these applications due to their limited energy density and quick discharge characteristics, the fuel cell battery hybrid system has provided a promising solution by extending the flight time.

In the study conducted, although the duration of flight was extended, the overall weight of the system ($m_{stack} + m_{H2} + m_{tank} + 2m_{battery}$) rose to 6.7 kg primarily attributable to the presence of the hydrogen tank, as opposed to the condition where solely the battery was employed.

However, fuel cell battery hybrid systems' longer flight hours and faster recharge times may occasionally offset the additional weight of hydrogen tanks.

IV. Conclusions

Replacing the DJI Matrice 30's TB30 flight battery with a fuel cell stack and two Li-Po batteries improved the endurance to 4 hours; however, the takeoff mass increased to 6.7 kg. In conclusion, fuel cell battery hybrid systems have significant potential in applications like precision agriculture, and this technology should be developed with further studies to increase the agricultural industry's efficiency.

Acknowledgments

We thank Hüseyin Devrim, who provided the facilities in Teksis A.Ş. Ege Koçak and Evren Tuncer are also acknowledged.

References

Devrim, Y., Devrim, H., & Eroğlu, İ. (2015). Development of 500 W PEM fuel cell stack for portable power generators. *International Journal of Hydrogen Energy*, *40*(24), 7707–7719. https://doi.org/10.1016/j.ijhydene.2015.02.005

DJI - Official Website. (n.d.). DJI Official. https://www.dji.com/global

Gong, A. (2014). Experimental Characterization of a Fuel Cell Hybrid Electrical UAVPropulsion System. *52nd Aerospace Sciences Meeting*. https://doi.org/10.2514/6.2014- 0017

Thunder Power RC. (n.d.). *Thunder Power RC*. https://www.thunderpowerrc.com/

Tsouros, D. C., Bibi, S., & Sarigiannidis, P. (2019). A review on UAV-Based Applications for Precision Agriculture. *Information*, *10*(11), 349. https://doi.org/10.3390/info10110349

Verstraete, D., Harvey, J. R., & Palmer, J. L. (2012). Hardware-In-The-Loop Simulation of Fuel-Cell-Based Hybrid-Electrical UAV Propulsion. *Hardware-in-the-Loop Simulation of Fuel-Cell-Based Hybrid-Electrical Uav Propulsion*.

Investigation of Methane Catalytic Decomposition over Mesoporous Carbon Supported Ni/La Based Catalysts

[1*]Hazal Pınar Köse, [2]Dilek Varişli
Gazi University, Faculty of Engineering, Chemical Engineering Department, Ankara, 06500, Türkiye

E-mail:hpinar.kose@gazi.edu.tr

Abstract
Nowadays, hydrogen as a clean energy source has gained an interest among researchers. Catalytic decomposition of methane is an alternative approach to produce COx-free hydrogen, and high-quality carbon with an economic value. This study examines the catalytic decomposition of methane using bimetallic Ni-La catalysts supported on mesoporous carbon. The activity tests were conducted in a microwave reactor which has many benefits over conventional heating like the formation of hot spots, quick heat up time, heating by volume, and quick start-up and shutdown. The effect of microwave energy on the catalytic activity and obtained solid carbon product will be examined and possible growth mechnanism will be discussed using the experimental data.

Keywords: Catalytic methane decomposition, microwave reactor, Lanthanum promoter

I. Introduction

The depletion of fossil fuels and the excessive greenhouse gas emissions to the environment are the two main issues facing the modern world. Therefore, the focus needs to be moved to the effective use of currently available technology to meet the world's energy demand while also reducing greenhouse gas emissions. (Raza,2022). Hydrogen is considered as an alternative and clean fuel to replace fossil fuels as it only creates water when it burns. When burning, hydrogen creates 39.4 kWh/kg, which is three times more energy than any other fuel, such as liquid hydrocarbons, which produce 13.1 kWh/kg (Ashik,2015). Catalytic decomposition of methane has been seen as promising to generate hydrogen free of COx in addition to high-quality carbon nanotubes. Methane is broken down by the endothermic process (eqn.1) which yields pure hydrogen and carbon (Mohamed, 2023).

$$CH_4 \rightarrow C + 2H_2 \qquad \Delta H = 74.9 \text{ kJ/mol} \qquad \text{(eqn.1)}$$

However, methane is one of the most inactive hydrocarbons due to its extremely strong C–H bond (440 kJ/mol) and high molecular structural symmetry. It can only be efficiently broken down at temperatures above 1200°C without the aid of a catalyst (Ashik,2015). Because of their partially filled 3d orbitals, which aid in the hydrocarbon dissociation process by partially accepting electrons, Ni, Co, and Fe are active in the breakdown of methane (Bayat, 2016). Nickel based catalysts are the most active, nevertheless they are not stable at temperatures higher than 650°C. (Alves, 2021). Adding rare earth metals like La, Ce, Pr, Nd, Sm, Gd, and Y plays an important role for Ni-based catalysts because of their distinct 4f electron structure. For example, the addition of La to a Ni-based catalyst provides a better nickel dispersion and the avoidance of graphite layer formation on nickel (Karimi, 2021). Microwave-based heterogeneous catalytic reactions have gained great importance due to the spectacular increase of catalytic reaction rates and selectivities that cannot be achieved by conventional heating (Xu, 2016). Application of microwave reator on the methane decomposition is still open to work especially ovet the metal incorporated catalysts. In the present study, the effect of microwave energy on the catalytic methane decomposition over mesoporous carbon supported nickel activated catalysts with and without promoter has been examined.

II. Experimental Set-up and Procedure

For the synthesis of Nickel-lanthanum catalysts, impregnation procedure was applied and lanthanum nitratehexahydrate ($La(NO_3)_3 \cdot 6H_2O$), and nickel nitratehexahydrate ($Ni(NO_3)_2 \cdot 6H_2O$), salts were used as the metal precursors. Catalysts were synthesized at different Ni/La molar ratio, which is presented in Table 1. The assynthesized samples were calcined 700°C for 5h and and reduced at 600°C for 4h. Reaction studies were carried out using dilute methane feed (0.7/0.3 nitrogen/methane gas) with a flow rate of 20 ml/min. Catalytic activity studies were carried out in the microwave reactor system which includes a microwave generator (SAIREM). Reaction temperatures were changed between 350-400°C by adjusting the set power in the generator. The unreacted methane and the possible products were analysed Gas Chromatography equipped with Carboxen column and TCD detector.

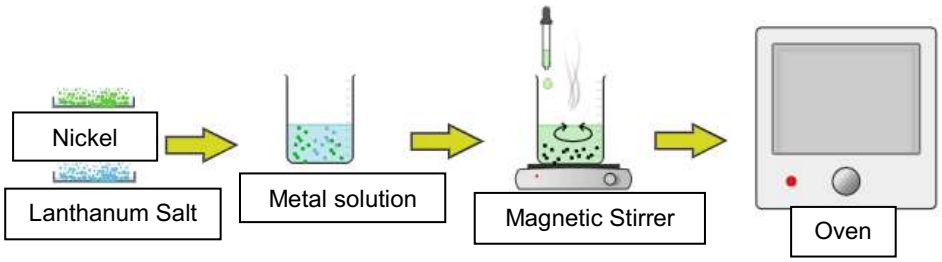


Fig 1. Experimental Setup for Syntesis of Catalysts

III.Analysis

The reduced forms of the synthesized catalysts were subjected to different characterization studies such as ICP-OES, XRD analysis and N_2 adsorption-desorption analysis. Conversion of methane was calculated using the data obtained from the effluent gas.

IV. Results and discussions

In the present study, catalysts were synthesized keeping the nickel loading at a constant value by changing the La/Ni mol ratio as 0.45/0.1, 2/0.25 and 2/0.002. The results of ICP-OES show that catalysts were prepared at the intended values of Ni and La (Table 1). Loading of nickel to the support, i.e. mesoporous carbon, significantly decreased the surface area of it. However, adding a small amount of lanthanum (50Ni-La(2/0.002)@MC) increased the surface area. In the 50Ni@MC catalyst, nickel particles may have clogged the pores and therefore the surface area decreased, and it is possible that these pores were opened by the addition of lanthanum. The surface area of the 50Ni-La(2/0.25)@MC catalyst slightly increased with an increase in lanthanum content, indicating the effect of lanthanum on increasing surface area. However, the surface area decreased with 50Ni-La(0.45/0.1)@MC catalyst with the highest lanthanum loading. It is seen that, lanthanum enhances the surface area of mesoporous carbon-supported nickel-loaded catalysts, but this effect decreases after a specific loading.

Table 1. Nickel Loaded Catalysts Synthesized on Mesoporous Carbon with Lanthanum Promoters

Catalyst	Ni Loading	La Loading	ICP %		BET
	%	%	Ni	La	Surface Area, m^2/g
50Ni-La(0.45/0.1)@MC	50	20.82	43±1	21±1	57.1
50Ni-La(2/0.25)@MC	50	12.89	55	15.6±0.3	68
50Ni-La(2/0.002)@MC	50	0.12	>60	0.23±0.01	53.24
50Ni@MC	50	-	56	-	43
Mesoporous Carbon	-	-	-	-	96

The results of XRD analyses shown in Figure 2 show that metallic nickel, carbon, and La peaks. La peaks may be both La_2O_3 and $La(OH)_3$ due to the hygroscopic nature of La_2O_3. It was emphasized by Pudukudy et al. (2019) that La_2O_3 is easily hydroxylated to form stable $La(OH)_3$ when exposed to air or moisture at room temperature. Lanthanum peaks were not observed in the 50Ni-La(2/0.002)@MC catalyst with the lowest lanthanum loading, likely due to the low amount of lanthanum and its high dispersion on the support. (Du et al., 2014).

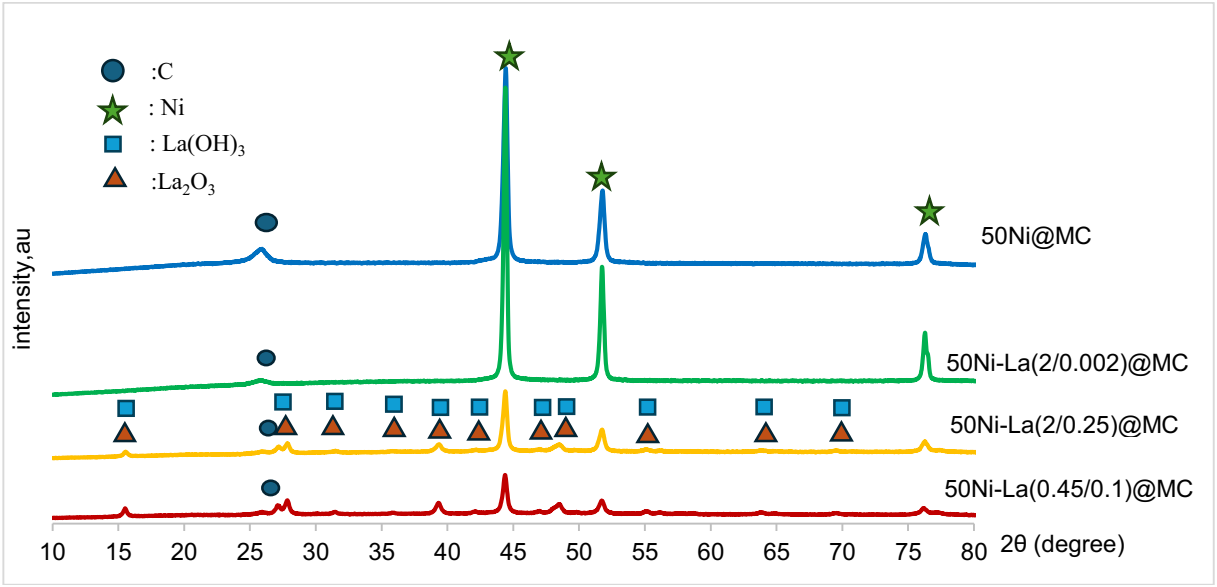
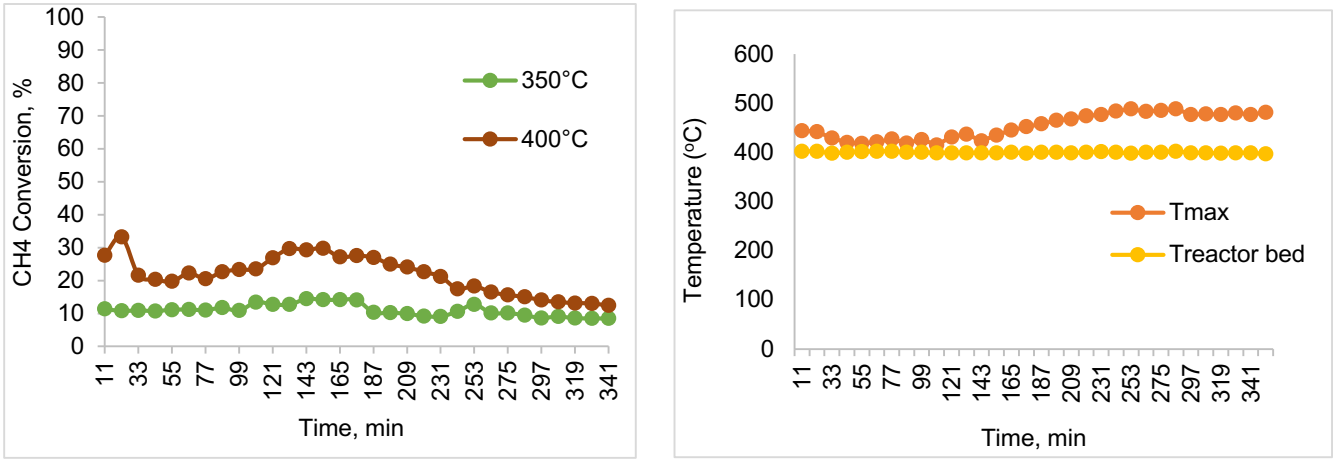


Fig. 2: XRD Analysis of Catalysts Supported by Mesoporous Carbon

The activity results of 50Ni-La(0.45/0.1)@MC catalyst tested for the decomposition of methane at 350 and 400°C in the microwave reactor are presented in Figure 3a. At lower temperatures, i.e., 250 and 300°C no significant conversion was observed. The highest CH_4 conversion was measured as 33.3% at 400°C during the initial 40 min of experiment time interval. During the experiments, power adjustment was done to keep the reaction temperature at a specified value. The front power, reflect power as well as the set power were recorded during the experiments. The difference between the front power and reflect power is a sign of the ability of material in the absorbing microwave energy. In addition, it is known that hot spots (microplasm) could be formed within the catalytic bed

during a chemical reaction, causing local temperature rise within the bed. For this reason, temperature of different points within the catalytic bed was measured with pyrometer until the end of reactor. Data obtained for the experiment of 50Ni-La(0.45/0.1)MC catalyst at 400°C was presented in Figure 3b. While the bulk temperature of the reactor bed stayed at 400°C, an increase was observed locally. After 110 minutes, there was an increase in methane conversion from 23% to 29% and it gave stable conversions for about 1 hour. At this time interval, maximum local temperature reached to 500°C was recorded. This increase is thought to be due to the carbon formed in the reaction, it is possibly absorbing the microwave energy and creates local maximum temperature inside enhancing the activity. But of course, although the carbon formed increased the maximum temperature and conversion slightly for a while, the catalyst was deactivated as the carbon formed and the conversion gradually decreased to 11% after about 6 hours.



(a) (b)

Fig. 3: a) Variation in methane conversion over 50Ni-La(0.45/0.1)MC catalyst with time, b)temperature variation in the catalytic bed for this experiment in case of 400oC.

In literature, catalytic methane decomposition is mostly studied in conventional reactor. Ying et al., (2014) investigated the effect of rare earth metals modified nickel-silicon catalysts. Ni-La-Si (0.45:0.45:0.1 mol ratio) catalyst gave no conversion at 350 and 400°C. Only at 500°C, the conversion reached 25%. In another example, Anjaneyulu et al., (2013) synthesized Ni-La-SiO_2 (2:0.1:0.9 mole ratio) and achieved 36% conversion at 600°C. In our research, 33% conversion is reached at the temperature of 400°C, indicating that microwave energy would be a good alternative for catalytic methane decomposition consuming lower energy. Characterization results which have been applied to the spent catalysts will give important information on the possible effect of microwave energy on the solid carbon product.

V. Conclusions

For this study bimetallic catalysts based on nickel-lanthanum metals and mesoporous carbon support were synthesized and tested in the reaction of catalytic methane decomposition, which is a potential way for producing hydrogen energy without the carbon emissions. The activity tests which were examined at 400°C give some details on the performance of the system. The lanthanum added catalyst gave higher conversion values compared to the literature at studied temperature. Future studies will give information about the solid carbon product and better operation conditions on microwave system.

Acknowledgements

This research was supported by TUBITAK 1001-Scientific and Technological Research Projects Support Program (Project No: 123M056).

References

Alves, L., Pereira, V., Lagarteira, T., & Mendes, A. (2021). Catalytic methane decomposition to boost the energy transition: Scientific and technological advancements. *Renewable and Sustainable Energy Reviews*, *137*, 110465.

Ashik, U. P. M., Wan Daud, W. M. A., & Abbas, H. F. (2015). Production of greenhouse gas free hydrogen by thermocatalytic decomposition of methane – A review. *Renewable and Sustainable Energy Reviews*, *44*, 221–256.

Bayat, N., Rezaei, M., & Fereshteh Meshkani. (2016). Hydrogen and carbon nanofibers synthesis by methane decomposition over Ni–Pd/Al2O3 catalyst. *International Journal of Hydrogen Energy*, *41*(12), 5494–5503.

Du, X., Almuqati, N., Kuznetsov, V. L., Zhao, Y., Zheng, J., Xiao, T., Bagabas, A., Almegren, H., & Edwards, P. P. (2014). The

effect of lanthanum addition on the catalytic activity of γ-alumina supported bimetallic Co–Mo carbides for dry methane reforming. *Applied Petrochemical Research*, *4*(1), 145–156.

Karimi, S., Bibak, F., Meshkani, F., Rastegarpanah, A., Deng, J., Liu, Y., Dai, H. 2021. 'Promotional roles of second metals in catalyzing methane decomposition over the Ni-based catalysts for hydrogen production: A critical review', Int. J. Hydrogen Energy, 46, 20435-20480.

Mohamed, A. T., Ali, S., Kumar, A., Mondal, K. C., & El-Naas, M. H. (2023). Evaluation of highly active and stable SiO2 supported Fe-based catalysts for the catalytic methane decomposition into COx free hydrogen and CNTs. *Catalysis Communications*, *180*, 106703.

Pudukudy, M., Yaakob, Z., Jia, Q., & Takriff, M. S. (2019). Catalytic decomposition of methane over rare earth metal (Ce and La) oxides supported iron catalysts. *Applied Surface Science*, *467-468*, 236–248.

Raza, J., Khoja, A. H., Anwar, M., Saleem, F., Naqvi, S. R., Liaquat, R., Hassan, M., Javaid, R., Qazi, U. Y., & Lumbers, B. (2022). Methane decomposition for hydrogen production: A comprehensive review on catalyst selection and reactor systems. *Renewable and Sustainable Energy Reviews*, *168*, 112774.

Xu, W., Zhou, J., Su, Z., Ou, Y., You, Z. 2016. 'Microwave catalytic effect: a new exact reason for microwave-driven heterogeneous gas- phase catalytic reactions.', Catal Sci Technol, 6, 698-702.

Development of Bimetallic Catalysts for CO_X-free Hydrogen Production by Microwave-Assisted Catalytic Methane Decomposition

[1]Ceren Acar, [2]Dilek Varışlı
Gazi University, Faculty of Engineering, Department of Chemical Engineering, Ankara, 06500, Türkiye

E-mail: ceren.acar@gazi.edu.tr

Abstract
In this study catalytic methane decomposition is carried out using carbon supported Ni-Fe bimetallic catalysts in the microwave reactor system. The effects of metal loading, the reaction temperature, the reduction time interval, on the catalytic activity of the catalyst as well as the characteristic of solid carbon product are evaluated. Mesoporous carbon and silicon carbide was selected as the supporting material due to their high microwave absorptive properties. In the literature, conventionally heated reactor systems have been frequently used with a reaction temperature higher 600°C. In the microwave reactor system, methane conversion of 33% is easily achieved even at a reaction temperature of 350°C, at the initially period of reaction. Indeed this methane conversion is higher than the corresponding equilibrium conversion. Possible presence of oxidized species in the catalysts structure due to the insufficient reduction time duration can be the reason of CO_2 formation.

Keywords: Catalytic methane decomposition, microwave heating, hydrogen, CO_X-free hydrogen

I. Introduction

Hydrogen is the most promising clean fuel due to its environmentally friendly property and fuel cell technology. Furthermore, the petroleum and petrochemical sectors have numerous uses for pure hydrogen as a raw material. Hydrogen produces nearly three times more energy during combustion (39.4 kWh/kg) than the liquid hydrocarbons (13.1 kWh/kg) (Rastegarpanah et.al.,2019). Hydrogen production involves the use of fossil fuels. On the other hand, they release a lot of pollutants that damage the earth and its ecosystem, including as CO_2, NO_x, and SO_x (Prasad et.al.,2011). Methane decomposition reaction is an alternative way to produce hydrogen and solid carbon and presented in Eq.(1).

$$CH_4 \rightarrow C + \ 2H_2 \qquad \Delta H^{\circ}_{298K} = 74.8 \ kJ/mol \tag{1}$$

Methane decomposition, which is an endothermic reaction, occurs in the absence of catalysts at a reaction temperature above 1200 K. To reduce the reaction temperature various transition metals have been used. Ni-based catalysts have been extensively studied for methane decomposition due to their higher activities. Fe-based catalysts are more stable at higher temperatures. Microwave heating technology is used in various chemical reactions and industrial processes in energy use (Chen et.al.,2019). It has been observed that the catalytic reaction rates and selectivity increase in microwave-based heating compared to conventional heating method (Xu et.al.,2016). In addition, microwave heating has advantages over conventional heating for chemical reactions such as high heating power, volumetric and fast heating, heating without contact, easy control for heating or drying, minimization of equipment size (Chen et.al.,2019). Application of microwave is a good alternative for methane decomposition due to these superior properties however limited number of studies are present in the literature. In this study, the activity of bimetallic catalysts on the microwave assisted catalytic methane decomposition to produce CO_x free hydrogen as well as high value-added solid carbon product is investigated.

II. Experimental Set-up and Procedure

In the synthesis of the catalysts, impregnation procedure was followed and two different carbon sources, namely Mesoporous carbon (MC) and silicon carbide (SiC) were used as support material. Bimetallic catalysts have been prepared using nitrate hexahydrate and iron nitrate nonahydrate salts. Calcination and reduction conditions for nickel-iron catalyst supported by mesoporous carbon and supported by silicon carbide were 750°C for 5h and 500°C for either 3h or 6h, respectively. Catalysts were called as (X)Ni-(Y)Fe@C where X refers to nickel metal loading (10wt % and 50 wt%) and Y refers to iron loading (6-15 wt%). A microwave reactor was used for evaluating the catalytic performance under the atmospheric pressure using 0.1g of catalyst with the gaseous feedstock (0.7/0.3 nitrogen/methane mixture gas) at a flow rate of 20 mL/min. Microwave generator was adjusted to reach the necessary reaction temperature and temperature change within the catalysts bed was recorded during the reaction. The reactant and products were analyzed with a Gas Chromatography device equipped with Thermal Conductivity Detector (TCD) and Carboxen column.

III. Analysis

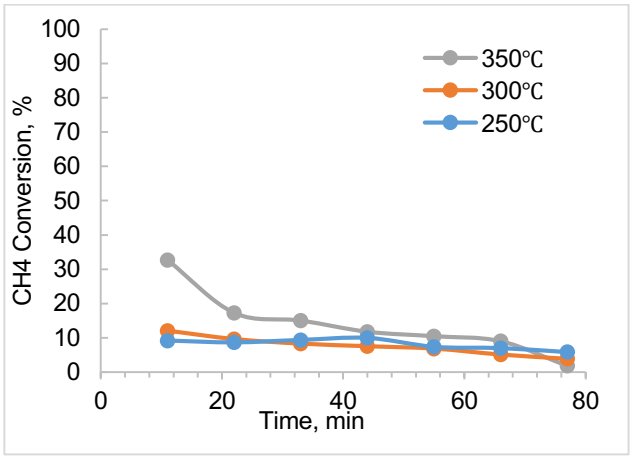
The fresh form of the synthesized catalysts were characterized via ICP-OES, XRD, XPS and SEM/EDS analyses. Methane conversions were calculated using Eq. 2 and the the amount of solid carbon product was calculated using the weight of fresh and spents for of the catalysts.

$$X = \frac{F^0_{CH_4} - F_{CH_4}}{F^0_{CH_4}} \times 100\% \tag{2}$$

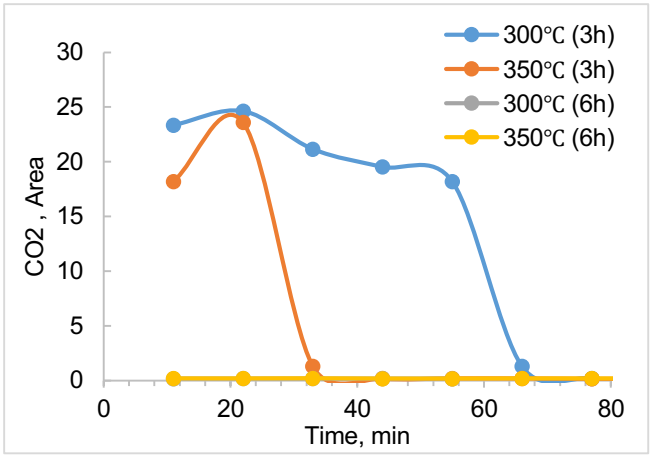
IV. Results and discussions

Results of ICP-OES studies showed that lower amount of iron than the expected value was present in both MC and SiC supported catalysts at 50 wt % of nikel loading. Graphitic carbon and metallic nickel peaks were found in the mesoporous carbon catalysts loaded with 50% nickel and different amounts of iron in XRD analyses. Ferronickel (FeNi) structure has been observed in catalysts loaded with 10% nickel due to the similar proximity of nickel and iron concentrations (Wang et al.,2020). Metallic nickel and metallic iron structures have been observed in silicon carbide-supported catalysts. In the XPS analysis performed for mesoporous carbon catalysts loaded with 50% nickel, NiO and Fe_2O_3 structures were also detected. However, these structures were not observed in the XRD analysis. In the SEM-EDS analysis, the shape of the oxide structure in the 50Ni-6Fe@SiC catalyst showed matches with the shape of the iron structure.

Catalytic methane conversion which was performed at different temperatures over 50Ni-6Fe@MC catalyst is presented in Figure 1.a. In the microwave reactor system about 0.02 kW energy was used by the catalyst to reach these temperature values rapidly. It has been observed that methane conversion at the initial period of reaction increases with increasing temperature and the highest methane conversion was observed at 350℃ with about 33%, which is over than the equilibrium value (Hamdan et al 2022). After 40 minutes later, conversion of methane decreased to 10% due to the formation of solid carbon product. In the conventionally heated system multiwall carbon nanotube is one kind of carbon product, this study will enable to see the effect of microwave exposure on the carbon structure. Main gaseous product was hydrogen, and negligible level of CO_2 formation was observed in the catalyst, which was reduced for 6 hours (Figure 1b). On the other hand, CO_2 formation was observed during activity studies over the 50Ni-6Fe@MC catalyst, which was reduced for 3 hours. Oxide species remained in the catalyst structure may give reaction directly methane to form of CO_2 (Yan et al., 2022). The results of the XPS analysis performed before the activity studies also confirmed this situation. When the weight of the spent form of 50Ni-6Fe@MC catalyst reduced at different time interval was determined, it was found that approximately 0.078 gr of solid carbon product was found for catalysts reduced for 6 h, and 0.141 g of solid carbon product was found for catalyst reduced for 3 h. This may be explained with methane reduction causing solid carbon formation, stated by Yan et al., 2022.



(a)



(b)

Fig. 1: (a) Methane conversion 50Ni-6Fe@MC catalyst reduced for 6 hours, (b) CO_2 area, obtained from GC analysis, of 50Ni-6Fe@MC catalyst at temperatures of 300-350℃, which have been pre-reduced for 3 hours and 6 hours.

V. Conclusions

In this study, synthesis, characterization and activity studies of bimetallic catalysts for catalytic decomposition of methane using microwave reactor were carried out. Methane conversion to high purity hydrogen could be observed at low reaction temperatures, which is promising. It is expected that further increase in the reaction temperatures may cause better activity and stability for these catalysts. Characterization studies, which are continued over spent form of the catalysts, will provide information about the effect of microwave exposure to the obtained carbon type which can be utilized in different area without any purification treatment.

Acknowledgements

This research is supported by TUBITAK 1001- Scientific and Technological Research Projects Support Program within the project 123M056.

References

Chen, W. H., Liou, H. J., & Hung, C. I. A numerical approach of interaction of methane thermocatalytic decomposition and microwave irradiation. *International journal of hydrogen energy*, *38*(30), 13260-13271, (2013).

Hamdan, M., Halawy, L., Aramouni, N. A. K., Ahmad, M. N., & Zeaiter, J. Analytical review of the catalytic cracking of methane. *Fuel*, *324*, 124455, (2022).

Rastegarpanah, A., Rezaei, M., Meshkani, F., Zhang, K., Zhao, X., Pei, W., ... & Dai, H. Mesoporous Ni/MeOx (Me= Al, Mg, Ti, and Si): Highly efficient catalysts in the decomposition of methane for hydrogen production. *Applied Surface Science*, *478*, 581-593, (2019).

Prasad, J. S., Dhand, V., Himabindu, V., & Anjaneyulu, Y. Production of hydrogen and carbon nanofibers through the decomposition of methane over activated carbon supported Ni catalysts. *International Journal of Hydrogen Energy*, *36*(18), 11702-11711, (2011).

Yan, P., Zhang, K., & Peng, Y. Study of Fe_2O_3-Al_2O_3 catalyst reduction parameters and conditions for catalytic methane decomposition. *Chemical Engineering Science*, *250*, 117410, (2022).

Wang, Y., Zhang, Y., Zhao, S., Zhu, J., Jin, L., & Hu, H. Preparation of bimetallic catalysts Ni-Co and Ni-Fe supported on activated carbon for methane decomposition. *Carbon Resources Conversion*, *3*, 190-197, (2020).

Xu, W., Zhou, J., Su, Z., Ou, Y., & You, Z. Microwave catalytic effect: a new exact reason for microwave-driven heterogeneous gas-phase catalytic reactions. *Catalysis Science & Technology*, *6*(3), 698-702, (2016).

A New Approach to Determine Model Parameters of Proton Exchange Membrane Fuel Cells Using Convolutional Neural Network

[1] Mustafa Tan, [1] Cem Emeksiz
[1] Tokat Gaziosmanpasa University, Faculty of Engineering and Architecture, Department of Electric-Electronic Engineering, Taslıciftlik Campus, Tokat, 60150, Türkiye

* E-mail: mustan79@gmail.com

Abstract
For PEMFC to perform reliably, it is essential to develop a suitable model. However, its nonlinearity and electrochemical nature make the system difficult to model. Therefore, a model based on a convolutional neural network (CNN) and a pool of probabilities method (PPM) is proposed to determine the PEMFC parameters. A classification map is used to identify the PEMFC parameters more accurately and quickly with the model). A new approach for data-driven modeling is proposed to address limited data and random factors. This study aims to optimize the unknown parameters of the data-driven model using PPM.

Keywords: Parameter estimation, probability pool, hydrogen energy, deep learning

I. Introduction

With the increasing demand for energy, the use of fossil fuels leads to environmental problems and energy security concerns. This situation further increases the need for clean and sustainable energy sources Hegazy et al. (2022) and Bayrak et al. (2016). Fuel cell (FC) technology has significant potential to meet this need. In particular, proton exchange membrane fuel cells (PEMFCs) have attracted attention due to their low operating temperatures and high-efficiency Nowotny and Veziroglu (2011). They are also used in various applications, from portable electronic applications to electric vehicles Dinçer (2012). However, the accuracy and complexity of mathematical models developed to optimize PEMFCs and improve their performance pose some challenges Petrone et al. (2013). To overcome these challenges, this study proposes an innovative method, the probability pooling method, which is independent of traditional approaches. This method will address the uncertainties of PEMFCs and optimize their performance, making a significant contribution in this field. However, besides the probability pool method, deep learning algorithms have also been used to improve the performance of PEMFCs Cho et al. (2022). In particular, convolutional neural networks (CNNs) have been effectively used to analyze and optimize complex systems. In this study, innovative methods such as OHT and ESAs provide a new approach to optimize the performance of PEMFCs. Thus, mathematical models of PEM fuel cells should be developed, and a framework should be provided to improve the performance of PEMFCs using innovative methods such as OHT and CNN to optimize the system's performance. By using these methods, the efficiency of PEMFCs can be increased and the development of clean energy technologies can be supported.

II. PEMFC modeling and identification

Fuel cells using a proton-conducting polymer membrane as the electrolyte have significant potential in clean energy applications. A fuel cell can be defined as an electrochemical cell that generates electrical energy from fuel through an electrochemical reaction. Equation 1 below describes an energy conversion that converts directly into electrical energy.

$$2H_2 + O_2 = 2H_2O\ (vapor) + \text{Energy} \quad (1)$$

Each FC has a cathode, an anode and an electrolyte between them. Fuel is connected to the catalyst via the anode. Likewise, the cathode provides the connection between O_2, the electrolyte and the catalyst. The electrolyte is a separator that separates O_2 and H_2. This part completes an electrical circuit by transporting H_2 ions to the cathode side Oruç and Dincer (2020). When PEMFC output voltage polarization curves are obtained, it can be said that three separate voltage losses are affecting the output voltage Özdemir (2021). These losses are activation, concentration and ohmic losses. The activation region represents the delayed chemical response from the activation barrier. The concentration region describes the concentration voltage drop caused by mass transfer processes. The ohmic losses region specifies the ohmic loss produced by different internal resistances.

$$V_T = N_S\ x\ (E_{nerst} - V_{act} - V_{con} - V_{ohm}) \text{n} \quad (2)$$

Here V_{act} represents the activation voltage drop, V_{ohm} denotes the ohmic losses voltage, V_{con} is the concentration voltage drops, and $E_{Nernest}$ is the Nernst voltage Yang et al. (2021). In this study, each voltage loss that affects the PEMFC output voltage is analyzed individually and the parameters that are effective in the related voltage drop are focused. The parameters of the losses that should ideally be obtained in the fuel cell model are three unknown parameters; ς2 for activation voltage losses, β for concentration voltage losses and ƛ for ohmic losses. Each parameter is bounded within a confidence interval.

The relevant limitations are presented in Table 1 Özdemir (2021).The perfect information taken as the basis

for the study was obtained from the database site "https://www.kaggle.com/code/thakursankalp/eda-visualisation-of-pem-fuel-cell-test." This dataset is related to Nafion 112 membrane standard tests and MEA activation tests of PEM fuel cells under various operating conditions. The dataset includes two general electrochemical analysis methods: Polarization and Impedance curves. The dataset can be used for in-depth analysis, simulation, and investigation of material performance in PEM fuel cell research.

Tab. 1. Max and Min limitations of PEMFC parameters.

Parameters	ς_2	λ	β
Min Limit	0.001	$1x10^{-4}$	0.0136
Max limit	0.005	$8x10^{-4}$	0.500

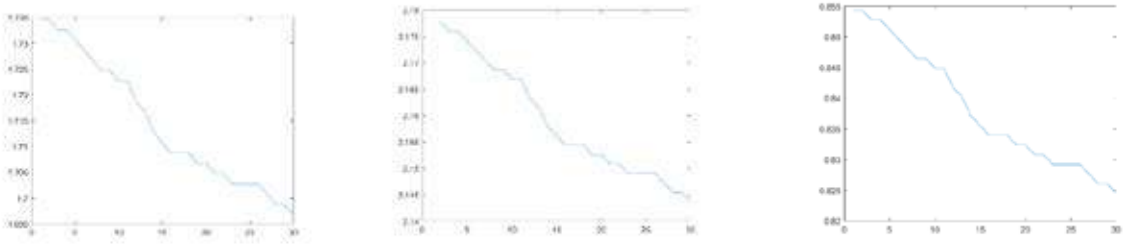
III. The Probability Pool Method

In the previous section, a new approach for accurately and precisely determining the model parameters is presented. The pool of probabilities method essentially refers to creating a pool of datasets obtained from the values of the relevant parameters that can be taken within the declared limits. In more detail, the model's parameters need to be calculated to improve their accuracy and better represent the physical performance. The results of the polarization curves obtained from the calculations are converted into a graph and (png) format and added to the probability pool. At the same time, classification mapping was created by assigning label information to unknown model parameters. The information about the probability pool obtained in the study is shown in Table 2.

Tab. 2. Probability pool dataset information

Label	Count
000	64
001	64
010	64
011	64
100	64
101	64
110	64
111	64

As can be seen in Table 2, a total dataset consisting of 512 data was obtained. Model parameters were estimated using this dataset. Figure 1 shows some of the sample data from the probability pool. As a prediction method, CNN convolutional neural network, a subject of deep learning, one of the artificial intelligence applications whose popularity is increasing rapidly, was used.



Label: 101 011 100
Count: 39 15 43

Fig. 1. Sample data from the pool of possibilities

In Figure 1, the data was resized to 64x64 dimensions to make it suitable for cnn input and trained with cnn. Then, the model parameters of PEMFC were determined by using the natural polarization curve of the data of nafion PEMFC (Table 3). The error correlation between the values of the extracted model parameters and the polarization curves of pemfc and nafion is shown in Figure 2.

Tab. 3. Optimal extracted parameters of Nafion 112 PEM using classification method.

Variables	ς_2	λ	B
Calculated Value	0.0045	10.2	0.08

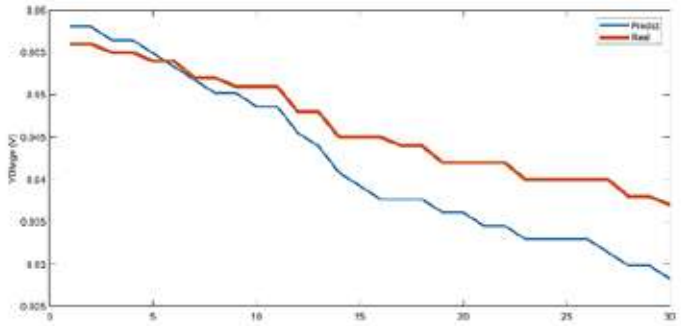


Fig. 2. Error correlation graph

IV. Conclusions

Proton exchange membrane fuel cells (PEMFC) are an essential technology for renewable energy production. In this study, a new method is proposed to determine unknown model parameters to improve the performance of PEMFC. This method is based on the probability pool method and is supported by classification mapping to increase the convergence time. PPM optimizes the system performance by using the probability distributions of the model parameters that describe the system's behavior. Convolutional neural networks (CNN) are used to train and classify the model, and the result shows high accuracy. This study analyzes the model parameters using data from the Nafian 112 membrane fuel cell dataset. Moreover, the parameter estimates of the CNN model were in good agreement with the actual measurements. The method is applicable to assess the efficiency and safety of fuel cells and improve parameter accuracy. Future work would provide recommendations for fault diagnosis of fuel cells and identification of other parameters

References

Bayrak Z.U., Bayrak G., Ozdemir M.T., Gencoglu M.T., Cebeci, M., A low-cost power management system design for residential hydrogen & solar energy based power plants, International Journal of Hydrogen Energy, Volume 41, Issue 29, Pages 12569-12581, (2016).

Cho Y., Hwang G., Quarme D.G., Hwang S., Artificial neural network based model predictive control for optimal operating conditions in proton exchange membrane fuel cells, Journal of Cleaner Production, Volume 380, 135049, ISSN 0959-6526 (2022).

Dinçer İ., Green methods for hydrogen production, International Journal of Hydrogen Energy, Volume 37, Issue 2, Pages 1954-1971, (2012).

Hegazy R., Olabi A.G., Seydali F., Sayed E.T., Accurate parameter estimation methodology applied to model proton exchange membrane fuel cell. Energy, Volume 255, 124454 (2022).

Nowotny J, Veziroglu T.N., Impact of hydrogen on the environment. Int J Hydrogen Energy 340:347-55 (2011).

Özdemir M.T., Optimal parameter estimation of polymer electrolyte membrane fuel cells model with chaos embedded particle swarm optimization, International Journal of Hydrogen Energy, Volume 46, Issue 30,16465-16480 (2021).

Oruç O., Dincer İ., Evaluation of hydrogen production with iron-based chemical looping fedy different biomass, International Journal of Hydrogen Energy, Volume 45, Issue 60, 4557-34565 (2020).

Petrone R, Zheng Z, Hissel D, Pera MC, Pianese C, Sorrentino M, Becherif M, Steiner NY, A review on model based diagnosis methodologies for PEMFCs. Int J Hydrogen Energy 38 (17):7077-7096 (2013).

Yang B., Zeng C., Wang L., Guo Y., Chen G., Guo Z., Chen Y., Li A., Cao P., Shu H., Tao Y., Zhu J., Parameter identification of proton exchange membrane fuel cell via Levenberg-Marquardt backpropagation algorithm, International Journal of Hydrogen Energy, 46: 22998-23012 (2021).

An Integrated Solution to Overcome Salt Lake Droughts with Hydrogen Production and Storage

[*1,2]Dogan Erdemir, [1,2]Ibrahim Dincer
[1]Ontario Tech University, Clean Energy Research Laboratory (CERL), Oshawa, Ontario, Canada
[2]Yildiz Technical University, Faculty of Mechanical Engineering, Department of Mechanical Engineering, Istanbul, Türkiye

* E-mail: dogan.erdemir@yildiz.edu.tr: dogan.erdemir@ontariotechu.ca

Abstract
Salt lakes, vital ecosystems, face increasing vulnerability to climate change-induced droughts, threatening their ecological integrity. This paper examines the complex dynamics of salt lake droughts and proposes a novel integrated system to combat them while enabling power generation, hydrogen production, and storage. Focusing on Lake Tuz in Türkiye, the study utilizes the organic Rankine cycle (ORC) to generate power from the lake's heat mass. Results from thermodynamic analysis indicate energy efficiency of 14.36% and exergy efficiency ranging from 14.08% to 15.47%. The system demonstrates potential for generating electricity, ranging from 822 GJ to 4157 GJ during 90-day summer operations. This integrated approach offers promise in mitigating salt lake droughts while advancing renewable energy and hydrogen technologies.

Keywords: Hydrogen storage, salt lake, hydrogen, droughts, organic Rankine cycle, energy, exergy.

1. Introduction

Salt lakes are unique ecosystems characterized by high salinity levels, creating habitats that support a diverse array of organisms specially adapted to thrive in such extreme conditions. These saline environments, often found in arid and semi-arid regions worldwide, play crucial roles in local hydrology, ecology, and socio-economic systems. However, salt lakes are increasingly vulnerable to the impacts of climate change, particularly in the form of droughts, which pose significant challenges to their ecological integrity and the services they provide. The multifaceted dimensions of salt lake droughts encompass a complex interplay of climatic, hydrological, ecological, and socio-economic factors. Understanding the underlying mechanisms driving salt lake droughts is essential for deciphering their impacts on ecosystems and communities, as well as for devising effective mitigation and adaptation strategies.

The use of salt lakes for storing natural gas is another significant feature. Salt lakes are geologic substances that provide a resilient, protected, and leak-proof environment for storing gases and liquids. Natural gas storage has been critical in the carbon age to provide temporary energy security. But now that we are in the hydrogen era, we must think about storing hydrogen—especially green hydrogen, which is derived from renewable resources that, by their very nature, have erratic availability.

In Turkiye, the Lake Tuz, nestled in the heart of central Türkiye, has long been a captivating landscape—a vast expanse of salt that shimmers under the relentless sun. Yet, beneath its crystalline surface lies a tale of ecological struggle and human impact. For centuries, Lake Tuz has hosted migratory flocks of flamingos, their vibrant plumage contrasting against the stark white salt flats. These elegant birds thrived on the algae-rich waters during warm seasons, creating a spectacle that drew photographers and nature enthusiasts alike. Approximately 5,000 young flamingos perished due to the absence of water. Experts attribute Lake Tuz's demise to a double assault: climate change-induced drought and decades of harmful agricultural practices. The underground water supply, once abundant, has been exhausted by unsustainable irrigation methods. As temperatures rise and rainfall dwindles, the lake's fate hangs in the balance Fraser and Guzel (2021) and Talf (2021).

There are other examples besides Lake Tuz. Multiple other lakes throughout Türkiye have also experienced the same phenomenon of drying up or receding to concerning levels. The scarcity of rainfall, combined with the redirection of water for agricultural and industrial purposes, intensifies the crisis. Rising temperatures further strain the delicate balance. In this research, we develop and evaluate a novel integrated system to fight droughts in basins of salt lakes while producing power and hydrogen and storing. The system has been evaluated based on the first and second laws of the thermodynamics.

2. System Description

Due to the shallow water, its immediate surroundings, and the bottom being covered with black slime, the water temperature of the salt lakes increases significantly in the summer. This makes the salt lakes a useful source of power generation with the organic Rankine cycle (ORC). This study develops a unique system that uses the hot water mass of salt lakes for power generation. The power generated is used for hydrogen production. The hydrogen produced is stored inside the salt caverns under the salt lakes. Figure 1 demonstrates the schematic illustration of the integrated system. As seen in Figure 1, a heat rejection mechanism is created to reduce the water temperature in the lake. The rejected heat is used for power generation via organic Rankine cycle. While the power generated can be used for grid supply, it can also be used for hydrogen production. In this study, The Lake Salt (Tuz Gölü) is selected as the case study.

The Lake Salt (Tuz Gölü), which is the second-largest lake in Türkiye by surface area, covering 1,665 km^2. Lake Tuz is a saline lake, meaning it has a high salt content. It is fed by two major streams, groundwater, and surface water, but it lacks an outlet. Lake Tuz is a vital source of salt production in Türkiye, contributing

approximately 60% of the country's total salt production. The salt extracted from Lake Tuz is rich and valuable. On the other hand, it is unique ecosystem that support diverse plant and bird species. For example, the Lake Tuz is home to the Mediterranean's largest flamingo population, which uses it as a breeding site. In order to save this habitat, novel techniques are required. With the project (Stage I) finished by the end of 2021 and further expansion (Stage II), the goal is to reach a storage capacity of 5.4 billion Sm3 and a daily back production capacity of 80 million Sm3. After completing the Phase I works, 1.2 billion Sm3 of working gas capacity and 40 million Sm3 of daily back production capacity were achieved. Salt Lake Natural Gas Storage Facility consists of a total of 52 caves, by pumping fresh water into salt wells opened 1.5 km underground, melting the salt. On the other hand, following the process of dissolving salt in subterranean wells using fresh water from Hirfanlı Dam, which is part of the storage project, salt water is pumped to the Salt Lake. As a result, Tuz Lake's water level rose daily, and the ecosystem within its basin was restored. However, recent development shows the Lake Salt has issues with droughts BOTAS (2024).

A complete thermodynamic analysis based on the first and second laws of thermodynamics is used for performance assessment. For this purpose, the overall energy and exergy efficiencies are calculated for the system proposed in this work as follows:

$$\eta_{en} = \frac{\left(\dot{m}_{h_2} * LHV_{H_2} \right) - \dot{W}_{H_2 compressor} - \dot{W}_{H_2\ cooling}}{\dot{Q}_{source}} \quad (1)$$

$$\eta_{ex} = \frac{\left(\dot{m}_{h_2} * ex_{H_2} \right) - \dot{W}_{H_2 compressor} - \dot{W}_{H_2\ cooling}}{\dot{E}x^{Q}_{source}} \quad (2)$$

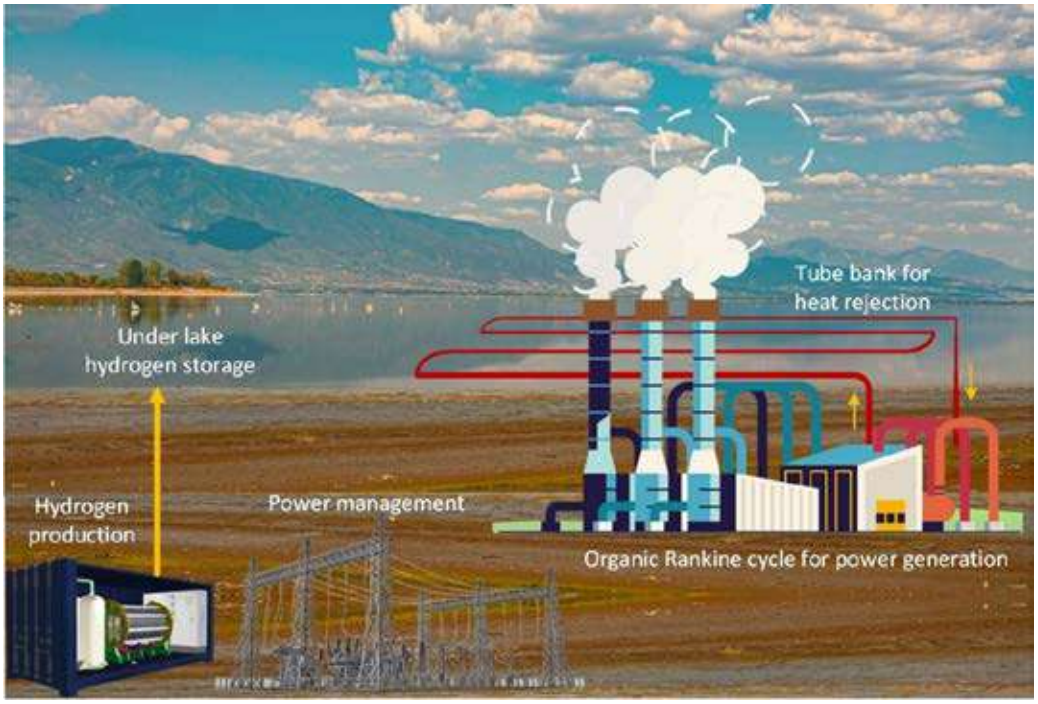
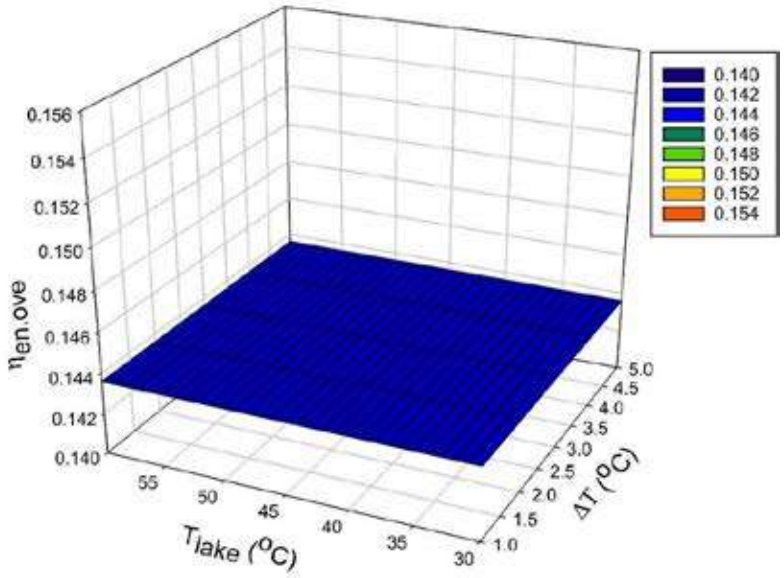


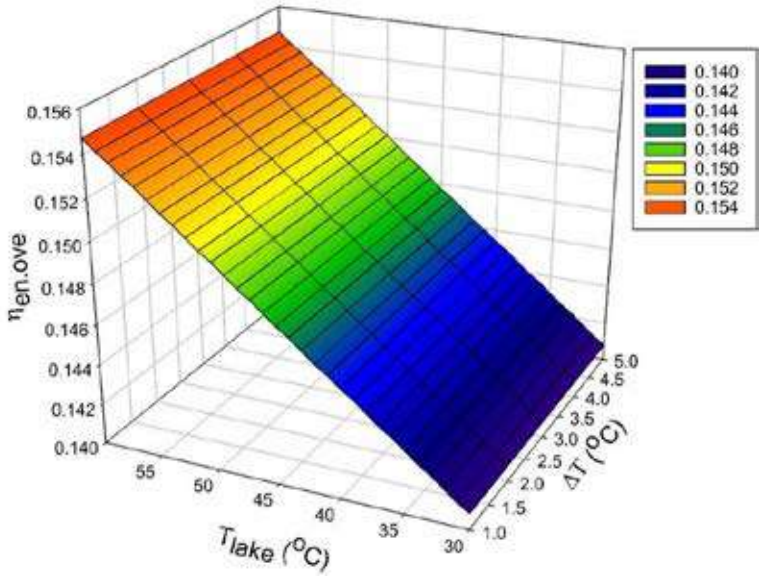
Fig. 1: The schematic illustration of the integrated system

3. Results and Discussion

In order to calculate the amount of heat rejected, first, it is required to know the volume of the water in the lake. The volume of water in the Lake Tuz, Türkiye, can vary significantly due to seasonal changes, climate variability, and human activities. Typically, Lake Tuz is very shallow, with an average depth of about 0.4 meters for most of the year. The total surface area of the lake and average depth are considered, the water volume of the lake is approximately 666,000 m^3. In order to control the evaporation rate, the temperature of the lake should be reduced by the tube banks which are placed inside the lake. Here, it should be noted that as the salt lakes are not deep, it makes the easy-to-apply for the tube banks. It is possible to control the evaporation rate in the lake by rejecting the heat from the lake via the tube bank, which is connected to the ORC's evaporator. The temperature of the lake and the temperature difference to control the evaporation are the main drivers. Fig. 2 demonstrates the energy and exergy efficiencies for the overall system. As seen in Fig. 2, while the overall energy efficiency has not changed significantly, the overall exergy efficiency has changed with the lake temperature and temperature difference. The overall energy efficiency for the system is observed to be 14.36% for all cases considered. The overall exergy efficiency varies from 14.08% to 15.47%. While increasing lake temperatures tend to increase the increase the exergy efficiency, there is no significant change depending on the operating temperature of the system. With 90 days of summer operation of the proposed system, it is possible to generate electricity from 822 GJ to 4157 GJ depending on the lake temperature and operating temperatures.



(a)



(b)

Fig. 2: Variation of the efficiencies with the lake temperature and temperature differences in the tube bank (a) energy efficiency (b) exergy efficiency

4. Conclusions

Despite the fact that salt lakes are vital for the storage of natural gas, they are currently experiencing severe droughts. Constantly, the water level is falling. This study proposes a novel integrated system to generate power, hydrogen production and storage along with the fight against droughts in salt lakes. The present study has chosen Lake Salt (Tuz Gölü) in Türkiye as a case study. It is found that the overall energy efficiency of the system is found to be 14.36% for all cases considered. The exergy efficiency ranges from 14.08% to 15.47% and is influenced by the operating temperature and lake water temperature. It is feasible to produce 4157 GJ of electricity during a 90-day period of summer operations.

References

BOTAŞ Petroleum Pipeline Corporation, Available online (April 1, 2024): https://www.botas.gov.tr/Sayfa/tuz-golu-dogal-gaz-depolama-tesisi/23#:~:text=Tuz%20G%C3%B6l%C3%BC%20Do%C4%9Fal%20Gaz%20Depolama%20Tesisi%2C%20yerin%201%2C5%20km,tesisi%20olma%20%C3%B6zelli%C4%9Fiyle%20%C3%B6ne%20%C3%A7%C4%B1kmaktad%C4%B1r.

Fraser S., Guzel M. Türkiye's Lake Tuz dries up due to climate change, farming. 2021. Available online (April 1, 2024): https://apnews.com/article/climate-science-business-droughts-environment-137e6f52a8fe14db981a45d19e8907d1

Talf M. Haunting Satellite Imagery Shows Türkiye's Second-Largest Lake Has Dried Up, 2021. Available online (April 1, 2024): https://gizmodo.com/haunting-satellite-imagery-shows-Türkiye-s-second-larges-1847983619

Leveraging Renewable Energy for Turkey's Future Hydrogen Supply Chain: A Stochastic Programming Model

[1*]Busenur Türkali Özbek, [2]Ahmet Erdoğan, [3]Mehmet Güray Güler
[1]Işık University, Faculty of Engineering and Natural Sciences, Department of Industrial Engineering, İstanbul, 34980, Türkiye
[1]Yıldız Technical University, Faculty of Mechanical Engineering, Department of Industrial Engineering, Istanbul, 34353, Türkiye
[2]Kayseri University, Faculty of Engineering, Architecture and Design, Department of Industrial Engineering, Kayseri, 38280, Türkiye
[3]İstanbul Technical University, Faculty of Management, Department of Industrial Engineering, İstanbul,34367, Türkiye

* E-mail: busenur.turkali@isikun.edu.tr

Abstract

Fossil fuel dependence and rising CO_2 emissions due to population growth and technological advancements necessitate a transition to clean energy sources. The transportation sector, a major contributor to CO_2 emissions, requires alternative solutions like hydrogen fuel cell electric vehicles (HFCVs). However, widespread adoption hinges on a reliable hydrogen supply chain (HSC). This study aims to design a HSC for Turkey's transportation sector in 2050, considering potential renewable energy sources. A scenario-based stochastic programming approach is employed to address the uncertainty in demand. Additionally, the Epsilon Constraint Method is used to incorporate multiple objectives, including cost, CO_2 emissions, and risk, into the model. The results show that the types of facilities opened are compatible with the renewable energy potential of each grid and there is a decentralized structure. This study contributes to the design of a sustainable HSC for Turkey, showcasing a methodology that can be adapted by other countries aiming to integrate renewable energy sources into their hydrogen supply chains.

Keywords: Hydrogen supply chain, Renewable Energy, Stochastic programming

I. Introduction

Technology advancements and population growth drive energy use higher, leading to fossil fuel depletion and environmental harm. Reducing carbon emissions, especially in transportation (second to electricity), is a major focus. Battery Electric vehicles help to reduce CO_2 emissions, but limited range and long charging times are drawbacks. Hydrogen fuel cell electric vehicles (HFCV) address these issues with fast refueling (like gasoline) and long range. However, a reliable hydrogen supply infrastructure is crucial for widespread adoption.

The most important points when planning the HSC are determining production locations, supplying raw materials, and delivering hydrogen to the end consumer. Like numerous other countries, research on HSC has been conducted and continues to be conducted in Turkey. Güler, et al. (2021) design a multi-period HSC for Turkey and then turn it into a single-period, multi-objective one (Erdoğan, et al., 2023). In (Erdoğan, et al., 2023), they combine these two studies and make a multi-objective and multi-period HSC plan. Nevertheless, one of the most crucial factors in HSC design in recent times, the green hydrogen production potential, is not addressed in these studies. Generally, coal, natural gas, biomass and a few renewable energy sources are used as primary energy sources (PES) in hydrogen production. However, obtaining the hydrogen obtained through green methods would be the most appropriate way to achieve the first purpose of using hydrogen. Green hydrogen is the type of hydrogen obtained from renewable sources such as wind, solar, hydroelectric, and geothermal. Sgarbossa, et al. (2023) propose an agenda about this topic in their study. A study undertaken by Seo, et al. (2023) focus on developing strategies for delivering hydrogen to customers from offshore production locations, where there is a higher potential for renewable energy. According to Jiang, et al. (2022), renewable energy resources that are overproduced should be converted to hydrogen for storage purposes; they develop an approach for carrying out this.

In this study, an HSC planning that considers renewable energy sources for Turkey is proposed. Although Turkey's renewable energy resources are not at a sufficient level at the moment, the potential is very high and studies on this subject are continuing. Based on this, Dinçer, et al. (2021) published a report revealing the hydrogen production potential in Turkey. We employed this report for our study.

II. Experimental Set-up and Procedure

Erdoğan, et al. (2023) propose the design of HSC in Turkey for 2050. Their model is a multi-objective model that minimizes cost, CO_2 emission and risk. In this study, this model is enriched by including stochasticity to minimize the problems arising from demand uncertainty and by using potential renewable energy resources in Turkey, addressed by (Dinçer, et al., 2021) report. The report indicates for each province how much hydrogen can be produced with potential renewable energy sources after deducting the electricity consumption in the province. To adapt this to our model, these hydrogen quantities are converted into units of primary energy sources. Based on our analysis, we project that the potential outlined in this report can be realized no earlier than 25 years from now.

Therefore, the model is created as a single period model for 2050.

Since HFCV is a new technology, there are uncertainties regarding its demand, hence a scenario-based stochastic programming approach with two stages is used to model this uncertainty. In stochastic programming, there are two kinds of variables. Even if the scenario changes, there will be no change in the values of *discrete control* (i.e., here-and-now) *variables*. They show the choices that need to be made at the beginning of the problem. The decision to open a plant in a grid can be given as an example. Another choice is the amount of hydrogen that will be transported or the amount that will be made in this plant. Their values depend on the scenario. *Continuous dispatch (i.e. wait-and-see) variables* show these kinds of choices. While determining the scenarios, the period between 2020 and 2050 is divided into three 10-year periods, and a total of eight scenarios is created by calculating how much the demand in 2050 would be, depending on whether the demand is high or low during these three periods. In addition, the Epsilon Constraint Method is employed to identify the optimal model that minimizes cost, risk, and CO_2 emissions as in (Erdoğan, et al., 2023).

There are two important points that distinguish this study from other multi-objective stochastic models. The first of these is the inclusion of potential renewable energy resources in Turkey into the model. Secondly, in CO_2 optimization, which is one of the model objectives, in addition to the CO_2 absorption resulting from production and transportation, the CO_2 emission resulting from the production of PES is also calculated as in Equation 1 and included in the objective function of CO_2 optimization. Therefore, the model is empowered to give greater consideration to the utilization of green hydrogen production.

$$TPESCO2_{e,k} = \sum_{p,j,g} PVar_{p,j,g,k} * U_{p,j,e} * PESCO2_e \quad (1)$$

TPESCO2, PVar, U and PESCO2 represent the total CO_2 emissions for each energy source and scenario; the production amount in each facility type, facility size, grid, and scenario; the usage amount of each PES in the facility of type p and size j; the CO2 emissions of each PES in electricity production, respectively.

III. Results and Discussions

The epsion constraint method yields the best solution as the one shown in Table 1.

Table 1. The Objective Results

Total Cost ($/day)	Total CO_2 (kg^{-1}/day)	Total Risk (unit)
103,404,474	34,828,652	3,925

Table 2 shows the number of facilities opened according to plant type and size, and in parantheses, the percentage of these facilities in the total number of plants.

Table 2. Number of facilities opened.

Plant Size/Type	SMR	ELE (Solar)	ELE (Wind)	ELE (Hydroelectric)	H_2S-ELE (Solar)	H_2S-ELE (Wind)	H_2S-ELE (Hydroelectric)
Small	0	118 (37.1%)	109 (34.3%)	20 (6.3%)	5 (1.6%)	12 (3.8%)	6 (1.9%)
Medium	1 (0.3%)	26 (8.2%)	13 (4.1%)	2 (0.6%)	1 (0.3%)	0	1 (0.3%)
Large	3 (0.9%)	1 (0.3 %)	0	0	0	0	0

According to the results, although Turkey's renewable energy resources are sufficient, it is observed that very few (only 1.2%) natural gas-powered SMR production facilities have been opened. This is because the cost of SMR facilities is less than electrolysis facilities and this affects the objective function. The facilities of the ELE, which rely on solar and wind energy, make up a significant share of Turkey's potential renewable energy sources, accounting for nearly 90% of all facilities. This rate also includes H2S-ELE facilities that produce by using sulfur in the Black Sea. It is seen that H2S-ELE facilities constitute approximately 8% of the total facilities.
Fig.1 shows the facilities opened in each grid and the flows between the grids according to the most likely scenario (where demand is low in all three periods).

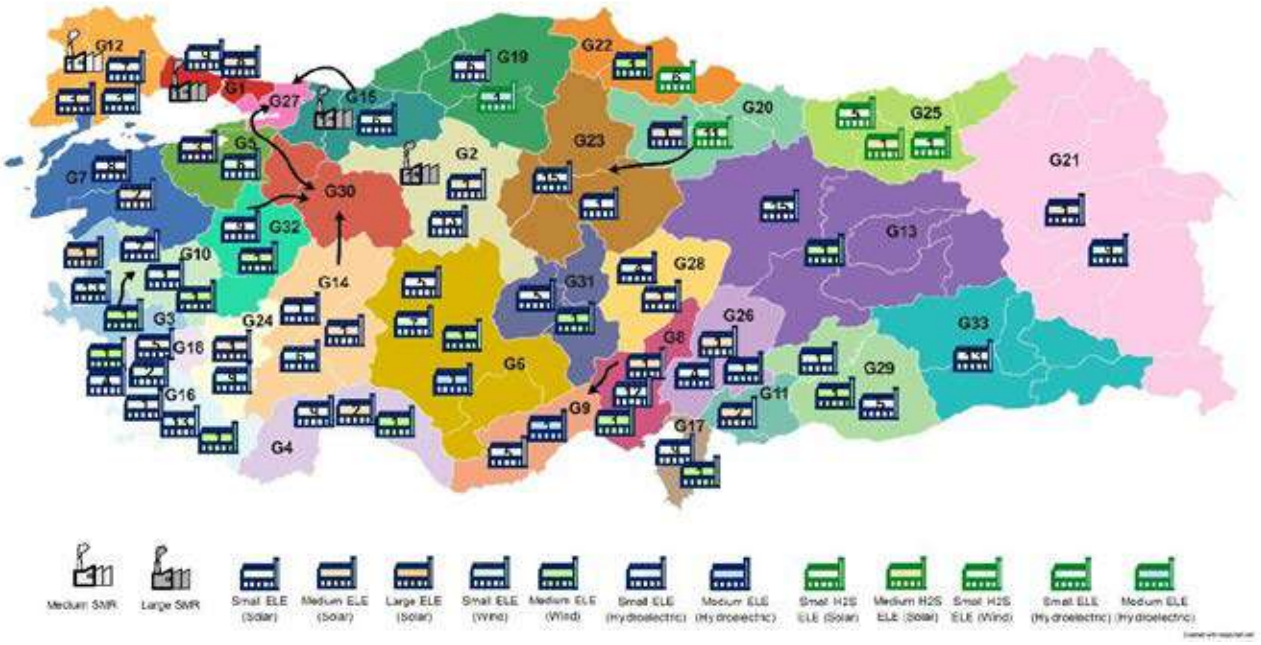


Fig.1: Plants opened in each grid.

It seems that the plant types opened are suitable for the renewable energy potential in the grids. In order to benefit from the sulfur in the Black Sea, H2S-ELE facilities are being opened in the grids on this coast. The network design appears to be decentralized. Plants are opened almost in each grid, usually in small sizes. This is because every grid is rich in renewable energy sources and can meet its own demand. Minimal flow rates between grids contribute to reducing both risk and emissions. Since no facilities have been opened in G30 and G27, the requirements of these grids are fulfilled by the neighboring grids. Moreover, although there are many facilities in G9, G10 and G23, there is also an inflow into these grids. This is because it is more economical to procure from nearby power grids rather than constructing a new plant to fulfill the remaining demand.

IV. Conclusion

In this study, assuming that renewable energy resources in Turkey are used, an HSC is designed for the transportation sector in 2050, which is considered as the earliest year in which this potential can be reached. Since it is impossible to know the hydrogen demand in 2050 in advance, scenario-based stochastic programming is used to control demand uncertainty and the Epsilon Constraint method is used to include all three objectives (i.e. cost, CO_2 emission, risk) in the model. According to the results, the types of plants opened in the grids are compatible with the renewable energy sources of those grids. In addition, since every region of Turkey is very rich in terms of renewable energy resource potential, plants are opened in almost every grid, meaning a decentralized structure is created.

References

Dinçer İbrahim, Javani N. and Karayel G.K, Türkiye için Hidrojen Çiftliği Konsepti Raporu,Report,İstanbul, (2021).

Erdoğan Ahmet and Güler Mehmet Güray, Optimization and analysis of a hydrogen supply chain in terms of cost, CO_2 emissions, and risk: the case of Turkey, International Journal of Hydrogen Energy, 60,48, 22752-22765, (2023).

Erdoğan Ahmet, Geçici Ebru and Güler Mehmet Güray, Design of a future hydrogen supply chain: A multi-objective model for Turkey, International Journal of Hydrogen Energy, 31 ,48, 1775-11789, (2023).

Güler Mehmet Güray, Geçici Ebru and Erdoğan Ahmet, Design of a future hydrogen supply chain: A multi period model for Turkey, International Journal of Hydrogen Energy, 30, 46, 16279-16298, (2021).

Jiang, H., Qi, B., Du, E., Zhang, N., Yang, X., Yang, F., and Wu, Z., Modeling Hydrogen Supply Chain in Renewable Electric Energy System Planning, IEEE Transactions on Industry Applications. 2, 58, 2780–2791, (2022).

Seo, Y., Park, H., Lee, S., Kim, J., and Han, S., Design concepts of hydrogen supply chain to bring consumers offshore green hydrogen, International Journal of Hydrogen Energy, 40, 48, 15126–15142, (2023).

Sgarbossa, F., Arena, S., Tang, O., and Peron, M., Renewable hydrogen supply chains: A planning matrix and an agenda for future research, International Journal of Production Economics, 255, 108674, (2023).

Developing exergetic sustainability indicators for Anion Exchange Membrane Electrolyzer

[1,2*]Furkan Şengüler, [3]Adnan Midilli
[1] PhD Student in Mechanical Engineering Department, Faculty of Mechanical Engineering, [2]Research Assistant in Energy Institute, Istanbul Technical University, Istanbul, Türkiye;
[3] Istanbul Technical University, Mechanical Engineering Faculty, Department of Mechanical Engineering, İnönü Street, No. 65, Gümüşsuyu, 34437, Beyoğlu, İstanbul, Türkiye

* E-mail: fursenguler@itu.edu.tr

Abstract

Hydrogen is crucial for sustainable development, decarbonization, and energy storage. Ensuring sustainability is essential for addressing the difficulties related to land, economics, and development. Energy policy makers globally should give top priority to promoting power-generating technologies that employ hydrogen in order to attain sustainability based on exergy. Anion Exchange Membrane Electrolysers can be important tools for minimizing the environmental impacts of the hydrogen production from coal and natural gas, etc. For better understanding, the environmental and sustainability aspects of the anion exchange membrane electrolysers, the required indicators should be taken into consideration. In this regard, the main objective of this study is to develop the exergetic sustainability indicators for Anion Exchange Membrane Electrolyzer.

Keywords: Hydrogen, Electrolyser, Efficiency, Exergy, Energy

I. Introduction

Sustainability is crucial for overcoming challenges in land, economy, and development. Energy policy makers worldwide should prioritize the promotion of power-producing technologies that utilize hydrogen, such as fuel cells, to achieve exergy-based sustainability (Dincer & Rosen, 2005). PEM fuel cells, which convert oxygen and hydrogen into water, electricity, and waste heat without generating harmful contaminants, are crucial for energy-based sustainability (Midilli & Dincer, 2009).

II. Main Consideration

The normal operating temperature for the anion exchange membrane electrolyser is between 50 and 60 degrees Celsius, as reported by Miller et al. in 2020. The operating pressure typically falls within the range of 1 to 30 bar (Vincent & Bessarabov, 2018). The cell voltage is typically between 1.8 and 2.2 volts, and the current density ranges from 0.2 to 1.0 Acm-2, as stated by (Miller et al., 2020).

III. Analysis

To establish the exergetic sustainability parameters of an AEM Electrolyzer, the first step is to conduct an exergy analysis of the AEM Electrolyzer using the principles of the second law of thermodynamics. The exergy data necessary for the calculation of exergy-based sustainability characteristics for an AEM Electrolyzer are obtained from the literature (Midilli & Dincer, 2009). The overall exergy balance equation for an AEM Electrolyzer can be expressed as

(Total exergy input) = (Total exergy of desired output) + (Total waste exergy output) + (Total exergy destruction)

$$\sum \dot{E}_{in} = \sum \dot{E}_{d,out} + \sum \dot{E}_{w,out} + \sum \dot{E}_{D} \quad (2)$$

Considering the operational concept of an AEM electrolyzer, the general exergy balance, as described by Equation (2), can be rewritten as follows:

$$\dot{E}_{Q_{heat},H_2O} + \dot{E}_{elec} + \dot{E}_{H2O} = \dot{E}_{H2} + \dot{E}_{O2} + \dot{E}_{D} \quad (3)$$

IV. Results and discussions

Tab. 1 Calculated exergetic sustainability parameters data table

Exergetic Sustainability Parameters	
Exergy Efficiency, η_{ex}	0.579
Waste exergy ratio, WER	0.420
Environmental effect factor, EEF	0.724

Environmental destruction coefficient, EDC	1.724
Exergetic sustainability index, ESI	1.380
Sustainability index, SI	2.380
Improvement potential, IP	4.943

V. Conclusions

A comprehensive framework for evaluating the environmental impact and efficiency of hydrogen production processes is established through the assessment of exergetic sustainability indicators in anion exchange membrane electrolyzers. By considering the exergetic sustainability indicators, one may effectively evaluate the exergetic sustainability aspects of an AEM electrolyser system.

References

Dincer, I., & Rosen, M. A. (2005). Thermodynamic aspects of renewables and sustainable development. In *Renewable and Sustainable Energy Reviews* (Vol. 9, Issue 2, pp. 169–189). Elsevier Ltd. https://doi.org/10.1016/j.rser.2004.02.002

Midilli, A., & Dincer, I. (2009). Development of some exergetic parameters for PEM fuel cells for measuring environmental impact and sustainability. *International Journal of Hydrogen Energy*, *34*(9), 3858–3872. https://doi.org/10.1016/j.ijhydene.2009.02.066

Miller, H. A., Bouzek, K., Hnat, J., Loos, S., Bernäcker, C. I., Weißgärber, T., Röntzsch, L., & Meier-Haack, J. (2020). Green hydrogen from anion exchange membrane water electrolysis: A review of recent developments in critical materials and operating conditions. In *Sustainable Energy and Fuels* (Vol. 4, Issue 5, pp. 2114–2133). Royal Society of Chemistry. https://doi.org/10.1039/c9se01240k

Vincent, I., & Bessarabov, D. (2018). Low cost hydrogen production by anion exchange membrane electrolysis: A review. In *Renewable and Sustainable Energy Reviews* (Vol. 81, pp. 1690–1704). Elsevier Ltd. https://doi.org/10.1016/j.rser.2017.05.258

Optimizing Underwater Hydrogen PEMFC Applications: A 2-D Mathematical Modeling Framework for Metal Hydride-Based Hydrogen Storage Systems

[1,2*]Berna Sezgin, [1]Tayfur Öztürk, [3]Inci Eroglu
[1] Middle East Technical University, Faculty of Engineering, Dept. of Metallurgical and Materials Eng., Ankara, 06800, Türkiye
[2] ROKETSAN Missiles Inc., New Generation Systems Dept., Elmadağ, Ankara, 06790, Türkiye
[3] Middle East Technical University, Faculty of Engineering, Dept. of Chemical Eng., Ankara, 06800, Türkiye

* E-mail:berna.sezgin@metu.edu.tr, berna.sezgin@roketsan.com.tr

Abstract

This study addresses the imperative for sustainable energy by focusing on hydrogen storage, mainly metal hydride-based systems for underwater applications. The research aims to develop a numerical model optimizing such systems, considering intricate factors like chemical kinetics, thermodynamics, and transport phenomena. Key challenges include absorption and desorption rates, thermodynamic properties, temperature and pressure effects, and material variability. The model predicts critical system specifications, such as mass and volume, essential for vehicular applications while also addressing heat management during hydrogen absorption by using a 2-D mathematical modeling approach. The study seeks to inform optimal system parameters and operational conditions through mathematical modeling and simulation, facilitating informed decision-making for designing and implementing metal hydride-based hydrogen storage systems.
Keywords: Hydrogen Storage, Metal Hydride, 2-D Modeling, Underwater Applications

I. Introduction

In recent years, our world has been thrust into an era of heightened environmental awareness, as the perils of air pollution and global warming. It has become abundantly clear that the status is unsustainable, necessitating a pivotal transition towards renewable and sustainable energy sources. In this perspective, hydrogen energy is one of the leading visions in sustainable energy systems. Hydrogen is acknowledged as a secondary energy form, serving as an energy carrier. To fully unlock the potential of hydrogen energy, it is imperative to thoroughly examine the challenges associated with the utilization, production, storage, and distribution of hydrogen. Hydrogen energy can be utilized by fuel cells, which convert chemical energy into electrical energy directly through an electrochemical reaction. Proton Exchange Membrane (PEM) fuel cells are the most common type of fuel cell, and a combination of hydrogen and fuel cells forms a symbiotic relationship that holds great potential for various applications. However, the bottleneck in developing hydrogen energy systems is its storage. Hydrogen storage can primarily occur through three methods: compressed gas, liquified hydrogen, and storage into solid materials, such as metal hydrides. The requirements of gravimetric and volumetric energy densities for hydrogen storage can differ from application to application. There are challenges related to energy storage, weight or volume considerations, and environmental impact for underwater applications powered by hydrogen energy. Metal hydride-based storage is preferable for volume considerations since it provides compact and safe storage solutions for underwater applications.

System performance optimization strongly depends on hydrogen storage system optimization since it enhances the vehicles' overall performance, efficiency, and practicality. This study aims to develop a model for metal hydride-based hydrogen storage systems for underwater applications to optimize system performance by determining key parameters with reduced time and resources. To investigate a metal hydride-based hydrogen storage system from the thermodynamic point of view, the heat analysis is based on two-dimensional mathematical modeling to attain an optimum mathematical model that represents the optimum system parameters.

II. Problem Definition

The behavior of different metal hydride materials during hydrogen absorption and desorption is intricate, encompassing chemical kinetics or thermodynamics and the mass, momentum, and heat transport process. This necessitates the design of the storage tank, which must consider which type of metal hydride material is used. Consequently, the effectiveness of a metal hydride-based hydrogen storage system relies on the interconnection between the metal hydride material and the storage tank. Designing such systems demands the application of thorough numerical models and experimental studies. An effective numerical model is crucial when considering the time-intensive nature of endeavors. This model should be capable of identifying coupled metal hydride material and storage system designs that are more likely to fulfill specified application performance criteria.

The problem definition for metal hydride-based hydrogen storage systems involves developing comprehensive numerical models to understand and optimize the complex processes associated with charging and discharging hydrogen in metal hydride materials. This encompasses addressing the intricate interplay of chemical kinetics, thermodynamics, mass, momentum, and heat transport phenomena. This includes addressing challenges related to:

- Modeling the rates of hydrogen absorption and desorption reactions within metal hydrides, considering factors such as reaction rates, activation energies, and reaction mechanisms,

•Analyzing the thermodynamic properties of the metal hydride-hydrogen system, including enthalpy and entropy changes during absorption and desorption processes,
•Understanding the impact of temperature and pressure variations on the absorption and desorption behavior, including the determination of optimal operating conditions,
•Accounting for the variability in hydrogen storage behavior among different metal hydride materials,
•Integrating the modeling of storage tank designs that are adjusted to the specific characteristics of metal hydride materials to enhance the efficiency of hydrogen absorption and desorption,
•Evaluating the performance of metal hydride-based hydrogen storage systems by considering the coupling between the metal hydride material and the storage tank.

III. Modeling

The model aims to predict the main specifications of a metal hydride storage system, such as mass and volume, which are critical for a vehicular application regarding vehicle design and space considerations. It uses the thermodynamic and transport properties of the metal hydride material to calculate the essential parameters needed to estimate the size of the metal hydride-based hydrogen storage tank. The heat balance of the metal hydride-based hydrogen storage tank is estimated as the storage system's property. While absorbing hydrogen, the reaction generates substantial heat, necessitating effective heat removal to enable the continuous absorption of hydrogen. Different types of cooling tube allocations can be considered for this heat removal. This study assumes a metal hydride-based hydrogen storage tank consists of axial coolant tubes. Moreover, the storage tank contents are divided into hypothetical unit cells, as shown in Figure 1(a). The representation of a unit cell is shown in Figure 1(b). The heat transfer fluid passes through cooling tubes, and exchanges heat with the metal hydride.

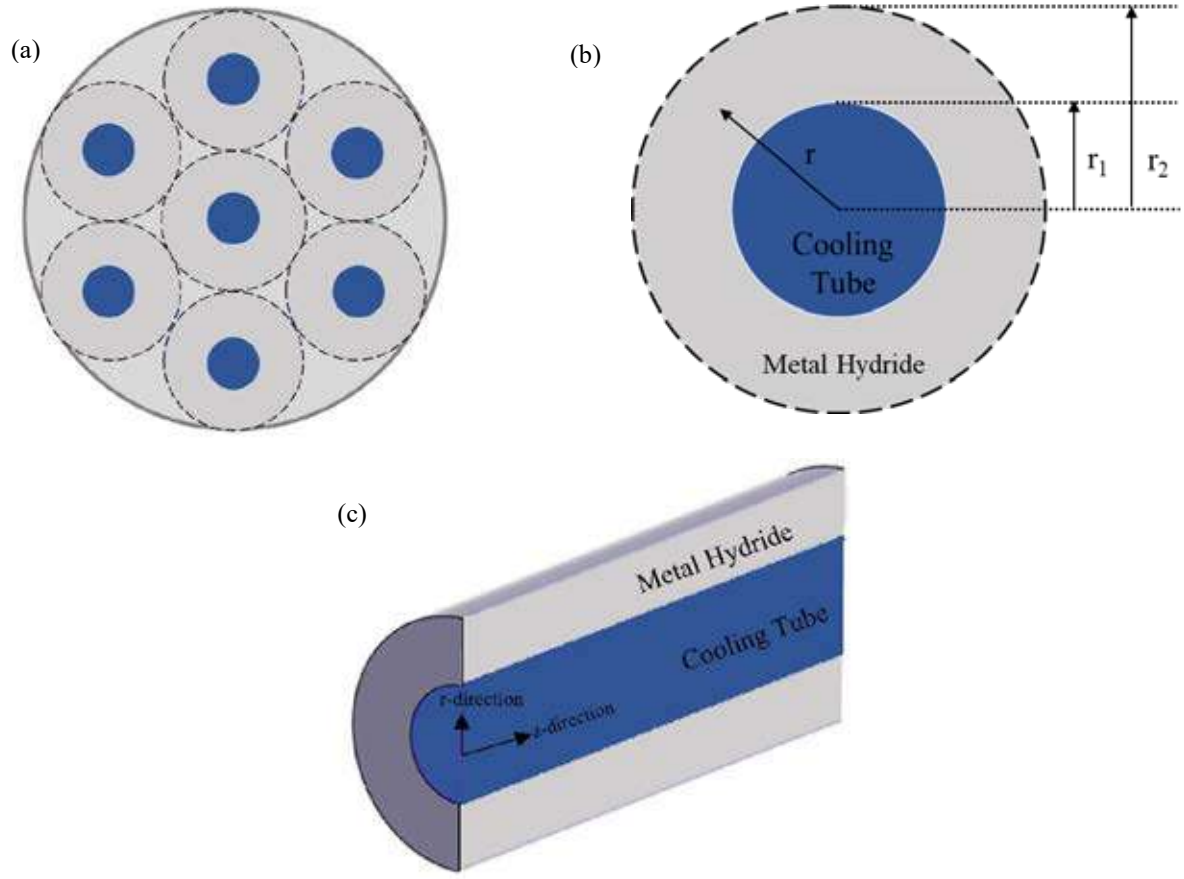


Fig. 1: (a) Cross-section of a cylindrical metal hydride tank containing hypothetical unit cells, (b) Cross-section of a unit cell in r-direction (a coolant tube surrounded by metal hydride material), (c) Cross-section of a unit cell in r and z directions

As can be seen from Figure 1(b), metal hydride material is filled in between r_1 and r_2. The energy balance written for metal hydride in a unit cell is as follows for cylindrical coordinates:

$$\rho c_p \frac{\partial T}{\partial t} = k \frac{1}{r}\frac{\partial}{\partial r}\left(r\frac{\partial T}{\partial r}\right) + \frac{1}{r^2}\frac{\partial^2}{\partial \theta^2}\left(k\frac{\partial T}{\partial \theta}\right) + \frac{\partial}{\partial z}\left(k\frac{\partial T}{\partial z}\right) + q''' \quad (1)$$

Where, ρ defines density (kg.m^{-3}); c_p, heat capacity (kJ.kg^{-1}K^{-1}); k, thermal conductivity (W.m^{-1}K^{-1}); q''', volumetric heat generation during hydrogen absorption (W.m^{-3}).

q''' can be found by the following equation:

$$q''' = -\Delta H \frac{\rho_{hydride}}{M_{hydride} MW_{H_2}} \frac{\Delta m_{H_2}}{\Delta t} \quad (2)$$

Where ΔH defines enthalpy of the hydrogen absorption on metal hydride (J.mol^{-1}); $\rho_{hydride}$the density of metal hydride (kg.m^{-3}); $M_{hydride}$mass of metal hydride required to load target amount of hydrogen (kg); MW_{H_2}, molecular weight of hydrogen (kg.mol^{-1}H_2); Δm_{H_2}, mass of hydrogen stored in metal hydride in time interval in kg.

The energy balance written for cooling fluid is as follows for cylindrical coordinates:

$$\rho_f c_{p,f} \left(\frac{\partial T_f}{dt} + u \frac{\partial T_f}{\partial z}\right) = \frac{1}{r}\frac{\partial}{\partial r}\left(k_f r \frac{\partial T_f}{\partial r}\right) + \frac{\partial}{\partial z}\left(k_f \frac{\partial T_f}{\partial z}\right) \quad (3)$$

Where, ρ_f defines density of the cooling fluid (kg.m^{-3}); $c_{p,f}$, heat capacity of the cooling fluid (kJ.kg^{-1}K^{-1}); k_f, thermal conductivity of the cooling fluid (W.m^{-1}K^{-1}); u, velocity of the cooling fluid (m.s^{-1}).

Assumptions are given below:

- 2-D heat transfer in radial and axial directions is assumed; i.e., heat transfer in angular (θ −Direction) is neglected.
- A mean value for q''' is considered, which is estimated by Equation 2. q''' is not position and temperature dependent.
- T and T_f are not changing with time.
- Thermal conductivity, k, is considered constant throughout the process.
- Convective heat transfer through the metal hydride bed is negligible.

Under these assumptions, Equation (1) and (3) can be re-written as follows, along with the provided inlet condition and boundary conditions below:

$$k\frac{1}{r}\frac{\partial}{\partial r}\left(r\frac{\partial T}{\partial r}\right) + \frac{\partial}{\partial z}\left(k\frac{\partial T}{\partial z}\right) + q''' = 0 \quad (4)$$

$$\rho_f c_{p,f} \left(u \frac{\partial T_f}{\partial z}\right) = \frac{1}{r}\frac{\partial}{\partial r}\left(k_f r \frac{\partial T_f}{\partial r}\right) + \frac{\partial}{\partial z}\left(k_f \frac{\partial T_f}{\partial z}\right) \quad (5)$$

Inlet Conditions:

- $T(0, 0) = T_{f, in}$
- $T_f(0, 0) = T_{f, in}$

Boundary Conditions:

- Convection boundary condition due to cooling fluid:
  $r=r_1$ ➔ $-k\frac{\partial T}{\partial r} = h(T - T_f)$ *at any z.*
- Insulated boundary condition:
  $r=r_2$ ➔ $dT/dr=0$ at any z.
- Symmetry boundary condition:
  $z=L$ ➔ $dT/dz=0$ and $dT_f/dz=0$

IV. Results and Discussions

The utilization of metal hydride materials holds promise as a viable strategy for creating a highly concentrated hydrogen medium for onboard vehicle applications such as underwater applications.

Analysis of absorption and desorption kinetics reveals distinct behaviors among metal hydride materials, impacting hydrogen storage's overall efficiency and effectiveness. Thermodynamic properties such as enthalpy and entropy changes during absorption and desorption processes are crucial in determining the system's performance under varying temperature and pressure conditions. Furthermore, the study highlights the importance of system design in enhancing hydrogen absorption and desorption rates. Optimal configurations of coolant tubes within the storage tank are identified, demonstrating improved heat transfer efficiency and enhanced system performance.

V. Conclusions

This paper introduces a modeling study that serves as a means to estimate the characteristics of a metal hydride-based hydrogen storage system intended for underwater vehicle use. Model estimates system mass and volume, enabling sensitivity analysis of different parameters. The model underscores that the hydrogen capacity alone does not fully determine a material's ability to meet the best performance criteria. Instead, the thermodynamic properties of the material can influence the adoption of a more compact and lighter tank configuration, along with lower

operating temperatures and reduced metal hydride mass. Physical properties like density and thermal conductivity can also impact the system's overall mass and volume. Although the analysis in this study is specific to a limited set of materials, the model can be positioned to guide researchers in developing future metal hydrides, thereby enhancing the model's applicability to alternative materials that may emerge.

References

Anderson, B., et al. (2023). Challenges in hydrogen energy systems: A comprehensive review. Renewable and Sustainable Energy Reviews, 45, 101325.

Chen, H., & Wang, Y. (2018). Environmental impact assessment of underwater applications powered by hydrogen energy. Environmental Impact Assessment Review, 75, 102356.

Gomez, R., et al. (2023). Modeling metal hydride-based hydrogen storage systems for underwater applications. Journal of Energy Conversion and Management, 150, 112345.

Hydrogen Quality Effect to Generator Performance

Kerim Kenan Kiremit
Eren Enerji Elektrik Üretim A.Ş., Kuzyaka Mahallesi Aras Sokak No:6
Çatalağzı, Kilimli, Zonguldak, 67150, Türkiye

kerimkenan.kiremit@erenenerji.com.tr

Abstract

Within the borders of Çatalağzı and Muslu Town of Zonguldak, we have units with a total installed power of 2790 MW, including 160 MWe with fluidized bed technology, 2x615 MWe and 2x700 MWe with super critical pulverized coal and and port facilities. Stator core and rotor of generator are cooled by hydrogen at 2x615 MWe and 2x700 MWe units. Hydrogen system of generator adopts closed circulation system. Hydrogen is produced in the hydrogen production facility within Eren. Hydrogen is at low density. Thus, it reduces air friction losses. Hydrogen has high heat conduction coefficient (Distributed Energy Systems, 2007). Hydrogen has lower corrosion effect than oxygen. Low gas density and closed loop reduce noise. Hydrogen is a clean gas in terms of being released into the atmosphere. Hydrogen is low cost. Leak detection was easy (David E. Wolff, 2009). This case study will present the hydrogen quality effect to generator performance.

Keywords: Hydrogen, windage loss, generator, power plant, efficiency, safety

I. Introduction

The quality of hydrogen used as cooling gas in the generator affects the generator operating conditions in three basic ways (Distributed Energy Systems, 2007).

- Hydrogen purity directly affects generator operating efficiency (Distributed Energy Systems, 2007).

The purity of hydrogen in the generator is very important for some reasons. The first and most important reason is safety. When the hydrogen content in the air inside the generator drops below %74, an explosive atmosphere occurs. In addition, the purity of the hydrogen in the generator is very important in reducing the friction losses of the windings. The increase in friction losses due to foreign substances causes a decrease in the revenues of the power plant.

- The amount of moisture contained in hydrogen affects the life of the generator windings (Distributed Energy Systems, 2007).

Water vapor causes the life of generator parts to shorten. High humidity causes stress corrosion failure of the protective seals, causing a short circuit in the stator windings. In most generators, it is recommended to keep the hydrogen dew point below 0°C. The most common source of moisture in hydrogen used as refrigerant is water combined with sealing oil. In general, the lower the dew point, the better. When moisture reaches the end of the rotor windings of the generator, it destroys the insulation and short-circuits the rotor windings. Unplanned downtimes and repair interventions due to damage caused by moisture result in very serious costs for power plants.

- The stability of the hydrogen gas pressure in the generator affects the maximum capacity of the generator (Distributed Energy Systems, 2007).

With increasing pressure, hydrogen becomes denser and absorbs heat faster and removes it faster. As a result, higher capacity can be achieved without temperature rise in the windings. The increased hydrogen pressure allows operation at normal load without increasing the cooling water temperature used in the cooler. When operating by maintaining the constant hydrogen pressure given by the manufacturer, the increased kVA output ensures that the power plant can operate at the highest electricity production capacity.

II. Experimental Set-up and Procedure

Air is the most likely impurity to affect hydrogen density within the generator casing. Air is 14,4 times as dense as hydrogen, so even relatively low levels of air increase the density of the hydrogen-air mixture considerably (David E. Wolff, 2009).

This is shown as (Distributed Energy Systems, 2007):

Gdens = (Hpur x 1) + (Abal x 14.4)
Gdens = Increase in Gas Density (%)
Hpur = Purity of Hydrogen in Generator Casing (%)
Abal = Balance of Impurity (air) in Generator Casing (%)

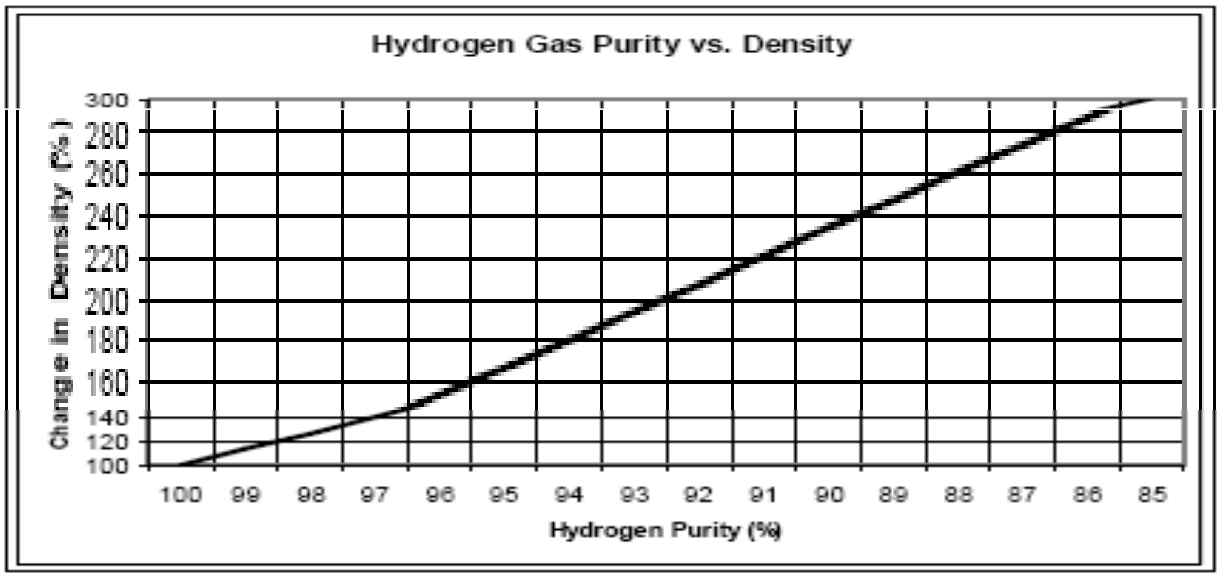


Fig. 1: The relationship between hydrogen gas purity and gas density

The change in gas density will have a negative affect on the windage loss of the generator. Windage losses are typically stated at nominal pressure above atmospheric pressure and at some nominal purity. The losses can be adjusted for actual operating conditions by simple calculations.

This is shown as (Distributed Energy Systems, 2007):

Gloss = Gwind x(Dact/ Dbase)x(Pact+14.7)/(Pspec+ 14.7)

Where:
Gloss = Total Generator Electrical Losses due to Windage (kW)
Gwind = Baseline Generator Windage Loss (kW)
Dact = Actual Gas Density due to Impurities (%)
Dbase = Gas Density Baseline (%)
Pact = Actual Generator Operating Pressure (psi)
Pspec = Generator Operating Pressure Specification (psi)

The improvement in the thermal capability of the generator is proportional to the square root of the absolute pressure increase in the generator casing (Distributed Energy Systems, 2007).

Gcap = √{(Pspec + 14,695) / (Plow + 14,695)} - 1

Where:
Gcap = Increase in Generator Capacity (%)
Plow = Pressure below OEM Max Specification (psi)
Pspec = Pressure at OEM Max Specification (psi)

The increased capacity is due to better heat removal from the copper windings associated with the higher density of the hydrogen gas. The higher density also has a small effect on the windage loss of the generator, but this is minimal in comparison to the gain in overall generating capacity.

III. Analysis

Generator technical data is given in Table 1 (Xie Hui, 2009).

Tab. 1: Generator Technical Data

Manufacturer	Shanghai Generator
Type	3 phase, synchronous generator
Model	QFSN-600-2
Rated active power	600 MWe
Maximum output power	642 MWe

Rated capacity	667 MVA
Rated frequency	50 Hz
Rotation speed	3000 rpm
Rated power factor	0,9
Number of poles	2
Genarator efficiency	%98,90
Rated hydrogen pressure	58,02 psi
Maximum permissible hydrogen pressure	63,82 psi
Genarator volume	90 m³
Genarator nominal hydrogen purity	≥%95
Genarator minimum hydrogen purity	≥%90
Genarator hydrogen dew point	-5≈-25 ºC

Tab. 2: Generator Capacity - Hydrogen Pressure Relationship

Gcap	Increase in Generator Capacity (%)	%	2,05
Plow	Pressure below OEM Max Specification	psi	55,11
Pspec	Pressure at OEM Max Specification	psi	58,02

According to generator technical data that is given in Table 1, genarator rated hydrogen pressure is 58,02 psi and generator maximum permissible hydrogen pressure is 63,82 psi (Shanghai Electric, 2008). In the past, our average generator hydrogen pressure was 55,11 psi. As a result of the studies and trials, we increased the generator hydrogen pressure to 58,02 psi. In this way, we increased the generator capacity by %2,05.

The windage loss curve depending on hydrogen purity provided by the generator manufacturer is given in Fig 2. Accordingly, every 1% increase in generator hydrogen purity increases the generator output power by 59,5 kW (Shanghai Electric, 2008).

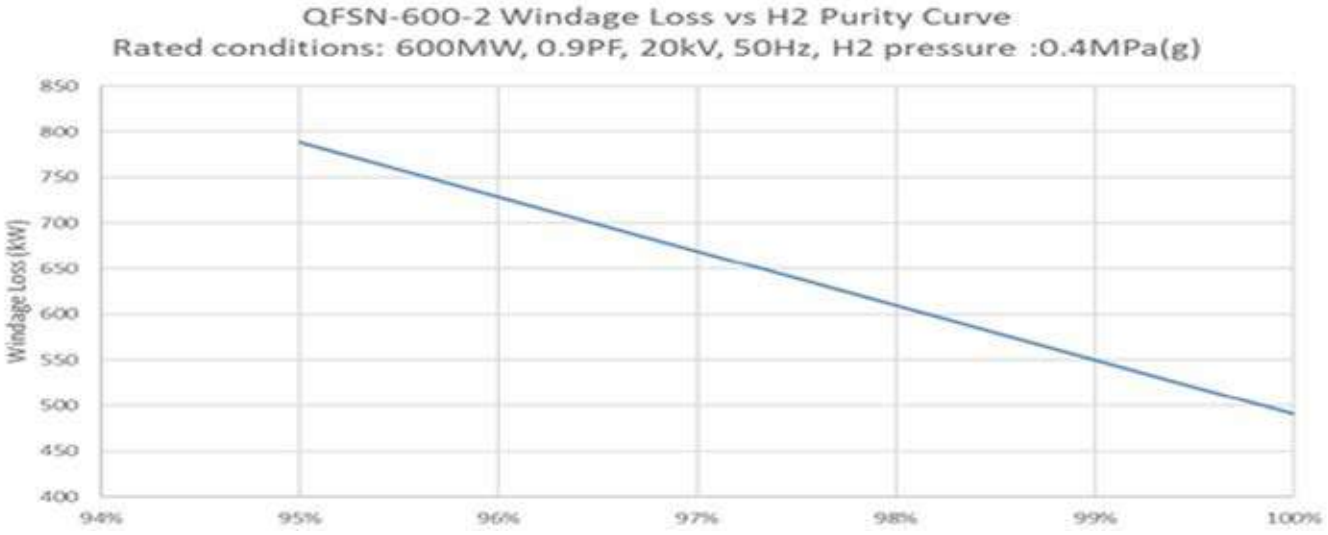


Fig. 2: “Generator Windage Loss&H2 Purity Curve

Tab. 3: Windage Loss - Hydrogen Purity Relationship

Hydrogen Purity Change			%99 to %98	%99 to %97	%99 to %96	%99 to %95
Gloss	Total Generator Electrical Losses Due To Windage	kW	563,00	622,49	681,99	741,49
Gwind	Baseline Generator Windage Loss	kW	503,50	503,50	503,50	503,50
Initial Hpur	Initial Hydrogen Purity	%	99,00	99,00	99,00	99,00
Final Hpur	Final Hydrogen Purity	%	98,00	97,00	96,00	95,00
Dact, Gdens	Actual Gas Density Due To Impurities	%	126,80	140,20	153,60	167,00

Dbase, Gdens	Gas Density Baseline	%	113,40	113,40	113,40	113,40
Pact	Actual Generator Operating Pressure	psi	58,02	58,02	58,02	58,02
Pspec	Generator Operating Pressure Specification	psi	58,02	58,02	58,02	58,02
Gnet	Net Windage Loss Associated With %1 Hydrogen Purity	kW	59,50	59,50	59,50	59,50

In the past, our average generator hydrogen purity was %97,00. As a result of the studies and trials, we increased the generator hydrogen purity to 98,00. In this way, we increased the generator output by 416.500 kWh at 7.000 hours of operation.

IV. Results and discussions

In a generator that uses hydrogen gas, the purity of the hydrogen gas is an important factor that can affect the performance and safety of the generator. If the hydrogen purity in a generator is too low, it can have several negative consequences, such as (Distributed Energy Systems, 2007):

Reduced efficiency: The lower the hydrogen purity, the less efficient the generator will be at producing hydrogen gas. This can result in a decrease in the amount of hydrogen gas produced, which can impact the performance of the application that requires the hydrogen gas.

Reduced safety: Hydrogen gas is highly flammable and can be explosive under certain conditions. If the hydrogen purity in a generator is too low, it can increase the risk of an explosion or fire.

Contamination: If the hydrogen purity in a generator is too low, it may contain impurities such as oxygen, nitrogen, or moisture, which can contaminate the hydrogen gas and impact the performance of the application that requires the hydrogen gas.

Damage to equipment: Impurities in the hydrogen gas can also damage equipment that comes in contact with the gases.

In summary, if the hydrogen purity in a generator is too low, it can lead to reduced efficiency, increased safety risks, contamination of the hydrogen gas, and damage to equipment. It's important to ensure that the generator is producing hydrogen gas at the required purity to ensure optimal performance and safety.

V. Conclusions

The purpose of the project is to assess the affect hydrogen purity and pressure stability has on the operating efficiency and capacity of the electrical generating assets of Zetes Power Plant. By ensuring high purity, controlling moisture content, optimizing pressure and temperature conditions, using clean hydrogen sources, and implementing proper storage and handling practices, operators can maximize the efficiency and performance of hydrogen-based generators while minimizing emissions and environmental impact. Further research and technological advancements in hydrogen production, purification, and utilization are essential for realizing the full potential of hydrogen as a clean and efficient energy carrier.

Acknowledgements

I would like to thank all managers who provided with their help and support during these research studies and tests.

References

David E. Wolff Proton Energy Systems, Hydrogen for Generator Cooling - The Pressure, Purity and Dewpoint Difference (2009)
Distributed Energy Systems Corp, Reducing 1.5 Million Tons Of CO_2 Annually in Europe (2007)
Distributed Energy Systems Corp, Mirant's Dickerson Generating Station (2007)
Shanghai Electric, Generator Technical Data Sheet, ER/YQ0A154F245 (2008)
Shanghai Electric, Turbine Generator Instruction Book, ER/YQ0A460F555 (2008)
Xie Hui, Training document for steam turbine operation (2009)

Thermodynamic Assessment Of an Improved Solar Powered Multi-Generation System Using A Thermoelectric Generator

[1]Mohammad Ali Sabbaghi, [2]Ehsan Baniasadi, [3]Hadi Genceli
[1] Department of Mechanical Engineering, Yazd University, Yazd, Iran
[2] Department of Mechanical Engineering, University of Isfahan, Isfahan, Iran
[3] Faculty of Mechanical Engineering, Yildiz Technical University, Besiktas, Istanbul, 34349, Türkiye

* E-mail: hgenceli@yildiz.edu.tr

Abstract
Employing multi-generation systems enables the simultaneous production of multiple forms of energy. The trend towards energy generating using multi-generation systems has increased notably in contrast to individual systems primarily owing to their enhanced efficiency and environmentally friendly features. This study focuses on the thermodynamic investigation of a modified organic Rankine cycle (ORC) with a thermoelectric generator (TEG) that uses solar energy for cogeneration of heat, hydrogen, and electricity. The results indicate that the proposed system has an energy and exergy efficiencies of 37.73% and 31.63% respectively, and can produce 1.93 kg/h hydrogen. The system efficiencies have optimal values with the turbine inlet pressure. In a portion of the ORC characterized by significant energy losses, the integration of a thermoelectric generator serves to decrease energy losses, resulting in a considerable 126.2 kW improvement in power generation. Additionally, this modification improves 10.21% and 8.55% in energy and exergy efficiencies of the system.

Keywords: Solar energy, Thermodynamic analysis, Hydrogen, Thermoelectric generator

I. Introduction

Multi-generation systems can generate multiple forms of energy from a single energy source. These systems can be considered as a valuable option that increases the production capacity of the system and also produces cooling, heating, and other forms of energy and uses it for various applications, Mirbagheri (2023), Sabbaghi (2024). Thermoelectric are one of the emerging technologies in energy production systems. This equipment operates based on exploiting temperature differences between their two ends to convert such thermal gradients into electrical energy. Previous research studies by Pourrahmani (2029) have examined the utilization of a thermoelectric generator instead of a condenser within the organic Rankine cycle, aiming to both prevent heat loss and generate power. Ziapour (2017) used thermoelectric generators in the conventional Rankine cycle and studied their potential as alternatives to condensers in other power generation cycles, including the Kalina cycle. In a study performed by Fan (2011), they conducted both theoretical and experimental analysis of a thermoelectric generator powered by solar thermal energy. Additionally, in the study by Kraemer (2011) conducted an evaluation of a flat plate solar collector integrated with an integrated thermoelectric generator. Their research aimed to explore the potential benefits of incorporating thermoelectric technology in the solar collector system and assess the resulting improvement in system efficiency. Amiri (2016) combined solar tower with a gas turbine cycle in a poly-generation energy system to decrease the consumption of fossil fuels. The findings showed that the productivity increased from 31% to 85%. As a result, utilizing solar energy to preheat the combustion chamber inlet air can reduce CO_2 emissions by approximately 400 kg/MWh.
The research literature emphasizes the importance of multi-generation systems in optimizing energy utilization. Specifically, the use of thermoelectric generators to harness excess heat and generate electricity has gained significant attention. In line with this, a new study presents a solar-powered multi-generation system that integrates thermoelectric generators. The main goal of this system is to improve electricity generation by effectively utilizing the excess heat. The integration of thermoelectric technology offers a promising approach to maximize energy conversion and utilization within the system. The findings of this research can present valuable insights to researchers, designer, engineers, and energy specialists in analysing multi-generation systems.

II. System Description

Figure 1 provides a schematic of the proposed multi-generation system employing solar energy as the primary source. The system comprises three subsystems: the ORC, the solar collector, and the PEME. The objective of the system is to generate electricity, hydrogen, and heating load. The operating fluid utilized in the ORC is R134a. It undergoes superheating to attain the highest temperature, facilitated by a series of heat exchangers. These heat exchangers encompass an economizer, an evaporator, and a super heater. Subsequently, the working fluid enters the turbine and generates power. To enhance efficiency and output power, the system employs a thermoelectric generator as a substitute for a condenser. The primary objective of using this equipment is to generate additional electrical power from wasted heat. The power generated by the thermoelectric generator is used to produce hydrogen by PEME.

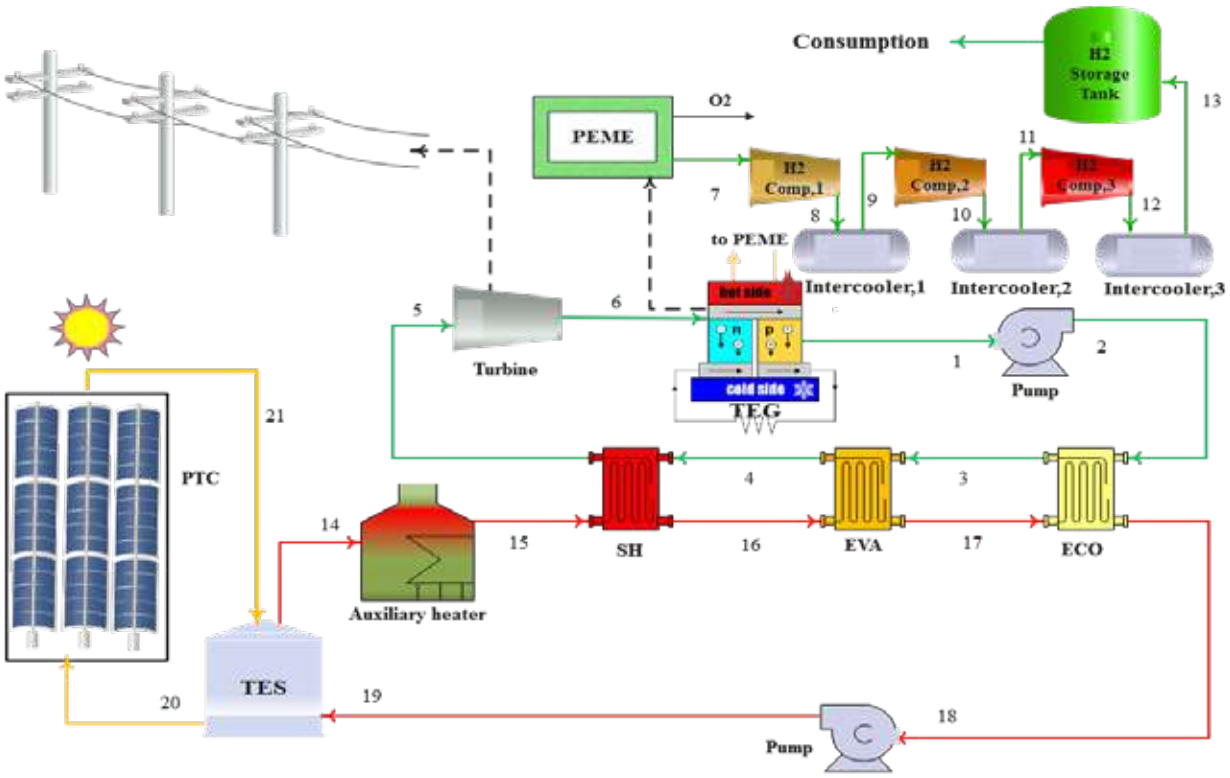


Fig 1. Schematic diagram of the studied system

III. Thermodynamic Modelling

For thermodynamic modelling, each component within the system is regarded as a control volume, and the both laws of thermodynamics are formulated for each component, Sabbaghi (2023).

$$\dot{Q} + \sum \dot{m}_i h_i = \dot{w} + \sum \dot{m}_e h_e \quad (1)$$

$$Ex_{ph} = (h - T_0 s) - (h_0 - T_0 s_0) \quad (2)$$

$$\bar{E}_{ch} = \left[\frac{\bar{e}^0_{ch,N_3}}{M_{N_3}}\right] X + \left[\frac{\bar{e}^0_{ch,H_2O}}{M_{H_2O}}\right](1 - X) \quad (3)$$

A thermoelectric generator (TEG) is equipment that functions on the Seebak effect. The Seebeck effect is a fundamental principle in thermoelectricity where a temperature difference between two different conductive materials or semiconductors generates an electric voltage. This voltage can then be utilized to produce electrical power. TEG efficiency is assessed through Equations 4-5, Pourrahmani (2019).

$$\eta_{teg} = \eta_{carnot} \frac{\sqrt{1 + zT_m} - 1}{\sqrt{1 + zT_m} + \frac{T_L}{T_H}} \quad (4)$$

$$\eta_{E} = \frac{\dot{W}_{teg}}{\dot{Q}_{elegant}} \quad \text{و} \quad \eta_{carnot} = 1 - \frac{T_L}{T_H} \quad (5)$$

The exergy efficiency of the studied system is determined from Equation 6.

$$\eta_{g} = \frac{\dot{W}_{net} + (\dot{E}x_{H2})}{\dot{E}x_{solar}} \quad (6)$$

IV. Results and Discussions

Initially, to ensure the accuracy of the analysis, it is necessary to perform validation. As depicted in Figure 2-3, a comprehensive comparison of the system's efficiency under identical operating conditions with reference results by Ya-Ling (2012) reveals a good agreement. Also, for the thermoelectric generator, a comparison was made between the obtained results and reference Habibollahzade (2018), which is shown in Figure 2.

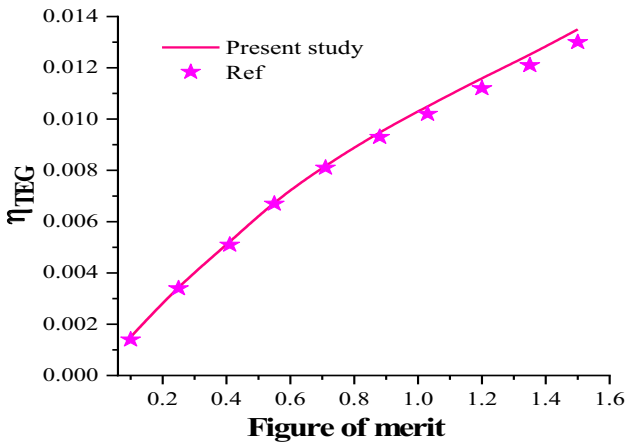


Fig 2. Comparison of the obtained results from modeling the TEG unit, Habibollahzade (2018)

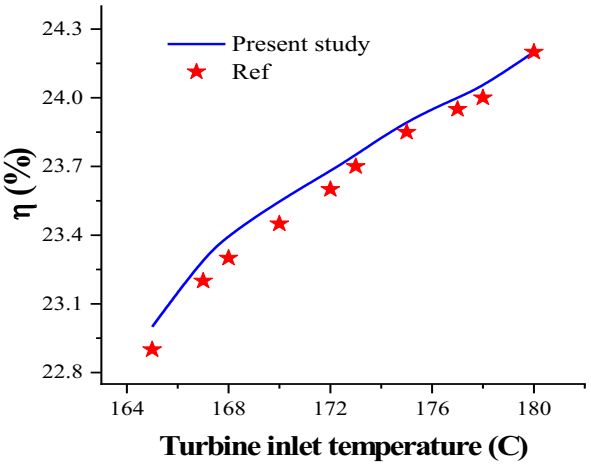


Fig 3. Comparison of the obtained results from modeling the ORC, Ya-Ling (2012)

The obtained results indicate that the investigated system has the capability to generate 1.93 kg/h of hydrogen and generate 126.2 kW of power through the TEG. These results showcase the system's potential for efficient energy production. The performance parameters of the system are highly influenced by solar radiation, as depicted in Figure 4. During the peak hours of solar radiation, typically occurring in the middle of the day, both the useful output heat and the production capacity of the system reach their maximum values. This suggests that the system operates most efficiently when solar radiation is at its highest. However, as the afternoon progresses and solar radiation decreases, the useful heat capacity and the outlet temperature of the fluid from the collector gradually decrease as well. This diminishing solar radiation has a direct effect on the production capacity and efficiencies of the system, leading to a decrease in overall performance. To optimize the efficiency of energy utilization, it becomes essential to precisely design solar systems that are efficient in capturing and harnessing solar radiation. This emphasizes the importance of accurate solar system design to maximize energy capture and utilization efficiency.

Overall, the analysis of the proposed system's results highlights the significance of solar radiation and its impact on system performance, underscoring the need for efficient solar system design for optimal energy utilization.

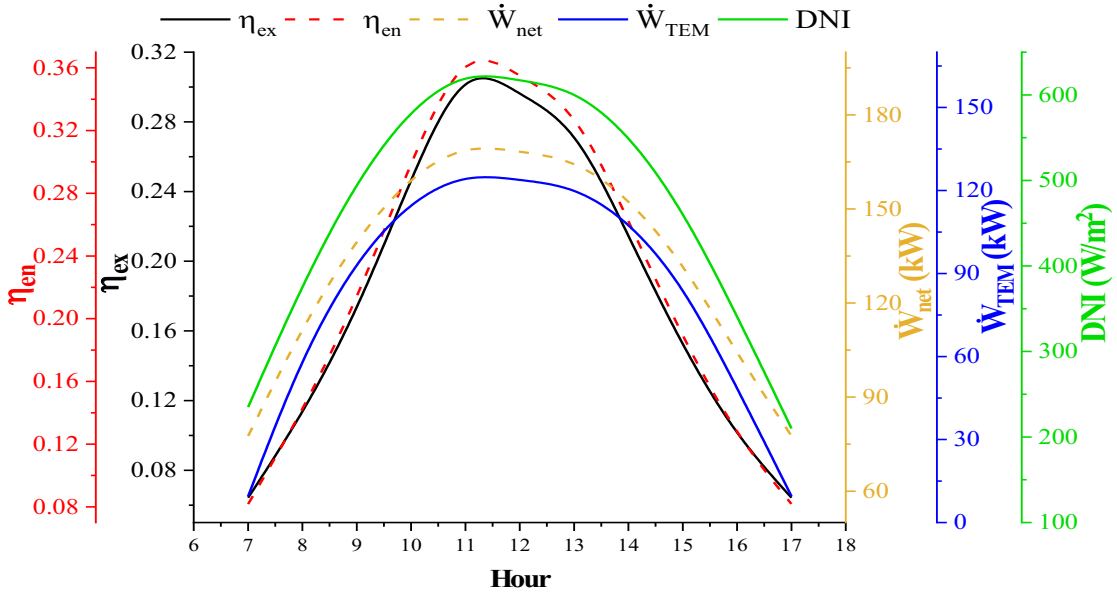


Fig 4. Variations in the system's performance parameters with solar radiation throughout the day

The diagram in Figure 5 illustrates the variations in the input pressure of the ORC turbine and its effect on the system's performance parameters. When the turbine input pressure increases to about 3500 kPa, the system's efficiencies increase. Beyond this point, however, a rise in input pressure results in a decrease in system efficiencies. When the input pressure to the turbine increases, it results in a higher enthalpy difference between the turbine's input and output, consequently increasing the turbine's output power. Conversely, an increase in the input pressure to the turbine reduces the amount of heat removed from the system. This reduction, in turn, decreases the output power of the TEG, indicating that a rise in the turbine's input pressure decreases the temperature difference across the TEG. Therefore, these two factors combined contribute to the establishment of an optimal

pressure point. The changes in the system's efficiencies and performance parameters with the turbine's outlet pressure are depicted in Figure 6. As the turbine's outlet pressure increases, the enthalpy difference in the turbine decreases, resulting in a reduction in the system's output powers.

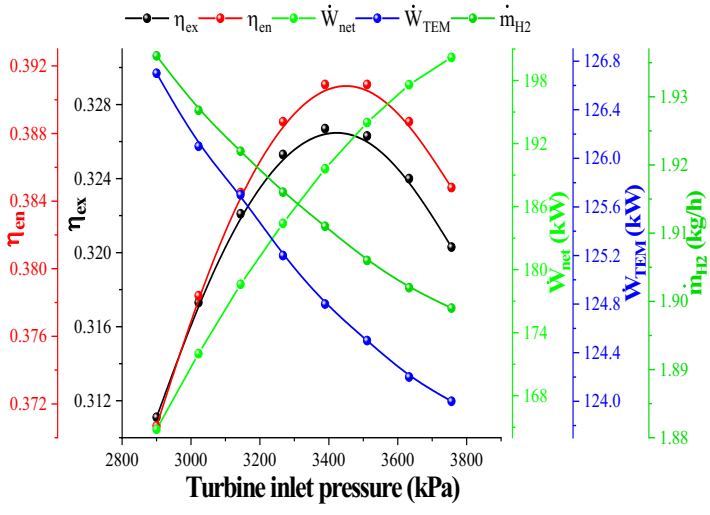


Fig 5. Effects of variations in turbine inlet pressure on system performance

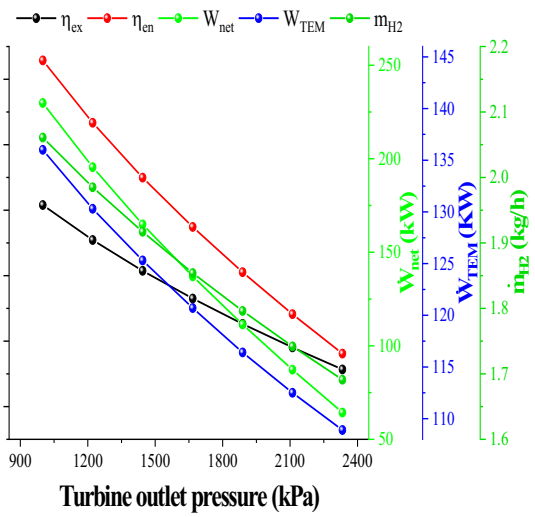


Fig 6. Effects of variations in turbine outlet pressure on system performance

V. Conclusion

The research explores a modified ORC featuring the integration of a TEG that uses solar energy to generate heat, hydrogen, and electricity simultaneously. The findings reveal energy and exergy efficiencies of 37.73% and 31.63%, respectively. During the middle hours of the day, solar irradiation reaches its peak. Peak solar irradiation maximizes useful heat and system power output. Elevating turbine pressure enhances enthalpy difference and turbine power, while higher turbine inlet pressure diminishes system heat removal, thereby reducing thermoelectric power generation. Consequently, an optimal operating pressure emerges as a cumulative effect of these factors.

References

Mirbagheri MH, Baniasadi E, Genceli H. Exploring the performance of an innovative integrated solar tower power plant with hydrogen generation and storage. Int J Hydrogen Energy, 48(99), 39271-39285 ,(2023).

Sabbaghi M A, & Sefid M. Risk, sensitive analysis, and optimization of a new multi-generation system activated by solar and biomass energies. Energy Report, 11, 1006-1018, (2024).

Pourrahmani H, Moghimi M. Exergoeconomic analysis and multi-objective optimization of a novel continuous solar driven hydrogen production system assisted by phase change material thermal storage system. Energy.189:116170, (2019).

Ziapour M.B., Saadat M., Palideh V., and Afzal S., Power generation enhancement in a salinity-gradient solar pond power plant using thermoelectric generator, Energy conversion and management, vol. 136, pp. 283-293, (2017).

Fan H, Singh R, Akbarzadeh A. Electric power generation from thermoelectric cells using a solar dish concentrator. Journal of Electronic Materials, 40(5), 1311-1320 , (2011).

Kraemer D, Poudel B, Feng H-P., Caylor, J, Yu B, Yan X. High-performance flat-panel solar thermoelectric generators with high thermal concentration. Nature Materials, (10) 532–538 , (2011).

Amiri, F., Tahouni, N., Azadi, M., & Panjeshahi, M. H. Design of a hybrid power plant integrated with a residential area. Energy, 115, 746-755, (2016).

Sabbaghi Ma, Sefid M. Exergy-environmental analysis and optimisation of the modified organic Rankine cycle driven by geothermal and biomass energies, Int J of exergy, 40(2): 144-161, (2023).

Ya-Ling He, Dan-Hua Mei, Wen-Quan Tao, Wei-Wei Yang, Huai-Liang Liu. Simulation of the parabolic trough solar energy generation system with Organic Rankine Cycle, Applied Energy. 630-641, (2012).

Habibollahzade A, Gholamian E, Ahmadi P, Behzadi A. Multi-criteria optimization of an integrated energy system with thermoelectric generator, parabolic trough solar collector and electrolysis for hydrogen production, Int. J. Hydrogen Energy. 43: 14140-14157, (2018).

Closed Loop Control Design for Enhanced Performance of Quasi-Switched Boost Inverters in PEM Fuel Cell-Based Residential Applications

[1*]Melike Esen Güngör, [2]Ozan Gülbudak, [2]Mustafa Gökdağ, [1]Mehmet Özdemir, [1]Ahmet Orhan
[1] Fırat University, Faculty of Engineering, Department of Electrical and Electronics Eng., Elazığ, 23100, Türkiye
[2] Karabük University, Faculty of Engineering, Department of Electrical and Electronics Eng., Karabük, 78050, Türkiye

* E-mail:melikeesen@firat.edu.tr"

Abstract

This study presents a closed-loop control design for residential PEM fuel cell applications. The proposed control design enhances the inverter's capability of adapting to dynamic input voltage and load changes while effectively handling the steady-state errors. The effectiveness of the proposed controller is examined and validated in MATLAB/Simulink.

Keywords: Quasi-switched boost inverter, Closed loop control design, PEM fuel cell

I. Introduction

With technological advancements, the increasing demand for electrical energy in residential settings, known as nano grids, is becoming more significant daily, alongside its established uses in the industrial, commercial, and transportation sectors. Renewable energy sources such as wind, solar, hydrogen, or hybrid energy systems, which are combinations of multiple sources, have become a solid alternative to fossil fuels in meeting the rising electricity needs across residential applications. (Sadeghian et al. 2024)

Proton Exchange Membrane (PEM) fuel cells are a type of hydrogen-based electricity generation system that operates at low temperatures, responds quickly to load changes, and is characterized by their compactness, quiet operation, and weight-optimized design (Wang et al. 2011). In addition to these benefits, since PEM fuel cells generate some heat as a byproduct during electricity production, this heat can be utilized in residential applications for heating and electricity generation. (Mamaghani et al. 2018)

Despite the numerous benefits of PEM fuel cells, they also face several drawbacks, including performance susceptibility to changes such as temperature and load, the necessity for power electronic circuits to adapt them for conventional grid use, and the inherently low DC voltage they produce. To obtain desired single-phase or three-phase AC output voltage, single-stage power conversion systems that use impedance or switched impedance source inverters can be low-cost, efficient, and reliable solutions for residential applications.

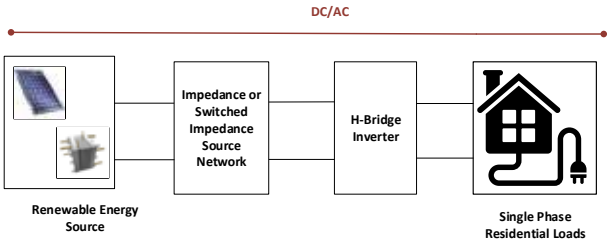


Fig. 1. Single-Stage Power Conversion System

Although there are many impedance source inverter topologies in the literature today, each distinguished by different features, some general advantages are common to all circuits. The occurrence of shoot-through, typically caused by electromagnetic interference or an incorrect switching signal in voltage source inverter (VSI) circuits, and known for its detrimental effects, is effectively managed in this circuit using suitable pulse width modulation (PWM) techniques. The duration of this short circuit is crucial, as it underpins the circuit's distinctive buck-boost capability. The Z-source inverter, proposed by Peng as a milestone for impedance source inverters, increases the inverter output voltage while utilizing the shoot-through switching condition. In this case, since dead-time circuits are not required, a more compact and reliable system is achieved (2003). Unlike traditional VSI circuits, this ability to increase the output voltage makes it particularly advantageous for renewable energy applications. (B. Ge et al. 2013) Another circuit design aimed at reducing voltage stress in capacitors and regulating the input current profile is the Quasi-Z-source inverter (q-ZSI), developed by Zeng and Andersen (2008). In the Quasi Z-Source inverter, continuity of the DC source current is maintained through an inductor connected in series with the source. However, these circuits are not cost-effective for low-power applications. The Quasi Switched Boost Inverter which is the inclusion of both a passive and an active switch allows for a reduction in both cost and size by halving the number of passive components ensuring continuous input current used in this study. (Nyguen et al. 2014).

In this study, the first section provides a general literature review related to the proposed inverter. The second and third sections include the operation of quasi-switched boost inverter and closed loop control of the impedance source inverters respectively. The subsequent section includes the simulation study along with the results. The final section presents the conclusions.

II. Operation of Quasi-Switched Boost Inverter

Embedded type-1 quasi-switched boost inverter topology is shown in Fig. 2. In the switched impedance network, there are two diodes, one active switch, one inductor, and one capacitor. Many PWM methods for the switching signal have been introduced by Nyguen et al. (2018). This study utilizes a simple boost control design introduced by Nyguen et al. (2014).

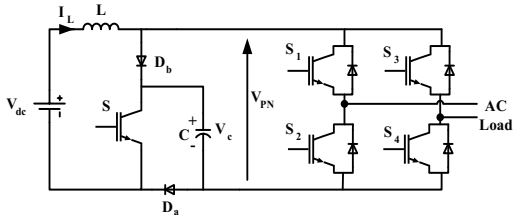


Fig. 2. Embedded type-1 quasi-switched boost inverter

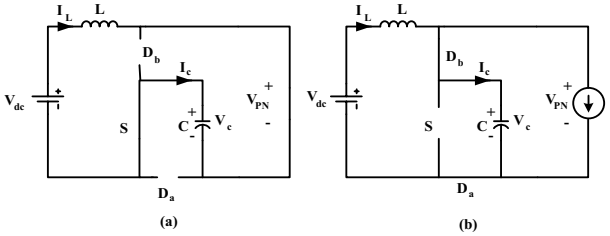


Fig. 3. Equivalent circuit during a) shoot-through interval and b) non-shoot-through interval

Equivalent circuits for two switching intervals are shown in Fig. 3.a and 3.b. The “shoot-through” switching interval is defined as $D_{st}T_s$, while T_s is the switching period of the inverter. The input voltage V_{PN} exceeds the V_{DC} source voltage hereby permitting the short-circuiting of both switches in the same leg, a condition that is typically prohibited in conventional VSIs. In the 'shoot-through' switching interval, while the switches in the bridge legs and the S are turned on, D_a and D_b are turned off. During this state, capacitor C discharges while inductor L accumulates energy. Due to the short-circuiting of the switches in the inverter legs, the inverter input voltage V_{PN} drops to 0 V. The inductor voltage and capacitor current can be expressed as follows:

$$L\frac{di_L}{dt} = V_c + V_{dc}, \quad C\frac{dV_C}{dt} = -i_L \tag{1}$$

In this circuit, the two switching states of traditional VSIs, namely zero switching and active switching, are collectively referred to as the 'non-shoot-through' switching condition. This switching interval can be represented as $(1 - D_{st})T_s$. During the 'non-shoot-through' state, diodes D_a and D_b are on while S is turned off. Capacitor C is charged by V_{dc}, and inductor L transfers energy from the DC voltage source to the AC load. The inductor voltage and capacitor current can be expressed as follows:

$$L\frac{di_L}{dt} = V_{dc} - V_c, \quad C\frac{dV_C}{dt} = i_L - i_{PN} \tag{2}$$

where L is the inductance, i_L denotes the inductance current, V_c is the capacitor voltage, C is the capacitor, i_{PN} is the input current of H-bridge and V_{dc} is the input voltage. The relationship between the peak value of the inverter output voltage $\hat{V}_0$ and V_C is shown below where m represents the modulation index

$$\hat{V}_0 = mV_C = m\frac{1}{1-2D_{st}}V_{dc} \tag{3}$$

In SBIs, there exists a limitation on the relationship between D_{st} value and m as $m + D_{st} \leq 1$. Therefore, these two variables cannot be considered independently.

III. Closed Loop Control Design

In addition to developing different topologies, the control of these inverters also holds an important place in the literature. There are many feedback control methods classified as single-loop, double-loop, linear, and non-linear methods. Compared to classical PI regulators, Sliding Mode Control (SMC) is a robust control method used in nonlinear systems, particularly when dealing with systems that have uncertainties or disturbances. It offers advantages such as fast dynamic response, output waveforms, stability of the impedance network, and robustness of transient response (Liu, Y. et al., 2016). The proposed control design adopted by Gautam et al. (2018) and its scheme is illustrated in Fig. 4. The primary aim of this control structure is to regulate the capacitor voltage by adjusting the shoot-through switching interval of the q-SBI. To produce the PWM signals, two sinus modulation signals, which have constant modulation index m, $V_{control}$ and $-V_{control}$ are compared with a high-frequency triangular waveform to generate control signals for switches S_1 to S_4. A constant voltage, V_{SH} $(1\text{-}D_{st})$ that is determined by

sliding mode controller, compared with another triangular waveform that has double the frequency and half the amplitude to generate the control signal for switch S. This shoot-through control signal is then combined with the control signals for switches S_1 to S_4 using OR gates to create shoot-through states in the inverter bridge.

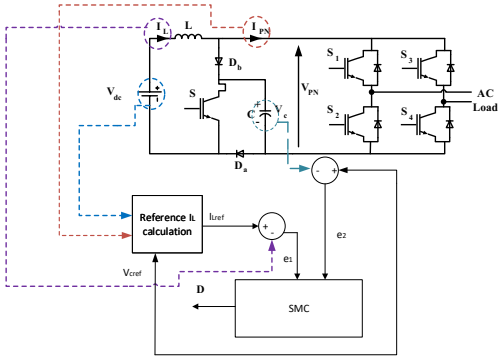


Fig. 4. Proposed control scheme

To generate the average dynamic model, we first define the state variables, the reference states, and the error state variables. After applying the duty cycle intervals for each mode, the average state-space model in error-space is obtained as

$$\dot{e}_1 = \frac{V_{dc}}{L} + \left(\frac{e_2+x_{2r}}{L}(-1+2D_{st})\right) \quad \dot{e}_2 = \frac{e_1+x_{1r}}{C}(1-2D_{st}) - \frac{(1-D_{st})i_{PN}}{C} \tag{4}$$

where $e_1 = i_L - i_{Lr} = x_1 - x_{1r}$ and $e_2 = V_C - V_{Cr} = x_2 - x_{2r}$ are the inductance current error and the capacitor voltage error, $i_L = x_1$ denotes the inductance current, $V_c = x_2$ is the capacitor voltage, and x_{1r} and x_{2r} denote the inductance current reference and capacitor voltage reference, respectively. A compact representation of the dynamic formulation is written as

$$\dot{e} = \nabla(f + gu) \tag{5}$$

where $\dot{e} = \begin{bmatrix}\dot{e}_1 \\ \dot{e}_2\end{bmatrix}$, $\nabla = \begin{bmatrix}1/L & 0 \\ 0 & 1/C\end{bmatrix}$, $f = \begin{bmatrix}V_{DC} - (e_2 + x_{2r}) \\ (e_1 + x_{1r}) - i_{PN}\end{bmatrix}$, $g = \begin{bmatrix}2(e_2 + x_{2r}) \\ -2(e_1 + x_{1r}) + i_{PN}\end{bmatrix}$ and $u = D_{st}$. In order to design the robust controller, we first define the sliding surface s as follows:

$$s = \alpha_1 e_1 + \alpha_2 e_2 = \begin{bmatrix}\alpha_1 & 0 \\ 0 & \alpha_2\end{bmatrix}\begin{bmatrix}e_1 \\ e_2\end{bmatrix} = \alpha\begin{bmatrix}e_1 \\ e_2\end{bmatrix} \tag{6}$$

where α_1 and α_2 are positive constant design parameters. The time derivative of the sliding surface is

$$\frac{ds}{dt} = \dot{s} = \alpha_1\dot{e}_1 + \alpha_2\dot{e}_2 = \alpha\begin{bmatrix}\dot{e}_1 \\ \dot{e}_2\end{bmatrix} = 0 \tag{7}$$

Substituting Eqs. (4) and (5) into Eq. (8), we obtain the equivalent control input as

$$u_{eq} = (\alpha\nabla g)^{-1}(-\alpha\nabla f) \tag{8}$$

To handle the uncertainties and disturbances, we develop the control input as

$$u = u_{eq} - k_1 \mathrm{sgn}(s) - k_2 s \tag{9}$$

where k_1 and k_2 are positive constant control design parameters, and sgn(s) is the signum function. In order to guarantee the system stability, we select the control design parameters according to the following stability analysis.

Let us choose a Lyapunov candidate function as $V = \frac{1}{2}s^2$ which is clearly positive definite. The derivative of the Lyapunov candidate function is

$$\dot{V} = s\dot{s} = s\alpha\nabla(f + gu) = s\alpha\nabla f + s\alpha\nabla g\, u < 0 \tag{10}$$

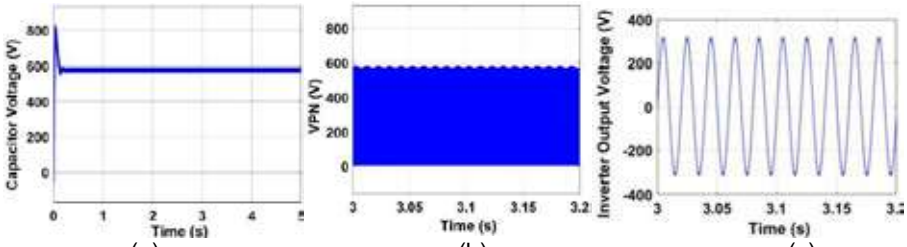
Substituting Eq. (9) into Eq. (11), we have

$$\dot{V} = -s\alpha\nabla g\, k_1\frac{|s|}{s} - s\alpha\nabla g\, k_2 s < 0 \tag{11}$$

To satisfy $\dot{V} < 0$, k_1 and k_2 should be selected according to $\begin{cases}k_1 > 0 \ \ and \ \ k_2 > 0, \ if \ g > 0 \\ k_1 < 0 \ \ and \ \ k_2 < 0, \ if \ g < 0\end{cases}$.

IV. Results and discussions

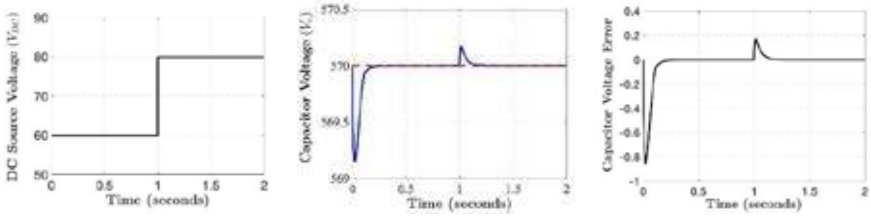
The simulation results for the open-loop control is shown for the capacitor voltage (V_c), the input voltage of H-bridge (V_{PN}), the output voltage of the inverter in Fig.5. The DC source voltage (V_{dc}), shoot-through duty cycle (D_{st}), and modulation index (*m)* are selected as 46 V, 0.46 and 0.54, respectively. In the steady state, the mean value of the capacitor voltage (V_c) is about 575 V. The peak voltage value of the inverter output voltage is about 311 V and 50 Hz which is suitable for residential loads.



(a) (b) (c)

Fig. 5.a) The capacitor voltage variation b) V_{PN} input voltage of H-bridge voltage variation c) The output voltage variation (open-loop conditions)

In order to evaluate the closed-loop control design performances, we present the simulation results in Fig. 6. The DC source voltage V_C is 60 V within the 0-1 second time interval, subsequently reaches 80 V as shown in Fig. 6.a. In Fig. 6.b, the inverter input voltage V_{PN} is maintained constant by ensuring that the measured capacitor voltage tracks the reference signal in response to the varying DC input voltage. As illustrated in Fig. 6.c, the steady-state error of the capacitor voltage converges to zero over time.



(a) (b) (c)

Fig. 6.a) The DC source voltage variation b) The reference and measured capacitor voltage variation c) The capacitor voltage error (closed-loop conditions)

V. Conclusions

In this study, the DC voltage from the PEM fuel cell is converted into usable AC voltage for residential loads utilizing a single-phase quasi-switched boost inverter circuit. The output voltage is elevated to the desired level by adjusting the duty cycle, which is determined by the shoot-through switching time interval. In the proposed approach, the duty cycle is determined via SMC design based on the error values generated from comparing the reference and measured values of the system's state variables.

References

Sadeghian, O., Shotorbani, A. M., Ghassemzadeh, S., & Mohammadi-Ivatloo, B., Energy management of hybrid fuel cell and renewable energy based systems-A review. International Journal of Hydrogen Energy, (2024).

Wang Y., Chen K.S., Mishler J. Cho S.C., Adroher X.C., A review of polymer electrolyte membrane fuel cells: Technology, applications, and needs on fundamental research, *Applied Energy*, *88*, 981–1007, (2011).

Mamaghani, A. H., Najafi, B., Casalegno, A., & Rinaldi, F. Optimization of an HT-PEM fuel cell based residential micro combined heat and power system: A multi-objective approach. Journal of cleaner production, 180, 126-138, (2018).

Peng, F. Z. Z-source inverter. IEEE Transactions on Industry Applications, 39(2), 504-510, (2003).

B. Ge *et al*., "An Energy-Stored Quasi-Z-Source Inverter for Application to Photovoltaic Power System," in *IEEE Transactions on Industrial Electronics*, vol. 60, no. 10, pp. 4468-4481, (2013).

Nguyen, M. K., Le, T. V., Park, S. J., & Lim, Y. C. A class of quasi-switched boost inverters. IEEE Transactions on Industrial Electronics, 62(3), 1526-1536, (2014).

Nguyen, Minh-Khai, Tan-Tai Tran, and Young-Cheol Lim. "A family of PWM control strategies for single-phase quasi-switched-boost inverter." *IEEE Transactions on Power Electronics* 34.2 (2018): 1458-1469, (2018).

Gautam, A. R., & Fulwani, D. Adaptive SMC for the second-order harmonic ripple mitigation: A solution for the micro-inverter applications. *IEEE Transactions on Power Electronics*, *34*(8), 8254-8264, (2018).

Liu, Y., Abu-Rub, H., Ge, B., Blaabjerg, F., Ellabban, O., & Loh, P. C. (2016). *Impedance source power electronic converters*. John Wiley & Sons.

Estimating the remaining useful life of PEM Fuel Cell with LSTM method

[1*] Mehmet İsmail Gürsoy
[1]Adıyaman University, Department of Elecrical Electronics Engineering, Adıyaman, 02040, Türkiye

* E-mail: mgursoy@adiyaman.edu.tr

Abstract
In this study, a method is proposed to estimate the remaining useful life (RUL) of proton exchange membrane fuel cells (PEMFC) using the Long Short Term Memory (LSTM) algorithm, one of the deep learning methods. In the developed method, 5-cell PEMFC stacks with and without current ripple disturbances were estimated with the PEMFC open data set provided by the Fuel Cell Laboratory (FCLAB). The obtained prediction results are compared using the coefficient of determination (R2), root mean square error (RMSE) and mean absolute percentage error (MAPE) statistical parameters. As a result, the average values of R2, RMSE and MAPE were obtained as 92.69%, 0.0041, 0.0010 for the FC1 dataset and 90.94%, 0.0044, 0.0012 for the FC2 dataset, respectively. With the developed model, it is shown that the RUL value of PEMFC can be predicted with high accuracy using the LSTM method.

Keywords: PEMFC, Remaining Useful Life, LSTM

I. Introduction

Proton exchange membrane fuel cells (PEMFC) are fuel cells used to produce electrical energy through a chemical reaction between hydrogen and oxygen. PEMFCs are zero-emission energy sources widely used in areas such as electric vehicles, energy storage and power generation facilities, and transportation (Sahajpal, Rana, and Kumar 2023). It is necessary to estimate the remaining useful life (RUL) of PEMFCs in order to improve system performance, increase their durability and maximize stable operation. RUL forecasting performs critical tasks such as evaluating the performance of PEMFC, tracking changes in the system, and determining maintenance and repair planning. To estimate RUL in a PEMFC-powered system, various parameters need to be measured temporally (Tian et al. 2023).

In this study, the publicly available IEEE 2014 PHM dataset provided by the FCLAB Research Federation in France was used (FCLAB Research. 2014). The test platform has a cross-sectional area of 100 cm2 with a power of 1 kW and consists of two piles. The first stack is called FC1. It was operated for 1155 hours with 70 A load current of 70 A. The second stack, designated FC2, was operated for 1021 hours at 70 A load current with a 7 A, 5 kHz triangular current swing. Data and parameters such as cell and stack voltages, currents, gas flow rate, temperature, humidity and pressure were recorded for 7 weeks.

II. Materials and methods

In this study, it is aimed to estimate the remaining useful life of PEMFC by using the Long Short Time Memory (LSTM) method, one of the deep learning algorithms of the IEEE 2014 PHM Data set provided by FCLAB Research Federation. LSTM method is a type of deep learning methods applied for estimation and classification of time data developed by Hochreiter & Schmidhubert. LSTM model is a special type of RNN model. RNN algorithm memorizes short-term information. LSTM, on the other hand, can analyze long-term time data (Hochreiter and Schmindhuber 1997).

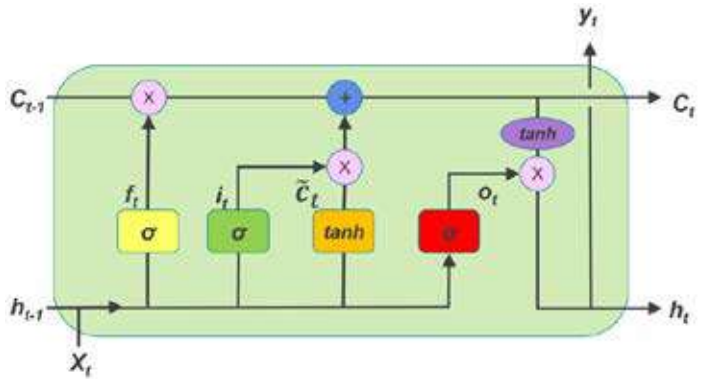


Fig. 1 LSTM unit

LSTM algorithm consists of sequential repetition of the blocks shown in Fig.1. LSTM architecture consists of 3 steps: input, forget and output. The input gate controls new information coming into the model. The Forget gate removes unimportant information from previous information. The output gate organizes the information coming out of the model and creates the output data (Gürsoy and Alkan 2022).

In this study, an LSTM layer consisting of 80 blocks was created for the prediction model. The tanh function was used as the activation function in the LSTM layer. Determining the accuracy of the developed model is an important factor. Coefficient of Determination (R2), Root Mean Square Error (RMSE) and Mean Absolute Percentage Error (MAPE) metrics were chosen to determine the performance of estimation problems commonly used in the literature.

Coefficient of Determination(R2): R2 is a measure used to evaluate the accuracy of the model developed in a forecasting problem. By determining the relationship between the predicted value and the real value in the model, it determines how close it can predict the real value. The R2 value is between 0 and 1. The closer the estimated value is to the real degree, the closer the R2 value is to 1 (Sahajpal, Rana, and Kumar 2023). The R2 value is calculated using Equation-1.

$$R^2 = 1 - \frac{Var\ (y_{true} - y_{pred})}{y_{pred}} \quad (1)$$

Root Mean Square Error (RMSE): RMSE is a widely used metric to evaluate model accuracy in forecasting problems. RMSE provides information on how different the predicted values obtained from the model are from the actual values (Liu et al. 2019). RMSE values can be obtained with Equation-2.

$$RMSE = \sqrt{\frac{1}{N}\sum_{i=1}^{N}(y_{pred} - y_{true})^2} \quad (2)$$

Mean Absolute Percentage Error (MAPE): The MAPE value calculates the average percentage difference between the predicted value obtained from the model and the actual value. In MAPE prediction problems, it shows the size of the errors in the predicted value compared to the actual values. A smaller MAPE value indicates better prediction performance (Hu et al. 2023). MAPE value is obtained using Equation-3.

$$MAPE = \frac{1}{N}\sum_{i=1}^{N}\frac{|y_{pred} - y_{true}|}{y_{true}}\ x\ 100\% \quad (3)$$

Where; y_pred represents the predicted voltage value and y_true represents the actual values from the PEMFC dataset.

III. Results and discussions

In this study, the estimation of the remaining useful lives of PEMFCs was investigated using the publicly available IEEE 2014 PHM data set provided by the FCLAB Research Federation in France. The FC1 dataset contains 143,862 data and the FC2 dataset contains 127,370 data. Data were first sampled from both datasets for 1 hour. 1155 hours of data were obtained for the FC1 data set and 1021 hours for the FC2 data set. The Savitzky-Golay Filter (SGF) was used to remove high-frequency noise in FC1 and FC2 data. There are two basic parameters for using this filter. It is the choice of polynomial degree and window width of the filter. As a result of the experiments in this study, the polynomial degree was chosen as 3 and the window width was chosen as 24. After applying the SGF filter to the data set, the failure threshold was determined to estimate RUL. The fault threshold determines the fault value that may occur if the PEMFC stack cannot provide a sufficient level of voltage. RUL is the period during which the voltage provided by the PEMFC stack can provide an output voltage equal to or greater than the fault threshold value. The fault threshold value, which is widely used in the literature, corresponds to 96% of the voltage of the PEMFC stack when it is at full energy. In this study, 3.202 V (=3.336 x 96%) for the FC1 dataset and 3.197 V (=3.3303 x 96%) for the FC2 dataset were determined as the failure threshold.

In this study, FC1 and FC2 datasets were analyzed separately with the LSTM method. In the LSTM method, the time step is determined as one. The datasets are divided into 60% train and 40% test. Thus, for the FC1 dataset, 692 hours were used as train and 462 hours as test, and for the FC2 dataset, 612 hours were used as train and 408 hours as test. FC1 and FC2 datasets were normalized to the [0 ,1] range using the min-max normalization method (Equation – 4).

$$\bar{x} = \frac{x - \min(x)}{\max(x) - \min(x)} \quad (4)$$

Here, $\bar{x}$ represents the scaled value and x represents the dataset input value

LSTM deep learning algorithm was used in the model developed with FC1 and FC2 data sets. In the LSTM model, the number of units was set to 80. The value 88 was selected as the model batcsize. 'tanh' was used as the activation function.

When the model was applied to the FC1 data set, 692 hours of data were used for training as shown in Fig.2. The average success rate of the model was 92.69%, a very high value.

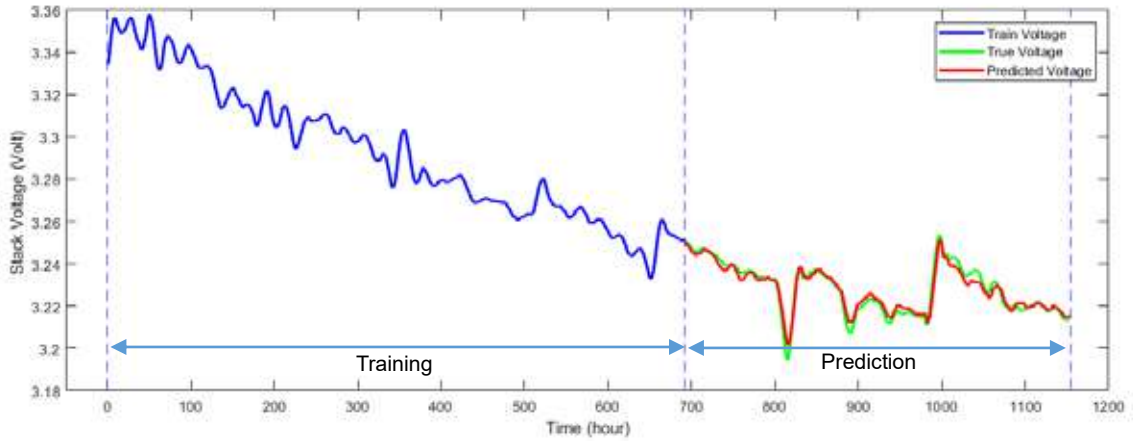


Fig. 2 Predicted voltage values for FC1

When the model is applied with the FC2 data set, the predicted voltage values are shown in Fig.3. 612 hours were used as training in the FC2 data set. Voltage values for the remaining 402 hours were estimated.

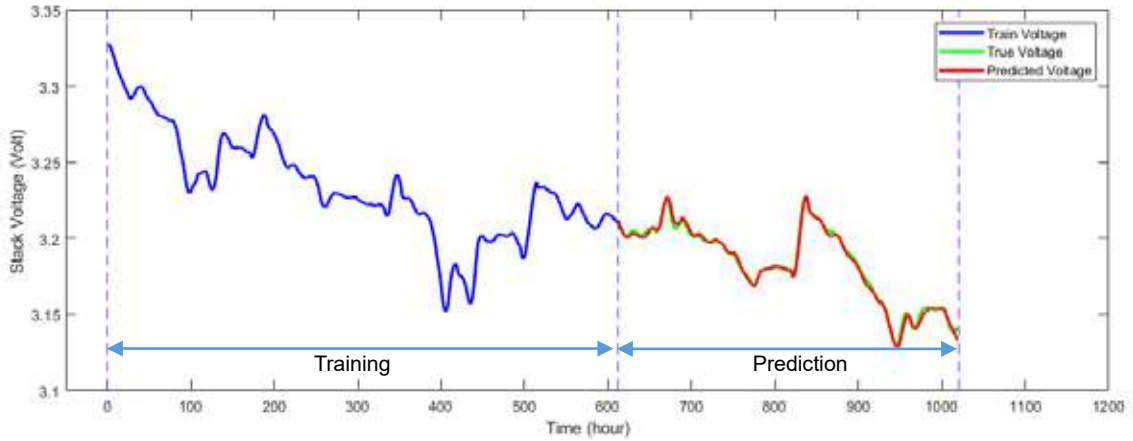


Fig. 3 Predicted voltage values for FC2

Tab. 1. Performance evaluations for FC1 and FC2 datasets

	R2 (%)			RMSE			MAPE		
	max	**min**	**mean**	**max**	**min**	**mean**	**max**	**min**	**mean**
FC1	*95,51*	*87,32*	*92,69*	*0,0056*	*0,0025*	*0,0041*	*0,0015*	*0,0006*	*0,0010*
FC2	*99,32*	*90,94*	*96,42*	*0,0074*	*0,0020*	*0,0044*	*0,0022*	*0,0005*	*0,0012*

The results obtained with the LSTM model developed using FC1 and FC2 datasets are shown in Tab.1. While analyzing the model, analyzes were performed 50 times for FC1 and FC2 data and the results of these analyzes are shown as min, max and mean in Tab.1. In the developed model, it is seen that 92.69% accurate prediction is made with the FC1 data set. In addition, it is seen that a high level of correct prediction is made in the FC2 data set, with 96.42%.

IV. Conclusions

In this study, a model was developed using the LSTM method, one of the deep learning algorithms, to estimate the remaining useful life of PEMFC. The proposed model was implemented with datasets of the IEEE PHM 2014 five-cell proton exchange membrane fuel cell (PEMFC). The prediction results obtained from the model show that RUL prediction can be achieved with the LSTM method. Since the dataset used covers limited working models, RUL prediction of PEMFCs can be investigated in different working models. Additionally, long-term RUL predictions can be made using different deep learning algorithms.

Acknowledgements
Many thanks to Adiyaman University for technical support.

References

FCLAB Research. "IEEE PHM Data Challenge." https://repository.lboro.ac.uk/articles/dataset/IEEE_-2014_Data_Challenge_Data/3518141 Accessed on 16 Jan 2023. (2014).

Gürsoy, Mehmet İsmail, and Ahmet Alkan. "Investigation Of Diabetes Data with Permutation Feature Importance Based Deep Learning Methods." Karadeniz Fen Bilimleri Dergisi 12(2): 916–30 (2022).

Hochreiter, Sepp, and Jürgen Schmindhuber. "Long Short-Term Memory." Neural Computation 9(8): 1–32 (1997).

Hu, Yanyan, Li Zhang, Yunpeng Jiang, Kaixiang Peng, and Zengwang Jin. "A Hybrid Method for Performance Degradation Probability Prediction of Proton Exchange Membrane Fuel Cell." Membranes 13(4): 1–16 (2023).

Liu, Jiawei, Qi Li, Weirong Chen, Yu Yan, Yibin Qiu, and Taiqiang Cao. "Remaining Useful Life Prediction of PEMFC Based on Long Short-Term Memory Recurrent Neural Networks." International Journal of Hydrogen Energy 4: 5470–80 (2019).

Sahajpal, Kartik, K. P.S. Rana, and Vineet Kumar. "Accurate Long-Term Prognostics of Proton Exchange Membrane Fuel Cells Using Recurrent and Convolutional Neural Networks." International Journal of Hydrogen Energy 48(78): 30532–55. https://doi.org/10.1016/j.ijhydene.2023.04.143 (2023).

Tian, Qiancheng, Haitao Chen, Shuai Ding, Lei Shu, Lei Wang, and Jun Huang. "Remaining Useful Life Prediction Method of PEM Fuel Cells Based on a Hybrid Model." Electronics (Switzerland) 12(18) (2023).

Investigation of Hydrogen Production from Brine by Using Membrane Cell Process Technology

[1,*]Haci Sogukpinar, [2]Ismail Bozkurt, [3]Serkan Cag, [1]M. Ismail Gursoy, [4]Ayhan Atiz, [4]Mehmet Karakilcik

[1]Department of Electric and Energy, Vocational School, University of Adıyaman, 02040, Türkiye
[2]Department of Mechanical Engineering, Faculty of Engineering, University of Adıyaman, 02040, Türkiye
[3]Department of Machinery and Metal Technology Vocational School, University of Adıyaman, 02040, Türkiye
[4]Department of Physics, Faculty of Sciences and Letters, University of Cukurova, Adana 01330, Türkiye

* E-mail: hsogukpinar@adiyaman.edu.tr

Abstract
In this study, hydrogen production was investigated by membrane cell process with brine by using commercial COMSOL software. Nernst-Planck equations were used to solve for the separate transport of charged and uncharged species in the electrolyte due to diffusion, migration, and convection and to find the current and potential distribution in the electrochemical cell. To provide charge transfer reactions, electrode kinetics were provided by using either arbitrary expressions or predefined Butler-Volmer and Tafel expressions. The current distributions, molar H_2, Cl_2, OH^-, and NaOH distributions within the cell were drawn and the results were discussed. 100 mol/m3 NaCl and water inflow were defined in the cell, and a potential difference of 3V was applied between the electrodes. While the maximum density of H_2 was 4000 mol/m^3 in the cathode region, Cl_2 was formed at a maximum density of 7000 mol/m^3 in the anode region.

Keywords: Hydrogen production, membrane cell process, NaOH production, Nernst–Planck

I. Introduction

As demand for sustainable energy sources increases, hydrogen emerges as a promising solution. Advances in hydrogen storage technologies encourage the widespread use of this technology (Hassan et al., 2023). Park et al. (2022) investigated the effect of voltage on NaCl poisoning in fuel cells with polymer electrolyte membranes and it was observed that the loss of performance was primarily due to the clogging of the active sites of the catalyst due to Cl^- adsorption. Erden and Karakilcik (2024) examined the hydrogen production of different salt solutions using a chlor-alkali reactor. Hydrogen production was compared depending on cell voltage, cell temperature and electrolyte flow rate by using aqueous solutions of NaCl, KCl and $CaCl_2$ salts. Merabet and Kerboua (2024) investigated the effect of the concentration of dissolved salts (KOH/NaOH) on hydrogen production depending on the electrolyte temperature with different electrode structures. At the same time, the effect of acoustic power was evaluated in two different ultrasound modes and the mechanism behind ultrasounds in sono-electrolysis was explained. Rossi et al. (2023) evaluated hydrogen production and reactor performance for specific concentrations using different alkaline electrolytes. At the same time, it was observed that 71.83 mL/min hydrogen production was achieved with 900 W/m2 solar radiation and 6.18 mol/L KOH concentration under optimized conditions using KOH electrolyte, stainless steel electrodes and photovoltaic panel. Contreras et al. (2024) economically analyzed a system in which hydrogen is produced together with value-added products such as chlorine and sodium hydroxide by using waste brine. It has been determined that sodium hydroxide, which constitutes 64% of the revenue from by-products, can reduce the cost of hydrogen production up to 0.78 \$/kgH_2 in optimum combinations.

In this study, the production of NaOH, Cl_2, and H_2 using cell membrane technology from salt water was investigated by using commercial COMSOL software. The concentration of the obtained products in the cell was determined and presented comparatively.

II. Materials and methods

Nernst-Planck equations were used to solve for the separate transport of charged and uncharged species in the electrolyte due to diffusion, migration, and convection, and to find the current and potential distribution in the electrochemical cell. To ensure charge transfer equality, the electrode kinetics are provided using arbitrary expressions or predefined Butler-Volmer and Tafel expressions. The overall mass balance of diluted species in an electrolyte is defined for each species i by the following equations (COMSOL, 2024):

$$\frac{\partial c_i}{\partial t} + \nabla . N_i = R_{i,total} \quad (1)$$

Where, N_i is the total flux of species i (mol/(m^2·s)). The amount of flux in an electrolyte is described by the Nernst–Planck equations and is used to describe the flow of charged ions through diffusion, migration, and convection; these are the first, second, and third terms on the right side of the equation below.

$$N_i = -D_i \nabla c_i - z_i u_{m,i} F c_i \nabla \Phi_l + c_i \mathbf{u} = \boldsymbol{J_i} + \boldsymbol{c_i}\mathbf{u} \quad (2)$$

Where, c_i is concentration, z_i is valence, D_i is diffusion coefficient, $u_{m,i}$ is mobility, F, is Faraday constant, Φ_l electrolyte potential, u is the velocity vector, J_i denotes the molar flux due to convective transport. The temperature in the electrolyte is defined as 77 K, and the diffusion coefficient of Na+ ions in water is 3e-8[m^2/s]. The potential difference between the anode and cathode is 3V, the Nernst-Einstein equation is used to ensure the conduction of charged particles in the electric field, the conductivity of the electrolyte was set as 50 S/n, the diffusion coefficient on the membrane was defined as 3e-8[m^2/s]. A reaction was defined to form NaOH from OH- and Na+ ions in the cathode region. An electrode reaction was defined, to produce Cl2 gas at the anode and to produce OH- and H2 gas at the cathode. In both reactions, electron exchange occurs between the anode and cathode. The anode and cathode were defined as 1x2mm rectangular, and membrane thickness was determined as 0.2 mm. Extra fine mesh type was chosen for mesh distribution and 9556 triangle mesh elements were obtained. By analyzing the mesh quality, the average mesh element quality was calculated as 0.88 and the worst mesh quality was 0.49. Mesh quality below 0.2 is undesirable and the best mesh quality is 1.

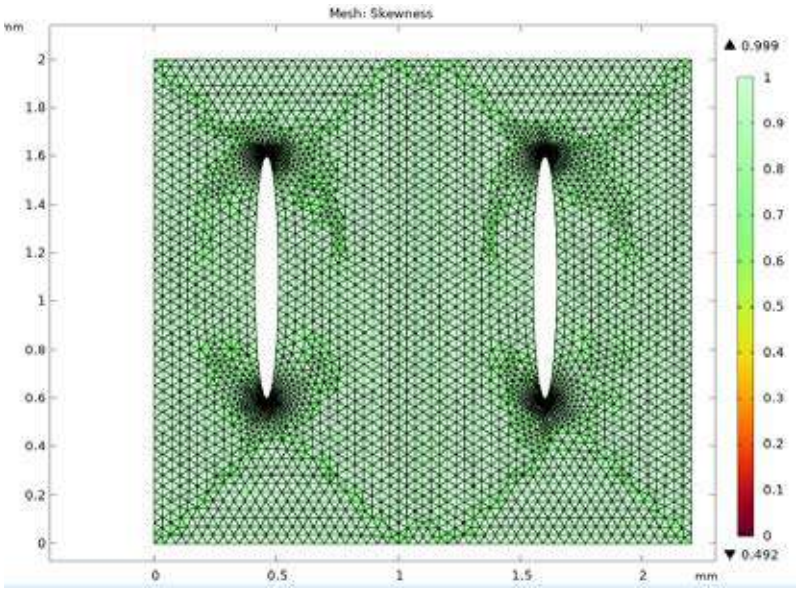


Fig.1: Mesh distribution

III. Results and discussions

Hydrogen production from brine with membrane technology was investigated numerically with the commercial software COMSOL. The amount of salt input to the cell was defined as 50 mol/m^3 and the potential difference between the anode and cathode was determined as 3 V. Electrolyte potential and the current density vector is given in Fig. 2.

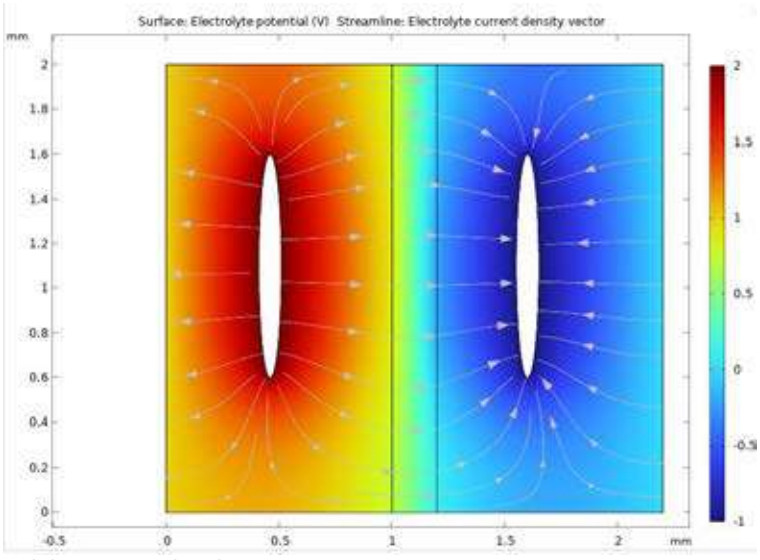


Fig. 2: Electrolyte potential and the current density vector

The surface and line graph of the Cl_2 concentration within the cell is given in Fig. 3. Cl_2 gas density appears to be concentrated at the spikes depending on the charge density on the electrode. In the simulation, the flow direction is defined from bottom to top within the cell. The Cl_2 concentration along a line just above the electrodes is calculated and given in the line graph. The Cl_2 gas density varies between 0 and 7000 mol/m^3.

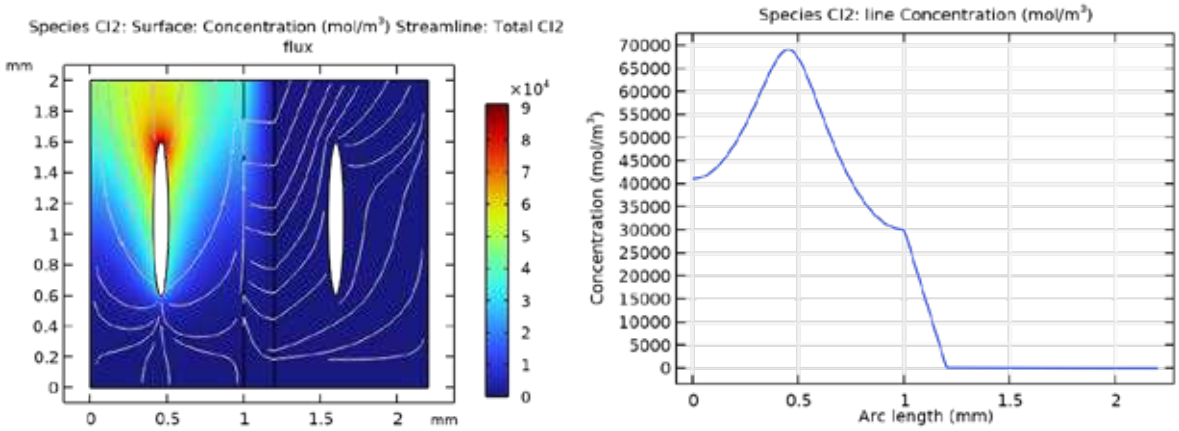


Fig. 3: Cl_2 concentration in the cell

H_2 concentration inside the cell was calculated and presented as both surface and line graphs and given in Fig. 4. A bottom-up flow was defined in the cell, and the Figure shows that the H_2 gases move in an upward direction. Depending on the charge density inside the cell, the accumulation of H_2 gas is concentrated at the sharp ends and becomes rare in other parts. The H_2 gas density varies between 0 and 3000 mol/m^3.

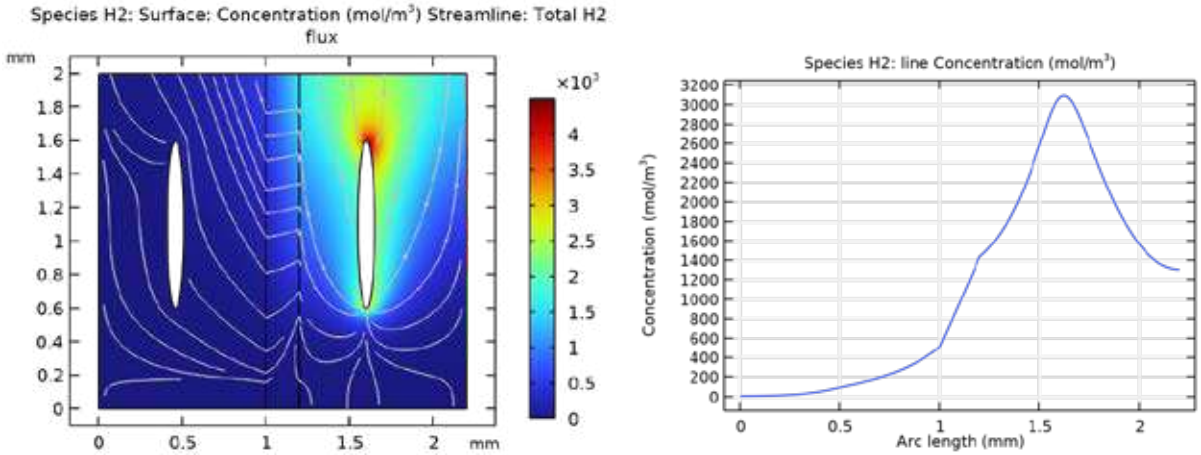


Fig.4: H_2 concentration in the cell

Apart from Cl_2 and H_2 gas, NaOH is also formed from salt water, and the distribution of NaOH production within the cell is given in Fig. 5, both as a surface and as a line graph. NaOH formation concentrates around the electrode and varies between 0 and 1600 mol/m^3.

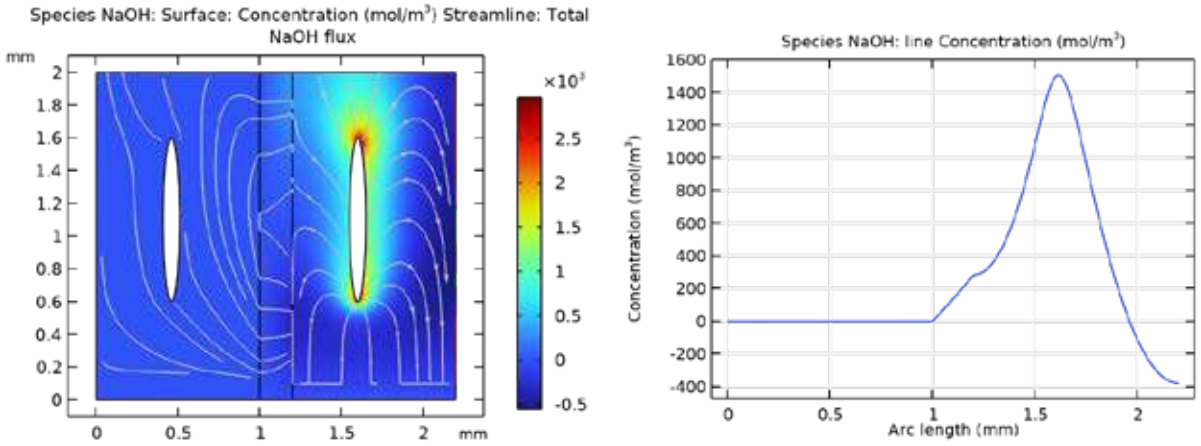


Fig.5: NaOH concentration in the cell

IV. Conclusions

In this study, the production of NaOH, Cl_2, and H_2 using cell membrane technology from salt water was investigated

numerically. All three products from salt water are commercially important and their raw material is seawater. Therefore, it is possible to establish a production facility on the seashore without paying any fee for raw materials. Today, the effects of global warming are increasing rapidly, it is an important mechanism for the production of H_2 gas, and its raw material is from salt water, covering 70% of the world.

Acknowledgements
Many thanks to Middle East Technical University and Adiyaman University for technical support

References

Contreras M., Mba-Wright M., Wulf C., Stanier CO., Mubeen S., Technoeconomic analysis of photoelectrochemical hydrogen production from desalination waste brine using concentrated solar flux, International Journal of Hydrogen Energy, 49, 360-372 (2024).

Erden M., Karakilcik M., Experimental investigation of hydrogen production performance of various salts with a chlor-alkali method, International Journal of Hydrogen Energy, 52, 546-560 (2024).

COMSOL ElectrochemistryModuleUsersGuide. http://www.comsol.com. 2024.

Hassan Q., Sameen AZ., Salman HM., Jaszczur M., Al-Jiboory AK., Hydrogen energy future: Advancements in storage technologies and implications for sustainability, Journal of Energy Storage, 72, 108404 (2023).

Merabet NH., Kerboua K., Membrane free alkaline sono-electrolysis for hydrogen production: An experimental approach, International Journal of Hydrogen Energy, 49, 734-753 (2024).

Park S., Shorova D., Kim H., Effect of operating cell voltage on the NaCl poisoning mechanism in polymer electrolyte membrane fuel cells, Journal of Power Sources, 538, 231590 (2022).

Rossi RAS., Palhares DDF., Cunha PCR., Damasceno JJR., Barrozo MAS., Vieira LGM., Operational and design parameters evaluation to improve hydrogen production using a low-cost alkaline water electrolysis cell in direct combination with a photovoltaic cell, Renewable Energy Focus, 47, 100510 (2023).

Fuel Cell and Battery Powered Brushless Direct Current Motor Control for Light Electric Vehicle Applications

[1*]Habip Şahin, [2]Muhammed Sefa Çetin, [2]Muhsin Tunay Gençoğlu, [3]Ozan Erdinç

[1] Fırat University, Vocational School of Technical Sciences, Department of Electricity and Energy, Elazığ, 23119, Türkiye
[2] Fırat University, Faculty of Engineering, Department of Electrical-Electronics, Elazığ, 23119, Türkiye
[3]Yıldız Technical University, Faculty of Electrical-Electronics, Department of Electrical Engineering, Istanbul, 34220, Türkiye

* E-mail: mscetin@firat.edu.tr

Abstract

Electrification in transportation is becoming more widespread day by day due to both environmental and economic concerns. For this purpose, vehicles suitable for many different purposes are designed and put on the market. Although battery electric vehicles are the first solution that comes to mind, their limited energy storage capacity and high charging times pose a major disadvantage. In order to overcome these disadvantages, technologies that use fuel cells as the primary energy source and batteries are used as secondary are also being developed. In this study, a hybrid power source consisting of fuel cell and battery is designed and the control of a brushless direct current motor that is assumed to drive a light electric vehicle is simulated in Matlab/Simulink. As a result, a system with 75% electrical efficiency is created and the motor is successfully controlled to ensure that it follows the reference speed and torque.

Keywords: Light electric vehicles, fuel cell, battery, brushless direct current motor, motor driver.

I. Introduction

Light electric vehicles (LEV) are environmentally friendly transportation solutions designed for short distances. This category includes various types of vehicles such as electric scooters, electric bicycles, electric skateboards, hoverboards, electric mini scooters, and small electric vehicles. Small electric vehicles are two-seater, fully electric, and due to their light and portable nature, they are suitable for short-distance use. These vehicles are increasingly preferred for urban use due to advantages such as reducing traffic congestion, ease of finding parking, and low operating costs. Skarlis et al. (2023).

The battery systems of LEV are a critical component that directly affects the performance of the vehicles. Lithium-ion batteries are commonly using in these vehicles due to their high-power densities, lightweight structures, and long lifespans. However, their disadvantages include limited electricity production capacity and lengthy charging times. Therefore, hybridizing with fuel cells (FC) that have higher energy densities can overcome these drawbacks. Battery management systems, on the other hand, ensure the safe and efficient use of batteries by protecting them from situations such as overcharging and discharging. Hwang and Chang (2012), Pramuanjaroenkij and Kakaç (2023).

When it comes to motor systems, it is evident that brushless direct current (BLDC) motors are frequently used in LEV due to their high efficiency, ease of control, and low maintenance requirements. While brushed motors are more cost-effective, they lag behind BLDC motors in terms of efficiency and lifespan. The motor driver optimizes the vehicle's speed, torque, and direction, enhancing performance and improving the user experience. All these components play a significant role in the overall performance of LEV. Mishra et al. (2022).

In this study, a BLDC motor control powered by a FC-battery hybrid power source was developed to drive a light electric vehicle. The FC is the primary energy source, while the battery is secondary. This allows both to be utilized at lower capacities than if used individually, creating a structure that is more suitable for motor control and capable of energy recovery during regenerative braking.

II. Materials and Methods

In this study, a hybrid power source consisting of FC and battery was used to power the BLDC motor. Although FC have higher energy density than battery, it has longer electrical response times and is disadvantageous in applications requiring high-frequency switching. Charging the battery, which has a relatively higher power density, requires long periods of time. In contrast, FC can produce energy as long as fuel is supplied, and refueling requires much shorter times. Kim et al. (2021). Thus, a proton exchange membrane FC (PEMFC) having a rated power of 500 W and 48 V 10 Ah Li-on battery are used to fed a 1 kW BLDC motor. Specifications of these three component are given in Tab.1.

Fuel cell

PEMFC offer some advantages such as; simplicity, mobility, fast response and low operation temperature. Therefore, in this study, PEMFC was chosen as primary energy source. A user-defined FC stack was used in Matlab/Simulink model. Polarisation and power curve data of the H-500 XP FC Stacks was entered as model parameter.

Battery

In battery pack, 3.7 V 3500 Ah Molicel M35A 18650 Lithium-iron-phosphate type cells were used. Battery was used as secondary energy source. It supplies power when load increases rapidly with fast response time and is charged

by FC during low loads.

Tab. 1: Technical specifications of FC, battery and BLDC motor.

	Specification	Value
BLDC	Motor power	1 kW
	Nominal speed	3000 rpm
	Nominal torque (@3000 rpm)	3 Nm
	Maximum torque (@0-1200 rpm)	6.8 Nm
Fuel Cell	Cell number	30
	Open circuit voltage	28.2 V
	Nominal power (21V, 23.8 A)	500 W
	Maximum power (18V, 41.7 A)	750 W
	Nominal efficiency	55 %
Battery	Number of cells (13Series×3Parallel)	39
	Nominal voltage	48 V
	Nominal capacity	10 Ah
	Battery energy	480 Wh

BLDC motor

A 3-phase, 1 kW BLDC type motor was selected considering its low cost and easy control. Motor has a nominal torque of 3 Nm at rated 3000 rpm and a maximum torque of 6.8 Nm between 0 to 1200 rpm. Thus, these values are enough to propel the LEV in daily use.

Driving cycle

In this study, it is assumed that designed propulsion system drives the LEV in Worldwide Harmonized Light Vehicle Test Procedure (WLTP) Class 1. Therefore, reference speed is determined to simulate average and maximum speed values.

The Matlab/Simulink model for the control of a BLDC motor fed from a FC, battery hybrid power source according to the reference speed and the associated torque is presented in Fig 1.

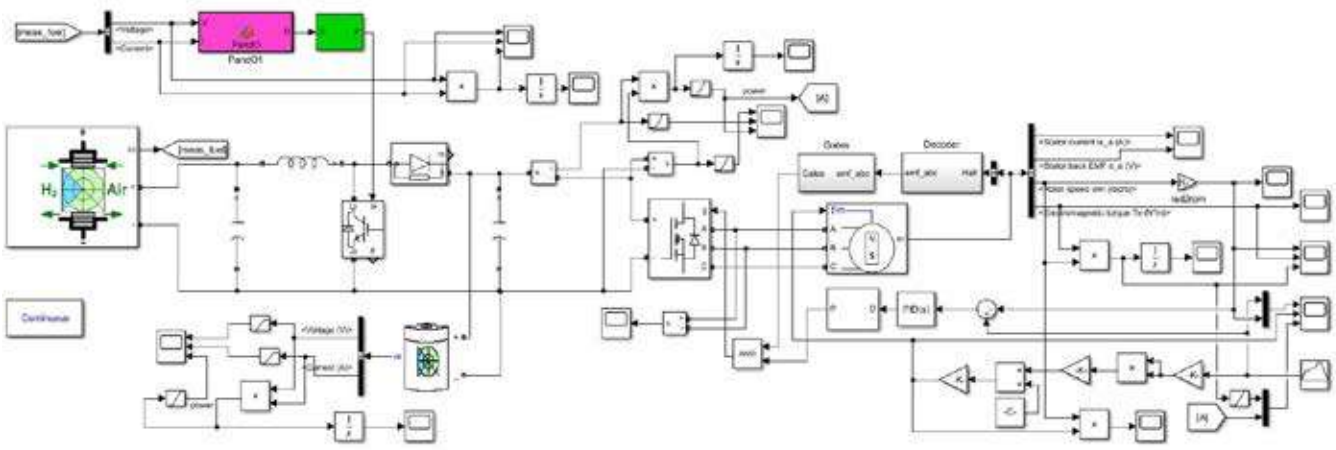


Fig. 1: Matlab/Simulink model

III. Analysis

The output voltage of the FC used as the primary energy source is 21 V at nominal power and 18 V at maximum power, and a boost converter was used to increase this value to 48 V. İnitial duty cycle is set to 0.5 and an step value of 5×10^{-6} is used to increase or decrease duty cycle. Maximum duty cycle is limited to between 0.08 and 0.9 to perform optimum operation conditions of FC. Especially, initial duty cycle is hold low value to prevent rapid decrease in FC voltage. Optimum voltage and capacity is selected for battery. Thus, it can be directly connected to system in parallel.

BLDC motor is fed by a six step voltage inverter. DC voltage is controlled by a speed regulator consisting a PID controller and DC-DC PWM generator. By decoding the hall effect signals, the inverter gates signals are produced and output of the inverter is applied to the BLDC motor stator windings (Tab. 2). Taking the average and maximum speed values of the WLTP Class 1 driving cycle as reference, a load torque that can drive a 400 kg LEV is simulated and applied to the motor shaft. Two control loops are used; inner one synchronizes the inverter gates

signals with the electromotive forces (EMF) and outer loop controls the speed of motor by varying the voltage.

Tab. 2: Truth table for driver gates signals

ha	hb	hc	emf_a	emf_b	emf_c	Q1	Q2	Q3	Q4	Q5	Q6
0	0	0	0	0	0	0	0	0	0	0	0
0	0	1	0	-1	1	0	0	0	1	1	0
0	1	0	-1	1	0	0	1	1	0	0	0
0	1	1	-1	0	1	0	1	0	0	1	0
1	0	0	1	0	-1	1	0	0	0	0	1
1	0	1	1	-1	0	1	0	0	1	0	0
1	1	0	0	1	-1	0	0	1	0	0	1
1	1	1	0	0	0	0	0	0	0	0	0

The reference speed is entered into the repeating sequence block, fed back with the motor mechanical (n_m) speed and controlled by the PID method. To simulate the torque (τ), the resistance forces (F) acting on the vehicle must be determined. By Eq 1-3, firstly the motor speed is converted to linear speed (v) then F and τ are calculated.

$$v = \frac{n_m \pi * r}{30 i} \quad (1)$$

$$F = mg\ c_{rr} + 0.5 \rho A_f c_d v^2 \quad (2)$$

$$\tau = Fr \quad (3)$$

where r is radius of wheel, i is gear ratio, m is mass, g is acceleration of gravity, c_{rr} is rolling resistance coefficient, ρ is the density of air, A_f is frontal area and c_d is air drag coefficient.

IV. Results and Discussions

With this study, a structure with the advantages of both FC and battery is created, such as high energy and power density, fast response times and more stable current and voltage characteristics. Fig. 2 shows the current, voltage and power graphs of each component when the FC and battery feed the motor driver together.

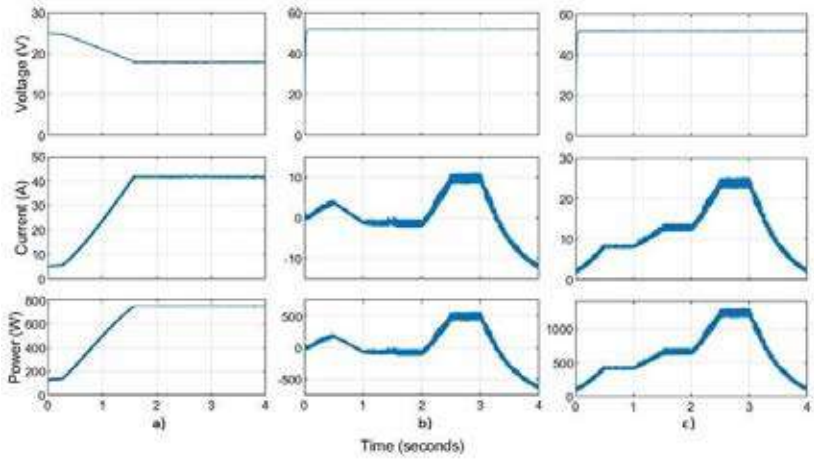


Fig. 2: Voltage, current and power graph of the hybrid drive system. a) FC b) Battery c) Motor driver.

Perturb and Observe (P&O) Algorithm is used for FC maximum power point tracking (MPPT). During startup, the increasing load demand is first met by the battery. Then FC, whose current is gradually increased, feeds the load. When the load demand exceeds the maximum power of the FC, the battery also comes into play and feeds the load together. During maximum power demand, FC and battery produce maximum power and feed the load. Then, as the load begins to decrease, the power of the battery used as the secondary power source also begins to decrease. When the load demand falls below the FC power, this time FC feeds the load and charges the battery. Thus, the FC and the battery perform well for the purpose of this study.

Considering that the cost is important since the system will be used in LEV, no active control mechanism is applied for the battery, and a passive power management is applied by connecting the battery with appropriate current and voltage values in parallel to the system. This also explains the similarity of battery and motor driver and current waveforms and voltages in Fig. 2. There is both an increase in speed and torque in the 0-0.5 s time interval, and in 0.5-1 s, both are constant. For 0-1 s interval, the phase-to-phase voltage, current and EMF voltage of the stator are observed and shown in Fig. 3.

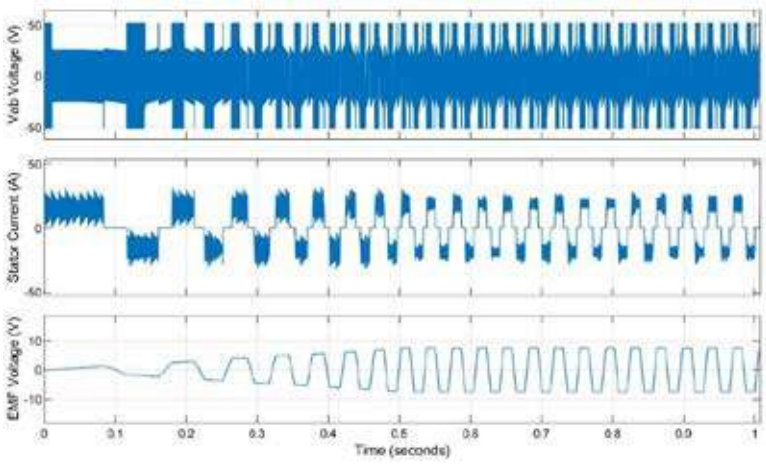


Fig. 3: phase-to-phase voltage, current and EMF voltage of stator windings.

While the switching frequency is increased to provide the reference speed, the average value of the current is increased to provide the required torque. During the all simulation, the motor is successfully controlled to follow the given reference speed and torque values (Fig. 4). While motor efficiency reaches 90% at full loads, it drops to 75% when motor drive losses are included.

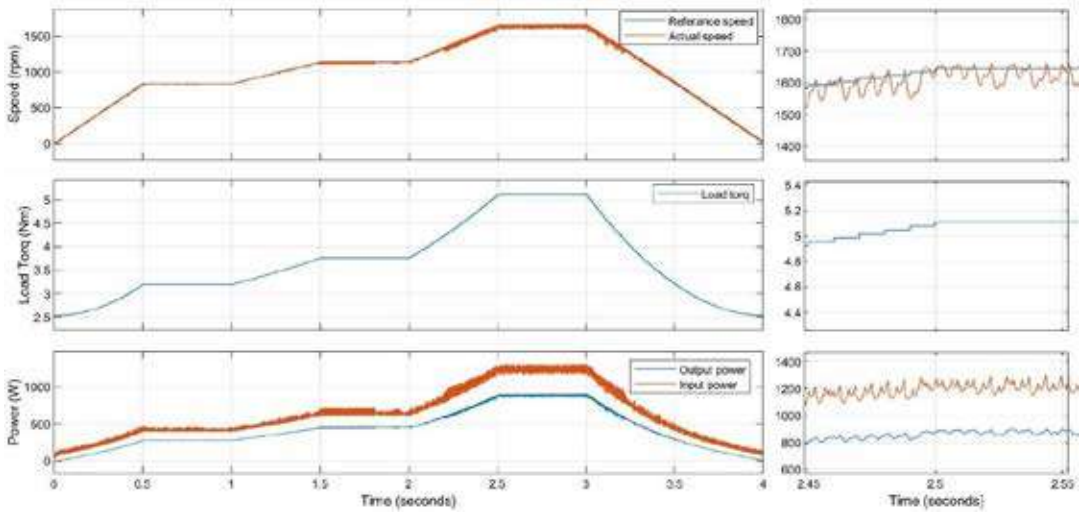


Fig. 4: Speed of motor, load torq and electrical input power of motor driver and mechanical output power of motor.

V. Conclusions

In this study, it is aimed to first eliminate the disadvantages of FC and battery by hybridizing them and obtain a power supply with the advantages of both. The second is to successfully drive the BLDC motor with this hybrid power supply. A boost converter was used to put the decreasing FC voltage into the appropriate form with the changing current demand. In order to keep the cost low in accordance with the application purpose, the battery is directly connected to the system. Thus, the required power is appropriately divided between both power sources and the load is successfully driven with components with smaller powers.

References

Hwang J. J., Chang W. R., Characteristic study on fuel cell/battery hybrid power system on a light electric vehicle, Journal of Power Sources, 207, 111-119, (2012).

Kim J. Y., Lee B. S., Lee Y. J., Kim J. K., Integrated multi mode converter with single inductor for fuel cell electric vehicles, IEEE Transactions on Industrial Electronics, 69(11), 11001-11011, (2021).

Mishra A. K., Singh A. K., Vishwanath G. M., A fuel-efficient BLDC motor-driven light electric vehicle with single-stage onboard charging system, IEEE Transactions on Transportation Electrification, 9(4), 4909-4921, (2022).

Pramuanjaroenkij A., Kakaç S., The fuel cell electric vehicles: The highlight review, International Journal of Hydrogen Energy, 48(25), 9401-9425, (2023).

Skarlis S., Molos T., Ayfantopoulou G., Nikiforiadis A., Bakouros L., Light commercial electric vehicles with hydrogen fuel-cell range extender: Refueling strategy evaluation, Research in Transportation Business & Management, 50, 101040, (2023).

Evaluation of a Decarbonized Combined Heat and Power (CHP) Plant, Incorporating Photovoltaic Panels and Hydrogen Re-electrification

[1*]Maryam Karami, [1]Parsa Fathi, [2]Parisa Heidarnejad
[1] Department of Machanical Engineering, Faculty of Engineering, Kharazmi Univeristy, Tehran, 15719-14911 Iran
[2] Department of Mechanical Engineering, Faculty of Engineering, Istanbul Gedik University, Istanbul, 34876, Türkiye

* E-mail:karami@khu.ac.ir

Abstract
This study presents an analysis of a combined heat and power plant incorporating solar photovoltaic panels, a gas engine, and a heat pump system. To mitigate the volatility of solar energy, an electrolyzer coupled with a storage tank is integrated into the system to produce green hydrogen using excess solar power for electrolysis. The performance of the system is evaluated based on solar radiation data from Ankara, Turkey. By utilizing zero-carbon solar energy and blending hydrogen with natural gas in the gas engine, the system contributes to decarbonization and reduces the carbon footprint. Mathematical modeling is employed to assess the performance of the system across four seasons in Ankara. The results indicate that on July 17, 2021, providing 50 kW of electric power requires 300 m^2 of PV panels, 18.08 kW power supply from the gas engine, and 6.18 kg/h of hydrogen production for storage. Additionally, a heat pump generating 11.21 kW of heat is sufficient to meet a 15 kW heating demand, with the remaining heat being recovered from the waste heat of the electrolyzer.

Keywords: CHP, Decarbonization, Re-electrification, PEM electrolyzer, PV panel

I. Introduction

The seasonal and daily fluctuations in renewable energy sources, particularly solar and wind energy, pose challenges to the reliability of power supply. One solution to address this issue is through storage and aggregation, as highlighted by Wu et al. (2022). A promising approach to mitigate fluctuation and intermittency is hydrogen re-electrification, which involves producing hydrogen via water electrolysis from surplus power and storing it in hydrogen tanks. This stored green hydrogen can then be utilized using standard methods for grid power production, such as fuel cells, gas turbine cycles, or gas engines, ensuring a stable power supply even when solar generation is unavailable. This storage method surpasses the capacity and duration of utility-scale batteries, as demonstrated by Zhang et al. (2017).

Given the imperative of decarbonizing the electricity sector to meet greenhouse gas emission reduction targets set after the Paris Agreement (Savaresi, 2016), reducing the utilization of fossil fuels has been emphasized. One strategy for reduction involves blending fossil fuels with carbon emission-free alternatives. Some studies have explored blending green hydrogen from water electrolysis with natural gas in gas turbine cycles or internal combustion engines. For example, Tebibel et al. (2014) proposed a sizing method for a system combining PV panels and a water electrolyzer to produce hydrogen for blending with compressed natural gas. Additionally, researchers have investigated renewable energy-based electrolyzers paired with storage tanks. Ghenai et al. (2020) proposed an off-grid hybrid solar PV/fuel cell system for a residential community in a desert region, demonstrating economic feasibility, environmental friendliness, and good technical performance. Zghaibeh et al. (2022) assessed the feasibility of a solar-based hydrogen electrolysis system in Oman for generating green fuel for fuel cells in transportation, with an investment cost of €5,301,760 for a capacity of 90,910 kg of hydrogen per year. Similarly, Nasser et al. (2022) analyzed the energy and exergy efficiencies of a PV panels/wind turbines hybrid system for green hydrogen generation and storage, with efficiencies calculated at 16.42% and 12.76% and a payback period of 7-13.85 years. Zhang et al. (2023) developed a PV-electrolyzer-fuel cell system for household power generation in China, achieving efficiency ranging from 6% to 7% under various conditions.

This study proposes an integrated system utilizing photovoltaic panels as the primary energy source for electricity generation. To mitigate solar energy fluctuations, surplus electricity is directed to a PEM electrolyzer to produce hydrogen as a storage medium, which is then utilized in gas engines during periods of insufficient solar energy. Before injection into the gas engine, hydrogen is blended with natural gas to reduce the required amount of natural gas. Additionally, the generated electricity is used to power a heat pump system to meet heating demands. Waste heat from the electrolysis process is also utilized to provide heat for users. The performance of the proposed system is analyzed through mathematical modeling to size the system and calculate power generation across four representative days, as detailed in the Analysis section.

II. Analysis

Figure 1 illustrates the configuration of the system under consideration. Solar radiation is captured by photovoltaic (PV) panels and converted into electrical energy. A portion of this generated power is supplied to the grid, while the remainder is directed to both the Proton Exchange Membrane (PEM) electrolyzer and the compressor of the heat pump. Within the PEM electrolyzer, water undergoes decomposition into hydrogen and oxygen gases. These gases are then stored in separate hydrogen and oxygen tanks. During periods of insufficient solar energy, the stored hydrogen is blended with natural gas and utilized in the gas engine to produce electricity. Concurrently, the heat pump utilizes the total electricity provided by the system. Additionally, heat recovery from the electrolyzer and

condenser of the heat pump is employed to maintain a constant heat supply for users. To size and evaluate the performance of the proposed system, mathematical modeling of the various subsystems is conducted using the equations provided below.

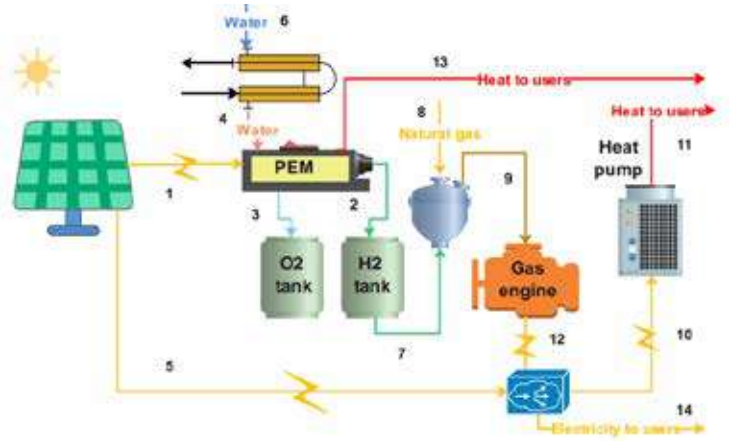


Fig. 1. The schematic of the considered system

PEM electrolyzer (Ni et al. 2008):

$$\dot{n}_{H_2} = \frac{n_c J}{2F} \quad (1)$$

$$\dot{n}_{O_2} = \frac{n_c J}{4F} \quad (2)$$

PV panels (Nasser et al. 2022):

$$\dot{W}_{PV} = N_{PV} \frac{G_t}{G_{t,ref}} \left[P_{PV,max} + \mu_p \left(T_{PV} - T_{PV,ref}\right)\right] \quad (3)$$

$$T_{PV} = T_a + G_t \left[\frac{NOCT - 20}{800}\right] \quad (4)$$

Overall system:

$$\dot{W}_{tot} = \dot{W}_{PV} - \dot{W}_{PEM} + \dot{W}_{GE} - \dot{W}_{HP} \quad (5)$$

$$\dot{Q}_{heating} = \dot{Q}_{HP} + \dot{Q}_{PEM} \quad (6)$$

III. Results and discussions

In this section, the results obtained from modeling the proposed system are presented and discussed, which are summarized in Table 1 and illustrated in Figure 2. To gain a comprehensive understanding of the system's performance, four representative days, each representing a season (spring, summer, fall, and winter) are selected. It is evident that the highest radiation occurs during July, resulting in the lowest power output from the gas engine and the lowest consumption of natural gas. Additionally, the maximum useful heat recovery from the electrolyzer for heating purposes is observed during this period. As the heating supply is derived from the heat loss of the electrolyzer and the heat pump condenser, the power consumption by the heat pump compressor is minimized. Conversely, the lowest radiation occurs in December, leading to the highest consumption of natural gas in the gas engine. Furthermore, the heat loss from the electrolyzer is minimized during this period, resulting in the maximum power consumption by the heat pump compressor to compensate for the heat supply.

Table 1. Performance of the proposed system on July 17, 2021

Parameter	Value
Irradiation on the tilted surface	1022 w/m^2
Number of PV modules	206
The total amount of power supply	50 kW
Power supply by PV	45.599 kW
Power supply by the gas engine	18.08 kW
Power consumption by the electrolyzer	13.68 kW
Total amount of heat supply	15 kW
Heat supply by heat pump	11.21 kW
Heat recovered from electrolyzer	3.79 kW
Electrolyzer hydrogen production	6.18 kg/h

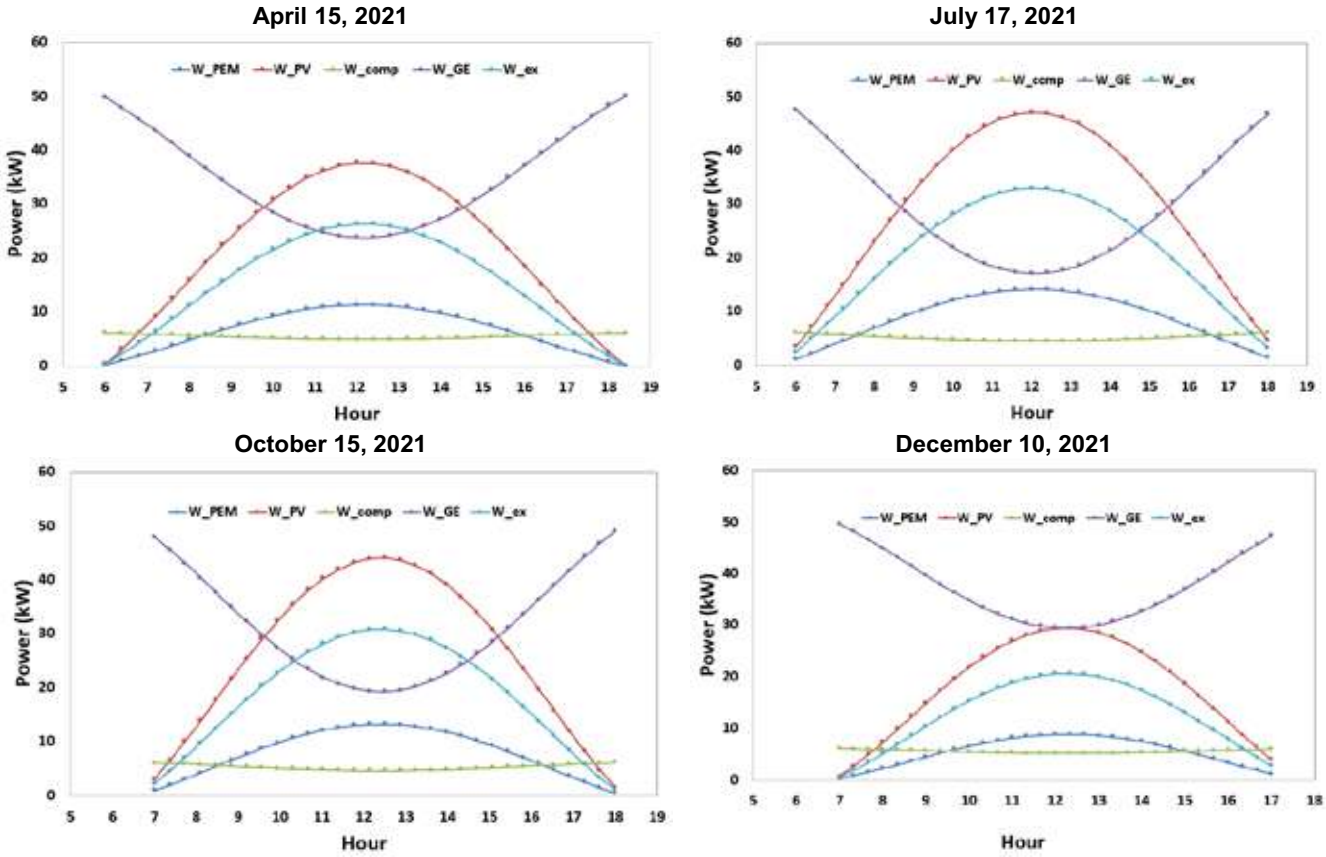


Fig. 2. The amount of power produced by PV, power produced by a gas engine, power consumed by electrolyzer, power consumed by heat pump compressor, and excessive power during different hours on April 15, July 17, October 15, and December 10, 2021.

IV. Conclusions

This study focuses on the performance evaluation of a combined heating and power plant integrating solar photovoltaic panels, a gas engine, and a heat pump system. The mathematical modeling is conducted using solar radiation data from Ankara, Turkey, and the analysis is carried out for four representative days, each representing a different season in Ankara. The results indicate that on July 17, 2021, to achieve 50 kW of electric power, 300 m^2 of PV panels, an 18.08 kW power supply from a gas engine, and the production of 6.18 kg/h of hydrogen as a storage medium are required. Additionally, utilizing a heat pump to generate 11.21 kW of heat is sufficient to meet a heating power demand of 15 kW, with the remaining heat recovered from the waste heat of the electrolyzer.

References

Ghenai C, Salameh T, and Merabet A. 2020. Technico-economic analysis of off grid solar PV/Fuel cell energy system for residential community in desert region. International Journal of Hydrogen Energy. 45(20): p. 11460-11470.

Nasser M, et al. 2022. Performance evaluation of PV panels/wind turbines hybrid system for green hydrogen generation and storage: Energy, exergy, economic, and enviroeconomic. 267: p. 115870.

Ni M, Leung M K H, and Leung D Y C. 2008. Energy and exergy analysis of hydrogen production by a proton exchange membrane (PEM) electrolyzer plant. Energy Conversion and Management. 49(10): p. 2748-2756.
Savaresi A. 2016. The Paris Agreement: a new beginning? Journal of Energy & Natural Resources Law. 34(1): p. 16-26.

Tebibel H and Labed S. 2014. Design and sizing of stand-alone photovoltaic hydrogen system for HCNG production. International Journal of Hydrogen Energy. 39(8): p. 3625-3636.

Wu C, Zhang X-P, and Sterling M. 2022. Solar power generation intermittency and aggregation. Scientific Reports. 12(1): p. 1363.

Zghaibeh M, et al. 2022. Analytical model for a techno-economic assessment of green hydrogen production in photovoltaic power station case study Salalah city-Oman. International Journal of Hydrogen Energy. 47(31): p. 14171-14179.

Zhang Y, et al. 2017. Comparative study of hydrogen storage and battery storage in grid connected photovoltaic system: Storage sizing and rule-based operation. Applied Energy. 201: p. 397-411.

Zhang F, et al. 2023. Development of photovoltaic-electrolyzer-fuel cell system for hydrogen production and power generation. Energy. 263: p. 125566.

Investigation of the Effects of Hydrogen and Water Vapor Addition on Compression Engine Performance and Exhaust Emissions

[1]Zafer Akbalık, [2*]Orhan Arpa
[1]Etibakır A.Ş. Mazıdağı İşletmesi / Mardin
[2]Dicle University Engineering Faculty Mechanical Engineering Department, 21000 Diyarbakır, Türkiye

* E-mail: orhana@dicle.edu.tr

Abstract
Increasing oil prices and environmental pollution have led to increased research on alternative fuels instead of petroleum fuels. In this single-cylinder, 4-stroke, air-cooled diesel engine, in addition to diesel fuel, hydrogen with a volumetric flow rate of 0.17 lt/min and water vapor with a mass flow rate of 250 g/h were supplied to the engine intake manifold. In this way, the engine's performance and exhaust emissions are revealed. In experiments where engine power and water vapor were added separately, an increase of 3.48% and 3.63%, respectively, was observed at 2000 rpm. However, a decrease in engine power was observed with the combination of diesel, hydrogen and water vapor (D+H+WS). The specific fuel varies somewhat with fuel storage, reduced by water vapor, and hydrogen + water vapor by fueling. The lowest fuel consumption was 307.17 g/kW.h at 1500 rpm, which decreased by 0.15% compared to diesel fuel. The lowest values for CO and NOx emissions were obtained at 900.5 ppm, 146 ppm and 459.5 ppm, respectively, in hydrogen, water and hydrogen-water conversion at 2500 rpm.

Keywords: Diesel Engine, hydrogen, water steam, performance, and emission.

I. Introduction

Today's energy requirements rapidly increase contrary to decrease of petroleum based fuels which cause to raise price of fuels, besides fossil fuel have harmful effect of emissions on environment with energy efficiency effects on engines. Thus, scientists aim to work on new fuel to use in engine or to add at various ratios like bioethanol. Due to European Union Commissions White Paper Report, target to minimize as 60 % of green-house gas emissions from vehicles by 2050 (EEA Report No 10/2013). Even though advance technological growth, Nitrogen Oxides and particulate matter emissions have increased at diesel transportation, however other emission are decreased at desired level (Liu Y et al).

Karagoz et al. studied on 25% and 50% of hydrogen injection into diesel engine to observed performance, emissions and combustion characteristics at full load with 900, 1100, 1400, 1750 and 2100 rpm. The test results of experiments can be declared as: engine effective power was decreased on contrary thermal efficiency was increased. The best results were obtained at 75% load conditions and 20% of hydrogen which lead to reduce thermal efficiency and volumetric yield as well as CO and CO2 emissions. And also NOx emissions were increased. Koten combusted different ratio of hydrogen (20%, 40%, 60% and 80%) at fixed speed (1800 rpm) with various load (20%, 40%, 60%, 80% and 100%) in a diesel engine. Test results can be items as specific fuel consumption decrease and thermal efficiency increase while CO and HC emissions reduce and, NOx emissions increase in a significant manner. Talibi et al. injected hydrogen directly in engine chamber and diagnosed that a reduce on particle amounts, meanwhile an increase at CO and HC emissions and especially at NOx emissions.

Zhao et al. added water vapor at different ratios for minimizing specific fuel consumption of diesel fuel which were carried out at 1000, 1300 and 1800 rpm.

II. Experimental Set-up and Procedure

Experimental studies were carried out on a single-cylinder, four-stroke, water-cooled and compression-ignition Antor 4LD 820L model diesel engine in Dicle University, Engineering Faculty, Mechanical Engineering Department Engine Laboratory.

To obtain these performance and emission values, the samples were tested in a diesel engine as shown schematically in figure 1. Testo 350 model exhaust emission measurement device was used in the experiments. The hydrogen used in the experiments was sent to the engine intake manifold by adjusting the pressure and flow rate. A flame protector has been installed at the regulator outlet to prevent the flame from flashing back, and a regulator adjustable up to a maximum of 16 bar has been used for hydrogen gas pressure control. An ultrasonic cold steam machine with a capacity of 5L and a maximum pressure rate of 250 g/h is used to add water vapor.

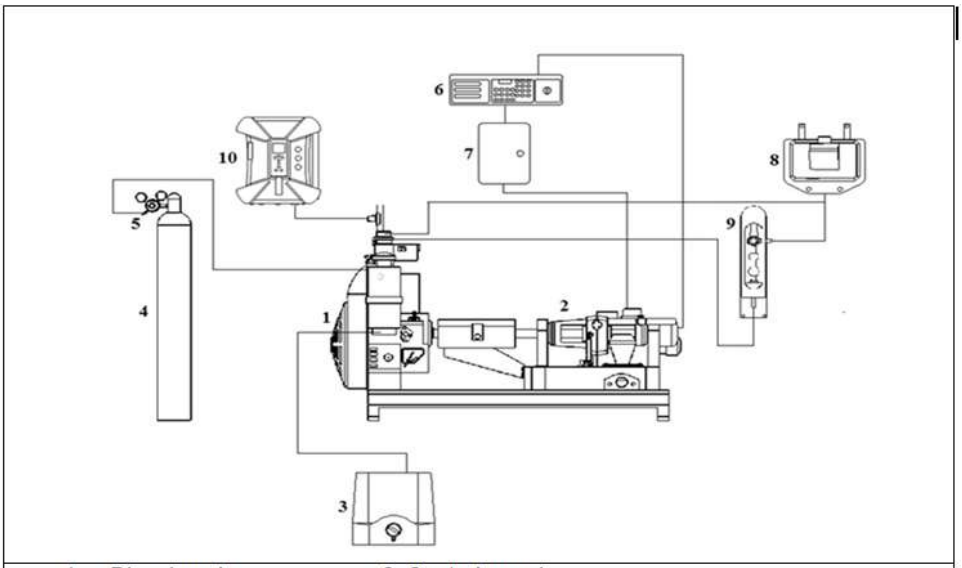


Fig.1: Schematically represation of experimental setup,

III. Results and Discussion

The obtained results were compared with standard diesel fuel, were given in Figures. The experiments were carried out at 1000, 1500, 2000 and 2500 rpm at full throttle opening valve, by injecting hydrogen, water vapor and hydrogen-water vapor simultaneously, respectively

III.I Engine Performance

The torque and power values obtained by adding hydrogen and water vapor to the diesel engine are given in Figure 2 and Figure 3 respectively. The engine torque was observed to increase by water vapor injection. The reason why the engine torque decreases when operating with D+H+WS can be explained by the fact that water vapor absorbs the heat in the cylinder due to its high molar heat capacity. The maximum engine power was 6.84 kW at 2000 rpm, with an increase of 3.48% due to the diesel fuel. And also, an increase of 0.68% and 1.35% in engine power at 1500 and 2500 rpm, respectively. The increase of engine power was related with rich combustion by high rate of hydrogen.

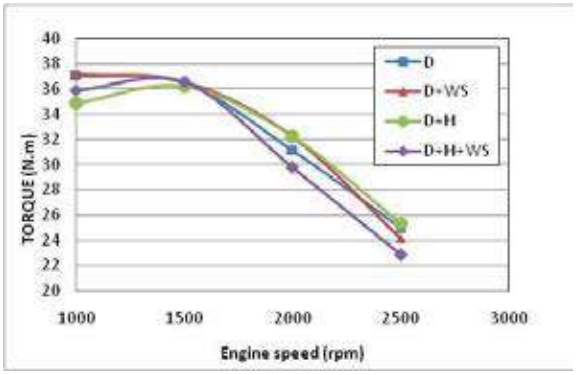


Fig. 2: Engine Torque variations at different speeds.

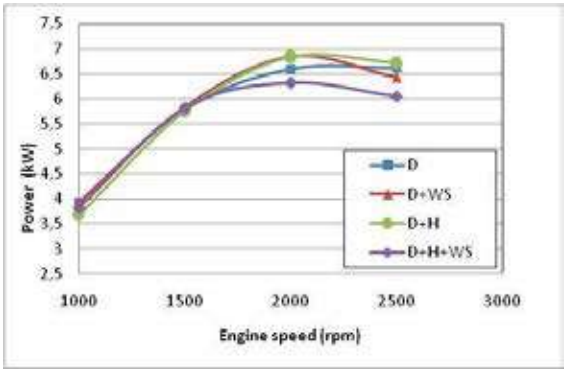


Fig. 3: Engine power variations at different speeds.

However, as seen that hydrogen and water vapor injection causes to decrease in engine power.

The lowest specific fuel consumption was calculated as 319.44 g/kWh at 1500 rpm for water vapor. This value is 3.38% higher when compared to diesel fuel. Specific fuel consumption increased by 3.17% with a value of 351.3 g/kWh at 1000 rpm where the maximum engine torque was seen, and decreased by 0.14% with a value of 366.76 g/kWh at 2000 rpm where the maximum engine power was seen.

For hydrogen-water mixture, maximum specific fuel consumption increased by 3.14% as 489.96 g/kW.h at 2500 rpm. And maximum engine torque at 1500 rpm and maximum engine power at 2000 rpm, fuel consumptions were 291.39 g/kW.h and 358.02 g/kW.h, respectively, 5.28% and 3.3% according to diesel fuel.

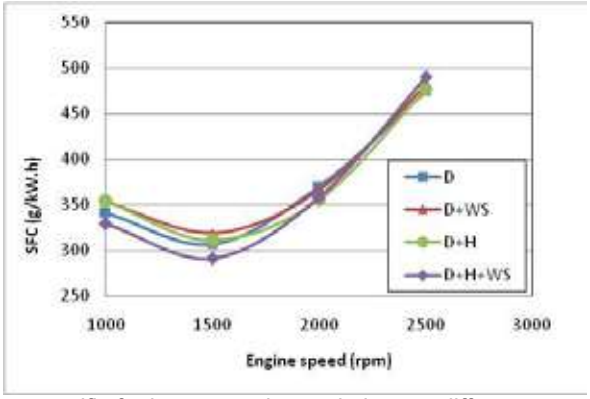


Fig. 4: Engine specific fuel consumption variations at different speeds.

III.II Exhaust Emissions

As seen from Figure 5 it was seen that hydrogen injection reduces NOx emissions in all speed. NOx emissions decreased by 26.63% according to 973.5 ppm diesel fuel at 1500 rpm of maximum engine torque while at 2000 rpm maximum engine power, 13.13% reduce observed as 678 ppm of diesel fuel. Figure 6 shows the change in CO emissions. With the addition of hydrogen, CO emission increased due to insufficient oxygen entering the cylinder. With the addition of water vapor, this drawback was corrected, especially after 1500 rpm.

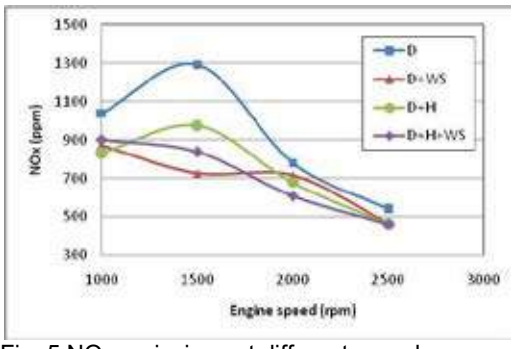


Fig. 5:NOx emissions at different speeds

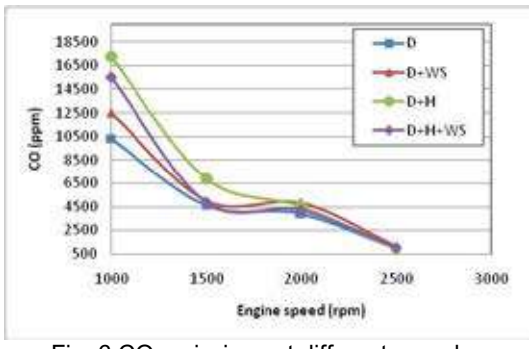


Fig. 6:CO emissions at different speeds.

IV. Conclusions

It has been observed that engine power decreases after 1500 rpm with the addition of water vapor and hydrogen.
The lowest specific fuel consumption values were obtained by adding water vapor and hydrogen at all engine speeds.
NOx emissions, which are considered the most important pollutants for diesel engines today, have decreased at all engine speeds with the addition of water vapor and hydrogen.
The addition of hydrogen to the diesel engine caused a significant increase in CO emissions at the 1500-2000 rpm range. In the 2000-2500 rpm range of the engine, the CO emission values of diesel fuel are approached. However, adding water vapor to the engine along with hydrogen significantly reduced CO emissions at speeds lower than 2000 rpm.

References

European Environment Agency (EEA). Trends and projections in Europe 2013: tracking progress towards Europe's climate and energy targets until 2020, Report No 10/2013, (2013).

Barrios, C. C.,Domínguez-Sáez, A., Hormigo, D., Influence of hydrogen addition on Combustion characteristics and particle number and size distribution emissions of a TDI diesel engine. Fuel, 199, 162–168, (2017).

Bose PK, Maji D. An experimental investigation on engine performance and emissions of a single cylinder diesel engine using hydrogen as inducted fuel and diesel as injected fuel with exhaust gas recirculation. Int J Hydrogen Energy, 34:4847-4854, (2009).

Gomes-Antunes JM, Mikalsen R, Roskilly AP. An investigation of hydrogen fuelled HCCI engine performance and operation.Int J Hydrogen Energy, 33:5823-5828, (2008).

Hu E, Huang Z, Liu B, Zheng J, Gu X, Huang B. Experimental investigation on performance and emissions of a spark ignition engine fuelled with natural gas hydrogen blends combined with EGR. Int J Hydrogen Energy, 34:528-539, (2009).

Karagoz Y, Yuksek L, Sandalcı T, Dalkılıc AS. Engine performance and emission effects of diesel burns enriched by hydrogen on different engine loads. İnternational journal of hydrogen energy, 40, 6702-6713, (2015).

Koten, H., Hydrogen effects on the diesel engine performance ande missions.International Journal of Hydrogen Energy, 43(22), 10511–10519, (2018)

Liu Y, Yang J, Sun J,Zhu A, Zhou Q. A phenomenological model for prediction auto-ignition and soot formation of turbulent diffusion combustion in a high pressure common rail diesel engine. Energies, 4(6), 894-912, (2011).

Romualdas Juknelevicius, Saugirdas Pukalskas, Alfredas Rimkus, Stanislaw Szwaja Investigation of Performance and Emission Parameters of Hydrogen (HHO)-Enriched Diesel Fuel with Water Injectionin the Compression Ignition Engine. CleanTechnol, 3, 537–562, (2021).

Sharma, P.,Dhar, A., 2018, Effect of hydrogen supplementation on engine performance and emissions, International Journal of HydrogenEnergy, 43(15), 7570–7580.

Talibi, M., Hellier, P., Ladommatos, N., 2017, Combustion and exhaust emission characteristics, and in-cylinder gas composition, of hydrogen enriched biogas mixtures in a diesel engine, Energy, 124, 397–412, (2017).

Supervised Learning Based PEM Fuel Cell Model

[1*]Soner Çelikdemir, [2]Burak Özdemir, [2]Mahmut Temel Özdemir
[1] Bitlis Eren University, Adilcevaz Vocational School, Electric and Energy, Bitlis, 13000, Türkiye
[2]Fırat University, Engineering Faculty, Electrical and Electronics Engineering, Elazığ, 23000, Türkiye

E-mail:celikdemirsoner@gmail.com

Abstract

Polymer Electrolyte Membrane Fuel Cells (PEMFC) have been preferred in important engineering applications in recent years due to their zero emission. In this study, it is aimed to predict the output voltage with minimum error by using regression learning methods, which is one of the machine learning classes. For this purpose, the suitability of different regression methods is compared. Root Mean Square Error (RMSE) values of the voltage value are taken into account while performing the regression method. The obtained results were only compared with a strictly verifiable reference and the performance of the proposed algorithm was tested. As a result, the supervised learning model with the lowest RMSE value is Gaussian Process Regression (Matern 5/2 GPR) with an RMSE value of 0.22 and a training time of 1.4388 seconds. The supervised learning model with the highest RMSE value is SVM Kernel with an RMSE value of 3.36 and a training time of 1.4645 seconds. This shows that the fuel cells will be predicted in a way that will enable them to operate more efficiently. In addition, the use of experimental data in such studies is important for objective evaluation.

Keywords: PEMFC, Supervised Learning, Root Mean Square Error

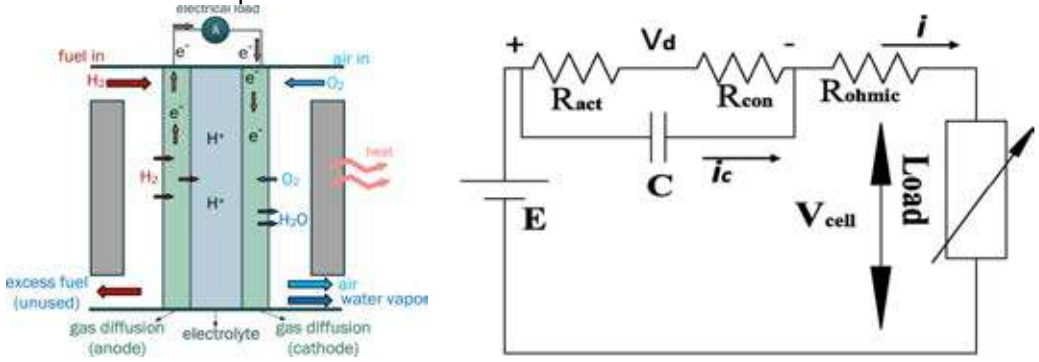
I. Introduction

In recent years, electric power systems have been continuously developing. In parallel with this development, the usage areas of fuel cells are also increasing. Fuel cells have the advantages of low noise, low temperatures, high electrical efficiency and current density, fast start-up, excellent transient response characteristics, and are highly modular for practical applications (Yang et al. 2016; Ijaodola et al. 2019). This has led researchers to focus on the development of fuel cells. Fuel cells are defined as an electrochemical device that converts chemical energy into electrical energy using hydrogen gas as input fuel and heat using oxygen/air as oxidant. Among the different types of FCs, PEMFCs are the most widely used type and have been used in many applications such as mobile, vehicle, transportation, industrial applications and distributed residential generation systems (S. Menesy et al. 2020). For this reason, the modeling of PEMFCs has received a great deal of attention in the literature.

There are various PEMFC modeling methods in the literature. These methods can be divided into two categories. The first one is called mechanistic modeling and describes the electrochemical phenomena occurring in FCs as well as heat and mass transfer. The second part is called empirical modeling and is described as semi-empirical and non-linear equations used to predict the effect of various parameters on current-voltage. In this study, the researchers have tried to predict the output voltage with minimum error by using regression learning methods, which is a class of machine learning. In this way, the suitability of different regression methods is compared. Root Mean Square Error (RMSE) values for the predicted voltage value were taken into account while performing the regression method. The obtained results are compared only with an absolutely verifiable reference and the performance of the proposed algorithm is tested.

II. System Description and Procedure

A conventional PEMFC employs a solid polymer electrode membrane to facilitate ion exchange between two electrodes. This membrane acts as an insulator for electrons while also serving as an efficient conductor for protons. Figure 3-a) illustrates a schematic illustration of the primary structure and components of PEMFCs, whereas Figure 3-b) presents the electrical equivalent circuit model.



a) b)

Figure 1. a) PEMFC structure (Özdemir 2021) b) Equivalent circuit model of PEMFC (Mitra, Arya, and Gupta 2023)

The PEM fuel cells consist of an anode, a cathode and a thin solid polymeric membrane. The PEM fuel cell is fed with a hydrogen-containing anode gas and an oxygen-containing cathode gas. Electrochemical reactions for

the PEM fuel cell are below (Ye, Wangb, and Xua 2009; Salim et al. 2015; Li et al. 2011; Isa and Rahim 2013; Chibante and Campos 2010)

$$\text{Anode: } H_2 \rightarrow 2H^+ + 2e^- \quad (1)$$
$$\text{Cathode: } 2H^+ + \tfrac{1}{2} O_2 + 2e^- \rightarrow H_2O \quad (2)$$
$$\text{Overall reaction: } H_2 + \tfrac{1}{2} O_2 \rightarrow H_2O \quad (3)$$

DC electricity, water vapour and heat are the products of the reactions. The PEM fuel cell output voltage is depended on some voltage drops such as activation, ohmic and concentration loss. If there is no load, the output of the fuel cell equals the open circuit voltage (E_0). Theoretically, E_0 is 1.2 V known as Nerst voltage. But it is less than this value for practically application.

III. Model Evaluation

Machine learning is a framework that focuses on building systems that learn or improve performance based on available data. In general, two main types of machine learning algorithms are used today: supervised training and unsupervised training. The difference between them is defined by how each learns from the data to make predictions. Supervised learning; with this model, the data expert acts as a guide and teaches the algorithm what conclusions to draw. During supervised learning, the algorithm tries to learn by memorization. As a result, it is trained with datasets that are already labeled and have a predefined output. Examples of supervised machine learning include algorithms such as linear and logistic regression, multi-class classification and support vector machines. Unsupervised machine learning, on the other hand, utilizes a more independent approach in which a computer learns complex processes and models without the constant and close guidance of a human. Unsupervised machine learning involves training based on data without labels or a specific, defined output. The general structure of machine learning is given in Figure 1.

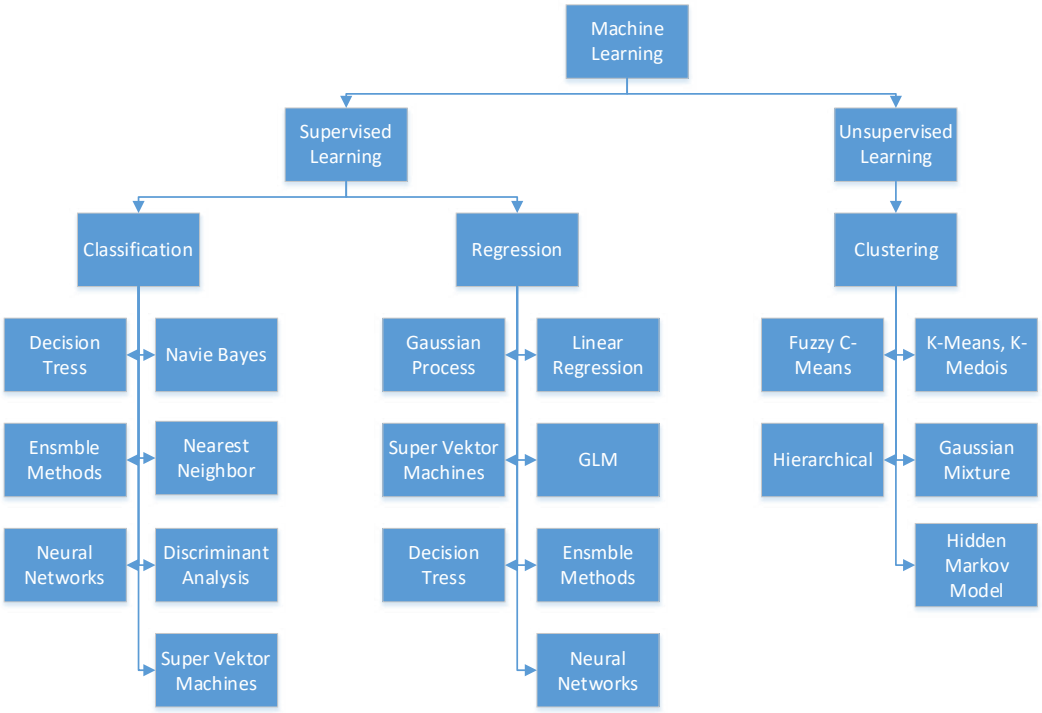


Figure 2. Machine learning techniques

In the study, 27 different supervised learning models were implemented and their results were compared. RMSE error values and training times of different algorithms are given in Figure 3.

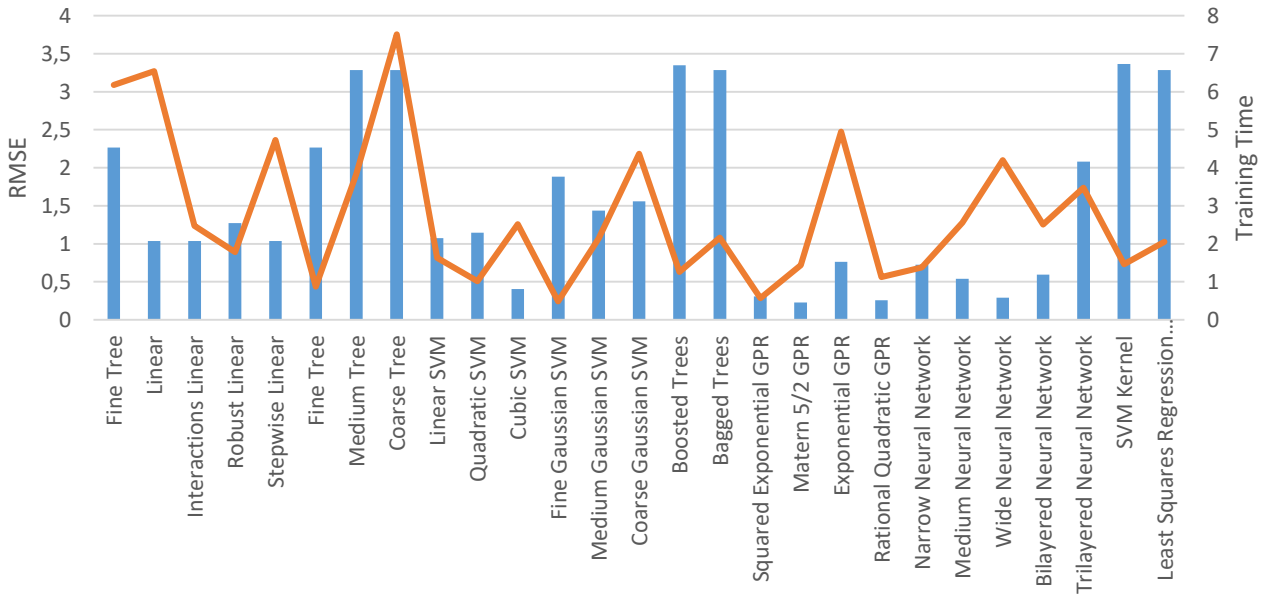
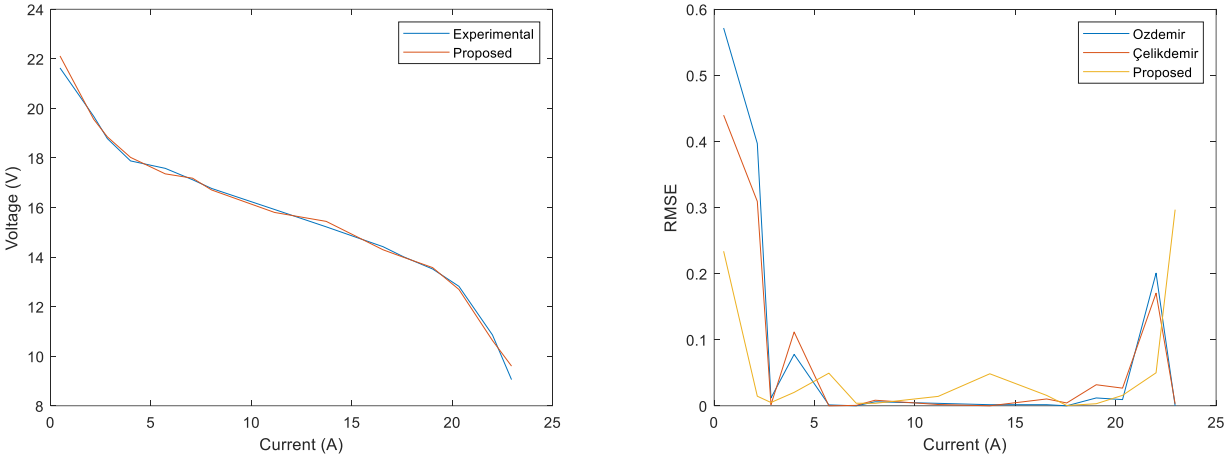


Figure 3. RMSE values and training times of classification models

Accordingly, the supervised learning model with the lowest RMSE is Gaussian Process Regression (Matern 5/2 GPR) with an RMSE of 0.22 and a training time of 1.4388 seconds. The supervised learning model with the highest RMSE value is SVM Kernel with an RMSE value of 3.36 and a training time of 1.4645 seconds. The polarization plots of the real data and those calculated using Gaussian Process Regression are given in Figure 4.

Table 1. PEMFC empirical and calculation results

Experimental Model		(Özdemir 2021)		(Çelikdemir 2023)		Proposed Model	
Current	Voltage	Voltage	Error	Voltage	Error	Voltage	Error
0.472	21.63	20.874	0.571	20.966	0.439	22.11	0.233
2.149	19.68	19.05	0.396	19.123	0.309	19.55	0.014
2.83	18.78	18.671	0.0118	18.738	0.00	18.85	0.004
3.983	17.88	18.159	0.0778	18.214	0.111	18.02	0.020
5.713	17.58	17.543	0.001	17.58	0	17.35	0.049
7.075	17.12	17.122	0	17.145	0	17.18	0.003
8.019	16.77	16.848	0.006	16.861	0.008	16.70	0.003
11.16	15.92	15.981	0.003	15.964	0.001	15.80	0.014
13.73	15.22	15.261	0.001	15.221	0	15.4	0.048
16.56	14.42	14.379	0.001	14.318	0.010	14.294	0.015
17.56	14.02	14.02	0	13.954	0.004	13.998	0
19.03	13.52	13.411	0.011	13.341	0.031	13.576	0.003
20.34	12.82	12.723	0.009	12.656	0.026	12.694	0.015
22.01	10.86	11.308	0.200	11.272	0.170	10.636	0.049
22.96	9.058	9.058	0	9.1132	0.003	9.602	0.296
	RMSE		**0.293**		**0.273**		**0.227**



a) b)

Fig.4: Result graphs a) I-V polarization graph b) RMSE graph

Accordingly, a model with lower error RMSE values than the existing literature is proposed to ensure that PEMFCs operate at high performances. According to the proposed model, the RMSE value is calculated as 0.22.

V. Conclusions

In this study, more realistic modeling of the current-voltage polarization graphs of PEMFCs is provided. For this purpose, the researchers tried to predict the output voltage with minimum error by using regression learning methods, which is one of the machine learning classes. In this way, the suitability of different regression methods was compared. The root mean square error (RMSE) values of the voltage value were taken into account while performing the regression method. The obtained results were only compared with a strictly verifiable reference and the performance of the proposed algorithm was tested. As a result, the supervised learning model with the lowest RMSE value is Gaussian Process Regression (Matern 5/2 GPR) with an RMSE value of 0.22 and a training time of 1.4388 seconds. The supervised learning model with the highest RMSE value is SVM Kernel with an RMSE value of 3.36 and a training time of 1.4645 seconds. This situation provides more efficient operation of fuel cells. The use of experimental data in such studies is important for objective evaluation.

References

Çelikdemir, Soner. 2023. “Parameter Estimation of the PEMFC Model with Coati Optimization Using New Objective Function.” In *IHTEC 2023*, 83–86. Elazığ.

Chibante, R., and D. Campos. 2010. “An Experimentally Optimized PEM Fuel Cell Model Using PSO Algorithm.” In *IEEE International Symposium on Industrial Electronics*. https://doi.org/10.1109/ISIE.2010.5637642.

Ijaodola, O.S., Zaki El- Hassan, E. Ogungbemi, F.N. Khatib, Tabbi Wilberforce, James Thompson, and A.G. Olabi. 2019. “Energy Efficiency Improvements by Investigating the Water Flooding Management on Proton Exchange Membrane Fuel Cell (PEMFC).” *Energy* 179 (July): 246–67. https://doi.org/10.1016/j.energy.2019.04.074.

Isa, Zainuddin Mat, and Nasrudin Abdul Rahim. 2013. “PEM Fuel Cell Model Parameters Optimization Using Modified Particle Swarm Optimization Algorithm.” In *2013 IEEE Conference on Clean Energy and Technology (CEAT)*, 442–45. IEEE. https://doi.org/10.1109/CEAT.2013.6775672.

Li, Qi, Weirong Chen, Youyi Wang, Shukui Liu, and Junbo Jia. 2011. “Parameter Identification for PEM Fuel-Cell Mechanism Model Based on Effective Informed Adaptive Particle Swarm Optimization.” *IEEE Transactions on Industrial Electronics* 58 (6): 2410–19. https://doi.org/10.1109/TIE.2010.2060456.

Mitra, Uliya, Anoop Arya, and Sushma Gupta. 2023. “A Comprehensive and Comparative Review on Parameter Estimation Methods for Modelling Proton Exchange Membrane Fuel Cell.” *Fuel*. https://doi.org/10.1016/j.fuel.2022.127080.

Özdemir, Mahmut Temel. 2021. “Optimal Parameter Estimation of Polymer Electrolyte Membrane Fuel Cells Model with Chaos Embedded Particle Swarm Optimization.” *International Journal of Hydrogen Energy* 46 (30): 16465–80. https://doi.org/10.1016/j.ijhydene.2020.12.203.

S. Menesy, Ahmed, Hamdy M. Sultan, Ahmed Korashy, Fahd A. Banakhr, Mohamed G. Ashmawy, and Salah Kamel. 2020. “Effective Parameter Extraction of Different Polymer Electrolyte Membrane Fuel Cell Stack Models Using a Modified Artificial Ecosystem Optimization Algorithm.” *IEEE Access* 8: 31892–909. https://doi.org/10.1109/ACCESS.2020.2973351.

Salim, Reem, Mahmoud Nabag, Hassan Noura, and Abbas Fardoun. 2015. “The Parameter Identification of the Nexa 1.2 KW PEMFC’s Model Using Particle Swarm Optimization.” *Renewable Energy* 82 (October): 26–34. https://doi.org/10.1016/j.renene.2014.10.012.

Yang, Shipin, Ryad Chellali, Xiaohua Lu, Lijuan Li, and Cuimei Bo. 2016. “Modeling and Optimization for Proton Exchange Membrane Fuel Cell Stack Using Aging and Challenging P Systems Based Optimization Algorithm.” *Energy* 109 (August): 569–77. https://doi.org/10.1016/j.energy.2016.04.093.

Ye, Meiying, Xiaodong Wangb, and Yousheng Xua. 2009. “Parameter Identification for Proton Exchange Membrane Fuel Cell Model Using Particle Swarm Optimization.” *International Journal of Hydrogen Energy* 34 (2): 981–89. https://doi.org/10.1016/j.ijhydene.2008.11.026.

Preparation and performance investigation of self-supported CoB catalysts for sodium borohydride hydrolysis reaction

[1]Jülide Hazal Özdemir, [2]Hüseyin Elçiçek, [2]Görkem Kökkülünk, [1*]Oğuz Kaan Özdemir
[1] YTU, Faculty of Chemistry-Metallurgy, Department of Metallurgy and Materials Engineering, Davutpaşa Mah. Davutpaşa Caddesi, Esenler, İstanbul, 34220, Türkiye.
[2] YTU, Faculty of Naval Architecture and Maritime, Department of Marine Machinery Management Engineering Barbaros Bulvarı İstanbul, 34349, Türkiye

* E-mail:kozdemir@yildiz.edu.tr

Abstract
The hydrolysis of sodium borohydride forms the basis for its widespread use as a hydrogen source. Hydrolysis usually occurs in the presence of a catalyst. Among different catalysts, CoB alloys are a good catalyst for the hydrolysis reaction. However, due to its magnetic feature, agglomeration occurs during the reaction and as a result, significant performance decreases in catalytic activity occur. For this reason, it is important to deposit catalysts on support materials with high surface area. In this study, it was determined that different cobalt oxide compounds were formed as a result of the addition of cetyl trimethyl ammonium bromide (CTAB), a cationic surfactant, during the synthesis of CoB catalysts and that these cobalt oxide phases served as support material for the CoB catalyst. The phases formed after the synthesis of the catalysts were examined by XRD technique, and the surface morphology was examined by FESEM.

Keywords: Sodium Borohydride, CoB Catalyst, Cetyl Trimethyl Ammonium Bromide (CTAB), Support Material

I. Introduction

The predominant energy infrastructure reliant on fossil fuels has been pinpointed as the primary contributor to both global climate alterations and regional air quality deterioration (Stern 2007). Hydrogen-powered fuel cells offer notable environmental benefits (Veziroglu 1998, Muradov and Veziroğlu 2005, Marbán and Valdés-Solís 2007, Midilli and Dincer 2008, Schlapbach and Borgschulte 2008). Nonetheless, the storage and transportation of hydrogen pose significant scientific and technological hurdles in the widespread adoption of a hydrogen-based economy, whether on a national or global level (Marrero-Alfonso, Beaird et al. 2009). The primary technologies devised for the storage and distribution of pure hydrogen encompass compressed gas(Ogden, Kreutz et al. 2000), cryogenic liquid(Qiu, Yang et al. 2021), adsorption on carbon materials (Xu, Sun et al. 2024), metal hydrides (Drawer, Lange et al. 2024), and chemical hydrides(Rampai, Mtshali et al. 2024). These storage techniques have been thoroughly assessed, with attention drawn to their potential for enhancement, as well as their inherent physical constraints (Bosu and Rajamohan 2024). Chemical hydrides, in particular, have garnered widespread recognition as promising storage mediums for supplying H_2 gas to fuel cells. Among these, sodium borohydride ($NaBH_4$) emerges as a standout candidate owing to its impressive hydrogen storage capacity of 10.8 wt% and potential for safe operation (Kaya, Özdemir et al. 2024). The methods for liberating stored H_2 within $NaBH_4$ encompass thermolysis(Fakioğlu, Yürüm et al. 2004), hydrolysis(Schlesinger, Brown et al. 1953, Shafirovich, Diakov et al. 2007), and hybrid approaches that combine elements of both processes(Marrero-Alfonso, Gray et al. 2007).

The efficiency of hydrogen production can be substantially boosted by employing catalysts during the hydrolysis reaction. While numerous organic and inorganic acids have the ability to accelerate the hydrolysis reaction rate, it often leads to uncontrollable reactions(Özkar and Zahmakıran 2005). These catalyst materials can be readily synthesized through a straightforward chemical reduction method, wherein transition metal ions are reduced to the metallic state by a reducing agent. In our prior research, Co-B catalysts fabricated in the form of nanoparticle-assembled films using pulsed laser deposition technique exhibited performance comparable to that of noble metals(Patel, Guella et al. 2007). However, the high surface energy and magnetic properties of Co–B catalysts make the particles easily agglomerate and have few active sites(Long, Chen et al. 2022). Support materials play a crucial role in catalyst design, not only providing a surface area for active ingredients but also enhancing the mechanical properties of the catalyst for prolonged use.

II. Experimental Set-up and Procedure

Cobalt (II) chloride hexahydrate ($CoCl_2.6H_2O$, 99.9%), sodium borohydride (NaBH4, min 98%), Cetrimonium bromide ($[(C_{16}H_{33})N(CH_3)_3]Br$), Sodium hydroxide (NaOH ≥97%) and ethanol (C_2H_6O, technical grade) were purchased from Merck.

Initially, a 0.02 M $CoCl_2.6H_2O$ solution was mixed with 80 ml ethanol and various quantities of CTAB surfactant to create a homogeneous suspension through ultrasonic bath and vigorous magnetic stirring. The pH of the mixture was adjusted to 4 for all solutions. The resulting solution was stirred at room temperature for 10 minutes, then further stirred for 30 minutes in a cryostat pre-set at 6°C. Subsequently, pure NaBH4 solution (10 mL) was added dropwise with stirring in a circulating water bath maintained at a constant temperature of 6 °C. The resulting black products were washed multiple times with distilled water and ethanol to eliminate unwanted ions from the catalyst. Finally,

the dried products were obtained in a vacuum oven at 110 °C. The abbreviations of the samples prepared using different amounts of CTAB are listed in Table 1.

Tab. 1: The abbreviations of the samples prepared using different amounts of CTAB

Amount of CTAB (mg)	Abbreviations
0	Co-B
25	Co-B/CTAB25
50	Co-B/CTAB50
75	Co-B/CTAB75
100	Co-B/CTAB100
150	Co-B/CTAB150

X-ray diffraction (XRD) analysis were performed on RIGAKU Smartlab X-ray diffractometer using Cu Kα radiation (α = 1.54 Å). The XRD data were collected in the range of 5°–95° 2θ and continuous scan mode. Morphology of catalysts and the elemental compositions of the catalysts were analyzed by scanning electron microscopy coupled with energy-dispersive X-ray spectroscopy (EDS), respectively.

Activity tests were conducted using 10 mg of dry catalyst and 10 ml of alkaline $NaBH_4$ solution in a batch-type reactor submerged in a thermostatic water bath to regulate the reactor temperature. The solution was stirred at 600 rpm using a Teflon-coated magnetic stirring bar.

III. Results and discussions

Fig. 1 illustrates both the final hydrogen generation rates for the various catalysts as a function of time, using 5% NaOH and 5% $NaBH_4$ concentrations. Hydrogen generation rates (HGR) are presented as HGR ($L.min^{-1}.g_{cat}^{-1}$).

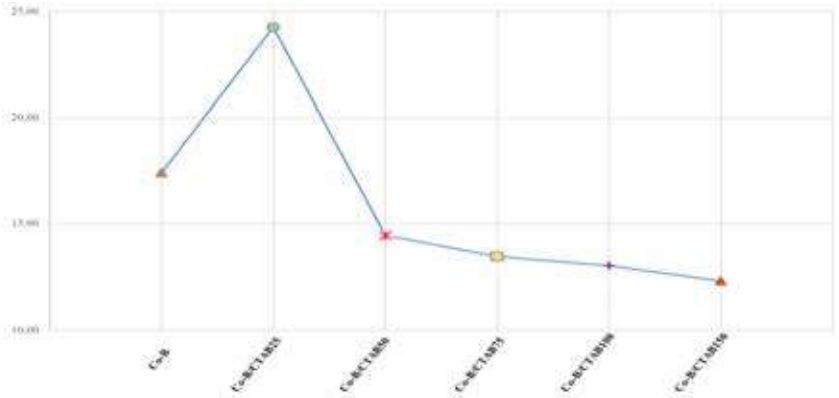


Fig.1: HGR results of different catalysts.

It was observed that the HGR value of the Co-B catalyst was 17.42 $L/(min.g_{cat})$ and increased to 24.25 $L/(min.g_{cat})$ after the addition of 25 mg CTAB. It was observed that the catalyst activity increased by approximately 40% as a result of the addition of 25 mg CTAB surfactant and with increasing CTAB amount, the catalytic activity shows a significant decrease.

The obtained otpimum Co-B/CTAB25 catalyst was used for kinetic studies to determine the activation energy. Temperature also plays a role in determining the rate of hydrogen generation. The Arrhenius equation provides a valuable framework for understanding the relationship between the rate of hydrogen generation and temperature. Kinetic studies were conducted at temperature values of 35, 45, 55, and 65 °C. The resulting graph is shown in Fig. 2.

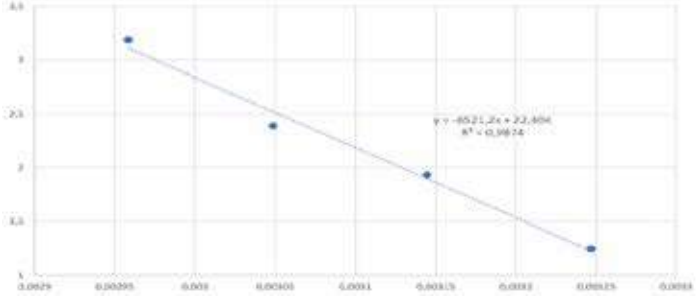


Fig.2. Temperature effect on HGR of CoB-/CTAB25.

As can be seen from the figure, there is a correlation coefficient value of 0.9874, indicating a good fit to the obtained

data. By using these data, the activation energy was determined to be 54.22 kJ/mol. Activation energy is an important indicator for reactions that indicates required barrier energy for reaction. It may be concluded that CoB/CTAB25 has relatively smaller value according to literature.

Fig. 3 shows the XRD patterns both of Co–B and CoB/CTAB25 samples. As observed in Fig. 3, a weak and broad diffraction peak is evident around 2θ = 45 for the Co-B sample. This peak signifies the characteristic feature of CoB alloys, indicating a short-range ordered structure typical of amorphous catalysts, with irregularity observed over longer distances. In contrast to Co-B catalysts, the addition of the surfactant leads to the disappearance of the Co-B peak, while different peaks emerge around 2θ = 35 - 40° and approximately 59.6°. These low-intensity Bragg peaks are attributed to the CoO phase. In the Co-B/CTAB25 and Co-B/CTAB150 samples, the CoO phase is distinctly identified. These peaks are also associated with the $Co(OH)_2$ phase (Huang, Wang et al. 2008).

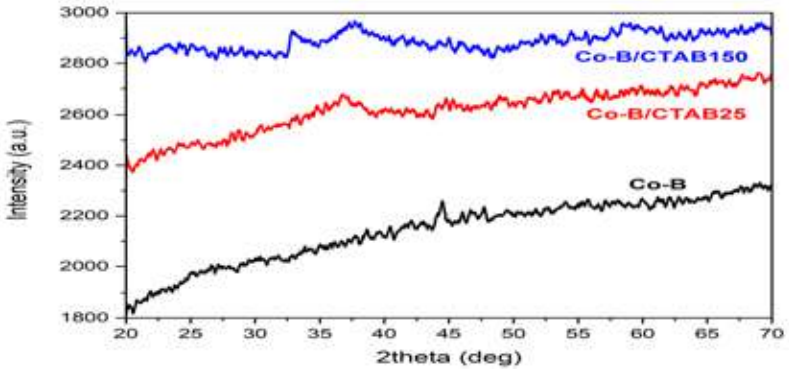


Fig.3. XRD patterns of Co–B, Co-B/CTAB150 and Co-B/CTAB25.

FESEM images were obtained to examine the morphology of the synthesized catalysts. Figure 5 depicts FESEM images of Co-B, Co-B/CTAB25, and Co-B/CTAB150 samples at different magnifications. It can be observed that the nanoparticles of the Co-B catalyst without CTAB surfactant have larger grains. Agglomeration of catalyst particles occurred due to the exothermic reaction during the preparation of the Co-B alloy via chemical reduction with NaBH4 and the magnetic properties of Co-B catalysts. EDS analyses indicate a significant presence of oxygen in the catalyst structure. Additionally, the percentage of oxygen increases with the addition of CTAB. It is believed that the cationic head (S+) of the CTAB surfactant cannot directly interact with the cobalt cations (Co^{+2}) in the solution, but rather interacts to a limited extent via the hydroxide anions ($S^{+}OH^{-}Co^{2+}$) present in the solution. As a result, compared to the Co-B alloy, XRD results show the formation of Co-O_x components during reduction. These oxide components serve as a kind of support for the catalysts, preventing agglomeration due to both the exothermic reactions during reduction and magnetic interactions. However, the formation of oxide phases at high CTAB concentrations leads to a significant decrease in hydrogen production rate due to reasons such as low catalytic activity and a decrease in the Co-B alloy. This suggests that the Co-B/CTAB25 catalyst may have a larger active surface area for the hydrolysis of NaBH4. The addition of 25 mg of CTAB surfactant resulted in the maximum hydrogen production rate. Table 2 and Figure 6 display the surface composition and spectra of the synthesized catalysts.

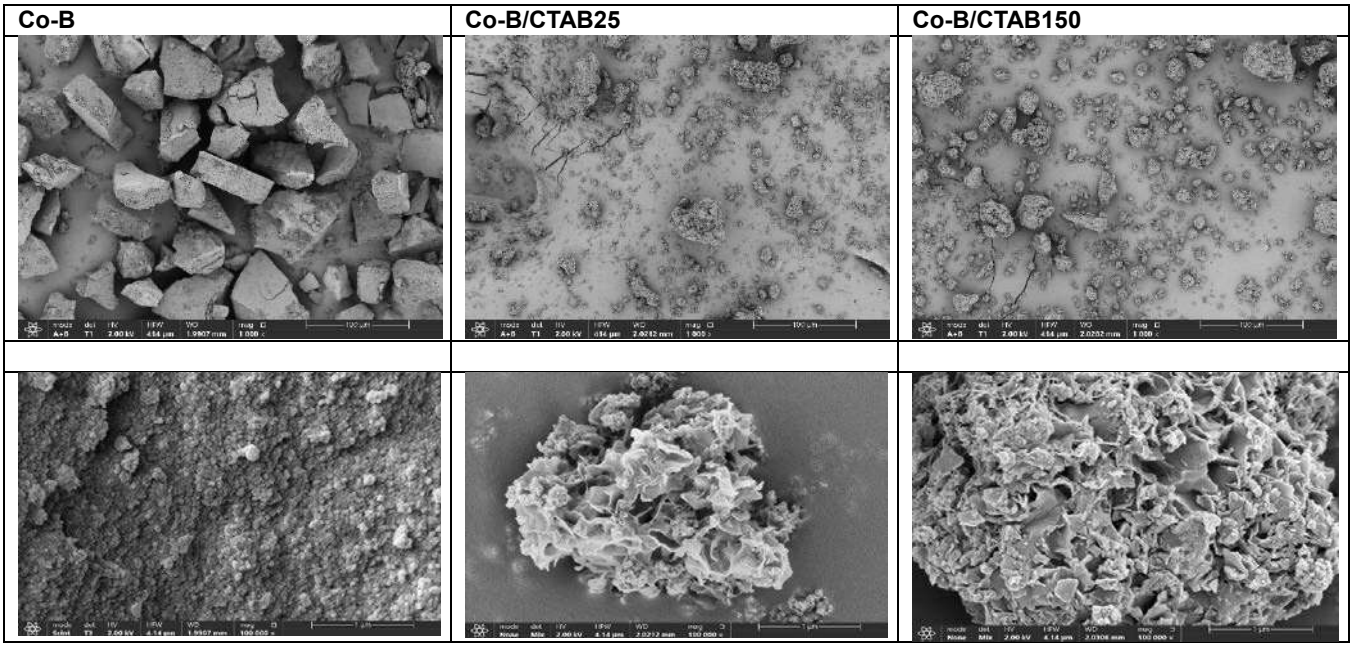


Fig.4. FESEM images at different magnifications of the synthesized catalysts.

Tab. 2: The EDS analysis of the catalysts

Element	Co-B		Co-B/CTAB25		Co-B/CTAB150	
	at%	wt.%	at%	wt.%	at%	wt.%
B	3.7	1.3	3.2	1.1	2.7	1.1
N	2.2	1.0	2.0	0.9	1.5	0.8
Br	0.0	0.0	0.0	0.0	0.0	0.0
C	9.7	3.8	6.9	2.7	6.4	2.8
O	49.1	25.7	51.3	26.4	62.9	37.3
Co	35.3	68.2	36.4	68.9	26.5	57.9

V. Conclusions

The highest hydrogen production rate was obtained with CoB/CTAB25 catalysts prepared with the addition of 25 mg CTAB, and a decrease in the efficiency of the catalysts was observed with increasing CTAB. XRD and FESEM analyzes of CoB, CoB/CTAB25 and CoB/CTAB150 catalysts, which have the lowest hydrogen production rate, were performed and the reason for the increase in catalytic activity was investigated. It was observed that different CoO phases were formed along with the CoB alloy during the preparation of the catalysts with the addition of CTAB. It is known that these CoO compounds formed do not have any activity for the hydrolysis reaction, but these oxidized phases serve as support material for CoB catalysts and prevent the catalysts from agglomerating under exothermic reaction conditions. As the amount of CoB catalysts decreases with increasing CTAB ratio, hydrolysis performance decreases.

Acknowledgements

This study was supported within the scope of the project numbered 122M515 by TÜBİTAK.

References

Bosu, S. and N. Rajamohan (2024). "Recent advancements in hydrogen storage-Comparative review on methods, operating conditions and challenges." International journal of hydrogen energy 52: 352-370.
Drawer, C., et al. (2024). "Metal hydrides for hydrogen storage–Identification and evaluation of stationary and transportation applications." Journal of energy storage 77: 109988.
Fakioğlu, E., et al. (2004). "A review of hydrogen storage systems based on boron and its compounds." International journal of hydrogen energy 29(13): 1371-1376.
Huang, Y., et al. (2008). "Accurately measuring the hydrogen generation rate for hydrolysis of sodium borohydride on multiwalled carbon nanotubes/Co–B catalysts." International journal of hydrogen energy 33(23): 7110-7115.
Kaya, C., et al. (2024). "Enhancing the efficiency of sodium borohydride hydrolysis with a novel CoB-Triton catalyst." International journal of hydrogen energy 51: 489-503.
Long, B., et al. (2022). "Synthesis of a Novel Ag/Co–B/CTAB Catalyst via Chemical Reaction at Room Temperature for Hydrolysis of Ammonia Borane." Energy Technology 10(9): 2200439.
Marbán, G. and T. Valdés-Solís (2007). "Towards the hydrogen economy?" International journal of hydrogen energy 32(12): 1625-1637.
Marrero-Alfonso, E. Y., et al. (2009). "Hydrogen generation from chemical hydrides." Industrial & Engineering Chemistry Research 48(8): 3703-3712.
Marrero-Alfonso, E. Y., et al. (2007). "Minimizing water utilization in hydrolysis of sodium borohydride: the role of sodium metaborate hydrates." International journal of hydrogen energy 32(18): 4723-4730.
Midilli, A. and I. Dincer (2008). "Hydrogen as a renewable and sustainable solution in reducing global fossil fuel consumption." International journal of hydrogen energy 33(16): 4209-4222.
Muradov, N. Z. and T. N. Veziroğlu (2005). "From hydrocarbon to hydrogen–carbon to hydrogen economy." International journal of hydrogen energy 30(3): 225-237.
Ogden, J. M., et al. (2000). "Fuels for fuel cell vehicles." Fuel Cells Bulletin 3(16): 5-13.
Özkar, S. and M. Zahmakıran (2005). "Hydrogen generation from hydrolysis of sodium borohydride using Ru (0) nanoclusters as catalyst." Journal of alloys and compounds 404: 728-731.
Patel, N., et al. (2007). "Thin films of Co–B prepared by pulsed laser deposition as efficient catalysts in hydrogen producing reactions." Applied Catalysis A: General 323: 18-24.
Qiu, Y., et al. (2021). "Research progress of cryogenic materials for storage and transportation of liquid hydrogen." Metals 11(7): 1101.
Rampai, M., et al. (2024). "Hydrogen production, storage, and transportation: recent advances." RSC advances 14(10): 6699-6718.
Schlapbach, L. and A. Borgschulte (2008). Hydrogen as a Future Energy Carrier, Wiley-VCH.
Schlesinger, H., et al. (1953). "Sodium borohydride, its hydrolysis and its use as a reducing agent and in the generation of hydrogen1." Journal of the American Chemical Society 75(1): 215-219.
Shafirovich, E., et al. (2007). "Combustion-assisted hydrolysis of sodium borohydride for hydrogen generation." International journal of hydrogen energy 32(2): 207-211.
Stern, N. H. (2007). The economics of climate change: the Stern review, cambridge University press.
Veziroglu, T. N. (1998). "Dawn of the hydrogen age." International journal of hydrogen energy 23(12): 1077-1078.
Xu, Z., et al. (2024). "Influence of different cone angles for hydrogen adsorption of cup-stacked carbon nanotube: A DFT study." International journal of hydrogen energy 50: 1174-1188.

Synthesis of $Cd_{0.7}Zn_{0.3}S/MoS_2$ Catalysts and Investigation of Their Activities in Photocatalytic H_2 Production

İbrahim Kaba, Özge Kerkez Kuyumcu*
Marmara University, Faculty of Engineering, Chemical Engineering Department, Maltepe, İstanbul, 34854, Türkiye

* E-mail: ozge.kuyumcu@marmara.edu.tr

Abstract

Photocatalytic hydrogen generation is a viable sustainable energy alternative. Solar energy will be converted into hydrogen using semiconductor photocatalysts. This study generated $Cd_{0.7}Zn_{0.3}S/MoS_2$, an effective photocatalyst, for the first time in solvothermally uniformly dispersed nanocomposite form using diaminopropane. The effect of the MoS_2 ratio on catalyst efficiency was investigated. The photocatalysts were characterized using X-ray diffraction (XRD), UV-visible diffuse reflectance spectroscopy (UV-Vis DRS), and transmission electron microscopy (TEM).

Keywords: Photocatalytic H_2 production, $Cd_{0.7}Zn_{0.3}S/MoS_2$, photocatalyst.

I. Introduction

Photocatalytic hydrogen production is a way to produce hydrogen in a renewable way. An important topic of study in converting solar energy into chemical energy is the use of sunlight and semiconductor catalysts that support it in the production of photocatalytic hydrogen. Water splitting using semiconductor photocatalysts is considered a positive and clean method for photocatalytic hydrogen production (Reddy et al. 2016).

The water decomposition reaction is a thermodynamically involuntary reaction; For this to happen, energy input must be given to overcome the energy barrier of 1.23 eV. For the photocatalytic dissociation reaction of water to occur, a semiconductor must be excited by a photon with energy equal to or greater than its band gap energy. In this case, electrons move from the valence band to the conduction band, leaving holes in the valence band. Electrons (e^-) and holes (h^+) produced by the photon are formed. If the conduction band (CB) of the photocatalyst is more negative than the H^+/H_2 reduction potential and the valence band (VB) is more positive than the O_2/H_2O oxidation potential, the electrons and holes produced by this photon have the capacity to oxidize H_2O by reducing the H^+ cation, respectively. (Wang et al., 2019).

CdS is one of the metals sulfides used for H_2 production among semiconductor materials (Huang et al., 2020). Due to its narrow band gap (2.4 eV), co-catalysts are used together with CdS to prevent the recombination of photon-generated charges and increase the efficiency of H^+ reduction (Wu et al., 2017). At the same time, zinc is added at different rates to prevent photocorrosion on CdS and $Cd_xZn_{1-x}S$ photocatalyst is synthesized. It has been shown that activity changes by changing the cadmium/zinc ratio (Chen vd., 2020; Yu vd., 2020; Huang vd., 2020).

Many studies have shown that MoS_2 can be a co-catalyst instead of Pt for different semiconductor photocatalysts (TiO_2, ZnS, CdS, $ZnIn_2S_4$ and CdZnS) (Li et al., 2020; Zhu et al., 2014; Wei et al., 2014; Zhao et al., 2014). Hinnemann et al., (2005) found in their study that MoS_2 increased the activity of the hydrogen production reaction and showed that it was promising as a low-cost alternative co-catalyst compared to platinum. Wei et al., (2014) synthesized $MoS_2/ZnIn_2S_4$ nanocomposite and found that MoS_2 significantly increased hydrogen production. As a most important result, Pt and MoS_2 were compared as co-catalysts, and it was shown that MoS_2 gave better results under the same conditions. MoS_2 has outstanding electronic, optical, and catalytic properties and increases H_2 production efficiency through its use with semiconductor catalysts (He et al., 2019). Its structure has strong intralayer covalent bonds separated by a weak van der Waals gap, which is important for catalysis (Ertis et al., 2017). Zhao et al., (2016) showed that the efficiency was increased by adding MoS_2 and found 12.3 mmol·g-1h-1 H2 production with the $MoS_2/Cd_{0.5}Zn_{0.5}S$ photocatalyst. The reason for this is the photocatalyst with the structure $MoS_2/Cd_{0.5}Zn_{0.5}S$; The electrons produced by the photon are transferred from the conduction band of the $Cd_{0.5}Zn_{0.5}S$ photocatalyst to the conduction band of MoS_2 to produce H_2, and the holes produced by the photon oxidize the sacrificial agents. Wang et al., (2023) 13.5 mmol using 0.8% $MoS_2/Cd_{0.6}Zn_{0.4}S$ catalyst. The amount of MoS_2 co-catalyst in the photocatalyst has been determined as a factor affecting H_2 production (Li et al., 2020; Li et al., 2021).

II. Experimental Set-up and Procedure

Synthesis of $Cd_{0.7}Zn_{0.3}S$.

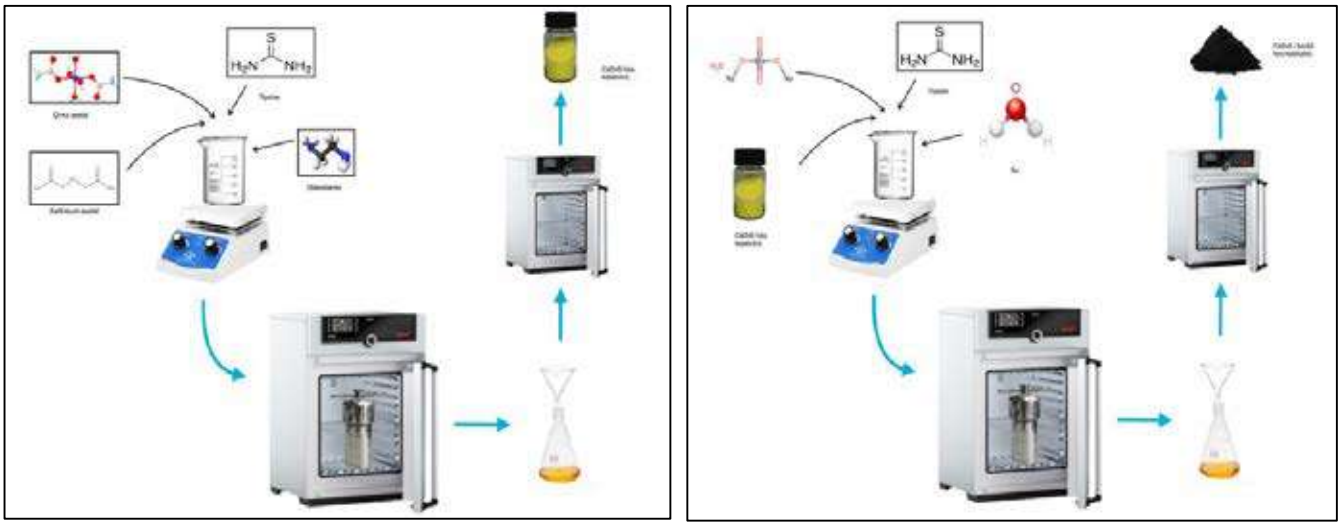
$Cd_{0.7}Zn_{0.3}S$ nanoparticles were produced using a solvothermal technique (Yu et al. 2020). $Cd(CH_3COO)_2 \cdot 2H_2O$ and $Zn(CH_3COO)_2 \cdot 2H_2O$ were dissolved (Cd/Zn = 7:3) in 1,3-DAP with vigorous magnetic stirring at room temperature. Then thiourea was added three times more than the total Cd and Zn mole number. After 60 minutes of stirring, the solution was transferred to a Teflon-coated stainless-steel autoclave and stored at 180°C for 24 hours. After the autoclave had naturally cooled down, the precipitate was filtered, washed several times with water, and dried overnight at 65°C.

Synthesis of $Cd_{0.7}Zn_{0.3}S/MoS_2$.

To create binary photocatalysts with varying MoS_2 content by weight, $Cd_{0.7}Zn_{0.3}S$ nanoparticles were suspended in water and $Na_2MoO_4 \cdot 2H_2O$ was added as a precursor. Thiourea was used as a sulfurizing agent. After 60 minutes in an ultrasonic bath, the suspension was transferred to a Teflon-coated stainless-steel autoclave and stored at 180°C for 24 hours. After the autoclave had naturally cooled down, the precipitate was filtered, washed several times with water, and dried overnight at 65°C.

Photocatalytic hydrogen generation

Photocatalytic hydrogen generation reactions were carried out in a 250 mL quartz reactor. In all studies, 150 ml of 0.25 M Na_2S-0.35 M Na_2SO_3 solution were utilized. The Philips 13095 halogen lamp was used to simulate sunlight, and the distance between the photocatalyst and the light source was adjusted to achieve a light intensity of 1000 W/m^2. The gas in the reactor was sampled using a gas syringe at regular intervals and examined using gas chromatography.



(A) (B)

Fig. 1: (A) Synthesis procedure of $Cd_{0.7}Zn_{0.3}S$ nanoparticle photocatalysts and (B) Synthesis procedure of $Cd_{0.7}Zn_{0.3}S$ / MoS_2 photocatalysts.

III. Analysis

Characterization of Photocatalyst

The characterization techniques briefly described below were applied to the synthesized solid photocatalysts. XRD (X-ray diffraction): The crystal structure of the synthesized catalysts was examined. TEM (Transmission electron microscopy): It was possible to visualize the surface and fine structures of the synthesized catalysts in more detail. Clusters, structure, and shape dimensions were examined. UV-vis DRS spectrophotometry: Band gaps of the samples were calculated using the obtained absorbance curves. The effect of co-catalysts on the band gap was demonstrated.

IV. Results and discussions

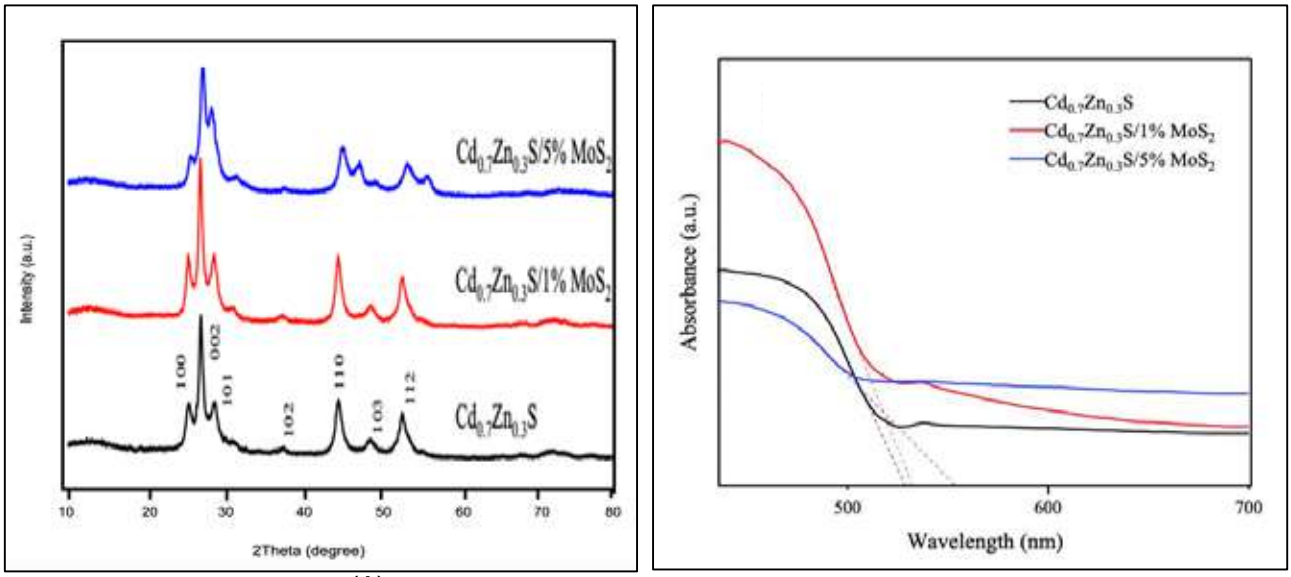


Fig. 2: (A) XRD patterns of $Cd_xZn_{1-x}S/MoS_2$ photocatalysts and (B) UV-vis absorbtion spectra of (a) $Cd_{0.7}Zn_{0.3}S$, $Cd_{0.7}Zn_{0.3}S$/1% MoS_2 and $Cd_{0.7}Zn_{0.3}S$/5% MoS_2.

Figure 2.A shows the XRD patterns of the photocatalysts containing CdZnS and MoS_2 contents. When $Cd_{0.7}Zn_{0.3}S$ samples are examined, it is observed that the diffraction patterns are like hexagonal phase CdS (JCPDS card No. 41–1049) (Rao et al., 2011). For the $Cd_{0.7}Zn_{0.3}S$ sample, peaks at 25.6, 27.09, 28.85, 37.72, 44.81, 48.88, and 53.11 are donated to the (100), (002), (101), (102), (110), (103), and (102) planes, respectively (Zhao et al., 2022). Figure 2.B indicates UV-vis absorption spectrum of the photocatalysts and the absorption wavelength edges and corresponded band gap values for each photocatalyst were calculated. Pure $Cd_{0.7}Zn_{0.3}S$ revealed an absorption edge at 528 nm, which corresponds to a 2.34 eV band gap. Furthermore, adding MoS_2 progressively to $Cd_{0.7}Zn_{0.3}S$ resulted in a shift across the visible range.

Figure 3.A shows the hydrogen production rate according to time. For hydrogen production, measurements were taken at 1 hour time intervals and the production rate was calculated. In Figure 3.B, three different samples were used as 10 mg and the production rates of each catalyst after 5 hours are given. It has been observed that when the amount of MoS_2 increases, the hydrogen production rate decreases. However, with the addition of MoS_2, the speed increased compared to the pure $Cd_{0.7}Zn_{0.3}S$ catalyst.

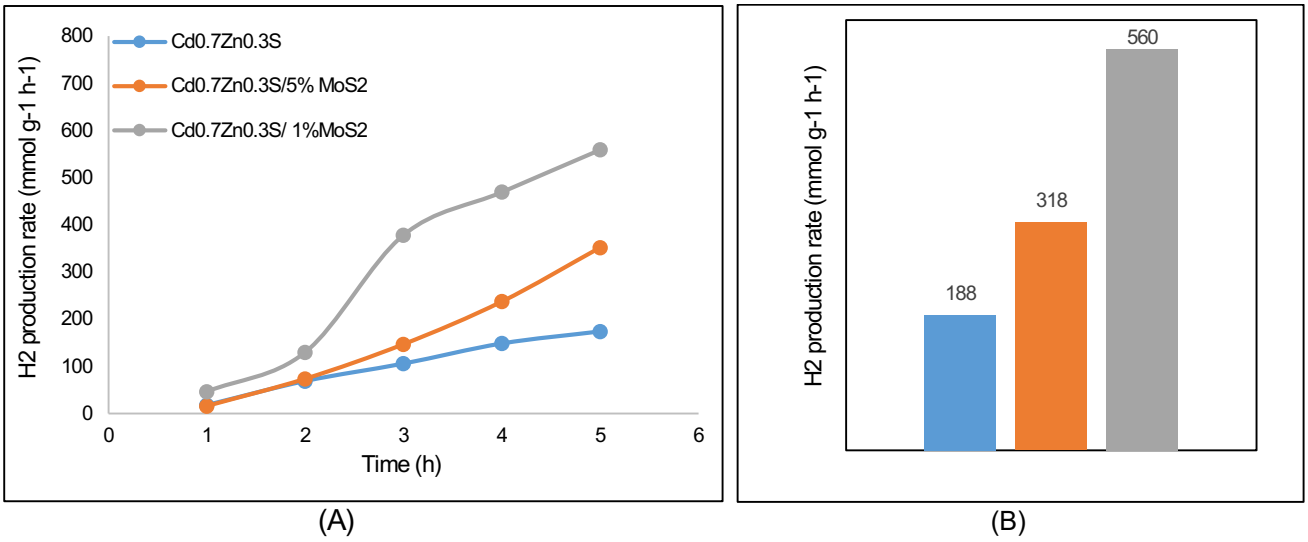


Fig. 3: (A) Time-dependent H_2 production activities and (B) Photocatalytic H_2 production rates of $Cd_{0.7}Zn_{0.3}S$, $Cd_{0.7}Zn_{0.3}S$/1 % MoS_2 and $Cd_{0.7}Zn_{0.3}S$/5 % MoS_2.

V. Conclusions

In the study, $Cd_{0.7}Zn_{0.3}S$ catalyst were synthesized as nanoparticles by a solvothermal method in an autoclave with using DAP. To increase the effectiveness of the catalyst, MoS_2 substituted for Pt was added hydrothermally at different mass percentages (1% and 5%). The $Cd_{0.7}Zn_{0.3}S$ /1%MoS_2 catalyst showed a hydrogen production rate of 560 mmol g^{-1} h^{-1}. The hydrogen production rate increased approximately 3 times compared to bare $Cd_{0.7}Zn_{0.3}S$.

Acknowledgements

This research was supported by TUBITAK 1002-A with Project No 123M629 and Scientific Research Projects Unit of Marmara University (Project No FYL-2024-11093).

References

Chen, Y. C., Huang, Y. S., Huang, H., Su, P. J., Perng, T. P., ve Chen, L. J., Photocatalytic enhancement of hydrogen production in water splitting under simulated solar light by band gap engineering and localized surface plasmon resonance of $Zn_xCd_{1-x}S$ nanowires decorated by Au nanoparticles, Nano Energy, 67, 104225, (2020).

Huang, H. B., Fang, Z. B., Yu, K., Lü, J., ve Cao, R., Visible-light-driven photocatalytic H_2 evolution over CdZnS nanocrystal solid solutions: interplay of twin structures, sulfur vacancies and sacrificial agents, Journal of Materials Chemistry A, *8*(7), 3882-3891, (2020).

Li, Y., Sun, B., Lin, H., Ruan, Q., Geng, Y., Liu, J., ... Tam, K. C., Efficient visible-light induced H_2 evolution from T-$Cd_xZn_{1-x}S$/defective MoS_2 nano-hybrid with both bulk twinning homojunctions and interfacial heterostructures, Applied Catalysis B: Environmental, 2*67*, 118702, (2020).

Li, Y., Wan, S., Lin, C., Gao, Y., Lu, Y., Wang, L., ve Zhang, K., Engineering of 2D/2D $MoS_2/Cd_xZn_{1-x}S$ photocatalyst for solar H_2 evolution coupled with degradation of plastic in alkaline solution, Solar RRL, *5*(6), 2000427, (2021).

Rao, B. S., Kumar, B. R., Reddy, V. R., Rao, T. S., & Chalapathi, G. J. C. L., Preparation and characterization of CdS nanoparticles by chemical co-precipitation techniqueü Chalcogenide Lett, 8(3), 177-185, (2011).

Reddy, D. A., Kim, H. K., Kim, Y., Lee, S., Choi, J., Islam, M. J., ... ve Kim, T. K, Multicomponent transition metal phosphides derived from layered double hydroxide double-shelled nanocages as an efficient non-precious co-catalyst for hydrogen production, Journal of Materials Chemistry A, *4*(36), 13890-13898, (2016).

Wang, Y., Yang, C., Guo, L., Yang, Z., Jin, B., Du, R., ... & Wang, D., Plate-on-plate structured $MoS_2/Cd_{0.6}Zn_{0.4}S$ Z-scheme heterostructure with enhanced photocatalytic hydrogen production activity via hole sacrificial agent synchronously strengthen half-reactions, Journal of Colloid and Interface Science, 630, 341-351, (2023).

Yu, K., Huang, H. B., Zeng, X. Y., Xu, J. Y., Yu, X. T., Liu, H. X., ... & Cao, R., CdZnS nanorods with rich sulphur vacancies for highly efficient photocatalytic hydrogen production, Chemical communications, 56(56), 7765-7768, (2020).

Zhao, H., Fu, H., Yang, X., Xiong, S., Han, D., & An, X., MoS_2/CdS rod-like nanocomposites as high-performance visible light photocatalyst for water splitting photocatalytic hydrogen production, International Journal of Hydrogen Energy, 47(13), 8247-8260, (2022).

Zhao, S., Huang, J., Huo, Q., Zhou, X., & Tu, W., A non-noble metal MoS_2–$Cd_{0.5}Zn_{0.5}S$ photocatalyst with efficient activity for high H_2 evolution under visible light irradiation, Journal of Materials Chemistry A, 4(1), 193-199, (2016).

Synthesis of $CuS/CuInS_2/TiO_2$ Catalysts and Investigation of Their Activities in Photocatalytic H_2 Production

Elif Tuğba Yilmaz, İbrahim Kaba, Özge Kerkez Kuyumcu*
Marmara University, Faculty of Engineering, Chemical Engineering Department, Maltepe, İstanbul, 34854, Türkiye

* E-mail: ozge.kuyumcu@marmara.edu.tr

Abstract

Photocatalytic hydrogen production is a sustainable energy alternative. Solar energy would be converted into hydrogen using semiconductor photocatalysts. This study aims to synthesize $CuS/CuInS_2/TiO_2$ nanocomposite to increase H_2 production under solar light. CuS, $CuInS_2$ and TiO_2 were combined in different proportions by two different routes: solid mixture and in-situ hydrothermally. The photocatalysts were characterized using X-ray diffraction (XRD), UV-visible diffuse reflectance spectroscopy (UV-Vis DRS), photoluminescence spectroscopy and scanning electron microscopy (SEM). As the result of the photocatalytic hydrogen production tests, $3\%CuS/10\%CuInS_2/TiO_2$ prepared by in-situ hydrothermal method showed the highest activity with 1165 μmol H_2 g^{-1} after 8 hours.

Keywords: Photocatalytic H_2 production, CuS, $CuInS_2$, TiO_2

I. Introduction

Semiconductor materials based on metal sulfides are used in hydrogen production due to their semiconductor and photoelectronic properties needed in hydrogen production, such as narrow band gaps, large specific surface areas and suitable band structures. Binary metal sulfides (BMS) and ternary metal sulfides (TMS) have been tried to support the hydrogen evolution rate of TiO_2 photocatalysts. TiO_2, which has a relatively wide band gap energy (about 3.2 eV), can be activated by UV radiation, which constitutes only about 5% of the sunlight spectrum [Li et al, 2014]. In this context, modification of TiO_2 with metal sulfides such as CdS, PbS, MoS_2, which have low band gap energy, and making it sensitive to the visible light region, which constitutes approximately 43% of the sunlight spectrum, are among the studies carried out [Zheng et al., 2019]. Compared with BMS, ternary metal sulfides (TMSs) generally have high activity, favorable chemical stability, flexible element compositions, and a tunable band structure. The scientific route of usage of BMS/TiO_2, and the combination of TMS and TiO_2, constructing $AgGaS_2/TiO_2$, $AgIn_5S_8/TiO_2$, $AgInS_2/TiO_2$, $AgBiS_2/TiO_2$, $CuInS_2/TiO_2$, and $ZnIn_2S_4/TiO_2$ heterojunction photocatalysts, have been developed for the application of photocatalytic hydrogen evolution via water splitting [Liu et al., 2022]. In a study conducted in 2018, it was reported that the H_2 production rate increased further by loading TiO_2 with $CuInS_2$ and MoS_2 structures together. It was noted that the highest H_2 production amount, 1034 μmol/g/h, was achieved by the $TiO_2/CuInS_2/MoS_2$ photocatalyst containing 0.6 mmol/g $CuInS_2$ and 0.5 wt% MoS_2 under visible light irradiation (λ>420 nm) [Yuan et al., 2018]. CuS, which has a relatively small band gap (about 2.13 eV) compared to TiO_2, promotes extensive photocatalytic hydrogen evolution in the visible light region. $CuInS_2$, a non-toxic, ternary semiconductor material, has many advantages such as a narrow band gap of approximately 1.53 eV, stable properties and a large absorption coefficient. In the light of this knowledge, this study investigated about the photocatalytic activity for the $CuS/CuInS_2/TiO_2$ catalysts.

II. Experimental Set-up and Procedure

Synthesis of TiO_2

First, solution A is prepared by mixing 3 ml of titanium tetra-isopropoxide and 10.6 ml of anhydrous propanol. Solution B is created by mixing 0.3 ml anhydrous propanol, 0.15 ml distilled water and 11.1 ml acetic acid. After both solutions are ready, solution B is added dropwise to solution A to obtain a clear transparent solution. After the solution reaches a milky consistency at room temperature after a few hours, it is waited for a few more hours and a gel consistency is obtained. Next, a drying step was performed at 120 °C for 5 h to remove volatile solvents, and then a xerogel was obtained and ground in an agate mortar. The final powder is achieved by calcining the precipitation at 500°C for 2 hours.

Synthesis of $CuS/CuInS_2/TiO_2$ by solid mixture method

For CuS synthesis, specified amounts of $Cu(NO_3)_2{\cdot}3H_2O$ and H_2NCSNH_2 are dissolved in 80 ml of deionized water under magnetic stirring. After 30 minutes, the solution is transferred to a 100 ml teflon-lined stainless steel autoclave and heated at 180°C for 5 hours. After the autoclave naturally cooled to room temperature, the resulting black CuS precipitates are collected by filtration and washed several times with distilled water and pure ethanol. Finally, the precipitate is dried in vacuum at 60°C.

For $CuInS_2$ synthesis, specified amounts of $Cu(NO_3)_2{\cdot}3H_2O$, H_2NCSNH_2 and $InCl_3{\cdot}4H_2O$ dissolved in 80 ml of

deionized water under magnetic stirring. After 30 minutes, the solution is transferred to a 100 ml teflon-lined stainless steel autoclave and heated at 180°C for 5 hours. After the autoclave naturally cooled to room temperature, the resulting black $CuInS_2$ precipitates are collected by filtration and washed several times with distilled water and pure ethanol. Finally, the precipitate is dried in vacuum at 60°C.
Certain proportions of CuS (0.5%, 1% and 3%), $CuInS_2$ (5%, 10% and 20%) and TiO_2 by weight were milled in an agate mortar. A few drops of ethanol were added to the powder mixture to ensure better mixing of the powder sample.

Synthesis of CuS/$CuInS_2$/TiO_2 by in-situ hydrothermal method
CuS/$CuInS_2$/TiO_2 photocatalysts were synthesized in autoclave using the in-situ method. The precursors of CuS and $CuInS_2$ were weighted as to achieve 3%CuS/(%5, %10, %20)$CuInS_2$/TiO_2.

Photocatalytic hydrogen production
160 ml, 0.25 M Na_2S-0.35 M Na_2SO_3 solution was loaded into a homemade quartz-based reactor to perform photocatalytic hydrogen production reactions. 50 mg photocatalyst was used for each experiment. HAL-320 Compact Xenon Light Source Solar Simulator was used as the source of light and the light intensity was adjusted to 1000 Wm^{-2}. A water manometer was used to measure the amount of gas that evolved. The gas collected was analyzed by GC (Agilent 6890); H_2 was qualitatively recognized.

III. Analysis

Characterization of Photocatalyst

The characterization techniques briefly described below were applied to the synthesized solid photocatalysts. XRD (X-ray diffraction): The crystal structure of the synthesized catalysts was examined. SEM (Scanning electron microscopy): It was possible to visualize the surface and fine structures of the synthesized catalysts in more detail. UV-vis DRS spectrophotometry: Band gaps of the samples were calculated using the obtained absorbance curves. The effect of co-catalysts on the band gap was demonstrated. PL (Photoluminescence spectroscopy): Photogenerated electron hole recombination rates were investigated.

IV. Results and discussions

Figure 1(a) represents XRD pattern of the photocatalysts. The characteristic peaks at 25.40º, 38.00º, 48.23º and 55.30º in the XRD pattern of the synthesized TiO_2 sample correspond to the (101), (112), (200) and (211) planes of the anatase phase, respectively. In addition, the peaks at 27.65º, 54.17º, 63.00º, 69.16º and 70.64º correspond to the (110), (211), (002), (301) and (112) planes of the rutile phase, respectively. It was determined that the TiO_2 synthesized in this study contained 85.5% anatase and 14.4% rutile phase. For as-prepared CuS sample the peaks observed at 27.24°, 29.35°, 31.81°, 32.81°, 47.93°, 52.73°, and 59.34° correspond to the direction of 101, 102, 103, 006, 110, 108, and 116, respectively [Li et al., 2012]. For as-prepared $CuInS_2$ sample the peaks located at 2θ values of 27.90°, 32.74°, and 55.05° can be assigned to (112), (200) and (312) planes of tetragonal structure of $CuInS_2$ respectively [Pervaiz et al., 2022]. 3%CuS/10%10$CuInS_2$/TiO_2 photocatalyst sample denoted as 3CS10CIST(in-situ); it shows the mainly the characteristic peaks of TiO_2 and additionaly it shows the CuS and $CuInS_2$ peaks that it is concluded CuS/$CuInS_2$/TiO_2 sample was prepared successfully. Figure 1(b) represents PL spectra of the photocatalysts. All of the modified TiO_2 photocatalyst samples demonstrate lower intensity than bare TiO_2, implying that CuS and $CuInS_2$ additon reduces the recombination of photogenerated electron hole pairs.

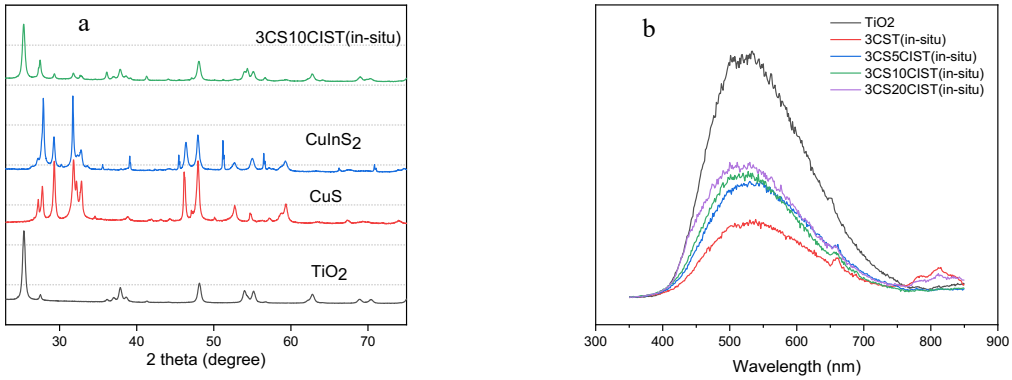


Fig. 1: (a) XRD Pattern of the photocatalyst samples, (b) PL spectra of the photcatalyst samples

Figure 2 represents the photocatalytic hydrogen production results of the 3%CuS/(5%, 10%, 20%)$CuInS_2$/TiO_2 photocatalysts prepared by two different method. 3%CuS/10%$CuInS_2$/TiO_2 prepared by in-situ hydrothermal

method showed the highest activity with 1165 μmol H_2 g^{-1} after 8 hours. While, 3%CuS/5%$CuInS_2$/TiO_2 prepared by solid mixture method showed 915 μmol H_2 g^{-1} after 8 hours.

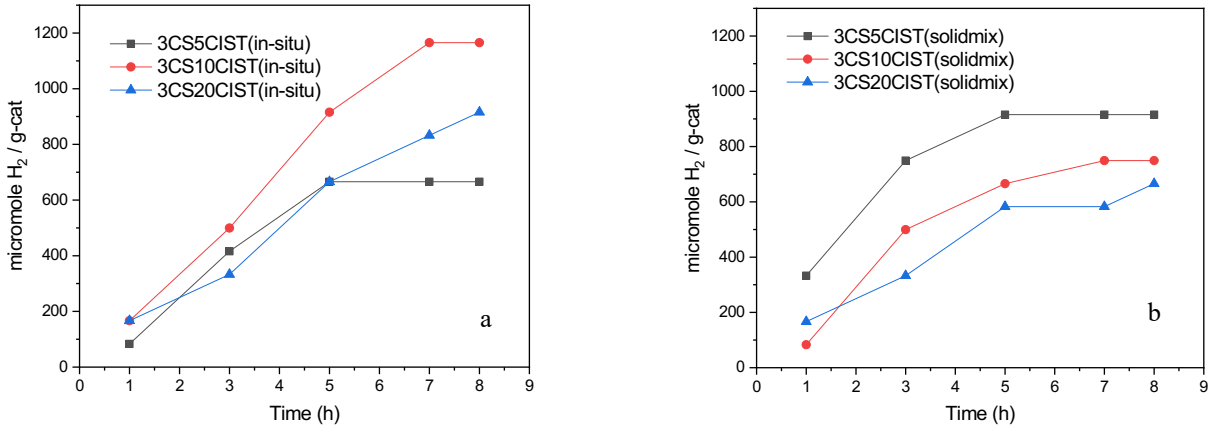


Fig. 2: Photocatalytic hydrogen production results under solar light by (a) photocatalysts prepared by in-situ hydrothermal method (b) photocatalysts prepared by solid mixture method

V. Conclusions

Photocatalytic hydrogen production activity of CuS/$CuInS_2$/TiO_2 photocatalysts were investigated in terms of the CuS and $CuInS_2$ proportions in the nanocomposite prepared by two different synthesis method. Moreover the use of TiO_2 with low band gap semiconductor metal sulfides has not only increased light absorption but also suppressed the recombination of photon-generated charge carriers, resulting in significant results in terms of hydrogen production amount.

Acknowledgements

This research was supported as TUBITAK 2209-A project.

References

Li Y.,Zhang Z., Zhang Y., Sun X., Zhang J., Wang C., Peng Z., Si H., Preparation of Ag doped Bi_2O_3 nanosheets with highly enhanced visible light photocatalytic performances, Ceramics International 40(8), Part B,13275-13280, (2014).

Li Z., Mi L., Chen W., Hou H., Liu C., Wang H., Zheng Z., Shen C., Three-dimensional CuS hierarchical architectures as recyclable catalysts for dye decolorization, CrystEngComm, 14, 3965-3971, (2012).

Liu Y., Zheng X., Yang Y., Li J., Liu W., Shen Y., Tian X., Photocatalytic Hydrogen Evolution Using Ternary-Metal-Sulfide/TiO_2 Heterojunction Photocatalysts, ChemCatChem,14, e202101439, (2022).

Pervaiz H., Khan Z. S., Shahzad N., Ahmed N., Jamil Q., Synthesis and characterization of $CuInS_2$ nanostructures and their role in solar cell applications, Materials Chemistry and Physics 290, 126602, (2022).

Yuan Y.-J., Fang G., Chen D., Huang Y., Yang L.-X., Cao D.-P., Wang J., Yu Z.-T., Zou Z.-G., High light harvesting efficiency $CuInS_2$ quantum dots/TiO_2/MoS_2 photocatalysts for enhanced visible light photocatalytic H_2 production, Dalton Trans., 47, 5652, (2018).

Zheng L., Teng F., Ye X., Zheng H., Fang X., Photo/Electrochemical Applications of Metal Sulfide/TiO_2 Heterostructures, Adv. Energy Mater., 10, 1902355, (2020).

Optimal design of a solar powered on-grid hybrid charging station for electric-hydrogen vehicles

[1*]Habip Sahin, [2]Cihangir Kale [2]Hikmet Esen

[1] Department of Electricity and Energy, Vocational School of Technical Sciences, Fırat University, Elazığ, Türkiye
[2] Department of Energy Systems Engineering, Faculty of Technology, Fırat University, Elazığ, Türkiye

* E-mail: hsahin@firat.edu.tr

Abstract
Nowadays, battery and plug-in hybrid electric vehicles are quite common, and hydrogen fueled electric vehicles are also started to be introduced to the market. For this reason, studies on environmentally friendly and economical optimum energy management systems for charging stations for electric and hydrogen fueled vehicles, which do not create excessive load on the existing network, are rapidly increasing.

In this study, an analysis of a solar powered on-grid hybrid charging station for electric-hydrogen vehicles installed in Diyarbakır, Turkey was carried out. The on-grid energy power system was designed to meet the load of 2514 kWh/d electric and 10 kg/d hydrogen. As optimal design results, the net present cost of the system is $7.81 million and the levelized cost of electricity is 0.435$/kWh with a renewable fraction of 59.6%.

Keywords: Electric vehicle charging stations, renewable energy sources, on-grid, HOMER.

I. Introduction

The number of electric vehicles (EV) is rapidly increasing at the global level, thanks to the introduction of EVs in many different classes and body structures to the market in recent years. The total number of EVs worldwide was 26 million in 2022. Forecasts show that the total number of EVs worldwide could reach 350 million units by 2030 (IEA, 2023). In response to these developments, the number of EVs in Türkiye, which was 14,500 by the end of 2022, reached 80,000 by the end of 2023 (TurkStat, 2024). This shows that EVs have just begun to develop their own markets in developing countries, and that there is a significant potential for increasing the use of EVs.
With the increase in EVs, electricity consumption demands will also increase, and in this respect, the issue of how to integrate them into the energy system is important for the electricity distribution system. It is obvious that charging the relatively small number of vehicles currently available will not require a large amount of electricity. However, it should be taken into consideration that charging stations (CS) will not be distributed homogeneously but will be clustered in residential groups in areas with high population density. For this reason, if EVs are charged in an uncontrolled manner without planning the CS infrastructure, it will negatively affect the functioning of distribution networks. Although they are not as popular as battery and plug-in hybrid electric vehicles, fuel cell electric vehicles (FCEV) will also become widespread in the near future. One of the most suitable solutions in this regard is renewable energy-supported energy storage CS solutions.
In this study, solar-powered on-grid hybrid EVCS that uses an electrolyzer and hydrogen tank system as a storage system was designed. When many vehicles need to be charged simultaneously, charging can be carried out without putting more pressure on the grid, especially during peak hours, by directly converting the hydrogen stored with excess power into electricity with a fuel cell (FC). Also, by this hybrid EVCS hydrogen refueling of FCEVs running on hydrogen can be carried out at the same time.

II. Experimental Set-up and Procedure

In this study, it is assumed that the solar-powered on-grid hybrid EVCS is located in Diyarbakır, Türkiye and that this EVCS has two Combined Charging System Combo 2 sockets with a maximum charging power of 150 kW each and is designed to meet the daily need for 10 kg of hydrogen. The electrical load profile of the hybrid EVCS is shown in Fig. 1. HOMER software is specifically designed to optimize the configurations of on-grid or off-grid power systems, and therefore, it is suitable to optimize the size of each component by techno-economic analysis.

PV array

A photovoltaic (PV) array was used as part of the hybrid EVCS system to limit the power drawn from the grid and to provide excess electricity to the electrolyzer. To calculate power output of a PV array Eq. 1 is used (HOMER, 2024).

$$P_{PV} = P_{PV,rated} f_{PV} \left(\frac{G_T}{G_{T,STC}} \right) \quad (1)$$

where $P_{PV,rated}$ rated power capacity of PV array (kW), G_T and $G_{T,STC}$ are solar radiation incident on the PV array at actual and standard test conditions (kW/m2), respectively and fPV is PV derating factor (%).

Elecrtolizer

PEM electrolyzers offer a number of advantages over other electrolyzers due to their simplicity, efficiency and hydrogen production capacity. Therefore, in this study, PEM electrolyzer was chosen as the hydrogen production system. Electrolyzer efficiency was taken as 80% (Gökek, 2010).

Hydrogen storage tank

The hydrogen tank is used to store produced hydrogen when there is an excess electricity or no hydrogen load to

meet the hydrogen or electricity demand when there is an excess hydrogen load or not enough electricity. It is assumed that there is no leakage, no treatment is needed and the initial amount of hydrogen is 50%.

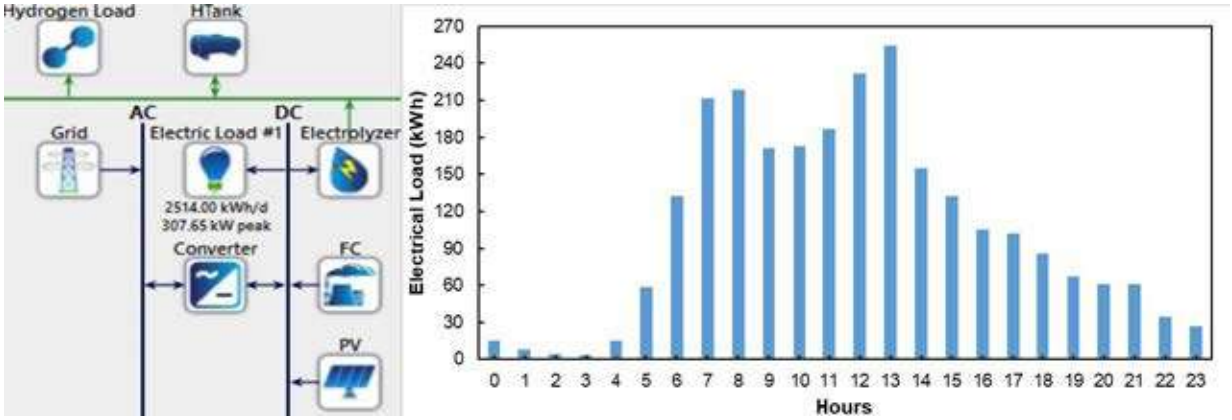


Fig. 1: Solar-powered on-grid hybrid EVCS and hourly electrical load profile

Fuel cell

PEMFC offer a number of advantages over other FCs due to their simplicity, mobility, fast response and low operation temperature. Therefore, in this study, PEMFC was chosen as a generator. PEMFC efficiency was taken as maximum 60%.

Converter

A converter both converts direct current (DC) to alternating current (AC) through a process known as inversion and AC to DC through a process known as rectification. The converter capacity was auto- in HOMER.

III. Analysis

Techno-economic analysis was performed using HOMER to evaluate the feasibility of hybrid EVCS based on net present cost (NPC). The NPC of the system is the difference between the present value of all expenses and the present value of all revenues earned over the lifetime of the system. The NPC of the system was determined using Eq. 2 (Homer Energy, 2016; Siyal et al., 2015).

$$C_{npc,tot} = \frac{C_{ann,tot}}{CRF} = \frac{C_{ann,tot}}{\frac{i(1+i)^n}{(1+i)^n-1}} = C_{ann,tot}\left\{\frac{\left(\frac{i'-f}{1+f}\right)\left(1+\left(\frac{i'-f}{1+f}\right)\right)^n}{\left(\frac{i'-f}{1+f}\right)\left(1+\left(\frac{i'-f}{1+f}\right)\right)^n-1}\right\}^{-1} \quad (2)$$

where, $C_{ann,tot}$ is the total annualised cost ($/yr),), *CRF* is the capital recovery factor, *i* is the annual real discount rate (%), *i'* is the nominal discount rate, *n* is the lifetime (year) and *f* is the expected inflation rate. In this study, the nominal discount rate and the expected inflation rate are taken into account as 5.5% and 3.2%, respectively (Central Bank of Republic of Türkiye, 2024). The economic analysis of the system considered was carried out by determining its life as 25 years. According to the definitions given in the HOMER database, levelised cost of electricity (LCOE) is the cost per kilowatt-hour of electricity produced. LCOE is determined by dividing the total annual cost by the amount of electricity produced, as given in Eq. 3 (Homer Energy, 2016).

$$LCOE = \frac{C_{ann,tot}}{E_{load}} \quad (3)$$

where E_{load} is the total electrical load (kWh/yr). Detailed technical and economic parameters for all components of the hybrid EVCS are specified in Table 1 (Babaei et al., 2022; HassanzadehFard et al., 2020; Rezk et al., 2019).

Tab. 1: Technical and economic parameters of components

Component	Capital Cost ($/kW)	Replacement ($/kW)	Operations & Maintenance Cost ($/kW)	Life Cycle (Year)	Capacity (kW)
Flat Generic Pv Panel	1000	1000	60	25	500
Electrolizer	1200	1200	20	25	150
Converter	300	300	-	25	207
Hydrogen Tank	500 ($/kg)	500 ($/kg)	-	25	800 (kg)
Fuel Cell	1200	1200	0.08 ($/kW/hr)	25	20

In the optimization process, all possible system configurations are listed, from the lowest NPC to the highest NPC, according to input parameters such as electricity and hydrogen load data, technical specifications and costs of the system components. Optimum configurations for different scenarios are given in Table 2.

The grid connection is provided by a 240 kVA transformer limited to a maximum capacity of 90%. When solar irradiation is sufficient, the electrical load is fed by solar power and hydrogen is produced through the electrolyzer

with the excess power. Otherwise, the difference between demand and solar power is primarily provided from the grid. In cases where neither is sufficient, remaining load demand is met by FC generating electricity from stored hydrogen. The system is fed by the grid at night, when there is no solar irradiation and the electrical load is low.

Tab. 2: Optimized scenarios for different configurations considered in the simulations.

Scenario	1	2	3	4
PV panel (kW)	500	500	500	496
Electrolizer (kW)	150	150	200	200
Fuel cell (kW)	20	20	30	30
Grid (kW)	216	216	216	216
Hydrogen tank (kg)	800	900	900	1000
Converter (kW)	207	207	207	207
NPC (M$)	7.81	7.88	7.96	8.03
LCOE ($/kWh)	0.435	0.439	0.453	0.458
Renewable Fraction (%)	59.6	59.6	59.6	59.3

IV. Results and discussions

As a result of the simulation, the scenario with the lowest NPC and LCOE and the highest capacity factors of the components is the first one, therefore the results of this scenario are examined. The aim of this study design a hybrid EVCS serving both battery EV and FCEV. By highlighting renewable energy sources (RES), dependence on the grid is reduced and the DC power produced is mostly used to feed the electrical load. Thus, no additional load is placed on the grid, especially at peak hours, and the disruptive effect on the grid due to DC-to-AC inversion is minimized (Fig. 2).

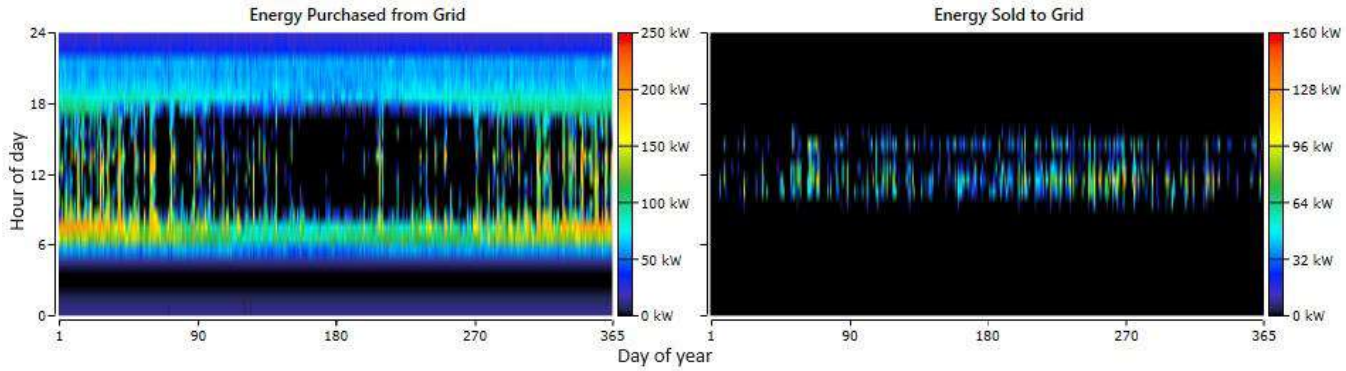


Fig. 2: Energy purchased from grid and sold to grid.

Annually, the energy drawn from PV, grid and FC is 779 MWh, 381 MWh and 18 MWh, respectively (Fig. 3). 27 MWh of this energy is sold to the grid, 213.5 MWh is spent in the electrolyzer, 20.5 MWh is lost in the converter and the remaining net 917 MWh is transferred to the load. Although FC production seems low, it fulfills the task of ensuring the energy supply security of the system and providing power to the load together with the grid and PV during peak hours and when solar power is low.

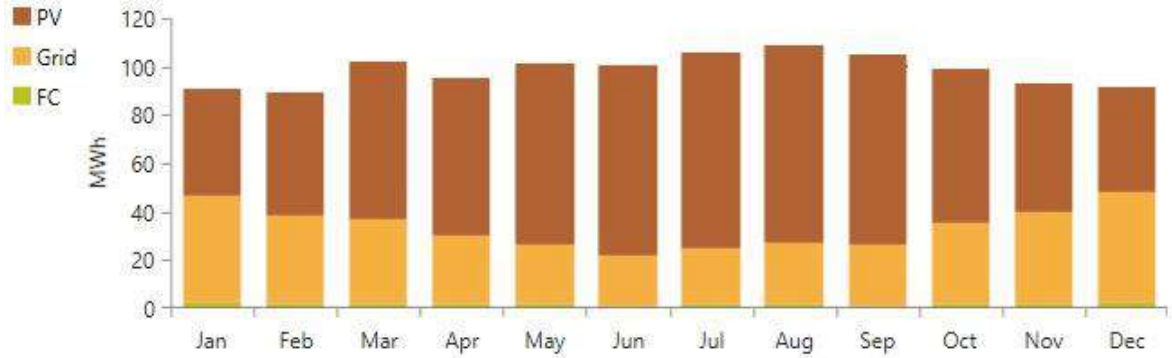


Fig. 3: Energy production from PV, Grid and FC.

The electrolyzer forms the energy storage function together with the hydrogen tank by producing fuel for the FC and hydrogen load. Annually, 4602 kg of hydrogen is produced by the electrolyzer, 3650 kg of which is consumed by FCEVs, which is assumed to be refueled with 5 kg twice a day, and 913 kg is consumed by FC. The electrolyzer is generally operated during hours when solar power is high, allowing excess power to be stored (Fig. 4).

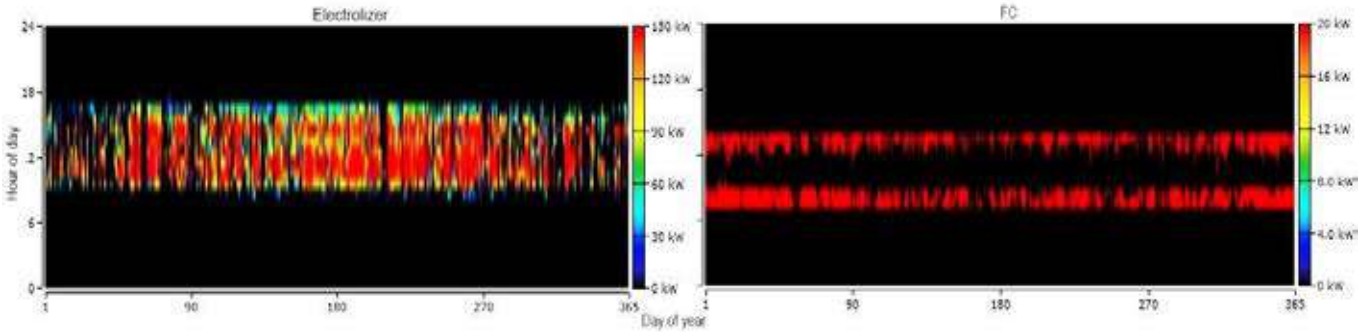


Fig. 4: Power of electrolyzer and FC

The hydrogen tank is important in terms of storing excess energy and meeting the fuel needs of hydrogen loads when needed. It is assumed that there is 400 kg (50%) hydrogen at the beginning, and at the end of the year the amount of hydrogen reaches 439 kg due to production being more than consumption (Fig. 5)

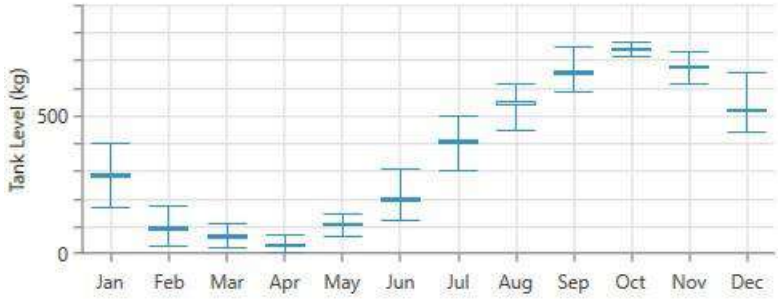


Fig. 5: Hydrogen tank level

As a result, 59.6% of the electrical and hydrogen loads are powered by RES, in accordance with the purpose of this study.

V. Conclusions

In this study, a techno-economic analysis was conducted to evaluate the feasibility of a solar powered on-grid hybrid EVCS installed in Diyarbakır, Türkiye, with a capacity of 2514 kWh/day and 10 kgH_2/day. The aim is to produce sustainable solutions by emphasizing the use of RES in order to meet the charging needs of rapidly expanding EVs without straining existing electrical infrastructures. The NPC and renewable fraction of the hybrid EVCS are $7.81 million and 59.6%, respectively. The LCOE for the system was found to be 0.435 $/kWh. These values will decrease further, especially with the decrease in electrolyzer and fuel cell costs.

References

Babaei, R., Ting, D.S.K., Carriveau, R., 2022. Optimization of hydrogen-producing sustainable island microgrids. Int. J. Hydrogen Energy 47, 14375–14392. https://doi.org/10.1016/J.IJHYDENE.2022.02.187

Central Bank of Republic of Türkiye, 2024. TCMB - Consumer Prices [WWW Document]. URL https://www.tcmb.gov.tr/wps/wcm/connect/EN/TCMB+EN/Main+Menu/Statistics/Inflation+Data (accessed 4.8.24).

Gökek, M., 2010. Hydrogen generation from small-scale wind-powered electrolysis system in different power matching modes. Int. J. Hydrogen Energy 35, 10050–10059. https://doi.org/10.1016/J.IJHYDENE.2010.07.149

HassanzadehFard, H., Tooryan, F., Collins, E.R., Jin, S., Ramezani, B., 2020. Design and optimum energy management of a hybrid renewable energy system based on efficient various hydrogen production. Int. J. Hydrogen Energy 45, 30113–30128. https://doi.org/10.1016/J.IJHYDENE.2020.08.040

HOMER, 2024. How HOMER Calculates the PV Array Power Output [WWW Document]. URL https://support.ul-renewables.com/homer-manuals-pro/how_homer_calculates_the_pv_array_power_output.html (accessed 4.8.24).

Homer Energy, 2016. HOMER Pro Version 3.7 User Manual. HOMER Energy 416.

IEA, 2023. Trends in electric light-duty vehicles – Global EV Outlook 2023 [WWW Document]. URL https://www.iea.org/reports/global-ev-outlook-2023/trends-in-electric-light-duty-vehicles (accessed 9.30.23).

Rezk, H., Sayed, E.T., Al-Dhaifallah, M., Obaid, M., El-Sayed, A.H.M., Abdelkareem, M.A., Olabi, A.G., 2019. Fuel cell as an effective energy storage in reverse osmosis desalination plant powered by photovoltaic system. Energy 175, 423–433. https://doi.org/10.1016/J.ENERGY.2019.02.167

Siyal, S.H., Mentis, D., Howells, M., 2015. Economic analysis of standalone wind-powered hydrogen refueling stations for road transport at selected sites in Sweden. Int. J. Hydrogen Energy 40, 9855–9865. https://doi.org/10.1016/J.IJHYDENE.2015.05.021

TurkStat, 2024. Distribution of Vehicles Registered to the Traffic by Fuel Type [WWW Document]. URL https://data.tuik.gov.tr/Bulten/Index?p=Road-Motor-Vehicles-February-2024-53454 (accessed 4.6.24).

Comparative Environmental Impact Evaluation of Diesel Fuels and Liquid Hydrogen in Transportation

*[2] Assem Abdurakhmanova and [1,2]Ibrahim Dincer
[1]Ontario Tech University, Clean Energy Research Laboratory, Oshawa, Ontario, Canada
[2]Yildiz Technical University, Clean Energy Technologies Institute, Istanbul, Türkiye

*Corresponding author's e-mail: assem.abdurakhman@gmail.com

Abstract
This study presents a comparative analysis between diesel fuels and liquid hydrogen as fuel sources across various transport modes, conducted using data from the GREET software. Four transport modes utilizing diesel fuels were examined: Car (CIDI ICEV - FT Diesel), Rail Commuter (FTD + Electricity), Rail Freight (FTD), and Rail Intercity (FTD + Electricity). For liquid hydrogen, identical transport modes were considered, with hydrogen production sourced from three pathways: The central Plants using natural gas, PEM electrolysis powered by solar or wind energy, and thermo-chemical cracking of water through nuclear energy. Emission indices including PM2.5, N_2O, CH_4, and CO_2 (kg/mile) were compared between diesel and hydrogen across the different transport modes and production pathways. The results indicate varying emissions profiles between diesel and hydrogen across the considered parameters, highlighting potential environmental implications and informing decision-making processes in transportation energy transitions. Specifically, the analysis revealed that while diesel exhibited lower CH_4 emissions (8.21E-04 kg/mi) compared to hydrogen in certain transport modes, hydrogen showed higher CO_2 emissions (0.4538 kg/mi), particularly when produced through central plants using natural gas.

Keywords: Hydrogen, Diesel, Life Cycle Assessment, Sustainable transport

1. Introduction
As the need to combat climate change increases, the transport sector is facing growing pressure to switch to sustainable fuel alternatives. Among these, liquid hydrogen appears to be a promising candidate. Hydrogen is a clean fuel and feedstock for making transport sector environmentally friendly. Hydrogen can play a major role in the transition to clean cities, especially in the transport sector, which is responsible for 26% of greenhouse gas emissions in Europe [1]. This study conducts a comparative life cycle assessment (LCA) of diesel and liquid hydrogen in different transport modes, including passenger, commuter, freight and intercity rail. Using data from GREET software, PM2.5, N_2O, CH_4, and CO_2 emissions per trip mile are estimated. The inclusion of three hydrogen production pathways - natural gas-fired central plants, PEM electrolysis using solar or wind power, and thermochemical water cracking at a nuclear plant - allows for a comprehensive analysis of environmental impacts across the entire fuel life cycle. Green hydrogen based on photovoltaics can reduce CO_2 emissions by 56% compared to a conventional diesel train [2]. By identifying both direct emissions and emissions associated with fuel production, this study helps contribute to decision-making on the transition to sustainable energy in transport.

2. Methodology
This study conducts a comparative life cycle assessment (LCA) of diesel fuels and liquid hydrogen across different modes of transport using data from the Greenhouse gases, Regulated Emissions, and Energy use in Transportation (GREET) software. Key pollutants including PM2.5, N_2O, CH_4, and CO_2 are evaluated to determine environmental impacts. Four modes of transport for diesel and hydrogen, representative of diverse transportation infrastructures, are considered:

- Transport 1 - Car: CIDI ICEV - FT Diesel
- Transport 2 - Rail: Commuter - FTD + Electricity
- Transport 3 - Rail: Freight - FTD
- Transport 4 - Rail: Intercity - FTD + Electricity

The liquid hydrogen is produced via three pathways:

- Pathway 1 - Central Plants: LH2 production from Natural Gas
- Pathway 2 - Central Plants: LH2 production from PEM Electrolysis - Solar (or Wind)
- Pathway 3 - Central Plants: LH2 production from Nuclear Energy (Thermo-Chemical Cracking of Water)

3. Results and Discussion
- Vehicle: CIDI ICEV - FT Diesel. Hydrogen production from natural gas yields the lowest emissions for all pollutants compared to PEM electrolysis and nuclear energy. However, the overall sustainability of hydrogen-based transport systems hinges on the energy sources employed for production. Figures 1 and 2 illustrate these findings graphically.
- Rail transport: commuter rail - FTD + electricity. PEM electrolysis powered by the solar or wind energy demonstrates the lowest emissions for all pollutants compared to other hydrogen production methods. This underscores the potential for significant environmental benefits when utilizing renewable energy for hydrogen production. Figures 3 and 4 visually depict these results.

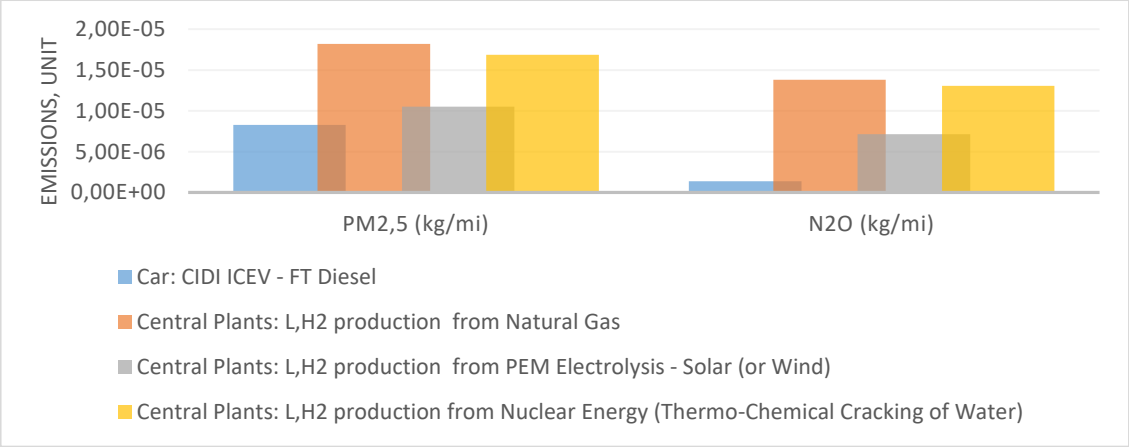


Figure 1. Comparison of PM2.5 and N_2O emissions in Transport-1 with Pathway-1, 2, 3

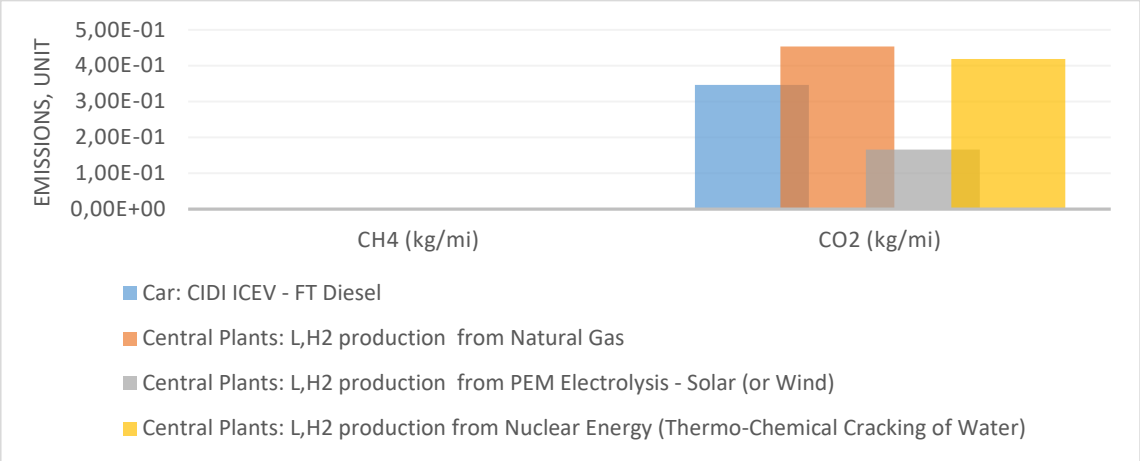


Figure 2. Comparison of CH_4 and CO_2 emissions indices in Transport-1 with Pathway-1, 2, 3

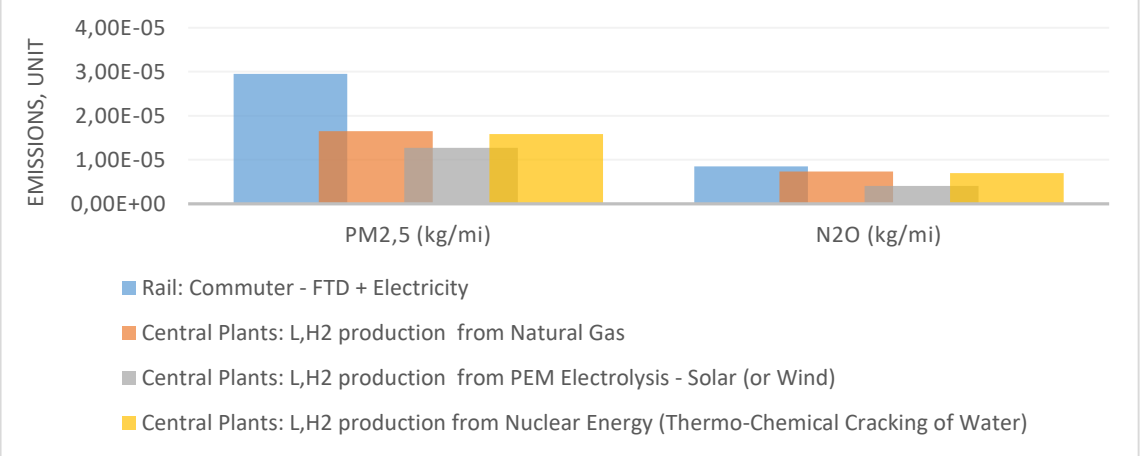


Figure 3. Comparison of PM2.5 and N_2O emissions in Transport-2 with Pathway-1, 2, 3

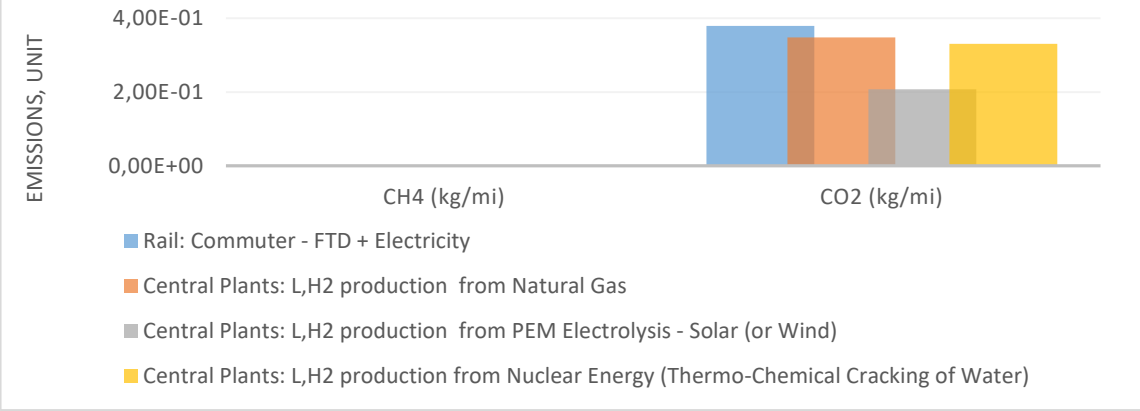


Figure 4. Comparison of CH_4 and CO_2 emissions indices in Transport-2 with Pathway-1, 2, 3

4. Conclusion

This study highlights the environmental performance differences between diesel fuels and liquid hydrogen across various transportation modes and production pathways. While diesel may emit fewer pollutants in certain scenarios, liquid hydrogen shows promise for reducing CO2 emissions, especially when sourced from renewable or nuclear energy. The selection of production pathway greatly influences environmental outcomes.

References

[1] E. Cutore, A. Fichera, G. Inturri, M. Le Pira, and R. Volpe, "Spatially-explicit optimization of an integrated wind-hydrogen supply chain network for the transport sector: The case study of Sicily," *International Journal of Hydrogen Energy*, vol. 52, pp. 761–774, 2024, doi: 10.1016/j.ijhydene.2023.10.105.

[2] M. Kolahchian Tabrizi, T. Cerri, D. Bonalumi, T. Lucchini, and M. Brenna, "Retrofit of Diesel Engines with H2 for Potential Decarbonization of Non-Electrified Railways: Assessment with Lifecycle Analysis and Advanced Numerical Modeling," *Energies*, vol. 17, no. 5, p. 996, 2024, doi: 10.3390/en17050996.

Exploring Novel Sustainable Energy Management Techniques: Unlocking the Potential of Black Sea Hydrogen Sulfide into Usable Energy

[1*]Elifnaz Unay, [1]Bestami Özkaya, [1]Doğukan Tunay, [2]Oğuz Kaan Özdemir
[1] Yildiz Technical University, Faculty of Civil Engineering, Environmental Engineering Department,
[2]Yildiz Technical University, Faculty of Chemical And Metallurgical Engineering, Department Of Metallurgical And Materials Engineering, Davutpaşa Caddesi, Esenler/İstanbul, 34220, Türkiye

*E-mail:elifnazunay@gmail.com

Abstract
This paper explores the potential of hydrogen sulfide (H_2S) in the Black Sea as a novel source for hydrogen energy and bio-batteries by utilization of sulfur in developing lithium-sulfur (Li-S) batteries, and the use of hydrogen to generate electric energy to charge the batteries in a sustainable energy management approach. The employment of the Claus process to effectively recover elemental sulfur, which is then used in the development of high-performance Li-S batteries. Furthermore, the integration of fuel cell technology to utilize the hydrogen extracted during the Claus process for generating clean electricity is analyzed. This dual approach not only mitigates the environmental impact of H_2S as a pollutant but also leverages it for critical energy storage solutions. The findings provide insight into the strategic potential of the Black Sea as a sustainable energy resource having the potential to address environmental challenges through innovative and transformative energy solutions

Keywords: hydrogen sulfide, Black Sea, sustainable energy management, H2S utilization, elemental sulfur, lithium-sulfur batteries

I. Introduction

The demand for sustainable sources of energy has become increasingly important as traditional resources such as fossil fuels are being depleted and leading to environmental issues like greenhouse gas emissions and global warming. Hence, there is growing interest in alternative sources like hydrogen energy to avert a future energy crisis while also offering environmentally friendly solutions. This interest has prompted researchers to explore and find new sources that minimize environmental effects and utilizing renewable feedstocks. In addition to finding new energy sources another important aspect is the energy storage as it is a critical component in the sustainable energy systems, as it allows for the efficient distribution of energy to achieve flexibility, power quality, and accommodate the scale-up of the new energy systems. With an increasing number of technologies being developed to increase energy storage efficiency, the industry is gathering strong momentum which is likely to carry through. This paper derives on the possiblities and challenges of sustainable energy management from Black Sea through decomposition and utilization of H2S closed circular energy system shown in the Fig.1.

II. Hydrogen Sulfide as a Source of Energy

One potential source of hydrogen-containing raw material is hydrogen sulfide (H_2S) which is an industrial byproduct as well as occuring naturally in many gas wells, gas saturated sediments. H_2S being an acid gas which is explosive and extremely poisonous environmental pollutant can be utilized as a potential energy source (Baykara et al., 2007). The Black Sea has caught the attention of researchers in recent years as a natural geobiotechnological reactor with its deep waters containing large amounts of H_2S with the sources from the gases erupted from volcanoes existing in the seabad and antropogenic pollution mostly from Danube area (Zaman & Chakma, 1995).

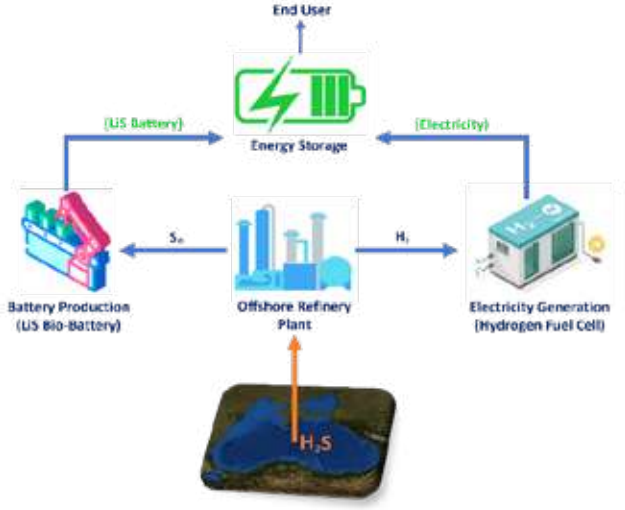


Fig.1: Proposed Approach for H2S Utilization in the Black Sea

Sulfur-reducing bacteria are consistently generating hydrogen sulfide at a rate of 10,000 tons/day in water and overall amount of H_2S in the Black Sea ranges from approximately 4-9 billion tons and is predominantly located

between depths of 500 and 2000 m (Haklidir, 2009)(Simova et.al,2023) (Симова et al, 2023).Such high levels of H_2S could lead to significant environmental disasters within decades while also holding potential for the hydrogen energy industry.The amount of H_2S in the sea continues to rise due to natural processes and significant human-caused activities, not only diminishes fish populations but also elevates pollution to the sea's surface, disturbing the destabilizes the entire ecosystem in the Black Sea. In this regard, a novel and innovative approach is suggested to recover H_2S and utilize it for the generation of hydrogen and sulfur (Figure 1), in an offshore floating refinery plant to generate bio-batteries (Li-S) and with the use of a fuel cell for generating electricity to charge the developed bio-batteries. As the hydrogen fuel cells are unique, they produce electricity only emitting water and heat as byproducts is an efficient and environmentally friendly method of providing electrical power for charging Li-S batteries, using direct electricity instead of grid electricity sources. This way, it is aimed to offer an innovative and sustainable solution for addressing the H_2S challenge in the Black Sea region, turning it into a potential advantage. The suggested approach faces two primary challenging routes and this paper concentrates on examining the feasability of this method in the analysis of LiS battery generation.

III. Addressing the Complexities in the Approach Challenge 1:

Extracting gaseous H2S from Black Sea and decomposing it as H_2 and S:

One of the main challenges in utilizing hydrogen sulfide is extracting it from the Black Sea and decomposing it into sulfur and hydrogen (Teimuraz et al., 2018). There are various technologies available for producing hydrogen and sulfur from hydrogen sulfide, such as electrochemical, thermochemical, photochemical, thermal, plasmochemical, and photoplasma methods. While photoplasma technologies are still in development and not yet advanced enough for large-scale application, the utilization of electrochemistry for H_2S needs further advancement to compete against current electricity costs (Al-Zareer&Dincer&Rosen, 2016) (Zaman & Chakma, 1995) (Baykara et al., 2007). Thermal and thermochemical approaches may serve as foundations for potential commercialization due to their capacity to directly obtain hydrogen and sulfur through the thermal decomposition of H2S. However, these reactions are highly endothermic with low equilibrium conversion even at high temperatures. To address these limitations, several two-step methods can be employed but they must demonstrate technical and economic feasibility for commercial viability in adjusting large-scale production. In addition, all methods for decomposing H_2S require electrical energy. Nevertheless, it is stated that the energy required is lower than that needed to produce hydrogen from H_2S by approximately 10 kWh/kg, while the net energy recovered from 1 kg of H_2 in a fuel cell system is around 25 kWh/kg (UAHE, 2010), resulting in an overall positive energy balance of nearly 15 kWh/kg making itself a self sustained system. This study focuses on using sulfur derived from H_2S as cathode material for Li-S batteries; therefore, the sulfur must be in elemental phase – hence why the Claus process emerges as a promising technology (Kohl&Nielsen,1997). The Claus process is a well-established technology used to produce elemental sulfur from hydrogen sulfide as it involves partial oxidation of hydrogen sulfide resulting in elemental sulfur along with low-quality steam.

IV. Addressing the Complexities in the Approach # Challenge 2:

Developing bio-batteries (LiS) from derived sulfur and analyzing their potential:

Developing bio-batteries from derived sulfur presents both challenges and opportunities. The use of sulfur as a cathode material for lithium-sulfur batteries has attracted attention due to its high theoretical specific capacity, low cost, and natural abundance. However, there are several challenges that must be addressed to optimize the performance and scalability of Li-S batteries (Hagen et al., 2015) (Zhao et al, 2018). In this study, the derived elemental sulfur from 120Y349 TÜBİTAK project is utilized to generate LiS batteries; test results (found in section IV below) demonstrate promising outcomes along with some shortcomings. One important challenge in the development of bio-batteries using derived sulfur is the need to address the issue of polysulfide dissolution, which leads to capacity fading and poor cycling stability in lithium-sulfur batteries. Additionally, the high-volume expansion of sulfur during lithiation and the insulating nature of sulfur are major hurdles in achieving long-term cycling stability and high energy density in Li-S batteries. These challenges call for innovative solutions in electrode design and electrolyte formulation to enhance the overall performance and lifespan of lithium-sulfur batteries. Addressing these limitations in future research will not only contribute to sustainable energy management but also pave the way for next-generation bio-batteries, promoting a more environmentally friendly and efficient energy infrastructure.

V. The Claus Process for Sulfur Recovery

The Claus process is a widely used technology by incomplete combustion of H_2S to produce elemental sulfur involves the following chemical reactions (gases containing more than 25% H_2S are ideal for Claus plants). The Claus process occurs in two main stages: the thermal stage, where hydrogen sulfide undergoes substoichiometric combustion at temperatures exceeding 850°C, and the catalytic stage, temperatures between 315°C to 330°C, where further conversion to sulfur is enhanced by activated aluminum or titanium oxide (Kohl&Nielsen,1997). Approximately 60 to 70% of the sulfur yield is obtained during the thermal stage, but the catalytic step is critical for increasing efficiency and to maximizing sulfur yield involving a series of processes including heating, reaction, and cooling to manage sulfur condensation and avoid catalyst fouling.

$H_2S + 3/2\ O_2 \rightarrow SO_2 + H_2O$ (thermal state) (ΔH = - 518 kJ mol^{-1}) (1)

$SO_2 + 2\ H_2S \rightarrow 3S_{(8)} + 2\ H_2O$ (catalytic stage) (ΔH = - 1165.6 kJ mol^{-1})

The formation of hydrogen gas as a side reaction in Claus process:

$2\ H_2S \rightarrow S_2 + 2\ H_2 \qquad (\Delta H > 0)$ (2)

Sulfur is generated in thermal stage as highly active S_2 diradicals, which then exclusively combine to form the S_8 allotrope.

$4\ S_{(2)} \rightarrow S_{(8)}$ (3)

The Claus process is widely used globally to produce large quantities of elemental sulfur from H_2S, including oil refining, cosmetics, mining, food processing, wood pulp processing, pharmaceuticals, agriculture, personal care products, water treatment, etc. The process not only recovers valuable sulfur but also contributes to environmental management by reducing sulfur emissions. Elemental sulfur can exist in various forms, ranging from S6 to S20, as shown in the Eq 3 the sulfur is derived in the Claus Process is in $S_{(8)}$ form which is the form that is needed for using sulfur in battery technology. The cyclic structure of this molecule provides the required properties for integration into battery technology to act as a key component in the cathode to ensure optimal performance and chemical stability by contributing to the overall efficiency and longevity of the battery. In this context, the Claus process has the potential to be integrated into sulfur production from H_2S for use in lithium-sulfur batteries. The resulting elemental sulfur can serve as a cathode material in these high-energy-density batteries, offering potential cost benefits. Additionally, the hydrogen extracted during the Claus process can be employed in fuel cells to generate electricity, which can then charge these bio-batteries, establishing a sustainable cycle of energy production and utilization. This holistic approach promotes advancements in energy storage technologies.

VI. Bio-Battery Development Using Elemental Sulfur

The demand for energy storage systems within the grid continues significantly and recognizing this unmet need, scientific efforts are focused on developing low-cost batteries to effectively address the market gap. Among emerging technologies, Lithium-Sulfur (Li-S) batteries stand out as particularly promising due to their exceptional energy density and cost effectiveness. Recent comparison studies of different battery types (Iclodean et al. 2017) clearly indicate that Li-S batteries demonstrate a 46% reduction in weight and a 17% decrease in cost compared to Li-ion batteries. The potential advantages of Li-S batteries play a significant role in advancing energy storage technology in terms of sustainability, cost-effectiveness, and high performance. Our preliminary studies with the use of purified $S_{(8)}$ in battery production also demonstrated a promising result in terms of performance, sustainability and cost-effectiveness. Li-S batteries were produced using elemental sulfur from project number 120Y349 TÜBİTAK project and the outcomes obtained demonstrate that recovered sulfur can indeed be utilized in energy storage applications. Also, the electrochemical tests of the Li-S batteries were conducted using a Swagelok setup. A cathode mixture of carbon black and sulfur in a 1:1 ratio and an electrolyte of 1M LiTFSI-0.5M LiNO3 in DOL:DME were used. The specific capacity of the half-cell at a potential of approximately 1.9V was around 550 mAh/g in the first cycle. With increasing cycle numbers, there was a significant decrease in the specific capacity. This decline in capacity is due to the dissolution/electrodeposition reaction over time causing unstable growth of the solid-electrolyte interface (SEI). This layer creates active sites for lithium nucleation and dendritic growth during reduction reactions. These formations present various challenges encountered with Li-S batteries, such as severe volume expansion, shuttle effect, and low conductivity, which restrict the widespread commercialization of lithium-sulfur batteries. To improve the longevity and performance of sulfur-based batteries, efforts should be made to enhance the purification and modification the sulfur (S_8 form and can exist in three different structures within S_8: α-sulfur, β-sulfur, and γ-sulfur. The variations between these forms can occur changes in physical conditions.) to mitigate the drawbacks in these batteries, thus extending their lifespan.

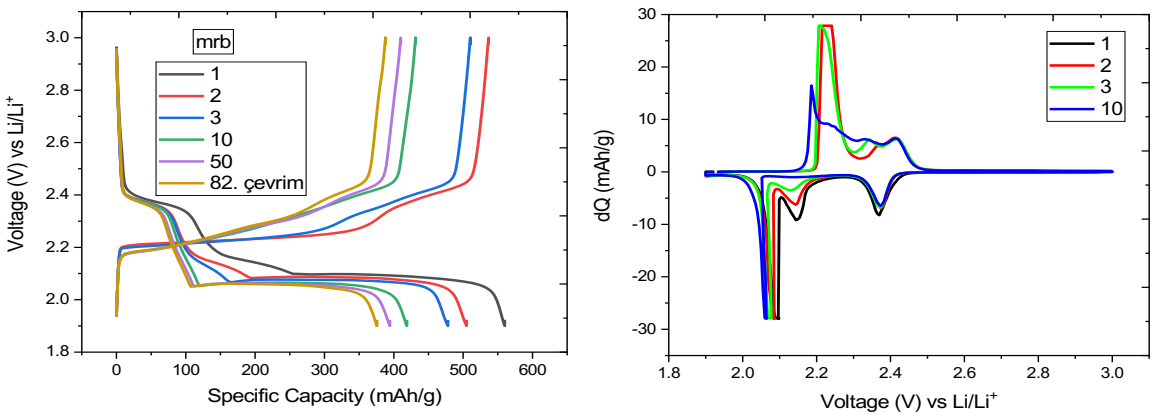


Fig. 2: Specific capacity relative to potential and CV curves, respectively

VII. Results and Conclusions

This paper has delved into the potential of hydrogen sulfide (H_2S) sourced from the sea sediments to be used as a novel energy storage solution. By extracting sulfur (S) and hydrogen (H_2) from this potent environmental pollutant, we not only mitigate its detrimental effect but also to utilize it as a valuable resource. The development of Li-S batteries from this pollutant provides a pathway for utilizing this sulfur in high-performance energy storage systems. With their unique properties, Li-S batteries stand out as an attractive option for various applications, including electric vehicles and renewable energy storage. These batteries have the potential to revolutionize the energy storage landscape due to their high theoretical energy density and cost-effectiveness, providing longer-lasting, environmentally friendly, and more efficient solutions compared to traditional lithium-ion batteries Moreover, the integrated approach of extracting H_2 and using it to generate electricity—which in turn charges the developed Li-S batteries—demonstrates a comprehensive and sustainable energy cycle. This enhances the viability of hydrogen as an energy source, thereby supporting the broader adoption of clean energy technologies. Continued research efforts focused on optimizing Li-S battery technology will be crucial for overcoming existing challenges while further expanding their application scope. Addressing technical considerations such as cycle life and safety measures is essential in accelerating its commercialization prospects. As research in this area progresses, enhancing the commercial viability and environmental benefits of novel technologies are essential to transition towards cleaner and more efficient energy storage technologies to unlock the full potential and pave the way for a greener and more sustainable future.

References

Al-Zareer M., Dincer I, Rosen Marc A. (2016) Development and analysis of an integrated system with direct splitting of hydrogen sulfide for hydrogen production, International Journal of Hydrogen Energy, Volume 41, Issue 44, Pages 20036-20062, ISSN 0360-3199, https://doi.org/10.1016/j.ijhydene.2016.08.217

Baykara, S., Figen, H E., Кале, A., & Везироглу, T H. (2007). Hydrogen from hydrogen sulphide in Black Sea. https://doi.org/10.1016/j.ijhydene.2006.07.021

C Iclodean, B Varga, N Burnete, D Cimerdean and B Jurchiş, (2017) "Comparison of Different Battery Types for Electric Vehicles," IOP Conference Series: Materials Science and Engineering, Volume 252, CAR2017 International Congress of Automotive and Transport Engineering - Mobility Engineering and Environment, 8–10 November 2017, Pitesti, Romania

Симова, И., Величкова, Р., Uzunova, M., Angelova, R A., Stankov, P., & Atanasov, K. (2023). On the possibility of the utilization of hydrogen sulfide from the Black Sea. https://doi.org/10.33223/epj/163372

Hagen, M., Hanselmann, D., Ahlbrecht, K., Maça, R., Gerber, D., Tübke, J., (2015). Lithium–Sulfur Cells: The Gap between the State-of-the-Art and the Requirements for High Energy Battery Cells. Advanced Energy Materials 5, 1401986. https://doi.org/10.1002/aenm.201401986

Haklidir, Mehmet & Tut Haklidir, Fusun. (2009). The possibilities for hydrogen production from H2S and storage in the Black Sea. International Journal of Nuclear Hydrogen Production and Applications. 2. 10.1504/IJNHPA.2009.023829.

Kohl Arthur L., Nielsen Richard B., (1997) Chapter 8 - Sulfur Recovery Processes,Gas Purification (Fifth Edition),Gulf Professional Publishing, Pages 670-730, ISBN 9780884152200, https://doi.org/10.1016/B978-088415220-0/50008-

Simova, I., Velichkova, R., Uzunova, M., Angelova, R., Stankov, P., Atanasov, K. (2023). On the possibility of the utilization of hydrogen sulfide from the Black Sea. Polityka Energetyczna – Energy Policy Journal, 26(2), 183-194. https://doi.org/10.33223/epj/163372

Teimuraz, K., Aleksandr, K., & Bachana, M. (2018). The difficulties of the extraction of hydrogen sulfide from the Black Sea water and methods to overcome them. https://cyberleninka.ru/article/n/the-difficulties-of-the-extraction-of-hydrogen-sulfide-from-the-black-sea-water-and-methods-to-overcome-them

Zaman, J., & Chakma, A. (1995). Production of hydrogen and sulfur from hydrogen sulfide. https://doi.org/10.1016/0378-3820(94)00085-8

Fault Diagnosis Method for Polymer Electrolyte Membrane Fuel Cells using Deep Learning Technologies

[1*]Meltem Yavuz Çelikdemir
[1] Bitlis Eren University, Tatvan Vocational School, Electric and Energy, Bitlis, 13000, Türkiye

E-mail:meltem.ycd@gmail.com

Abstract

Effective and accurate diagnostic methods are necessary to ensure the stable and efficient operation of Polymer Electrolyte Membrane Fuel Cells (PEMFCs). One of the most common failures encountered by PEMFCs is water flooding. In practice, voltage drop is commonly used as an indicator of water flooding failure. This paper proposes a data-driven method for PEMFC using machine learning technologies that can automatically extract fault characteristics from raw data to better diagnose water flooding failure under changing conditions. For this, different Machine learning classification algorithms are used in the study. Performance metrics are compared using these classification algorithms. As a result, the classification model with the highest accuracy is Narrow Neural Network (99.96%) and the classification model with the lowest accuracy is Boosted Tresss Ensemble (65.7%). At the same time, when the training times are analyzed, the classification model with the shortest training time is Gaussian Naive Bayes (4.47 s) and the classification model with the longest training time is Kernel Naive Bayes (172.06 s).

Keywords: PEMFC, Water flooding, Machine learning classification algorithms

I. Introduction

Today, there is an increasing interest in alternative energy sources. Among these energy sources, Polymer Electrolyte Membrane Fuel Cells (PEMFC) have remarkable features. These features include zero emissions, low noise and high efficiency compared to other energy sources. It also produces only water and heat as by-products. These advantages have made PEMFCs widely used (Razi and Dincer 2022). However, PEMFCs can experience operational failures during operation, such as waterlogging, air starvation and membrane drying. These failures can often lead to performance degradation and reduced lifetime. Therefore, fault diagnosis methods are important to increase durability and reduce maintenance costs. Due to this importance, the operational reliability of PEMFCs can be increased and commercialization can be achieved.

A PEMFC basically consists of an anode, cathode and membrane. The membrane allows the passage of protons but not electrons. In the anode catalyst, hydrogen atoms are split into protons and electrons. The protons and electrons pass through the membrane and external circuits respectively, generating electrical energy for the external electrical charges. Water and heat are also generated in the cathode catalyst layer. These electrical reactions are expressed as follows;

$$\text{Anode: } H_2 \rightarrow 2H^+ + 2e^- \quad (1)$$

$$\text{Cathode: } 2H^+ + \tfrac{1}{2}\,O2 + 2e^- \rightarrow H_2O \quad (2)$$

$$\text{Overall reaction: } H_2 + \tfrac{1}{2}\,O2 \rightarrow H_2O \quad (3)$$

In high power applications, PEMFCs produce excess water as given in Equation 2. This can cause water to accumulate in the flow channel. This is referred to as flow channel blockage or water flooding failure. Water accumulation hinders the delivery of reactants, reduces the active area of the catalyst and can lead to gas starvation. Gas starvation can lead to irreversible and permanent failure of PEMFCs. Therefore, water flooding diagnostics is important to increase the lifetime of PEMFCs.

Nowadays, fault detection is a current issue that is frequently addressed by researchers. Numerous diagnostic methods have been proposed for this purpose, including electrochemical impedance spectroscopy-based methods, physical model-based methods and data-driven methods (Mao et al. 2020; Zuo et al. 2022).

For PEMFC systems, the monitoring signals of auxiliary systems can represent the operating status of the fuel cell. Although voltage drop is commonly used as an indicator of flooding fault detection, the change of load may also affect the output voltage of the fuel cell, which may reduce the diagnostic accuracy. To solve the problem, inspired by previous diagnostic studies, a data-driven diagnostic method is proposed to detect the flooding fault of the fuel cell.

Diagnostic selection for data-driven methods is very important for model performance. To ensure proper fuel cell operation, the membrane must contain enough water to allow protons to pass through it. Water transport in FC stacks includes Electro-Osmotic Drag (EOD), Back Diffusion (BD), Hydraulic Permeability (HP), water transport and diffusion, and convective mass transfer in the gas channel. Water is produced at the cathode and is expelled or purified by the flow of unreacted gas. The water content in the fuel cell is affected by various transport channels. The process by which water entrained by protons passes through the membrane is called electro-osmotic entrainment (Berning 2011). Back Diffusion (BD) refers to the diffusion of excess water produced at the cathode back to the anode (Kong et al. 2017). Durring operation of the fuel cell stack, water molecules are produced on the cathode by the oxygen reduction reaction. The water molecules diffuse into the membrane and the gas diffusion layer (Kandlikar, Garofalo, and Lu 2011). The amount of water produced is proportional to the current density of the

cell. Therefore, the current density of the FC is chosen as an indicator in this study.

In this study, machine learning classification algorithms are used as PEMFC fault diagnosis method. These classification algorithms include discriminant analysis, naive bayes, support vector machines, neural networks, decision trees, logistic regression, ensemble classifier, nearest neighbor algorithms. Performance metrics were compared using these classification algorithms in fault detection with the dataset.

II. System Description and Procedure

Experimental data of 80 W PEMFC is used in the study. In the experimental study, the temperature of the PEMFC is reduced to obtain water flooding failure data. In this case, water condensation and then water unitization is achieved. A voltage drop of 5% of the PEMFC output voltage is referred to as water flooding (Mao et al. 2020). In the study, the temperature was increased to remove water and improve the performance of the fuel cell by observing the PEMFC voltage drop. In the study, machine learning is used for PEMFC water flood fault detection.

Machine learning is divided into two classes as supervised learning and unsupervised learning. The classification technique algorithm used in the study is a supervised learning technique. In this algorithm, it is supervised machine learning where an algorithm learns to classify new observations from labeled data samples. In this study, different classification algorithms are used and their results are compared. These results are called model performance evaluation metrics. Accuracy (ACC), Sensitivity (SEN), Specificity (SPE) and Precision (PRC) parameters are used as metrics. Equation 4-8 is used to calculate these parameters.

.

$$A_{CC} = \frac{tp + tn}{tp + tn + fp + fn} \tag{4}$$

$$S_{EN} = \frac{tn}{tn + fn} \quad S_{EN} = \frac{tp}{tp + fp} \tag{5}$$

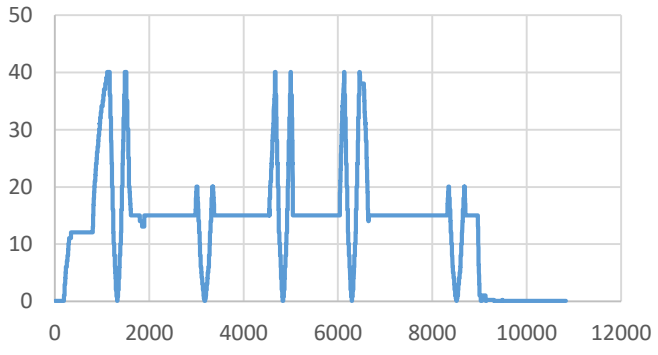
$$S_{EE} = \frac{tp}{tp + fp} \quad S_{EE} = \frac{tn}{tn + fn} \tag{6}$$

$$P_{RC} = \frac{tn}{tn + fp} \quad P_{RC} = \frac{tp}{tp + fn} \tag{7}$$

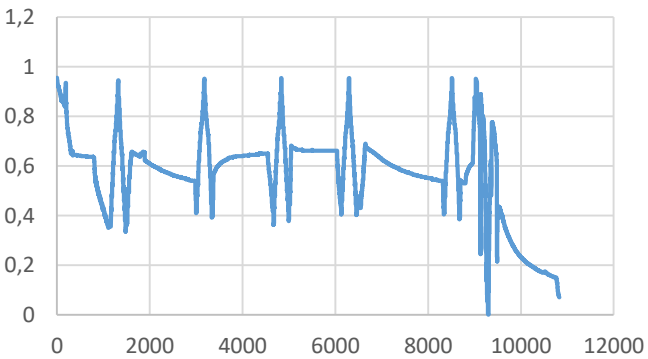
$$F - score = \frac{2 * tn}{2 * tn + fp + fn} \quad F - score = \frac{2 * tp}{2 * tp + \mathrm{fp} + fn} \tag{8}$$

Here, true positive (tp), true negative (tn), false positive (fp), and false negative (fn) represent the coefficients of the confusion matrix. In addition, the Area Under the Curve (AUC) parameter shows the discrimination success of the model classes. AUC refers to the area under the Receiver Operating Characteristic (ROC) curve. The ROC curve is an increasing function between (0,0) and (1,1) and shows that the higher the AUC value, the higher the classification success of the model. While an AUC value of "0.5" indicates that the model has failed, the highest value of "1" indicates maximum success.

The graphics of the data set used in the study for water flooding are given in Figure 1. In the study, 37899 pieces of data were used.



a)



b)

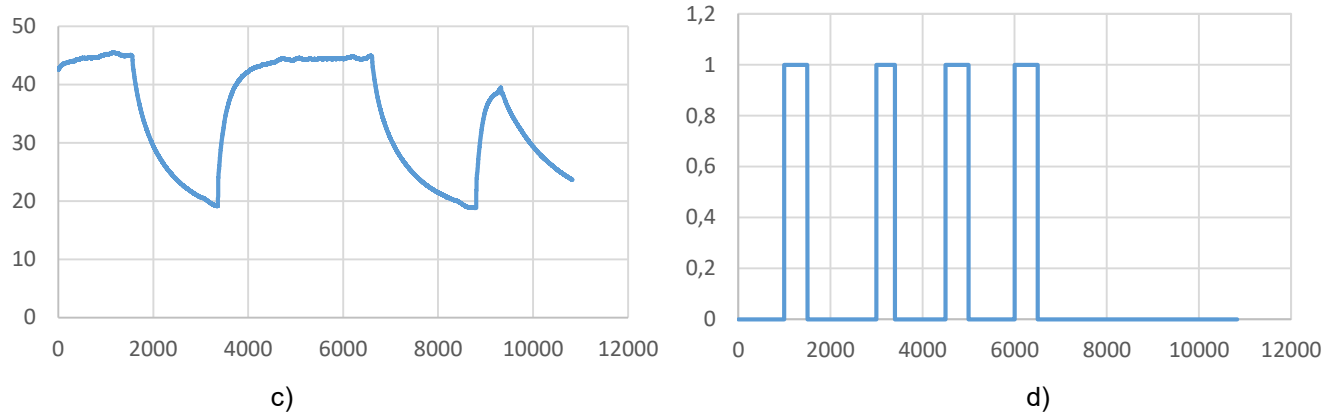


Fig.1: Data graphs a) current-time graph b) voltage-time graph c) temperature-time graph d) faulted state graph used in training

III. Model Evaluation

Accuracy rates and training times for different classification models of machine learning used in the study are given in Figure 2.

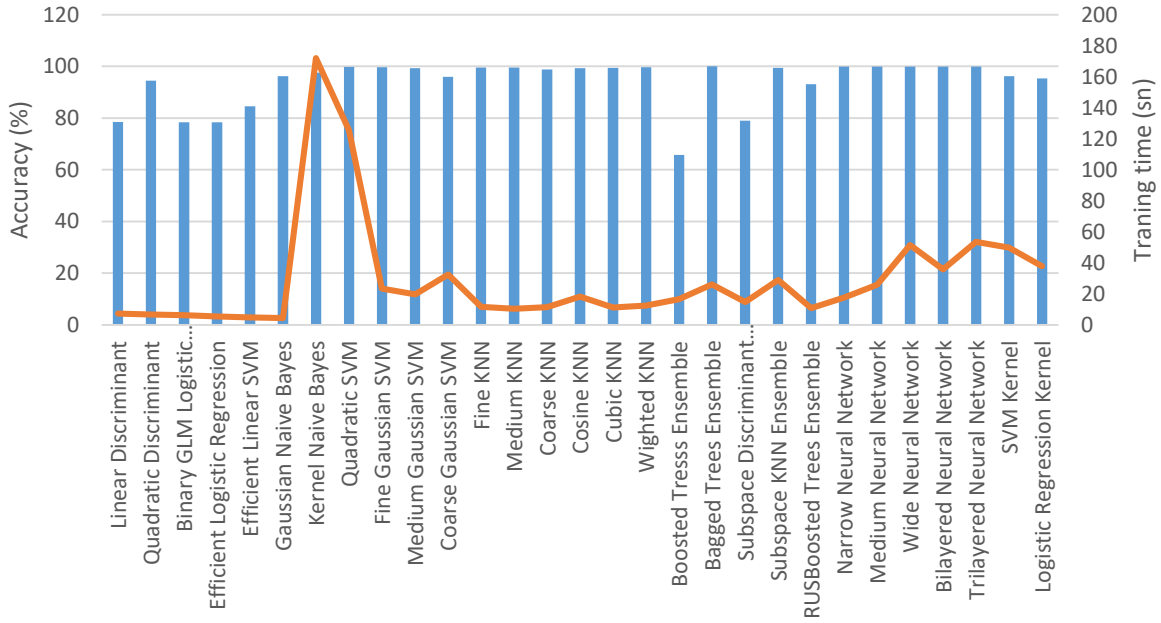
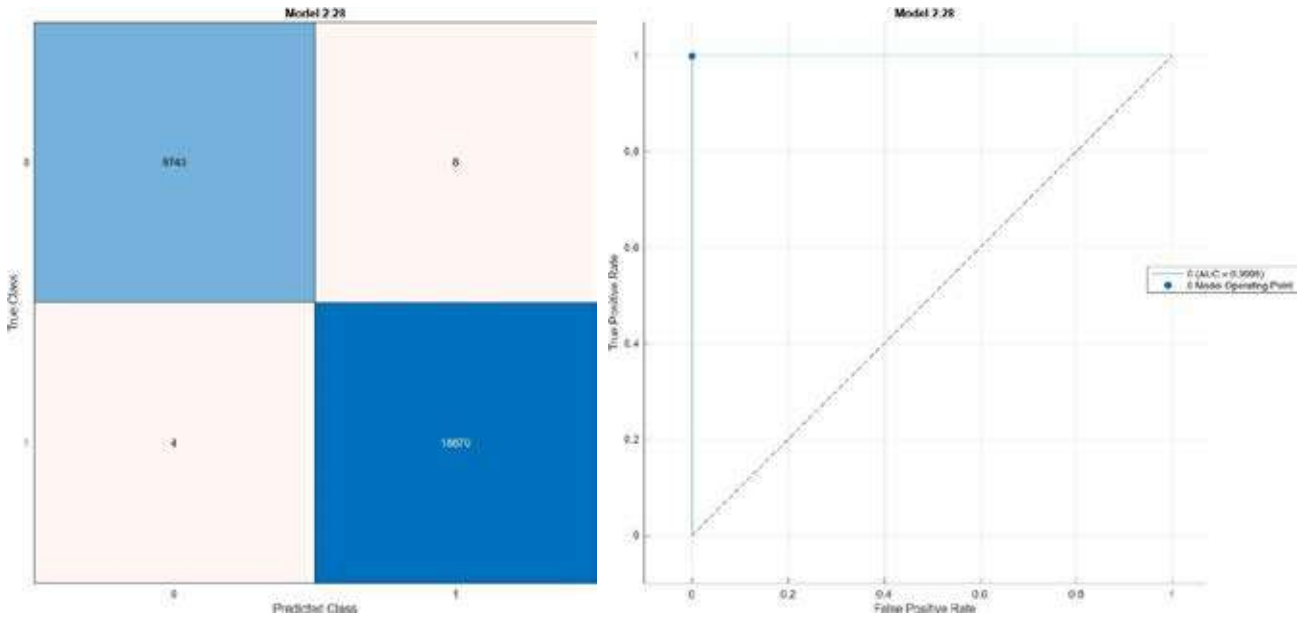


Fig. 2: Accuracy rates and training times for classification models

Accordingly, the classification model with the highest accuracy is Narrow Neural Network (99.96%) and the classification model with the lowest accuracy is Boosted Tresss Ensemble (65.7%). At the same time, when the training times are analyzed, the classification model with the shortest training time is Gaussian Naive Bayes (4.47 s) and the classification model with the longest training time is Kernel Naive Bayes (172.06 s). The confusion matrix components of the Narrow Neural Network classification model, which has the best accuracy rate in the study, are given in Figure 3-a and the ROC curve is given in Figure 3-b.



a) b)

Fig. 3: a) Confusion matris b) ROC curve

In the study, 9743 true negatives (tn), 8 false negatives (fn), 4 false positives (fp) and 18670 true positives (tp) were calculated. According to the performance metrics obtained from the confusion matrices of machine learning algorithms; accuracy was 99.95%, sensitivity 99.91%, specificity 99.97%, precision 99.95% and F1 score 99.93%.

IV. Conclusions

In the study, different machine learning classification algorithms are used to diagnose the water flooding failure of PEMFCs. Performance metrics are compared using these classification algorithms. As a result, the classification model with the highest accuracy is Narrow Neural Network (99.96%) and the classification model with the lowest accuracy is Boosted Tresss Ensemble (65.7%). At the same time, when the training times are analyzed, the classification model with the shortest training time is Gaussian Naive Bayes (4.47 s) and the classification model with the longest training time is Kernel Naive Bayes (172.06 s). This will enable the detection of water flooding faults with high accuracy and thus increase the lifetime of PEMFCs.

References

Berning, Torsten. 2011. “On Water Transport in Polymer Electrolyte Membranes during the Passage of Current.” *International Journal of Hydrogen Energy* 36 (15): 9341–44. https://doi.org/10.1016/j.ijhydene.2011.04.079.

Kandlikar, S. G., M. L. Garofalo, and Z. Lu. 2011. “Water Management in A PEMFC: Water Transport Mechanism and Material Degradation in Gas Diffusion Layers.” *Fuel Cells* 11 (6): 814–23. https://doi.org/10.1002/fuce.201000172.

Kong, Im Mo, Aeri Jung, Young Sang Kim, and Min Soo Kim. 2017. “Numerical Investigation on Double Gas Diffusion Backing Layer Functionalized on Water Removal in a Proton Exchange Membrane Fuel Cell.” *Energy* 120 (February): 478–87. https://doi.org/10.1016/j.energy.2016.11.100.

Mao, Lei, Lisa Jackson, Weiguo Huang, Zhinong Li, and Ben Davies. 2020. “Polymer Electrolyte Membrane Fuel Cell Fault Diagnosis and Sensor Abnormality Identification Using Sensor Selection Method.” *Journal of Power Sources* 447 (January): 227394. https://doi.org/10.1016/j.jpowsour.2019.227394.

Razi, Faran, and Ibrahim Dincer. 2022. “Challenges, Opportunities and Future Directions in Hydrogen Sector Development in Canada.” *International Journal of Hydrogen Energy* 47 (15): 9083–9102. https://doi.org/10.1016/j.ijhydene.2022.01.014.

Zuo, Bin, Zehui Zhang, Junsheng Cheng, Weiwei Huo, Zhixian Zhong, and Mingrui Wang. 2022. “Data-Driven Flooding Fault Diagnosis Method for Proton-Exchange Membrane Fuel Cells Using Deep Learning Technologies.” *Energy Conversion and Management* 251 (January): 115004. https://doi.org/10.1016/j.enconman.2021.115004.

The Effective Parameter Estimation for a PEMFC Based on Archimedes optimization Algorithm

[1]Abuzer Caliskan, [2*]Hasan Bektas Percin
[1] Firat University, Faculty of Engineering, Department of Electrical and Electronics Engineering, Elazığ, 23119, Türkiye
[2] Firat University, Elazığ, 23119, Türkiye

* E-mail: hbpercin@firat.edu.tr

Abstract
Designing and developing an accurate model of fuel cell systems, particularly Proton Exchange Membrane Fuel Cells (PEMFCs), is crucial for simulating, controlling, managing, and accurately optimizing system parameters. For this purpose, it is very important to detect unknown parameters. To get the optimal parameters, this paper introduces a novel approach where Archimedes optimization method is effectively employed to estimate the unknown parameters of Proton Exchange Membrane Fuel Cell (PEMFC) model. After introducing the optimization problem and solving the problem based on the presented equations in the fuel cell, an Archimedes Optimization Algorithm (AOA) model is presented. The proposed optimization algorithm has been tested on commercial PEMFC stack, experimental data.

KeywordsPEMFC, Optimization, Parameter identification, Sum of squared errors”

I. Introduction

Intensifying global energy demand, industrialization, and technological advancements, has strained traditional fossil energy sources. These finite resources not only contribute to air and water pollution but also exacerbate climate change through greenhouse gas emissions However, numerous alternative approaches can mitigate environmental concerns and circumvent resource depletion. As one of these, Fuel cells (FC)s have gained significant interest due to their remarkable feature in directly converting the chemical energy of hydrogen and oxygen into electricity through electrocatalytic reactions. Over the past few decades, considerable researches have been directed towards advancing fuel cell technology to a commercial scale. Blanco-Cocom (2023). When compared to other types of fuel cells, Proton Exchange Membrane Fuel Cells (PEMFCs) offer a combination of high efficiency, power density, low operating temperatures, and environmental sustainability making them well-suited for a wide range of applications Alsaidan (2022).

Accurate modeling of PEMFCs is essential for optimizing their performance and ensuring their effective utilization in various applications Poor or inaccurate modeling of of PEMFCs can lead to inefficient utilization, limiting their potential project lifetime. This minvolves a set of parameters, which are often not directly obtained but are essential for analyzing Therefore, parameter estimation becomes necessary to effectively utilize PEMFCs. Algorithms inspired by nature and stochastic characteristics are widely favoured due to their capability to effectively navigate complex parameter spaces and handle situations with multiple minima Mossa (2021).

A diversity of research exists concerning parameter estimation, These researches encompass various modifications aimed at enhancing standard algorithms to achieve better performance when using different objective functions Cao (2019), Mo (2006)

The study proposes a new model estimation of a PEMFC, such that the parameters of the model have been optimized using Archimedes Optimization Algorithm (AOA). The simulation results achieved by AOA are validated by comparing them with measured experimental data. In this context, the mathematical model incorporates seven unknown design variables. The primary objective of the optimization problem presented is to minimize the sum of squared errors (SSE).

II. Experimental Set-up and Procedure

A fuel cell is commonly regarded as a straightforward process wherein chemical energy is directly converted into electrical energy. The end product for the entire electrochemical process is water and heat. Fig. 1 illustrates the typical construction of traditional PEMFCs.

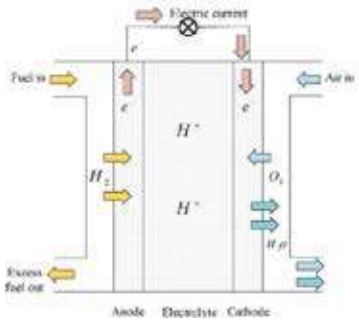


Fig. 1: The general structure of a polymer electrolyte membrane fuel cell stack

In PEMFCs, there are two electrodes known as the anode and the cathode, separated by an electrolyte. At the anode, hydrogen undergoes a catalytic reaction, resulting in the production of a positively charged ion and a negatively charged electron. While the positively charged ion moves through the electrolyte, the electron travels through an external circuit, generating an electric current Yuan (2020). Dynamic modeling of PEMFCs enables the evaluation of system response to dynamic loads, disturbances, and transient events, providing valuable information for system optimization and robust control design. The impact of different parameters, such as pressure, temperature, and current density can be evaluated on the performance of PEMFCs. Hossain (2023) With this knowledge, the primary aim of this study is to optimize the estimation of the unknown parameters aiming to achieve a model that exhibits satisfactory agreement with experimental data.

There are numerous methods available for parameter identification of Proton Exchange Membrane Fuel Cells (PEMFCs), broadly categorized into two classes: classical methods and modern optimization techniques. Classic methods, while exact and theoretically rigorous, do exhibit significant drawbacks that can limit their effectiveness. To address these challenges, modern optimization techniques, such as evolutionary algorithms, swarm intelligence approaches, or machine learning-based methods, have gained popularity Guo (2020).

III. Analysis

In this section, to achieve an accurate model for Proton Exchange Membrane PEMFCs, it is essential to employ an efficient and versatile optimization approach to assess the PEMFC's parameters effectively. We validate the efficiency of the proposed algorithm by assessing its performance across various assessment criteria. Additionally, we analyze the obtained results to demonstrate the superiority of our approach across the selected features. The proposed algorithm works based on the phenomenon explained by Archimedes' law of physics. This principle is concerned with an object completely or partially submerged in a fluid Hashim etal. (2021). The application of the Archimedes optimization algorithm is given in Fig. 2.

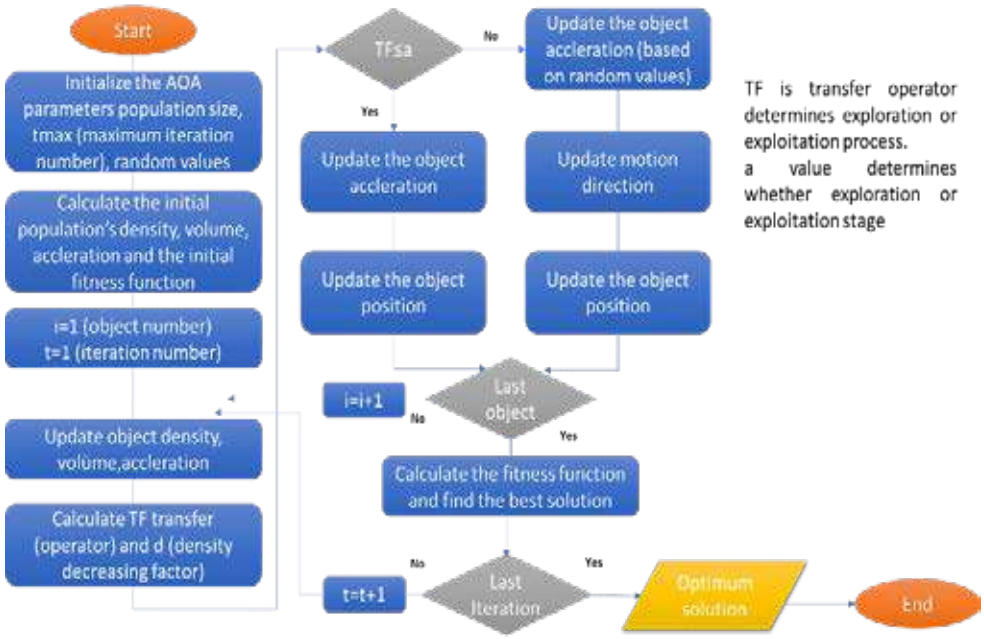


Fig. 2: The flowchart of Archimedes Optimization Algorithm

The study utilizes the Sum of Squared Errors (SSE) between the estimated model and the actual dataset as the objective function. The goal is to minimize this function to obtain the optimal model of the PEMFC. Therefore, the objective function for the studied PEMFC model is formulated as follows: Yuan (2020).

$$obj_{sse} = \min(sse) = min\left\langle \sum_1^m \left(X_i - \hat{X}_i\right)^2 \right\rangle \quad (1)$$

where i stands for the iteration number, m represents the number of measured points, and X_i and $\hat{X}_i$ describe the model and the PEMFC experimental output measurements, respectively. The Sum of Squared Errors (SSE) has been effectively minimized using the (AOA) algorithm to estimate the parameters of the model. This optimization process involves iteratively adjusting the model parameters within the proposed algorithm until certain stopping criteria are met.

IV. Results and discussions

In this section, The proposed AOA is used to estimate the model parameters of ξ1, ξ2, ξ3, ξ4, β, RC, and λ. For this purpose, the algorithm has been tested 30 times to evaluate its robustness. The obtained parameter values

are shown in Table 1.

Tab. 1: Estimated parameters for the optimization algorithm used in the study

Parameters	Estimated values
ξ1	*-0.9712*
ξ2,	*2. 7704x10^{-3}*
ξ3,	*4.302x10^{-5}*
ξ4	*-1.952x10^{-4}*
β	*0.01540*
R_C	*1.772x10-4*
λ	*19.976*

Where ξ1, ξ2, ξ3, ξ4 denote the semi-empirical coefficients. β expresses the regulating parametric coefficient. R_C represents the corresponding resistance that protons experience when passing through the membrane. λ expresses a variable parameter indicating the water content of the membrane material. The SSE value for the proposed algorithm is 0.1229. the efficiency of the presented algorithm is verified based on specific PEMFC 500 W characteristics. Analysis is carried out by comparing the parameters obtained with the optimization algorithm and the parameters obtained experimentally. The conducted analysis involves studying the voltage and power curves in relation to the current for the selected PEMFC as seen in Fig. 3.

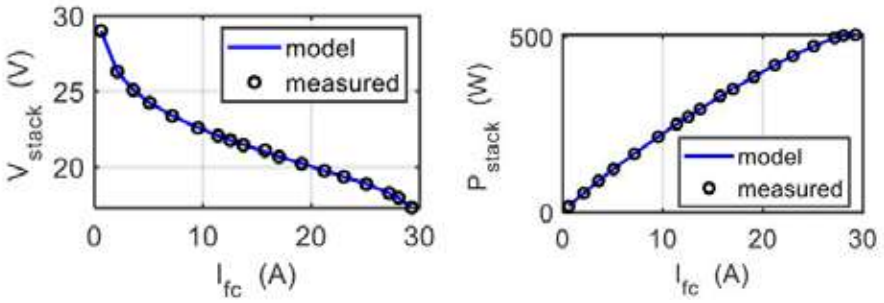


Fig. 3: The I-V and I-P curves for the study

As seen in Figure 3, the fact that the curves obtained according to the estimated parameters converges as closely as possible with the measured curves show the effectiveness and efficiency of the study used here. The lower the SSE value obtained, the better the performance of the optimisation algorithm. In addition to these curves, comparisons can be made for varying temperature values or varying membrane water content values to demonstrate performance.

V. Conclusions

This paper addresses the formulation of an optimization problem aimed at the optimal identification of the unknown parameters associated with the PEMFC. The algorithm, originally inspired by Archimedes' law of physics, is adapted and improved to effectively address the optimization problem by leveraging the unique characteristics of the optimization algorithm, aiming to efficiently navigate the parameter space and converge towards optimal solutions. For further studies, alternative optimization algorithms, artificial intelligence (AI) and machine learning techniques, can be utilized to asess the challenging problem of PEMFC parameter estimation comparatively.

References

Alsaidan, I., Shaheen, M. A. M., Hasanien, H. M., Alaraj, M., & Alnafisah, A. S. A PEMFC model optimization using the enhanced bald eagle algorithm. Ain Shams Engineering Journal, 13(6), 101749. (2022).

Blanco-Cocom, L., Botello-Rionda, S., Ordoñez, L. C., & Valdez, S. I. (2023). Design optimization and parameter estimation of a PEMFC using nature-inspired algorithms. Soft Computing, 27(7), 3765-3784. (2023).

Cao Y, Li Y, Zhang G, Jermsittiparsert K, Razmjooy N. Experimental modeling of PEM fuel cells using a new improved seagull optimization algorithm. Energy Rep.5:1616-1625. (2019);

Hashim, F. A., Hussain, K., Houssein, E. H., Mabrouk, M. S., & Al-Atabany, W. Archimedes optimization algorithm: a new metaheuristic algorithm for solving optimization problems. Applied Intelligence, 51(3), 1531–1551. (2021).

Hossain, Md. A., Islam, Md. R., Hossain, Md. A., & Hossain, M. J. Control strategy review for hydrogen-renewable energy power system. Journal of Energy Storage, 72, 108170. (2023).

Guo, H., Tao, H., Salih, S. Q., & Yaseen, Z. M. Optimized parameter estimation of a PEMFC model based on improved Grass Fibrous Root Optimization Algorithm. Energy Reports, 6, 1510-1519. (2020).

Mo, Z.-J., Zhu, X.-J., Wei, L.-Y., & Cao, G.-Y. Parameter optimization for a PEMFC model with a hybrid genetic algorithm. International Journal of Energy Research, 30(8), 585-597. (2006).

Mossa, M. A., Kamel, O. M., Sultan, H. M., & Diab, A. A. Z. Parameter estimation of PEMFC model based on Harris Hawks' optimization and atom search optimization algorithms. Neural Computing and Applications, 33(11), 5555-5570. (2021).

Yuan, Z., Wang, W., & Wang, H. Optimal parameter estimation for PEMFC using modified monarch butterfly optimization. International Journal of Energy Research, 44(11), 8427-8441. (2020).

Enabling Interactive G2V and V2G Integration through Smart Fault Protection and Bi-Directional Power Flow Control in EV Charging Stations

[1]Samet Öner, [1*]Gökay Bayrak
[1]Bursa Technical University, Renewable Energy Systems and Smart Grids Laboratory, Department of Electrical and Electronics Engineering, 16300, Bursa, Türkiye
* E-mail: gokay.bayrak@btu.edu.tr

Abstract

The widespread use of electric vehicles (EVs) and the associated EV charging stations can result in overloads on the electricity grid and different power quality issues. To deal with overloads, peak loads need to be minimized by using supplemental energy sources. Vehicle-to-grid (V2G) technology allows energy transfer from the electric vehicle battery to the grid. V2G technology is a promising solution that can support the grid by mitigating the negative impacts of electric vehicles on the grid. During off-peak hours, EV owners can charge their vehicles at a lower energy price. Even during peak load times, the required energy for a house can be supplied from the battery of the electric vehicle. This study aims to enable EVs to contribute to the smart grid by implementing intelligent charging and discharging methods, specifically by employing bidirectional Grid-to-Vehicle (G2V) and V2G solutions instead of traditional, unidirectional systems. A single-phase bidirectional converter (BDC) circuit was designed and implemented to transfer energy using both G2V and V2G technology. The BDC prototype includes voltage and frequency protection functions according to IEEE 929-2000 standards and grid code, providing intelligent protection functions for safe operation with the grid. The results verify the reliable operation of the proposed system. The developed prototype was designed for high-power applications, making it suitable for widespread use in future V2G/G2V applications.

Keywords: Electric Vehicles, EV Charger, V2G, G2V, Bidirectional Power Flow

I. Introduction

The development of smart grids has been influenced by the increasing consumption of electricity, the integration of renewable energy, and advancing technology (Hou et al., 2023). However, one significant challenge in smart grids is the expected rapid increase in the number of electric vehicles in the near future (Li et al., 2022). As the number of electric vehicles on the grid increases, it can overload existing power systems, transformers, and power lines, leading to quality degradation and power outages (Mehrjerdi, 2019). To maximize the potential of electric vehicles, they can be connected to the grid through bidirectional charging and discharging solutions via charging stations, known as two-way G2V-V2G connections (Wang et al., 2020). This approach can allow electric vehicles to provide energy to the grid only when needed, instead of being a burden on the grid. This study aims to provide an example of this approach.

According to a recent publication by (Wong et al. 2022), a single-stage three-phase bidirectional charger was developed using zero voltage switching (ZVS) and soft switching methods. The suggested circuit achieved a high efficiency of 95.2% in G2V mode and 91.2% in V2G mode. The charger's performance was confirmed through experimental results. A recent study by Liu et al. (2022) proposed a new type of wireless power transfer converter. The converter is soft-switched, single-phase, single-stage, and bidirectional. Its primary objective is to reduce the number of semiconductor power elements and the device's total cost. The proposed converter stands out with higher efficiency when compared to traditional single-phase single-stage bidirectional AC-DC topologies.

This study investigates the design and implementation of a single-phase AC-DC converter circuit with bidirectional energy flow. The circuit was created as a prototype charger, which consists of an H-bridge made of IGBT and diodes, a step-down converter, and a boost converter circuit, all connected to the same circuit. The charger has two modes of operation: V2G and G2V. In V2G mode, the DC power source is the DC source on the DC side, and the resistive load is applied as the DC load at the output. In G2V mode, the power network is used as the AC source on the AC side, and there is no output load in V2G mode. An external intelligent protection circuit was implemented on the mains part of the charger as a protection function.

The proposed structure has several advantages over previous studies in the literature. It is more compact and has a smart breaker (SB) and AC-DC rectifier converter, step-down converter, step-up converter, and DC-AC converter circuits, all connected on a single line and synchronized to provide energy flow in both directions. Voltage and frequency values obtained from the input line with SB were transferred to the internet using the ESP8266 WiFi module. Working simulations of the G2V-V2G circuit were carried out in a MATLAB-Simulink environment. In the application phase, the switchings were made using the signal generator and the Arduino platform, and the smart protection function was made using the Arduino platform.

The proposed structure is a prototype system that can transfer power from the grid to the vehicle and from the vehicle to the grid, has smart protection functions, and can be securely connected to the EV charging stations and the grid. It is believed that this prototype system can also be applied to EVs with high battery capacity, with models to be developed in practice at high currents and powers of the proposed structure.

This study's contributions can be summarized as follows:

- A single-phase bidirectional converter (BDC) circuit was designed and implemented to transfer energy using both G2V and V2G technology. The BDC was designed with IGBT elements switched with standard PWM and sinusoidal PWM (SPWM) control methods at a frequency of 30 kHz.
- The study includes an applied aspect, which is a novelty compared to studies that typically present simulations in the literature. The circuit can perform both V2G and G2V modes of operation, which is again a unique feature.
- The BDC prototype includes top/bottom voltage and frequency protection functions according to IEEE 929-2000 standards and grid code, providing intelligent protection functions for safe operation with the grid.
- The developed prototype was designed for high-power applications, making it suitable for widespread use in future V2G/G2V applications.
- This study provides a foundation for future widespread use of V2G/G2V applications and contributes to the development of sustainable transportation systems.

II. Proposed G2V-V2V EV Charger

In conventional charging stations, there are circuits between the EV battery and the grid that convert the energy flow from the grid to the vehicle, with a unidirectional flow. However, in the proposed system, there is an additional smart breaker (SB) that provides under/over voltage and under/over frequency protection. The energy flow in the proposed system is bidirectional, unlike the traditional unidirectional flow. The detailed model of the V2G EV charger prototype is given in Fig. 1.

In G2V mode, the energy is transferred to the transformer through a fuse when the energy, voltage, and frequency values comply with the standards. The energy flow is rectified by passing through an AC-DC converter after reducing the mains voltage with the transformer and then transferring to the load with the step-down converter.

In V2G mode, the voltage source is amplified with an amplifier, turned into AC with a DC-AC converter, and then amplified with a transformer. The AC voltage amplified by the transformer is transferred to the grid via SSR. In the studies, the mains will be the AC source in G2V mode, the rheostat will be the load, the DC power supply will be the DC source and the output will be unloaded in the V2G mode.

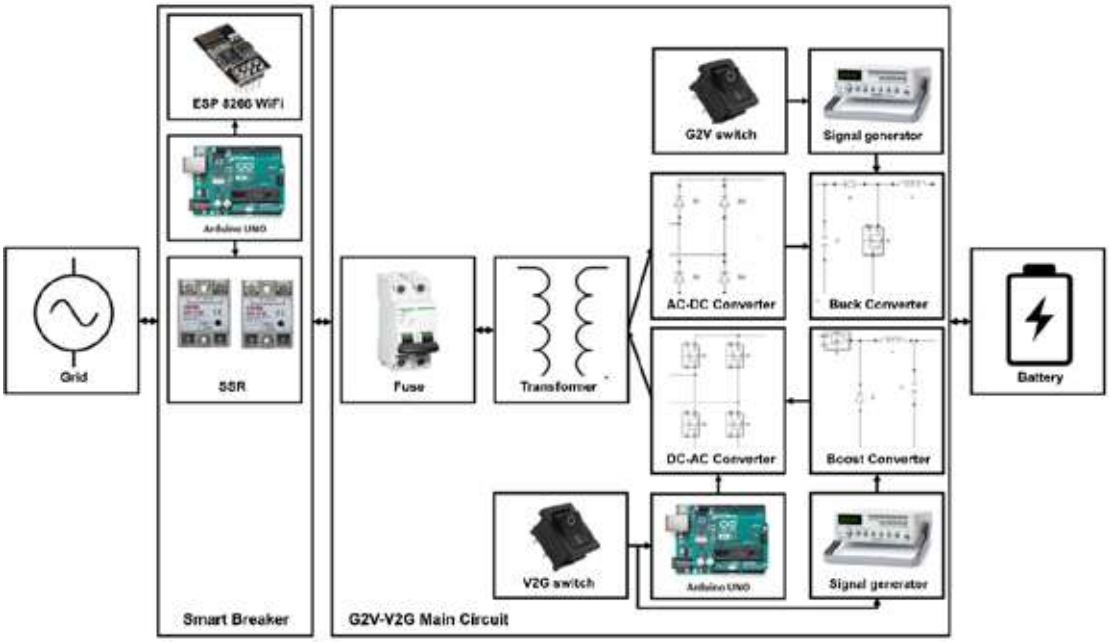


Fig. 1: Proposed G2V-V2G system.

In the diagram, the primary G2V circuit is illustrated in Fig. 1. The circuit diagram for the G2V mode during the test phase is presented in Fig 2. a. The energy flow is from the grid to the vehicle. The power analyzer, which measures the current at the field input network number 2, acts as the power source that supplies the driver for TLP350. This driver triggers the IGBT in the field reducer circuit number 3, and its voltage is 14.5 V. Area 4 shows the waveform of the voltage at the G2V output. Area 5 displays the multimeter that reveals the mains voltage, and its value is read at 228 Vrms. Area 6 illustrates the multimeter that displays the voltage at the output, and its voltage is 12 V. A signal generator, set to a 30 kHz frequency and 35% loop cycle, is used to trigger the IGBT in the field reducer circuit number 7 by providing a signal to the driver for TLP350. Area 8 illustrates the rheostat with a 24 Ω value that works as a load at the G2V output.

In V2G mode, the circuit diagram in Fig.2.b shows the detailed view of the main circuit. The input of the circuit is given in area 1, consisting of an input terminal and boost converter circuit. The DC source output adjusted to 12 V is connected to the input terminal. One TLP350 driver shown in field 2 is used for switching the IGBT in the boost converter. The driver is switched with a signal generator at 30 kHz and 65% duty cycle. The cable coming out of the input terminal is connected to the amplifier converter input. The boost converter increases the 12 V to 34 V, and the step-up converter output is connected to the input line of the H-bridge indicated by field 3. Four IGBTs connected

as H-bridges are switched with the SPWM method using an Arduino Uno development board with four TLP250 drivers in area 4. Then, the H-bridge output is connected to the 24 V low voltage input of the transformer shown in area 5. The transformer increases the 24 V SPWM output to 220 VAA, and the output voltage is measured as 214 VAA with a multimeter from the 6-output terminal.

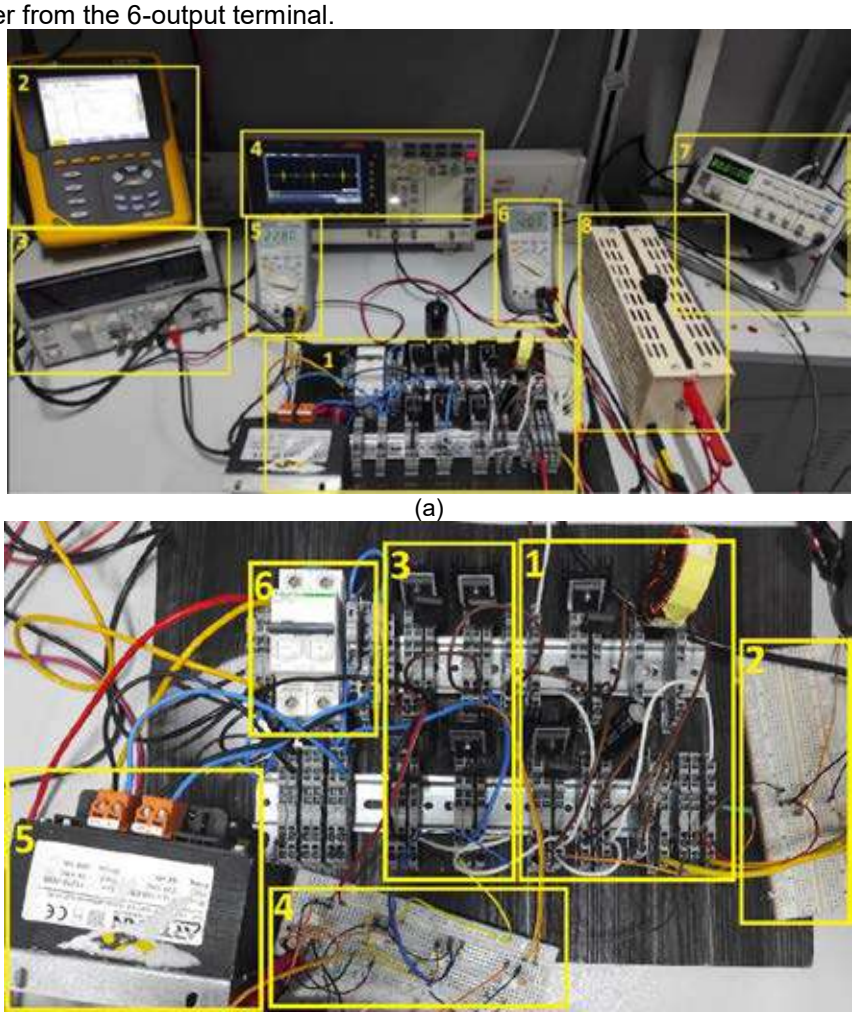


Fig. 2: (a) Developed G2V circuit, and (b) V2G main circuit

IV. Results

A two-way energy flow over a single circuit has been successfully carried out using the designed G2V-V2G circuit. This circuit works in two modes - G2V mode and V2G mode. In G2V mode, there is an electrical network at the circuit input. The AC mains are first reduced with a transformer and then rectified with a full bridge diode and capacitor. Finally, a constant voltage of 12V is obtained at the output with the help of a step-down circuit. The IGBT switch used in the step-down converter is switched with 30 kHz and a 35% duty cycle by the PWM method. The input mains current analyzer image for G2V mode is given in Figure 3. a, and the output voltage wave oscilloscope image is given in Figure 3. b. In V2G mode, there is a DC voltage source at the circuit input.

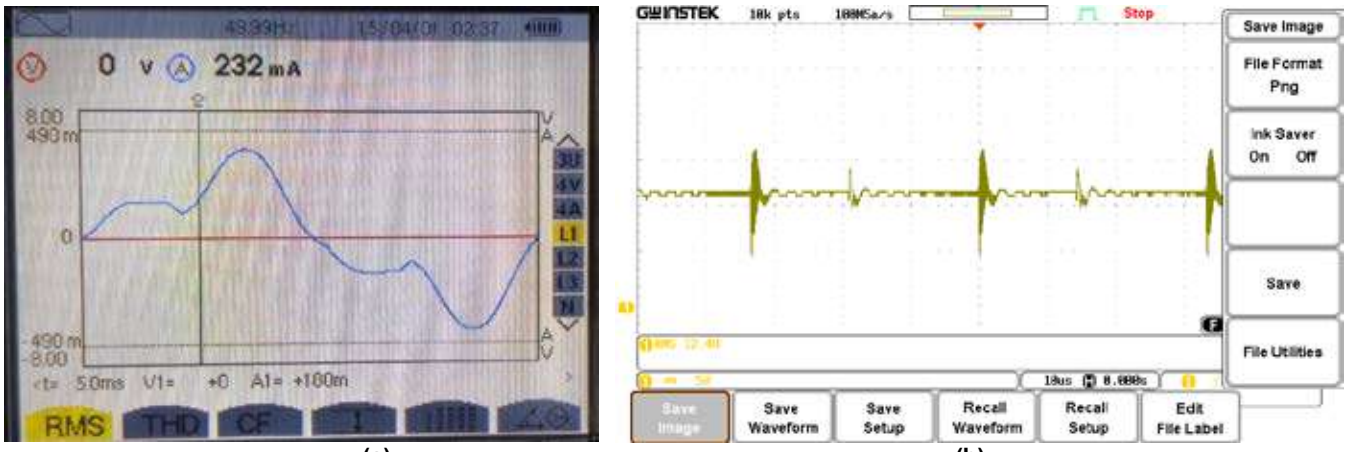


Fig. 3: (a) G2V grid input current, (b) G2V Output Voltage Oscilloscope Display

In V2G mode, the DC source voltage was increased from 12V to 34V using a step-up converter. An H-bridge, consisting of 4 IGBTs, was connected to the input of the transformer and switched using the SPWM method. The voltage amplified by the transformer was measured at 214V at the output. The IGBT switch used in the boost converter was switched with 30kHz and 65% duty cycle using the PWM method. [Plate_number_1] and [Plate_number_2] drivers were used for the H-bridge IGBT switches due to their high performance in step-down and step-up switches. The switching graph of the [Plate_number_2] output used for the H-bridge IGBT is shown in Fig. 4 of the oscilloscope output.

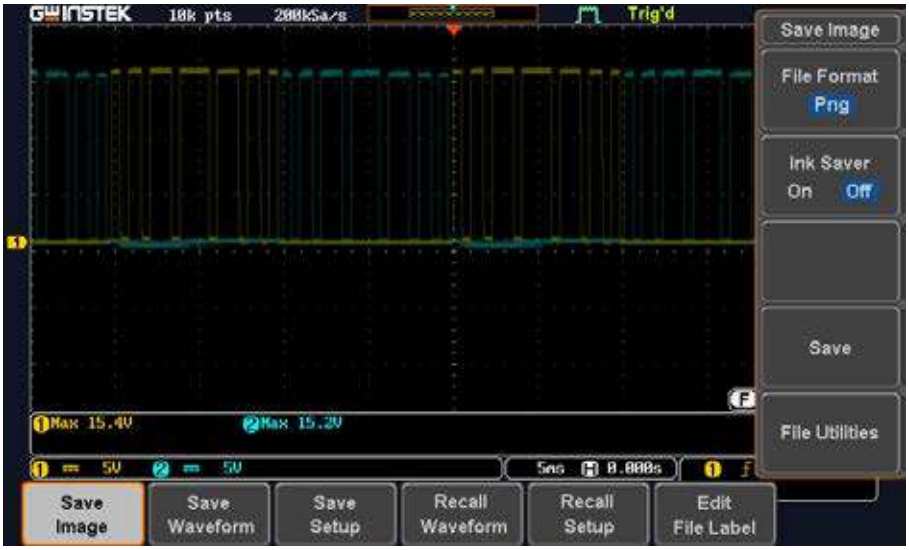


Fig. 4: V2G operation of Inverter output

V. Conclusions

In this study, a prototype of a charger with bidirectional energy flow and protection functions over a single circuit has been designed and implemented. The charger is intended for use in EV charging stations and can effectively transfer energy from the grid to the load in the G2V mode, and from the DC source to the grid in the V2G mode. The charger is equipped with an IoT-based SB that performs protection functions independently of the inverter while complying with the grid codes for voltage and frequency. It is believed that this prototype system can also be used for EVs with high battery capacity. Further models will be developed to test the high current and power capabilities of the proposed structure.

Acknowledgment

This thesis was supported by Bursa Technical University Scientific Research Project Unit (BTU-BAP) within the scope of the Master's Thesis Research Project with project number 220Y020.

References

Hou, L., Dong, J., Herrera, O. E., and Mérida, W., Energy management for solar-hydrogen microgrids with vehicle-to-grid and power-to-gas transactions, International Journal of Hydrogen Energy, 48(5), 2013-2029, (2023).

Li, H., Sun, B., Hao, J., Zhao, J., Li, J., and Khakichi, A., Economical planning of fuel cell vehicle-to-grid integrated green buildings with a new hybrid optimization algorithm. International Journal of Hydrogen Energy, 47(13), 8514-8531, (2022).

Mehrjerdi, H., Off-grid solar-powered charging station for electric and hydrogen vehicles including fuel cell and hydrogen storage. International journal of hydrogen Energy, 44(23), 11574-11583, (2019).

Wang, Y., Kazemi, M., Nojavan, S., and Jermsittiparsert, K., Robust design of off-grid solar-powered charging station for hydrogen and electric vehicles via a robust optimization approach. International Journal of Hydrogen Energy, 45(38), 18995-19006, (2020).

Wong, C. S., Liu, J., Cao, L., and, Loo, K. H., A SWISS-Rectifier-Based Single-Stage Three-Phase Bidirectional AC–DC Inductive-Power-Transfer Converter for Vehicle-to-Grid Applications, IEEE Transactions on Power Electronics, 38(3), 4152-4166, (2022).

Liu, J., Xu, F., Sun, C., and Loo, K. H., A soft-switched power-factor-corrected single-phase bidirectional AC–DC wireless power transfer converter with an integrated power stage, IEEE Transactions on Power Electronics, 37(8), 10029-10044, (2022).

CFD Combustion Model Optimization for Hydrogen Blended Combustion in Furnace Experimental System

[1*]Onur Salcı, [2]Semiha Öztuna
[1] Termo Isı Sistemleri Tic. ve San. A.Ş., R&D Department, Tekirdağ, 59850, Türkiye
[2] Trakya University, Engineering Faculty, Mechanical Engineering Department,Institute of Natural and Applied Sciences, Edirne, 22030, Türkiye

* E-mails: onur.salci@ecostar.com.tr , semihae@trakya.edu.tr

Abstract
Industrial burners have large heat input ranges. Prototype optimization experiments of the burners could be expensive or impossible. Combustion numerical studies are very efficient method to predict combustion variables instead of experiments. In the present study, EDC (eddy dissipation combustion), NPC (Non premixed combustion) and PPC (partially premixed combustion) models have been performed for NG (natural gas) combustion and compared with experimental results. Optimum realistic values have been calculated by using PPC model. After, determination of combustion model, H_2 (hydrogen) blending ratio has been increased up to 20% in NG fuel. Greenhouse gases ratios have been decreased, NO_x pollutants and flue gas temperatures have been increased by resulted of H_2 blended NG fuelled combustion.

Keywords: Combustion model, Hydrogen, Hydrogen blended combustion

I. Introduction

Eco-friendly energy demands in the world are increasing day by day. Fossil fuels used due to increasing energy demands create greenhouse gases as a result of combustion. CO_2 (carbon dioxide) is an important heat-trapping gas, also known as a greenhouse gas (Change, n.d.).

H_2 is an efficient alternative fuel for decarbonization studies in industry. It is not released CO_2, CO (carbon monoxide) and unburned hydrocarbon emissions when it burned purely. Greenhouse gas emissions can be reduced by burning H_2 as a blending gas into NG fuel.

Various studies about hydrogen blended combustion have been conducted in literature. NPC model has been used by Büyükakın and Öztuna (2020) to investigate combustion performance of nozzle-mix gas burner in back pressurized water cooled boiler. As the H_2 content in the fuel increased, the NO_x (nitric-oxides) rate increased. Effect of swirl number on the combustion characteristics of H_2 containing fuel blends in a gas fired combustor using a numerical CFD code have been investigated by İlbaş et al. (2016). The PDF Mixture Fraction combustion model was used due to its accuracy for blending fuels. Temperature distributions and gas emissions from the combustion of various H_2-CH_4 fuel blends in a model combustor have been conducted by Yılmaz and İlbaş (2008). The results showed that increasing the H_2 content in the fuel blend increased the temperature and reduced CO and CO_2 emissions. Effects of H_2 blending on ammonia combustion in a model combustor have been investigated by Kekul et al. (2023). hydrogen addition improves flame stability and increases flame temperature, but also increases NO emissions.Turbulent non premixed H_2 and H_2 – C_xH_y (hydrocarbon) flame with different radiation models and without radiation has been modelled by İlbaş (2008). Using radiation models in calculation resulted with similar values according to experimental values. Lower temperatures and NO_x emissions were calculated using with radiation models compared with non-radiation model.

In the present study, Fluent codes of different combustion models have been performed and compared with the experimental results. Then, H_2 blending rate has been increased in NG and investigated of combustion variables numerically and experimentally.

II. Experimental Set-up and Procedure

Experiments of the study have been conducted in the R&D laboratory of Ecostar, located in Tekirdağ, Türkiye, using a PLC controlled combustion experimental system. The combustion experimental system includes NG, H_2, a gas blending unit, and pressurized air lines. Leakage and safety controls were performed before each experiment. The experimental system provides a maximum heat input of 150 kW with a blending of 20% H_2 gas and 80% NG.

The experiments utilized an Ecostar FPB 200 (FPB 200 - Ecostar, n.d.) process gas burner. This type of burner is primarily used in industry for heat treatment, melting, drying and various process heating applications. Features of the burner are dual-stage, direct ignition and ionization with electrodes.

The schematic view of the combustion experiment system is given in **Fig.1**. Fuel types in experiments are 100% NG and 5%, 10%, 15%, 20% H_2 blended in NG respectively. NG was supplied by Çordaş Çorlu NG Distribution Co. and the compositional values of NG used in the experiments are given in **Tab 1**. H_2 was supplied by Habaş Industrial and Medical Gases Production Industry Inc. as pressurized cylinder tanks (Salcı, O., 2023).

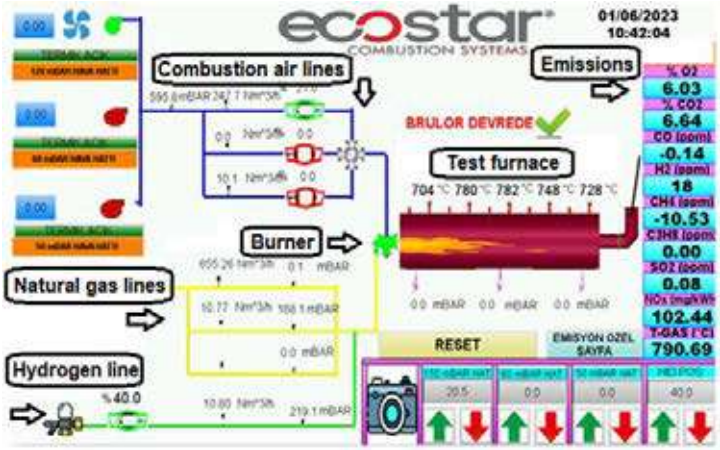


Fig. 1: The schematic view of the combustion experiment system (Salcı, O., 2023).

Tab 1. Natural gas compositions (Salcı, O., (2023).

Content	CH_4	C_2H_6	C_3H_8	C_4H_{10}	C_5H_{12}	C_6H_{14}	N_2	CO_2
Mole (%)	*96.068*	*2.198*	*0.654*	*0.194*	*0.0131*	*0.01*	*0.668*	*0.0177*

Combustion experiments were conducted in the test furnace to measure flue gas emissions and temperature variations.The experiments were conducted again at atmosphere ambient conditions to observe of H_2 effects on flame. Heat input of 150 kW was applied in the combustion experiments with constant λ (excess air ratio) of 1.2. The fuel and combustion air flow rates required for combustion are given in **Tab 2**.

Tab 2. Fuel and combustion air flow rates depending on blended fuel composition and constant λ=1.2 (Salcı, O., (2023).

Blended Fuel Composition	Heat Input (kW)	$\dot{V}_{fuel,N}$ (Nm³/h)	$\dot{V}_{fuel,H2}$ (Nm³/h)	$\dot{V}_{air}$ (Nm³/h)
100 % NG + 0 % H_2	*150*	*16*	*0*	*183.4*
95 % NG + 5 % H_2	*150*	*15.7*	*0.8*	*179.9*
90 % NG + 10 % H_2	*150*	*15.4*	*1.8*	*179,1*
85 % NG + 15 % H_2	*150*	*15.1*	*2.7*	*178.7*
80 % NG + 20 % H_2	*150*	*14.8*	*3.7*	*176.2*

The furnace internal pressures measured from different points are -0.1 mbar constantly. Main flue suction line created vacuum condition in furnace during combustion experiments and any pressure rises didn't occur. O_2, CO_2, CO, CH_4, NO, and temperature were measured with MRU MGA Prime gas analyzer after all values were stabilized.

III. Analysis

In the present study, simulation of combustion involves of the equations governing the conservation of mass, momentum, and energy within the fluid domain. Continuity equation, conservation of momentum, energy equation and ideal gas equation are given between Eq. (1) and Eq. (3), (Yılmaz et al., 2017):

$$\frac{\partial}{\partial t}(\rho) + \nabla.(\rho\vec{v}) = 0 \quad (1)$$

$$\frac{\partial}{\partial t}(\rho\vec{v}) + \nabla.(\rho\vec{v}\vec{v}) = -\nabla p + \nabla(\bar{\bar{\tau}}) + \rho\vec{g} + \vec{F} \quad (2)$$

$$\frac{\partial}{\partial x_j}(\rho u_j h + F_{hj}) = u_j\frac{\partial p}{\partial x_j} + \tau_{ij}\frac{\partial u_i}{\partial x_j} \quad (3)$$

Energy equation (3) non-adiabatic NPC model is enabled, the total enthalpy form of the energy equation is given Eq (4) (ANSYS Fluent 2023R2, 2023):

$$\frac{\partial}{\partial t}(\rho H) + \nabla.(\rho\vec{v}H) = -\nabla.\left(\frac{k_{eff}}{c_p}\nabla H\right) + S_h \quad (4)$$

PPC model solves a transport equation for the mean mixture fractions and reaction progress variables to determine the position of the flame front. f (mean mixture fraction) equation PDF (probably density function) is given Eq (5) and Eq (6), (ANSYS Fluent 2023R2, 2023):

$$f = \frac{Z_i - Z_{i,oxidizer}}{Z_{i,fuel} - Z_{i,oxidizer}} \quad (5)$$

$$\bar{\Phi} = \int_0^1 \int_0^1 \Phi \ (f,c) p(f,c) df dc \quad (6)$$

Eq (5) and Eq (6) have been solved both NPC and PPC combustion models. The net rate of production of species i due to reaction r for the EDC model is given by Eq (7),(ANSYS Fluent 2023R2, 2023):

$$R_{i,r} = (v''_{i,r} - v'_{i,r}) M_{w,i} A \ \frac{\varepsilon}{k} \dot{m} \ _R(\frac{Y_R}{v'_{R,r} M_{w,R}}) \quad (7)$$

Realizable k - ε turbulence model has been used for (RANS) (reynolds averaged navier stokes) simulations. Discrete ordinates (DO) model have used for radiation modelling of gas fuelled combustion. After combustion cases converged for all species, NO values were solved as slow chemistry.

CFD model mesh properties are polyhedral cell types 2,896,126 cells, 505,174 nodes, and maximum skewness is 0.79. At the furnace flue exit, atmospheric pressure have been defined. Inner walls of the furnace are firebrick material and average temperature is 1000 K and emissivity value is 0.33 (Bergman et al., 2011). Air temperature is approximately 298 K and fuel temperature is approximately 293 K. Boundary conditions of fuel and air inlet are given by **Tab 2** (Salcı, O., 2023).

Tab 2. Fuel properties, Re (Reynolds) numbers, and mass flow rates of fuel and air (Salcı, O., 2023).

Fuel Type	λ	LHV (kcal/Nm³)	ρ_{fuel} (kg/m³)	Re_{fuel}	Re_{air}	$\dot{m}_{fuel}$ (kg/s)	$\dot{m}_{air}$ (kg/s)
100 % NG	*1.2*	*8066*	*0.6893*	*12600*	*85100*	*0.00306*	*0.06151*
95 % NG + 5 % H_2	*1.2*	*7798*	*0.6599*	*13000*	*84800*	*0.00303*	*0.06131*
90 % NG + 10 % H_2	*1.2*	*7518*	*0.6293*	*13500*	*84600*	*0.003*	*0.06115*
85 % NG + 15 % H_2	*1.2*	*7246*	*0.5994*	*14000*	*84300*	*0.002964*	*0.06093*
80 % NG + 20 % H_2	*1.2*	*6970*	*0.5693*	*14600*	*82900*	*0.002916*	*0.05994*

IV. Results and discussions

In the present study 3 different Fluent combustion model have been analysed and compared with experimental results. Total operating pressures of fuel and air have been compared with the experimental results given in **Tab 3**.

Tab 3. Comparison of total operating pressures of fuel and air; FPB 200, 150 kW, NG fuelled, λ:1.2.

Combustion Models	EDM	NPC	PPC	Experiment
P_{fuel} (mbar)	*15.9*	*14.29*	*14.38*	*13.7*
P_{air} (mbar)	*16.57*	*15.54*	*16.14*	*14.9*

Operating pressures at NPC and PPC of fuel and air have been validated by experimental results, but EDM results have been different from experimental results. Emissions and flue gas temperatures compared in **Tab 4**. O_2 emissions of all models are similar to experimental result. CO_2 emissions of EDM and NPC are different from experimental result, but CO2 value of PPC model is similar to experimental result. NO value of EDM is higher, NO value of NPC is lower than experimental result. NO value of PPC is similar to experimental result. CO and CH_4 pollutants of EDM are calculated higher and CO and CH_4 pollutants of NPC are lower than experimental result. and CO and CH_4 pollutants of PPC are similar to experimental result. Flue gas temperatures have been calculated higher than experimental result approximately 150 – 200 °C in all cases. PDF. table calculation of temperatures are higher than exact temperatures, that is known by literature. Therefore, $T_{flue\ gas}$ temperatures have been corrected.

Tab 4. Comparison of emissions and flue gas temperatures ; FPB 200, 150 kW, NG fuelled, λ:1.2.

Combustion Models	O_2 (%)	CO_2 (%)	NO (ppm)	CO (mass fraction)	CH_4 (mass fraction)	$T_{flue\ gas}$ (°C)
EDM	*3.7*	*9.32*	*73*	*4.97E-31*	*6.50E-11*	*910*
NPC	*3.6*	*9.44*	*36*	*1.24E-05*	*1.29E-06*	*907*
PPC	*3.6*	*9.5*	*44*	*1.11E-07*	*0*	*913*
Experiment	*3.5*	*9.5*	*42*	*11E-06*	*0*	*887*

H_2 has been blended with NG up to 20% by volume. Comparison of numerical and experimental results given in Fig 2.

In Fig 2. depending on increasing H_2 content in NG fuel, O_2 emissions kept constant with low fluctuations, CO_2 emissions reduced approximately 5.8%, NO emissions increased approximately 21%, T_{flue_gas} increased approximately 12.5%.

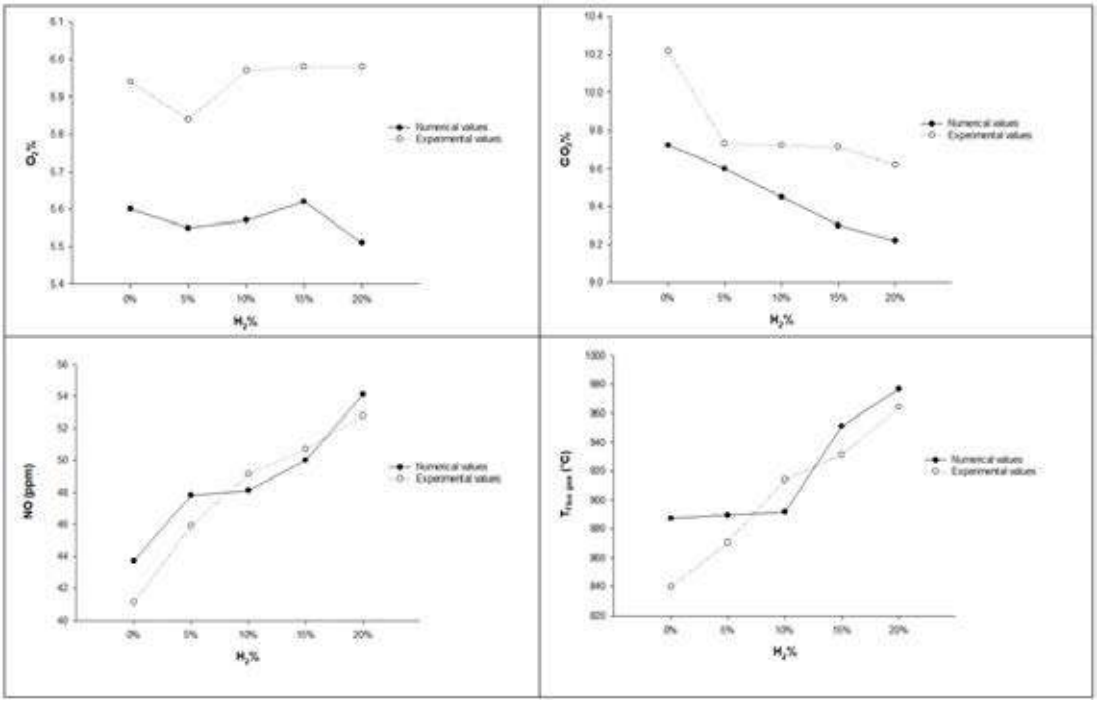


Fig 2. Comparison of numerical and experimental O_2 (%), CO_2 (%), NO (ppm) and $T_{flue\ gas}$ (°C) ; FPB 200, 150 kW, 100 – 80 % NG + 0 – 20 % H_2 fuelled, λ:1.2 .

V. Conclusions

In the present study, different Fluent combustion models are EDC, NPC and PPC have compared each other and experimental results. PPC model has been provided optimum realistic results for NG and H_2 blended NG fuelled combustion. Additionally, H_2 blending ratio in NG fuel has been increased up to 20% percent. Decarbonizaton has been provided by reducing greenhouse gas emissions. Though, low blending ratios of H_2 in NG fuel, combustion efficiency of the burner has been improved.

Acknowledgements

We would like to thank the management of Ecostar and our colleagues, TÜBİTAK, TÜBAP and our families for their supports.

References

ANSYS Fluent 2023R2, Theory guide. July 2023.

Bergman, T. L., Lavine, A. S., Incropera, F. P., & DeWitt, D. P. (2011). Introduction to heat transfer. John Wiley & Sons.

Büyükakın, M. K., & Öztuna, S. (2020). Numerical investigation on hydrogen-enriched methane combustion in a domestic back-pressure boiler and non-premixed burner system from flame structure and pollutants aspect. International Journal of Hydrogen Energy, 45(60), 35246 35256. https://doi.org/10.1016/j.ijhydene.2020.03.117

Change, N. G. C. (n.d.). Carbon dioxide concentration | NASA Global Climate Change. Climate Change: Vital Signs of the Planet. https://climate.nasa.gov/vital-signs/carbon-dioxide/?intent=111

FPB 200 - Ecostar. (n.d.). https://www.ecostar.com.tr/en/products/industrial-burners/process/fpb/fpb-200

İlbaş, M. (2005). The effect of thermal radiation and radiation models on hydrogen–hydrocarbon combustion modelling. International Journal of Hydrogen Energy, 30(10), 1113–1126. https://doi.org/10.1016/j.ijhydene.2004.10.009

İlbaş, M., Karyeyen, S., & Yılmaz, İ. (2016). Effect of swirl number on combustion characteristics of hydrogen-containing fuels in a combustor. International Journal of Hydrogen Energy, 41(17), 7185–7191. https://doi.org/10.1016/j.ijhydene.2015.12.107

Salcı, O. (2023). Fırın sisteminde hidrojen gazı katkılı doğal gaz yakıtlı proses brülörü yanma analizleri ve optimizasyonu (Master's thesis, Trakya Üniversitesi Fen Bilimleri Enstitüsü)

Yılmaz, H., Çam, Ö., Tangöz, S., & Yılmaz, İ. (2017). Effect of different turbulence models on combustion and emission characteristics of hydrogen/air flames. International Journal of Hydrogen Energy, 42(40), 25744–25755. https://doi.org/10.1016/j.ijhydene.2017.04.080

Yılmaz, İ., & İlbaş, M. (2008). An experimental study on hydrogen–methane mixtured fuels. International Communications in Heat and Mass Transfer, 35(2), 178–187. https://doi.org/10.1016/j.icheatmasstransfer.2007.06.004

Hydrogen Blended Natural Gas Fuelled A Process Heating Application

[1*]Onur Salcı, [2]Semiha Öztuna, [3]Mustafa İlbaş,
[1] Termo Isı Sistemleri Tic. ve San. A.Ş., R&D Department, Tekirdağ, 59850, Türkiye,
[2] Trakya University, Engineering Faculty, Mechanical Engineering Department,Institute of Natural and Applied Sciences, Edirne, 22030, Türkiye
[3] Gazi University, Engineering Faculty, Mechanical Engineering Department, Graduate School of Natural and Applied Sciences, Ankara, 06500, Türkiye

* E-mails: onur.salci@ecostar.com.tr , semihae@trakya.edu.tr , ilbas@gazi.edu.tr

Abstract
H_2 (Hydrogen) is an alternative eco-friendly fuel in process burners by blending it with NG (natural gas) in different ratios. In the present study, H_2 blended fuel effect to combustion performance of a process burner were investigated. 100% NG, 30%, 40% and 50% H_2 blended NG fuels were used. Heat input of the burner is 120 kW. Equivalence ratio is kept constant as 0,77. Experimental studies were validated by Fluent codes. Partially premixed combustion model was used in combustion cases. Resulting by up to 50 %H_2 blended NG combustion by volume, O_2 (oxygen) remained constant with low fluctuations, CO_2 (carbon dioxide) decreased by up to 21%, H_2O (water vapor) increased by up to 16%, CO (carbon monoxide) decreased by up to 82%, CH_4 (methane) decreased by up to 79,6% and nitric oxide (NO) increased by up to 26,5%.

Keywords: Hydrogen, Hydrogen Blended Fuel, Process Heating, Decarbonization

I. Introduction

COP28, signaling a transition towards a carbon-free future by moving away from fossil fuels, will play a significant role in meeting global energy needs and decarbonizing industries as part of the transition to human-centered net zero energy, with renewable and low-carbon hydrogen based technologies (COP28 Declaration of Intent - Hydrogen, n.d.).

Passing to low carbon technologies in current industrial processes, accelerating the use of renewable energy alone is not sufficient. Using of eco-friendly renewable fuels blending and adapting with fossil fuels should be expanded. Lower greenhouse gas emissions and pollutants can be achieved by blending different proportions of H_2 into NG fuelled burner that require heat power in the continuous operation.

The effects of hydrogen blended in different ratios with NG on combustion and diffusion flame structure have been investigated by Öztuna and Büyükakın (2020) in a non-premixed, pressure-swirl burner and back pressured water-cooled boiler system. As the blending rate of hydrogen in combustion increased, the flame has become less dense and flow velocities of the flame have increased. The effect of CO_2 on combustion efficiency of CH_4 and H_2 have been investigated by Ilbas and Candan (2023b) using a small swirl burner and furnace combustion system. At higher CO_2 dilution rates, combustion instability has decreased. The gas emissions resulting from turbulent reactive flow using composite fuels of H_2 and CH_4 at different blending ratios have been investigated by Ilbas and Yılmaz (2011) in a model burner. As the blending rate of H_2 in the fuel increases, combustion efficiency has increased, and CO emissions have decreased. The effect of flame behavior and combustion performance resulting from the combustion of NG mixed with 30 % H_2 by volume in different gas stove geometries have been investigated by Sorgulu et al. (2024b). H_2 blending rate in combustion increases, shorter flame length, altered flame color to bluish and improved combustion efficiency has been occurred. Experiments involving different ratios of H_2 blended with NG in identical gas stoves have been conducted by Öztürk et al. (2023). Despite decreased in CO_2 and CO emissions, fluctuation in NO_x emissions has been measured.

II. Experimental Set-up and Procedure

Experiments of the study have been conducted in the R&D laboratory of Ecostar, located in Tekirdağ, Türkiye, using a combustion experimental system with blending of NG and H_2. The combustion experimental system includes NG, H_2, a gas blending unit, and pressurized air lines. Leakage and safety controls were performed before each experiment. The experimental system provides a maximum heat input of 120 kW with a blending of 50 % H_2 gas and 50 % NG.

The experiments utilized an Ecostar FPB 200 (FPB 200 - Ecostar, n.d.) process gas burner. This type of burner is primarily used in industry for process heating, heat treatment, melting, drying, and various applications. In the experiments, the burner was used with dual-stage, direct ignition, and ionization features (Salcı, O., 2023).

The control of the burner, fuel and air lines, and emission variations were provided by the PLC (Programmable Logic Controller) operating the combustion experiment system. The schematic view of the combustion experiment system is given in **Fig.1**. Fuel types in experiments are 100% NG, 70% NG and 30% H_2, 60% NG and 40% H_2, and 50% NG and 50% H_2, respectively. NG was supplied by Çordaş Çorlu NG Distribution Co. and the compositional values of NG used in the experiments are given in **Tab 1**. H_2 was supplied by Habaş Industrial and Medical Gases Production Industry Inc. as pressurized cylinder tanks (Salcı, O., 2023).

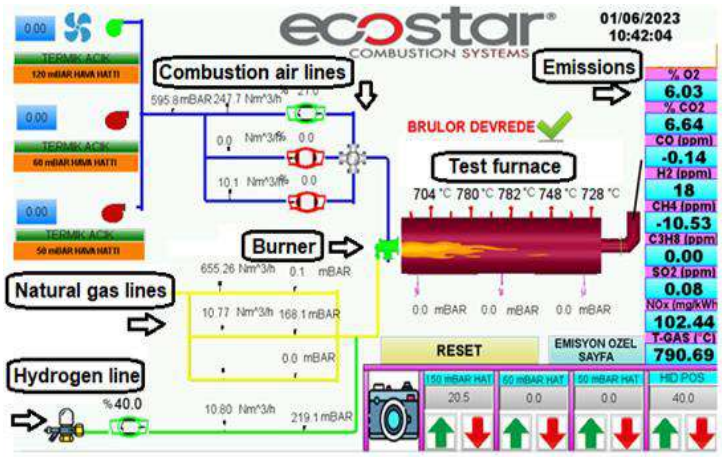


Fig. 1: The schematic view of the combustion experiment system (Salcı, O., 2023).

Tab 1. Natural gas compositions (Salcı, O., 2023).

Content	CH_4	C_2H_6	C_3H_8	C_4H_{10}	C_5H_{12}	C_6H_{14}	N_2	CO_2
Mole %	*96.068*	*2.198*	*0.654*	*0.194*	*0.0131*	*0.01*	*0.668*	*0.0177*

Four different combustion experiments were conducted in the test furnace to measure flue gas emissions and temperature variations.The experiments were conducted again at atmosphere ambient conditions to observe of H_2 effects on flame. Heat input of 120 kW was applied in the combustion experiments with constant φ (equivalence ratio) of 0.77. The fuel and combustion air flow rates required for combustion are given in Tab 2.

Tab 2. Fuel and combustion air flow rates depending on blended fuel composition and constant $\varphi = 0.77$

Blended Fuel Composition	Heat Input (kW)	$\dot{V}_{fuel,NG}$ (Nm^3/h)	$\dot{V}_{fuel,H2}$ (Nm^3/h)	$\dot{V}_{air}$ (Nm^3/h)
100 % NG + 0 % H_2	*120*	*12.5*	*0*	*195.1*
70 % NG + 30 % H_2	*120*	*14.1*	*6.1*	*192.2*
60 % NG + 40 % H_2	*120*	*13.2*	*8.8*	*189.3*
50 % NG + 50 % H_2	*120*	*12.1*	*12.1*	*187.4*

The furnace internal pressures measured from different points are -0.1 mbar constantly. Main flue suction line created vacuum condition in furnace during combustion experiments and any pressure rises didn't occur. O_2, CO_2, CO, CH_4, NO, and temperature were measured with MRU MGA Prime gas analyzer after all values were stabilized.

III. Analysis

CFD model mesh properties are polyhedral cell types 2,896,126 cells, 505,174 nodes, and maximum skewness is 0.79 .

At the furnace flue exit, atmospheric pressure have been defined. Inner walls of the furnace are firebrick material and average temperature is 1000 K and emissivity value is 0.33 (Bergman et al., 2011). Adiabatic wall boundary condition has been defined for other furnace and burner surfaces. Heat input of the burner was set to 120 kW constantly.

The measured average combustion air temperature was 298 K, and fuel temperature was 293 K. Hydraulic diameters are 0.0272 m for fuel, 0.091 m for air, and 0.22 m for flue gas.

NG consists of approximately 96% CH_4 by volume given in Tab 2. Therefore, CH_4 was used instead of NG in numerical analyses. Boundary conditions of fuel and air inlets are given in Tab 3.

Tab 3. Boundary conditions of fuel and air inlets (Çengel and Cimbala, 2004),(ANSYS Fluent 2023R2, 2023)

Blended Fuel Composition	$\dot{m}_{air}$ (kg/s)	$\dot{m}_{fuel}$ (kg/s)	ρ_{fuel} (kg/m^3,)	Hu ($kcal/Nm^3$)	Air/Fuel (m^3/m^3)	I_{fuel} (%)	I_{air} (%)
100 % CH_4	*0.04984*	*0.00228*	*0.683*	*8570*	*12.38*	*4.75*	*4.3*
70 % CH_4 + 30 % H_2	*0.04890*	*0.00213*	*0.504*	*6770*	*9.59*	*4.62*	*4.3*
60 % CH_4 + 40 % H_2	*0.04846*	*0.00206*	*0.444*	*6170*	*8.66*	*4.56*	*4.3*
50 % CH_4 + 50 % H_2	*0.04793*	*0.00198*	*0.384*	*5570*	*7.74*	*4.51*	*4.3*

PPC (partially premixed combustion) model was used for all combustion cases. PPC model solves a transport equation for the mean mixture fractions and reaction progress variables to determine the position of the flame front (ANSYS Fluent 2023R2,2023). f (mean mixture fraction) equation is given Eq (1).

$$f = \frac{Z_i - Z_{i,oxidizer}}{Z_{i,fuel} - Z_{i,oxidizer}} \quad (1)$$

In Eq.(1) Z_i is the elemental mass fraction for element, i (ANSYS Fluent 2023R2,2023). $Z_{i,fuel}$ and $Z_{i,oxidizer}$ defines gas fuel and combusiton air.

Chemical equilibrium model and PDF (probably density function) were solved for diffusion flames. Density weighted mean scalars (such as temperature and species fractions) defines as $\bar{\Phi}$, are calculated from the probablity density function (PDF) equation of mean reaction progress (c) , and local mixture fraction (f) is given Eq(2) (ANSYS Fluent 2023R2,2023).

$$\bar{\Phi} = \int_0^1 \int_0^1 \Phi \ (f,c) p(f,c) df dc \quad (2)$$

DO (discrete ordinates) model was used for radiation modelling. In the present study, the flow characteristics of fuel and air are determined as turbulent flow for all cases (Tab 3.). Realizable k - ε turbulence model has been used. After all variables converged, NO_x post processing have been done.

IV. Results and discussions

The comparison of numerical calculations and experimental measurements in the present study is given in Tab 4. Experimental and numerical results conducted φ=0.77 and four different fuel blending ratios, differences of O_2, CO_2, CO, CH_4, NO, and $T_{flue\ gas}$ have been examined. H_2O emissions in the flue gas composition were not measured by gas analyser and were only estimated based on CFD calculations. O_2 emissions remained constant with small fluctuations due to the increased proportion of hydrogen gas in fuel blends, as a result of constant φ=0.77 combustion. CO_2 emissions decreased by 21% as the volumetric percentage of H_2 in fuel blend increased to 50%. As the proportion of H_2 in the fuel content increased up to 50%, there was a 16% increase in H2O emissions.

CO and CH_4 greenhouse gas emissions result from incomplete combustion of hydrocarbon-based fuels. As the proportion of these emissions increases, incomplete combustion and unnecessary fuel consumption also increase. Although CO and CH_4 greenhouse gas emissions were too low to be measured in the experiments, numerical calculations showed low levels of emissions, which decreased significantly with an increase in H_2 gas content. CO emissions decreased by -82%, and CH_4 emissions decreased by -79.6% due to the increase in H_2 content in the blended fuel.

NO_x pollutant emissions are mostly composed of NO. As the proportion of H_2 in the fuel increased, NO emissions increased by 26.5% in the experiments and by 29.8% in the CFD calculations. Since, increase in flame peak temperature as the proportion of H_2 gas in combustion increased, NO_x emissions increase. NO_x emission rates can be reduced with NO_x reduction methods applied in current burner technology.

Tab 4. Comparison of experimental and numerical results

Blended Fuel Composition	O_2 (%)	CO_2 (%)	H_2O (%)	CO (mass fraction)	CH_4 (mass fraction)	NO (ppm)	$T_{fluegas}$ (K)
100 % CH_4, EXP	*4.86*	*9.23*	-	*0*	*0*	*36.4*	*1302.1*
100 % CH_4, CFD	*4.95*	*8.97*	*15.2*	*1.13E-05*	*4.57E-07*	*40.6*	*1330.2*
70 % CH_4 + 30 % H_2, EXP	*4.78*	*8.39*	-	*0*	*0*	*48.3*	*1310.9*
70 % CH_4 + 30 % H_2, CFD	*4.95*	*8.19*	*16.6*	*2.51E-06*	*1.16E-07*	*44.7*	*1336.4*
60 % CH_4 + 40 % H_2, EXP	*4.88*	*8.06*	-	*0*	*0*	*45.8*	*1318.8*
60 % CH_4 + 40 % H_2, CFD	*4.83*	*7.88*	*17.4*	*2.12E-06*	*1.07E-07*	*48.4*	*1342.4*
50 % CH_4 + 50 % H_2, EXP	*4.81*	*7.39*	-	*0*	*0*	*49.5*	*1347.6*
50 % CH_4 + 50 % H_2, CFD	*5.05*	*7.3*	*18.1*	*2.04E-06*	*9.33E-08*	*52.7*	*1351.3*

Flame center velocities formed on the central axis from the burner and furnace to the chimney exit are shown in Fig 2.. As the proportion of H_2 in combustion increased, the flow velocity at the center of the flame increased, resulting in a decrease in flame diameter.

In experimental studies and CFD calculations, flue gas increased relative to the fuel content as the proportion of H_2 increased. This can be explained by the increase in flame peak temperature as the proportion of H_2 increased in combustion.

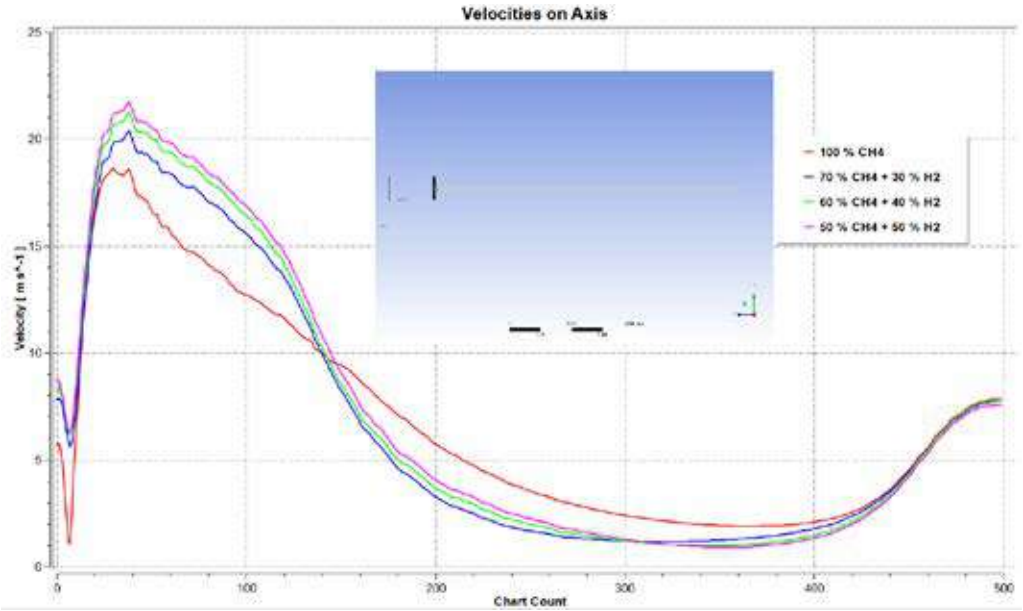


Fig. 2: Combustion flow velocities at burner and furnace axis depending on fuel type

V. Conclusions

Process burners are commonly used in industry. In the present study, NG fulelled combustion performance of a process burner and NG blended with up to 50% hydrogen by volume have been investigated using experimental and numerical methods. As the proportion of H_2 increases, greenhouse gas emissions decrease, leading to eco-friendly combustion. However, flame peak temperature and NO_x pollutants increase with increase of H_2 in combustion. NO_x could be reduced by adapting the burner and using traditional NOx reduction methods. Higher flame temperatures and flame front flow velocity with H_2 fuel might be useful for process applications requiring rapid heating.

Acknowledgements

We would like to thank the management of Ecostar and our colleagues, TÜBİTAK, TÜBAP and our families for their supports.

References

ANSYS Fluent 2023R2, Theory guide. July 2023.

Bergman, T. L., Lavine, A. S., Incropera, F. P., & DeWitt, D. P. (2011). Introduction to heat transfer. John Wiley & Sons.

Çengel, Y. A., & Cimbala, J. M. (2004). Fluid Mechanics: Fundamentals and Applications. http://ci.nii.ac.jp/ncid/BB04830554

COP28 Declaration of Intent - hydrogen. (n.d.). https://www.cop28.com/en/cop28-uae-declaration-on-hydrogen-and-derivatives

FPB 200 - Ecostar. (n.d.). https://www.ecostar.com.tr/en/products/industrial-burners/process/fpb/fpb-200

İlbaş, M., & Candan, G. (2023b). Küçük Bir Girdaplı Yakıcı ve Fırında CO_2 Seyreltmesinin Alev Stabilizasyonu ve NO_X Emisyonu Üzerindeki Etkileri. Politeknik Dergisi, 26(2), 603–608. https://doi.org/10.2339/politeknik.1026159

İlbaş, M., & Yılmaz, İ. (2011). Experimental analysis of the effects of hydrogen addition on methane combustion. International Journal of Energy Research, 36(5), 643–647. https://doi.org/10.1002/er.1822

Öztuna, S., & Büyükakın, M. K. (2020). Effects of hydrogen enrichment of methane on diffusion flame structure and emissions in a back-pressure combustion chamber. International Journal of Hydrogen Energy, 45(10), 5971–5986. https://doi.org/10.1016/j.ijhydene.2019.09.187

Öztürk, M., Sorgulu, F., Javanı, N., & Dinçer, İ. (2023). An experimental study on the environmental impact of hydrogen and NG blend burning. Chemosphere, 329, 138671. https://doi.org/10.1016/j.chemosphere.2023.138671

Salcı, O. (2023). Fırın sisteminde hidrojen gazı katkılı doğal gaz yakıtlı proses brülörü yanma analizleri ve optimizasyonu (Master's thesis, Trakya Üniversitesi Fen Bilimleri Enstitüsü)

Performance Evaluation for an Hybrid E-scooter Worked with FC/Battery Integration

[1]*Sencer Ünal, [1]Hilal Biyik
[1] Fırat Üniversity, Engineering Faculty, Electrical Electronics Engineering, Enstitute of Science, Elazığ, 23000, Türkiye

*E-mail:sencerunal@firat.edu.tr

Abstract
The increase in individual vehicle use in the worldwide has caused users to prefer light electric vehicles such as scooters and mopeds. However, due to the negative effects such as long charging time and short charging life in electric scooters, manufacturers have started to work on producing fuel cell electric scooters. Fuel cells have low power density and slow power response compared to internal combustion engines. This undesirable situation can be eliminated with lithium-ion batteries with high power density. Fuel cell/battery integration promises importance in the future as both sources have the potential to eliminate each other's negativities. In this manuscript, a model is proposed consisting of combination of PEM fuel cell and lithium-ion battery. Additionally, regenerative braking and an energy management system is used to control the commissioning of resources. With this system, system inefficiency in case of separate use of power supplies in the scooter will be minimized with this hybrid design.

Keywords: Hydrogen fuel cell, Lithium ion battery, hybrid scooter, energy management system

I. Introduction

Although there are many studies related to electric cars to minimize emission value emitted to the environment and fuel consumption, research on two-wheeled vehicles in the group of light electric vehicles has not been very widespread(Yap and Karri, 2008).Hybrid types of these vehicles have great power in achieving net zero emission values and minimizing fuel demand(Tso and Chang, 2003).HEVs produced using more than one power sources are becoming increasingly common due to their net zero emission value and maximum mileage (Mulla etal., 2020).Fuel cell HEVs, which are seen as the cleanest technology of recent times, have many positive aspects such as the low operating temperature of the fuel cells, fast start-up and response to load changes, easy use, high power density, long life, less noise, net zero emission value, high energy efficiency.However, the difficulty of operating fuel cells, the slow dynamic response time, and the high system cost create requirements for more suitable features for operating conditions(Du etal., 2022).In addition, the fuel cell has also disadvantage of not being able to store the regenerative energy that occurs during braking in the hybrid system(Fathabadi, 2018).At this point, an integration that includes the battery can be used to ensure the adequacy and stability of the system(Boumediene etal., 2021).In such systems, energy management control strategies are also used to improve the power performance of the vehicle and to keep fuel consumption and economy at more reasonable levels(Du et al., 2022). A prototype of a fuel cell hybrid system was created and the system performance was found to be quite good in a study by Fathadabi (2018). In this manuscript, a hybrid model was proposed to eliminate the drawbacks of an e-scooter with FC/battery power supply that arise when both sources are in a system alone. In this hybrid model, an energy management strategy was used to control the activation of power supplies, and the WMTC drive cycle was preferred for the behavior of the system.

II. System Modeling

The diagram of the model created with the energy management system of the hydrogen fuel cell hybrid electric scooter and developed according to the WMTC driving mode is shown in Figure 1. While the driving cycle determined for the system behavior is added to the mechanical part as a changeable input, the scooter driver model is determined as a fixed input. Additionally, regenerative braking has been added to the system to save energy. This will also enable in scooter to travel further than if a battery or fuel cell is used. In addition, Proton Exchange Membrane Fuel Cell (PEMFC) was preferred as the fuel cell.

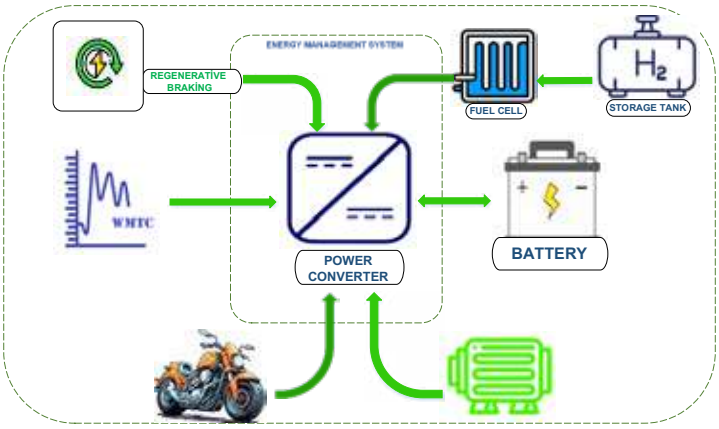


Fig.1: Model of a hybrid scooter with WMTC drive cycle

World Motorcycle Test Cycle *(*WMTC*)*

Driving cycles are the speed-time profile of vehicles driving in the city or outside the city depending on certain conditions and provide accurate results in estimating fuel consumption (Tong and Hung, 2010). In this article was used, the World Harmonized Motorcycle Test Cycle (WMTC) part 1, which has an average speed of 24.4 km/h is shown in Figure 2 (Steven, 2002).

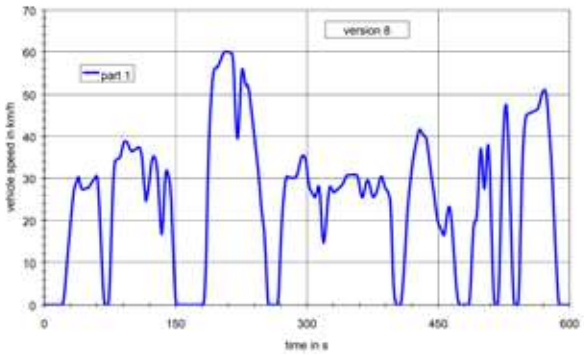


Fig.2: WMTC (part-1) driving cycle speed change

Kinetic energy recovery system (KERS)

KERS, or regenerative braking, is a system that stores the kinetic energy of a vehicle lost during deceleration and returns this energy to the vehicle's powertrain, allowing the vehicle's power to increase (Menon etal., 2013). Regenerative braking is seen as an important development that increases travel distance in vehicles while consuming electricity (Serykhanovna etal., 2023).

Energy Manangement System (EMS)

In electric vehicles, EMS is a control strategy that increases system efficiency, slows down degradation and directly affects the performance of the vehicle. A correct EMS applied to the system increases fuel economy and strengthens durability (Du etal., 2022). Figure 3 shows the management scheme of the control algorithm of battery and fuel cell which duties are different. Regenerative braking system is active as long as the scooter is running. Control of power supplies according to the charging status of the system is carried out with this EMS.

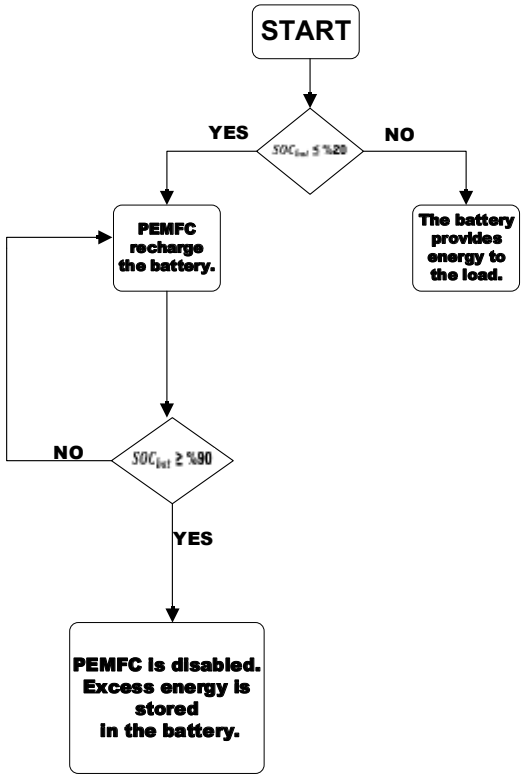


Fig. 3: Energy management system control schema

III. Results and discussions

According to the results obtained from the simulated model, the behavior of FC/battery integration was examined according to the WMTC driving cycle of the hybrid electric scooter. In the model, the energy management system that controls the activation of power sources according to the situation will also maximize energy savings. Figure 4 (a) the results of SOC behavior with and without regenerative braking in the model and in Figure 4 (b), the results of the voltage and SOC behavior of the battery are given. As seen in Figure 4 (a), the hybrid electric scooter consisting of FC/battery integration moved for approximately 137 minutes. With regenerative braking, this time increased by 15 minutes and ensured the scooter to move for approximately 152 minutes. This shows that with regenerative braking, the vehicle's energy increases by approximately 10% and the distance it travels also increases. In the graph in Figure 4 (b), the battery continues to charge the load for 108.33 minutes. At this moment, SOC_{bat} drops to 20%. When SOC_{bat} was 20%, PEMFC started to provide energy to the battery. After PEMFC charges the battery and load for approximately 25 minutes, PEMFC is disabled when SOC_{bat} is 90% and excess energy is stored in the battery.

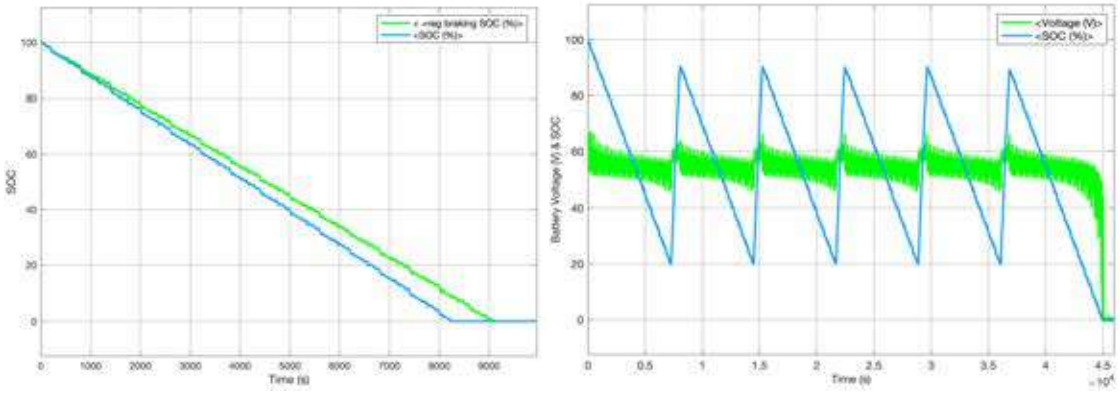


Fig. 4 : Behavior of the scooter modeled for the WMTC drive cycle: (a) SOC behavior with and without regenerative braking, (b) battery voltage and SOC behavior

The graph in Figure 5 shows the simulation result of the range of the scooter during its entire movement. As can be seen from the graph, when SOC_{bat} is 20%, the scooter has traveled approximately 50 km. During the 25 minutes that PEMFC charged to 90% the battery and load, the scooter traveled 3 km. In addition, it was seen from the simulation results that the scooter traveled approximately 300 km during its entire movement.

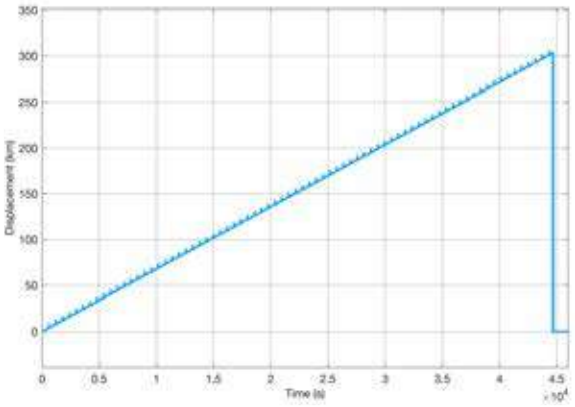


Fig. 5: Range of the scooter modeled for the WMTC driving cycle

IV. Conclusions

Short charging life and long charging time in e-scooters negatively affect the users. The fuel cell, which has attracted attention recently as another power source, cannot respond to sudden changes in the load and creating the need for an additional power source. In this manuscript, a hybrid model is proposed where both power sources support each other and will eliminate the negative effects they create when used separately in a scooter. Regenerative braking and a control strategy have also been added to the proposed model.In this way it has been observed that system performance, SOC and distance traveled are improved.

References

Boumediene S., Abdelfatah N., Hamza T., Hicham C., Novel energy management policy based on Fuel cell/battery power sources for scooter electric supply, In 2021 7th International Conference on Electrical Energy Systems (ICEES), (pp. 129-134), IEEE, (2021).

Du C., Huang S., Jiang Y., Wu D., Li Y., Optimization of energy management strategy for fuel cell hybrid electric vehicles based on dynamic programming, Energies, 15(12), 4325, (2022).

Fathabadi H., Fuel cell hybrid electric vehicle (FCHEV): Novel fuel cell/SC hybrid power generation system, Energy Conversion and Management, 156, 192-201, (2018).

Menon S. S., Sooraj M. S., Mohan S., Disney, R., Sukumaran S., Design and analysis of kinetic energy recovery system in bicycles, IJIRSET, ISSN, 2319-8753, (2013).

Mulla M. J. G., Rathod M. S. B., Mallinath M. M. S., Cost Analysis of MotoGine Hybrid Scooter, International Journal of Innovations in Engineering Research and Technology, 1-4, (2020).

Serykhanovna B. Z., Utebayev R., Baktybayev M., Temirzhanov A., Kunelbayev M. M., Development of a method for regenerative braking of an electric scooter, International Journal of Power Electronics and Drive Systems (IJPEDS), 14(3), 1331, (2023).

Steven H., Worldwide harmonised motorcycle emissions certification procedure,Institute for Vehicle Technology, (2002).

Tong H. Y., Hung W. T., A framework for developing driving cycles with on-road driving data, Transport reviews, 30(5), 589-615, (2010).

Tso C., Chang S. Y., A viable niche market—fuel cell scooters in Taiwan, International Journal of Hydrogen Energy, 28(7), 757-762, (2003).

Yap W. K., Karri V., Modeling and Simulation of a Hybrid Scooter, International Journal of Mechanical and Mechatronics Engineering, World Academy of Science, Engineering and Technology, Vol:2, No:11, (2008).

Optimization Of Electrospinning Parameters To Get Nano Hematite Fibers As A Photo Anode For Hydrogen Production Through Water-Splitting

[1,2*]Şükrü Kaya [1,2**]Cevat Sarıoğlu
[1] Marmara University, Department of Metallurgical and Materials Engineering, Istanbul, 34840, Türkiye
[2] Marmara University, Institute of Pure and Applied Sciences, Istanbul, 34722, Türkiye

E-mail: cevat.sarioglu@marmara.edu.tr, sukru.kaya@marmara.edu.tr

Abstract

In this study, hematite nanofibers were effectively produced by the electrospinning technique, implementing various electrospinning process parameters. The scanning electron microscopy (SEM) technique was used to characterize the surface morphology of the fibers. An investigation was conducted to examine the effect of electrospinning parameters, including the inner diameter of the needle and voltage, on the diameters of the fibers. The electrospun composite fibers of PVP/$Fe(NO_3)_3$ were subjected to annealing at 550°C in air. The effect of this heat treatment on the diameter of the fibers was investigated. When the inner diameter of the needle is reduced from 0.127 mm (26G) to 0.108 mm (32G), there was a corresponding decrease in the average fiber diameter after annealing from 558 nm to 227 nm. The average diameter of hematite fibers decreased significantly after annealing due to PVP decomposition. This reduction is anticipated to enhance the efficiency of hydrogen production due to the increased surface area.

Another parameter, which is electrospinning voltage was investigated from 2kV to 30kV with 32G needle tip. The smallest and most uniform fibers were obtained with annealed hematite fibers at 30kV with 32G needle tip. Hematite fibers produced in this study have one of the smallest average diameters with continuous form as compared with the literature (135nm ±22nm)(Li et al., 2014) .

Parameters were optimized and uniform nanoscale fibers (227nm) were successfully produced in comparison with our previous study (5.99 µm) (KAYA, 2023).

Keywords: Nano Fiber, Hematite, Photoelectrochemical, Annealing, Photoelectrode, Hydrogen production, Water splitting, Electrospinning

I. Introduction

In the near future, hydrogen energy will be a highly significant and anticipated renewable energy source. The sustainability and environmental friendliness of hydrogen energy production derive from its exclusive generation of water vapor, in contrast to fossil fuels which emit greenhouse gases such as carbon dioxide and carbon monoxide. Moreover, the energy content of 1 kilogram of hydrogen gas is about equivalent to that of 2.8 kilograms of gasoline. (Pareek et al., 2020).

An effective substitute in this situation is to split water into hydrogen and oxygen using photocatalytic and photo-electrochemical processes. Because of its non-toxic nature, abundance in nature, relative economic viability, thermodynamic stability at high temperatures (up to 1457°C), and chemical stability at high pH levels, hematite (α-Fe_2O_3) is particularly appealing for this use (Liu, Le Formal, Boudoire, & Guijarro, 2019).

Hematite (α-Fe_2O_3) is a very suitable photoanode material for photoelectrochemical (PEC) water splitting due to its cost-effectiveness, widespread availability, and favorable bandgap range of 1.9-2.2 eV (Sivula, Le Formal, & Grätzel, 2011). Electrospinning is a flexible way to make nanoscale hematite fibers that are then used to make photoelectrodes with a significant amount of surface area and better light absorption (Huang, Zhang, Kotaki, & Ramakrishna, 2003). The procedure involves the extruding of a polymer solution by a high-voltage electric field, resulting in the formation of ultrafine fibers that are collected on a conductive substrate. The electrospinning solution for hematite photoelectrodes usually consists of an iron precursor and a polymer that is dissolved in a solvent. Electrospinning has been identified as an efficient technique for the production of hematite fibers suitable for photoelectrodes due to its ability to generate fibrous networks characterized by diverse fiber sizes and morphologies (Lu, Zhang, Wang, Wen, & Wei, 2011).

In this work, the effect of electrospinning parameters such as needle's inner diameter and voltage on hematite fiber morphologies and average fiber diameters were investigated.

II. Experimental Procedures

In accordance with the data provided in Table 1 and Table 2, a solution was made by combining polyvinylpyrrolidone (PVP), iron (III) nitrate, absolute ethanol and distilled water. The solution was mixed by a magnetic stirrer up to totally dissolved of PVP and iron (III) nitrate. Afterwards, the solution was transferred into a blunt-tipped syringe and connected to the syringe pump of the Inovenso NE200 Electrospinning, as depicted in Figure 1. The production and deposition of electrospun fibers on a collector were accomplished effectively. Table 1 shows the electrospinning solution utilized for the manufacture of the samples.

The composite fibres of PVP/$Fe(NO_3)_3$ were subjected to thermal oxidation in a Protherm box furnace at a temperature of 550℃ under ambient environment. The furnace's heating rate was adjusted to 3℃/min. The specimens were positioned within a porcelain crucible and positioned at the heat source of the furnace, where they were kept at a temperature of 550℃ for a duration of 3 hours. Upon completion of the annealing process, the samples were allowed to undergo a cooling process within the furnace until they reached ambient temperature.

The Bruker D2 Phaser was utilised to acquire and examine the X-ray diffraction (XRD) pattern of the annealed fibres. The FEI Sirion Scanning Electron Microscope SEM was used to capture fibre pictures, while the diameters were measured using ImageJ Software.

Table 1. Electrospinning solution recipe

Compound	Function	Amount (w%)	Amount (g.)	Volume (cc.)
Water	Solvent	53.82	9.60	9.6
Ethanol	Solvent	28.37	5.06	6.4
PVP	Carrier	11.21	2	-
$Fe(NO_3)_3$	Fe Precursor	6.60	1.178	-

To observe the effect of needle tip inner diameter effect on fiber production by electrospinning method, 4 samples were produced by parameters as seen Table 2.

Table 2. First set of experimental parameter of fiber production by electrospinning for investigation needle effect

	Needle Universal Gauge Number	Spinner Voltage (kV)	Needle-Collector Distance (cm)
Sample 1	26G	30	10
Sample 2	28G	30	10
Sample 3	30G	30	10
Sample 4	32G	30	10

To observe the effect of electrospinning voltage effect on fiber production by electrospinning method, 4 samples were produced by parameters as seen Table 3.

Table 3. Second set of experimental parameter of fiber production by electrospinning for investigation voltage effect

	Needle Universal Gauge Number	Spinner Voltage (kV)	Needle-Collector Distance (cm)
Sample 5	32G	2	10
Sample 6	32G	10	10
Sample 7	32G	20	10
Sample 8	32G	30	10

III. Results

In figure 1, with decreasing needle tip, the more smooth surface morphology was observed. When the needle used 26G and 28G, some bead-like structures occurred on the fibers. From 30G to 32G, the more smooth and without bead-like fibers were produced. As shown in Figure 2, the more uniform distribution and thinner fiber diameter were observed. The average fiber diameter after annealing was decreased from 558nm to 237nm as the inner diameter of the needle was reduced from 0.127mm (26G) to 0.108mm (32G) at a voltage of 30kV.

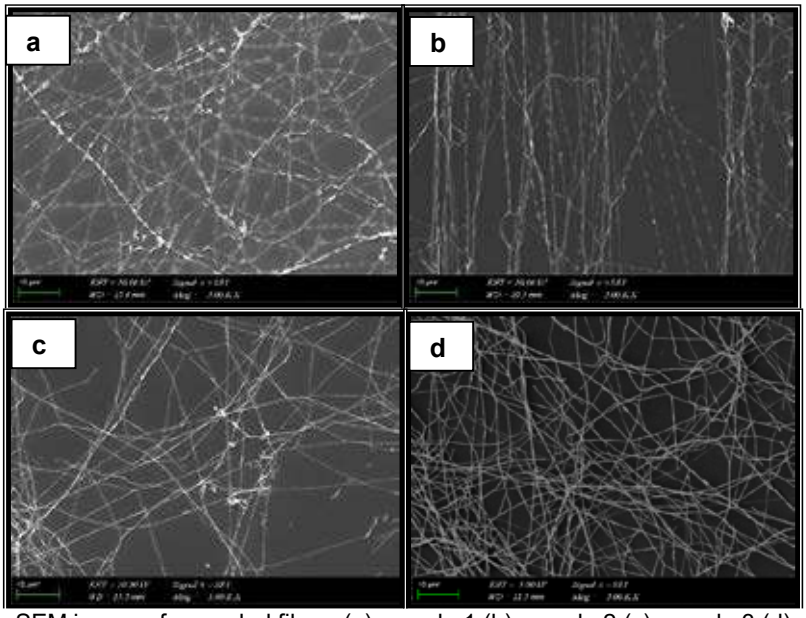


Figure 1. SEM image of annealed fibers (a) sample 1 (b) sample 2 (c) sample 3 (d) sample 4

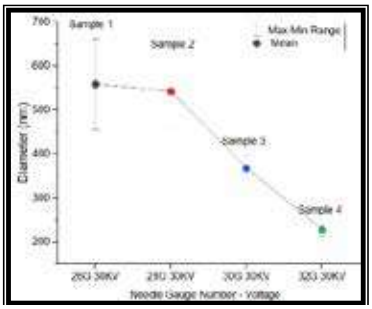


Figure 2. Fiber diameter distribution and mean based on needle gauge number

In figure 3, with increasing voltage, the more smooth surface morphology was observed. When the applied voltage was 10kV, 20kV, 30kV, smoother and straight line-shaped fibers occurred. As shown in Figure 4, uniformity was disrupted dramatically at 2kV critical voltage. Uniformity increased as the voltage increased. The fiber diameter decreased from 453 nm to 227nm as the voltage was increased from 2 kV (the critical voltage at which the minimum voltage fiber can be produced) to 30 kV (with 32G needle tip). The diameter of the fiber decreased as the voltage increased in agreement with literature (Haider, Haider, & Kang, 2018).

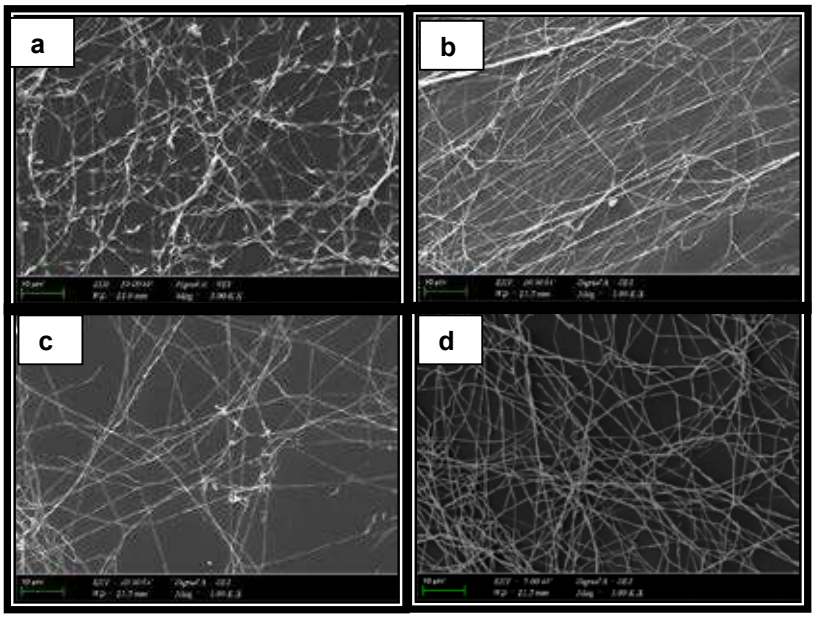


Figure 3. SEM image of annealed fibers sample 5 (a) sample 6(b) sample 7 (c) sample 8 (d)

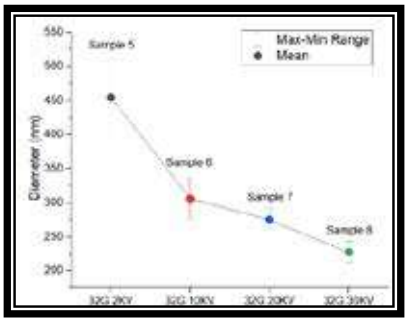


Figure 4. Fiber diameter distribution and mean based on voltage

The XRD pattern of the one of annealed fibers was given in Figure 5. It was confirmed that the annealed fibers were α-Fe_2O_3 (hematite). The XRD spectrum of the fibers contains eleven peaks, which are clearly observable. In peak position, all of them may be precisely indexed to rhombohedral Fe_2O_3 (JCPDS No. 24-0072), space group R3.(148).

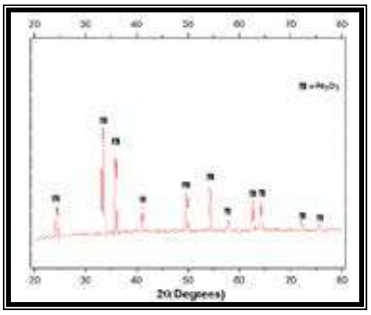


Fig. 5. The XRD pattern of annealed fiber

IV. Conclusion

1. Hematite fibers were effectively manufactured using the electrospinning technique.
2. The fiber diameters were analyzed using SEM and measured using ImageJ software after annealing. The precision of fiber diameter measurements is enhanced by the use of scanning electron microscope (SEM) images, as they offer a larger field of depth in comparison to optical microscope images.
3. The average fiber diameter after annealing was decreased from 558nm to 237nm as the inner diameter of the needle was reduced from 0.127mm (26G) to 0.108mm (32G) at a voltage of 30kV.
4. The fibre diameter decreased from 453 nm to 227nm as the voltage was increased from 2 kV (the critical voltage at which the minimum voltage fiber can be produced) to 30 kV (with 32G needle tip).
5. As the voltage increases from 2kV to 30kV, a more uniform distribution of fibre diameter is observed.
6. As the number of needle tips rises, a more uniform distribution of fibre diameter was observed.
7. For the future work, hematite fibers will be produced in the form of photoanode electrodes on the fluorine doped tin oxide (FTO) substrate and photoelectrochemical characterization will be performed to improve hydrogen production efficiency.

Acknowledgements

This research was supported by Marmara University through Coordination Scientific Research Project (BAPKO) with project no: FDK-2022-10753.

References

Haider, A., Haider, S., & Kang, I.-K. (2018). A comprehensive review summarizing the effect of electrospinning parameters and potential applications of nanofibers in biomedical and biotechnology. *Arabian Journal of Chemistry, 11*(8), 1165-1188.

Huang, Z.-M., Zhang, Y.-Z., Kotaki, M., & Ramakrishna, S. (2003). A review on polymer nanofibers by electrospinning and their applications in nanocomposites. *Composites science and technology, 63*(15), 2223-2253.

KAYA, Ş. (2023). Synthesis of hematite fibers by electrospinning for producing photoanode for hydrogen production by water splitting.

Li, N., Jayaraman, S., Tee, S. Y., Kumar, P. S., Lee, C. J. J., Liew, S. L., . . . Luo, H.-K. (2014). Effect of La-Doping on optical bandgap and photoelectrochemical performance of hematite nanostructures. *Journal of Materials Chemistry A, 2*(45), 19290-19297.

Liu, Y., Le Formal, F., Boudoire, F., & Guijarro, N. (2019). Hematite photoanodes for solar water splitting: a detailed spectroelectrochemical analysis on the pH-dependent performance. *ACS Applied Energy Materials, 2*(9), 6825-6833.

Lu, X., Zhang, W., Wang, C., Wen, T.-C., & Wei, Y. (2011). One-dimensional conducting polymer nanocomposites: Synthesis, properties and applications. *Progress in Polymer Science, 36*(5), 671-712.

Pareek, A., Dom, R., Gupta, J., Chandran, J., Adepu, V., & Borse, P. H. (2020). Insights into renewable hydrogen energy: Recent advances and prospects. *Materials Science for Energy Technologies, 3*, 319-327.

Sivula, K., Le Formal, F., & Grätzel, M. (2011). Solar water splitting: progress using hematite (α-Fe2O3) photoelectrodes. *ChemSusChem, 4*(4), 432-449.

Energy Management Strategy for Improving Flight Performance of Fuel Cell Hybrid Quadrotor UAV

[1]*Sencer Ünal,[1]Murat Kayaoğlu
[1]Fırat Üniversity, Engineering Faculty, Electrical Electronics Engineering, Enstitute of Science, Elazığ, 23000, Türkiye

*E-mail:sencerunal@firat.edu.tr

Abstract
The advancements in the defense industry today have greatly contributed to the significant development of technology known particularly as drones or Unmanned Aerial Vehicles (UAVs) in both military and civilian domains. Due to their ability to hover, low cost, reduced carbon footprint, and quiet operation, UAVs have become increasingly popular. However, UAVs face a range limitation that needs to be addressed. Therefore, this paper aims to increase the flight range of UAVs through the integration of PEM fuel cell/battery hybrid design.
Keywords: Quadrotor, PEM Fuel Cell, Unmanned Aerial Vehicle, Power Management

I. Introduction

Unmanned Aerial Vehicles (UAVs), also known by names such as remotely piloted vehicle (RPV), drone, robotic aircraft, and unmanned aircraft, are capable of autonomous flight or remote control(Bone and Bolkcom,2003). Especially when it comes to market and application research of mini-UAVs, they become quite popular due to reasons such as lower costs and infrastructure requirements associated with investments(Lapena-Rey etal., 2017). As mini-UAV technology continues to advance, it also brings along some challenges. One of the most significant issues is the limited flight time when powered solely by batteries and the difficulties in balance/control. Depending on the usage purposes, these flight durations often prove insufficient in many applications. There are many studies in the literature focusing on supercapacitors (SC) and fuel cells (FC) in relation to this topic, and these two energy sources are seen as solutions for insufficient flight time. Especially, Proton Exchange Membrane (PEM) fuel cells are notable for their small size, low cost, long operational duration, and high energy densities in increasing flight time(Dudek etal., 2013). In this regard, it is observed that there are fewer studies on rotary-wing UAVs compared to fixed-wing UAVs. In the study conducted by Arat and Sürer, the aim was to increase the flight time of a rotary-wing UAV using PEMFC. They achieved a 2-minute improvement with the designed four-rotor UAV(Turan and Sürer, 2020).
Taking into account the literature research, in this study, a 4-winged UAV model consisting of PEMFC integration has been designed. With this model, especially during takeoff, climb, and descent phases, the sudden power demand will be met by the battery PEMFC combination. Since the power demand of the UAV during cruising is low, PEMFC also charges the battery according to the power situation. At the same time, an energy management system that controls power supplies has been added to this model consisting of FC/battery integration.

II. System Set-up and Procedure

The configurations of mini UAVs, also known as drones, vary significantly depending on different parameters within a system and application.
Figure 1(a) and Figure 1(b) respectively illustrate the overall forces when a drone moves vertically at a constant speed and when it flies horizontally at a constant speed. The sum of weight and drag is equal to thrust in both cases(Chen etal., 2018).

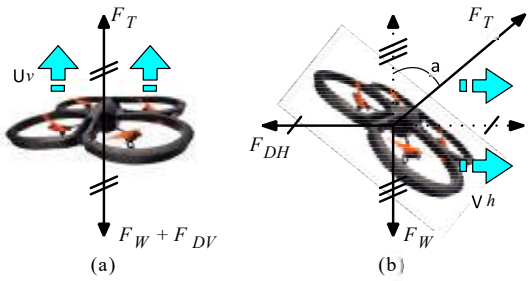


Fig. 1: Forces acting on a drone(Chen etal., 2018)

In Equations 1 and 2, the forces acting on the UAV during hover, horizontal flight, and vertical flight are depicted. In Equation 1, F_W, exerted by gravity, pulls the UAV downward, representing the total weight of the drone along with its payload. In Equation 2, F_{DH} and F_{DV} represent the drag forces in the horizontal and vertical directions, respectively, caused by the disturbance of the airflow. Additionally, drag opposes the UAV's motion in both horizontal and vertical directions.F_T, which sustains the altitude and velocity of the drone by counteracting the weight and drag, is the thrust generated by the drone's rotating propellers(Chen etal., 2018).

$$F_W = (m_d + m_p)g \quad (1)$$

$$F_{DV} = \frac{1}{2}\rho A_t C_d v_v^2 \; ; \quad \frac{1}{2}\rho A_f C_d v_h^2 \quad (2)$$

Where, m_d and m_p respectively represent the mass of the drone and the payload, g is the acceleration due to gravity, A_F and A_t are the cross-sectional areas in the horizontal and vertical directions, C_d is the drag coefficient, and ρ is the air density. The required thrusts are defined as $F_{T,v}$ and $F_{T,h}$.

$$F_{T,v} = F_W + F_{DV} = \left(m_d + m_p\right)g + \frac{1}{2}\rho A_t C_d v_v^2 \quad (3)$$

$$F_{T,h} = \sqrt{F_W^2 + F_{DH}^2} = \sqrt{((m_d + m_p)g)^2 + (\frac{1}{2}\rho A_F C_d v_h^2)^2} \quad (4)$$

The thrust required to balance the weight and drag force is obtained from the effective air passing through the rotating propeller. A fundamental formula for thrust is as follows: (Chen etal., 2018)

$$F_T = 2\rho A p \vartheta i^2 \quad (5)$$

III. Analysis

During the design phase of a UAV, a mission profile outlining the fundamental characteristics of the UAV and the mission should be elaborated in detail, along with the requirements. A simple mission may include five flight phases: takeoff, climb, cruise, descent, and landing. Accordingly, the UAV's characteristics encompass elements such as takeoff weight, takeoff distance, operating altitude, climb or descent rate, and endurance. Once these factors are determined, the power requirements of the mission can be estimated after thorough analysis(Aslam etal., 2023).
In this study, a 4-rotor UAV model consisting of FC/battery hybrid integration and controlled by an energy management system has been designed. Considering the dynamics of the established system, brushless DC motors have been preferred in the design due to their high efficiency and maintenance-free characteristics. Additionally, for providing energy to the UAV in the model, a high-energy-density PEMFC and a high-power-density lithium polymer battery have been used. Lithium-based batteries, with their relatively higher power density ranging from approximately 500 to 2800 W/kg and faster response times compared to FC systems, are a highly notable technology in UAV applications. Especially, lithium-ion and lithium-polymer technologies are more commonly used in commercial UAVs. However, due to their low energy density, lithium-based batteries alone are not sufficient to power UAVs. Therefore, hybridizing a fuel cell with a battery is a very good solution to mitigate the drawbacks of both power sources. (Wang et al., 2020) Furthermore, due to its characteristics such as high energy density and short start-up time compared to other types of fuel cells, PEM fuel cell is the most suitable type for mini UAVs, and it has been chosen in this study (Oh, 2018).

IV. Results and discussions

The climb profile of the UAV should be designed according to the capacity of the battery and the output performance. During the climb, the battery will provide peak power, and the maximum climb power should not exceed the peak power of the battery and the total peak power of the FC.(Wang etal., 2020)
The schematic of the modeled system is shown in Figure 3. During peak times when the power demand of the UAV is high and cannot be met instantly, the majority of the energy requirement will be supplied by the battery. However, PEMFC is also operational during these peak moments. During the cruising phase, since the power requirement is at a minimum level, PEMFC can meet all power demands, and if the battery level is low, excess energy will charge the battery. Thus, energy management is achieved, maximizing flight time. Energy distribution is carried out through the DC bus, and energy distribution to the motors is ensured with the help of ESC.

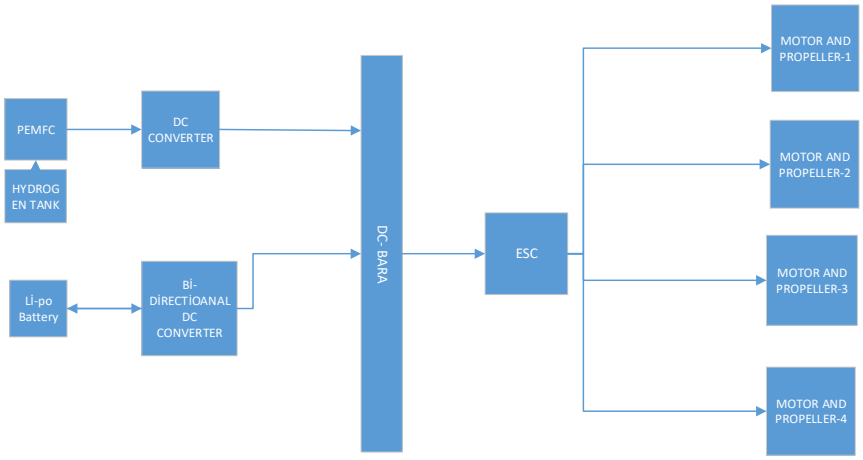


Fig. 3: System model

In Figure 4, the trajectory of the UAV fulfilling the given mission is depicted. It is crucial for the UAV to move with minimum error rate, avoiding excessive influence from external disturbances, in order to fulfill the mission effectively.

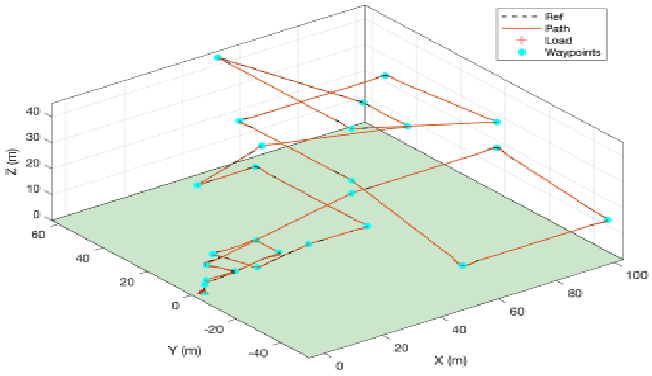
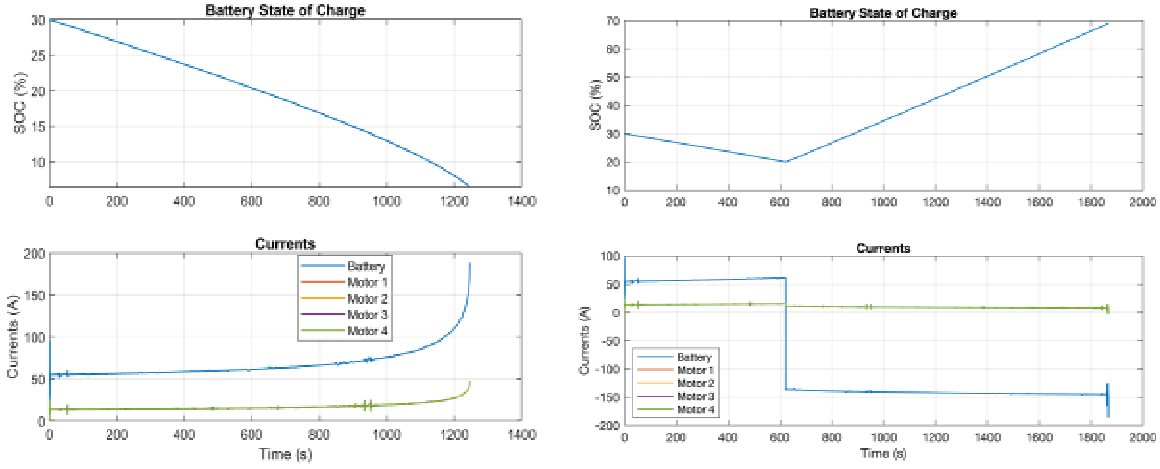


Fig. 4: Quadrotor Trajectory

In Figure 5 (a), the SOC and current behavior of the UAV when powered only by the battery is provided. As seen from the graph, the UAV starts operating with a 30% SOC. The battery has powered the UAV for approximately 22 minutes, after which its charge is depleted. Figure 5 (b) presents the results of the hybrid system consisting of both the battery and FC. From these results, it can be observed that when the SOC drops to 20%, the FC kicks in to charge the battery and supply energy to the UAV motors. Where, thanks to the FC, the UAV's energy needs are met, enabling it to complete the mission flight.



(a) (b)

Fig. 5: For the modeled mini UAV, the power sources are as follows:(a) State of Charge (SOC) and current behavior when only the battery is used. (b) SOC and current behavior for the FC/battery integration.

V. Conclusions

This study aims to increase the flight time and manage energy for a four-rotor PEMFC/battery hybrid UAV. The model created in MATLAB/Simscape has attempted to fulfill the mission on the specified trajectory with minimum error rate. The obtained results are quite promising in terms of increasing flight time, energy management, and tracking the trajectory with minimum error. Additionally, the choice of Maximum Power Point Tracker (MPPT) has helped us use power most efficiently.

References

B. Wang *vd.*, "Current technologies and challenges of applying fuel cell hybrid propulsion systems in unmanned aerial vehicles", *Progress in Aerospace Sciences*, c. 116, s. 100620, doi: 10.1016/j.paerosci.2020.100620, (2020).

Bone E, Bolkcom C., "Unmanned Aerial Vehicles: Background and Issues for Congress", (2003).

Arat H.T., Sürer M.G., "Experimental investigation of fuel cell usage on an air Vehicle's hybrid propulsion system", *International Journal of Hydrogen Energy*, c. 45, sy 49, ss. 26370-26378, doi: 10.1016/j.ijhydene.2019.09.242, (2020).

Dudek M., Tomczyk P., Wygonik P., Korkosz M., Bogusz P., Lis B., "Hybrid Fuel Cell – Battery System as a Main Power Unit for Small Unmanned Aerial Vehicles (UAV)", *International Journal of Electrochemical Science*, c. 8, sy 6, ss. 8442-8463, doi: 10.1016/S1452-3981(23)12901-4, (2013).

Lapeña-Rey N., Blanco J.A., Ferreyra E., Lemus J.L., Pereira S., Serrot E., "A fuel cell powered unmanned aerial vehicle for low altitude surveillance missions", *International Journal of Hydrogen Energy*, c. 42, sy 10, ss. 6926-6940, doi:

10.1016/j.ijhydene.2017.01.137, (2017).

Oh T.H., "Conceptual design of small unmanned aerial vehicle with proton exchange membrane fuel cell system for long endurance mission", *Energy Conversion and Management*, c. 176, ss. 349-356, doi: 10.1016/j.enconman.2018.09.036, (2018).

Chen Y., Baek D., Bocca A., Macii A., Macii E., ve Poncino M., "A Case for a Battery-Aware Model of Drone Energy Consumption", içinde *2018 IEEE International Telecommunications Energy Conference (INTELEC)*, Turin: IEEE, ss. 1-8. doi: 10.1109/INTLEC.2018.8612333, (2018).

Aslam A., Felix A., Kalyvas C., Chizari M., "Design of a Fuel Cell/Battery Hybrid Power System for a Micro Vehicle: Sizing Design and Hydrogen Storage Evaluation", *Vehicles*, c. 5, sy 4, ss. 1570-1585, doi: 10.3390/vehicles5040085, (2023).

Analysis of a Microgrid with Hydrogen Storage from a Technoeconomic Perspective

[1*]Elifnur Bayraktar, [2]Yahya Akil, [1]Faruk Barlaz, [1]Husnugul Tekin, [1]Servan Marşil, [3]Heybet Kilic
[1] Dicle University, Institute of Science and Technology, Renewable Energy Sources, Diyarbakır, 21000, Türkiye
[2] Dicle University, Electrical Electronics Engineering, Diyarbakır, 21000, Türkiye
[3] Dicle University, Diyarbakir Vocational School of Technical Sciences, Electricity and Energy, Diyarbakır, 21000, Türkiye

* E-mail:Elifnur.bayraktar@dedas.com.tr

Abstract
This study is based on the Devegeçidi Dam in Diyarbakır. There are small stream mouths and agricultural areas around the dam lake. This research work is analysed to design a technical and economical hybrid system in the vicinity of Devegeçidi Dam. The proposed site is analysed to find the potential of renewable energy such as solar and hydrogen. The proposed renewable energy options include a 152 kW Solar Power Plant, 11 kW Hydroelectric Power Plant, 250 kW Electrolyser, 1000 kg Hydrogen Tank, 10,000 kW Converter and a simulated grid. Hybrid Optimisation Model (HOMER) software was used for all simulations and techno-economic perspective of the system for this analysis. The study reveals that the hybrid system has reached a significant share of 42.57%. It shows an NPC cost of $41,937.68 and a CoE production of 52,658.90 kWh, resulting in a levelled energy cost of $0.0701/kWh. At a carbon abatement cost of approximately $37,58.47 per t/CO2 e, the system demonstrates the potential to reduce CO2 emissions by 70,529.80 tonnes over its 20-year lifetime.

Keywords: Devegeçidi Dam, Hybrid System, Techno-Economic Perspective, HOMER Pro

I. Introduction
Energy is an essential tool for every country [1]. In various studies for the electrification of rural areas of Diyarbakır, hydrogen energy has been found to be the best energy that can reliably provide power supply to the ever-increasing load demand and can be an effective alternative way to replace conventional power sources. Several research studies based on renewable resources have been completed. Worldwide, hybrid system analysis is one of the versatile methods that should be used predominantly in Diyarbakır. Hybrid system technique includes many system configurations of renewable energy sources [2]. In this analysis, the location 20 kilometres northwest of Diyarbakır 'Devegeçidi Dam' has been selected for the techno-economic analysis of power backup and hydrogen storage system for the grid with Hydro Electric Power Plant. The site where the proposed system will be evaluated is located in the vacant land in the vicinity of Devegeçidi Dam and has coordinates 38°3.5'N and 39°59.2'E respectively. The mentioned study is about optimising the cost of electricity generation with hybrid power plants using HOMER Pro software [3]. This study aims to encourage the use of renewable energy instead of coal, gas and oil in the country. The aim of the study is to perform a techno-economic analysis and optimise renewable energy systems for the vacant land around Diyarbakır Devegeçidi Dam using HOMER Pro software. The novelty of this research is that it focuses on the optimisation of Hydrogen Energy and Solar Energy systems and the configurations of the existing Hydroelectric Power System.

II. Experimental Set-up and Procedure
The representation of the Renewable Energy System location on HOMER Pro is shown in Fig. 1, and the components used in the Hybrid Renewable Energy System are shown in Fig. 2. The site selected for this study is Devegeçidi Dam (38°3.5'N and 39°59.2'E), Kayapınar Neighbourhood, Diyarbakir. Currently, the island's electricity is provided by the Hydroelectric Power Plant (1,800 MWe installed capacity) already located on the island. The study was carried out with the inclusion of renewable energy sources such as solar panels, hydrogen energy and storage as part of the existing Hydroelectric Power Plant.



Fig. 1: Location of Devegeçidi Dam on the World and Map View of the Facility

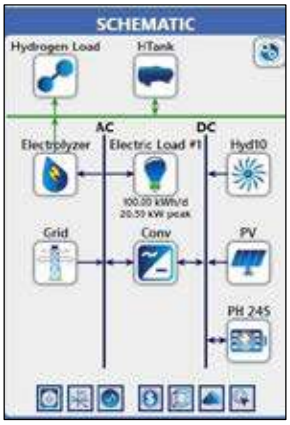


Fig. 2: Hybrid Renewable Energy System Configuration

Properties of the components used in the Hybrid Renewable Energy System; Generic Flat Plate PV, Generic 245 kWh Pumped Hydro Storage, 10 kW Generic Hydro, Generic Large Free Converter, Electric Load, Grid, Generic Electrolyzer and Hydrogen Load values are entered for optimisation. Recommended configuration values after optimisation; 152 kW PV, 10.000 kW Converter, 250 kW Electrolyzer, 1000 KG Hydrogen Tank and 11 kW Hydropower are recommended.

III. Analysis

Before simulating a renewable energy system, the system architecture must be designed [4]. In this case, the system design consists of generators, solar panels and hydrogen plant as the storage equipment of the study. All selected equipment and their specifications are listed below.

- Average Electric Load Demand

In order to determine the optimised system with the best output and lowest cost for this hybrid renewable energy system, a data set based on January 2024 is used. This data is used to estimate the load demand of the system based on the commercial HOMER Pro electricity load [5]. The average electrical load of the island is presented in Fig. 3.



Fig. 3: Estimated Average Electricity Load of Camelgorge Dam in January

- Electrolyser Analysis

The electrolyser is the central element of hydrogen production. Alkaline Electrolyser is used in the current design. The electrolyser used in the system produces 4,504 kg per year with a capacity of 250 kW. The levelised energy cost is calculated as 11.7. The highest production of the year was calculated in July with an energy production of 15.3 kW. Hydrogen production by month is presented in Fig. 4.

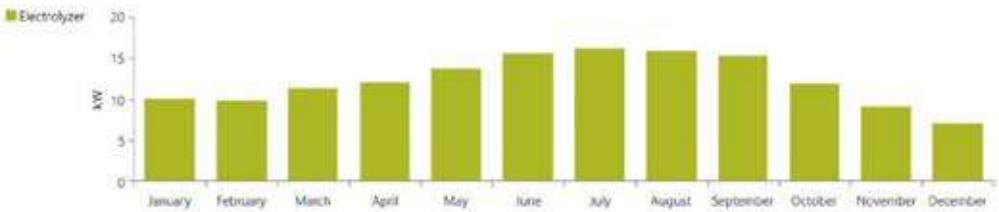


Fig. 4: Monthly Values of Electrolysis Used in kW

- Hydrogen Tank Analysis

The hydrogen produced by the electrolyser was stored in a 1000 kg hydrogen tank. The specification parameters of the hydrogen tank installed in the 3rd quarter of the year with a period of 282.19 and an energy storage capacity of 33.33 kWh are shown in Fig. 5.

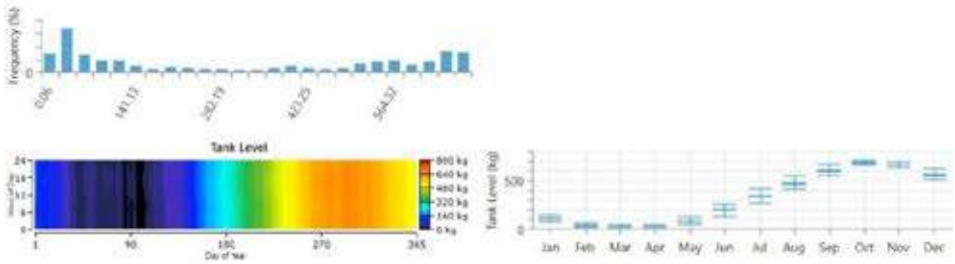


Fig. 5: Data of the Hydrogen Tank Used

- Solar Panel Analysis

The power generation of a PV array is expressed as $P_{PV} = n_{PV} U_{PV} i_{PV}$. In the designed system; Nominal Capacity: 152 kW, Average Output: 27 kW and 649 kWh/d, Capacity Factor: 17.8%, Total Generation: 236,854 kWh/yr, Maximum Output: 158 kW, 4,384 Operating Hours and Levelised Cost: 0.130 $/kWh. The specification parameters of the installed Solar Panels are shown in Fig. 6.

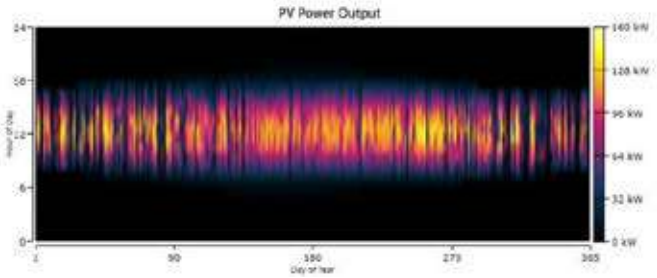


Fig. 6: Data on Solar Panels Used

IV. Results and Discussions

An average of 72.38% of the simulated solutions were found to be feasible. It was also noticed that the inclusion of electrolysis and hydrogen tank to produce hydrogen in the design of all electricity demand categories in the studied site increased the feasibility of the solutions. It is important to summarise the calculation report in HOMER Pro in terms of feasibility and techno-economic analysis (see Fig. 7).

Component	Capital ($)	Replacement ($)	O&M ($)	Fuel ($)	Salvage ($)	Total ($)
10kW Generic	$6,188.35	$0.00	$2,400.00	$0.00	$0.00	$8,588.35
Generic 245kWh Pumped Hydro	$185.65	$263.73	$24.00	$0.00	($19.06)	$454.32
Generic Electrolyzer	$5,801.58	$2,461.46	$2,500.00	$0.00	($463.27)	$10,299.76
Generic flat plate PV	$29,297.97	$0.00	$1,515.00	$0.00	$0.00	$30,812.97
Grid	$0.00	$0.00	$1,789.36	$0.00	$0.00	$1,789.36
Hydrogen Tank	$464.13	$0.00	$250.00	$0.00	$0.00	$714.13
System	$41,937.68	$2,725.19	$8,478.36	$0.00	($482.33)	$52,658.90

Fig. 7: $ Values of Components Entered into the System

If we look at the emission values of the system; Carbon Dioxide: 11.309 kg/yr, Carbon Monoxide: 0 kg/yr, Unburned Hydrocarbons: 0 kg/yr, Particulate Matter: 0 kg/yr, Sulphur Dioxide: 49.0 kg/yr and Nitrogen Oxide: 24.0 kg/yr calculated by the system.

Optimisation results of the system are shown as a result of HOMER calculations for these scenarios. The total capital cost of the system is calculated as $542,150.00 and the total cost of the system is calculated as $680,748.76 when the annual replacement and repair-maintenance costs of the system are added.

The reason for the appearance of carbon dioxide in the system is due to the presence of the grid. Since Solar and Hydrogen Energy does not contain carbon and sulphur, there is no CO, CO2 and HC among the combustion products [6].

V. Conclusions

HOMER Pro allows modelling and optimising risk mitigation techniques of low-cost renewable energy systems by

simulating the technical and economic feasibility of microgrid or distributed energy systems [7]. The programme shows how to combine conventional power generation with renewable energy, storage, grid resources and load control based on techno-economic analysis. The program simulates the operation of a hybrid microgrid or distributed energy system for one year by evaluating and optimising the electrical system architecture, load profiles, components, fuel prices and environmental factors in the run of input data. The results section summarises the research findings, first with the optimisation results and then with the economic evaluation results. The optimisation results for the location of the 1,800 MWe Devegeçidi Dam in Diyarbakır (38°3.5'N and 39°59.2'E) show the best probability. The simulated microgrid uses 1470 kWh of energy per day. The simulation process calculated a list of selected system configurations and capacities according to the lowest CoE and NPC. This research selects the optimum system design that best suits the identified site configuration system. The optimised component detail is presented in Table. 1.

Component	Capacity	Total ($)
10 kW Generic	11.0 kW	$8,588.35
Generic 245 kWh Pumped Hydro	12.0 string	$454.32
Generic Electrolyzer	250 kW	$10,299.76
Generic Flat Plate PV	152 kW	$30,812.97
Grid	∞	$1,789.36
Hydrogen Tank	1000 kg	$714.13
System		$52,658.90

Table. 1: Capacity and Total Cost Values of Components in the System

In this study, electricity and hydrogen production was carried out on Devegeçidi Dam in Kayapınar neighbourhood of Diyarbakır by using PV module, hydrogen plant, hydrogen tank, water electrolyser, grid, converter, hydroelectric power plant and storage technology. The results obtained from this system are given below.

- The use of storage in the simulation resulted in minimum energy cost in terms of electricity demand.
- Although the hydrogen produced in this study is costly, the use of the produced hydrogen in fuel cells and its storage in the hydrogen tank resulted in the availability of green energy in the determined region.
- Overall emission rates have decreased compared to grid-connected direct systems, except for microgrids [8].

Acknowledgements
I would like to thank Dicle Elektrik Dağıtım A.Ş. and Eksim Holding for their support during the conduct of this study.

References

[1] A. Bowen., Regional Planning Strategies for Hybrid Energy Optimization Solar Energy Conversion, 587-628, (1979).

[2] S. Rahman., K.S. Tam., A Feasibility Study of Photovoltaic-Fuel Cell Hybrid Energy System IEEE Trans Energy Convers, 50-55, (1988).

[3] S.B. Silva., M.A. De Oliveira., M.M. Severino., Economic Evaluation And Optimization Of A Photovoltaic-Fuel Cell-Batteries Hybrid System For Use In The Brazilian Amazon Energy Pol, 6713-6723, (2010).

[4] D. Rekioua., S. Bensmail., N. Bettar., Development Of Hybrid Photovoltaic-Fuel Cell System For Stand-Alone Application, 1604-1611, (2014).

[5] N. Mezzai., D. Rekioua., T. Rekioua, A. Mohammedi., K. Idjdarane., S. Bacha., Modeling Of Hybrid Photovoltaic/Wind/Fuel Cells Power System, 15158-15168, (2014).

[6] J. Armijo et al., Flexible Production Of Green Hydrogen And Ammonia From Variable Solar And Wind Energy: Case Study Of Chile And Argentina, (2020).

[7] M. Raab et al., Techno-Economic Assessment Of Renewable Hydrogen Production And The Influence Of Grid Participation, (2022).

[8] https://www.iea.org/reports/co2-emissions-in-2023/executive-summary

Hydrogenation of Safflower Oil for Sustainable Biocomposite Production: Process Optimization and Characterization

[1*]Ercan Aydoğmuş, [2]Cenk Yanen
[1]Fırat University, Engineering Faculty, Chemical Engineering, Elazığ, 23119, Türkiye
[2]Fırat University, Engineering Faculty, Mechanical Engineering, Elazığ, 23119, Türkiye

*Corresponding Author E-mail:ercanaydogmus@firat.edu.tr

Abstract
In this research, modified safflower oil reinforced biocomposite material is obtained by using hydrogen gas and nickel catalyst. Hydroxylation of safflower oil is a chemical transformation that occurs with the use of hydrogen gas. This process is generally carried out by a reaction mechanism called catalytic hydrogenation. Triglycerides containing double bonds in safflower oil are hydroxylated with the help of hydrogen gas and nickel metal catalysts. Experimental studies are being carried out on the borosilicate glass reactor system that is resistant to high temperature and pressure. Modified safflower oil (MSO), hydrogen gas, and catalyst (nickel) are combined in the reaction vessel. In this environment, hydrogen is added to the carbon atoms in the double bonds. As a result of this chemical modification, the double bonds in safflower oil are partially or completely transformed into saturated fatty acids. Biocomposite is produced by adding a crosslinker to the synthesized raw material under appropriate conditions. This process can generally take place at a temperature of 150 °C, and as the temperature increases, the reaction rate increases, and undesirable side reactions are prevented. The hydrogenation process is carried out under 2 atmospheres of pressure. As the pressure increases, the solubility of hydrogen increases and the efficiency of the chemical reaction rises. The experimental parameters in this study are optimized by the response surface methodology (RSM. According to the results obtained, it has been determined that both the physical and chemical properties of the biocomposite with approximately 5 wt.% MSO addition is optimum. However, higher MSO reinforcement reduces both the density and hardness of the biocomposite. When the surface morphology of the obtained composites is examined, highly irregular pore structure and distribution are observed. The thermal conductivity coefficient of the highly MSO reinforced biocomposite also increases due to this matrix structure.

Keywords: Safflower oil**,** hydrogen gas, hydroxylation**,** biocomposite, characterization

I. Introduction

The increasing demand for sustainable and environmentally friendly materials is encouraging extensive research into the development of biocomposite materials derived from renewable resources. Among these sources, vegetable oils emerge as promising candidates for the synthesis of biocomposite matrices due to their versatile chemical properties (Bharath and Basavarajappa, 2016). The use of vegetable oils in various industrial applications is increasing and they are attracting great attention due to their high content of unsaturated fatty acids that can be chemically modified (Sharma et al., 2006).

In recent years, there has been increasing interest in using this type of oil as a matrix material in biocomposite production. In particular, catalytic hydrogenation of vegetable oil occurs by adding hydrogen gas to the carbon-carbon double bonds in triglyceride molecules under controlled conditions (Veldsink et al., 1997). This chemical transformation leads to partial or complete saturation of double bonds, resulting in the formation of saturated fatty acids. Modified vegetable oils exhibit improved thermal stability, oxidative resistance and mechanical properties, making them suitable for use as matrix materials in biocomposites (Quirino et al., 2014).

Biocomposite materials are obtained by reinforcing natural fibers or nanoparticles into modified vegetable oil-based polymer matrices (Mosiewicki et al., 2013). Due to their low cost and favorable mechanical properties, biocomposites have a significant potential for widespread use in the future. The use of biocomposite materials enables the development of sustainable and environmentally friendly materials with various applications. Through ongoing research and innovation, these materials have the potential to drive advances in the field of biomaterials and contribute to a more sustainable future (Chakraborty and Chatterjee, 2020).

The production and characterization of biocomposite materials using hydrogen gas-modified vegetable oil is an interesting field of research that combines the principles of polymer chemistry, materials science, and green chemistry (Kumar et al., 2003). Biocomposite materials are composite materials consisting of a matrix (usually a polymer) and reinforcement derived from renewable biological resources such as natural fibers, starch, or vegetable oils (Rus, 2010). They offer potential advantages over traditional petroleum-based composite materials due to their biodegradability, renewability, and potentially lower environmental impact. Hydrogenation is a chemical process in which hydrogen gas is added to the unsaturated bonds in vegetable oils, converting them into saturated fats. This process can be catalyzed by metal catalysts such as nickel or palladium. Hydrogenation of vegetable oils improves their oxidative stability and changes their physical properties, making them suitable for a variety of industrial applications, including the production of biocomposite materials (Karmakar et al., 2020). Production of biocomposite materials using hydrogenated vegetable oils typically involves mixing the modified oil with a suitable reinforcing agent (such as natural fibers or nanoparticles) and other additives (such as cross-linkers or fillers) to achieve the desired properties. The mixture is then processed using techniques such as compression molding, extrusion, or injection molding to create the final composite material. Biocomposite materials find applications in a variety of

industries, including automotive, construction, packaging, and consumer goods. They can be used to produce lightweight, environmentally friendly products with special properties for specific applications.

Characterization processes are carried out by performing some physical tests and chemical analyses to evaluate the properties of biocomposite materials (Aydoğmuş, 2022). Mechanical tests are carried out, especially by performing tensile, compression, and bending tests on the biocomposite. Differential scanning calorimetry (DSC) and thermogravimetric analysis (TGA) are used to study the thermal behavior and stability of materials. Scanning electron microscopy (SEM) and transmission electron microscopy (TEM) provide information about the distribution and morphology of the reinforcement within the matrix. Fourier transform infrared spectroscopy (FTIR) and nuclear magnetic resonance (NMR) spectroscopy are used to analyze the chemical composition and structure of materials (Şahal and Aydoğmuş, 2023).

Research in the field of biocomposite materials using hydrogenated vegetable oils continues, focusing on the development of new formulations, optimizing processing techniques, and exploring new applications. Future efforts may also aim to improve the performance and sustainability of these materials through the use of advanced additives and processing methods. Overall, the production and characterization of biocomposite materials using hydrogen gas-modified vegetable oil offer promising opportunities for the development of sustainable and environmentally friendly materials with diverse applications in various industries (El-Qelish et al., 2024).

This research focuses on the development of biocomposite materials using natural fibers or modified safflower oil as a matrix reinforced with nanoparticles. Safflower oil, a renewable and abundant resource, is chemically modified through hydrogenation to improve its properties and make it suitable for use as a matrix material in biocomposites. Hydroxylation of safflower oil involves the addition of hydrogen gas to the carbon-carbon double bonds found in the oil's triglyceride molecules. This process, catalyzed by the nickel catalyst, leads to partial or complete saturation of the double bonds, leading to the formation of saturated fatty acids. Catalytic hydrogenation is a well-established reaction mechanism used in the food and chemical industries to change the physical and chemical properties of oils and fats (Abdulkareem-Alsultan et al., 2019). Experimental studies are carried out using a borosilicate glass reactor system that can withstand high temperatures and pressures. Safflower oil, hydrogen gas, and nickel catalyst are combined in the reactor vessel where hydrogen is added to the carbon-carbon double bonds under controlled conditions. The reaction temperature is maintained at 150°C because higher temperatures promote faster reaction rates while minimizing undesirable side reactions. The hydrogenation process is carried out under a pressure of 2 atmospheres since increased pressure increases the solubility of hydrogen and increases the efficiency of the chemical reaction. After the modification of safflower oil, biocomposite materials are produced by adding a crosslinker to the synthesized raw material under appropriate conditions. The cross-linker helps strengthen the matrix and improve the mechanical properties of the biocomposite (Mohammad et al., 2013).

The manufacturing process is carefully controlled to ensure uniform distribution of the reinforcement and proper curing of the matrix material. Experimental parameters, including reaction temperature, pressure, and catalyst concentration, were optimized using response surface methodology (RSM). RSM is a statistical technique used to design experiments, analyze data, and optimize process parameters to maximize the desired response (Aydoğmuş et al., 2021). By systematically varying the experimental conditions, researchers can determine the optimal set of parameters that provide the desired properties of the biocomposite material (Aydoğmuş et al., 2022). The resulting biocomposite materials are subjected to extensive physical and chemical characterization to evaluate their properties. Techniques such as mechanical testing, thermal analysis, microscopy, and spectroscopy are used to evaluate the structural integrity, thermal stability, morphology, and chemical composition of biocomposites. These characterization processes provide valuable information about the performance and suitability of materials for various applications. In summary, this research aims to develop sustainable and environmentally friendly biocomposite materials by using modified safflower oil as matrix material. Through careful control of the hydrogenation process and optimization of experimental parameters, researchers aim to produce biocomposites with special properties suitable for a wide range of applications.

II. Experimental Set-up and Procedure

Materials used in experimental studies

Commercially available safflower oil (purity: 99%) was obtained from a local supplier. Hydrogen gas, with high purity (99%), is used with the help of a gas cylinder equipped with a pressure regulator. Nickel catalyst is used in the form of nickel powder or nickel supported on a suitable substrate for catalytic hydrogenation. Methylene diphenyl disocyanate functional crosslinker was preferred to develop biocomposite material. Commercial polyol (CP) and methylene diphenyl diisocyanate (MDI) were supplied by Puryap Company.

The preferred method in experimental studies

Safflower oil (100 g) was placed in the borosilicate glass reactor equipped with a magnetic stirrer and reflux condenser. The nickel catalyst (1% w/w oil) was added to the reactor, followed by hydrogen gas at a flow rate of 100 mL/min. The reaction was carried out at 150 °C, under 2 atmospheres of pressure, with continuous stirring for 4 hours. After the reaction, washing, neutralization, and purification processes were performed and hydrogenated safflower oil was prepared for biocomposite production (Yenumala et al., 2016). In the biocomposite preparation process, modified safflower oil (MSO) was mixed homogeneously with natural straw fibers under room conditions. After adding MDI crosslinker to the mixture, it was cast into standard molds. After waiting 24 hours for the curing process, the necessary physical tests and chemical analyses were carried out (Dağ et al., 2023). Table 1 lists each

component and mixture ratios used in experimental studies.

Tab. 1: Experimental study plan for the biocomposite production

Experiments	MSO (wt.%)	CP (wt.%)	MDI (wt.%)
1	*0.0*	*50.0*	*50.0*
2	*2.5*	*47.5*	*50.0*
3	*5.0*	*45.0*	*50.0*
4	*7.5*	*42.5*	*50.0*
5	*10.0*	*40.0*	*50.0*

Response surface methodology (RSM)

A central composite design (CCD) was used to optimize experimental parameters including reaction temperature, pressure, catalyst concentration, cross-linker concentration, and fiber content. The experimental design consists of a series of factorial points, axial points, and center points to explore the response surface. Responses such as the degree of hydrogenation, mechanical properties, and thermal stability of the biocomposite were evaluated using regression analysis to determine the optimal conditions. Data obtained from the experiments were subjected to analysis of variance (ANOVA) to evaluate the significance of the factors and their interactions. Regression models were developed to predict response variables based on experimental data. To maximize the desired properties of the biocomposite, optimum process conditions were determined by solving regression equations and performing desirability analysis.

IV. Results and Discussions

According to the results obtained from experimental studies, some thermophysical properties of the biocomposite have been examined. Bulk density, hardness, and thermal conductivity coefficient measurements are expressed in the graphs below. It has been observed that as the MSO ratio in the mixture increases, the density of the biocomposite tends to decrease (Fig. 1). When calculating bulk density, it is determined after measuring the masses of samples with a certain volume in standard molds. After measuring the dimensions of the samples with the help of a digital caliper, shrinkage after curing is also taken into account. The bulk density of the biocomposite is calculated by the mass divided by volume ratio.

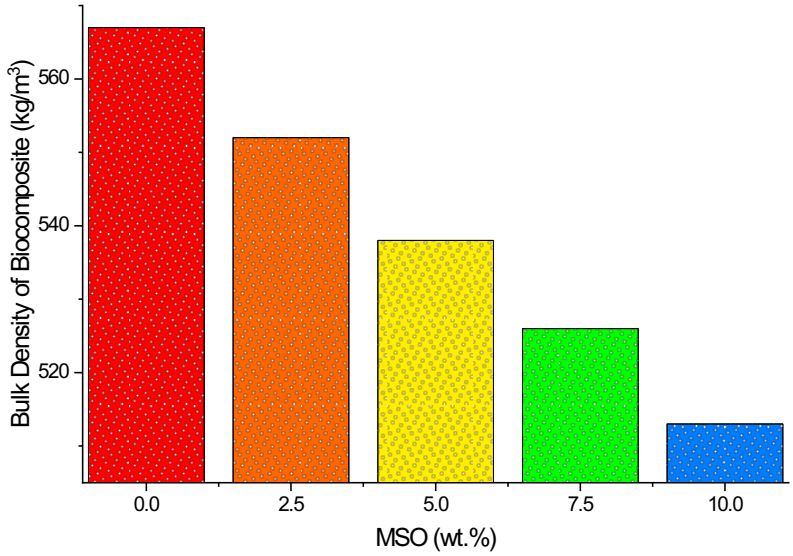


Fig. 1: Effect of MSO addition on bulk density of the biocomposite

Shore D hardness testing is performed according to ASTM D2240 standard. ASTM (American Society for Testing and Materials) is an organization that develops standards for evaluating the physical and mechanical properties of materials. The ASTM D2240 standard specifies a test method used to measure the hardness of elastomeric and rubber-like materials (Calvert et al., 2010). As seen in Figure 2, the hardness of the biocomposite decreases as the MSO ratio increases.

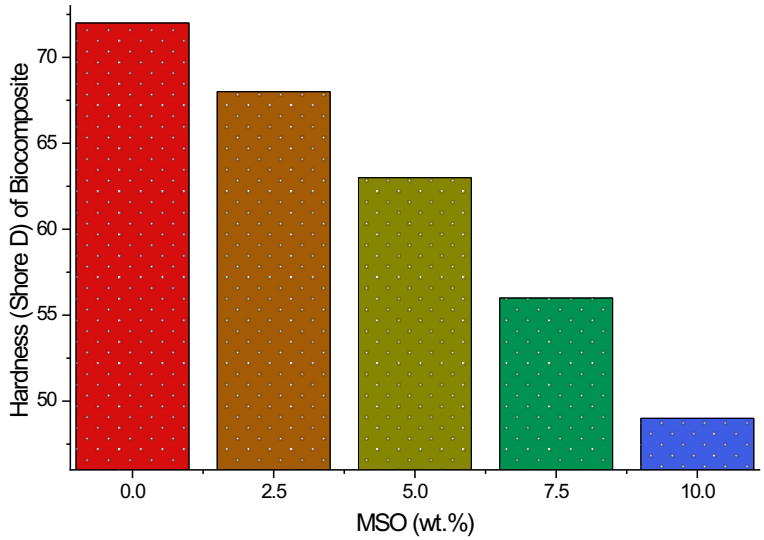


Fig. 2: Change of Shore D hardness of biocomposite with MSO ratio

In thermal conductivity coefficient measurements, MSO reinforcement increases the thermal conductivity of the biocomposite. When Figure 3 is examined, the pure biocomposite has a thermal conductivity of approximately 0.026 W/m·K, but with 10 wt.% MSO reinforcement, this coefficient approaches 0.039 W/m·K.

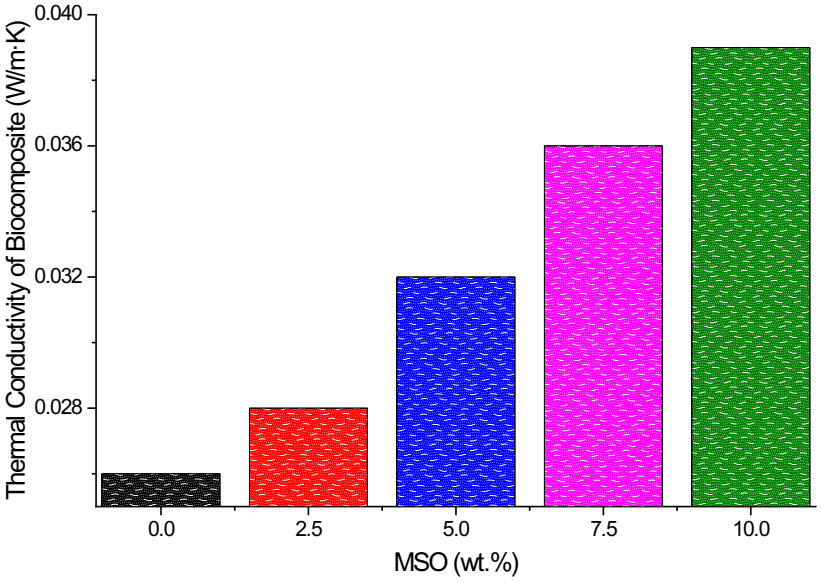


Fig. 3: Variation of thermal conductivity coefficient of biocomposite with MSO reinforcement

V. Conclusions

Safflower oil undergoes a hydroxylation process using hydrogen gas and nickel, a catalyst. This process involves the hydroxylation of triglycerides containing double bonds in safflower oil. With the help of hydrogen gas and the nickel catalyst, this process is accomplished through a reaction mechanism called catalytic hydrogenation. Experiments are carried out in borosilicate glass reactor systems that are resistant to high temperatures and pressure. These systems allow the reaction to occur in a controlled manner. Bio-composite material is produced by adding a crosslinker to hydroxylated safflower oil under appropriate conditions. This process usually takes place at a temperature of 150 °C, and as the temperature increases, the reaction rate increases, and unwanted side reactions are prevented. The hydrogenation process is carried out under 2 atmospheres of pressure. As the pressure increases, the solubility of hydrogen increases and the efficiency of the chemical reaction increases. In this study, experimental parameters are optimized using response surface methodology (RSM). This methodology requires less experimental work than the trial-and-error method and helps determine the interactions of experimental parameters. The physical and chemical properties of the resulting biocomposite material are characterized. This characterization process is aimed at determining the structural, thermal, mechanical, and surface properties of the material.

The results indicate that the addition of approximately 5 wt.% MSO leads to the optimal balance of properties in the biocomposite. Both physical and chemical properties exhibit favorable characteristics at this level of reinforcement. However, it was observed that higher levels of MSO reinforcement resulted in a reduction in both the density and

hardness of the biocomposite. This suggests that there exists an optimum MSO content beyond which further reinforcement may compromise certain mechanical properties of the material. Furthermore, analysis of the surface morphology revealed a highly irregular pore structure and distribution in the biocomposite with higher MSO content. This irregularity may affect the overall structural integrity and performance of the material in certain applications. Interestingly, the thermal conductivity coefficient of the biocomposite increased with higher MSO reinforcement, likely due to the altered matrix structure caused by the irregular pore distribution. This finding suggests that MSO reinforcement not only influences mechanical properties but also affects thermal characteristics, which could be advantageous in specific thermal management applications. Therefore, this study provides valuable insights into the effects of MSO reinforcement on biocomposite properties. The optimized MSO content identified in this research can serve as a guideline for future biocomposite development efforts. However, further research is warranted to explore the full potential of MSO reinforcement and to address the challenges associated with pore structure irregularities observed at higher reinforcement levels. Overall, the findings of this study contribute to the advancement of sustainable and environmentally friendly biocomposite materials with potential applications in various industries.

References

Abdulkareem-Alsultan, G., Asikin-Mijan, N., Lee, H. V., Rashid, U., Islam, A., & Taufiq-Yap, Y. H. (2019). A review on thermal conversion of plant oil (edible and inedible) into green fuel using carbon-based nanocatalyst. Catalysts, 9(4), 350.

Aydoğmuş, E. (2022). Biohybrid nanocomposite production and characterization by RSM investigation of thermal decomposition kinetics with ANN. Biomass Conversion and Biorefinery, 12(10), 4799-4816.

Aydoğmuş, E., Arslanoğlu, H., & Dağ, M. (2021). Production of waste polyethylene terephthalate reinforced biocomposite with RSM design and evaluation of thermophysical properties by ANN. Journal of Building Engineering, 44, 103337.

Aydoğmuş, E., Dağ, M., Yalçın, Z. G., & Arslanoğlu, H. (2022). Synthesis and characterization of waste polyethylene reinforced modified castor oil‐based polyester biocomposite. Journal of Applied Polymer Science, 139(27), e52526.

Bharath, K. N., & Basavarajappa, S. (2016). Applications of biocomposite materials based on natural fibers from renewable resources: a review. Science and Engineering of Composite Materials, 23(2), 123-133.

Calvert, K. L., Trumble, K. P., Webster, T. J., & Kirkpatrick, L. A. (2010). Characterization of commercial rigid polyurethane foams used as bone analogs for implant testing. Journal of materials science: Materials in medicine, 21, 1453-1461.

Chakraborty, I., & Chatterjee, K. (2020). Polymers and composites derived from castor oil as sustainable materials and degradable biomaterials: current status and emerging trends. Biomacromolecules, 21(12), 4639-4662.

Dağ, M., Aydoğmuş, E., Yalçin, Z. G., & Arslanoğlu, H. (2023). Diatomite reinforced modified safflower oil-based epoxy biocomposite production: Optimization with RSM and assessment of outcomes by ANN. Materials Today Communications, 35, 106327.

El-Qelish, M., El-Shafai, S. A., Azouz, R. A., Rashad, E., & Elgarahy, A. M. (2024). From seashells to sustainable energy: Trailblazing the utilization of Anadara uropigimelana shells for sustainable biohydrogen production from leftover cooking oil. Journal of Environmental Chemical Engineering, 12(2), 111914.

Karmakar, G., Ghosh, P., Kohli, K., Sharma, B. K., & Erhan, S. Z. (2020). Chemicals from vegetable oils, fatty derivatives, and plant biomass. Innovative Uses of Agricultural Products and Byproducts, 1-31.

Kumar, M. S., Ramesh, A., & Nagalingam, B. (2003). Use of hydrogen to enhance the performance of a vegetable oil fuelled compression ignition engine. International Journal of Hydrogen Energy, 28(10), 1143-1154.

Mohammad, M., Hari, T. K., Yaakob, Z., Sharma, Y. C., & Sopian, K. (2013). Overview on the production of paraffin based-biofuels via catalytic hydrodeoxygenation. Renewable and Sustainable Energy Reviews, 22, 121-132.

Mosiewicki, M. A., & Aranguren, M. I. (2013). A short review on novel biocomposites based on plant oil precursors. European Polymer Journal, 49(6), 1243-1256.

Quirino, R. L., Garrison, T. F., & Kessler, M. R. (2014). Matrices from vegetable oils, cashew nut shell liquid, and other relevant systems for biocomposite applications. Green Chemistry, 16(4), 1700-1715.

Rus, A. Z. M. (2010). Polymers from renewable materials. Science Progress, 93(3), 285-300.

Şahal, H., & Aydoğmuş, E. (2023). Production of SBS Reinforced Polyester Composite: Characterization of Physical and Chemical Properties. Journal of the Turkish Chemical Society Section A: Chemistry, 10(3), 827-834.

Sharma, B. K., Adhvaryu, A., Liu, Z., & Erhan, S. Z. (2006). Chemical modification of vegetable oils for lubricant applications. Journal of the American Oil Chemists' Society, 83, 129-136.

Veldsink, J. W., Bouma, M. J., Schöön, N. H., & Beenackers, A. A. (1997). Heterogeneous hydrogenation of vegetable oils: a literature review. Catalysis Reviews, 39(3), 253-318.

Yenumala, S. R., Maity, S. K., & Shee, D. (2016). Hydrodeoxygenation of karanja oil over supported nickel catalysts: influence of support and nickel loading. Catalysis Science & Technology, 6(9), 3156-3165.

A New Controller Design for Fuel Cells

[1*]Serhat Dogan, [1]Cem Haydaroglu, [1]Bilal Gumus
[1] Dicle University, Faculty of Engineering, Department of Electrical & Electronics Engineering, Diyarbakır, 21280, Türkiye

* E-mail:serhat.dogan@dicle.edu.tr

Abstract

With the rapid growth in population and technological advancements, global energy demand has significantly increased. However, environmental impacts of fossil fuels and issues like climate change have triggered energy crises, increasing interest in alternative energy production systems. One such alternative is Proton Exchange Membrane Fuel Cells (PEMFCs). PEMFCs are notable for their low operating temperatures, high power densities, and clean energy production capacities. These characteristics make PEMFCs an eco-friendly and economical energy source for various applications. However, the performance of PEMFC systems is dependent on non-linear operating conditions such as temperature, gas pressure, and membrane water content. To maximize efficiency and ensure a longer operational lifespan under these adverse conditions, appropriate control methods are required. In this study, a Fuzzy Logic control-based maximum power point tracking (MPPT) controller for a PEMFC system was developed. To validate this Fuzzy Logic-based controller, the PEMFC system was analyzed and compared with different control algorithms in MATLAB/Simulink, and the results were evaluated.

Keywords: Fuel Cell, MPPT, Fuzzy Logic

I. Introduction

In recent years, global energy demand has increased significantly due to population growth and rapid technological advancements. Additionally, concerns about fossil fuel depletion and climate change have accelerated investments in renewable energy. Market fluctuations and rising fossil fuel prices have led to energy crises worldwide, making renewable energy more competitive. Fuel cells, with their low operating temperatures, high power density, clean and efficient energy production, low noise, and cost-effectiveness, have emerged as a preferred alternative energy source. These technologies are used in distributed generation, residential and industrial co-generation, maritime applications, military equipment, and transportation sectors. (Cigolotti, 2021), (Akinyele, 2020), (Van Biert, 2016), (Fan, 2021).

Despite the high efficiency of PEMFCs, the power output is not always optimal due to variables such as hydrogen and oxygen gas pressures, stoichiometry, cell temperature, and membrane water content. Like other renewable energy sources, PEMFCs require maximum power point tracking (MPPT). In the literature, MPPT algorithms used in photovoltaic (PV) systems can be effectively applied to PEMFCs. For example, (Ahmadi, 2017) designed a particle swarm optimization (PSO)-based proportional-integral-derivative (PID) controller to estimate the maximum power point of a PEMFC system. Another study by (Percin, 2023) developed a whale optimization algorithm (WOA)-based method for MPPT in PEMFC systems.

In this study, a Fuzzy Logic control-based MPPT system for a PEMFC was developed and implemented in MATLAB/Simulink. The performance of the Fuzzy Logic controller was compared with that of the traditional Perturb & Observe (P&O) algorithm. The aim was to enhance MPPT performance using Fuzzy Logic control and to highlight the differences between this method and the conventional P&O algorithm. The advantages and accuracy of the Fuzzy Logic control method were examined, and the results were analyzed and compared with those obtained using the P&O algorithm.

II. Simulation Set-up and Procedure

The fuel cell model used in this study is a detailed Proton Exchange Membrane Fuel Cell (PEMFC) model configured in MATLAB/Simulink. The model provides a power output of 1.26 kW and a nominal voltage of 24 Vdc. To observe the effects of different control structures on fuel cell performance, the diagram shown in Figure 1 was created. This setup allows for a comprehensive analysis of various control methods and their impact on the efficiency and performance of the PEMFC system.

Furthermore, Figure 2 illustrates the power-current relationship of the fuel cell stack. The graph shows that as current increases, the power output also increases. Two critical points are highlighted: 1.26 kW at 52 amperes and 2 kW at 100 amperes. These points represent the nominal and maximum power outputs of the fuel cell stack, respectively. The nominal power output indicates the power provided under normal operating conditions, while the maximum power output represents the point of highest efficiency.

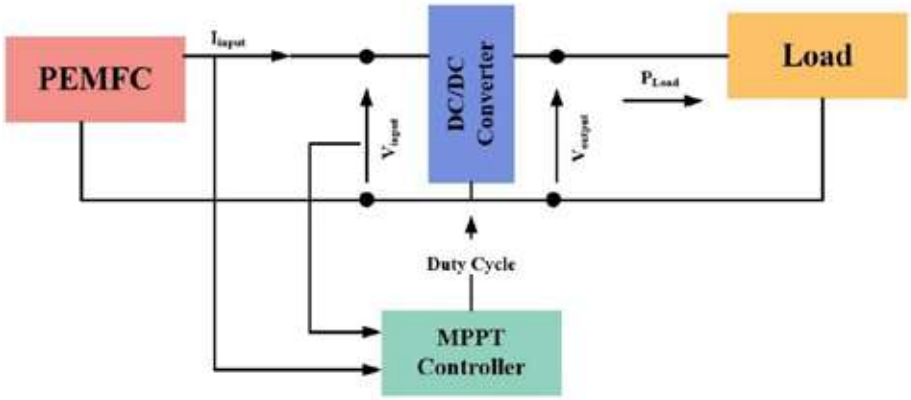


Fig. 1: MPPT controlled DC/DC converter diagram for a PEMFC

This graph serves as a crucial reference for evaluating the fuel cell's performance, enabling observation of power production at various current levels. Based on these data, the fuel cell was operated at its nominal power point.

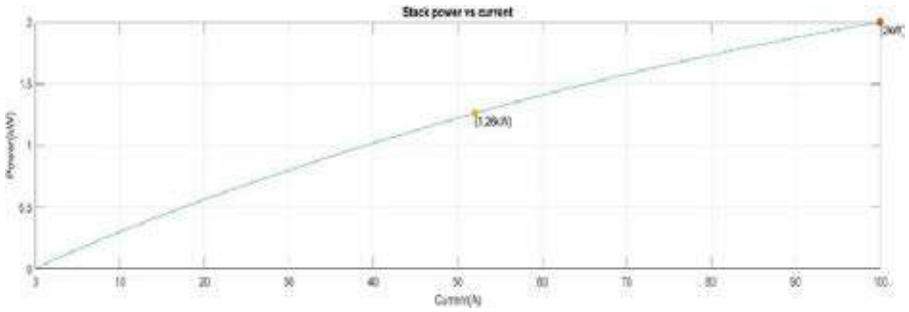


Fig. 2: Power-current curve for fuel cell

In applying the Fuzzy Logic control method for both Type 1 and Type 2, the boundaries were determined based on the condition $dP/dI = 0$. According to the membership function shown in Figure 3, the error input variable is defined in the range of [-200, -150]. This range represents the control errors determined relative to the point where the rate of change of power and current is zero. These boundaries are critical for the accurate and effective operation of the Fuzzy Logic controller in tracking the maximum power point (MPP) of the PEMFC system.

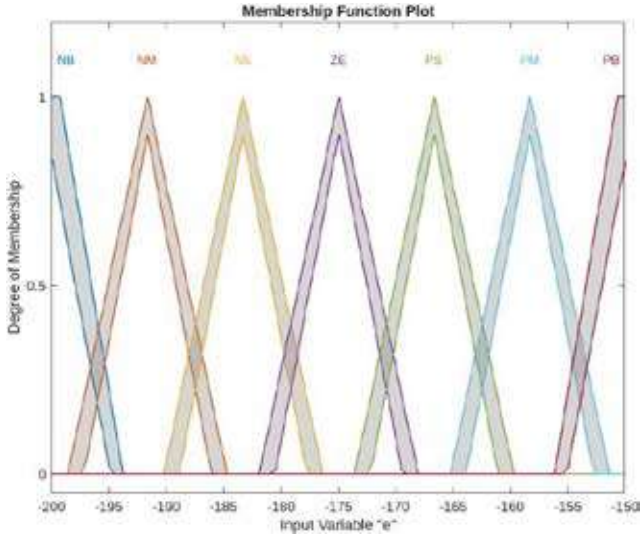


Fig. 3: Fuzzy logic membership functions graph

The membership functions are named Negative Big (NB), Negative Medium (NM), Negative Small (NS), Zero (ZE), Positive Small (PS), Positive Medium (PM), and Positive Big (PB). Each membership function is modeled using triangular or trapezoidal shapes representing the degree of error. This modeling ensures the Fuzzy Logic controller responds sensitively to different operating conditions of the system. By utilizing these membership functions, the controller tracks the system's maximum power point based on the condition $dP/dI = 0$, thereby achieving optimal

performance. This approach effectively enhances the efficiency of fuel cell systems under dynamic and varying conditions.

The equation $dP/dI = 0$ is an optimization criterion used to determine the maximum power point (MPP) of a fuel cell. When the partial derivative of this equation is taken, the maximum power point, similar to that in photovoltaic systems, is obtained (Gulzar, 2023):

$$\frac{dP}{dI} = \frac{d(V.i)}{dI} \tag{1}$$

$$\frac{dP}{dI} = V + i.\frac{d(V)}{dI} \tag{2}$$

$$V + i.\frac{d(V)}{dI} = 0 \tag{3}$$

These equations illustrate the similarities in determining the maximum power point (MPP) for both fuel cell and photovoltaic systems. They are used to identify the optimal operating conditions for efficient performance in both types of systems.

III. Analysis

In this simulation, the performances of Perturb & Observe (P&O), Fuzzy Logic Type 1, and Fuzzy Logic Type 2 control structures were compared in detail. The comparison was conducted based on the nominal power of the fuel cell, with the nominal power curve obtained at a temperature of 328 °F. The results are shown in Figure 4.

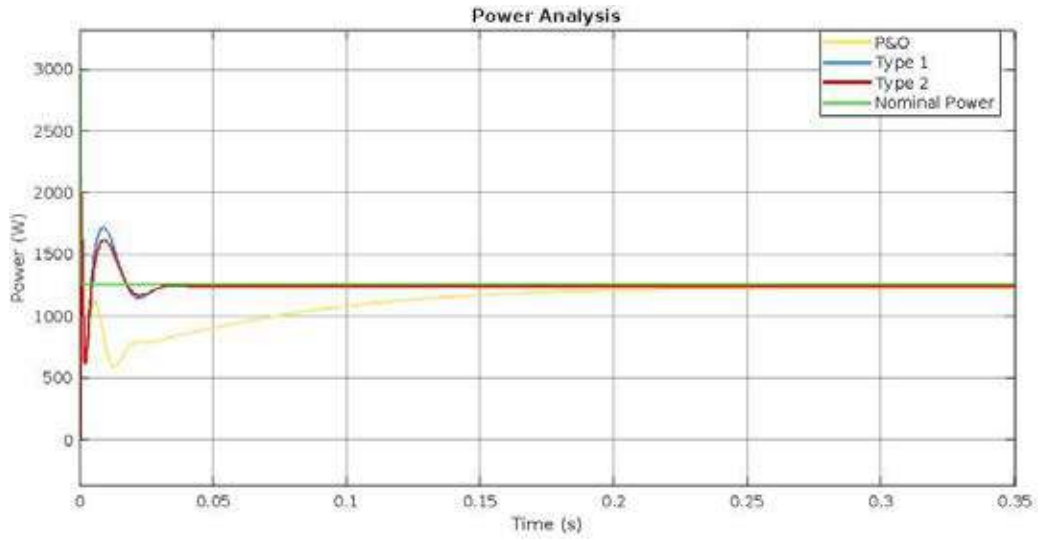


Fig. 4: Fuel cell power analysis and performance comparison of different MPPT algorithms

According to the analysis results, the Fuzzy Logic Type 2 controller demonstrated superior performance in tracking MPP and optimizing energy efficiency of the fuel cell compared to other algorithms. The Fuzzy Logic Type 2 algorithm, with its rapid response time and low oscillation characteristics, reached nominal power the quickest, making it the most efficient method for optimizing energy systems. Conversely, the P&O algorithm exhibited high initial power fluctuations and took longer to stabilize, revealing its disadvantages in dynamic and varying conditions. The Fuzzy Logic Type 1 controller showed a fast and stable performance, closely approximating nominal power with minimal fluctuations, but had a higher oscillation rate compared to the Type 2 controller.

IV. Results and discussions

With its fast response time and low oscillation characteristics, the Type 2 algorithm significantly enhanced the efficiency of energy systems by reaching nominal power the quickest. Conversely, the P&O algorithm experienced high initial power fluctuations and took longer to stabilize, highlighting its disadvantages. The Type 1 controller delivered a fast and stable performance but exhibited higher oscillation compared to the Type 2 controller. Future research could focus on exploring different Fuzzy Logic types and advanced control algorithms to further improve fuel cell system performance and energy efficiency. In this context, employing more advanced Fuzzy Logic controllers, such as Type 3, could yield better results under dynamic and varying operating conditions.

References

Cigolotti V., Genovese M., Fragiacomo P., Comprehensive Review on Fuel Cell Technology for Stationary Applications as Sustainable and Efficient Poly-Generation Energy Systems, Energies, 14, 16, 4963, (2021).

Akinyele D., Olabode E., Amole A., Review of Fuel Cell Technologies and Applications for Sustainable Microgrid Systems, Inventions, 5, 3, 42, (2020).

Van Biert L., Godjevac M., Visser K., Aravind P. V., A review of fuel cell systems for maritime applications, Journal of Power Sources, 327, 345-364, (2016).

Fan L., Tu Z., Chan S. H., Recent development of hydrogen and fuel cell technologies: A review, Energy Reports, 7, 8421-8446, (2021).

Boscaino V., Miceli R., Capponi G., MATLAB-based simulator of a 5 kW fuel cell for power electronics design, International Journal of Hydrogen Energy, 38, 19, 7924-7934, (2013).

Karami N., El Khoury L., Khoury G., Moubayed N., Comparative study between P and O and incremental conductance for fuel cell MPPT, 2014 International Conference on Renewable Energies for Developing Countries, REDEC 2014, 2, 17-22, (2014).

Ahmadi S., Abdi S., Kakavand M., Maximum power point tracking of a proton exchange membrane fuel cell system using PSO-PID controller, International Journal of Hydrogen Energy, 42, 32, 20430-20443, (2017).

Percin H. B., Caliskan A., Whale optimization algorithm based MPPT control of a fuel cell system, International Journal of Hydrogen Energy, 48, 60, 23230-23241, (2023).

Gulzar M. M., Maximum Power Point Tracking of a Grid Connected PV Based Fuel Cell System Using Optimal Control Technique, Sustainability, 15, 3980, (2023).

Control Parameters Optimization of HHO Dry Cell by Metaheuristic Algorithms

[1]Caglar Conker, [1*]Mustafa Kaan Baltacioglu
[1] Iskenderun Technical University, Department of Mechatronics Engineering, Hatay, 31200, Turkey

* E-mail:mkaan.baltacioglu@iste.edu.tr

Abstract
Simulation studies that examined the effects of search algorithm and fitness functions on controller performance were verified in HHO Dry Cell system. The proposed approach has been validated by testing both theoretically and experimentally. Using a hydroxyl dry cell system consisting of 13 plates (14x14 cm and 316 stainless stell each), an electrolyte has been prepared in compliance with the literature. Taking into account temperature and safety criteria, PID control parameters for the dry cell have been determined. These control parameters were optimized using artificial bee colony and genetic algorithm methods, and the results were compared with two basic control methods: on-off and fuzzy-PID. The obtained results are presented comparatively with graphs.

Keywords: Artificial Bee Colony, Genetic Algorithm, HHO Dry Cell, Optimization, Electrochemistry

I. Introduction

Commercial application of electrolyzers commenced in the 1920s with alkaline variants but experienced an economic downturn circa the 1970s with the advent of hydrogen production from natural gas and steam methane. In this investigation, the primary aim is maintaining the temperature within the HHO reactor below 60°C through the modulation of Pulse Width Modulation (PWM) settings during hydrogen generation operations. Absent the utilization of PWM techniques, conventional HHO gas generator systems typically operate at full load, which may result in an elevation of the generator temperature to approximately 90°C (Baltacioglu, 2019). Such elevated temperatures may precipitate critical damage to the tube material within the HHO generators. Furthermore, it is recognized that elevated temperatures within the reactor yield several adverse consequences. Firstly, heightened temperature levels contribute to increased water evaporation, consequently elevating the moisture content within the produced gas, thereby compromising the quality of the resultant hydrogen gas. Secondly, elevated temperature levels within the reactor curtail the operational lifespan of the system. It is suggested by literature that optimal temperature levels for HHO gas generators reside below 70°C (Conker, 2019, Conker ve Baltacıoglu, 2020). The temperature control of HHO reactors emerges as a complex optimization problem. In this context, the necessity of utilizing modern artificial intelligence techniques alongside traditional control methods becomes apparent. Meta-heuristic optimization techniques inspired by natural intelligence, such as genetic algorithms and artificial bee colony, could play a significant role in managing the temperature of HHO reactors. These techniques offer potential in effectively navigate through multiple variables in complex systems, thereby potentially yielding optimized and energy-efficient solutions for temperature control in HHO reactors. Therefore, artificial intelligence-based methods such as genetic algorithms and artificial bee colony present themselves as significant tools in managing the temperature of HHO reactors.

II. Experimental and Numerical Set-up

The regulation of temperature in a dry cell HHO reactor is a commonplace endeavor within temperature control systems. This process can be aptly characterized mathematically through the formulation of a first-order system transfer function. The transfer function is expressed as:

$$G(s)=\frac{K}{Ts+1}e^{-\tau s}=\frac{56.8}{1780s+1}e^{-50s} \tag{1}$$

Wherein, K signifies the static gain inherent to the controlled process, τ delineates the pure lag time exhibited by the system, and T denotes the time constant characterizing the controlled process. Consequently, the representation of the dry cell HHO reactor system's dynamics finds articulation through Equation 1.

The on-off controller is often considered the most basic form of feedback control. Its implementation typically requires minimal tuning, usually limited to determining the on-value, off-value, and threshold level of the controller output. When applied, the on-off control system tends to oscillate and typically exhibits a non-zero offset between the mean value of the control error and the set point. The function of an on-off controller can be defined as follows:

$$u(t)_{on-off}=\begin{cases}u_{on} \; for \; e(t)>0\\ u_{off} \; for \; e(t)<0\end{cases} \tag{2}$$

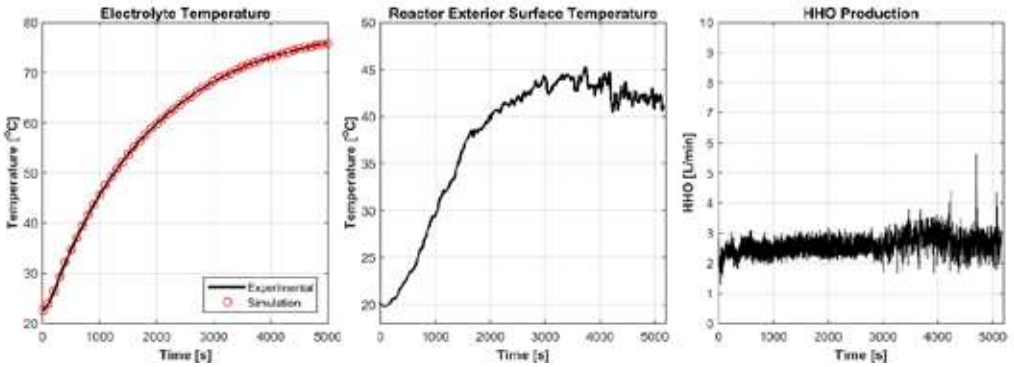


Fig.1.Surface & electrolyte temperatures and hydroxy production rates of the HHO dry cell (Conker ve Baltacıoglu, 2020)

In this context, the output signal from the controller is denoted by *u(t)*, while the actuating error signal is presented by *e(t).*

A PID (Proportional-Integral-Derivative) controller is a ubiquitous feedback control mechanism extensively utilized in industrial control systems due to its favorable attributes, such as high reliability, stability, and computational simplicity. The PID controller aims to minimize the discrepancy between a measured process variable and a desired set point by computing and implementing corrective actions promptly to regulate the process effectively and minimize errors. The conventional transfer function of a PID controller can be expressed as follows:

$$u(t)_{PID} = K_p e(t) + K_i \int_0^t e(t)dt + K_d \frac{d\left(e(t)\right)}{dt} \tag{3}$$

The suitability of a PID (Proportional-Integral-Derivative) controller is primarily limited to linear systems with well-defined mathematical models. However, the regulation of temperature in an HHO (Hydrogen-Hydrogen-Oxygen) reactor poses a distinct challenge due to its inherently non-linear, time-delayed, and time-varying characteristics.

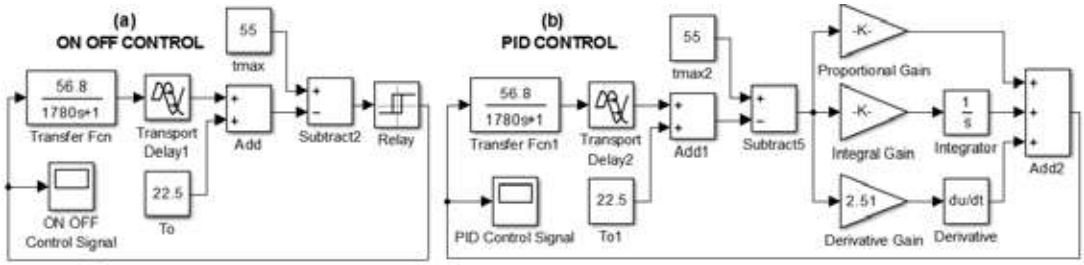


Fig.2. Flow chart of on-off (a) and fuzzy PID (b) structures

III. Analysis

Genetic Algorithm (GA)

The genetic algorithm commences by generating chromosomes randomly, which form the foundation for subsequent generations. These subsequent generations evolve through iterative processes, leveraging the preceding ones. Evaluation of these new generations is conducted based on a defined objective function, guiding natural selection. Following selection, both crossing and mutation processes come into play. Crossing facilitates minor alterations in chromosomes, driven by genetic mutation, thus generating a new generation with modified gene sequences from selected chromosomes. This iterative cycle persists, aiming for each successive generation to surpass its predecessors by selecting more favorable chromosomes. The algorithm continues until termination criteria and a predefined number of iterations are met. Key parameters like population size, crossing, and mutation rates directly impact the algorithm's performance. A flowchart depicting the progression of the genetic algorithm is presented in Figure 3.a.

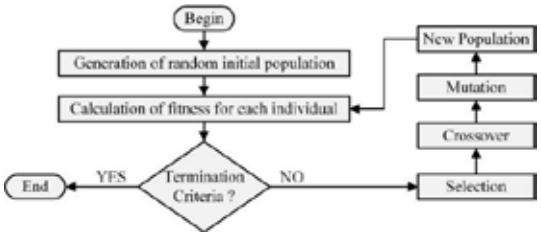


Fig.3.a Genetic Algorithm Flowchart

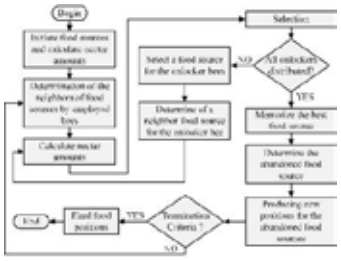


Fig.3.b. Artificial Bee Colony Algorithm Flowchart

Artificial Bee Colony (ABC) Algorithm

The algorithm is structured around three distinct types of bee species. Firstly, there are employed bees tasked with gathering nectar from known sources. These bees communicate the location of the nectar to their peers through intricate dances. Secondly, there are onlooker bees, which rely on the information provided by the employed bees to locate and pursue the nectar sources. The colony is evenly split between employed and onlooker bees. When the nectar supply is depleted, both groups transition into scout bees, forming the third category. These scout bees roam the vicinity of the hive aimlessly, without any specific information. The ABC algorithm strives to identify the location with the highest nutrient content, seeking to optimize or minimize the problem within the solution space. The algorithm's flowchart is presented in Figure 3.b.

Fitting Functions

This section elaborates on the tuning methods utilized for various performance metrics, including Integral Square Error (ISE), Integral Absolute Error (IAE), Integral Time Absolute Error (ITAE), and Mean Square Error (MSE); Eq.4 to 7 respectively (Furat ve Eker, 2014).

$$IAE = \int_0^t |e(t)|\,dt \tag{4}$$

$$ISE = \int_0^t e^2(t)dt \tag{5}$$

$$ITAE = \int_0^t t\,|e(t)|\,dt \tag{6}$$

$$MSE = \frac{1}{N}\sum_{k=1}^{N} e^2(k) \tag{7}$$

The primary control objective is to maintain various performance specifications, including rise time, settling time, maximum overshoot, and steady-state error, within desirable limits. To further validate the proposed technique and demonstrate its practical effectiveness compared to conventional methods, a series of experiments are conducted.

IV. Results and Discussions

The system, controller and optimization process are presented in Figure 4. Beside, optimization results of GA and ABC due to ISE, IAE, ITAE, MSE are presented in Table 1 in numerical form. Graphical resresentation of them are shown in Figure 5 and 6, respectively.

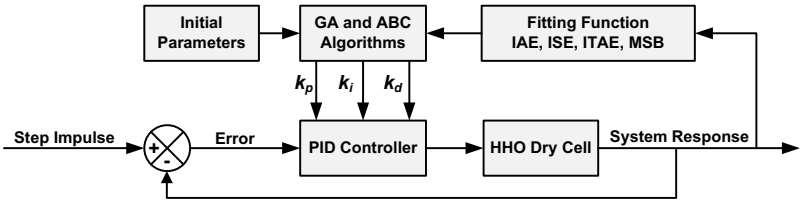


Fig.4. Optimization and Controller Structure

Tab. 1. Optimization results for GA and ABC algorithms

		Population Size 20		Population Size 30		Population Size 40		Population Size 50	
		GA	ABC	GA	ABC	GA	ABC	GA	ABC
ISE	Kp	3.1702	10	9.993619	9.645	4.2184	7.818	4.2184	7.9998
	Kd	0.0960	9.8621	9.91224	0.0815	9.9078	9.856	9.9078	9.867
	N	77.380	50	109.033	50	140.241	51.81	140.24	52.02
	Time	458.46	637.79	568.6452	928.84	825.994	1847.03	825.99	1705.67
IAE	Kp	6.1228	8.782	0.6606	10	4.14549	1.3937	9.2162	4.820
	Kd	1.06741	9.8737	-1.3782	0.080	9.90487	0.081	9.0375	0.0813
	N	70.878	52.32	109.986	93.301	117.85	50	92.490	50
	Time	328.731	648.23	470.243	928.48	667.71	1573.86	845.22	1655.34
ITAE	Kp	2.5397	0.800	1.2700	1.1698	3.9232	1.2524	0.2372	4.2993
	Kd	-1.260	0.943	-1.6050	1.1655	-1.9868	3.4279	0.2119	1.8568
	N	124.472	92.17	108.576	50	111.321	69.23	110.06	50
	Time	329.22	604.33	554.559	900.26	693.62	1206.21	864.04	1.5820
MSE	Kp	2.1797	3.5124	0.9048	10	5.1772	9.608	1.7123	6.3524
	Kd	0.0248	2.8795	0.0922	4.244	0.5145	1.0468	0.9368	0.8492
	N	111.14	105.13	110.911	81.979	111.28	150	106.97	50.855
	Time	362.073	607.98	514.818	941.87	716.18	1243.54	900.47	1658.78

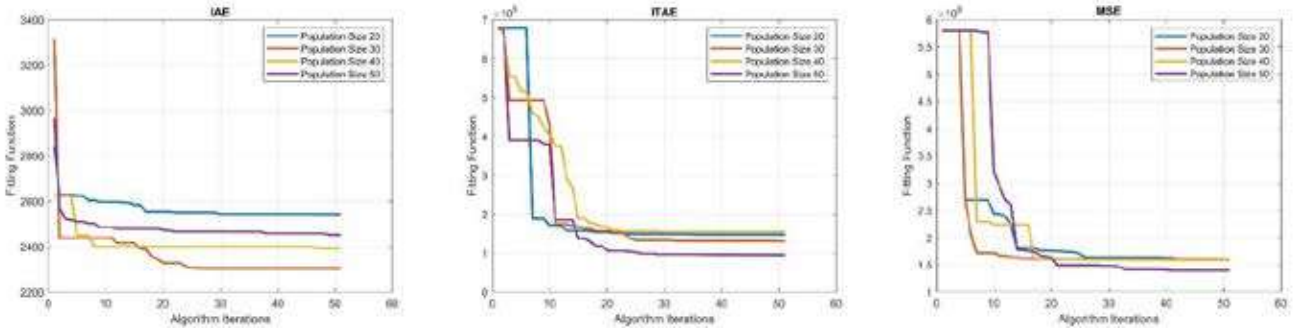


Fig.5.Convergence histories of the GA for different values of population size for IAE, ITAE and MSE

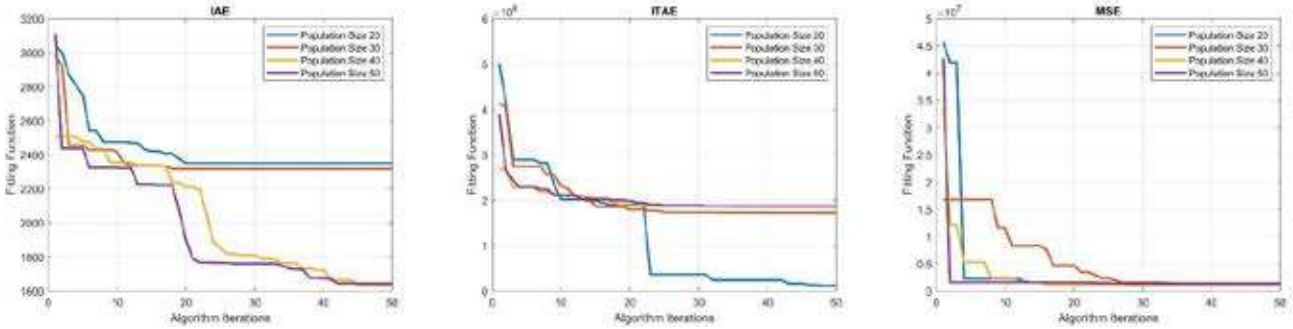


Fig.6. Convergence histories of the ABC for different values of population size for IAE, ITAE and MSE

Figure 7.a and 7.b present system respons graphs of GA and ABC, respectively below.

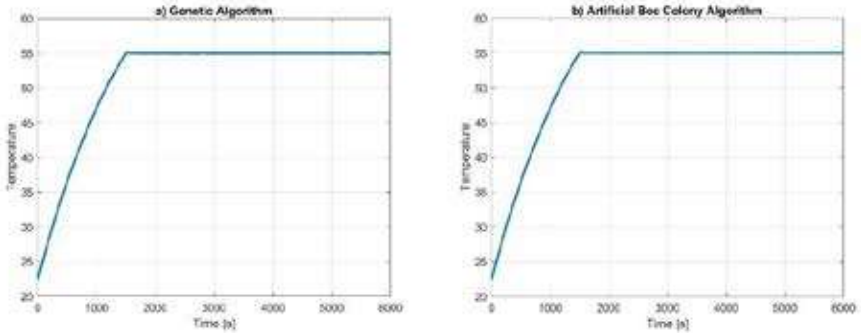


Fig. 7. HHO Dry Cell sytem response for Genetic Algorithm (a) and Artificial Bee Colony (b) based proportional-integral-derivative (PID) controller

The results indicate that, in comparison to the On-Off, PID, and Fuzzy controllers, the metaheuristic-based PID controller displays notable advantages. These include the absence of overshoot, a shorter adjustment time, improved dynamic response, and enhanced steady-state characteristics.

V. Conclusions

This paper presents the design and performance analysis of metaheuristics search techniques (Genetic Algorithm and Artificial Bee Colony Algortihm) for optimal tuning of Proportional-Integral-Derivative (PID) controller for a HHO Dry Cell temperature control. It is aimed to minimize Integral Square Error (ISE), Integral Absolute Error (IAE), Integral Time Absolute Error (ITAE), and Mean Square Error (MSE), which are frequently preferred fitness functions in the literature, in determining optimum controller gains. The presented results also confirm the successful implementation of the proposed approach. Although two of the most commonly used models within the scope of optimization of control systems were analyzed in this study, it is important to use other optimization techniques to be compared in future studies.

References

Baltacıoğlu, M. K. (2019). A novel application of pulse width modulation technique on hydroxy gas production. International Journal of Hydrogen Energy, 44(20), 9726-9734.

Conker, Ç. (2019). A novel fuzzy logic based safe operation oriented control technique for driving HHO dry cell systems based on PWM duty cycle. International Journal of Hydrogen Energy, 44(20), 9718-9725.

Conker, C., & Baltacioglu, M. K. (2020). Fuzzy self-adaptive PID control technique for driving HHO dry cell systems. International Journal of Hydrogen Energy, 45(49), 26059-26069.

Furat, M., & Eker, I. (2014). Second-order integral sliding-mode control with experimental application. ISA transactions, 53(5), 1661-1669.

Synthesis of Titanium Dioxide (TiO_2) Based Photocatalyst and Investigation of Hydrogen Production Activity

[1]Beyza Yıldırım, [2]Muhammed İberia Aydın, [1,2]Aysel Kantürk Figen
[1]Yıldız Technical University, Faculty of Chemistry and Metallurgy, Department of Chemical Engineering, Istanbul, 34220, Türkiye
[2]Yıldız Technical University, Clean Energy Technologies Institute, Istanbul, 34220, Türkiye

E-mail: akanturk@yildiz.edu.tr

Abstract
Hydrogen production through water splitting provides a clean and sustainable energy carrier, with oxygen being the only by-product. This minimizes harmful emissions and greenhouse gas releases, reducing dependence on fossil fuels and enhancing energy sustainability. Titanium dioxide (TiO_2) is the most used photocatalyst in semiconductor-based photocatalytic hydrogen production due to its properties such as photocatalytic stability, non-toxicity, accessibility. This work investigates the function of a sacrificial agent of 25% MeOH in the production of hydrogen in a photoelectrochemical reactor utilizing hydrothermally synthesized TiO_2 and Degussa P25 photocatalyst. The potential of sacrificial agent to optimize the photocatalytic process and increase hydrogen production efficiency is examined. Hydrothermal synthesis offers advantages such as easy preparation, rapid reaction, low cost, good dispersibility, and high purity. Characterization methods have confirmed that the crystal structure resulting from hydrothermal synthesis contains only the anatase phase, which is known to increase the rate of hydrogen production and the hydrogen activity has been investigated using a solar simulator.

Keywords: water splitting, photocatalyst, titanium dioxide, hydrothermal, solar simulator

I. Introduction

Low-emission hydrogen production constitutes less than 1% of all production, and various technologies are being researched to produce green hydrogen from environmentally friendly sources (2023 Global Hydrogen Review). Recently, water electrolyzers utilizing electricity generated from renewable energy sources such as wind and solar power, are widely preferred for hydrogen production. However, due to efficiency losses in these electrolyzers, there is an increasing focus on research aimed at directly utilizing solar energy for hydrogen production (Tentu and Basu, 2017). The goal of the recently popular photocatalytic decomposition method for direct utilization of solar energy is to use semiconductor materials to transform photonic energy from the sun into chemical energy. The fundamental idea behind the photocatalytic water splitting process is that when photons with energy exceeding the band gap are absorbed by the photocatalyst, it creates electron-holes for oxidation and reduction reactions. The resulting electric charge enables the production of H_2 (Li et al., 2024). The photocatalyst must have its conduction and valence bands positioned correctly in order to facilitate the occurrence of redox reactions during the photocatalytic water splitting reaction. Since 1960, TiO_2 has been a material studied in various fields such as air and water purification, health, energy conversion, electrical appliances, due to its superior photocatalytic activity, non-toxicity, accessibility, environmental friendliness, biological and chemical stability, and resistance to photodegradation. (Singh and Dutta, 2018; Sari et al., 2024). However, despite its many advantages, the efficiency of photocatalytic water splitting with solar energy is significantly low for TiO_2 due to reasons such as its tendency to readily form water through hydrogen and oxygen recombination, and its band gap of 3.2 eV, which only activates the photocatalyst with UV light. (Liao et al., 2012). TiO_2 can be doped with various metals or non-metals to achieve important properties like more effectively adsorption, band energy gap adjustment, stability, and enhanced hydrogen production performance (Fajrina and Tahir, 2019).

In this study, the hydrogen production activity of TiO_2 powders synthesized by hydrothermal method (indexed as T2) and commercially Degussa P25 TiO_2 powder (indexed as T1) with deionized water (DW) and sacrificial agent of 25% methanol (MeOH) will be examined in the photoelectrochemical reactor.

II. Experimental Set-up and Procedure Synthesis of Pure TiO_2 Photocatalyst

Titanium (IV) N-butoxide (TBOT, Alfa Aesar 99%) was dissolved in ethanol (EtOH, Honeywell >99,8%) under magnetic stirring and deionized water (DW) was added (2:30:2). Figure 1 shows the schematic of catalyst preparation process. After mixing until a transparent colour was obtained, it was transferred to an 85 ml Teflon-coated stainless-steel autoclave and kept at 200°C for 24 hours. It was filtered by centrifuge and washed 3 times with DW and 1 time with EtOH. TiO_2 powder was obtained by drying in an oven at 90°C for 30 minutes.

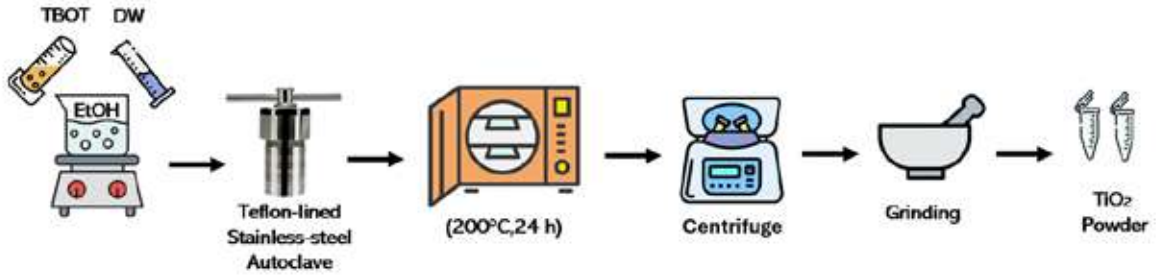


Fig. 1: Schematic of catalyst preparation process.

Examination of Hydrogen Production Activity: In the experimental procedure, hydrogen production was measured with a mass control system under the FYTRONIX-branded solar simulator (Fig. 2). Firstly, the solar simulator and hydrogen production experimental setup were established. For the photocatalytic reaction, 0.2 g of catalyst (T1 or T2 was taken and mixed in DW, and MeOH (25% by volume) sacrificial agent solution to ensure homogeneous distribution. During the experiment, the solar simulator was adjusted to the desired light intensity and spectral distribution (400-1000 nm). During the hydrogen production process, the amount of hydrogen was measured over time along with the accumulation of hydrogen gas through the mass controller system. The obtained data were evaluated about hydrogen production rate and efficiency and the results were reported. The same procedure steps were followed for the synthesized TiO_2 powders.

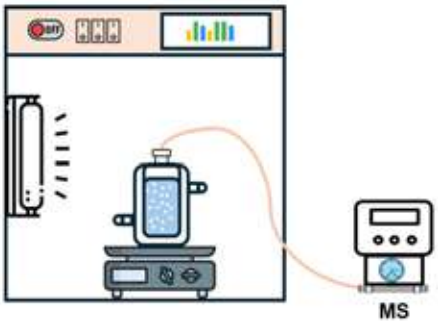


Figure 2: Hydrogen production activity test in solar simulator.

III. Analysis

XRD: The crystal structure of the catalysts were investigated using a Philips Panalytical X'Pert Pro XRD device with CuKα tube at 45 kV and 40 mA. The powdered samples were emptied into an aluminum sample holder, ensuring a flat surface, and prepared for analysis. XRD analyses were conducted with a step size of 0.01 2θ° and a scan time of 1.2 seconds.

Hydrogen Production Profile: The amount of H_2 production is determined based on the volumetric flow rate using a solar simulator from the Fytronix brand with wavelengths ranging from 400 to 1000 nm in the photoelectrochemical reactor prepared with sacrificial agent and a specific amount of catalyst. The obtained values are plotted as graphs of µmol H_2-hour and µmol H_2 $g_{cat}^{-1}h^{-1}$-hour.

IV. Results and discussions

In this study synthesized TiO_2 powder firstly analyzed XRD technic and compared with supplied TiO_2. CuKα radiation (λ = 1.5406 Å) was employed in the powder X-ray diffraction (PXRD) investigation, which was conducted using the PANalytical X'Pert Pro diffractometer. The XRD patterns of supplied TiO_2 and hydrothermally synthesized TiO_2 are compared in Figure 3. The Fig 3.b shows that XRD patterns of the supply TiO_2 exhibit prominent peaks at 25.5°, 38°, and 48° which signify the anatase phase, and rutile peaks at 27.5°, 36°, and 54.2°.The predicted XRD peaks were found when compared to the literature. The XRD patterns of TiO_2 synthesized using a hydrothermally method (200°C, 24 hours) is displayed in Figure 3.a. The distinctive peaks are found for the sample synthesized TiO_2 at 2θ angles 25.5°, 38°, 48° indicate anatase phase. The highly tetragonal system crystallized anatase structure without rutile phase appears in the XRD pattern. All the sharp peaks could be indexed as anatase TiO_2 with crystalline cell constants a=3.7760 c=9.4860 Å, which are basically in agreement with the reported values.

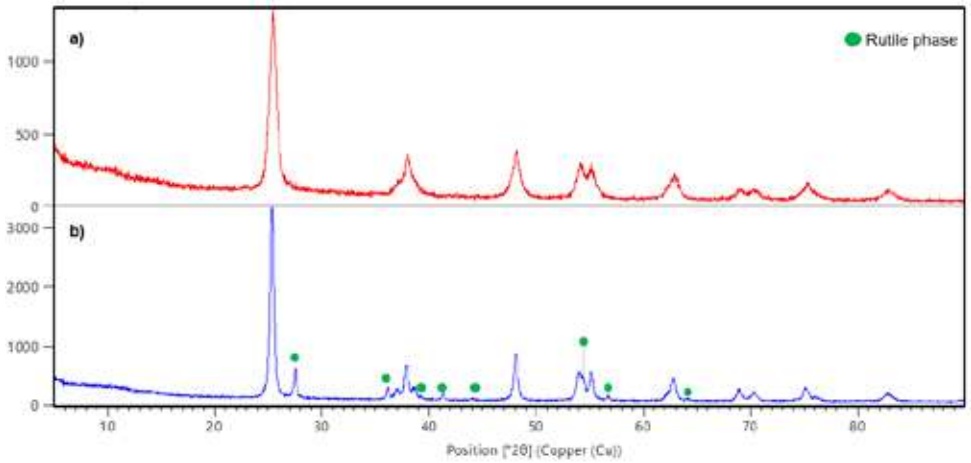


Figure 3: (a) XRD pattern of TiO_2 nanoparticles synthesized via hydrothermal method. (b) XRD diffractograms of Degussa P25's anatase and rutile phases.

Hydrogen production rates of photocatalysts synthesized via the hydrothermal method and supported TiO_2 were determined in a solar simulator, utilizing sacrificial agents and catalysts in a photoelectrochemical reactor. The presence of an alcohol-based sacrificial agent, such as methanol, facilitates the separation of electron-hole pairs due to properties such as the number of OH groups and polarity, aiming to enhance the efficiency of H_2 production by facilitating the migration of electrons to the photocatalyst surface for the reduction of water to hydrogen gas (Chen et al., 2020). Analysis revealed that while approximately 90 µmol of H_2 was produced at the 50th minute for the sample labeled DW-T1 (100% pure water + P25), MeOH-T1 (P25 catalyst in 25% methanol) yielded 200 µmol of H_2, emphasizing the significance of the sacrificial agent (Fig. 4). The same procedure was conducted for TiO_2 powders synthesized via the hydrothermal method (DW-T2, MeOH-T2), and it was observed that the presence of only the anatase phase within the structure increased the quantity of H_2 produced during the photoelectrochemical reaction.

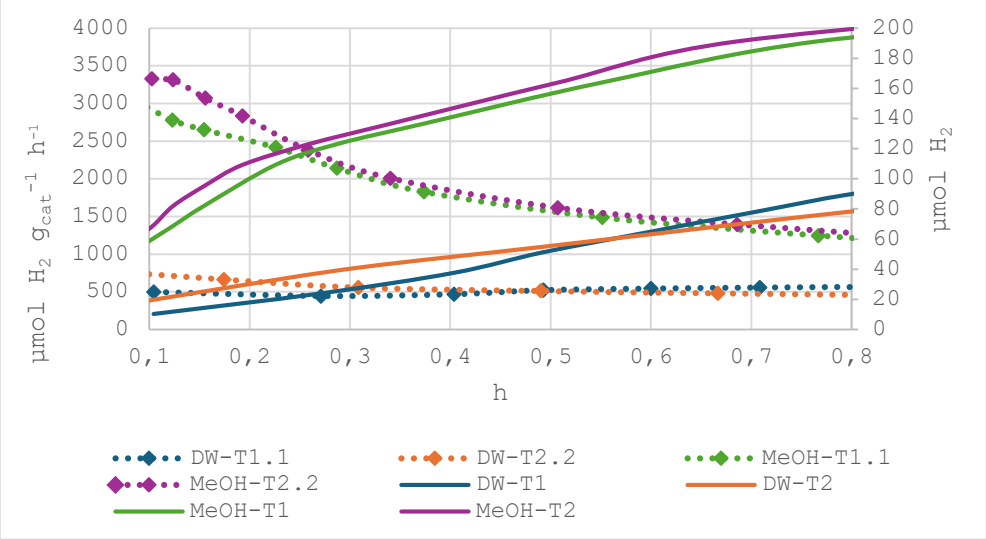


Fig. 4: Hydrogen production values in solar simulator.

V. Conclusions

Hydrogen emerges as a prominent energy carrier, with low-emission production achieved through alternative processes such as utilizing direct solar energy in photoelectrochemical reactions, a method known as water splitting. This study explores the hydrogen production potential of semiconductor TiO2 photocatalysts, known for their stability and resistance to degradation, in a solar simulator. Comparing hydrothermally synthesized TiO2 to commercial Degussa P25 samples reveals the performance of the pure anatase phase (DW-T1: 78 µmol H2, DW-T2: 92 µmol H2). Emphasizing the use of MeOH as a sacrificial electron donor significantly boosts hydrogen production, marking a 2.5-times increase compared to pure water.

Acknowledgements
The authors are gratefully acknowledged for financial support of solar simulator system (Yildiz Technical University Research Foundation, Project No: FBA-2023-5648).

References

International Energy Agency, Global Hydrogen Review 2023, (2023).

Tentu R. D., Basu S., Photocatalytic water splitting for hydrogen production, Current Opinion in Electrochemistry, 5(1), 56-62 (2017).

Li, T., Tsubaki, N., Jin, Z., S-scheme heterojunction in photocatalytic hydrogen production, Journal of Materials Science & Technology, 169, 82-104 (2024).

Singh, R., Dutta, S., A review on H_2 production through photocatalytic reactions using TiO_2/TiO_2-assisted catalysts, Fuel, 220, 607-620 (2018).

Sari, Y., Gareso, P. L., Armynah, B., Tahir, D., A review of TiO_2 photocatalyst for organic degradation and sustainable hydrogen energy production, International Journal of Hydrogen Energy, (2024).

Liao, C. H., Huang, C. W., Wu, J. C., Hydrogen production from semiconductor-based photocatalysis via water splitting, Catalysts, 2(4), 490-516 (2012).

Fajrina, N., Tahir, M., A critical review in strategies to improve photocatalytic water splitting towards hydrogen production, International Journal of Hydrogen Energy, 44(2), 540-577 (2019).

Chen, W. T., Dong, Y., Yadav, P., Aughterson, R. D., Sun-Waterhouse, D., & Waterhouse, G. I., Effect of alcohol sacrificial agent on the performance of Cu/TiO_2 photocatalysts for UV-driven hydrogen production, Applied Catalysis A: General, 602, 117703 (2020).

Impacts of Hydrogen Fuel Stations on Distribution Networks

[1*]Halil İbrahim TEKİN, [2]Bilal GÜMÜŞ
[1-2] Dicle University, Engineering Faculty, Department of Electrical and Electronics Engineering Department, Sur, Diyarbakır, 21280, Türkiye

* E-mail:halilibrahimtekin@outlook.com.tr

Abstract
This study investigated the integration of hydrogen refuelling stations (HRS) into modern energy networks, focusing on their impact on sustainable energy systems. The study, which analyses the HRS infrastructure, aims to investigate capacity problems in the network and provide solutions by emphasising adaptable configurations according to operational needs. In the study, the capacity issues were identified by evaluating the impact of HRS integration on urban medium voltage feeders through simulations. As a result of the study, a holistic approach to HRS integration is recommended, emphasising technological innovation, infrastructure improvements and a supportive policy framework for a sustainable hydrogen economy.

Keywords: Hydrogen refueling stations, hyrdogen, electrolyser, FCEV's, distribution networks

I. Introduction

I.I Hydrogen Refueling Stations

The basic components of a refuelling station are: hydrogen production unit, storage tanks, compression systems, dispensers and control systems. While these components form the core infrastructure of hydrogen refuelling stations, their arrangement and technological specifications may vary depending on factors such as geographical location, scale of operation and intended use. The general operation of a refuelling station powered by the grid is shown in Figure 1.

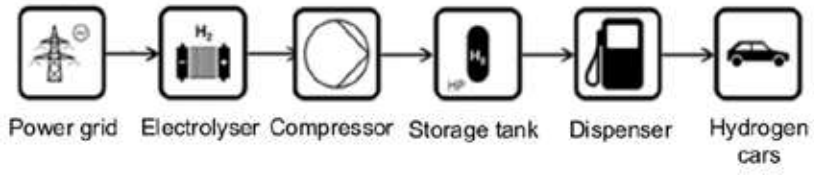


Fig. 1: Generic model of the hydrogen refueling station with power-to-gas production and grid connection (Sun & Harrison, 2021)

The hydrogen required at hydrogen refuelling stations can be sourced from external suppliers or produced on site. The general operation of an externally supplied hydrogen refuelling station is shown Figure 2. In both cases, energy needs to be identified and managed.

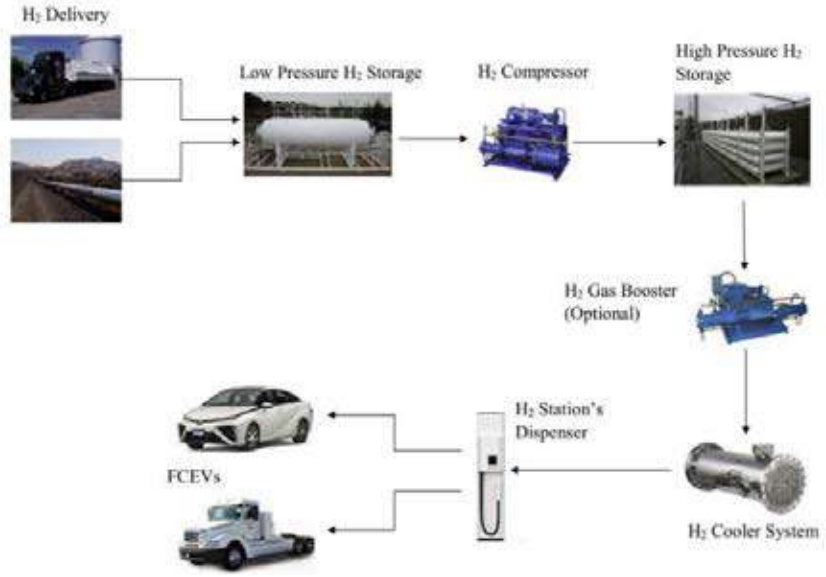


Fig. 2: Off-site H2 production-hydrogen gas refueling station's main components (Apostolou & Xydis, 2019)

It is important that the control of the hydrogen frefuelling station is in accordance with the requirements of the market operators and the power quality parameters. Figure 3 shows the general operation of an on-site hydrogen refuelling station and an example of a control mechanism.

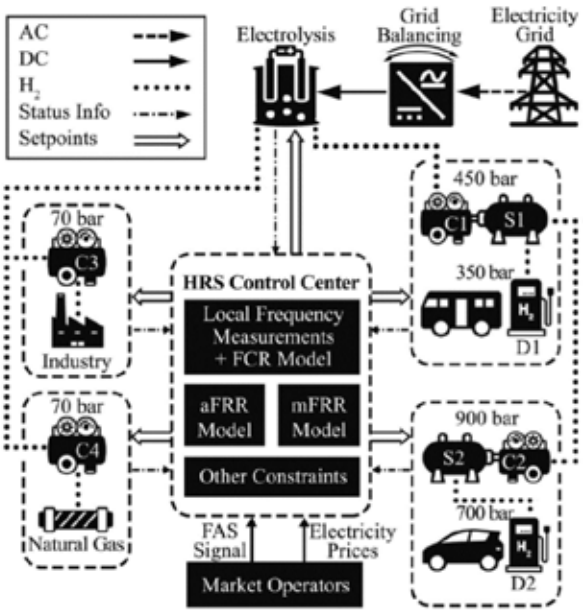


Fig. 3: On-site H2 production-hydrogen gas refueling station's main components (Dadkhah et al., 2022)

By the end of 2021, the number of FCEVs worldwide will reach 51,600, while there will be a total of 730 HRS. (*IEA*, 2022).

I.II Power Requirements of Hydrogen Refueling Stations

The power requirements of hydrogen refuelling stations depend on many factors, such as whether the hydrogen is produced at the station, the production capacity of the station, the stage at which the hydrogen is put into service, the types of vehicles served, the size of the area in which the station is located and the climatic conditions. In general, however, the electricity requirements of a hydrogen refuelling station are quite high. The factors that determine the power requirements of a hydrogen refuelling station are as follows:

Electrolysis process: Hydrogen is generally produced by electrolysis of water. In this process, an electric current splits water molecules into hydrogen and oxygen. The electrolysis process requires a large amount of electrical energy and is therefore the main source of electricity consumption at the refuelling station.

Compression and storage: The hydrogen gas produced is compressed into smaller volumes and then stored. The compression process is also powered by electricity, increasing the overall electricity demand.

Cooling systems: Cooling systems are required to manage the heat generated during the compression and storage of hydrogen. These systems also use electricity and increase the total electricity consumption.

Station internal requirements: As with any station, the service area has energy needs such as lighting, air conditioning, a service area, security systems and other operational needs.

Safety and security systems: Hydrogen refuelling stations have safety systems and electrical back-up systems for emergencies. These systems operate continuously and contribute to electricity consumption to ensure operational safety.

II. Materials-Method

In order to determine the impact of the hydrogen refuelling station on the power grid, a simulation model is created on the basis of realistic network data. The simulation model is used to analyse the impact of the hydrogen refuelling station on the network

II.I. Research Constraint on Learning the Demand Profile of Hydrogen Refueling Stations

Although the general capacity characteristics of electric vehicle charging stations are known, even at module level, this situation is quite uncertain for hydrogen refuelling stations. This is because, as mentioned above, many factors can change the characteristics of hydrogen refuelling stations. Due to the lack of research on net electricity consumption data, this study has used appropriate values from studies in the literature. (For this study (Minutillo et al., 2021))

II.II. Simulation Structure

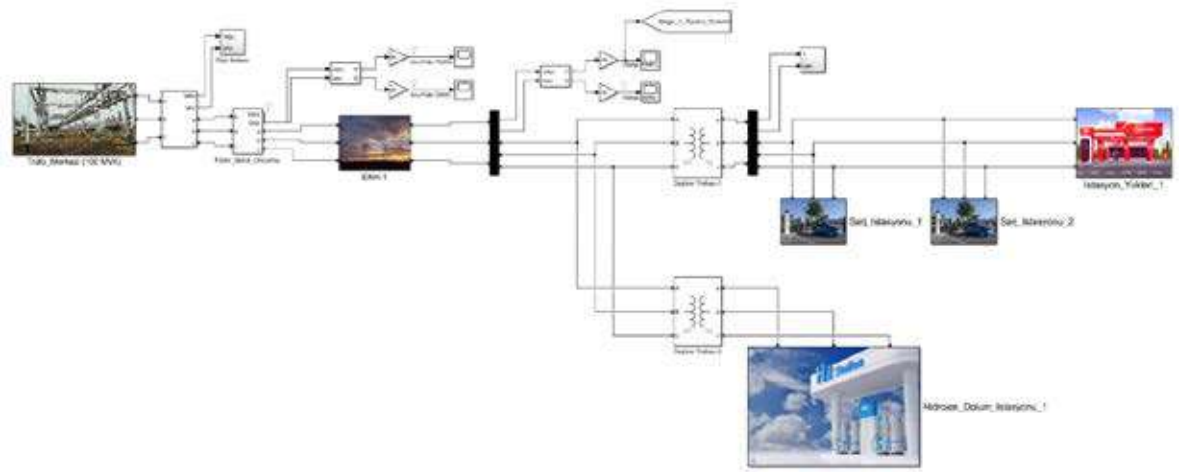


Fig. 4: Simulation Structure

A test environment was set up in the MATLAB Simulink software to evaluate the issue at hand. In this test environment, the time-domain effects of the electric vehicle charging stations and the hydrogen refuelling station installed on the transformer poles feeding the receiver groups connected to the urban medium-voltage feeder were studied.In the simulation topology, there is a feeder connected to a substation and two separate transformers connected to this feeder. One of these transformers (1,600 kVA) has two electric vehicle charging stations and a permanent load. The other transformer (1,250 kVA) has a hydrogen refuelling station as a load (Fig.4)

For each EV charging station, 65 kW rated power, 90% charging system efficiency, fixed controller gain values and different connection profiles that change within 24 hours were used. The internal load of the transformer to which the DC fast charging stations are connected has a different load profile that changes within 24 hours. For the hydrogen refuelling station, a load profile with a daily consumption of 3,150 kWh was defined. The characteristic of the 3 km long distribution feeder is "3AWG Swallow" and the simulation in question was run on a 24 hour basis.The simulation was run in two stages and the total power at the feeder head was recorded. In the first stage the hydrogen refuelling station is not connected to the existing grid, whereas in the second stage it is connected to the grid. In this way, it is possible to investigate the impact on the network capacity of the hydrogen refuelling station added later to the feeder with an electric vehicle charging station.

IV. Results and discussions

The simulation showed that the EV charging stations in a network could reach their maximum capacity without becoming overloaded. However, an additional transformer was integrated to accommodate the hydrogen charging station, but its capacity was occasionally overloaded. The flow profile of the feeder connecting the two stations was disturbed by coincident peaks from both groups, triggering the primary protection system. This was caused by higher inrush currents at the hydrogen refuelling stations. Fuel cell vehicles can reduce charging times to 8 minutes, but the high-power consumption of hydrogen refuelling stations increases operational difficulties. To reduce sustainability and environmental impact, measures such as producing hydrogen from renewable sources and increasing energy efficiency should be implemented. The impact of hydrogen refuelling stations on distribution networks is a complex aspect of the energy transition and requires a comprehensive approach.

References

Apostolou, D., & Xydis, G. (2019). A literature review on hydrogen refuelling stations and infrastructure. Current status and future prospects. Renewable and Sustainable Energy Reviews, 113, 109292. https://doi.org/10.1016/j.rser.2019.109292

Berg, H. (2015). Batteries for Electric Vehicles: Materials and Electrochemistry (1st ed.). Cambridge University Press. https://doi.org/10.1017/CBO9781316090978

Chau, K. T. (Ed.). (2016). Energy Systems for Electric and Hybrid Vehicles. The Institution of Engineering and Technology.

Dadkhah, A., Bozalakov, D., De Kooning, J. D. M., & Vandevelde, L. (2022). Techno-Economic Analysis and Optimal Operation of a Hydrogen Refueling Station Providing Frequency Ancillary Services. IEEE Transactions on Industry Applications, 58(4), 5171–5183. https://doi.org/10.1109/TIA.2022.3167377

Genovese, M., & Fragiacomo, P. (2023). Hydrogen refueling station: Overview of the technological status and research enhancement. Journal of Energy Storage, 61, 106758. https://doi.org/10.1016/j.est.2023.106758

IEA (2022). Global Electric Vehicle Outlook 2022

Minutillo, M., Perna, A., Forcina, A., Di Micco, S., & Jannelli, E. (2021). Analyzing the levelized cost of hydrogen in refueling stations with on-site hydrogen production via water electrolysis in the Italian scenario. International Journal of Hydrogen Energy, 46(26), 13667–13677. https://doi.org/10.1016/j.ijhydene.2020.11.110

Sun, W., & Harrison, G. P. (2021). Active Load Management of Hydrogen Refuelling Stations for Increasing the Grid Integration of Renewable Generation. IEEE Access, 9, 101681–101694. https://doi.org/10.1109/ACCESS.2021.3098161

A Review of Performance, Combustion, and Emissions of Diesel Engines Fuelled with Hydrogen

*Mert Gülüm
Karadeniz Technical University, Engineering Faculty, Mechanical Engineering Department, Trabzon, 61080, Türkiye

* E-mail: gulum@ktu.edu.tr

Abstract
Presently, there is a scarcity of global petroleum resources, and the extensive utilization of diesel engines is closely linked with significant environmental pollution. This situation has prompted researchers to explore more environmentally friendly alternative fuels. In recent years, there has been a deepening focus on hydrogen as a viable alternative fuel. This paper conducts a comprehensive review of recent articles on the performance, combustion, and emission characteristics of diesel engines fuelled with hydrogen under different conditions.
Keywords: Internal combustion engines, diesel engines, performance, combustion, emissions, hydrogen

I. Introduction

Energy stands as a cornerstone for the sustainability and advancement of society. The increase in global energy demand, fueled by population growth, improving living standards, and expanding industrialization, is projected to double by 2050, as outlined by the International Energy Agency (EIA,2016). Currently, fossil fuels like petroleum, coal, and natural gas account for over 80% of the world's energy supply (Bahrami etal.,2019). However, alongside the depletion of fossil fuel resources, their extraction, processing, and combustion in the internal combustion engines have led to significant environmental problems (global warming, air pollution, acidic rains, and respiratory problems) (Hosseini etal.,2023). To eliminate these problems, alternative fuels have been explored by scientists for a long time.

Among various alternative fuels, hydrogen emerges as one of the most promising options to fulfill the energy demands of diesel engines. This study has reviewed the effects of hydrogen on the performance, combustion, and emissions of diesel engines under different operating conditions.

II. The use of hydrogen in diesel engines

In this section, a literature review on the use of hydrogen is given as follows: Koten investigated the effects of hydrogen addition on the performance and emissions of a diesel engine. The engine was operated at a constant speed of 1800 rpm with different loads (20%, 40%, 60%, 80%, and 100%). Hydrogen was fed by a hydrogen injector on the intake port at different amounts (0.20, 0.40, 0.60, and 0.80 lpm). The maximum brake thermal efficiency of 27.3% was achieved for 0.80 lpm hydrogen enrichment, compared to diesel fuel of 24.9% (Koten,2018).

Karagöz et al. investigated the effect of hydrogen enrichment on the performance, combustion, and emissions of a diesel engine. All tests were performed at the constant engine speed of 1100 rpm and full load condition. Three different hydrogen energy fractions (0%, 22%, and 53%) were used. CO emissions decreased by 67.2% and 69.2% for the 22% and 53% hydrogen enrichment, compared to diesel fuel, due to its higher diffusion coefficient (Karagöz etal.,2016).

Köse and Acaroğlu investigated the effects of different fuels on performance, combustion, and emissions of a diesel engine at full load between 1000 rpm and 4000 rpm. Biodiesel was produced from Cynara cardunculus seed oil. CO emissions (%) averagely decreased by 82.8%, 50.3%, 52.3%, 62%, and 64% for biodiesel, diesel fuel-hydrogen blend, biodiesel-diesel fuel-hydrogen blend, and biodiesel-hydrogen blend (Köse and Acaroğlu,2020).

Jamrozik et al. analyzed combustion stability, performance, and emission of a diesel engine fuelled by diesel fuel and diesel fuel-hydrogen blends (including various hydrogen contents 2%-30% by volume) at a constant engine speed of 1500 rpm and full load. The diesel fuel-hydrogen blends were named DH02, DH08, DH14, DH25, and DH30 to show the hydrogen volume content. The assessment of the combustion stability was performed by determining the coefficient of variation in the indicated mean effective pressure (COV_{IMEP}) and the maximum pressure (COV_{Pmax}). Adding hydrogen up to 25% did not cause significant changes in the COV_{IMEP} (between 1.49% and 1.74%) and COV_{Pmax} (between 0.79% and 1.82%). After 25% hydrogen content, the largest increases in COV_{IMEP} (3.89%) and COV_{Pmax} (2.43%) were obtained for DH30 (Jamrozik etal.,2020).

III. Conclusions

This study presents a comprehensive review of recent studies focusing on the effects of the utilization of hydrogen on the performance, combustion, and emissions of diesel engines under different operating conditions. Compared to pure diesel fuel operation, adding hydrogen generally improves peak pressure, peak heat release rate, brake power and brake thermal efficiency, while decreases ignition delay and some emissions (CO, smoke, and HC). The

main disadvantages of hydrogen include issues with knocking and backfiring, as well as higher NO_x emissions.

References

Bahrami A., Teimourian A., Okoye C.O., Shiri H., Technical and economic analysis of wind energy potential in Uzbekistan, Journal of Cleaner Production, 223, 801-814, (2019).

EIA U.S., International energy outlook 2016 with projections to 2040. Office of energy analysis US department of energy: Washington, DC, USA, (2016).

Hosseini S.H., Tsolakis A., Alagumalai A., Mahian O., Lam S.S., Pan J., Peng W., Tabatabaei M., Aghbashlo M., Use of hydrogen in dual-fuel diesel engines, Progress in Energy and Combustion Science, 98, 101100, (2023).

Jamrozik A., Grab-Rogaliński K., Tutak W., Hydrogen effects on combustion stability, performance and emission of diesel engine, International Journal of Hydrogen Energy, 45(38), 19936-19947, (2020).

Karagöz Y., Güler I., Sandalcı T., Yüksek L., Dalkılıç A.S., Effect of hydrogen enrichment on combustion characteristics, emissions and performance of a diesel engine, International Journal of Hydrogen Energy, 41(1), 656-665, (2016).

Koten H., Hydrogen effects on the diesel engine performance and emissions, International Journal of Hydrogen Energy, 43(22), 10511-10519, (2018).

Köse H., Acaroğlu M., The effect of hydrogen addition to Cynara biodiesel on engine performance and emissions in diesel engine, Energy Sources, Part A: Recovery, Utilization, and Environmental Effects, 1-20, (2020).

Analyzing Energy Efficiency in Hydrogen Energy from Agriculture: A Bibliometric Approach

[1]Masud Kabir and [1*]Sami Ekici
[1] Firat University, Faculty of Technology, Department of Energy Systems Engineering, Elazığ, 23200, Türkiye

* E-mail: sekici@firat.edu.tr

Abstract

An extensive bibliometric analysis is presented in this study with the goal of clarifying the patterns, relationships, and new directions in the realm of energy efficiency within the context of producing hydrogen energy from agricultural resources. This interdisciplinary field study provides insights into the evolution of scholarly discourse, patterns of collaboration, and theme shifts through methodical data collecting and analysis. There are numerous important steps in the methodology used in this study. To find relevant publications, a first step systematic search was performed using predetermined search terms in the Web of Science database. Bibliographic information, including the year of publication, authors, titles of the publications, keywords, and the number of citations, were then extracted for analysis. Keyword analysis for determining the recurring topics and research goals in the field, and network analysis to find collaborations between authors and institutions and get insights into knowledge distribution and interdisciplinary collaboration, were conducted, respectively. By providing an interdisciplinary, thorough and organized investigation of energy efficiency in hydrogen energy production from agricultural sources, this study offers fresh perspectives on growing research fields, citation trends, and publication trends. Researchers, practitioners, and other stakeholders will potentially benefit greatly from the practical recommendations this study offers by combining quantitative data analysis and qualitative interpretation to advance sustainable energy solutions.

Keywords: Energy Efficiency, Hydrogen Energy, Agriculture, Bibliometric Analysis, Sustainability

I. Introduction

In the world of today, growing concerns over climate change, environmental degradation, and energy security have shaped the global energy conversation in recent decades. As countries endeavor to shift towards more environmentally friendly energy sources, hydrogen has surfaced as a potentially viable substitute for conventional fossil fuels (Joseph 2023). Hydrogen presents a strong answer to the urgent problems of decarbonization and the energy transition because of its high energy density, zero-emission combustion, and adaptability to a wide range of industries (Filippov and Yaroslavtsev 2021).

Simultaneously, the agricultural industry has experienced notable changes due to breakthroughs in technology, shifting consumer preferences, and growing environmental restrictions (Vourdoubas and Dubois 2016). Previously linked mainly to the production of food, agriculture is today acknowledged as a diverse industry with substantial potential to support sustainable development objectives (Ghosh 2023; Jarzebski et al. 2023). Agriculture influences the future of energy and environmental sustainability in a variety of ways, from bioenergy generation to carbon sequestration (Brennan and Owende 2010; Liu, Zhang, and Bae 2017; Stamenkovic et al. 2020).

Hydrogen energy from agricultural sources is an idea that sits at the junction of these two realms. The creation of hydrogen from agricultural waste, leftovers, and biomass presents a special chance to combine the production of renewable energy with environmentally friendly farming methods. Through techniques like biomass gasification, pyrolysis, or electrolysis, we may effectively employ agricultural resources to meet energy demands while lowering greenhouse gas emissions and environmental footprints (Das and Peu 2022; Sharma et al. 2023). This method turns organic materials into hydrogen fuel.

One cannot emphasize how important it is to research energy efficiency in hydrogen energy from agriculture. The usable energy output to energy input ratio, or energy efficiency, is a crucial parameter for evaluating the sustainability and feasibility of energy production systems. Optimizing energy efficiency is crucial for hydrogen energy from agriculture in order to increase resource usage, reduce energy losses, and improve overall system performance. The production of hydrogen from agricultural sources requires careful consideration of a wide range of technological, economic, and policy factors in order to maximize energy efficiency. Many tactics can be used to improve energy efficiency throughout the production process, ranging from sophisticated conversion technology to integrated supply networks and market incentives. But reaching maximum energy efficiency necessitates a comprehensive strategy that takes the whole value chain, from biomass sourcing and preprocessing to hydrogen production, storage, and utilization.

This article can bridge a research gap. There have been no prior investigations on the connection between agricultural hydrogen energy and energy efficiency, according to the literature review. The current study has been centered on investigating potential ways to improve the connection between these two domains. Through a thorough examination of the body of literature, we want to clarify current research directions, recognize significant figures in the field, and highlight frontiers for innovation and expansion. Our goal is to provide insights that can guide future research endeavors, policy decisions, and technology improvements in the field through a systematic examination of peer-reviewed articles, conference proceedings, and other scholarly publications.

II. Methodology

The study's methodology comprised a methodical approach to doing an extensive bibliometric analysis at the nexus of energy efficiency and hydrogen energy produced from agriculture. To collect, examine, and evaluate the pertinent literature, the following procedures were followed: Initially, the main instrument for bibliometric analysis was chosen to be the Bibiliometrix library, specifically the "Biblioshiny" program developed by (Aria and Cuccurullo 2017) that can be accessed using R and RStudio. This tool, which is well-known for its strong capabilities in the analysis of bibliographic data, was shown to be appropriate for investigating citation networks, co-authorship analysis, and keyword mapping. We then searched the Web of Science database, which is well-known for its broad coverage of academic articles in a variety of fields, for relevant material. A search query was created using the terms "energy efficiency" AND "hydrogen energy from agriculture." To ensure relevance to current research trends, the search parameters were limited to publications indexed between January 1, 2000, and December 31, 2023. After the search, 958 bibliographic files that included references and full-text articles were obtained from the Web of Science database. To enable additional analysis, these files were then combined into a single BibTeX (.bib) file.

The Bibiliometrix library in RStudio was then used to do the bibliometric study. Investigating publishing trends, citation patterns, co-authorship networks, and keyword distributions required importing the bibliographic data from the .bib file into RStudio and running a number of analyses. The bibliographic data was then organized and processed in RStudio to produce metrics and visualizations for examination. To assess the state of the field's research generally, descriptive data were calculated, such as the number of publications over time and the number of citations. Prominent authors and research collaborations were identified and co-authorship networks were visualized using network analysis techniques.

III. Results and discussions

A thorough summary of the bibiliometric dataset is presented in Table 1. This dataset represents a varied and multifaceted approach to investigating the complexity of hydrogen energy production and consumption, where contributions extends from 356 different sources, including books, journals, and other scientific publications. With 958 papers total—from reviews to research articles—this body of knowledge shows a consistent upward trend, averaging 5.95% annually, thus reflecting the substantia interest growth and financial support for hydrogen as a sustainable energy source. A comparatively young average age of the documents was observed to be 5.35 years, indicating a concentration on modern and cutting-edge research developments in the field. With an average citation rate of 37.99 per document, this body of research has a considerable impact on the academic world, as demonstrated by its high citation rate. Moreover, the vast network of references—49,877 in total—reflects the depth and breadth of the dataset's citation and literature review networks. There are 3593 unique authors in this collaborative project, and there is a significant emphasis on collaboration as seen by the 5.85 co-authors on average per document and the large percentage (36.53%) of international co-authorships. The dataset provides insights into the wide range of themes and focal areas investigated by researchers in the field through the analysis of keywords and terms supplied by the authors.

Table 1 Bibliometric Dataset Summary

DESCRIPTION	RESULTS	DESCRIPTION	RESULTS
Main Information about Data		**Document Types**	
Timespan	2000:2024	article	790
Sources (Journals, Books, etc.)	356	article; book chapter	4
Documents	958	article; early access	8
Annual Growth Rate (%)	5.95	article; proceedings paper	40
Document Average Age	5.35	proceedings paper	25
Average citations per doc	37.99	review	89
References	49877	review; early access	2
Document Contents		**Authors Collaboration**	
Keywords Plus (ID)	3108	Single-authored docs	7
Author's Keywords (DE)	3112	Co-Authors per Doc	5.85
AUTHORS		International co-authorships (%)	36.53
Authors	3593	Authors of single-authored docs	6

The field of hydrogen production research is a multidisciplinary one, encompassing chemistry, materials science, engineering, and environmental sciences. This approach reflects the growing importance of hydrogen as a clean and sustainable energy carrier, driving research efforts across various fields to develop efficient and environmentally friendly hydrogen production technologies. The International Journal of Hydrogen Energy is a primary source for research in hydrogen energy, covering topics such as production, storage, and utilization. Other journals, such as Energy Conversion and Management, Chemical Engineering Journal, Journal of Cleaner Production, and Journal of Environmental Chemical Engineering, focus on clean and environmentally friendly approaches to hydrogen production. The study further examined that the publication dynamics ranges across six key sources (as in **Fig**. **1**): International Journal of Hydrogen Energy, Bioresource Technology, Energy Conversion and Management, Chemical Engineering Journal, Energies, and Energy. The results show consistent increases in publication output, with a notable acceleration from 2016 onwards. The International Journal of Hydrogen Energy shows a consistent increase

in publication output, possibly driven by advancements in the field and increasing attention to energy efficiency in the eyes of sustainable energy solutions. Bioresource Technology exhibits steady growth in publication output, indicating the ongoing significance of research related to bioenergy, biotechnology, and waste management. Energy Conversion and Management shows a relatively stable publication output until around 2018, possibly due to a surge in research focusing on energy conversion technologies and management strategies. The Chemical Engineering Journal shows a gradual increase in publication, particularly in areas intersecting with energy and sustainability.

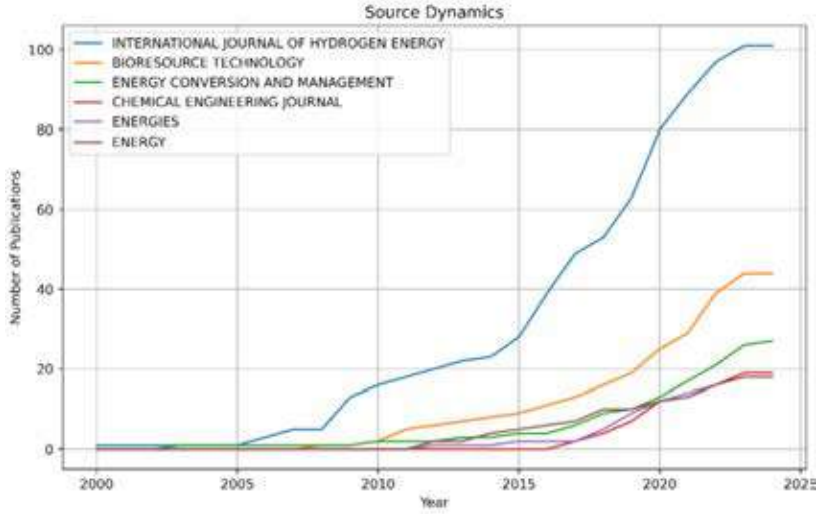


Fig. 1: Source Dynamics

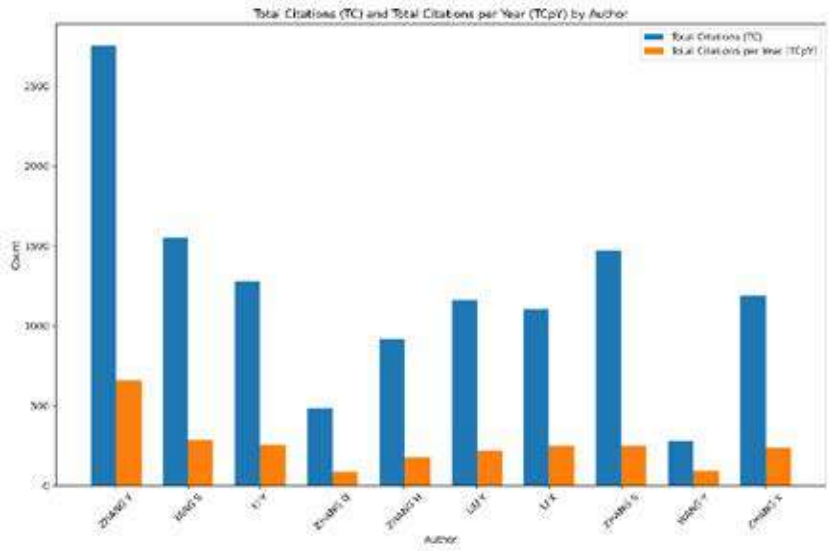


Fig. 2: Most relevant authors

The study also examines the citation analysis of highly cited papers and influential authors, institutions, and journals in the field of hydrogen energy research. The study of author production over time (see

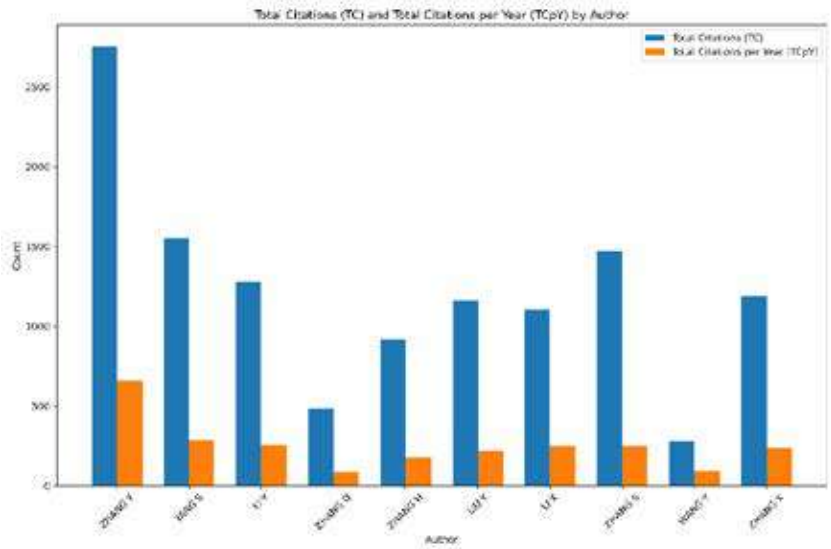


Fig. *2*) provides insights into the influence and output of scholars in the aspect of energy efficiency in hydrogen energy research. The data shows patterns and trends, with Li X showing a notable increase in total citations between 2015 and 2022. Other authors, such as Liu Y and Zhang Q, have had a steady increase in total citations. The most cited papers discuss the role of microalgae-based biofuels in sustainable energy strategies, electrochemical reduction processes, and sustainable nitrogen fixation technologies. The collection of articles focuses on hydrogen energy and energy efficiency, with 40% addressing hydrogen energy issues and 35% examining technologies and processes. Others weren't found to suit the discourse of energy efficiency in hydrogen energy from agriculture research due to most likely search terminology limits and datasource limits.

The study of coutries impact results show that China leads the field in energy efficiency in hydrogen energy from agricultural research, with an average article citation rate of 32.60. The USA has a higher citation rate, while Ireland has a high average article citation rate of 637.80. Canada has a significant research output and impact, while India has a lower impact per article. Ireland and Belgium has the highest average article citation rates, indicating the largest share of research impact in the subject, while Italy, the Netherlands, and Australia have high citation rates. Iran, Korea, and Malaysia have moderate citations, while Egypt and Greece show potential for major contributions in the future of energy efficiency in hydrogen energy research from agriculture.

The subject research from great scientific sources (universities) is significant, with South China Agricultural University, Henan Agricultural University, University of Tehran, Pennsylvania State University, and Indian Institute of Technology leading global contributions significantly. These institutions are actively involved in sustainable energy solutions, collaborating with stakeholders, and fostering cross-disciplinary research. Collaborations and knowledge-sharing networks among these institutions perhaps can promote innovation and sustainable energy technologies. Moreover, the data shows a significant increase in research output from various agricultural institutions, including China Agricultural University, Huazhong Agricultural University, Henan Agricultural University, South China Agricultural University, South China University of Technology, and University of Tehran, respectively. These institutions have shown a focus on research innovation and excellence, contributing to the scholarly literature and tackling global issues, including hydrogen energy, efficiency, and sustainability. However, ongoing funding is needed reiteratively to maintain this momentum and propel hydrogen energy efficiency further.

In addition, the research on the subject was observed to be multidisciplinary, focusing on various aspects such as hydrogen production, biomass, photocatalysis, biohydrogen, anaerobic digestion, gasification, methane, biogas, and fermentation. The focus is on reducing carbon emissions, promoting a low-carbon economy, and integrating renewable energy sources into energy systems. The field also explores biogas production, optimizing anaerobic digestion processes, and optimizing fermentation processes. The research aims to reduce environmental impact, increase productivity, and enhance efficiency. The multidisciplinary nature of these fields underscores the importance of innovation and collaboration across various scientific disciplines in addressing global energy concerns.

The global network of cooperation in hydrogen energy from agricultural sources is diverse, involving European, Chinese, USA, Canada, Australia, India, Saudi Arabia, and potential developing countries like Nigeria, Egypt, Turkiye and South Africa. This collaboration demonstrates both national and scientific efforts to develop sustainable energy alternatives and promotes global synergy. It aims to address energy security, climate change, and agricultural sustainability, promoting open communication, knowledge sharing, and resource exchange. From the keyword analyses, the dataset highlights the growing interest in using agricultural resources for hydrogen production, particularly "biomass".

Researchers are exploring various biomass sources, including crop residues, organic waste, and energy crops, but further research is needed to improve feedstock selection, preprocessing methods, and conversion pathways. Techno-economic analyses are needed to determine the viability and scalability of biomass-based hydrogen production in agricultural settings. Photocatalysis is also being explored as a viable method for producing hydrogen from agricultural materials. Nanoparticles play a crucial role in various aspects of agricultural hydrogen production,

such as catalysis, photocatalysis, and biomass conversion. Combining anaerobic digestion and fermentation can improve process efficiency and hydrogen yield.

V. Conclusions

This research paper analyzes energy efficiency in hydrogen energy from agricultural sources using a bibliometric approach. It highlights the growing interest in sustainable energy solutions and identifies research gaps in bioreactor optimization, hydrogen storage technologies, and life cycle assessments. The study suggests future research directions and innovation to enhance energy efficiency in agricultural hydrogen production by optimizing bioreactor systems, addressing storage and distribution issues, and using comprehensive life cycle evaluations to evaluate the environmental sustainability of hydrogen production. Using agricultural waste streams can also be a sustainable way to produce hydrogen, promoting a more circular economy and providing additional income for farmers and rural communities.

References

Aria, Massimo, and Corrado Cuccurullo. 2017. "Bibliometrix: An R-Tool for Comprehensive Science Mapping Analysis." *Journal of Informetrics* 11(4): 959–75.

Brennan, Liam, and Philip Owende. 2010. "Biofuels from Microalgae-A Review of Technologies for Production, Processing, and Extractions of Biofuels and Co-Products." *Renewable and Sustainable Energy Reviews* 14(2): 557–77.

Das, Arnob, and Susmita Datta Peu. 2022. "A Comprehensive Review on Recent Advancements in Thermochemical Processes for Clean Hydrogen Production to Decarbonize the Energy Sector." *Sustainability* 14(18).

Filippov, Sergey P., and Andrey B. Yaroslavtsev. 2021. "Hydrogen Energy: Development Prospects and Materials." *Russian Chemical Reviews* 90(6): 627–43. https://iopscience.iop.org/article/10.1070/RCR5014 (April 9, 2024).

Ghosh, Aritra. 2023. "Nexus between Agriculture and Photovoltaics (Agrivoltaics, Agriphotovoltaics) for Sustainable Development Goal: A Review." *Solar Energy* 266: 112146.

Jarzebski, Marcin Pawel et al. 2023. "Developing Biodiversity-Based Solutions for Sustainable Food Systems through Transdisciplinary Sustainable Development Goals Labs (SDG-Labs)." *Frontiers in Sustainable Food Systems* 7: 1144506.

Joseph, Jo. 2023. "Green Energy Transmission Chain of Climate Management and Smart Transition." *SSRN Electronic Journal*. https://papers.ssrn.com/abstract=4417370 (November 3, 2023).

Liu, Xuyi, Shun Zhang, and Junghan Bae. 2017. "The Nexus of Renewable Energy-Agriculture-Environment in BRICS." *Applied Energy* 204: 489–96.

Sharma, Mukesh et al. 2023. "Premier, Progress and Prospects in Renewable Hydrogen Generation: A Review." *Fermentation-basel* 9(6).

Stamenkovic, Olivera S et al. 2020. "Production of Biofuels from Sorghum." *Renewable and Sustainable Energy Reviews* 124.

Vourdoubas, John, and Olivier Dubois. 2016. "Energy and Agri-Food Systems: Production and Consumption." In *Mediterra 2016. Zero Waste in the Mediterranean. Natural Resources, Food and Knowledge/International Centre for Advanced Mediterranean Agronomic Studies (CIHEAM) and Food and Agriculture Organization of the United Nations (FAO)–Paris: Presses de Sciences*, , 155.

USE OF FIELD WOUND SYNCHRONOUS MOTOR IN FUEL CELL ELECTRIC VEHICLES

[1*]Kıvanç Doğan, [1]Ahmet Orhan, [1]Abuzer Çalışkan
[1] Fırat University, Faculty of Engineering, Electrical and Electronics Engineering, Elazığ, 23100, Türkiye

* E-mail:kivanc.dogan@firat.edu.tr

Abstract
This study examines the potential advantages of wound-rotor synchronous motors (WRSMs), which can serve as an alternative to asynchronous motors and permanent magnet synchronous motors (PMSMs) commonly used in fuel cell electric vehicles (FCEVs), and investigates the control method that could provide these motors with superior performance. WRSMs offer significant potential for the electric vehicle industry due to their capabilities in power factor control, high speed, high torque, compact power electronics circuits, low maintenance requirements with brushless excitation systems, and superior control characteristics. This research highlights the potential of WRSMs to extend the range of electric vehicles and reduce the reliance on PMSMs. WRSMs can deliver superior performance even at high speeds through flux adjustment with field current. These features indicate that the use of WRSMs could significantly contribute to the development of zero-emission, long-range electric vehicles. Furthermore, it can be emphasized that WRSMs represent a strategic technology for systems powered by hydrogen obtained from renewable energy sources and could be a critical step towards reducing carbon emissions in the global transportation sector. In conclusion, this study demonstrates that WRSMs have the potential to create a significant transformation in the electric vehicle industry and play a central role in developing environmentally friendly transportation solutions.

Keywords: Fuel cell, Field wound synchronous motor, Electric vehicle

I. Introduction

In recent years, the electric vehicle sector has shown rapid development. The demand for electric vehicles at various power levels has necessitated the exploration of alternative motor types. Permanent magnet synchronous motors (PMSMs), generally preferred as traction motors, have driven the electric vehicle market to seek alternatives due to price fluctuations caused by China's monopoly. Additionally, the toxic acid produced during the extraction of rare earth elements has led the World Health Organization to impose restrictions on these products, which are considered carcinogenic. For these reasons, many countries around the world, particularly the European Union, have begun to support the development of motors with high torque and efficiency that can be used in electric vehicles instead of permanent magnet motors subject to price fluctuations and health restrictions under China's monopoly.

WRSMs offer numerous advantages over PMSMs and asynchronous motors, which are commonly preferred in electric vehicles (Cao et al. 2021; Liu et al. 2021; Ramya et al. 2022). These advantages can be summarized as follows:

Synchronous motor drive systems have a higher torque/inertia ratio, lower noise, and robust motor control algorithms compared to asynchronous motor drive systems. This is because the rotor diameter of synchronous motors is smaller than that of equivalent power asynchronous motors.
Synchronous motors are practically essential for high power and high-speed applications.
The lower efficiency and power factor of asynchronous motors compared to synchronous motors limit their use at high power and speed levels. This is because a low power factor means higher volume and lower-cost power electronics circuits.
The ability to control the power factor with rotor excitation current in synchronous motors makes them unrivaled in applications requiring high torque.
Considering the cost of inverters, synchronous motors can form a more attractive drive system compared to asynchronous and PMSMs.
When considering the load on the motor and the power electronics supplying the motor, it is important to achieve torque with the lowest stator current. This means that there is only an exchange of active power between the motor and the power circuits supplying the motor.
Operating close to unity power factor reduces current, simplifies transmission, decreases copper losses, and reduces inverter size and cost. Therefore, WRSMs offer higher degrees of freedom in both design and control compared to other motor types used in electric vehicles (Park et al. 2019).

The motivation for the proposed study on fuel cell electric vehicles (FCEVs) is the numerous significant features of WRSMs, including:

- High torque and high efficiency
- Power factor control capability via rotor current
- High torque/inertia ratio

- Low noise and robust motor control algorithms
- Capability to operate at high power and high speeds
- Lower motor cost compared to permanent magnet motors
- More attractive drive system compared to asynchronous motors and PMSMs when considering inverter cost
- Control method that allows only active power exchange between the motor and motor power circuits
- Low current, low copper loss, low cost, and low volume through unity power factor control
- Higher degree of freedom provided by magnetic flux control via field current

This study highlights the potential of wound-rotor synchronous motors (WRSMs) as an innovative motor technology for fuel cell electric vehicles (FCEVs). The cost-effectiveness, superior control capability, and stable performance of WRSMs even at high speeds have the potential to create a significant transformation in the electric vehicle industry. Additionally, this study emphasizes that WRSM technology could accelerate the development of systems powered by hydrogen derived from renewable energy sources and is expected to be a critical step towards significantly reducing carbon emissions in the global transportation sector.

II. System Description

The block diagram of the fuel cell system with stator flux field-oriented control structure is given in Figure 1.

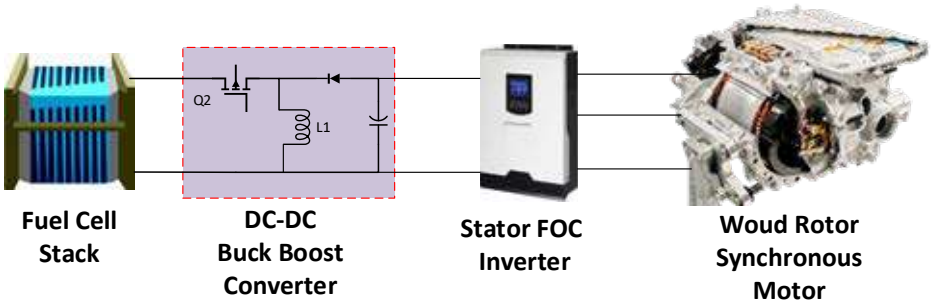


Fig. 1: Block Diagram of the Proposed System

In the proposed system, the WRSM is powered by a fuel cell. A DC-DC Buck Boost converter is utilized at the output of the fuel cell. This converter is employed to maintain the stability of the fuel cell output and to control the torque required by the load. The inverter is powered from the output of the converter.

The stator flux-oriented control method is used for controlling the synchronous motor. In this flux orientation method, the torque and flux components of the stator current are decoupled. This decoupling positively affects the dynamic response of the system. The reactive component of the stator current and power factor control are achieved most simply through stator flux orientation. Under unity power factor conditions, the stator voltage and current are in phase, and the stator flux vector is perpendicular to the current vector. Stator flux-oriented control, which meets unity power factor conditions, is the most critical control method for reducing the inverter size and cost. The FOC (Field-Oriented Control) method is a control strategy for AC motors based on the decoupling and control of the torque and flux components of the stator current. The decoupling of the torque and flux components of the stator current and the control of torque using only the torque component positively influence the dynamic response of the control system. Among the synchronous motor FOC methods, Stator Flux-Oriented Control is the most important control method in terms of inverter size and cost since it also meets the unity power factor conditions. FOC also improves the dynamic response of torque and speed (Amin, F., Sulaiman, E., & Soomro, 2019). The phasor diagram related to stator flux orientation is shown in Figure 2.

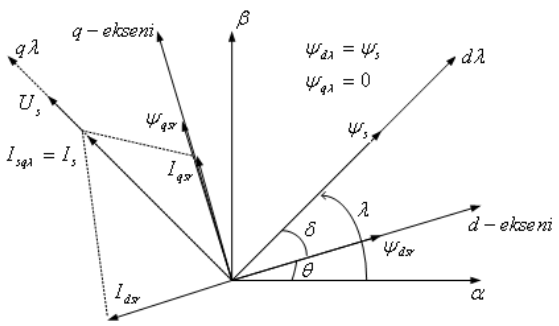


Fig.2: Phasor diagram for stator flux field orientation

The proposed system is simulated in Matlab/Simulink environment and the simulation results are analyzed in terms of the use of WRSM in fuel cell electric vehicles.

III. Result and Discussion

Figure 3 shows the Matlab/Simulink model of the synchronous motor for the case of feeding from a six-step current source inverter and the stator flux field orientation for power factor control.

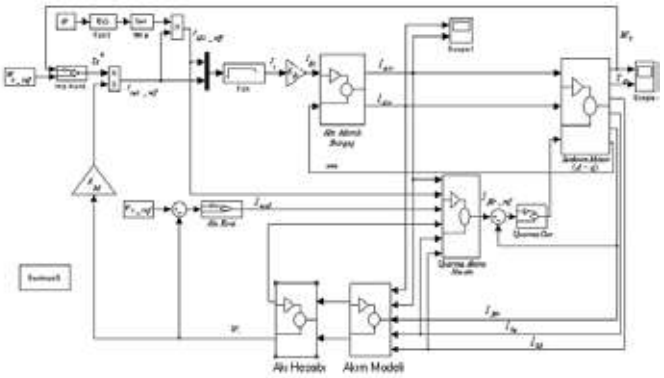


Fig.3: Matlab / Simulink Model for Stator Flux Field Orientation of Inverter-Fed Synchronous Motor

In the aforementioned model, the actual speed is compared with the reference speed, and the resulting speed error is processed by a PI (Proportional-Integral Controller). The output of this PI controller provides the reference torque. The flux component of the stator current is obtained as a reference from the external input (the phase difference between U_s and I_s) and the multiplication of the torque component of the stator current. When the motor is loaded with a constant load torque, the simulation program is run, and the variation of speed, torque, and stator q-axis current over time is shown in Figure 4.

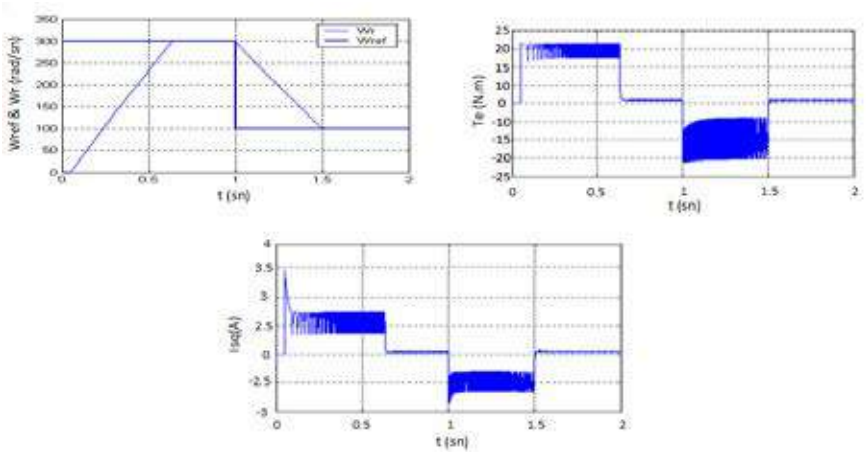


Fig.4: Variation of Speed, Torque and Stator Q-axis Current of Synchronous Motor Fed by Stator Flux Field-Oriented Inverter

IV. Conclusions

In this study, the potential positive impacts of using wound-rotor synchronous motors (WRSM) in fuel cell electric vehicles (FCEVs) were examined through the implementation of the stator flux-oriented control method. A model related to the stator flux-oriented control system was created using the Simulink simulation program. This model was run for approximately 2 seconds, and the variations in speed, torque, stator current, voltage, and the phase difference between these variables were analyzed.

The stator flux-oriented control method has achieved results at unity power factor. The stator current orientation, which ensures the highest torque per ampere of stator current, offers a new perspective for synchronous motor drives. Design improvements in WRSM can introduce a new outlook for the automotive industry in terms of cost and energy efficiency when WRSM is used in fuel cell electric vehicles.

References

Amin, F., Sulaiman, E., & Soomro, H. A. 2019. “Field Oriented Control Principles for Synchronous Motor.” *International Journal*

of Mechanical Engineering and Robotics Research 8(2):284–88.
Cao, Zhi, Amin Mahmoudi, Solmaz Kahourzade, and Wen L. Soong. 2021. "An Overview of Electric Motors for Electric Vehicles." Pp. 1–6 in *2021 31st Australasian Universities Power Engineering Conference (AUPEC)*. IEEE.
Chae, Woong-Chan, Mi-Jung Kim, Ki-Doek Lee, Jae-Jun Lee, Jung-Ho Han, Tae-Chul Jung, and Ju Lee. 2012. "High Speed Performance Improvement of the WRSM and Its Comparison with the IPMSM." *The Transactions of The Korean Institute of Electrical Engineers* 61(11):1595–1600. doi: 10.5370/KIEE.2012.61.11.1595.
Ding, Ning, K. Prasad, and T. T. Lie. 2017. "The Electric Vehicle: A Review." *International Journal of Electric and Hybrid Vehicles* 9(1):49. doi: 10.1504/IJEHV.2017.082816.
Hwang, Daeyeon, and Bon-Gwan Gu. 2020. "Field Current Control Strategy for Wound-Rotor Synchronous Motors Considering Coupled Stator Flux Linkage." *IEEE Access* 8:111811–21. doi: 10.1109/ACCESS.2020.3001866.
Liu, Chunhua, K. T. Chau, Christopher H. T. Lee, and Zaixin Song. 2021. "A Critical Review of Advanced Electric Machines and Control Strategies for Electric Vehicles." *Proceedings of the IEEE* 109(6):1004–28. doi: 10.1109/JPROC.2020.3041417.
Park, Min-Ro, Dong-Min Kim, Young-Hoon Jung, Myung-Seop Lim, and Jung-Pyo Hong. 2019. "Modeling, Design and Control of Wound-Field Synchronous Motor for High Energy Efficiency of Electric Vehicle." Pp. 3960–67 in *2019 IEEE Energy Conversion Congress and Exposition (ECCE)*. IEEE.
Pramuanjaroenkij, Anchasa, and Sadık Kakaç. 2023. "The Fuel Cell Electric Vehicles: The Highlight Review." *International Journal of Hydrogen Energy* 48(25):9401–25. doi: 10.1016/j.ijhydene.2022.11.103.
Ramya, K. C., J. Geetha Ramani, A. Sridevi, Rajakumar S. Rai, and D. Ruth Anita Shirley. 2022. "Analysis of the Different Types of Electric Motors Used in Electric Vehicles." Pp. 43–57 in.

Thermodynamic analysis of hydrogen production with different solar collectors

[1*]Arif Karabuga
[1] Sustainable Energy Systems Application and Research Center, Haliç University, 34445, Istanbul, Türkiye

* E-mail:arif.karabuga@gmail.com

Abstract
In order to prevent or reduce global warming, the most important choice for states is renewable energy sources. This study uses a solar energy-supported ORC system and PEM electrolyzer to produce renewable energy-supported hydrogen, in other words, green hydrogen. To benefit from solar energy, evacuated tube heat pipe solar collector (ETHPSC) and parabolic trough collector (PTC) are used together. ETHPSC is positioned before PTC for preheating purposes. The electricity required for the PEM electrolyzer is fed from the ORC system. All of the electricity obtained from the micro ORC system with a capacity of 1.189 kW is spent on hydrogen production. As a result of thermodynamic analysis, the energy efficiency of the whole system was calculated as 14.32%. In addition, as a result of the experimental study, the amount of hydrogen produced was found to be 87.05 kg/annual.

Keywords: Hydrogen production, Solar energy, Parabolic trough collector

I. Introduction

One of the main causes of global warming is the release of emissions based on human impacts (Hamed, 2019; Karabuga et al., 2022). In order to prevent this, the use of carbon-free energy sources must be expanded. Renewable energy, especially solar energy, comes to the fore as a carbon-free energy source. There are two basic methods to benefit from solar energy. These; (i) photovoltaic (PV) systems that produce direct electricity and (ii) solar collector systems that produce thermal energy (Kandukuri et al., 2024). There are many methods to benefit from thermal energy production from solar energy. Evacuated tube heat pipe solar collector (ETHPSC) and parabolic trough collector (PTC) are two of them (Sathish et al., 2024). ETHPSCs are planar collectors with low and medium temperature densities. It is widely used in roof-type applications due to its ease of installation and low cost (Zhang et al., 2024). PTCs are chambered collectors with medium and high-temperature density (Ahmad et al., 2023). It is used in industrial applications and energy production facilities due to its high collector outlet temperature. Due to these advantages, ETHPSC and PTC are used for thermal energy production in this study.

Thermal energy obtained from ETHPSC and PTC is used as a heat source in the organic Rankine cycle (ORC) system used for electricity generation. ORC systems have been discussed by many researchers for many years as an energy conversion technology from thermal energy sources with a low temperature density (Wang et al., 2013; Karabuga et al., 2023; Fatigati et al., 2024). In recent years, researchers have given importance to the use of the ORC system with different configurations for sustainable energy production by taking advantage of low temperatures (Boyaghchi and Sohbatloo, 2018; Kutlu et al., 2020; Bozgeyik et al., 2022; Bozgeyik et al., 2023). Gursoy and Dincer (2023) presented the thermodynamic analysis of a solar powered power, heating, hot water and cooling system. Focused solar collector was used for the thermal energy production and ORC system was used for a power generation. The energy and exergy efficiency of the study in which the multiple production method was used were calculated as 22.64% and 21.8%, respectively. Sharifishourabi et al. In their study (2023), presented the thermodynamic analysis of electricity and hydrogen production in an energy production system using solar energy. At the end of the study, the hydrogen production amount was calculated as 0.04 kg/s and the exergy efficiency of the ORC system was calculated as 23.23%.

The aim of this study is to examine the thermodynamic analysis of a solar energy-assisted hydrogen production system in which two different solar collectors are used together. When the literature studies are examined, it is seen that there are more theoretical studies and only a single collector system is used in experimental studies. For this reason, in order to fill this gap in the literature, it is aimed to experimentally use two different solar collectors for the same purpose.

II. Experimental Set-up and Procedure

The presented study deals with the solar energy-supported electricity and hydrogen production system. Two different solar collectors have been used to benefit from solar energy. The heat transfer oil (1 point) coming out of the pump enters the ETHPSC, which is a type of flat solar collector. The heat transfer oil leaving the ETHPSC with a difference of about ΔT=20° C enters the linearly oriented PTC (2 point). The preview for ETHPSC PTC is shown. Thanks to this, there is a possibility of PTC operation at a higher temperature. The transport stream exiting the PTC enters the view source change 1 (HE-1) for the ORC system (3 point). The thermal energy coming out of HE-1 enters pump 1 to ensure circulation in the production area (4 point). Another current line of the flow coming out of the HE-1 is the turbine inlet for electrical energy production (5 point). The highest pressure in the system is located at this point. It has a capacity of 5 kW. The main difference is that all the electricity generated is spent on hydrogen production. R1234yf is used as the working flow in the ORC system. Ultra-pure water is used to clean the pores of the PEM electrolyzer membrane. The purity of the water used directly affects the use time of the electrolyzer. The

water in PEM electrolyzer is about 0.055 μs.

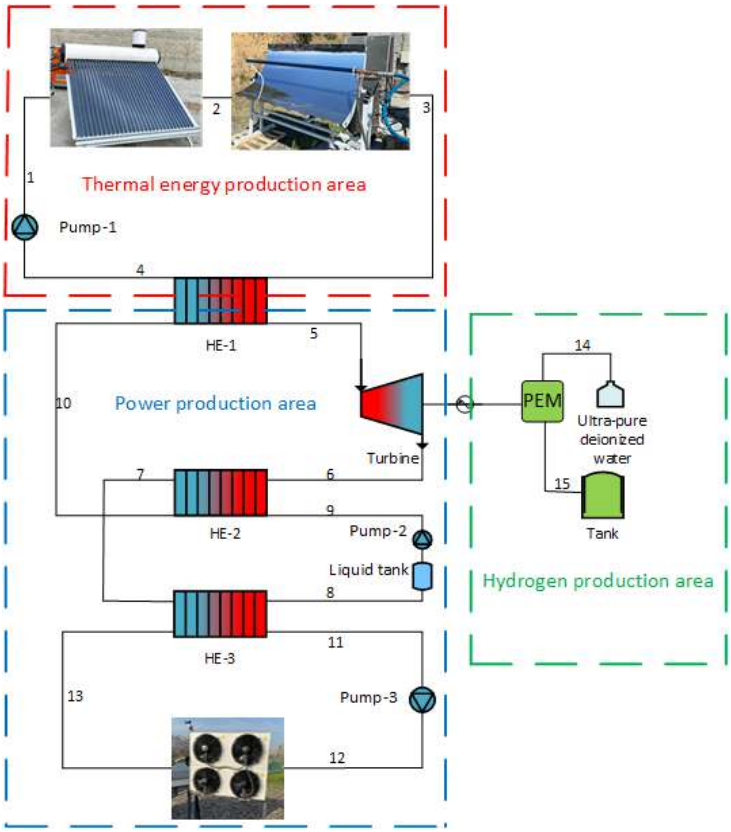


Fig. 1: Schematic diagram of the experimental study

III. Analysis

The following assumptions have been made in order to simplify the mathematical modeling of the solar energy-based electricity and hydrogen production cycle and energy and exergy analysis processes.

- Steady-state conditions are valid for all process.
- The change in kinetic and potential energies is considered to be negligible.
- The ambient temperature and pressure were accepted to be 22°C and 101.325 kPa.
- The power consumption of the fans in the condenser is considered to be negligible.
- Pumps and turbine are considered adiabatic throughout the process.
- The efficiency of heat exchangers is considered to be 1.
- Pressure and temperature losses in pipes and equipment are ignored decently.

While performing thermodynamic performance analysis, energy analysis method was used for various parameters that ambient temperature, mass flow, and turbine inlet temperature, and a package program called Engineering Equation Solver (EES) was used. The energy equations applied to each component in the proposed system are given below;

$$\sum \dot{m}_{in} = \sum \dot{m}_{out} \quad (1)$$

$$\Delta E = \sum \dot{Q} - \sum \dot{W} + \sum \dot{m}_{in} h_{in} - \sum \dot{m}_{out} h_{out} \quad (2)$$

$$\dot{Q}_{col} = I \rho_{ref} \rho_{ref} \varepsilon_{ref} A_n A_{rec} \quad (3)$$

$$\dot{Q}_{solar} = \mathrm{IA}\sigma\alpha \quad (4)$$

$$\eta_{sys} = \frac{\dot{m}_{H_2} LHV}{\dot{Q}_{solar}} \quad (5)$$

IV. Results and discussions

In this section, the results obtained by transferring the values measured via experimental equipment to the EES program are presented. Table 1 shows the energy efficiency and hydrogen production amount of the main equipment used in the experiment. The flow rate of the working fluid in the ORC system is 0.04 kg/s. Figure 2 shows

the change in the energy efficiency of the entire system and the change in the amount of hydrogen production depending on the temperature of the fluid coming out of the PTC collector. If the collector output temperature increases from 90°C to 170°C, the energy efficiency of the entire system increases from 1.15% to 31.57%. It is observed that an increase in the collector output temperature has a positive effect on the system efficiency. A similar trend is also observed for hydrogen production. Depending on the collector output temperature given previously, the amount of hydrogen produced from the system increases from 7.015 kg/year to 196.7 kg/year. Figure 3 shows the change in the turbine energy production value and the amount of energy spent for hydrogen production depending on the increase in the PTC outlet temperature. If the collector outlet temperature increases from 90°C to 170°C, the production capacity of the turbine will increase from 0.5988 kW to 3.342 kW. A similar curve is seen for the energy consumption of the hydrogen production system. Due to the abovementioned in the collector, energy consumption increases from 0.0355 kW to 2.77 kW.

Table 1: Obtained results from presented study

Component	**Value**
ETHPSC energy efficiency	57.64 %
PTC energy efficiency	47.89 %
Turbine energy efficiency	9.69 %
ORC energy efficiency	19.3 %
PEMe energy efficiency	32.54 %
Whole system energy efficiency	14.32 %
Hydrogen production amount	87.05 kg/annual

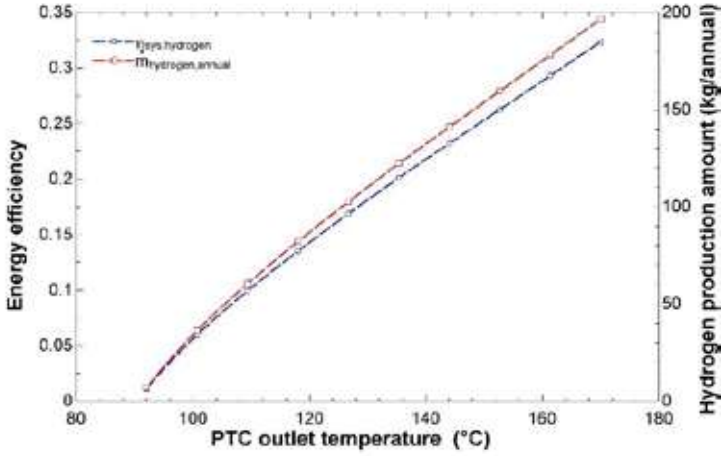


Fig. 2: Change in energy efficiency of the presented system and hydrogen production amount depending on PTC outlet temperature

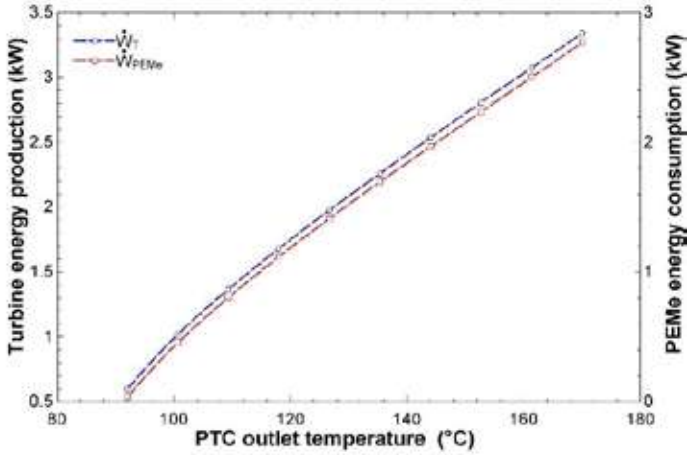


Fig. 3: Change in turbine energy production and PEMe energy consumption depending on PTC outlet temperature

V. Conclusions

In this study, the solar energy-assisted hydrogen production system was evaluated in terms of energy efficiency. Electricity was produced by integrating two different and interconnected solar collectors into the ORC system. All of the electrical energy produced was spent on hydrogen production. Some important results obtained as a result of the study are given below;

• The highest energy efficiency among all components was calculated as 57.64% in ETHPSC.
• The energy efficiency of the ORC unit and hydrogen production systems was calculated as 18.01% and 32.54%, respectively.
• The net power produced was 1.189 kW and the amount of hydrogen produced was 87.05 kg/annual.
• The energy efficiency of the entire system was calculated as 14.32%.

References

Hamed, S.G., 2019, The Share of Cooling Electricity in Global Warming: Estimation of the Loop Gain for the Positive Feedback, *Energy*, vol. 179: p.747-761.

Karabuga, A., Yakut, M.Z., Utlu, Z., 2022, Evaluation of the Thermodynamic Analysis of Hydrogen Production from a Middle-Temperature Intensity Solar Collector, a Case Study, *International Journal of Hydrogen Energy,* vol. 47, no. 74: p. 31821-31832.

Kandukuri, K., Sharma, P.K., Arun R.K., 2024, A comparative assessment of distributive mode active solar dryers: Flat plate collector vs evacuated tube collector with thermal energy storage and perforated baffled trays, *Solar Energy,* vol. 271: p. 112421.

Sathish, T., Kathirvel, S., Dwivedi, Y.D., Stalin, N., Giri, J., Saravanan, R., Makki, E., 2024, Performance enhancement by tungsten trioxide and silicon dioxide mixed nanofluids in solar collector of evacuated tube type, *Case Studies in Thermal Engineering,* vol. 55: pp. 104098.

Zhang, Y., Liu, H., Zhou, X., Hu, Z., Wang, H., Kuang, M., Li, J., Zhang, H., A novel photo-thermal-electric hybrid system comprising evacuated U-tube solar collector and inhomogeneous thermoelectric generator toward efficient and stable operation, *Energy,* vol. 292: p. 130616.

Ahmad, A., Prakash, O., Kausher, R., Kumar, G., Pandey, S., Hasnain, S.M.M., 2024, Parabolic trough solar collectors: A sustainable and efficient energy source, *Materials Science for Energy Technologies*, vol. 7: p. 99-106.

Wang, M., Wang, J., Zhao, Y., Zhao, P., Dai, Y., 2013, Thermodynamic analysis and optimization of a solar-driven regenerative organic Rankine cycle (ORC) based on flat-plate solar collectors, *Applied Thermal Engineering,* Vol. 50, no. 1: p. 816-825.

Karabuga, A., Yakut, M.Z., Utlu, Z., 2023, Assessment of thermodynamic performance of a novelty solar-ORC configuration based hydrogen production: An experimental study, *International Journal of Hydrogen Energy,* vol. 48, no. 99: p. 39154-39168.

Fatigati, F., Vittorini, D., Cipollone, R., 2024, Dynamic response of a micro-scale ORC-based power unit fed by solar flat panels, *Applied Thermal Engineering,* vol. 243: p. 122546.

Boyaghchi, F.A., and Sohbatloo, A., 2018, Assessment and optimization of a novel solar driven natural gas liquefaction based on cascade ORC integrated with linear Fresnel collectors, *Energy Conversion and Management,* vol. 162: p. 77-89.

Bozgeyik, A., Altay, L., and Hepbasli, A., 2022, A parametric study of a renewable energy based multigeneration system using PEM for hydrogen production with and without once-through MSF desalination, *International Journal of Hydrogen Energy*, vol. 47, no. 74: p. 31742-31754.

Bozgeyik, A., Altay, L., and Hepbasli, A., 2023, Energetic, exergetic, exergoeconomic, environmental and sustainability analyses of a solar, geothermal and biomass based novel multi-generation system for production of power, hydrogen, heating, cooling and fresh water, *Process Safety and Environmental Protection,* vol. 177: p. 400-415.

Kutlu, C., Li, J., Su, Y., Wang, Y., Pei, G., and Riffat, S., 2020, Investigation of an innovative PV/T-ORC system using amorphous silicon cells and evacuated flat plate solar collectors, *Energy,* vol. 203: p. 117873.

Gursoy, M., and Dincer, I., 2023, A solar based system for integrated production of power, heat, hot water and cooling, *Energy,* vol. 282: p. 128943.

Sharifishourabi, M., Dincer, I., and Mohany, A., 2023, Performance assessment of a novel solar heliostat and digester-based multigeneration system with hydrogen production, *Applied Thermal Engineering*, vol.232: p. 121094.

Catalyst selection for microplastic photodegradation via MCDM analysis

Hülya Civelek Yörüklü[1,2]

[1]Yıldız Technical University, Faculty of Civil Engineering, Department of Environmental Engineering, 34220, Istanbul, Türkiye
[2]Yıldız Technical University, Clean Energy Technologies Institute, 34220, Istanbul, Türkiye

* E-mail: hcivelek@yildiz.edu.tr

Abstract
Microplastics are considered one of the most urgent environmental problems due to their high consumption rates and high resistance in nature. Photocatalytic methods get attention not only for being environmentally friendly and effective methods for microplastic degradation but also for serving as hydrogen gas producing opportunities. The number of studies on simultaneous microplastic removal and hydrogen production is quite low. Therefore, there are no decision mechanisms that can enlighten future studies. In this study, photocatalytic methods were ranked for simultaneous microplastic removal and hydrogen production using MCDM. Results showed that the power of the lamp and catalyst to microplastic ratio were effective parameters in determining the most economical and effective catalyst and method.

Keywords: Photodegradation, Hydrogen production, Microplastic photodegradation

I. Introduction

There has been an increase in the use of plastic worldwide due to its attractive properties such as low cost and versatility. 155–265 Mt of plastic are projected to be produced yearly by 2060, unless a restriction was handled (Chia et al., 2021). As a result of high plastic production and the high stability and anti-oxidation properties of plastics, plastics get attention due to being one of the most urgent environmental problems. Microplastics (MPs), which are plastic particles having a size smaller than 5 mm, pose a serious threat to aquatic life and ultimately human health through the food chain, in particular (Thacharodi et al., 2024). MPs can be dispersed into different media such as air, water, and soil (Jiang et al., 2020). They can also be encountered in deep-sea sediments and polar glaciers because they may move over great distances when carried by wind and ocean currents.

Several technologies such as thermal or catalytic degradation procedures, and enzymatic degradation methods, have been developed to manage MPs pollution. Among these strategies, photocatalysis is an effective and environmentally friendly strategy via degrading the microplastics and hydrogen (H_2) gas producing opportunity based on catalyst used (Praus et al., 2024). Microplastics are seen as a substrate in these systems for H_2 production. However, it could be confusing to determine the most ideal photocatalytic methodology for simultaneous H_2 producing and microplastic degradation.

Several elements should be considered carefully to determine the most sustainable and feasible alternatives among different options. A significant and useful method known as multiple criteria decision-making (MCDM) offers a methodical way to support decision makers. The TOPSIS technique, which is one of the most used MCDM techniques, finds the answer that is the closest to the ideal solution and the furthest from the negative-ideal solution.

In this study, photocatalysis studies that performed simultaneous microplastic removal and hydrogen production were examined in detail. Among the reviewed studies, the most suitable method was determined by TOPSIS analysis, taking into account the hydrogen production efficiency, the power of the lamp used, the amount of catalyst used per microplastic and the duration of the reaction parameters.

II. Experimental Set-up and Procedure

The literature data listed in this paper were mainly obtained from the scientific databases of Google Scholar and Science Direct via using specific keyword groups such as "photocatalytic microplastic degradation" and "hydrogen production". Considering that review, many different catalyst for photocatalytic reactions and hydrogen production efficiency were obtained.

III. Analysis

The parameters were subjected through Multi-Criteria Decision Making Analysis (MCDA), which involved the criteria weighting and the creation of alternatives. By evaluating each criterion between 1 and 9, the Analytical Hierarchy Process (AHP) method was utilized to determine the criteria weighting (Yoruklu et al., 2023). Criterion were selected as (i) the hydrogen production efficiency, (ii) the power of the lamp used, (iii) the amount of catalyst

used per microplastic and (iv) the duration of the reaction. The consistency of the results was checked after criterion weighting was calculated by computing the consistency index (CI) in AHP method. CI value was found less than 0.1, which indicates that the consistency of the criterion weighting.

The unit-equalized value of each parameter and the criterion weights assigned to the criteria were taken into account while creating the normalized decision matrix. In the end, Euclidian distance was used to compute the positive and negative ideal solutions, and the optimum option was identified by comparing each one's proximity to the ideal solution.

IV. Results and discussions

The hydrogen production yields of different catalysts for simultaneous hydrogen production and microplastic photodegradation were compared using the TOPSIS method. Detailed summary of the studies carried out on the subject were listed in Tab. 1. All criterion data were converted to a unique unit to be able to compare.

Tab. 1. Studies used in TOPSIS analysis

Plastic used	Wavelength (nm)	Type of the lamp	Watt of the lamp (W)	Catalyts	H_2 evolution	Duration (h)	Catalyst : MP amount	Plastic removal	References
PET[(a)]	>420 nm	Xenon	300	$Z_{0.6}C_{0.4}S$	6.68 mmol/g/h	4	0.10 mg : 50 mg	-	Cao et al., 2022
PET	>420 nm	Xenon	300	M-2/$Z_{0.6}C_{0.4}S$	14.17 mmol/g/h	4	0.10 mg : 50 mg	-	Cao et al., 2022
PS[(b)]	365 nm	LED	5	FeB/TiO_2	103.5 µmol	12	50 mg : 30 mg	-	He et al., 2023
PET and PLA[(c)]	≥ 700 nm	Near ınfrared lamp	0.1	h-BN/PDA/MoS_2	5.33 mmol/g/h	30	0,1g : 1.5g	92% for T	Xu et al., 2023
PLA	≥ 700 nm	Near ınfrared lamp	0.1	h-BN/PDA/MoS_2	3.07 mmol//g/h	30	0,1g : 1.5g	34% for PLA	Xu et al., 2023
PEG [(d)]	420 nm	Xenon	300	Ag_2O/Fe-MOF	6.2 mmol/g	3	0.1 g : 0.5 g	27.5 mg PEG	Qin et al., 2022
PET	>420 nm	Xenon	300	CdS-16% $CuInSe_2$	4382 µmol/g/h	3	30 mg : 3 g	-	Liu et al., 2024
PLA	430 nm	Solar light simulator	150	CdS/CdO_x QDs	64.3 mmol/g/h	24	272,89 mg : 50 mg	38,8% PLA	Uekert et al., 2018
PET	431 nm	Solar light simulator	150	CdS/CdO_x QDs	3.42 mmol/g/h	24	272,89 mg : 50 mg	16,6% PET	Uekert et al., 2018
PU [(e)]	432 nm	Solar light simulator	150	CdS/CdO_x QDs	0.85 mmol/g/h	24	272,89 mg : 50 mg	22,5% PUR	Uekert et al., 2018
PET	420 nm	Xenon	300	CPDs-CN 7%	1034 µmol/g/h	22	20mg : 1.25g	-	Han et al., 2022
PET	420 nm	Xenon	300	30% WO_3/g-C_3N_4	14.20 mM/g/h	0.5	0.2 g : 50 mg	-	Wang et al., 2023
PET	420 nm	Metal halide lamp	45	Au/TiO_2	0.81 µmol/g/h	20	0.5 g : 0.5 g	-	Edirisooriya et al., 2023
PET	365 nm	UV mercury vapor lamp	160	Pt/TiO_2	1.28 µmol/h/g catalyst	20	0.5 g : 0.5 g	-	Edirisooriya et al., 2023
PET	>420 nm	Xenon	300	TP-PCN in 75% KI soln	600.3 µmol/g/h	4	30 mg : 650 mg	-	Liu et al., 2023
PES [(f)]	480-950 nm	Xenon	150	n-p heterojunction g-C_3N_4/$CuFeO_2$	241 µmolg/h	12	2 mg : 0.35 mg	-	Lai et al., 2023

[(a)]: PET: Polyethylene terephthalate, [(b)]: PS: Polystrene, [(c):] PLA: Polylactic acid, [(c):] PEG: Polyethylene glycol, [(e)] PU : Polyurethane, [(f)] PES : Polyester

The experimental data given in the Tab.1 were ranked by using TOPSIS analysis based on 4 criterion (hydrogen production efficiency, power of the lamp used, amount of catalyst used per microplastic and duration of the reaction). The ranking obtained from the TOPSIS analysis is given in Tab. 2.

Tab. 2: TOPSIS results for simultaneous H_2 production MP degradation

Plastic used	Catalyts	H_2 evolution	Watt of the lamp (W)	Catalyst : MP amount	Duration (h)	Ranking	References
PET[(a)]	$Z_{0.6}C_{0.4}S$	6.68 mmol/g/h	300	0.10 mg : 50 mg	4	7	Cao et al., 2022

PET	M-2/$Z_{0.6}C_{0.4}S$	14.17 mmol/g/h	300	0.10 mg : 50 mg	4	2	Cao et al., 2022
PS[(b)]	FeB/TiO_2	103.5 µmol	5	50 mg : 30 mg	12	5	He et al., 2023
PET, PLA[(c)]	h-BN/PDA/MoS_2	5.33 mmol/g/h	0.1	0,1g : 1.5g	30	3	Xu et al., 2023
PLA	h-BN/PDA/MoS_2	3.07 mmol//g/h	0.1	0,1g : 1.5g	30	4	Xu et al., 2023
PEG [(d)]	Ag_2O/Fe-MOF	6.2 mmol/g	300	0.1 g : 0.5 g	3	10	Qin et al., 2022
PET	CdS-16% $CuInSe_2$	4382 µmol/g/h	300	30 mg : 3 g	3	8	Liu et al., 2024
PLA	CdS/CdO_x QDs	64.3 mmol/g/h	150	272,89 mg : 50 mg	24	1	Uekert et al., 2018
PET	CdS/CdO_x QDs	3.42 mmol/g/h	150	272,89 mg : 50 mg	24	14	Uekert et al., 2018
PU [(e)]	CdS/CdO_x QDs	0.85 mmol/g/h	150	272,89 mg : 50 mg	24	16	Uekert et al., 2018
PET	CPDs-CN 7%	1034 µmol/g/h	300	20mg : 1.25g	22	12	Han et al., 2022
PET	30% WO_3/g-C_3N_4	14.20 mM/g/h	300	0.2 g : 50 mg	0.5	15	Wang et al., 2023
PET	Au/TiO_2	0.81 µmol/g/h	45	0.5 g : 0.5 g	20	6	Edirisooriya et al., 2023
PET	Pt/TiO_2	1.28 µmol/h/g catalyst	160	0.5 g : 0.5 g	20	9	Edirisooriya et al., 2023
PET	TP-PCN in 75% KI soln	600.3 µmol/g/h	300	30 mg : 650 mg	4	11	Liu et al., 2023
PES [(f)]	n-p heterojunction g-C_3N_4/$CuFeO_2$	241 µmolg/h	150	2 mg : 0.35 mg	12	13	Lai et al., 2023

According to Tab. 2, the highest hydrogen yield was at the top of the ranking list, which indicates that hydrogen yield is the most important parameter. However, although the hydrogen yield obtained by Cao et al (6.68 mmol/g/h) is higher than the hydrogen yield obtained by Xu et al (5.33 mmol/g/h), the TOPSIS ranks are 7 and 3. This shows that the lamp power is also an important parameter in photodegradation to obtain an energy efficient system.

V. Conclusions

A MCDM analysis was conducted to determine the best alternative for simultaneous microplastic photodegradation and hydrogen production by using TOPSIS analysis. Results showed that the power of the lamp and catalyst to microplastic ratio were effective parameters in determining the most economical and effective catalyst and method. Therefore, further studies should be carried out also to optimize different parameters such as cost and microplastic removal efficiency.

References

Cao, B., Wan, S., Wang, Y., Guo, H., Ou, M., Zhong, Q. Highly-efficient visible-light-driven photocatalytic H2 evolution integrated with microplastic degradation over MXene/ZnxCd1-xS photocatalyst. Journal of Colloid and Interface Science, 605, 311-319 (2022).

Chia, R. W., Lee, J. Y., Kim, H., Jang, J. Microplastic pollution in soil and groundwater: a review. Environmental Chemistry Letters, 19(6), 4211-4224 (2021).

Edirisooriya, E. T., Senanayake, P. S., Wang, H. B., Talipov, M. R., Xu, P., Wang, H. Photo-reforming and degradation of waste plastics under UV and visible light for H2 production using nanocomposite photocatalysts. Journal of Environmental Chemical Engineering, 11(2), 109580 (2023).

Han, M., Zhu, S., Xia, C., & Yang, B. Photocatalytic upcycling of poly (ethylene terephthalate) plastic to high-value chemicals. Applied Catalysis B: Environmental, 316, 121662 (2022).

He, J., Han, L., Ma, W., Chen, L., Ma, C., Xu, C., Yang, Z. Efficient photodegradation of polystyrene microplastics integrated with hydrogen evolution: Uncovering degradation pathways. Iscience, 26(6) (2023).

Jiang, R., Lu, G., Yan, Z., Liu, J., Wu, D., Wang, Y. Microplastic degradation by hydroxy-rich bismuth oxychloride. Journal of Hazardous Materials, 405, 124247 (2021).

Lai, Y. H., Yeh, P. W., Jhong, M. J., Chuang, P. C. Solar-driven hydrogen evolution in alkaline seawater over earth-abundant g-C3N4/CuFeO2 heterojunction photocatalyst using microplastic as a feedstock. Chemical Engineering Journal, 475, 146413 (2023).

Liu, X., Yang, Y., Wan, S., Li, S., Ou, M., Song, F., Fan, X., Zhong, Q. Tuning the surface hydrophilicity of a C3N4 nanosheet for efficient photocatalytic H2 evolution coupled with microplastic degradation. International Journal of Hydrogen Energy, 48(71), 27599-27610 (2023).

Liu, Y., Zeng, Q., Ning, S., Gan, Y., Fujita, T., Wei, Y., Wang, X., Zeng, D. CuInSe2 nanoplatelets decorated CdS nanosheets as

2D-2D S-scheme photocatalyst for photocatalytic H2 generation coupled with benzyl alcohol oxidation and microplastic degradation. Journal of Solid State Chemistry, 124645 (2024).

Praus, P. Photoreforming for microplastics recycling: a critical review. Journal of Environmental Chemical Engineering, 112525 (2024).

Qin, J., Dou, Y., Wu, F., Yao, Y., Andersen, H. R., Hélix-Nielsen, C., Lim, S.Y., Zhang, W. (2022). In-situ formation of Ag2O in metal-organic framework for light-driven upcycling of microplastics coupled with hydrogen production. Applied Catalysis B: Environmental, 319, 121940 (2022).

Thacharodi, A., Hassan, S., Meenatchi, R., Bhat, M. A., Hussain, N., Arockiaraj, J., Ngo, H.H., Sharma, A., Nguyen, H.T., Pugazhendhi, A. Mitigating microplastic pollution: A critical review on the effects, remediation, and utilization strategies of microplastics. Journal of Environmental Management, 351, 119988 (2024).

Uekert, T., Kuehnel, M. F., Wakerley, D. W., Reisner, E. Plastic waste as a feedstock for solar-driven H 2 generation. Energy & Environmental Science, 11(10), 2853-2857 (2018).

Wang, X., Zhu, Z., Jiang, J., Li, R., Xiong, J. Preparation of heterojunction C3N4/WO3 photocatalyst for degradation of microplastics in water. Chemosphere, 337, 139206 (2023).

Xu, N., Chen, J., Hu, C., Zhu, Z., Wang, W., Liu, B. Near-infrared-dominated photothermal nanofluids for degradation and H2-producing photochemical reforming of fiber-based microplastics. Ceramics International, 49(15), 24730-24743 (2023).

Evaluation of Exergy Efficiency of a PEM Fuel Cell System

[1*]Sinan Kapan, [2]Zehra Ural Bayrak, [1]Nevin Celik
[1] Fırat University, Engineering Faculty, Mechanical Engineering Department, Elazığ, 23200, Türkiye
[2] Fırat University, School of Aviation, Department of Avionics, Elazığ, 23200, Türkiye

* E-mail:skapan@firat.edu.tr

Abstract

In this study, standard exergy analysis of a PEM fuel cell system planned to be used in a zero-energy building is presented. A thermodynamic analysis is carried out to examine the effect of varying operating temperatures and pressures on the exergy and efficiency of a 6 kW PEMFC system. Calculation of physical and chemical exergies, mass flow rates, and exergy efficiencies are performed for temperature (T) and pressure (P) ranging from 313 to 353 K and 1.5 to 2.5 bar, respectively. Results from the exergy analysis reveal that the overall exergy efficiency of the fuel cell system vary between 53% and 55%.

Keywords: Exergy, PEM, Fuel Cell, zero-energy building.

I. Introduction

A fuel cell type known as a proton exchange membrane fuel cell (PEMFC) uses a polymer electrolyte membrane to conduct protons and may function at comparatively low temperatures. It is thought to be vitally important to ascertain how best to use a PEMFC and gauge its actual performance using the laws of thermodynamics. The efficiency of a PEMFC determined by applying the first law of thermodynamics theoretically does not indicate the fuel cell's optimal performance and may thus be deceptive. However, a more accurate indicator of a PEMFC's performance may be provided by its second law efficiency, also known as exergetic efficiency. This is calculated as the electrical output divided by the greatest amount of work that may be produced. Exergy analysis, sometimes referred to as availability analysis, is the study of energy applied to a system using the second law of thermodynamics.

Exergy deals with both the quantity and quality of energy, in contrast to energy, which only addresses the quantity of energy (Cengel and Boles, 1994). Physical exergy, which is related to the matter's temperature and pressure, and chemical exergy, which is related to a system's chemical composition diverging from that of its surroundings, make up the total exergy (Dincer, 2002).

Numerous types of fuel cells have been the subject of in-depth research on energy and energy analysis, which has shown the importance of the second law efficiency to hydrogen and the functioning of the fuel cell system (Rosen and Scott, 1987; Jung et al., 2023).

The efficiency of a PEMFC, its economics at different loads and its possible uses, especially in transportation, have been studied in the literature (Cownden et al., 2001). In an effort to find and create fuel cell systems with more energy-saving and cost-effective attributes than conventional power generation plants, other studies have conducted energy and exergy evaluations of PEMFC systems with various degrees of cogeneration (Liu et al., 2017). For this purpose, the usage area of PEMFC is developing day by day and application studies in net zero-energy buildings are gaining importance (Baniasadi et al., 2023)

It is important for sustainability parameters to meet the heating, cooling, electrical energy and hot water demands of a net zero energy building from the fuel cell system and to evaluate this system with energy-exergy analysis methods. For this purpose, a 6 kW PEMFC developed by Matlab/Simulink software, is handled to analyze the second law efficiency in this study. The supply pressure of air and operating temperatures vary in the range of 313-353 K and 1-2.5 bar, respectively. The exergy of the reactants as O_2 and H_2 and the exergies of products as air and waste water are estimated by conducting physical and chemical exergy balances.

II. Materials and Methods

The model is a 6 kW & 45 V PEMFC stack that is chosen using the commercial program Matlab/Simulink's SimPowerSystem Toolbox. Air and hydrogen are the inputs of fuel cell stack. It is assumed that 56 cm^2 is the activation area. DC/DC converter is used to increase the voltage and produce

a constant direct voltage. The current and voltage values are measured by connecting the load to the output of the DC/DC converter. The system was previously created by the co-authors of this study and a detailed parametric evaluation of the system was presented (Ural Bayrak and Celik, 2023).

The number of cells in the stack is 65, the nominal current and voltages are assumed to be 133.3 A and 45 V, respectively. The nominal air flow rate and fuel flow rate are respectively 300 lpm and 50 lpm. The nominal value of air supply pressure is 1 bar. The fuel supply pressure varies as 1.5, 2 and 2.5 bar. The operating temperature varies as 313, 323, 333, 338, 343 and 353 K. In this study, thermodynamic analysis of the PEMFC is carried out, as shown in Fig.1. The effects of temperature and pressure parameters on exergy efficiency are investigated. This study will be used in the analysis of a zero-energy building that produces its own energy, as designed in Fig. 2.

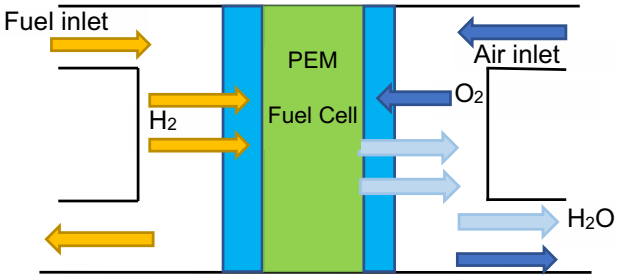


Fig. 1. Schematic representation of PEM fuel cell

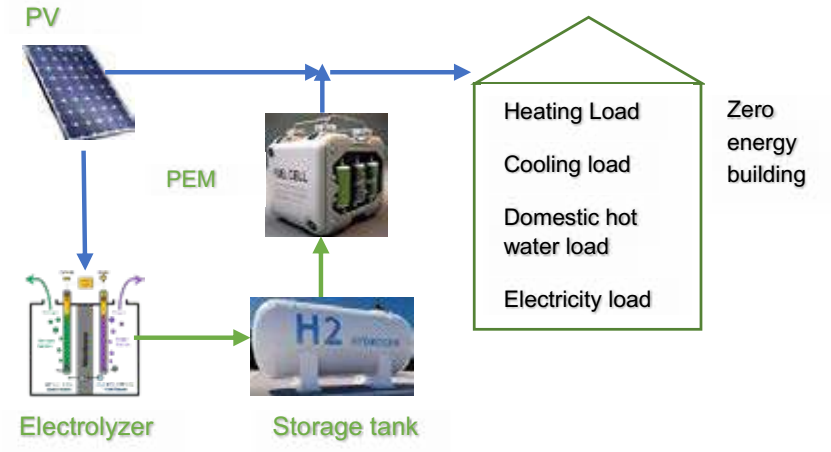


Fig. 2. Schematic representation of the system to meet the energy requirements of the building

The mass flow rates of the entering air and hydrogen are obtained by Eq. (1-2).

$$\dot{m}_{air,in} = 3{,}57x10^{-7}\ (\frac{\lambda \dot{W}}{V}) \quad (1)$$

$$\dot{m}_{H_2,in} = 1{,}05x10^{-8}\ (\frac{\dot{W}}{V}) \quad (2)$$

The mass flow rate of the exiting air is obtained by subtracting the oxygen consumed during the reaction from the air entering the fuel cell in Eq. (3).

$$\dot{m}_{air,out} = 3{,}57x10^{-7}\ (\frac{\lambda \dot{W}}{V}) - 8{,}29x10^{-8}\ (\frac{\dot{W}}{V}) \quad (3)$$

The amount of water released as a result of the reaction is calculated with Eq. (4).

$$\dot{m}_{water,out} = 9{,}34x10^{-8}\ (\frac{\dot{W}}{V}) \quad (4)$$

The exergy efficiency of the system as shown in Fig.1, is obtained by dividing the amount of power produced by the fuel cell to the difference between the exergy of the reactants (air + hydrogen) and the exergy of the products (air + water).

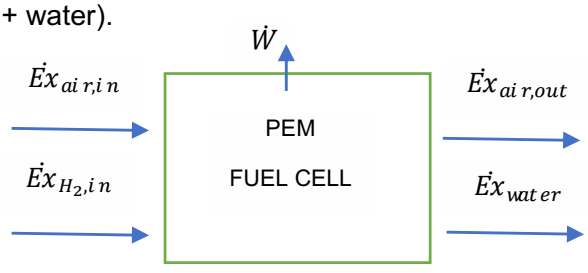


Fig. 3. Exergy balance of PEMFC

Exergy efficiency of the PEM fuel cell is calculated by Eq. (5).

$$\eta_{II} = \frac{\dot{W}}{(\dot{E}x_{air,in} + \dot{E}x_{H_2}) - (\dot{E}x_{air,out} + \dot{E}x_{water,out})} \quad (5)$$

where $\dot{E}x_{air,in}$, $\dot{E}x_{H_2,in}$, $\dot{E}x_{air,out}$, and $\dot{E}x_{water}$ are the exergy values of input air, input hydrogen, output air and waste water. Only physical and chemical exergy were taken into account when calculating the exergy value. For the PEM fuel cell subsystem, the reactants are treated as ideal gases with constant specific heat. Therefore, the physical and chemical exergies is calculated by following equations.

$$\dot{E}x = \dot{E}x^{phy} + \dot{E}x^{ch} \quad (6)$$

and

$$\dot{E}x^{phy} = c_p(T - T_0) - T_0\left[c_p\, l\, n\frac{T}{T_0} - Rl\, n\frac{P}{P_0}\right] \quad (7)$$

where P_0 = 101.325 kPa and T_0 = 298.15 K are the standard conditions of pressure and temperature, respectively.

$$\dot{E}x^{ch} = \sum_k y_k\, \bar{\varepsilon}^0{}_k + RT_0 \sum_k y_k\, l\, ny_k \quad (8)$$

where y_k in the equation refers to the ratio of the number of moles of each component forming the gas to the total number of moles, and $\bar{\varepsilon}^0{}_k$ refers to the standard chemical exergy of each component.

III. Results and Discussions

In this study, an exergy analysis of a PEM fuel cell is performed at different operating temperatures and pressures. Exergy input to the system occurs with air and hydrogen. Since air enters the system under ambient conditions (298 K, 1 atm), so its physical exergy is zero. However, the chemical exergy of the oxygen contained in the air (assumed that air contains 0,21 O_2) and the entering hydrogen is calculated with Eq. (8) and presented in Table 1. The physical exergy of H_2 entering the system is presented in Fig.4, and the temperature and pressure values vary between 313 to 353 K and 1.5 to 2.5 bar, respectively. Additionally, the chemical exergies of water and air leaving the system are given in Table 2.

Tab. 1. Chemical exergies entering to the system

Element	$\dot{m}$ (kg/s)	Standart chemical exergy (kJ/kg)	$\dot{E}x^{ch}$ (W)
H_2	0,000091	118050	10742,55
O_2	0,00194922	124,06	241,82

Tab. 2. Chemical exergies leaving from the system

Element	$\dot{m}$ (kg/s)	Standart chemical exergy (kJkg)	$\dot{E}x^{ch}$ (W)
Air	0,001230753	124,06	152,69
H_2O	0,000809	50	40,47

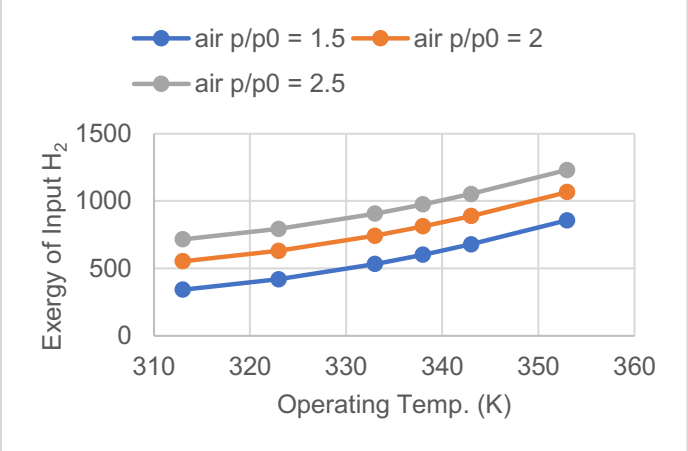


Fig. 4. Physical exergy of input H_2

In Fig. 5, it is seen that as temperature and pressure increase, the exergy carried from the system by the products increases. Fig. 6 shows the variation of the exergy efficiency. Exergy efficiency decreases with increasing temperature and pressure because the output power is constant. Therefore, the desired output power can be achieved by using the initial values of temperature and pressure.

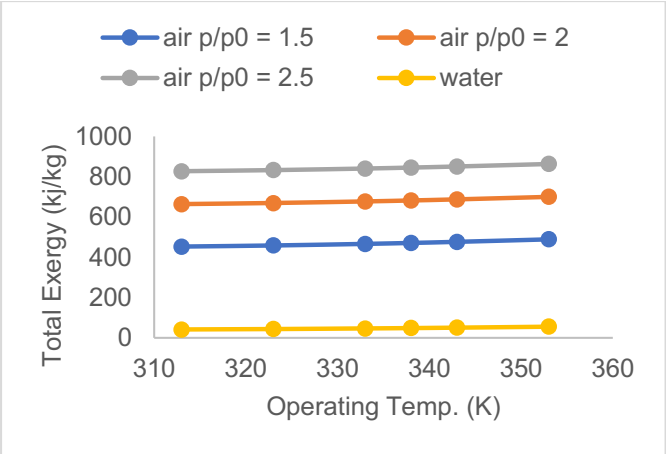


Fig. 5. Total exergy leaving the system by products

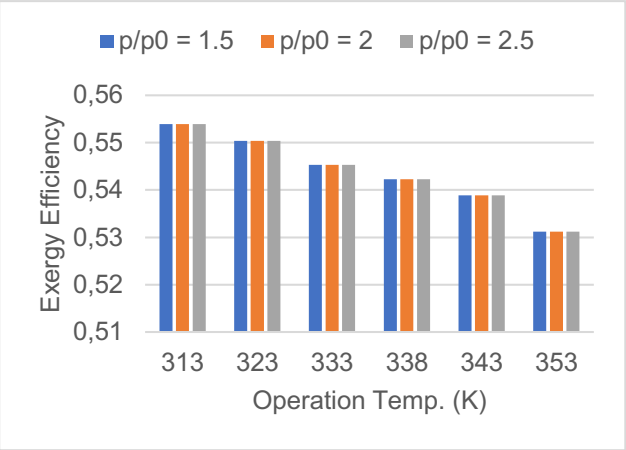


Fig. 6. Variation of exergy efficiency of the system

IV. Conclusions

The efficiency of the PEM fuel cell, which is planned to be used in a zero-energy building, was evaluated in terms of exergy analysis. The relationship of variables such as operating pressure and temperature with the total performance of the fuel cell has been demonstrated. According to the analysis, a fuel cell system's exergy efficiency is calculated as the fuel cell's power output divided by the total exergies of the reactants and products of the electrochemical process that drives the fuel cell. Each element in the electrochemical process has a physical and chemical exergy, which adds up to the overall exergy of the reactants and products. The present results showed that the exergy efficiency of the fuel cell increased with different combinations of the variable parameters studied.

References

Baniasadi E., Ziaei-Rad M., Behvand M.A., Javani N. Exergy-economic analysis of a solar-geothermal combined cooling, heating, power and water generation system for a zero-energy building, International Journal of Hydrogen Energy, 48 (99), 39064-39083 (2023).

Cengel Y., Boles M.A. Thermodynamics—An Engineering approach. 2nd ed. Mc Graw-Hill, Inc.; (1994).

Cownden R, Nahon M, Rosen M. Exergy analysis of a fuel cell power system for transportation applications. Exergy, An International Journal, 1(2),112–121 (2001). https://doi.org/10.1016/S1164-0235(01)00017-6.

Dincer I. Technical, environmental and exergetic aspects of hydrogen energy systems. Int J Hydrogen Energy, 27(3), 265–285 (2002).

Jung Y., Heo Y., Cho H., Kang Y.T., Kim Y., Lee H. A plan to build a net zero energy building in hydrogen and electricity-based energy scenario in South Korea, Journal of Cleaner Production, 397, 136537 (2023).

Liu J., Zhao T., Chen Y.Q. Maximum Power Point Tracking with Fractional Order High Pass Filter for Proton Exchange Membrane FC. IEEE/CAA Journal of Automatica Sinica, 4(1), 70-79 (2017).

Rosen M.A., Scott D.S. An energy-exergy analysis of the Koppers–Totzek process for producing hydrogen from coal. Int J Hydrogen Energy 12, 837–845 (1987).

Ural Bayrak Z., Celik N., Determining the Effects of Operating Conditions on Current Density of a PEMFC by Using Taguchi Method and ANOVA, Arabian Journal for Science and Engineering, Article in Press (2023), DOI: 10.1007/s13369-023-08470-9.

Heterojunction Cr_2O_3/CuO photocathode for photoelectrochemical hydrogen production

[1*]Ender FAKI, [2]Fatih TEZCAN, [1]Gökmen SIĞIRCIK, [1]Gülfeza KARDAŞ,
[1]Çukurova University, Science and Letters Faculty, Chemistry Department, Adana, 01330, Türkiye
[2]Tarsus University, Vocational School of Technical Sciences at Mersin Tarsus Organized Industrial Zone, Chemistry and Chemical Process Technology, Mersin, 33100, Türkiye

* E-mail: enderfaki@gmail.com

Abstract
One of the promising applications for bringing carbon dioxide emissions closer to zero is the importance of hydrogen gas produced from renewable energy sources. Solar energy uses n/p-type semiconductors in the photo-electrochemical cell to generate hydrogen. In a photoelectrochemical cell, p-type semiconductors are used in the production of hydrogen gas in the reaction of oxygen-forming n-type semi-conductors. The paper presents synthesized photoelectrodes Cr_2O_3, CuO, and Cr_2O_3/CuO for use in the photo-electrochemical cell's hydrogen production process. The p-type Cr_2O_3 is obtained by hydrothermal and CuO is synthesized by electrochemical deposition. Scanning Electron Microscopy images show that Cr_2O_3 is synthesized by the hydrothermal method in the form of a nanoball, while CuO is formed in a nanocube. The XRD pattern depicts that Cr_2O_3 and CuO crystal phases are orthorhombic and cubic, respectively. The photoelectrochemical performance test was performed by linear sweep voltammetry (LSV), electrochemical impedance spectroscopy (EIS) and chronoamperometric measurements. The binary Cr_2O_3/CuO heterostructure performs the most catalytically, with a current density value of -0.834 mA cm^{-2} (-0.6 V vs. Ag/AgCl) under solar irradiation.

Keywords: Photoelectrochemical hydrogen production, p-type semiconductor, photocathode, water splitting

I. Introduction

Fossil fuel usage leads to elevated amounts of CO_2 emissions in the environment. Researchers suggest that we are close to a looming tragedy because of the escalating severity of the climate change crisis (Chehade and Dincer, 2021). To reverse this disastrous scenario and return it to its former state, transferring from fossil fuels to energy from renewable sources is the only way to proceed (Acar and Dincer, 2016; Anctil et al., 2023). Solar energy usage is of the utmost significance currently. The hydrogen gas produced using sunlight photon rays is considered an important breakthrough in addressing the global warming crisis, due to its zero CO_2 emissions into atmosphere. Hydrogen production can be achieved in photoelectrochemical cells (PECs) with a photoanode for the oxygen evolution reaction (OER) and a photocathode for the hydrogen evolution reaction (HER). The photocathode and photoanode are consisted of p-type and n-type semiconductors in PECs. Additionally, there are plenty of studies on n-type semiconductive photoelectrodes in the literature, but there has been a lack of research on p-type semiconductors (Li et al., 2020). It is possible to find an abundance of research on n-type semiconductive photoelectrodes in the literature, but there is a lack of comparable studies on p-type semiconductors. Furthermore, p-type semiconductors have not reached the desired photocurrent density. The CuO semiconductor is preferred for use in PEC applications as a p-type semiconductor owing to its absorption in the spectrum of visible light and its cost-effectiveness (Siavash Moakhar et al., 2021). The CuO band is particularly disadvantageous due to its susceptibility to cathode corrosion. Heterostructure designs may boost the photocatalytic efficiency by decreasing sunlight scattering and adjusting the absorption threshold to the visible and near-infrared spectrum for improved sunlight absorption. It reduces the recombination of holes and electrons between semiconductors, which accelerates the movement of electrons between energy levels within semiconductors (Joy et al., 2018). Photoelectrochemical hydrogen production employs CuO photoelectrodes in conjunction with semiconductor heterostructures such as TiO_2 (Zhang et al., 2022), Cu_2O (Jeong et al., 2022), and MoS_2 (Tiwari et al., 2022). Additionally, Cr_2O_3 is a p-type semiconductor, serving the photostability of heterostructures, visible light absorption, and decreasing the cost of photoelectrodes (Mohd Nasir and Mat-Teridi, 2020).

The study presents a photocathode material consisting of CuO and Cr_2O_3 heterostructures for photoelectrochemical hydrogen production under solar light irradiation. CuO nanofilm is coated by electrochemical deposition, applying a current density of -0.3 mA cm^{-2}. Cr_2O_3 nanoballs are synthesized by hydrothermal deposition. Cr_2O_3/CuO heterostructure enabled broad light absorption and decreased the corrosion of the photocathode. The combined Cr_2O_3/CuO heterostructure enhances photocatalytic performance with a current density value -0.834 mA cm^{-2} (-0.6 V vs. Ag/AgCl) compared to pristine CuO and Cr_2O_3 under solar irradiation.

II. Experimental Set-up and Procedure

D-glucose, KCl, $Cr(NO_3)_3{\times}5H_2O$, $CuSO_4{\times}5H_2O$, lactic acid, Na_2SO_3, phosphate buffer, acetone and ethyl alcohol were obtained from Sigma–Aldrich. Fluorine-doped tin oxide (FTO, ~8 Ω/Sq.) was purchased from Teknoma Company. Furthermore, all materials were employed without purification procedures.

The Cr_2O_3 nanoball synthesis was conducted on the FTO substrate by the hydrothermal deposition method. The deposition of Cr_2O_3 was carried out in the autoclave at 90 °C for 24 h. The hydrothermal deposition bath was consisted of 50 mM $Cr(NO_3)_3{\times}5H_2O$, 50 mM D-glucose and 50 mM KCl. Cr_2O_3 nanoball were washed with distilled

water and dried in a furnace of 40 °C. Subsequently, Cr_2O_3 nanoballs were calcinated in furnace at 500 °C for 2 hours under air.

The heterojunction of CuO on Cr_2O_3 nanoballs were performed by electrochemical deposition. It was carried out at -0.25 mA cm^{-2} at 45 °C. The electrochemical deposition bath included 1.0 M lactic acid – 0.1 M $CuSO_4 \times 5H_2O$. The chronoamperometric deposition was conducted by a conventional three electrode set-up, including Cr_2O_3, Ag/AgCl (3.0 M KCl), and Pt sheet (2 cm^2) as the actual working electrode, reference electrode, and counter electrode, respectively. The photoelectrodes were washed with distilled water, and they were calcinated at 500 °C for 2 hours under air.

III. Analysis

The electrode's surface assessment was observed using a Field-Emission Scanning Electron Microscope (FESEM). The electrode crystal structure was evaluated using X-Ray Diffractometers (XRD) throughout the 2θ° range of 20° - 80°. The photoelectrode's light absorbance was determined with a UV-Vis spectrometer in an applied range of 350 and 900 nm.

The photocatalytic experiments were carried out using an electrochemical analyzer in a conventional three-electrode setup. The photocathodes, Ag/AgCl (3.0 M KCl), and Pt sheet (2 cm^2) were employed as the actual working electrode, reference electrode, and counter electrode, respectively. The electrolyte was contained 0.1M phosphate buffer and 0.1M Na_2SO_3. A Xe arc lamp was used to imitate solar power of 100 mW cm^{-2} which is used for all photoelectrochemical tests. LSV tests were conducted using a scan rate of 5 mV s^{-1}, covering a potential value range of 0.0 V to -0.6 V.

IV. Results and discussions

We applied ultraviolet-visible (UV-Vis) spectroscopy to evaluate the sunlight absorbance properties of photoelectrodes. Fig. 1(a) displays the UV-Vis spectrum of photoelectrons within the wavenumber range of 350–900 nm. The pristine Cr_2O_3 has an absorption beginning peak around 540 nm and a final absorbance of 400 nm, allowing solar light to be effectively used in the visible region. The pristine CuO possesses a peak of absorption that begins at 840 nm, and extends throughout the visible region, revealing its broad solar efficiency from near infrared to visible light. Furthermore, as seen in Fig. 1(a), the Cr_2O_3/CuO heterostructure enhances solar light absorption compared to pristine CuO and Cr_2O_3 photoelectrodes. It can be suggested that binary heterostructures improve light absorption through their energy levels.

Fig. 2(b) shows XRD pattern of photoelectrodes. The Cr_2O_3 XRD pattern peaks at 2θ° of 24.44°, 36.45° and 41.55° correspond to hkl parameters (012), (110), (006), respectively. It suggests that Cr_2O_3 is a rhombohedral structure characteristic (JCPDS NO-98-020-2619). The XRD pattern peaks of CuO at 2θ° of 32.57°, 35.49°, 38.71°, 48.82°, 53.41°, 66.24° and 68.05 correspond to hkl parameters (110), $(11\bar{1})$, (111), $(20\bar{2})$, (020), $(31\bar{1})$ and (220), respectively. It indicates that CuO is characteristic a monoclinic crystal structure (JCPDS NO-98-062-8616). Furthermore, the XRD pattern of the Cr_2O_3/CuO heterostructure shows similar characteristic peaks instead of disappearing the 2θ° peak of Cr_2O_3 at 24.44°. It could be explained by the second calcination process for CuO synthesis.

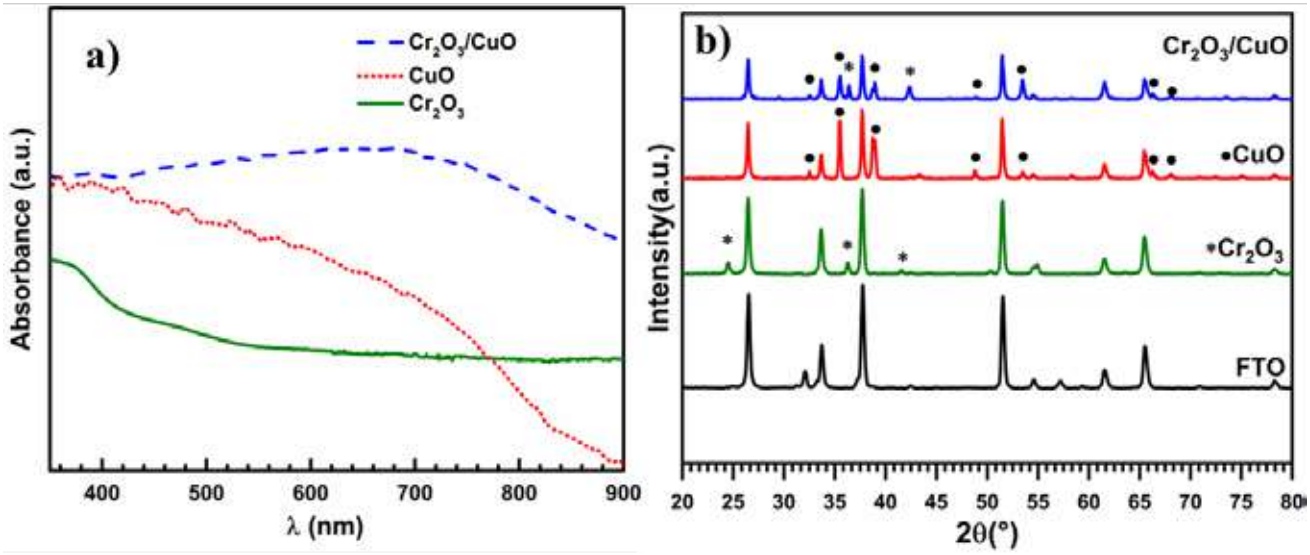


Fig. 1: UV-Vis spectra (a) and XRD pattern (b) of photoelectrodes.

Fig. 2 shows FESEM images of the samples at 5–20 kx magnified. The Cr_2O_3 surface morphology indicates nanoball structures that exhibit growth with gaps throughout the entire surface, suggesting the crystal growth of the Cr_2O_3 is performed regionally instead of covering the entire FTO substrate. CuO surface topography shows complete coverage of the FTO surface by forming diverse dimensions of nanocubes. Furthermore, the surface images of the Cr_2O_3/CuO heterostructures indicate that both Cr_2O_3 and CuO structure growth occur with similar surface morphology on the FTO. Therefore, it can be concluded that the synthesis of Cr_2O_3/CuO heterostructures was achieved by hydrothermal and electrochemical deposition.

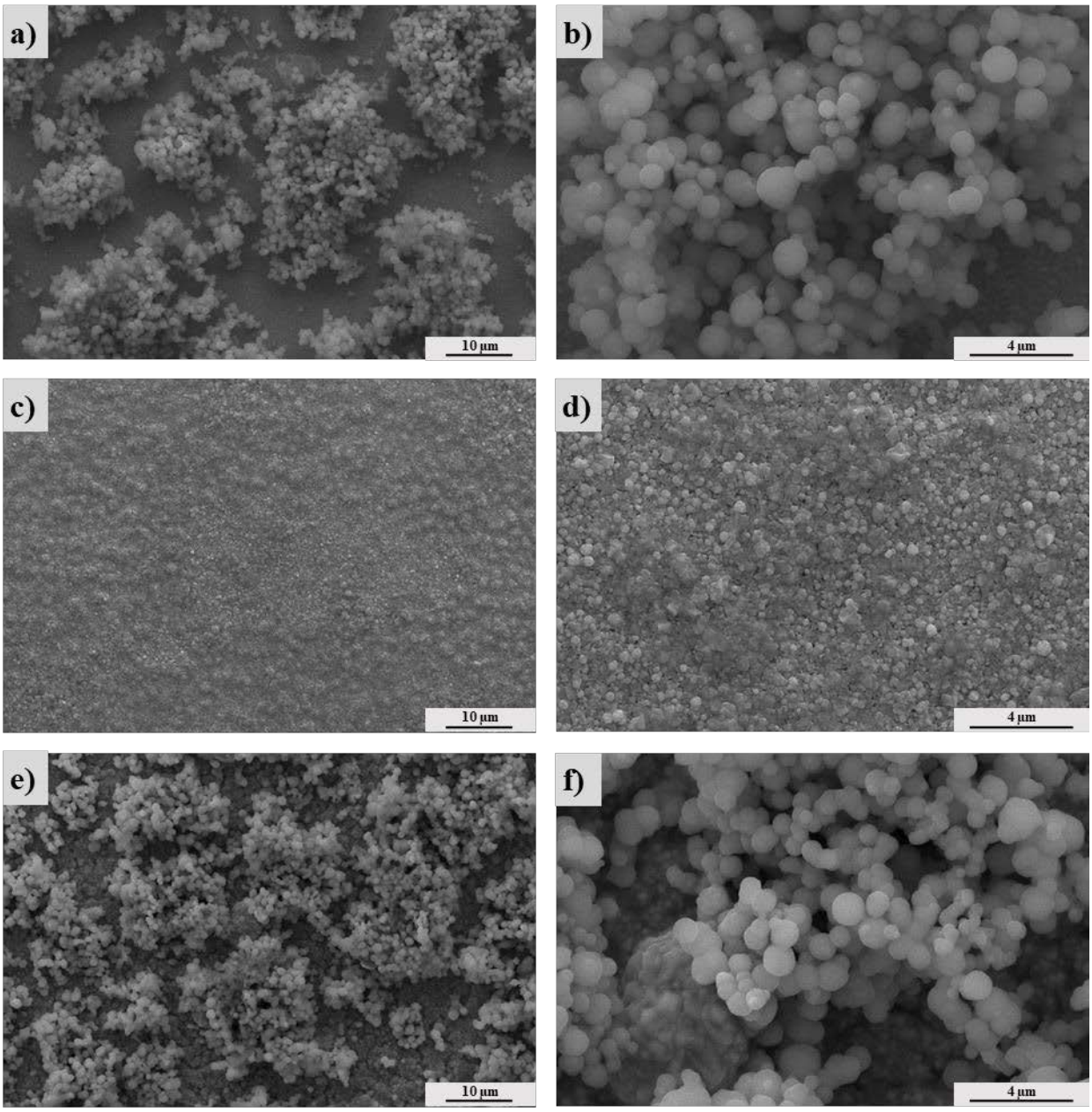


Fig. 2: Cr_2O_3 (a-b), CuO (c-d) and Cr_2O_3/CuO (e-f) FESEM images.

LSV tests were utilized to assess the photocatalytic performance of the synthesised photoelectrodes. Fig. 3 represents the measurements of photoelectrodes in a voltage range of 0.0 to -0.6 V. LSV measurement was carried out cathodic scan to enlighten the photocathode performance of samples. It indicates that the photocurrent density of electrodes increases in the sequence of Cr_2O_3, CuO and Cr_2O_3/CuO (0.0237 mA cm^{-2}, 0.780 mA cm^{-2} and -0.834 mA cm^{-2} vs. Ag/AgCl). Cr_2O_3/CuO heterostructure performs the most catalytic activity in the hydrogen evolution reaction (HER). It can be suggested that the photocatalytic efficiency is enhanced by decreasing the recombination of holes and electrons between semiconductors, which accelerates the movement of electrons between energy levels within semiconductors. Therefore, the synthesis of Cr_2O_3/CuO conforms to accomplish of heterostructure in HER process.

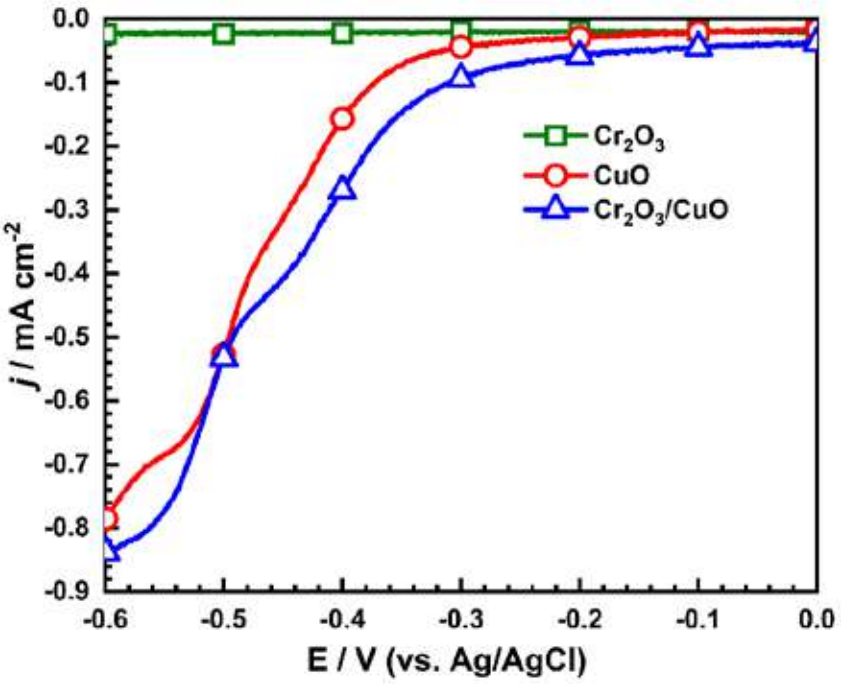


Fig. 3: LSV measurement of photoelectrodes.

V. Conclusions

We achieved Cr_2O_3/CuO heterostructures and tested their photocatalytic properties as a photocathode for solar driven water splitting to hydrogen gas production. The heterojunction of CuO on Cr_2O_3 nanoballs was performed by electrochemical deposition. The Uv-Vis showed that the Cr_2O_3/CuO heterostructure enhances solar light absorption compared to pristine CuO and Cr_2O_3 photoelectrodes. FESEM images depict that Cr_2O_3 surface morphology resembles nanoball structures and CuO surface involves diverse dimensions of nanocubes. The XRD pattern suggests that Cr_2O_3 and CuO are rhombohedral and have a monoclinic crystal structure, respectively. LSV and chronoamperometric measurement indicated that the most photocatalytic electrode under solar irradiation was the Cr_2O_3/CuO heterostructure -0.834 mA cm^{-2} (-0.6 V vs. Ag/AgCl) compared to pristine CuO and Cr_2O_3.

Acknowledgements

The authors are thankful to Çukurova University, Science and Letters Faculty, Chemistry Department, Physical Chemistry Research Laboratory and Tarsus University for laboratory studies.

References

Acar, C., & Dincer, I. A review and evaluation of photoelectrode coating materials and methods for photoelectrochemical hydrogen production. International Journal of Hydrogen Energy, 41, (2016).

Anctil, A., Beattie, M. N., Case, C., Chaudhary, A., Chrysler, B. D., Debije, M. G., Essig, S., Ferry, D. K., Ferry, V. E., & Freitag, M.. Status report on emerging photovoltaics. Journal of Photonics for Energy, 13, (2023).

Chehade, G., & Dincer, I. Progress in green ammonia production as potential carbon-free fuel. In Fuel, 299, (2021).

Jeong, D., Jo, W., Jeong, J., Kim, T., Han, S., Son, M. K., & Jung, H. Characterization of Cu_2O/CuO heterostructure photocathode by tailoring CuO thickness for photoelectrochemical water splitting. RSC Advances, 12, (2022).

Joy, J., Mathew, J., & George, S. C. Nanomaterials for photoelectrochemical water splitting – review. In International Journal of Hydrogen Energy, 43, (2018).

Li, X., Zhao, L., Yu, J., Liu, X., Zhang, X., Liu, H., & Zhou, W. Water Splitting: From Electrode to Green Energy System. In Nano-Micro Letters,12, (2020).

Mohd Nasir, S. N. F., & Mat-Teridi, M. A. Photoelectrochemical tandem cell of Se/BiVO4 photoanode and Cr_2O_3/CuO:Ni photocathode in aqueous medium. Journal of Sol-Gel Science and Technology, 93, (2020).

Siavash Moakhar, R., Hosseini-Hosseinabad, S. M., Masudy-Panah, S., Seza, A., Jalali, M., Fallah-Arani, H., Dabir, F., Gholipour, S., Abdi, Y., Bagheri-Hariri, M., Riahi-Noori, N., Lim, Y. F., Hagfeldt, A., & Saliba, M. Photoelectrochemical Water-Splitting Using CuO-Based Electrodes for Hydrogen Production: A Review. In Advanced Materials, 33, (2021).

Tiwari, S., Kumar, S., & Ganguli, A. K. Role of MoS2/rGO co-catalyst to enhance the activity and stability of Cu_2O as photocatalyst towards photoelectrochemical water splitting. Journal Of Photochemistry and Photobiology A-Chemistry, 424, (2022).

Zhang, X., Zhang, S., Cui, X., Zhou, W., Cao, W., Cheng, D., & Sun, Y. Recent Advances in TiO_2-based Photoanodes for Photoelectrochemical Water Splitting. In Chemistry - An Asian Journal 17, (2022).

Hydrogen generation from ethylenediamine bisborane solution with metal catalyst coated on metal oxide / reduced graphene oxide

[1]Burak Uygar Mert Yorgun, [1*]Gülay Özkan, [2]Göksel Özkan
[1]Ankara University, Engineering Faculty, Department of Chemical Engineering, Ankara, 06100, Türkiye
[2] Gazi University, Faculty, Department of Chemical Engineering, Ankara, 06570 Maltepe, Türkiye

* E-mail: gozkan@ankara.edu.tr

Abstract
Hydrogen generation by the hydrolysis of aqueous ethylenediamine bisborane (EDAB) solutions was studied using lithium cobalt oxide ($LiCoO_2$) and reduced graphene oxide (rGO) supported Pd catalysts. Initially, graphene oxide was synthesized by the Hummers and Tour methods. Then, 3.75%, 7.5% Pd@rGO and 3.75% Pd@$LiCoO_2$ catalysts by mass were synthesized. Characterization of the catalysts was determined by FTIR, SEM-EDX, BET, XPS, TEM and XRD analyses. Hydrolysis reactions were carried out at two different temperatures (50, 70℃) and EDAB concentrations (0.02M, 0.03M). The performance of the rGO supported catalyst was better then that of $LiCoO_2$ supported catalyst. The highest hydrogen generation rate (HGR) was obtained in 0.02M EDAB hydrolysis as 502,5 mL/min.$g_{catalyst}$ for 7,5% Pd@rGO catalyst at 70℃.

Keywords: Etylenediamine bisborane, dehydrogenetion, graphene oxide, lithium cobalt oxide

I. Introduction

Hydrogen production from non-fossil sources is important for sustainable energy. Since transporting explosive and flammable hydrogen gas is dangerous, hydrogen production by hydrolysis of stable hydrogen-rich materials has been studied by several researcher in literature (Özkan et al., 2019, Önder et al 2020, Bayram et al.,2024). Hydrolysis of boron derivatives such as $LiBH_4$ (18.5wt% hydrogen), $NaBH_4$ (10.8wt% hydrogen), NH_3BH_3 (AB,19.6wt% hydrogen), ethane 1,2 diamine borane (EDAB, $BH_3NH_2CH_2CH_2NH_2BH_3$,11.4wt% hydrogen) can produce hydrogen rapidly, in large quantities and without any fuel cell poisons. In this study, EDAB was chosen as the hydrogen storage material. EDAB exhibits good kinetic stability at ambient conditions and more stable than AB at temperatures below 100°C.

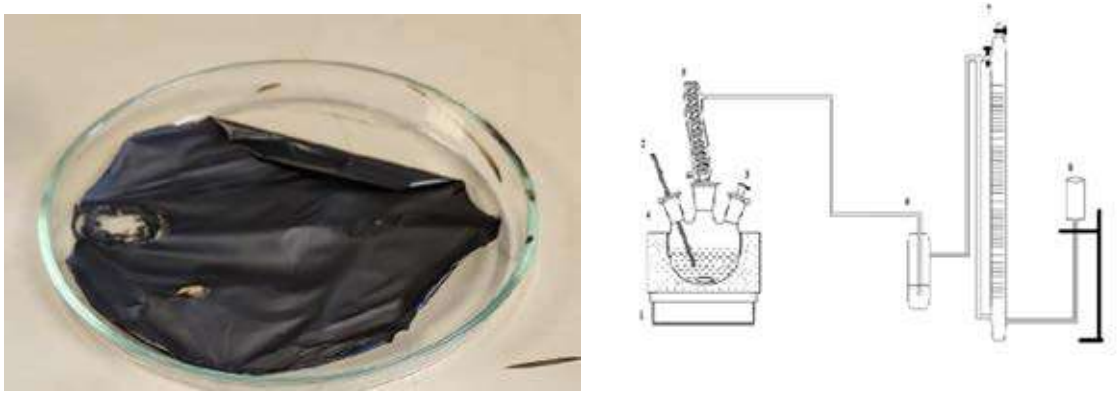
Carrying out hydrolysis quickly and efficiently requires the presence of active catalysts. For this reason, metal nanocatalysts such as Ag, Cu, Co, Ni, Pd are used in EDAB hydrolysis. (Durgut et al., 2020; Ozay et al., 2020). Graphene is simply just a single atomic layer of graphite. It has created an increase in nanometric-scale research activities in recent years due to its high current density, chemical inertness, high thermal conductivity, optical transmittance, unique surface area and superhydrophobicity. Today, graphene-based nanostructures are at the top of candidate lists for many new advanced applications, from energy storage to encapsulation and medical applications. Graphene nanostructures should be used as graphene oxide(GO), reduced graphene oxide(rGO), nanocomposites and hybrid nanostructures to reach their full potential in these applications (Choi et al. 2011).

A limited number of catalyst systems have been studied so far in hydrogen production from EDAB. Palladium and nickel-based catalysts have been shown to facilitate the dehydrogenation of EDAB, AB. However, there has been no information in the published literature that would give catalytic hydrolysis of EDAB performed in the presence of Pd@rGO(H), Pd@rGO(T) and Pd@$LiCoO_2$ catalysts. Therefore, we focused hydrolysis of EDAB and in the presence of Pd doped rGO and $LiCoO_2$ catalysts. First, GO was synthesized by the Hummers(H) and Tour(T) methods. Then, catalysts (Pd@rGO(H), Pd@rGO(T), Pd@$LiCoO_2$) loaded with different amounts of Pd metal were obtained using the hydrothermal method. Finally, EDAB hydrolysis was carried out.

II. Experimental Set-up and Procedure

Graphene oxide was produced from graphite powder by the hummers (Figure 1a, GO(H)) and tour (GO(T)) methods according to the literature (Hummers et al., 1958; Tour et al., 2010). Using $PdCl_2$ solution, 3,75% Pd@rGO, 7,5% Pd@rGO catalysts (Hummers) by weight were produced by hydrothermal method in a stainless-steel autoclave (Cao et al., 2015). Pd@$LiCoO_2$ catalyst was obtained by first wet impregnation and then reduction in a tube furnace in He and H_2 atmosphere. Additionally, 5%Pd@rGO(T) catalyst was synthesized by hydrothermal method.

The hydrolysis experimental system is shown in Figure 1(b). EDAB used for hydrolysis experiments was synthesized in the laboratory with high purity (Schneider et al, 1961). In the experiments, EDAB was dissolved in 3 mL of pure water with the help of sonication. When the mixture became homogeneous, it was drawn into the syringe until there was no air left in it. The determined amount of catalyst (0.02g) was placed in the 3-neck reactor by adding 3mL of pure water and a magnetic stirrer. When the expected temperatures were reached, after checking for leaks, the syringe was injected into the system and the experiment was started, and the magnetic stirrer was started at the same time. The hydrogen formed in the gas burette was observed, measured and recorded. In order to prevent the formation of different gases, 0.3M HCl was filled into the washing solution. In this way, experiments were carried out with high accuracy. In the experiments, temperatures (50℃, 70℃), metal loading and EDAB concentration (0.02 M, 0.03 M) parameters were examined.

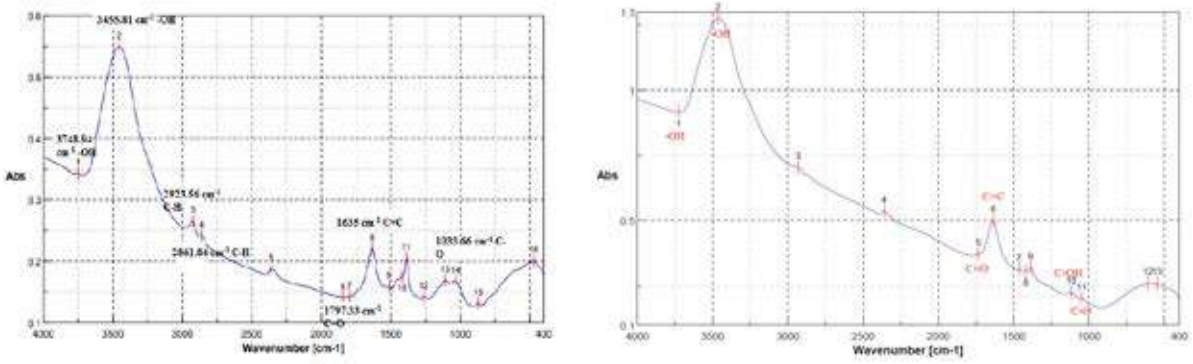


(a) (b)

Fig. 1: (a) GO(H) in the form of an oven-dried film (b) Catalytic hydrolysis experimental setup of EDAB (1) heater-magnetic stirrer plate, (2) thermometer, (3) EDAB-water solution, (4) three-necked glass flask (5) reflux, (6) washing bottle, (7) gas burette system (8) dropping funnel (Angı et al., 2022).

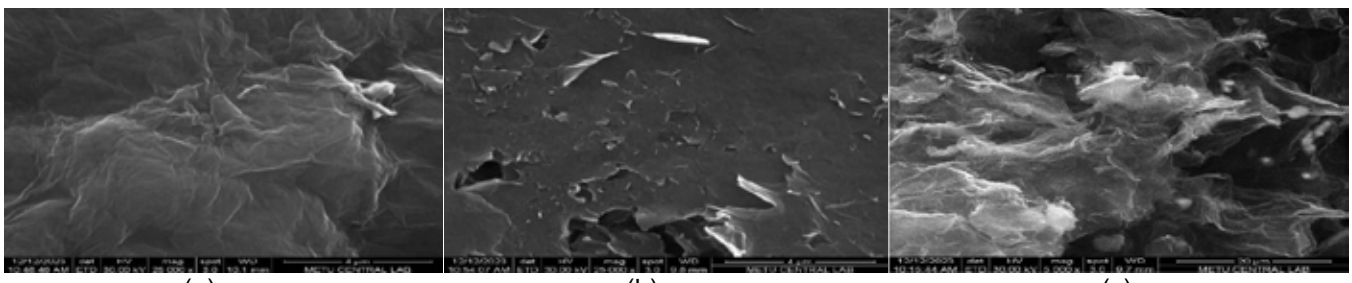
III. Analysis

FTIR spectra of GO(H) and GO(T) structures between 4000-400 cm^{-1} are shown in Figure 2. For GO(H), the bands of 3748.94 cm^{-1} and 3455.81 cm^{-1} in the high frequency area, with a broad peak, correspond to the stretching and bending vibration of –OH groups originating from water molecules adsorbed on graphene oxide. The band belonging to the carbonyl group (C=O) stretching was observed at 1797.33 cm^{-1}. Finally, the absorption peaks at 1385 and 1033.66 cm^{-1} correspond to stretching vibration of carboxylic acid (C-O) and stretching vibration of alcohol (C-OH), respectively. Presence of these oxygen-containing groups reveals that graphite is oxidized. Polar groups cause hydrogen bonds to form between graphite and water molecules. This also explains the hydrophilic nature of graphene oxide (Shahriary et al., 2014). Similarly characteristic peaks of GO(T) was marked in Figure 2(b).



(a) (b)

Fig.2: FTIR analysis for GO(H) (a) and GO(T) (b).



(a) (b) (c)

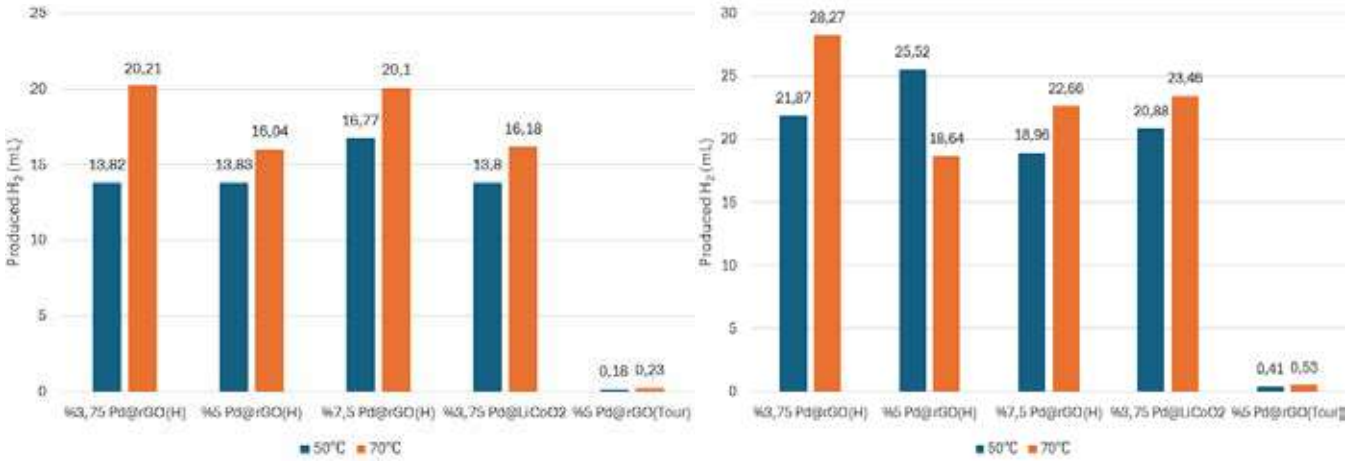
Fig. 3: SEM images of GO(H) (a), GO(T) (b) and (c) %3,75 Pd@rGO.

SEM images of GO(H), GO(T) and %3,75 Pd@rGO catalyst are shown in Figure 3. Figure 3(a) shows structure consisting of well-separated graphite layers due to high oxygen contents and more efficient insertion of oxygen atoms between graphene layers. In recent study observed large and rather wrinkled graphite layers means that there was a deterioration in graphene layers due to oxygen binding and that large nanolayer sizes were preserved (Muzyka et al., 2017). While GO(H) images showed a wavy, wrinkled and layered structure with a larger layer size,

GO(T) exhibited a smoother surface with an ultra-thin film morphology (Yadav et al., 2019). The only difference is the occasional erosion and layered structures. It is thought that this may be due the drying temperature being 70 °C and not using a vacuum oven. Figure(c) shows Pd nanoparticles distributed almost evenly throughout, clearly visible as white dots, and exhibiting no agglomeration.

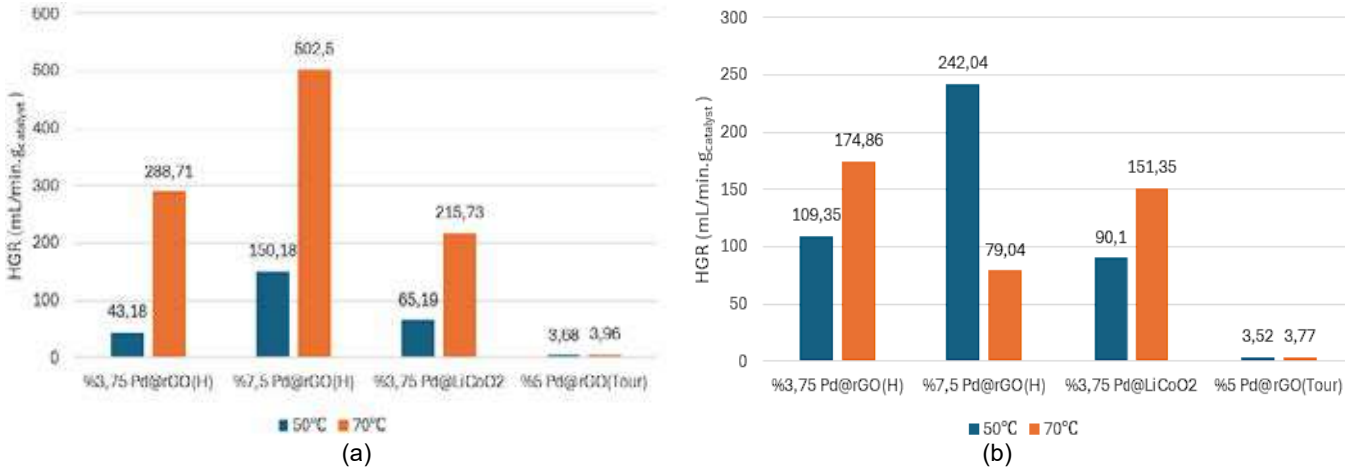
IV. Results and discussions

Characterization of the catalysts was determined by FTIR, SEM-EDX, BET, TEM, XPS and XRD analyses. Using the synthesized catalysts, catalytic hydrolysis reactions were carried out at two different EDAB concentration (0.02M, 0.03M), metal loading and temperatures (50,70℃). As shown in Fig.4, no hydrogen generation was observed for 5% Pd@rGO(T) suggesting that rGO(T) have no catalytic activity for the hydrolysis of EDAB due to defects caused by the surface morphology (low-layer, impermeable) as seen in the SEM images. 7,5% Pd@rGO catalyst completed the reaction in the shortest time (120 seconds) in the hydrolysis of 0.02M EDAB at 70℃. The longest reaction was found in 0.02M EDAB hydrolysis with 3.75% Pd@rGO catalyst (960 seconds). Hydrogen generation rates (HGR) was calculated and shown in Fig.5(a,b). The highest HGR was calculated as 502,5 mL/min.$g_{catalyst}$ for 7,5% Pd@rGO catalyst in 0.02M EDAB hydrolysis at 70℃. The highest HGR for 0.03M EDAB hydrolysis was calculated as 242,04 mL/min.$g_{catalyst}$ for 7,5% Pd@rGO catalyst at 50℃.



(a) (b)

Fig. 4: Amounts of H_2 produced by EDAB hydrolysis (a) 0.02M EDAB, (b) 0.03M EDAB



(a) (b)

Fig.5: Hydrogen generation rates (HGR) for EDAB hydrolysis (a) 0.02M EDAB, (b) 0.03M EDAB

V. Conclusions

We observed that activity of Pd@rGO/$LiCoO_2$ catalysts in hydrogen production by EDAB hydrolysis varies with loading rates and reactor temperature. The folded, wrinkled, layered structure of rGO catalyst has increased the catalytic effect positively as support material. In the 0.02M EDAB parameter, reaction time decreased significantly as the temperature increased. Reaction times for the 0.03M EDAB parameter took longer compared to the 0.02M EDAB parameter. The increase in the amount of EDAB in solution had a limiting effect on the reaction speed and hydrogen production.

Acknowledgements

We are thankful to ANKARA University BAP for financially supporting this work (FYL-2022-2329)

References

Angı O.S., Murathan H.B., Özkan G., Özkan G., Non-linear kinetics analysis of catalytic hydrolysis of ethylenediamine bisborane with nano-structured Pd/TiO2 catalyst, International Journal of Hydrogen Energy, 47, 40430-40444, (2022)

Bayram O, Murathan HB, N, Angı Os, Özkan G, Özkan G Innovation in the synthesis of hydrazine borane by mechanochemical method and hydrolysis of hydrazine borane with Pd/TiO2 catalyst, Materials Chemistry and Physics, 2024 be press.

Durgut, S., & Ozay, H. , Ag (0) nanocatalyst stabilized with networks of p (SPA-co-AMPS) for the hydrogen generation process from ethylenediamine bisborane hydrolysis. International Journal of Hydrogen Energy, 45(35), 17649-17661 (2020).

Hummers, W. S., & Offeman, R. E. , Functionalized graphene and graphene oxide: materials synthesis. J Am Chem Soc, 80, 1339-1344 (1958).

Mishra, S. S., Yadav, T. P. , Mukhopadhyay, N. K., & Srivastava, O. N.. Synthesis of fine skeletal structure on Al–Cu–Co decagonal quasicrystals for hydrogen production through steam reforming of methanol. International Journal of Hydrogen Energy, 45(46), 24491-24501 (2020).

Muzyka, R., Kwoka, M., Smędowski, Ł., Díez, N., & Gryglewicz, G. Oxidation of graphite by different modified Hummers methods. New Carbon Materials, 32(1), 15-20 (2017).

Onder, A., & Ozay, O., Fly ash as catalyst support material in the hydrolysis of ethylenediamine bisborane for hydrogen production: The use of coal-fired power plant waste. International Journal of Hydrogen Energy, 45(20), 11651-11661 (2020).

Ozkan G., Akkuş M., Ozkan G.,The effects of operating conditions on hydrogen production from sodium borohydride using Box-Wilson optimization technique,International Journal of Hydrogen Energy, 44, 9811-9816 (2019).

Wang, C., Wang, Q., Fu, F., & Astruc, D., Hydrogen generation upon nanocatalyzed hydrolysis of hydrogen-rich boron derivatives: recent developments. Accounts of Chemical Research, 53(10), 2483-2493 (2020).

Yadav, N., & Lochab, B. , A comparative study of graphene oxide: Hummers, intermediate and improved method. FlatChem, 13, 40-49 (2019).

INVESTIGATION OF THE USE OF CARBON-BASED SUPPORTS IN THE CATALYTIC HYDROLYSIS OF ETHYLENEDIAMINE BISBORANE

[1]Bensu Naz Örs, [1*]Gülay Özkan, [2]Göksel Özkan
[1] Ankara University, Engineering Faculty, Department of Chemical Engineering, Ankara, 06100, Türkiye
[2] Gazi University, Engineering Faculty, Department of Chemical Engineering, Ankara, 06570 Maltepe, Türkiye

* E-mail:gozkan@ankara.edu.tr

Abstract
In this study, the effect of the heterogeneous catalysis systems formed by reduced graphene oxide and activated carbon, which are carbon-based support materials, with Pd and Co metals, on the hydrolysis of ethylenediamine bisborane (EDAB) was observed. For this purpose, activated carbon obtained from the Pavlonia tree and graphene oxide produced using the Hummers method were used as support materials. Pd and Co metals were loaded onto the support materials by the impregnation-reduction method, first separately at 5% by mass, and then together at 2.5% by mass of each. EDAB hydrolysis was carried out at 50 and 70℃ temperatures and different EDAB concentrations (0.02 M, 0.03 M) using the gas burette system. Catalyst characterizations were carried out by FTIR, SEM-EDX, TEM, BET, XRD and XPS analyses.

Keywords: Etyhlenediamine bisborane, catalytic hydrolysis, hydrogen generation

I. Introduction

As fossil fuels, which provide our energy needs, are becoming depleted and environmental concerns have led to a trend towards hydrogen energy, one of the renewable energy sources(Schlapbach et al., 2001). Sodium borohydride, ammonia borane and ethylenediamine bisborane (EDAB) stand out with their high hydrogen storage capacities (10.8%, 19.6%, 11.5%, respectively). Since EDAB is a substance that does not release volatile borazine and its derivatives as a result of hydrolysis, releases hydrogen quickly and has a low exothermic enthalpy. Metals and their alloys such as Ag, Au, Co, Pd and Pt are generally used as catalysts in hydrogen production (Angı et al.,2022). When metals are used alone as catalysts, they can oxidize and lose their stability, and particle agglomeration may occur. Therefore, homogeneous distribution of the catalyst must be ensured by using support material (Leardini et al., 2014).

Carbon-based support materials are frequently used today because they have a large surface area, large pore volume, and can be produced easily and cost-effectively (Onder et al., 2020). Graphene oxide (GO), a carbon-based support material, can be produced from graphite, with high efficiency using chemical methods. Due to the oxygen and hydroxyl groups in its structure, it dissolves easily in solvents and this feature prevents clumping. By removing the oxygen-containing groups in its structure, it turns into reduced GO, a graphene-like structure. There are many methods (Brodie, Staundenmaier, Tour and Offeman-Hummers) in the production of GO, but GO can be produced more safely with the Hummers method.

Activated carbon (AC) is one of the most preferred adsorbents due to its large surface area, high adsorption capacity and ability to be produced at low cost. AC was previously generally obtained from coal, but since this method is costly, studies have been carried out on methods of obtaining activated carbon from vegetable raw materials. In this way, waste plant materials are brought into the economy and it is more economical to obtain activated carbon. (Yorgun et al., 2016)

In the article, firstly, the PdCo@AC, Co@AC, PdCo@RGO, and Co@RGO catalysts prepared by the impregnation method are studied. Secondly, Cataltyic hydrolysis of EDAB was carried out.

II. Experimental Set-up and Procedure

The activated carbon used in the study was obtained from the Pavlonia tree (Yorgun et al., 2016). Graphene oxide was produced by the Hummers method. To load the metal nanoparticles, the wet impregnation method was applied by taking the required amounts of $PdCl_2$ and $CoCl_2$ solutions and adding them to the support materials. The catalysts subjected to the wet impregnation method were then thermally reduced in a tube furnace in a hydrogen and helium atmosphere at 550℃ for 2 hours. EDAB, used as a hydrogen source, was synthesized under laboratory conditions for experimental studies (Murathan et al., 2024, Murathan et al.,2023). The synthesized EDAB was dissolved in 2.5 ml of pure water in an ultrasonic bath, withdrawn with the help of a syringe, and fed into the batch reactor during the experiment. In order to prevent gases other than hydrogen from reaching the burette during feeding, 0.2 M HCl was placed in the middle of the experimental system as a washing solution. The three-mouthed flask used as a batch reactor contains 0.02 grams of catalyst, 2.5 ml of water and a magnetic stirrer. Hydrolysis experiments are started when the system temperature becomes stable and gas leakage checks are completed. The gas volume values coming out of the burette were measured and noted. Temperature (50, 70℃) and EDAB concentration (0.02 M, 0.03 M) were selected as experimental parameters.

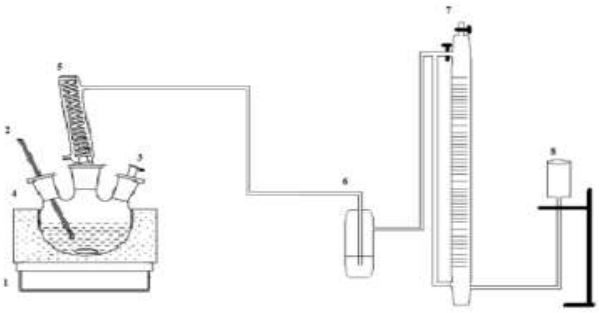


Fig. 1: Catalytic hydrolysis of EDAB experimental setup ((1) heater-magnetic stirrer plate, (2) thermometer, (3) EDAB-water solution, (4) three-necked glass flask (5) reflux, (6) washing flask, (7) gas burette system (8) dropping funnel

III. Analysis

The FTIR spectrum of graphene oxide produced by the Hummers method is as shown in the Figure 2. It can be said that the stretch in the 3741 cm^{-1}, 3455 cm^{-1} and 3424 cm^{-1} bands belong to -OH stretching. It is estimated that the stretch observed at 1797 cm-1 belongs to the C=O stretch and at 1619 cm^{-1} is C=C sp^2 stretch band. The characteristic peaks that graphene oxide should have were obtained in accordance with the literature. (Marcano et al., 2010)

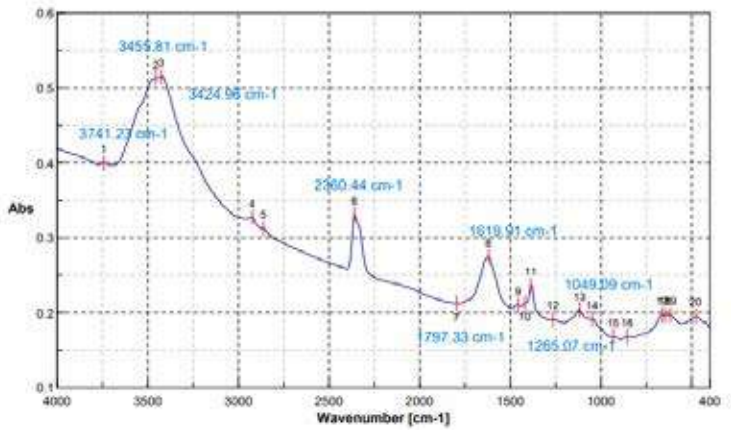


Fig. 2: Graphene Oxide FTIR Spectrum

Table 1.Graphene oxide FTIR results

Wavelength (this study)	Literature (cm^{-1})	Surface group
3741 *3455* *3424*	*3420*	*-OH stretch band*
1797	*1720-1740*	*C=O stretch band*
1619	*1590-1620*	*C=C sp^2 stretch band*
1265 (epoxy) *1049 (alkoxy)*	*1250*	*C-O stretch band*

The FTIR spectrum for activated carbon produced from the pavlonia plant is shown in the Fig 3. The stretches in the 2923.56 cm^{-1} and 2861.84 cm^{-1} bands show CH_2 stretches. The stretch in the 1612.2 cm^{-1} band symbolizes the C=C stretches in the aromatic ring. The stretch at 1457.92 cm^{-1} represents the C=O stretch in the ether group. The 1249.65 cm^{-1} stretch belongs to the C=O stretch in the ester or epoxy group. (Terzyk et al., 2001)

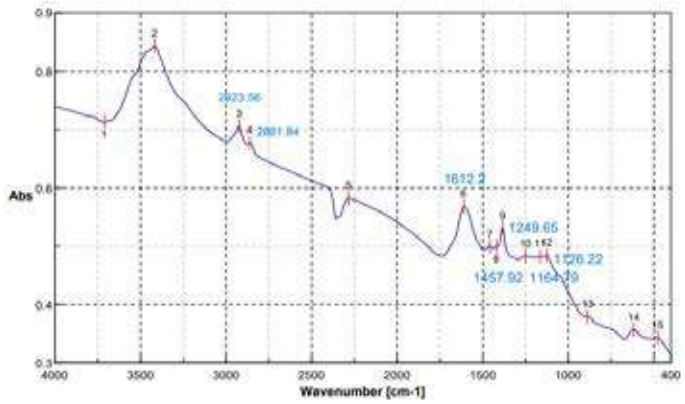


Fig. 3: Activated carbon FTIR spectrum

Table 2. Activated carbon FTIR results

Wavelength (this study)	Literature (cm^{-1})	Surface group
2923.56	*2921.88*	*CH_2 asymmetrical stretch band*
2861.84	*2852.74*	*CH_2 symmetrical stretch band*
1612.2	*1629.33*	*C=C stretch band (aromatic rings)*
1457.92	*1458.80*	*C=O stretch band (ethers)*
1249.65	*1243.13*	*C=O stretch band (esters or epoxides)*
1164.79	*1157.69*	*C=O=C stretch band*
1126.22	*1111.98*	*-OH stretch band*

SEM images of the synthesized PdCo@AC catalyst obtained at different magnification rates are shown in the Fig.4. RGO surface topography shows a wavy structure and its layers are intertwined. Van der Waals bonds in its structure cause it to have a membranous appearance and it can be said that it has a translucent structure. Metal particles are evenly distributed on the RGO support material. (Gul et al., 2023)

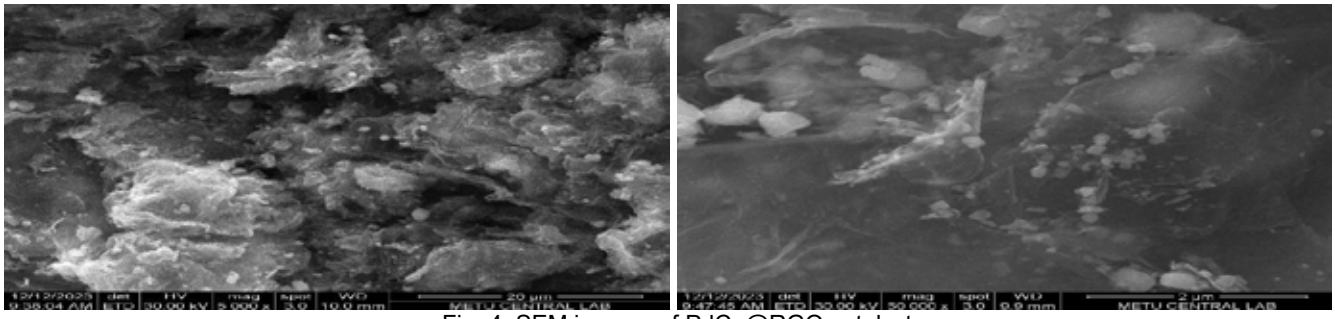


Fig. 4: SEM images of PdCo@RGO catalyst

SEM images of the synthesized PdCo@AC catalyst using the impregnation method at different magnituede is given in the Figure 5. As can be seen, the surface topography of activated carbon has a hexagonal honeycomb-like appearance. Metal nanoparticles are distributed homogeneously within these structures. The porous structure of activated carbon exposed to a carbonization temperature of 500 ^{0}C (Saka et al., 2012)

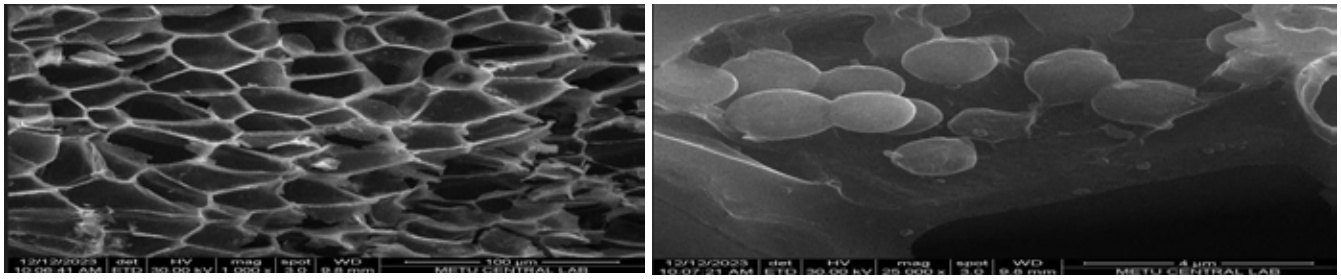


Fig. 5: SEM images of PdCo@AC catalyst

IV. Results and discussions

Catalytic hydrolysis experiments were carried out at the different experimental conditions. As seen in the Fig 6., The PdCo@AC catalyst provided the highest H_2 volume at both temperatures, but the experiment time for this catalyst was longer than other catalysts. According to the hydrogen production rate (HGR) comparison, PdCo@RGO catalyst was the most effective catalyst in the EDAB hydrolysis experiments within the scope of this study, at 70 ℃ temperature and 0.03 M EDAB concentration, with 563,03 ml/min.g cat.

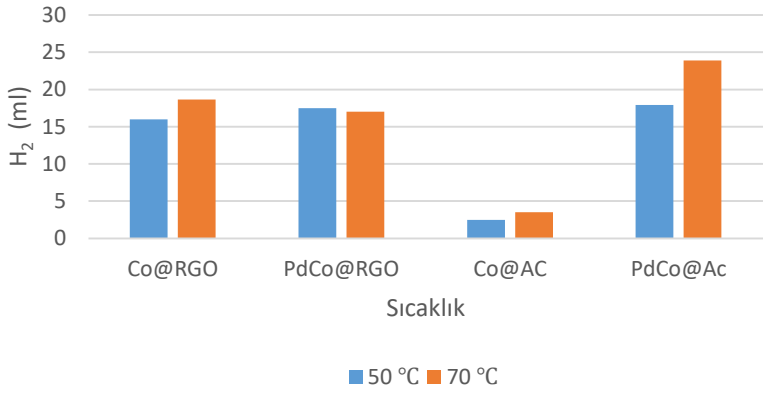


Fig. 6: Hydrolysis results at two different temperatures and EDAB concentrations

V. Conclusions

In this study, the performances of heterogeneous catalysis systems formed by loading Pd-Co nanoparticles on RGO and AC supports in the catalytic hydrolysis of EDAB were examined. When the performances of the catalysts were compared in terms of hydrogen production rates (HGR), it was observed that the PdCo@RGO catalyst exhibited the best performance with 563,03 ml/min.gcat. Although activated carbon-supported catalysts provide high hydrogen volume, hydrogen production rates were observed to be lower than graphene based catalysts. As a result of the studies, it was observed that the Co@AC catalyst did not show catalytic activity in EDAB hydrolysis in these parameters.

Acknowledgements

The authors appreciate the financial support from the TUBITAK within the application “1649B022305595" . Also, The authors would like to thank Prof.Dr. Said Yorgun (Department of Chemical Engineering, Engineering and Architecture Faculty, Eskisehir Osmangazi University, Eskisehir, Turkey) who supplied the Active carbon

References

Angı, O. S.,Murathan,H. B., Ozkan G. and Ozkan G. Non-linear kinetic analysis of catalytic hydrolysis of ethylenediamine bisborane with nanostructured Pd/TiO_2 catalyst. Int J Hydrogen Energy, 47, 40430-4044 (2022).

Murathan H. B., Özkan G., Özkan G., Catalytic dehydrogenation of ethylene diamine bisborane in ethylene diamine media , Int J Hydrogen Energy,51,38-3978 (2024)

Murathan H. B., Özkan G., Özkan G., Hydrogen generation from the hydrolysis of ethylenediamine bisborane using Ni/NixBy-Zr and Pd-Ni/NixBy-Zr as highly active catalysts, Environmental Progress and Sustainable Energy , 42, 4 (2023)

Gul, W., Akbar Shah, S. R., Khan, A., Ahmad, N., Ahmed, S., Ain, N., ... & Khan, R. Synthesis of graphene oxide (GO) and reduced graphene oxide (rGO) and their application as nano-fillers to improve the physical and mechanical properties of medium density fiberboard. *Frontiers in Materials*, *10*, 1206918. (2023).

Leardini, F., Valero-Pedraza, M. J., Perez-Mayoral, E., Cantelli, R., & Bañares, M. A.,Thermolytic decomposition of ethane 1, 2-diamineborane investigated by thermoanalytical methods and in situ vibrational spectroscopy. The Journal of Physical Chemistry C, 118(31), 17221-17230 (2014).

Marcano, D. C., Kosynkin, D. V., Berlin, J. M., Sinitskii, A., Sun, Z., Slesarev, A., ... & Tour, J. M., Improved synthesis of graphene oxide. ACS nano, 4(8), 4806-4814(2010).

Saka, C., BET, TG–DTG, FT-IR, SEM, iodine number analysis and preparation of activated carbon from acorn shell by chemical activation with $ZnCl_2$. Journal of Analytical and Applied Pyrolysis, 95, 21-24.(2012).

Schlapbach, L. and Zuttel, A. Hydrogen-storage materials for mobile applications. Nature, 414, 353-358 (2001).

Terzyk, A. P., The influence of activated carbon surface chemical composition on the adsorption of acetaminophen (paracetamol) in vitro: Part II. TG, FTIR, and XPS analysis of carbons and the temperature dependence of adsorption kinetics at the neutral pH. Colloids and Surfaces A: Physicochemical and Engineering Aspects, 177(1), 23-45 (2001).

Yorgun, S., Yıldız, D., & Şimşek, Y. E., Activated carbon from paulownia wood: Yields of chemical activation stages. Energy Sources, Part A: Recovery, Utilization, and Environmental Effects, 38(14), 2035-2042 (2016).

Analysis of Real Grid Voltage Fluctuation Problem with Nickel Hydrogen Batteries Using DIGSILENT Program

[1*]Hulusi Faik Orhan, [1]Abuzer Çalişkan
[1]Fırat University, Faculty of Engineering, Electrical and Electronics Engineering, Elazığ, 23100, Türkiye

* E-mail: hulusiorhn98@gmail.com

Abstract
The studies related to the storage of electrical energy in the world date back to the early 1800s. One of the most significant limitations to the use of solar energy and wind energy, which will see increased effective usage in the coming years, is their intermittency. These energies can be used effectively during their availability, but they become inactive during periods without radiation or wind. This situation has brought up the necessity of storing the energy obtained from these systems for later use. Besides being stored for the sake of supply security, energy storage systems have become crucial for preventing line fluctuations that may occur when energy is not drawn from the interconnected system and for maintaining grid quality. In recent years, fuel cell systems, which have also started to be used in storage systems, have been examined on an actual grid using the DIgSILENT Power Factory program with Nickel Hydrogen Storage systems. There is no study in the literature that operates and analyzes storage systems using the DIgSILENT Power Factory program. In this study, Nickel Hydrogen battery systems, which will bring a new perspective to the batteries in storage systems, will be examined in terms of grid solutions.

Keywords: Hydrogen Storage System, Nickel Hydrogen, Digsilent Power Factor

I. Introduction

The climate crisis caused by carbon emissions has made alternative energy systems and energy storage systems crucial for a sustainable world. The European Union aims for solar power plants and wind farms to produce 50% of the countries' electricity by 2030 and 80% by 2050 from renewable energy sources (Manthiram, 2015). Furthermore, as a result of the requirements of the Paris Climate Agreement, the EU has set its goal to reduce greenhouse gas emissions across the economy by at least 40% by 2030. Achieving such a significant contribution from renewable energy sources necessitates the use of storage systems. The primary issue with these energy systems arises during periods of minimum consumption. This situation brings many problems in interconnected systems (such as system outages and consumer product failures due to line voltage increases). In recent years, storage systems have emerged as the most critical systems to be considered for maintaining high-quality energy and balancing energy supply and demand. Energy storage systems balance the supply of electricity and load demand (Wen, J, 2012). Even when connected to the grid, a storage device is needed to smooth out the output. Additionally, when the input from renewable sources to the grid exceeds approximately 10%, energy storage becomes necessary (Lin, RH, 2019). Efficient energy storage is considered the key to a successful and holistic transition to renewable energy sources. Electrochemical energy storage technologies play and will continue to play a significant role in achieving this desirable goal, particularly for mobile devices and the transportation sector, as well as for stationary storage (Du, Z, 2021). In this context, nickel hydrogen storage systems stand out in the field of energy storage systems. The supply of hydrogen for fuel cells is the most significant barrier to their being considered green storage solutions. This is because, in most cases, hydrogen is produced from fossil fuels and has a carbon footprint. Ideally, however, fuel cells would use "green" hydrogen obtained from renewable sources such as solar and wind energy. A fuel cell combines oxygen and hydrogen to produce electricity, resulting in water as its byproduct. The production of water as waste makes the fuel cell a promising power source (Barbir, F, 2005). Hydrogen energy is regarded as the ultimate energy source of the 21st century due to its low carbon emissions, flexibility, and high efficiency in harnessing various sources. Hydrogen is a promising energy source with the potential to play a significant role in the global energy mix in the coming years. Its unique properties make it a versatile fuel source that can be used in various applications, from transportation to power generation and industrial processes. Hydrogen is the most abundant element in the universe and can be obtained from a wide range of sources, including water, natural gas, and biomass. The production of water vapor as waste highlights its potential to significantly reduce greenhouse gas emissions and air pollution (Dincer, İ, 2020).

Currently, hydrogen can be stored either as a compressed gas or in liquid form. Depending on the type of storage method used, the ratio of stored hydrogen to the weight of the storage container varies between 2% and 68% (Gao, D.,2014)

The utilization of excess electrical energy from alternative energy sources for hydrogen production through electrolysis presents a significant opportunity to mitigate or eliminate the adverse effects of this energy on interconnected systems and loads. Additionally, hydrogen storage provides the advantage of low-loss storage during extended periods of adverse weather conditions (Gray, E. M., 2011)

Storing energy obtained from renewable sources that is not consumed during the production process will be one of the most critical research topics in the coming periods. In this system, hydrogen produced in processes where electrical energy is generated but not consumed will be stored, and fuel cells will ensure the continuity of energy supply in processes where electrical energy cannot be produced, but demand is high.

This study particularly aims to create high-quality energy systems by using storage systems to prevent voltage rise

and fall problems experienced in interconnected systems, through reliable and realistic grid simulation with DIgSILENT analysis. No previous studies in the literature have addressed this issue using the DIgSILENT program.

II. A New Perspective on Energy Storage: Nickel-Hydrogen Batteries

Nickel-hydrogen batteries, which can last for decades with high efficiency and long lifespan, are used in many satellites. Nickel-hydrogen batteries (NHB) have the potential to revolutionize renewable energy and grid-scale energy storage, providing a new perspective on renewable energy sources on Earth. Widely used in spacecraft for their robustness and power, it is worth questioning why these batteries have not yet been utilized in storage systems. Why has such a perfect storage system not been considered until now? The unique chemistry and engineering of these batteries allow them to retain 86% of their capacity after 30,000 cycles or approximately 30 years with zero maintenance. This value translates to a warranty of 20 years/20,000 cycles. Additionally, these batteries are extremely resistant to temperature and can operate very well in extreme temperatures. Nickel-hydrogen batteries can function within a temperature range of -40°C to 60°C. The efficiency of the battery varies between 80% and 90%, depending on the cycle rate. The leveled storage cost for hydrogen storage systems is estimated to be between $200 and $600 per MWh. Hydrogen storage technologies offer a significant advantage in terms of life cycles, with electrolyzers and fuel cells having an operational life of 40,000 to 80,000 hours and storage tanks offering nearly unlimited cycles.

One of the safety concerns with nickel-hydrogen batteries is the storage of hydrogen gas under high pressure. However, tests have shown no explosions or fires in storage systems. Additionally, nickel-hydrogen chemistry does not form dendrites—small, sharp metal structures that accumulate on the anode during charging. Repeated charging cycles can cause dendrites to grow, potentially leading to short circuits that can result in fires or other battery failures.

Nickel-hydrogen storage systems are referred to as "maintenance-free" systems. Hydrogen is the most abundant element in the universe (J.E. Miller, 2017). This abundance simplifies the supply chain and cost issues for nickel-hydrogen batteries (storage systems) compared to other emerging battery technologies (Purushothaman, B. K., 2012). EnerVenue reports that Ni-H batteries are nearly 100% recyclable.

Theoretically, it is reported that the cost of nickel-hydrogen batteries will become competitive in large, grid-scale conditions. This is the area where these batteries are most needed. Nickel-hydrogen storage systems do not require a heating or cooling system. Even in a storage system in the middle of the desert, no maintenance or heating issues arise.

Recent studies have shown that significant cost savings can be achieved by replacing the expensive platinum anode with another anode material. This work was developed by Stanford materials science professor Yi Cui. The latest developments indicate that the platinum catalyst in nickel-hydrogen batteries has been replaced with a bifunctional nickel-molybdenum-cobalt alloy catalyst.

The technologies developed by EnerVenue were commercially successfully implemented in 2022. It is projected that these battery systems will become widespread in the market by the first quarter of 2024. Whether these batteries can solve energy storage issues will be a significant research topic in the coming period.

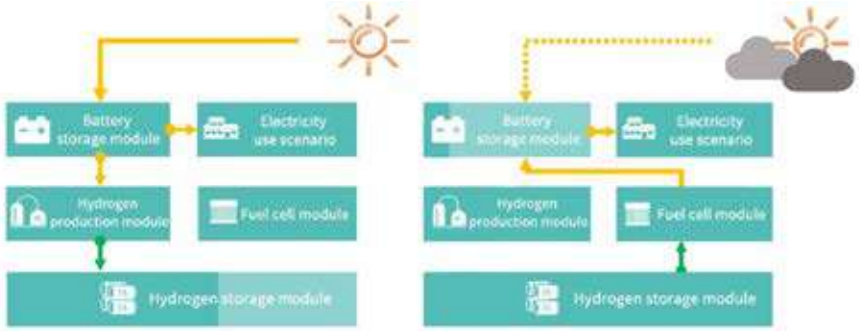


Fig. 1: Grid Energy Transport

Figure 1 illustrates the installation of a fuel cell at a distribution center in a real electrical grid using the DIgSILENT program. Analyses were conducted on this system within the DIgSILENT program. Nickel-Hydrogen batteries, in particular, become challenging in the grid under high power demands. Analyses conducted using DIgSILENT have enabled the reliable evaluation of real field analyses and the achievement of optimal results.

III. DigSILENT Analysis

In Figure 2, a feeder with an average daily active energy demand of 9 MW from the grid was identified as a result of a study conducted under real grid conditions. In Figure 3, approximately 9.5% voltage drop was detected as the line progresses towards the 40th kilometer.

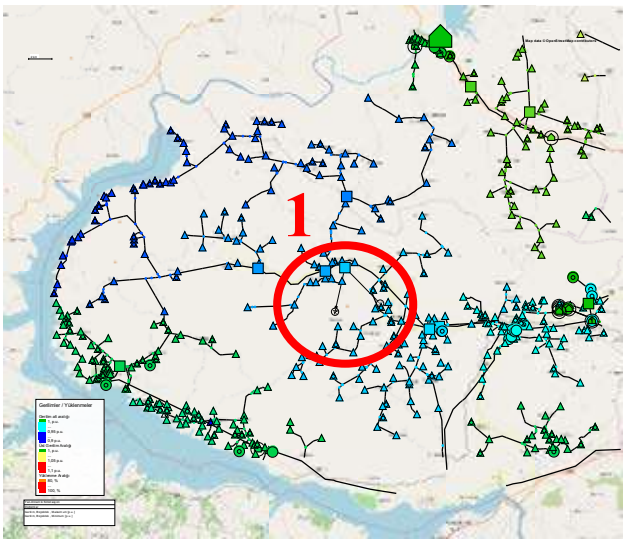


Fig. 2: DigSILENT Grid without Storage System connected

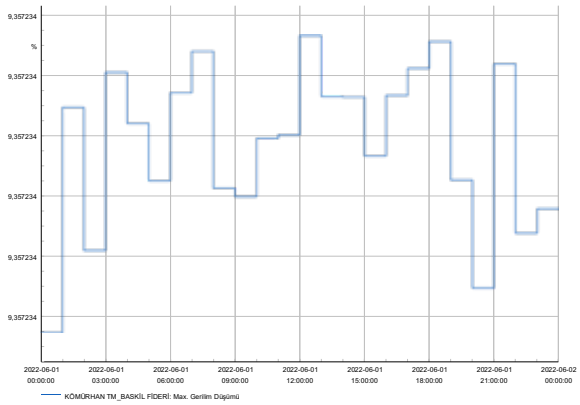


Fig. 3: DıgSILENT Grid Voltage Drop without Storage System connected

Demand load analyses were performed using DIgSILENT, considering one day's working conditions. The legend graph shows a transition from green to dark blue, indicating a percentage increase in voltage drop. The area studied is also indicated within a circle in the figure. Considering the legend graph, it is observed that a voltage drop occurs in this area. In the area marked as number 1 in the figure, hydrogen storage were integrated at the optimum point determined, and analyses of technological differences, triggering counts, and lifespan were conducted regarding the voltage drop.

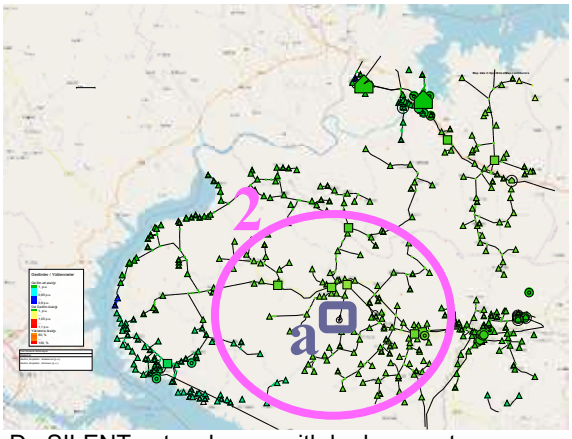


Fig. 4: DıgSILENT network map with hydrogen storage connected

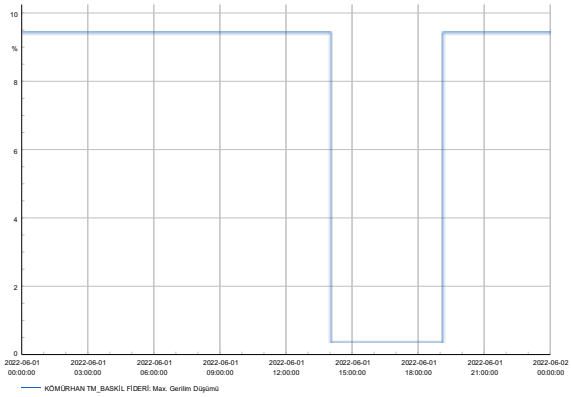


Fig. 5: DıgSILENT grid voltage drop with hydrogen storage connected

In Figure 4, the connection of the hydrogen storage system with the identified optimum point is shown with the gray area. The voltage drop resulting from the analysis conducted with the hydrogen storage system is given in Figure 5. According to the analysis, the hydrogen storage system operated for 4 hours daily, undergoing 3 cycles per day, similar to the lithium-ion battery system. After completing the full charge-discharge cycle, it was observed that it underwent approximately 1000 cycles annually. As a result, unlike lithium-ion batteries, an approximately 10-fold longer lifespan and a usage period of 30 years were determined in the designated area.

IV. Conclusions

In this study, it has been demonstrated that the contribution of storage systems to grid quality can provide a solution, especially in preventing system outages and device damages resulting from voltage surges. This study, which has no counterpart in the literature, will provide a new perspective on storage systems, particularly fuel cells, and create a multiplier effect.

The commercialization process of Nickel-Hydrogen fuel cells and their ability to demonstrate a charge-discharge capacity of 30,000 cycles highlight the necessity for a new analysis of these storage systems using the DIgSILENT program. Following this analysis, the establishment and operational costs of commercialized Nickel-Hydrogen battery systems should also be examined in comparison to lithium-ion battery systems. In these analyses, the ability of Nickel-Hydrogen battery systems to operate over a wide temperature range, and thus not require cellular cooling or heating during operation, may also reveal notable cost differences.

References

Manthiram, A. An outlook on lithium ion battery technology. ACS central science, 3(10), 1063-1069, (2017).

J.E. Miller, F. Lyons, E.L. Christiansen, D.M. Lear, Failure mechanisms of Ni-H2 and Li-Ion batteries under hypervelocity impacts, Procedia Engineering, Volume 204, 2017,Pages 239-246

Purushothaman, B. K., & Wainright, J. S. (2012). Analysis of Pressure Variations in a Low-Pressure Nickel-Hydrogen Battery – Part 1. Journal of power sources, 206, 429.

Gray, E. M., Webb, C. J., Andrews, J., Shabani, B., Tsai, P. J., & Chan, S. L. I. (2011). Hydrogen storage for off-grid power supply. International Journal of Hydrogen Energy, 36(1), 654-663.

Wen, J., Yu, Y., Chen, C. A review on lithium-ion batteries safety issues : existing problems and possible solutions. Materials express , 2 (3), 197-212, (2012).

Lin, RH, Xi, XN, Wang, PN, Wu, BD, & Tian, SM. on hydrogen fuel cell condition monitoring and prediction methods. International Journal of Hydrogen Energy , 44 (11), 5488-5498, (2019).

Du, Z., Liu, C., Zhai, J., Guo, X., Xiong, Y., Su, W., & He, G. A review of hydrogen purification technologies for fuel cell vehicles. Catalysts , 11 (3), 393, (2021).

Barbir, F., PEM “Fuel Cells: Theory and Practice”, Elsevier Academic Press, 2005

Dincer, İ., Ezan, M. A. Tüba-Enerji Depolama Teknolojileri Raporu. (2020)

Gao, D., Jiang, D., Liu, P., Li, Z., Hu, S., & Xu, H. (2014). An integrated energy storage system based on hydrogen storage: Process configuration and case studies with wind power. Energy, 66, 332-341.

Leveraging Machine Learning Methods to Determine the Charging Status and Capacity of Hydrogen-Based Batteries Through Current Analysis

[1*]Yasin Sönmez
[1] Batman University, Technical Vocational School, Computer Technology, Batman, 72100, Türkiye

* E-mail:yasin.sonmez@batman.edu.tr

Abstract

Hydrogen-Based Lithium-ion and lithium-polymer batteries are increasingly prevalent in high-discharge rate applications, particularly in military and civilian systems. These batteries are capable of operating at C-rates exceeding 1 in various applications, from small aerial vehicles to energy transfer systems. However, accurate and precise real-time estimation of the state of charge (SoC) and capacity of the battery is crucial under such high discharge rates. This study aims to conduct a detailed investigation using machine learning methods to categorize the battery's SoC and capacity during discharge based on battery current. Achieving a consistent and accurate estimation with an error margin below 1%, which is not feasible with traditional methods, is essential for ensuring the health, performance, and usability of the battery. Experimental measurements were conducted on lithium-polymer battery cells to collect performance parameters such as battery current, capacity, temperature, and voltage. These data were processed using machine learning algorithms to develop models for predicting the SoC and capacity of the battery during discharge. The results demonstrate that machine learning methods, particularly the Feed Forward Neural Network modeling approach using Butterworth and Hampel filters, can accurately predict the real-time SoC and capacity of the battery with a root-mean-square error (RMSE) below 1%. This achievement represents a significant step forward in battery management and control, offering substantial potential for improving battery performance, durability, and reliability.

Keywords: Hydrogen-Based Battery, Battery status, Battery capacity, Machine learning methods, ANN

I. Introduction

Energy storage systems are becoming increasingly important today due to the widespread use of renewable energy sources, leading to an increased demand for energy storage. Therefore, battery technologies, especially emerging technologies like hydrogen batteries, hold significant potential in the field of energy storage. Batteries have a wide range of applications, from portable devices to electric vehicles and energy storage systems Fei Xia et all (2023). Particularly with the rise of electric vehicles and renewable energy systems, the importance of batteries has further increased. Batteries provide flexibility in energy conversion processes by storing energy and helping balance supply and demand Dos Reis et all (2020).

Hydrogen batteries are a technology of interest, especially in the field of energy storage and portable energy sources Tianhan Gao and Wei Lu (2021). These batteries enable the storage of hydrogen as chemical energy and can be converted back to electrical energy as needed Martin Pham (2023). The charge-discharge processes form the main operational mechanism of hydrogen batteries. There are several advantages to hydrogen batteries, including high energy density, environmental friendliness, ease of integration with renewable energy sources, and long lifespan. These advantages indicate that hydrogen batteries may find a broader range of applications in the future. In conclusion, the importance of battery usage is increasing, and with the development of new technologies, the potential in this field is also growing. Innovative technologies like hydrogen batteries can be a significant solution for energy storage and portable energy solutions Saphra et all (2023).

In the second section of this study, Single-Layer ANN, Cross-validation (with 5-folds cross-validation results presented in the article), and Validation parameters are provided. In the third section, detailed results of battery condition detection with ANN are presented. The final section presents the conclusions of the study.

II. Method

In this study, the open source Hydrogen Fuel Cell Anomoly Detection dataset published by Ranit Sarkar on the Kaggle data sharing platform was used Ranit Sarkar (2024). This data set includes experimental data examining Lithium Ion (Li-ion) charge, discharge and impedance cycles at every stage. The charging cycle process was continued by charging the batteries used during the experiment at a constant current of 1.5A until it reached 4.2V, and then remaining at a constant voltage until the current dropped to 20mA, and the obtained values were added to the data set. Following this process, the batteries were subjected to the discharge process and a different minimum voltage value was determined for each battery used and the discharge cycle was completed with SA constant current. The valuable information obtained during this process was recorded and stored in the data set. In the impedance measurement cycle, data obtained using electrochemical impedance spectroscopy at frequencies from 0.1Hz to 5kHz were recorded. In this study, the data in the Hydrogen Fuel Cell Anomaly Detection dataset was trained using various machine learning models and the K-Fold cross-validation parameter.

ANN – Artificial Neural Network

Artificial neural networks (ANN) are a sub-branch of machine learning. The functioning of the human brain and the communication between neurons are taken as an example in the development of artificial neural networks and are defined as the biggest role model used in the development of this technology Agatonovic-Kustrin, S., and Beresford, R. (2000). ANNs have a wide range of application areas, including image processing, natural language processing, speech recognition, and signal processing. This structure is defined as a program design consisting of mathematical operations known as neurons. Figure 1 shows that the developed artificial neurons are designed to resemble the functions of real neurons in the human brain Kanat, (2020). Transactions in this structure; It proceeds by importing the input data received by the artificial neuron, processing the necessary processing steps and functions, and obtaining the final outputs.

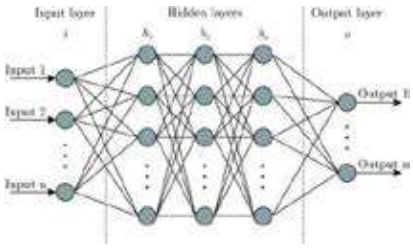


Fig. 1: Artificial neural network architecture

Similar to the human learning process, ANNs follow the path of improving their learning performance through cause and effect relationship. Network performance can be improved by understanding the relationship between input and output data Agatonovic-Kustrin, S., and Beresford, R. (2000). ANNs continue the process by labeling and testing a certain part of the data transferred to the system as a result of the learning process. The network uses certain input and output values obtained from the training data for the labeling process. These values change the parameters of the network, allowing its performance to be increased. ANN structures have three basic layers. These layers are called input layer, hidden layer and output layer. In the input layer, inputs to the neural network and data that can be processed in the network are accepted. Input data received from the network is processed in hidden layers, output results are calculated and transmitted to the output layer Ataseven, B. (2013). Finally, the output layer contains the results. The number and size of hidden layers determine the main differences in ANNs. Features in these layers greatly affect network performance.

Extreme Learning Machines (ELM)

Extreme Learning Machines (ELM) can be defined as a single-layer feedforward neural network. It is a fast and successful learning algorithm based on this definition. ELM includes input layer, hidden layer and output layer structures, similar to feedback ANN structures, as seen in Figure 2. The difference between this structure and ANNs is that it contains a single hidden layer. Thanks to the single hidden layer used, it is aimed to make the training process faster and more effective Wang et all (2022), Huang et all (2011). In this layer, weights are chosen randomly and are not updated, operations continue with fixed weights. It appears that a significantly faster training process is achieved when compared to traditional ANN methods.

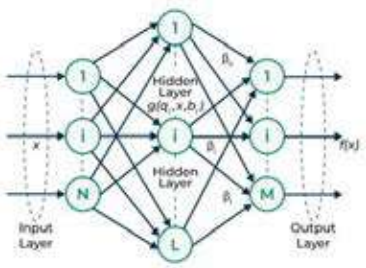


Fig. 2: Extreme Learning Machines architecture

In this study, the ELM method was used on Hydrogen Fuel Cell Anomaly Detection data and was evaluated by subjecting it to a comparative study. Classification and regression models were used in this study. It was used together with AAN and ELM models. As shown in Figure 3, 18 different machine learning methods were used for the classification method and 8 different machine learning methods for the regression method. For the classification method; AdaBoost, Bagging, DecisonTree, ExtraTrees, GradientBoosting, IsolationForest, K-Nearest Neighbors, LinearSVC, Logistic Regression, Naive Bayes, NuSVC, Passive Aggressive, Perceptron, Random Forest, Ridge, Stacking, SVM (RBF Kernel), Voting models were used.

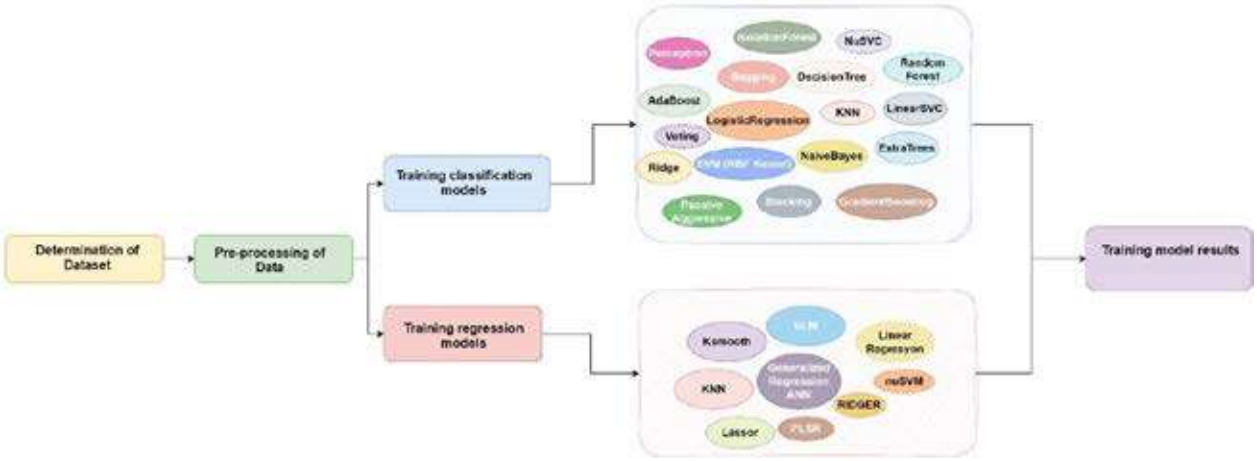


Fig. 3: Architecture of the method.

These models used include traditional machine learning models for classification, as well as ensemble methods such as Stacking and Voting. Ensemble learning models have emerged as relatively newer and more advanced techniques in the field of machine learning. Stacking is a method that develops a new model training by combining the predictions of different models. Ensemble learning with this technique Stacking ensemble learning; It basically uses the outputs and predictions of the machine learning models it uses as input. At the stage where the final predictions are made, it uses another learning algorithm called meta-model. This approach aims to increase the overall performance of the model. In this way, it is aimed to make more accurate predictions and obtain strong results in various problem types Pavlyshenko, B. (2018). .

III. Results

In this section, the values obtained as a result of the steps described in the method title are presented in tables and figures. First of all, an attempt was made to detect the battery status with ANN. In addition to separate findings for B05, B06 and B07, predictions were also obtained for the combination of these three.

18 different classification methods were used to determine battery status. Accuracy, precision, recall, f1-score and support values are presented in Table 1, which will allow a comprehensive evaluation of the classification results. While 13 out of 18 methods showed 100% success, very high successful results were obtained, except for one or two methods.

Tab. 1:“ Detection of battery status with ANN for B05+B06+B07

	Train Accuracy					Test Accuracy				
	'sig'	'sin'	'tribas'	'radbas'	'hardlim'	'sig'	'sin'	'tribas'	'radbas'	'hardlim'
2	2,92	19,99	69,97	3,68	45,14	2,92	22,49	69,95	3,73	45,08
3	17,05	15,60	93,99	3,32	45,24	16,92	15,78	93,95	3,41	45,24
4	1,14	4,30	81,65	1,23	45,24	0,92	4,27	81,68	1,30	45,24
5	1,50	7,14	98,38	2,23	71,30	1,51	6,59	98,27	2,27	69,03
10	4,53	3,10	99,39	9,92	74,94	4,16	3,19	99,35	10,05	74,97
20	4,29	6,66	100,00	13,15	94,21	4,11	7,30	100,00	13,41	94,22
30	14,29	15,59	100,00	10,78	99,28	14,27	15,57	99,95	10,70	98,97
40	10,47	15,25	100,00	21,12	97,35	10,65	15,41	99,89	21,24	97,35
50	14,84	6,41	100,00	11,84	99,13	14,97	6,76	99,95	11,46	99,14
60	11,06	9,69	100,00	13,15	86,27	10,27	9,51	99,89	13,35	86,22
70	10,84	14,37	100,00	12,98	99,03	10,76	13,84	99,95	13,03	98,97
80	17,27	6,54	100,00	14,74	92,31	17,62	6,70	99,84	14,76	92,32
90	14,05	13,44	100,00	24,61	100,00	13,35	13,51	99,89	24,59	99,95
100	13,23	12,94	100,00	15,32	100,00	12,49	12,92	99,84	15,57	99,95
125	11,98	9,39	100,00	14,93	100,00	11,57	9,89	99,84	14,59	99,95
150	13,03	10,77	100,00	16,68	100,00	13,03	10,49	99,78	17,46	99,95
175	15,28	15,28	100,00	14,48	100,00	14,43	14,49	99,78	14,27	99,84
200	14,11	16,40	100,00	14,63	100,00	13,95	15,19	99,89	14,05	100,00
225	12,53	12,65	100,00	12,29	100,00	12,27	11,57	99,62	12,05	99,89
250	11,34	10,32	100,00	11,42	100,00	10,92	9,35	99,78	11,89	100,00

Tab. 2:“ Estimation of battery capacity based on current and usage ID for B05+B06+B07

	R²	MAE	MSE	RMSE	RMSPE	MARE	MAPE
ELM	*0,990*	*0,007*	*0,000*	*0,010*	*1,191*	*0,009*	*0,877*
Generalized Regression ANN	*0,737*	*0,043*	*0,003*	*0,054*	*7,420*	*0,057*	*5,737*
Linear Regresyon	*0,992*	*0,007*	*0,000*	*0,009*	*1,108*	*0,008*	*0,819*
Support Vector Machine	*0,894*	*0,051*	*0,004*	*0,060*	*7,853*	*0,066*	*6,602*
K Nearest Neighbor	*0,984*	*0,008*	*0,000*	*0,013*	*1,531*	*0,010*	*1,013*
RIDGER	*0,990*	*0,007*	*0,000*	*0,010*	*1,222*	*0,009*	*0,897*
Lassor	*0,992*	*0,007*	*0,000*	*0,009*	*1,127*	*0,008*	*0,839*
Ksmooth	*0,794*	*0,038*	*0,002*	*0,049*	*6,637*	*0,051*	*5,085*
PLSR	*0,989*	*0,008*	*0,000*	*0,011*	*1,250*	*0,009*	*0,940*

The R-squared value indicates how well the independent variables explain the dependent variable. The R-squared value takes a value between 0 and 1. The closer it is to 1, the better the model fits the data. In general, the higher the R-squared value, the better the model is considered to fit the data. Therefore, in order to better evaluate the compatibility of predicted and actual values, R² graphs of each machine learning are given in Figure 4.

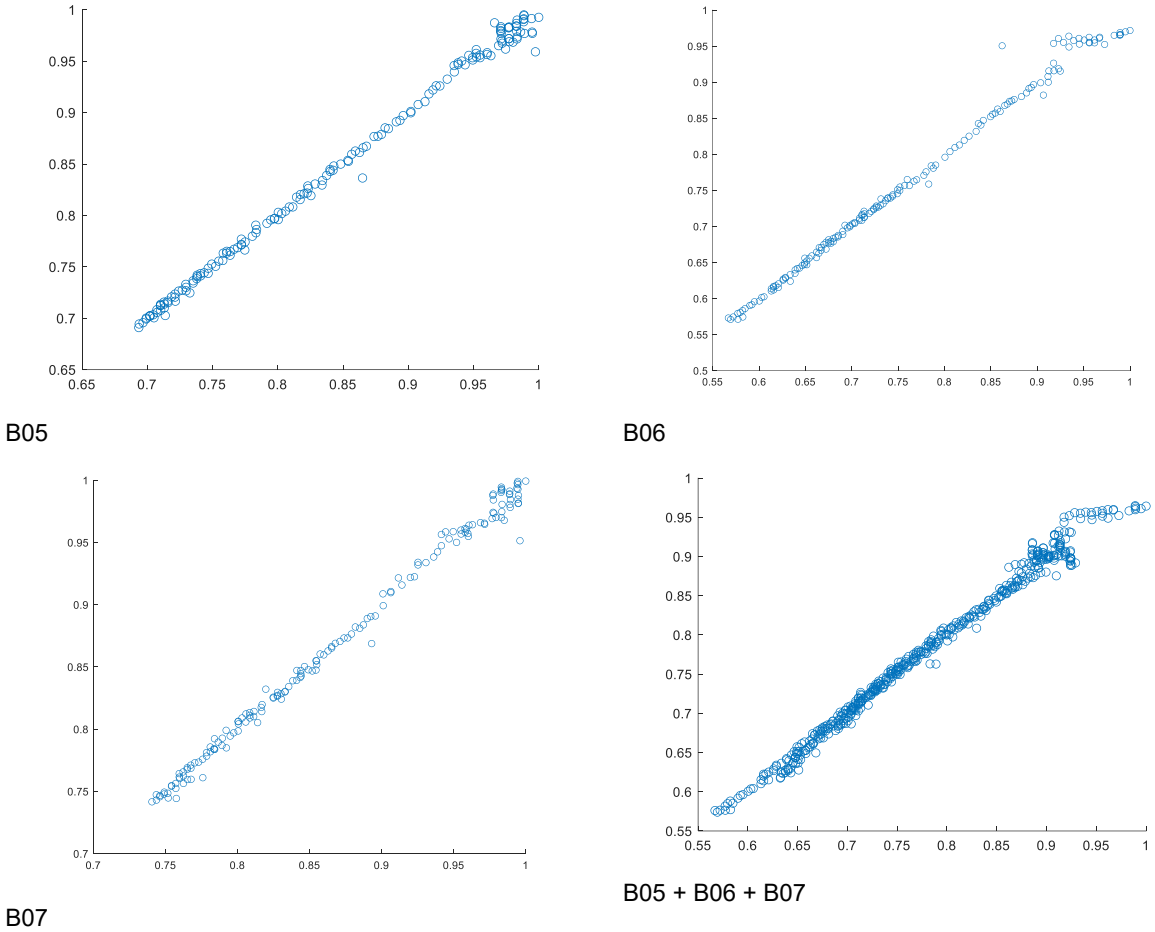


Fig. 3: R² for Estimation of battery capacity

VI. Conclusions

In conclusion, this study has focused on the application of machine learning methods for identifying the battery status and capacity during discharge based on battery current. Through the use of advanced algorithms and data analysis techniques, we have demonstrated the potential of machine learning in improving battery management systems for enhanced performance and efficiency. By analyzing the battery current, we have successfully developed and implemented artificial neural networks (ANN) to predict the battery status and capacity. The results obtained from the ANN models indicate the accuracy and reliability of the predictions, as demonstrated in the presented tables and figures.

The findings of this study highlight the effectiveness of machine learning in detecting battery status, both independently for individual batteries (B05, B06, and B07) and collectively for the combined dataset. The accuracy values obtained for different activation functions provide insights into the performance of the ANN models.These results have significant implications for the field of battery technology and its application in various industries, particularly in the development of eite devices. By accurately identifying battery status and capacity during discharge, we can enhance battery management, optimize energy consumption, and prolong battery life. Moving forward, further research and development in machine learning techniques for battery monitoring and management are necessary. The continuous refinement of algorithms and the integration of real-time monitoring capabilities will contribute to the advancement of battery technology and its practical implementation.

In summary, this study has demonstrated the potential of machine learning methods in identifying battery status and capacity based on battery current during discharge. The findings underscore the importance of leveraging advanced data analysis techniques to improve battery management systems for enhanced performance, efficiency, and overall user experience in eite devices.

References

Agatonovic-Kustrin, S., & Beresford, R. (2000). Basic concepts of artificial neural network (ANN) modeling and its application in pharmaceutical research. Journal of pharmaceutical and biomedical analysis, 22(5), 717-727.

Agatonovic-Kustrin, S., & Beresford, R. (2000). Basic concepts of artificial neural network (ANN) modeling and its application in pharmaceutical research. Journal of pharmaceutical and biomedical analysis, 22(5), 717-727.

Ataseven, B. (2013). Yapay sinir ağlari ile öngörü modellemesi. Öneri Dergisi, 10(39), 101-115.

Dos Reis, Gonçalo & Fermin Cueto, Paula & Medina-Lopez, Encarni & Anjos, Miguel & McTurk, Euan & sylvester, Joel &

Allerhand, Michael. (2020). Identification and machine learning prediction of knee-point and knee-onset in capacity degradation curves of lithium-ion cells. 10.1016/j.egyai.2020.100006.

Fei Xia, Kangan Wang, Jiajun Chen, State of health and remaining useful life prediction of lithium-ion batteries based on a disturbance-free incremental capacity and differential voltage analysis method, Journal of Energy Storage, Volume 64, 2023, 107161, ISSN 2352-152X,

Huang, G. B., Wang, D. H., & Lan, Y. (2011). Extreme learning machines: a survey. International journal of machine learning and cybernetics, 2, 107-122.

Hydrogen Fuel Cell—Anomoly_detection. (t.y.). Geliş tarihi 11 Mayıs 2024, gönderen https://www.kaggle.com/datasets/ranitsarkar01/hydrogen-fuel-cell-anomoly-detection

Kanat, E. (2020). Determination of Optimum Artificial Neural Network in the Stock Market. Turkish Studies-Economics, Finance, Politics, 15(1), 239-252.

Martin Pham, Acoustic and X-ray Characterisation of Lithium-Ion Battery Failure, Electrochemical Innovation Lab, Department of Chemical Engineering, University College London, 2023

Pavlyshenko, B. (2018, August). Using stacking approaches for machine learning models. In 2018 IEEE second international conference on data stream mining & processing (DSMP) (pp. 255-258). IEEE.

Sapra, H., Elfimova, O., Upadhya, S., Desorcy, L. et al., "Estimating Battery State-of-Charge using Machine Learning and Physics-Based Models," SAE Technical Paper 2023-01-0522, 2023, https://doi.org/10.4271/2023-01-0522.

Tianhan Gao and Wei Lu, Machine learning toward advanced energy storage devices and systems, iScience, Volume 24, Issue 1, 101936, January 22, 2021

Wang, J., Lu, S., Wang, S. H., & Zhang, Y. D. (2022). A review on extreme learning machine. Multimedia Tools and Applications, 81(29), 41611-41660.

Hydrogen Production with Cu-Cl Thermochemical Cycle Integrated into Next-Generation Nuclear Power Plant for Sustainable Cities

[1*]Muhammet Mert Dincer, [1,2]Merve Ozturk
[1] Yildiz Technical University, Faculty of Mechanical Engineering, Department of Mechanical Engineering, Besiktas, Istanbul, 34349, Türkiye
[2] Yildiz Technical University, Clean Energy Technologies Institute, Esenler, Istanbul, 34200, Türkiye

* E-mails: muhammet.dincer@std.yildiz.edu.tr, merveoz@yildiz.edu.tr

Abstract
In the present study, a modular helium reactor with 250 MW thermal capacity integrated with a Cu-Cl thermochemical cycle to produce low-carbon hydrogen is designed to change a landlocked city into a sustainable city. The system includes a gas turbine modular helium reactor, an organic Rankine cycle (ORC), a five-step Cu-Cl thermochemical cycle, and greenhouse and residential heating subunits. For this developed system, thermodynamic analysis is conducted by employing Engineering Equation Solver software. The useful outputs arising are electricity, heating for greenhouse and houses, and hydrogen. Some parametric analyses are made in order to obtain critical parameters for system efficiencies and hydrogen production rate. The overall exergy and energy efficiencies are found to be 41% and 45% while hydrogen production capacity is 19.03 kg/s.

Keywords: Nuclear, sustainable city, hydrogen, thermochemical cycle, exergy.

I. Introduction

80% of the world's total energy supply is still derived from fossil fuels, of which oil accounts for around 30%, coal (27%), and natural gas (24%). The rising use of fossil fuels, in line with increased energy demand, causes rising greenhouse gas (GHG) emissions (IEA, 2023). Reducing greenhouse gas emissions can be accomplished through multigeneration systems that utilize sustainable and renewable energy sources. The direct reduction of greenhouse gas emissions occurs when zero-carbon energy production systems replace fossil fuel-based power production. GHG emissions are reduced by improving efficiencies by utilizing excess energy in various forms in integrated systems.

The generation of low-carbon hydrogen is emerging as another barrier in the struggle against greenhouse gas emissions. The adaptation of nuclear reactors with different systems that generate valuable outputs, such as hydrogen, has been investigated for some countries, in the literature. Cany et al. (2017) aimed to assess the potential contribution of surplus nuclear power to the production of low-carbon hydrogen in France. For this purpose, they created scenarios involving nuclear and renewable energy sources, modeled and analyzed possible nuclear hydrogen production costs and volumes, and assessed the possibility of CO_2 reduction. Temiz and Dincer (2021) designed a nuclear and solar-based integrated system that generated several beneficial outputs, such as food, fuel, and energy, allowing indigenous communities to meet some of the United Nation's sustainability goals and attain sustainable development. The developed integrated system offered an overall energy efficiency of 62.64% and an overall exergy efficiency of 68.91% under ambient conditions. Wang et al. (2023) stated that employing a complex Brayton cycle for the Gas Turbine Modular Helium Reactor (GT-MHR) plant could have some benefits. They analyzed a modular nuclear plant with a thermal capacity of 250 MW. The plant comprised an energy conversion unit and a nuclear reactor cooled by helium. The findings demonstrated that if the optimal design parameters for every in-plant component are presently attained in the existing power engineering and gas turbine sectors, high cycle efficiency in electricity generation could be achieved.

In this study, a nuclear energy-based multigeneration system is developed and analyzed thermodynamically to transform a landlocked province into a sustainable city by exporting hydrogen and reducing carbon emissions. The useful outputs of this system are hydrogen, which is produced by a five-step Cu-Cl thermochemical cycle, electricity, and heat.
helium

II. System Description

The proposed multigeneration system layout is shown in Fig. 1. This system consists of a Gas Turbine Modular Helium Reactor with a 250 MW thermal capacity, a five-step Cu-Cl thermochemical cycle, and an organic Rankine cycle. Helium with a mass flow rate of 165.9 kg/s is fed to the modular reactor and its temperature is increased from 560 °C to 865 °C. In the organic Rankine cycle, the working fluid is R-134a. Electricity is produced by gas turbine and organic Rankine cycles. While the heat obtained from the first heat exchanger is used to produce hydrogen by a five-step Cu-Cl thermochemical cycle, heat from heat exchanger 3 is used for residential heating and greenhouse heating.

III. Analysis

Engineering Equation Solver (EES) software is employed for the thermodynamic analysis of the nuclear-based multigeneration system. Some assumptions are made during the analysis as listed below:

- Isentropic efficiencies of low-pressure and high-pressure compressors are 0.875 and 0.85, respectively.
- For the turbine 1, the isentropic efficiency is 0.93.

- In ORC, pressure ratio is taken as 3 and the isentropic efficiencies of pump and turbine are 0.80 and 0.70, respectively (Tchanche, 2010).
- The boundary temperature of the heat exchangers 1 and 3 are taken as 645 K and 285 K, respectively.
- The ratio of pressure for the turbine 1 is taken as 1.85.
- The exergy and energy efficiencies of the Cu-Cl thermochemical cycle are assumed to be 0.73 and 0.45, respectively (Orhan et al., 2008).
- Evaporating and condensing temperatures are taken as 75 °C and 35 °C, respectively (Tchanche, 2010). Pressure drops through the heat exchangers are neglected.

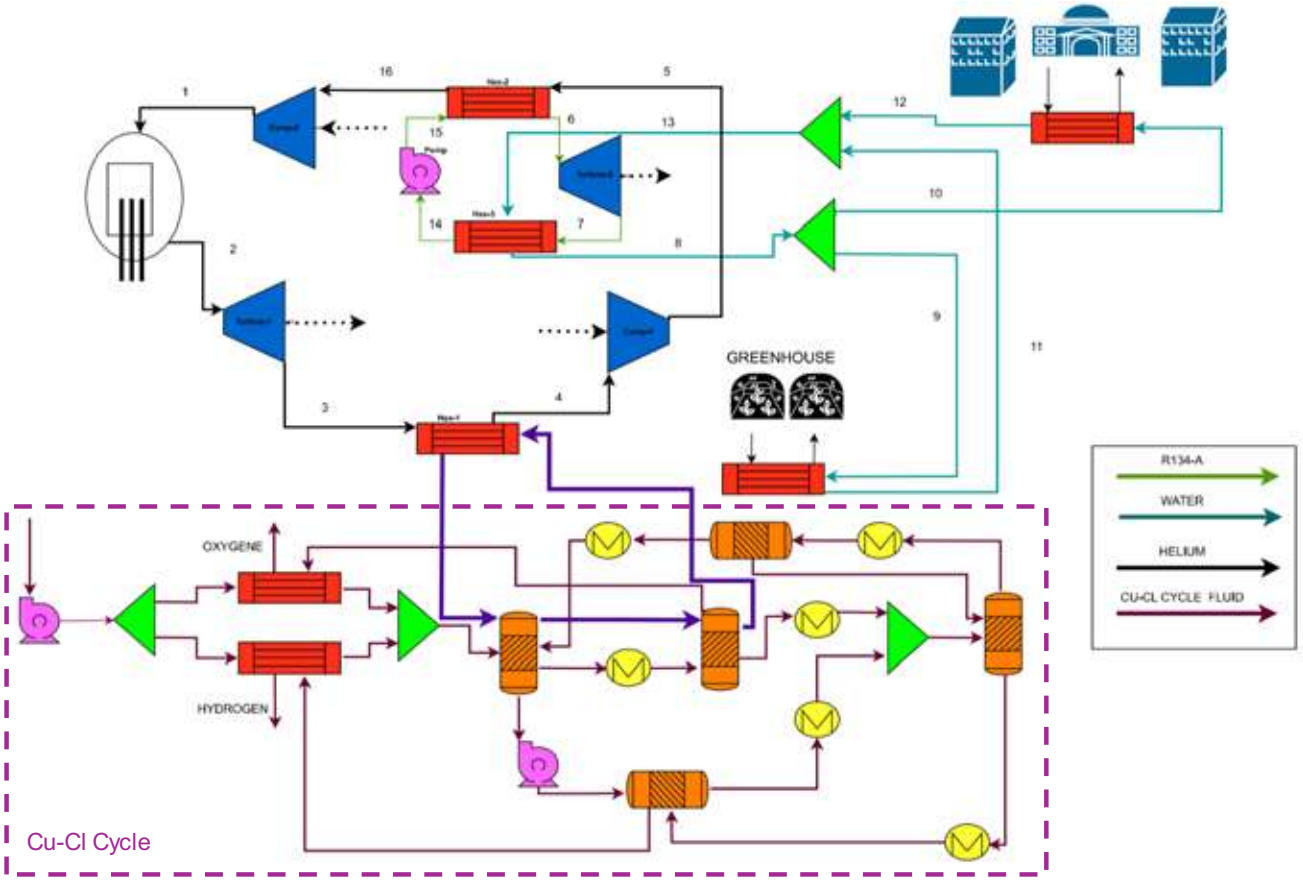


Fig. 1: Layout of the developed multigeneration system

Overall energy and exergy efficiencies for the nuclear-based multigeneration system are calculated as follows:

$$\eta_{en,overall} = \frac{\dot{W}_{net} + \dot{m}_{H_2} LHV_{H_2} + \dot{Q}_{Greenhouse} + \dot{Q}_{Houses}}{\dot{Q}_{Reactor,in}} \quad (1)$$

where, $\dot{m}_{H_2}$ defines the mass flow rate of hydrogen produced by the Cu-Cl cycle, $\dot{Q}_{Greenhouse}$ and $\dot{Q}_{Houses}$ are heat rates provided to the greenhouse and residential buildings, respectively. LHV is the lower heating value of hydrogen and $\dot{Q}_{Reactor,in}$ is the heat extracted from the modular nuclear reactor by helium.

$$\eta_{ex,overall} = 1 - \frac{\dot{E}x_{d,total}}{\dot{E}x^{\dot{Q}_{Reactor,in}}} \quad (2)$$

where $\dot{E}x_{d,total}$ is the total exergy destruction rate and $\dot{E}x^{\dot{Q}_{Reactor,in}}$ is the thermal exergy of heat received rate.

IV. Results and discussions

Thermodynamic analysis results show that rising the pressure ratio of turbine 1 raises the heat rate extracted from the condenser in the ORC, as given in Fig. 2. On the other hand, the work rate produced by the system increases as the pressure ratio increases until the pressure ratio reaches 1.8. After this value, it starts to decrease with the pressure ratio.

Besides, the hydrogen generation rate reduces with the pressure ratio due to the decrease in heat fed to the Cu-Cl thermochemical cycle. In Fig. 3, the effect of turbine 1 pressure ratio on overall system exergy and energy efficiency values. A greater pressure ratio of the turbine provides greater energy efficiency. However, overall exergy efficiency diminishes with a growing pressure ratio because of the higher heat rate generated rather than the work rate.

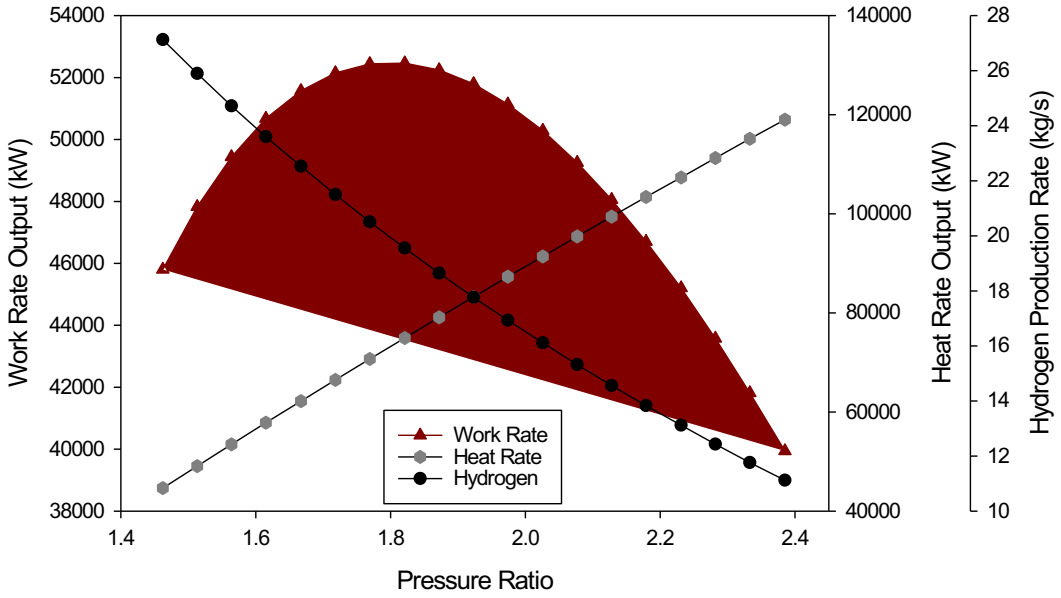


Fig. 2: Variation of work rate produced and heat rate output with the pressure ratio of helium turbine

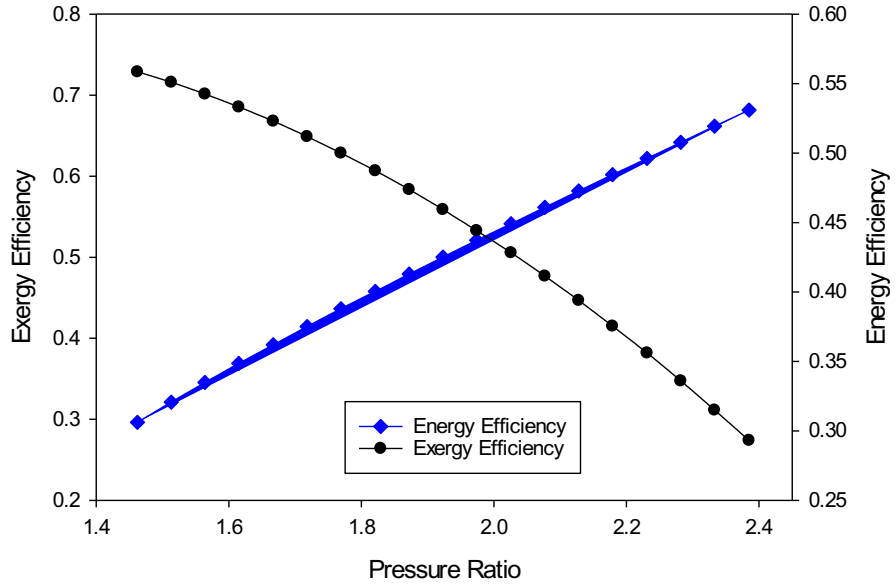


Fig. 3: Change of overall system exergy and energy efficiencies with pressure ratio of helium turbine

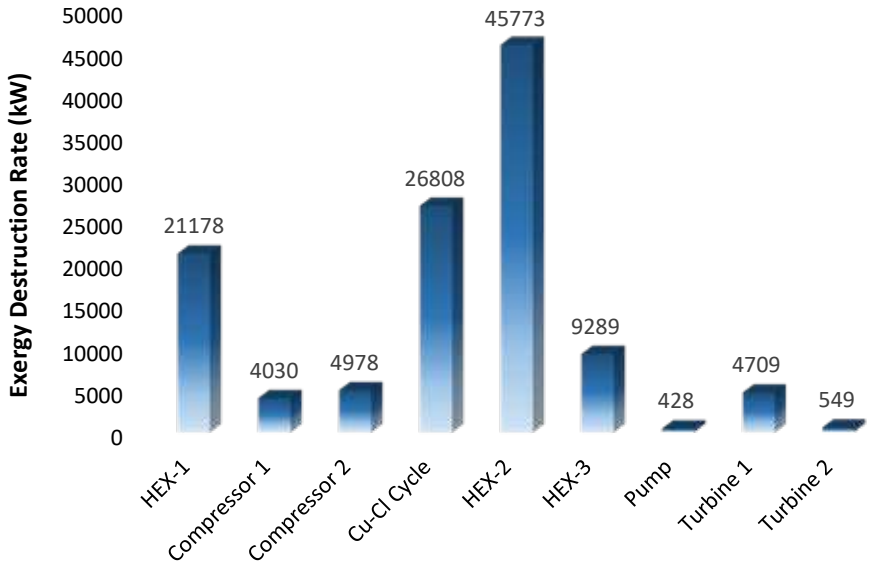


Fig. 4: Exergy destruction rates for each unit in the analyzed system

For the developed system, each component has some exergy destructions due to the irreversibilities. These destructions are determined with the exergy balance equations and given in Fig. 4. The highest value of exergy destruction belongs to heat exchanger 2 due to the high heat output. The change in total exergy destruction and exergy efficiency of the overall integrated system with ambient temperature is shown in Fig. 5. When ambient temperature has a higher value total exergy destruction rate is increased, therefore, exergy efficiency is decreased accordingly.

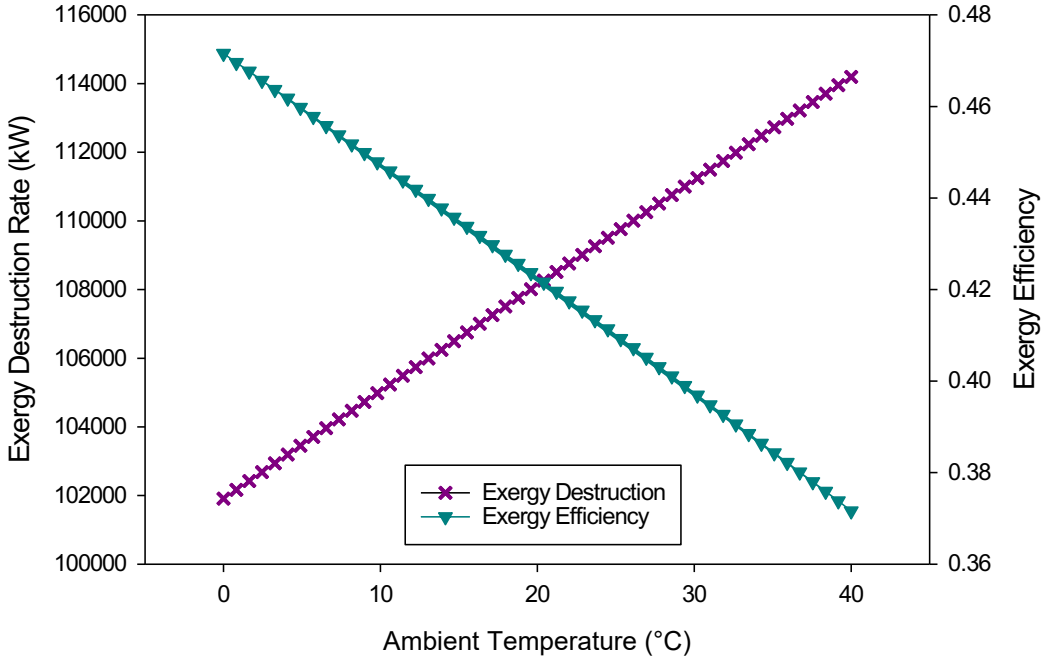


Fig. 5: Variation of environment temperature on exergy efficiency and total exergy destruction rate

V. Conclusions

In the current study, a multigeneration system based on a next-generation nuclear power plant is developed and analyzed. The conclusions arising from the present work are obtained as follows:

- The hydrogen production capacity is 19.03 kg/s, and it reduces with the enhancing ratio of the pressure for the turbine 1.
- The work rate produced raises with the improving ratio of pressure for the turbine 1 until the pressure ratio reaches 1.8; after that value, it reduces with the enhancing pressure ratio.
- The heat rate output from the condenser of ORC is enhanced by the growing ratio of pressure for the turbine 1.
- Overall energy efficiency increases while exergy efficiency reduces with enhancing the ratio of pressure for the turbine 1.
- Greater ambient temperature leads to greater exergy destruction and therefore, lower exergy efficiency.

References

IEA, Greenhouse Gas Emissions from Energy Data Explorer, (2023).

Cany, C., Mansilla, C., da Costa, P., Mathonnière, G., Adapting the French nuclear fleet to integrate variable renewable energies via the production of hydrogen: Towards massive production of low carbon hydrogen? International Journal of Hydrogen Energy, 42(19), 13339-13356, (2017).

Orhan, M.F., Dincer, I., Rosen, M.A., Thermodynamic analysis of the copper production step in a copper–chlorine cycle for hydrogen production. Thermochimica Acta, 480(1-2), 22-29, (2008).

Tchanche, B.F. Low-Grade Heat Conversion into Power Using Small Scale Organic Rankine Cycles, Doctoral Thesis. Agricultural University of Athens, (2010).

Temiz, M., Dincer, I., Development of an HTR-Type nuclear and bifacial PV solar based integrated system to meet the needs of energy, food and fuel for sustainable indigenous cities. Sustainable Cities and Society, 74, 103198, (2021).

Wang, D., Khalatov, A., Shi-Ju, E., Donyk, T., Shikhabutinova, O., Thermodynamics of GT-MHR-250 modular nuclear plant with helium reactor and gas turbine based on the complex Brayton cycle. Thermal Science and Engineering Progress, 39, 101686, (2023).

Comparative Analysis of YSZ and SCSZ Electrolytes in Solid Oxide Fuel Cells (SOFCs) with novel PrCeMn electrocatalyst

[1*]Esra Balkanlı Ünlü, [2] Meltem Karaismailoğlu Elibol, [1,3] Halit Eren Figen
[1] Yildiz Technical University, Faculty of Chemical and Metallurgical Engineering, Department of Chemical Engineering, Istanbul, 34220, Türkiye
[2] Turkish-German University, Department of Energy Science and Technology, Istanbul, 34820, Türkiye
[3] Yildiz Technical University, Clean Energy Technologies Institute, Istanbul, 34220, Türkiye

* E-mail: balkanliesra@hotmail.com

Abstract

Solid oxide fuel cells are known for their wide fuel diversity, high efficiency of operation and high temperature requirements. The electrolyte material used is critical to the performance of SOFCs. Moreover, a most commonly used electrolyte, YSZ (yttria-stabilized zirconia) may require high temperatures depending on how designed on a cell. This study presents a comparative analysis of two prominent electrolyte materials, YSZ (yttria-stabilized zirconia) and SCSZ (scandia stabilized zirconia) with using PrCeO as a catalyst. The PrCeO electrocatalysts were synthesized using the sol-gel combustion method, followed by electrocharacterization analysis conducted via Electrochemical Impedance Spectroscopy (EIS) on half-cells for each electrolyte. The experimental comparison revealed that the half cell prepared with the ScSZ electrolyte showed a 28% reduction in resistance compared to the YSZ electrolyte.

Keywords: Solid Oxide Fuel Cell, SCSZ electrolyte, Prasedium catalyst

I. Introduction

In order to overcome the political and climatic problems defined globally, the orientation towards alternative energy sources is gaining momentum (de Sa, 2024). As an alternative solution, fuel cells are attracting a lot of attention with their emission-free, highly efficient electrical conversion. Therefore solid oxide fuel cell stands for its fuel flexibility and hig efficiency among fuel cells.

At high temperatures, oxygen ions are carried from the cathode to the anode through a solid oxide electrolyte. The oxygen ions then react with hydrogen or hydrocarbon fuels at the anode to produce water and/or carbon dioxide, releasing electrons, which are conducted through an external load to the cathode, resulting in an electric current. The reactions that occur at the anode and cathode are as follows for hydrogen (Chen et al. 2018);

Anode: $H_2+O^{2-} \rightarrow H_2O+2e^-$ (1)

Cathode: $1/2O_2 + 2e^- \rightarrow O^{2-}$ (2)

The electrolyte used in solid oxide fuel cells is the most important feature that determines the operating temperature and fuel diversity. Electrolytes must be capable of good oxygen ion conductivity, high chemical stability, low electronic conductivity, acceptable mechanical properties. YSZ is an oxygen ion conductor and has been widely used in SOFCs, which YSZ shows high chemical and mechanical strength and stability (Ivers-Tiffée et al., 2019). However, YSZ requires high temperatures (>800 °C) to achieve good performance in an electrolyte-supported cell, which makes it susceptible to system-related failures (Zakaria et al., 2020).

Although zirconia remains the preferred electrolyte material for SOFCs, scandia-stabilized zirconia shows potential for lower operating temperatures and enhanced conductivity (Lakshmi, 2011). Studies have shown that when ScSZ is used as the electrolyte, intermediate operating temperatures of 600-800 °C can be achieved on SOFCs (Zhigachev et al., 2021).

To this extend, EIS technique with the different temperature range have been used to examine YSZ and SCSZ which have been selected on the basis of their differing electrical behavior on literature. Half-cells were prepared using PrCeMn catalyst with selected electrolytes and oxygen vacancy of PrCeMn were analyzed via O_2-Temperature Programmed Desorption method.

II. Experimental Set-up and Procedure

Synthesis of the PrCeMn eletrocatalyst. PrCeMn electrocatalysts were prepared by the sol-gel combustion method with a ratio of metal to glycine to citric acid of 1:1.5:1.5 in the starting solution. In preparing the perovskite electrocatalyst, the metal ratios of the A-side (praseodymium and cerium) and B-side (manganese) were adjusted to 1:1 as well as the ratio of the A-side metals within themselves was maintained at 1:1 in the starting solution. The pH of the starting solution was then adjusted to 7 with a 1 M ammonia solution and the gel was formed by evaporation at 80 °C. Final product was obtained after the formed gel was oven dried at 250 °C and calcined at

1000 °C.

Preparation of half cells. To evaluate the comparisons between the YSZ and ScSZ electrolytes by EIS, half cells were prepared as a electrolyte support design with press method. In order to obtain homogenous powder, YSZ were ballmilled at 100 rpm rotation speed for 24 hours by wet milling. Prepared powder then were sieved through 100 micron. YSZ powders were transformed into pellets by applying 5 tonnes of pressure and, the final shape of the 2cm diameter, 1mm thick pellets was achieved after heat treatment at 1450°C for 3 hours. SCSZ could be milled through a 100 micron sieve and therefore did not need to be pre-treated with a ball mill. ScSZ powder were pressed through pellets same as YSZ and final product of 2 cm diameter pellets were obtained after heat treatment at 1400°C for 3 hours.
PrCeMn electrocatalyst was coated on the both side of the prepared electrolyte pellets via spray coating method. The spray solution was prepared using 30% alpha-terpineol and 70% powder (containing 95% catalyst and 5% ethyl cellulose) dispersed in isopropanol and then mixed by ball milling at 150 rpm for 1 hour. The final half-cells were obtained after both side of the electrolyte pellets coated and calcined at 1100 °C for 4h.

III. Characterization Method

Temperature programmed desorption (TPD), analysis were conduct to help with the understanding of the PrCeMn catalysts oxygen diffusion characteristic. TPD reactşon were carried out on tubular reactor with continuous flow and analysis were performed by mass spectrometry (Hiden Analytical QGA). 100 mg of catalyst loaded on quartz wool in the reactor was pretreated in an argon-balanced 10% oxygen environment (total flow: 40 ml/min) which heated to 750 °C and cooled to room temperature in a controlled manner. When sample reached room temperature, the flow was switched to argon (40 ml/min) and after stabilization in the mass spectrometer (MS), the temperature was increased to 900 °C at 3 °C/min (Choi et all., 2012).
Impedance measurements of symmetrical half-cells are analysed at different temperatures using a probostat apparatus, data was collected by controlling with versestat4 potentiostat. Impedance measurements of PrCeMn catalyst coated ScSZ and YSZ half-cells were carried out in dry air at 600-950 °C and 100000-0.001 Hz frequency range with 40 amplitude.

IV. Results and discussions

O2-TPD Result. PrCeMn catalyst was prepared for electrolyte comparison and was analyzed by O_2 TPD as shown in Fig. 1 for the desorption behaviour.

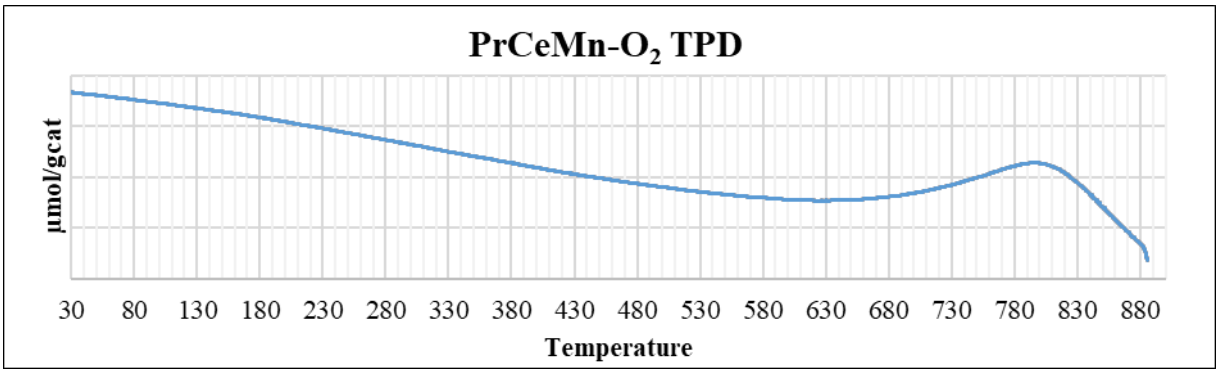


Fig. 1. Desorption profile of PrCeMn electrocatalysts versus temperature (°C)

The only clear peak were observed between 700-850 °C, which indicates desorped bulk oxygen (β-oxygen). There for β-oxygen desorption reflects oxygen mobility in the PrCeMn electrocatalyst, which is oxygen exchange between the bulk oxygen and surface oxygen vacancies (Zhang et al., 2018; Gu et al., 2019).

EIS Results. Fig. 2. Shows the Nyquist Plot of PrCeMn-ScSZ and PrCeMn-YSZ halcells measured at 700 °C to 850 °C in air environment.

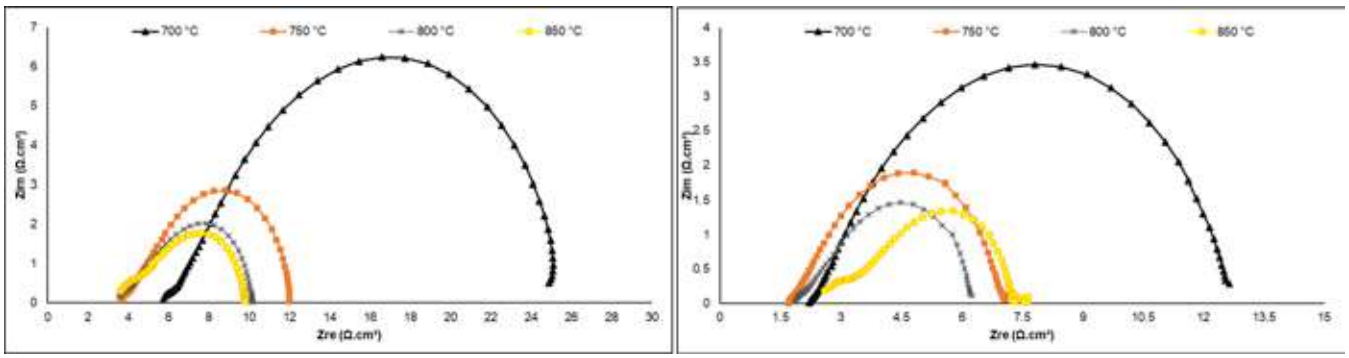


Fig. 2. EIS measurements at 700 C to 850 C for a) PrCeMn-YSZ, b) PrCeMn-ScSZ half-cells

Cathode polarization resistances for PrCeMn on YSZ electrolyte are 19.12, 8.37, 6.61, and 6.17 Ω.cm² while on ScSZ electrolyte; 12.63, 7.07, 4.4, and 4.97 Ω.cm² for 700, 750, 800, and 850 °C, respectively.To higher temperature, ionic conductivity and surface exchange kinetics increased for both electrolyte, meanwhile degradation between ScSZ and cathode electrocatalyst was occured at 850 C. Studies with ScSZ electrolyte shows lower resistance results by 28% than YSZ by at midpoint temperature which is 800 °C for all cells.

V. Conclusions

The comparative analysis between YSZ and ScSZ electrolytes in Solid Oxide Fuel Cells (SOFCs) has provided valuable material based insights. While YSZ remains a widely used electrolyte material, the experimental studies indicate that ScSZ electrolyte has lower resistance by 28% than YSZ at 800 °C. The ScSZ electrolyte demonstrated lower resistance and the ability to operate at lower temperatures compared to YSZ. These initial results highlight the importance of further research and optimisation of scandia-stabilised zirconia electrolytes to improve the performance for further studies.

Acknowledgements

This research was supported by Yildiz Technical University BAP (Scientific Research Projects Coordination Unit) under Doctoral Thesis Project (FDK-2021-4211) and TUBITAK under 2211-A program.

References

Chen, Y.; Zhou, W.; Ding, D.; Liu, M.; Ciucci, F.; Tade, M.; Shao, Z., Advances in Cathode Materials for Solid Oxide Fuel Cells: Complex Oxides without Alkaline Earth Metal Elements. Adv. Energy Mater. 5 (18), 1500537, (2015).

Choi, H., Fuller, A., Davis, J., Wielgus, C., & Ozkan, U. S., Ce-doped strontium cobalt ferrite perovskites as cathode catalysts for solid oxide fuel cells: Effect of dopant concentration. Applied Catalysis B: Environmental, 127, 336-341, (2012).

de Sá, M. H., Electrochemical Devices to Power a Sustainable Energy Transition-An Overview of Green Hydrogen Contribution. Applied Sciences 14.5: 2168, (2024).

Gu, Y., Zhang, Y., Zheng, Y., Chen, H., Ge, L., & Guo, L., $PrBaMn_2O_{5+\delta}$ with praseodymium oxide nano-catalyst as electrode for symmetrical solid oxide fuel cells. Applied Catalysis B: Environmental, 257, 117868, (2019).

Ivers-Tiffée, E.; Weber, A.; Herbstritt, D., Materials and Technologies for SOFC-Components. J. Eur. Ceram. Soc., 21 (10), 1805–1811, (2001).

Lakshmi, V. V., Bauri, R., Gandhi, A. S., & Paul, S., Synthesis and characterization of nanocrystalline ScSZ electrolyte for SOFCs. International journal of hydrogen energy, 36(22), 14936-14942, (2011).

Zakaria, Z.; Mat, Z. A.; Hassan, S. H. A., Kar, Y. B. A, Review of Solid Oxide Fuel Cell Component Fabrication Methods toward Lowering Temperature. Int. J. Energy Res., 44 (2), 594–611, (2020).

Zhang, X., Song, Y., Guan, F., Zhou, Y., Lv, H., Wang, G., & Bao, X., Enhancing electrocatalytic CO_2 reduction in solid oxide electrolysis cell with $Ce_{0.9}Mn_{0.1}O_{2-\delta}$ nanoparticles-modified LSCM-GDC cathode. Journal of Catalysis, 359, 8-16, (2018).

Zhigachev, A. O., Rodaev, V. V., Zhigacheva, D. V., Lyskov, N. V., & Shchukina, M. A., Doping of scandia-stabilized zirconia electrolytes for intermediate-temperature solid oxide fuel cell: A review. Ceramics International, 47(23), 32490-32504, (2021).

Circle-Inspired Optimization Algorithm for Parameter Estimation in Photovoltaic and Fuel Cell Systems

[1*]Süleyman Yıldız
[1] Mus Alparslan University, Department of Electricity and Energy, Mus, 49250, Türkiye

* E-mail: s.yildiz@alparslan.edu.tr

Abstract
This study introduces the Circle-Inspired Optimization Algorithm (CIOA) for predicting optimal parameters in PEMFC and PV systems. Addressing the escalating demand for renewable energy sources, the article emphasizes the pivotal role of PV and FC technologies in sustainable energy production. Through a comparative evaluation with existing literature and experimental data, the efficacy of CIOA in parameter identification for both single-diode PV and PEMFC models is demonstrated. The proposed algorithm exhibits superior performance, affirming its potential for enhancing the design and optimization of renewable energy systems.

Keywords: PEM Fuel Cell, PV System, Parameter Estimation, Circle-Inspired Optimization Algorithm.

I. Introduction

Nowadays, there is a rapid increase in demand for renewable energy sources to meet the current energy needs and ensure environmental sustainability. This demand can be fulfilled by renewable sources such as solar, wind, hydroelectric, and biomass. However, the unpredictable nature of renewable energy sources due to natural conditions highlights the importance of energy production and storage methods. In this context, photovoltaic (PV) systems and fuel cell (FC) technologies play a significant role in electricity generation and storage processes.

Fuel cells are a type of renewable energy source that convert chemical potential into electrical energy. There are various types of fuel cells, including Direct Methanol Fuel Cell (DMFC), Alkaline Fuel Cell (AFC), Solid Oxide Fuel Cell (SOFC), Phosphoric Acid Fuel Cell (PAFC), and Proton Exchange Membrane Fuel Cell (PEMFC) (Tariq, 2021). PEMFCs are particularly well-suited for small-scale devices such as vehicles, portable electronic devices, and other mobile applications. Their suitability for mobile applications has increased the popularity of PEMFCs due to features like rapid startup and high efficiency.

The modeling of PEMFCs is mostly carried out through three different methods. One of them is mechanical modeling, which involves simulations of heat/mass transfer, and the study of electrochemical events. The second approach is black-box modeling. The third is empirical modeling based on semi-experimental and nonlinear equations to predict the effect of specific parameters on the current-voltage polarization curve of PEMFCs (Özdemir, 2021).

PV systems, on the other hand, are technologies that directly convert sunlight into electrical energy and have vast potential for electricity generation. The proportion of renewable energy generated through PV systems has been rapidly increasing in recent years, and it is predicted to become one of the main energy sources in the future. Extensive research efforts to enhance the performance and optimize the efficiency of PV systems focus on effectively modeling PV cells or modules.

Accurately predicting the parameters that determine the performance of photovoltaic and fuel cell systems is crucial. Well-modeled FC and PV modules are of critical importance for improving system design, optimizing energy production, and reducing costs (Yan etal, 2023). The methods used for parameter estimation should have the following characteristics:

- The parameter estimation method should not be complex and should be easily applicable.
- It should accurately predict FC and PV performance and produce results as close to real data as possible.
- It should be applicable to different FC and PV cell structures and be applicable across a wide range.

In light of the above information, this article focuses on the intuitive estimation of parameters for photovoltaic and fuel cell systems. For the first time, this study proposes a circle-inspired optimization algorithm for predicting FC and PV parameters.

II. The Mathematical Model of PEMFC

The modeling of a PEMFC entails the representation of electrical, chemical, and thermal processes under various operating conditions. Accurate determination of numerical parameters is crucial for the precision of the model. Current studies indicate that as computational efficiency improves, the accuracy of the modeling decreases. The operation of a PEMFC is inherently intricate, encompassing factors such as electrochemical reactions, gas transport phenomena, and chemical equilibria. Therefore, modeling the PEMFC accurately necessitates accounting for this complexity. Figure 1 illustrates the fundamental operation of a PEMFC.

,

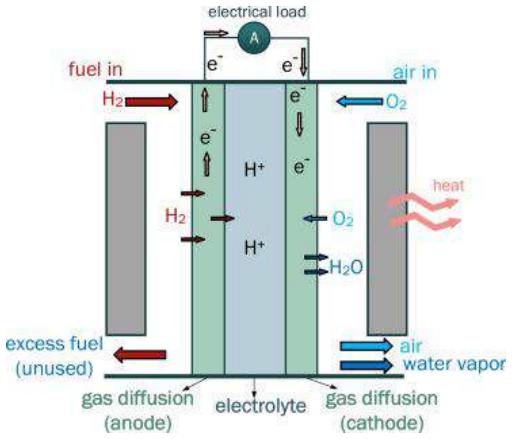


Fig. 1: Structure of PEMFC *(Özdemir, 2021)*

Equation 1 defines the DC voltage at the output of the PEMFC, taking into account various losses such as concentration loss, ohmic loss, and activation loss.

$$V = (E_0 - V_{act} - V_{ohmic} - V_{conc})N_s \quad (1)$$

Here, , V_{conc}, V_{ohmic} and V_{act} respectively represent concentration loss, ohmic loss, and activation loss. N_s represents the number of fuel cells in the stack.

II. The Mathematical Model of PV

An appropriate circuit model is one that accurately reflects the electrical behavior of a physical PV cell while minimizing complexity. When selecting a circuit model for a PV cell, a balance must be struck between accuracy and simplicity. To this end, this section introduces and examines the Single-Diode PV model. The Single-Diode PV model is a representation of the fundamental electrical behaviors of a photovoltaic cell (Nunes etal, 220). This model describes the current-voltage characteristics of the cell and typically consists of a diode, series resistance, and parallel resistance. Figure 2 provides a schematic representation of this model.

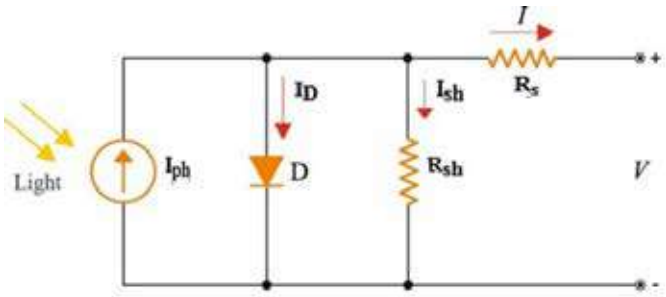


Fig. 2: Equivalent circuit diagram of the Single-Diode PV model

In the circuit depicted in Figure 2, the output current (I), diode current (I_D), and current passing through the shunt resistance (I_{sh}) are calculated using Equations 2, 3, and 4, respectively.

$$I = I_{ph} - I_D - I_{sh} \quad (2)$$

$$I_D = I_0 \left\{ exp\left(\frac{q(V+IR_s}{nkT}\right) - 1 \right\} \quad (3)$$

$$I_{sh} = \frac{V+IR_s}{R_{sh}} \quad (4)$$

In these equations, I_0 represents the reverse saturation current of the diode, q denotes the electron charge, V represents the output voltage, n signifies the ideality factor of the diode, k denotes the Boltzmann constant, and T represents the temperature in Kelvin. Here, there are five parameters $(I_{ph}, I_0, n, R_s, R_{sh})$ which are unknown but can be estimated.

III. Proposed Circle-Inspired Optimization Algorithm

CIOA is an optimization algorithm developed taking inspiration from the geometric properties of a circle. The symmetry of the circle, including its center and radius, provides a fundamental model for the distribution and

movement of solution candidates in the problem domain. The algorithm involves individuals moving symmetrically around the circle and dynamically adjusting the center and radius of the circle according to the fitness function. This allows for optimizing interactions among individuals while exploring a wide search space. CIOA has been applied to various research and optimization problems, and the results obtained have demonstrated its greater efficiency compared to other well-known algorithms, contributing to the accurate and rapid resolution of complex optimization problems (de Souza and Miguel,2022). The flowchart for CIOA is presented in Figure 3.

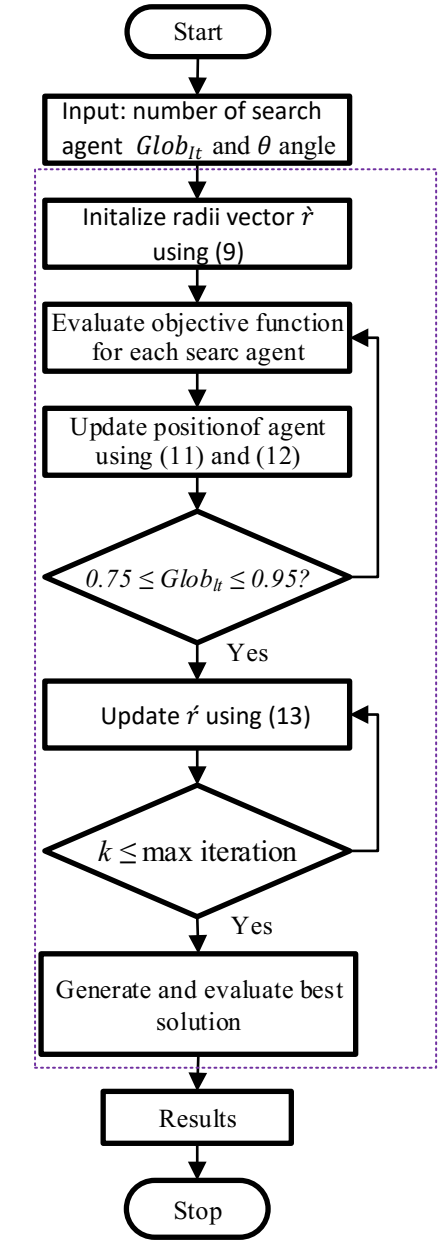


Fig. 3: Flow Chart of CIOA (Yıldız etal, 2024).

IV. Results and discussions

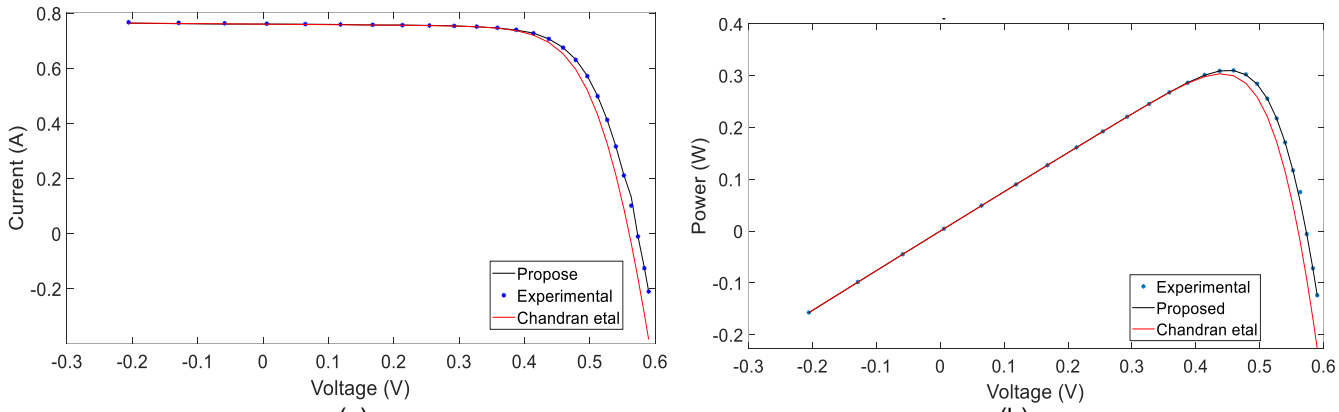
In this subsection, the effectiveness of the CIO algorithm in parameter estimation is validated through the estimation of parameters for a single-diode PV model and a 250W PEMFC fuel cell model. The current-voltage (I-V) characteristics are obtained based on the estimated parameters. The obtained I-V values are compared with parameters determined in previous studies in the literature and experimentally obtained I-V data. The upper and lower limits of the parameters estimated with the proposed CIOA are presented in Table 1.

Table 1: The upper and lower limits of the parameters

PEMFC Parameters			PV Parameters		
Parameter	lower limit	upper limit	Parameter	lower limit	upper limit
ξ_1	-1.25	0.75	I_{ph}	0	1
ξ_2	8e-4	6e-3	I_0	0	1
ξ_3	3.5e-5	1e-4	n	1	2
ξ_4	-3e-4	-8e-5	R_s	0	0.5

λ	9	25	R_{sh}	0	100
R_c	8e-4	9.9e-4			
β	0.01	0.65			
ξ_5	1e-6	1e-5			
ξ_6	0	6			
ξ_7	0	6			

PV system:
In this subsection, the parameters of the single-diode PV model were determined using the CIOA algorithm, and the I-V and P-V characteristics of the model were obtained based on these parameters. The obtained results were then compared with the characteristic curves derived from the parameter values reported by Chandran etal (2021), as well as those determined experimentally. The comparison results are presented in Figure 4.

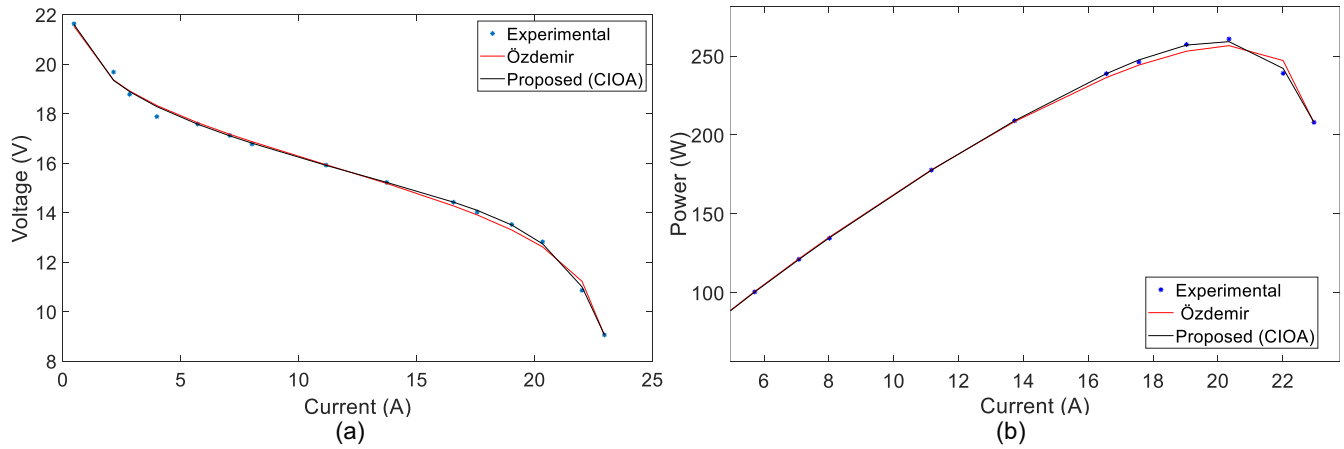


(a) (b)

Fig. 4: Single Diode model (a) I-V Characteristics (b) P-V Characteristics.

Figure 4 demonstrates that the characteristic curves drawn for the parameter values obtained with the CIOA algorithm are closer to the experimentally obtained characteristic curves.

FC system:
In this subsection, the parameters of the 250W PEMFC fuel cell model were determined using the CIOA algorithm, and the I-V and I-P characteristics of the model were obtained based on these parameters. The obtained results were then compared with the characteristic curves derived from the parameter values reported by Özdemir (2021), as well as those determined experimentally. The comparison results are presented in Figure 5.



(a) (b)

Fig. 5: 250W PEMFC model (a) I-V Characteristics (b) I-P Characteristics.

Upon scrutiny of Figure 5, the efficacy of CIOA in parameter estimation for PEMFC is unequivocally discernible.

V. Conclusions
In conclusion, this study introduces the Circle-Inspired Optimization Algorithm (CIOA) for predicting the optimal parameters of PEMFC and PV systems. The performance of this algorithm was evaluated by comparing it with current literature findings and experimental results for determining the parameters of PV and FC systems. The proposed algorithm demonstrated superior results for both single-diode PV and PEMFC models. Thus, the efficiency of the proposed CIOA algorithm in parameter identification for PEM fuel cells and solar panels was tested and validated.

References

Chandran, B. P., Selvakumar, A. I., Let, G. S., & Sathiyan, S. P. (2021). Optimal model parameter estimation of solar and fuel cells using improved estimation of distribution algorithm. Ain Shams Engineering Journal, 12(2), 1693-1700.
de Souza, O. A. P., & Miguel, L. F. F. (2022). CIOA: Circle-Inspired Optimization Algorithm, an algorithm for engineering optimization. SoftwareX, 19, 101192.
Nunes, H. G. G., Silva, P. N. C., Pombo, J. A. N., Mariano, S. J. P. S., & Calado, M. R. A. (2020). Multiswarm spiral leader particle swarm optimisation algorithm for PV parameter identification. Energy conversion and management, 225, 113388.
Özdemir, M. T. (2021). Optimal parameter estimation of polymer electrolyte membrane fuel cells model with chaos embedded particle swarm optimization. International Journal of Hydrogen Energy, 46(30), 16465-16480.
Tariq, A. H., Kazmi, S. A. A., Hassan, M., Ali, S. M., & Anwar, M. (2023). Analysis of fuel cell integration with hybrid microgrid systems for clean energy: A comparative review. International Journal of Hydrogen Energy.
Yan, Y., Wang, B., Wang, C., Zhao, D., & Xiao, C. (2023). Adaptive maximum power point tracking based on Kalman filter for hydrogen fuel cell in hybrid unmanned aerial vehicle applications. International Journal of Hydrogen Energy, 48(66), 25939-25957.
Yıldız, S., Yildirim, B., & Özdemir, M. T. (2024). Enhancing load frequency control and cybersecurity in renewable energy microgrids: A fuel cell-based solution with non-integer control under cyber-attack. International Journal of Hydrogen Energy.

Utilization of Modular Floating Offshore Energy Islands with High Green Hydrogen Production: A P2X Example

[1*]Alper Nabi Akpolat
[1] Marmara University, Faculty of Technology, Department of Electrical-Electronics Engineering, Maltepe, Istanbul, 34854, Türkiye

* E-mail: alper.nabi@marmara.edu.tr

Abstract

Over the past decades, eliminating the ongoing problems of global warming has been one of the world's current aims. Therefore, renewable energy systems allow humanity to produce zero-carbon energy. Recent developments regarding renewable-based generation have led to utilize effectively. On the other hand, hydrogen production, storage, and utilization as fuel for different applications like re-electrification or catalysis for natural gas are attracting considerable interest due to their stable nature and resource diversity, contrary to solar and wind. In this context, energy islands have been established near consumption points to serve as energy hubs by producing energy with photovoltaics (PVs) and wind turbines (WTs). In these islands, the utilization of renewable-based green hydrogen production has witnessed a huge growth in hydrogen storage and its flexibility. As known, green hydrogen is generated by an electrolyzer device that is decomposed water. This paper proposes the utilization of a modular floating offshore energy island. This study is a preliminary attempt and effective solution to establish these energy islands, including green hydrogen production, considering feasibility criteria.

Keywords: Renewable, energy Islands, green hydrogen, fuel cells, distributed energy resources, power-to-X.

I. Introduction

Nowadays, 85% of the energy demand is supplied by conventional sources such as oil, coal, and natural gas. Regarding Turkiye's oil, coal, and gas reservoir, there is no promising leadership among the top countries in the world. Thus, Turkiye has such good renewable potential to produce zero-carbon energy. Reducing energy dependence is one of the national goals of our country. It is anticipated that shortly, there will be a swift transition towards RESs like solar, wind, and hydrogen energy, focusing on these three primary resources due to their effectiveness by Akpolat et al. (2024). Turkiye shows a growing trend in renewable energy market share. The government is actively promoting renewable energy sources such as wind, solar, and hydropower to diversify the country's energy mix and reduce dependence on fossil fuels. In recent years, Turkiye has significantly invested in renewable energy projects, increasing renewable energy capacity. However, Turkiye's market share of renewable energy may vary depending on factors such as government policies, economic conditions, and technological developments. Overall, the trend is favorable, and renewable energy plays an increasingly important role in Turkiye's energy sector, according to CSB data (2021). The ratios of wind and solar energy usage shares to other access resources produced from the graphs are 26.5% and 11.76%, respectively, as seen in Fig.1.

As seen by the figure above, there is no electricity production from hydrogen; however, according to the EU projections, it is aimed to meet approximately $ of the total energy need from hydrogen by 2050 and to prevent 560 Million Tonnes of CO_2 annually. Following the EU's 2050 net zero emission target, Turkiye also ratified the Paris Climate Agreement and set a net zero emission target for 2053. In line with this target, wind, solar, bioenergy, and hydroelectricity from renewable energy sources are primarily on the agenda. Still, hydrogen energy has also been on the agenda in recent years. Turkiye has a green hydrogen production potential between 1.2 and 1.6 USD/kg, according to IDB data (2022).

Green hydrogen is an essential renewable energy source alternative for meeting Turkiye's energy needs, reducing dependence on energy imports, and creating a new export item. In this context, the utilization of RESs near consumption points must be one of the primary goals for achieving these official figures, as reported by ministries. This study aims to present the design, criteria, and utilization of modular floating offshore energy islands with high green hydrogen penetration.

With the increase in energy demand, the trend towards renewable energy is also increasing. The share of renewable energy in Turkiye's total installed capacity increased from 43.3% in 2015 to 56.1% in 2024. The Turkish government is proactively supporting renewable energy sources such as wind, solar, and hydroelectric power to diversify its energy mix and lessen reliance on fossil fuels. In recent years, substantial investments in renewable energy projects have increased Turkiye's renewable energy capacity by Yuksel et al. (2013).

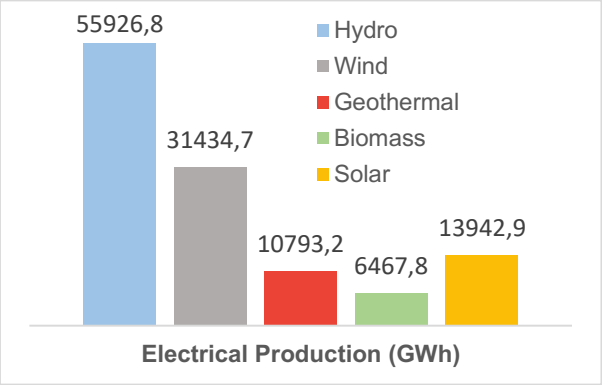


Fig. 1: Produced Electricity Ratio from Renewable Sources in Turkiye CSB data (2021).

The country plans to further boost this share to 65% by 2035 by Anadolu Ajansi (2023). As global energy demands increase and climate change concerns intensify, offshore wind energy has emerged as a promising renewable energy source with great potential. However, implementing offshore wind energy projects successfully depends on comprehensive technical feasibility assessments.

Some advances in the literature are held by Gokcek et al. (2024) about a techno-economic analysis of an on-site hydrogen station supplied via renewables in HOMER, evaluating and analyzing the potential of solar power generation using PVsyst by Endiz et al. (2023) and presenting an insight into the potential situation for the rooftop solar photovoltaic system designing and calculation for the faculty building with PV*SOL package software program by Akpolat et al. (2019). To identify encouraging offshore wind farm locations, the wind atlas program is utilized by Argin et al. (2019). Similarly, Satir et al. (2018) have investigated the feasibility potential of offshore wind farms in the Egean Sea to reduce energy dependence, although the mentioned sea has large continental shelves compared to the Marmara Sea. Also, we can see a fresh study on green hydrogen production potential conducted in Canada by Karayel et al. (2024). This study emphasizes the combined utilization of modular offshore wind-solar and hydrogen energy sources covering the P2X scheme.

II. General System Description of Modular Floating Offshore Energy Islands

The site selection phase begins by considering factors such as wind resource availability, water depth, seabed conditions, and proximity to the power grid. Comprehensive environmental impact assessments are required to ensure sustainable development and minimize environmental impacts. This process examines the impacts of offshore wind farms on marine ecosystems and migratory bird routes. Strategies such as restrictions on turbine spacing and construction period are implemented to reduce negative impacts. In the design of offshore wind energy projects, elements such as turbine selection, foundation design, substation layout, and transmission infrastructure are carefully analyzed to optimize energy production and transmission efficiency and ensure structural integrity. Additionally, technologies such as floating wind turbines and dynamic cables are being investigated to increase the feasibility of projects in deep waters.

Risk assessment is critical to the technical feasibility of these projects. Factors such as extreme weather conditions, corrosion, foundation stability, and electrical grid integration are examined to identify potential challenges and develop risk mitigation strategies. Advanced modeling techniques help predict and optimize system performance. Economic analysis and financing strategies are necessary to determine the project's economic viability. Cost-benefit analyses, energy cost calculations, and evaluation of government incentives are performed. Collaboration between project developers, financial institutions, and regulatory bodies is critical to secure financing and ensure successful implementation.

The general overview of the Power-to-X (P2X) scheme includes green ammonia, which is already utilized in fertilizer production, and green methane. Additionally, synthetic natural gas can be a transitional resource in replacing fossil fuels with synthetic alternatives. P2X technology also enables the production of liquid fuels such as diesel, gasoline, and synthetic kerosene for aviation and shipping industries, as can be seen in Fig. 2.

III. Potential Areas for Modular Energy Islands to

The Ministry of Energy and Natural Resources (MENR) in Turkiye has granted an international project from the European Union toward the cost of the EU Instrument for Pre-Accession (IPA) Energy Sector Program Phase IV Project by performing some part of proceeds for consulting services by MENR (2023). The aforementioned service consists of analysis, measurement, and survey activities with the help of applying meteorological and oceanographic measurement systems. Also, the system should acquire a large amount of reliable meteorological and oceanographic data and yield a report to be analyzed data. Furthermore, this project's goal is to produce technical,

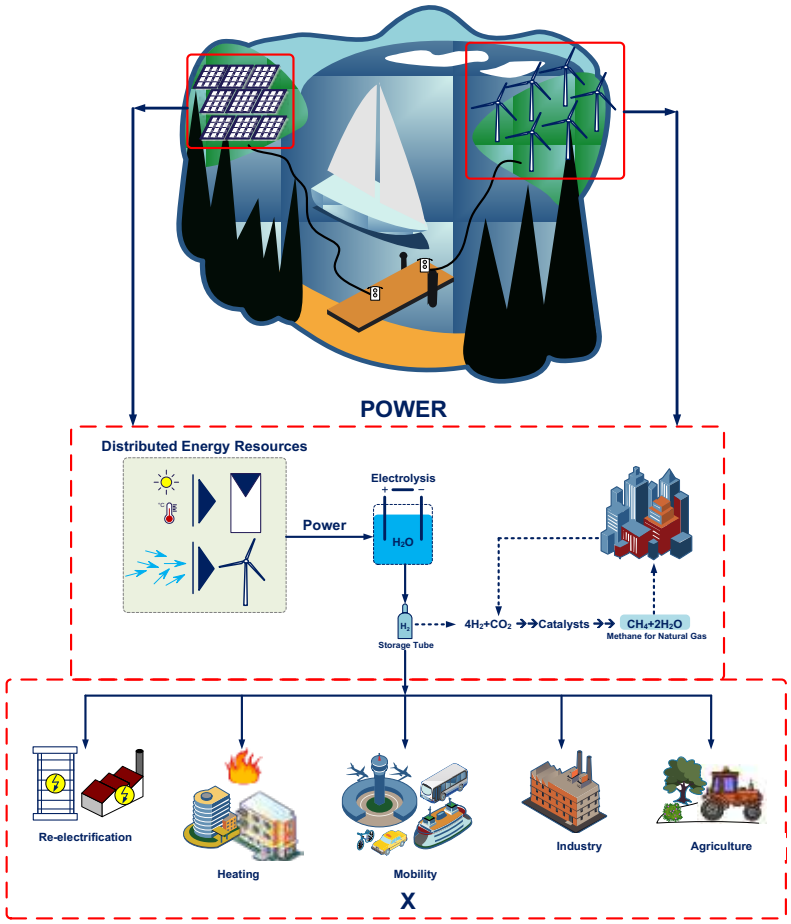


Fig. 2: Modular floating offshore energy island with green energy production: General overview of P2X structure.

legalization, and economic analysis reports, including an oceanographic report with wave model and wind resource assessment and recommendations on offshore wind turbine location, type, sizing, etc. It is worth mentioning that some issues should be considered before advancing. Economic and financial pre-feasibility reports or analyses should be carried out correctly. A detailed high-level grid connectivity assessment should be analyzed to utilize and integrate this offshore wind turbine power plant. Establishing offshore wind development is enabled in advance to ensure this project will avoid facing relevant existing legislation problems. Fig. 3 shows three different development zones (red shaded area) for potential offshore wind turbine projects in the Marmara Sea. It is logical because the selected areas have large continental shelves and are close to electricity consumption points.

On the other hand, the renewable energy production potential of the islands near Istanbul and their support to the general grid are essential for energy continuity. In this context, the potential of solar PV production is presented to establish natural islands close to Istanbul's coast, as this big city needs considerable energy procurement. Regarding this case study, the technical and economic analysis of the photovoltaic system that will meet the energy needs of these households is performed using PV*SOL software, one of the industry's leading solar software programs. It offers detailed configuration and shade analysis for photovoltaic systems. Since the building structures on the island are similar, the studies will be carried out on one household and will also apply to other households on the island. The nine islands in the northeastern part of the Marmara Sea and on the Anatolian side of Istanbul are called the Prince Islands. Five of these nine islands are inhabited. As seen in Fig.3, Sedef Island has a total area of 1.43 km^2 and 114 detached households. According to the results, the electricity fee per kWh is calculated as 0.0633 £, a total of 1906.46 £ is saved according to the results. Financially, the Internal Rate of Return (IRR) is % 10.88. The average performance ratio of the system is 87.14 % with an annual specific yield of 1313.49 kWh/kWp, showing that yearly CO_2 emission can be avoided as 14.131 kg/year, which has noteworthy results.

IV. Conclusion

This study highlights the importance of stakeholder engagement and regulatory compliance throughout the technical feasibility assessment process. Community consultations, environmental permits, and adherence to national and international regulations are essential to gain public acceptance and ensure project sustainability. The technical feasibility assessment for potential offshore wind power projects involves a multidisciplinary approach, encompassing site selection, environmental impact assessment, design optimization, risk analysis, economic evaluation, and regulatory compliance. This simulation study for Sedef Island demonstrates that the 22.89-kWp connected to this PV power plant can produce remarkable power with 42 panels. Detailed financial and performance analysis of the grid-connected RSPS for a sample summer house with various parameters is also carried out in this study. With the help of the calculations, the hour of daily-based annual average



Fig. 3: Selected potential offshore wind turbine MENR (2023) and solar photovoltaic power plant areas in the Marmara Sea.

the duration of sunshine-produced power is 3.6 hours, which is reasonable for the location. Wind and PV-based DERs can contribute to the island's electricity demand and store green hydrogen to supply different purposes, with the aim of covering the P2X structure.

References

Akpolat A. N., Dursun E., Kuzucuoğlu A. E., Modeling and operation of a fuel cell stack for distributed energy resources: A living lab platform, *International Journal of Hydrogen Energy*, (2024), https://doi.org/10.1016/j.ijhydene.2024.03.353.

11.7 Yenilenebilir Kaynaklardan Üretilen Elektrik Oranı, (2021), https://cevreselgostergeler.csb.gov.tr/yenilenebilir-kaynaklardan-uretilen-elektrik-orani-i-85810

Türkiye'nin yeşil hidrojen potansiyeli ve hidrojen teknolojileri, (2022), https://iklim.gov.tr/turkiye-nin-yesil-hidrojen-potansiyeli-ve-hidrojen-teknolojileri-degerlendirildi-haber-31#:~:text=Bu%20hedef%20do%C4%9Frultusunda%20yenilenebilir%20enerji,ye%C5%9Fil%20hidrojen%20%C3%BCretimi%20potansiyeli%20bulunuyor.

Yuksel I., Kaygusuz K., Renewable energy sources for clean and sustainable energy policies in Turkey. *Renewable and Sustainable Energy Reviews*, *15*(8), 4132-4144, (2011).

Renewables total 99.5% of Türkiye's electricity capacity growth in 2023: Energy minister, (2023), https://www.aa.com.tr/en/world/renewables-total-995-of-turkiye-s-electricity-capacity-growth-in-2023-energy-minister/3115824.

Gökçek M. et al., Optimum sizing of hybrid renewable power systems for on-site hydrogen refuelling stations: Case studies from Türkiye and Spain. International Journal of Hydrogen Energy, 59, 715-729, (2024).

Endiz M. S., Coşgun A. E., Assessing the potential of solar power generation in Turkey: A PESTLE analysis and comparative study of promising regions using PVsyst software. *Solar Energy*, *266*, 112153, (2023).

Akpolat A. N. et al., Performance analysis of a grid-connected rooftop solar photovoltaic system. *Electronics*, *8*(8), 905, (2019).

Argin M. et al., Exploring the offshore wind energy potential of Turkey based on multi-criteria site selection. *Energy Strategy Reviews*, *23*, 33-46, (2019).

Satir M., Murphy F., McDonnell K., Feasibility study of an offshore wind farm in the Aegean Sea, Turkey. *Renewable and Sustainable Energy Reviews*, *81*, 2552-2562, (2018).

Karayel G. K., Dincer I., A study on green hydrogen production potential of Canada with onshore and offshore wind power. *Journal of Cleaner Production*, *437*, 140660, (2024).

The Ministry of Energy and Natural Resources, EU Instrument for Pre-Accession (IPA) Energy Sector Program Phase IV Project, (2023), https://enerji.gov.tr/Media/Dizin/BHIM/tr/Duyurular//EK-1_%C4%B0lgi_Beyan%C4%B1_Talebi_%20ve_%C5%9Eartname_202306021410.pdf.

Enhancing Operation Reliability of PV/FC/Battery-Based Distributed Generation via Supervised Deep Learning Approach

[1*]Alper Nabi Akpolat
[1] Marmara University, Faculty of Technology, Department of Electrical-Electronics Engineering, Maltepe, İstanbul, 34854, Türkiye

* E-mail: alper.nabi@marmara.edu.tr

Abstract

Machine learning (ML) has received much attention and has become widespread in energy system problems. To enhance operation sustainability, stability, and reliability of renewable-based distributed energy generation (DEG) systems, AI can be a remedy. Power electronics converters have such a duty as being the backbone of transferring energy. Power electronics' stability and reliability have gained importance for smoothly dispatching energy from renewable energy sources (RESs) to the load side. The crucial matter is here to keep the inputs and outputs of the converters as stable as possible. In this context, this paper outlines the supervised deep learning (SDL) approach to enhance reliability, which is a subset of ML. SDL approach can play a key role in energy transition, especially in the main inverter of the system from the DC bus to the AC bus. As the main power is transferred to the DC bus and then the AC side via the inverter, stabilizing the DC bus voltage with the help of the SDL method has satisfactory results in DC bus voltage and also an easy solution to voltage imbalance.

Keywords: Distributed energy generation, photovoltaics, fuel cells, machine learning, supervised deep learning, reliability.

I. Introduction

In today's world, diminishing carbon footprints and producing zero-carbon energy are primary sustainability aims across the world. An easy step to achieve these aims is to generalize the feasibility of distributed generation (DG). DG systems are scaled-down versions of conventional utility grids and incorporate various renewables such as photovoltaic (PV) panels, wind turbines (WTs), hydrogen fuel cells (FCs), and biomass with battery energy storage (BES) units. The variable nature of renewables on the production side affects the power system adversely. This situation necessitates the development of more intelligent and flexible approaches to improve energy reliability and efficiency. With the technological developments, artificial intelligence (AI) is deployed in nearly every field of science. Originally, AI has been struggling to resemble the mindset of a human brain. The human brain contains many neurons associated with biological neural networks facilitating behavior.

A fully renewable-based distributed generation (DG) system has some challenges. These challenges are solved with the help of modern control methodologies, which sometimes require a heavy mathematical burden for the mentioned system. Therefore, AI can be considered a black box system since it does not require knowledge or a mathematical model of the system to which it will be applied and does not carry any computational burden by Akpolat et al. (2020). Zhao et al. (2021) analyzed AI applications in power electronics in three main aspects: design, control, and maintenance.

Artificial neural networks (ANNs) are a neat solution for estimating energy consumption, management, or load forecasting.SDL strategies have been applied to solve challenges in RES-based DG, e.g., power applications. For better illustration, an SDL-based sensorless control approach has been implemented in PV/BES–based DGs by Akpolat et al. (2021). In Nam et al. (2020), DL-based models estimate voltage and frequency variations in electrical energy production and consumption.

As another example, the SDL-based model has been implemented to analyze and forecast considering factors with an industrial PV power plant's generation by Chandel et al. (2023). With a similar topology, Sabzalian et al. (2022) proposed a novel approach for energy management in PV/FC/BES-based DG systems with DL type-2 fuzzy logic controllers. Apart from these studies, a deep reinforcement learning-based optimal scheduling for rural energy system approach has been conducted with high computational efficiency for the system's energy supply reliability by Liu et al. (2023).

Compared to simpler structures such as ANNs, where an extensive data set is not required for the training process, a deep neural network (DNN) structure based on supervised learning can make short-term forecasts hourly, daily, or weekly using a small amount of data and with minimal error rates as DNN structure has more complexity than in ANNs. In this context, SDL algorithms play an important role in requiring less amount of datasets.

The rest of this study is organized as follows: Section 2 describes an overview of a PV/FC/BES-based distributed generation system. Section 3 provides a deployment of a supervised deep learning approach. In Section 4, findings, obtained results, and discussions on the studied system are given. Lastly, Section 5 elucidates conclusion remarks.

II. Overview of PV/PEMFC/BES-Based Distributed Generation System

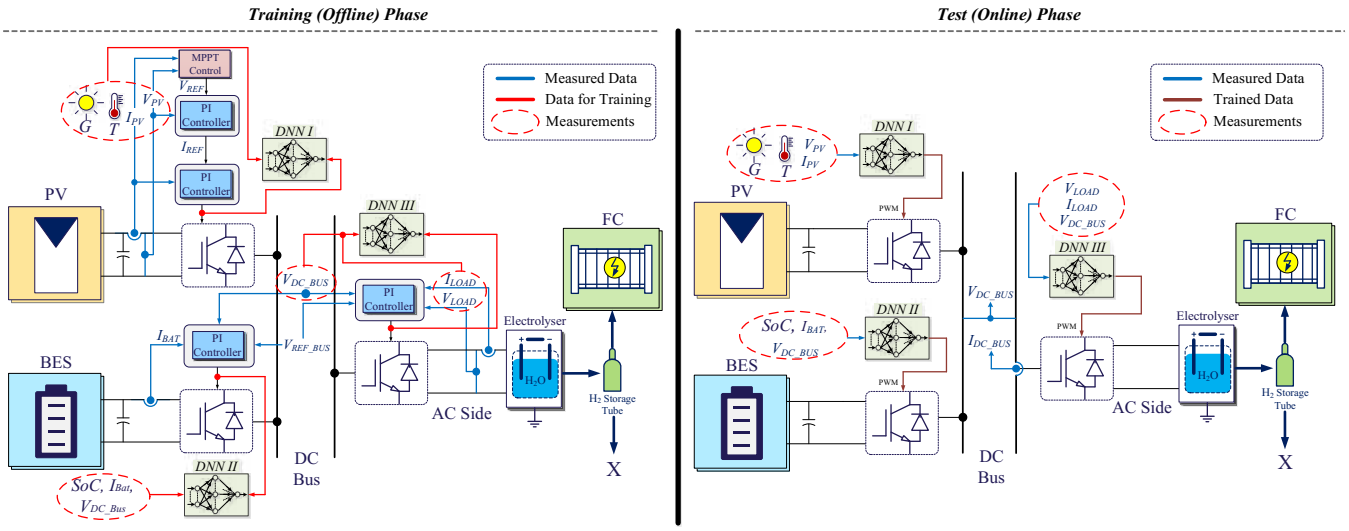


Fig. 1: Operation overview of PV/FC/BES-based DG structure and its controller scheme for training and exploitation phases.

Fig.1 depicts two phases of the whole process: training and operating. The training phase is deployed to gather the training data for DNNs, and then the operating phase is the online phase, which is exploited to see what the DNNs provide output data after the offline phase. After checking the accuracy of the trained network for the system, the system is ready for usage with random datasets as inputs. The trained DNNs provide optimum duty cycles with DC pulse width modulation (PWM) signals to the power electronics quickly without any communication delay and computation effort.

While the PV system is established as a main power source, the BES has the duty of an auxiliary service to energize the electrolyzer. As known, an electrolyzer is a device that separates hydrogen from water by electrolysis. Electrolysers decompose water molecules into oxygen and hydrogen gases using electrical energy. This process allows water to be divided into its two components using an electrical current. Alcalin, proton exchange membrane, and solid oxide electrolyzer types exist. One of the paper's most desired aims is to keep the system stable and transfer sustainable energy for hydrogen production. Hydrogen production is utilized with the help of fully penetrated RESs; thus, it can be noted that this system produces green hydrogen. This green hydrogen can benefit such as different applications like re-electrification with FCs.

This topology can be asserted as a power-to-X (P2X) structure. While the power side can be categorized as the PV/BES-based production part, the X part can be mentioned with different applications. For better illustration, a P2X enables the creation of carbon-neutral resolutions, addressing unavoidable emissions from industries. For instance, synthetic natural gas can serve as a transition source for the eventual replacement of fossil fuels with synthetic fuels. Also, green ammonia and green methane, currently used in fertilizer production, can also be produced. In addition, liquid fuels such as diesel, petrol, and synthetic kerosene can be produced for use in the aviation and marine sectors. In this context, hydrogen-based electricity infrastructures have been becoming more common in Akpolat et al. (2024).

III. Deployment of a Supervised Deep Learning Approach

If we assume that AI is a big cluster, machine learning (ML) is a subset of AI, which includes many specific mathematical algorithms. As seen in Fig. 2, deep learning (DL) is a subset of ML known as a neural network with many hidden layers. Supervised deep learning (SDL) is an ML method in which DL models are trained using labeled data. This method enables a model to learn the information required to perform a specific task from examples in the dataset. In the supervised learning process, the model is fed with the correct outputs (labels) corresponding to the inputs and tries to learn this relationship, as explained by Habibi et al. (2023).

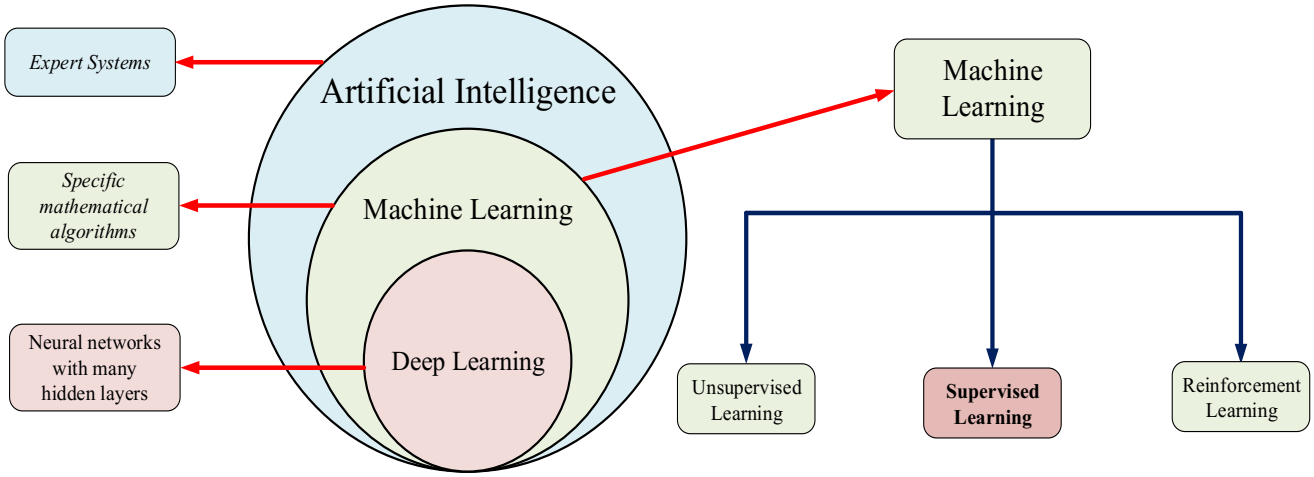


Fig. 2: Artificial intelligence (AI) family and machine learning (ML) methods.

SDL carries out some processes, such as data collection, and a large amount of labeled data is required to train the model. Each data sample is associated with a label indicating the correct output. The second primary step is to model training. During training, the model uses the data to learn the relationship between inputs and outputs. This allows the model to predict the outputs corresponding to the inputs accurately. After this step, an error measurement is achieved, and the backpropagation algorithm is initialized. The difference between the model's predictions and the actual outputs is measured. Thus, an error is calculated. This error is used to update the model's parameters so that the model makes more accurate predictions over time. Lastly, after complete training, the model is tested with data it has not seen before. This evaluates the model's ability to generalize and perform in the real world by Akpolat et al. (2021).

It is important to mention that we have used a back-propagation algorithm based on networks of DNNs and supervised learning. Supervised learning has such a process that correct output (y_{co}) is known by output (y_o) gathered in the offline phase. The error (e) should be calculated between y_{co} *and* y_o.

$$e = y_{co} - y_o, \tag{1}$$

These error values are transferred back to hidden layers to set the weights of DNN nodes; thus, y_{co} is defined again. This process has a systematic way of updating the weight of the nodes, which denotes a "learning rule." Delta learning rule and rectified linear unit (ReLU) function as an activation function is adopted. According to the errors, the weights should be updated with the help of satisfying as follows

$$w_{ij} \leftarrow w_{ij} + \Delta w_{ij}, \tag{2}$$

$$\Delta w_{ij} = \alpha \delta_i x_j, \tag{3}$$

then,

$$\delta_i = \varphi'(v_i) e_i, \tag{4}$$

$$w_{ij} \leftarrow w_{ij} + \alpha \varphi'(v_i) e_i x_j, \tag{5}$$

where, α is the learning rate that should be between zero and one ($0 < \alpha < 1$), φ is the derivative of the activation function, and v_i represents α weighted sum of the output node (i-namely i^{th} neuron).

$$\Delta w_{ij} = \frac{1}{n} \sum_{r=1}^{n} \Delta w_{ij}(r), \tag{6}$$

where, $\Delta w_{ij}(r)$ is the weight update for r_{th} training data, n denotes the total number of the training data. To evaluate the performance criteria for the trained network, Equation (7) gives the mean squared error (*MSE*), which is used as a loss function as follows:

$$MSE = \frac{1}{n} \sum_{i=1}^{n} e_i^2 = \frac{1}{n} \sum_{i=1}^{n} |y_{co} - y_o|^2. \tag{7}$$

IV. Results and Discussion

It is distinct that DNN-aided operation shows superior performance than conventional control. As observed from Fig. 3, V_{DC_BUS} in the operating phase, i.e., after the training phase, looks more stable than the training phase. Furthermore, damping the fluctuations of V_{DC_BUS} is crucial for feeding the AC side and producing green hydrogen, as the single-phase full-bridge pure sinus inverter topology needs a stable DC bus voltage. Thereby, the inverter can produce a pure sinus wave with less harmonic. On the other hand, the DNN-aided system has placed steady-state operation sooner than the conventional one since it has no computational burden, which results in a communication delay. The best performance of *MSE* has been obtained as 3.96e-4.

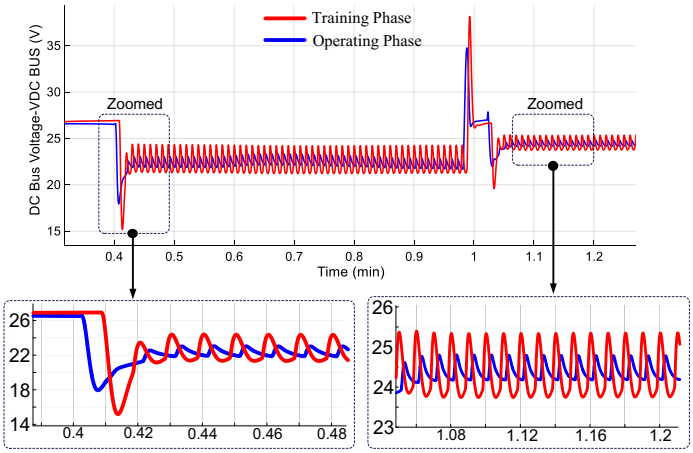


Fig. 3: DC Bus voltage V_{DC_BUS} on the BS bus under variable input and output (load) change.

V. Conclusion and Future Remarks

This study has highlighted the importance of providing sustainable energy from renewables to the AC side to produce green hydrogen for the P2X structure. The proposed design has obtained satisfactory results, proving that less voltage oscillation, faster slew rate, and sooner time response. The fluctuations of V_{DC_Bus} under variable input-output (load) conditions have achieved better performance and operation conditions that enhance the system's stability and reliability. This approach can be applied where it needs more reliable operation. With the help of gathered big data from the system, remaining useful lifetime estimation or predictive maintenance for the system's component can be implemented in future work.

References

Akpolat A. N., Dursun E., Kuzucuoğlu A. E., AI-aided control of a power converter in wind energy conversion system. In *2020 Innovations in Intelligent Systems and Applications Conference (ASYU)*. pp. 1-6, IEEE, (2020, October).

Zhao S., Blaabjerg F., Wang, H., An overview of artificial intelligence applications for power electronics. *IEEE Transactions on Power Electronics*, *36* (4), pp. 4633–4658, (2021).

Akpolat A. N., Dursun E., Kuzucuoğlu A. E., Deep learning-aided sensorless control approach for PV converters in DC nanogrids. *IEEE Access*, *9*, pp.106641-106654, (2021).

Nam K., Hwangbo S., Yoo C., A deep learning-based forecasting model for renewable energy scenarios to guide sustainable energy policy: A case study of Korea. *Renewable and Sustainable Energy Reviews*, 122, 109725, (2020).

Chandel S. S., Gupta A., Chandel R., Tajjour S., Review of deep learning techniques for power generation prediction of industrial solar photovoltaic plants. *Solar Compass*, *8*, 100061, (2023).

Sabzalian M. H., et al., A new immersion and invariance control and stable deep learning fuzzy approach for power/voltage control problem. *IEEE Access*, *10*, 68-81, (2021).

Liu B., Liao J., Xu L., Huang Q., A Deep-Reinforcement-Learning-based Optimal Scheduling for Rural Integrated Energy System Considering the Uncertainties of Renewable Energies and Loads. In *2023 3rd New Energy and Energy Storage System Control Summit Forum (NEESSC)*, pp. 1-6, IEEE, (2023, September).

Akpolat A. N., Dursun E., Kuzucuoğlu A. E., Modeling and operation of a fuel cell stack for distributed energy resources: A living lab platform. *International Journal of Hydrogen Energy*, (2024), https://doi.org/10.1016/j.ijhydene.2024.03.353.

Habibi M. R., Golestan S., Guerrero J. M., Vasquez J. C., Deep Learning for Forecasting-Based Applications in Cyber–Physical Microgrids: Recent Advances and Future Directions. *Electronics*, *12* (7), 1685, (2023).

Transition to Fuel Cells in Diesel Fueled Locomotives: An Environmental and Technological Change

[1]Kenan Dogan, [1*]Zehra Ural Bayrak
[1] Firat University, School of Aviation, Department of Avionics, Elazığ, 23200, Türkiye

* E-mail:zural@firat.edu.tr

Abstract
Nowadays, environmental sustainability is becoming increasingly important, and in this context, the transportation sector, especially railway transportation, is entering a process of transformation towards green technologies. This study deals with a research on the use of fuel cell systems instead of traditional diesel-fueled locomotives. Diesel engines are known for their harmful effects on the environment, such as atmospheric pollution and greenhouse gas emissions. To reduce these impacts, alternative fuel sources and clean energy technologies are being investigated. Fuel cells are an energy conversion technology that attracts attention with its low carbon emissions and high efficiency. Fuel cell locomotive systems consist of various main components such as battery groups, fuel cells, inverters, converters and engines. The integration of these components enables a cleaner and more efficient rail transport system. This study discusses the advantages and disadvantages of using fuel cell systems to reduce the environmental impact of diesel-fueled locomotives and highlights the potential of future green rail transport.

Keywords: Fuel cell, Diesel Locomotive, Green Energy, Hydrogen Technologies

I. Introduction

Rail transport plays a vital role in economic growth and the mobility of societies around the world. However, the environmental impacts of diesel-fueled locomotives, one of the traditional power sources of this sector, are causing increasing concerns. Diesel engine locomotives pose restrictions on energy efficiency and operating costs, as well as environmental problems such as greenhouse gas emissions and air pollution.

In the search for an alternative and environmentally friendly solution, the transition to a power source based on fuel cells has significant potential. Diesel engines convert the heat energy generated by the combustion of fuel into mechanical energy using a mechanism known as internal combustion engines. In this process, various greenhouse gases and particles are released as a result of the burning of petroleum-derived fuels. Fuel cells produce electrical energy by combining hydrogen and oxygen through chemical reactions. This reaction produces clean byproducts such as water and heat, resulting in zero emissions and higher efficiency. In this study, the environmental impacts of existing diesel locomotives and the difficulties in reducing these impacts will be examined. Next, the operating principle of the diesel-fueled locomotive will be explained. Finally, the technical and economic benefits of switching to fuel cells in diesel-fueled locomotives will be discussed.

II. Operation of Diesel-Electric Locomotives

Diesel engines, one of the internal combustion engine types, have higher torque and fuel efficiency, have a longer life and provide high performance at low revs. They are more advantageous than other engines in heavy load transportation and long-distance roads. The main parts of a standard Diesel-Electric locomotive are shown in Figure 1.

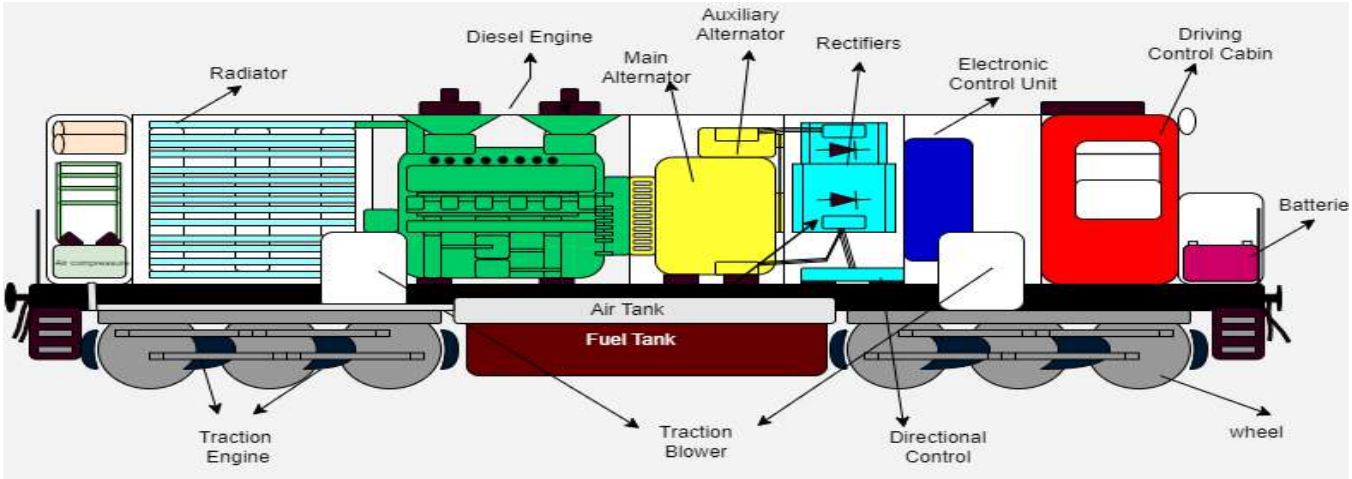


Fig. 1: Main parts of a standard Diesel-Electric locomotive

In Diesel-Electric Locomotives, the source of energy is diesel engines. The mechanical energy obtained in diesel engines is converted into three-phase AC electrical energy in the Main Alternator connected to the crankshaft. The diesel engine turns the rotor shaft in the main alternator. On the rotor shaft are the rotor windings of the main

alternator, which rotate inside the stator windings. The stator windings are fixed to the body of the main alternator. In order for the main alternator to produce energy, it must be excited by the auxiliary alternator. Three-phase AC voltage is produced depending on the amount of excitation and engine speed. This three-phase electrical energy is controlled in different ways according to the control system of the locomotive and used to rotate the traction motors located on the axles and turning the wheels of the locomotive. The mechanical energy produced by the diesel engine is converted into 3-phase alternating current electrical energy in the alternator and then rectified by full-wave rectifiers. The direct current electrical energy obtained is converted back into mechanical energy in the DC traction motors located in the front and rear wheel groups and is transferred to the wheels through pinion gears.

In this type of applications, speed control of traction motors is done by directly changing the alternator excitation current. Diesel-electric locomotive power transmission diagram is given in Figure 2. As shown in Figure 2, the auxiliary alternator, which takes its action from the diesel engine, excites the main alternator by being excited through the excitation regulator. This current applied to the main alternator terminals produces three-phase energy at the levels of 225-1440 volts, depending on the power of the main alternator. After this voltage is rectified at the output of the main alternator, it is applied to the traction motors placed in the wheel groups in proportion to the desired power in the locomotive.

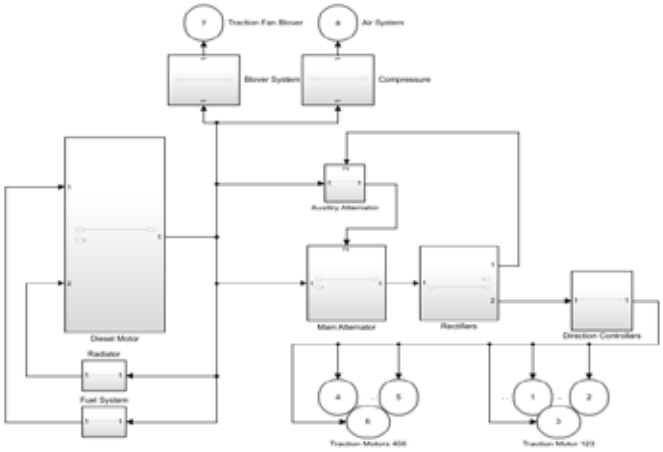


Fig. 2: Diesel-Electric Locomotive Power Transmission

III. Fuel Cell Locomotive Technology

Fuel cell locomotives are an energy conversion technology that converts chemical energy directly into electrical energy. These locomotives work with electric motors. As in diesel locomotives, there are traction motors in the wheel groups. In place of the diesel engine, there are fuel cells in which hydrogen comes into contact with oxygen. As shown in Figure 3, the system consists of hydrogen tanks, fuel cells and battery groups, unlike diesel locomotives. When the driver wants to move the locomotive, a power request is sent to the electronic control unit. The electronic control unit activates the relevant valves connected to the system and provides hydrogen flow from hydrogen tanks to fuel cells. The flowing hydrogen is directed to the anode plates of the fuel cell. Oxygen taken from the open air through air filters travels towards the cathode plates. Electrical energy is produced by reacting with hydrogen and oxygen between these plates. Fuel cells provide the environment necessary for this reaction. Such locomotives can also generate electricity during dynamic braking (regenerative braking). Battery groups are charged with this generated energy. While the battery groups store the energy produced during regenerative braking, they also provide extra energy to the traction motors during the traction of the locomotive. The inverter section in our system converts energy at different voltage levels. The 220 V energy need in the driver's cabin or the supply voltage of the electronic control unit can be given as examples of this situation. An electric fan should be used instead of a snail type blower to cool the traction motors.

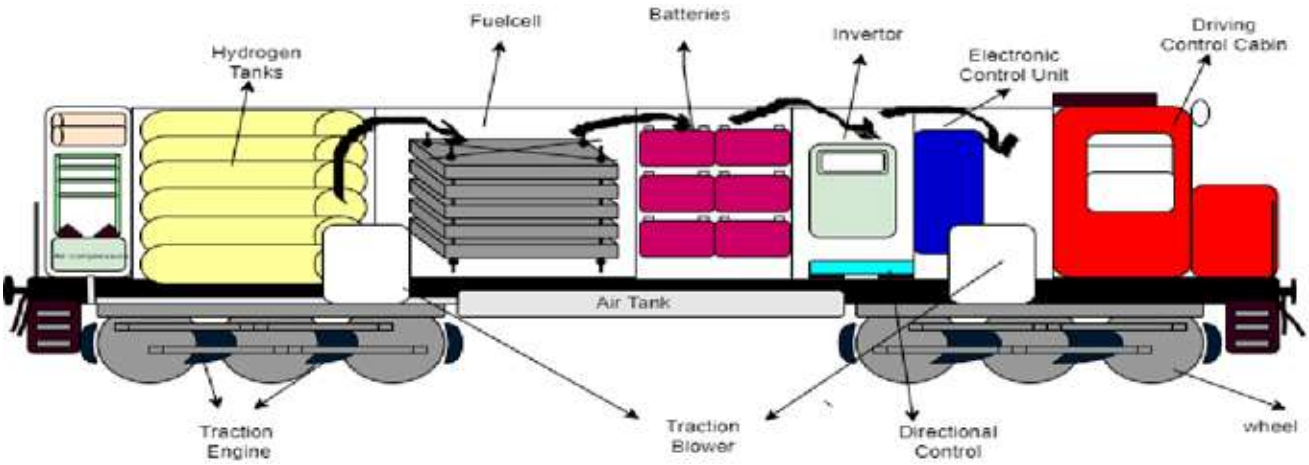


Fig. 3: Main parts of Fuel Cell-Electric Locomotive

DE24000 type locomotives used in the state railways of the Republic of Turkey have an average power of 2400hp. To provide this very high power, one of SOFC or PEM fuel cells can be used. SOFC can operate at high temperature and is often used in industrial facilities and large-scale power generation. This type of fuel cell can provide high power production and low costs, but may require a more complex system. The PEM fuel cell can operate at low temperature and offers faster starting and stopping capabilities, making it more suitable for vehicles and portable applications. However, it may have higher costs and maintenance requirements in high power applications. As a result, certain requirements and constraints must be taken into account to decide which fuel cell to use to deliver 2500hp.

IV. Results and discussions of two systems

The contribution of diesel locomotives to atmospheric pollution and greenhouse gas emissions is significantly high. During the combustion process, particulate matter, nitrogen oxides (NO_x), carbon dioxide (CO_2) and other harmful gases are released into the atmosphere. These emissions cause environmental problems such as air pollution, health problems and climate change.

Hydrogen fueled locomotives offer a clean and zero-emission alternative. Hydrogen fuel produces only water vapor and heat during the combustion process, so no harmful emissions are released into the atmosphere. This improves air quality and reduces environmental impact.

Diesel locomotives produce electrical energy from the combustion process of fuel. However, energy efficiency is low and energy losses occur during combustion. Therefore, the fuel consumption of diesel locomotives is high and increases operational costs.

Hydrogen-fueled locomotives directly produce electrical energy using fuel cell technology. This increases energy efficiency and enables longer ranges with lower fuel consumption. This saves on operating costs. Diesel locomotives operate based on existing fuel supply and infrastructure. The widespread availability of fuel stations and storage facilities increases the operational flexibility of diesel locomotives. The use of hydrogen-fueled locomotives may encounter technical difficulties such as hydrogen storage and distribution. The expansion of hydrogen filling stations and infrastructure is necessary and may be costly and complex initially.

V. Conclusions

In this study, the environmental impacts, technological features and advantages of diesel locomotives and hydrogen fueled locomotives were compared. Both technologies have certain advantages and disadvantages, and these factors shape the future of rail transportation.

Diesel locomotives have been a widely used technology for many years and enable a rapid transition based on existing infrastructure. However, the environmental impacts of diesel engines, such as atmospheric pollution and greenhouse gas emissions, cause serious concerns. Therefore, the search for environmentally friendly and sustainable alternatives is increasing.

Hydrogen-fueled locomotives offer a clean, zero-emission alternative. Hydrogen fuel produces only water vapor and heat during the combustion process, so no harmful emissions are released into the atmosphere. This improves air quality and reduces environmental impact. Additionally, hydrogen fueled locomotives are more energy efficient and enable long ranges to be achieved. However, there are some difficulties with the use of hydrogen fueled locomotives. Technical challenges may be encountered, such as hydrogen storage and distribution, and infrastructure requirements may be initially costly. Therefore, infrastructure development and costs need to be reduced for wider adoption of hydrogen-fueled locomotives.

Consequently, the comparison between diesel locomotives and hydrogen-fueled locomotives plays an

important role in the search for sustainable alternatives to improve the environmental impacts and energy efficiency of rail transport. Hydrogen-fueled locomotives are seen as a promising solution for a clean and environmentally friendly future, but infrastructure and technological developments need to progress further.

References

Siddiqui O., Dincer I., A Review on Fuel Cell-Based Locomotive Powering Options for Sustainable Transportation, Arabian Journal for Science and Engineering, 44, 677–693, (2019).

Nylund, N.O. et al., Hydrogen and fuel cells in maritime and rail transportation: A review, Renewable and Sustainable Energy Reviews, 118, 109502, (2020).

United Nations. The Environmental Benefits of Rail Transport, Retrieved from: https://www.unece.org/fileadmin/DAM/trans/doc/2018/ecfwp2018/UN_ECE_WP29_Greener_Transport.pdf. (2019).

Zhang, Y. et al. Energy and Environmental Assessment of Hydrogen Fuel Cell Locomotives Compared with Electric and Diesel Locomotives, Energy, 174, 1164-1174, (2019).

European Railway Agency. "Rail in Figures." Retrieved from: https://www.era.europa.eu/content/rail-figures_en. (2021).

https://earsiv.anadolu.edu.tr/xmlui/bitstream/handle/11421/6008/12056.pdf?sequence=1&isAllowed=y

Multi-optimization of Hydrogen Production of a Solar-based S-I Thermochemical Cycle

[1,] Ramazan Çakıroğlu, [2]Gamze Şener, [1]*Oguz Kaan Çinici, [1,2]Adem Acir,
[1]Gazi University, Faculty of Technology, Department of Energy Systems Engineering, Ankara, 06000, Türkiye
[2]Gazi University, Graduate School of Natural and Applied Sciences, Department of Nuclear Sciences, Ankara, 06000, Türkiye

* E-mail: oguzkaancinici@gazi.edu.tr

Abstract
The aim of this study is to examine the multi-optimization of hydrogen production with by using solar based sulfur-Iodine (S-I) thermochemical cycle. Experimental design is planned according to $L9$ orthogonal array with by using Taguchi method. The overall efficiency of the system ($\eta_{overall}$) and hydrogen production ($\dot{m}_{H_2}$) have been optimized for receiver height (A), receiver radius (B) and wind velocity (C) with ANOVA analysis. The best results have been obtained as A1B1C1 for $\eta_{overall}$ and $\dot{m}_{H_2}$ of the optimum parameters. The percent contribution rates (PCR) for $\eta_{overall}$ and $\dot{m}_{H_2}$ have been computed as 38.84 %, 44.90 % and 0.1% for for receiver height (A), receiver radius (B) and wind velocity (C), respectively.

I. Introduction

Energy need increases with the increasing population rate. Today, energy needs are met from fossil fuels. Fossil fuels emit environmentally harmful gases such as CO_2, SO_x and NO_x. For this reason, the search for clean and renewable alternative fuels continues [1, 2]. Hydrogen energy, which is a clean energy, comes to the fore in the search for alternative energy. Hydrogen can effectively reduce greenhouse gas emissions. In recent years, hydrogen production has been carried out through hydrogen production processes integrated with renewable energy sources. Hydrogen production from solar energy is considered sustainable and clean solutions. Hydrogen production was carried out by Emre and Dinçer [3] through a solar heliostat-based hybrid system integrated with NaOH PCM. Ratlamwala et al. [4] investigated hydrogen production by developing an integrated system including the heliostat area, steam cycle, organic Rankine cycle and electrolyzer. In this study, multi-objective optimization of the hydrogen production of a solar-based sulfur-Iodine (S-I) thermochemical cycle with grey relational analysis (GRA) has been performed. The hydrogen production ($\dot{m}_{H_2}$) at optimum design, parameters were calculated and compared.

II. Problem Description

The solar-powered hydrogen production system consists of a solar heliostat field, a central receiver, a phase change material (PCM) unit and a hydrogen production facility. In this study, it is aimed to produce hydrogen using the sulfur iodine (S-I) thermochemical cycle. The solar energy-based hydrogen production system flow chart is shown in Figure 1. In this system, analyzes were made for six-month average solar flux values. Additionally, in addition to solar flux values, a Taguchi experiment design was made for receiver height (A), receiver radius (B) and wind velocity (C) with ANOVA analysis. The parameters determined for hydrogen production are given in Table 1. To determine the optimum design parameters, depending on the parameters selected in the experimental design, receiver height (A), receiver radius (B) and wind velocity (C) with ANOVA analysis for $\eta_{overall}$ and $\dot{m}_{H_2}$. Experimental design using L_9 orthogonal array have been given in Table 2. Sulfur-iodine cycle is one of the most widely used water splitting methods for hydrogen production [5]. The sulfur-iodine cycle consists of three thermochemical reactions that occur at different temperatures. All process fluids are recycled and all harmful chemicals are kept in the loop; The high temperature (~900 °C) stage can be integrated into a solar reactor as shown in Fig. 1.

Table 1. Assignment of the levels to the factors

Symbol	Parameters	Levels		
		1	**2**	**3**
A	Receiver height, H (m)	8	12	18
B	Receiver radius, R (m)	4	6	9
C	Wind velocity (m/s)	4	6	8

Table 2. Experimental design using L9 orthogonal array

Experiment no.	A	B	C
1	1	1	1
2	1	2	2
3	1	3	3
4	2	1	2
5	2	2	3
6	2	3	1
7	3	1	3
8	3	2	1
9	3	3	2

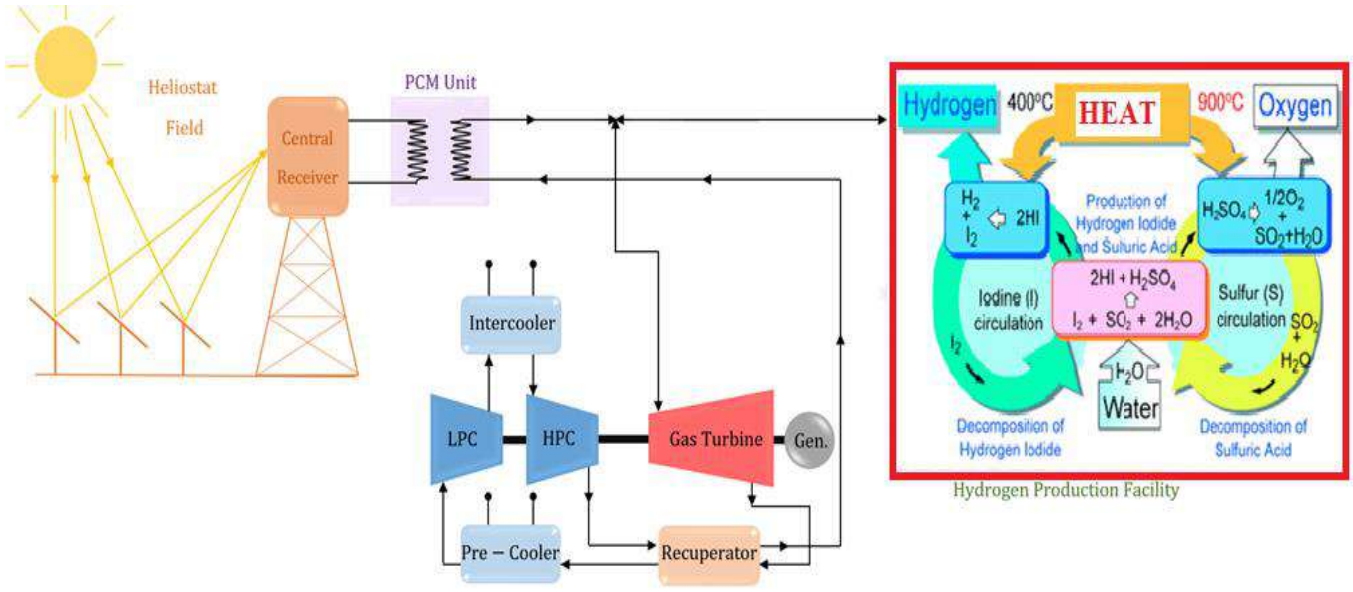


Fig. 2. Schematic description with S-I cycle

The mass flow rate of the generated hydrogen (kg/s) has been determined using mass ratio balance equations, specifically, Eqs. (1-4). The comprehensive explanations and further details regarding these mass flow ratio balance equations can be found in Refs. [6-7].

$$\sum \dot{m}_{in} = \sum \dot{m}_{out} \tag{1}$$

$$\dot{m}_x = \frac{\dot{Q}_{abs}\,\varphi}{q_{tot}} \tag{2}$$

$$\dot{m}_y = \dot{m}_x \frac{u_y}{u_x}\eta \tag{3}$$

Finally, the overall efficiency of the system is calculated with Eq. (4)

$$\eta_{overall} = \frac{\dot{m}_{H_2} \times HHV}{\dot{Q}_{field}} \tag{4}$$

IV. Results and discussions

The effecting the amount of hydrogen produced by the solar-based cobalt-chlorine (Co-Cl) thermochemical cycle using the GRA method have been performed with various parameters. The overall efficiency of the system ($\eta_{overall}$) and hydrogen production ($\dot{m}_{H_2}$) have been optimized for receiver height (A), receiver radius (B) and wind velocity (C) with parameters as presented in Table 1. The experimental design with three factors and levels have been performed by using Minitab software and the obtained results are normalized between zero (0) and one (1) in GRA. The normalization of the $\eta_{overall}$, $\dot{m}_{H_2}$have been conducted in the case of the “higher the better” process as given in Eq. (5).

$$\frac{S}{N} = -10\left(log\frac{1}{n}\sum_{i=1}^{n}\frac{1}{y_i^2}\right) \tag{5}$$

The thermal energy required by the S-I thermochemical cycle is provided by the solar heliostiat system. Experimental results and S/N ratio have been given Table 3. The optimum parameters with S/N ratio have been obtained as presented Figs. 2 and 3. As presented in Fig. 2-3 and Table 3-4-5, The $\eta_{overall}$, $\dot{m}_{H_2}$optimal performances for "higher the better" have been provided in the A1-B1-C1 optimum sequence as receiver height (A)=8 m, receiver radius (B)= 4 m and wind velocity (C)= 4m/s, respectively.

Table 3. Experimental results and S/N ratio

Experiment no.	A	B	C	$\dot{m}_{H_2}$		$\eta_{overall}$	
				Calculated (kg/s)	S/N (dB)	Calculated	S/N (dB)
1	8	4	4	0.2488	-12.0844	0.3427	-9.3011
2	8	6	6	0.2387	-12.4446	0.3288	-9.6613
3	8	9	8	0.2226	-13.0505	0.3066	-10.2672
4	12	4	6	0.2393	-12.4212	0.3297	-9.6379
5	12	6	8	0.2238	-13.0031	0.3083	-10.2198
6	12	9	4	0.2127	-13.4450	0.2930	-10.6617
7	18	4	8	0.2249	-12.9597	0.3099	-10.1764
8	18	6	4	0.2137	-13.4056	0.2944	-10.6223
9	18	9	6	0.1817	-14.8122	0.2504	-12.0289

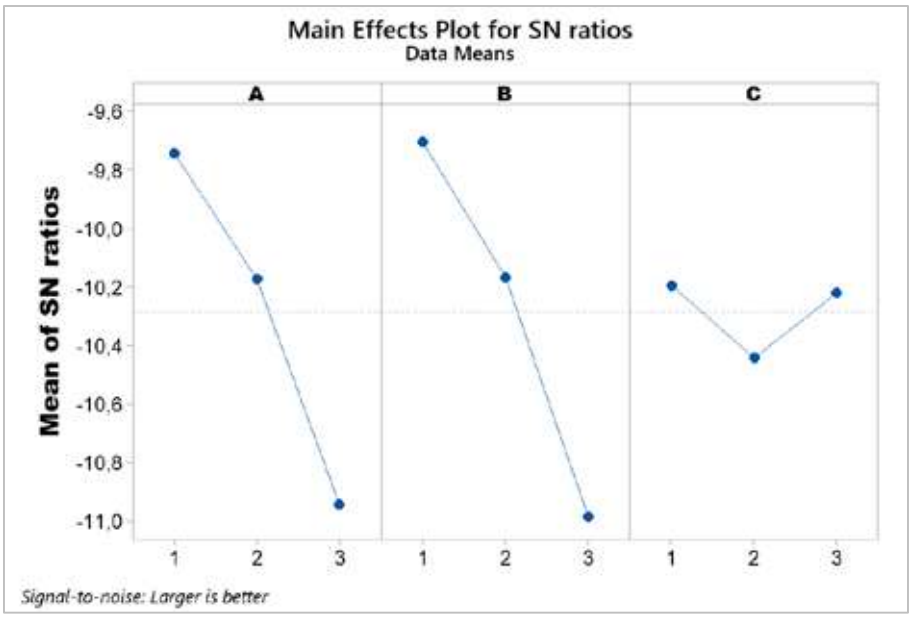


Fig. 3. Mean S/N ratio graph for $\eta_{overall}$

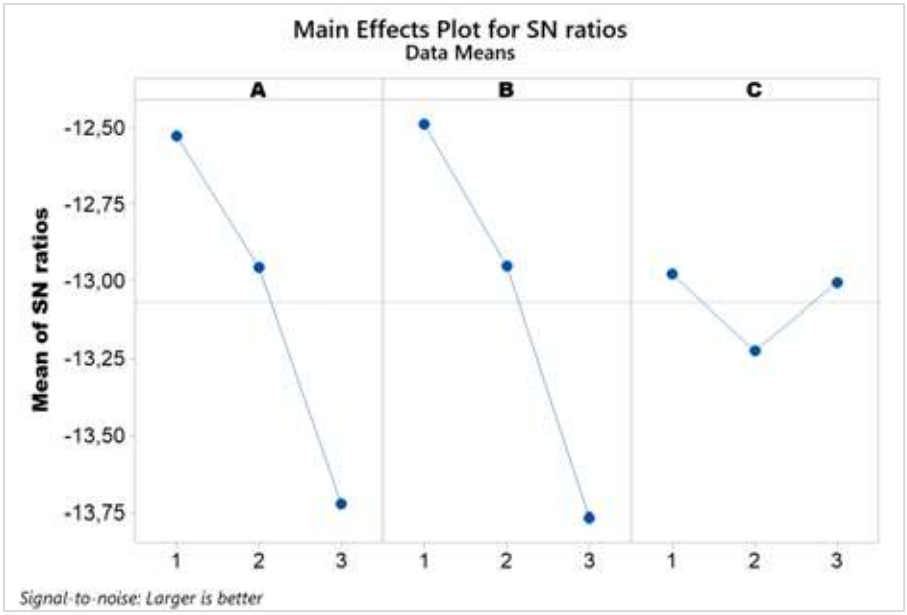


Fig. 4. Mean S/N ratio graph for $\dot{m}_{H_2}$ (kg/s)

This quantitative effect on the outputs has been calculated as the percent contribution rate (PCR) given in Eq. (6).

$$PCR\ \% = \left(\frac{SS_A - (V_e).(\upsilon_A)}{SS_T}\right) x100 \quad (6)$$

where SS_A is the sum of squares, υ_A is the degree of freedom, SS_T has represented the total sum of squares, V_e has indicated variance of error.

Table 4. ANOVA results for $\eta_{overall}$ (for S/N ratios)

Source	Degrees of freedom (DoF)	Sequential sum of squares (SS)	Mean sum of squares (MS)	F-test	P-coefficient	PCR (%)
A	2	2.2153	1.10764	9.28	0.097	38.84
B	2	2.5239	1.26196	10.57	0.086	44.90
C	2	0.1111	0.05557	0.47	0.682	0.10
Residual error	2	0.2388	0.11942			16.6
Total	8	5.0892				100

Table 5. ANOVA results for $\dot{m}_{H_2}$, (kg/s) (for S/N ratios)

Source	Degrees of freedom (DoF)	Sequential sum of squares (SS)	Mean sum of squares (MS)	F-test	P-coefficient	PCR (%)
A	2	2.2153	1.10764	9.28	0.097	38.84
B	2	2.5239	1.26196	10.57	0.086	44.90
C	2	0.1111	0.05557	0.47	0.682	0.10
Residual error	2	0.2388	0.11942			16.6
Total	8	5.0892				100

As shown in Table 4 and Table 5, the PCR values of each parameter have been computed for $\eta_{overall}$, $\dot{m}_{H_2}$ with ANOVA analysis. The PCR values for $\eta_{overall}$, $\dot{m}_{H_2}$ have been computed as 38.84 %, 44.90 % and 0.1% for for receiver height (A), receiver radius (B) and wind velocity (C), respectively. The results of confirmation tests for $\eta_{overall}$ and $\dot{m}_{H_2}$have been given in Table 6 and 7. According to the ANOVA results, the improvement of S/N ratio have been computed as 0.9188 dB and 0.9199 dB for $\eta_{overall}$ and $\dot{m}_{H_2}$

Table 6. Results of confirmation tests for $\eta_{overall}$

	Starting parameters	Optimal parameters	
		Prediction	Experimental
Level	A2B2C3	A1B1C1	A1B1C1
n, overall	0.3083	0.3493	0.3427
S/N ratio (dB)	-10.2205	-9.0707	-9.3017
Improvement of S/N ratio	0.9188 dB (8.99%)		
Prediction error (dB)	0.231		

Table 7. Results of confirmation tests for $\dot{m}_{H_2}$, (kg/s)

	Starting parameters	Optimal parameters	
		Prediction	Experimental
Level	A2B2C3	A1B1C1	A1B1C1
mH2. (kg/s)	0.2238	0.2536	0.2488
S/N ratio (dB)	-13.0028	-11.8540	-12.0829
Improvement of S/N ratio	0.9199 dB (7.07%)		
Prediction error (dB)	0.2289		

V. Conclusions

The following results have been given as below:

- ✓ The optimum levels for $\eta_{overall}$, $\dot{m}_{H_2}$ have been computed as A1-B1-C1 which has i receiver height (A)=8 m, receiver radius (B)= 4 m and wind velocity (C)= 4m/s, respectively.
- ✓ The PCR of the $\eta_{overall}$, $\dot{m}_{H_2}$ have been computed as as 38.84 %, 44.90 % and 0.1% for for receiver height (A), receiver radius (B) and wind velocity (C), respectively.
- ✓ The produced hydrogen amount ($\dot{m}_{H_2}$) in optimum design parameters have been calculated as 0.2488 kg/s.

References

[1] Veziroğlu T. N. and Şahin S. 21st Century's energy: Hydrogen energy system. Energy Convers. Manag. 2008; 49(7):1820–31.

[2] Paparao J. and Murugan S. Oxy-hydrogen gas as an alternative fuel for heat and power generation applications - A review Hydrogen enriched Compressed Natural Gas. Int. J. Hydrogen Energy 2021;46(76):37705–35.

[3] M. Emre and I. Dincer. Development of a hybrid solar thermal system with TEG and PEM electrolyzer for hydrogen and power production. Int. J. Hydrogen Energy. 2017;42(51):30044–56.

[4] T. A. H. Ratlamwala, I. Dincer, and M. Aydin. Energy and exergy analyses and optimization study of an integrated solar heliostat field system for hydrogen production. Int. J. Hydrogen Energy. 2012;37(24):18704–12.

[5] D. O'Keefe, et al. Preliminary results from bench-scale testing of a sulfur-iodine thermochemical water-splitting cycle Int J Hydrogen Energy, 7 (5) (1982), pp. 381-392

[6] Ş. Asal and A. Acır. Utilization of the Cu–Cl thermochemical cycle for hydrogen production using a laser driver thorium molten salts. Int. J. Hydrogen Energy. 2021:6(61):31133-42.

[7] Cengel Y, Boles M. In: Thermodynamics an engineering approach. 2012.

Novel Bi_2S_3 and $NiBiS_3$ electrocatalysts for alkaline hydrogen evolution reactions

[1*]Goncagül Aksaray, [2]Mehmet Erman Mert, [3]Başak Doğru Mert, [1*]Gülfeza Kardaş

[1]Çukurova University, Science and Letters Faculty, Chemistry Dep., Adana, 01330, Türkiye
[2]Adana Alparslan Türkeş Science and Technology University, Advanced Technology Research and Application Center, 01250, Adana, Türkiye
[3]Adana Alparslan Türkeş Science and Technology University, Engineering Faculty, Energy Systems Engineering Dep., 01250, Adana, Türkiye

* E-mail: goncagulaksaray@gmail.com, gulfeza@gmail.com

Abstract
Hydrogen's role as an energy carrier is expected to grow due to its status as a clean energy source. The cathode material is crucial for the electrolysis of water, which is the most suitable method for its production. The selection of cathode endeavors to enhance hydrogen production and decrease energy consumption. In this study; Bi_2S_3 and $NiBiS_3$ were synthesized as catalysts for the hydrogen evolution reaction (HER), using a facile and available process. The characterization was achieved via XRD analysis, and electrochemical behavior was analyzed via cyclic voltammetry, Tafel polarization, electrochemical impedance spectroscopy, and chronoamperometry in a 1 M KOH solution. The graphite electrode was preferred as a substrate due to several characteristics, such as its low price, electrical conductivity, mechanical advantages, etc. Nickel and bismuth sulfides are of considerable attention for their potential applications in many areas, especially photovoltaics, due to their reasonably low band gap energy (almost 2 eV), high absorption coefficients, but neither Bi_2S_3 nor $NiBiS_3$ have been used as HER catalysts. According to the obtained results, polarization resistance was decreased almost 15 times at -1.4 V, the current density was increased almost a hundred times via $NiBiS_3$ catalyst. The durability test showed that the catalytic performance of $NiBiS_3$ was protected in chronoamperometry analysis during 6000 s.

Keywords: Electrocatalysts, HER, Bi_2S_3, $NiBiS_3$

I. Introduction

Energy demand has risen dramatically in parallel with the world's population's ongoing growth. Due to environmental concerns raised by carbon dioxide emissions and the unsustainability of fossil fuels, which are the world's primary energy sources, research into alternative sustainable energy has advanced (Chen et al., 2023; Zou et al., 2022). Renewable and clean energy sources aim to reduce greenhouse gas emissions without compromising modern life. The intermittency of renewable clean energies such as wind or solar power limits their direct and widespread application (Yue et al., 2021; Zhou et al., 2020). However, it is thought that energy conversion based on electrochemical techniques can solve this problem and realize a sustainable energy cycle. Thus, an efficient water splitting reaction that may promote the green hydrogen economy requires a technological advance (Martin et al., 2020; Yusaf et al., 2023. Hydrogen energy has become the most promising renewable energy source of the twenty-first century due to its high energy density and low pollution emissions. However, due to the high thermodynamic oxidation potential and the high cost of the metal electrodes used, problems are encountered in decomposing water and obtaining hydrogen (Pareek at al., 2020). Therefore, developing cost-effective and efficient HER catalysts to replace expensive metals for HER catalysis is very important. In this study, Bi_2S_3 and $NiBiS_3$ electrocatalysts were prepared via hydrothermal reaction. The characterization was achieved through X-ray diffraction analysis (XRD). The synthesized catalysts were operated on graphite electrodes via Dr. Blade method. The activity and stability of the prepared electrocatalyst were tested in 1 M KOH solution using cyclic voltammetry (CV), cathodic current-potential curves, electrochemical impedance spectroscopy (EIS) and chronoamperometry (CA) analysis.

II. Experimental

Synthesis of Bi_2S_3; 2 mmol bismuth nitrate pentahydrate (1.692 g) and 8 mmol thiourea (0.608 g) were dissolved in 80.0 mL of aqueous solvent (1:3 distilled water-ethylene glycol) under constant magnetic stirring for 30 minutes. Then it was mixed in an ultrasonic bath for 5 minutes. The resulting mixture was transferred to a 100 mL Teflon–lined stainless steel autoclave and dried in an oven at 150 °C for 24 hours. Then it was filtered by washing distilled water, ethyl alcohol, and distilled water. The prepared powder material was dried at 80°C for 2 hours (Cai et al.,2019; Ismail et al., 2023). Synthesis of $NiBiS_3$; 2 mmol bismuth nitrate pentahydrate (1.692 g), 2 mmol nickel nitrate hexahydrate (0.582 g) and 16 mmol thiourea (1.216 g) were dissolved in 80.0 mL of aqueous solvent (1:3 distile water-ethylene glycol) under constant magnetic stirring for 30 minutes. Then it was mixed in an ultrasonic bath for 5 minutes. The resulting mixture was transferred to a 100 mL Teflon–lined stainless steel autoclave and dried in an oven at 160 °C for 16 hours. Then it was filtered by washing distilled water, ethyl alcohol, and distilled water. The prepared powder catalyst was dried at 80°C for 2 hours (Fig.1).



Fig. 1. Schematic route for the synthesis of Bi_2S_3 and $NiBiS_3$

A slurry containing 80% acetylene black (AB), 10% Bi_2S_3 and 10% polyvinylidenedifluoride (PVDF) in N-methyl pyrrolidone (NMP) as the binder was prepared for the electrocatalyst material. The graphite (G) electrode with a radius of 0.5 cm^2 was coated with the slurry using the Dr. blade method, then dried in an oven at 70°C for 15 minutes. All electrochemical experiments were performed using a CHI660b potentiostat/galvanostat. The Ag/AgCl (3M KCl) electrode was utilized as the reference electrode, and a 2 cm^2 Pt sheet was employed as the counter electrode. Before each experiment, the G electrode surface was mechanically cleaned using emery paper from 320 to 1200. After that, the electrode surface was thoroughly rinsed with double-distilled water. Using an CHI660b electrochemical workstation at room temperature in an open atmosphere, the electrochemical experiments were performed in a 1 M KOH solution. XRD analysis was achieved with EMPYREAN X-ray diffractometer. The cyclic voltammetry analysis was obtained between -1.6 V and 0.8 V with a 100 mV s^{-1} scan rate. Electrochemical Impedance Spectroscopy (EIS) measurements were taken with an amplitude of 5 mV and a frequency range of 10^5 -0.1 Hz at several cathodic potentials. The EIS data were fitted via the ZView program with a Randless equivalent circuit. Tafel analysis was done with a 5 mV s^{-1} scan rate. The chronoamperometry analysis was performed with 50 mV s^{-1} at -1.3 V.

III. Results and discussion

The synthesized catalysts were analyzed via XRD. In Fig. 2, the peaks at 2 θ values of 15.66, 17.56, 22.35, 23.67, 25.10, 28.53, 31.79, 32.93, 33.90, 35.57, 40.29, 42.57, 45.52, 46.52, 49.08, 52.65, 54.63, 59.21 and 62.60 can be indexed to the (200), (120), (220), (101), (310), (211), (221), (410), (311), (240), (430), (421), (440), (501), (160), (312), (360), (640) and (152) planes of Bi_2S_3, respectively (JPDS 170320) (Dutta et al., 2014).

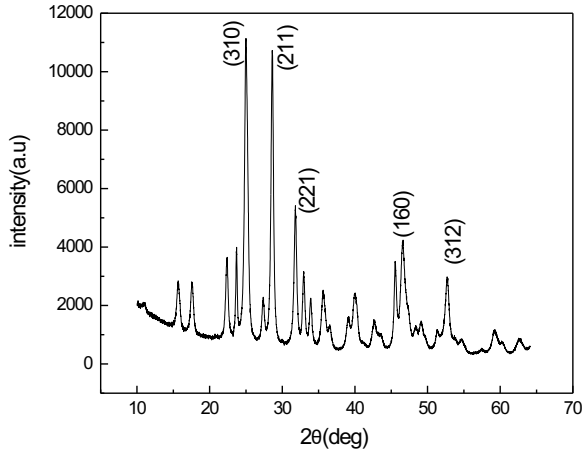


Fig. 2. XRD spectra of Bi_2S_3

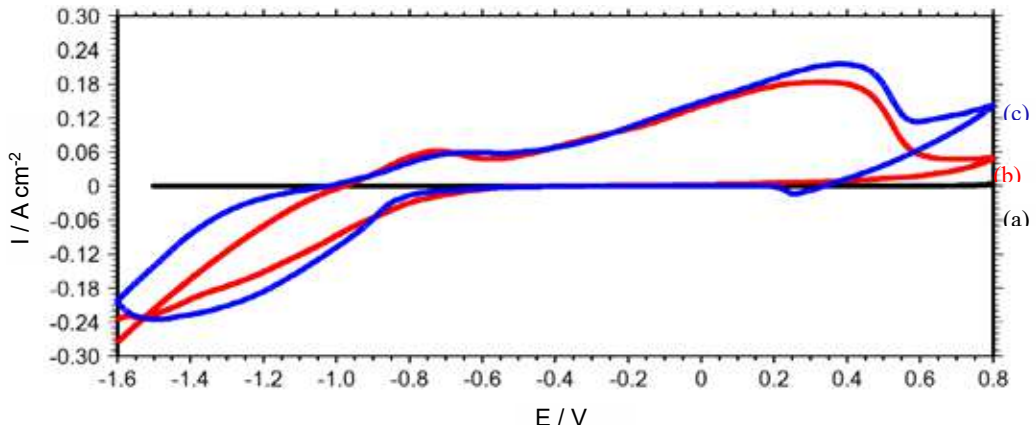


Fig. 3. The cyclic voltammograms of bare graphite (G) (a), G/Bi_2S_3 (b) and G/$NiBiS_3$ (c) in 1M KOH

As seen in Fig. 3a, for the bare electrode, neither forward nor reverse scanning revealed the presence of anodic or cathodic currents or the accompanying electrochemical transition. While obvious peaks were detected for G/Bi_2S_3 and G/$NiBiS_3$. In Fig. 3b, the oxidation peak was observed at -0.75, demonstrating the oxidation of Bi_2O_3 to Bi_4O_7. The BiH_3 production and then immediately hydrogen evolution reactions were detected at the reverse scan from -0.80 to upper cathodic potentials, respectively. In Fig. 3c, the anodic oxidation peak was observed at 0.40 V, demonstrating nickel oxidation. Firstly, metallic nickel oxidation occurs and continuing the transition from α-$Ni(OH)_2$ to β-$Ni(OH)_2$ and then Ni^{2+}/Ni^{3+} oxidation. The reduction of Ni^{2+} detected at nearly 0.25 V in the subsequent scan during the backward route.

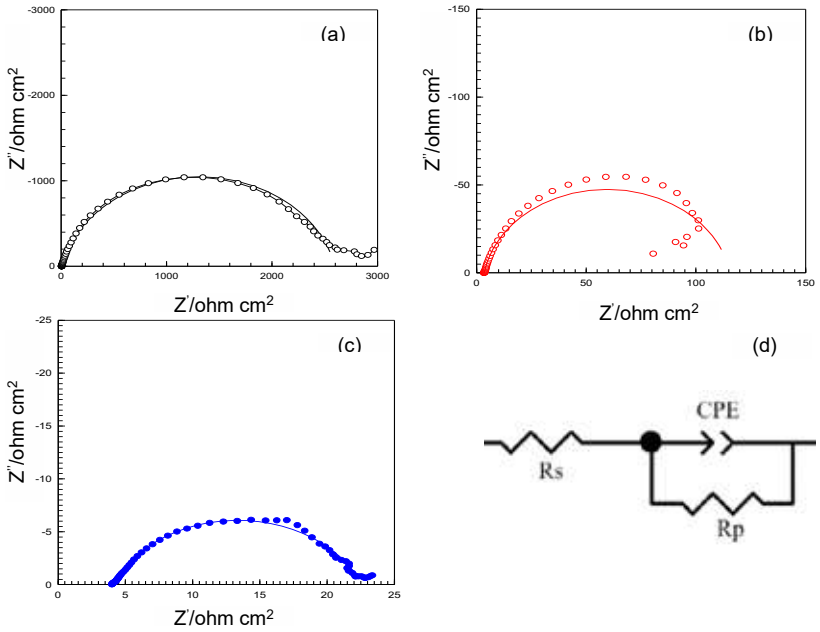


Fig. 4. Nyquist diagrams of G (a), G/Bi_2S_3 (b), G/$NiBiS_3$ (c) in 1M KOH at -1.4 V (the fitted data were given as solid line) and equivalent circuit diagram (d).

The Nyquist diagrams of all electrodes were presented in Figure 4, as seen from the curves; a charge transfer- controlled reaction mechanism was detected. The curves started as semi-elliptical in the high frequency region, continued at the middle frequency and ended at the low frequency. The depressed shape was illustrated by surface inhomogenity. The diameter of the curves was attributed to polarization resistance (R_p), which decreased in the presence of the catalyst. The obtained values were ~3000; 111.5; 18.55 ohm cm^2 for G, G/Bi_2S_3 and G/$NiBiS_3$ respectively.

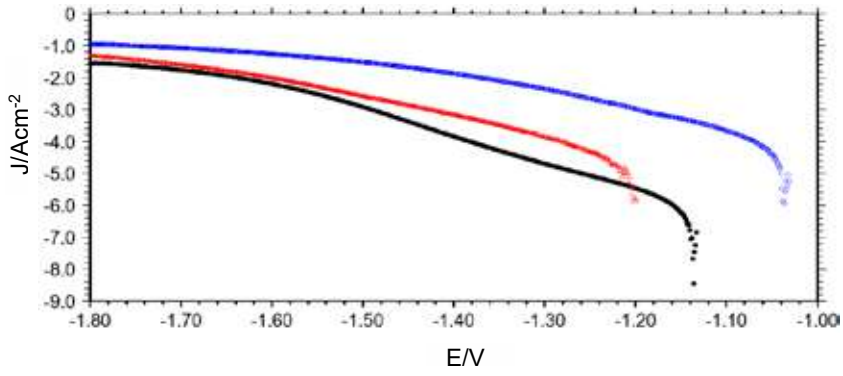


Fig.5. Cathodic current-potential curves of G, G/Bi_2S_3 and G/$NiBiS_3$

Fig. 5 shows the cathodic current -potential curves of the catalyst obtained in the open atmosphere. The cathodic current density values proved that higher catalytic activity was detected for G/$NiBiS_3$ electrode. The current density values were -1.0x10^{-5}; -0.7x10^{-4} and -2.3x10^{-3} A cm^{-2} at -1.30 V, for G, G/Bi_2S_3 and G/$NiBiS_3$ respectively. The values increased with increasing cathodic potential, which were -7.2x10^{-5}; -3.4x10^{-4} and -6.7x10^{-3} A cm^{-2} at -1.40 V, for G, G/Bi_2S_3 and G/$NiBiS_3$ respectively. Furthermore, the cathodic polarization measurements were obtained after chronaamperometric (CA) analysis after 6000 s and the obtained data are given inset in Fig. 6.

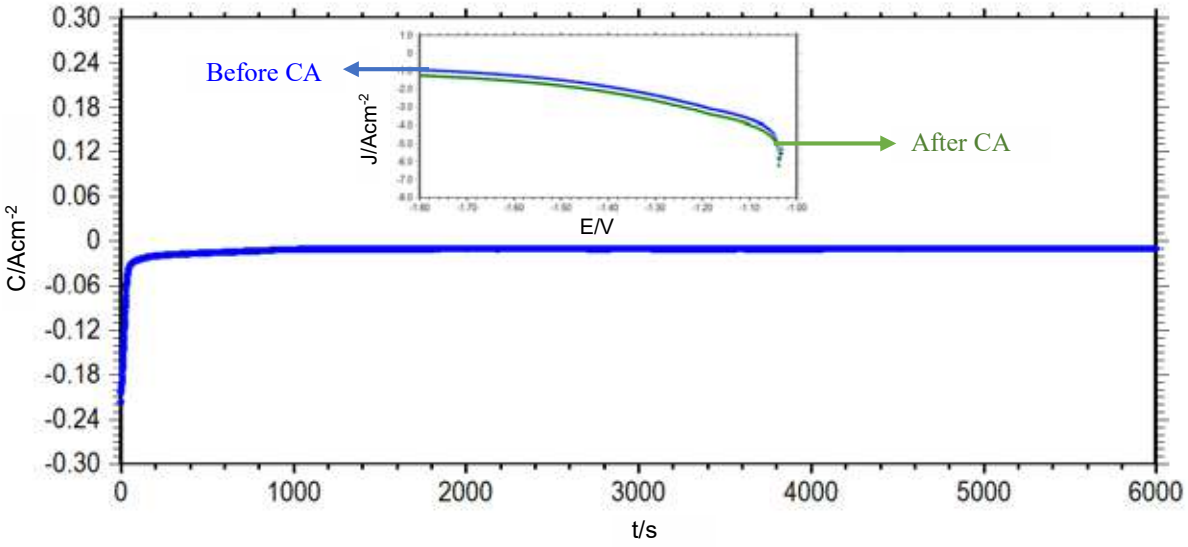


Fig.6. The chronoamperometric analysis of G/$NiBiS_3$ (inset: the cathodic current-potential curves of G/$NiBiS_3$ before and after CA)

As seen from Fig. 6, during the long CA period, the current density values were almost stable at -0.015 A cm^{-2} at -1.30 V, the initial and final analysis of polarization curves also proved the G/$NiBiS_3$ protected the activity during CA analysis. The current density which was obtained from the cathodic polarization curve after CA was $-2.2x10^{-3}$ A cm^{-2}.

IV. Conclusions

Bi_2S_3 and $NiBiS_3$ were produced for the hydrogen evolution reaction (HER) catalyst using an accessible and uncomplicated method. The distinct peaks in the XRD spectra indicated that Bi_2S_3 was formed in an amorphous state. The electrochemical tests demonstrated that the hydrogen evolution reaction (HER) efficiency of graphite was significantly improved by the produced catalysts. These electrodes (G/Bi_2S_3 and G/$NiBiS_3$) attained greater current density values and reduced polarization resistances. The durability test conducted using CA and Tafel polarization analysis demonstrated the stability of G/$NiBiS_3$.

Acknowledgments

The authors would like to thank to Çukurova University and Adana Alparslan Türkeş Science and Technology University.

References

Cai, F., Chen, X., Qiu, L., Jiang, L., Ma, S., Zhang, Q., & Zhao, Y. (2019). Controlled hydrothermal synthesis and photoelectrochemical properties of Bi2S3/TiO2 nanotube arrays heterostructure. Journal of Alloys and Compounds, 808, 151770. https://doi.org/10.1016/j.jallcom.2019.151770

Chen, Z., Yun, S., Wu, L., Zhang, J., Shi, X., Wei, W., ... & Ni, B. J. (2023). Waste-derived catalysts for water electrolysis: circular economy-driven sustainable green hydrogen energy. Nano-Micro Letters, 15(1), 4.

Dutta, A. K., Maji, S. K., Mitra, K., Sarkar, A., Saha, N., Ghosh, A. B., & Adhikary, B. (2014). Single source precursor approach to the synthesis of Bi2S3 nanoparticles: a new amperometric hydrogen peroxide biosensor. Sensors and Actuators B: Chemical, 192, 578-585. https://doi.org/10.1016/j.snb.2013.11.030

Ismail, K. B. M., Kumar, M. A., Jayavel, R., Arivanandhan, M., & Ismail, M. A. M. (2023). Enhanced electrochemical performance of the MoS_2/Bi_2S_3 nanocomposite-based electrode material prepared by a hydrothermal method for supercapacitor applications. RSC advances, 13(35), 24272-24285. DOI: 10.1039/D3RA03892K

Martin, A., Agnoletti, M. F., & Brangier, E. (2020). Users in the design of Hydrogen Energy Systems: A systematic review. International Journal of Hydrogen Energy, 45(21), 11889-11900. https://doi.org/10.1016/j.ijhydene.2020.02.163

Pareek, A., Dom, R., Gupta, J., Chandran, J., Adepu, V., & Borse, P. H. (2020). Insights into renewable hydrogen energy: Recent advances and prospects. Materials Science for Energy Technologies, 3, 319-327. https://doi.org/10.1016/j.mset.2019.12.002

Yue, M., Lambert, H., Pahon, E., Roche, R., Jemei, S., & Hissel, D. (2021). Hydrogen energy systems: A critical review of technologies, applications, trends and challenges. Renewable and Sustainable Energy Reviews, 146, 111180. https://doi.org/10.1016/j.rser.2021.111180

Yusaf, T., Mahamude, A. S. F., Kadirgama, K., Ramasamy, D., Farhana, K., Dhahad, H. A., & Talib, A. R. A. (2023). Sustainable hydrogen energy in aviation–A narrative review. International Journal of Hydrogen Energy. https://doi.org/10.1016/j.ijhydene.2023.02.086

Zhou, L., Yang, T., Chen, S., Gao, J., Wang, X., He, P., ... & Zhang, H. (2020). Tunably fabricated nanotremella-like Bi_2S_3/MoS_2: An excellent and highly stable electrocatalyst for alkaline hydrogen evolution reaction. International Journal of Hydrogen Energy, 45(16), 9535-9545. https://doi.org/10.1016/j.ijhydene.2020.01.168

Zou, C., Li, J., Zhang, X., Jin, X., Xiong, B., Yu, H., ... & Pan, S. (2022). Industrial status, technological progress, challenges, and prospects of hydrogen energy. Natural Gas Industry B, 9(5), 427-447. https://doi.org/10.1016/j.ngib.2022.04.006

NiP Cathode Catalyst For Alkaline Water Electrolyser

[1*]Goncagül Aksaray, [1]Ender Faki, [1]Yakubu Sawadogo Adam,[1]Patrick Marcel Seumo Tchekwagep, [2]Murat Farsak [1*]Gülfeza Kardaş

[1]Çukurova University, Arts and Sciences Faculty, Chemistry Department, Adana, 01330, Türkiye
[2]Osmaniye Korkut Ata University, Department of Battery Systems and Hydrogen Technologies, Osmaniye, Türkiye

* E-mail:goncagulaksaray@gmail.com, gulfeza@gmail.com

Abstract
In this study, the hydrogen evolution reaction (HER) catalyst was prepared on a 2x2 cm perforated stainless steel support for the synthesis of a highly efficient alkaline electrolyser's cathode. The perforated stainless steel surface was coated in two layers with nickel film. Then, CuZn was deposited on the nickel-coated electrode in a copper-zinc bath using the chronopotentiometry method, and zinc was leached in an alkaline solution to produce a highly porous surface. Finally, the electrode was doped with NiP by using an electroless coating. The efficiency of the catalyst was tested by electrochemical impedance spectroscopy (EIS) and linear sweep voltammetry (LSV). The NiP coated electrode shows the highest HER efficiency. The current density of NiP deposited electrode is measured100 mA cm^{-2} at -1.66 V for NiP catalyst.

Keywords: catalysts, electrolysis, NiP, hydrogen evolution reaction

I. Introduction

The rising need for fossil fuels has resulted in significant environmental contamination, prompting contemporary society to confront the advancement of innovative energy technologies that are green, renewable, and highly efficient (Martin-Sabi et al., 2018; Ghorbani-Choghamarani et al., 2021; Yang et al., 2021). Recent innovations and advancements, such as fuel cells, electrolyzers, batteries, and supercapacitors, have significantly aided in the development of sustainable energy. These technologies have played a crucial role in diminishing the reliance on fossil fuels and enhancing the efficiency of current energy resources (Zhu et al., 2018; Lui et al., 2020 ; Duan et al., 2023). Hydrogen is important in the energy transition because it offers a clean and versatile energy source. Diverse domestic resources can produce it with near-zero greenhouse gas emissions, making it a sustainable option. Scientific research has identified electrolysis as the most efficient technique for generating hydrogen. Although water electrolysis is the most straightforward way to produce hydrogen gas, using an efficient catalyst is crucial because high overvoltages in the system increase the cost (Bai et al., 2014; Ma et al., 2022). Synthesizing extremely efficient catalysts as a substitute for the expensive platinum electrode for the activity of HER is important to decrease the cost. For this purpose, researchers have created numerous catalysts and are constantly exploring new ones.
In this study, a cathode catalyst was prepared by nickel, copper zinc coating, and nickel phosphorous doping on the perforated 304 stainless steel surface. Scanning electron microscopy (SEM) and energy dispersive X-ray spectroscopy (EDX) analysis were used to characterize the material. The activity and stability of the prepared electrocatalyst were tested in a 1 M KOH alkaline solution using cyclic voltammetry (CV), linear sweep voltammetry (LSV) and electrochemical impedance spectroscopy (EIS).

II. Experimental

Preparation of electrodes: 2x2 cm perforated 304 stainless steel (SS) were electrochemically coated with nickel in a nickel bath by applying a current of 0.005 A for 200 s to form a thin nickel film on the surface and ensure good adhesion of nickel carbonyl to the surface (composition of nickel bath: 30% $NiSO_4.7H_2O$, 1.25 H_3BO_3, 1.10 $NiCl_2.6H_2O$; pH=3.5) (Solmaz et al., 2009). The thin-layer nickel surface was coated with nickel powder. Then the electrode was placed in a high-temperature furnace and heated at 950 °C for 15 minutes in an argon atmosphere, increasing at a rate of 10 °C per minute, and then cooled to room temperature.
A thin nickel film was created by the chronopotentiometry approach and then covered with nickel powder over perforated 304 stainless steel, as illustrated in Figure 1.

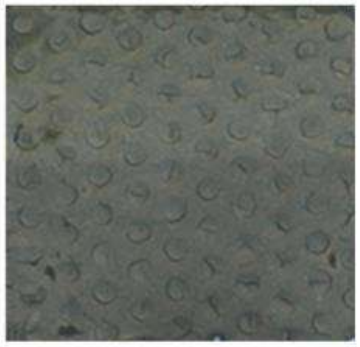


Fig. 1. Perforated 304 stainless steel, the surface of which is coated with nickel and nickel powder

CuZn coating was done using the chronopotentiometry technique with a current density of 10 mA cm^{-2} for 120 seconds (Döner et al., 2015; Mert et al., 2017) on the two layer nickel coated SS. The zinc leaching process was applied to the electrode to increase the surface area by creating a porous structure on the CuZn coated electrode and to fill the resulting gaps with NiP. NiP doping was done by immersing the electrodes in the NiP bath for 1 minute at 80 ^oC.
All electrochemical experiments were performed using a Gamry 1000 Interface Instrument. The 2x2 cm^2 Pt mesh was used as a counter electrode, and Ag/AgCl (3M KCl) electrode was used as a reference electrode. The HER efficiencies of the catalysts were determined by using LSV in a 1.0 M KOH solution in the cathodic direction with a scanning rate of 1 mV/s from -1.0 V to -1.8 V.

III. Results and discussion

In Figure 2, the SEM images of CuZn coated (a), CuZn leached (b) and NiP deposited electrodes are presented to demonstrate their surface characteristics. The SEM images of the CuZn electrode (Figure 2 a) reveal a uniform and spherical structure at the coating layer, indicating a successful deposition process. On the other hand, CuZn leached (Figure 2 b) exhibits a rough and porous surface due to the removal of zinc during the leaching process. The SEM images reveal a more irregular and rough surface, indicating the incorporation of NiP into the electrode structure (Figure 2 c). This suggests that the presence of NiP doping alters the overall structure and morphology of the electrode, potentially affecting its electrochemical performance. These SEM images provide valuable insights into the surface characteristics of these electrodes.

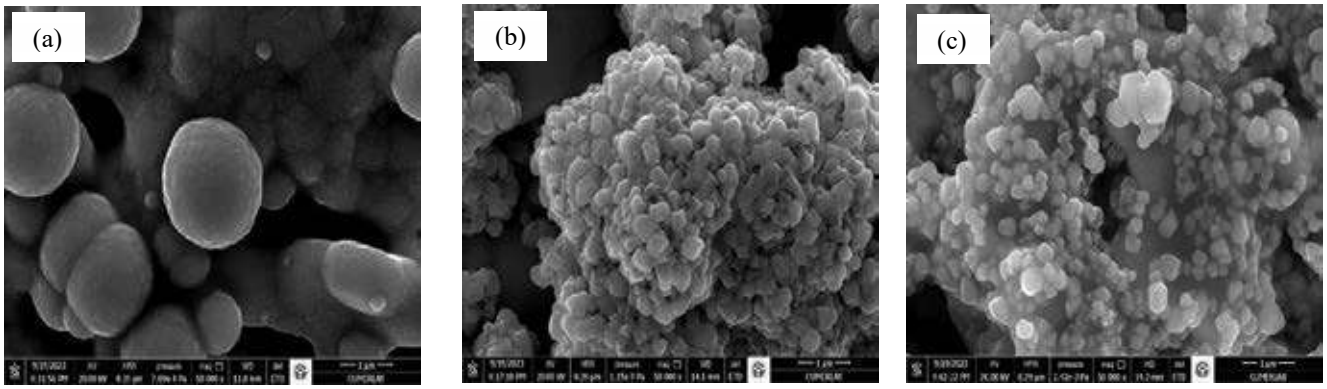


Fig. 2. SEM images (X50000) of CuZn(a), CuZn leached (b) and NiP deposited (c) electrodes

Table 1: EDX analysis of the prepared electrodes

Elements	CuZn electrode (%wt)	CuZn leached electrode (%wt)	NiP deposited on CuZn leached electrode (%wt)
O	3.2	5.4	8.12
Ni	72.52	64.26	54.13
Cu	23.34	27.35	16.43
Zn	0.95	-	-
Fe	-	0.7	14.7
P	-	-	0.44

EDX analysis found high levels of nickel and copper elements, as expected, in the CuZn coated electrode. It is seen that when zinc is leached from the electrode, the amount of nickel element decreases, while the amount of copper element increases, and zinc is removed from the surface. EDX results of the NiP deposited electrode show the presence of phosphorus on the surface.
Electrochemical Impedance Spectroscopy (EIS) measurements were taken with an amplitude of 10 mV and a frequency range of 10^5 - 0.1Hz. Nyquist diagrams of the electrodes are seen in Figure 3.

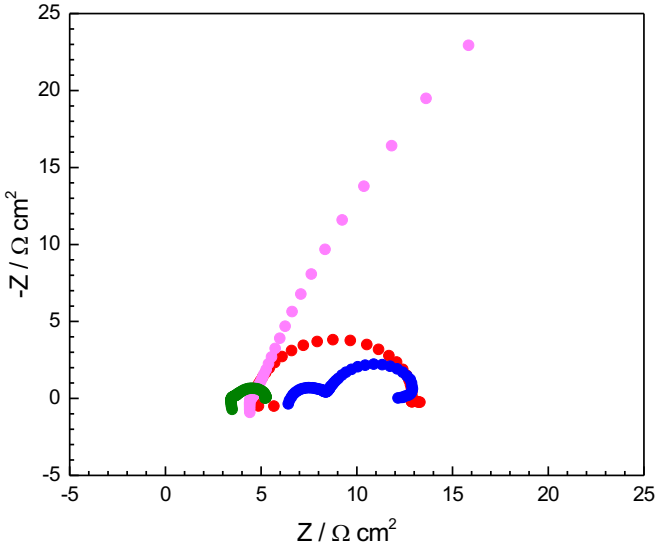


Fig. 3. Nyquist diagrams of the nickel (red), nickel carbonyl (blue), CuZn leached (pink) and NiP deposited (green) electrodes at -1.3 V potential in 1.0 M KOH

Nyquist diagrams of the electrodes obtained at -1.3 V, the hydrogen evolution potential of the electrodes are seen in Figure 3. The loop of the curves which is related to polarization resistance decreases with doping on the electrode surface. The lowest polarization resistance for HER is obtained with NiP electrode. This shows that the catalytic efficiency of the electrode increases with doping. The polarization resistance of the Ni electrode calculated from Figure 3 is ~12 Ω cm^2 while that of the NiC electrode is ~8 Ω cm^2. While holes produced in the structure by leaching zinc from the surface improved the polarization resistance (~11 Ω cm^2), the polarization resistance decreases dramatically at the NiP deposited electrode (~2 Ω cm^2).
HER activities of the electrodes were determined by obtaining current potential curves in the cathodic direction with a scan rate of 1 mV/s between the range of -1.0 V to -1.8 V in 1.0 M KOH solution.

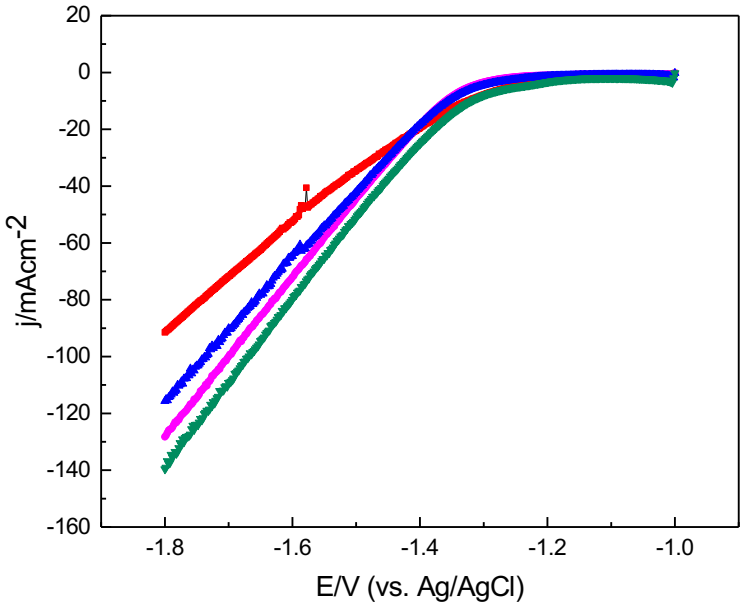


Fig. 4. Cathodic current-potential curves of Ni (red), NiC (blue), CuZn leached (pink) and NiP deposited (green) electrodes in 1.0 M KOH

When the current-potential curves are examined in Figure 4, it is seen that the overvoltage decreases and the current density increases in the NiP deposited electrode. It can be seen that hydrogen evolution starts at a lower potential in the NiP deposited electrode. At the same time, overvoltage decreases at the NiP deposited electrode and current density increases under polarization conditions. This can be explained by the fact that NiP on the electrode surface increases HER efficiency and reduces overvoltage. At 100 mA cm^{-2} we can observe on effective performance of NiP catalyst with -1.66 V.

Table 2: Current densities of the electrodes at different cathodic potentials

E/V	Nickel coated SS (mA cm^{-2})	Nickel carbonyl coated (mA cm^{-2})	CuZn coated (mA cm^{-2})	NiP deposited (mA cm^{-2})
-1.4	18.43	16.82	18.15	25.26
-1.5	34.61	44.39	42.01	51.31
-1.6	52.45	72.10	66.64	80.20

Table 2 gives the HER efficiency of all electrodes at different potentials. The best HER efficiency was obtained when -1.3V potential was applied.

IV. Conclusions

According to the experimental findings of the study, the NiP deposited electrode is an effective electrocatalytic efficiency for HER. According to electrochemical measurements, electrochemical coatings and chemical doping on the perforated 304 stainless steel, a significant increase in hydrogen evolution reaction was observed on the surface. Better catalytic activity with surface modifications was exhibited by the NiP with 80.20 mA cm^{-2} curent densities at -1.6V (vs. Ag/AgCl) potential.

Acknowledgments

We acknowledge support from Turkey's Scientific and Technological Research Council (TUBITAK-Grant Number: 121C260) within the “2247 – A National Outstanding Researchers Program” program

References

Bai, S. and al (2014) Surface polarization matters: Enhancing the Hydrogen evolution reaction by shrinking pt shells in Pt-Pd-graphene stack structures. Angewandte Chemie International Edition,doi.org/10.1002/anie.201406468.

Döner, A. and al (2015) Fabrication and characterization of alkaline leached CuZn/Cu electrode as anode material for direct methanol fuelcell.Energy,doi.org/10.1016/j.energy.2015.06.058.

Duan, Y., Zhang, X. L., Gao, F. Y., Kong, Y., Duan, Y., Yang, X. T., ... & Yu, S. H. (2023). Interfacial engineering of Ni/V2O3 heterostructure catalyst for boosting hydrogen oxidation reaction in alkaline electrolytes. Angewandte Chemie, 135(10), e202217275.

Ghorbani-Choghamarani, A., Taherinia, Z., & Mohammadi, M. (2021). Facile synthesis of Fe3O4@ GlcA@ Ni-MOF composites as environmentally green catalyst in organic reactions. Environmental Technology & Innovation, 24, 102050.

Liu, Z., Zhang, C., Liu, H., & Feng, L. (2020). Efficient synergism of NiSe2 nanoparticle/NiO nanosheet for energy-relevant water and urea electrocatalysis. Applied Catalysis B: Environmental, 276, 119165.

Ma, S., and al (2022) Pollen-like self-supported FeIr alloy for improved hydrogen evolution reaction in acid electrolyte. Journal of Energy Chemistry, doi.org/10.1016/j.jechem.2021.08.066

Martin-Sabi, M., Soriano-López, J., Winter, R. S., Chen, J. J., Vilà-Nadal, L., Long, D. L., ... & Cronin, L. (2018). Redox tuning the Weakley-type polyoxometalate archetype for the oxygen evolution reaction. Nature catalysis, 1(3), 208-213.

Mert, M. E., and al. (2017) The photoelectrocatalytic activity, long term stability and corrosion performance of NiMo deposited titanium oxide nano-tubes for hydrogen production in alkaline medium. AppliedSurface,doi.org/10.1016/j.apsusc.2017.06.216

Solmaz, R. and al. (2009) Electrochemical deposition and characterization of NiFe coatingsas electrocatalytic materials for alkaline water electrolysis,ElectrochimicaActa,doi.org/10.1016/j.electacta.2009.01.064.

Yang, L., Liu, Z., Zhu, S., Feng, L., & Xing, W. (2021). Ni-based layered double hydroxide catalysts for oxygen evolution reaction. Materials Today Physics, 16, 100292.

Zhu, S., Zhao, X., Li, H., & Chu, L. (2021). Catalytic three-component dicarbofunctionalization reactions involving radical capture by nickel. Chemical Society Reviews, 50(19), 10836-10856.

The effect of using nanofluid in a parabolic trough collector on its thermodynamic performance and hydrogen production

[1*]Orhan Şahmerdan, [2]Canan Cimşit, [3]Müslüm Arıcı,
[1] Kocaeli University, Engineering Faculty, Mechanical Engineering Department, Umuttepe Campus, Kocaeli, 41001, Türkiye
[2] Kocaeli University, Golcuk Vocational School of Higher Education, Golcuk, 41650, Türkiye
[3] Kocaeli University, Engineering Faculty, Mechanical Engineering Department, Umuttepe Campus, Kocaeli, 41001, Türkiye

* E-mail:orhansahmerdan@hotmail.com

Abstract
In this paper, nanoparticle use to improve the hydrogen production of an solar-driven integrated system is proposed and analyzed. The system includes a parabolic trough solar collector mounted to an organic Rankine cycle to generate electricity for a polymer electrolyte membrane electrolyzer producing hydrogen. The system performance is evaluated for the use of nanofluid which contains Cu nanoparticles with the volumetric fraction of 2% in the solar collector and contrasted with a scenario where the heat transfer medium is a pure base fluid. Thermodynamic models for both the parabolic trough collector and organic Rankine cycle, in addition to an approach of hydrogen production in the electrolyzer, are employed for the Kocaeli location across all months of the year. To the results, using nanofluid increases the thermal and exergy efficiencies of the collector mostly by 4.5% and 1.38%, respectively, while it improves hydrogen production rate from 37,906 kg/year to 40,006 kg/year.

Keywords: Nanofluid, parabolic trough solar collector, hydrogen production.

I. Introduction

To devise an alternative to fossil fuels and address the issue of CO_2 emissions they cause, hydrogen can be considered as a potential energy carrier in the production of sustainable and environmentally friendly energy. (Abbas, 2023).On the other hand, in the quest for sustainable energy options, solar energy is one of the most promising renewable sources (Fang et al, 2023). It can be converted into electricity power by transferring heat attracted via a parabolic trough solar collector (PTC) to a power cycle for hydrogen production in an electrolyzer. In this process nanofluid use in the PTC can increase the system's thermodynamic efficiencies and hydrogen production rate (HPR).

In this regard, Ju et al. (2023) utilized a PTC, Kalina cycle (KC) and polymer electrolyte membrane (PEM) electrolyzer to investigate the impact of CuO, SiO_2 and Al_2O_3 nanoparticles dispersed into Syltherm-800 base fluid. Their findings revealed that CuO nanoparticles exhibited the most significant enhancement, resulting in a 9.63% increase in exergy efficiency and a hydrogen production enhancement of 0.033 kg/h. Satish et al. (2023) compared the effects of CuO and Al_2O_3 nanoparticles with WO_3 nanoparticles, using water as the base fluid in a PTC. They employed a Rankine cycle (RC) and solid oxide electrolyzer. In this system, CuO is recognized as the most efficient nanoparticle, too. Abid et al. (2017) applied an organic Rankine cycle (ORC) to generate power for an electrolyzer. They separately dispersed Al_2O_3, and Fe_2O_3 nanoparticles into water, and also used molten salts in the PTC cycle. The use of nanofluids resulted in higher HPRs, reaching up to 0.02454 g/s. Toghyani et al. (2019) used CuO nanoparticles in the PTC to supply required heat loads for a RC linked with a PEM electrolyzer for hydrogen production and absorption cooling system. To the results, increasing the volumetric fraction of nanoparticles ca higher amount of hydrogen production.

In this study, Cu nanoparticles are dispersed into Syltherm-800 base fluid in a PTC cycle connected to an ORC producing electricity for hydrogen production in an electrolyzer to investigate the impact of these nanoparticles on the PTC's thermodynamic efficiencies along with the hydrogen production.

II. Procedure

In this study, solar calculations for the proposed system were conducted for Kocaeli (40°N, 29°E). Monthly average total daily solar irradiance, sunning time, and wind speeds were collected for this location across all months of the year. The system was assumed to operate throughout the duration of sunning time every day of the year. The schematic view of the system is illustrated in Fig. 1.

In the studied system, the mirror of the PTC focuses solar radiation onto the absorber, which is placed along the central axis of the collector. This absorber is surrounded by tempered glass cover, and there is air between the cover and the absorber. The solar radiation absorbed by the absorber is transferred to the heat transfer fluid (HTF) flowing through the absorber via convection. In this study, two scenarios of HTF for the PTC were compared: one using Silterm-800 base fluid and the other incorporating Cu nanoparticles at a volumetric concentration of 2% into the base fluid to obtain a nanofluid for higher thermal performance. The HTF enters the absorber at 400 K and absorbs heat, so its temperature increases as it passes through this component. Subsequently, it enters the evaporator and transfers its heat to benzene what is the working fluid in the ORC. After this, the HTF returns to the inlet of the PTC at 400 K. Meanwhile, benzene, which turns from compressed liquid to superheated vapor due to the heat it absorbs in the evaporator, expands as it passes through the turbine of the ORC. This causes an electrical power generation by the turbine. Then, benzene exits the turbine as superheated vapor at low pressure. Following this, it condenses to saturated liquid at 313 K temperature after passing through the condenser. Consequently, it is compressed back to evaporator pressure by a pump. The fluid flow in the ORC continues in this manner.

Simultaneously, the electricity generated by the turbine is converted into direct current by a rectifier and then supplied to a PEM electrolyzer. With this electricity, water is electrolyzed in the electrolyzer to produce hydrogen and oxygen

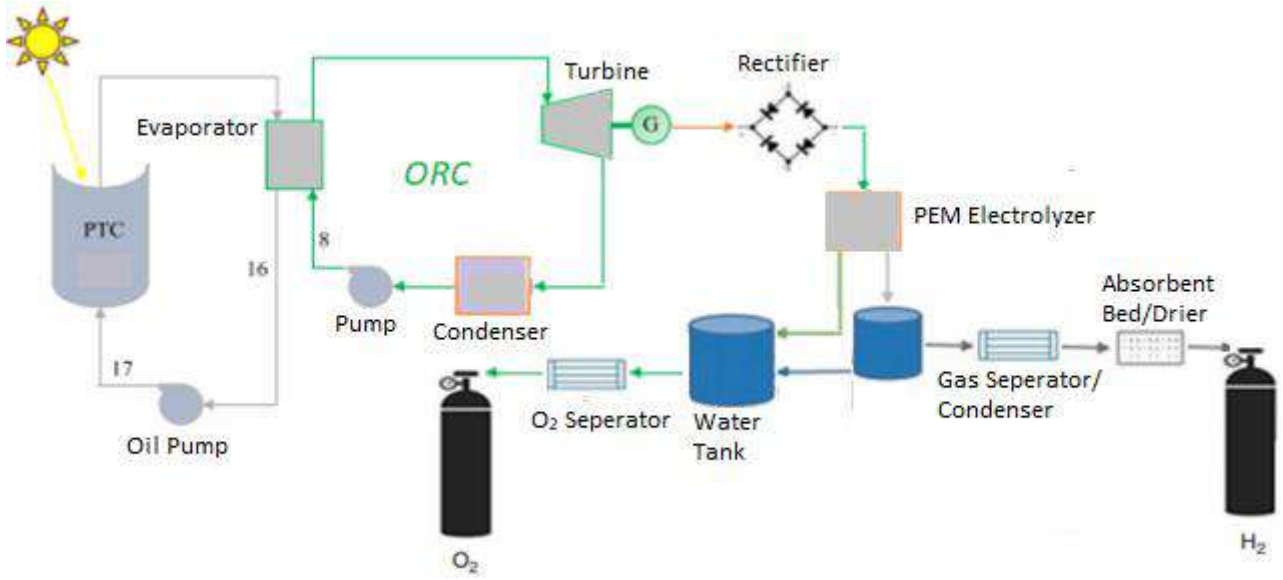


Fig. 1: Schematic view of the hydrogen production system

III. Analysis

Thermophysical properties of Syltherm-800 and Cu at 400 K are given in Table 1.

Table 1. Thermophysical properties of Syltherm-800 and Cu at 400 K (Dou et al. 2023)

Property	Syltherm-800	Cu
ρ [kg/m^3]	*840.067*	*8933*
C_P [J/kg K]	*1791*	*396.370*
k [W/m K]	*0.114927*	*393.170*
μ [Pa s]	*0.002186*	-

The total collector efficiency is computed by Equation 5. Here, the parameter η_{el} indicates the electrical efficiency of the power block whose value is 0.327.

$$\eta_{en} = \frac{Q_u - (W_P/\eta_{el})}{Q_s} \quad (1)$$

The total available solar energy (Q_s) is found by multiplying direct solar radiation (I_b) with the aperture area of the PTC (A_a).

$$Q_s = A_a \ . I_b \quad (2)$$

The useful energy gain of the PTC (Q_u) and the exit temperature of the nanofluid ($T_{nf,out}$) are detected by following equations:

$$Q_u = F_R \ . A_a \ . \left(I_b - \left(\frac{A_r}{A_a}\right) . U_L . \left(T_{nf,in} - T_{amb}\right) \right) \quad (3)$$

.

$$T_{nf,out} = T_{nf,in} + \left(\frac{Q_f}{\dot{m}_{nf} \ . C_{P,nf}}\right) \quad (4)$$

The loss coefficient (U_L) is determined using Equation 8. Then, the value of this parameter is used to find the the factors of collector efficiency (F_{EF}), collector flow (F_{EF}), and heat removal (F_R), respectively.

$$U_L = \frac{Q_{loss}}{A_r.(T_{abs} - T_{amb})} \quad (5)$$

$$F_{EF} = \frac{\frac{1}{U_L}}{(1/U_L)+\left(\frac{d_{ao}}{h_{nf} d_{ai}}\right)+\left(\left(\frac{d_{ao}}{2k_a}\right).ln(d_{ao}/d_{ai})\right)} \quad (6)$$

$$F_{FF} = \left(\frac{m_{nf} C_{P_{nf}}}{A_r \ .U_L \ .F_{EF}}\right) \ .\left(1 - exp\left(-\left(\frac{A_r \ .U_L \ .F_{EF}}{m_{nf} \ .C_{P_{nf}}}\right)\right)\right) \quad (7)$$

$$F_R = F_{FF} \ .F_{EF} \quad (8)$$

Where d_{ao}, d_{ai}, k_a, A_r, m_{nf} and h_{nf} are absorber outer diameter, inner diameter, thermal conductivity, outer surface area, nanofluid mass flow rate and convection heat transfer coefficient (do Carmo Zidan et al. 2022).

The PTC exergy efficiency (η_{ex}), useful exergy gain (E_u), and available solar exergy (E_s) are calculated by the following equations (Bellos and Tzivanidis, 2019):

$$\eta_{ex} = \frac{E_u}{E_s} \quad (9)$$

$$E_u = Q_u - m_{nf} \ .C_{P_{nf}}.T_{amb} \ .\ln\left(\frac{T_{nf,out}}{T_{nf,in}}\right) - \ m_{nf} \ .T_{amb} \ .\frac{\Delta P}{\rho_{nf} \ .T_{mean}} \quad (10)$$

$$E_s = Q_s \ .\left(1 - \frac{4}{3}\frac{T_{amb}}{T_{in}} + \frac{1}{3}\left[\frac{T_{amb}}{T_{in}}\right]^4\right) \quad (11)$$

The modeling parameters of the PTC, along with the methodology and equations for calculating heat loss (Q_{loss}), PTC cycle pumping power (W_p), nanofluid properties and net power production by the ORC can be derived from do Carmo Zidan et al. 2022. Some design parameters related to the ORC and PEM electrolyzer are given in Table 2.

Table 2. Design parameters for the ORC and PEM electrolyzer

Parameters	Value	Unit
Temperature difference between turbine and evaporator inlet of source	*10*	°C
Temperature difference between turbine inlet and evaporator	*5*	°C
Pinch point temperature difference (at least)	*5*	°C
Condenser temperature	*40*	°C
Rectifier efficiency	*0.796*	-
Cell number of the electrolyzer	*19*	-

The HPR per cell of the PEM electrolyzer (m_{el}) can be calculated in g/h by Equation 12 (Budak and Devrim, 2019).

$$m_{el} = 1.43 \times 10^{-3} + 2.39 \times 10^{-2} E_{el} - 4.32 \times 10^{-5} E_{el}^2 \quad (12)$$

where E_{el} is electrical power provided to one cell of the electrolyzer.

IV. Results and discussions

The monthly useful energy and exergy amounts, as well as energy and exergy efficiencies of the PTC, are presented in Table 3. According to the data, the amounts of useful energy and exergy transferred from the collector's absorber to the HTFs increase from January to July, due to the monthly direct solar radiation exposure of the collector. However, from July to the end of the year, they gradually decrease. This trend is also available for the energy and exergy efficiencies. The highest useful energy and exergy amounts, and energy and exergy efficiencies, were obtained with values of 8551 W, 2250 W, 94.38%, and 26.67%, respectively, when using nanofluid, The addition of Cu nanoparticles at a 2% of volumetric concentration into the base fluid, Syltherm-800, resulted in approximately 4% and 4.3% increases in the useful energy and exergy rates, respectively, while leading to approximately 3.5% and 1% increases in energy and exergy efficiencies, respectively.

In the study, the monthly average hydrogen production quantities produced by the system through electrolysis are also calculated and the results are presented in Table 4. According to the results, the HPR increased from January to July, reaching a maximum amount of 7.092 kg/month in July when using nanofluid. However, after this month, they gradually decreased due to the reasons mentioned above. The use of nanofluid increased the HPR by

4.184% to 4.495%, leading to an increase in the annual HPR from 37,904 kg/year to 39,562 kg/year.

Tab. 3: Monthly average thermodynamic values of the PTC system.

Months	Useful Energy (W)		Useful Exergy (W)		Energy Efficiency (%)		Exergy Efficiency (%)	
	Base Fld.	Nanofluid	Base Fld.	Nanofluid	Base Fld.	Nanofluid	Base Fld.	Nanofluid
January	*2466*	*2567*	*633,5*	*660,4*	*83,35*	*86,77*	*22,99*	*23,96*
February	*3618*	*3768*	*933,1*	*973,7*	*86,3*	*89,88*	*23,9*	*24,94*
March	*4676*	*4871*	*1210*	*1264*	*87,86*	*91,54*	*24,42*	*25,5*
April	*5945*	*6187*	*1546*	*1614*	*89,23*	*92,87*	*24,91*	*26*
May	*7453*	*7753*	*1948*	*2034*	*90,28*	*93,9*	*25,33*	*26,45*
June	*8015*	*8331*	*2099*	*2191*	*90,68*	*94,26*	*25,5*	*26,61*
July	*8229*	*8551*	*2157*	*2250*	*90,83*	*94,38*	*25,56*	*26,67*
August	*7832*	*8138*	*2050*	*2138*	*90,68*	*94,22*	*25,48*	*26,58*
September	*6540*	*6800*	*1704*	*1778*	*89,92*	*93,49*	*25,15*	*26,24*
October	*4586*	*4770*	*1187*	*1237*	*88,19*	*91,73*	*24,5*	*25,55*
November	*3334*	*3468*	*859,1*	*895,2*	*86,11*	*89,57*	*23,82*	*24,82*
December	*2427*	*2525*	*623,4*	*649,4*	*83,37*	*86,74*	*22,99*	*23,95*

Tab. 4: Monthly average hydrogen production amounts of the system in kilograms.

Fluid	Jan	Feb	Mar	Apr	May	Jun	Jul	Aug	Sep	Oct	Nov	Dec	Total
Base Fld.	*0,570*	*0,907*	*1,734*	*2,877*	*4,868*	*6,272*	*6,795*	*6,125*	*4,101*	*2,051*	*1,020*	*0,584*	*37,904*
Nanofluid	*0,594*	*0,947*	*1,812*	*3,004*	*5,085*	*6,548*	*7,092*	*6,386*	*4,283*	*2,140*	*1,064*	*0,609*	*39,562*

V. Conclusions

In this study, the effect of Cu nanoparticle usage in a PTC cycle connected to an ORC producing electricity for hydrogen production in an electrolyzer is analyzed. The highest useful energy and exergy rates, and energy and exergy efficiencies, are found to be 8551 W, 2250 W, 94.38%, and 26.67%, respectively, when using nanofluid. The use of nanofluid leads to approximately 4%, 4.3%, 3.5% and 1% increases in the useful energy, exergy rates and energy and exergy efficiencies, respectively. It also increases the HPR by 4.184% to 4.495%, resulting in an annual increase from 37,904 kg/year to 39,562 kg/year.

References

Abbas M.K., Hassan Q., Tabar V.S., Tohidi S., Jaszczur M., Abdulrahman I.S., Salman H.M., Techno-economic analysis for clean hydrogen production using solar energy under varied climate conditions, International Journal of Hydrogen Energy, 48, 2929-2948, (2023).

Abid M., Ratlamwala T. A., Atikol U., Solar assisted multi-generation system using nanofluids: A comparative analysis, International Journal of Hydrogen Energy, 42, 21429-21442, (2017).

Bellos E., Tzivanidis C., Alternative designs of parabolic trough solar collectors, Progress in Energy and Combustion Science, 71, 81-117, (2019).

Budak Y., Devrim Y., Comparative study of PV/PEM fuel cell hybrid energy system based on methanol and water electrolysis. Energy Conversion and Management, 179, 46-57, (2019).

do Carmo Zidan D., Maia C. B., Safaei, M. R., Performance evaluation of various nanofluids for parabolic trough collectors, Sustainable Energy Technologies, 50, 101865 (2022).

Dou L., Ding B., Zhang Q., Kou G., Mu M., Numerical investigation on the thermal performance of parabolic trough solar collector with synthetic oil/Cu nanofluids. Applied Thermal Engineering, 227, 120376 (2023).

Fang J., Yang M., Cui L., Yi X., Huo H., Wen Z., Liu X., Efficient hydrogen production system with complementary utilization of methane and full-spectrum solar energy, Energy Conversion and Management, 283, 116951 (2023).

Ju Y., Abdalla A.N., Wang S., Hai T., Wei H., Wang M., Exergetic evaluation of the effect of nanofluid utilization for performance enhancement of a solar driven hydrogen production plant, International Journal of Hydrogen Energy, 52, 302-314, (2024).

Sathish T., Sailaja C., Saravanan R., Suresh P., Anish, M. An absorber of parabolic trough collector for hydrogen production in a solid oxide fuel cell, Fuel, 343, 127982 (2023).

Toghyani S., Afshari E., Baniasadi E., Shadloo M.S., Energy and exergy analyses of a nanofluid based solar cooling and hydrogen production combined system, Renewable Energy, 141, 1013-1025, (2019).

The performance comparison of a hydrogen production system utilizing solar energy with nanofluid in its parabolic trough collector for Antalya and Kocaeli

[1*]Orhan Şahmerdan, [2]Canan Cimşit, [3]Müslüm Arıcı,
[1] Kocaeli University, Engineering Faculty, Mechanical Engineering Department, Umuttepe Campus, Kocaeli, 41001, Türkiye
[2] Kocaeli University, Golcuk Vocational School of Higher Education, Golcuk, 41650, Türkiye
[3] Kocaeli University, Engineering Faculty, Mechanical Engineering Department, Umuttepe Campus, Kocaeli, 41001, Türkiye

* E-mail:orhansahmerdan@hotmail.com

Abstract
In this study, energy and exergy analyses are conducted on the parabolic trough collector (PTC) component of a simple hydrogen production system from solar energy which consists a PTC, organic Rankine cycle (ORC), and polymer electrolyte membrane (PEM) electrolyzer, with the utilization of nanofluid in its PTC. Additionally, the hydrogen production values for the entire system are determined. The Syltherm-800/Cu is used as the nanofluid, which was obtained by dispersing Cu nanoparticles into Syltherm-800 by 2% of volumetric fraction. The study is carried out for Antalya and Kocaeli provinces using daily average meteorological values on a monthly basis, and the results are compared. The results indicate that installing the system in Antalya rather than Kocaeli leads to a 50% and 25% increase in the energy and exergy efficiency of the PTC, respectively, while also resulting in a 36 kg increase in the annual hydrogen production of the entire system.

Keywords: Nanofluid, parabolic trough solar collector, hydrogen production.

I. Introduction

To explore alternatives to fossil fuels and mitigate CO_2 emissions, hydrogen emerges as a promising energy carrier for sustainable and eco-friendly energy production (Abbas, 2023). Concurrently, solar energy stands out as a leading renewable resource in the pursuit of sustainable energy solutions (Fang et al., 2023). Through the utilization of a parabolic trough solar collector (PTC), solar energy can be harnessed to power cycles for hydrogen generation in electrolyzers. Introducing nanofluids into the PTC system can enhance its thermodynamic efficiencies and increase hydrogen production rates (HPR).

In this context, Khan et al. (2020) conducted a comparison between Fe_2O_3/therminol VP1, SiO_2/therminol VP1, and Cu/therminol VP1 nanofluids within a Parabolic Dish Collector (PDC), which is connected to a combined cycle for power and hydrogen production. Their investigation revealed that SiO_2/therminol VP1 exhibited superior characteristics compared to the other nanofluids studied. Ju et al. (2023) explored the effects of CuO, SiO_2, and Al_2O_3 nanoparticles dispersed in Syltherm-800 base fluid within a PTC, Kalina cycle (KC), and polymer electrolyte membrane (PEM) electrolyzer setup. Their research highlighted CuO nanoparticles as particularly effective, resulting in a 9.63% increase in exergy efficiency and a 0.033 kg/h improvement in the HPR. İbrahim et al. (2022) employed silver and graphene nanoparticles dispersed in ethylene glycol within the Compound Parabolic Concentrator (CPC) of a solar-biomass hybrid multigeneration system. The findings also demonstrated enhanced system performance with the utilization of nanofluids as working fluids in solar collectors. Furthermore, Abid et al. (2017) investigated the integration of nanofluids, including Al_2O_3 and Fe_2O_3 nanoparticles dispersed in water, as well as molten salts, into an organic Rankine cycle (ORC) to power an electrolyzer. Their findings indicated increased HPRs, reaching up to 0.02454 g/s.

In this study, the impact of Cu nanoparticle-dispersion into Syltherm-800 base fluid within a PTC cycle integrated with an ORC for electricity generation to be consumed in a PEM electrolyzer for hydrogen production is thermodynamically investigated for the cases of founding the system in Antalya and Kocaeli. Then, the thermodynamic findings and HPRs for the two cases are compared with each other.

II. Procedure

In this study, solar computations for the investigated system are performed for Antalya (36°N, 30°E) and Kocaeli (40°N, 29°E). Total daily average meteorological values on monthly basis are used and the results are obtained for all months of the year. The system is assumed to work during the sunlight hours on every day of the year. Fig. 1 represents the system.

In the examined system, the PTC mirror directs solar radiation onto the absorber, positioned along the collector's central axis. This absorber is enclosed by tempered glass, with air filling the space between the glass cover and the absorber. Solar radiation acquired by the absorber is then conveyed to the heat transfer fluid (HTF) flowing inside the absorber. Two HTFs in the PTC are thermodynamically compared in this study: The Silterm-800, and Silterm-800 /Cu nanofluid which contains Cu nanoparticles in the base fluid at a volumetric fraction of 2% to improve the thermal performance of the PTC.

The operating principle of the system can be explained as follows: The HTF enters the absorber at 400 K, absorbing heat and increasing its temperature as it traverses the component. It subsequently moves to the evaporator, where it conducts its heat to the ORC whose working fluid is benzene. After this heat transfer, the temperature of the HTF decreases to 400 K and reaches the PTC inlet again. In the ORC cycle, benzene, transitioning from compressed liquid to superheated vapor via heat transfer in the evaporator, expands while

passing through the ORC turbine and leads to an electrical power generation. The expanded benzene leaves the turbine at low pressure in the phase of superheated vapor. Then, benzene undergoes a condensation at 313 K what converts it to the saturated liquid at the outlet of the condenser. Afterward, it is compressed back to the pressure of the evaporator and sent back to this device. On the other hand, the turbine-generated electricity is transformed into direct current via a rectifier and directed to a PEM electrolyzer. This electricity is then utilized to conduct electrolysis on water within the electrolyzer, resulting in the production of hydrogen.

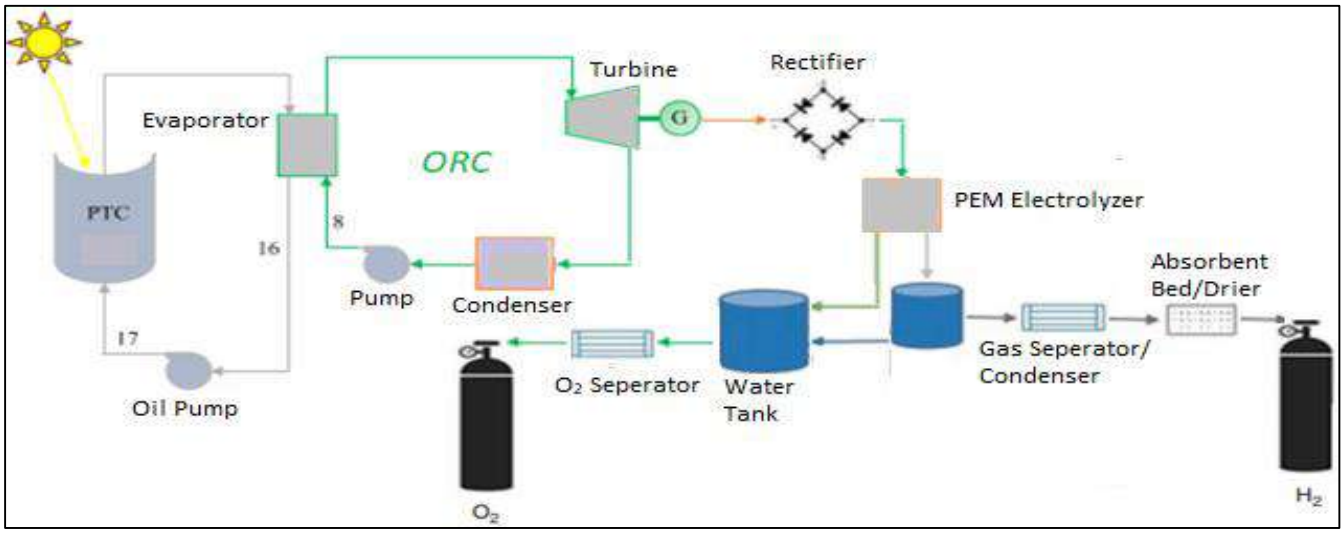


Fig. 1: The configuration of the system.

III. Analysis

Thermophysical properties of Syltherm-800 and Cu at 400 K are given in Table 1.

Table 1. Thermophysical properties of Syltherm-800 and Cu at 400 K (Dou et al. 2023)

Property	Syltherm-800	Cu
ρ [kg/m^3]	*840.067*	*8933*
C_P [J/kg K]	*1791*	*396.370*
k [W/m K]	*0.114927*	*393.170*
μ [Pa s]	*0.002186*	-

The equations to compute the total solar energy incident on the PTC (Q_s), the useful energy gain of the fluid in the PTC (Q_u), the PTC's energy efficiency (η_{en}), the exergy efficiency of the PTC (η_{ex}), useful exergy gain of the fluid flowing inside the PTC (E_u), and total available solar exergy that exposing the PTC (E_s) can be listed as follows (do Carmo Zidan et al. 2022) and (Bellos and Tzivanidis, 2019):

$$\eta_{en} = \frac{Q_u - (W_P/\eta_{el})}{Q_s} \quad (1)$$

$$Q_s = A_a \ . I_b \quad (2)$$

$$Q_u = F_R \ . A_a \ . \left(I_b - \left(\frac{A_r}{A_a}\right) . U_L . \left(T_{nf,in} - T_{amb}\right) \right) \quad (3)$$

$$T_{nf,out} = T_{nf,in} + \left(\frac{Q_f}{\dot{m}_{nf} \ . C_{P,nf}} \right) \quad (4)$$

$$U_L = \frac{Q_{loss}}{A_r . (T_{abs} - T_{amb})} \quad (5)$$

$$F_{EF} = \frac{\frac{1}{U_L}}{(1/U_L) + \left(\frac{d_{ao}}{h_{nf} d_{ai}}\right) + \left(\left(\frac{d_{ao}}{2k_a}\right) . ln(d_{ao}/d_{ai})\right)} \quad (6)$$

$$F_{FF} = \left(\frac{m_{nf} C_{P_{nf}}}{A_r \ .U_L \ .F_{EF}}\right) \ .\left(1 - exp\left(-\left(\frac{A_r \ .U_L \ .F_{EF}}{m_{nf} \ .C_{P_{nf}}}\right)\right)\right) \quad (7)$$

$$F_R = F_{FF} \ .F_{EF} \quad (8)$$

$$\eta_{ex} = \frac{E_u}{E_s} \quad (9)$$

$$E_u = Q_u - m_{nf} \ .C_{P_{nf}}.T_{amb} \ .\ln\left(\frac{T_{nf,out}}{T_{nf,in}}\right) - \ m_{nf} \ .T_{amb} \ .\frac{\Delta P}{\rho_{nf} \ .T_{mean}} \quad (10)$$

$$E_s = Q_s \ .\left(1 - \frac{4}{3}\frac{T_{amb}}{T_{in}} + \frac{1}{3}\left[\frac{T_{amb}}{T_{in}}\right]^4\right) \quad (11)$$

The structural specifications of the PTC, the method used to determine nanofluid properties, heat loss (Q_{loss}), pump power in the PTC cycle (W_p), and net power production by the ORC are available in the study by do Carmo Zidan et al. (2022). Additionally, Table 2 provides some design parameters relevant to the ORC and PEM electrolyzer.

Table 2. Design parameters for the ORC and PEM electrolyzer

Parameters	Value	Unit
Temperature difference between turbine and evaporator inlet of source	*10*	*°C*
Temperature difference between turbine inlet and evaporator	*5*	*°C*
Pinch point temperature difference (at least)	*5*	*°C*
Condenser temperature	*40*	*°C*
Rectifier efficiency	*0.796*	*-*
Cell number of the electrolyzer	*19*	*-*

Equation 12 is used to calculate the HPR per cell of the PEM electrolyzer in g/h (m_{el}) (Budak and Devrim, 2019).

$$m_{el} = 1.43 \times 10^{-3} + 2.39 \times 10^{-2} E_{el} - 4.32 \times 10^{-5} E_{el}^2 \quad (12)$$

where E_{el} is electrical power acquired by one electrolyzer cell.

IV. Results and discussions

Table 3 illustrates the monthly quantities of useful energy and exergy, along with the corresponding energy and exergy efficiencies of the PTC system. The efficiency values in the table are rounded. According to the results, the useful energy and exergy transferred from the absorber to the collector, as well as the energy and exergy efficiencies, increase from January to July in both the Antalya and Kocaeli cases. However, after this month, they gradually decrease until the end of the year because of meteorological reasons. The peak values for useful energy and exergy rates, energy and exergy efficiencies, are achieved with nanofluid in Antalya, reaching 9994 W, 2644 W, 95%, and 27%, respectively. Adding Cu nanoparticles at a volumetric concentration of 2% into the base fluid, Syltherm-800, resulted in approximately 3.80%-4.13% and 4.26%-4.48% enhancements in the rates of useful energy and exergy, respectively. Also, there are approximately 4% and 1% improvements in energy and exergy efficiencies, respectively, for the Antalya case. Establishing the system with nanofluid in Antalya instead of Kocaeli enables the transfer of 64.74% and 65.90% more energy and exergy to the fluid in January. while it causes a 1%-4% enhancement in energy efficiency and a 0%-1% enhancement in exergy efficiency.

Tab. 3: Monthly average thermodynamic values of the PTC system.

	Useful Energy (W)				**Useful Exergy (W)**				**Energy Efficiency (%)**				**Exergy Efficiency (%)**			
	Kocaeli		**Antalya**		**Kocaeli**		**Antalya**		**Kocaeli**		**Antalya**		**Kocaeli**		**Antalya**	
	BF	**NF**	**BF**	**NF**	**BF**	**NF**	**BF**	**NF**	**BF**	**NF**	**BF**	**NF**	**BF**	**NF**	**BF**	**NF**
January	*2466*	*2567*	*4061*	*4229*	634	660	*1049*	*1095*	*83*	*87*	*87*	*91*	*23*	*24*	*24*	*25*
February	*3618*	*3768*	*5101*	*5312*	933	974	*1323*	*1381*	*86*	*90*	*88*	*92*	*24*	*25*	*25*	*26*
March	*4676*	*4871*	*6400*	*6664*	1210	1264	*1667*	*1741*	*88*	*92*	*89*	*93*	*24*	*26*	*25*	*26*
April	*5945*	*6187*	*7669*	*7980*	1546	1614	*2006*	*2096*	*89*	*93*	*90*	*94*	*25*	*26*	*25*	*26*
May	*7453*	*7753*	*8800*	*9150*	1948	2034	*2311*	*2413*	*90*	*95*	*91*	*95*	*25*	*26*	*26*	*27*
June	*8015*	*8331*	*9450*	*9816*	2099	2191	*2487*	*2595*	*91*	*94*	*91*	*95*	*26*	*27*	*26*	*27*
July	*8229*	*8551*	*9628*	*9994*	2157	2250	*2535*	*2644*	*91*	*94*	*92*	*95*	*26*	*27*	*26*	*27*
August	*7832*	*8138*	*9416*	*9775*	2050	2138	*2478*	*2584*	*91*	*94*	*91*	*95*	*25*	*27*	*26*	*27*
September	*6540*	*6800*	*8271*	*8591*	1704	1778	*2168*	*2261*	*90*	*93*	*91*	*94*	*25*	*26*	*26*	*27*
October	*4586*	*4770*	*6486*	*6743*	1187	1237	*1690*	*1762*	*88*	*92*	*90*	*93*	*25*	*26*	*25*	*26*

November	*3334*	*3468*	*5072*	*5277*	859	895	*1315*	*1372*	*86*	*90*	*89*	*92*	*24*	*25*	*25*	*26*
December	*2427*	*2525*	*3860*	*4018*	623	649	*997*	*1039*	*83*	*87*	*87*	*91*	*23*	*24*	*24*	*25*

BF: Base Fluid, NF: Nanofluid

The study also analyzes the monthly average quantities of hydrogen production generated by the electrolysis system. The findings are presented in Table 4. The results indicate that the HPR raised from January to July, peaking at 10.95 kg/month in July when nanofluid is employed in Antalya. However, thereafter, it gradually declines, attributed to the reasons mentioned earlier. Adding nanoparticles to the base fluid increases the HPR by approximately the same percentage of 4.184% to 4.495% in both cities. However, in the case of Antalya, the annual HPRs are 69,762 kg/year and 72,756 kg/year when using both the base fluid and nanofluid, respectively, which are 84% higher than those in the Kocaeli case.

Tab. 4: Monthly average hydrogen production amounts of the system in kilograms.

City	Fluid	Jan	Feb	Mar	Apr	May	Jun	Jul	Aug	Sep	Oct	Nov	Dec	Total
Koc.	**BF**	*0,57*	*0,90*	*1,734*	*2,877*	*4,868*	*6,272*	*6,795*	*6,125*	*4,101*	*2,051*	*1,020*	*0,584*	*37,904*
	NF	*0,59*	*0,94*	*1,812*	*3,004*	*5,085*	*6,548*	*7,092*	*6,386*	*4,283*	*2,140*	*1,064*	*0,609*	*39,562*
Ant.	**BF**	*2,09*	*2,72*	*4,153*	*5,537*	*7,968*	*9,746*	*10,51*	*9,954*	*7,428*	*4,878*	*2,934*	*1,844*	*69,765*
	NF	*2,19*	*2,84*	*4,338*	*5,782*	*8,314*	*10,16*	*10,95*	*10,37*	*7,742*	*5,088*	*3,061*	*1,925*	*72,756*

V. Conclusions

This study examines the impact of incorporating Cu nanoparticles into a PTC cycle linked to an ORC for electricity generation for hydrogen production in an electrolyzer. The system achieves its highest useful energy and exergy rates, and energy and exergy efficiencies, at 9994 W, 2644 W, 95%, and 27%, respectively, when utilizing nanofluid in Antalya. This scenario notably boosts the energy and exergy efficiencies of the PTC by at most 64.74% and 65.90%, respectively, compared to the Kocaeli case. Setting up the system in Antalya instead of Kocaeli results in an 84% increase in the annual HPR, reaching 72.756 kg.

References

Abbas M.K., Hassan Q., Tabar V.S., Tohidi S., Jaszczur M., Abdulrahman I.S., Salman H.M., Techno-economic analysis for clean hydrogen production using solar energy under varied climate conditions, International Journal of Hydrogen Energy, 48, 2929-2948, (2023).

Abid M., Ratlamwala T. A., Atikol U., Solar assisted multi-generation system using nanofluids: A comparative analysis, International Journal of Hydrogen Energy, 42, 21429-21442, (2017).

Bellos E., Tzivanidis C., Alternative designs of parabolic trough solar collectors, Progress in Energy and Combustion Science, 71, 81-117, (2019).

Budak Y., Devrim Y., Comparative study of PV/PEM fuel cell hybrid energy system based on methanol and water electrolysis. Energy Conversion and Management, 179, 46-57, (2019).

do Carmo Zidan D., Maia C. B., Safaei, M. R., Performance evaluation of various nanofluids for parabolic trough collectors, Sustainable Energy Technologies, 50, 101865 (2022).

Dou L., Ding B., Zhang Q., Kou G., Mu M., Numerical investigation on the thermal performance of parabolic trough solar collector with synthetic oil/Cu nanofluids. Applied Thermal Engineering, 227, 120376 (2023).

Fang J., Yang M., Cui L., Yi X., Huo H., Wen Z., Liu X., Efficient hydrogen production system with complementary utilization of methane and full-spectrum solar energy, Energy Conversion and Management, 283, 116951 (2023).

İbrahim A.A., Kayfeci M., Georgiyev A.G., Dolgun G.K., Keçebaş A., Performance assessment of a novel solar and biomass-based multi-generation system equipped with nanofluid-based compound parabolic collectors, Energies, 15(23), 8911, (2022).

Ju Y., Abdalla A.N., Wang S., Hai T., Wei H., Wang M., Exergetic evaluation of the effect of nanofluid utilization for performance enhancement of a solar driven hydrogen production plant, International Journal of Hydrogen Energy, 52, 302-314, (2024).

Khan M.S., Amber K.P., Ali H.M., Abid M., Ratlamwala T.A.H., Javed S., Performance analysis of solar assisted multigenerational system using therminol VP1 based nanofluids: a comparative study, Thermal Science, 24, 865-878, (2020).

Effects of Chemical Machining Characteristics of Aluminum as Metallic Bipolar Material

[1*]Deniz Okka, [1]Orhan Çakir
[1] Yıldız Technical University, Faculty of Mechanical Engineering, Mechanical Engineering, Beşiktaş, İstanbul, 34349, Türkiye

* E-mail: denizokka.34@gmail.com

Abstract
Chemical machining is typical nontraditional machining method that is based on controlled corrosion of material. The process is unique which the selected chemical solution that is named as etchant, is employed to corrode unmasked areas of workpiece. Aluminum is an engineering material and used as metallic bipolar material in fuel cell that is main equipment of hydrogen energy technology. In this experimental study, aluminum alloy (Al6061-T651) is selected for examining chemical machining performance in three different sodium hydroxide (NaOH) etchant concentrations (1 Mol, 2 Mol and 3 Mol). Depth of etch and surface roughness parameters have been determined.

Keywords: Chemical Machining, Aluminum, Bipolar Plates

I. Introduction

Metallic bipolar material is vital part of fuel cells and different metallic materials such as aluminum, copper, stainless steel, nickel can be named. Their good mechanical properties, very high electrical and thermal conductivity, and easy manufacturability give advantages against graphite and composite bipolar materials. Additionally, the requirement of lightweight construction in bipolar plates, the thickness of the plate plays an important factor. The thin metallic bipolar plates present better gas-impermeable and durability to mechanical vibrations. They are capable to be manufactured as thin as 1-2 mm, causing smaller and lighter fuel cell stack compare to similar graphite bipolar plates Gautam et al. (2015).

Chemical machining is a nontraditional machining method that takes advantages of corrosion mechanism, weakens atomic and metallic bonds, and removes material atom-by-atom. Therefore, chemical machining is useful manufacturing method due to various advantages over other manufacturing methods.

Although the first evidence written about chemical machining process related to armour etching is revealed in 15th century, the origins of chemical machining trace back to the Ancient Egyptian W. T. Harris (1976). Nowadays, chemical machining is desired for manufacturing a variety of devices, such as aircraft and spacecraft parts, PCBs, capacitors, fuel cells, heat exchangers etc.

The bipolar plates are opposing channeled surfaces for delivery of hydrogen to the anode of electrochemical cell and for delivery of oxygen to the cathode cell. Bipolar plates are structured in different ways, generally cladded with more conductive materials than structural metal, and then flow fields are chemically etched. These flow fields have intricated shapes and are dimensioned between 0.25 – 2.5 mm. Photochemical machining of bipolar plates is a common production method, because of the advantages of chemical etching and mass production David J. Edlund et al. (2006).

This study aims to determine the machining characteristics of chemical machining of aluminum alloy Al6061-T651 as metallic bipolar plate. The selected etchant is sodium hydroxide (NaOH) at different concentrations and process temperatures.

II. Experimental Set-up and Procedure

The experiments of chemical machining of aluminum alloy, Al6061-T651 (chemical composition is given in Table 1), is carried out in glass baker. The experiments were conducted at 20°C room temperature. The illustration of experimental apparatus and set-up are given in Fig.1, the system is included in magnetic stirrer, baker, heat controller, thermometer, water jacket and specimen holder. Chemical machining process consists of several steps, that's why process is difficult. To avoid operator and application errors, standard operating procedures (SOPs) should be prepared for even simple steps. The study also tries to express purpose, scope, circumstance, and responsibilities of SOPs, and that can guide to prepare of SOP.

Table 1 Chemical composition of Al6061-T651

Specimen	Al	Si	Fe	Cu	Mn	Mg	Cr	Zn	Ti	Others
Al 6061-T651	97	0.53	0.26	0.22	0.10	1.01	0.08	0.02	0.02	0.08

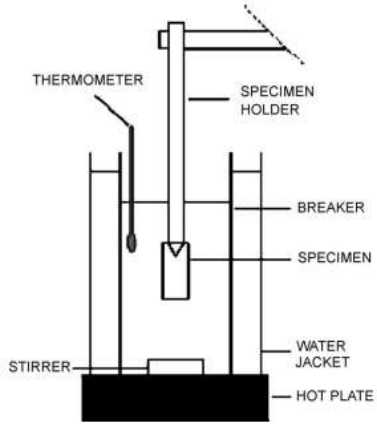


Fig.1: Experimental set-up of aluminum etching tests

The experimental work is included in two process steps, cleaning (Fig.2) and etching (Fig. 3). The first step (cleaning specimen) purpose is to remove surface contaminations, such as oxide layer, clad, grease or other type of oils, marker sign etc. These contaminations result in non-uniform surface and cause material removal gradients. Consequently, specimens should be cleaned carefully. However, some reactive materials, like aluminum, were impacted easily by cleaning agents; also, excessive contaminations of copper, iron, zinc in the solution may have negative impacts on the surface quality. The purpose of the second step (etching specimen) is controllable material removing with corrosive effect. The temperature and molarity of etchant have an important effect on etching rate and surface finish conditions. Since chemical machining is an exothermic reaction, it is important to maintain the solvent temperature within the desired range.

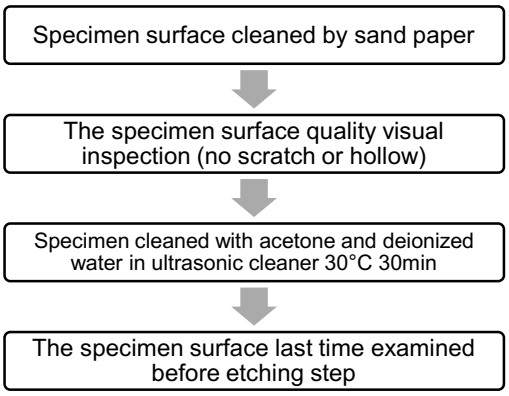


Fig.2: Experiment Surface Cleaning Process Steps

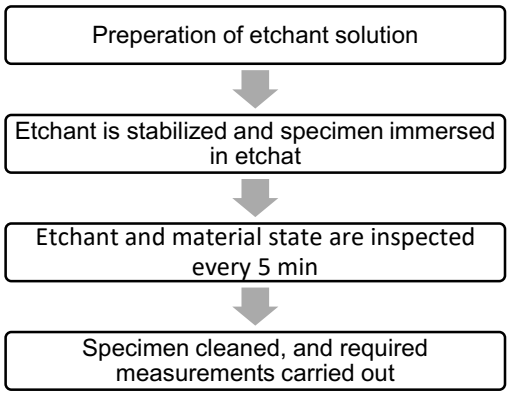


Fig. 3: Experiment Etching Process Steps

Specimens are dimensioned 100x25x8 mm (h x d x t). Since chemical machining process reproduce surfaces again, the material stock surface quality has a great effect on surface finish. Therefore, on surface of specimens, there should be no damage or process errors. Specimens cleaned carefully by sandpapering and ultrasonic cleaner (30°C 30 min).

In the experiment, the both-side-etched immersion etching method is carried out. The sodium hydroxide is supplied from laboratory, graded %99 percent. Tests carried out 1 Mol, 2 Mol, and 3 Mol NaOH dissolution with deionized water and 20°C, 30°C, 40°C and 50±1°C. Every 5 min intervals, specimens are washed with pressurized water and then the depth of etch and surface roughness are measured. Chemical machining depth is measured by caliper (±0.01) and surface roughness is measured by Mitutoyo SJ-210 (2CR-75 measurement filter, stylus type 2µm radius and 60° profile angle).

III. Results and discussions

The study aims to determine the chemical machining characteristics of aluminum alloy Al6061-T651 and application potential and advantages on metallic bipolar plates. The experimental study is carried out to optimize two main controlling parameters of the chemical machining processes, temperature and etchant molarity, depending on surface conditions O. Çakır (2008). Obtained results show that chemical machining process is suitable for micromachining processes and for developing surface condition David J. Edlund et al. (2006).

CHM is an appropriate application for machining complex peripheral shapes as bipolar plates. There are no thermal and mechanical effects on material, thus material physical and chemical opportunities do not change. The partition between chemical etch depth (s) and chemical machining time (t) determines the etching rate (E), Equation (1. In Fig.4 and Fig.5, the effects of temperature and molarity on chemical etch depth is compared. The etching rate increases C/C_0 times for each etchant molarity (C_0=1) change and approximately 2 times for every 10°C.

$$E = s/t \quad (1)$$

Surface roughness is an important parameter for disclose material behaviours. Although increasing surface roughness provides higher chargeability and reactivity, the mechanical strength of workpiece decreasing. As a result, the etching rate should be optimized based on surface roughness. In the study of O. Çakır (2011) about chemical machining of aluminum the results show that the speed-up of obtained surface roughness decreases until optimum etch rate and then increases again. The impact of molarity on surface roughness is shown in Fig.7. In Fig.7, optimum value 1.6 µm Ra is obtained at 2 Mol, low etch rate (1 Mol) and high etch rate (3 Mol) shows higher surface roughness (respectively 1.8 and 2.1 µm Ra). Depends on the temperature, surface roughness variation is given in Fig.6. Between 30-40°C and 2 Mol NaOH dissolution determines optimum conditions.

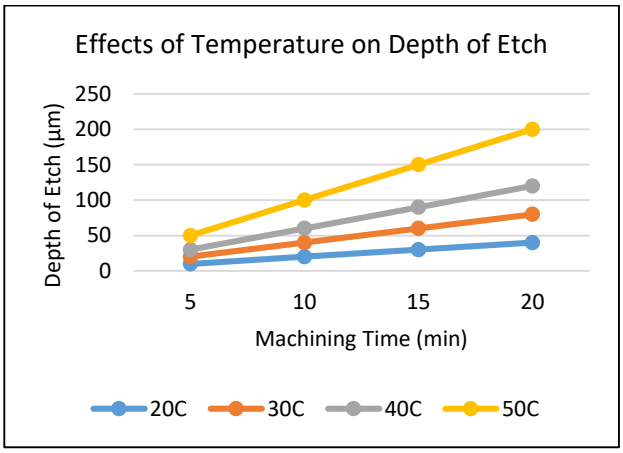


Fig.4: Chemical Etch Depth Examined Depending on Temperature

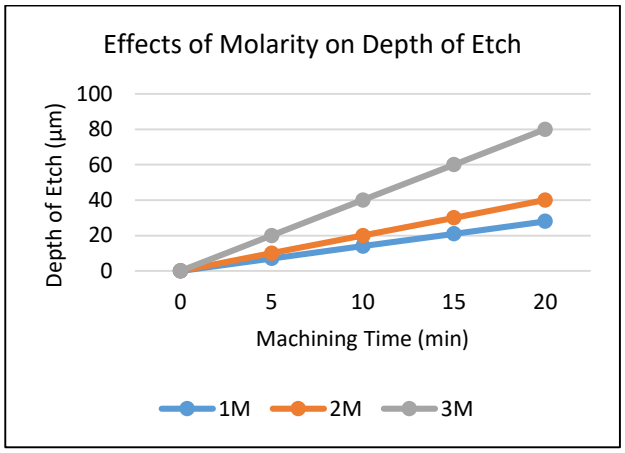


Fig.5: Chemical Etch Depth Examined Depending on Temperature

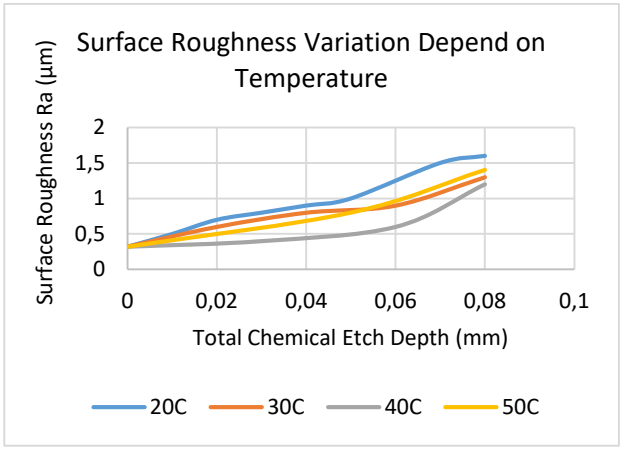


Fig.6: Surface Roughness Variation Depends on Temperature

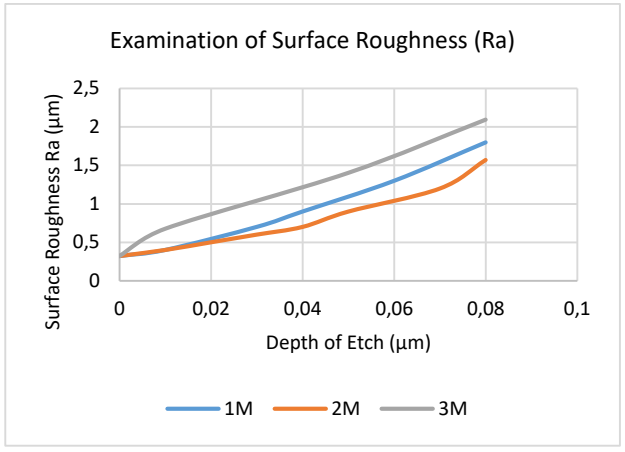


Fig.7: Examination of Surface Roughness Variation (NaOH 2M 20°C)

The surface development applications are also utilized for fabrication hydrophilic surfaces Tao Zie (2006). In hydrogen fuel cells, reaction of oxygen and hydrogen brings about water on cathode part exhaust flow field, and it aggregates on bipolar plate and cathode electrode. Formed water slug inhibits gas flow and decreases in surface area of electrode. Therefore, hydrophilic surfaces eliminate water slug formation and increase reaction potential.

Although the chemical machining is suitable for micromachining processes, very tiny bubbles and foam appeared in etchant solution. The trapped bubbles may prevent machining, especially in porous constructs, like aluminum foams Y. Matsumoto (2007). The amount of formed foam and corrosive evaporation increase with temperature, especially after 40°C. Over 40°C temperature conical machining or nonuniform-graded machining process is not applicable without specific apparatus. In etchant solution, the formation of sludge is also seen, this sludge may be caused by non-soluble contaminants in specimen, as copper.

IV. Conclusions

The study aims to clarify advantages of chemical machining on metallic bipolar plates, also provides a comprehensive data to literature. Atom-by-atom material removing by corrosion mechanism provides to machine high accuracy intricated shapes easily. However, chemical machining process reproduce own surfaces, thus the surface roughness increases with depth of etch. Surface roughness is also affected by etch rate and stock surface quality. Chemical machining of Al6061-T651 by using NaOH is carried out with different temperatures and comcentrations. Optimum result is emerged at 2 Mol NaOH dissolution and between 30-40°C. Experiments also

show that only controllable parameter is temperature while machining, this emphasizes the importance of temperature.

Chemical machining produces high chargeable and catalytic layers on bipolar plate with ability of increasing surface area by fine etched tunnels. Chemical etching may increase the efficiency of the system. In addition, CHM present the possibility of development of hydrophilic surfaces for fuel cells. The reaction of hydrogen and oxygen in cathode cell produces water molecules, and water slug inhibits gas flow and electrode surface area. Formed water molecules can remove easily on hydrophilic surfaces.

In experiments, formation of foam and sludge is observed, they may cause material removing gradients. However, it doesn't prevent to machine small gaps like aluminum foam Y. Matsumoto (2007). Formed sludge is not much sticky, it does not form scale on specimens.

According to experiment and research results, chemical machining is more suitable for processes of channelling intricate-shaped plates, of surface development, of machining small porosities. This takes an important advantage for developing small electronic devices or improving performance of them.

References

Çakır,O., Chemical Etching of Aluminium, Journal of Materials Processing Technology, vol. 99, 337-340, (2008)

Çakır O., Etchants For Chemical Machining of Aluminum and Its Alloys, Acta Physica Polonica, 135, 4, 586-587 (2019)

David J. Edlund et al., Bipolar Plate Assembly Fuel Cell Stacks and Fuel Cell Systems Incorporating The Same, US. Patent 7,147,677 B2 (2006)

Gautam R.K., Soma B.S., Kar K.K., Bipolar Plate Materials for Proton Exchange Membrane Fuel Cell Application, Recent Patents on Materials Science, 8, 15-45 (2015)

Matsumoto, Y., Brothers, A., Stock, S., Dunand, D., Uniform and graded chemical milling of aluminum foams, Materials Science and Engineering A 447 (2007) 150–157 (2007)

Tao Zie, et al., Hydrophilic Bipolar Plates, US Patent 20060172172A1, (2006)

W. T. Harris, W.T., Chemical Milling, Clarendon Press Oxford, (1976)
,
Wei Yuan et al., Porous metal materials for polymer electrolyte membrane fuel cells – A review, vol. 94, (2012)

Thermodynamic Analysis of The Integration of Reverse Osmosis Desalination, Reverse Electrodialysis and Photo-Chloralkaline System Using Renewable Energy for Enhanced Brine Management and Hydrogen Production

*Nadira Salsabila, Muhammad Usman Sajid, Yusuf Bicer
Division of Sustainable Development (DSD), College of Science and Engineering (CSE), Hamad Bin Khalifa University (HBKU), Qatar Foundation (QF), Education City, Doha, Qatar

* E-mail:nasa49089@hbku.edu.qa

Abstract
This study explores an innovative integrated system combining Reverse Osmosis (RO), Reverse Electrodialysis (RED), and Photo-Chloroalkali (PCA) processes, powered by renewable solar energy for enhanced brine management and hydrogen production. We conduct a thorough thermodynamic analysis to assess the synergy between these technologies in utilizing brine from desalination processes. The integrated approach not only aims to mitigate the environmental impact of high salinity waste but also enhances energy recovery and resource efficiency. Results demonstrate the potential for substantial energy and exergy efficiencies across the systems, highlighting significant improvements in sustainable water treatment and energy production. The findings advocate for a paradigm shift in handling desalination byproducts, proposing a model that maximizes renewable energy use while producing valuable byproducts like hydrogen and chlorine, essential for further industrial applications.

Keywords: Reverse Osmosis, Reverse Electrodialysis, Photo-Chloroalkali, Hydrogen Production, Brine Management, Renewable Energy, Thermodynamic Analysis

I. Introduction

Wastewater and brine management are critical for environmental sustainability, public health, and economic growth, as highlighted by the increasing global population and urbanization. Effective management is essential to mitigate the adverse impacts on ecosystems and human health. Proper wastewater treatment is crucial for disease prevention and ecosystem protection, and conserving water resources for various uses (Corcoran, 2010). Similarly, managing brine from desalination processes is vital due to its high salt content and potential harm to marine life (Meehan et al., 2017).

The adoption of sustainable management practices is gaining momentum, driven by technological advancements, best practices, and increased awareness and education (Corcoran, 2010). Desalination, especially through reverse osmosis, offers a solution to water scarcity but poses environmental challenges due to brine production. This concentrated salt solution can significantly impact marine ecosystems if not properly managed (Lim et al., 2021; Panagopoulos et al., 2019).

Reverse electrodialysis (RED) presents a promising approach by using the salt gradient in brine to generate electricity, showcasing an innovative way to address brine disposal challenges while supporting renewable energy production (Nazif et al., 2022). Moreover, this technology not only facilitates electricity generation but also enables the production of valuable byproducts like chlorine gas and hydrogen, enhancing its economic viability and environmental benefits (Ranade et al., 2022). This multifaceted approach underscores the importance of ongoing research into RED's applications, particularly in optimizing its efficiency and integration into broader environmental management strategies.

Other methods capable of producing hydrogen while treating brine or seawater include the photo-chloroalkali system. Research on this system has explored its integration with photoelectrodialysis (Mir et al., 2021), among other attempts to optimize its capabilities and assess its benefits for producing both hydrogen and chlorine, which is used as a disinfectant. This approach presents a promising method for exploring similar objectives. The study examines the integration of reverse osmosis (RO) with reverse electrodialysis (RED) and the photo-chloroalkali (PCA) process for hydrogen production and brine management, utilizing renewable solar energy. It delves into the potential for integration and conducts a thermodynamic assessment of these capabilities.

II. System Diagram

An integrated system was analyzed thermodynamically, which involved utilizing RO brines in an RED system for power and hydrogen generation. Another system, PCA was also integrated using seawater to produce chlorine valuable products for disinfectants and also hydrogen. The hydrogen output of both systems was compressed, stored, and then processed in a fuel cell to generate electricity using a PEM cell. Additionally, the entire integrated system was powered by photovoltaic thermal technology, and the thermal energy was used for cooling via an ejection cooling system. The cold air produced by the cooling system was utilized in the intercooler of the hydrogen compressors to maximize the system's efficiency. Fig. 1 is a full systematic diagram of the proposed integrated system.

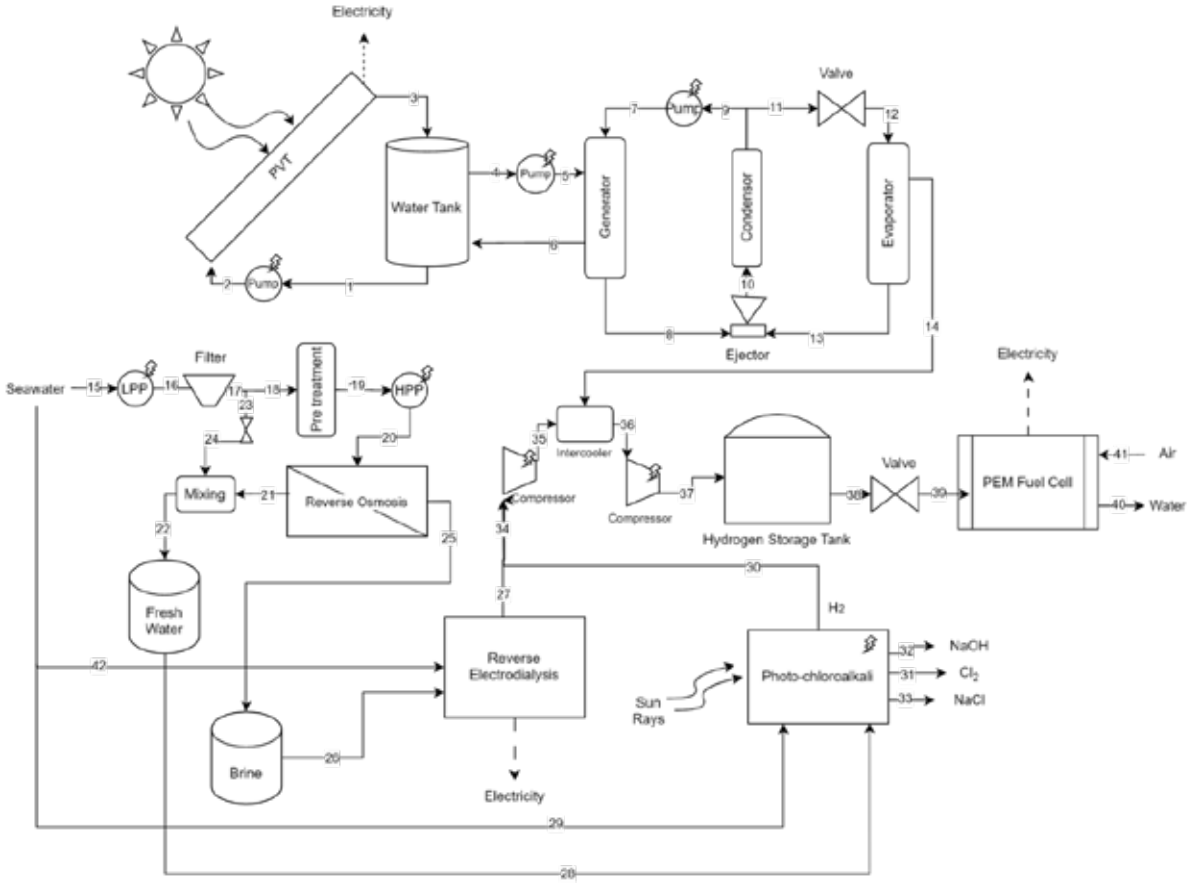


Fig. 1: Full systematic diagram of the proposed integrated system.

III. Analysis

Thermodyanamic assessments were conducted using engineering equation solver on each subsystem where mass balance equation, energy balance equation, entropi balance equations and exergy balance equations wer calculated. Energy and exergy analysis was also performed for each subsystem and overall system where efficiency equations are shown below:

1. Reverse osmosis system

$$\eta_{\text{en, RO}} = \frac{\dot{m}_{22}\cdot h_{22}}{W_{\text{dot, in, pump4}} + W_{\text{dot, in, pump5}} + \dot{m}_{15}\cdot h_{15}} \quad (1)$$

$$\eta_{\text{ex , RO}} = \frac{\dot{m}_{22}\cdot \text{ex}_{22}}{W_{\text{dot, in, pump 4}} + W_{\text{dot, in, pump5}} + \dot{m}_{15}\cdot \text{ex}_{15}} \quad (2)$$

2. Reverse electrodialysis system

$$H_{\text{en-RED}} = \frac{P_{\text{gros}}}{Ex_{\text{in}} - E} \quad (3)$$

3. Photo-chloroalkali system

$$\eta_{en;PCA} = \frac{\dot{m}_{30}\cdot h_{30} + \dot{m}_{31}\cdot h_{31} + \dot{m}_{32}\cdot h_{32}}{W_{CA;PV} + \dot{m}_{28}\cdot h_{28} + \dot{m}_{29}\cdot h_{29}} \quad (4)$$

$$\eta_{ex;PCA} = \frac{\dot{m}_{30}\cdot ex_{30} + \dot{m}_{31}\cdot ex_{31} + \dot{m}_{32}\cdot ex_{32}}{W_{CA;PV} + \dot{m}_{28}\cdot ex_{28} + \dot{m}_{29}\cdot ex_{29}} \quad (5)$$

4. PVT System

$$\eta_{\text{en,PVT}} = \frac{W_{\text{dot,PVT}} + (\dot{m}_3\cdot h_3 - \dot{m}_2\cdot h_2)}{Q_{\text{dot,PVT}}} \quad (6)$$

$$\eta_{\text{ex,PVT}} = \frac{W_{\text{dot,PVT}} + (\dot{m}_3\cdot \text{ex}_3 - \dot{m}_2\cdot \text{ex}_2)}{Q_{\text{dot,PVT}}\left(1 - \frac{T_0+273}{T_{\text{sun}}+273}\right)} \quad (7)$$

5. PEM fuel cell system

$$\eta_{\text{en,PEM}} = \frac{W_{\text{dot,FC, net}}}{\dot{m}_{H_2} \cdot \text{HHV}_{H_2,\text{pem}}} \quad (8)$$

$$\eta_{\text{ex,PEM}} = \frac{W_{\text{dot,FC, net}}}{\dot{m}_{H_2} \cdot \text{ex}_{ch,H_2,\text{pem}} + \dot{m}_{\text{air}} \cdot \text{ex}_{ch,\text{air}}} \quad (9)$$

IV. Results and discussions

The result from this study was compared to the results found in literature to validate the findings of this study. Tab. 2 shows the efficiency results of each subsystem of this study in comparison to literature.

Tab. 1: The efficiency results of each subsystem of this study in comparison to literature.

Subsystem	This Study Results	Literature
PVT	η_{energy} =0.585 η_{exergy} =0.212	η_{energy} =051 (Çiftçi et al., 2021) η_{exergy} =0.08 (Çiftçi et al., 2021)
RO	η_{energy} =0.623 η_{exergy} =0.065	η_{energy} =0.6 (Siddiqui et al., 2018) η_{exergy} =0.3 (Siddiqui et al., 2018)
RED	η_{exergy} =0.309	η_{energy} = 0.30 (Ranade et al., 2022)
PCA	η_{energy} =0.475 η_{exergy} =0.129	η_{energy} =0.48 (Mir et al., 2021) η_{exergy} =0.10 (Mir et al., 2021)
PEM	η_{energy} =0.206 η_{exergy} =0.242	η_{energy} =0.47 (Taner, 2018) η_{exergy} =0.50 (Taner, 2018)

In this system, a total of 6 different useful outputs were produced. PVT resulted in electricity and heat energy where the heat was used for an ejector cooling system making cooling another useful output. RO system desalinated sweater and produced brine and freshwater this brine is the given to the RED system producing power and hydrogen. Another stream of seawater was used in the PCA system where it is used to produce hydrogen, NaOH and Cl_2 for disinfectant purposes. Hydrogen is eventually run through a PEM fuel cell making more electricity.

Tab. 2: Outputs of different subsystems

Subsystems	**Outputs**
Electrical energy from PVT	121.6 kW
Thermal energy from PVT	347.4 kW
Cooling capacity from ejector cooling system	192.5 kW
Fresh water from RO system	6 kg/s
Brine from RO system	3.993 kg/s
Power from RED	1.163 kW
Hydrogen from RED	0.0004146 kg/s
NaOH from PCA system	0.01497 kg/s
CL2 from PCA system	0.005436 kg/s
H2 from PCA system	0.00017821kg/s
Electricity from PEM	8.686 kW

Energy and exergy efficiency of every sub system was also calculated as well as the overall system efficiencies when integrated. Overall system energy efficiency is 69.23% and overall exergy efficiency is 22.43%.

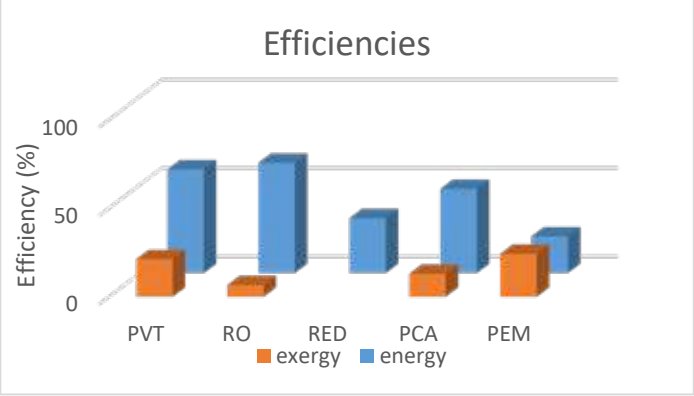


Fig. 2: The energy efficiency and the exergy destruction for each subsystem

The PVT subsystem demonstrates an energy efficiency of 58.5% and an exergy efficiency of 21.1%, indicating effective solar energy conversion but with potential for exergy improvement. The Reverse Osmosis (RO) unit achieves a higher energy efficiency of 62.2% but a lower exergy efficiency of 6.5%, highlighting its effective

desalination process albeit with optimization potential in exergy use. The Reverse Electrodialysis (RED) subsystem, assessed solely on exergy efficiency, shows a moderate performance at 30.9%. In contrast, the PCA system stands out with an energy efficiency of 47.5% and an exergy efficiency of 12.8%, showcasing effective production of valuable products. The Proton Exchange Membrane (PEM) electrolyzer, however, records a lower energy efficiency of 20.6% but a comparable exergy efficiency of 24.1%, suggesting a need for improvement in energy conversion despite a balanced exergy performance.

V. Conclusions

The designed integrated system resulted in efficiencies, with the Photovoltaic Thermal (PVT) subsystem achieving an energy efficiency of 58.5% and an exergy efficiency of 21.1%, highlighting its effective conversion of solar energy. The Reverse Osmosis (RO) process demonstrates a notable energy efficiency of 62.2% with a lower exergy efficiency of 6.5%, indicating a proficient desalination process that has room for optimization in energy usage. Furthermore, the Reverse Electrodialysis (RED) subsystem, with an exergy efficiency of 30.9%, and the Photochloro-alkali (PCA) system, boasting an energy efficiency of 47.5% and an exergy efficiency of 12.8%, both exhibit efficient energy storage and conversion capabilities. The Proton Exchange Membrane (PEM) fuel cell system, although showing a lower energy efficiency of 20.6%, maintains a balanced exergy efficiency of 24.1%, suggesting an area for energy conversion improvements. The overall system energy efficiency is reported at 69.2%, and the overall exergy efficiency is at 22.4%, indicating a highly efficient integrated system that optimally utilizes renewable energy sources for multiple generations, including electricity, hydrogen, and valuable byproducts from waste management.

Acknowledgements

The authors acknowledge the support provided by the Hamad BinKhalifa University, Qatar Foundation, Education City, Doha, Qatar (210049089).

References

Çiftçi, E., et al. Energy and exergy analysis of a photovoltaic thermal (PVT) system used in solar dryer: A numerical and experimental investigation. *Renewable Energy*, *180*, 410–423. (2021).

Corcoran, Emily. Sick water? : the central role of wastewater management in sustainable development : a rapid response assessment. In *GRID-Arendal*. (2010).

Lim, Y. J., et al. Seawater desalination by reverse osmosis: Current development and future challenges in membrane fabrication – A review. *Journal of Membrane Science*, *629*, 119292. (2021).

Meehan, M., et al. Environmental Impacts of Brine (Produced Water). *North Dakota State University*, *June*. (2017).

Mir, N., et al. Thermodynamic modeling of a combined photo-electrodialysis-chloralkali system for sustainable desalination. *Desalination*, *499*. (2021).

Nazif, A., et al. Recent progress in membrane development, affecting parameters, and applications of reverse electrodialysis: A review. *Journal of Water Process Engineering*, *47*, 102706. (2022).

Panagopoulos, A., et al. Desalination brine disposal methods and treatment technologies - A review. *Science of The Total Environment*, *693*, 133545. (2019).

Ranade, A., et al. Feasibility of Producing Electricity, Hydrogen, and Chlorine via Reverse Electrodialysis. *Environmental Science & Technology*, *56*(22), 16062–16072. (2022).

Siddiqui, O., et al. Examination of a new solar-based integrated system for desalination, electricity generation and hydrogen production. *Solar Energy*, *163*, 224–234. (2018).

Taner, T., et al. Energy and exergy analyze of PEM fuel cell: A case study of modeling and simulations. *Energy*, *143*, 284–294. (2018).

The Effect of TiO_2 Coating on PEC Efficiency of Hematite Photoanode Produced by Thermal Oxidation of Electrodeposited Fe Thin Films

[1,2*]Uğur Oktay, [1,2*] Cevat Sarıoğlu
[1] Marmara University, Department of Metallurgical and Materials Engineering, Istanbul, 34840, Türkiye
[2] Marmara University, Institute of Pure and Applied Sciences, Istanbul, 34722, Türkiye

** Corresponding author: cevat.sarioglu@marmara.edu.tr, * uguroktay674@gmail.com

Abstract

Surface modification of semiconductor photoelectrodes with passivation overlayers has garnered significant interest due to its potential to enhance charge separation and charge transfer processes across semiconductor-liquid interfaces. In this study, hematite thin films were produced by the thermal oxidation of Fe electrodeposited on a FTO substrate in an air atmosphere. Subsequently, a water-soluble titanium complex was used to deposit TiO_2 overlayers using a facile water-based solution method for the modification of the hematite photoanode. This work demonstrates the effect of the TiO_2 overlayers on the PEC efficiency of hematite photoanodes.

Keywords: Hematite Photoanodes, Passivation Overlayers, TiO_2 Coating, Water Splitting, Hydrogen Production

I. Introduction

Today the global energy supply is still reliant on fuels and their use releases great amounts of carbon dioxide and other greenhouse gases into the atmosphere,which causing to global warming and climate changes. Fossil fuel combustion also emits pollutants such as sulfur dioxide, nitrogen oxides, particulate matter, and volatile organic compounds, which can lead to air pollution and adverse health effects. Therefore renewable energy resources are gaining interest to maintain and protect a clean environment.

Among other renewable energy resources, the interest in hydrogen energy is increasing rapidly due to its abundance and versatility. The PEC (photoelectrochemical) water splitting method, which utilizes solar energy to produce hydrogen gas is a promising method. However, one of the barriers that needs to be overcome prior to a widespread use of this technology will be the discovery and development of stable and efficient photoelectrodes. Among the usage of photoelectrodes, the hematite a is promising candidate due to its abundance, low cost and has the most ideal bandgap with a 2.0 eV bandgap, and is stable iron oxide in an aqueous environment (Sivula et al., 2011). According to the previous studies, photocurrent efficiencies that were reported for hematite remained below the theoretical hydrogen production efficiency levels due to their poor electrical conductivity, low hole diffusion length and high overvoltage requirements. The surface modification of semiconductor photoelectrodes with passivation overlayers has recently attracted great attention as an effective strategy to improve the charge-separation and charge-transfer processes across the semiconductor−liquid interfaces.

In the literature, the effect of TiO_2 overlayers on hematite have been investigated (Ahmed, M. G., 2015) It has been determined that the modification of hematite photoanodes employing a simple facile surface modification with using water-soluable titanium complex have been dramatically improved the photocurrent density.

In this study, hematite films were prepared by thermal oxidation of Fe films electrodeposited on FTO substrate at 550°C in air atmosphere. Afterwards, TiO_2 overlayers over the hematite films have been developed and were characterized to evaluate their hydrogen production efficiency using I-V data.

II. Experimental Set-up and Procedure

The electrodeposition of Fe on the fluorine-doped tin oxide (FTO) coated glass was carried out in a two-electrode setup cell in a galvanostatic mode in a solution of 0.02 M $FeSO_4.7H_2O$, 0.5 M H_3BO_3 and 0.5 M Na_2SO_4. Before the film deposition, the FTO substrates were carefully cleaned by ultrasonic rinsing in deionized water, ethanol and acetone. The potential was controlled by a Bio-Logical potentiosat / galvanostat. FTO substrate was used as a working electrode and a platinum wire was used as a counter electrode. The distance between the working and the counter electrode was about ~1.5 cm and was kept constant during the deposition process. The electrochemical deposition was carried out for 50 s. In the galvanostatic mode, the current density of 5 mA/cm^2 was obtained with the applied voltage of 2.7 V.

The Fe thin film samples were submitted to thermal oxidation under air atmosphere, and at the temperature of 550°C in a Protherm furnace. For 30 min samples were heat treated Table 1. At the end of the thermal oxidation the samples were left to cool in the furnace to room temperature. Later the as prepared hematite films were immersed in aqueous TALH (titanium bis(ammonium lactate) dihydroxide) solution (2.5 mmol L^{-1} at pH 5.5) for 1 hour, Table 2. Afterward, the films were rinsed with distilled water and then heat treated at 350°C for 1 hour, Table 3. The furnace was maintained at the same temperature for 1 hour, afterwards the samples were left to cool in the furnace to room temperature.

Tab. 1 : The details of the annealing process for the samples

Sample Code	Atmosphere	Temperature (°C)	Time (min)
A	Air	550	30
B	Air	550	30

Tab. 2: The details of the immersion process for the sample

Sample Code	Temperature (°C)	Solutions pH	Concentration
B	24	5-6	

Tab. 3: The details of the calcination process for the sample

Sample Code	Atmosphere	Temperature (°C)	Time (min)
B	Air	350	60

III. Analysis

The electrodeposited photoelectodes were connected to the copper wire using conductive copper band. Photoelectrochemical tests (I-V curves) were performed in a three electrode system with a platinum counter electrode and a saturated calomel electrode as the reference electrode in 0.1 M sodium hydroxide electrolyte using a potentiostat (Bio-Logic VSP) under AM 1.5G solar irradiation from an Abet solar simulator.

Results and discussions

The I-V curves in Fig. 1 shows the bare hematite versus TiO_2 coated hematite photocurrent densities. The TiO_2 coated samples photocurrent density decrased from 0.15 to 0.11 mA/cm^2 at 0.5 V.

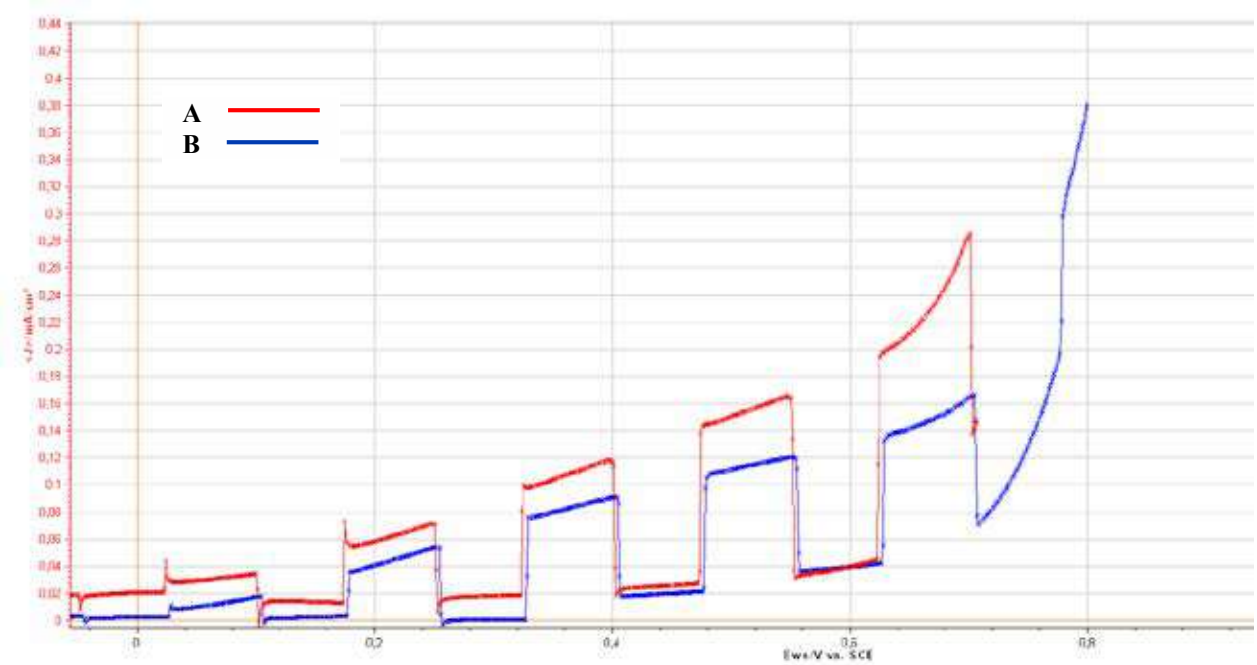


Fig. 1: Current densities of A (bare hematite) and B (TiO_2 coated hematite)

While the previous works showed that the surface modification with TiO_2 showed 2.5 times higher photocurrent densities this experiment showed that surface modified hematite has lower photocurrent density than bare hematite produced with thermal oxidation. Further research will be performed to optimize the thickness of TiO_2 overlayers and characterization of TiO_2 overlayers.

V. Conclusions

As a result of this experiment, the hematite sample modified with TiO_2 overlayers showed a photocurrent density of 0.11 mA/cm^2 at 0.5 V, while the bare hematite exhibited a photocurrent density of 0.15 mA/cm^2. During the modification process, parameters including immersion time, solution molarity, heat treatment time, and temperature for calcination will be evaluated for further research to optimize the thickness of TiO_2 overlayers and improve the PEC efficiency of the photoanodes.

References

Ahmed, M. G., Kretschmer, I. E., Kandiel, T. A., Ahmed, A. Y., Rashwan, F. A., & Bahnemann, D. W. (2015). A facile surface passivation of hematite photoanodes with TiO2 overlayers for efficient solar water splitting. ACS applied materials & interfaces, 7(43), 24053-24062.

Liu, R.; Zheng, Z.; Spurgeon, J.; Yang, X. Enhanced Photoelectrochemical Water-Splitting Performance of Semiconductors by Surface Passivation Layers. Energy Environ. Sci. 2014, 7, 2504−2517.

Lewis, N. S.; Nocera, D. G. Powering the Planet: Chemical Challenges in Solar Energy Utilization. Proc. Natl. Acad. Sci. U. S. A. 2006, 103, 15729−15735.

Klahr, B.; Gimenez, S.; Fabregat-Santiago, F.; Hamann, T.; Bisquert, J. Water Oxidation at Hematite Photoelectrodes: The Role of Surface States. J. Am. Chem. Soc. 2012, 134, 4294−4302.

Ahmed, A. Y.; Oekermann, T.; Lindner, P.; Bahnemann, D. Comparison of the Photoelectrochemical Oxidation of Methanol on Rutile TiO2 (001) and (100) Single Crystal Faces Studied by Intensity Modulated Photocurrent Spectroscopy. Phys. Chem. Chem. Phys. 2012, 14, 2774−2783.

Design, Data Analysis and Prototype Manufacturing of Off-Grid Domestic Refrigerator Systems

[1]Burak Halis Güneş, [1]Bahattin Sevinçli, [1]Ufukhan Acar, [1]Tahsin Altuğ Özden, [1]Olgun Konur, [1]Süleyman Aykut Korkmaz, [2]Anıl Erdoğan, [2]Rüstem Aşık
[1] Dokuz Eylül University, Maritime Faculty, Marine Engineering, Kuruçeşme, DEÜ Kaynaklar Yerleşkesi No:13, İzmir, 35390, Türkiye
[2] Vestel Home Appliances, Technology Development Department, Manisa, Türkiye

E-mail:burakhalissguness@gmail.com

Abstract

Addressing the urgent need for sustainable energy solutions, this thesis investigates the integration of off-grid solar energy with hydrogen-operated proton exchange membrane fuel cell (PEMFC) technology for domestic refrigerator systems. Aligned with the European Union's Green Deal Action Plan, which targets carbon neutrality by 2050, this research aims to contribute to reducing greenhouse gas emissions and advancing sustainability in refrigeration. The study explores various system configurations, performance evaluations, and cost analyses to identify optimal solutions that balance environmental objectives with economic viability. Through theoretical research, technical analysis, and simulations, the most efficient configuration incorporating solar panels and PEMFC technology is identified. Despite challenges related to cost-effectiveness, the focus remains on creating environmentally friendly solutions aligned with the goals of the Green Deal. Ongoing advancements in renewable energy and fuel cell technologies offer opportunities to overcome current limitations and further optimize system performance, paving the way for a more sustainable future.

Keywords: Off-grid solar energy, hydrogen-operated proton exchange fuel cell technology, Green Deal Action Plan.

I. Introduction

In response to the urgent global imperative to mitigate climate change and reduce greenhouse gas emissions, the pursuit of sustainable energy solutions has become paramount (IPCC, 2018). The European Union's ambitious Green Deal Action Plan epitomizes this commitment, aiming for carbon neutrality by 2050 (European Commission, 2019). Central to this endeavor is the transition towards zero-emission technologies across various sectors, including refrigeration systems, which are integral to modern life yet notorious for their environmental impact (Pilla et al., 2017). This project endeavors to contribute to the realization of the Green Deal's objectives by exploring the integration of off-grid solar energy with hydrogen-operated proton exchange membrane fuel cell (PEMFC) technology. By leveraging the synergies between these renewable energy sources, our aim is to advance the sustainability of refrigeration systems while concurrently addressing challenges related to energy efficiency, emissions reduction, and cost-effectiveness. The rationale behind this research lies in the unique advantages offered by combining off-grid solar energy with hydrogen-operated PEFCs. Solar energy, abundant and renewable, presents an opportunity for localized energy generation, reducing reliance on fossil fuels and mitigating carbon emissions (Kademli, 2017). Concurrently, hydrogen-operated PEMFCs offer a clean and efficient means of converting hydrogen fuel into electricity, emitting only water vapor and heat as byproducts (Abderezzak et al., 2020). This combination not only aligns with the zero-emission goals of the Green Deal but also offers the potential for decentralized and sustainable energy solutions.

However, despite the promise of this integrated approach, significant challenges remain, particularly in terms of cost-effectiveness compared to conventional grid connections. This thesis seeks to address these challenges through a comprehensive analysis of system configurations, performance evaluations, and cost assessments. By employing methodologies ranging from literature reviews (Li et al., 2019) and software simulations to detailed calculations and discussions, we aim to identify optimal solutions that balance environmental sustainability with economic viability. Through this interdisciplinary inquiry, we endeavor to contribute to the advancement of sustainable energy solutions, thereby supporting the overarching goals of the Green Deal Action Plan and fostering a more resilient and environmentally conscious society.

II. Experimental Set-up and Procedure

Our project began with careful planning using a Gantt Chart, focusing on design work supported by literature reviews and software tools like SOLIDWORKS and MATLAB. We analyzed different configurations integrating fuel cells and batteries, considering energy production, consumption, cost, and efficiency with software tools like SOLIDWORKS and MATLAB. After thorough calculations and discussions, we selected the most optimal and cost-effective equipment. We used a Mervesan-300 Watt 24 Vdc-220 Vac Inverter to convert DC to AC. Lexron LXR-50-Watt Monocrystalline Photovoltaic Panels captured sunlight and converted it into electricity. A Maximum Power Point Tracking (MPPT) algorithm optimized power extraction from the panels. Batteries stored electrical energy, while a Proton Exchange Membrane Fuel Cell (PEMFC) generated electricity through an electrochemical reaction. In our off-grid refrigeration system, photovoltaic panels generated electricity, which was directed to charge batteries through an MPPT Solar Charge Controller. These batteries supplied power to the inverter, which converted it to 220

V AC. This AC power then operated the compressor of the Vestel SB14001 121 L Mini Refrigerator using the vapor compression cycle.

Also, this off-grid refrigeration system integrates photovoltaic panels and Proton Exchange Membrane Fuel Cell (PEMFC) technology which shown below as Fig. 1 for supplying running power of refrigerator. Photovoltaic panels generated electricity stored in batteries for the refrigerator's operation. When battery levels were low, the PEMFC produced energy from stored hydrogen. To minimize PEMFC hydrogen consumption, a Maximum Power Point Tracker stored daytime photovoltaic-generated DC in batteries. The inverter then converted stored DC into AC, powering the refrigeration cycle. Furthermore, to minimize hydrogen consumption, system always using batteries to run compressor while starting-up.

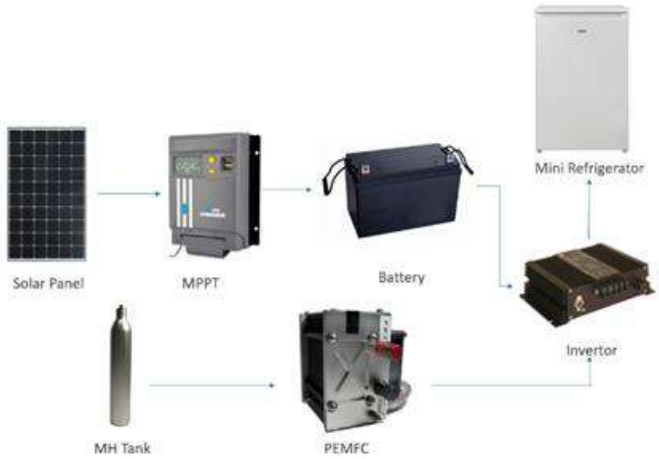


Fig. 1: Case 1 for Designing of System

This system aligned with the Green Deal Action Plan, aiming for zero emissions. Metal hydride storage was chosen for safety and efficiency. Monocrystalline photovoltaic panels ensured effectiveness and portability. The mini refrigerator, powered by a combination of photovoltaic panel and PEMFC, offered a unique off-grid solution. Despite challenges with PEMFC, this innovation addressed sustainability, supporting diverse applications. The PEMFC and photovoltaic panel combination mini refrigerator held promise for a sustainable, portable, and off-grid technology, contributing to various sectors and environmental objectives.

III. Analysis

After project assembly, thermodynamic analyzes will be divided into two parts. photovoltaic panel and PEMFC will be thermodynamically examined, tested and data analyzed separately if all the conditions meet. In case of cost risk, photovoltaic panel and PEMFC tests and modelling will be examined as theoretically, photovoltaic panel system examined and tested as experimentally. We have summarized used equations in Table 1 as shown below.

Table 1. Used Equations Through the Analysis

Equation	No	Description	Reference
$\eta_{pv} = P_{pv}/(S * A_{pv})$	(1)	Photovoltaic panel efficiency	Sugianto, 2020
$E_{bat} = V_{bat} * C_{bat}$	(2)	Calculation for battery energy storage	
$P_{pv_final} = P_{pv} * \eta_{MPPT}$	(3)	Power calculation considering MPPT efficiency limitations	
$E_{pv_final} = E_{PV} * \eta_{MPPT}$	(4)	Energy calculation considering MPPT efficiency limitations	
$P_{PEMFC} = P_{ref} * BOP$	(5)	Energy calculation considering MPPT efficiency limitations	
$HydCon\,s_{ave} = 7 * (10\text{^} - 17) * (P\text{^}6) - 2 * (10\text{^} - 13) * (P\text{^}5) + 1 * (10\text{^} - 10) * (P\text{^}4) + 7 * (10\text{^} - 8) * (P\text{^}3) - 9 * (10\text{^} - 5) * (P\text{^}2) + 0.034 * P - 0.5805$	(6)	Formula for PEMFC average fuel consumption	(H-1000 XP Fuel Stacks User Manual)
$m_{H2} = \dot{m}_{H2,ave} * t$	(7)	Total Consumed Hydrogen	
$\eta_{PEFMC} = \frac{P_{PEFMC}}{HydCon\,s_{ave} * 178.361} * 100$	(8)	PEMFC efficiency	(H-1000 XP Fuel Stacks User Manual)
$CRF = i.(1+i)^{LT}/[1+\dot{\imath})^{LT} - 1]$	(9)	Capital Recovery Factor	Yang, 2018; Tian, 2021
$LEC = (CRF.Cost_{ini} + Cost_{om})/(\dot{W_{net}}.t)$	(10)	Levelized Energy Cost	Tian, 2021; Rodriguez, Paleta, Ochoa and Grijalva, 2012

According the Table 1. η defines efficiency (percentage); P, power (W); S, solar irradiance (W/m^2); A, area (m^2); E, energy (W.t where t is time); V, voltage (V); C, coulomb (A.t); BOP, balance of plant (percentage); HydCons, hydrogen consumption (L/min); m, fluid mass (kg); ṁ, mass flow rate (kg/s); t, time (hour, minute or second); CRF, capital recovery factor; i, annual interest rate (percentage); LT, life time of system (year); LEC, levelized energy cost ($/kW.h); $Cost_{ini}$, initial cost for experimental set-up ($); $Cost_{om}$, operating and maintenance cost ($) and W_{net}, net work (W/t).

IV. Results and discussions

In response to the growing demand for sustainable energy, our project focuses on theoretical research and configuration development using renewable resources like hydrogen and solar power. Sustainability is at the core of our system, achieved through optimized configurations for photovoltaic panels and fuel cell power.

According to our multidimensional approach, involving theoretical research, technical analysis, and simulations in MATLAB and Excel, 20 different configuration was constituted and evaluated. Also, 120 different configuration was calculated for economical analysis. These configurations were produced, incorporating fuel cells and batteries with different ampere-hours and voltages and more which shown below in Table 2, to identify the optimal combination. Running time and consumption calculations informed the selection of battery type and capacity, factoring in activation of fuel cell.

Table 2. Equipment List Used in Theorotical Calculations

Equipment Number and List	
Photovoltaic Panel	PEMFC
Lexron 50 W Monocrystal (1) Argeus 50 W Monocrystal (2)	H-20 Horizon Fuel Cell (9) H-30 Horizon Fuel Cell (10) H-100 Horizon Fuel Cell (11) H-300 Horizon Fuel Cell (12) H-1000 Horizon Fuel Cell (13)
Inverter	
24 V - 200 W Powermaster (3) 24 V - 350 W Powermaster (4) 24 V - 1200 W Powermaster (5)	Battery
Hydrogen Storage Tank	12 V 12 Ah AGM Battery (14) 12 V 18 Ah AGM Battery (15) 12 V 24 Ah Gel Battery (16) 12 V 30 Ah Gel Battery (17)
MyH2® 300 (6) MyH2® 600 (7) MyH2® 900 (8)	

Fig 2. shows that PEMFC may not work for some days depends on battery storage capacity. On the other hand, PEMFC will eventually run and running time will be fixed at a point since PEMFC generation power is same due to the starting power of the compressor is supplied from batteries despite battery storage increase. According to the Fig. 3 the most efficient configuration identified incorporates the H-30 PEMFC and a 12V30Ah battery which consume less hydrogen. Our theoretical research indicates power consumption fluctuates is 20W as a average value, affirming the suitability of the H-20 and H-30 PEMFC for our setup. Furthermore, while PEMFC power capacity is increased or battery storage capacity is decreased, hydrogen consumption will increase.

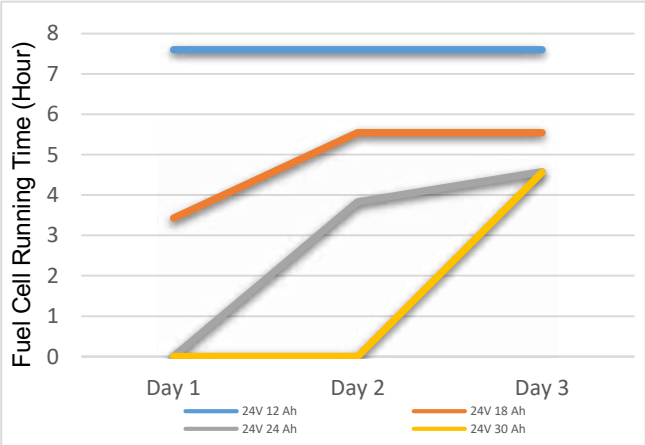


Fig. 3: Fuel Cell Running Time with Different Batteries for 3 Batteries for 3 Days

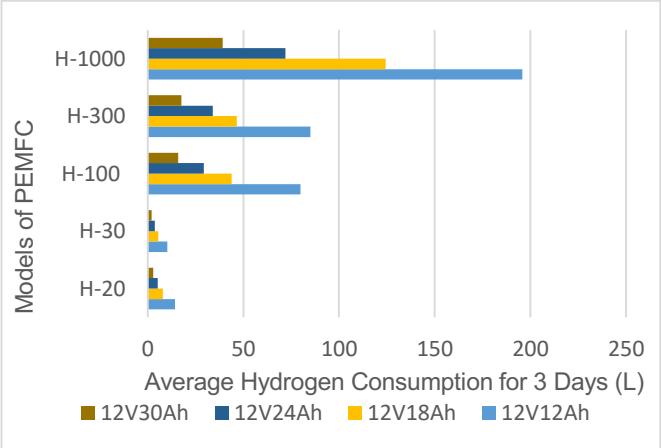


Fig. 3: Average Hydrogen Consumption of Cells and Different Fuel for 3 Days

Economic availability of configurations were evaluated based on CRF and LEC values, involving various components. H-20 and H-30 PEMFC configurations are more cost effective against high power capacity PEMFC's which shown below in Fig 4, in lower power demand. However, configurations are not suitable for daily using and do not have payback period because of higher LEC. It's important to note that the primary aim of the system is to create an environmentally friendly solution and bigger plants may have lower LEC. Also, the system's efficiency

and availability can be further enhanced by incorporating electrolysis. It lowers overall system costs by generating hydrogen, enhancing the system's sustainability.

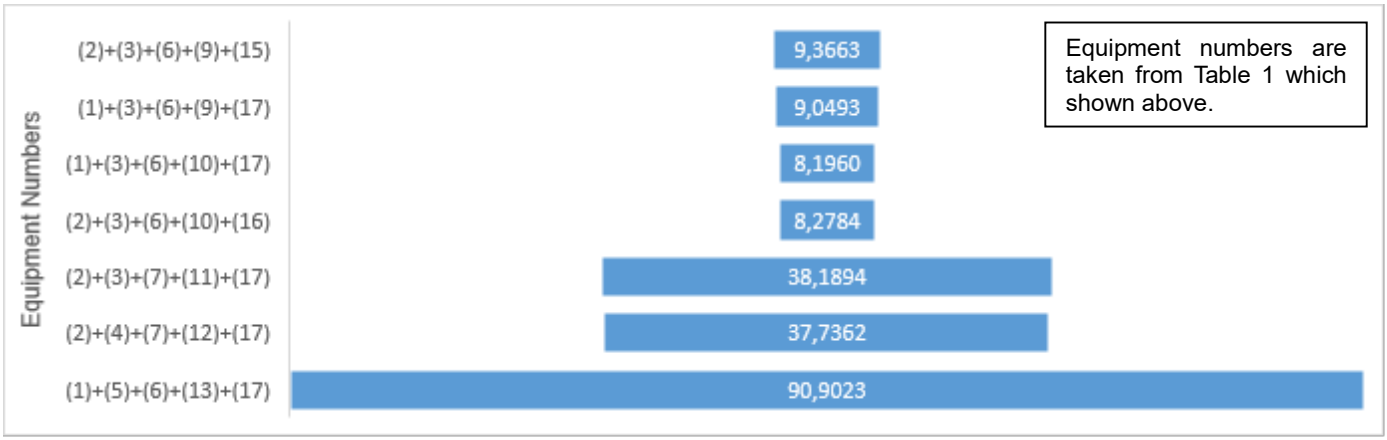


Fig. 4: Lec Values for Different Configurations

V. Conclusions

Based on the comprehensive research conducted on off-grid solar energy integrated with PEMFC, it is evident that this innovative approach holds significant promise for achieving zero emissions in critical sectors. Despite challenges related to cost-effectiveness compared to conventional grid connections, the primary focus remains on creating environmentally friendly solutions. Additionally, ongoing advancements in renewable energy and fuel cell technologies offer opportunities to overcome current limitations and further optimize system performance. By continuing to innovate and refine these technologies, we can accelerate the transition towards a carbon-neutral society in line with the ambitious goals of the Green Deal Action Plan.

Acknowledgements

The authors express our gratitude to TÜBİTAK for their support of this project (Project Number: 1139B412300257).

References

Kademli, M., Hidrojen Teknolojisi, Potansiyeli ve Geleceği. Mesleki Bilimler Dergisi (MBD), 6(2), 106-110, (2017).

Sugianto, Comparative Analysis of Solar Cell Efficiency between Monocrystalline and Polycrystalline. INTEK Jurnal Penelitian, 7 (2), 92-100, (2020).

Abderezzak, B., Binns, R., D., Busawon, Douine, B., Guilbert, D., Hinaje, M., & Rekioua, K., Technical feasibility assessment of a PEM fuel cell refrigerator system, International Journal of Hydrogen Energy, 45, (2020).

Busquet, S., Domain, F., Mayer D., & Metkemeijer, R., A new approach to empirical electrical modelling of a fuel cell, an electrolyser or a regenerative fuel cell, (2004).

Koşar, C., Hidrojen Depolama Yöntemleri, Open Journal of Nano, 6(1), 1-10, (2021).

Karaca, G., & Ural, T., Hidrojen Ekonomisi, Küresel Mühendislik Çalışmaları Dergisi, 3(2), 145-154, (2016).

Usman, R. M., Hydrogen storage methods, Renewable and Sustainable Energy Reviews, Elsevier, vol. 167(C), (2022).

Demir, F., & Yeşilata, B., Fotovoltaik ve Yakıt Pili Birleşik Sisteminin, Isı Bilimi Ve Tekniği Dergisi, 26(1), 37-44, (2006).

S. A. Korkmaz Et Al. , Environmental and economic analyses of fuel cell and battery-based hybrid systems utilized as auxiliary power units on a chemical tanker vessel, International Journal of Hydrogen Energy , vol.48, no.60, pp.23279-23295, (2023).

C. M. Bautista-Rodríguez, D. Sánchez-Grijalva, N. Tepale-Ochoa, & M. G. A Rosas-Paleta, FEL Methodology for Stationary Domestic Electrical Service: PEMFC Technology, Costs and Risk Analysis, Int. J. Electrochem. Sci., 3903 – 3918, 7 (2012).

Modeling and Control of the PEMFC Energized Mobile Robot

[1*]Tevfik YIGIT
[1] Niğde Ömer Halisdemir University, Faculty of Engineering, Mechatronics Engineering Department, Niğde, 51240, Türkiye

* E-mail:tevfikyigit@ohu.edu.tr

Abstract
Mobile robots are robots that can move freely and perform tasks in areas defined by their types. Movements of mobile robots can be achieved by combustion energy, such as internal-combustion engines, or by mootors that use electricity. While mobile robots with internal combustion engines are very advantageous in range, the considerable increase in size and weight of these robots, their noise and non-environmental exhaust gas emissions are the disadvantages. In electric mobile robots, chemical batteries are often used to store electricity. To take advantage of the efficiency of electric motors, to keep the robot's size small, and at the same time to increase the range in an environmentally friendly way, it is suggested to use a PEMFC instead of batteries. The results show that it is possible to longer range using hydrogen technologies.

Keywords: PEM Fuel Cell, Mobile Robot, BLDC Motor, Control

I. Introduction

Mobile robots can be studied in three main sections, depending on the environment in which they are used, such as land, water and air. The land robots that are the subject of this study can be divided into classes such as wheeled, leged, and palleted. Among land robots, wheeled robots stand out for their speed and range advantages, while lagging behind for their sluggish terrain performance. In recent years, hybrid wheel-legged or convertible wheeled ground robots have been frequently studied to overcome this situation (Yigit and Celik, 2023). While wheeled robots have range advantages because of their lower power consumption compared to legged robots, the range of these robots powered by a chemical electric battery is rather limited. When the battery capacity is increased and the range is extended, this can be applied linearly up to a certain level, but an added inefficiency from a point of view arises, due to the ratio of battery weight to total weight. This is why researchers have recently been working on optimum battery weight, especially in today's electric vehicles (Shui et al., 2018). Other technologies that exist today need to be considered as alternatives until battery technologies reach a higher level.

One of today's most advanced energy sources is hydrogen. The PEM Fuel Cell (PEMFC) is one of the most important fuel cell technologies that can convert the chemical energy of hydrogen into electricity (Barbir, 2013). It was first developed by General Electric in the 1960s for use in NASA's Gemini missions (Benz et al., 2009). Considering the advantages of PEMFC, first of all it is suitable for use in off-grid, uninterruptable and back-up systems. It was first chosen for a space mission like Gemini because of its superiority and reliability. However, since some important patents on critical parts of this system are not public and have not spread to general consumer products, it has remained a more niche product and therefore has not become widespread at the desired level as an expensive system (Yang et al., 2023). For this reason, this system needs to be used more frequently in developing areas, developed and turned into an alternative. In this study, it is aimed to energize the mobile robot designed to benefit from its advantages with PEMFC and to compare the systems with standard chemical batteries in terms of weight and range.

Brushless DC Motor (BLDCM), which is highly efficient and frequently preferred in the field of robotics, was used as the drive element of the mobile robot (Yigit and Celik, 2020). BLDCMs stand out with their torque/size advantages as well as low maintenance needs. However, they are quite difficult to control compared to standard DC motors (Mohanraj et al., 2022). This study also aims to demonstrate the high-performance controllability of these motors with PEMFC.

II. Design and modeling of the system

A four-wheel-drive mobile robot with omniwheel type wheels has been modeled. BLDCMs with appropriate moment values were selected according to the dimensions and calculated weight of this mobile robot to be used in the solid design and MATLAB/Simulink model. Eq 1. was used in BLDCM selection.

$$T = M_m \,.(a + g.sin\theta).r \quad (1)$$

Here, M_m is weight of the mobile robot, a is desired acceleration, g is gravity, θ is desired climb slope angle. According to this calculation, A BLDCM has a motor torque of 1 Nm was selected for a robot that weight 20 kg and can reach a speed of 5 km/h in 2 seconds on a 10-degree slope. The solid design shown in Fig. 1 is also obtained using the drawing of the selected BLDCM.



Fig. 1: Solid design of the mobile robot

The electrical model was builded in the Simulink environment using the parameters of the selected BLDCM. This model was prepared using the electrical elements of the Simulink/Simscape library in order to draw current from the PEMFC model and obtain a model closer to reality.

Each motor consumes 200 W power. Accordingly, PEMFC was chosen as 1.2 kW so that it can power all motors, its own cooling system and other electronic components at full load. Accordingly, a PEMFC with 42 cells, a nominal power of 1.2 kW and an output of 52 V, 25 A was selected. The selected PEMFC weight is approximately 3 kg. At nominal load, it consumes approximately 900 standard liters of hydrogen per hour. A storage tank weighing 4 kg with a storage capacity of 900 liters was selected for 1 hour of operation of the mobile robot. Thus, the total weight of the hydrogen energy system is approximately 7 kg. I-V and I-W characteristics of the PEMFC is given in Fig. 2.

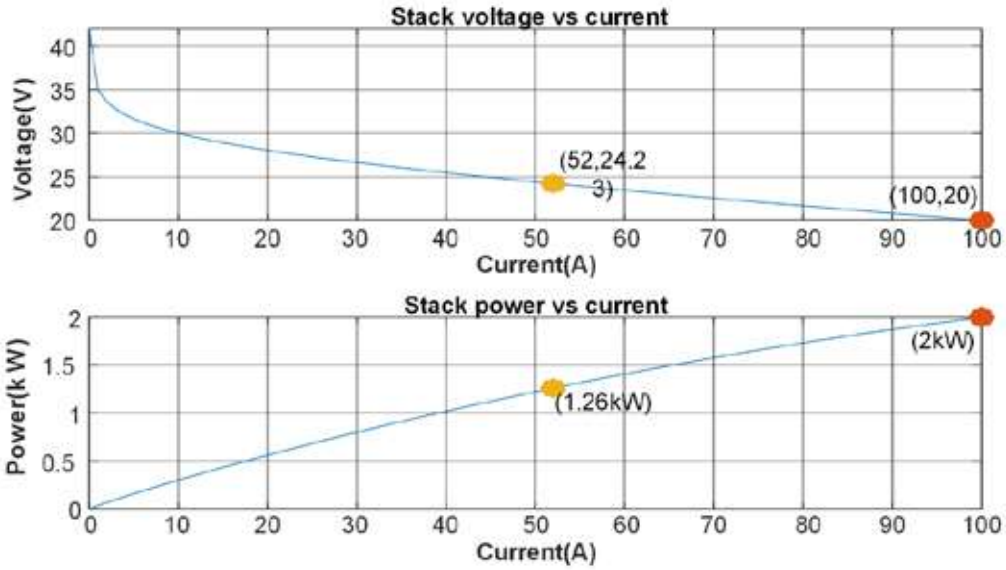


Fig. 2: I-V and I-W characteristics of the PEMFC

All the calculated system elements were brought together in the Simulink environment and the PEMFC energized Mobile Robot model shown in Fig.3 was obtained.

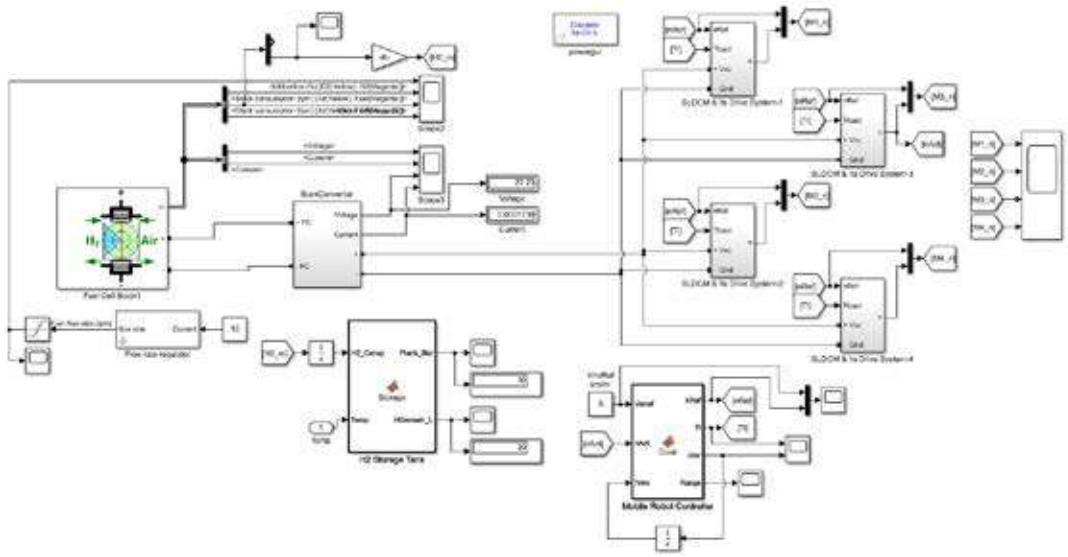


Fig. 3: MATLAB/Simulink model of the PEMFC energized Mobile Robot

To simulate the energy consumption of the mobile robot under different conditions, a route of 15 meters with a slope of 0%, 10% and -5% was prepared and hydrogen consumption was monitored along this route. Along this route, dynamic load moments were calculated and applied to the motors according to the weight of the robot and the current slope of the route. In order to make these calculations, a robot control model was added to the model.

In addition, in order to obtain optimum control performance from the engines along this route, separate PID controllers were used in each motor and these controllers were optimized and designed with Particle Swarm Algorithm (PSO). In addition to the motor controllers, a PID controller was designed using PSO for the DC/DC converter used, thus providing the appropriate voltage level for the motors in variable situations.

III. Results and discussion

Speed changes of the robot's wheel motors and the distance traveled by the mobile robot along this planned route is given in Fig. 4.

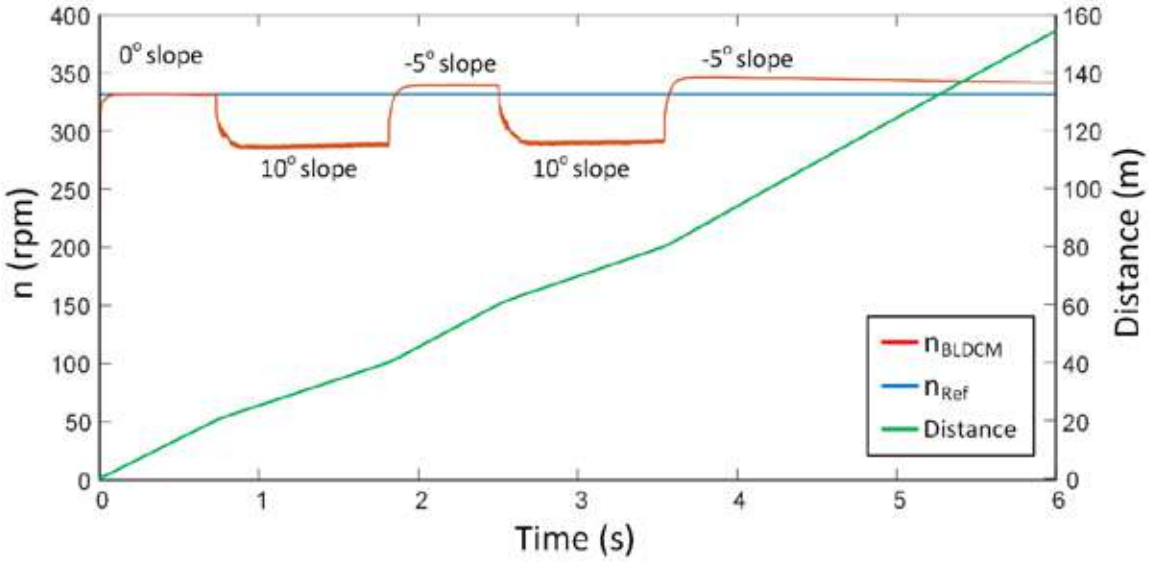


Fig. 4: BLDCM speed changes and distance traveled by the mobile robot during planned route

When Fig. 4 is examined, it can be seen that the robot slows down a little when going uphill and accelerates a little when going downhill. The controller designed for BLDCM has successfully managed to keep the motor speeds close to the desired reference speed in these variable situations.

Fig. 5 shows the PEMFC output voltage and DC/DC controller voltage during this scenario.

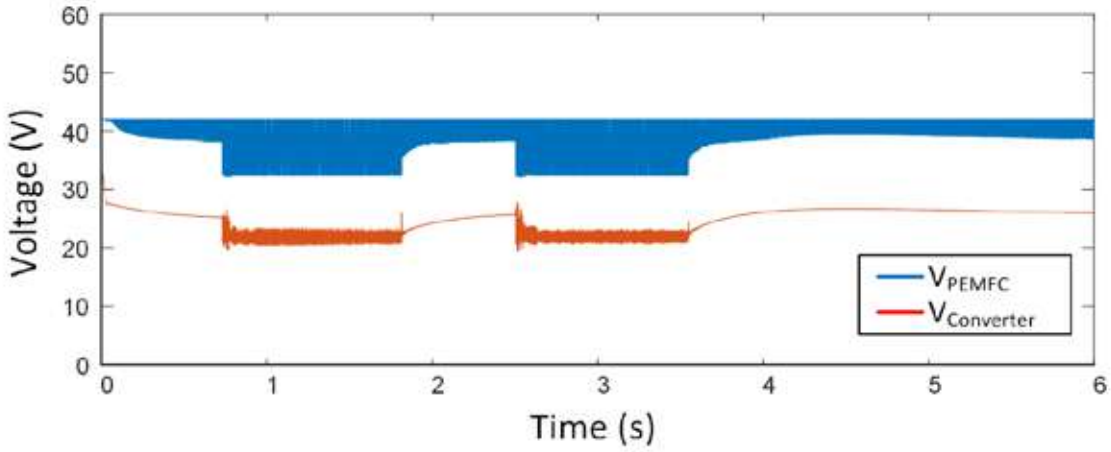


Fig. 5: Voltages of the PEMFC and DC/DC converter output during planned route

When Figure 4 is examined, the voltage at the PEMFC output fluctuates a lot as the motors demand high current, especially going uphill. The DC/DC converter tolerated this fluctuation well and managed to keep it within the desired range thanks to designed PID controller.

IV. Conclusions

When the results obtained are examined, it can be seen that the mobile robot, which has very high power motors and a total energy consumption of 1 kW/h, is powered quite successfully using PEMFC. By optimizing the

controller used in the DC/DC converter, BLDCM motors, which are very sensitive to voltage changes, can be energized with PEMFC, which can behave quite variablely. Compared to a chemical battery of the same weight, higher current levels can be achieved with PEMFC and considerably higher ranges can be achieved.

References

Barbir, F., 2013. PEM fuel cells: theory and practice, 2. ed. ed. Elsevier/Acad. Press, Amsterdam.

Benz, U., Busche, D., Lutterbeck, D., 2009. APPLICATIONS – STATIONARY | Uninterruptible and Back-up Power: Fuel Cells, in: Garche, J. (Ed.), Encyclopedia of Electrochemical Power Sources. Elsevier, Amsterdam, pp. 135–145. https://doi.org/10.1016/B978-044452745-5.00347-6

Mohanraj, D., Aruldavid, R., Verma, R., Sathiyasekar, K., Barnawi, A.B., Chokkalingam, B., Mihet-Popa, L., 2022. A review of BLDC motor: state of art, advanced control techniques, and applications. Ieee Access 10, 54833–54869.

Shui, L., Chen, F., Garg, A., Peng, X., Bao, N., Zhang, J., 2018. Design optimization of battery pack enclosure for electric vehicle. Structural and Multidisciplinary Optimization 58, 331–347.

Yang, D., Lee, J., Song, N.C., Lee, Sangseon, Kim, S., Lee, Sukho, Choi, S., 2023. Patent analysis on green hydrogen technology for future promising technologies. International Journal of Hydrogen Energy.

Yigit, T., Celik, H., 2023. Designing and FOPID Controlling of the Wheeled-Legged Mobile Robot with Adjustable Height, in: 2023 10th International Conference on Signal Processing and Integrated Networks (SPIN).npp. 854–859. https://doi.org/10.1109/SPIN57001.2023.10116238

Yigit, T., Celik, H., 2020. Speed controlling of the PEM fuel cell powered BLDC motor with FOPI optimized by MSA. International Journal of Hydrogen Energy. https://doi.org/10.1016/j.ijhydene.2020.04.091

Use of Hydrogen as Secondary Fuel in Internal Combustion Engines: A approach on combustion, performance and emissions

[1]Süleyman Şimşek, [1*]Muhammed Uçum

[1]İstanbul Aydın University, Graduate Education Institute, Mechanical Engineering Department, Beşyol Mah. İnönü Cad. No: 38, Küçükçekmece, İstanbul, 34290, Türkiye

*E-mail: muhammeducum@stu.aydin.edu.tr

Abstract

Hydrogen is an important fuel type that is abundant in nature, is economical, easy to produce, has no toxic properties and does not harm the environment. This feature of hydrogen; It has become important to use it as fuel in internal combustion engines. Unlike fossil fuels, it does not create polluting gases (carbon dioxide, carbon monoxide, hydrocarbon, etc.) and prevents the release of these gases into nature, making it attractive to use this type of fuel as an alternative in the transportation and industrial sectors. In this article, the literature on hydrogen has been scanned and information on its use in internal combustion engines has been explained. Additionally, current studies showing the effect of hydrogen on engine combustion, emissions and performance are included.

Keyword: Hydrogen, İnternal Combustion Engines, Performance, Emission

I. Introduction

The discovery of internal combustion engines contributed significantly to the development of industrialization. The increase in population, the development of industrialization and the expansion of urbanization have brought about a significant increase in energy consumption. However, in our age, the growth of industrialization causes fossil fuel costs to rise. This is a disadvantage for industries that depend on fossil fuel use. Researchers; In order to get rid of this addiction, they have attempted to research a new motor fuel that can be an alternative to traditional fossil fuels. As a result of the studies, one of the most important fuels that has been studied intensively is hydrogen. Hydrogen is an important fuel type that is the most economical, non-toxic, sustainable and does not harm the environment among alternative fuels. In addition, the fact that it is a flammable gas, approximately 14 times lighter than air, abundant in nature, and easy to produce reveals the importance of this type of fuel.

Hydrogen, in its pure form, is not suitable for use in piston engines due to its low energy density and difficulty in storing **(Xiumin et al., 2016).** In order to use hydrogen in its pure form, a new engine design or modification is required. That's why it is used as secondary fuel in piston engines. It does this by mixing a certain amount of fossil fuels in gasoline and diesel engines. In this study, studies using various fuel injection methods in the literature were examined and the effects of hydrogen use on the engine were compared.

II. Use of Hydrogen in İnternal Combustion Engines

Hydrogen; It is a colorless, odorless, flammable substance that does not harm humans and the environment. It is an important alternative fuel due to its physical and chemical properties. Compared to other types of fossil fuels; It has unique features such as high flammability rate and high diffusion coefficient **(Karagöz Y. et al, 2019).**

The properties of other fuel types and hydrogen are given in Table 1. Table 1 shows that the physical and chemical properties of hydrogen and other fuels are different. Hydrogen's high characteristic structure such as flammability rate, auto-ignition temperature and stoichiometric ratio makes it different from others. These properties make hydrogen an excellent fuel for combining with other fuels

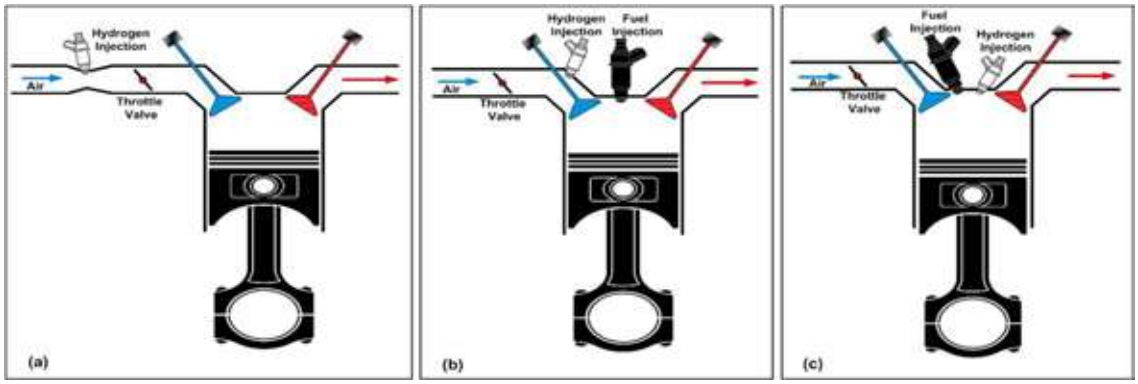
Tab.1: The properties of other fuel types and hydrogen

Properties of Fuel	Diesel	Gasoline	Hydrogen
Molecular Structure	$C_{12}H_{26}$	$C_nH_{1.8n}$	H_2
Density (kg/m^3)	821,5	700-780	0,08
Diffusion Coefficient (cm^2/s)	0,189	0,05	0,61
Higher Heating Value at 25° and 1 atm (kj/g)	44,8	47,5	141,86
Lower Heating Value at 25° and 1 atm (kj/g)	44	43,5	120
Flash Point (°C)	55	-43	<-253

Auto-İgnition Temperature (°C)	210	280	585
Laminar Flame Speed (cm/s)	33	51	291
Laminar Burning Velocity (m/s)	0,3	0,5	3,2
Stoichiometric A/F ratio	14,4	14,7	34,3
Octane Number	30	87	130+ (Lean Burn)
Cetane Number	40-55	-	-

The use of hydrogen as additional fuel in internal combustion engines without the need for any modification is done with the injector method system. There are three most common forms in the literature. These; The fuel carburetion method, intake manifold or intake port injection and direct injection.

Fig. 1: Fuel Induction Technics for Hydrogen **(Nemitallah Methad et al., 2024)**



a) Fuel Carburetion Method b) Port Fuel İnjection (PFI) c) Direct İnjection (DI)

a) **Fuel Carburetion Method**: Carburetion by the use of a gas carburetor has been the simplest and the oldest technique. This system has advantages for a hydrogen engine. Firstly, central injection does not require the hydrogen supply pressure to be as high as for other methods. Secondly, central injection or carburetors are used on gasoline engines, making it easy to convert a standard gasoline engine to hydrogen or a gasoline/hydrogen engine. The disadvantage of central injection in international combustion engine, the volume occupied by the fuel is about 1.7% of the mixture whereas a carbureted hydrogen engine, using gaseous hydrogen, results in a power output loss of 15%. Thus, carburetion is not at all suitable for hydrogen engine, because it gives rise to uncontrolled combustion at unscheduled points in the engine cycle. Also the greater amount of hydrogen/air mixture within the intake manifold compounds the effects of pre-ignition **(Ciniviz, M.,et al., 2012).**

b) **Port Fuel Injection (PFI):** The port injection fuel delivery system injects fuel directly into the intake manifold at each intake port by using mechanically or electronically operated injector, rather than drawing fuel in at a central point. Typically, the hydrogen is injected into the manifold after the beginning of the intake stroke. Electronic injectors are robust in design with a greater control over the injection timing and injection duration with quicker response to operate under high speed conditions. In port injection, the air is injected separately at the beginning of the intake stroke to dilute the hot residual gases **(Ciniviz, M.,et al., 2012)..**

c) **Direct Injection (DI):** In direct in-cylinder injection, hydrogen is injected directly inside the combustion chamber with the required pressure at the end of compression stroke. As hydrogen diffuses quickly the mixing of hydrogen takes flame instantaneously. For ignition either diesel or spark plug is used as a source. The problem of drop in power output in manifold induction/injection can be completely eliminated by in-cylinder ignition. During idling or part load condition the efficiency of the engine may be reduced slightly. This method is the most efficient one compared to other methods of using hydrogen. The power output of a direct injected hydrogen engine was 20% more than for a gasoline engine and 42% more than a hydrogen engine using a carburetor. With hydrogen directly injected into the combustion chamber in a compression ignition (CI) engine, the power output would be approximately double that of the same engine operated in the pre-mixed mode **(Ciniviz, M.,et al., 2012).**

III. Experimental Set-up and Procedure

The literature data listed in this study were collected from Google Scholar and Sciencedirect databases using keywords such as internal combustion engine and hydrogen. It has been concluded that the effects of hydrogen on engine performance are variable when used in different proportions.

IV. Results and Discussions

Tab. 2: Studies using different injection methods

Fuel	Engine Specifications	Hydrogen Induction System	Hydrogen mixture as volumetric (%)	Performance	Combustion	Emission	Reference
Hydrogen	Single cylinder, four stroke, SI engine, Compression ratio 8:1, Power (kW) 3.2 @1500 rpm	Port Fuel Injection (PFI)	1,2	BP; 19,06% decreased BTE; 3,16% decreased	NHRR; two times higher, PCP; increased	NOx; decreased after engine speed of 1700 rpm	Navale, S. J., et al., 2017
Hydrogen	Single cylinder, four stroke Air cooled SI engine, , Compression ratio 6.6-8.1, Power (kw) 8,8 @1600 rpm	Port Fuel Injection (PFI)	1,5	BP; increased @-10 TE increased	@-10 CABTDC EE; increased	NOx; decreased after @-10 CABTDC	Şöhret, Y., et al.,2019
Hydrogen	Single-cylinder, four stroke, air-cooled DI SI engine, Compression ratio 11.5:1, 3.8 kW@2000 rpm	Port Fuel Injection (PFI)	8-14	BTE; increased	HRR; increased, PCP; increased	NOx; increased	Purayil, S. T. P., et al., 2024
Hydrogen	Single-cylinder four-stroke, SI engine, air-cooled, carburetor fuel system, @300 rpm	Port Fuel Injection (PFI)	24-49	BTE; increased, TE; increased	CP; increased	CO; decreased HC; decreased	Elsemary, I. M. et al., 2016
Hydrogen	Single-cylinder four-stroke, SI engine, air-cooled, Compression ratio 8.5:1, 6.3 kW@3600 rpm	Port Fuel Injection (PFI)	0,15-1,5	BTE; increased	CP; increased	CO; neglect, NOx; increased	Karagöz, Y., et al. 2019
Hydrogen	Single-cylinder four-stroke, CI engine, water-cooled, Compression ratio 20.5:1, 3,5 kW@1500 rpm	Port Fuel Injection (PFI)	15-35	BTE; increased	CP; increased, HRR; increased	NOx; increased	Bakar, R. A., et al., 2022
Hydrogen	Single-cylinder four-stroke, CI engine, water-cooled, Compression ratio 17,5:1 5,2 kW@1500 rpm	Port Fuel Injection (PFI)	0-20	BTE; decreased at max load, VE; decreased	-	NOx; increased, PM; decreased	Sharma, P., & Dhar, A. (2018).
Hydrogen	Two-cylinder four-stroke, CI engine, water-cooled, Compression ratio 18.5, 21 kW@2000 rpm	Direct Injection (DI)	10-30	BTE; increased, BP; increased	-	NOx; increased, HC; decreased, CO; decreased	Wu, Y., Devi et al., 2022
Hydrogen	Four-cylinder four-stroke, CI engine, water-cooled, Compression ratio 18.5:1, 260 kW@1800 rpm	Direct Injection (DI)	20-80	BTE; increased, TE; increased	-	NOx; decreased, CO; decreased, CO2; decreased	Koten, H. (2018).

Hydrogen	Single-cylinder four-stroke, CI engine, air-cooled, Compression ratio 16.5:1, 3,7 kW@1500 rpm	Port Fuel Injection (PFI)	7,5-20	BTE; increased	CP; increased	NOx; increased,	Jabbr, A. I., & Koylu, U. O. (2019

VE: Volumetric Efficiency, **BTE**: Brake Thermal Efficiency, **CP**: Cylinder Pressure, **PCP**: Peak Cylinder Pressure **HRR**: Heat Release Ratio, **NHRR**: Net Heat Release Ratio **BP**: Brake Power, **TE**: Thermal Effciency **HC**: Hydro Carbon, **CO**: Carbon monoxide, **CAbTC**: Crank Angle Top Dead Center, **NOx**: Nitrogen Oxide, **EE**: Exergy Efficiency

Table 2 shows the performance, emission and combustion analysis results of diesel and gasoline engines using different hydrogen induction methods. The results were examined by adding a certain volumetric amount of hydrogen for both engine types. The changes in performance depending on the injection type used are shown in table 2.

When table 2 is examined; It can be seen how adding hydrogen to the fuel affects the engine characteristics in the same number of engine types. In particular, using different injection types reveals their effects on performance, combustion and emissions. It can be said that among the injectors used in the studies, the one that preferred the direct injection method was the one with the highest efficiency. There are many similar studies in the literature. Here, the technique of taking hydrogen into the cylinder is important.

With the addition as volumetric a large amount of hydrogen to the engine;

-In terms of performance; An increase in brake thermal efficiency, brake power and volumetric efficiency was observed.

-In the combustion process; net heat release rate, peak cylinder and cylinder pressures increased.

-İf as emissions; there was an increased in NOx rate, but there was a decrease in carbon monoxide, carbon dioxide and other hydrocarbon emissions.

V. Conclusions

When the studies that form the basis of our article are examined; It is seen that hydrogen is added to gasoline and diesel engines using port fuel injection and direct injection methods. Here, in addition to the fact that the two techniques are the most preferred methods in the studies, when looking at the data, it is also concluded that the direct injection method is the one with the highest efficiency.

Reference

Navale, S. J., Kulkarni, R. R., & Thipse, S. S. (2017). An experimental study on performance, emission and combustion parameters of hydrogen fueled spark ignition engine with the timed manifold injection system. *international journal of hydrogen energy*, *42*(12), 8299-8309.

Şöhret, Y., Gürbüz, H., & Akçay, İ. H. (2019). Energy and exergy analyses of a hydrogen fueled SI engine: Effect of ignition timing and compression ratio. *Energy*, *175*, 410-422.

Purayil, S. T. P., Al-Omari, S. A. B., & Elnajjar, E. (2024). Experimental investigation of spark timing on extension of hydrogen knock limit and performance of a hydrogen-gasoline dual-fuel engine. *International Journal of Hydrogen Energy*, *49*, 910-922.

Elsemary, I. M., Attia, A. A., Elnagar, K. H., & Elaraqy, A. A. (2016). Experimental investigation on performance of single cylinder spark ignition engine fueled with hydrogen-gasoline mixture. *Applied Thermal Engineering*, *106*, 850-854.

Karagöz, Y., Balcı, Ö., & Köten, H. (2019). Investigation of hydrogen usage on combustion characteristics and emissions of a spark ignition engine. *International Journal of Hydrogen Energy*, *44*(27), 14243-14256.

Bakar, R. A., Kadirgama, K., Ramasamy, D., Yusaf, T., Kamarulzaman, M. K., Aslfattahi, N., ... & Alwayzy, S. H. (2022). Experimental analysis on the performance, combustion/emission characteristics of a DI diesel engine using hydrogen in dual fuel mode. *International Journal of Hydrogen Energy*.

Sharma, P., & Dhar, A. (2018). Effect of hydrogen supplementation on engine performance and emissions. *International Journal of Hydrogen Energy*, *43*(15), 7570-7580.

Wu, Y., Devi, P. B., Anbarasu, A., Sołowski, G., Chanh, H. C., Chi, N. T. L., ... & Xia, C. (2022). Estimation of the engine performance and emission characteristics of hydrogen feed vehicles with modified injection fuel system. *Fuel*, *329*, 125339.

Koten, H. (2018). Hydrogen effects on the diesel engine performance and emissions. *International journal of hydrogen energy*, *43*(22), 10511-10519.

Jabbr, A. I., & Koylu, U. O. (2019). Influence of operating parameters on performance and emissions for a compression-ignition engine fueled by hydrogen/diesel mixtures. *International Journal of Hydrogen Energy*, *44*(26), 13964-13973.

El-Adawy, M., Nemitallah, M. A., & Abdelhafez, A. (2024). Towards sustainable hydrogen and ammonia internal combustion engines: Challenges and opportunities. *Fuel*, *364*, 131090.

Sun, Y., Yu, X., & Jiang, L. (2016). Effects of direct hydrogen injection on particle number emissions from a lean burn gasoline engine. *International journal of Hydrogen energy*, *41*(41), 18631-18640.

Ciniviz, M., & Köse, H. (2012). Hydrogen use in internal combustion engine: a review. *International Journal of Automotive Engineering and Technologies*, *1*(1), 1-15.

Renewable Energy Supported and Hydrogen Energy Storing Off-Grid Smart City Design

[1*]Emrullah Kocaman, [1]Hüseyin Yağlı, [1]Recep Yumrutaş, [2]Ali Koç, [2]Yıldız Koç

[1] Gaziantep University, Engineering Faculty, Mechanical Engineering Department, University Boulevard 27310 Şehitkamil - Gaziantep, Türkiye
[2] Iskenderun Technical University, Faculty of Engineering and Natural Sciences, Mechanical Engineering Department, Hatay, Türkiye

* E-mail:emrullahkocaman@gmail.com

Abstract
In this study, by using mathematical modelling methods, a simulation model is designed for Araban district of Gaziantep province, which can meet daily and annual energy needs by using its own local energy resources in a region of 8500 households. For this selected pilot region, it is aimed to obtain steam in the solar tower by using the annual radiation amount data obtained from the General Directorate of Meteorology. A steam Rankine Cycle system is used to convert the steam into power. On a daily basis, molten salt energy storage method is used to provide the energy needed in cases such as overcast weather or night when sunlight is not sufficient. In cases where sufficient radiation cannot be received in the winter months, hydrogen fuel stored in the summer months when the radiation is high is used to meet the missing energy requirement.

Keywords: Off-grid cities, Rankine cycle, Solar tower power

I. Introduction

Nowadays, it is inevitable that interruptions in electricity grids, natural disasters and other adverse events will negatively affect cities. Therefore, the importance of smart, self-sufficient cities that are independent from the electricity grid is increasing. Such cities are characterised by having renewable energy-based systems that operate on the basis of environmentally friendly energy sources and generate and store energy on their own. In this way, cities can be self-sufficient even in the event of energy shortages. In addition, independent energy systems are also important with their positive impact on the environment. Off-grid cities are likely to play a major role in shaping urban life in the future Munro and Samarakoon (2023).

Off-grid cities play an important role to increase environmental sustainability by providing energy independence Uddin et all (2021). Such cities meet their energy needs by using local energy production facilities based on solar energy, wind energy, hydraulic energy, biomass and other renewable energy sources.

Renewable energy-based, off-grid smart cities can increase environmental sustainability by providing energy independence. They meet their electrical energy needs by using local energy production facilities based on renewable energy sources. In this way, the use of fossil fuels can be reduced and the carbon footprint can be reduced Calado and Castro (2021).

Off-grid smart cities are important not only for environmental sustainability, but also for social and economic sustainability Afaneh and Alshafei (2023). Digital technologies can help improve people's quality of life by providing innovative solutions in areas such as education, healthcare and job opportunities.

Smart cities independent from the electricity grid are also becoming more resilient against natural disasters. Thanks to sensors and developing artificial intelligence algorithms, data collection and analyses are performed before and after the disaster. In this way, disasters can be responded to faster and the recovery process after the disaster is accelerated Yamagat et all (2016).

II. System Description

In this study, by using mathematical modelling methods, a simulation model is designed for Araban district of Gaziantep province, which can meet daily and annual energy needs by using its own local energy resources in a region of 8500 households. For this selected pilot region, it is aimed to obtain steam in the solar tower by using the annual radiation amount data obtained from the General Directorate of Meteorology. A steam Rankine Cycle system is used to convert the steam into power. On a daily basis, molten salt energy storage method is used to provide the energy needed in cases such as overcast weather or night when sunlight is not sufficient. In cases where sufficient radiation cannot be received in the winter months, hydrogen fuel stored in the summer months when the radiation is high is used to meet the missing energy requirement.

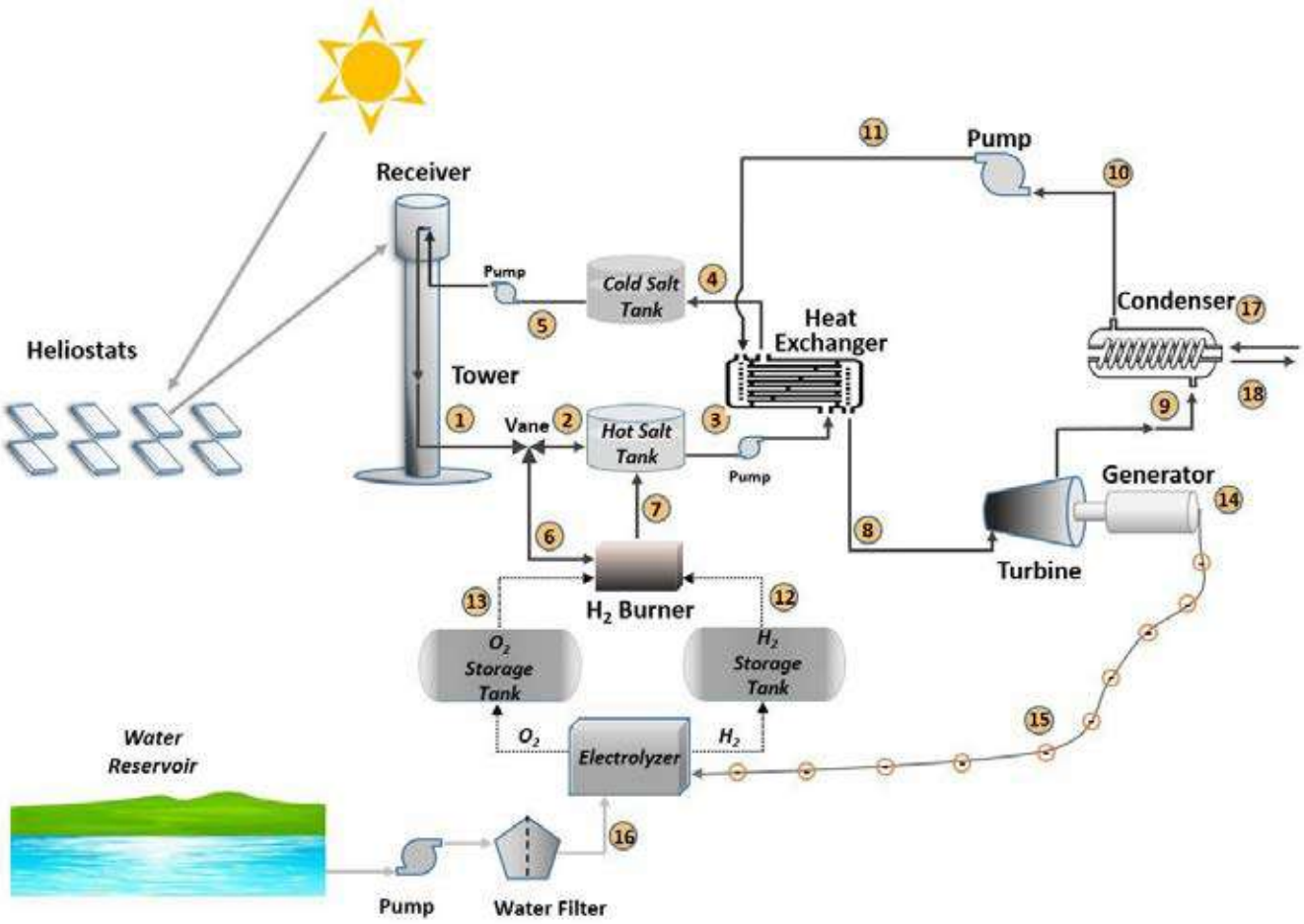


Fig. 1: Schematic representation of solar tower based power generation plant

Figure 1 shows a schematic representation of a solar tower based power generation plant. The designed system consists of three interconnected basic cycles. The first cycle consists of solar tower, cold molten salt, hot molten salt storage tank and heat exchanger. The second cycle is a steam rankine cycle consisting of heat exchanger, turbine, condenser and pump. The third cycle is the hydrogen storage cycle obtained by electrolysis of water.

III. Results and discussions

Tab. 1: Hydrogen production-consumption by month and the amount of energy produced by Heliostats

Mounths	Monthly total Required electricity	Hydrogen Production		Hydrogen Consumption		$Q_{heliostat}$
	MWh	MWh	kg	MWh	kg	kW
January	2232			545,5	14024	7256
February	2016			28,7	742	9465
Marc	2232	355,7	9146			14018
April	2160	517,3	13303			16238
May	2232	859,8	22111			20276
June	2160	986,7	25374			22260
July	2232	951,3	24462			21411
August	2232	729,7	18765			18661
September	2160	479,0	12318			15747
October	2232	149,7	3849			11460
November	2160			242,0	6227	8526
December	2232			672,7	17294	6709

Tab. 1 shows the amount of hydrogen required according to the months and the amount of energy obtained from heliostats. Hydrogen was produced and stored in the summer months from March to October when the amount of radiation was high. In the winter months when the sunlight is low, the stored hydrogen is used in the system and the required monthly energy amount is provided.

Tab. 2: Pump condenser and net work quantities obtained according to months

Mounths	$W_{net;src}$	$W_{net;overall}$	$W_{pump;salt}$	$W_{pump;cw}$	Q_{cond}	m_{cw}
	kW	kW	kW	kW	kW	kg/s
January	2267	2194	73,7	29,1	4862	232,5
February	2958	2861	96,08	37,97	6342	303,3
Marc	4380	4238	142,3	56,24	9393	449,1
April	5074	4909	164,8	65,15	10881	520,3
May	6336	6130	205,8	81,35	13587	649,6
June	6956	6730	226	89,31	14916	713,2
July	6990	6473	217,3	85,9	14347	686
August	5831	5642	189,4	74,87	12504	597,9
September	4921	4761	159,9	63,18	10552	504,5
October	3581	3465	116,3	45,98	7679	367,2
November	2664	2578	86,55	34,21	5713	273,2
December	2096	2028	68,1	26,92	4496	215

When the net work amounts given according to the months in Tab. 2 are analysed, it is seen that the system reached the maximum net work in June with approximately 7MW.

References

Afaneh, A. and Alshafei, I. (2023). The influence of smart technologies: a comparative study on developing large to small scale smart cities and smart campuses.. Iop Conference Series Earth and Environmental Science, 1210(1), 012015. https://doi.org/10.1088/1755-1315/1210/1/012015

Calado, G. and Castro, R. (2021). Hydrogen production from offshore wind parks: current situation and future perspectives. Applied Sciences, 11(12), 5561. https://doi.org/10.3390/app11125561.

Munro, P. G., & Samarakoon, S. (2023). Off-grid electrical urbanism: Emerging solar energy geographies in ordinary cities. Journal of Urban Technology, 30(2), 127-149.

Uddin, R., Khan, H., Arfeen, A., Shirazi, M., Rashid, A., & Khan, U. (2021). energy storage for energy security and reliability through renewable energy technologies: a new paradigm for energy policies in Turkey and Pakistan. sustainability, 13(5), 2823. https://doi.org/10.3390/su13052823.

Yamagata, Y., Murakami, D., Minami, K., Arizumi, N., Kuroda, S., Tanjo, T., & Maruyama, H. (2016). Electricity self-sufficient community clustering for energy resilience. Energies, 9(7), 543.

Development of optimization-based energy management system in hybrid charging stations

[1]Abuzer Caliskan, [2*]Hasan Bektas Percin
[1] Firat University, Faculty of Engineering, Department of Electrical and Electronics Engineering, Elazığ, 23119, Türkiye
[2] Firat University, Elazığ, 23119, Türkiye

* E-mail: hbpercin@firat.edu.tr

Abstract
The Hydrogen/Electric Vehicle Charging Station (HEVCS) is widely regarded as a highly attractive system for facilitating the popularisation of hydrogen and electric vehicles in the future. This paper considers multiple electricity-hydrogen integrated charging stations for charging plug-in electric vehicles and refilling hydrogen fuel vehicles
To address the challenge of power allocation and coordinated operation for these type stations. A power allocation strategy and control method based energy management system have been proposed.

Keywords: Energy management, Charging station Hydrogen, Optimization

I. Introduction

Hydrogen fuel vehicles and plug-in electric vehicles are considered promising due to their fast-refuelling rate, high mileage range, and lack of pollution, in contrast to internal combustion engine vehicles. maintaining instant balance in dual-function charging stations powered by renewable energy sources requires adaptive energy management strategies, including energy storage integration, grid interaction, and smart charging infrastructure. These measures are essential for optimizing energy efficiency, reducing reliance on non-renewable resources, and supporting the transition towards sustainable transportation systems. Bansal (2020)

Renewable energy sources can be used in charging stations for off-grid systems to meet consumer demand to a certain extent without creating an extra burden on the main power grid. Renewable energy sources such as solar and wind are inherently variable, with power generation levels influenced by weather conditions and time of day. This variability can result in fluctuations in energy production, leading to challenges in matching supply with demand. Energy consumption patterns at charging stations can also vary significantly throughout the day, depending on factors like vehicle charging demand, time of use, and grid conditions. Rapid changes in consumption levels require agile response mechanisms Tostado-Véliz etal (2021). To address these problems, an optimization strategy is proposed to handle different uncertainties for the energy management problem. This management contains instant balance involves adjusting energy supply and demand in real-time to match the available renewable energy production. This balance ensures efficient utilization of renewable resources and minimizes reliance on grid electricity during peak periods. To achieve instant balance, charging stations employ advanced energy management systems that integrate smart algorithms and predictive analytics Xu, et al (2021). These systems continuously monitor energy generation and consumption patterns to anticipate fluctuations and adjust operations accordingly. A comprehensive review of existing literature highlights a common trend where research on Hydrogen Refueling and charging stations is often conducted independently, with limited studies focusing on their integration. Predicting the future dominance of either vehicle type. A hybrid station integration holds substantial promise for advancing clean production and fostering sustainable development within the transportation sector. The energy management problem is investigated using a optimization strategy. The objective function of the energy management problem is to minimize the total operational cost of the hybrid charging station

II. Experimental Set-up and Procedure

The EMS subject of study in this paper was implemented on a hybrid charging station with pre-defined EV fast charging units and a hydrogen dispenser for Fuel cell and hydrogen fuel vehicles. Fig.1 illustrates the proposed system Triviño etal. (2019).

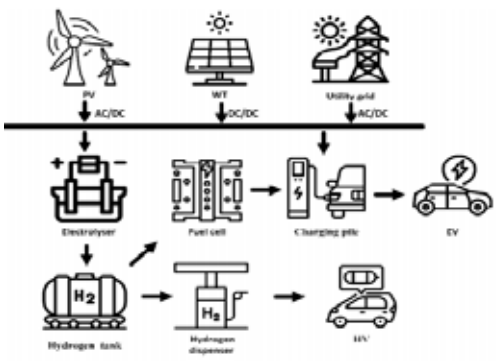


Fig. 1: The schematic diagram of a hybrid charging station

Fig. 1 presents the schematic diagram of the proposed hybrid station containing a hybrid PV/wind power plant, an electrolyzer, a Hydrogen Tank, a fuel cell, a hydrogen dispenser system. The power produced by the hybrid PV/wind power plant flows to two directions: one is supplied to EVs directly when the PV and wind power generation is sufficient, the other one flows to the PEM electrolyzer to produce hydrogen. Hydrogen tank as the storage device of hydrogen provides hydrogen to fuel cell to generate electricity for EVs Overall, the energy management strategy of the charging station ensures efficient utilization of renewable energy sources, seamless integration of fuel cell technology, and reliable service delivery to electric and hydrogen-powered vehicles, while minimizing reliance on conventional grid electricity during peak demand periods Chen etal. (2023).

III. Analysis

The setup for the electric/hydrogen charging station involves configuring essential equipment such as electrolyzers, fuel cells, and hydrogen storage tanks. These components form the backbone of the station's infrastructure, enabling efficient production, storage, and distribution of hydrogen for vehicle refueling Fang (2023). The primary optimization goal, reflected in the objective function, is to minimize the comprehensive cost of the electric/hydrogen charging station. This objective is crucial for ensuring optimal investment allocation, avoiding equipment shortages, and eliminating redundant construction Li, etal (2023). The objective function be expressed as (1)

$$mi\ \eta_{bj} = C_{st} + C_{en} + C\,a \quad + C\,b \tag{1}$$

Where, C_{st} denotes the construction cost of electric/hydrogen charging station. C_{en}denotes the generation cost of energy equipment. Ca denotes the abandoned power cost. Cbdenotes the purchased power cost. There are also Constraints that need to be defined. The proposed objective functions are optimized regarding several economicaltechnical constraints. These can be exemplified by electrical balance storage sizing and cost.

IV. Results and discussions

The aim of the proposed model in this paper is to: 1) minimize the operation cost, 2) maximize reliability, and 3) minimize the deviation of the energy consumption from its desired value as described in Fig. 2. The methodology followed for developing the optimization is shown in Fig. 2

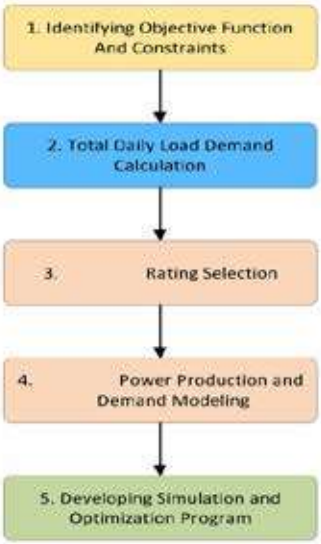


Fig. 2: Methodology followed for optimizing the station

Daily resource change and daily demand in the process are defined as follows

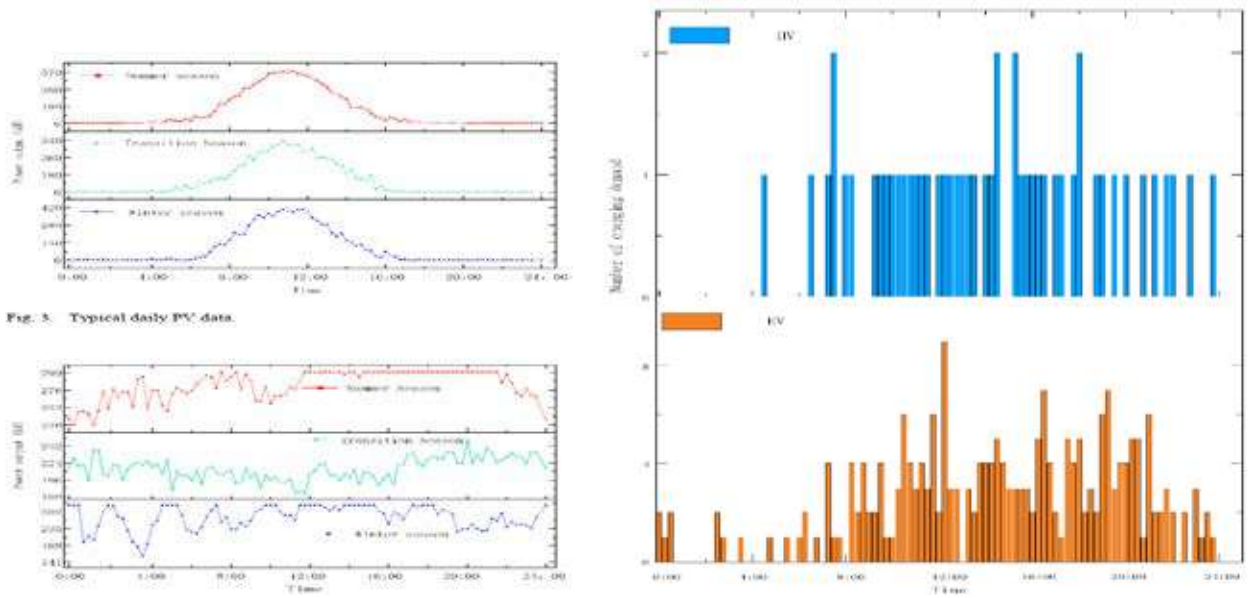


Fig. 3: Daily production potential and demand graphs

The charging station operates dynamically by allocating power from each unit based on real-time demand from both Electric Vehicles (EVs) and Hydrogen Vehicles (HVs). The state of the fuel cell is directly affected by the operational status of each unit within the system. In situations where the output power from renewable sources like wind turbines and photovoltaic units is insufficient to meet the charging demand of EVs and HVs, the fuel cell utilizes hydrogen from the storage tank to generate additional electricity. This ensures continuous charging capability regardless of fluctuating renewable energy production. Conversely, if the power supplied by the fuel cell becomes insufficient to meet demand, the charging station must draw electricity from the grid to supplement the shortfall. This approach ensures uninterrupted service and reliable operation even under varying renewable energy conditions.

In scenarios where the output power from wind turbines and photovoltaic units exceeds the immediate charging requirements of EVs and HVs, the excess electricity is not wasted. Instead, it can be diverted for other purposes energy storage for future use, or powering auxiliary systems within the charging station. This optimized utilization of renewable energy resources maximizes efficiency and minimizes waste, contributing to the overall cost-friendly sustainability of the charging station.The system costs in €/h are shown in Fig. 4

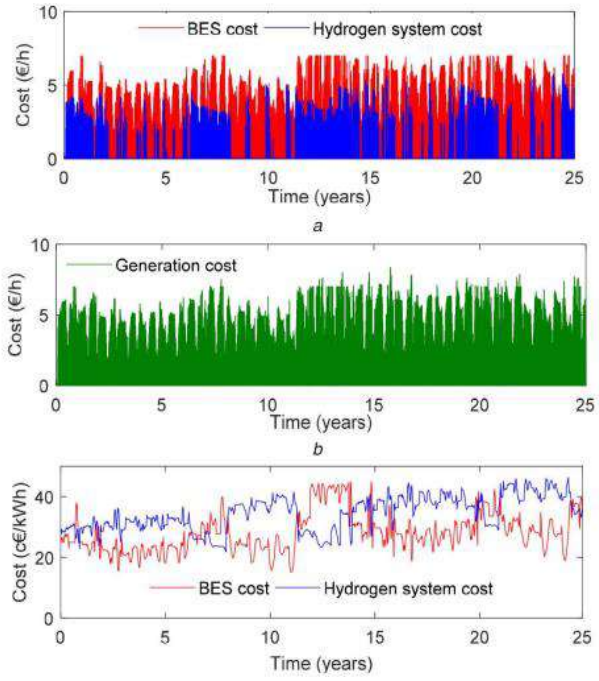


Fig. 4: The overall cost graphs for hybrid charging station

These costs are calculated by the multiplication between their powers and the utilisation pre defined costs. Besides, It can be observed that the utilisation costs evolve according to their utilisation rate. Thus, although the utilisation

cost is generally higher for hydrogen than for the system, in some periods it is reversed

V. Conclusions

In conclusion, effective energy management is a cornerstone of sustainable hydrogen and electric charging stations. By leveraging smart technologies and renewable energy integration, these stations can operate efficiently while supporting the transition to cleaner transportation alternatives. One key contribution was the development of an Energy Management System (EMS) designed to optimize the overall system cost over long-term simulations. This approach differs from traditional methods that focus solely on optimizing component sizes. By incorporating EMS into the optimization process, the study aimed to achieve cost-effective system operation and management, considering dynamic operational conditions and varying demand profiles.

References

Bansal, Saumya, et al. "Technical and economic analysis of one-stop charging stations for battery and fuel cell EV with renewable energy sources." Energies 13.11 (2020): 2855.

Chen, Xiaoyuan, et al. "Techno-economic study of a 100-MW-class multi-energy vehicle charging/refueling station: Using 100% renewable, liquid hydrogen, and superconductor technologies." Energy Conversion and Management 276 (2023): 116463.

Fang, Xiaolun, et al. "Optimal energy management of multiple electricity-hydrogen integrated charging stations." Energy 262 (2023): 125624.

García‐Triviño, Pablo, et al. "Optimised operation of power sources of a PV/battery/hydrogen‐powered hybrid charging station for electric and fuel cell vehicles." IET renewable power generation 13.16 (2019): 3022-3032.

Li, Jiurong, et al. "Optimal Configuration of Electric/hydrogen Charging Station Based on User Behavior Characteristics." 2023 8th Asia Conference on Power and Electrical Engineering (ACPEE). IEEE, 2023.

Tostado-Véliz, Marcos, Paul Arévalo, and Francisco Jurado. "A comprehensive electrical-gas-hydrogen Microgrid model for energy management applications." Energy conversion and management 228 (2021): 113726.

Xu, Xiao, et al. "Risk-based scheduling of an off-grid hybrid electricity/hydrogen/gas/refueling station powered by renewable energy." Journal of Cleaner Production 315 (2021): 128155.

Some Policies on Green Hydrogen Use for Decarbonization of Steel Industry

[1*]Ali Eren Aluç, [1,2]Adnan Midilli
[1] Istanbul Technical University, Energy Institute, Ayazaga, Istanbul, 34469, Türkiye
[2] Istanbul Technical University, Faculty of Mechanical Engineering, Gümüşsuyu, Istanbul, 34437, Türkiye

* E-mail: aluc23@itu.edu.tr

Abstract

Even now, the world is facing with a chain of disasters such as air pollution, ozone layer depletion, global warming because of the fossil fuels usage. The research continues to decrease the impacts of these problems in order to prevent the dangers that may arise in the future. In this regard, decarbonization has become one of the top topics of the 21st Century. Even the strongest nations that can influence variety parts of the world, put their differences aside and gather about this issue. Steel industry is very important sector affected by carbon tax in the near future. Therefore, decarbonization in steel industry is very important topic. In this regard, the main objective of this paper is to develop some policies of decarbonization in steel industry. One of the best ways is to perform this target is to use green hydrogen in steel production processes.

Keywords: Decarbonization, Hydrogen, Steel Industry

I. Introduction

World produced 1.88 billion tone of steel in 2022 (World Steel Association, 2023). Countries like China, India, United States and Japan are leading the way in steel industry, and it can be said that one of the common issues of these countries is air pollution. The production of 1 kg steel generates 1.6-1.7 kg of carbon emissions and this number of production is responsible for almost 9% of the the world's carbon emissions (International Energy Agency [IEA], 2020). In respond to this, researchers have turned to alternative fuels that would reduce carbon emissions. This is where hydrogen becomes one of the most important solutions for decarbonization in this industry (Scott, 2019).

III. Some Policies

These are some policies about decarbonization of steel industry with use of green hydrogen.

- Promoting steel production through Direct Reduced Iron technology using green hydrogen.
- Promoting the use of natural gas instead of coke gas for reheating in furnaces so that the gas can be enriched with green hydrogen.
- Green hydrogen use for other heating processes in steel industry.
- Combination of Direct Reduction method and Carbon Capture Technologies.

IV. Results and discussions

The steel industry is a sector where fuels with high carbon emissions, such as coal and natural gas, are frequently used. Replacing them with green hydrogen is a hard processes due to high cost. However, decarbonization process of the steel industry has to be done. Therefore people did start from somewhere. With the development of carbon capture technologies and electrolyzers, combination of the policies above will gain meaning in the near future. In order to achieve this, countries around the world should continue to encourage the companies for green hydrogen use wherever possible, not only in the steel sector.

V. Conclusions

Steel industry is one of the key sectors for sustainable development and therefore decarbonization in this sector is vital. The use of green hydrogen could play a important role, if we can make electricity produced from renewable sources widely used and cheaper, and the electrolyzer more efficient to produce green hydrogen.

References

IEA (International Energy Agency), Iron and Steel Technology Roadmap, (2020). (https://www.iea.org/reports/iron-and-steel-technologyroadmap)

IEA (International Energy Agency), Global Hydrogen Review 2023.

Scott K., Introduction to Electrolysis, Electrolysers and Hydrogen Production (2019).

World Steel Association, World Steel in Figures, (2023).

Securing the Future: A Comprehensive Study on the Implications of Cyber Intrusions on Battery Management in Fuel Cell Electric Vehicles

[1*]Hasan Gunduz
[1] Muş Alparslan University, Department of Electricity and Energy, Muş, 49210, Türkiye

* E-mail: h.gunduz@alparslan.edu.tr

Abstract
The surge in popularity of Fuel Cell Electric Vehicles (FCEVs) has prompted a corresponding rise in the utilization of management systems to oversee and regulate the functionality of their fuel cell batteries. However, this increased reliance on such systems has also amplified the threat of cyber-intrusions to FCEV users. This research seeks to evaluate the potential impacts of cyber-intrusion on the control mechanisms of FCEVs. Employing a simulation-based methodology, the study assesses the effects of cyber-intrusion on FCEVs. The investigation utilized Matlab to simulate FCEVs and employed randomized cyber-intrusion processes targeting fuel cell controllers. Results indicate that cyber-attacks can inflate the total power consumption of FCEVs by up to 94%. Furthermore, the study reveals that such attacks can inflict significant harm on the battery system, leading to diminished performance and, in severe instances, complete system failure. These findings offer crucial insights into the risks posed by cyber-intrusions into FCEV management systems.

Keywords: Battery Monitoring Systems, Cybersecurity Breaches, Hydrogen Fuel Cells, Fuel Cell-Powered Vehicles, Hydrogen Technology

I. Introduction

The The rapid expansion of the transportation sector has led to a surge in carbon emissions, contributing to environmental degradation and climate change. In response, Fuel Cell Electric Vehicles (FCEVs) have emerged as a promising alternative to traditional internal combustion engine vehicles, offering a cleaner and more sustainable means of transportation. FCEVs utilize fuel cells that convert hydrogen and oxygen into electricity to power electric motors, emitting only water vapor as a byproduct (Pramuanjaroenkij and Kakaç, 2023).

However, as the adoption of FCEVs grows, concerns have arisen regarding the cybersecurity risks associated with the reliance on battery management systems. The integration of connected technologies, like telematics and remote monitoring, has expanded the vulnerability of EVs to cyber-intrusions (Guo et al., 2020). Yet, within the realm of FCEV management systems, comprehensive investigations into complex and sophisticated cyberattacks remain limited as of current knowledge.

Cyber-intrusions pose a myriad of threats, ranging from performance degradation and compromised safety to complete system failure (Gunduz and Jayaweera, 2020). The potential consequences of such intrusions on FCEVs could be severe, resulting in harm to individuals, infrastructure damage, and financial losses. Therefore, it is imperative to comprehend the potential impact of cyber-intrusions on management systems to ensure the safe and reliable operation of FCEVs. Fig.1 illustrates the generic architecture of the FCEV powertrain (Luciani and Tonoli, 2022).

This impact study seeks to evaluate the potential effects of cyber-intrusion on FCEV Battery Management Systems (BMSs) through simulation-based assessments of cyber-attacks on FCEV control systems. The findings of this study will offer valuable insights into the associated risks of cyber-intrusions and advocate for enhanced cybersecurity measures to mitigate these risks.

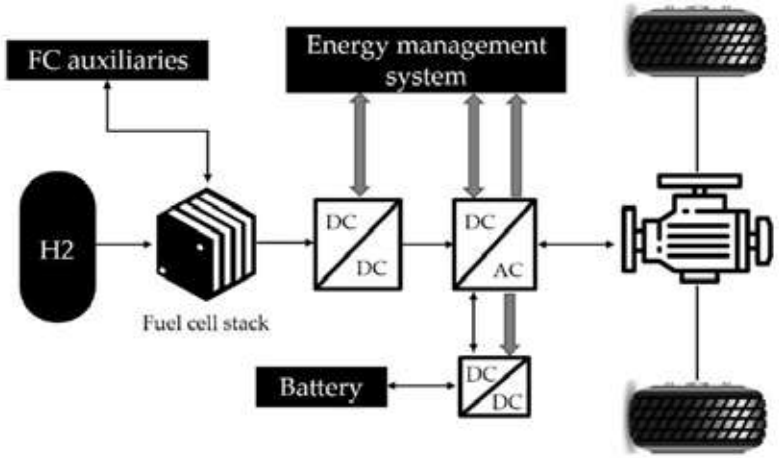


Fig. 1: Basic Configuration of Fuel Cell Electric Vehicles (Luciani and Tonoli, 2022)

II. Experimental Set-up, Procedure, and Analysis

The The Fuel Cell (FC) stacks and their accompanying subsystems constitute the core of a fuel cell electric vehicle (FCEV). In this setup, the FC system converts chemical energy into electrical energy to power the electric motor, as illustrated in Fig. 1. Apart from the electric motor, there are four other essential subsystems: air supply, hydrogen

supply, heat management, and water management. The primary function of the hydrogen supply system is to deliver hydrogen from the tank to the stack. Meanwhile, the air supply system ensures the FC stack receives oxygen, facilitated by components such as air filters, humidifiers, and compressors. The heat and water management systems play crucial roles in separating water and redistributing cabin heat efficiently. The generated electrical power from the FC is then transmitted to the electric motor via the control unit. Additionally, the battery in the FCEV operates in parallel with the FC stack, providing supplementary electrical power, when necessary, as depicted in Fig. 1.

Research by Miller (2023) elucidates the FCEV's configuration, highlighting the symbiotic relationship between the fuel cell stack and the battery. Specialized monitoring tools, such as MATLAB-Simulink, are employed for designing and integrating various components of the FCEV. Furthermore, MATLAB-Simulink aids in modeling cyber-intrusion scenarios and deriving equations to validate the vehicle's components.

The Urban Driving Cycle (UDC), exemplified by the ECE cycle in Fig. 2, is a typical driving scenario encountered in urban environments. This cycle is characterized by lower vehicular speeds, decreased engine load, and reduced exhaust emissions, reflecting real-world urban driving conditions.

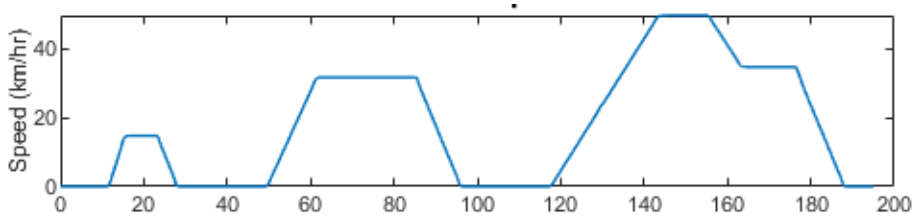


Fig. 2: Driving cycle of FCEV (as the Urban Driving Cycle)

Cyber-intrusion models have been developed for both the FC control system (1) and the boost converter (2).

$$F_{cyber_control1}(t) = 5 \times a \times rand(b) \rightarrow a = \sin t,\ b = (0,1) \quad (1)$$

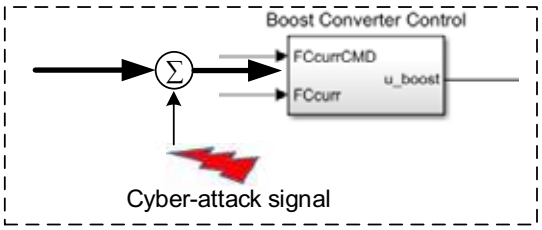


Fig. 3: Framework for Cyber-Attack on Boost Converter Module (1)

$$F_{cyber_control2}(t) = 100 \times a \times rand(b) \rightarrow a = \sin t,\ b = (0,1) \quad (2)$$

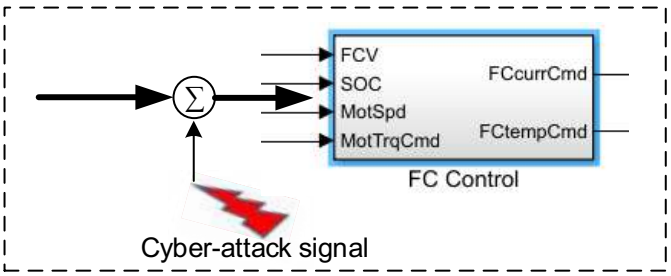


Fig. 4: Framework for Cyber Attacks Targeting Fuel Cell Control Module (2)

The depicted indicators of the proposed cyber-attack can be observed in Fig. 5.

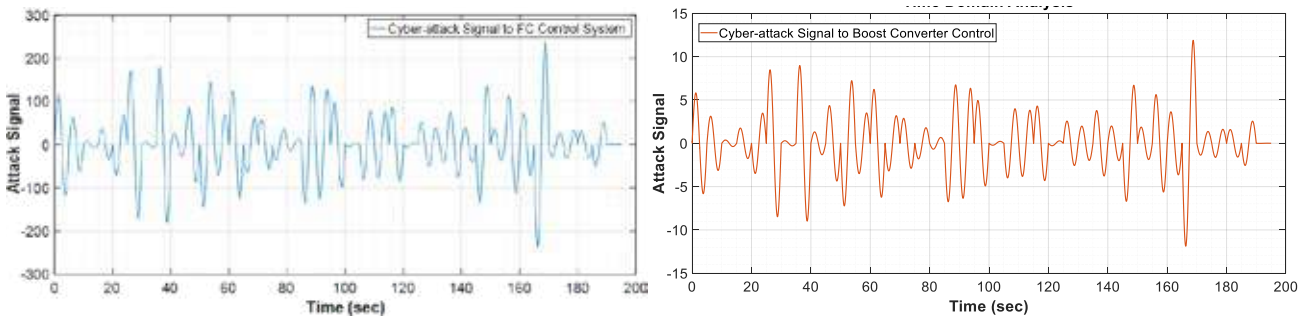


Fig. 5: Proposed cyber-attack signals targeting the FC control system (on the left) and boost converter (on the right).

IV. Results and discussions

This study utilizes a cyber-attack signal FC control and Boost converter system to demonstrate the impact of cyber-intrusion. In Fig. 6, the fluctuation in hydrogen levels in fuel cell electric vehicles (FCEVs) is illustrated under both normal (blue line) and abnormal (orange line) operating conditions throughout a specific driving cycle.

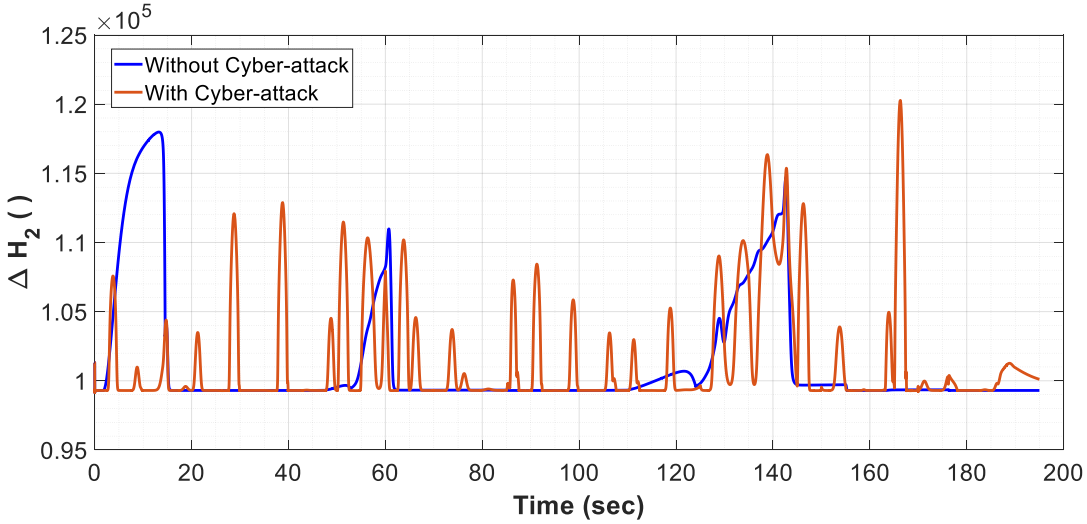


Fig. 6: Variation in Hydrogen Pressure Levels in Fuel Cell Electric Vehicles (FCEVs) with and without Cyber Intrusion

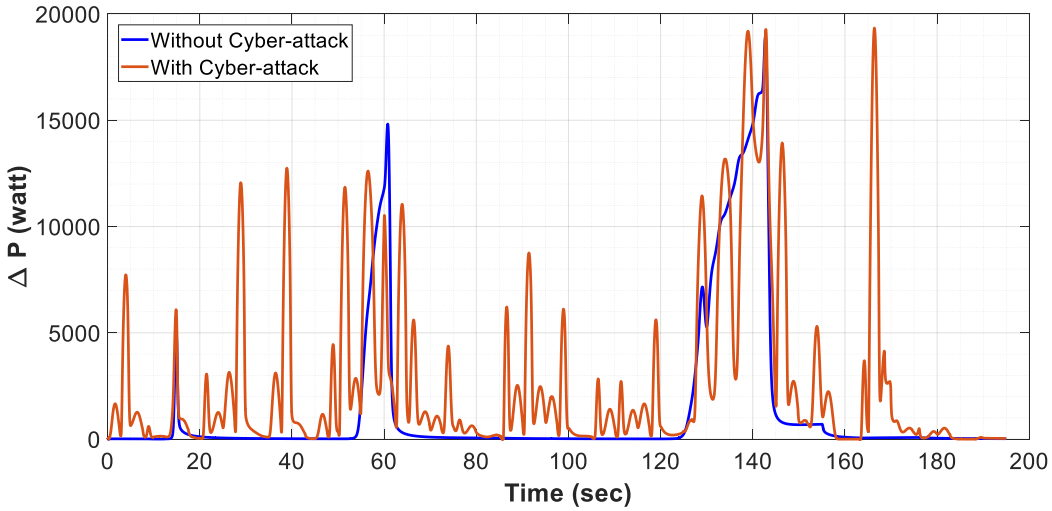


Fig. 7: Quantifying the Impact of Cyber Intrusion on Total Power for FCEVs

Fig. 7 displays the dynamic fluctuations in total power changes of fuel cell electric vehicles (FCEVs) under standard (blue line) and unusual (orange line) operational conditions across a defined driving scenario. Both Fig. 6 and Fig. 7 depict the notable influence of cyber-attacks on power usage and hydrogen reserves. Intrusions in cyber security notably elevate total power consumption, showing an approximate surge of 94%.

V. Conclusions

The surge in demand for Fuel Cell Electric Vehicles (FCEVs) has led to an increase in the deployment of management systems aimed at regulating their fuel cell batteries. However, this heightened reliance on such

systems has made users of FCEVs more susceptible to cyber intrusions. This study aims to assess the potential impact of cyber-intrusions on the control mechanisms of FCEVs. Using simulation methodology, we evaluate how cyber-attacks affect FCEVs by employing Matlab software to simulate both FCEVs and unpredictable cyber-attacks targeted at their fuel cell controllers. The results reveal that these cyber-attacks can cause a substantial increase in power consumption, up to 94%, potentially leading to significant harm to the battery infrastructure. This damage can result in reduced efficiency and, in extreme cases, complete system failure. The findings shed light on the risks associated with cyber intrusions on FCEV control systems.

References

Gunduz, H. and Jayaweera, D., Modern power system reliability assessment with cyber-intrusion on heat pump systems. IET Smart Grid, 3(5), pp.561-571, (2020).

Guo, L., Ye, J. and Du, L., Cyber–physical security of energy-efficient powertrain system in hybrid electric vehicles against sophisticated cyberattacks. IEEE transactions on transportation electrification, 7(2), pp.636-648, (2020).

Luciani, S. and Tonoli, A., Control strategy assessment for improving PEM fuel cell system efficiency in fuel cell hybrid vehicles. Energies, 15(6), p.2004, (2022).

Miller S., Fuel Cell Vehicle Model in Simscape (https://github.com/mathworks/Fuel-Cell-Vehicle-Model-Simscape/releases/tag/22.2.1.5), GitHub, (2023).

Pramuanjaroenkij, A. and Kakaç, S., The fuel cell electric vehicles: The highlight review. International Journal of Hydrogen Energy, 48(25), pp.9401-9425 (2023).

Hydrogen-Based Mobile Fast Charging Station for Disasters and Emergencies

[1]Tevfik Yigit, [2*]Hakan Celik, [3]Zehra Ural Bayrak, [4]Yavuz Erol
[1] Niğde Ömer Halisdemir University, Engineering Faculty, Department of Mechatronics, Niğde, 51240, Türkiye
[2*] Fırat University, Engineering Faculty, Department of Mechatronics, Elazığ, 23119, Türkiye
[3] Fırat University, School of Aviation, Department of Avionics, Elazığ, 23119, Türkiye
[4] Fırat University, Engineering Faculty, Department of Electrical Electronics Engineering, Elazığ, 23119, Türkiye

* E-mail: hakancelik@firat.edu.tr

Abstract

In cases of natural disasters such as earthquakes, fires and floods, the ability of renewable energy sources to operate independently of the grid is of great importance for energy uninterruptedly. In this study, PEMFC and solar cells, which are renewable energy conversion technologies, are combined in a single system to be used as a mobile charging station in times of natural disasters. In this proposed system, if the grid connection is interrupted after natural disasters, the energy required by the mobile charging station will continue to be produced uninterruptedly. In the system, the DC power obtained from the Photovoltaic (PV) panel and PEMFC will be transferred to a bus, and the energy required for the DC and AC loads of the mobile power station will be provided uninterruptedly. In order to use energy resources efficiently and effectively, an energy management system (EMS) will be created and energy resources will be managed according to energy needs with this system. In addition, DC/DC converters connected to both the PV panel and PEMFC output will be controlled according to the Maximum Power Point Tracking (MPPT) control algorithm.

Keywords: PEM Fuel Cell, PV, MPPT, EMS, Fast-Charging.

I. Introduction

The ability of renewable energy sources to operate independently of the grid brings these energy sources to the fore in cases of natural disasters such as earthquakes, fires and floods. However, some of these resources have continuity problems due to climatic conditions (Choobineh and Mohagheghi, 2015; Maghami et al., 2016). For this reason, hybrid use of energy resources is very important in terms of energy efficiency and sustainability (Candan et al., 2023; Kumar and Jaya Laxmi, 2018).

Fuel cells are one of the most promising technologies that will meet future energy needs by reducing carbon footprint. Unlike PV panels, which produce energy depending on weather conditions and daylight, PEMFCs are an energy conversion technology that produces energy uninterruptedly. The efficiency of PEMFCs, which convert the energy of hydrogen and oxygen into electrical energy through an electrochemical process, is increasing day by day due to research and development studies. The PEMFC will continuously produce DC power as long as hydrogen is supplied.

In this study, PEMFCs, which can operate independently of the grid without being affected by climate conditions, and PV panels, another renewable energy source, were combined in a single concept and proposed as an alternative energy source solution for mobile charging stations. These recommended energy sources will continue to produce the energy needed by the mobile charging station uninterruptedly, even if the grid connection is damaged after natural disasters and emergencies.

Solar energy has a non-linear current-voltage characteristic depending on environmental factors such as temperature and radiation. For this reason, a constant energy production cannot be expected from PV panels at every moment of the day. In PV systems, Maximum Power Point Tracker (MPPT) algorithms are used to maximize the output power by adjusting the switching periods of DC/DC converters (Chittoor and Chokkalingam, 2021). The input of the MPPT algorithm will be the current and voltage of the PV panel and will control the duty period of the MOSFETs used in DC/DC converters (Doğmuş and Kılıç, 2017). The efficiency of this algorithm also determines the efficiency of the PV system.

PEMFCs can produce variable voltage depending on the current drawn by the load. For this reason, a DC/DC converter circuit was used to regulate the voltage at the PEMFC output. With the MPPT algorithm, the PEMFC will be operated at maximum power and the duty periods of the semiconductor power switches in the converters will be adjusted.

The most commonly used traditional MPPT algorithms in PV systems are perturb&observe (P&O) algorithm, incremental conductivity (IC) and constant voltage methods (Gürkan and Güner, 2024). In the literature, the same methods are also used for PEMFC MPPT control (Perçin and Çalışkan, 2023). In this study, the IC algorithm, which is among the traditional methods and widely used for both PV and PEMFC MPPT control, will be used.

Multiple cell phones can be charged at the same time from the DC outputs at the mobile charging station. In addition, a DC bus-powered inverter circuit allows other devices to be charged from the AC network.

This study proposed an Energy Management System (EMS) for efficient use of energy resources. With this system, the solar battery will first energize the DA bus when there is sunlight, and PEMFC will be activated when the irradiance is reduced.

II. Hydrogen-Based Mobile Fast Charging Station

The general structure of the system proposed in this study is given in Figure 1. As seen in Figure 1, the energy produced by the PV panel and PEMFC is transferred to the DC bus and the DC charging units are fed uninterruptedly through this bus. AC charging units are fed uninterruptedly thanks to the single-phase inverter (DC/AC converter) connected to the DC bus output. In hybrid power systems existing in the literature, energy continuity is generally achieved by using batteries. However, as seen in Figure 1, in this study, energy continuity is ensured with a completely green system in which the battery is not used due to its negative effects on the environment.

In the system, the DC bus voltage will be adjusted to approximately 3.7 V for fast charging of mobile communication devices. The inverter will be fed directly with 3.7 V DC bus voltage and the AC charging units will be fed with 220 V, 50 Hz mains voltage at its output via a transformer. In addition, DC/DC converters connected to the both PV panel and PEMFC output will be controlled with the MPPT algorithm to ensure efficient operation of the system.

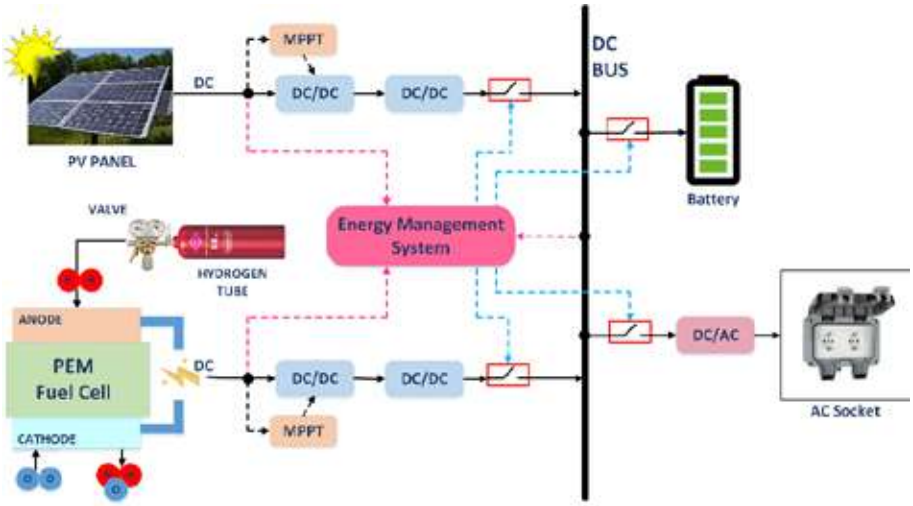


Fig. 1: General block diagram of the system

EMS application will be carried out so that the energy sources in the system can provide the energy required for the DC bus regardless of climatic conditions. This will ensure that the mobile charging station operates uninterruptedly in times of disaster and emergencies. In the study, rule-based method has been used for EMS application, and IC method has been used for the MPPT algorithm.

III. Modelling and Simulation

All the elements of the system are modeled one by one in the Simulink environment, and the whole system is created. For a more realistic modeling of the system, it was requested that the loads can draw current in the simulation. Therefore, the entire model has been electrically modeled.

Initially, PV and PEMFC were modeled, and the output voltages of the two models were adjusted by converters that consisting MPPT, and outputs of the models put together on a DC bus. Two converters are used at PV and PEMFC outputs, the first of which is to perform the MPPT task and the second is to control the DC bus voltage level. It is planned to add both AC and DC loads to the system. To simulate mobile phone charging, batteries selected at appropriate values were used as DC load. As an AC load, an RL load that can draw 15 W-15 VAr power has been added. An inverter and a transformer were used to feed the 220 V AC load.

According to the planned scenario, it is planned to initially consider that the hydrogen tube is full, the system will be put into use in an emergency, and the system fed by PV will be supported with PEMFC according to the variable irradiance gathering by the PV. An EMS model was developed and added to the system to manage this scenario. EMS provides uninterrupted power by activating PEMFC when the output power of PV is insufficient or during night conditions.

The MATLAB/Simulink model of the system is given in Figure 2.

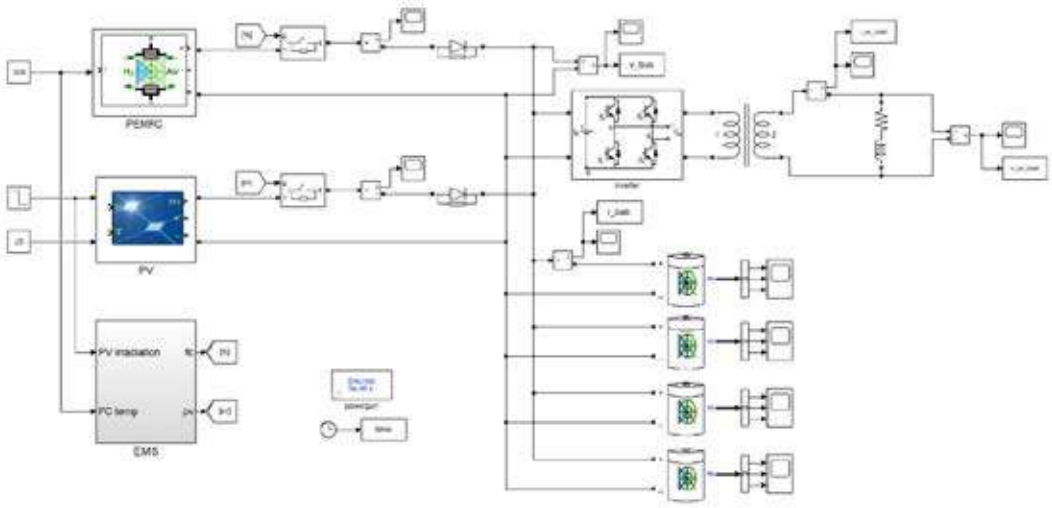


Fig. 2: MATLAB/Simulink model of the system

IV. Results and discussions

The simulation was run for 15 s and different irradiance values were applied. Irradiance was applied as 1000 W/m^2 for the first 5 s, 500 W/m^2 for the next 5 s, and 0 W/m^2 for the last 5 s. Meanwhile, all loads continued to draw power from the system.

In this process, the power values provided by PV and PEMFC and the State of Charge (SoC) of the four batteries connected to the system are given in Fig. 3.

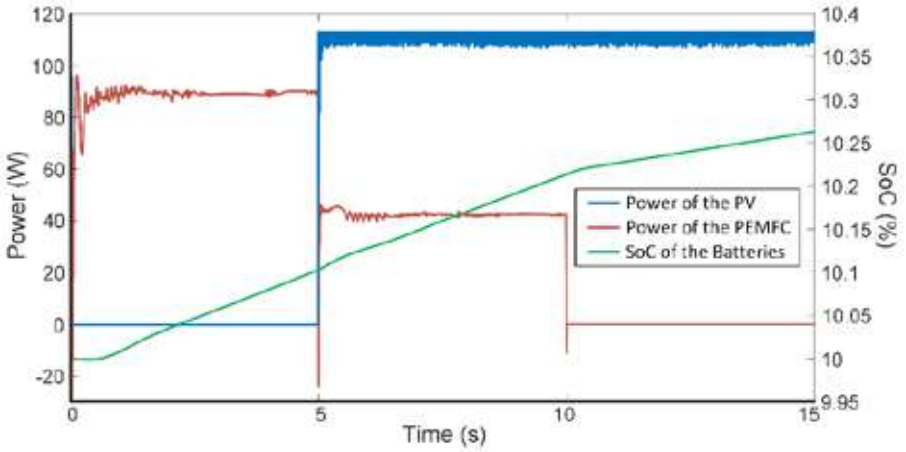


Fig. 3: SoC of the batteries according to PV and PEMFC power changes

As can be seen in Fig. 3, the batteries started charging when they were at 10% SoC and reached 10.27% SoC in 15 seconds. Meanwhile, a constant AC load continued to be fed from the system. Current and voltage values of the AC load given in Fig. 4.

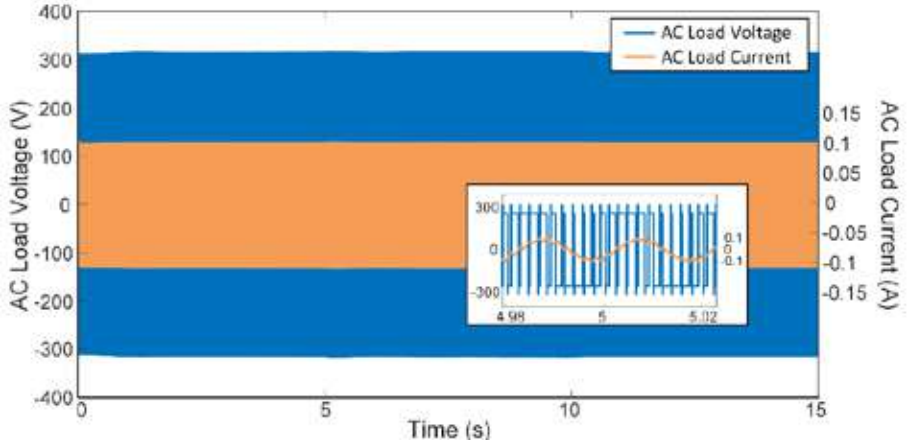


Fig. 4: Voltage and current values of the AC load

Batteries used as DC loads were charged directly via DC bus. The voltage on the batteries and the amount of current drawn during the 15 s simulation are given in Fig. 5.

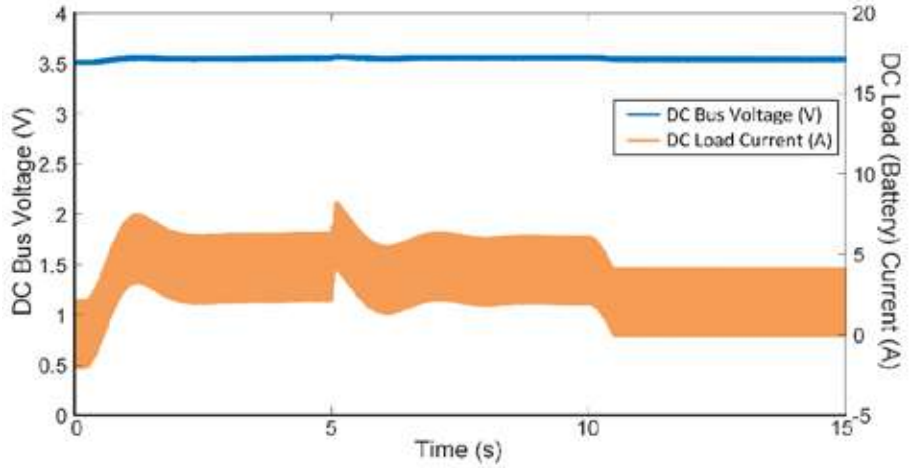


Fig. 5: Voltage and current values of the DC load

As seen in Figure 5, the batteries were charged with an average current of 5 A in total. The current change varies depending on the charging characteristics of the battery and the total power provided via the DC bus.

V. Conclusions

In this study, a fast-charging system consisting of PV and PEMFC is proposed to be used in emergencies and disasters. Thanks to both AC and DC output, the proposed system will be able to charge multiple communication devices at the same time and devices with AC input up to 15 W-15 VAr. When the results obtained are examined, it is seen that the system offers an uninterrupted charging opportunity. Thanks to the MPPT algorithms used, both PV and PEMFC were operated with maximum efficiency. When the results obtained were examined, it was seen that the batteries were charged in accordance with the fast-charging criteria. As a result, the proposed system can be used to charge communication devices or other vital devices in the post-disaster period and can operate uninterruptedly for at least a few days.

References

Candan, A.K., Boynuegri, A.R., Onat, N., 2023. Home energy management system for enhancing grid resiliency in post-disaster recovery period using Electric Vehicle. Sustainable Energy, Grids and Networks 34, 101015.

Chittoor P.R., Chokkalingam B., Solar Integrated Wireless Drone Charging System for Smart City Applications, IEEE 6th International Conference on Computing, Communication and Automation (ICCCA), Aurel Vlaicu University of Arad, Romania. Dec 17-19, (2021).

Choobineh, M., Mohagheghi, S., 2015. Emergency electric service restoration in the aftermath of a natural disaster. Presented at the 2015 IEEE Global Humanitarian Technology Conference (GHTC), IEEE, pp. 183–190.

Doğmuş O., Kılıç E., Şit S., Güneş M., PSO Algoritması ile Optimize Edilmiş PID Denetleyicinin Fotovoltaik MPPT Sistemine Uyarlanması, KSU Mühendislik Bilimleri Dergisi, 20 (4), 1-8. (2017).

Gürkan E., Güner A., Comparative performance analysis of metaheuristic algorithms for maximum power point tracking under partial shading conditions in PV systems, Pamukkale Üniversitesi Mühendislik Bilimleri Dergisi, in press, (2024). DOI: 10.5505/pajes.2024.61667.

Kumar, M.A., Jaya Laxmi, A., 2018. Power restoration based on intentional islanding algorithm for distributed energy resources in disaster management. International Journal of Modelling and Simulation 38, 189–206.

Maghami, M.R., Maghoul, A., Dehkohneh, S.S., Gomes, C., Hizam, H., Othman, M.L.B., 2016. Hybrid renewable energy as power supply for shelter during natural disasters. Presented at the 2016 IEEE International Conference on Automatic Control and Intelligent Systems (I2CACIS), IEEE, pp. 34–39.

Perçin, H.B., Çalışkan, A., Whale optimization algorithm based MPPT control of a fuel cell system, International Journal of Hydrogen Energy, 48 (60) 23230-23241, (2023). https://doi.org/10.1016/j.ijhydene.2023.03.180

Comperative Evaluation of Non-Precious Material Catalysts for PEM Fuel Cells in Terms of Cost, Stability and Activity

[1*]Erman Çelik
[1] Fırat University, Faculty of Technology, Mechanical Engineering Department, Elazığ, 23119, Türkiye

* E-mail:ecelik@firat.edu.tr

Abstract
Catalyst layer is one of the most important component of PEM fuel cells since it has crucially important role on electrochemical processes occur during energy conversion phenomena. Recently due to the high cost of Pt, efforts have been made to develop non-precious material catalysts that can be produced at low cost while offering high performance and stability. In this study, the properties of the most frequently used non-precious materials were discussed and their cost, stability and activity level properties were analyzed comparatively. Thus, it is aimed to more clearly express the technical and economic obstacles to the commercialization of non-precious material catalysts and to reveal the features that need to be developed.

Keywords: PEM Fuel Cells, Non-Precious Catalyst, Technoeconomic Analysis

I. Introduction

Proton Exchange Membrane (PEM) fuel cells are considered a promising technology for sustainable energy conversion due to their high efficiency and low environmental impact. However, the widespread commercialization of PEM fuel cells is hindered by the high cost of platinum (Pt)-based electrocatalysts, which are a significant component of the overall system cost. Pt-based catalysts, while highly efficient and stable, contribute substantially to the high manufacturing expenses, making the technology less economically viable for large-scale applications [1,2].

Recent research has focused on developing non-precious metal catalysts (NPMCs) as alternatives to Pt-based electrocatalysts. Among these, Fe-N-C, Co-N-C, Mn-N-C, Ni-N-C, Fe-Co-N-C, and Fe-Ni-N-C catalysts have shown considerable potential [3,4]. These NPMCs are evaluated based on three critical parameters: cost, stability, and activity. Cost-effectiveness is a primary consideration, as NPMCs are generally less expensive due to the abundance and lower price of base metals compared to platinum. Stability, or the ability to maintain performance over time, is crucial for ensuring the longevity and reliability of fuel cells. Activity, measured in terms of catalytic performance, determines the efficiency of the fuel cell reactions and overall energy output. Fe-N-C catalysts have been widely studied and have demonstrated significant promise due to their high catalytic activity and stability in acidic environments. Co-N-C catalysts also exhibit good activity and are particularly noted for their enhanced durability. Mn-N-C and Ni-N-C catalysts offer a balance between cost and performance, with Mn-N-C showing favorable stability and Ni-N-C providing competitive activity levels [5,6]. The combination of metals in Fe-Co-N-C and Fe-Ni-N-C catalysts aims to synergize the properties of individual metals, potentially leading to improved overall performance [7–9].

This comparative evaluation aims to provide a comprehensive analysis of these NPMCs in relation to Pt-based catalysts. By assessing their cost, stability, and activity, we seek to identify viable alternatives that could reduce the economic barriers to PEM fuel cell commercialization without compromising performance. This work contributes to the ongoing effort to develop sustainable and cost-effective energy solutions, highlighting the importance of innovative material science in addressing the challenges faced by current fuel cell technologies.

II. Analysis

In this study, the cost of the electro catalyst will be divided into two sections: the mining costs of the precursor material used in the catalyst and the energy costs required for the process of converting the material. Mining costs and process costs were calculated using Open LCA software. The performance and stability values of the electro catalyst were obtained from the literature. However, since each of these tests in the literature was conducted under different conditions, the net energy production was calculated by normalizing the differences in the literature based on the total energy produced over the total lifetime of the electro catalyst, taking into account the variable degradation rate of the electro catalyst. To normalize the variation in endurance tests conducted at different current densities, voltages, or power values across different studies, an efficiency coefficient was determined as seen in Eq.(1)

$$\eta = \frac{V_{operation}}{Vo} \quad (1)$$

Degradation at nominal current density is presented as a function of time and rate constants of demetallation degradation as in the Eq(2).

$$I_{nom} = I_{slow} e^{k_{slow} t} + I_{fast} e^{k_{fast} t} \quad (2)$$

Energy production as function of time (t) given in Eq(3).

$$W(t) = I_{nom} \cdot V_{operation} \cdot t \quad (3)$$

Total energy produced by the cell during its productive operating period via integration of energy until cell expiration time as given in Eq.(4).

$$W = \int_{t_o}^{t_{expiration}} I_{nom} \cdot V_{operation} \cdot t \quad (4)$$

Cost of electrocatalyst depending on mining and process expenses per unit mass of loading is given as Eq.(5).

$$C = C_{m,n,ng} + C_{process} \quad (5)$$

Cost for total mass of loading is given as Eq.(6).

$$C_{Total} = C \cdot m_{loading} \quad (6)$$

The cost per unit of energy was calculated as shown in Eq.(7).

$$C_{perunit\ energy} = \frac{C_{Total}}{W \cdot \eta} \quad (7)$$

III. Results and discussions

The cost per unit mass of the electrocatalyst was calculated by considering the mining costs. The costs for each electrocatalyst are presented in Figure 3. According to these calculations, the highest manufacturing cost is associated with the Pt-C catalyst, amounting to $46.28. In contrast, the lowest cost is attributed to the Co-N-C catalyst, at $8.11. The costs for catalysts based on Mn, N, and Fe, including mining costs, range between $8.60 and $18.00. This comprehensive analysis provides a clear comparison of the economic feasibility of different electrocatalyst materials based on their production costs.

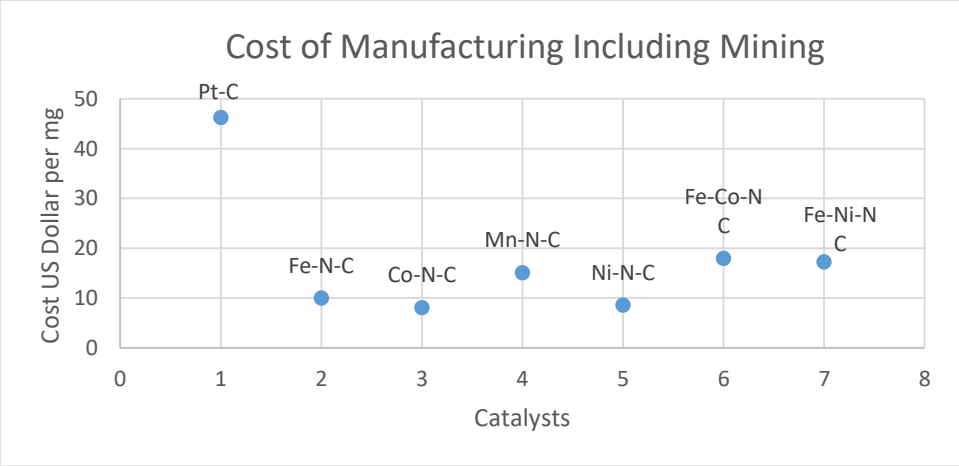


Fig. 1: Costs of Pt and non Pt group electrocatalysts including mining expences.

The unit costs of Pt-based and non-Pt-based electrocatalysts were calculated excluding mining expenses. The unit costs, excluding mining expenses, are presented in Figure 2. It was observed that the unit cost of Pt-based electrocatalysts, excluding mining costs, is lower than that of some non-Pt-based electrocatalysts. Notably, Fe-based catalysts have higher production costs due to the long-duration pyrolysis processes at high temperatures required for their synthesis. This analysis highlights the economic considerations of manufacturing different types of electrocatalysts, emphasizing the impact of processing conditions on overall production costs.

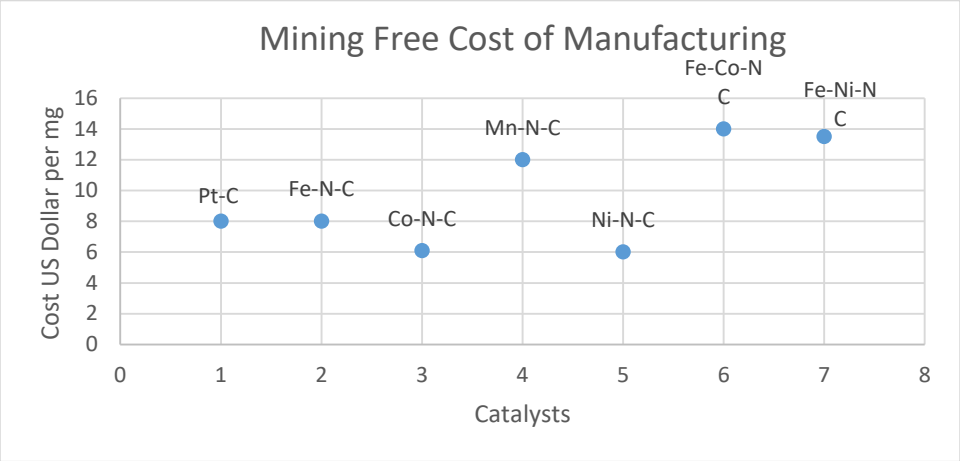


Fig. 2: Costs of Pt and non Pt group electrocatalysts excluding mining expences.

The proportions of mining expenses, early degradation, and process costs within the total cost were determined and are presented in Figure 3. It was observed that, for Platinum-based catalysts, the majority of the cost is attributed to mining expenses. Despite their high activity, Fe-based catalysts exhibit significant cost increases primarily due to their rapid degradation. Conversely, Co- and Ni-based catalysts have demonstrated higher stability, contributing to lower overall costs. This comprehensive analysis provides insight into the cost distribution and highlights the economic challenges and advantages associated with different electrocatalyst materials.

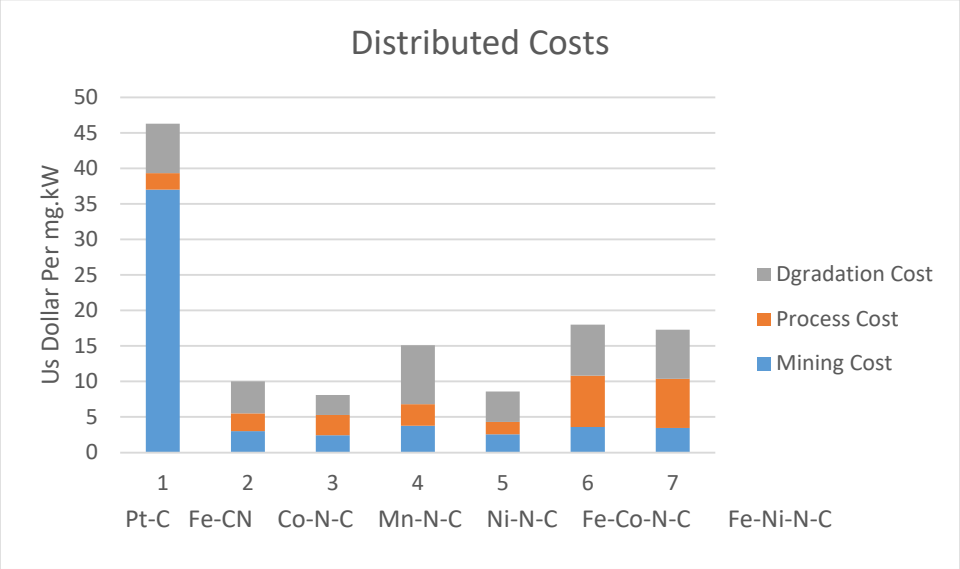


Fig. 3: Distributed expences of manufacturing costs regarding Pt and non-Pt group electrocatalysts.

IV. Conclusions

A method for economically recycling Pt would significantly reduce the cost of Pt-based catalysts. Although Fe-based catalysts have high activity, their stability is low. Developing new agents to enhance their stability could make Fe a leading alternative. Materials like Co and Ni have shown promise as components that support stability. By addressing these factors, Fe-based catalysts could become highly viable, while Co- and Ni-based catalysts continue to be seen as promising for their stability-enhancing properties.

References

Banham, D., Ye, S., Pei, K., Ozaki, J., Kishimoto, T., & Imashiro, Y. A review of the stability and durability of non-precious metal catalysts for the oxygen reduction reaction in proton exchange membrane fuel cells, *Journal of Power Sources*, *285*, 334–348 (2015).

Gollasch, M., Müller-Hülstede, J., Schmies, H., Schonvogel, D., Wagner, P., Dyck, A., & Wark, M. Elucidating synergistic effects of different metal ratios in bimetallic Fe/Co-NC catalysts for oxygen reduction reaction, *Catalysts*, *11*(7), 841 (2021).

Liu, D., Ding, S., Wu, C., Gan, W., Wang, C., Cao, D., ur Rehman, Z., Sang, Y., Chen, S., & Zheng, X. Synergistic effect of an atomically dual-metal doped catalyst for highly efficient oxygen evolution, *Journal of Materials Chemistry A*, *6*(16), 6840–6846

(2018).

Pan, F., Jin, T., Yang, W., Li, H., Cao, Y., Hu, J., Zhou, X., Liu, H., & Duan, X. Theory-guided design of atomic Fe–Ni dual sites in N, P-co-doped C for boosting oxygen evolution reaction. *Chem Catalysis*, *1*(3), 734–745 (2021).

Shen, H., Thomas, T., Rasaki, S. A., Saad, A., Hu, C., Wang, J., & Yang, M.. Oxygen reduction reactions of Fe-NC catalysts: current status and the way forward, *Electrochemical Energy Reviews*, *2*, 252–276 (2019).

Sun, Z., Zhang, S., Zheng, B., Zhou, Y., Chen, W., Liu, R., Liu, G., & Lang, L. Metal–Organic Framework-Derived Mn/Ni Dual-Metal Single-Atom Catalyst for Efficient Oxygen Reduction Reaction, *Inorganics*, *11*(3), 101(2023).

Wang, J., Wang, H., & Fan, Y. Techno-economic challenges of fuel cell commercialization, *Engineering*, *4*(3), 352–360 (2018).

Wang, Y., Wang, D., & Li, Y. A fundamental comprehension and recent progress in advanced Pt-based ORR nanocatalysts, *SmartMat*, *2*(1), 56–75 (2021).

Wu, H., Qu, B., Nguyen, T., Lorenz, J. C., Buono, F., & Haddad, N., Recent Advances in Non-Precious Metal Catalysis, *Organic Process Research & Development*, *26*(8), 2281–2310 (2022).

Off-grid cities with an Environmental Analysis Approach for Sustainability: An Overview Considering Alternative Fuels, Renewable Energy Sources and Energy Storing

[1*]Emrullah Kocaman, [1]İbrahim Furkan Korkmaz, [1]Hüseyin Yağlı, [2]Özkan Köse

[1] Gaziantep University, Engineering Faculty, Mechanical Engineering Department, University Boulevard 27310 Şehitkamil - Gaziantep, Türkiye
[2] Iskenderun Technical University, Faculty of Engineering and Natural Sciences, Mechanical Engineering Department, Hatay, Türkiye

* E-mail:emrullahkocaman@gmail.com

Abstract

This study, which deals with the environmental impacts and benefits of Off-Grid Cities, is the result of the examination of three main topics. The first is the reduction of carbon emissions and environmental footprint. Here, the effects of off-grid cities on reducing carbon emissions and carbon footprint are examined. Secondly, studies on the protection of natural resources and biodiversity of self-sufficient cities are discussed. Finally, in the third section, the role of off-grid smart cities in mitigating climate change impacts is discussed. The method used is discussed from the perspective of geographical and regional best renewable energy sources, energy storage methods and alternative energy sources in order to provide optimum benefit.

Keywords: Off-Grid cit, Environmental Sustainability, Carbon Emissions

I. Introduction

The increase in the human population and the increase in the rate of migration to cities and the rapid consumption of resources lead to the insufficiency of basic resources such as energy, food, water, health and education Aliyu and Amadu (2017). It is aimed to take advantage of the possibilities of technology, to increase the possibilities of sustainable energy production and to use the resources of cities with high population much more effectively Omer, A. M. (2008). Many cities, municipalities and living regions around the world have contributed to designing strategies to transform their region's energy supply into a sustainable energy system for the future. Studies on more effective use of resources are being carried out. It is inevitable to switch to advanced engineering technologies in terms of energy production and to reorganise the systems. Grand economies of the world today look to fossil fuels. Nevertheless, as fossil fuels are rapidly diminishing, dependence on these fuels has become a worldwide economic problem. It was speculated that the existing fossil fuel reserves could sustain petroleum for up to 40 years, natural gas for 60 years, and coal for 156 years Midilli etal (2005).

The consumption of fossil fuels, global warming and rapid changes in climate have led to the need to develop green energy systems technologies for a livable World. Unlike fossil fuels, alternative energy sources that are harmless to nature, highly efficient and low-cost can be used. Renewable energy sources include, Hydrogen, while considered a viable alternative fuel, tends to promise a lot but delivers very little. Hydrogen has the potential to significantly contribute to a low-carbon future as a zero-carbon energy carrier that is easily storable and transportable. It is enhanced energy security by reducing reliance on fossil fuels and has the flexibility to be used in transportation, heating, industry, and electricity sectors. Totally, these sources contribute to two-thirds of the world's CO_2 emissions Gökçek and Kale (2018). Wind energy results from the movement of atmospheric air from high-pressure areas to neighboring low-pressure regions, with the wind speed depending on the pressure gradient. Over oceans, deep bodies of water, and lakes, winds tend to be stronger and appear calmer during the day compared to the adjacent land areas Dhunny etal (2019).

II. Method

This study, which deals with the environmental impacts and benefits of Off-Grid Cities, is the result of the examination of three main topics. The first is the reduction of carbon emissions and environmental footprint. Here, the effects of off-grid cities on reducing carbon emissions and carbon footprint are examined. Secondly, studies on the protection of natural resources and biodiversity of self-sufficient cities are discussed. Finally, in the third section, the role of off-grid smart cities in mitigating climate change impacts is discussed. The method used is discussed from the perspective of geographical and regional best renewable energy sources, energy storage methods and alternative energy sources in order to provide optimum benefit.

Solar energy can be effectively converted into photovoltaic electricity. Photovoltaic generation involves the conversion of solar radiation into usable electrical energy through the photoelectric effect, utilizing solar cells that exhibit the photovoltaic effect.

Geothermal energy comprises wide diversity of uses, suc as heating and cooling, industry, greenhouse and health spas. It typically employs established technology and straightforward engineering principles. This technology, trustworthiness, environmental admissibility, and economics use of this geothermal energy have been exemplified along the World Fridleifsson (2001). For many years, biomass has been effectively utilized to produce alternative fuels for ground transportation. Similarly, biomass is likely to be the most promising option for use in the aviation sector, a major global transportation mode. Any agricultural or animal feed-based biological material containing carbohydrates qualifies as a biomass energy resource, and fuels derived from biomass are termed biofuels. As a sustainable energy resource, biomass reduces greenhouse gas emissions, improves air quality, decreases oil dependence, and generates new employment opportunities. Countries with significant biomass potential typically possess large reserves of vegetable oils, inedible materials, and bio-alcohols.

III. Analysis

Biomass can be utilized in two primary ways: first, through direct combustion for the generation of electricity or heat; second, through conversion into biofuels via biochemical and thermochemical processes, such as the production of biodiesel and other fuels. Biodiesel is an eco-friendly fuel compatible with any gas turbine. Biodiesel surpasses diesel fuel in various aspects including flash point, aromatic content, sulfur content, and biodegradability. Renewed interest in vegetable oil-derived biodiesel stems from its reduced environmental impact and renewable nature compared to conventional petroleum-based diesel fuel. As a result of its environmental benefits, the market share of biodiesel in the automotive fuel sector is experiencing rapid growth Demirbas (2007). It must be stored in case of excess energy produced and in case of insufficient energy deficiency. There are various storage methods that are currently used or will be used in the future. Energy Storage Systems play a crucial role in addressing grid challenges arising from the intermittent nature of Renewable Energy Sources (RESs). These systems offer a wide range of services, encompassing short-term balancing and reserve capacity, ancillary services aimed at enhancing grid stability, as well as long-term energy storage and grid restoration in blackout scenarios Díaz-gonzález (2016). There are a wide variety of storage techniques, some of them are hydrogen mechanic, flywheels, DLC, Superconducting magnetic energy Ge (2024).

References

Aliyu, A. A., & Amadu, L. (2017). Urbanization, cities, and health: the challenges to Nigeria–a review. Annals of African medicine, 16(4), 149-158.

Demirbas A. Progress and recent trends in bio-fuels. Progress in Energy and Combustion Science 2007;33:1–18.

Dhunny, A. Z., Allam, Z., Lobine, D., & Lollchund, M. R. (2019). Sustainable renewable energy planning and wind farming optimization from a biodiversity perspective. Energy, 185, 1282-1297.

F. Díaz-gonzález, Energy Storage in Power Systems, John Wiley & Sons, Ltd, Chichester, UK, 2016, pp. 143–162, URL https://onlinelibrary.wiley.com/doi/ 10.1002/9781118971291.ch5

Fridleifsson, I. B. (2001). Geothermal energy for the benefit of the people. Renewable and sustainable energy reviews, 5(3), 299-312.

Ge, L., Zhang, B., Huang, W., Li, Y., Hou, L., Xiao, J., ... & Li, X. (2024). A review of hydrogen generation, storage, and applications in power system. Journal of Energy Storage, 75, 109307.

Gökçek, M., & Kale, C. (2018). Optimal design of a hydrogen refuelling station (HRFS) powered by hybrid power system. Energy Conversion and Management, 161, 215-224.

International Enerw Agency, Technolog Roadmap: Hydrogen and Fuel Cells, Paris, 2015.

Midilli A, Ay M, Dincer I, Rosen M. Hydrogen and hydrogen energy strategies I: current status and needs. Renew Sustain Energy Rev 2005;9:255e71.Energy Agreement of 29 June 2018

Omer, A. M. (2008). Energy, environment and sustainable development. Renewable and sustainable energy reviews, 12(9), 2265-2300.

Cooperative Games to Support the Development of the Hydrogen Economy

[1*]Sofía De-León Almaraz, [2]Andrea Gelei, [3]Tamás Solymosi
[1] Corvinus University of Budapest, Institute of Operations and Decision Sciences, Department of Supply Chain Management, 8 Fővám tér, 1093 Budapest, Hungary
[2] Corvinus University of Budapest, Institute of Operations and Decision Sciences, Department of Supply Chain Management, 8 Fővám tér, 1093 Budapest, Hungary
[3] Corvinus University of Budapest, Institute of Operations and Decision Sciences, Department of Operations Research, 8 Fővám tér, 1093 Budapest, Hungary

* E-mail: de.sofia@uni-corvinus.hu

Abstract
In order to deploy new hydrogen technologies, cooperation is essential. Cooperative game models can assist in determining the most advantageous coalitions and guaranteeing equitable benefit sharing. The new "tree-enterprise" game has been applied to a case study for low-carbon hydrogen production, addressing greenhouse gas emissions employing nucleolus-type allocations in hierarchies. The definition of the most significant scenarios for cooperation within hydrogen supply chains is not an easy task and can be hindered by the uneven distribution of the utilities that can stem from a potential cooperative effort. The problem can be overcome by predefined allocation rules. In the hydrogen supply chain, the proposed cooperative game is a helpful tool for allocating value among coalition members.
Keywords: Hydrogen, cooperative games, fair allocation, hydrogen supply chain.

I. Introduction

Energy security and the energy transition must be accelerated in order to provide inexpensive and clean energy, as energy consumption is expected to rise (IEA, 2021). Renewables intermittency has been a limitation to the penetration of renewable energy sources (RES) in the energy mix. To meet this challenge, hydrogen (H_2) represents a promising alternative to recover the overproduction of electricity (e.g., from solar and wind parks) creating greater flexibility in energy systems (Azzaro-Pantel, 2018). The European Commission (2020-2021) has announced an ambitious goal to bring the hydrogen cost below 1.8 EUR per kg by 2030 [~$2] and to increase Europe's annual production of green hydrogen to 10 million tonnes by 2030.

The decade from 2020-2030 is crucial to ensure a sustainable hydrogen supply chain development and cooperation of different countries and stakeholders is decisive. Scientific analysis of strategical competition in the HSC has been widely explored in the last 15 years. Today, the analysis of cooperation seems more relevant to make possible the hydrogen deployment. Cooperation and collaboration are two keywords that are always present in hydrogen discussion at a global, regional and local levels. To do so, several actors or stakeholders are invited to participate, and financial support can be granted to some proposals to work mainly on R&D initiatives. The expected outcome of those projects is to have an effect on the large-scale deployment of clean hydrogen technologies from 2030 through international networking by involving industrial and government representatives. Even if a large number of financial programs are promoting cooperation, there is a lack of scientific works that study the effect of cooperation for the different stakeholders. The research proposed here aims to work on this gap.

II. Experimental Set-up and Procedure

There are some works applying cooperative games by using collaborative allocation for energy systems (Gately, 1974; Li et al., 2021; Tan et al., 2021). In cooperative or coalitional games the players can communicate and decide to form coalitions between each other in order to improve their payoff from the game (Moncecchi et al., 2020); the Shapley value has been one of the most referred methods for cooperative games and is reported to be the most fair method to allocate costs and profits of shared infrastructures. The nucleolus is another frequently applied solution of cooperative games. It shares several appealing properties with the Shapley value, but in many models, especially in the network-structured ones, the nucleolus has two advantages over the Shapley value: it provides Pareto-efficient allocations which are stable against group deviations, and computationally it is more tractable (Solymosi et al., 2005; Sziklai et al., 2017) .

In this work, we propose a new cooperative model: the "tree-enterprise" game. It uses nucleolus-type allocations in hierarchies when cooperation is costly. The new model is inspired in the computation of the nucleolus in peer-group games presented by (Brânzei et al., 2005). The key feature of the new game is that the hierarchy is important in decision making. In this sense, a multi-agent decision situation can be considered when cooperation is possible but constrained by a hierarchy of the agents.

The problem can be represented by a rooted tree graph, both vertically (highest positions have the highest impact in decision making), or horizontally (higher influence depending on the root side). The definition of scenarios and case studies is a complex task because cooperation can take place at different levels and for diverse markets (H_2 products, H_2 applications, etc.). In this sense, many different players can be involved, e.g, large, medium and small companies or organizations. Same happens with the producers of hydrogen technology (e.g., electrolysers, and fuel cells). An illustrative hypothetical example for a cooperative game with the purpose of installing electrolysis

technology in 2030 with the objective of achieving a predefined capacity while decreasing carbon emissions is presented in the following sections.

III. Case study

The structure taken into account consist of a hydrogen supply chain with 3 levels of echelons (Figure 1). On the top level (Level 1) there is the storage technology agent (hydrogen gaseous storage). In Level 2, the centralization degree is given. Nodes 2 and 3 consist of agents for electrolysis production by using directly renewable sources, solar or wind in place without transportation needs (descentralized options). Node 4 represents the centralized alternative with an agent in charge of the transportation of gaseous hydrogen in tube trailers. Node 4 is connected to agents in Level 3 which are those for which the facilities are transported far away from the user point (storage), and for that reason, depend on a more complex logistics system. Nodes 5, 7 and 8 are agents using electrolysis production with different electricity types (nuclear, solar and wind, respectively). Node 6 is an agent producing H_2 by using steam methane reforming (SMR) coupled with carbon capture and storage (CCS). The formulated case study uses as a reference the emissions of the status quo technology (SMR) vs low-carbon alternatives. In this sense, it is possible to identify environmental impacts (costs) for the different technologies or agents (Table 1).

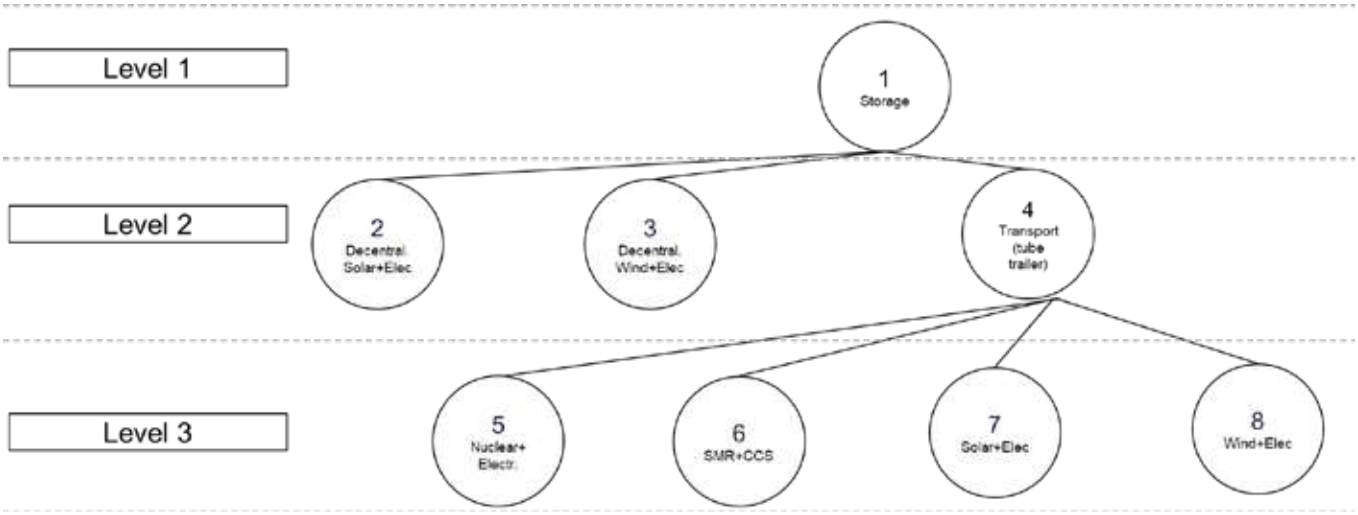


Fig. 1: Structure of the hydrogen supply chain

Tab. 1: Information of the relevant nodes for the hydrogen supply chain considered in the case study

Node or Agent (i)	Agent (technology) name	c_i: cost per agent (kg $CO_{2\text{-eq}}$ /kgH_2)	Reference	b_i	Comment
Status quo	Steam methane reforming (SMR)	10.30	(Sadeghi et al., 2020)	0	Reference technology for grey H_2 (no benefit)
1	Gaseous storage	1.00	assumption	0	Can be used for any H_2 color (no benefit)
2,7	Electrolysis + Solar power	3.08	(Sadeghi et al., 2020)	7.22	cost status quo – ci
3,8	Electrolysis + Wind power	0.98	(Bhandari et al., 2014)	9.32	
4	Gaseous transportation	1.00	assumption	0	Can be used for any H_2 color (no benefit)
5	Electrolysis + Nuclear power	2.15	(Bhandari et al., 2014)	8.15	cost status quo – ci
6	SMR + carbon capture and storage	3.40	(Sadeghi et al., 2020)	6.9	
C: total cost of the coalition (nodes 1-8)		15.67			

IV. Analysis

In the "tree-enterprise" game, agents in a hierarchical supply chain need a “resource” (i.e., hydrogen infrastructure) in order to materialize their potential profits or cost (i.e., CO_2 emissions). For the selected case study, the infrastructure has fixed CO_2 emissions per technology and is capable to serve all or any subgroup of the agents. The supply chain is hierarchical, represented by a tree graph (Figure 2) and the given potential emissions of an agent (a node, except the root in the graph) can only be made if all the upstream agents (all nodes on the path from the node to the root) are participating. In Figure 2, the root of the tree is not a stakeholder but represents the resource (hydrogen infrastructure) to be created by a coalition of agents in order to make their capabilities work. The game calculations can be summarized in Equations 1-4 and solved in Figure 2.

$$v(N) = -C + \sum_{j \in N} b_j \quad (1)$$

$$Q = \sum_{i \in N} q_i \quad \text{where } q_i = \min\{v(N), \sum_{j \in R(i)} b_j\} \text{ and R(i) is the set of node } i \text{ and all its dependents} \quad (2)$$

$$t = \frac{v(N)}{Q} \quad (3)$$

$$x_i = q_i t \quad (4)$$

Where, *j* is the reference unit (CO_2 equivalent), *i* is the agent, b_j is the potential benefit per node, *C* is the total fixed cost of the coalition, *v(N)* is the total net benefit (the value) of the coalition (Eq. 1), q_i is the claim of agent *i* on the value *v(N)* (i.e. the feasible total potential benefit of agent *i* and all his dependents, at most *V(N)*), *Q* is the total claim of agents (Eq. 2), *t* is the value-portion per unit claim (Eq. 3). The allocation of v(N), that is x_i ($i \in N$), is in proportion to the claims of agents: q_i ($i \in N$) (Eq. 4).

IV. Results and discussions

The value of a coalition of agents is the sum of the potential profits/cost of the member agents (shared CO_2 emissions for the coalition) who are connected to the root via other members within the coalition minus the fixed (independent of the group to be served) emissions savings of the “source”. The reason is that the root represents a "crucial resource", each other node of the tree represents one of the agents with a given profit-making potential that can only materialize if all agents on the path to the root are also participating (Figure 2).

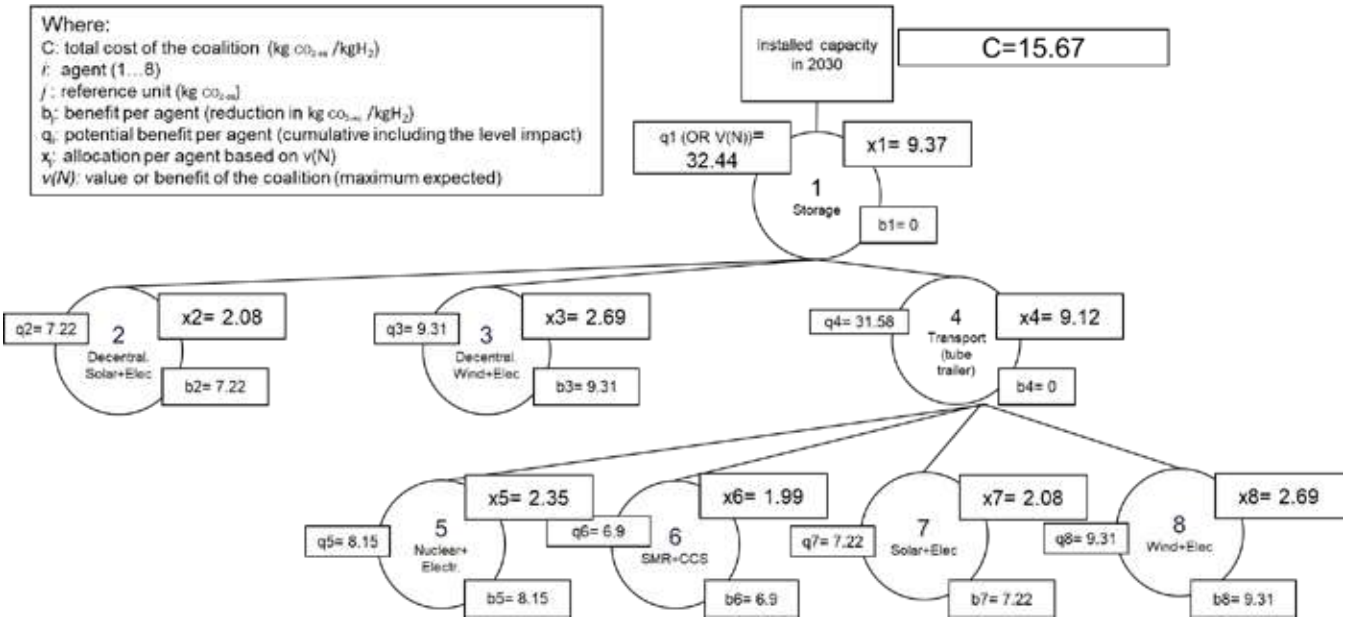


Fig. 2: Example of a cooperative tree-enterprise game applied to the installation of hydrogen technologies.

Having access to the "crucial resource" is necessary for being able to materialize the potential profit-making capabilities of the agents. Making this resource, capable of serving any subgroup of the agents, available has a fixed environmental impact. The value of a coalition of agents is defined as the sum of the individual potential profits of those members who are connected to the root via other members within the coalition minus the fixed (independent of the coalition to be served) investment cost of the "crucial resource" (electrolyser technology installation). The stakeholders’ interaction level requires a careful analysis (Gelei & Dobos, 2016). For the treated case, it can be highlighted that the relevance of the proposed model clearly displays the importance of the position in the hierarchy. For example, even if the transportation of hydrogen offers zero benefit when considered independently, when placed in the coalition it plays a crucial role due to its logistics relevance which makes it necessary for centralized production options.

V. Conclusions

Cooperation is crucial in the deployment of new hydrogen technologies, and cooperative game models can help identify the best coalitions and ensure fair distribution of benefits. The "tree-enterprise" game, using nucleolus-type allocations in hierarchies, has been applied to a case study for low carbon hydrogen production, addressing

greenhouse gas emissions. This cooperative game formulationcan be a useful tool for distributing value among coalition players in the hydrogen supply chain.

Acknowledgements

The project is supported by the National Research, Development and Innovation Fund of Hungary [grant number: OTKA FK 146575].

References

Azzaro-Pantel, C. (2018). Hydrogen Supply Chains. In *Academic Press* (1st ed.).

Bhandari, R., Trudewind, C. A., & Zapp, P. (2014). Life cycle assessment of hydrogen production via electrolysis – a review. *Journal of Cleaner Production*, *85*, 151–163. https://doi.org/10.1016/J.JCLEPRO.2013.07.048

Brânzei, R., Solymosi, T., & Tijs, S. (2005). Strongly essential coalitions and the nucleolus of peer group games. *International Journal of Game Theory*, *33*(3), 447–460. https://doi.org/10.1007/s00182-005-0213-9

European Commission. (2021). *Opening keynote by the President: European Hydrogen Week*. Https://Ec.Europa.Eu/. https://ec.europa.eu/commission/presscorner/detail/en/speech_21_6421

Gately, D. (1974). Sharing the Gains from Regional Cooperation: A Game Theoretic Application to Planning Investment in Electric Power. *International Economic Review*, *15*(1), 195. https://doi.org/10.2307/2526099

Gelei, A., & Dobos, I. (2016). Mutual trustworthiness as a governance mechanism in business relationships — A dyadic data analysis. *Acta Oeconomica*, *66*(4), 661–684. https://doi.org/10.1556/032.2016.66.4.5

IEA. (2021). *Global Hydrogen Review 2021*.

Li, D., Gao, C., Chen, T., Guo, X., & Han, S. (2021). Planning strategies of power-to-gas based on cooperative game and symbiosis cooperation. *Applied Energy*, *288*, 116639. https://doi.org/10.1016/J.APENERGY.2021.116639

Moncecchi, M., Meneghello, S., & Merlo, M. (2020). A Game Theoretic Approach for Energy Sharing in the Italian Renewable Energy Communities. *Applied Sciences 2020, Vol. 10, Page 8166*, *10*(22), 8166. https://doi.org/10.3390/APP10228166

Sadeghi, S., Ghandehariun, S., & Rosen, M. A. (2020). Comparative economic and life cycle assessment of solar-based hydrogen production for oil and gas industries. *Energy*, *208*, 118347. https://doi.org/10.1016/J.ENERGY.2020.118347

Solymosi, T., Raghavan, T. E. S., & Tijs, S. (2005). Computing the nucleolus of cyclic permutation games. *European Journal of Operational Research*, *162*(1), 270–280. https://doi.org/10.1016/J.EJOR.2003.02.003

Sziklai, B., Fleiner, T., & Solymosi, T. (2017). On the core and nucleolus of directed acyclic graph games. *Mathematical Programming*, *163*(1–2), 243–271. https://doi.org/10.1007/S10107-016-1062-Y/FIGURES/8

Tan, C., Geng, S., Tan, Z., Wang, G., Pu, L., & Guo, X. (2021). Integrated energy system–Hydrogen natural gas hybrid energy storage system optimization model based on cooperative game under carbon neutrality. *Journal of Energy Storage*, *38*, 102539. https://doi.org/10.1016/J.EST.2021.102539

Nano Iron Powder Usage in HHO Dry Cell Electrolyte Solution

[1*]Mustafa Kaan Baltacioğlu, [2]Onur Bulut
[1] İskenderun Technical University, Faculty of Engineering and Natural Science, Mechatronics Engineering Department, Hatay,31200, Türkiye
[2] İskenderun Technical University, Faculty of Engineering and Natural Science, Mechanical Engineering Department, Hatay, 31200, Türkiye

* E-mail: mkaan.baltacioglu@iste.edu.tr

Abstract
Nowadays, renewable energy sources are more important than ever due to environmental reasons and sustainability of humanbeing. Hydrogen can be used as an alternative clean fuel and most promising candidate as an energy carier. One of the common hydrogen production methods is electrolysis process. Electrolysis is the process of disintegration of water. There are many types of electrolysis process. One of them is using HHO dry cells. Investigations are continuing to improve the HHO dry cell efficiency and hydroxyl production rate. In order to increase the efficiency, nano iron powder addition is examined to the electrolyte solutions and investigated it in two different types, which distilled and ultrapure water. 30% (w/L) potassium hydro oxide (KOH) prefered for electrolyte solution and 2 g/L nano iron used in order to increase conductivity. Encountered problems are determined such as precipitation and temperature increase.

Keywords: Hydrogen, HHO, dry cell, electrolyte, nanoparticles, electrochemistry

I. Introduction

Today, the use of fossil fuels has increased. Fossil fuels damage the atmosphere and cause global warming. For this reason, the use of fossil fuels is being reduced and alternative clean fuels are being used. (Tamer et al., 2018) Alternatively, hydrogen can be used as a cleaner fuel. In this study, water electrolysis method, one of the hydrogen production methods, was used. HHO works on the principle of water electrolysis in dry cell. thus, hydroxy (HHO) or also known as Browns gas is obtained. There are many factors affecting HHO production. Some of them are electrode arrangement, electrolyte type, applied voltage, applied current, temperature, time, catalysts. Studies on the factors affecting HHO production are ongoing. (El Kady et al., 2020).

Nanoparticles are used in many applications today. One of these applications is electrolysis. Nanoparticles can be used in electrolyte solution to increase energy efficiency in electrolysis application. In their study, Uddin et. al used graphene, multi-wall carbon nanotubes and indium tin oxide in electrolysis electrolyte solution. They encountered some difficulties in their study. One of them is that nanomaterials do not mix in water. In order to eliminate this problem, they tried the mechanical mixing method. The most successful of the nanomaterials examined here was multi-wall carbon nanotubes. However, we used nano iron powder in this study because MWCNTs are costly. (Uddin et al., 2020).

Various studies have been carried out for electrolyte solution in the literature. However, nanoparticles have not been tried in the electrolyte solution in HHO dry cell. Since iron is a good conductor, we predicted that the temperature of the dry cell would increase. In the study conducted by Baltacıoğlu et. al; the temperature changes between distilled water and ultrapure water used in the HHO dry cell were beneficial on the mixture of potassium hydroxide (KOH) and nano iron powder that we will use in the electrolyte solution (Baltacıoğlu et al., 2019)
In this study, KOH and nano iron powder in the electrolyte solution, distilled water and ultrapure water were tested separately in HHO dry cell. Research was carried out on HHO production, temperature effects and cost.

II. Experimental Set-up and Procedure

HHO dry cell works on the principle of electrolysis. Electrolysis is the breakdown of water by chemical reaction using electrical energy. In this study, a 316L stainless steel plates with a size of 14 cm x 14 cm were used as electrode. A total of 13 plates were used. Heat resistant rubber was used as a gasket between the plates. Pure water, KOH, and nano iron powder were used as components of the electrolyte solution. Distilled water and ultrapure water were separately analyzed under identical conditions as pure water. Complementary equipment of the system such as a dehumidifier, volumetric flowmeter, and changes in the hydroxy gas produced with a microcontroller were recorded. The schematic diagram of the experimental setup is shown in Figure 1. HHO gases were passed through a dehumidification filter before the flowmeter. Experiments were conducted under constant KOH ratio, constant nanoparticle ratio, and constant current conditions, and the effects of the electrolyte solution as the sole variable were analyzed. Nano iron powder, commonly used in typical electrode production and found in the literature, was integrated into the system without requiring additional processing. The effects were initially visually observed during the electrolysis process and subsequently tested in the dry cell. Firstly, 1 L distilled water, 300 g/L KOH and 2 g/L nano iron powder were mixed with a magnetic stirrer at 80 rpm for 1 hours. The solution was cooled steadily to room temperature. At the second step, similar procedure is repeated for ultrapure water with same w/v ratios.

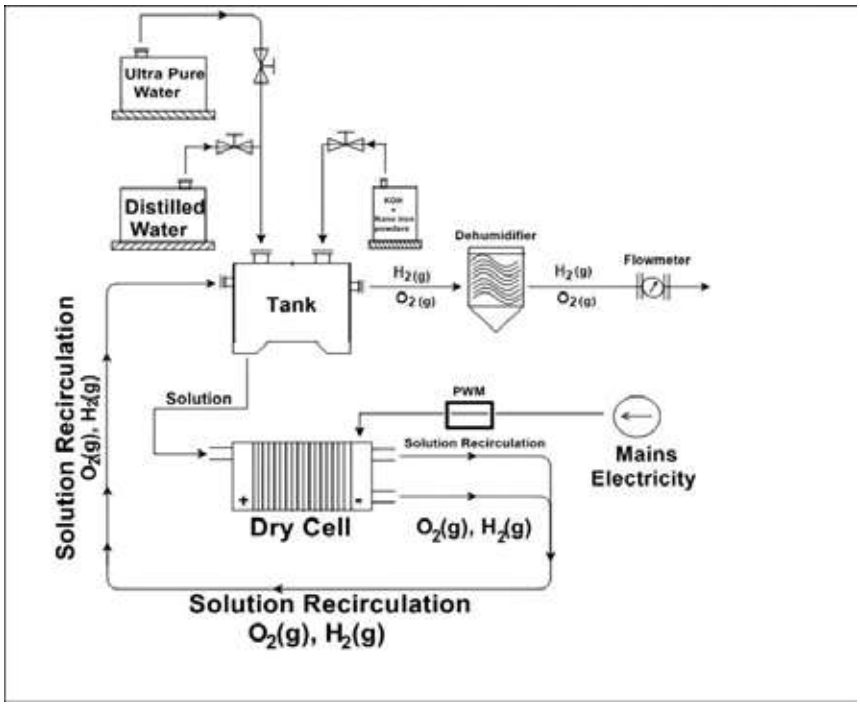


Fig. 1: HHO Dry Cell experimental set-up

Equal conditions were provided in the tests performed at the same voltage level values. The temperature changes of the solutions, HHO production amount and reactor outer surface temperatures were measured for two different waters as a function of time and taken into account in the experimental studies. Finally, the effects of the first electrolyte on the temperature and production results are presented graphically with the effects of the second electrolyte.



Fig.2: Ultra-pure water device

Tab.1: Technical properties of nano iron powder

Density (g/cm^3)	*7,9*
Purity	*99.9%*
Color	*Dark Grey-Black*
Crystal Structure	*Cubic*
$T_{melting}$ (°C)	*1538*
$T_{boiling}$ (°C)	*2862*
Particle Size (nm)	*800*

III. Results and discussions

Among the pure waters, distilled water without nanoparticles (Dist_NoNano) 19,4% more hydroxy gas produced than ultrapure water (Ult_NoNano) in the temperature range of 25°C - 60°C. Ultrapure water provided 17,54% better results between 60°C - 80°C compared to Dist_NoNano.

The nano iron powder caused a faster temperature rise and improved the performance of HHO production from ultrapure water (Ult_Nano), which had lower conductivity. On the other hand, since the average temperature at which distilled water provides relatively more production shortens the time between 25°C and 60°C, the total production decreased and the peak production point increased for nano iron added distilled water (Dist_Nano). Since there will be instantaneous high consumption and it is suitable for use in environments where there will be an

opportunity to cool down afterwards, the cumulative efficiency of the systems can be improved by using control strategies and optimisation methods such as Fuzzy PID and Metaheuristic Algorithms (Conker and Baltacıoglu, 2020).

As seen in Figure 3, one of the important zone is between 50-60 °C. Becaouse of that variaton of hydroxyl production rate would be separate in two control zone; which are 23-55 °C (zone 1) and 55-80 °C (zone 2). Under zone 1 conditions, mean effect of nano iron addition to distilled and ultra-pure water were 5,54%,9,19%, respectively. For zone 2, improvement ratios on distilled and ultra-pure water were 3,62%,4,94%, respectively. The detected situation between 50-60 °C is also compatible with the literature (Baltacıoglu, 2019).

Considering the cost analysis of the use of nanoparticles; nano iron powder costs $ 295 per kilogram. In this study, 2 g/L of nanoparticles used which cause extra 0.6 $ process cost. However, this cost is about 6% compared to the system cost, which is quite acceptable since the change in production is 9,19% more. A sustainable increase in efficiency can be created by including the importance of removing precipitation over time and various comparison methods.

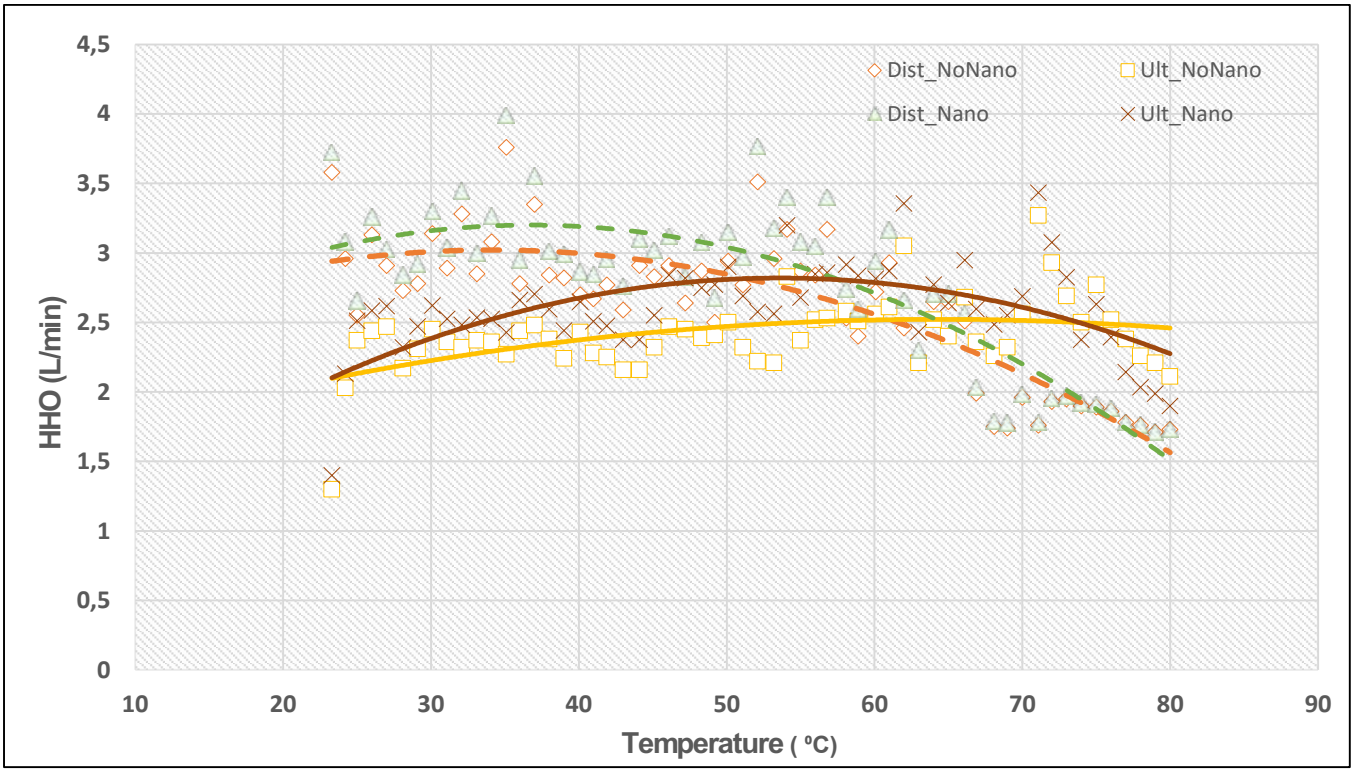


Fig. 3: Comparison of HHO production rates for distilled and ultrapure water with and without nano iron additive

IV. Conclusions

In order to increase energy efficiency in water electrolysis, it is extremely important to improve the HER (Hydrogen Evoulation Reaction) and OER (Oxygen Evoulation Reaction) processes required in electrolysis. In the literature, nano electrocatalysts have been tried to improve OER and HER processes in various electrolysis applications. The best electrocatalysts on the market are noble metals. However, since noble metals are costly and scarce in nature, alternative methods have been used. Some of these are changing the material composition and morphology. (El Soly et al., 2021). So, with in the scope of this study, a simple and effective method has been investigated and results were promising to go forward and develop new opportunities to improve hydroxyl production rate. As a result of analysis, a typical cooling system which has renewable energy source and more comlex magnetic mixer would be offered as future study topics.

Acknowledgement

The authors acknowledge for ultra-pure water supply to the Ministry of Commerce of the Republic of Turkey, Eastern Mediterranean Regional Customs and Foreign Trade Regional Directorate, Iskenderun Customs Laboratory Directorate.

References

Baltacıoğlu, M. K.. A novel application of pulse width modulation technique on hydroxy gas production. International Journal of Hydrogen Energy, 44(20), 9726-9734. (2019)

Baltacıoğlu M. K., Mustafa Tunahan Başar, Feride Cansu Iskenderoğlu, Çağlar Conker, Ahmet Atçı, Experimental Investigation of Hydroxyl Gas Production by Using Distilled and Ultra-Pure Water, International Hydrogen Technologies Congress (IHTEC-2019), (2019).

Conker, C., & Baltacioglu, M. K. Fuzzy self-adaptive PID control technique for driving HHO dry cell systems. International Journal of Hydrogen Energy, 45(49), 26059-26069. (2020).

El Kady M. A., Ahmed El Fatih Farrag, M.S. Gad, A.K. El Soly, H.M. Abu Hashish, Parametric study and experimental investigation of hydroxy (HHO) production using dry cell, Fuel 282, 118825 (2020).

El Soly A.K., M.A. El Kady, Ahmed El Fatih Farrag, M.S. Gad, Comparative experimental investigation of oxyhydrogen (HHO) production rate using dry and wet cells, International Journal of Hydrogen Energy 46, 12639-12653 (2021).

Tamer M. Ismail, Khaled Ramzy, M.N. Abelwhab, Basem E. Elnaghi, M. Abd El-Salam, M.I. Ismail, Performance of hybrid compression ignition engine using hydroxy (HHO) from dry cell, Energy Conversion and Management 155 287–300 (2018).

Uddin M. N., V. V. Nageshkar, R. Asmatulu, Improving water-splitting efficiency of water electrolysis process via highly conductive nanomaterials at lower voltages, Volume 5, pages 108–117, (2020).

Exergetic Sustainability Indicators of E-methanol Production depending on green hydrogen

[1*]Selcuk Inac, [2]Adnan Midilli
[1] Department of Mechanical Engineering, Engineering Faculty, Dogus University, 34775, Istanbul, Türkiye
[2] Department of Mechanical Engineering, Mechanical Engineering Faculty, Istanbul Technical University, 34437 Beyoglu, Istanbul, Türkiye

* E-mail:sinac@dogus.edu.tr

Abstract

Methanol is not only used as a raw material in the production of many chemical substances but also employed as an effective solution in energy generation, hydrogen storage, and transportation. Methanol can be produced by certain processes. However, more sustainable, and cleaner methanol production can be achieved by synthesizing the hydrogen obtained from the renewable energy-supported electrolyzer with CO_2. In this context, as the first stage of this study, the main concept design of the renewable hydrogen-assisted methanol production system is made. Later, exergetic sustainability indicators are developed for this system. In this designed system, hydrogen production is provided by the wind energy-supported electrolyzer. In addition, the CO_2 gas required for methanol production is obtained by capturing CO_2 from the flue gas released by the combustion of fuels such as biomass or biogas plant. As a result of this study, when the methanol conversion rate is 0.2, the exergy efficiency, environmental effect factor and exergetic sustainability index of the system were calculated to be 16.25%, 1.851 and 0.54, respectively.

Keywords: Methanol, Renewable Hydrogen, Wind Energy, Exergy Analysis, Sustainability.

I. Introduction

Climate change is one of the most important factors that humanity seriously threaten today. Globally, carbon dioxide emissions have seriously increased in the last century. Many scientists argue that the increasing amount of CO_2 in the atmosphere will markedly increase global warming. Therefore, green energy sources are considered the most effective solutions to reduce the CO_2 level in the atmosphere (Inac and Midilli, 2024). There are various utilization methods of CO_2. Among these, methanol production from CO_2 both reduces CO_2 emissions and enables the production of clean fuels and other methanol derivatives. In this context, methanol production via hydrogenation of CO_2 has recently attracted increasing attention (Huang et al., 2023).

Methanol has many advantages such as high energy density, easy storage and transportation, low toxicity, and low environmental pollution. It can also be used as raw material in the production of various basic chemicals. On the other hand, a large amount of hydrogen is required for methanol production via hydrogenation of CO_2. In this context, renewable energy-supported green hydrogen production systems such as wind, solar and geothermal can be used for the required hydrogen (Nazerifard et al., 2021).

Green energy has emerged as a clean and sustainable alternative to fossil fuels. In this context, it becomes imperative to utilize thermodynamic systems integrated with highly efficient and sustainable energy sources. Evaluating the efficiency of a thermodynamic system requires defining its exergetic performance. Furthermore, sustainability is crucial for these systems, allowing local and national authorities to integrate environmental factors into energy planning (Bozoglan et al., 2012).

In this study, exergy-based sustainability indicators of the green hydrogen supported e-methanol production system were developed and examined. Thanks to these parameters, the environmental, sustainability and exergetic performances of the system were parametrically examined and discussed depending on certain operating conditions.

II. Main concept design

The basic concept diagram of the wind energy-assisted e-methanol production system is given in Fig. 1. The system designed as shown in Fig.1. consists of three subsystems: Wind energy-assisted hydrogen production system, methanol production system and CO_2 capture system. In the system, the electricity required for the methanol production system, hydrogen production system and CO_2 capture system is provided by wind energy. On the other hand, the working principles, and parameters of the PEM electrolyzer, methanol production system and CO_2 capture system have been detailed in (Bellotti et al., 2019, Inac and Midilli, 2024).

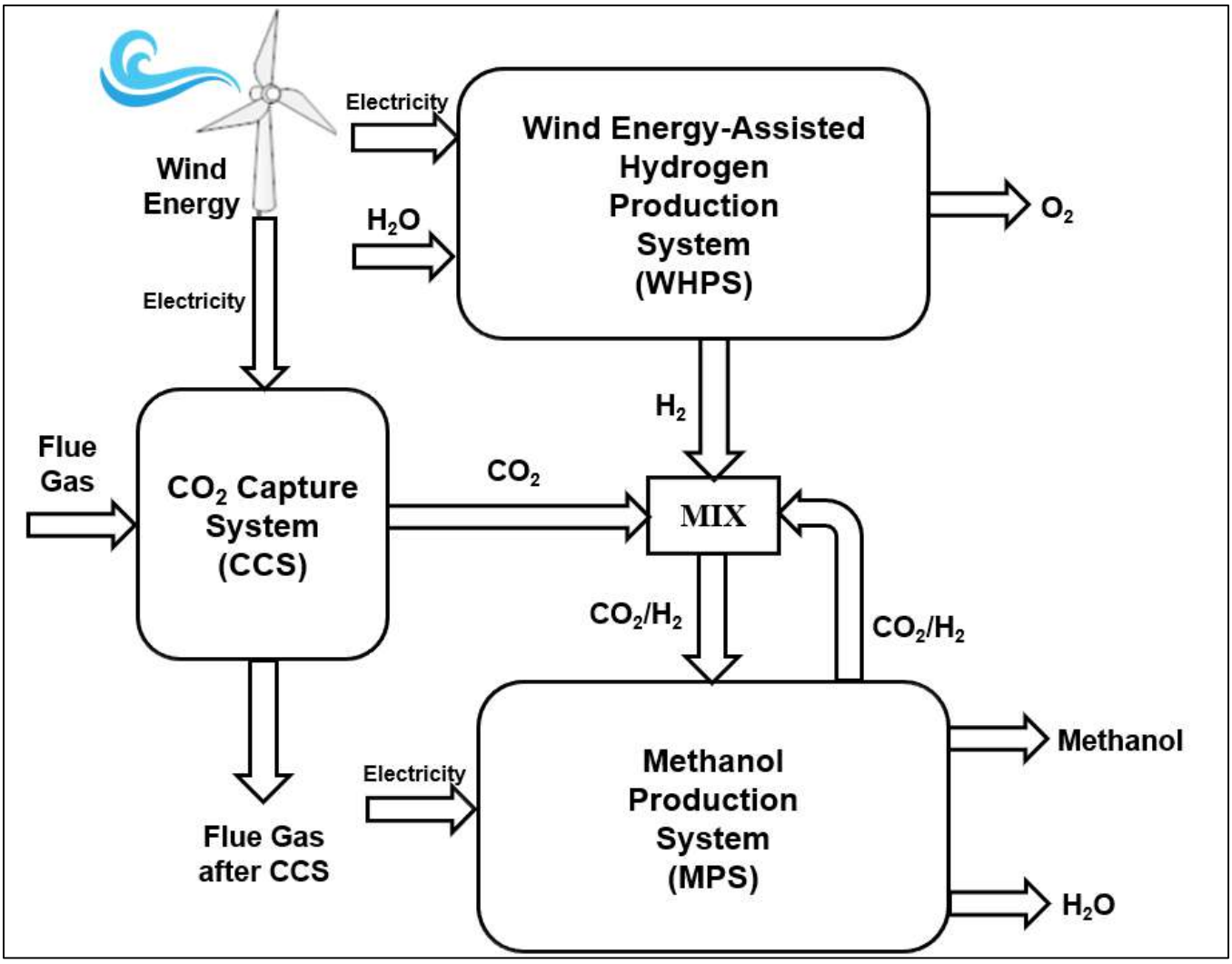


Fig. 1: Schematic illustration of wind energy-assisted e-methanol production system.

III. Analysis

In this section, the exergetic sustainability parameters of the designed system are developed. Before these exergetic sustainability analyzes are carried out, energy and exergy analyzes of the system must be carried out. In this context, the mass, energy, and exergy balance equations of all equipment in the subsystems that make up the system can be written as follows, respectively (Bejan et al., 1995):

$$\sum \dot{m}_{in} = \sum \dot{m}_{out} \tag{1}$$

$$\dot{Q}_{in} + \dot{W}_{in} + \sum \dot{E}_{in} = \dot{Q}_{out} + \dot{W}_{out} + \sum \dot{E}_{out} \tag{2}$$

$$\sum \dot{m}_{in} ex_{in} + \dot{E}x_{Q_{in}} + \dot{E}x_{W_{in}} = \sum \dot{m}_{out} ex_{out} + \dot{E}x_{Q_{out}} + \dot{E}x_{W_{out}} + \dot{E}x_{d} \tag{3}$$

Electrical power generated from the wind turbine can be obtained from the following equation (Ishaq and Dincer, 2020):

$$\dot{E}_{wt} = \frac{1}{2} \eta_{wt} \rho_{air} V_w^3 A_{wt} C_{p,wt} \tag{4}$$

In the developed system, exergy efficiency, waste exergy ratio, exergy recoverability ratio, exergy destruction ratio, environmental effect factor and exergetic sustainability index were taken into account as exergetic sustainability indicators. Detailed information about these indicators is given in previous studies (Inac et al., 2020, Midilli and Dincer, 2009).

IV. Results and discussions

Fig. 2. shows the change in system exergetic sustainability indicators as a function of PEM electrolyzer capacity.

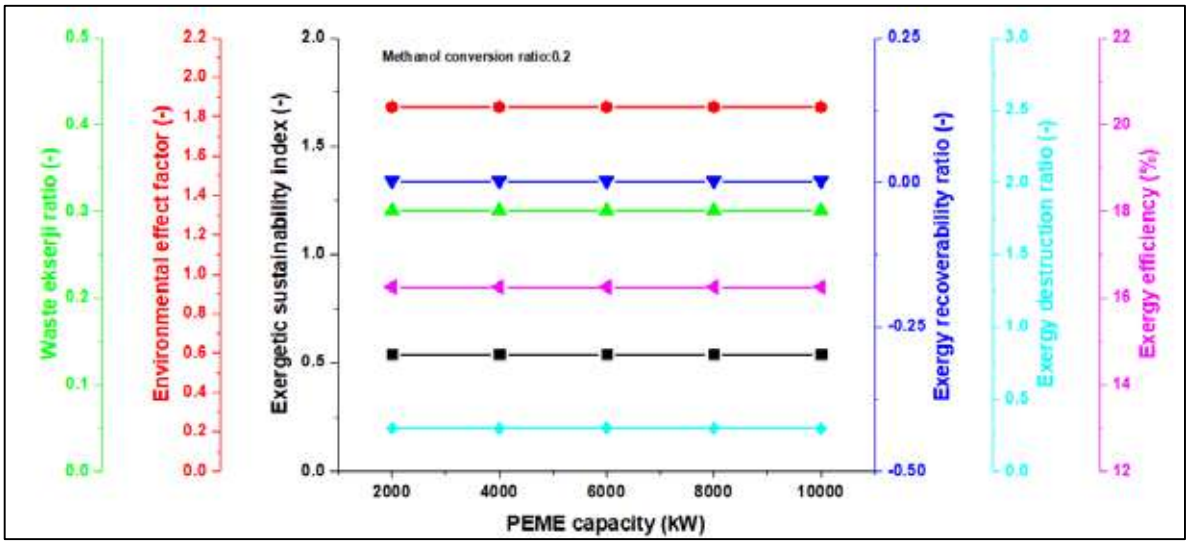


Fig. 2: The change of system exergetic sustainability indicators with PEM electrolyzer capacity.

V. Conclusions

In this parametric study, the methanol conversion ratio was taken to be 0.2. Fig. 2. illustrated that when the PEM electrolyzer capacity increases, there is slightly change in the exergetic sustainability indicators of the system. This is because the amount of methanol produced from the system depends on the amount of hydrogen obtained from the PEM electrolyzer.

Acknowledgements

We would like to thank Dogus University and Istanbul Technical University in Turkey for their support of this study.

References

Bellotti D, Cassettari L, Mosca M, Magistri L. RSM approach for stochastic sensitivity analysis of the economic sustainability of a methanol production plant using renewable energy sources. J Clean Prod, 240,117947 (2019).

Bejan, A., Tsatsaronis, G., Moran, M. J., Thermal design and optimization. John Wiley & Sons, (1995).

Bozoglan, E., Midilli, A., Hepbasli, A., Sustainable assessment of solar hydrogen production techniques. Energy, 46(1), 85-93, (2012).

Huang, Y., Zhu, L., He, Y., Wang, Y., Hao, Q., Zhu, Y., Carbon dioxide utilization based on exergoenvironmental sustainability assessment: A case study of CO2 hydrogenation to methanol. Energy, 273, 127219, (2023)

Ishaq, H., Dincer, I., Evaluation of a wind energy based system for co-generation of hydrogen and methanol production, Int. J. Hydrogen Energy 45, 15869–15877, (2020).

Inac, S., Unverdi, S. O., Midilli, A., Global warming, environmental and sustainability aspects of a geothermal energy based biodigester integrated SOFC system. International Journal of Hydrogen Energy, 45(60), 35039-35052, (2020)

Inac, S., Midilli, A., The integrated hydro-solar e-fuel production for a tea factory: Preliminary design and thermodynamic analysis. International Journal of Hydrogen Energy, In press, (2024).

Midilli A, Dincer I., Development of some exergetic parameters for PEM fuel cells for measuring environmental impact and sustainability. Int J Hydrogen Energy ,34, 3858-72, (2009).

Nazerifard, R., Khani, L., Mohammadpourfard, M., Mohammadi-Ivatloo, B., Akkurt, G. G., Design and thermodynamic analysis of a novel methanol, hydrogen, and power trigeneration system based on renewable energy and flue gas carbon dioxide. Energy Conversion and Management, 233, 113922, (2021).

Ni-Modified Self-Assembled Monolayer Films of Bingöl Pollen on Copper Substrate as a Novel Anode Catalyst for Methanol Electrooxidation Reaction

[1,2*] Yeşim Aydın Dursun, [2*] Ramazan Solmaz
[1] Bingöl University, Science and Letters Faculty, Chemistry Department Bingöl, Türkiye
[2] Bingöl University, Health Sciences Faculty, Occupational Health and Safety Department, 12000, Bingöl, Türkiye

[*] e-mail: yesimaydindursun@gmail.com; rsolmaz@bingol.edu.tr; rsolmaz01@gmail.com

Abstract
In this study, a natural film of Bingöl pollen extract (BPE) was prepared on a Cu substrate (Cu/BPE-SAM) as an anode for direct methanol fuel cells (DMFC). The surface of the film was modified by electrochemical deposition of a small amount of Ni (Cu/BPE-SAM/Ni) to further enhance the electrocatalytic activity of the electrode. The methanol electrooxidation activity of the modified electrode was carried out in 0.1 M KOH solution containing 1 M CH_3OH using electrochemical techniques. The surfaces of the electrodes were characterized using scanning electron microscopy (SEM). Compared to Cu, the peak current density of methanol oxidation increased from 21.33 mA cm^2 to 41.54 mA cm^2 at the Cu/BPE-SAM electrode and to 44.51 mA cm^2 at the Cu/BPE-SAM/Ni electrode. The enhanced activity at the BPE-SAM modified surface was associated with the enhanced real surface area and charge transfer capaility of the film. Moreover, the Ni-mofied electrode showed better activity due to the good intsic activity of the metal. It was concluded that the BPE-SAM demonstrates significant potential as an effective support material for the electrooxidation of methanol, thus offering promising prospects in fuel cell technology.

Keywords: Fuel Cell, Ni-modified, Self-Assembled Monolayer, Pollen

I. Introduction

From the past to the present, humans have required energy to meet many of their needs, and this energy has typically been derived from fossil fuels. The rapid depletion of fossil fuel resources, coupled with increasing industrialization and population growth, has accelerated research into new and renewable energy sources (Kivrak and Ulas, 2017). To effectively utilize renewable energy sources, there is a need to develop environmentally friendly and highly efficient energy conversion devices. Fuel cells are environmentally friendly devices with high energy conversion efficiency that convert chemical energy into electrical energy [Zhu, 2020].

Fuel cells come in many varieties, with DMFCs being the most preferred type. The advantages of using DMFCs can be attributed to their high power density, ease of use and portability (Zhang, 2016). DMFCs are electrochemical cells that require electrocatalysts for oxygen reduction at the cathode and fuel oxidation at the anode (Huang and Wang, 2014). Various catalysts are employed to enhance the kinetics of methanol oxidation. Although Pt is the most active electrocatalyst in methanol electrooxidation, its use is limited due to disadvantages such as high cost, limited availability, and susceptibility to poisoning by products such as CO (Yüce and Ark, 2013; Li et al., 2018; Baştürk et al., 2019; Abdel-Karim et al., 2018).

The literature shows that these disadvantages can be eliminated with many anode materials that have been developed and reported. Self-assembled monolayer films (SAM) can also be used for this purpose. (Prashar, 2012; Zhang et al., 2017). Recently, it was noted that the enhancement of Cu with Ni-modified rhodanine-SAM film could enhance the rate of the methanol electrooxidation reaction (Salcı et al., 2019). The beneficial effect of this metal-organic composite film can be attributed to the presence of active sites in rhodanine and the high electrocatalytic activity of Ni.

The good charge transfer effect of organic products may be due to the fact that they contain multiple bonds and active centers. In our previous studies, we indicated that mounting Sivan MM-SAM on the Cu surface increased the anodic activity for alcohol oxidation (Dursun and Solmaz, 2022). In this study, the BPE-SAM films were deposited on Cu substrate and modified with a small amount of Ni to enhance the methanol oxidation performance of the electrocatalyst. Bee pollen is rich in healthy components such as phenolic compounds, nutrients, amino acids, vitamins, proteins and fatty acids (Li et al., 2018; Xi et al., 2018; Dursun, et al., 2024). Therefore, the green BPE-SAM film can be safely used for the practical applications.

The main objective of this study was to prepare metal-organic multilayer coatings from natural products for the methanol electrooxidation reaction. Electrochemical experiments were conducted in a 0.1 M KOH solution containing 1 M CH_3OH. The modified electrodes were characterized by SEM.

II. Experimental Set-up and Procedure

A Cu substrate was used for the film modification. The BPE-SAM film was prepared on the Cu substrate as described earlier (Dursun and Solmaz, 2024; Solmaz et al., 2024; Salcı and Solmaz, 2019). The solution for film formation was sealed to prevent air exposure and passed through with pure nitrogen gas. After polishing and cleaning the Cu substrates, they were immersed in a 1000 ppm BPE aqueous solution for 24 hours. Following the film formation, the electrodes were cleaned with the same solution, and dried was achieved with nitrogen gas. For Ni-modification, a special deposition bath containing 1% $NiCl_2.6H_2O$ was prepared. A galvanostatic deposition process was performed to deposit 1 mg/cm^2 Ni at 5 mA cm^{-2}.

The surface characterization was conducted using SEM technique. The catalytic activity of the modified electrode was investigated in a 0.1 M KOH solution containing 1 M CH_3OH by cyclic voltammetry (CV). The electrochemical performance of the electrode was studied using electrochemical studies. A Pt sheet with a surface area of 2 cm^2 was used as the counter electrode, while an Ag/AgCl (3 M KCl) electrode was used as the reference electrode.

III. Results and discussions

Figure 1 shows the SEM image of the Cu/BPE-SAM/Ni surface. The SEM image demonstrates the homogeneous distribution of the BPE-SAM film on the Cu substrate. Island-like and almost uniformly distributed Ni deposits are observed on the top layer of the SAM-modified Cu. These deposits exhibit strong adhesion to the surface, which is beneficial for the physical stability and electrochemical durability of the electrode.

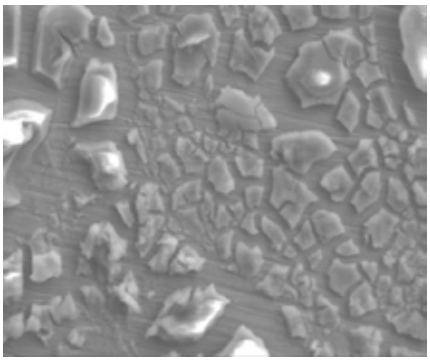


Fig.1. SEM image of the Cu/BPE-SAM/Ni surface

The electrooxidation activity of the modified electrode was examined in a 0.1 M KOH solution containing 1 M CH_3OH by CV) technique. In order to compare the CVs of the same electrodes, measurements were also conducted in the alkaline solution without CH_3OH. The data obtained at uncoated Cu electrode are shown in Fig. 2a. A peak at 0.874 V was observed in the presence of CH_3OH, which is attributed to alcohol oxidation. The current density of this peak was 2.13 mA cm^{-2}. In Fig. 2b, the methanol oxidation behavior of the modified Cu/BPE-SAM/Ni electrode was compared with that of the bare Cu and BPE-SAM modified Cu electrodes. The BPE-SAM modification leads to an increase in the electroactivity of the substrate. A significant enhancement in the alcohol oxidation performance of the Ni-modified electrode was observed. The peak current densities of Cu/BPE-SAM and Cu/BPE-SAM/Ni electrodes increased from 2.13 mA cm^{-2} to 4.06 mA cm^{-2} and 4.32 mA cm^{-2}, respectively. The increase in the real surface area, the presence of active centers, and Ni islands serving as catalytic centers on the surface can explain the increase in the activity.

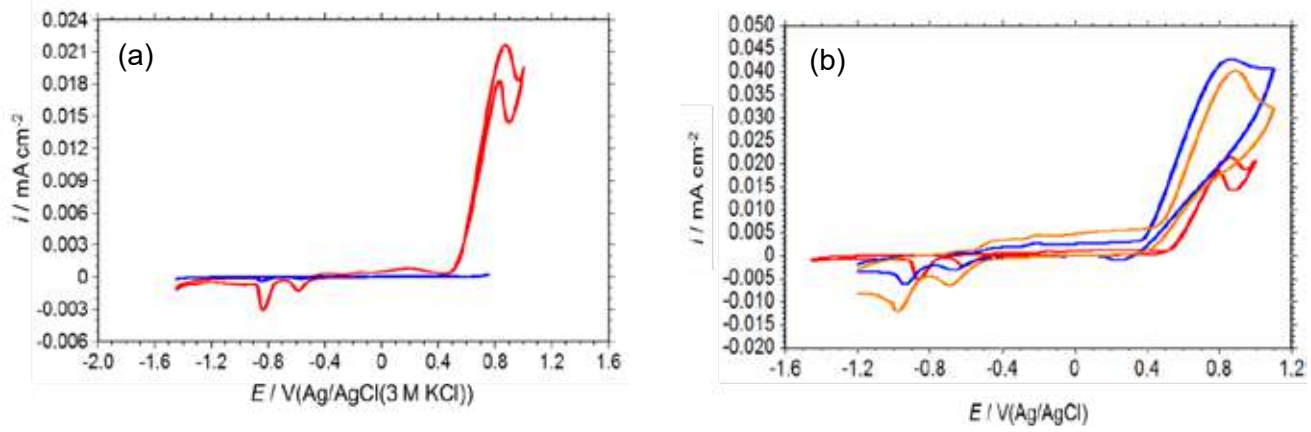


Fig. 2. CVs of bare Cu in 0.1 M KOH solution in the absence (—) and presence (—) of 1M CH_3OH (a). Comparison of methanol oxidation activities of bare Cu (—), BPE-SAM coated Cu (—) and BPE-SAM/Ni coated Cu (—) electrodes under identical idential conditions (b) (scan rate: 100 mV s^{-1})

IV. Conclusions

An organic-metal multilayer of BPE-SAM/Ni was prepared on a Cu substrate. The film was characterized by SEM technique. The methanol electrooxidation activity of the electrode was investigated in a 0.1 M KOH solution containing 1 M CH_3OH. The key points of the study are summarized below.

- A uniform and tightly bonded BPE-SAM film was successfully formed on the Cu substrate.
- Homogeneously dispersed Ni island-like structures were electrochemically deposited on the BPE-SAM film.

- The BPE-SAM film can also be utulized for decorative purposes due to its good appearence.
- The modification of Cu surface with the BPE-SAM film enhances the electrocatalytic activity of the electrode. However, the deposition of 1 mg cm^{-2} Ni on the film significantly enhances the rate of the methanol electrooxidation reaction.
- While the focus of this study was primarily on the enhanced electrocatalytic activity achieved through the deposition of Ni on the BPE-SAM film, future research will address into the stability of the electrode as well as potential poisoning effects that may arise during electrochemical reactions.

Acknowledgements
The authors are greatly thankful to Bingöl University, Health Sciences Faculty, Occupational Health and Safety Department for conducting the electrochemical experiments and to the Bingöl University Central Laboratory for performing the characterization measurements. Some data were obtained by developing the outputs of 2017K124000-BÜBAP and PİKOM-Arı.2018.006 projects data. We would like to thank Bingöl University Scientific Research Projects Coordination Unit and project team.

References

Abdel-Karim R., Ramadan M., El-Raghy S. M. Morphology and Electrochemical Characterization of Electrodeposited Nanocrystalline Ni-Co Electrodes for Methanol Fuel Cells. *Journal of Nanomaterials*, 1–13, (2018).

Dursun Y.A., Solmaz R., Take your energy using servi dut pekmezi (mulberry molasses): A novel electroactive film for water electrolysis, 23rd World Hydrogen Energy Conference (WHEC2022) Proceedings Book, 62, June 26-30, İstanbul, Türkiye, (2022).

Baştürk F., Yüksel H., Solmaz R. Fabrication of three-dimensional copper nanodomes as anode materials for direct methanol fuel cells. International Journal of Hydrogen Energy, 44(27), 14235-14242, (2019).

Dursun Y.A., Solmaz R. Fabrication of Bingöl pollen self-assembled monolayer films on copper as a novel cathode for electrochemical hydrogen production. *International Journal of Hydrogen Energy*, *52*, 1280-1290, (2024).

Dursun İ., Felek İ., Çobanoğlu D. N. Analyzing the antioxidant activity and fatty acid composition of monofloral mullein (Verbascum sp.) pollen oil obtained via various extraction techniques. Chemistry & Biodiversity, e202400117, (2024).

Huang H., Wang X.. Recent progress on carbon-based support materials for electrocatalysts of direct methanol fuel cells. Journal of Materials Chemistry A, 2 (18): 6266-6291, (2014).

Li J., Rong H., Tong X., Wang P., Chen T., & Wang Z. Platinum–silver alloyed octahedral nanocrystals as electrocatalyst for methanol oxidation reaction. J*ournal of colloid and interface science*, 513, 251-257, (2018).

Li, Q. Q., Wang, K., Marcucci, M. C., Sawaya, A. C. H. F., Hu, L., Xue, X. F., ..., Hu, F. L. Nutrient-rich bee pollen: A treasure trove of active natural metabolites. Journal of Functional Foods, 49, 472-484, (2018)

Kivrak H., Ulas, B. Doğrudan metanol yakıt pili karbon destekli pt-ru anot katalizörlerinin sıralı indirgeme yöntemi ile sentezi ve geliştirilmesi. *Journal of the Institute of Natural & Applied Sciences*, 22(1), 21-32, (2017).

Prashar D. Self assembled monolayers-a review. *International Journal of ChemTech Research*, 4(1), 258-265, (2012).

Salcı A, and Solmaz R. Hydrogen Evolution Reaction Activity of Rhodanine Self Assembled Monolayer Films. 4th International Hydrogen Technologies Congress, Proceedings Book, 192-195 pp., Edirne, Türkiye (2019).

Salcı A., Şahin E.A., Solmaz R., Methanol electrooxidation at nickel-modified rhodanine self-assembled monolayer films: A new class of multilayer electrocatalyst, International Journal of Hydrogen Energy 44:14228-34 – 404, (2019).

Solmaz R., Dursun Y.A, Şahin E.A., Geçibesler İ.H., Doğrubaş M., Tunç M.,…, Kardaş G. Bingöl propolis self-assembled monolayer films: Preparation, characterization and application as corrosion inhibitors for copper protection in NaCl environment. Materials Chemistry and Physics, 315, 128956, (2024).

Xi, X., Li, J., Guo, S., Li, Y., Xu, F., Zheng, M., ..., Han, C., The potential of using bee pollen in cosmetics: a review. Journal of Oleo Science, 67(9), 1071-1082, (2018).

Yüce A. O., Döner, A., Kardaş, G. NiMn composite electrodes as cathode material for hydrogen evolution reaction in alkaline solution. *International journal of hydrogen energy*, 38(11), 4466-4473, (2013).

Zhang X., Zhu J., Tiwary C.S., Ma Z., Huang H., Zhang J., ... & Wu Y. Palladium nanoparticles supported on nitrogen and sulfur dual-doped graphene as highly active electrocatalysts for formic acid and methanol oxidation. ACS applied materials & interfaces, 8 (17): 10858-10865, (2016).

Zhang B., Feng, H., Lin, F., Wang, Y., Wang, L., Dong, Y., & Li, W. Superhydrophobic surface fabricated on iron substrate by black chromium electrodeposition and its corrosion resistance property. *Applied Surface Science*, 378, 388-396, (2017).

Zhu, B., Raza, R., Fan, L., and Sun C. “Solid Oxide Fuel Cells" Energy, (2020).

Electrochemical Hydrogen Production Activity of Self-Assembled Monolayer Film Prepared from Bingöl Walnut Leaf Extract on Copper Surface

[1,2*] Yeşim Aydın Dursun, [2*] Ramazan Solmaz
[1] Bingöl University, Science and Letters Faculty, Chemistry Department Bingöl, Türkiye
[2] Bingöl University, Health Sciences Faculty, Occupational Health and Safety Department, 12000, Bingöl, Türkiye

[*] e-mail: yesimaydindursun@gmail.com; rsolmaz@bingol.edu.tr; rsolmaz01@gmail.com

Abstract
In this study, self-assembled monolayer thin films (SAM) of walnut leaf extract (WLE) were spontaneously assembled on a copper surface (Cu/WLE-SAM). The walnut leaves were collected from Bingöl province. The presence of adsorption active centers, such as S, N, and O in the chemical structure of these natural product provides an advantage for surface binding. The films were assembled in methanol solvent containing 1000 ppm Bingöl WLE for 24 hours to be attached to the Cu surface. The Cu/WLE-SAM was employed as cathode for the electrochemical production of hydrogen in a 6 M KOH solution at 298 K. Subsequently, 1 mg of Ni was deposited onto the prepared electrode, and it was observed that the resulting CY-SAM/Ni films effectively adhered to the Cu surface and exhibited remarkable stability during the electrochemical process. It was deduced that the CY-SAM/Ni modified electrode facilitates hydrogen gas production and functions as a suitable metal-organic substrate for cathode manufacturing.

Keywords: Hydrogen Production, Self-Assembled Monolayer Films, Walnut Leaf, Ni deposition

I. Introduction

Hydrogen, as a clean energy carrier, has the potential to replace hydrocarbons and plays a significant role in sustainable energy systems (Shih and Haile, 2022). The electrolysis of water has become very popular for many researchers as an ideal hydrogen production method (Li et al., 2020; Zhang et al., 2021; Xie et al., 2022). However, the slow reaction kinetics and the presence of excessive overpotential lead to an increase in the cost of hydrogen gas production (Wang et al., 2020). Therefore, it is necessary to improve electrocatalysts with high stability and activity. The most electroactive for water electrolysis is Pt. However, the limited reserves of Pt and its high cost restrict its practical usage (Li et al., 2018; Deng e tal., 2019; Qian et al., 2021). Therefore, it is necessary to produce electrochemically active electrodes having low hydrogen overpotential, large surface area, high stability, and low cost. Cu, which has high thermal and electrical conductivity, is preferred in many fields (Bi et al., 2016). However, the corrosion of Cu limits its usage as an electrocatalyst in many environments. Therefore, the corrosion resistance of Cu in alkaline and acidic solutions needs to be enhanced.

Modifying metal surfaces with an organic film can improve the stability and corrosion resistance of Cu. Simultaneously, the prepared surface film should not reduce the electrocatalytic activity of the elecytrode. To address these issues, self-assembled monolayer films (SAM) with nano-scale dimensions and electroactive properties can be employed to modify Cu surface. The highly adhesive surface films are generally stable and can be modified by metal modifications (Dursun and Solmaz, 2024). Studies have reported that SAM films, facilitate charge transfer at the metal/solution interface and enhance the rate of hydrogen gas evolution (Dursun and Solmaz, 2024; Solmaz et al., 2024; Salcı and Solmaz, 2019). Walnut leaves have been reported to possess anticancer, antioxidant, and antifungal efficacy. Juglone (5-hydroxy-1,4-naphthoquinone) has been identified in fresh walnut leaves. Therefore the extarcts of this natural product can be safely used as a green film (Ara et al., 2023).

In this study, SAM films of walnut leave extrcats (Bingöl walnut leaf, WLE) were assembled on a Cu surface in methanol solvent containing 1000 ppm Bingöl WLE for 24 hours (Cu/WLE-SAM). In the second stage, the surface of SAM film was modified by elecrodeposition of small amount of Ni (Cu/WLE-SAM/Ni). Cu/WLE-SAM and Cu/WLE-SAM/Ni electrodes were applied as cathode materials in 6 M KOH solution at 298 K to test their electrocatalytic activies for water splitting. For this aim, potentiodynamic polarization and electrochemical impedance spectroscopy (EIS) measurements. Surface characterization studies of the electrodes were performed using as scanning electron microscopy (SEM), atomic force microscopy (AFM) and energy dispersive X-ray spectroscopy (EDX).

II. Experimental Set-up and Procedure

WLE-SAM films were prepared on the Cu surface in methanol as solvent. The WLE concentration in methanol was 1000 ppm, and the metal was exposed to this solution at room temperature for 24 hours for film formation as previously described (Dursun and Solmaz, 2024; Solmaz et al., 2024). After the film formation, the electrode was removed from the solution, cleaned with the same solvent, dried with nitrogen gas, and stored in a desiccator until used in experiments. The structure of the WLE-SAM/Ni film surfaces were examined using SEM, AFM and EDX techniques.

The electrochemical activity of the electrodes for hydrogen gas production was investigated using EIS and potentiodynamic polarization techniques in 6 M KOH solution at 298 K. The electrochemical experiments were performed using a three-electrode CHI electrochemical analysis device. Polarization studies were conducted

between -1.8 V and the open-circuit potential (E_{ocp}). The frequency range was between 100 kHz and 0.1-0.01 Hz. A Pt plate with dimensions of 10mm x 10mm x 1mm was used as the counter electrode, and an Ag/Ag/AgCl (3 M KCl) electrode was used as the reference electrode.

III. Results and discussions

Fig. 1 displays the SEM, AFM, and EDX spectrum of the electrode surface modified with WLE-SAM/Ni. The SEM and AFM images demonstrate the homogeneous distribution of the WLE-SAM/Ni film on the Cu surface. Obviously, a homogenous and adherent film was formed on the surface. Ni particles were homogenously distributed on the previously assembled SAM film. Since pure Cu does not contain elements C, N, Ni, S, or O, the presence of these elements in the EDX spectrum indicates presence of WLE-SAM/Ni film. The uniformity of this film on the surface and enhanced surface area provide a significant advantage for the hydrogen gas production.

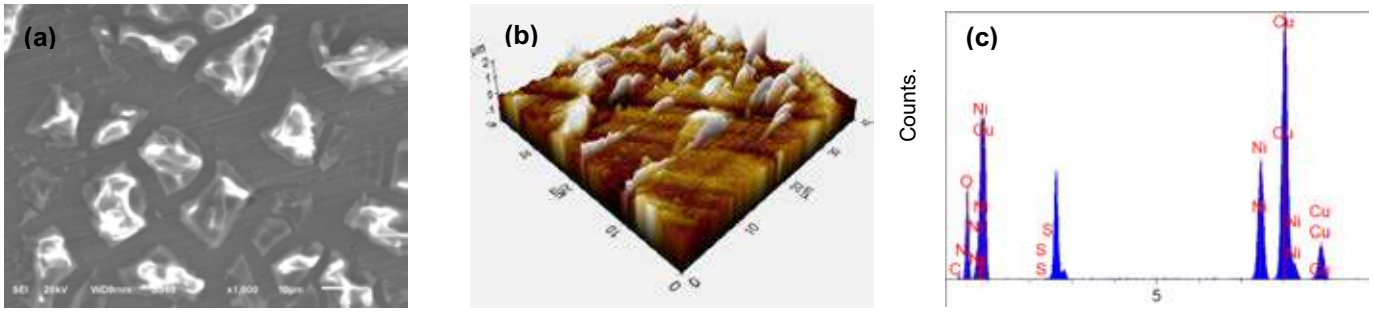


Fig.1. SEM (a), AFM (b), EDX spectrum (c) of the Cu/WLE-SAM/Ni surface

The water splitting activity of the Cu/WLE-SAM/Ni electrode was investigated in 6 M KOH solution at 298 K. For comparision the similar data of Cu and Cu/WLE-SAM elecrodes were also obtained and presented. EIS and semi-logarithmic current-potential curves of the electrodes were presented in Fig. 2. A comparison between uncoated Cu and WLE-SAM modified electrodes reveals that in (Fig. 2a), the higher current density, namely the rate of hydrogen gas evoluiiton was significantly enhanced at a certain overpotential in the case of the Cu/WLE-SAM/Ni electrode. This means that the Cu/WLE-SAM/Ni modified electrode requires less energy for hydrogen gas production compared to the other electrodes. This increased activity suggests can be assigned to the facilitaded charge transfer activity of the film, high intrinsic activity of Ni and large surface area (Dursun and Solmaz, 2024; Solmaz et al., 2024).

The similar results were supported by the EIS studies. The corresponding Nyquist plots of the same electrodes are shown in Fig. 2b. As seen from Fig. 2b, the resistance corresponding to the charge transfer resistance at the metal/solution interface reduced after assembling WLE-SAM film on the metal. The decrease in the charge transfer resistance indicates a facilitated reaction with lower resistance. However, modifying the surface with a small amount of Ni further enhances the hydrogen evolution activity of the electrode. This means that a lower energy is required to produce the same amount of hydrogen gas production in the case of Cu/WLE-SAM/Ni electrode compared to the Cu and WLE-SAM electrodes (Dursun and Solmaz, 2024; Solmaz et al., 2024).

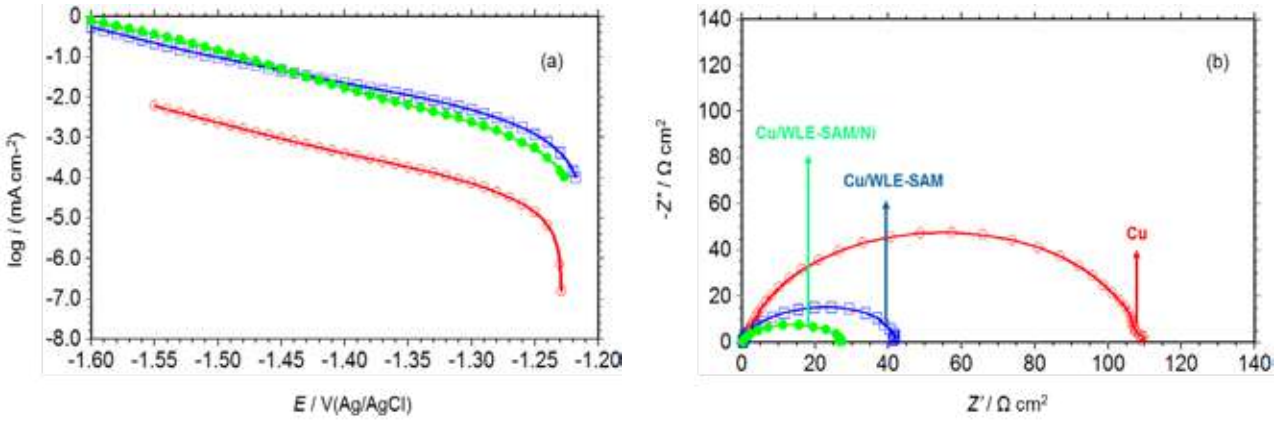


Fig. 2. Semi logarithmic current-potential curves (a) Nyquist plots (b) and of Cu, Cu/WLE-SAM and Cu/WLE-SAM/Ni electrodes obtained in 6 M KOH solution at 298 K

IV. Conclusions

WLE-SAM films were assembled on a Cu surface in methanol solvent containing 1000 ppm Bingöl WLE for 24

hours. Then, the surface of WLE-SAM was modified by elecrodeposition of small amount of Ni. Cu/WLE-SAM and Cu/WLE-SAM/Ni electrodes were applied as cathode materials in 6 M KOH solution at 298 K to test their electrocatalytic activies for water splitting using electrochemical techniques. Their surface structures were analysed by SEM, AFM and EDX. The key points of the study can be summarized as follows:

- WLESAM and WLE-SAM/Ni films were uniformly prepared on Cu.
- The films were adhered to the metal surface and was stable.
- The modification of Cu with WLE-SAM enhances water splitting activity of the electrode in 6 M KOH solution. However, deposition of small amount of Ni further enhances the rate of hydrogen evolution performance of the electrode.
- Current densities are higher and charge transfer resistance corresponding to the rate of hydrogen evolution reaction was lower at the Cu/WLE-SAM/Ni electrode at a specific potential.
- The study will be further elaborated in the next studies.

Acknowledgements
The authors are greatly thankful to Bingöl University, Health Sciences Faculty, Occupational Health and Safety Department for conducting the electrochemical experiments and to the Bingöl University Central Laboratory for performing the characterization measurements.

References

Ara, T., Shafi, S., Ghazwani, M., Mir, J. I., Shah, A. H., Qadri, R. A., ..., Wahab, S. In vitro potent anticancer, antifungal, and antioxidant efficacy of Walnut (Juglans regia L.) Genotypes. *Agronomy*, *13*(5), 1232 (2023).

Bi, J., Yao, L., Ao, J., Gao, S., Sun, G., He, Q., ... & Zhang, Y. Pulse electro-deposition of copper on molybdenum for Cu (In, Ga) Se2 and Cu2ZnSnSe4 solar cell applications. Journal of Power Sources, 326, 211-219 (2016).

Deng, S., Zhang, K., Xie, D., Zhang, Y., Zhang, Y., Wang, Y., ..., Tu, J. High-index-faceted Ni 3 S 2 branch arrays as bifunctional electrocatalysts for efficient water splitting. *Nano-Micro Letters*, *11*, 1-12 (2019).

Dursun, Y.A., Solmaz, R. Fabrication of Bingöl pollen self-assembled monolayer films on copper as a novel cathode for electrochemical hydrogen production. *International Journal of Hydrogen Energy*, *52*, 1280-1290 (2024).

Li, J., Xu, W., Luo, J., Zhou, D., Zhang, D., Wei, L., ..., Yuan, D. Synthesis of 3D hexagram-like cobalt–manganese sulfides nanosheets grown on nickel foam: a bifunctional electrocatalyst for overall water splitting. *Nano-micro letters*, *10*, 1-10 (2018).

Li, X., Zhao, L., Yu, J., Liu, X., Zhang, X., Liu, H., & Zhou, W. Water splitting: from electrode to green energy system. *Nano-Micro Letters*, *12*, 1-29 (2020).

Qian, G., Chen, J., Yu, T., Luo, L., …, Yin, S. N-doped graphene-decorated NiCo alloy coupled with mesoporous NiCoMoO nano-sheet heterojunction for enhanced water electrolysis activity at high current density. *Nano-micro letters*, *13*, 1-13 (2021).

Solmaz R., Dursun Y.A., Şahin E.A., Geçibesler İ.H., Doğrubaş M., Tunç M.,…, Kardaş G. Bingöl propolis self-assembled monolayer films: Preparation, characterization and application as corrosion inhibitors for copper protection in NaCl environment. Materials Chemistry and Physics, 315, 128956 (2024).

Salcı A, and Solmaz R. 2019. Hydrogen Evolution Reaction Activity of Rhodanine Self Assembled Monolayer Films. 4th International Hydrogen Technologies Congress, Proceedings Book, 192-195 pp., Edirne, Türkiye.

Shih, A. J., & Haile, S. M. Electrifying membranes to deliver hydrogen. *Science*, *376*, 6591, 348-349 (2022).

Wang, J., Yue, X., Yang, Y., Sirisomboonchai, S., Wang, P., Ma, X., ..., Guan, G. Earth-abundant transition-metal-based bifunctional catalysts for overall electrochemical water splitting: A review. Journal of Alloys and Compounds, 819, 153346, (2020).

Xie, H., Zhao, Z., Liu, T., Wu, Y., Lan, C., Jiang, W., …, Shao, Z. A membrane-based seawater electrolyser for hydrogen generation. *Nature*, *612*(7941), 673-678 (2022).

Zhang, X., Zhang, M., Deng, Y., Xu, M., Artiglia, L., Wen, W., …, Ma, D. A stable low-temperature H2-production catalyst by crowding Pt on α-MoC. *Nature*, *589*(7842), 396-401 (2021).

Advancing Power System Reliability with AI-Driven Monte Carlo Simulations for Hydrogen Fuel Cell Integration

[1*]Dogan Urgun and [2]Gokhan Gungor
[1] Department of Electrical and Electronics Engineering, Karabük University, Karabük, Türkiye
[2] Department of Mechatronics Engineering, Karabük University, Karabük, Türkiye

* E-mail:durgun@karabuk.edu.tr

Abstract
This paper presents an advanced method for evaluating the reliability of hydrogen-integrated composite power systems using AI-optimized Sequential Monte Carlo simulations. Traditional reliability assessment techniques have not adequately investigated the complexities of integrating hydrogen technologies in power systems. Our approach utilizes artificial intelligence to enhance the computational efficiency of Monte Carlo simulations, making detailed reliability studies more feasible and economically viable. We integrate deep learning techniques to streamline the computational process, focusing on the critical integration of hydrogen technologies for sustainable energy solutions. The effectiveness of this method is demonstrated through various case studies and comparisons with traditional methods, showing significant improvements in computational speed without compromising accuracy.

Keywords: Composite Power System Reliability Evaluation, Hydrogen Fuel Cell Integration, Deep Learning, Sequential Monte Carlo Simulation

I. INTRODUCTION

Hydrogen serves as a clean energy source, offering a potential solution to the worldwide energy shortage and environmental degradation. Recent advancements in hydrogen production, transmission, and storage technologies have enhanced their applications in decarbonizing the power and energy sectors (Veziroğlu et al., 2019). Unlike renewable energy sources like wind and solar, which are subject to fluctuations, hydrogen technology, such as fuel cells, offers a reliable and almost carbon-free power supply. Furthermore, excess renewable electricity is converted into hydrogen via water electrolysis and stored in various forms like salt caverns or compressed tanks, facilitating flexible energy storage and release to enhance renewable energy system efficacy. Integrating renewable power sources with hydrogen technologies is essential to achieving a carbon-neutral future (Dincer and Acar, 2015). The development of hydrogen-based power systems has garnered significant attention in recent research due to their potential environmental benefits. Recent studies have explored various applications and benefits of these systems. Notably, hydrogen storage stations are being explored for their potential to enhance the capacity of power systems and provide essential services like demand response and power regulation. Khani et al. (2019) discussed how these stations could optimize hydrogen storage scheduling to support fuel supply and capacity-based demand response under dynamic pricing conditions. Pan et al. (2020) developed a long-term planning model for an electricity-hydrogen-integrated energy system that includes power-to-hydrogen-and-heat (P2HH) devices and seasonal hydrogen storage. Khan et al. (2023) introduces a techno-economic analysis and predictive operation framework for Power-to-Hydrogen systems within renewable microgrids, aiming to optimize power flow and operational costs through advanced mathematical solutions and AI-driven forecasting models. Ramesh et al. (2023) examined the integration of artificial intelligence in hydrogen and battery technologies, highlighting how AI enhances hydrogen production, storage, transportation, smart battery manufacturing, and optimization.

Based on available research, the aspect of reliability in hydrogen-integrated composite power systems has not been thoroughly investigated. Despite the crucial role that reliability plays in ensuring these systems have adequate generation capacity to meet energy demands, the field remains underexplored. Existing studies on this topic are relatively few and tend to focus on narrow aspects of the subject (Chen et al., 2022). This observation highlights a significant research gap and underscores the urgent need for more comprehensive investigations into the reliability of these power systems. In addressing this gap, it is crucial to recognize that traditional random Monte Carlo simulations, while popular for their broad applicability, do not suit the specific demands of hydrogen-based systems due to their inability to capture the sequential dependencies and complexities inherent in such systems. Instead, Sequential Monte Carlo simulations, which are more adept at handling these complexities, are required. However, the transition to Sequential Monte Carlo simulations introduces a significant challenge due to their extensive computational demands (Shu et al., 2014). Considerable effort has been dedicated to increasing the computational efficiency of MCS methods in the reliability analysis of large power systems. Techniques such as variance reduction, state space pruning, and more efficient sampling techniques like Importance Sampling (IS) or Latin Hypercube Sampling (LHS) have been explored. Furthermore, approaches like fuzzy optimal power flow and population-based intelligence search (PIS) methods have been utilized to refine the search for meaningful states, thus enhancing computational efficiency. Pattern

classification techniques, such as those using Least Squares Support Vector Machines (LSSVM) and Artificial Neural Networks (ANN), have become pivotal in reducing the computational load by effectively characterizing system states before conducting detailed power flow analysis (Pindoriya et al., 2011). These techniques have proven effective in decreasing the number of states needing evaluation, thus reducing the overall computation time (Singh and Wang, 2008). While these advancements have enhanced the efficiency of simulations, the accuracy of state classification and the flexibility of models remain areas needing improvement, particularly when adapting these techniques to the specific complexities of hydrogen-integrated composite power systems. Building upon these established methods, this paper proposes the integration of artificial intelligence to further enhance the computational processes in Sequential Monte Carlo simulations, specifically tailored to the reliability studies of hydrogen-integrated systems. By employing AI for algorithm optimization and process simplification, we aim to significantly reduce the computational costs associated with these simulations. This approach not only makes detailed and accurate simulations more feasible but also contributes to more cost-effective and sustainable research practices. Ultimately, the goal is to ensure that hydrogen power systems are not only economically viable but also reliably meet energy demands. The main contributions of this paper are as follows: i) introduction of AI-optimized Sequential Monte Carlo simulations designed explicitly for reliability assessments in hydrogen-integrated composite power systems, addressing complex system behaviors more effectively than traditional methods and ii) enhancement of computational efficiency through advanced AI techniques, significantly reducing the time and computational resources needed for detailed reliability simulations. The structure of this paper is organized as follows: Section II, "Methodology", offers a brief overview of the mathematical background of the proposed method. In Section III, the application steps of the proposed method are described. Section IV provides the results obtained from this study. The paper concludes with Section V.

II. METHODOLOGY

To enhance the computational efficiency of the power system reliability analysis, an artificial intelligence (AI) model, specifically a 1-dimensional Convolutional Neural Network (1-D CNN), was employed to pre-classify system states before applying the traditional Optimal Power Flow (OPF). This method leverages a Sequential Monte Carlo simulation to generate a robust dataset reflecting a diverse array of possible system states under varying operational conditions. The dataset was generated using a Sequential Monte Carlo simulation that meticulously accounts for the stochastic nature of power system components, including the operational uncertainties of generation units and the dynamic integration of hydrogen-based energy storage and generation systems. This simulation produced a multitude of system states, each annotated with operational parameters and the resultant need for OPF application. Each system state in the dataset is labelled as '0' Successful (no OPF intervention needed) or '1': Failure (requires OPF intervention). The 1-D CNN architecture is tailored for sequence data processing, making it ideal for time-series-like data encountered in power systems. The model comprises several convolutional layers that automatically detect patterns and features in the input data, crucial for making accurate predictions. The CNN model is trained on the labeled dataset using the loss function $L(y, y') = [y \log(y') + (1 - y) \log(1 - y')]$ where y is the true label, and y' is the predicted probability of the state, an adaptive learning rate optimization algorithm commonly used for training deep learning models, and metrics such as accuracy, sensitivity and specificity to evaluate performance of the proposed architecture. Once trained, the CNN model operates in real-time, classifying incoming sequences of system state data. If the model predicts a '0', the system bypasses the computationally intensive OPF process, directly enhancing efficiency. Conversely, a prediction of '1' triggers the application of OPF to ensure system reliability. The architecture of the 1-D CNN used in this study. The integration of hydrogen technologies into the power system simulation involves detailed modeling of hydrogen production (via electrolyzers), storage, and electricity generation (via fuel cells). These components are pivotal in our study for their role in enhancing grid stability and providing energy during demand peaks or renewable intermittency. Electrolyzers convert excess electricity into hydrogen when renewable energy production exceeds demand. The rate of hydrogen production H_{prod} by the electrolyzers is given by: $H_{prod} = \eta_{P2H} P_{excess}$ where η_{P2H} is the efficiency of the electrolyzer and P_{excess} is the excess power available from renewable sources. The hydrogen storage unit acts as a buffer to balance supply and demand for hydrogen. The change in stored hydrogen over time is modeled as $\Delta H_{storage} = H_{prod} - H_{used}$, $H_{min} \leq H_{storage} \leq H_{max}$ where H_{used} represents the hydrogen consumed by fuel cells to generate electricity. H_{min} and H_{max} are the minimum and maximum storage capacities, respectively. Fuel cells generate electricity by converting hydrogen back to electrical energy. The electric power output P_{FC} from the fuel cells is modeled as: $P_{FC} = \eta_{H2P} H_{used}$ where η_{H2P} is the conversion efficiency of hydrogen to power. The operational states of the hydrogen components are updated at each step in the Sequential Monte Carlo simulation to reflect real-time interactions and dependencies. The availability and operational status of each hydrogen component are determined based on a probabilistic model that considers typical failure rates and repair times, akin to other power system components. The probabilistic nature of component failures and repairs is captured through: $P_{fail} = 1 - e^{-\lambda}$, $P_{repair} = 1 - e^{-\mu t}$ where λ and μ represent the failure and repair rates, respectively, and t denotes time. At each time step, the overall system state, including the hydrogen subsystem, is classified as either successful or requiring OPF intervention based on the AI model's prediction. This classification effectively directs the simulation process, minimizing

unnecessary OPF computations. The introduction of an AI-based state classification system not only streamlines the process of determining the need for OPF but also quantifies the extent of computational savings. This section details the equations that model these processes. The AI model classifies system states based on a set of input features, X derived from the current operational data of the power system. The classification function, $f(X)$, outputs a binary decision, d, indicating whether the OPF should be executed: $d = f(X) = \begin{cases} 0 & if\ OPF\ not\ needed \\ 1 & if\ OPF\ needed \end{cases}$.

Here, X typically includes power generation levels, load demands, and the status of hydrogen storage and conversion units. The performance of our proposed method was evaluated using statistical metrics such as Sensitivity, Specificity, and Accuracy, which are derived from the concepts of True Positive (TP), False Positive (FP), True Negative (TN), and False Negative (FN). Here, 'True' and 'False' indicate whether the classification is correct, and 'Positive' or 'Negative' refers to the classifier's prediction. Sensitivity, which is the ratio of correctly predicted positive observations to all actual positives, helps gauge the method's efficiency in reducing the need for complete MCS computations. It is computed as follows: $Sensitivity = \frac{TP}{TP+FN}$. Specificity assesses the proportion of actual negatives that are correctly identified and is crucial for accurately estimating reliability parameters. It is defined as: $Specifidity = \frac{TN}{TN+FP}$. Accuracy measures the overall effectiveness of the classifier in identifying both positive and negative states accurately and is calculated by: $Accuracy = \frac{TP+TN}{Number\ of\ States\ Classified}$. Additionally, the performance in estimating the power system reliability indices was also examined through the Loss of Load Probability (LOLP), which represents the fraction of time the system is in a failure state relative to the total simulation time: $LOLP = \frac{Total\ Failure\ Time}{Simulation\ Time}$. These metrics collectively offer a comprehensive view of the classifier's performance in both computational efficiency and reliability prediction.

III. Application of Proposed Method

In a Sequential MCS, the system state is simulated over a sequence of time steps. Each power system component is represented using a Markov Model (MM). There are two primary methods to progress the simulation in time: using fixed time intervals or based on the next event. In this study, we employ the fixed time interval approach for Sequential MCS, which is outlined in the following steps: i) initialize the system with an assumption of all component states are up, then calculate a transaction probability matrix for the next state of each component, ii) determine the status of each generation unit in the next transaction then calculate the total generation for each bus of the system, iii) generate the system load level *L*, and iv) evaluate the reliability indices for current state. If the converging criteria are satisfied, stop the simulation; otherwise, go back to step 2. This study chooses the coefficient of variation (COV) for stopping criteria (for both training and testing stages) as it represents the estimated uncertainty. Instead of COV, a specified number of samples can be used as well. COV is explained in $\beta = \frac{\sqrt{V(E(F))}}{(E(F))}$ where $V(E(F))$ represents the variance of estimated value E(F). The performance of our proposed method is benchmarked against a Crude Monte Carlo Simulation (CMCS) to assess the effectiveness of our classifier. During the training phase, the CMCS runs until the coefficient of variation (COV) hits a 10% threshold. The states generated are logged and evaluated using OPF, with generation and load data consolidated into input vectors, and state outcomes labeled as 0 (success) or 1 (failure). For testing, Sequential MCS is utilized to simulate the power system until the COV reaches a 5% threshold. The classifier then determines the status of each system bus state. States identified as failures are subsequently analyzed via OPF. Ultimately, a comparison is drawn between the results from the CMCS and those from the proposed method. A comprehensive schematic of the proposed method is illustrated in Fig. 1.

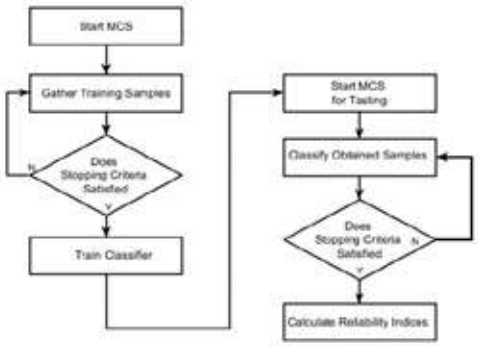


Fig. 1: General diagram of the proposed CNN architecture

IV. RESULTS

The proposed method is applied to the IEEE RTS test system (RTS) which has 24 buses (10 of them are generation buses), 38 transmission lines and 32 generation units. The total installed capacity is 3405 MW and the system has 2850 MW at annual peak. In this section, sequential MCS is performed for original data of RTS then the performance metrics are evaluated by comparing the results obtained from CMCS benchmark and proposed method. A hydrogen energy system, encompassing production, storage, and conversion facilities, is installed at bus 18. The performance metrics are evaluated by comparing the results obtained from CMCS benchmark and proposed method. It should be mentioned that transmission lines in this study are considered available at all the time since failure rate of transmission lines are much lower than generation units. The capacity constraints of transmission lines are, however, considered. To train classifier, sequential MCS is run until COV reaches 10%, approximately 800 years in simulation time. After obtaining the training samples, proposed LSTM architecture is trained for 100 iterations. After classifier is successfully trained, the proposed system is tested until COV reaches the limit of ≤ 5%, approximately 2250 years in simulation time. The results for this case study are presented in Tab. 1.

Tab. 1: Performance Comparison of the Proposed Method with CMCS for RTS

	CMCS	Proposed Method
Success States	12,721,456	12,689,842
Failure States	11789	12921
Loss of Load Probability	0.0011	0.0012
Sensitivity	N/A	0.98
Specificity	N/A	0.94
Accuracy	N/A	0.95
Analysis Time (Hr)	~21	~1

This case study shows that the proposed method shows superior performance on identifying overall system status of RTS while reducing computational time significantly.

V. CONCLUSION

This study shows the effectiveness of AI-enhanced Sequential Monte Carlo simulations for assessing the reliability of hydrogen-integrated power systems. Our method significantly boosts computational efficiency without sacrificing accuracy, facilitating more sustainable and reliable energy solutions. Future research will aim to broaden the model's applicability across various system configurations and operational conditions.

References

Chen, W., Zhang, J., Ma, D., Sun, X., Chen, J. and Zhang, R., 2022, April. Reliability Assessment of Hydrogen-Based Carbon-Neutral Power Systems Using Improved Quasi-Sequential Monte Carlo Simulation. In *2022 7th Asia Conference on Power and Electrical Engineering (ACPEE)* (pp. 2008-2012). IEEE.

Dincer, I. and Acar, C., 2015. Review and evaluation of hydrogen production methods for better sustainability. *International Journal of Hydrogen Energy*, *40*(34), pp.11094-11111.

Khan, M.A., Bayati, N. and Ebel, T., 2023. Techno-economic analysis and predictive operation of a power-to-hydrogen for renewable microgrids. *Energy Conversion and Management*, *298*, p.117762.

Khani, H., El-Taweel, N.A. and Farag, H.E.Z., 2019. Supervisory scheduling of storage-based hydrogen fueling stations for transportation sector and distributed operating reserve in electricity markets. *IEEE Transactions on Industrial Informatics*, *16*(3), pp.1529-1538.

Pan, G., Gu, W., Lu, Y., Qiu, H., Lu, S. and Yao, S., 2020. Optimal planning for electricity-hydrogen integrated energy system considering power to hydrogen and heat and seasonal storage. *IEEE Transactions on Sustainable Energy*, *11*(4), pp.2662-2676.

Pindoriya, N.M., Jirutitijaroen, P., Srinivasan, D. and Singh, C., 2011. Composite reliability evaluation using Monte Carlo simulation and least squares support vector classifier. *IEEE Transactions on Power Systems*, *26*(4), pp.2483-2490.

Ramesh, A.S., Vigneshwar, S., Vickram, S., Manikandan, S., Subbaiya, R., Karmegam, N. and Kim, W., 2023. Artificial intelligence driven hydrogen and battery technologies–A review. *Fuel*, *337*, p.126862.

Singh, C. and Wang, L., 2008. Role of artificial intelligence in the reliability evaluation of electric power systems. *Turkish Journal of Electrical Engineering and Computer Sciences*, *16*(3), pp.189-200.

Shu, Z., Jirutitijaroen, P., da Silva, A.M.L. and Singh, C., 2014. Accelerated state evaluation and latin hypercube sequential sampling for composite system reliability assessment. *IEEE Transactions on Power Systems*, *29*(4), pp.1692-1700.

Veziroğlu, T.N. and Şahi, S., 2008. 21st Century's energy: Hydrogen energy system. *Energy Conversion and Management*, *49*(7), pp.1820-1831

Integrating RLS and FCS-MPC for Enhanced Control in Hydrogen Fuel Cell and Grid Inverter Systems

[1,2*] Sulman Shahzad, [1]Muhammad Abbas Abbasi
[1]Department of Electrical Engineering, Islamia University of Bahawalpur, Bahawalpur 63100, Pakistan
[2] National Transmission & Despatch Company Limited, 60600, Multan, Pakistan

* E-mail: salmanshahzad05@gmail.com

Abstract
The integration of hydrogen fuel cells with grid inverters presents unique challenges, primarily due to the highly dynamic nature of fuel cell responses and grid demands. This paper proposes a novel control strategy that combines Recursive Least Squares (RLS) and Finite Control Set Model Predictive Control (FCS-MPC) to enhance the operational efficiency and stability of hydrogen fuel cell systems integrated with grid inverters. The RLS algorithm is utilized for real-time system identification, providing accurate model parameters that are fed into an FCS-MPC framework to optimize control actions dynamically. The results demonstrate the effectiveness of the integrated approach in improving response times, efficiency, and system robustness against disturbances
Keywords: Predictive control, hydrogen energy, fuel cell, model-free, inverter

I. Introduction

Hydrogen fuel cells are emerging as a pivotal technology in renewable energy systems, particularly for their high energy efficiency and low environmental impact. However, the integration of these systems with electrical grids, via grid inverters, introduces complexities due to the variable nature of electrical demand and the intrinsic characteristics of fuel cell dynamics (Bermudez et al., 2021).. Traditional control methods often fall short in handling these complexities, leading to suboptimal performance and reduced reliability. This research introduces a sophisticated control mechanism integrating Recursive Least Squares (RLS) with Finite Control Set Model Predictive Control (FCS-MPC) to address these challenges effectively. Existing control strategies in renewable energy systems often rely on model-based predictive controls that necessitate precise and often rigid models. However, the variable parameters of hydrogen fuel cells, such as changing load conditions and fuel flow rates, make static models inadequate (He et al., 2019). Previous research has explored various adaptive control strategies, but few have seamlessly integrated real-time parameter estimation with predictive control to cater to both the accuracy and flexibility required in renewable energy systems (Kazemian et al., 2021).

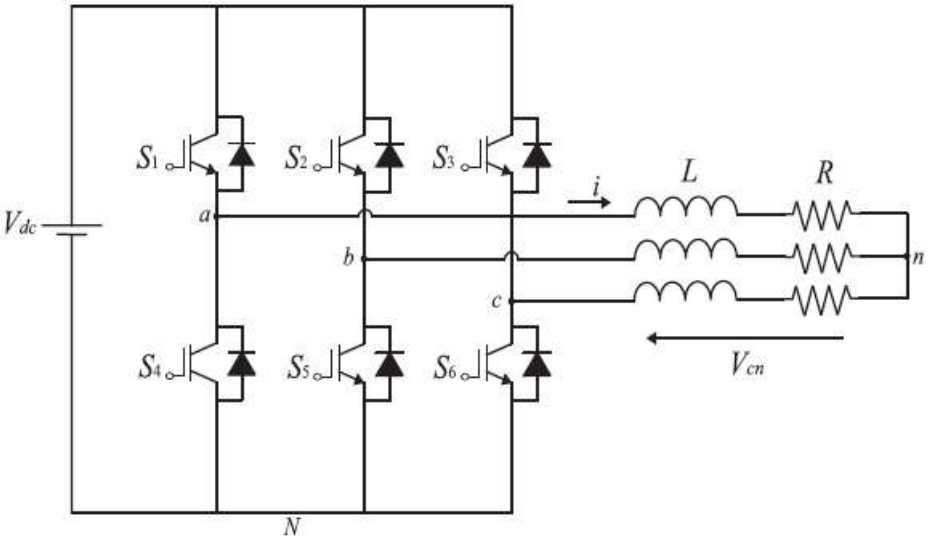


Fig.1: Generic system model

II. Methodology

The RLS algorithm was implemented for continuous real-time system identification. This method adapts to changes in system dynamics by updating the parameters of the model incrementally, ensuring that the control system always reflects the current state of the hydrogen fuel cell. FCS-MPC was chosen for its ability to handle multivariable control problems effectively. It uses the updated parameters from the RLS to predict future states of the system and compute control actions that optimize a predefined cost function (Prasanth et al., 2020). This function was designed to minimize energy consumption while maximizing output efficiency and maintaining grid stability. The integration process involves feeding the parameters estimated by the RLS algorithm into the FCS-MPC to dynamically adjust the control actions (Xu et al., 2020). This integration was implemented on a test bench setup involving a real hydrogen fuel cell and a grid-tied inverter, with various load scenarios to evaluate performance under realistic conditions.
The cost function for the suggested technique has a similar structure to the traditional FCS-MPC.

$$C = |i_\alpha^*(j+1) - i_\alpha'(j+1)| + \left|i_\beta^*(j+1) - i_\beta'(j+1)\right| \quad (1)$$

in equation (1) $i_\alpha^*(j+1)$ and $i_\beta^*(j+1)$ represent real and imaginary parts of reference current and $i_\alpha'(j+1)$ and $i_\beta'(j+1)$ represent real and imaginary parts of load current. In model-free approach the dynamic system is represented using an autoregressive structure (ARX) and its parameters are computed using an adaptive recursive least square (ARLS) technique. The transfer function using ARX structure in α-β stationary reference frame is defined as

$$i_\alpha'(j) = \frac{B^{\alpha\alpha}(z^{-1})}{A^{\alpha}(z^{-1})} v_\alpha(j) + \frac{B^{\alpha\beta}(z^{-1})}{A^{\alpha}(z^{-1})} v_\beta(j) \quad (2)$$

$$i_\beta'(j) = \frac{B^{\beta\alpha}(z^{-1})}{A^{\beta}(z^{-1})} v_\alpha(j) + \frac{B^{\beta\beta}(z^{-1})}{A^{\beta}(z^{-1})} v_\beta(j) \quad (3)$$

Here $i_\alpha'(j)$ and $i_\beta'(j)$ represent real and imaginary parts of load current while $v_\alpha(j)$ and $v_\beta(j)$ are inverter voltages. The A and B represent coefficients of autoregressive model. The adaptive recursive least square (ARLS) technique is used for computing the coeffiecnts in equation (2) and (3). The ARLS algorithm at present time t'(j) is represented by equation (4)

$$t'(j) = t'(j-1) + G(j)e(j) \quad (4)$$

$$G(j) = \frac{Q(j-1)u(j)}{u^S(j)Q(j-1)u(j) + \lambda} \quad (5)$$

$$Q(j) = \frac{1}{\lambda}\left(V - G(j)\lambda^T(j)\right)Q(j-1) \quad (6)$$

III. Results

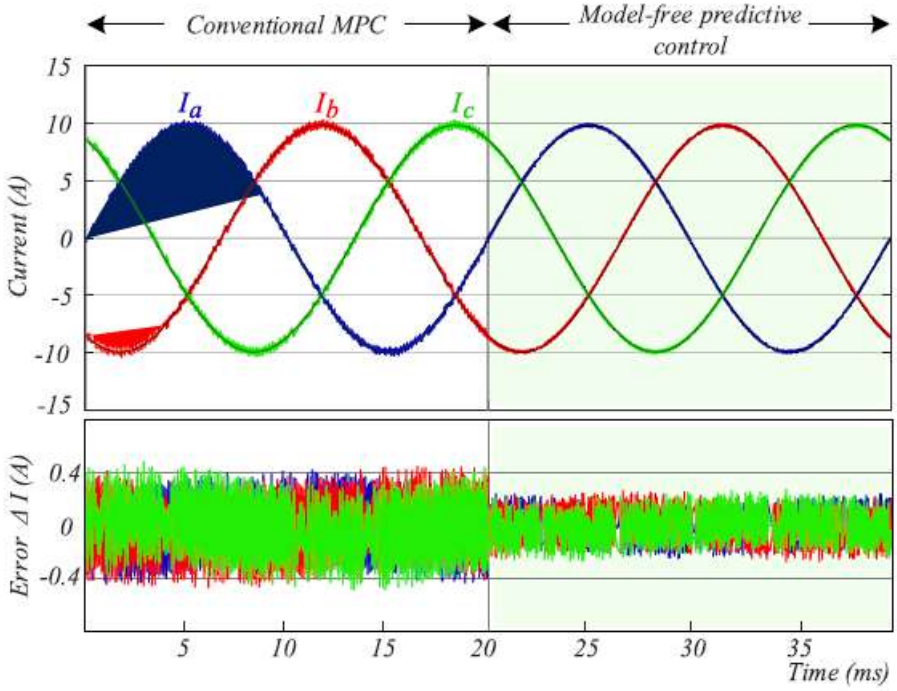


Fig.2: Currents under Scenario 1

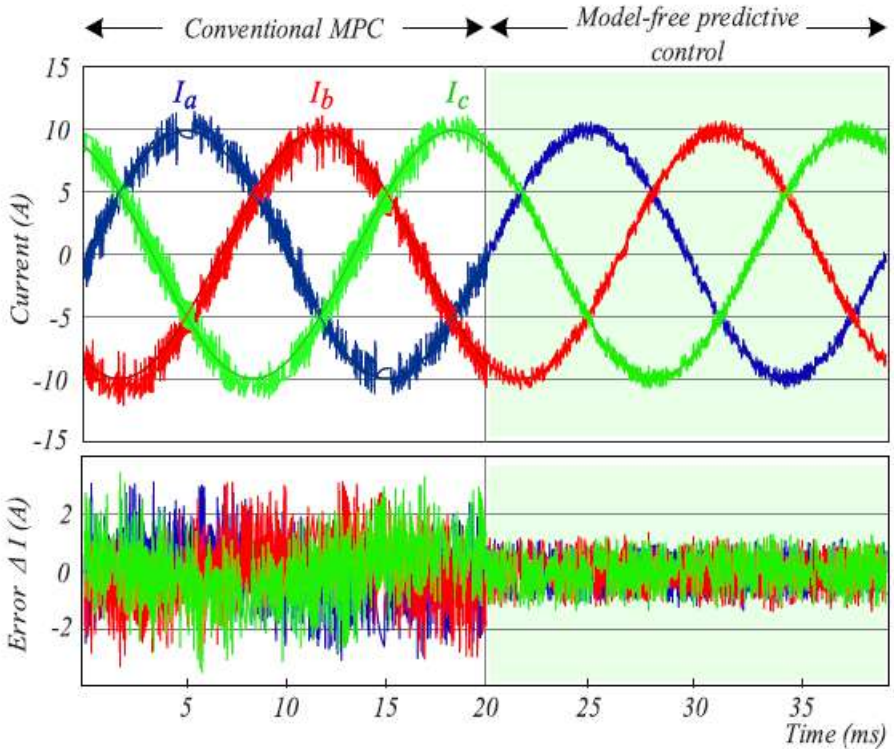


Fig.3: Currents under Scenario 2

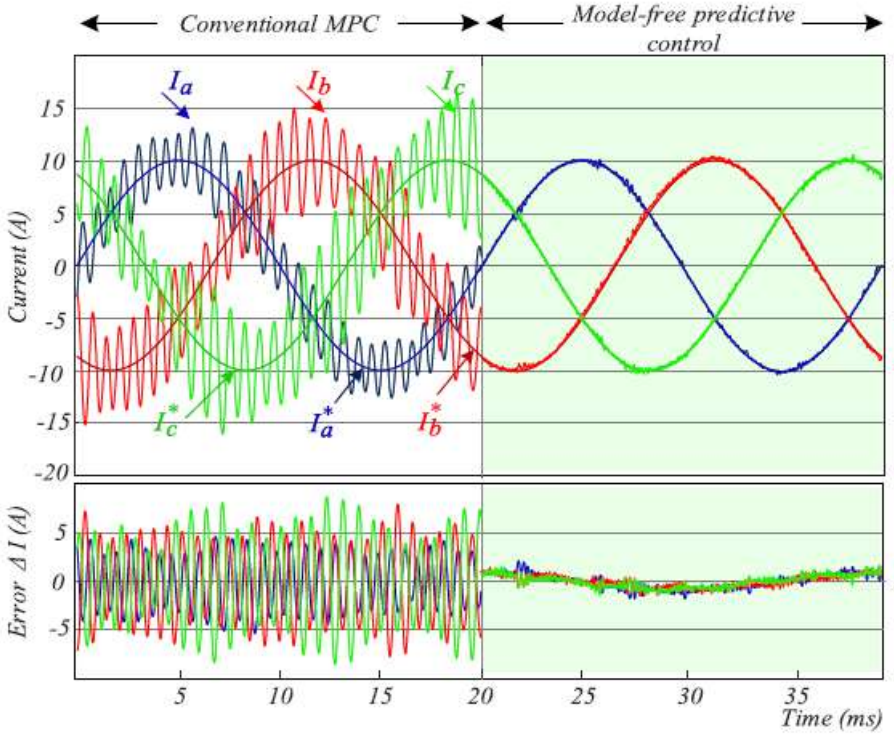


Fig.4: Currents under Scenario 3

IV. Conclusions

This paper has presented a new strategy for predictive current control in a two-level voltage-source inverter without using the physical model and the parameters of the system under control. For this reason, the strategy is named ``model-free predictive control''. The strategy presented in this paper is based on an estimation of the controlled variables using the Recursive Least Squares (RLS) method which is a standard systems identication technique. Simulation and experimental results conrm that it is not necessary to have previous knowledge of the physical model of the inverter and the load to apply predictive control. In addition, these results conrm that this new strategy is very robust in relation to parameter and model mismatch in comparison to standard model predictive control. In the light of these results, it is possible to consider the robust application of predictive control in power electronics systems with higher complexity in a very simple and systematic way, opening a new eld of research and industrial application.

References

Bermudez, M., Arahal, M. R., Duran, M. J., & Gonzalez-Prieto, I. (2021). Model Predictive Control of Six-Phase Electric Drives Including ARX Disturbance Estimator. IEEE Transactions on Industrial Electronics, 68(1), 81–91. https://doi.org/10.1109/TIE.2019.2962477

He, F., Zhou, J., Feng, Z. kai, Liu, G., & Yang, Y. (2019). A hybrid short-term load forecasting model based on variational mode decomposition and long short-term memory networks considering relevant factors with Bayesian optimization algorithm. Applied Energy, 237, 103–116. https://doi.org/10.1016/J.APENERGY.2019.01.055

Kazemian, A., basati, Y., Khatibi, M., & Ma, T. (2021). Performance prediction and optimization of a photovoltaic thermal system integrated with phase change material using response surface method. Journal of Cleaner Production, 290. https://doi.org/10.1016/j.jclepro.2020.125748

Prasanth, V., Natarajan, V., & Basu, K. (2020). Continuous Control Set Model Predictive Control of Buck Converter. IECON Proceedings (Industrial Electronics Conference), 2020-Octob, 1297–1302. https://doi.org/10.1109/IECON43393.2020.9254921

Xu, W., Elmorshedy, M. F., Liu, Y., Rodriguez, J., & Garcia, C. (2020). Maximum Thrust per Ampere of Linear Induction Machine Based on Finite-Set Model Predictive Direct Thrust Control. IEEE Transactions on Power Electronics, 35(7), 7366–7378. https://doi.org/10.1109/TPEL.2019.2960280

Investigation of hydrogen production potential by using the concentrated multi-junction photovoltaic solar cell

[1*]Cihangir Kale [1]Hikmet Esen,
[1] Department of Energy Systems Engineering, Faculty of Technology, Fırat University, Elazığ, Türkiye

* E-mail: ckale@firat.edu.tr

Abstract
Hydrogen, seen as the largest energy carrier of the future, is rapidly entering our lives every day. Hydrogen is generally produced from fossil sources by steam reforming due to its low efficiency and cheapness. With the development of technology, hydrogen can be produced from renewable energy sources in a more environmentally friendly, relatively more economical and highly efficient way.
In this study, the hydrogen production potential with concentrated photovoltaic solar cells and solid oxide electrolyzers was investigated. Analyzes were carried out at a concentration ratio of 500X in the system using a concentrated solar cell with an active area of 10x10 mm^2. According to the results obtained, the electrical production efficiency of the optical system was determined as 32.6%, while the hydrogen production efficiency of the total system was calculated as 33.5% in the analyzes carried out based on the assumption that the thermal load required for the operation of the solid oxide electrolyzer is used from waste heat. It has been observed that this efficiency value is approximately 3 times the hydrogen production efficiency of PEM and Alkaline electrolyzers used with silicon-based conventional solar cells.

Keywords: Hydrogen production, renewable energy, multi-junction solar cell, solid oxide electrolyzer.

I. Introduction

The increase in energy demand in all sectors, the growth of the world population and the decrease in low-cost fossil fuels are becoming one of the most important problems faced by the world in the 21st century.
With an upper calorific value of hydrogen of 140 MJ/kg, it is a fuel with the highest energy content by weight of any fossil fuel. In addition, it is energy efficient and has little harm to the environment since only water and a small amount of NO_x are released when burned with air. However, although hydrogen is an abundant element on earth, it is not found in nature alone as a gas (H_2). Therefore, hydrogen is not a natural fuel, but a synthetic fuel, that is, an energy carrier, that can be produced from different raw materials such as water, fossil fuels and biomass by utilizing primary energy sources [1].
Nowadays, hydrogen is still produced cheaply from fossil fuels by reaction with steam [2]. However, this method increases dependence on fossil resources and also causes air pollution. Using renewable energy sources to produce hydrogen is of great importance for a faster transition to a sustainable-clean environment [3].
Solar energy is the richest renewable energy source in the world. The simplest and most applied method of producing hydrogen from solar energy is the production of electrical energy from solar energy with PV solar cells and the production of hydrogen by separating water into its components by using an electrolyser.
PV cells, which are widely used commercially today, are single-layer silicon-based solar cells and their electrical efficiency is approximately between 16% and 22% [4]. Developing technology has developed PV solar cells, also called multi-junction or III-V group. Since these cells can use a wider part of the sunlight spectrum between 350-1850 nm, the efficiency of these cells reaches 30-46% [5]. Systems that produce electricity from PV cells by concentrating sunlight using optical materials are called concentrated PV (CPV) systems.
Electrolysers are used for the electrolysis process. There are three main electrolyser technologies: Polymer Electrolyte Membrane (PEM), Alkaline and Solid oxide electrolyser (SOE). PEM and alkaline electrolysers are frequently used in industry with their low operating temperature (70-100 °C) and advanced technologies. The conversion efficiency of these electrolysers from electrical energy to hydrogen varies between 56-70% [6]. SOE is a relatively new electrolyser that operates at high temperatures (700-1000 °C) and is the subject of research. The ionic conductivity of the electrolyte and the rate of electrochemical reactions on the electrode surfaces increase at high temperature [7].
In this study, the hydrogen production potential was investigated by performing optimal system sizing of CPV and SOE

II. Material and methods

In this study, the hydrogen production potential of the system was examined in the case of using SOE with CPV. To achieve this, optical system, electrical of CPV solar cell, thermal of CPV solar cell and solid oxide electrolyzer models were created. Analyzes were carried out by optimal sizing so that no DC-DC converter was required in the system.

CPV solar cell electrical model

In this study, due to the availability of more accessible data, the high-efficiency triple-junction concentrated solar cell with GaInP/GaInAs/Ge layer and 10x10 mm^2 dimensions belonging to the Azur Space company was modeled and used in the analysis. The performance of the CPV solar cell at 250X, 500X and 1000X concentration values is given in Table 1 [8].

Tab. 1: The performance of the CPV solar cell at 250X, 500X and 1000X concentration.

Sun Concentration	I_{sc} [A]	V_{oc} [V]	I_{MPP} [A]	V_{MPP} [V]	P_{MPP} [WMPP]	FF [%]	Ŋ [%]
X 250	3.82	3.07	3.76	2.80	10.55	89.9%	41.9
X 500	7.61	3.11	7.50	2.81	21.04	88.8%	41.8
X 1000	15.36	3.15	14.98	2.70	40.46	83.8%	40.2

In order to model the CPV solar cell more accurancy, it is important to consider the relationship between solar cell performance and cell temperature. The relationship between the cell temperature increase and the performance of the CPV solar cell is given in Table 2 [8].

Tab. 2: The relationship between temperature and performace of CPV solar cell.

Parameter	$(\Delta I_{sc} / I_{sc}(25°C)) / \Delta T$	$(\Delta V_{oc} / V_{oc}(25°C)) / \Delta T$	$(\Delta P_{mpp} / P_{mpp}(25°C))/\Delta T$	$(\Delta \eta / \eta(25°C)) / \Delta T$
Value	0.080%/K	-0.135%/K	-0.106%/K	-0.106%(rel)/K
Parameter	$\Delta I_{sc} / \Delta T$	$\Delta V_{oc} / \Delta T$	$\Delta P_{mpp} / \Delta T$	$\Delta \eta / \Delta T$
Value	6.1 mA/K	-4.2 mV/K	-22.5 mW/K	-0.045%(abs)/K

The current-voltage characteristic produced by the CPV solar cell can be found according to the Shockley single diode model given Eq. 1 [9]:

$$I = I_{ph} - I_0\left(\exp\frac{q(V+I.R_s)}{n_i.K_b.T_c} - 1\right) - \frac{V+I.R_s}{R_{sh}} \quad (1)$$

where, V is the cell voltage, R_s is the series resistance, R_{sh} is the shunt resistance, I_0 is the reverse saturation current, n_i ideality factor and I_{ph} stands for photocurrent. The photocurrent is equal to the short-circuit current under ideal conditions ($I_{ph} = I_{sc}$).

In this study, a CPV solar cell model using a single diode model was carried out by creating a script in Python. Unknown parameters (R_s , R_{sh} , n_i) in the model were estimated using the reference values in the Table 1-2 and the CPV solar cell I-V graph was obtained with high accuracy.

CPV solar cell thermal model

In this study, the receiver module containing the CPV solar cell was numerically modeled using COMSOL Multiphysics software according to the outdoor conditions of Elazig province. The thermophysical and geometric properties of the components used in the model are given in Table 3.

Tab. 3: The thermophysical and geometric properties of the components.

Component	Thermal Conductivity k (W/m.K)	Specific Heat Capacity C_p (J/g-°C)	Emissivity	Width (mm)	Area (mm^2)
Homogenizer	1.40	0.858	0.84	22	10x10
Silicone Adhesive	0.15	0.7		0.2	10x12
Cell	60	0.32		0.19	10x10
Soldering	65	0.22		0.05	10x12
Top Copper	400	0.385		0.3	25x25
Alumina	24	0.800		0.38	26x26
Bottom Copper	400	0.385		0.3	25x25
Thermal Interface Rubber	3.3	0.83		0.5	30x30
AL base	138	0.880		4	40x40
Oil Compound	0.7	1		0.2	40x40
Heat Sink	200	0.9	0.8	40	50x50

Optical model

In this study, the optical system consists of a silver-plated primary parabolic mirror with a high transmission rate and a receiver part. The receiver part is basically a secondary optical element (homogenizer), cpv solar cell and heat sink for passive cooling. The optical system concentration ratio was chosen as 500X to both protect the solar cell from high temperatures and allow it to operate at high efficiencies. Since the heat sink, which has the largest surface area on the receiver side with 50x50 mm^2, will create a shadowing area on the primary mirror, the primary mirror dimensions of approximately 230x230 mm^2 square for a 500x concentration ratio were determined for this study. The optical system efficiency, including the shadowing area, was kept constant at 85% for this study.

Solid oxide electrolyser model

In this study, a solid oxide electrolyser (SOE) operating at high temperature (800 °C) was modeled as three-dimensional small size (active area= 0.1 cm^2) single-cell and single-channel using COMSOL Multiphysics software. In the model, results were obtained by performing analyzes with 0.01 V differences between 1 V and 1.6 V voltage values.

The layers and isometric view of single-cell and single-channel SOE modelled by COMSOL Multiphysics software are shown in Figure 1.

For electrolysers, faraday efficiency (η_{soe}), is a ratio between the theoretical maximum and the actual amount of hydrogen produced in the electrolyzer. It can be expressed as in Eq. 2 [10]:

$$\eta_{soe} = \frac{N_{H_2} I_e}{2.F} \quad (2)$$

where, N_{H_2} expresses the amount of moles of hydrogen produced per second and I_e is the he electrolyser current. The total system hydrogen production efficiency can be expressed simply as in Eq 3.

$$\eta_{tot} = \eta_{opt} \times \eta_{cpv} \times \eta_{soe} \quad (3)$$

where η_{opt}, η_{cpv} and η_{soe} are refer to optical, CPV solar cell and SOE efficiencies, respectively.

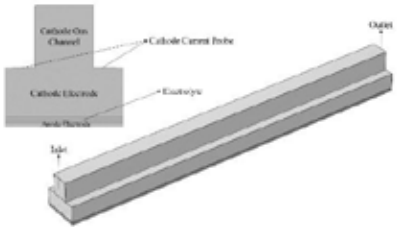
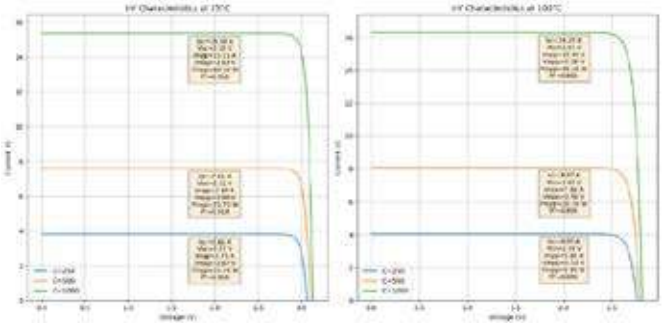


Fig. 1: The layers and isometric view of single-cell and single-channel SOE

III. Results and discussions

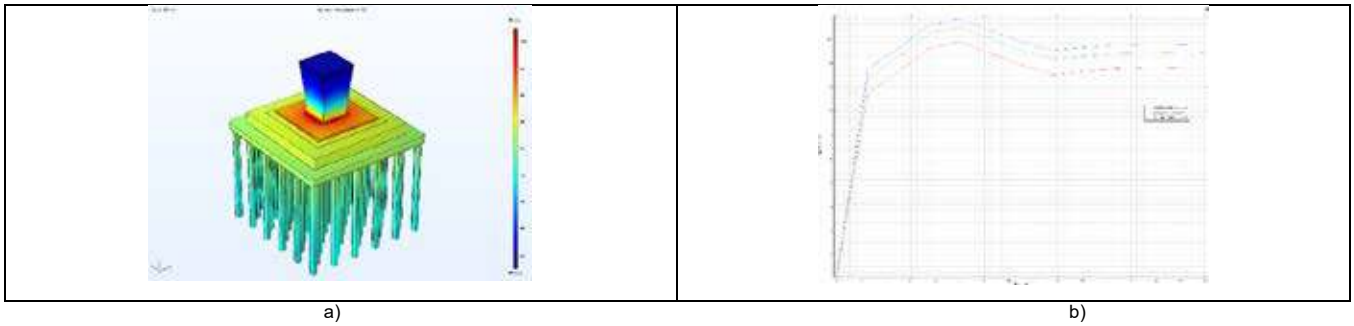
For the CPV solar cell electrical model, optimum values (R_s, R_{sh}, n_i) were estimated by a script created in Python and I-V graphs were obtained under 250X, 500X and 1000x concentration ratio at 25 °C and 100 °C. The obtained I-V graphs are given in Figure 2. The high-precision model was confirmed by comparing the solar cell values taken at 25 °C in Figure 2 with the values in the datasheet shared in Table 1.



a) b)

Fig. 2: The I-V graph of CPV solar cell under 250X, 500X and 1000x a) at 25 °C b) at 100 °C

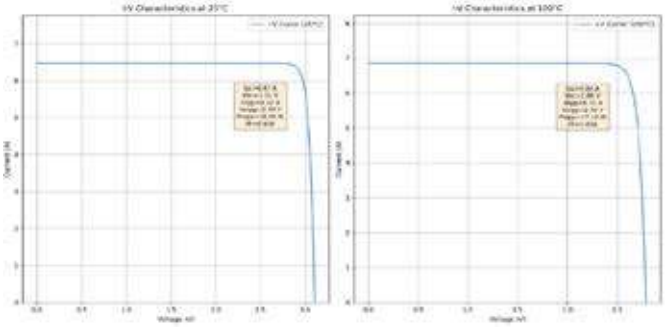
Considering the 230x230 mm^2 primary mirror area, the amount of radiation entering the system was calculated as 52.5 W, and under 85% optical efficiency, the amount of radiation coming to the CPV solar cell was determined as 44.625 W radiation. Since the electrical efficiency of the CPV solar cell at 25 °C under 500X concentration is 41.8%, 25.97 W thermal load remains on the cell. The receiver time-dependent temperature results under 25.97 W thermal load of the receiver modeled in COMSOL under the outdoor conditions of Elazığ province are given in Figure 3. According to these results, the system becomes steady state within 35 minutes and the average temperature of the CPV solar cell reaches 100 °C.



a) b)

Fig. 3: a) Temperature distribution of the receiver part b) the maximum, minimum and average cell temperature over time.

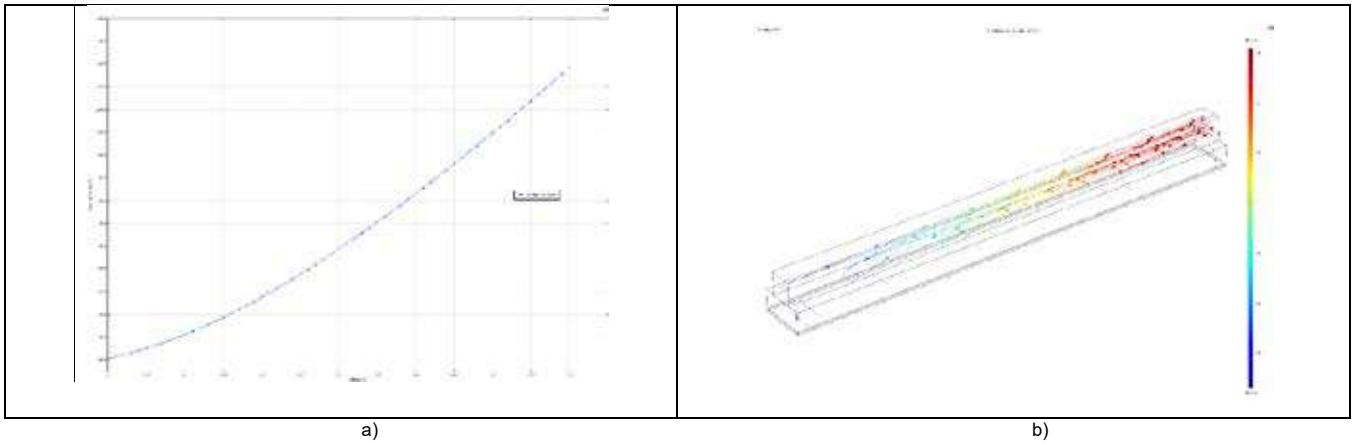
After obtaining cell values under 500X at 25 °C with 85% optical efficiency with the validated electrical model, cell performance at 100 °C was determined according to the results obtained from the thermal model and the results are shown in Figure 4. As can be clearly seen in Figure 4, while the CPV solar cell I_{mpp} was 6.71 A at 100 °C, the V_{mpp} value was found to be 2.55 V.



a) b)

Fig. 4: The I-V graph of CPV solar cell under 500X and with 85% optical efficiency a) at 25 °C b) at 100 °C

Current values of SOE modeled by the COMSOL software were obtained between 1 and 1.6 V with 0.01 V differences. In addition, considering that the CPV solar cell V_{mpp} value is 2.55 V, it was concluded that SOE should be operated in the 1.27 V range and formed in the form of a 2 cell stack. Current values at diffrenet cell voltage and hydrogen molar concentration results in the cell at 1.27 V are given in Figure 5. At the cell value of 1.27 V, the molar concentration value was 0.26 mol/m^3 at the inlet and reached 1.62 mol/m^3 at the outlet.



a) b)

Fig. 5: The I-V graph of CPV solar cell under 250X, 500X and 1000x a) at 25 °C b) at 100 °C

In this study, optimum sizing for SOE was achieved in the light of the results obtained from the CPV solar cell electrical model and the results obtained from the SOE modeled by COMSOL software. According to the results obtained, it was concluded that the optimum form for SOE should be a stack with 2 cells which is consist of 64 channels of each. The I-V graph of SOE and CPV solar cell is shown in Figure 6.

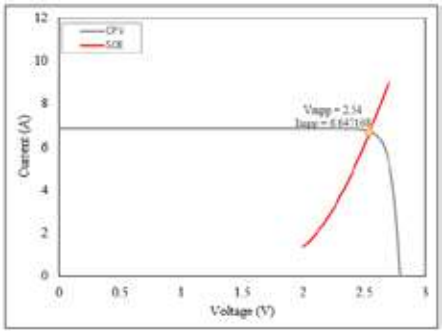


Fig. 6: The I-V graph of CPV solar cell and SOE

IV. Conclusions

In this study, the optimum design of a system using SOE with a triple-junction CPV solar cell with high electrical efficiency was carried out and the hydrogen production potential was investigated. According to the results obtained, the total electrical efficiency of the system was calculated as 32.6%, while the total hydrogen production efficiency of the system was calculated as 33.5%. According to the results obtained, it has been observed that the CPV-SOE hydrogen production system has the highest efficiency among systems producing hydrogen from renewable energy sources.

References

[1]Hosseini SE, Wahid MA. Hydrogen production from renewable and sustainable energy resources: Promising green energy carrier for clean development. Renew Sustain Energy Rev 2016. https://doi.org/10.1016/j.rser.2015.12.112.

[2]Manage MN, Hodgson D, Milligan N, Simons SJR, Brett DJL. A techno-economic appraisal of hydrogen generation and the case for solid oxide electrolyser cells. Int J Hydrogen Energy 2011;36:5782–96. https://doi.org/10.1016/J.IJHYDENE.2011.01.075.

[3]Ghazvini M, Sadeghzadeh M, Ahmadi MH, Moosavi S, Pourfayaz F. Geothermal energy use in hydrogen production: A review. Int J Energy Res 2019;43:7823–51. https://doi.org/10.1002/ER.4778.

[4]Zhang L, Jing D, Zhao L, Wei J, Guo L. Concentrating PV/T hybrid system for simultaneous electricity and usable heat generation: A review. Int J Photoenergy 2012;2012. https://doi.org/10.1155/2012/869753.

[5]Wiesenfarth M, Philipps SP, Bett AW, Horowitz K, Kurtz S. Current Status Of Concentrator Photovoltaic (CPV) Technology Version 1.3. 2017.

[6]Parra D, Patel MK. Techno-economic implications of the electrolyser technology and size for power-to-gas systems. Int J Hydrogen Energy 2016;41:3748–61. https://doi.org/10.1016/J.IJHYDENE.2015.12.160.

[7]Burgess G, Fernández-Velasco JG. Materials, operational energy inputs, and net energy ratio for photobiological hydrogen production. Int J Hydrogen Energy 2007. https://doi.org/10.1016/j.ijhydene.2006.10.055.

[8] AZUR SPACE Solar Power GmbH n.d. https://www.azurspace.com/index.php/en/ (accessed April 18, 2024).

[9]Segev G, Mittelman G, Kribus A. Equivalent circuit models for triple-junction concentrator solar cells. Sol Energy Mater Sol Cells 2012;98:57–65. https://doi.org/10.1016/J.SOLMAT.2011.10.013.

[10]Yodwong B, Guilbert D, Phattanasak M, Kaewmanee W, Hinaje M, Vitale G. Faraday's efficiency modeling of a proton exchange membrane electrolyzer based on experimental data. Energies 2020;13. https://doi.org/10.3390/EN13184792.

Thermodynamic Performance Assessment of PEMFC Powered Air to Water Heat Pump

[1,2*]Anil Erdogan, [3]Ozge Ozcan Bilgilioglu, [3]Oguz Yildirim, [4,5]S. Aykut Korkmaz, [1]Omer Can Inci, [2]C. Ozgur Colpan

[1] Vestel Home Appliances, Department of Technology Development, Manisa, Türkiye
[2] Dokuz Eylül University, Faculty of Engineering, Department of Mechanical Engineering, Buca, Izmir, Türkiye
[3] Vestel Home Appliances, R&D Department of Air Conditioning, Manisa, Türkiye
[4] Dokuz Eylul University, Maritime Faculty, Buca, Izmir, Türkiye
[5] Department of Civil, Maritime and Environmental Engineering, University of Southampton, Southampton, UK

* E-mail: anil.erdogan@vestel.com.tr

Abstract
Heat pumps play a crucial role in future energy solutions due to their energy efficiency, sustainability, and environmental friendliness. Heat pumps can be classified according to the type of heat source, such as air source, water source, ground source, and hybrid heat pumps (which use both air and water). This study presents the system design and thermodynamic analysis of a 9 kW air-to-water heat pump (AtW) integrated with a proton exchange membrane fuel cell (PEMFC) that uses R290 as the working fluid. The performance of the system is evaluated using thermodynamic balance equations, including mass balance, energy balance, and exergy balance. Furthermore, a parametric study is conducted to assess the effect of operational parameters, such as air temperature, and working fluid type, on the performance of the AtW heat pump. The performance parameters considered are coefficient of performance (COP), exergy destruction rate, and hydrogen consumption rate, respectively. The results show that ambient temperature affects directly to the performance of the system. In addition, R290 gets the best performance in heating mode; whereas R1234yf has favorable performance in cooling mode. This study results guide researchers, academicians, and industrial partners working in the field of heat pumps as well as HVACs to develop systems efficiently.
Keywords: Air to Water Heat Pump, Thermodynamic Analysis, PEMFC, Performance Assessment

I. Introduction

A heat pump uses similar technology to a refrigerator or air conditioner. A heat pump increases heat by taking it from a source (e.g. outside air, nearby water source, factory waste and process heat), subjecting it to a thermodynamic cycle and then transferring it to where it is needed. It is more efficient and environmentally friendly than traditional heating solutions (combi boiler, electric heater) (Chua et al., 2010). Heat pump systems can also be operated in hybrid mode.

Heat pump systems consist of a compressor that increases the pressure and temperature of the refrigerant, a heat exchanger that extracts heat from the source, and then another heat exchanger that transfers the resulting heat to another source. The heat generated in buildings and homes is transmitted via hydronic systems. Heat pumps can generally provide space heating in winter and space cooling in summer and can also provide hot water.

Fuel cells, one of the clean and sustainable energy technologies, are electrochemical devices that convert the chemical energy of the fuel into electricity through electrochemical reactions. There are several types of fuel cells that can be used. The most commonly used type of fuel cell is the Proton Exchange Membrane Fuel Cell (PEMFC) (Mench, 2008). This is due to the fact that PEM fuel cells have high power density, low operating temp (typically between 40-80°C), fast start capabilities and are easily integrated into many systems.

According to the IEA (IEA,2023), sales of heat pumps in Europe increased by almost 40% in 2023. Among the heat pump types, air-to-water heat pumps, which are popular in the market, their sales increased by about 50% in Europe in the year of 2023. Meanwhile, China has the largest heat pump market in the world.

Several studies have been conducted on thermodynamic modelling of air-to-water heat pump systems. For instance, Voloshchuk et al. (2023) developed a mathematical model for a reversible air-to-water heat pump that uses R290 as a working fluid. They investigated the system's performance under various conditions, such as different temperatures and heat loads. The study results indicate that heat exchanger sizing significantly impacts the distribution of exergy destruction within the system components. Furthermore, it was found that when the heating design loads to cooling design loads ratio is less than 1.2, the system should be sized based on the cooling design loads. Kumar et al. (2023) developed an integrated model that includes thermodynamic and control models for an air-to-water heat pump. The model was used to investigate the performance of an air-to-water heat pump that serves an office building in Italy. The results of their study showed that the average coefficient of performance increased from 17% to 50%. Kinab et al. (2010) performed a performance assessment of a reversible air-to-water heat pump using R410a as the working fluid under off-design conditions. They then validated the developed model using seasonal weather and experimental data. The study results indicated that the model agreed with the experimental data, with an error rate of 5% for cooling mode and 8% for heating mode. Furthermore, it was suggested that optimizing operating parameters, such as air and water temperature, and flow rates of air, water, and refrigerant, would lead to maximum annual system efficiency. Madonna and Bazzochi (2013) developed a model for simulating the hourly performance of a reversible air-to-water heat pump. Their study showed that the heating and cooling load at the peak point is significant, as indicated by the authors. Therefore, in buildings where the heating load differs from the cooling load, the seasonal efficiency can decrease by up to 25%. While there are numerous studies on

designing and thermodynamically modelling air-to-water heat pump systems that use various refrigerants such as R32 and R410a, there are few studies, to the authors' knowledge, on thermodynamically modelling integrated PEMFC and R290-based air-to-water heat pumps. This study presents a thermodynamic model for integrating an air-to-water heat pump and a PEMFC, considering both heating and cooling modes. Parametric studies were conducted to evaluate the system's performance under different operating conditions, such as ambient and water temperatures. The performance parameters considered were the coefficient of performance (COP) and exergy destruction rate. The modeling equations are solved using the Engineering Equation Solver (EES) environment.

II. Mathematical Modeling

This section presents the modeling equations for the integrated system under study and introduces the modeling approach. Fig. 1 shows the schematic diagram for the air-to-water heat pump integrated with PEMFC.

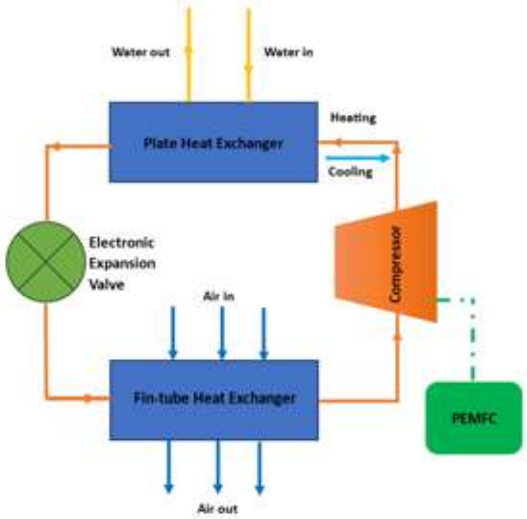


Fig. 1. The schematic representation of PEMFC integrated with the air-to-water heat pump system

Assumptions were made for the modelling of the integrated system.

- The system operates under the steady-state conditions
- Changes in the kinetic and potential energy can be ignored
- The pressure drops in the tubes as well as heat exchangers can be neglected
- Air is taken as ideal gas that means the thermophysical properties only depend on the temperature.
- The pinch point temperature of the heat exchangers is assumed to be as 5 K.

The open system energy balance equation under steady-state conditions can be applied in order to find the unknown properties (Moran et al. 2019).

$$0 = \dot{Q}_{cv} - \dot{W}_{cv} + \sum_i (\dot{m}_i \cdot h_i) - \sum_e (\dot{m}_e \cdot h_e) \quad (1)$$

Here, $\dot{Q}_{cv}$ is the heat transfer rate from the component to the environment, $\dot{m}$ is the mass flow rate, h is the specific enthalpy, and i and e express the inlet and exit, respectively.

Isentropic efficiency of the compressor is evaluated using Eq. (2).

$$\eta_{i\,sen\,compressor} = \frac{h_{comp,o,s} - h_{comp,i}}{h_{comp,o} - h_{comp,i}} \quad (2)$$

The power required by the compressor can be calculated using Eq. (3)

$$\dot{W}_{comp} = \dot{m}_{ref} \cdot \left(h_{comp,o} - h_{comp,i}\right) \quad (3)$$

The heat capacity of evaporator and condenser can be found using Eqs. (4) and (5), respectively.

$$\dot{Q}_{evap} = \dot{m}_{ref} \cdot \left(h_{evap,o} - h_{evap,i}\right) \quad (4)$$

$$\dot{Q}_{cond} = \dot{m}_{ref} \cdot \left(h_{cond,i} - h_{cond,o}\right) \quad (5)$$

Finally, the coefficient of performances (COP) for both heating and cooling modes are calculated below.

$$COP_{heating} = \frac{\dot{Q}_{cond}}{\dot{W}_{comp}} \quad (6)$$

$$COP_{cooling} = \frac{\dot{Q}_{evap}}{\dot{W}_{comp}} \quad (7)$$

After finding the state properties, the open system exergy balance equation under the steady state condition can be applied in order to find the exergy destruction of each component. This equation is presented in Eq. (8) (Moran et al. 2019).

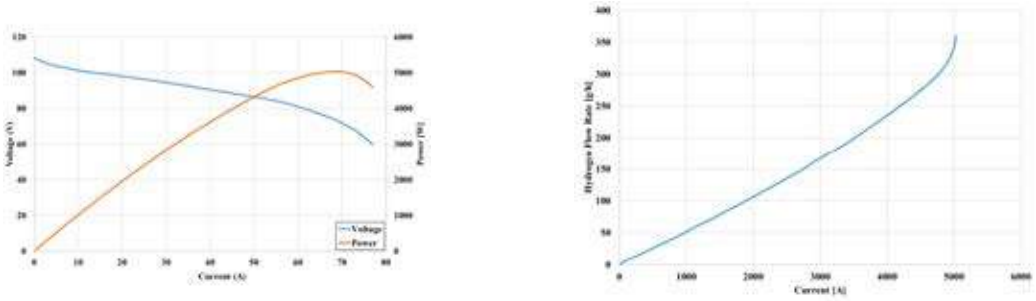
$$0 = \dot{E}x_Q - \dot{E}x_W + \sum_i \left(\dot{m}_i \cdot ex_{f,i}\right) - \sum_e \left(\dot{m}_e \cdot ex_{f,e}\right) - \dot{E}x_{D,k} \quad (8)$$

Here, $\dot{E}x_Q$ is exergy transfer rate by heat, $\dot{E}x_W$ is the exergy transfer by work, $ex_{f,i}$ and $ex_{f,e}$ are specific flow exergy of inlet and exit streams, and $\dot{E}x_{D,k}$ is the exergy destruction rate of kth component. The specific flow exergy can be calculated below.

$$e\,x_{f,j} = \left((h_j - h_0) - T_0 \cdot (s_j - s_0)\right) \quad (9)$$

Here, h_0 and s_0 are specific enthalpy and entropy at the dead state condition, respectively.

Regarding the basic PEMFC modeling, a commercially available 5kW Horizon H5000 product was used. In this regard, the voltage, the current and the hydrogen consumption values are taken from technical document published by the company. The technical document can be found in the reference of (Horizon Fuel Cell – H5000). The performance and hydrogen flow rate curves extracted from the document are presented below.

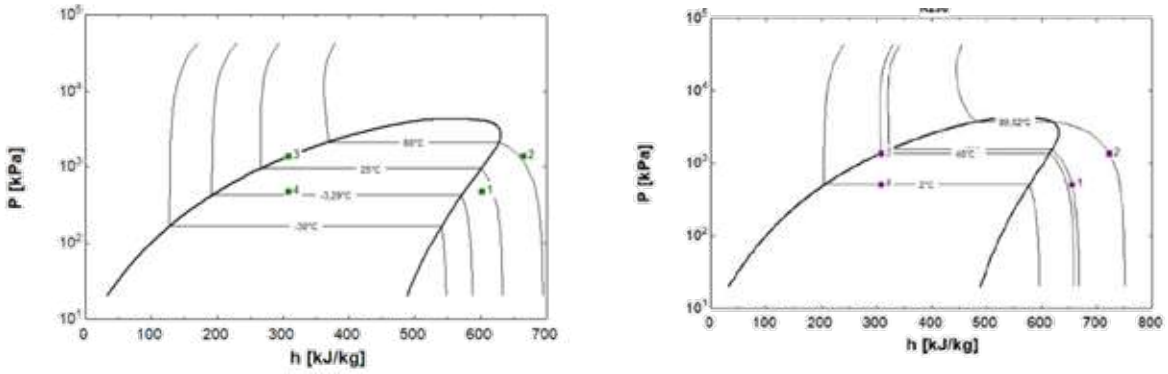


(a) (b)

Fig. 2. (a) the polarization and power curves, (b) hydrogen consumption curve for PEMFC used in air-to-water heat pump

IV. Results and discussion

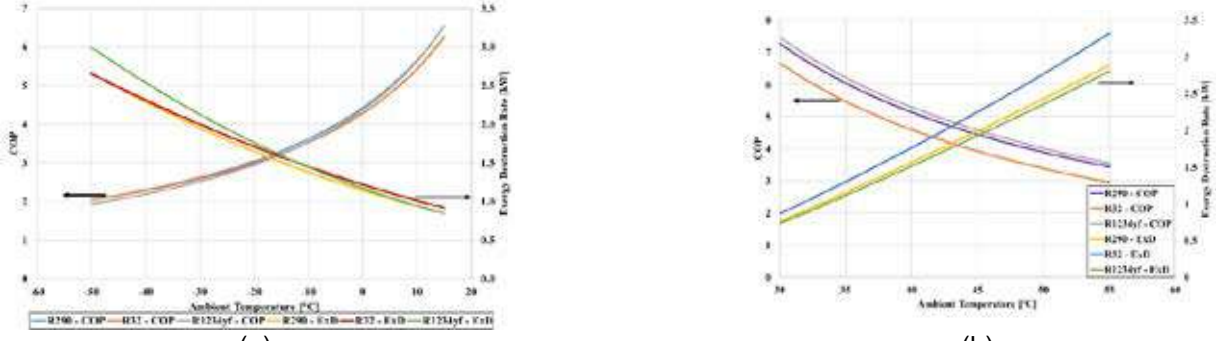
In this section, the results derived from the study are presented and discussed. The lnP – h diagram of the air-to-water heat pump for both heating and cooling modes are presented in Figs. 3(a) and 3(b), respectively.



(a) (b)

Fig. 3. lnP – h diagram of air-to-water heat pump (a) heating mode, (b) cooling mode

The effect of ambient temperature on coefficient of performance and the total exergy destruction rate according to different refrigerants for heating and cooling modes are demonstrated in Figs. 4(a) and 4(b), respectively. For heating mode (as presented in Fig. 4(a)), when the ambient temperature varies between -50°C and 15°C, COP value increases. This trend mainly due to the increase in evaporation temperature as well as decrease in compressor power. On the other hand, as the ambient temperature increases, the total exergy destruction rate decreases. In addition, it was found that under the same ambient temperature, R290 has the minimum exergy destruction rate compared to the other working fluids studied. For cooling mode (as shown in Fig. 4(b)) when the ambient temperature increases from 30°C to 55°C COP decreases. The reason of this trend is increase in condensation temperature as well as the compressor power. On the other hand, as the ambient temperature increases, the total exergy destruction rate increases. Moreover, it was obtained that R1234yf has the minimum exergy destruction rate compared to the other working fluids.

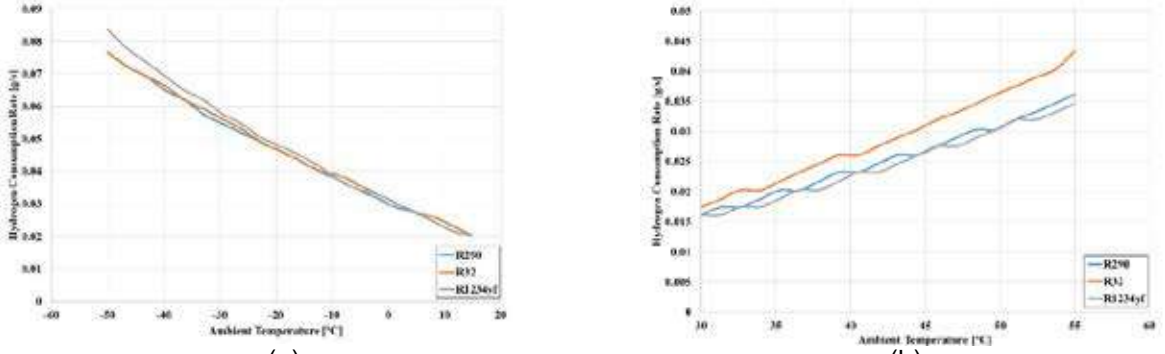


(a) (b)

Fig. 4. The effect of ambient temperature on (a) the COP (b) the exergy destruction rate according to different refrigerants

Figs. 5(a) and 5(b) demonstrates the effect of ambient temperature on the hydrogen consumption rate according to

different refrigerants for heating and cooling modes, respectively. For heating mode, as the temperature increases the hydrogen consumption rate decreases for all refrigerants. It was found that when R290 is used as working fluid for air-to-water heat pump, the hydrogen consumption rate has the minimum values for all temperatures. For cooling mode, as the temperature increases the hydrogen consumption increases. It was obtained from the figure that R1234yf has the minimum hydrogen consumption rate compared to the others.



(a) (b)

Fig. 5. The effect of ambient temperature on the hydrogen consumption rate for (a) heating mode, (b) cooling mode

The component-based exergy analysis under the baseline conditions analysis shows that the condenser has the highest exergy destruction rate for both heating and cooling modes and found as 0.8299 kW and 1.421 kW, respectively. In addition, this analysis displays that the condenser should be optimized in order to decrease the irreversibilities.

V. Conclusions

In this study, a detailed thermodynamic analysis, including energy and exergy, is carried out for an integrated PEMFC and air-to-water heat pump under heating and cooling conditions. For this purpose, mass and energy balance equations are applied to determine the state characteristics. Then, an exergy balance equation including the components of the system is applied to find the irreversibilities. Furthermore, a parametric study is carried out to evaluate the effect of ambient temperature and different working fluids on the performance of the system. The results derived from the study carried out are listed below.

- Ambient temperature affects the performance of the system. It was found that the cold and harsh climatic conditions the performance of the integrated system gets minimum. Whereas, the hot climatic conditions, the performance of the system gets minimum.
- For heating mode, R290 yields the best performance; whereas R1234yf has appropriate performance for cooling mode, in terms of exergetic point of view.
- Regarding the hydrogen consumption rates, the hydrogen consumption in PEMFC decreases with an increase in the ambient temperature. On the other hand, the hydrogen consumption rate increases with an increase in the ambient temperature for cooling mode.
- For both modes, the condenser has the highest irreversibilities.

Future studies on this topic will include a life cycle assessment of an air-to-water heat pump system using different refrigerants, the development of a detailed electrochemical model for PEMFC, and a techno-economic analysis of the system.

References

Chua, K. J., Chou, S. K., & Yang, W. M. (2010). Advances in heat pump systems: A review. *Applied energy*, *87*(12), 3611-3624.

Horizon Fuel Cell, Link: https://www.horizoneducational.com/h-5000-pem-fuel-cell-5kw/p1361 Last Access Date: 18.04.2024.

Kinab, E., Marchio, D., Rivière, P., & Zoughaib, A. (2010). Reversible heat pump model for seasonal performance optimization. *Energy and Buildings*, *42*(12), 2269-2280.

Kumar, D.M.; Catrini, P.; Piacentino, A.; Cirrincione, M. Integrated Thermodynamic and Control Modeling of an Air-to-Water Heat Pump for Estimating Energy-Saving Potential and Flexibility in the Building Sector. Sustainability 2023, 15, 8664

Madonna, F., & Bazzocchi, F. (2013). Annual performances of reversible air-to-water heat pumps in small residential buildings. *Energy and Buildings*, *65*, 299-309.

Mench, M. M. (2008). *Fuel cell engines*. John Wiley & Sons.

Moran, M. J., Shapiro, H. N., Boettner, D. D., & Bailey, M. B. (2019). *Fundamentals of engineering thermodynamics*. John Wiley & Sons.

The Future of Heat Pumps (2023), World Energy Outlook Special Report, IEA

Voloshchuk, V., Gullo, P., Stepanets, O., & Nikiforovich, E. (2023). Exergy-based sizing of a R290 air-to-water reversible heat pump for space heating and cooling purposes. In *36th International Conference on Efficiency, Cost, Optimization, Simulation and Environmental Impact of Energy Systems, ECOS 2023* (pp. 851-862). International Conference on Efficiency, Cost, Optimization, Simulation and Environmental Impact of Energy Systems.

Hydrogen and Hydrogen Technologies in Healthcare Institutions

[1*]Duygu Yildirim, [2]Cem Haydaroğlu, [3]Burak Yildirim, [4]Mahmut Temel Özdemir, [5]Ozan Erdinç
[1] Fırat University, Kovancılar Vocational School, Kovancılar, Elazığ, 23850, Türkiye
[2] Dicle University, Department of Electrical and Electronics Engineering, Diyarbakır, 21100, Türkiye
[3] Bingöl University, Voc. and Tech. High School, Bingöl, 12100, Türkiye
[4] Fırat University, Department of Electrical and Electronics Engineering, Elazığ, 23100, Türkiye
[5] Yıldız Technical University, Department of Electrical Engineering, İstanbul, 34220, Türkiye

* E-mail:dyildirim@firat.edu.tr

Abstract
The worldwide challenges posed by climate change, energy security disruptions caused by conflicts, and production and supply chain outages resulting from COVID-19 have underscored the necessity for global readiness in confronting future crises. Hospitals and healthcare institutions are substantial consumers of energy, leading to increased operational costs, diminished competitiveness, and negative environmental impacts. The COVID-19 pandemic has emphasized the importance of ensuring an uninterrupted provision of oxygen and executing stringent sanitation and disinfection measures in hospitals and healthcare institutions. This study investigates the utilization of hydrogen and hydrogen technologies in hospitals and healthcare institutions. This study provides an examination of hydrogen and its related technologies in the context of energy generation, medical applications, sterilization and disinfection, as well as laboratory utilization in hospitals and healthcare institutions.

Keywords: Hydrogen, Hydrogen Technologies, Hospital, Healthcare Institutions

I. Introduction

The exponential growth of the global population and the process of industrialization have resulted in a significant surge in the demand for energy. This surge results in an escalation in the utilization of fossil fuels and significant harm to the environment. Because of this, there is a very strong potential to employ sustainable energy sources such as solar and wind energy (Temiz and Javani, 2020). Hospitals and healthcare institutions are recognized as the primary consumers of energy in the construction industry (Vaziri, Rezaee, and Monirian, 2020). One of the major concerns is meeting the energy requirements of hospitals and healthcare institutions. These institutions must operate continuously 365 days a year. Administrations are highly concerned with cost reduction because of the competitive commercial environment. Specifically, the energy consumption of hospitals and healthcare institutions soared during the Corona epidemic (Izadi et al., 2023).

Hydrogen is playing an increasingly important role in efforts to reduce carbon emissions. Furthermore, hydrogen has the capability to provide energy to the three most energy-intensive sectors, namely transportation, heating, and electricity, thereby enabling sector coupling. Fuel cell methods for energy conversion have been documented since 1839. However, in recent years, there has been a resurgence of interest in these technologies due to their distinctive properties as potential solutions for the energy transition (Lamagna et al., 2021).

Hydrogen is the lightest element in the periodic table and the most abundant chemical substance in the universe. Recent data indicates that hydrogen possesses strong antioxidant, antiapoptotic, and anti-inflammatory properties, suggesting its potential for medicinal uses in cells, tissues, and organs. Accordingly, the use of hydrogen as a medical gas has aroused great interest worldwide, and scientists have investigated the therapeutic value of hydrogen in many disease models (Shen et al., 2014). Additionally, hydrogen peroxide has an important use in hospitals and healthcare institutions as a sterilant and disinfectant (Bharti et al., 2022).

The COVID-19 epidemic and other factors, such as global warming and the depletion of fossil resources, have highlighted how critical it is for healthcare facilities to use cutting-edge technologies in everything from energy to cleanliness. Hydrogen is extensively utilized in healthcare institutions for several purposes, including energy generation, cleanliness maintenance, therapeutic procedures, and laboratory applications. This research provides a comprehensive outlook by integrating the energy and health dimensions of hydrogen and hydrogen technology in various applications inside healthcare organizations.

II. The use of hydrogen as a energy source and storage

Hospitals and healthcare institutions are the most important energy consumers in the field of buildings, and most of their energy needs come from fossil fuel sources. Additionally, energy continuity is vital for these organizations. Healthcare facilities have the potential to use large amounts of oxygen. Figure 1 presents a comprehensive energy flow diagram for a hospital based on hydrogen and hydrogen technologies. The figure illustrates the production of green hydrogen, which relies on renewable energy sources. The oxygen acquired during this phase is also utilized as a source of oxygen in the hospital. The hydrogen acquired is utilized immediately for therapeutic reasons in medical facilities. Hydrogen is utilized for heating, generating power, and serving as a fuel for vehicles (Izadi et al., 2023; Yin, Xu, and Wang, 2023).

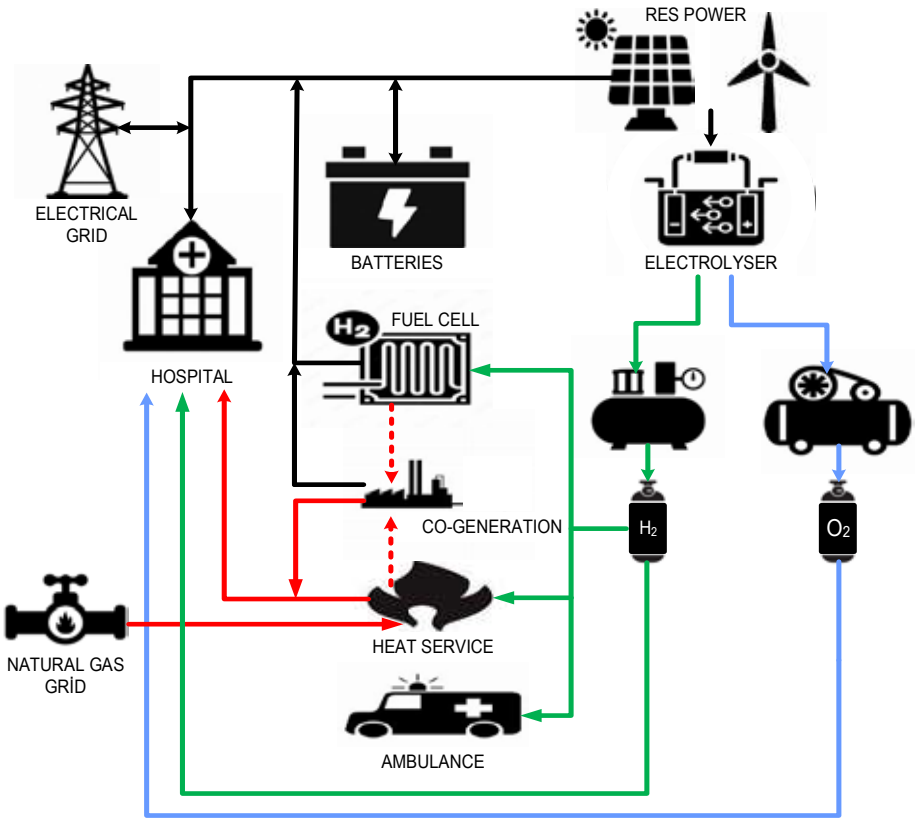


Fig. 1: An overview of hospital energy flow based on hydrogen and hydrogen technologies

III. The use of hydrogen as a sterilization and disinfection

Sterilization refers to the complete eradication or elimination of all microorganisms, including bacterial spores. Disinfection is the process of removing various disease-causing microorganisms, excluding bacterial spores (Tao et al., 2021). The sterilization techniques employed in healthcare facilities may be classified into two categories: high-temperature procedures and low-temperature approaches. However, recent improvements in sterilization technology employed in healthcare institutions have mostly focused on low-temperature sterilization systems. Hydrogen peroxide is widely recognized for its versatile use as a disinfectant, sterilant, fumigant, antiseptic, and preservative. The environmental sustainability of hydrogen peroxide is acknowledged due to its ability to break down into oxygen and water (Bharti et al., 2022). Figure 2 provides examples of hydrogen peroxide uses in the healthcare sector.

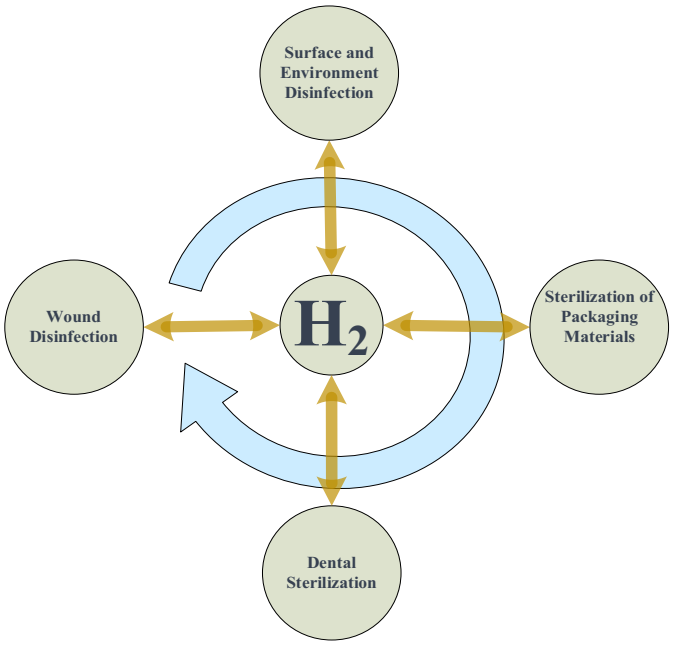


Fig. 2: The use of hydrogen and hydrogen technologies for sterilization and disinfection purposes in hospitals and healthcare institutions

IV. The use of hydrogen as a medicinal agent

Various cellular, animal, and clinical studies have demonstrated the biological effects of hydrogen molecules, focusing on their anti-inflammatory, antiapoptotic, and antioxidant properties. Molecular hydrogen (H2) has demonstrated potent antioxidant and anti-inflammatory properties in several illnesses via modulating the activity and expression of molecules. Studies have also shown that H2 therapy improves the wound healing process in many models of skin injury illnesses, including burn wounds, pressure ulcers, diabetic wounds, and radiation-induced dermatitis. These findings indicate that H2 therapy has significant promise as an effective method in the realm of therapeutic wound care. Empirical studies have demonstrated that individuals suffering from various chronic respiratory conditions exhibit favorable reactions to H2 treatment. Figure 3 presents a comprehensive compilation of the therapeutic applications of hydrogen molecules (Perveen et al., 2023; Zhao et al., 2023).

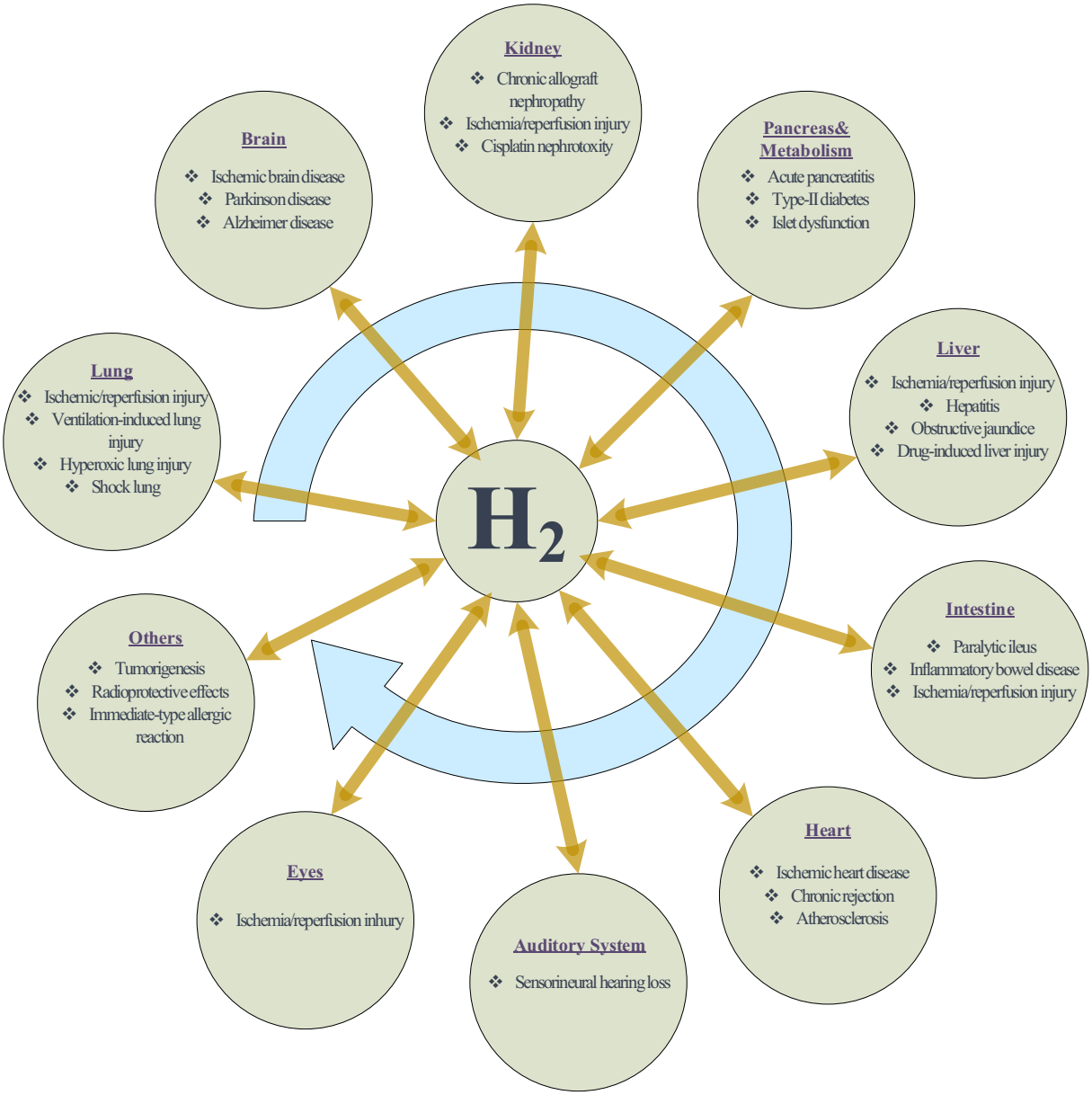


Fig. 3: The use of hydrogen for therapeutic purposes in humans.

V. Conclusions

This study examines the application areas of hydrogen and hydrogen technologies in hospitals and healthcare institutions. The use of hydrogen and hydrogen technologies in these settings significantly contributes to the energy supply and security of these institutions, which are major energy consumers. Additionally, energy production from renewable sources makes significant contributions to the carbon reduction of hospitals. Hydrogen molecules also have notable biological effects, making hydrogen a vital medical gas for direct treatment purposes. Hydrogen peroxide is crucial for sterilization and disinfection in hospitals due to its properties as a disinfectant, sterilant, fumigant, antiseptic, and preservative.

References

Bharti, Bandna, Hanliang Li, Zhaoyong Ren, Rongshu Zhu, and Zhenye Zhu. 2022. “Recent Advances in Sterilization and Disinfection Technology: A Review.” *Chemosphere* 308:136404. doi: 10.1016/j.chemosphere.2022.136404.

Izadi, Ali, Masoomeh Shahafve, Pouria Ahmadi, and Pedram Hanafizadeh. 2023. “Design, and Optimization of COVID-19 Hospital Wards to Produce Oxygen and Electricity through Solar PV Panels with Hydrogen Storage Systems by Neural Network-Genetic Algorithm.” *Energy* 263:125578. doi: 10.1016/j.energy.2022.125578.

Lamagna, Mario, Benedetto Nastasi, Daniele Groppi, Caroline Rozain, Massimiliano Manfren, and Davide Astiaso Garcia. 2021. “Techno-Economic Assessment of Reversible Solid Oxide Cell Integration to Renewable Energy Systems at Building and District Scale.” *Energy Conversion and Management* 235:113993. doi: 10.1016/j.enconman.2021.113993.

Perveen, Ishrat, Bakhtawar Bukhari, Mahwish Najeeb, Sumbal Nazir, Tallat Anwar Faridi, Muhammad Farooq, Qurat-ul-Ain Ahmad, Manal Abdel Haleem A. Abusalah, Thana’ Y. ALjaraedah, Wesal Yousef Alraei, Ali A. Rabaan, Kirnpal Kaur Banga Singh, and Mai Abdel Haleem A. Abusalah. 2023. “Hydrogen Therapy and Its Future Prospects for Ameliorating COVID-19: Clinical Applications, Efficacy, and Modality.” *Biomedicines* 11(7):1892. doi: 10.3390/biomedicines11071892.

Shen, Meihua, Hongying Zhang, Congjun Yu, Fan Wang, and Xuejun Sun. 2014. “A Review of Experimental Studies of Hydrogen as a New Therapeutic Agent in Emergency and Critical Care Medicine.” *Medical Gas Research* 4(1):17. doi: 10.1186/2045-9912-4-17.

Tao, Meihan, Tianrang Ao, Xiaoyan Mao, Xinzhu Yan, Rabia Javed, Weijian Hou, Yang Wang, Cong Sun, Shuang Lin, Tianhao Yu, and Qiang Ao. 2021. “Sterilization and Disinfection Methods for Decellularized Matrix Materials: Review, Consideration and Proposal.” *Bioactive Materials* 6(9):2927–45. doi: 10.1016/j.bioactmat.2021.02.010.

Temiz, Mert, and Nader Javani. 2020. “Design and Analysis of a Combined Floating Photovoltaic System for Electricity and Hydrogen Production.” *International Journal of Hydrogen Energy* 45(5):3457–69. doi: 10.1016/j.ijhydene.2018.12.226.

Vaziri, Shabnam Mahmoudzadeh, Babak Rezaee, and Masoud Amel Monirian. 2020. “Utilizing Renewable Energy Sources Efficiently in Hospitals Using Demand Dispatch.” *Renewable Energy* 151:551–62. doi: 10.1016/j.renene.2019.11.053.

Yin, Hang, Yue Xu, and Jiahuan Wang. 2023. “Deep Learning-Based Optimization of a Hydrogen and Oxygen Production System for Patients in Hospital with Alkaline Electrolyzer.” *Fuel* 333:126441. doi: 10.1016/j.fuel.2022.126441.

Zhao, Pengxiang, Zisong Cai, Xujuan Zhang, Mengyu Liu, Fei Xie, Ziyi Liu, Shidong Lu, and Xuemei Ma. 2023. “Hydrogen Attenuates Inflammation by Inducing Early M2 Macrophage Polarization in Skin Wound Healing.” *Pharmaceuticals* 16(6):885. doi: 10.3390/ph16060885.

Fabrication of 3D ordered mesoporous 1T-phase MoS_2@C for electrochemical hydrogen evolution

[1*]Derya Ozgur, [2]Filiz Akti
[1] Gazi University, Engineering Faculty, Chemical Engineering Department, Ankara, 06570, Türkiye
[2] Hitit University, Engineering Faculty, Chemical Engineering Department, Çorum, 19030, Türkiye

* E-mail:deryaoncel@gazi.edu.tr

Abstract
MoS_2 is a highly active catalyst for the hydrogen evolution reaction (HER), but its active sites are limited to the edges. Therefore, structures that expose many edges are desired for the application of MoS_2 in HER. To address this goal, a phase transition was first applied to convert the 2H-MoS_2 phase into the 1T-MoS_2 phase, which exhibits higher conductivity and catalytic activity. Morphological design was also achieved by incorporating the synthesized 1T-MoS_2 onto a mesoporous carbon support (CMK-3). The 3D-ordered mesoporous structure of the catalyst provides a high specific surface area and ensures efficient transport channels for both the material and electrons during the electrochemical HER. Consequently, the composite demonstrated efficient HER activity, exhibiting lower overpotential and Tafel slope under acidic conditions. This study lays the groundwork for constructing a 3D HER catalyst with a high specific surface area and uniformly dispersed, few-layered MoS_2.

Keywords: 3D ordered mesoporous structure, 1T-phase MoS_2, high specific surface area, hydrogen evolution reaction

I. Introduction

The use of fossil fuels, along with the development of modern society and industry, has constantly increased, resulting in greenhouse gas emissions. The global climate scenario, combined with the gradual depletion of fossil reserves and rapid increase in energy consumption, has revealed the necessity of developing alternative energy sources that are renewable, clean, and promising in the future.

Hydrogen is a potential candidate for future energy systems because it is an environmentally friendly energy carrier with a high gravimetric energy density (Zhu et al., 2019). Approximately 90% of the current hydrogen production comes from fossil energy sources (Hota et al., 2022). However, a clean, renewable, and efficient hydrogen production route is required to sustain a hydrogen economy. Water electrolysis has been accepted among green and sustainable hydrogen production technologies with zero carbon emissions (Sun et al., 2022). Electrocatalytic hydrogen production requires electricity from renewable sources (wind, water, or sun); therefore, the intermittent nature of renewable sources can be converted into hydrogen fuel and stored. The Pt catalyst is the most effective for electrocatalytic hydrogen production, but its high cost has driven the search for alternative electrocatalysts to replace Pt catalysts. Among the abundant non-noble-metal catalysts, MoS_2 is the most promising for HER applications (Hellstern et al., 2017). Despite its potential, MoS_2 is highly anisotropic; its activity for HER is limited to the edge regions because the basal regions lack catalytic activity, and its semiconductor properties make it less efficient than Pt-based catalysts. Nevertheless, shaping the morphology of MoS_2 improves its catalytic performance. Placing the MoS_2 structure into a mesoporous conductive structure allows the electrons from the electrode to reach the active sites and quickly overcome ion transfer resistances, significantly increasing the HER performance.

In this study, the CMK-3 mesoporous carbon structure was preferred to increase the effectiveness of MoS_2. A procedure was developed to modify CMK-3, safeguarding the pores in the hybrid structure during the incorporation of MoS_2 into CMK-3 and preventing MoS_2 stacking. This approach maintained the surface area of the modified MoS_2 without a significant reduction compared to previous work.

II. Materials Synthesis and Characterization

For the synthesis of CMK-3, SBA-15 silica mesoporous material was used as the replica, sucrose as the carbon source, deionized water as the solvent, H_2SO_4 as the acid source, and HF acid to remove the replica. SBA-15 was synthesized as described by Akti et al. (2019). Pluronic 123 was dissolved in deionized water, and HCl solution was added. TEOS was then added and the mixture was stirred for 24 h at 37 °C. At the end of this period, the obtained mixture was placed in an autoclave and heated in an oven at 100 °C for 48 h. Finally, the obtained solid gel was filtered and dried at RT. The dried samples were calcined in air at 550 °C at a rate of 1 °C/min for 6 h.

CMK-3 was synthesized as follows. SBA-15 and sucrose were dissolved in a mixture of H_2SO_4 and distilled water, respectively. After mixing for 1 h, the solution was first dried in an oven at 100 °C for 6 h and then dried in an oven at 160 °C for 6 h. The resulting solid was again treated with sucrose, H_2SO_4, and distilled water after mixing for 1 h. The drying process was repeated as previously described. The samples were then carbonized in a tube furnace under nitrogen atmosphere at 900 °C for 3 h. Finally, HF acid was treated several times to remove the replica from the structure. After the samples were filtered, they were washed several times with an ethanol/water mixture and dried in an oven at 40 °C for 24 h.

In the synthesis of 1T-MoS_2@CMK-3, CMK-3 was initially modified, and then MoS_2 was added to the mixture.

MoS_2 was synthesized according to the method determined by Oncel Ozgur in 2022. The final product was then dried in a vacuum oven at 60 °C.

Surface area, pore volume, and pore diameter values were determined from nitrogen adsorption/desorption isotherms data using the procedure described by Lowell et al. 2012. Nitrogen adsorption/desorption isotherm experiments were performed using a Quanthrocrome Autosorb 1C instrument at 77 K.

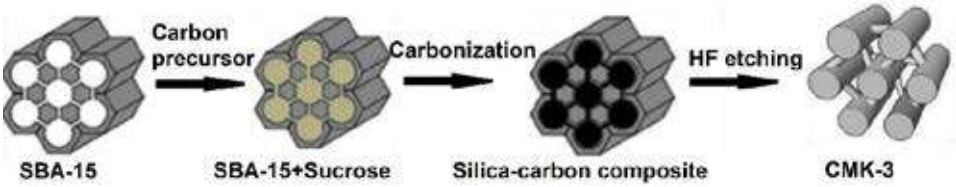


Fig. 1: Synthesis step of CMK-3.

III. Electrocatalytic Performance of Materials

An electrochemical workstation (Ivium CompactStat potentiostat/galvanostat) was configured with three electrodes: an Ag/AgCl (3 M KCl) reference electrode and a graphite rod serving as the counter electrode. The electrochemical reactions were conducted in a 0.5 M H_2SO_4 solution. The prepared electrocatalysts were applied to a glassy carbon electrode (2 mm in diameter) that served as the working electrode. The catalyst ink was prepared by combining 4 mg of catalyst with 750 µL of deionized water, 250 µL of ethanol, and 20 µL of 0.5 wt% Nafion solution. Subsequently, 5 µL of the catalyst ink was deposited onto the cleaned glassy carbon electrode. Polarization curves were recorded using linear sweep voltammetry (LSV) at a scan rate of 5 mV/s.

IV. Results and discussions

Nitrogen adsorption/desorption isotherms of CMK-3 & 1T-MoS_2@CMK-3

The nitrogen ad/des isotherms of CMK-3 and 1T-MoS_2@CMK-3 are shown in Fig. 2a, and the isotherm behavior was examined according to the IUPAC classification. The samples exhibited a Type IV isotherm behavior, which is a typical characteristic of mesoporous materials containing micropores. With the inclusion of MoS_2 in the structure, the surface area decreased from 1364 m^2/g to 843 m^2/g. This decrease indicated that MoS_2 was included in the structure. Although the mesopore volume values were close to each other, the micropore volume value exhibited a 50% reduction (Table 1). This decrease was thought to be due to the MoS_2 settlingng into the structure, which blocked the micropores. The pore size distributions of CMK-3 and 1T-MoS_2@CMK-3 are shown in Fig. 2b. The mesopore diameter values obtained are similar for both catalysts. The lack of change in either mesopore volume or mesopore diameter values demonstrated that incorporating MoS_2 into the structure after modifying CMK-3 was an effective method.

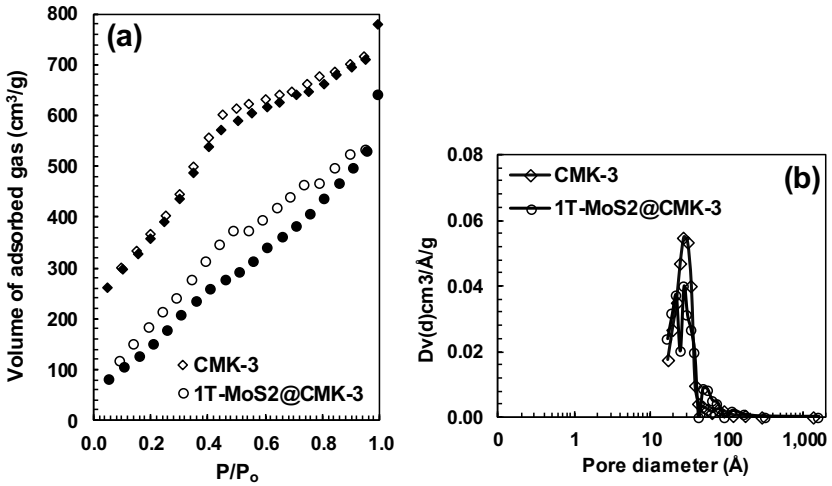


Fig. 2: (a) Nitrogen adsorption/desorption isotherm (b) Pore size distribution of CMK-3 and 1T-MoS2@CMK-3.

Table 1: Physical properties of CMK-3 and 1T-MoS_2@CMK-3 samples.

Sample	Surface area (m^2/g)		Pore volume (cm^3/g)		Porediameter (Å)
	Multi point	BJH	Meso (BJH)	Micro (SF)	Meso (BJH)
CMK-3	1364	1428	1.194	0.523	27.5
1T-MoS_2@CMK-3	843	1282	1.220	0.203	26.5

Electrochemical performance of 1T-MoS_2@CMK-3 hybrids

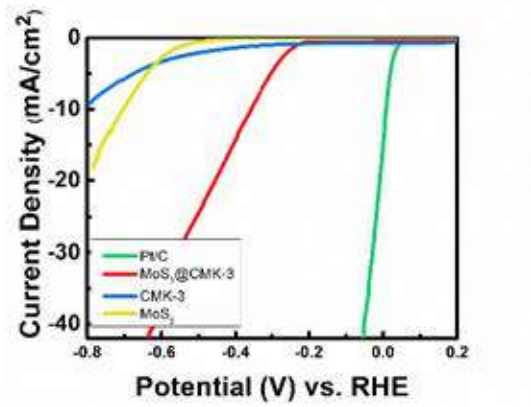


Fig.3: Polarization curves of the as-synthesized catalysts.

Fig. 3 shows the polarization curve of the synthesized 1T-MoS_2@CMK-3 cathode. In addition to pristine MoS_2 (2H-MoS_2), CMK-3, and Pt/C were used as electrocatalysts to better understand the HER performance of the 1T-MoS_2@CMK-3 hybrid. As anticipated, Pt/C exhibited the highest activity in terms of the onset potential (~ 0 mV) and an overpotential of 83 mV at 10 mA/cm², with a low Tafel slope of 35 mV dec^{-1}. The 1T-MoS_2@CMK-3 hybrid demonstrated a slight increase in overpotential (350 mV) at a current density of 10 mA/cm² compared to that of the Pt/C. However, the overpotentials of pristine MoS_2 (705 mV) and CMK-3 (817 mV) are 2.0 to 2.63 times higher than that of 1T-MoS_2@CMK-3. The synthesized 1T-MoS_2@CMK-3 exhibited the lowest Tafel slope of 88 mV dec^{-1}, whereas pristine MoS_2 and CMK-3 exhibited higher Tafel slopes of 140 and 550 mV dec^{-1}, respectively. A lower Tafel slope indicates faster kinetics and is more favorable for the HER.

V. Conclusions

In summary, MoS_2 nanosheets with enhanced 1T phase were successfully deposited onto mesoporous CMK-3. The synthesized 1T-MoS_2@CMK-3 catalysts exhibited low Tafel slopes and low overpotential values in HER reactions. This can be attributed to (i) the increased number of active sites and conductivity for hydrogen adsorption in 1T-MoS_2 and (ii) the 3D CMK-3 carbon matrix, which not only provides the inherent electrical conductivity of carbon-based materials but also limits the size and aggregation of in situ deposited active MoS_2 materials. Importantly, these accessible 3D mesoporous structures significantly enhanced electron/ion transport kinetics. We anticipate that the 1T-MoS_2@CMK-3 materials investigated in this study will play a significant role in the design of high-performance materials for energy storage and conversion.

Acknowledgements

This work was supported by the Scientific and Technological Research Council of Turkey (TUBITAK Project Nos 123M875).

References

Akti F., Balci S., Dogu T., Role of synthesis media on properties of tin and copper incorporated SBA-15 catalysts and their activity in selective oxidation of ethanol, Materials Chemistry and Physics, 223, 249-259 (2019).

Hellstern T. R., Kibsgaard J., Tsai C., Palm D. W., King L. A., Abild-Pedersen F., Jaramillo T. F., Investigating Catalyst–Support Interactions To Improve the Hydrogen Evolution Reaction Activity of Thiomolybdate [Mo3S13]2– Nanoclusters. ACS Catalysis, 7(10), 7126-7130 (2017).

Hota P., Das A., Maiti D. K., A short review on generation of green fuel hydrogen through water splitting. International Journal of Hydrogen Energy, 48(2), 523-541 (2022).

Sun L., Han L., Huang J., Luo X., Li X., Single-atom catalysts for photocatalytic hydrogen evolution: A review. International Journal of Hydrogen Energy, 47(40), 17583-17599 (2022).

Lowell S., Shields J. E., Thomas M. A., Thommes M., Characterization of porous solids and powders: surface area, pore size and density (Vol. 16). Springer Science & Business Media (2012).

Oncel Ozgur D., 2A novel 0D/2D/2D hetero-layered nitrogen-doped graphene/MoS2 architecture for catalytic hydrogen evolution reaction. Fuel, 328, 125538 (2022).

Zhu J., Hu L., Zhao P., Lee L. Y. S., Wong K.Y., Recent advances in electrocatalytic hydrogen evolution using nanoparticles. Chemical reviews, 120(2), 851-918 (2019).

HOPat: A new feature extraction function based on the atomic orbitals of the hydrogen atom

[1*]Habip Sahin, [2]Sengul Dogan, [3]Turker Tuncer
[1] Fırat University, Technical Vocational School, Hybrid and Electric Vehicles Technology, Elazığ, 23119, Türkiye
[2,3] Fırat University, Technology Faculty, Department of Digital Forensics Engineering, Elazığ, 23119, Türkiye

* E-mail: habipsahin@firat.edu.tr

Abstract
In this study, our primary objective was to identify a novel attribute of hydrogen with potential applications in machine learning. To develop a new quantum-based feature extraction function, we analyzed the orbitals of the hydrogen atom and modeled them as directed graphs. Using these models, we proposed a feature extraction function termed the Hydrogen Orbit Pattern (HOPat). To demonstrate HOPat's classification ability, we have presented a feature engineering model employing a public vowel dataset to detect specific language impairments.
Our feature engineering model yielded a classification accuracy of 97.33%. These results strongly demonstrate that hydrogen orbits can be utilized as feature extractors; we have discovered a new attribute of the hydrogen.

Keywords: HOPat, Hydrogen-inspired feature extraction, Quantum-inspired machine learning, Atomic orbital modelling, Specific language impairment (SLI), INCA feature selector, BGLMLR classifer.

I. Introduction

Atomic orbitals describe regions where electrons are most likely to be found around the nucleus of an atom and chemistry and quantum mechanics sciences have been interested in atomic orbital Qiao et al. (2020). Thus, the classical understanding of atoms changed, and 3-dimensional orbits began to be defined with probabilistic models being created. These three-dimensional diagrams inspire machine learning algorithms Anusuya and Kumar (2023). This study has presented the modeling of diagrams describing atomic orbitals using 2D directed graphs. This approximation helps researchers to translate complex models of atomic structure into a format suitable for digital machine learning algorithms, and the Hydrogen Orbital Pattern (HOPat) feature extraction method has been proposed using this approach. HOPat starts by splitting the input signals into overlapping blocks, and the resulting blocks are then converted into matrices. By applying the four suggested patterns to the matrices, binary features are extracted, and these binary features are converted to decimal numbers to obtain four map signals. The histograms of the map signals are combined to obtain the ultimate feature vector. The main motivation for presenting HOPat, the steps of which are given, is to show the effect of hydrogen in the machine learning research field, which is popular today, and in this respect, this study aims to discover new properties of hydrogen.
The capabilities of HOPat are demonstrated using a publicly available vowel dataset for the detection of specific language disorders (SLI) Grill et al. (2016). The model demonstrates the classification ability of HOPat by achieving a classification accuracy of 97.33%.
The integration of quantum-inspired Tasci et al. (2023) models with traditional machine learning paradigms Tuncer et al. (2022) represents a significant advance by bridging the theoretical foundations of quantum mechanics with practical applications in data analysis. It aims to inspire future studies, and our ultimate goal is to create an atomic model that can perform machine learning calculations.
In future research, we aim to develop a hydrogen-based artificial intelligence model by using unique pattern creators derived from each hydrogen atom's electronic configuration and hydrogen-based neural processing units can be developed.

II. The proposed hydrogen orbit pattern

In this research, we have proposed a new quantum-inspired feature extraction function named HOPat. This model utilizes the atomic orbitals of hydrogen atoms Orchin et al. (2005). We modeled four directed graphs to generate patterns, employing them in a local binary pattern-like feature extraction scheme due to its histogram-based nature. Firstly, we divided the signal into overlapping blocks of length 25, creating 5x5 matrices. The generated patterns (directed graphs) were embedded within these matrices for feature extraction. We applied the signum function to obtain binary features Pietikäinen (2010), which were then used to construct four map signals. Finally, we extracted histograms from these map signals, merging them to yield a 1024-length feature vector. To clarify the presented feature extractor, we gave graphical explaination of the recommended HOPat in Figure 1.

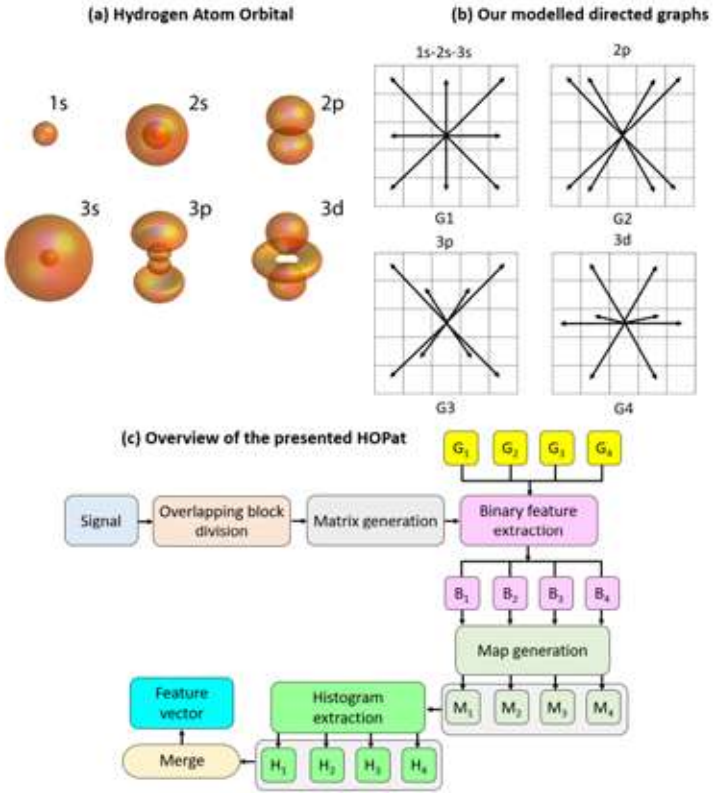


Fig. 1. The graphical outline of the proposed HOPat.

The steps of the recommended HOPat are given below.

S1: Load signal.

S2: Divide signal to overlapping data block and the length of each data block is 25.

$$dt(j) = signal(i + j - 1), i \in \{1,2, \dots, len(signal)\}, j \in \{1,2, \dots ,25\} \quad (1)$$

where dt: data block, $len(.)$: length measure function.

S3: Transform the data block to matrix with a length of 5 x 5.

S4: Extract binary features by using the presented patterns and signum function.

$$\begin{aligned} &bit_1(1) = \varphi\big(mt(3,3), mt(1,1)\big), bit_1(2) = \varphi\big(mt(3,3), mt(1,3)\big), \\ &bit_1(3) = \varphi\big(mt(3,3), mt(1,5)\big), bit_1(4) = \varphi\big(mt(3,3), mt(3,5)\big), \\ &bit_1(5) = \varphi\big(mt(3,3), mt(5,5)\big), bit_1(6) = \varphi\big(mt(3,3), mt(5,3)\big), \\ &bit_1(7) = \varphi\big(mt(3,3), mt(5,1)\big), bit_1(8) = \varphi\big(mt(3,3), mt(3,1)\big) \end{aligned} \quad (2)$$

$$\begin{aligned} &bit_2(1) = \varphi\big(mt(3,3), mt(1,1)\big), bit_2(2) = \varphi\big(mt(3,3), mt(1,2)\big), \\ &bit_2(3) = \varphi\big(mt(3,3), mt(1,4)\big), bit_2(4) = \varphi\big(mt(3,3), mt(1,5)\big), \\ &bit_2(5) = \varphi\big(mt(3,3), mt(5,5)\big), bit_2(6) = \varphi\big(mt(3,3), mt(5,4)\big), \\ &bit_2(7) = \varphi\big(mt(3,3), mt(5,1)\big), bit_2(8) = \varphi\big(mt(3,3), mt(5,2)\big) \end{aligned} \quad (3)$$

$$\begin{aligned} &bit_3(1) = \varphi\big(mt(3,3), mt(1,1)\big), bit_3(2) = \varphi\big(mt(3,3), mt(1,5)\big), \\ &bit_3(3) = \varphi\big(mt(3,3), mt(5,5)\big), bit_3(4) = \varphi\big(mt(3,3), mt(5,1)\big), \\ &bit_3(5) = \varphi\big(mt(3,3), mt(2,2)\big), bit_3(6) = \varphi\big(mt(3,3), mt(2,4)\big), \\ &bit_3(7) = \varphi\big(mt(3,3), mt(4,4)\big), bit_3(8) = \varphi\big(mt(3,3), mt(4,2)\big) \end{aligned} \quad (4)$$

$$\begin{aligned} &bit_4(1) = \varphi\big(mt(3,3), mt(1,2)\big), bit_4(2) = \varphi\big(mt(3,3), mt(1,4)\big), \\ &bit_4(3) = \varphi\big(mt(3,3), mt(5,4)\big), bit_4(4) = \varphi\big(mt(3,3), mt(5,2)\big), \\ &bit_4(5) = \varphi\big(mt(3,3), mt(3,2)\big), bit_4(6) = \varphi\big(mt(3,3), mt(3,4)\big), \\ &bit_4(7) = \varphi\big(mt(3,3), mt(3,1)\big), bit_4(8) = \varphi\big(mt(3,3), mt(3,5)\big) \end{aligned} \quad (5)$$

$$\varphi(a,b) = \begin{cases} 0, a - b < 0 \\ 1, a - b \geq 0 \end{cases} \quad (6)$$

Herein, bit binary features, mt: matrix with a size of 5 x 5 and $\varphi(.)$: signum function. By deploying the created four patterns, four binary features vectors been extracted.

S5: Compute map signal by deploying binary to decimal transformation.

$$map_k(i) = \sum_{j=1}^{8} bit_k(j) * 2^{j-1}, k \in \{1,2, \dots ,4\} \quad (7)$$

where map: map signal.

S6: Extract histograms of the map signals.

S7: Merge the extracted histograms to create feature vector with a lenfgth of 1024.

III. Feature engineering model

To demonstrate the classification ability of the presented HOPat, we have designed/created a simple feature engineering model. This model has three main phase and these are:

- The proposed HOPat-based feature extraction,
- The most informative features selection deploying Iterative Neighborhood Component Analysis (INCA) feature selector Tuncer et al. (2020)
- Binary Generalized Linear Model Logistic Regression (BGLMLR) classifier-based classification Schein et al. (2003).

Furthermore, Figure 2 summarizes the presented HOPat-based signal classification model graphically.

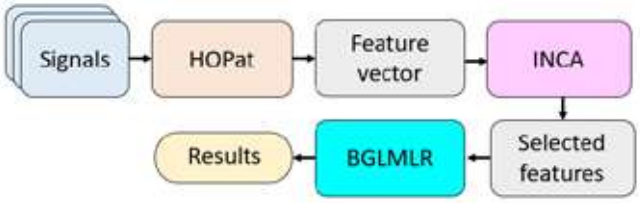


Fig. 2. The graphical depiction of the proposed model.

The steps of the presented feature engineering model are:

Step 1: Extract features from the signal using the proposed HOPat, obtaining 1024 features for each signal.

Step 2: Select the most informative features from the extracted feature set using the INCA feature selector.

Step 3: Classify the selected features with a BGLMLR classifier, employing 10-fold cross-validation (CV).

This model is designed to demonstrate the classification capabilities of the proposed HOPat. Therefore, we have intentionally kept its structure simple.

IV. Results and discussions

The proposed HOPat-based signal classification model was implemented using MATLAB (version 2024a) programming environment, utilizing .m files to create functions which are HOPat, INCA, BGLMLR and main functions. This model was executed on a standard (simple configured) personal computer with 32 gigabytes of main memory, a 3.6 GHz central processing unit (CPU), and the Windows 11 operating system. The implementation operated in CPU mode and we did not use any parallel programming model. Moreover, our HOPat-based classification model does not necessitate specialized hardware such as a graphical processing unit (GPU) since it has linear time complexity.

To evaluate classification performance, we employed a publicly available vowel signal dataset containing two classes: (i) specific language impairment (SLI) and (ii) control. This dataset was compiled by researchers at the Czech Technical University Grill et al. (2016). The attributes of this dataset has been given below.

Table 1. The characteristics of the collected vowel signal dataset.

Attribute	Value
Audio signal	Vowel sounds
Signal acquisition	Digital microphone
Sampling frequency	44.1 KHz
Subject by class	54 SLI (35 Male, 19 Female), 44 control (15 Male, 29 Female)
Number of sounds	2173 SLI, 1680 control

To comprehensively evaluate the model's classification capabilities, we utilized various metrics. These include sensitivity, specificity, geometric mean, precision, F1-score, and classification accuracy Zhu et al. (2010). We present their mathematical definitions in the following section.

$$sensitivity = \frac{tp}{tp + fn} \quad (8)$$

$$specificity = \frac{tn}{tn + fp} \quad (9)$$

$$geometric\ mean = \sqrt{sensitivity * specificity} \quad (10)$$

$$precision = \frac{tp}{tp + fp} \quad (11)$$

$$F1 - score = 2\frac{sensitivity * precision}{sensitivity + precision} \quad (12)$$

Here, tp: true positive, tn: true negative, fp: false positive and fn: false negative.

To compute the given performance evaluation metrics, we have used the confusion matrix and the computed confusion matrix have been given in Figure 3.

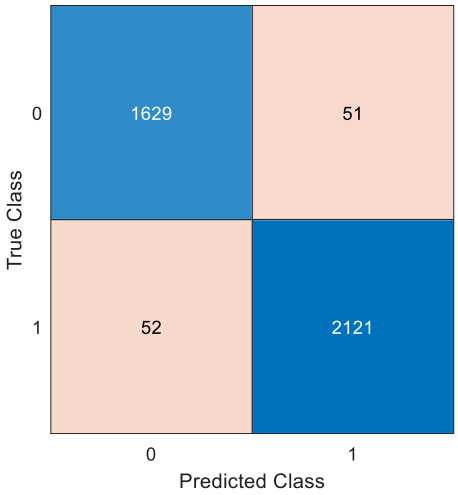


Fig. 3. The confusion matrix of the presented HOPat-based feature engineering model. 0: Control, 1: SLI.

Table 2 summarizes the computed performance evaluation metrics.

Table 2. The results of the HOPat-based model on the used SLI vowel dataset.

Performance metric	Result (%)
Classification accuracy	97.33
Sensitivity	97.61
Specificity	96.96
Geometric mean	97.28
Precision	97.65
F1-score	97.63

As shown in Table 2, the proposed model achieved a classification accuracy of 97.33%, with high sensitivity (97.61%), specificity (96.96%), geometric mean (97.28%), precision (97.65%), and F1-score (97.63%). These results strongly indicate the model's robust classification performance.

The most important points of this research are:

- A new quantum-inspired feature extraction function which is HOPat has been proposed.
- The atomic orbitals are modeled as directed graphs, which are then utilized in a feature extraction process.
- We have proposed a feature engineering model to get classification performance of the HOPat and our proposal attained 97.33% of classification accuracy on a public vowel sound dataset.
- In this research, we have discovered feature extraction ability of the hydrogen.

V. Conclusions

This research investigated a novel attribute of hydrogen by modeling its atomic orbits, leading to the development of the quantum-inspired feature extraction function, HOPat. To evaluate HOPat, we designed a feature engineering model using an SLI vowel sound dataset. This model involved feature extraction with HOPat, feature selection using INCA, and classification with a BGLMLR classifier, achieving 97.33% accuracy. These results suggest the potential of hydrogen-based models for machine learning applications. Future work will explore new hydrogen-based feature extractors derived from wave equations.

Acknowledgements

References

Anusuya, T., and Vivek Kumar. "DFT study of hydrogen interaction with transition metal doped graphene for efficient hydrogen storage: effect of d-orbital occupancy and Kubas interaction." Physical Chemistry Chemical Physics 25.1 (2023): 262-273.

Grill, Pavel, and Jana Tučková. "Speech databases of typical children and children with SLI." PloS one 11.3 (2016): e0150365.

Orchin, Milton, et al. "Atomic orbital theory." The Vocabulary and Concepts of Organic Chemistry, Second Edition, John Wiley & Sons, Inc., Hoboken, NJ, USA. doi 10 (2005): 0471713740.

Pietikäinen, Matti. "Local binary patterns." Scholarpedia 5.3 (2010): 9775.

Qiao, Zhuoran, et al. "OrbNet: Deep learning for quantum chemistry using symmetry-adapted atomic-orbital features." The Journal of chemical physics 153.12 (2020).

Schein, Andrew I., Lawrence K. Saul, and Lyle H. Ungar. "A generalized linear model for principal component analysis of binary data." International Workshop on Artificial Intelligence and Statistics. PMLR, 2003.

Tasci, Gulay, et al. "Automated accurate detection of depression using twin Pascal's triangles lattice pattern with EEG Signals." Knowledge-Based Systems 260 (2023): 110190.

Tuncer, Turker, et al. "Novel multi center and threshold ternary pattern based method for disease detection method using voice." IEEE Access 8 (2020): 84532-84540.

Tuncer, Turker, et al. "A novel Discrete Wavelet-Concatenated Mesh Tree and ternary chess pattern based ECG signal recognition method." Biomedical Signal Processing and Control 72 (2022): 103331.

Zhu, Wen, Nancy Zeng, and Ning Wang. "Sensitivity, specificity, accuracy, associated confidence interval and ROC analysis with practical SAS implementations." NESUG proceedings: health care and life sciences, Baltimore, Maryland 19 (2010): 67.

Alternative Fuel Mixtures and Sustainable Development: An Energy and Environmental Perspective Evaluation of Diesel, Biodiesel, and Alcohol Blends

*Halis Deviren
Dicle University, Diyarbakır Vocational School of Technical Sciences, Department of Motor Vehicles and Transportation Technologies, Diyarbakır, 21280, Türkiye.

* E-mail:halis.deviren@dicle.edu.tr

Abstract
This study examined biodiesel synthesized from oil extracted from safflower seeds grown under arid conditions and butanol that can be produced through the fermentation of lignocellulosic materials. The remaining cake, with a 22-24% crude protein content after oil extraction from safflower seeds, can be used as a valuable alternative animal feed. Additionally, along with biodiesel produced from this oil, n-butanol was also mixed with fossil-based diesel fuel (DF), which has a high carbon/hydrogen ratio, to examine the effects on emissions. The obtained mixtures have resulted in a 17.47% reduction in carbon monoxide (CO) emissions and a 21.05% reduction in nitrogen oxides (NOx) emissions compared to diesel fuel (DF). The results demonstrate that alternative fuels provide cleaner combustion and produce fewer harmful gas emissions. These findings demonstrate the potential to develop sustainable transportation solutions while complying with environmental regulations.

Keywords: Carbon/hydrogen ratio, n-bütanol, biodiesel, Sustainable fuel solutions, Emissions mitigation

I. Introduction

Compression Ignition (CI) engines offer advantages over gasoline engines due to their high brake thermal efficiencies and superior combustion characteristics. Reduced fuel consumption and increased durability contribute to their preferred use in the energy, agriculture, and transportation sectors. (Heywood, 1988; V. Kumar et al., 2020). However, the widespread use of CI engines increases fossil fuel consumption, jeopardizing the sustainability of energy resources and contributing to global air pollution and climate change. Strict emission regulations are implemented to mitigate these issues (Agarwal et al., 2020; Chen et al., 2023). In this context, considering sustainable energy solutions and environmental impacts, interest in renewable energy sources is increasing, and research in this area is intensifying (Çılğın, 2015). Renewable energy sources such as alcohol, vegetable oils, and biodiesel are considered effective alternatives for meeting energy needs and reducing emission levels (Imdadul et al., 2016). However, some studies indicate that at low engine loads, the inadequate atomization of biodiesel during the combustion of the air-fuel mixture slightly increases CO and hydrocarbon (HC) emissions (M. S. Kumar et al., 2010; Sahoo et al., 2009). The high viscosity of biodiesel adversely affects fuel injection, atomization, and combustion processes, leading to challenges (Gaur et al., 2022). Additionally, the use of biodiesel in CI engines is associated with increased NOx emissions due to its high viscosity and oxygen richness (Bitire & Jen, 2022; Hazar et al., 2019; Hoekman & Robbins, 2012). To address this issue, instead of viscosity-reducing preheating techniques and engine design and operational settings, which would entail significant costs and technical challenges, the use of various additives and technologies that enhance combustion efficiency and reduce emissions is recommended.

Biobutanol, as an additive, possesses advantages such as high energy density, less tendency to create water pollution, low corrosiveness, improved blend stability, and a higher cetane number compared to lighter alcohols. Biobutanol is a renewable fuel produced through the alcoholic fermentation of biomass-based raw materials. The sustainability of its production depends on the raw materials used and the process involved. Both the raw materials (such as corn, sugarcane, sugar beet) and the processes used for ethanol production can be easily adapted for butanol production. Bütanol üretiminin sürdürülebilirliği, fermantasyon yoluyla lignoselülozik malzeme kullanımı ile artırılabilir. However, this technology is still in the development stage and requires additional research to advance (Rakopoulos et al., 2011). Additionally, crude glycerol, a byproduct of biodiesel production, can be used for butanol production through anaerobic fermentation. This method offers an efficient alternative by enabling the effective utilization of crude glycerol (Sukjit et al., 2013). Bio-alcohols like butanol offer significant advantages for internal combustion engines due to their high hydrogen/carbon ratio, existing oxygen content, and molecular structures, achieving high fuel standards (Jung et al., 2020; Munfarida et al., 2021; Nogueira et al., 2021; Voloshin et al., 2016). Particularly, recent research has determined that adding oxygenated alcohols, primarily n-butanol and isobutanol, to biodiesel-diesel-nanoparticle mixtures enhances performance parameters and reduces pollution (Pullagura et al., 2022, 2023). The carbon-hydrogen bonds in these alcohols are positioned differently, which increases the combustion rate and their structures inherently oppose the formation of NOx. Consequently, the combustion process is improved, and NOx emissions are reduced (Gu et al., 2013; Ozsezen et al., 2011). In this context, the use of biodiesel and bio-alcohols stands out among sustainable fuel alternatives, contributing to both environmental and technological innovations.

II. Experimental Set-up and Procedure

The oil required for biodiesel production was extracted from safflower seeds using a hydraulic press and converted into biodiesel through the transesterification process shown in Figure 1.

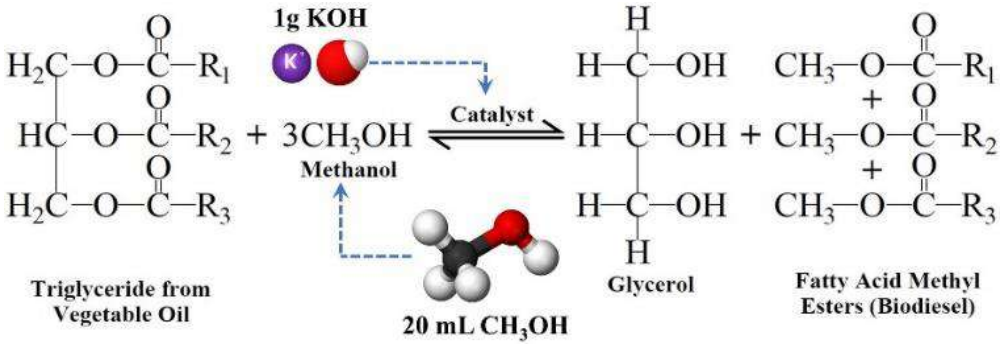


Fig. 1: Biodiesel synthesis from safflower seed oil through the transesterification process

As described in the literature and Figure 1, the conversion of safflower seed oil into fatty acid methyl esters (FAME) has been successfully carried out, and as a result, biodiesel (B100) has been produced from safflower seed oil (Deviren & Aydın, 2023). This conversion process was conducted using 1% potassium hydroxide (KOH) catalyst based on the mass of the oil and the addition of methanol equivalent to 20% of the oil's volume, at a temperature of 60°C and a mixing speed of 600 rpm. (Deviren et al., 2023).

In this study, without additives DF was used as the reference fuel for comparative analysis. A mixture created by adding 50% biodiesel by volume to DF has been named DF50B50. Similarly, a fuel mixture prepared by adding 50% 1-butanol by volume to DF has been named DF50BÜ50, and a mixture prepared by adding 25% biodiesel and 25% 1-butanol to DF has been named DF50B25BU25. The basic properties of the tested fuels are given in Table 1.

Tab. 1: Specification of tested fuels

Properties	DF[a]	Biodiesel (B100)[b]	1-butanol[c]
Density at 15 °C (kg m^{-3})	*827.1*	*886.6*	*809.5*
Cetane number	*53.9*	*54.8*	*17*
Kinematic viscosity at 40 °C (mm^2 s^{-1})	*2.70*	*4.444*	*2.23*
Lower heating value (kJ kg^{-1})	*43,11*	*39,700*	*33.12*
Latent heat of vaporization[a] (kJ kg^{-1})	*243*	*221*	*581.4*
Surface tension (mN/m)	*36.85*	*44.91*	*24.2*
Chemical formula	$C_{14}H_{25}$	$C_{17.88}H_{32.69}O_2$	C_4H_9OH
Carbon (mass%)	*87.05*	*76.78*	*64.78*
Hydrogen (mass%)	*12.95*	*11.78*	*13.63*
Oxygen (mass%)	*0*	*11.44*	*21.59*
Carbon/Hydrogen	*6.72*	*6.51*	*4.75*

[a]These values were adopted from Ref. (Sukjit et al., 2013)
[b]These values were adopted from Ref. (Deviren & Aydın, 2023)
[c]Values determined by the supplier

Based on the data presented in Table 2 and using the percentages of the main FAME identified by GC-MS (Gas Chromatography-Mass Spectrometry) analysis of biodiesel, calculations were performed using Python on the Google Colaboratory platform. As a result, the chemical formula of biodiesel and the mass percentages of carbon, hydrogen, and oxygen elements specified in Table 1 were obtained. This process is crucial for a detailed analysis of the chemical structure and properties of biodiesel.

Tab. 2: GC-MS analysis of biodiesel components and molar mass

Compound	Percentage	Formula	Molar Mass (g/mol)	Element Counts
Metil palmitat	*6.1%*	$C_{16}H_{32}O_2$	*256*	*{'C': 16, 'H': 32, 'O': 2}*
Metil stearat	*2.5%*	$C_{18}H_{36}O_2$	*284*	*{'C': 18, 'H': 36, 'O': 2}*
Metil oleat	*28.9%*	$C_{18}H_{34}O_2$	*282*	*{'C': 18, 'H': 34, 'O': 2}*
Metil elaidat	*0.7%*	$C_{18}H_{34}O_2$	*282*	*{'C': 18, 'H': 34, 'O': 2}*
Metil linoleat	*59.2%*	$C_{18}H_{32}O_2$	*280*	*{'C': 18, 'H': 32, 'O': 2}*
Metil α-linolenat	*0.7%*	$C_{18}H_{30}O_2$	*278*	*{'C': 18, 'H': 30, 'O': 2}*
Metil palmitat	*6.1%*	$C_{16}H_{32}O_2$	*256*	*{'C': 16, 'H': 32, 'O': 2}*
Metil stearat	*2.5%*	$C_{18}H_{36}O_2$	*284*	*{'C': 18, 'H': 36, 'O': 2}*

In this study, a single-cylinder, four-stroke, naturally aspirated Kirloskar TV1 diesel engine with a maximum power output of 5.2 kW and a working speed of 1500 rpm was used. The engine load was adjusted using an eddy current type dynamometer integrated into the engine and controlled by a unit.

The emission values such as CO, NO, NOx, and smoke opacity in the engine's exhaust gases were measured on a dry basis using the Testo 350 brand analyzer. In order to obtain highly accurate measurement results, the device's calibration, zeroing, and contamination tests were meticulously conducted prior to analysis. The measurements were repeated three times, and the results were determined by taking the averages of the obtained data.

III. Results and discussions

The data collected from the test engine were thoroughly analyzed based on the average values of all loads during the tests (AAL), to better represent the real-world usage conditions of vehicles. As can be seen in Figure 2(a), the engine produces high levels of CO emissions for all fuels under low load conditions. As the load increases, the observed decrease in CO levels can be explained by the increased amount of oxygen in high load conditions, which promotes the oxidation of CO, resulting in reduced emissions. Additionally, the rise in cylinder temperature under nominal load conditions is another factor contributing to the decrease in CO emissions (Atmanli & Yilmaz, 2020; Thiyagarajan et al., 2020).

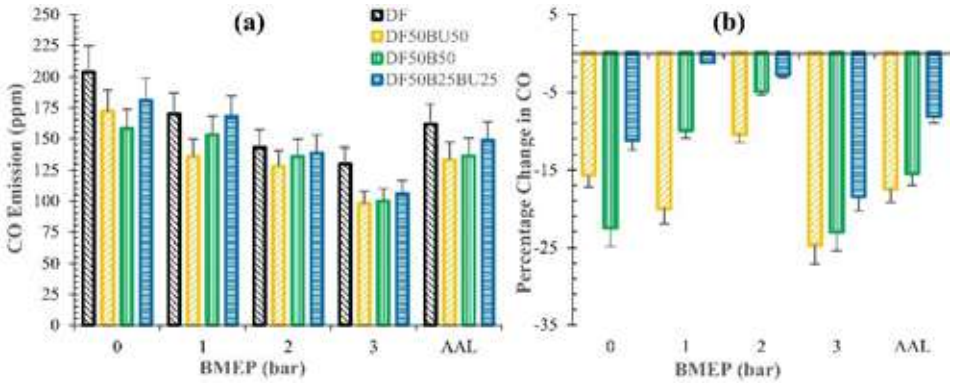


Fig. 2: (a) CO values of the fuels and (b) Percentage differences of other fuels compared to DF based on BMEP

As shown in Figure 3(a), the increase in engine load raises combustion temperatures, linearly increasing NOx emissions. At high temperatures, prolonged interaction between oxygen and nitrogen triggers NOx release. As the engine load increases, the pressure and temperature in the combustion chamber also rise, which leads to an increase in NOx emissions (Nour et al., 2019). Figure 3(b) comparatively displays the percentage changes in NOx emissions for different fuels tested under various load conditions, in comparison with DF.

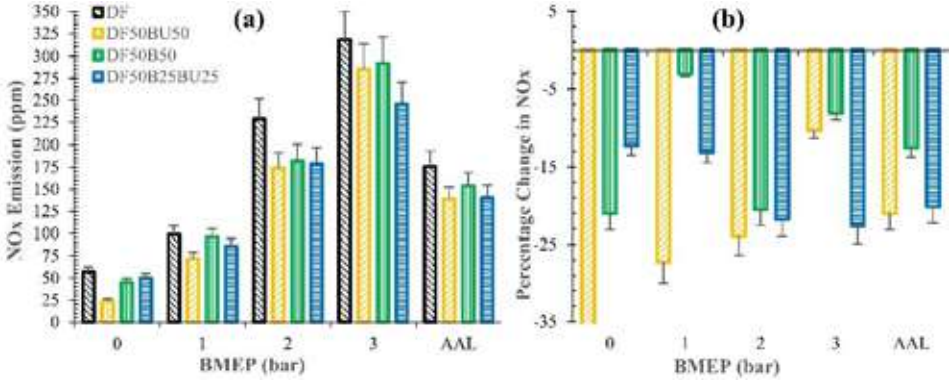


Fig. 3: (a) NOx values of the fuels and (b) Percentage differences of other fuels compared to DF based on BMEP

V. Conclusions

Based on the data obtained from GC-MS analysis, the chemical formula of the synthesized biodiesel has been determined to be $C_{17.88}H_{32.69}O_2$. The carbon/hydrogen ratios for DF, biodiesel, and n-butanol have been calculated as 6.72, 6.51, and 4.75, respectively. In the conducted tests, when averaged motor loads were compared with DF, the DF50BU50 dual fuel blend achieved the best results with a 17.47% reduction in CO emissions and a 21.05% reduction in NOx emissions. In conclusion, the binary and ternary fuel blends prepared by adding biodiesel and n-butanol to DF fuel have significantly reduced emissions compared to DF alone. These results demonstrate the potential of alternative fuel blends to reduce environmental impacts.

References

Agarwal, A. K., Singh, A. P., Gupta, T., Agarwal, R. A., Sharma, N., Pandey, S. K., & Ateeq, B. (2020). Toxicity of exhaustparticulates and gaseous emissions from gasohol (ethanol blended gasoline)-fuelled spark ignition engines. *Environmental Science: Processes and Impacts*, *22*(7), 1540–1553. https://doi.org/10.1039/d0em00082e

Atmanli, A., & Yilmaz, N. (2020). An experimental assessment on semi-low temperature combustion using waste oil biodiesel/C3-C5 alcohol blends in a diesel engine. *Fuel*, *260*, 116357. https://doi.org/10.1016/j.fuel.2019.116357

Bitire, S. O., & Jen, T. C. (2022). The role of a novel green synthesized nanoparticles added parsley biodiesel blend on the performance-emission characteristics of a diesel engine. *South African Journal of Chemical Engineering*, *41*(1), 161–175. https://doi.org/10.1016/j.sajce.2022.06.007

Chen, Y., Alizadeh, A., Abed, A. M., Nasajpour-Esfahani, N., Smaisim, G. F., Hadrawi, S. K., Zekri, H., Sabetvand, R., & Toghraie, D. (2023). The combustion process of methyl ester-biodiesel in the presence of different nanoparticles: A molecular dynamics approach. *Journal of Molecular Liquids*, *373*, 121232. https://doi.org/10.1016/j.molliq.2023.121232

Çılğın, E. (2015). 3. Nesil Biyoyakıt Teknolojisi Alglerin bir Dizel Motorunda Performans ve Egzoz Emisyonlarına Etkisinin

Araştırılması. *Iğdır Üniversitesi Fen Bilimleri Enstitüsü Dergisi*, *5*(3), 33–41. http://dergipark.gov.tr/igdirfbed/issue/15545/385065
Deviren, H., & Aydın, H. (2023). Production and physicochemical properties of safflower seed oil extracted using different methods and its conversion to biodiesel. *Fuel*, *343*, 128001. https://doi.org/10.1016/j.fuel.2023.128001
Deviren, H., Çılgın, E., & Aydin, S. (2023). Study on using nano magnesium oxide (MNMgO) nanoparticles as fuel additives in terebinth oil biodiesel blends in a research diesel engine. *Energy Sources, Part A: Recovery, Utilization and Environmental Effects*, *45*(4), 12181–12200. https://doi.org/10.1080/15567036.2023.2270559
Gaur, A., Dwivedi, G., Baredar, P., & Jain, S. (2022). Influence of blending additives in biodiesel on physiochemical properties, engine performance, and emission characteristics. *Fuel*, *321*, 124072. https://doi.org/10.1016/j.fuel.2022.124072
Gu, X., Li, G., Jiang, X., Huang, Z., & Lee, C. F. (2013). Experimental study on the performance of and emissions from a low-speed light-duty diesel engine fueled with n-butanol-diesel and isobutanol-diesel blends. *Proceedings of the Institution of Mechanical Engineers, Part D: Journal of Automobile Engineering*, *227*(2), 261–271. https://doi.org/10.1177/0954407012453231
Hazar, H., Sevinc, H., & Sap, S. (2019). Performance and emission properties of preheated and blended fennel vegetable oil in a coated diesel engine. *Fuel*, *254*, 115677. https://doi.org/10.1016/j.fuel.2019.115677
Heywood, J. B. (1988). Internal combustion engine fundamentals. In *Choice Reviews Online* (Vol. 26, Issue 02). McGraw-Hill Education. https://doi.org/10.5860/choice.26-0943
Hoekman, S. K., & Robbins, C. (2012). Review of the effects of biodiesel on NOx emissions. *Fuel Processing Technology*, *96*, 237–249. https://doi.org/10.1016/j.fuproc.2011.12.036
Imdadul, H. K., Masjuki, H. H., Kalam, M. A., Zulkifli, N. W. M., Alabdulkarem, A., Rashed, M. M., & Ashraful, A. M. (2016). Influences of ignition improver additive on ternary (diesel-biodiesel-higher alcohol) blends thermal stability and diesel engine performance. *Energy Conversion and Management*, *123*, 252–264. https://doi.org/10.1016/j.enconman.2016.06.040
Jung, S., Kim, H., Tsang, Y. F., Lin, K. Y. A., Park, Y. K., & Kwon, E. E. (2020). A new biorefinery platform for producing (C2-5) bioalcohols through the biological/chemical hybridization process. *Bioresource Technology*, *311*, 123568. https://doi.org/10.1016/j.biortech.2020.123568
Kumar, M. S., Ramesh, A., & Nagalingam, B. (2010). A comparison of the different methods of using jatropha oil as fuel in a compression ignition engine. *Journal of Engineering for Gas Turbines and Power*, *132*(3). https://doi.org/10.1115/1.3155400
Kumar, V., Singh, A. P., & Agarwal, A. K. (2020). Gaseous emissions (regulated and unregulated) and particulate characteristics of a medium-duty CRDI transportation diesel engine fueled with diesel-alcohol blends. *Fuel*, *278*, 118269. https://doi.org/10.1016/j.fuel.2020.118269
Munfarida, I., Munir, M., & Rezagama, A. (2021). The use of banana peels as raw materials of bio-alcohol production. *IOP Conference Series: Earth and Environmental Science*, *896*(1), 12019. https://doi.org/10.1088/1755-1315/896/1/012019
Nogueira, C. da C., Padilha, C. E. de A., Dantas, J. M. de M., Medeiros, F. G. M. de, Guilherme, A. de A., Souza, D. F. de S., &Santos, E. S. dos. (2021). In-situ detoxification strategies to boost bioalcohol production from lignocellulosic biomass. *Renewable Energy*, *180*, 914–936. https://doi.org/10.1016/j.renene.2021.09.012
Nour, M., Attia, A. M. A., & Nada, S. A. (2019). Improvement of CI engine combustion and performance running on ternary blends of higher alcohol (Pentanol and Octanol)/hydrous ethanol/diesel. *Fuel*, *251*, 10–22. https://doi.org/10.1016/j.fuel.2019.04.026
Ozsezen, A., Turkcan, A., Sayin, C., & Canakci, M. (2011). Comparison of performance and combustion parameters in a heavy-duty diesel engine fueled with iso-butanol/diesel fuel blends. *Energy Exploration and Exploitation*, *29*(5), 525–541. https://doi.org/10.1260/0144-5987.29.5.525
Pullagura, G., Bikkavolu, J., Vadapalli, S., Chebattina, K. R. R., & Kuchipudi, V. (2022). Comparative Study of TiO2 Nanoparticles and Alcoholic Fuel Additives-Biodiesel-Diesel Blend for Combustion, Performance, and Emission Improvements. *International Journal of Heat and Technology*, *40*(5), 1249–1257. https://doi.org/10.18280/ijht.400517
Pullagura, G., Vadapalli, S., Prasad, V. V. S., Datla, S. V., Makkena, A. J. S., Chilla, A. S. R., Velisala, V., & Chebattina, K. R. R. (2023). *Aluminum Oxide as Potential Additives to N-Butanol-Diesel Blends on Emission and Performance Characteristics of the Diesel Engine BT - Recent Advances in Thermal Sciences and Engineering: Select Proceedings of ICAFFTS 2021* (H. B. Mehta, M. K. Rathod, R. Abiev, & M. Arıcı (eds.); pp. 241–256). Springer Nature Singapore. https://doi.org/10.1007/978-981-19-7214-0_20
Rakopoulos, D. C., Rakopoulos, C. D., Papagiannakis, R. G., & Kyritsis, D. C. (2011). Combustion heat release analysis of ethanol or n-butanol diesel fuel blends in heavy-duty di diesel engine. *Fuel*, *90*(5), 1855–1867. https://doi.org/10.1016/j.fuel.2010.12.003
Sahoo, P. K., Das, L. M., Babu, M. K. G., Arora, P., Singh, V. P., Kumar, N. R., & Varyani, T. S. (2009). Comparative evaluation of performance and emission characteristics of jatropha, karanja and polanga based biodiesel as fuel in a tractor engine. *Fuel*, *88*(9), 1698–1707. https://doi.org/10.1016/j.fuel.2009.02.015
Sukjit, E., Herreros, J. M., Dearn, K. D., Tsolakis, A., & Theinnoi, K. (2013). Effect of hydrogen on butanol-biodiesel blends in compression ignition engines. *International Journal of Hydrogen Energy*, *38*(3), 1624–1635. https://doi.org/10.1016/j.ijhydene.2012.11.061
Thiyagarajan, S., Sonthalia, A., Edwin Geo, V., Prakash, T., Karthickeyan, V., Ashok, B., Nanthagopal, K., & Dhinesh, B. (2020). Effect of manifold injection of methanol/n-pentanol in safflower biodiesel fuelled CI engine. *Fuel*, *261*, 116378. https://doi.org/10.1016/j.fuel.2019.116378
Voloshin, R. A., Rodionova, M. V., Zharmukhamedov, S. K., Nejat Veziroglu, T., & Allakhverdiev, S. I. (2016). Review: Biofuel production from plant and algal biomass. *International Journal of Hydrogen Energy*, *41*(39), 17257–17273. https://doi.org/10.1016/j.ijhydene.2016.07.084

Assessment of Sensitivity to Temperature and Feedstock Characteristics in Biomass Pyrolysis using Aspen Plus

[1*]Kaan Erdem, [1]Duygu Gündüz Han, [2]Adnan Midilli
[1] Medeniyet University, Faculty of Engineering and Natural Sciences, Mechanical Engineering Department, Ünalan Mah. Ünalan Sk. D100 Karayolu Yanyol 34700, İstanbul, Türkiye
[2] Istanbul Technical University, Faculty of Mechanical Engineering, Department of Mechanical Engineering, İnönü Caddesi, No. 65, Gümüşsuyu, 34437, İstanbul, Türkiye

* E-mail: kaan.erdem@medeniyet.edu.tr

Abstract

Pyrolysis represents an advanced method for harnessing energy from biomass sources. Given the significance of pyrolysis, accurately modeling this process to forecast the final product holds considerable importance. In this regard, a steady-state simulation model was created using Aspen Plus. A comparative study was conducted on five biomass feedstocks; Cherry Pits (CP), Coffee Husk (CH), Mint Straw (MS), Rice Husk (RH), and Tea Waste (TW). Moreover, TW was specifically employed to investigate the temperature sensitivity of the pyrolysis between 300-600°C. The research primarily focused on analyzing the composition of pyrolysis products, encompassing solid (bio-char), liquid (bio-oil), and gas phases. The findings indicate CP pyrolysis generates the most bio-char at 41.4%, while MS pyrolysis yields the highest bio-oil content at 43.0%. CH pyrolysis displays the highest proportion of gaseous products, reaching 22.8%. With increasing temperature, solid and liquid contents decline in TW pyrolysis products, while gas products exhibit an increase.

Keywords: Aspen plus, pyrolysis, biomass, bio-char, bio-oil.

I. Introduction

Biomass based fuels are emerging as a practical alternative to conventional fossil fuels with global energy consumption on the rise and increasing concerns about environmental impacts and sustainability. Therefore the effective utilization of biomass has gained attraction in recent years. Pyrolysis, a widely employed method for extracting energy from waste biomass, involves heating the material feed to high temperatures in an inert environment. This process yields a carbon-rich solid residue namely bio-char, liquids namely bio-oils, and gases. There has been a growing interest in biomass pyrolysis experimentally with an aim of producing renewable fuels by researchers (Midilli et al., 2000; Ronsse et al., 2013).

On the other hand, the usage of Aspen Plus for simulations has proven to be efficient and economical way to assess process conditions. Many researchers have conducted numerical studies using Aspen Plus, resulting in the creation of computer based simulations for biomass pyrolysis (Rosha et al., 2022; Ighalo & Adeniyi, 2019).

This study fills a gap in the literature by examining and comparing the pyrolysis of various biomass types such as Cherry Pits (CP), Coffee Husk (CH), Mint Straw (MS), Rice Husk (RH), and Tea Waste (TW) using the Aspen Plus simulator. Additionally, TW was selected to explore the temperature impact (300-600 °C) on the pyrolysis process due to its widespread availability in Türkiye. The research analyzes the effects of feedstock characteristics and pyrolysis temperature by evaluating the fractions of bio-char, bio-oil and pyrolysis gas in the final product. The findings offer valuable insights for such systems.

II. Modeling and Analysis

Feedstock Properties

Cherry Pits (CP), Coffee Husk (CH), Mint Straw (MS), Rice Husk (RH), and Tea Waste (TW) were chosen as the fuel sources. A comprehensive overview of the feedstock characteristics is given in Table 1.

Modeling

The pyrolysis procedure was examined using Aspen Plus, where evaluation of mass and energy balance, along with chemical equilibrium, was carried out throughout the entire process, as depicted in Figure 1. To conduct this investigation, the composition of the feedstocks were obtained from literature (Kartal and Özveren, 2020; Demirbaş, 1997).

In the modeling and analysis phase, several fundamental assumptions were made. Aspen Plus categorized material streams into three groups: mixed, conventional solids, and nonconventional solids. The physical characteristics of traditional components involved in the gasification process were assessed using the Peng-Robinson equation with Boston-Mathias modification (PR-MB), a recommended method for thermochemical processes (Pala et al., 2017). In the numerical model devoid of kinetics, both stoichiometric and non-stoichiometric methodologies were employed to maintain thermodynamic equilibrium. The model was developed under several assumptions, such as operating under steady-state, steady-flow conditions, ensuring isothermal temperature, neglecting pressure fluctuations in the system, assuming ideal gas behavior for all gases, and treating char solely as pure carbon (AlNouss et al., 2021).

Table 1. Characteristics of feedstocks (Kartal and Özveren 2020; Demirbaş, 1997)

	Cherry Pits, CP	Coffee Husk, CH	Mint Straw, MS	Rice Husk, RH	Tea Waste, TW
		Proximate Analysis (wt%, dry basis)			
Fixed Carbon	17.10	31.30	19.42	14.42	13.60
Volatile Matter	82.00	64.60	69.80	65.67	84.90
Ash	0.90	4.10	10.78	19.91	1.5
Moisture Content (MC)	6.00	11.40	16.82	3.92	6.5
		Ultimate Analysis (wt%, dry basis)			
C	53.41	42.10	45.22	28.85	51.98
H	7.04	4.60	5.52	3.96	5.91
N	0.30	1.53	2.47	0.68	0.53
S	0.30	0.10	0.25	1.17	0
O	38.05	47.57	35.76	45.43	40.08

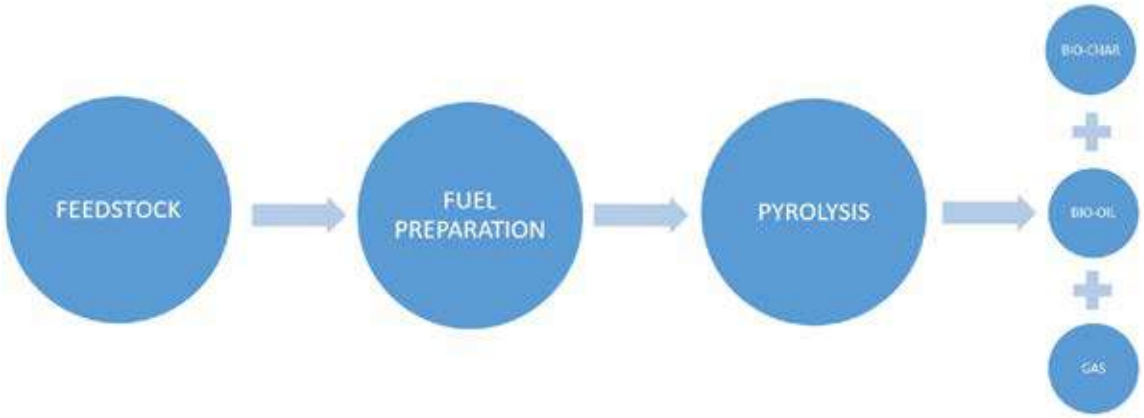


Fig. 1: A diagram showing the creation of pyrolysis products from biomass feedstocks.

III. Results and discussion

Initially, the developed model was validated with the results of the experimental study by Shah et al. (2012) on corn stover pyrolysis, as shown in Table 2. Additionally, the simulation results are provided and compared to the experimental findings. Therefore, the proposed model demonstrates high compatibility with the experimental data.

Table 2. Model validation results

	Experimental (Shah et al., 2012)	Model
Feedstock	Corn Stover	Corn Stover
Feeding rate	1 kg/h	1 kg/h
Pyrolysis temperature	500°C	500°C
Yield of products (wt%)		
Solid	36.1	37.3
Liquid	45.0	43.8
Gas	15.2	16.5

Following the validation of the model, the pyrolysis product yields of five different biomass samples were investigated. The simulations were carried out under conditions set at 500 °C and atmospheric pressure. Biomass feedstocks are utilized in pyrolysis process to create products in solid, liquid, and gaseous states. The resulting gas product predominantly comprises hydrogen, carbon monoxide, carbon dioxide, methane, and several other light hydrocarbons.

Figure 2 illustrates the production of bio-char (solid), bio-oil (liquid), and non-condensable gases from various biomass samples, ranging from 22-42%, 37-43%, and 16-23% by weight, respectively. Among all biomass types, cherry pits pyrolysis yields the highest bio-char content (41.4%), whereas the pyrolysis of rice husk yields the lowest bio-char content (22.9%). Additionally, mint straw yields the maximum bio-oil content at 43.0%, while rice husk yields the least bio-oil at 37.9%. Furthermore, coffee husk produces the highest fraction by weight of pyrolysis gas products at 22.8%, whereas cherry pits yield the lowest fraction at 16.8%.

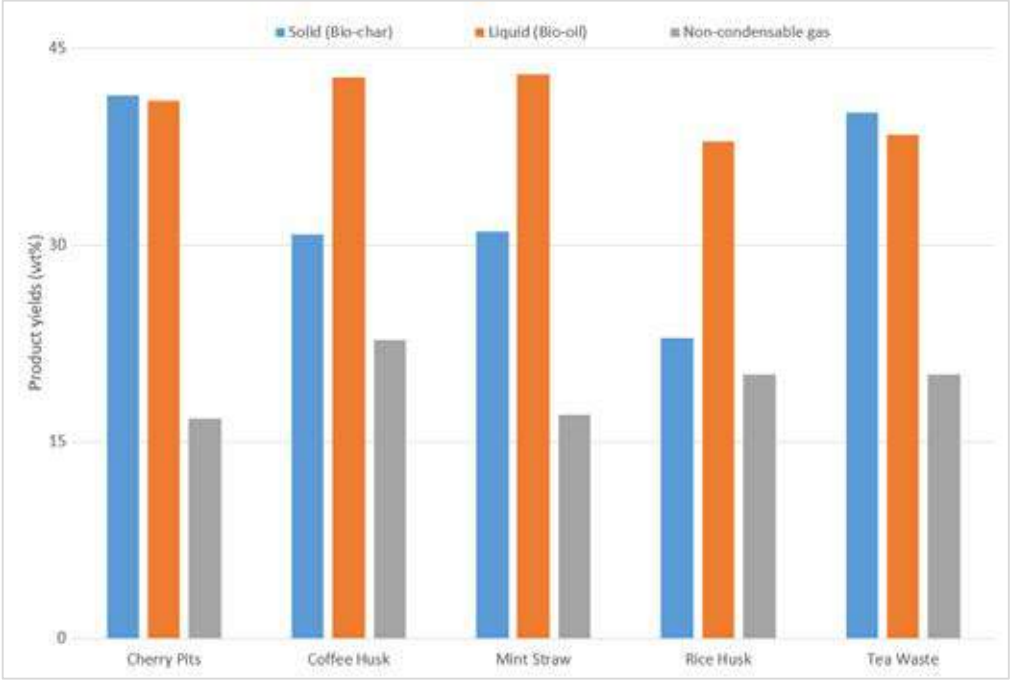


Fig. 2: Product yields for different biomass types during pyrolysis at 500°C and 1 atm.

Figure 3 depicts the alteration in the mass fraction of pyrolysis products relative to temperature for tea waste as feedstock. The reactor temperature was increased from 300°C to 600°C. With this increase, the bio-char and bio-oil content in the final product decrease from 42.3% to 38.9% and from 42.7% to 34.1%, respectively, while the gas content increases from 13.6% to 25.6%. A similar trend has been observed in other studies in the literature (Ighalo & Adeniyi, 2019). This phenomenon can be explained by the endothermic water gas reaction ($C + H_2O \rightarrow CO + H_2$). Additionally, the higher heating value of pyrolysis gas experiences a slight decrease from 36.2 MJ/kg to 34.9 MJ/kg as the temperature increases.

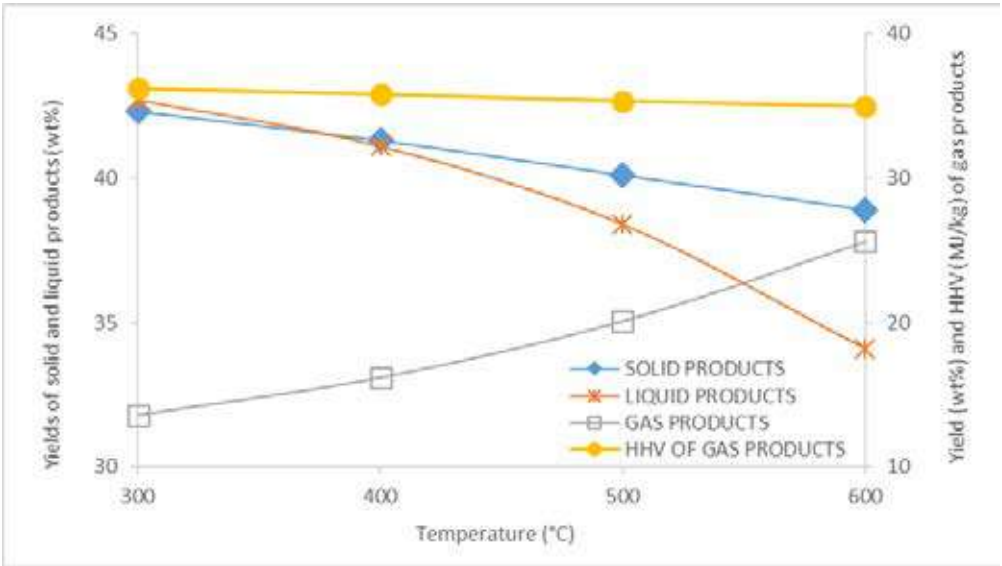


Fig. 3: Variation of pyrolysis product yields by weight with temperature during tea waste pyrolysis.

IV. Conclusions

The following concluding observations can be made:

- Cherry pits pyrolysis yields the highest bio-char content (41.4%), while mint straw pyrolysis produces the highest bio-oil content (43.0%).
- Coffee husk exhibits the highest proportion of gaseous products from pyrolysis with 22.8%.
- As temperature rises, the solid and liquid contents of tea waste pyrolysis products decrease, whereas gas products show an opposite trend.
- The HHV of pyrolysis gas is not significantly affected by temperature changes.

Acknowledgements

This study was supported by Istanbul Medeniyet University (BAP Project number: F-GAP-2022-1782).

References

AlNouss, A., Parthasarathy, P., Mackey, H. R., Al-Ansari, T., & McKay, G. (2021). Pyrolysis study of different fruit wastes using an Aspen Plus model. Frontiers in Sustainable Food Systems, 5, 604001.

Demirbaş, A. (1997). Calculation of higher heating values of biomass fuels. Fuel, 76(5), 431-434.

Ighalo, J. O., & Adeniyi, A. G. (2019). Thermodynamic modelling and temperature sensitivity analysis of banana (Musa spp.) waste pyrolysis. SN Applied Sciences, 1(9), 1086.

Kan, T., Strezov, V., & Evans, T. J. (2016). Lignocellulosic biomass pyrolysis: A review of product properties and effects of pyrolysis parameters. Renewable and sustainable energy reviews, 57, 1126-1140.

Kartal, F., Özveren, U., (2020) A deep learning approach for prediction of syngas lower heating value from CFB gasifier in Aspen plus®. Energy 209, 118457.

Midilli, A., Rzayev, P., Olgun, H., & Ayhan, T. (2000). Solar hydrogen production from hazelnut shells. International journal of hydrogen energy, 25(8), 723-732.

Pala, L. P. R., Wang, Q., Kolb, G., & Hessel, V. (2017). Steam gasification of biomass with subsequent syngas adjustment using shift reaction for syngas production: An Aspen Plus model. Renewable Energy, 101, 484-492.

Ronsse, F., Van Hecke, S., Dickinson, D., & Prins, W. (2013). Production and characterization of slow pyrolysis biochar: influence of feedstock type and pyrolysis conditions. Gcb Bioenergy, 5(2), 104-115.

Rosha, P., Kumar, S., & Ibrahim, H. (2022). Sensitivity analysis of biomass pyrolysis for renewable fuel production using Aspen Plus. Energy, 247, 123545.

Shah, A., Darr, M. J., Dalluge, D., Medic, D., Webster, K., & Brown, R. C. (2012). Physicochemical properties of bio-oil and biochar produced by fast pyrolysis of stored single-pass corn stover and cobs. Bioresource technology, 125, 348-352.

Power to Hydrogen: Assessing the Transition of Electric Charging Stations to Green Hydrogen

[1*]Meltem Yavuz Çelikdemir, [2]Hasan Gündüz
[1] Bitlis Eren University, Tatvan Vocational School, Electric and Energy, Bitlis, 13000, Türkiye
[2] Muş Alparslan University, Department of Electricity and Energy, Muş, 49250, Türkiye

* E-mail:meltem.ycd@gmail.com

Abstract

The study proposes a conversion model of electric charging stations to green hydrogen. In this study, RES potentials were determined from the coordinates of electric charging stations in Bitlis province. Then, a solar and RES hybrid energy system model was proposed according to the full operating scenarios of these charging stations. Next, we scrutinized the model for green hydrogen production within the hybrid energy system. Two different alternative models have been proposed for hydrogen production from RES, such as using the electrolysis method and pressurized gas storage and cryogenic liquid storage of the produced hydrogen. Then, the conversion model from hydrogen to electrical energy with fuel cells was examined. Finally, techno-economic cost analyses were made regarding these transformation models. In the case 5 kW SPP and 5 kW WPP are proposed in the determined coordinates, a total of 69553.32 kWh of energy will be produced, including 7732.5 kWh of SPP and 61820.82 kWh of WPP. This amount of energy produced will meet the entire energy needs of the electric charging station, and the remaining amount will produce additional hydrogen. In this case, 353 kg of extra hydrogen are produced at the end of the year.

Keywords: Electric charging station, Green hydrogen, Renewable energy sources

I. Introduction

Electric Vehicles (EVs) significantly contribute to reducing air pollution and greenhouse gas emissions, which are today's pressing issues. Electric vehicles have more efficient electric motors than traditional internal combustion engines. They also have the advantages of high efficiency and less noise. Today's increasing demands for electric vehicles also increase the required charging station infrastructure (Chen et al., 2023). These charging stations often use existing electricity grids (Benmouna, Borderiou, and Becherif 2024). However, when renewables and sustainability are taken into consideration, it is important that these demands are met by Renewable Energy Resources (RES). Although the use of renewable energy sources has the advantage of alleviating the use of the existing electricity grid, it also requires the construction of extra energy storage equipment because RES are not continuous. Today, batteries, supercapacitors, and flywheels are used to balance this storage and instantaneous power. Diesel generators serve as a long-term solution. Some studies use fuel cells as an alternative. Fuel cells use hydrogen as a raw material and produce only water as a combustion product (Das et al., 2024; Palanisamy and Lala, 2024).

The use of hydrogen in refueling stations is an important energy storage concept. Refueling stations employ two distinct methods for supplying hydrogen. These are centralized hydrogen supply and distributed hydrogen supply methods. In the central hydrogen supply method, it refers to the production of hydrogen centrally and then transporting it by different transportation methods. Pipelines and tankers are the two types of transportation. The distributed hydrogen supply method is expressed as the on-site production and use of hydrogen. Although there are different methods of hydrogen production, the electrolysis method is important for zero-carbon hydrogen production. Electrolysis is the process of decomposing water into hydrogen and oxygen under the influence of an applied current (Dudkina et al., 2024).

There are different concepts for hydrogen storage. Among these, high-pressure gas storage stands out. This is due to the fact that it is the most suitable storage method for investment costs, operating costs, and system optimization (Yang et al., 2024). It has been stated that this situation will be sufficient when the daily energy supply and demand of electric charging stations are taken into account. The proposed working concept is given in Fig. 1.

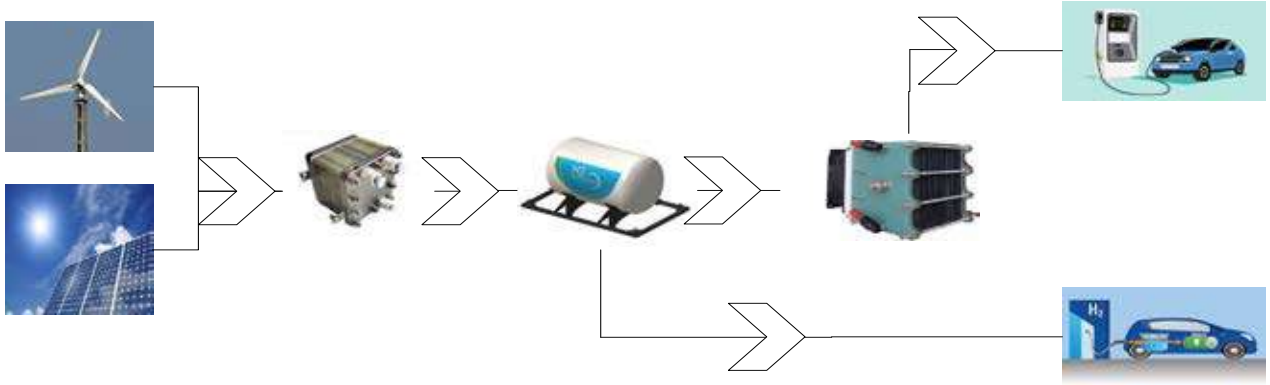
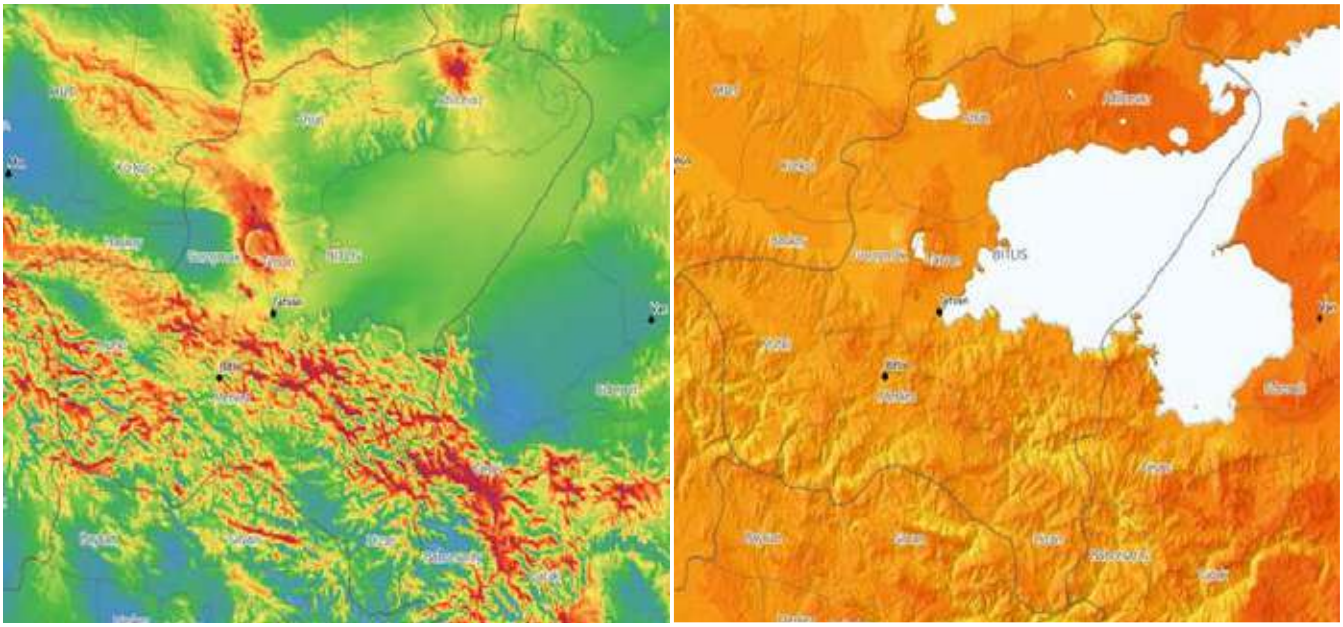


Fig. 1: Proposed operating concept

The research investigated the transition to green hydrogen utilization within electric charging infrastructure. To achieve this objective, a focused case study was undertaken, centering on Bitlis province as a representative locale. Ten electric charging stations, operated by distinct entities within Bitlis province, were subjected to thorough analysis. The proposition put forth entails leveraging Renewable Energy Sources (RES) to fulfill the energy demands of these stations through the adoption of green hydrogen, thereby establishing an autonomous energy supply mechanism detached from the incumbent electricity grid infrastructure.

II. System Description and Procedure

In contemporary times, Renewable Energy Sources (RESs) have garnered escalating attention, primarily driven by the depletion of conventional fuel reservoirs and the irreparable ecological ramifications thereof. The viability of RESs is contingent upon geographical and geological attributes. Among the array of RESs, wind and solar energy emerge as prominent contenders, particularly due to their discernible potential. Notably, Turkey exhibits substantial promise in both solar and wind energy domains. The solar energy potential in Turkey is characterized by an annual average of 2741 hours and 1527 kWh/m^2 (Colak, Memisoglu, and Gercek 2020). Conversely, the wind energy potential is assessed based on specific criteria, with an acknowledgment that wind power plants boasting a 5 MW capacity per square kilometer can be established in areas featuring altitudes of 50 meters and annual average wind speeds surpassing 7.5 m/s. The aggregate capacity of wind power plants deemed feasible in Turkey is estimated at 47.84 GW. Against this backdrop, the delineation of wind and solar energy potential maps for the Bitlis province is illustrated in Fig. 2.



a) b)

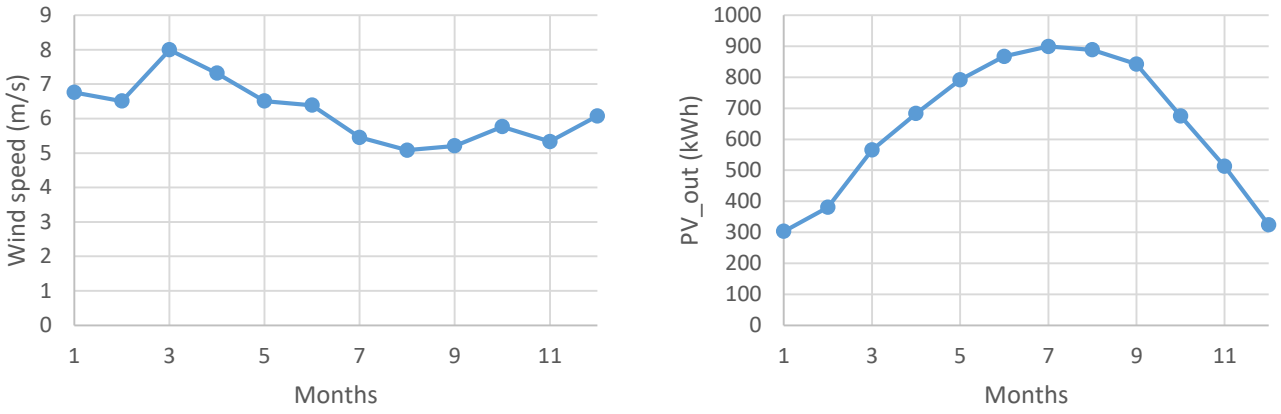
Fig. 2: Wind and solar energy map a) Wind energy b) Solar energy

The average wind speed value for Bitlis province is 4.79 m/sec, and the average power density is 162,122 W/m2. Similarly, the annual sunshine duration is 2690 hours, and the annual radiation value is 1604 kWh/m^2. These values show that Bitlis province has exploitable wind and solar energy potential. Table 1 provides data on electric charging stations in Bitlis province and RES potential data for these coordinates.

Table 1. Station and RES data

Charging station	Latitude	Longitude	Power (kVA)	WPP (W/m^2)	SPP (W/m^2)
Voltrun- AC	38.521100	42.266975	3.7	223	1610.5
Trugo-DC	38.450805	42.146000	22	554	1607.1
Trugo-DC	38.762973	42.519657	22	161	1677.8
Voltrun- AC	38.525180	42.266657	3.7	221	1614.4
ZES-AC	38.453995	42.147657	22	546	1607.1
Eşarj-DC	38.390648	42.102970	50	304	1591.8
Trugo-DC	38.511451	42.227687	22	347	1608.3
Trugo-DC	38.469454	42.316313	22	504	1589.5
ZES-AC	38.506372	42.221000	22	319	1609.8
ZES-AC	38.508563	42.278627	22	288	1603.5

Among the electric charging stations in Bitlis province, the station determined as a case study is the Trugo-DC station with coordinates 38.511451 and 42.227687. Wind and solar energy graphs of this station are given in Fig. 3.



a) b)

Fig. 3: Wind and solar energy graphs a) wind energy graph b) solar energy graph

III. Techno-economic analysis

In the study, it was suggested that the energy needed for electric charging stations should be completely met by RES. It has also been suggested to convert the generated electrical energy into hydrogen as an alternative to storing it in backup batteries. The basis of this suggestion is that hydrogen has a high energy rate. Hydrogen is an energy carrier, and hydrogen can be transported more efficiently than electrical energy. It was stated by Dinçer that the hydrogen age has begun today (Dincer 2020). As a result, hydrogen production now emerges as an important engineering application. Although hydrogen is the most abundant and cleanest energy source, it is not easily found pure in nature because it is mostly bound to other molecules. Therefore, it must be produced before use. Various methods are available in the literature to produce hydrogen. However, in order to be considered an alternative energy source, it must have a renewable and sustainable-based process. In this context, water electrolysis is the only viable technology to produce large-scale 'green and clean' hydrogen. Water electrolysis is the process of decomposing water into hydrogen and oxygen under the influence of an applied current. In line with this proposal, the electrical energy produced by RES will meet the energy needs of electrical charging stations, and the excess energy will be stored as hydrogen to be used later as needed. Techno-economic cost data for this proposed system are given in Table 3.

Table 2. Equipment costs (Chen et al. 2023)

Component	Capital Cost	OM Cost
PV	625 $/kw	6.25 $/kw
Wind turbine	1197 $/kw	23.93 $/kw
PEMEC	1326 $/kw	13.26 $/kw
PEMFC	4486 $/kw	44.86 $/kw
Compressor	8879 $/kw	159.79 $/kw
Liquefier unit (15 ton)	75185000 $/unit	751850 $/unit
Dispenser with precooling	185878 $/unit	1858.78 $/unit
Fast charging pile	27899 $/unit	893 $/unit
GH_2	1538 $/kg	15.38 $/kg
LH_2 main tank	73 $/kg	0.73 $/kg
Gasifier	133 $/kg	13.3 $/kg
Li-on battery (200 kWh)	678 $/unit	135.6 $/unit

Main Table 2 provides the primary component parameter data used in the study's economic evaluation. The study proposed two main hydrogen storage technologies. These are high-pressure gas storage and cryogenic liquid storage technologies. For production and storage equipment, compressors and high-pressure tanks are used in high pressure gas storage, while liquefiers and cryogenic tanks are used in cryogenic liquid storage.

The Trugo-DC station, located at coordinates 38.511451 and 42.227687 in Bitlis province, was the subject of a case study in Table 1. As a result, 195 minutes are required to charge an average 90 kWh electric vehicle to 80%. In this average two-vehicle scenario, the daily amount of energy required by the charging station will be 144 kWh. In the case 5 kW SPP and 5 kW WPP are proposed in the determined coordinates, a total of 69553.32 kWh of energy will be produced, including 7732.5 kWh of SPP and 61820.82 kWh of WPP. This amount of energy produced will meet the entire energy needs of the electric charging station, and the remaining amount of excess hydrogen can be produced and stored. Additionally, it can serve as a hydrogen filling station, positioning itself as the fuel of the future.

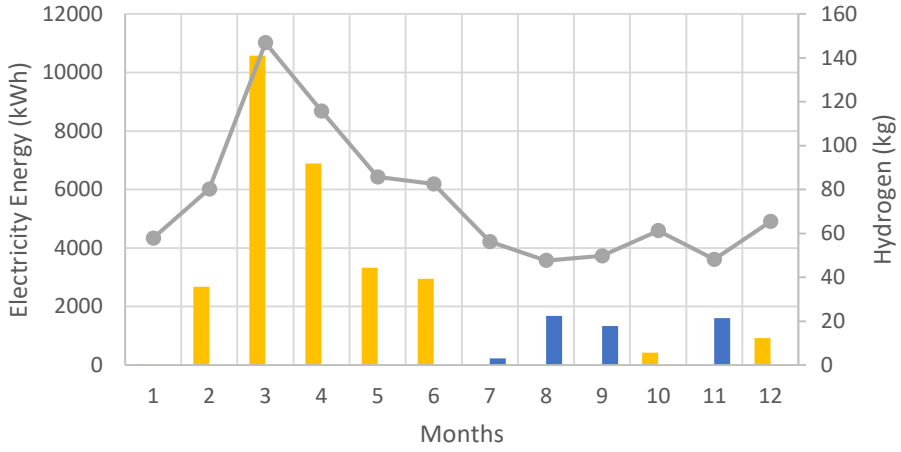


Fig. 4: Electricity production and hydrogen production/consumption graphs

As a result of the calculations, the monthly amounts of electrical energy produced from SPP and WPP are given as a line graph in Fig 4. As a result of charging an average of 2 electric vehicles per day at the electric charging station, the remaining amount of electrical energy is converted into hydrogen, with a conversion rate of 47.5 kWh/kg. This situation is given as a yellow column chart in Fig 4. In some months, when the amount of electrical energy produced by RES does not cover the charging of electric vehicles, electrical energy is produced from previously produced and stored hydrogen with a conversion rate of 33.3 kg/kWh. This situation is given as a blue column chart in Fig 4. In this case, 353 kg of extra hydrogen are produced at the end of the year.

V. Conclusions

In the study, techno-economic analyses of the conversion of electric charging stations in Bitlis province into green hydrogen were made. In this direction, RES potentials were determined from the coordinates of electric charging stations in Bitlis province. Then, a solar and RES hybrid energy system model was proposed according to the full operating scenarios of these charging stations. Then, the green hydrogen production model from the hybrid energy system model was examined. Two different alternative models have been proposed for hydrogen production from RES, such as using the electrolysis method and pressurized gas storage and cryogenic liquid storage of the produced hydrogen. Then, the conversion model from hydrogen to electrical energy using FC was examined. Contributions to the study:

- It has been suggested to use RES to meet the energy needs of fuel filling stations with green hydrogen, independent of the existing electricity grid.
- It has been proposed to convert the generated electrical energy into hydrogen as an alternative to storing it in backup batteries.
- It can be used as a hydrogen filling station without any additional investment in hydrogen, which is seen as the fuel of the future.

In this way, an important step will be taken to provide a more livable environment and reduce the carbon footprint.

References

Benmouna, Amel, Laurence Borderiou, and Mohamed Becherif. 2024. “Charging Stations for Large-Scale Deployment of Electric Vehicles.” *Batteries* 10 (1): 33. https://doi.org/10.3390/batteries10010033.

Chen, Xiaoyuan, Zhou Pang, Mingshun Zhang, Shan Jiang, Juan Feng, and Boyang Shen. 2023. “Techno-Economic Study of a 100-MW-Class Multi-Energy Vehicle Charging/Refueling Station: Using 100% Renewable, Liquid Hydrogen, and Superconductor Technologies.” Energy Conversion and Management 276 (January): 116463. https://doi.org/10.1016/j.enconman.2022.116463.

Colak, H. Ebru, Tugba Memisoglu, and Yasin Gercek. 2020. “Optimal Site Selection for Solar Photovoltaic (PV) Power Plants Using GIS and AHP: A Case Study of Malatya Province, Turkey.” Renewable Energy. https://doi.org/10.1016/j.renene.2019.12.078.

Das, Deboleena, Ishan Chakraborty, Aashish Kumar Bohre, Prince Kumar, and Raja Agarwala. 2024. “Sustainable Integration of Green Hydrogen in Renewable Energy Systems for Residential and EV Applications.” Edited by Subhashree Choudhury. International Journal of Energy Research 2024 (January): 1–20. https://doi.org/10.1155/2024/8258624.

Dincer, Ibrahim. 2020. “Covid - 19 Coronavirus: Closing Carbon Age, but Opening Hydrogen Age.” International Journal of Energy Research 44 (8): 6093–97. https://doi.org/10.1002/er.5569.

Dudkina, Ekaterina, José Villar, Ricardo Jorge Bessa, and Emanuele Crisostomi. 2024. “The Role of Batteries in Maximizing Green Hydrogen Production with Power Flow Tracing.” In 2024 4th International Conference on Smart Grid and Renewable Energy (SGRE), 1–6. IEEE. https://doi.org/10.1109/SGRE59715.2024.10428749.

Palanisamy, Sekar, and Himadri Lala. 2024. “Optimal Sizing of Renewable Energy Powered Hydrogen and Electric Vehicle Charging Station (HEVCS).” IEEE Access 12: 48239–54. https://doi.org/10.1109/ACCESS.2024.3383960.

Yang, Jie, Fan Yu, Kai Ma, Bo Yang, and Zhiyuan Yue. 2024. “Optimal Scheduling of Electric-Hydrogen Integrated Charging Station for New Energy Vehicles.” Renewable Energy 224 (April): 120224. https://doi.org/10.1016/j.renene.2024.120224.

Experimental Investigation of Distinct Surface Geometries of Nickel Coated 3D Printed Electrodes

Ibrahim Eren Dincer*, Martin Agelin-Chaab
Clean Energy Research Laboratory (CERL), Faculty of Engineering and Applied Science,
Ontario Tech. University, 2000 Simcoe Street North, Oshawa, Ontario L1G 0C5, Canada

E-mails: ibrahimeren.dincer@ontariotechu.net, Martin.Agelin-Chaab@ontariotechu.ca

Abstract
The current study investigates the use of nickel coated 3D printed electrodes with distinct surface geometries for hydrogen evolution reaction in alkaline media. Three different surface geometries, circular, triangular, and rectangular, are utilized for the 3D printed electrodes in addition to the flat surface geometry. The electrodes are 3D printed with conductive polylactic acid (PLA) filament and coated with nickel through an electrodeposition process. The C3 electrode, which is the circular design with the highest aspect ratio, exhibited greater current densities compared to the other surface geometries investigated. It was concluded that modification of the surface geometry enabled enhanced catalytic performance by achieving relatively low overpotentials of 269 mV and 290 mV for the R3 and T2 electrodes, respectively.
Keywords: Hydrogen Evolution Reaction (HER), 3D Printed Electrode, Electrodeposition, Catalysts, Current Density

I. Introduction

The rapidly growing energy consumption due to factors such as population growth and industrialization, primarily through the utilization of nonrenewable energy sources, has resulted in an increase in anthropogenic greenhouse gas emissions that significantly impact global warming and climate change (Lee et al., 2023). The utilization of clean and renewable energy sources is essential to mitigate the harmful impacts caused by human activity. Hydrogen is one of the carbon-free energy carriers that will play a crucial role in achieving net zero emissions when it is produced through the utilization of clean and renewable energy sources, which is defined as green hydrogen. Currently, the mass production of hydrogen is done by utilizing nonrenewable energy sources, such as fossil fuels. Alkaline water electrolysis, which is a process of hydrogen production through the water splitting process with the use of direct current supplied to the électrodes, only accounts for approximately 4% of global hydrogen production (Acar & Dincer, 2018), yet water is a highly abundant source. Alkaline water electrolysis technologies require further research and development to achieve lower hydrogen production costs compared to non renewable based hydrogen production systems. The use of 3D printing technology emerging in electrochemical applications, such as 3D printed électrodes, is a relatively new topic that has been gaining interest in research and development (Lee et al., 2019). The fundamental benefits of utilizing 3D printing in these applications are its rapid manufacturing process, ease of design implementations, and cost reduction.

II. System description and analysis

The electrodes with distinct surface geometries and aspect ratios are shown in Fig. 1, where all the electrodes are coated with nickel (Ni).

The active surface area of the electrodes varied according to the geometries and aspect ratios utilized. The highest active surface area for the 3D printed electrodes was observed for the lowest aspect ratio utilized for the same surface geometry. The electrodeposition system utilized to deposit thin Ni films on electrodes consisted of a DC power supply, a platinized titanium anode, a heating and stirring pad, 3D printed electrodes acting as the working electrode, and a Ni electrolyte bath that is the source of Ni ions being deposited. The Ni electrolyte bath consisted of nickel (II) sulfate hexahydrate ($NiSO_4 \cdot 6H_20$), nickel (II) chloride ($NiCl_2$), and boric acid (H_3BO_3) for deposition of Ni (Khalil & Dincer, 2024). The electrodeposition of Ni was driven at an average current of 0.450 A for the 3D printed electrodes, where the electrodes with the metal depositions observed had an average of 0.470 g.

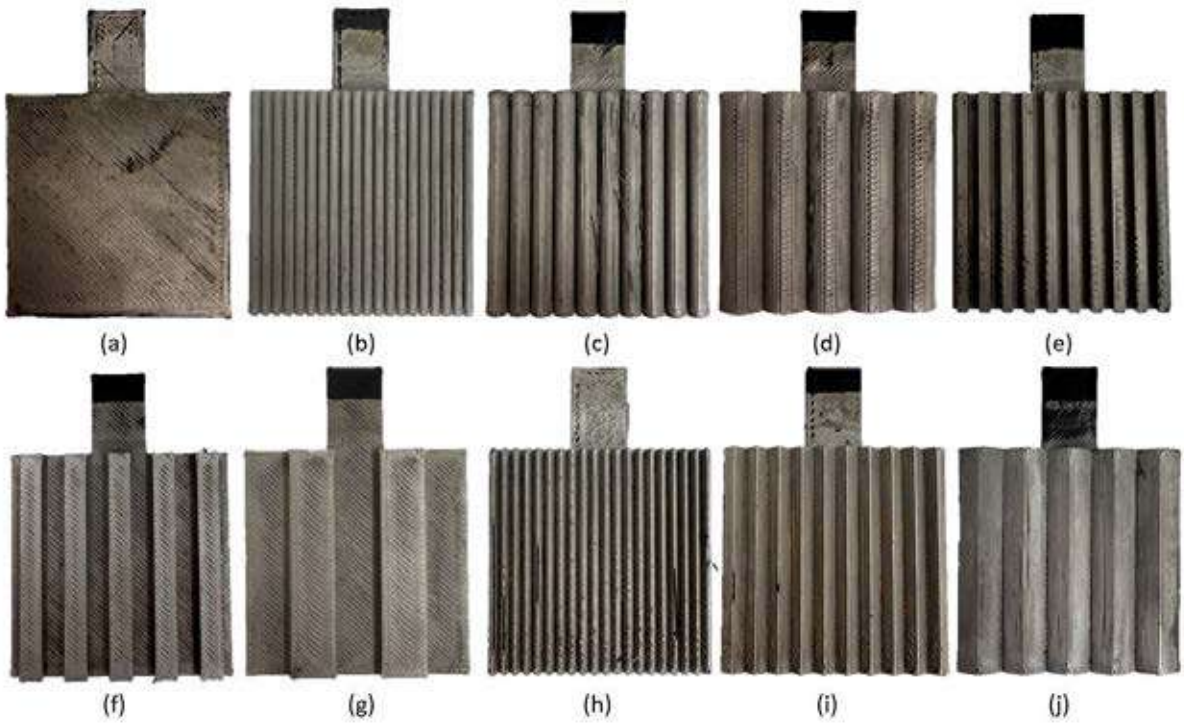


Fig. 1: Nickel Coated 3D printed electrodes with (a) flat (b) C1 (c) C2 (d) C3 (e) R1 (f) R2 (g) R3 (h) T1 (i) T2 (j) T3 geometries

The electrochemical setup utilized to evaluate the performance of the electrodes consisted of a Gamry 3000 reference potentiostat and an electrolytic cell consisting of a reference electrode, platinized titanium mesh electrode, 3D printed electrodes, and an electrolyte solution of KOH with a molarity of 1 M.

III. Results and discussions

The 3D printed electrodes fabricated with the FDM technique and coated with Ni through electrodeposition are tested in an alkaline medium of 1M KOH solution to evaluate their electrochemical performance. The electrochemical tests included linear sweep voltammetry (LSV), cyclic voltammetry (CV), and electrochemical impedance spectroscopy (EIS).

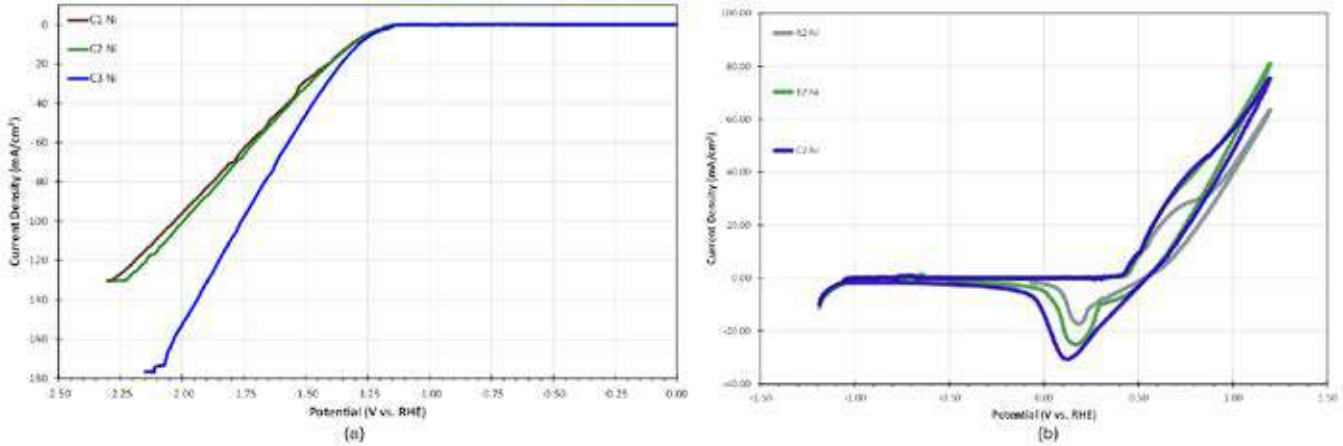


Fig. 2: Electrochemical measurements (a) LSV of Ni coated circular electrodes, and (b) CV of T2, C2, and R2 Ni coated electrodes

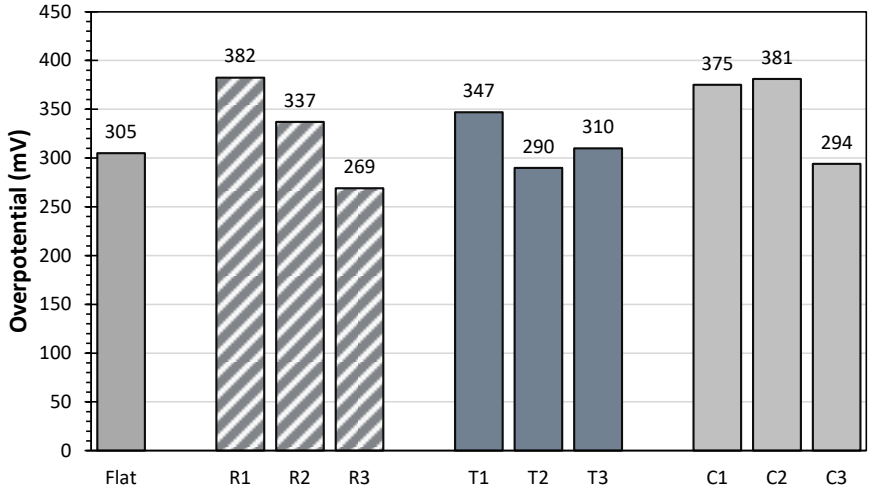


Fig. 3: Overpotential of the Ni coated electrodes at a current density of 10 mA/cm^2

The LSV measurements provided in Fig. 2(a) demonstrated that the C3 Ni coated electrode achieved a current density of -176.67 mA/cm^2 at a voltage of -2.14 V, where the C2 and C1 Ni coated electrodes had current densities of -119.60 mA/cm^2 and -113.37 mA/cm^2, respectively. In addition, the CV measurements taken from -1.2 V to 1.2 V demonstrated that R2 achieved slightly greater current densities at -1.2 V, indicating its performance towards HER surpasses the T2 and C2 electrodes. The activation overpotential, which demonstrates the energy required to initiate and overcome the activation energy to drive the reaction at a specified current density of the Ni coated electrodes at a current density of 10 mA/cm^2 is represented in Fig 3. It could be observed that for electrodes with the same surface geometries and higher aspect ratios, the latter yielded lower active surface areas, and exhibited lower overpotentials. It was concluded that modification of surface geometry resulted in lower overpotentials, such as C3 exhibiting an overpotential of 294 mV, whereas R3 had an overpotential of 269 mV, which is 35 mV lower than that of the C3 electrode. This indicates that the R3 electrode would consume less energy than the C3 electrode to drive HER at a current density of 10 mA/cm^2.

IV. Conclusions

The use of distinct surface geometries and aspect ratios for Ni coated 3D printed electrodes are experimentally investigated in this study to evaluate their performance towards HER. The electrodes were tested in an electrolytic cell with a 1 M KOH solution to determine their electrochemical performance, where LSV, CV, and EIS tests were conducted. The LSV measurements demonstrated that current densities reaching up to -176.67 mA/cm^2 were achieved for the Ni coated 3D printed electrodes, where it was concluded that for equal amounts of metal deposits, electrodes with smaller surface areas exhibited greater current densities. It was concluded that modification of surface geometry can enhance the performance of the electrodes towards HER by achieving lower overpotentials.

References

Acar, C., & Dincer, I. (2018). 3.1 Hydrogen Production. *Comprehensive Energy Systems: Volumes 1-5*, *3*, 1–40.

Khalil, M., & Dincer, I. (2024). An investigation of hydrogen production using 3D-printed cathodes for alkaline water electrolysis. *Energy Conversion and Management*, *302*, 118169.

Lee, C. Y., Taylor, A. C., Nattestad, A., Beirne, S., & Wallace, G. G. (2019). 3D Printing for Electrocatalytic Applications. *Joule*, *3*(8), 1835–1849.

Lee H, Calvin K, Dasguta D, et al. Synthesis Report of the IPCC Sixth Assessment Report Climate Change 2023. Intergovernmental Panel on Climate Change 2023.

Classification of Organic and Recyclable Waste used in Green Hydrogen Production with Deep Learning Models

Hüseyin Firat
Dicle University, Faculty of Engineering, Department of Computer Engineering, Sur, Diyarbakır, 21280, Türkiye

E-mail:huseyin.firat@dicle.edu.tr

Abstract
This paper investigates the classification of recyclable and organic waste used in green hydrogen production through the application of deep learning (DL) models. With the increasing demand for sustainable energy solutions, green hydrogen has emerged as a promising alternative, requiring efficient classification of waste materials to serve as feedstocks. Traditional waste classification methods are labor-intensive and error-prone, prompting the exploration of DL models for automating this process. Specifically, the study focuses on employing the VGG19 DL model to classify recyclable and organic waste. Experimental evaluations demonstrate the effectiveness of the proposed DL model, achieving high levels of accuracy, F1-score, recall, and precision. The findings underscore the potential of DL models in advancing green hydrogen production by optimizing waste classification processes.

Keywords: Green Hydrogen Production, Organic and Recyclable Waste, Classification, Deep Learning

I. Introduction

Green hydrogen (GH) refers to hydrogen produced using renewable energy sources, such as hydroelectric power, solar, or wind through a process called electrolysis. In this process, water (H2O) is split into hydrogen (H2) and oxygen (O2) using electricity generated from renewable sources. Unlike conventional hydrogen production methods, which often rely on fossil fuels and emit greenhouse gases, green hydrogen production produces zero carbon emissions, making it an environmentally friendly and sustainable alternative (Squadrito, Maggio, & Nicita, 2023).

Amidst the ongoing debate within the renewables and fossil fuel sectors over the optimal production methods for green hydrogen needed for the energy transition, a new contender has emerged. This alternative presents a cost-effective approach to GH production compared to both fossil fuels and renewables: the utilization of organic and recyclable waste (Santhosh, Sarkar, & Venkata Mohan, 2021). The expense associated with manufacturing 1 kg of GH derived from organic and recyclable waste amounts to approximately $3 per kg. In comparison, the production cost of GH from solar or wind sources ranges from $11 to $16 per kg. Additionally, each tonne of dry waste can yield approximately 40–50 kg of GH. Conversely, the output of GH from organic and recyclable waste may range from 30 kg to 120 kg per tonne, contingent upon the moisture content present in the waste materials (Torky, Dahy, & Hassanein, 2023).

The pursuit of sustainable energy solutions has spurred interest in harnessing GH as a clean and renewable energy carrier. A crucial step towards realizing the potential of GH lies in the efficient classification of organic and recyclable waste, which serve as key feedstocks for its production. Traditional methods of waste classification often rely on manual sorting and are labor-intensive, time-consuming, and prone to errors. In contrast, leveraging deep learning (DL) models presents a promising avenue for automating and optimizing the classification process. By harnessing the power of artificial intelligence, DL models can analyze vast amounts of waste data with remarkable speed and accuracy, enabling the identification and segregation of organic and recyclable materials with unprecedented efficiency. This paper explores the application of DL models, specifically VGG19, for the classification of organic and recyclable waste, with the ultimate goal of advancing GH production. Through experimental studies and performance evaluations, the effectiveness of the proposed model in accurately categorizing waste materials is assessed, laying the groundwork for enhanced sustainability and resource efficiency in the GH production process.

II. Organic and Recyclable Waste Dataset

In this study, a dataset consisting of recyclable (R) and organic (O) waste, available on the Kaggle platform, was utilized (Sekar, 2019). The original dataset on Kaggle is divided into two subfolders: Train and test. The train folder contains a total of 22564 images. Among these, 9999 images contain recyclable waste items (such as plastic bottles, medicine bottles, glass bottles, cans, etc.), while 12565 images contain organic waste items (such as napkins, rags, toothpicks, chopsticks, watermelon rinds, nuts, leftovers, bread, etc.). The test folder, on the other hand, contains a total of 2513 images. Among these, 1401 images contain organic waste items, while 1112 images contain recyclable waste items.

III. Methodology

Transfer learning (TL) based VGG19 DL model was used to classify recyclable and organic waste. The TL involves utilizing a DL technique whereby a model trained for a particular task is repurposed as the initial framework for a model targeting a different yet related task (Gao & Mosalam, 2018). Instead of commencing the learning process from scratch, the model leverages knowledge gained from solving a related problem. This approach is particularly useful when the new task has less data available for training, as the pre-trained model has already acquired knowledge about features that can be adapted to the novel task. In practical terms, the TL entails the utilization of

a pre-trained model, often trained on an extensive dataset (such as ImageNet), for a general task like image classification. Subsequently, the model is fine-tuned on a smaller dataset specific to the new task. Fine-tuning typically involves adjusting the weights of the pre-trained model's layers to better align with the new data while preserving the fundamental knowledge gleaned from the original task (Hussain, Bird, & Faria, 2019). In addition, it enables faster development of models and often leads to improved results compared to training models from scratch, especially when dealing with tasks with limited data availability.

VGG19 represents a convolutional neural network model developed by scholars affiliated with the Visual Geometry Group (VGG) at the University of Oxford (Simonyan & Zisserman, 2015). An advancement of the VGG16 model, VGG19 is specifically tailored for image classification assignments. Notably, VGG19 is distinguished by its depth, comprising 19 layers (hence the nomenclature) with adjustable parameters, encompassing 16 convolutional layers followed by three fully connected layers. Principal attributes of the VGG19 model encompass:

Convolutional (Conv) Layers: The VGG19 is equipped with 16 convolutional layers, where each layer is succeeded by a ReLU activation function and utilizes a 3x3 filter size. These layers are specifically engineered to extract hierarchical features from input images.

Max Pooling Layers: Following every pair of Conv layers, VGG19 incorporates max pooling layers with a window size of 2x2 and a stride of 2. The inclusion of max pooling aids in decreasing spatial dimensions while preserving critical features.

Fully Connected (FC) Layers: The final layers of VGG19 consist of three FC layers, followed by a softmax layer for classification. These layers join high-level features learned by earlier Conv layers to make predictions about the input image classes.

Fig. 1 illustrates the VGG19 model used for the classification of recyclable and organic waste. Prior to performing convolution, pooling, and FC operations in this model, the sizes of the waste objects are adjusted. The input size for all waste objects is taken as 224x224x3. Subsequently, these input images are fed into the VGG19 model. In the VGG19 model, 16 Conv layers with a filter size of 3x3 and 5 max pooling operations with a filter size of 2x2 are applied. Following Conv and max pooling, global average pooling (GAP) is implemented to the obtained feature maps instead of FC layers. The GAP significantly reduces the number of parameters in the network compared to FC layers. Instead of flattening the feature maps and connecting each neuron to every neuron in the next layer (as in FC layers), the GAP computes the average of each feature map, resulting in a fixed-size vector regardless of the input image size. Since the GAP involves only a simple averaging operation, it requires fewer computations, reducing both training and inference time. In addition, the GAP acts as a form of regularization by reducing the model's capacity to memorize noise or irrelevant details in the training data. This can help prevent overfitting and improve the generalization performance of the model. After the GAP process, batch normalization (BN), FC layer with 128 neurons, another BN, dropout layer with 0.3 dropout ratio and softmax function are used as the final classifier. In VGG19 model, BN improves neural network training by stabilizing learning, accelerating convergence, and enhancing generalization performance. It does this by ensuring stable input distributions across layers, reducing sensitivity to parameter initialization, introducing regularization, enabling the use of higher learning rates, and improving gradient flow. The use of dropout layers is advantageous because they prevent overfitting by randomly disabling neurons during training, leading to more robust and generalizable models. They also facilitate ensemble learning, improve training efficiency by reducing the need for manual hyperparameter tuning, and enhance the model's ability to generalize to new data by encouraging the learning of diverse features.

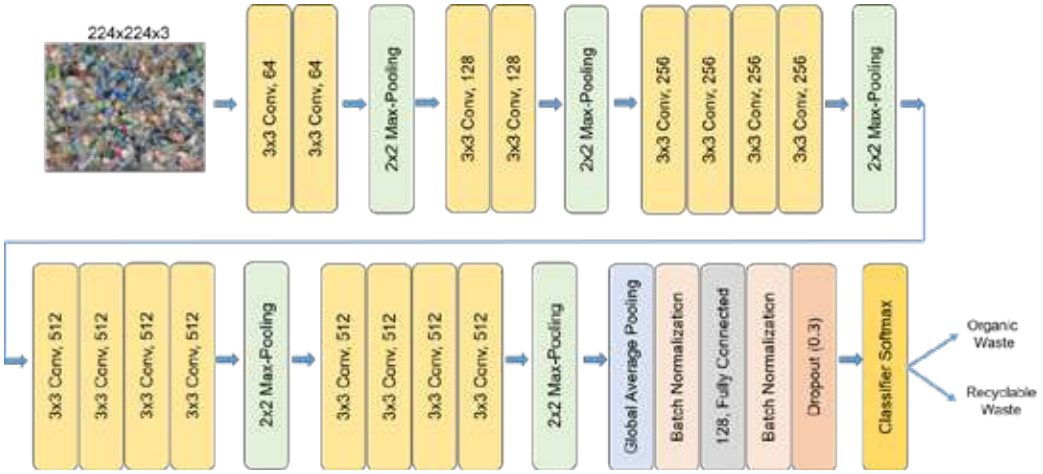


Fig. 1: Proposed VGG19 model

IV. Results and discussions

In experimental studies, the Kaggle platform and Python programming language were utilized. The preference for the Kaggle platform stemmed from its provision of TPU (Tensor Processing Unit) as a hardware accelerator. Out of the total 22564 training examples in the dataset, 30% were allocated for validation. For testing purposes, 2513 images from the original dataset were used. No data augmentation was applied to the dataset during experiments. Among other hyperparameters, a batch size of 128 was chosen, and training continued for 100 epochs.

With the proposed VGG19 model, four different evaluation criteria were utilized to evaluate the performances of different models: accuracy, F1 score, recall, and precision. The basis of these evaluation metrics is based on the confusion matrix. The confusion matrix provides a detailed breakdown of the model's predictions, showing the number of true positive, false positive, true negative, and false negative predictions for each class. It helps identify specific areas of improvement and potential sources of misclassification. *True Positive (TP):* These are cases where the model correctly predicts the positive class when the actual class is indeed positive. In other words, the model correctly identifies instances of the positive class. *False Positive (FP):* These are cases where the model incorrectly predicts the positive class when the actual class is negative. In other words, the model incorrectly identifies instances as belonging to the positive class when they actually belong to the negative class. *True Negative (TN):* These are cases where the model correctly predicts the negative class when the actual class is indeed negative. In other words, the model correctly identifies instances of the negative class. *False Negative (FN):* These are cases where the model incorrectly predicts the negative class when the actual class is positive. In other words, the model incorrectly identifies instances as belonging to the negative class when they actually belong to the positive class.

The accuracy, precision, recall and F1 score values obtained using the confusion matrix are as follows: The accuracy measures the proportion of correctly classified instances among all instances in the dataset. It provides an overall indication of the model's effectiveness in correctly classifying organic and recyclable wastes. The formula required to calculate the accuracy value is as in Equation (1). The precision measures the proportion of true positive predictions out of all positive predictions made by the model, while recall measures the proportion of true positive predictions out of all actual positive instances in the dataset. The precision and recall provide insights into the model's ability to correctly classify each class without misclassification or omission. While the precision is calculated as in Equation (2), the recall is calculated as in Equation (3). The F1 score is the harmonic mean of the precision and recall and provides a balance between the two metrics. It is particularly useful when there is an imbalance between the classes in the dataset. Calculation of the F1 score is as in Equation (4).

$$Accuracy = \frac{TP+TN}{TP+TN+FP+FN} \quad (1)$$

$$Precision = \frac{TP}{TP+FP} \quad (2)$$

$$Recall = \frac{TP}{TP+FN} \quad (3)$$

$$F1-score = 2 \; x \; \frac{Precision \; x \; Recall}{Precision + Recall} \quad (4)$$

The confusion matrix for the proposed VGG19 model is provided in Fig. 2. In the confusion matrix, 'O' represents the organic waste class, and 'R' represents the recyclable waste class. Upon examination of the confusion matrix, it is observed that out of a total of 1401 organic waste images, 1343 were correctly classified, and out of 1112 recyclable waste images, 986 were correctly classified. A total of 2329 images out of 2513 were classified correctly. The ratio of correctly classified images to the total number of test images gives the test accuracy rate. The test accuracy rate for the proposed VGG19 model is calculated as (2329/2513)*100=%92.68.

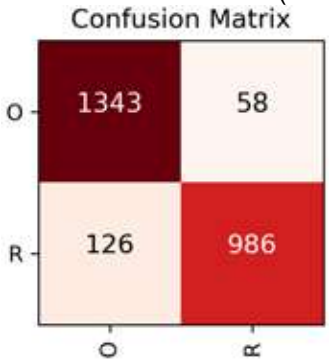


Fig. 2: Confusion matrix of proposed VGG19 model

Table 1 presents the classification results obtained with different models for the task of classifying organic and recyclable wastes. The models evaluated include VGG16, MobileNet, ResNet50, Xception, and the proposed VGG19. Accuracy, precision, recall, and F1-score metrics are reported for each model. The proposed VGG19 model outperforms the other models with an accuracy of 92.68%, demonstrating its effectiveness in accurately classifying waste images. Additionally, the proposed VGG19 model achieves high precision, recall, and F1-score values, indicating its ability to achieve a balance between precision and recall while maintaining high overall classification performance. These results highlight the superiority of the proposed VGG19 model for the given task compared to the other models evaluated.

Table 1: Classification results obtained with different models

Model	Accuracy (%)	Precision (%)	Recall (%)	F1-score (%)
VGG16	91.96	92.41	91.4	91.8
MobileNet	91.64	92.86	90.8	91.4
ResNet50	91.08	91.63	90.5	90.9
Xception	86.39	89.82	84.7	85.5
Proposed VGG19	92.68	92.93	92.3	92.5

V. Conclusions

In this study, a VGG19 deep learning model is proposed for the classification of organic and recyclable wastes, which are crucial for green hydrogen production. In the proposed VGG19 model, instead of fully connected layers, global average pooling, batch normalization, and dropout layers are added in the final layers, distinguishing it from the standard VGG19 model. Experimental studies were conducted on a dataset obtained from the Kaggle platform containing organic and recyclable objects. The experimental results show that the proposed VGG19 model achieved an accuracy of 92.68%, precision of 92.93%, recall of 92.3%, and F1-score of 92.5%. Comparisons with different deep learning models demonstrate the effectiveness of the proposed VGG19 model in achieving promising results.

References

Gao Y., Mosalam K. M., Deep Transfer Learning for Image-Based Structural Damage Recognition. Computer-Aided Civil and Infrastructure Engineering, 33(9), 748–768, (2018). https://doi.org/10.1111/mice.12363

Hussain M., Bird J. J., Faria D. R., A study on CNN transfer learning for image classification. Advances in Intelligent Systems and Computing, 840(October), 191–202, (2019). https://doi.org/10.1007/978-3-319-97982-3_16

Santhosh J., Sarkar O., Venkata Mohan S., Green Hydrogen-Compressed natural gas (bio-H-CNG) production from food waste: Organic load influence on hydrogen and methane fusion. Bioresource Technology, 340(July), 125643, (2021). https://doi.org/10.1016/j.biortech.2021.125643

Sekar S., Waste Classification data. Retrieved from Kaggle website: https://www.kaggle.com/datasets/techsash/waste-classification-data, (2019).

Simonyan K., Zisserman A., Very deep convolutional networks for large-scale image recognition. 3rd International Conference on Learning Representations, ICLR 2015 - Conference Track Proceedings. International Conference on Learning Representations, ICLR (2015).

Squadrito G., Maggio G., Nicita, A., The green hydrogen revolution. Renewable Energy, 216(March), 119041, (2023). https://doi.org/10.1016/j.renene.2023.119041

Torky M., Dahy G., Hassanein A. E., GH2_MobileNet: Deep learning approach for predicting green hydrogen production from organic waste mixtures. Applied Soft Computing, 138(March), 110215, (2023). https://doi.org/10.1016/j.asoc.2023.110215

Economic And Strategic Evaluation Of Underground Hydrogen Storage Areas

[1,*]Hatice Karakilcik

[1] Department of Geology Engineering, Faculty of Engineering, University of Cukurova Adana, 01250, Türkiye

* E-mail: hkilcik@cu.edu.tr

Abstract
This study investigates underground hydrogen storage (UHS) areas in terms of their economic and strategic importance. It is observed that the most significant UHS areas can be established within massive underground geological structures known as salt domes. These structures provide the opportunity for the construction of vast salt caverns, which offer a crucial economic and strategic advantage for storing hydrogen generated from solar and wind energy sources. Salt caverns are found worldwide at depths ranging from approximately 500 to 2000 meters below the surface. Within the salt dome, caverns are constructed as cylindrical tubes, approximately 300 meters in height and 50-100 meters in diameter. In optimal conditions, these structures can serve as long-term storage facilities. The hydrogen storage potential of salt caverns is enormous, while the storage cost is significantly low. Therefore, they ensure rapid and secure energy supply-demand balance and are also economically advantageous. From the perspective of ensuring the security and sustainability of the energy supply chain, they hold strategic importance. Consequently, large-scale underground storage facilities play a crucial role in resolving short-term energy crises that may arise in international conflicts, maintaining the supply-demand balance, and facilitating the import and export of hydrogen.

Keywords: Underground hydrogen storage, Salt dome, Salt cavern, Hydrogen economic and strategic

I. Introduction

The energy produced from renewable sources such as solar and wind can be used to generate hydrogen through water electrolysis, which can then be stored in large volumes (e.g. $0.5\times10^6 – 1\times10^6$ m^3) as a gas. UHS facilities hold significant economic and strategic potential for countries producing hydrogen based on renewable energy. In addition to the need for clean and reliable energy, these massive hydrogen reservoirs can also compete cost-effectively with other energy sources.

Shortly, energy will be generated by multi-megawatt capacity power plants based on wind and solar energy. Consequently, there will be a need for multi-megawatt capacity storage systems (Tarkowski and Uliasz-Misiak, 2022). Electricity generated in large quantities from wind and solar energy can be stored either as electricity in batteries or as hydrogen through electrolysis, which can then be stored in tanks or underground storage caverns (Karakilcik, 2022; Atız et. al. 2022). However, the storage method is selected based on various criteria, including the amount of energy stored, storage duration, response time, round-trip efficiency, energy density, and cost (Luo et al., 2015; Behabtuet et al., 2020). Underground hydrogen energy storage differs from other storage types primarily due to the volume of stored hydrogen, average (seasonal) or long storage duration, and significant capital expenditures associated with constructing underground storage facilities. Hydrogen is a special gas that must be compressed to occupy the smallest possible volume. Compared to other gases, it has the lowest molecular weight (2.016 g/mol), low density (0.08375 kg/m^3), low solubility in water (0.00016 g /100 g), low dynamic viscosity (0.88×10^{-5} Pa S), high mass-energy density (120 MJ/kg), and very low volumetric energy density (0.01079 MJ/L) (Tarkowski et al., 2021). Underground hydrogen storage, in terms of economic sustainability, requires high-budget investments for the electricity required for water electrolysis and the construction of storage sites (Noussan et al., 2020; Abdalla et al., 2018). Above-ground hydrogen storage sites such as pipelines or tanks have limited storage capacities (MWh; hours-days). Therefore, areas allowing much larger storage capacities, measured in GWh or TWh (weeks-months), must be used to store energy on a large scale. These areas include underground hydrogen storage (UHS) in salt caverns and geological structures consisting of porous rocks, depleted oil and natural gas reservoirs, and deep aquifers (Zivar et al., 2021; Heinemann et al., 2021; Lankof et al., 2020; Tarkowski, 2017).

Unlike above-ground storage systems, underground gas storage offers several advantages. These include lower storage costs, greater security against fires and terrorist attacks, and less land requirement (Matos et al., 2019; Tarkowski, 2019).

This makes large-scale hydrogen storage facilitated by pipeline transportation, which is considered the most economical transportation method compared to other storage technologies (Michalski, 2017; Garcia et al., 2016) an attractive option.

As the demand for renewable and sustainable energy sources increases, hydrogen is emerging as a promising solution. Advances in hydrogen storage technologies encourage widespread use of this technology (Hassan et al., 2023). The most commonly used underground geological storage sites on a large scale are depleted oil and gas fields and natural aquifer formations. However, salt domes are important geological structures that allow the formation of salt caves in various geometric forms and large volumes. These structures are relatively easy to build and cost-effective in the long run. Additionally, salt extracted from salt caves has an important economic value in the chemical industry. In this study, underground storage caverns with very large-scale hydrogen storage capacity were evaluated from an economic and strategic perspective.

II. Materials and methods

Approximately three-quarters of the Earth's surface is covered by water, and solar energy is a significant energy source in the existence of living organisms. Efficient electrolysis systems using both resources can produce large amounts of hydrogen. Furthermore, underground storage areas and pipeline transportation can be utilized for storing, transporting, and distributing hydrogen in vast quantities. Numerous individuals, institutions, and organizations contribute to the journey of hydrogen from producers to end-users. Therefore, making informed decisions about investing in underground hydrogen storage areas requires comprehensive economic and strategic evaluations, considering both financial feasibility and broader strategic implications. At the forefront of these evaluations, as depicted in Figure 1, economic and strategic assessments should be conducted.

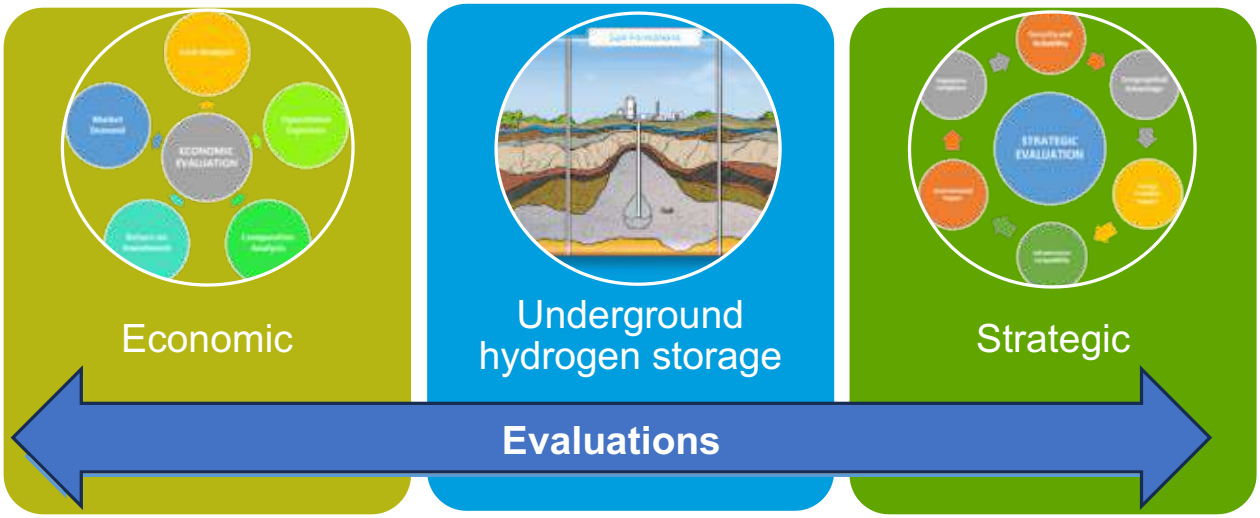


Fig. 1: Economic and Strategic Evaluations (ESEs)

III. Results and discussions

Economic Evaluation:



Fig. 2: Economic evaluation of UHS

In the economic evaluations, generally outlined in Figure 2;

The costs associated with the development of underground storage facilities are assessed, including drilling, construction, security measures, and maintenance.

Ongoing expenses such as monitoring systems, leakage prevention measures, and personnel costs are considered for operational expenditures.

Comparative analysis compares the costs of underground hydrogen storage with alternative storage methods such as above-ground tanks or compressed hydrogen.

The potential return on investment (ROI) is estimated over the project's lifespan by considering the savings from efficient storage and potential revenue from hydrogen sales.
Market analysis examines current and projected market demand for hydrogen by considering applications in industries such as transportation, energy production, and manufacturing.

Strategic Evaluation:



Fig. 3: Strategic evaluation of UHS.

Strategic evaluations, generally depicted in Figure 3;

Assess the safety and reliability of underground storage compared to above-ground storage facilities, considering risks such as natural disasters, sabotage, or accidents.

The strategic advantage of placing storage facilities near hydrogen production sites, transportation hubs, or major demand centers to minimize transportation costs and optimize supply chain efficiency is evaluated for geographical advantages.

For supporting energy transition, the role of underground hydrogen storage in facilitating the transition to renewable energy sources by storing surplus renewable energy in the form of hydrogen is considered.

Infrastructure compatibility assesses the compatibility of underground storage with existing energy infrastructure, including pipelines, power plants, and transportation networks.

Environmental impact evaluates the environmental benefits and risks associated with underground storage, including potential groundwater contamination, methane leakage, or land subsidence.

Compliance with safety standards ensures regulatory compliance for underground storage facilities, including environmental regulations and permits.

IV. CONCLUSIONS

In this study, underground hydrogen storage areas were generally evaluated from economic and strategic perspectives. When hydrogen energy is produced based on renewable energy sources, it is considered the cleanest and greenest energy of the future. It plays a significant role in meeting the demand for clean energy and being storable in large quantities. Therefore, it holds high environmental and economic value. The conversion of renewable energy into hydrogen and its storage in underground structures are strategically important for energy supply. Consequently, the construction of underground storage areas was evaluated both economically and strategically. As a result, some assessments were made, such as cost analysis, operational expenses, and estimating the potential return on investment over the project's lifespan by considering savings from efficient storage and potential revenue from hydrogen sales. It was observed that analyzing the current and projected market demand for hydrogen, considering applications in industries such as transportation, energy production, and manufacturing, is important. Factors such as natural disasters, geographic strategic advantage, support for energy transition by storing surplus renewable energy in hydrogen form, and the role of underground hydrogen storage were identified as crucial. It was also emphasized that considering factors such as compatibility with existing energy infrastructure, environmental benefits, and risks is essential. Ensuring compliance with security standards and regulations was deemed a significant strategic advantage.

References

Tarkowski R., Uliasz-Misiak B., Towards underground hydrogen storage: A review of barriers Renewable and Sustainable Energy Reviews, 162, 112451 (2022).

Karakilcik H., Investigation of infrastructure study and operation planning of underground hydrogen storage area, Proceedings of WHEC 2022 - 23rd World Hydrogen Energy Conference: Bridging Continents by H2, WHEC 2022 Istanbul 26-30 June 2022, 638 – 640 (2022).

Atiz A., Erden M., Karakilcik M., Hydrogen production flat plate solar collector integrated with PV-T, Proceedings of WHEC 2022 - 23rd World Hydrogen Energy Conference: Bridging Continents by H2, WHEC 2022 Istanbul 26-30 June 2022, 177–179 (2022).

Behabtu HA, Messagie M, Coosemans T, Berecibar M, Fante KA, Kebede AA, et al. A review of energy storage technologies' application potentials in renewable energy sources grid integration, Sustainability, 12,1–20 (2020).

Luo X., Wang J., Dooner M., Clarke J., Overview of current development in electrical energy storage technologies and the application potential in power system operation, Appl Energy, 137, 511–36 (2015).

Tarkowski R., Uliasz-Misiak B., Tarkowski P., Storage of hydrogen, natural gas, and carbon dioxide-geological and legal conditions, Int J Hydrogen Energy, 46, 20010–22 (2021).

Noussan M., Raimondi PP., Scita R., Hafner M., The role of green and blue hydrogen in the energy transition - a technological and geopolitical perspective, Sustainability, 13(1), 298 (2020).

Abdalla AM., Hossain S., Nisfindy OB., Azad AT., Dawood M., Azad AK., Hydrogen production, storage, transportation and key challenges with applications: a review, Energy Convers Manag, 165, 602–27 (2018).

Zivar D, Kumar S, Foroozesh J. Underground hydrogen storage: a comprehensive review. Int J Hydrogen Energy, 46, 23436–62 (2021).

Heinemann N., Alcalde J., Miocic JM., Hangx SJT., Kallmeyer J., Ostertag- Henning C., Enabling large-scale hydrogen storage in porous media – the scientific challenges, Energy Environ Sci, 14, 853–64 (2021).

Lankof L, Tarkowski R. Assessment of the potential for underground hydrogen storage in bedded salt formation. Int J Hydrogen Energy, 45, 38, 19479-19492 (2020).

Tarkowski R., Some aspects of underground hydrogen storage, Przeglad Geol, 65, 282–91 (2017).

Matos CR., Carneiro JF., Silva PP., Overview of large-scale underground energy storage technologies for integration of renewable energies and criteria for reservoir identification, J Energy Storage, 21, 241–58 (2019).

Tarkowski R., Underground hydrogen storage: characteristics and prospects. Renew Sustain Energy Rev 105, 86–94 (2019).

Michalski J., Investment decisions in imperfect power markets with hydrogen storage and large share of intermittent electricity, Int J Hydrogen Energy, 42, 19,13368–81 (2017).

Garcia DA., Barbanera F., Cumo F., Matteo U Di., Nastasi B., Expert opinion analysis on renewable hydrogen storage systems potential in Europe, Energies, 9, 963 (2016).

Hassan Q., Sameen AZ., Salman HM., Jaszczur M., Al-Jiboory AK., Hydrogen energy future: Advancements in storage technologies and implications for sustainability, Journal of Energy Storage, 72, 108404 (2023).

Development of a High-Performance Fully Automatic PEM Water Electrolyser Control System for Solar Energy-Assisted Hydrogen Production

[1,4,5]Eda Nur Çakıraslan, [1,2,3,4,5,6]Emre Özdoğan, [4,5]Eren Batuhan Orhan, [4,5]Ahmet Altun, [1,3,5,6]Murat Kıstı and [1,2,3,5 *]Mehmet Fatih Kaya

[1] Erciyes University, H2FC Hydrogen Energy Research Group, 38039, Kayseri, Türkiye
[2] BATARYASAN Enerji ve San. Tic. Ltd.Şti, Yıldırım Beyazıt Mah., Erciyes Teknopark, Aşık Veysel Bul., ERÜ TGB İdare ve Kuluçka , No: 63/B, 38010, Melikgazi, Kayseri, Türkiye
[3] Erciyes University, Engineering Faculty, Energy Systems Engineering Department, Heat Engineering Division, Kayseri, 38039, Türkiye
[4] Erciyes University, Engineering Faculty, Electrical and Electronics Engineering Department, Kayseri, 38039, Turkey
[5] Erciyes University, ArGePark Research Building, Kayseri, Türkiye
[6] Erciyes University, Graduate School of Natural and Applied Sciences, Energy Systems Engineering Department, 38039 Kayseri, Türkiye

* E-mail: kayamehmetfatih@erciyes.edu.tr

Abstract
Water electrolysis stands out as a prominent method among various hydrogen production techniques. It is especially recognized for its ability to generate hydrogen with higher purity than other methods and plays a crucial role in the production of green hydrogen as an emission-free technology. Compared to other electrolysis technologies, Proton Exchange Membrane Water Electrolysis (PEMWE) offers numerous advantages. The performance of PEMWE is influenced by various parameters, including activation, ohmic, and mass transfer losses. These parameters are largely dependent on factors such as the temperature of the water tank, cell temperature, water flow rate, and cell design. Additionally, the output voltage of the photovoltaic (PV) panel can vary based on the temperature and irradiance values at its location. To ensure stable power supply to the system despite changing weather conditions, a DC/DC buck converter is utilized to deliver the required power value at the PV output. For this purpose, the DC-DC buck converter, controlled by Perturb and Observe (P&O) and Fuzzy Logic (FL) Maximum Power Point Tracking (MPPT) algorithms, is simulated using MATLAB/Simulink software. Based on the simulation results, an algorithm suitable for the control card was developed.

Keywords: Energy Efficiency, Water Electrolysis, PEMWE, Hydrogen Production.

I. Introduction

Factors such as the rapid development of technology, a growing population, and increasing energy demand in daily life lead to a continuous increase in energy demand. In this situation, meeting the increasing energy demand without causing environmental impacts or negative consequences worldwide emerges as an important challenge. (Zhiznin, Shvets et al. 2023). At this point, it is vital to turn to alternative energy sources for a sustainable energy future. In this context, hydrogen energy, which is considered a secondary energy source, plays an important role in meeting the energy demand. In water electrolysis technologies there are four different technologies available. These are included as alkaline water electrolysis (AWE), PEMWE, solid oxide water electrolysis (SOWE), and anion exchange membrane water electrolysis (AEMWE). PEMWE has many advantages compared to other electrolysis technologies. It has higher energy efficiency than other methods at temperatures below 100 °C. Moreover it has compact dimensions, and the potential for direct, high-pressure hydrogen storage (Wang, Xiao et al. 2024). These features make PEMWE as a preferred technology over other electrolysis methods. The main components of PEMWE include a catalyst-coated membrane (CCM), gas diffusion layers (GDL), and bipolar layers (BP) (Qiu, Xu et al. 2024). At PEMWE, the production of hydrogen is realized through the electrochemical reactions oxygen evolution reaction (OER) and hydrogen evolution reaction (HER). This process is integrated with PEMWE's wind, solar, and other renewable energy sources, making hydrogen production sustainable (Chu and Meisen 2011). However, there are various parameters, such as activation, ohmic, and mass transfer losses, that affect the performance of PEMWE during the electrolysis process. These parameters largely depend on the cell design and other parameters such as temperature, pressure flow rate, working voltage etc. Antonios Antoniou et al. (Antoniou, Celis et al. 2024) designed an innovative control system to optimize the stability and functionality of a solar electrolysis plant. The system works by adapting to environmental conditions such as varying solar radiation, ambient temperature, and wind speed and precisely controlling the functional parameters of the electrolyser, such as cell voltage, current, temperature, and pressure. The proposed control system has been proven to minimize power fluctuations by regulating the appropriate components and can increase the system efficiency by up to 20% depending on the ambient conditions. In this study, a control card is designed to investigate the effects of solar PEMWE on parameters such as water tank temperature, cell temperature, and water flow rate. A DC/DC Buck converter is used to provide the required power value at the PV output to provide stable power to the system despite the changing weather conditions. In order for the PV panel to provide high current and low voltage to the PEMWE, MPTT needs to be monitored. This power monitoring will ensure more stable operation of the PEMWE system under varying radiation and temperature conditions, and power losses will be prevented by providing the required voltages. For this purpose, the DC-DC Buck converter controlled by P&O and FL MPTT algorithms has been simulated using

MATLAB/Simulink software. It is also an important problem to balance hydrogen production and water treatment and to minimize energy losses. This issue has not been a focus in the literature. By applying various control algorithms to the DC/DC buck converter, the system is fully controlled by comparing the amount of hydrogen to be produced and the amount of water to be treated, and the hydrogen production performance is improved by minimizing energy losses. This innovative approach can contribute to the performance optimization and commercialization of solar PEMWE technology in a wider range of parameters.

II. Experimental Set-up and Procedure

The proposed system consists of a PV, control card, PEMWE, hydrogen dryer tank, and pure water tank, as shown in Fig. 1. The output voltage of PVs can vary depending on the temperature and irradiance values of the location. In this study, a 36-cell monocrystalline PV panel is selected. For this purpose, the DC-DC buck converter controlled by P&O and FL MPTT algorithms is simulated using MATLAB/Simulink software.

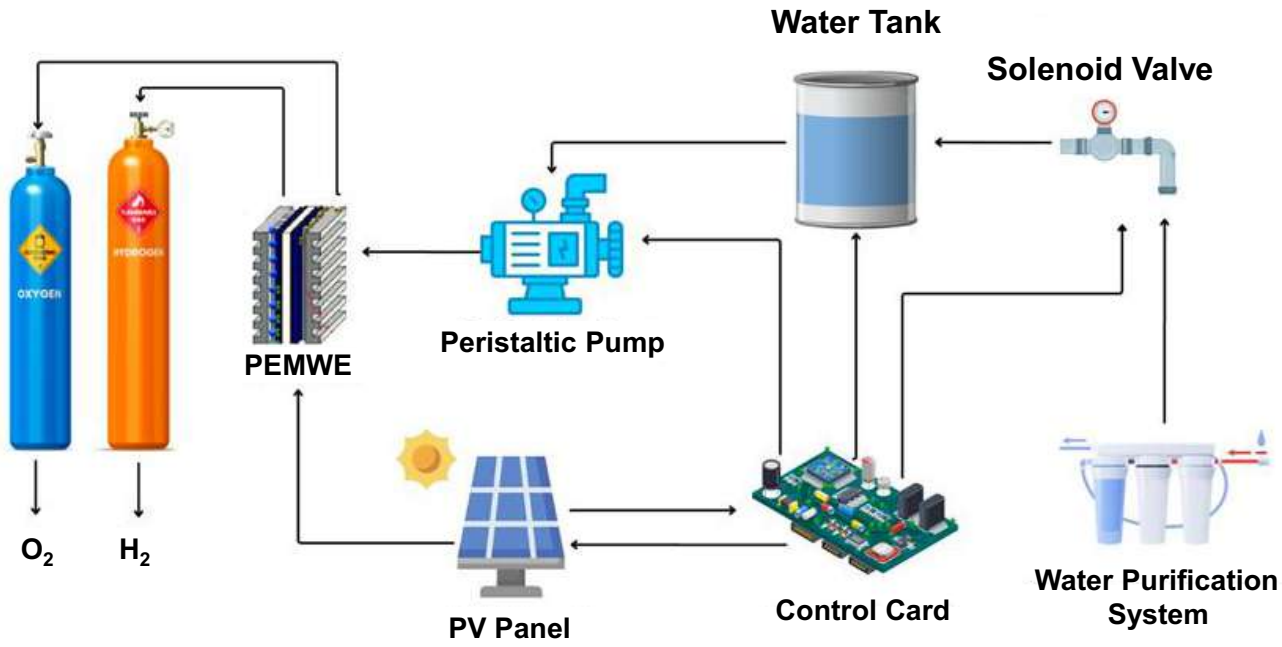


Fig. 1: Schematic of Solar Energy Assisted Hydrogen Production System

Fig. 2 shows the MATLAB/Simulink simulation model for the DC-DC buck converter system. The simulation results allow us to better understand the performance of the system and determine the necessary steps to optimize the system.

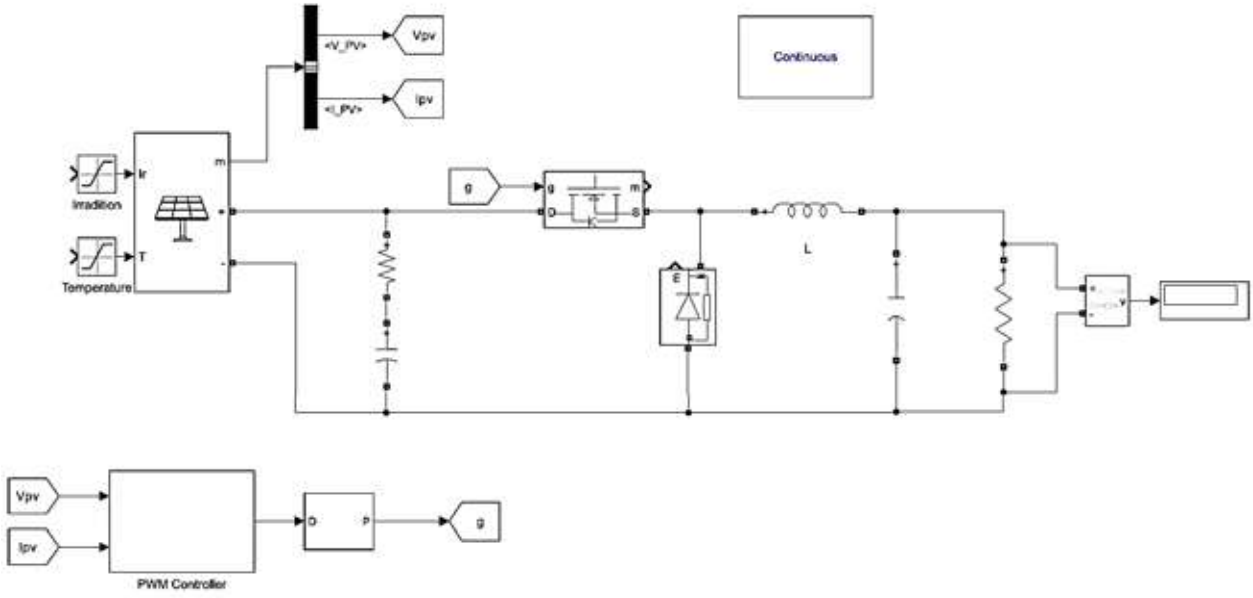


Fig. 2: MATLAB/Simulink simulation model for DC-DC buck converter system

According to the simulation results, an algorithm suitable for the control card was created. Tab. 1 shows the radiation values for Kayseri published by the Solar Energy Potential Atlas (GEPA), and Tab. 2 shows the temperature values (Hansen 2023).

Tab.1: Monthly Radiation Values of Kayseri

Months	1	2	3	4	5	6	7	8	9	10	11	12
Radiation (kWh/m^2day)	1.93	2.59	4.1	5.04	6.33	6.74	6.86	5.98	5.03	3.62	2.28	1.73

Tab. 2: Monthly Temperature Values of Kayseri

Months	1	2	3	4	5	6	7	8	9	10	11	12
Temperature (°C)	19,3	22,6	28.6	31.2	34.2	37.6	40.7	40.6	38.4	33.6	26.0	21.0

The control card then compares the amount of hydrogen to be produced with the water consumption, depending on the duration of the duration of the sunshine at this location. In this step, the water tank is maintained at a certain level and refilled, when necessary, by a water level comparison based on the PV panel power. This step optimizes water consumption with the required panel power. Furthermore, the control card ensures that the water temperature control and the cell temperature remain within the optimum range of the operating temperature of the PEMWE.

III. Results and discussions

Thanks to this control system, continuous hydrogen production is achieved and PEMWE performance is improved by controlling the optimum cell conditions with the control circuit. The proposed system ensures sustainable hydrogen production and minimises energy losses. It is also noted that the control of electrochemical systems is very important to improve the PEMWE performance.

Acknowledgements

The authors would like to give thanks for the financial support from the Scientific and Technological Research Council of Turkey (TUBITAK) 1001 Research Projects Funding Program with project number 120M234. The authors also would like to thank the Scientific Research Projects Unit of Erciyes University for funding and supporting the project under the contract number FBA-2024-13646. Finally, authors would like to thank Erciyes University dean of research for providing the necessary infrastructure and laboratory facilities at the ArGePark Research Building.

References

Antoniou, A., C. Celis, R. Mas, A. Berastain, N. Xiros, G. Papageorgiou, A. Maimaris and T. Wang, "Effective thermal-electric control system for hydrogen production based on renewable solar energy." International Journal of Hydrogen Energy 53: 173-183, (2024).

Chu, Y. and P. Meisen, "Review and comparison of different solar energy technologies." Global Energy Network Institute (GENI), San Diego, CA 1: 1-52, (2011).

Hansen, M., "Enhancing polymer exchange membrane water electrolyser's performance and efficiency by utilising electromagnetic solar radiation and magnetic field applications: Hydrogen production.", (2023).

Qiu, C., Z. Xu, F.-Y. Chen and H. Wang ,"Anode Engineering for Proton Exchange Membrane Water Electrolyzers." ACS Catalysis 14(2): 921-954, (2024).

Wang, G., L. Xiao and L. Zhuang, "General definition of hydrogen energy and related electrochemical technologies." Chinese Journal of Catalysis 56: 1-8, (2024).

Zhiznin, S., N. Shvets, V. Timokhov and A. Gusev , "Economics of hydrogen energy of green transition in the world and Russia. Part I." International Journal of Hydrogen Energy 48(57): 21544-21567, (2023).

Solar Tracking Systems Applications in Planar Solar Panels

[1*]Gizem Gül Katırcıoğlu, [2]Mehmet Daş, [3]Ebru Akpınar
[1,2,3] Fırat University, Faculty of Engineering, Department of Mechanical Engineering, Elazığ, 23119, Türkiye

* E-mail: ggkatircioglu@firat.edu.tr

Abstract
From the history of mankind to the present day, especially in recent years when technology has developed rapidly, studies on solar energy and solar energy panels have become more widespread among renewable energy sources in order to investigate alternative renewable energy sources and to meet this need due to the environmental impacts of existing fossil resources and nuclear power plants. Planar solar panel systems are one of the most common methods used to utilize solar energy. The most common areas of use of solar panels are heat and electricity generation. Various methods have been developed to increase the energy production efficiency of planar solar panels. The most effective of these is solar tracking systems. This study reviews studies for photovoltaic (PV), pneumatic, and concentrator-type solar panels and examines the effects of solar tracking systems on performance. As a result of the analyzed studies, energy performance has increased between 10-50% thanks to solar tracking systems. Solar tracking systems are expected to be studied and developed in parallel with the decrease in installation cost in the future.

Keywords: Solar energy, solar tracking, energy performance

I. Introduction

Energy has an important place in the social and economic progress of societies, as it has been in all civilizations formed by human beings since the existence of humanity, especially today, which is the age of technology. With the increase in the world population, the need for energy is also increasing (Liu et al., 2022). Individual energy consumption increases due to technological developments and the increase in living standards. In order to meet the energy need in the world, research on the research and use of environmentally friendly, economical and sustainable energy sources has been increasing in recent years. The first among these energy sources is solar energy. Studies show that the world's energy demand will increase in the coming years (Ihoume et al., 2022).

In recent years, the number of researches on alternative energy sources is increasing day by day in order to meet the increasing energy demand. Solar energy is the most researched renewable energy source due to its potential. Even a low proportion of the energy coming to the world from the sun meets the total energy needed by the world. It is predicted that the demand for energy in the world will be very high in the future and fossil resources will not be able to meet this need (Dong et al., 2021).

By the end of February 2023, Turkey's installed capacity reached 104,496 MW. As of the end of February 2023, the distribution of our installed capacity by resources is as follows: 30.2% hydraulic energy, 27% natural gas, 27.5% coal, 11% wind, 4% solar, 4% geothermal and 2.5% other resources.[5]

Planar solar panel systems are one of the most common methods used to utilize solar energy. The most common areas of use of solar panels are heat and electricity generation. Various methods have been developed to increase the energy production efficiency of planar solar panels. The most effective of these is solar tracking systems.

Why is a solar tracking system needed?

- Inability to utilize solar energy continuously due to the movement of the Sun and the Earth,
- Photovoltaic cells give maximum efficiency when the sun's rays are perpendicular,
- Failure to receive the desired amount of radiation in bad weather and climatic conditions,
- Increased cost due to the need for large surface area to achieve high powers,
- Unfavorable terrain, site conditions

In this study, 3 different solar panel systems are investigated to examine the effects of solar tracking systems on power generation performance. The selected planar solar panel systems are PV, parabolic reflector and air heated solar panel systems, respectively.

II. Solar Tracking For Planar Solar Panels

Solar tracking systems (STS) are systems designed to condition the rays coming from the sun perpendicular to the panel surface. STS is designed to have two different structures. This structure is divided into two as single axis and dual axis control.

According to the number of rotation axes; there are single axis tracking systems and double axis tracking systems. According to the control method; there are closed loop (passively controlled) and open loop (actively controlled) controls.

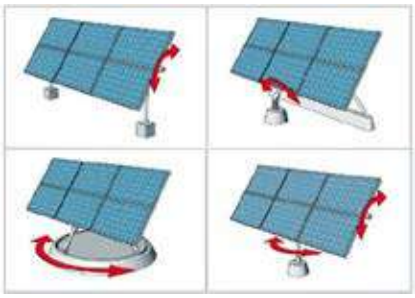


Fig. 1: Single axis tracking systems and double axis tracking systems

For the highest efficiency in planar solar panels, the sun's rays should be perpendicular to the panel, considering the geographical location. Regarding their efficiency, the advantage of dual-axis controlled STS makes itself evident. The efficiency of panels with the STS system can be increased up to approximately 50% compared to fixed panels. [9]

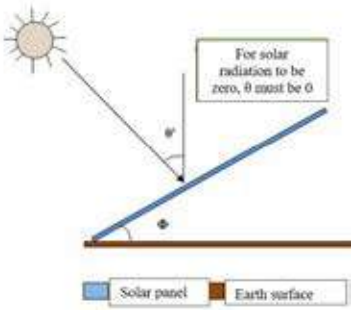


Fig. 2: Solar tracking system working principle

One of the leading methods to improve the performance of planar solar panels is solar tracking systems. Solar tracking systems for PV, parabolic, and air-heated panels are given below as headings.

Solar Tracking for PV solar panels

In Ismail Kayri's study, a single-axis solar tracking system was developed. The daily efficiency increase obtained by the solar tracker system was distributed according to the radiation and sunshine duration of the relevant day. According to the results obtained at the end of the experiment, the solar monitor system achieved a 30.84% efficiency increase annually (İsmail Kayri, 2023).

The study by Abdulwaheed Musa et al. is a comprehensive analysis of time-based solar tracking systems, considering various axis rotation and motion types. The widely used fuzzy logic method was also examined. The findings were clear: the hybrid solar tracking system emerged as the most efficient (Abdulwaheed Musa et al. 2023).

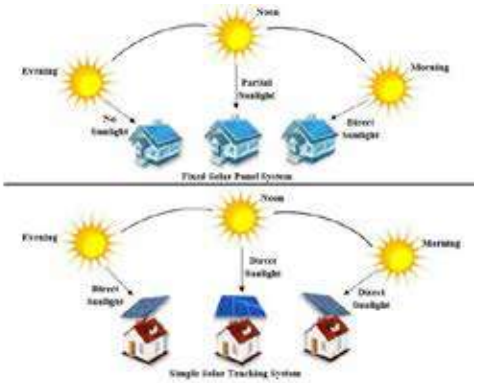


Fig. 3: Solar Tracking for PV solar panels

In the study by Azwaan Zakariah et al., a dual-axis sun-tracking system was used. Arduino was used as the hardware system. A microcontroller was used as the control device, and an LDR sensor was used for light detection. Glass motors were used for movement on both axes. These motors move according to the inputs from LDR sensors. As a result of this study, it was observed that the efficiency increased by 18.33% compared to fixed systems (Azwaan Zakariah et al., 2015).

Huiling Shang et al. designed and built a novel dual-axis solar tracking system. The photoelectric method was used to realize the tracking process. The solar radiation values of the designed system and a fixed panel system are theoretically estimated and compared, and it was shown that the proposed system was more efficient in

collecting solar energy than a fixed solar panel with a fixed 30◦ inclined surface facing south. The experimental results confirmed the validity of the prediction as well as the efficiency of the proposed solar tracking system. A comparison of the data obtained from the measurements showed that 24.6% more energy was obtained in the dual-axis solar tracking system compared to the fixed system. (Huiling Shang et al., 2023)



Fig. 4: PV solar panels with solar tracking system (Azwaan Zakariah ve Ark.,2015).

Solar Tracking for parabolic solar panels

Asif Ahmed Rahimoon et al. studied a parabolic solar tracking system. The dish has a polished surface on which the sun's rays fall and are collected. However, this prototype is configured with an anti-lock hybrid (L298) module to overcome the control circuit complexity. Two 12V rotary motors of 4*4ft design are mounted. The jolts between the trackers are also reduced while the prototype maintains the experimental results. The declination angle is approximately 22.47°. In this study, Asif Ahmed Rahimoon et al. showed that the parabolic solar dish tracking system is 3.43% more efficient than the solar dish tracking system (Asif Ahmed Rahimoon et al., 2020).



Fig. 5: Parabolic solar panels with solar tracking system (Asif Ahmed Rahimoon et al., 2020)

In this study, Ganime Tuğba Ercoşkun et al. designed a parabolic solar collector consisting of double parabolic troughs with a 90cm opening and an edge angle (Qr) of 83 degrees. In order to reduce heat losses in the system, a glass pipe was placed concentrically with the receiving pipe, and the air between the two pipes was evacuated by vacuuming. The designed parabolic collector has a two-axis solar tracking system. Performance tests using water as heat transfer fluid were carried out in Tarsus climate conditions. The system's measured minimum and maximum efficiency values are 37.59% and 50.60%, and the average efficiency is 43.03%. The system is environmentally sensitive because it uses solar energy, is practical in terms of manufacturing, accessible in terms of supply of materials, and more efficient than planar collectors in everyday use because it works based on concentration (Ganime Tuğba Ercoşkun et al., 2013).

In the study by Naseer T. Alwan et al., two types of parabolic solar dishes were considered. The first was fixed, and the second was a rotating dish. It was observed that the water heater output of the rotating dish was 22% higher than that of the fixed dish type. For both types, the temperature recorded at 1:00 p.m. was 76.9 W for the rotating dish and 54.7 W for the fixed dish. It was also observed that the highest energy loss occurred during the installation of the fixed dish type (Naseer T. Alwan et al., 2021)



Fig. 6: Fixed and solar tracking parabolic solar panels (Naseer T. Alwan et al., 2021)

Solar Tracking for air heated solar panel

The main objective of the study by Ramadan ElGamal et al. was to develop an integrated solar tracking system to maximize the efficiency of solar heaters manufactured from recyclable aluminum cans (RAC) for optimal drying of apple slices. The results revealed that the thermal efficiency of the solar air heater combined with a tracking unit was significantly improved by about 45% compared to conventional stationary heaters at all tested air flow rates. The highest thermal efficiency of 87.1% of the solar air heater equipped with the tracking unit was achieved at the highest air flow rate of 44 m3 h-1. The drying rate of apple slices under such a tracking module was significantly higher than that of the conventional stationary system or drying in the ambient sun. (Ramadan ElGamal et al., 2021).

Daş has developed two equal-sized SAHs (Solar Air Heaters). A solar tracking system was integrated into one of the systems. The thermal efficiency values of the SAHs were calculated using the "I" and "II" laws of Thermodynamics according to three different mass flow values of the air inside the SAH. As a result of the experiment, the mobile SAH has twice the average heat transfer value and 47.8% more energy efficiency. These results show that a solar tracking system is an essential method for solar energy utilization (Das, 2022).



Fig. 7: Solar Tracking for air heated solar panel (Das, 2022)

III. Conclusions

When examining the studies on STS, it becomes evident that this system, despite its disadvantages, offers significant advantages. These key benefits are outlined below.

Advantages:

- Since STSs position the sun's rays perpendicular to the panel, they can produce more energy than fixed panels. This capacity can vary between 10 and 50% depending on the geographical location of the system.
- STS provide optimum space in terms of land use compared to fixed-angle systems. At peak times of the day, STS contribute to the generation of more electricity, maximizing the gain obtained at these times.
- In recent years, software, technological developments, and related electronic developments in mechanics have significantly reduced STS monitoring systems' long-term maintenance and operation problems.

Disadvantages:

- STSs are slightly more expensive than their stationary counterparts due to the more complex technology and moving parts required for operation.
- Despite the high efficiency, STSs generally require more maintenance than a conventional fixed system.
- Initial installation costs of STSs are high.

As a result of the studies carried out, it is anticipated that solar tracking systems, with their significant performance improvements and potential for decreased installation costs, will continue to be a focus of future research and development.

References

Abdulwaheed M., Emmanuel A., Suleiman A., John A., Agbotiname I. A Review of Time-Based Solar Photovoltaic Tracking Systems, (2023).

Asif Ahmed R., Mohd Noor A., Dur Muhammed S., Murad Yahya N., Design of parabolic solar dish tracking system using arduino, Indonesian Journal of Electrical Engineering and Computer Science, 914~921, (2019).

Azwaan Z., Jasrul J., Coutanceau M., Bouard R., Dual-Axis Solar Tracking System Based on Fuzzy Logic Control and Light Dependent Resistors as Feedback Path Elements, 5 IEEE Student Conference on Research and Development, (2015).

Huiling S., Wei S., Design and Implementation of a Dual-Axis Solar Tracking System, Journal of Energies (2023).

Ganime Tuğba E., Ali K., Metin G., Duran A., Fabrication and Performance Investigation of Double Trough Parabolic Trough Type Solar Collector, Journal of Gazi Üniversitesi faculty of engineering gazi university, 855-863 (2013).

İsmail K., Design and Implementation of a Stable Uniaxial Solar Tracking System for Photovoltaic Applications, Journal of Yüzüncü Yıl University Graduate School of Science and Technology, 432-450 (2023).

Mehmet D., Comparison of the performance of fixed and two-axis movable solar air heaters with different methods, Journal of Energy Sources, Part A: Recovery, Utilization, and Environmental Effects (2022).

Naseer T. A., Milia H. Dual axis solar tracking system for a parabolic dish CPU water heaterJournal of Physics: Conference Series, (2021).

Ramadan El G., Sameh K., Salim A., Gamal E., Incorporation of a solar tracking system for enhancing the performance of solar air heaters in drying apple slices , Journal of Renewable Energy., 676-684, (2020).

2D Transition Metal Carbide (MXene) as Promising Catalyst for Fuel Cells

Emre Oguz Koroglu
Kahramanmaraş Sütçü İmam University, Department of Environmental Engineering, Kahramanmaraş, Türkiye

* E-mail:emreoguzkoroglu@gmail.com

Abstract
MXenes, discovered in 2011, represent a versatile family of 2D transition metal compounds, including carbides, nitrides, borides, and carbonitrides. They are synthesized by selectively etching A layers from the MAX phase. MXenes exhibit abundant surface functional groups like -O, -OH, and -F, enhancing their reactivity. This makes them promising catalysts for fuel cell applications. Their high surface area, tunable electronic properties, and excellent conductivity facilitate efficient catalysis. MXenes like $Ti_3C_2T_x$, Ti_2CT_x, and Mo_2CT_x have shown potential as catalysts in fuel cells due to their ability to catalyze oxygen reduction reactions (ORR) and hydrogen evolution reactions (HER). Additionally, theoretical calculations predict the synthesis of more MXene variants with tailored properties for enhanced catalytic performance, making them attractive candidates for advancing fuel cell technology.

Keywords: 2D nanomaterials, MXene, catalyst, fuel cells

I. Introduction

As far as the various types of fuel cells are considered, like polymer electrolyte membrane fuel cells (PEMFCs), direct methanol fuel cells (DMFSs), alkaline fuel cells (AFCs), phosphoric acid fuel cells (PAFCs) and microbial fuel cells (MFCs), still rely on platinum (Pt) supported on high surface area carbon as the state of the art electrocatalyst. Besides, Pt has a relatively high work function, corrosion resistance than other materials and thus is the most desired/preferred catalyst for fuel cell application. However, a cell operated at variable load condition (0.6–1 V) and vigorous operation will gradually decrease the Pt active area due to Pt agglomeration followed by dissolution, structural, and morphology changes on the carbon layer leading to decreased fuel cell performance (Dhanasekaran et al., 2022, Dhanasekaran et al., 2016). Exploring innovative catalysts with well-ordered nanostructures is crucial for enhancing catalytic activity, power density, durability, and efficiency in fuel cell applications (Khan et al., 2018). 2D nanomaterials, including metal nitrides, carbides, graphene, and modified metal oxides, are highly favored for their larger surface area and active sites, facilitating rapid electron or interfacial charge transfer.2D nanomaterials like metal nitrides, carbides, graphene, and modified metal oxides are the most sought-after supports/composites for noble metal for actual fuel cell application. These materials serve as promising supports/composites for noble metals in fuel cells, acting as both cathode and anode catalysts, thereby addressing issues related to reaction kinetics and reducing costs (Gupta, 2022). MXenes, a novel 2D nanomaterial, offer unique properties such as electrical conductivity and surface functional groups, making them ideal for enhancing fuel cell electrocatalytic performance by modifying electrode surfaces (Bilibana, 2023).Utilizing restacked and aggregated MXene nanosheets as electrode modification materials can lead to improved fuel cell performance through increased specific surface area, surface hydrophilicity, and electropositivity. This chapter aims to review fuel cell stability by depositing MXene-based 2D nanostructures and comprehensively understanding the structural characteristics and synthesis of MXenes.

II. Structural Characteristics and Synthesis of MXenes

MXenes, a novel category of 2D nanomaterials, are synthesized through selective etching, typically from transition metal carbides or nitrides. They are characterized by a general formula $M_{n+1}X_nT_x$, where M denotes the pre-transition metal, X represents carbon or nitrogen, and T_x denotes surface end groups such as -O-, –OH, –F, and others (Sajid et al., 2024, Oyehan et al., 2023, ampong et al., 2023). Among synthesized numerous MXenes, $Ti_3C_2T_x$ is the most widely researched (Cai et al., 2024). The surface of $Ti_3C_2T_x$ contains numerous hydrophilic groups like -O-, –OH, and –F, exhibiting strong hydrophilicity, exceptional thermal stability, and high conductivity. Due to these properties, it finds extensive applications across various fields including electronics, biomedicine, sensors, biosensors, photothermal conversion, water purification, and catalysis (Ampong et al., 2023, Peng et al., 2021, Saeidi et al., 2023) (Tab.1). With a 2D structure akin to graphene but boasting superior conductivity, MXenes are extensively researched as electrocatalysts for clean energy conversion reactions. These encompass the oxygen reduction reaction (ORR), methanol oxidation reaction (MOR), nitrogen reduction reaction (NRR), and electrochemical water splitting reactions, including the hydrogen evolution reaction (HER) and oxygen evolution reaction (OER) (Wu et al., 2024). This demonstrates that numerous studies indicate MXenes' potential as promising electrocatalysts in the mentioned reactions, offering an alternative to costly platinum-based catalysts.

Tab. 1: The general applications of 2D nanomaterial MXene till date

Energy	Environment	Biomedical	Electronics	Optical
Super capacitors	*Water desalination*	*Cancer treatment*	*Gas sensors*	*Laser*
Ion batteries	*Water purification*	*Drug delivery*	*Electrical conductivity*	*Surface-enhanced Raman spectroscopy*
HER	*Air purification*	*Biosensors*	*Magnetic*	*Photo detectors*
OER	*Membrane*	*Electrodes*	*Laser*	
CO_2 reduction	*Bioelectrochemical fuel cells*	*Antimicrobial activity*	*Gas/humidity/strain sensors*	
Fuel cells				
Sensors				

MXenes are conventionally synthesized from MAX phase materials, characterized by the general formula $M_{n+1}AX_n$, where ‘‘M” represents transition metal such as Sc, Ti, V, Cr, Zr, Nb, Mo, Hf, Ta and “A” represents group IIIA or IVA element elements such as Al, Si, Ga or Ge and and “X” represents C, N or B element (Oyehan et al., 2023). During MXene synthesis, the A element is selectively etched away, leaving behind only M and X, the primary components of MXenes. Various etching techniques contribute to the diversity of MXene types, properties, and functionalities. Top-down methods involve removing the ' elements, typically Al, Si, or Ga, from either the MAX phase or non-MAX phase. These methods can broadly be classified into wet chemical approaches and dry selective extraction (DSE) methods (Rems et al., 2023). The Dry Selective Extraction (DSE) method represents an innovative fluoride-free halogen etching approach guided by computation (Jawaid et al., 2021). It employs iodine vapor to selectively remove the A element from the MAX phase. Wet chemical methods, on the other hand, utilize strong chemicals, electrochemical exfoliation, and mechanical/hydrothermal techniques to target the A element for etching. These methods are widely favored and extensively researched in synthesis approaches. For instance, the well-known $Ti_3C_2T_x$ was synthesized by etching aluminum from Ti_3AlC_2 using HF (50%) (Naguib et al., 2011). Typically, chemical exfoliation precedes intercalation with cations or organic molecules (Alhabeb et al., 2017), which facilitates delamination, the process of separating the synthesized MXene into 2D layers (Rasool et al., 2019). While alternative etching solutions exist, fluoride-containing acids such as HF and NH4F remain prevalent in chemical etching due to their potent ionizing properties. Nonetheless, in light of environmental and safety considerations, fluoride-free etchants have recently garnered increased attention (Oyehan et al., 2023).

III. MXene for Fuel Cell Applications

MXene has excellent electrochemical stability and has been widely studied in energy-related fuel cell applications. MXene is especially attractive in terms of outstanding chemical and thermal stability and excellent electron inter-conducting behavior compared to various carbon and metal oxide systems (Dhanaeskaran et al., 2022). Especially, a two- layer MXene-based system has essential characteristics that can utilize for energy conversion applications. MXene-based 2D nanomaterials also act as a catalyst as well as support materials for fuel cell application. The strong interaction between MXene-based 2D nanomaterials and Pt metal might be ameliorating the catalytic activity and stability. As suggested by Gao et al. (2019) through density functional theory (DFT) calculations, the robust interaction between MXene-based 2D nanomaterials and Pt metal likely enhances catalytic activity and stability. Pt metal nanoparticles exhibit excellent adsorption energies, particularly when supported by $Ti_3C_2T_x$. Uniform deposition of Pt nanoparticles on well-layered $Ti_3C_2T_x$ nanosheets forms higher intermetallic compounds, resulting in improved selectivity.

Efficient electrocatalysts are crucial for high-capacity energy systems to facilitate clean and sustainable development. Notably, the direct methanol fuel cell (DMFC) has garnered significant interest owing to its cost-effectiveness and the safe, convenient storage and transfer of liquid methanol. Therefore, a high-performance direct methanol fuel cell (DMFC) necessitates a highly active anode electrocatalyst for the methanol oxidation reaction (MOR) and a highly active oxygen reduction reaction (ORR) electrocatalyst with methanol-tolerant properties at the cathode. Yang et al. (2019) synthesized a non-Pt electrocatalyst MoS_2QDs@$Ti_3C_2T_x$QDs@MWCNTs composite for ORR and MOR in alkaline solution. The MoS_2QDs@$Ti_3C_2T_x$QDs@MWCNTs showed good electrocatalytic activity for methanol oxidation reaction in alkaline media with a high maximum current density of 160 A/g at the potential of 2.2 V. In an alkaline medium, the MXene composite demonstrated superior stability, maintaining 93% of its initial activity compared to Pt/C (63%) at 0.6 V even after 6,000 cycles.

Durability poses the primary challenge in the long-term operation of PEMFCs (Ahmad et al., 2021; Xie et al., 2014). Carbon corrosion remains the principal obstacle in achieving stability with Pt/C catalysts, a challenge yet to be overcome. During standard PEMFC operation, the density of the Pt catalyst may decline due to carbon support degradation, primarily attributed to carbon corrosion. In contrast, MXene demonstrates remarkable durability in both acidic and alkaline environments, resulting in a more pronounced interaction between Pt and the support compared to carbon. Through density functional theory (DFT) calculations, Xie et al. (2013) illustrated that the binding energy of Pt on Ti_3C_2 is 5.499 eV, exceeding that of Pt on carbon support clusters (Ebind = 3.362 eV). This highlights a robust interaction between Pt and Ti_3C_2 MXenes. Additionally, Xie noted that after 10,000 cycles of accelerated durability testing (ADT), Pt/C experienced a 21 mV decrease in the half-wave potential, whereas Pt/$Ti_3C_2X_2$ exhibited no such decrease.

Numerous MXene-based nanostructures have been explored and studied as electrocatalysts for the HER. The unique surface chemistry and electronic structure of MXenes facilitate strong hydrogen adsorption and desorption, leading to enhance HER performance (Yang et al., 2021). It exhibits remarkable efficiency in catalyzing the Hydrogen Evolution Reaction (HER). Studies have shown that MXenes, particularly $Ti_3C_2T_x$, significantly enhance HER kinetics due to their high surface area, conductivity, and abundant active sites. For instance $T_{i3}C_2T_x$-based catalysts achieved lower overpotentials and higher current densities compared to traditional Pt based catalysts (Zhang et al., 2018, Li et al., 2019). The $Mo_2TiC_2T_x$-PtSA electrode exhibited a remarkably current density of 1.54 mA/cm^2 for HER, surpassing pristine $Mo_2TiC_2T_x$, $Mo_2TiC_2T_x$-VMo, and Pt/C by approximately 15.4, 3.1, and 1.1 times, respectively (Zhang et al., 2018).

Yang et al. (2022) examined the utilization of the 2D nanomaterial MXene in anion exchange membranes for alkaline fuel cells. They found that 2D MXenes, including LiF-$Ti_3C_2T_x$ and NH_4HF_2-$Ti_3C_2T_x$, enhanced both ionic conductivity and power density, resulting in improved cell performance. This development offers the potential for more efficient and sustainable energy storage in alkaline fuel cell technology.

The MXene has also been used in bioelectrochemical fuel cells. Tahir et al. (2020) investigated the MXene as cathode catalyst to improve microbial electrosynthesis (MES) performance. The MXene-coated biocathode enhanced MES efficiency by facilitating electron transfer between microorganisms and electrodes. This improvement leads to higher production rates of valuable chemicals and fuels through MES processes. Liu et al. (2018) investigated the use of Ti_3C_2 MXene as an anode material in microbial fuel cells (MFCs). The results showed that a two-dimensional Ti_3C_2 MXene anode enhanced MFC performance, with higher power output and improved stability compared to traditional anode materials. The study demonstrates Ti_3C_2 MXene's potential for advancing MFC technology, offering a sustainable and efficient approach for electricity generation through microbial processes, with implications for various applications in renewable energy and wastewater treatment.

IV. Conclusion

The review discusses the significance of MXenes in fuel cell applications, primarily focusing on their role as catalysts. They are explored as alternatives to platinum-based catalysts due to their superior stability and catalytic activity. Their applications extend to various fuel cells, where they improve electron transfer efficiency, leading to increased production rates of valuable chemicals and fuels. In the future, 2D MXene nanostructures offer potential for enhancing fuel cell performance by improving chemical and thermal stability. Lightweight MXene-coated engineering components could reduce costs and enhance durability. Consequently, MXene-based catalysts hold great potential for improving the efficiency of fuel production in various applications, including fuel cells and electrolyzers.

References

Ahmad Junaidi, N. H., Wong, W. Y., Loh, K. S., Rahman, S., & Daud, W. R. W., A comprehensive review of MXenes as catalyst supports for the oxygen reduction reaction in fuel cells, *International Journal of Energy Research*, *45*(11), 15760-15782, (2021).

Alhabeb, M., Maleski, K., Anasori, B., Lelyukh, P., Clark, L., Sin, S., & Gogotsi, Y., Guidelines for synthesis and processing of two-dimensional titanium carbide (Ti3C2T x MXene), *Chemistry of Materials*, *29*(18), 7633-7644, (2017).

Ampong, D. N., Agyekum, E., Agyemang, F. O., Mensah-Darkwa, K., Andrews, A., Kumar, A., & Gupta, R. K., MXene: fundamentals to applications in electrochemical energy storage, *Discover Nano*, *18*(1), 3, (2023).

Bilibana, M. P., Electrochemical Properties of MXenes and Applications, *Advanced Sensor and Energy Materials*, 100080, (2023).

Cai, Y., Chen, X., Xu, Y., Zhang, Y., Liu, H., Zhang, H., & Tang, J., Ti3C2Tx MXene/carbon composites for advanced supercapacitors: Synthesis, progress, and perspectives, *Carbon Energy*, 501, (2024).

Dhanasekaran, P., & Selvaganesh, S. V., MXene-Based 2D Nanomaterials for Fuel Cells. In Energy Applications of 2D Nanomaterials, CRC Press,, 39-57, (2022).

Dhanasekaran, P., Selvaganesh, S. V., & Bhat, S. D., Nitrogen and carbon doped titanium oxide as an alternative and durable electrocatalyst support in polymer electrolyte fuel cells, Journal of Power Sources, 304, 360-372, (2016).

Gao, Y., Cao, Y., Gu, Y., Zhuo, H., Zhuang, G., Deng, S., ... & Wang, J. G., Functionalization Ti3C2 MXene by the adsorption or substitution of single metal atom, *Applied Surface Science*, *465*, 911-918, (2019).

Gupta, R. K. (Ed.), *Energy Applications of 2D Nanomaterials*, CRC Press, (2022).

Jawaid, A., Hassan, A., Neher, G., Nepal, D., Pachter, R., Kennedy, W. J., ... & Vaia, R. A., Halogen etch of Ti3AlC2 MAX phase for MXene fabrication, *ACS nano*, *15*(2), 2771-2777, (2021).

Khan, K., Tareen, A. K., Li, J., Khan, U., Nairan, A., Yuan, Y., ... & Ouyang, Z., Facile synthesis of tin-doped mayenite electride composite as a non-noble metal durable electrocatalyst for oxygen reduction reaction (ORR), *Dalton Transactions*, *47*(38), 13498-13506, (2018).

Li, N., Zhang, Y., Jia, M., Lv, X., Li, X., Li, R., ... & Tao, X., 1T/2H MoSe2-on-MXene heterostructure as bifunctional electrocatalyst for efficient overall water splitting, *Electrochimica Acta*, *326*, 134976, (2019).

Liu, D., Wang, R., Chang, W., Zhang, L., Peng, B., Li, H., ... & Guo, C., Ti 3 C 2 MXene as an excellent anode material for high-performance microbial fuel cells, *Journal of Materials Chemistry A*, *6*(42), 20887-20895, (2018).

Naguib, M., Kurtoglu, M., Presser, V., Lu, J., Niu, J., Heon, M., ... & Barsoum, M. W., Two-dimensional nanocrystals produced by exfoliation of Ti3AlC2, In *MXenes*, Jenny Stanford Publishing, 15-29 (2011).

Oyehan, T. A., Salami, B. A., Abdulrasheed, A. A., Hambali, H. U., Gbadamosi, A., Valsami-Jones, E., & Saleh, T. A., MXenes: Synthesis, properties, and applications for sustainable energy and environment, *Applied Materials Today*, *35*, 101993, (2023).

Peng, Z., Zhang, X., Zhao, C., Gan, C., & Zhu, C., Hydrophobic and stable MXene/reduced graphene oxide/polymer hybrid materials pressure sensors with an ultrahigh sensitive and rapid response speed pressure sensor for health monitoring, *Materials Chemistry and Physics*, *271*, 124729, (2021).

Rasool, K., Pandey, R. P., Rasheed, P. A., Buczek, S., Gogotsi, Y., & Mahmoud, K. A., Water treatment and environmental remediation applications of two-dimensional metal carbides (MXenes), *Materials Today*, *30*, 80-102, (2019).

Rems, E., Anayee, M., Fajardo, E., Lord, R. L., Bugallo, D., Gogotsi, Y., & Hu, Y. J., Computationally Guided Synthesis of MXenes by Dry Selective Extraction, *Advanced Materials*, *35*(45), 2305200, (2023).

Saeidi, M., Chenani, H., Orouji, M., Adel Rastkhiz, M., Bolghanabadi, N., Vakili, S., ... & Simchi, A., Electrochemical wearable biosensors and bioelectronic devices based on hydrogels: mechanical properties and electrochemical behavior, *Biosensors*, *13*(8), 823, (2023).

Sajid, I. H., Iqbal, M. Z., & Rizwan, S., Recent advances in the role of MXene based hybrid architectures as electrocatalysts for water splitting, *RSC advances*, *14*(10), 6823-6847, (2024).

Tahir, K., Miran, W., Jang, J., Shahzad, A., Moztahida, M., Kim, B., & Lee, D. S., A novel MXene-coated biocathode for enhanced microbial electrosynthesis performance, *Chemical Engineering Journal*, *381*, 122687, (2020).

Wu, X., Wang, Y., & Wu, Z. S., Recent advancement and key opportunities of MXenes for electrocatalysis, *Iscience*, (2024).

Xie, X., Chen, S., Ding, W., Nie, Y., & Wei, Z., An extraordinarily stable catalyst: Pt NPs supported on two-dimensional Ti 3 C 2 X 2 (X= OH, F) nanosheets for oxygen reduction reaction, *Chemical Communications*, *49*(86), 10112-10114, (2013).

Xie, X., Xue, Y., Li, L., Chen, S., Nie, Y., Ding, W., & Wei, Z., Surface Al leached Ti 3 AlC 2 as a substitute for carbon for use as a catalyst support in a harsh corrosive electrochemical system, *Nanoscale*, *6*(19), 11035-11040, (2014).

Yang, C., Huang, H., He, H., Yang, L., Jiang, Q., & Li, W., Recent advances in MXene-based nanoarchitectures as electrode materials for future energy generation and conversion applications, *Coordination Chemistry Reviews*, *435*, 213806, (2021).

Yang, X., Jia, Q., Duan, F., Hu, B., Wang, M., He, L., ... & Zhang, Z., Multiwall carbon nanotubes loaded with MoS2 quantum dots and MXene quantum dots: Non–Pt bifunctional catalyst for the methanol oxidation and oxygen reduction reactions in alkaline solution, *Applied Surface Science*, *464*, 78-87, (2019).

Yang, Z., Zhang, M., Zhao, Z., Lan, W., Zhang, X., & Fan, M., Application of 2D nanomaterial MXene in anion exchange membranes for alkaline fuel cells: Improving ionic conductivity and power density, *International Journal of Hydrogen Energy*, *47*(41), 18122-18138, (2022).

Zhang, J., Zhao, Y., Guo, X., Chen, C., Dong, C. L., Liu, R. S., ... & Wang, G., Single platinum atoms immobilized on an MXene as an efficient catalyst for the hydrogen evolution reaction, *Nature Catalysis*, *1*(12), 985-992, (2018).

A Strategy Study on Green Hydrogen Valleys

Adnan Midilli
Mechanical Engineering Department, Faculty of Mechanical Engineering, Istanbul Technical University, Gümüşsuyu Campus, 34437, İstanbul, Türkiye

* E-mail: amidilli@itu.edu.tr

Abstract
Green hydrogen production has become one of the most important aims of green industry, which requires sustainable supply of water, green energy, investment, and clean hydrogen technologies, is an important target of hydrogen valleys. Green Hydrogen Valley (GHV) concept includes, in addition to the hydrogen supply chain, the sectors that use hydrogen, technology producers, critical technology and raw material suppliers, research and educational institutions, public and private sectors, non-governmental organizations, all patners in society. Briefly, it is an important concept that concerns stakeholders, in short, all areas from health to economy. On the other word, A GHV is an energy-strategic area where green hydrogen contributes to multiple sectors or applications in mobility, decarbonization, green transformation, digitalization, transportation, energy, etc. Briefly, a GHV, which includes hydrogen production, hydrogen storage, hydrogen distribution and hydrogen use, is a technological and industrial park focusing on contribution to the development of the hydrogen economy and hydrogen-based sustainable development.
Uder these considerations, the main aim of this study is to develop sustainability indicators of hydrogen valleys in terms of a preliminary design approach to GHVs. In this regard, technological alternatives are taken into account and examined depending on the infrastructure of green hydrogen valleys, including green hydrogen supply chain processes containing hydrogen production, hydrogen storage, hydrogen distribution and hydrogen use. Additionally, the design criteria that should be taken into account in the establishment of hydrogen valleys are investigated in detail. Accordingly, considering the sustainability indicators, hydropower integrated hydrogen valley concept is developed.

Keywords: Hydrogen, green energy, hydrogen valley, sustainability

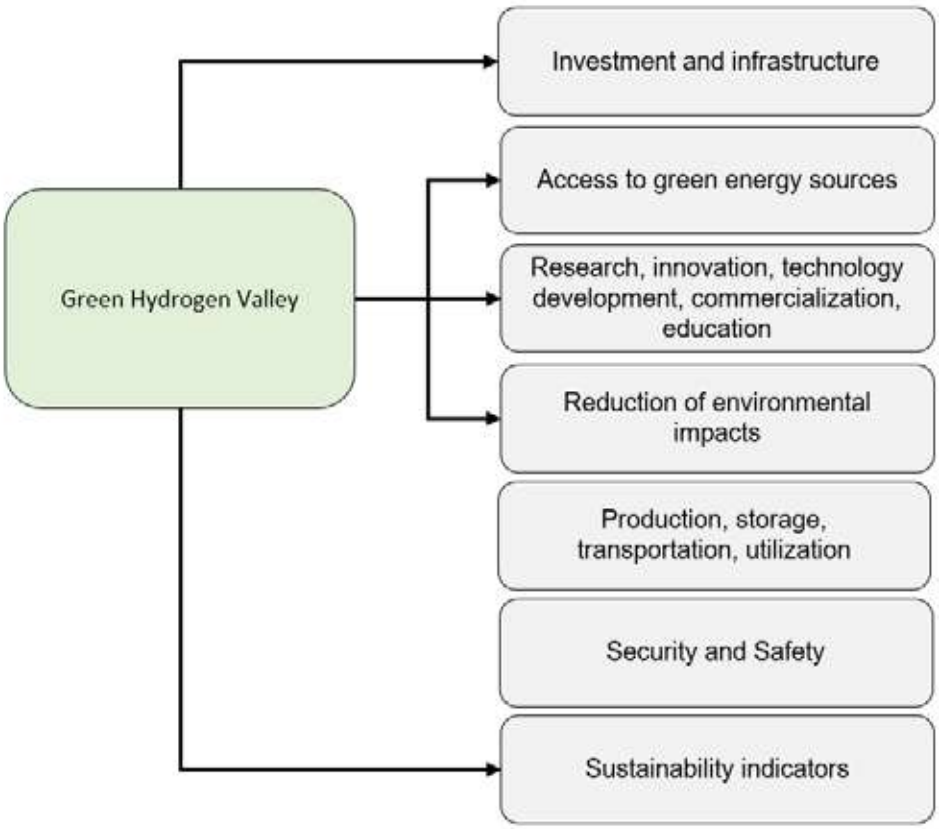


Fig.1: A basic strategy on a Green Hydrogen Valley

Energy Management in Microgrids with Hybrid Energy Storage Systems Utilizing Batteries and Proton Exchange Membrane/Fuel Cells

[1*]Ömer Faruk Özcan, [1]Heybet Kılıç, [2]Ömerül Faruk Özgüven

[1] Dicle University, Department of Electric Power and Energy System, Sur, Diyarbakır, 21280, Türkiye
[3] İnönü University, Engineering Faculty, Electric and Electrical, Battalgazi, Malatya, 44280, Türkiye

* E-mail: omerfaruk.ozcan@dicle.edu.tr

Abstract
The rapid depletion of fossil fuels and the increasing demand for energy have led to the replacement of centralized and traditional power plants with distributed systems based on renewable energy, referred to as clean energy. The concept of microgrids has emerged as a potential solution for integrating distributed energy sources, such as primary sources like solar (PV) and wind, and energy storage systems based on hydrogen and batteries, into the grid. This study addresses the intermittent nature of renewable energy sources by presenting a control strategy for the energy management of an energy storage system comprising hydrogen and batteries. The proposed control strategy is based on Grey Wolf Optimization (GWO) and Takagi-Sugeno-Kang (TSK) fuzzy logic, inspired by nature. The GWO-TSK based control also facilitates Maximum Power Point Tracking (MPPT) to extract maximum power from PV and Proton Exchange Membrane Fuel Cell (PEM FC) systems. The proposed control strategy determines the amount of power to be produced or stored in the energy storage system under different scenarios by considering the grid's load demand, the currently generated power, and the battery's state of charge. This approach aims to enhance the sustainability of energy systems by ensuring the effective and efficient utilization of renewable energy sources.
Keywords:“ Energy management system, hybrid energy storage system, gwo-tsk

I. Introduction

The transition towards renewable energy sources in electricity generation has become imperative due to the escalating global energy demand, the depletion of fossil fuels, their environmental repercussions, and the surge in energy costs (Marks-Bielska et al., 2020). Microgrids have emerged as a promising solution for integrating distributed energy resources, including renewable sources like photovoltaic (PV) solar power and wind energy, along with energy storage systems based on hydrogen and batteries. The concept of microgrids involves creating self-contained systems composed of distributed energy resources capable of operating independently during grid disruptions (J. Albarakati et al., 2022). The intermittent and unpredictable nature of renewable energy sources poses challenges for maintaining grid stability and efficient energy management within microgrids. To address this, research has focused on optimal energy management strategies using a combination of renewable energy sources and energy storage systems (Tomin et al., 2022). These systems can be controlled using advanced technologies such as artificial intelligence, fuzzy logic controllers, and metaheuristics to ensure stable and efficient operation (Sumarmad et al., 2022; Deng et al., 2022; Arrar & Xioaning, 2022).

This study introduces an advanced energy management strategy for microgrids utilizing a hybrid energy storage system (HESS) that combines batteries and PEM FC. The proposed approach leverages Grey Wolf Optimization (GWO) and Takagi-Sugeno-Kang (TSK) based fuzzy control to enhance the performance and reliability of the energy storage system. GWO, inspired by the social hierarchy and hunting behavior of grey wolves, is an effective optimization technique known for its simplicity and ability to avoid local minima. TSK fuzzy logic, on the other hand, offers a robust framework for handling uncertainty and imprecision in complex systems (Liu et al., 2021). By integrating GWO with TSK fuzzy logic, the proposed control strategy aims to optimize the power flow within the microgrid, ensuring maximum power extraction from renewable sources through Maximum Power Point Tracking (MPPT) and efficient energy distribution between the battery storage and PEM FC systems. The study's control strategy dynamically adjusts to load demands, power levels, and battery state, improving microgrid efficiency and renewable energy utilization, contributing to a sustainable and resilient energy infrastructure.

II. System Component and Modelling

Figure 1 illustrates the configuration of a grid-connected hybrid microgrid system with the proposed GWO-TSK-based energy management system.Grid-connected hybrid micro-grid system that combines solar PV, wind turbine-based PMSG, a dual-input DC-DC converter, battery energy storage system, hydrogen system, DC load, AC load, and additional components.The hybrid renewable energy system’s primary energy sources are two- blade wind turbines and photovoltaic (PV) panels (HRES).Through the DC bus, power converters are connected to both energy sources using the Maximum Power Point Tracking (MPPT) technique.

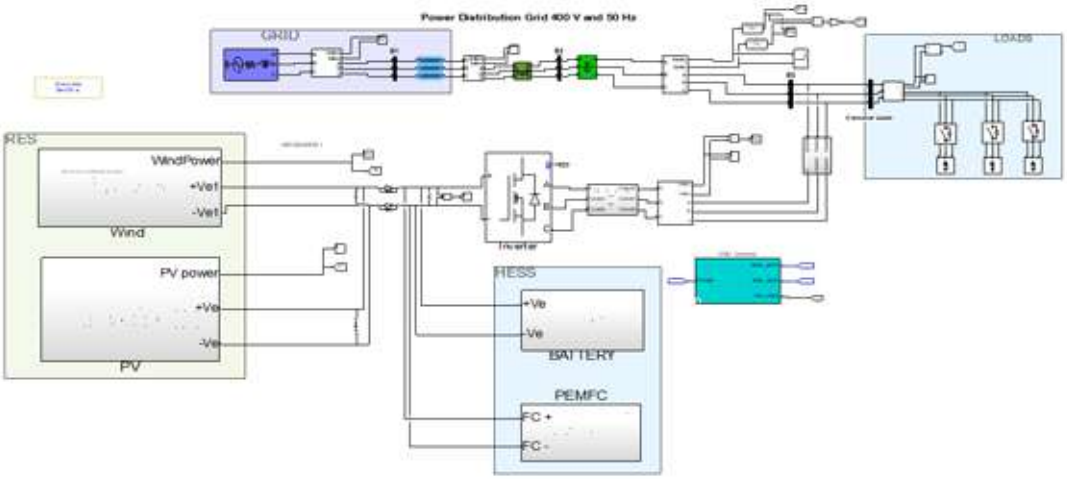


Fig.1: The Configuration of a Grid-connected Hybrid Microgrid System

The hybrid renewable energy system's primary energy sources are two- blade wind turbines and photovoltaic (PV) panels (HRES).Power converters utilize MPPT control and unidirectional DC/DC converters to extract maximum power from both sources. However, converting the three-phase voltage generated by the wind turbine requires an AC/DC converter (rectifier). One system integrates a Proton Exchange Membrane (PEM) fuel cell, hydrogen tanks, and an electrolyzer. The hydrogen system enhances the stability of HRES and balances energy production with demand. However, it exhibits a slow dynamic response to rapid load fluctuations, necessitating a storage device with fast dynamic response, such as a lead-acid battery.

III. GWO-TSK ALGORITM

Within the realm of renewable energy systems, such as fuel cell, solar, and wind power systems, the utilization of Maximum Power Point Tracking (MPPT) plays a vital role in optimizing power production despite fluctuations in hydrogen availability, sun irradiation, and wind speed. Traditionally, it has been typical to use separate controllers for each component in hybrid renewable energy systems (HRES), such as fuel cell, solar, and wind producing units. The pseudocode summary for this control algorithm is shown below.

```
Function hybridGWOTSK_MPPT(pvVoltage, pvCurrent)
    // Parameters
    Initialize maxIterations, wolfCount, alpha, beta, delta
    Initialize fuzziness
    Initialize wolf positions randomly

    // Optimization loop
    For each iteration up to maxIterations
        Evaluate fitness for each wolf
        Identify best wolf as alphaPosition
        Update positions using GWO formula
        Perform TSK fuzzy inference for duty cycle
    End For

    Return final dutyCycle
End Function

Function evaluateFitness(positions, pvVoltage, pvCurrent, fuzziness)
    Calculate power output for each wolf position
    Return negative power output as fitness
End Function

Function calculatePowerOutput(positions, pvVoltage, pvCurrent, fuzziness)
    For each wolf position
        Extract a1 and a2
        Apply TSK fuzzy rules to compute aggregated output
        Calculate dutyCycle based on fuzziness and aggregated output
        Clamp dutyCycle within valid range
        Set powerOutput (replace with actual calculation)
```

```
    End For

    Return powerOutput
End Function

Function tskFuzzyInference(alphaPosition, pvVoltage, pvCurrent, fuzziness)
    Extract a1 and a2
    Apply TSK fuzzy rules to compute aggregated output
    Calculate dutyCycle based on fuzziness and aggregated output
    Clamp dutyCycle within valid range
    Return dutyCycle
End Function
```

IV. Results and discussions

• The graph obtained at the end of the simulation is shown in Figure 2a. Accordingly, the radiation is given at variable values [1000 500 800 400] according to time [0 0.5 1 1.5 2] and according to the examined graph, it is seen that the MPPT control works stably and the noise levels are at a minimum.

• The maximum power point output graph obtained from the wind with the GWO-TSK fuzzy logic method above is as shown in figure 2b.
• The mppt algorithm applied according to a time-varying wind speed provides maximum power stably.

• Figure 2c and 2d show the dc bus voltage obtained before and when the pem fc is included in the microgrid structure. When GWO-TSK based mppt applied pem fc was included in the system, a more stable dc bus voltage was obtained by reducing the discontinuous nature of the dc bus voltage and wind.

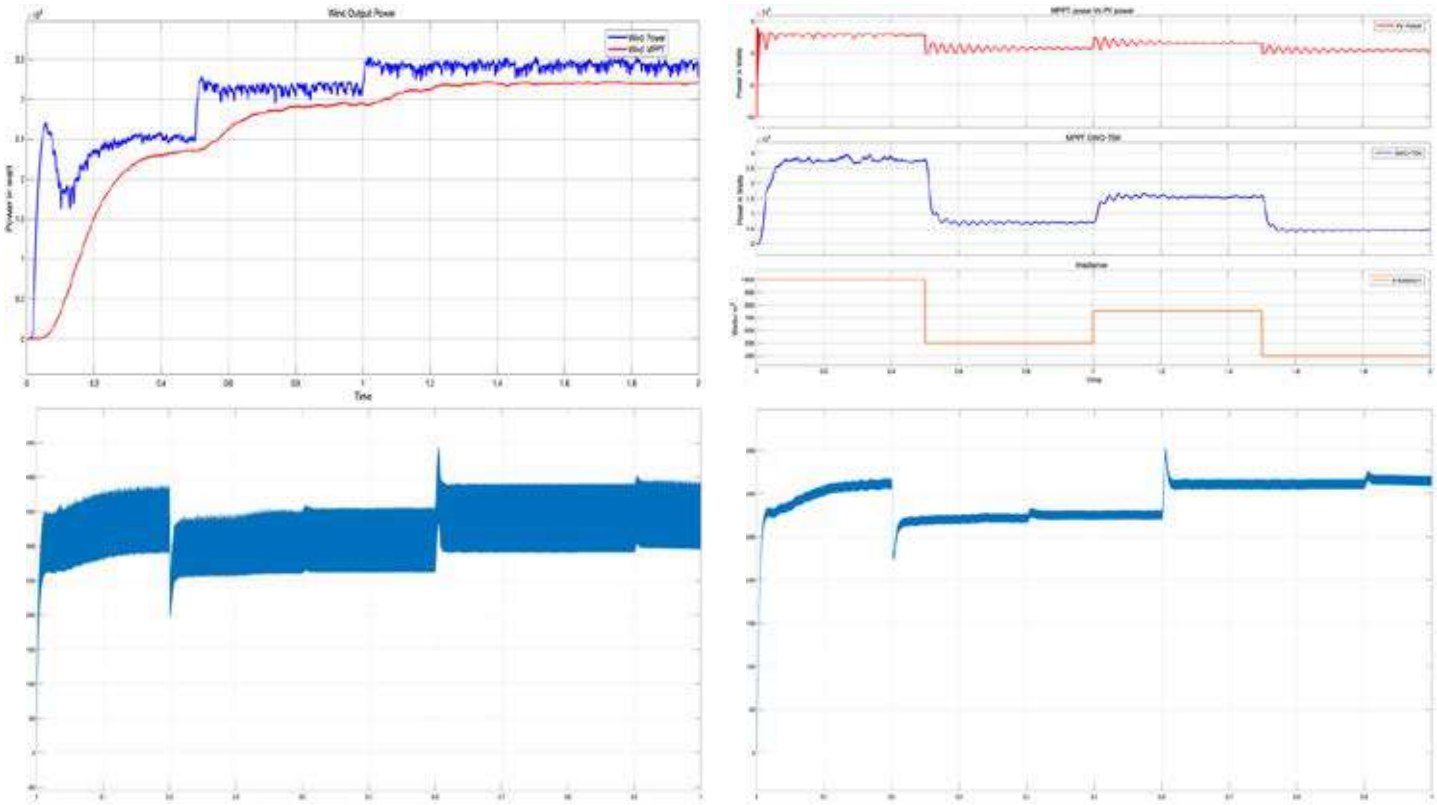


Fig.2: a) PV MPPT output graph b) Wind MPPT output graph c-d) Dc bus voltage with pem fc and without

• The result graph of the battery management system is given in figure 3 below.
• PV, WT and LP (load power) are given as input and the duty cycle, which adjusts the charging and discharging status of the battery by switching, is given as output.

• In this management system, an algorithm has been created according to the scenarios created depending on whether the load power is less or more than the total power.

• At 0.2 seconds, when the total load power starts to exceed the total generated power, the battery power tries to cover the difference between the total load and the generated power. At this stage, the power drawn from the battery increases and the battery power shows an upward trend in the graph.

Between 0.2 and 0.6 seconds, when a constant load power is more than the generated power and is constant, it remains constant because the battery capacity is full. 0.4. Battery power decreases as the load decreases slightly per second. 0.6. In seconds, the total load falls below the total generated power and the battery power decreases accordingly.

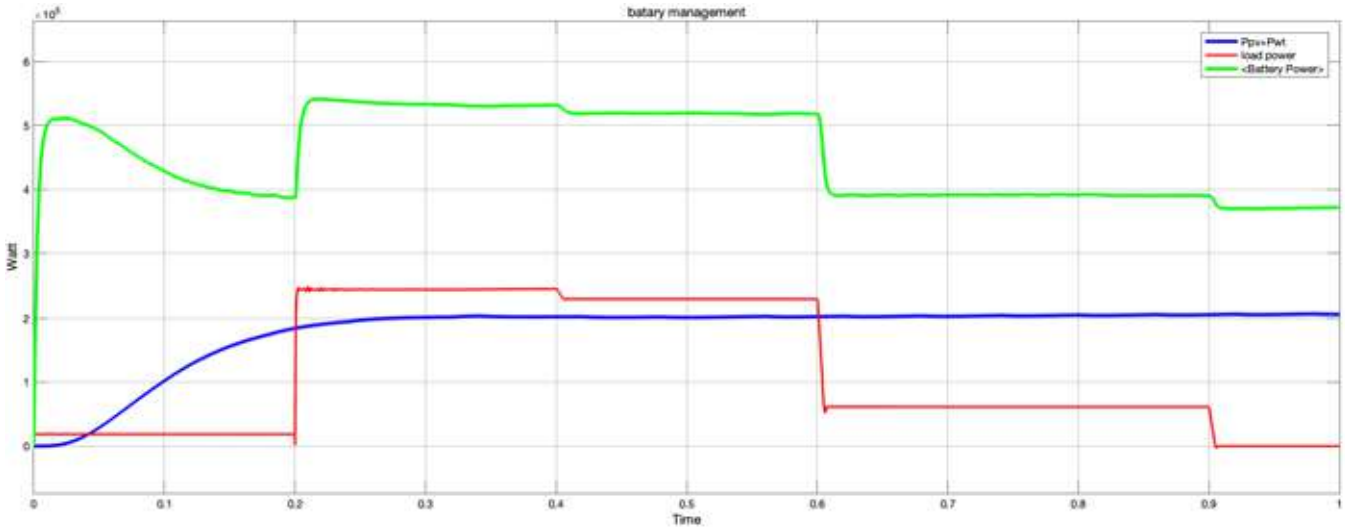


Fig. 3: Battery management Simulation results

V. Conclusions

This study proposed an energy management strategy using Grey Wolf Optimization (GWO) and Takagi-Sugeno-Kang (TSK) fuzzy logic to address the intermittency of renewable energy sources in microgrids. The strategy integrates solar (PV), wind, and energy storage systems like hydrogen and batteries. It also incorporates Maximum Power Point Tracking (MPPT) to optimize power extraction from PV and Proton Exchange Membrane Fuel Cell (PEM FC) systems. By considering load demand, generated power, and battery charge state, the GWO-TSK control effectively determines power production and storage. This approach enhances energy efficiency and sustainability in microgrids.

References

Albarakati AJ, Boujoudar Y, Azeroual M, Eliysaouy L, Kotb H, Aljarbouh A, Khalid Alkahtani H, Mostafa SM, Tassaddiq A and Pupkov A (2022) Microgrid energy management and monitoring systems: A comprehensive review. *Front. Energy Res.* 10:1097858. doi: 10.3389/fenrg.2022.1097858

Arrar, S., & Xioaning, L. (2022). Energy Management in Hybrid Microgrid using Artificial Neural Network, PID, and Fuzzy Logic Controllers. *European Journal of Electrical Engineering and Computer Science*, *6*(2), 38–47. https://doi.org/10.24018/ejece.2022.6.2.414

Liu, J., Wei, X., & Huang, H. (2021). An improved grey wolf optimization algorithm and its application in path planning. Ieee Access, 9, 121944-121956.

Marks-Bielska, R., Bielski, S., Pik, K., & Kurowska, K. (2020). The importance of renewable energy sources in poland's energy mix. Energies, 13(18), 4624.

Sumarmad, K., Sulaiman, N., Wahab, N., & Hizam, H. (2022). Energy management and voltage control in microgrids using artificial neural networks, pid, and fuzzy logic controllers. Energies, 15(1), 303.

Tomin, N., Shakirov, V., Kozlov, A., Sidorov, D., Kurbatsky, V., Rehtanz, C., … & Lora, E. (2022). Design and optimal energy management of community microgrids with flexible renewable energy sources. Renewable Energy, 183, 903-921.

Steam Reforming of Sugar Beet Pulp in the Presence of Ni/Dolomite Catalyst for the Synthesis of Hydrogen-Rich Gas

Tolga Kaan Kanatlı[1], Nasrin Pourmoghaddam[1], Serkan Karadeniz[1], Nezihe Ayas[1,*]

[1]Department of Chemical Engineering, Faculty of Engineering, Eskisehir Technical University, Eskisehir 26555, Türkiye

*E-mail:nazcan@eskisehir.edu.tr

Abstract
In this work, hydrogen-rich gas synthesis through the gasification and steam reforming of sugar beet pulp sourced from Eskişehir Kazım Taşkent Sugar Factory was investigated in the presence of Ni/Dolomite catalysts. To the best of the authors' knowledge, no other steam reforming studies on sugar beet pulp using Ni/Dolomite as a catalyst exist in the literature. The catalysts were synthesized using the impregnation method and were characterized by XRD, FT-IR, TGA, BET, XRF, and SEM. The sugar beet pulp's physical and chemical characterizations were carried out to determine its composition. At the steam reforming tests, a steam-to-biomass ratio of 3:1 was employed, and the impact of the air-fuel equivalence ratio (0 and 0.04), temperature (600, 700, and 800 °C), and catalyst (uncatalyzed, 10% Ni/Dolomite, 20% Ni/Dolomite) was investigated. The highest molar concentration of hydrogen in the syngas was obtained as 51.0% at 700 °C, without air, in the presence of 10% Ni/Dolomite.

Keywords: Biomass, Sugar beet pulp, Steam reforming, Dolomite, Hydrogen

I. Introduction

The depletion of fossil fuels and the environmental risks associated with these fuels has resulted in an increased interest in clean, sustainable, and renewable energy sources. Among these sources, hydrogen energy is seen as a viable alternative, as it provides energy security, can be obtained through various methods, has a high energy content, and emits only water vapor as the product of its combustion.

Biomass is being investigated as a potential feedstock for renewable hydrogen production. Sugar beet pulp, which is a waste product from the sugar production industry, contains valuable substances like cellulose and hemicellulose. According to the information provided by The Eskişehir Kazım Taşkent Sugar Factory, the average amounts of bagasse and pulp produced from sugar beet processed in Turkey between the years 2018 and 2022 are 312.679 and 22.137 tons, respectively. Utilizing sugar beet pulp for fuel production would have environmental benefits, support the energy need, and reduce dependence on external sources of energy. Turkey, one of the largest sugar beet producers, has a significant amount of sugar beet pulp available for conversion into hydrogen, which can be achieved through thermochemical methods such as gasification. The process of gasification involves the conversion of carbon-containing materials into flammable or synthetic gases, including hydrogen (H_2), carbon monoxide (CO), carbon dioxide (CO_2), and methane (CH_4).

A literature survey shows that sugar beet industry waste has been utilized in various works such as pyrolysis of sugar beet pulp (Aho et al., 2013; Yılgın et al., 2010), gasification as a waste-to-energy strategy for sugar beet industry (Rajaeifar et al., 2019), investigation of possible routes for synthesis of biofuels through gasification (Nicodème et al., 2018), supercritical water gasification of sugar beet pulp (Babatabar et al., 2023), there are very limited studies on the gasification of sugar beet industry waste.

To the best knowledge of the authors, there are no studies that focus on catalyst synthesis and the parametric gasification of sugar beet pulp. Therefore, in this study, dolomite-supported Ni catalysts (10% and 20% wt./wt.) were synthesized through the impregnation method, and characterized by XRD and SEM. Parametric gasification studies were conducted at a steam-to-biomass ratio of 3:1, air-fuel equivalence ratio of 0 and 0.04, and gasification temperatures of 600, 700, and 800 °C.

II. Experimental Set-up and Procedure

Pre-treatment procedure and proximate analysis of sugar beet pulp have been carried out as described in a previous work (Ayas & Karadeniz, 2017).

To synthesize the Ni/Dolomite catalysts, the calculated amount of nickel nitrate hexahydrate salt was dissolved in pure water and mixed with the dolomite support material in a magnetic stirrer at 80 °C for six hours, after which the mixture was aged at room temperature for 24 hours. Subsequently, the obtained catalyst was dried in an oven at 105 °C for 24 hours and pulverized in a mortar. Finally, it was calcined at 800°C for 3 hours with a heating rate of 10 °C/min and air flow rate of 400 mL/min. The calcined catalysts were reduced at 800 °C for 60 minutes with an H_2/N_2 gas mixture containing 20% H_2 by volume at a 400 mL/min flow rate (Kiren & Ayas, 2022).

For XRD analysis, the Rigaku MiniFlex 600 was employed. For SEM imaging, the Zeiss Supra 50 VP was utilized to characterize the catalysts.

Parametric gasification and the steam reforming process were carried out in an updraft 316 stainless steel tubular updraft gasification reactor described in previous work (Ayas & Karadeniz, 2017). For steam generation, a peristaltic pump is used to feed the calculated amount of water (Steam:Biomass ratio of 3:1) to the reactor through a 1.5 m long heated line operating at 150 °C. For all experiments, 2 g of sugar beet pulp was mixed with 0.4 g catalyst, achieving a 20 wt% catalyst:biomass ratio. The reaction duration was kept constant at 15 minutes for all

experiments. The product gas was collected in a Tedlar™ Bag and analyzed using a μ-GC.

III. Analysis

As seen in Fig. 1, the XRD pattern of dolomite has mostly CaO and MgO peaks. Calcined dolomite exhibits the corresponding characteristic CaO peaks at 2θ = 32.2, 37.6, 53.8, 64.1 and MgO peaks at 2θ = 43.1, 62.8, 74.9. Fig. 1 also shows the presence of $NiMgO_2$, CaO, and MgO in the 10% Ni/Dolomite catalyst. Srinakruang et al. (2006) examined the effect of calcination temperature on a 10% Ni/dolomite catalyst using XRD analysis. They found that the $NiMgO_2$ phase was present in all Ni/dolomite catalysts calcined at various temperatures, while the NiO phase was present only for the catalyst calcined at 500 °C. It is also evident from the XRD patterns that the peak of $NiMgO_2$ becomes gradually stronger as the amount of Ni gradually increases.

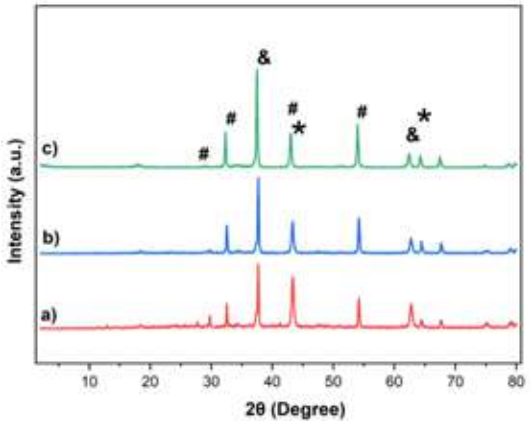


Fig.1 . XRD patterns of a) calcined-Dolomite, b) %10 Ni/Dolomite, c) %20 Ni/Dolomite (#: CaO &: MgO *: $NiMgO_2$)

SEM analyses were carried out to obtain information about the morphology, shape, and size of the synthesized catalysts. Fig. 2 shows the SEM images of calcined dolomite and Ni/Dolomite catalysts with different Ni loadings. SEM image of calcined dolomite reveals an irregular structure. Similarly, as seen in Fig. 2, homogeneous and porous textures occur on the dolomite when the nickel loading ratio rises from 10% to 20%. In comparison to other nickel-loaded catalysts, the agglomeration structure on the catalyst surface of the 20% Ni/Dolomite is observed to exhibit a homogeneous distribution, completely covering the dolomite surface, and displaying a compact structure.

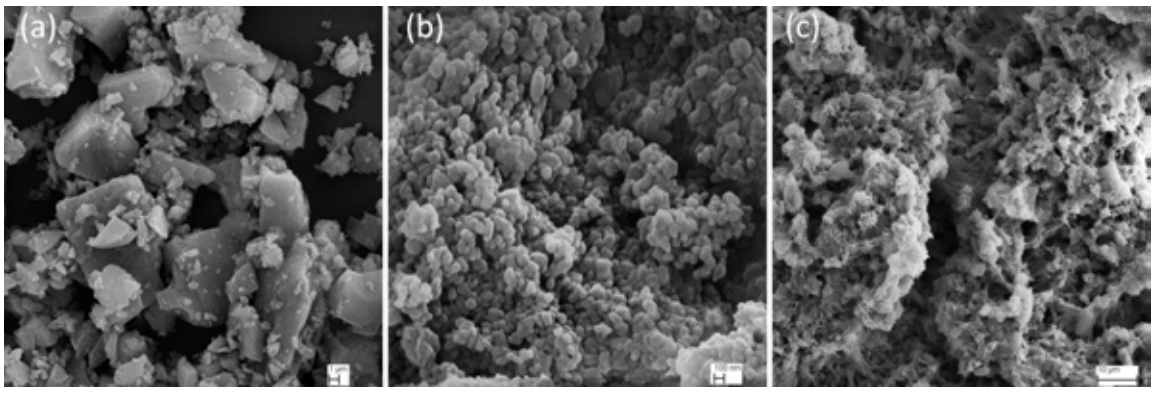


Fig. 2. SEM images of Ni/Dolomite catalysts: a) Calcined Dolomite, b) 10% Ni/Dolomite, c) 20% Ni/Dolomite

IV. Results and discussions

The impact of air feed was examined at an ER of 0.04 and in the absence of air, at a temperature of 700 °C, a steam-to-biomass ratio of 3:1 (0.33 g/min water feed rate). It was determined that the removal of the air feed resulted in a 24% increase in hydrogen concentration due to the elimination of nitrogen from the product gas considering that at an ER of 0.04, nitrogen constitutes 17% of the product gas. The observed decrease in CO and CO_2 yields, along with the increase in hydrogen yield, indicates that the removal of the air supply prevented combustion reactions and increased hydrogen conversion.

Steam reforming experiments were conducted at temperatures of 600, 700, and 800 °C to determine the effect of temperature in the presence of a 10% Ni/Dolomite catalyst in an air-free environment. The resulting gas product concentrations and yields are presented in Fig. 3.

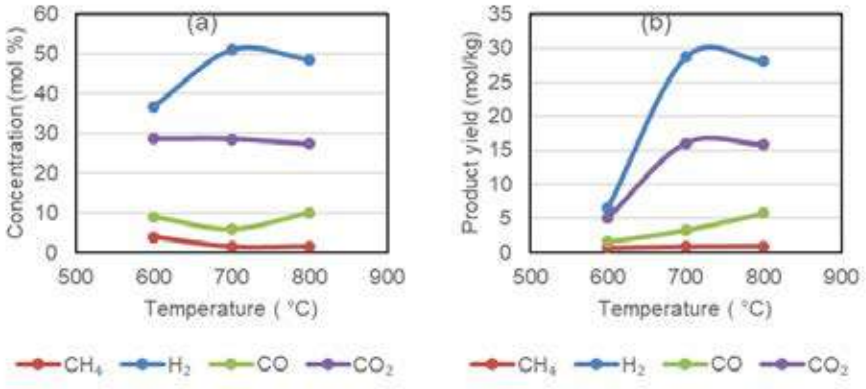


Fig. 3. Effect of temperature on the steam reforming process (10% Ni/Dolomite catalyst, air-free environment, S:B ratio 3:1)

Increasing the temperature from 600 to 700 °C resulted in a more than 2-fold increase in gas volume while increasing the temperature from 700 to 800 °C only caused a 3% increase. The hydrogen yield increased by 3.3 times at 700 °C but decreased by 2% at 800 °C. The increase in gas volume indicates that 600 °C is not sufficient for efficient gasification. The increase in temperature accelerated the reverse water-gas displacement reaction, consuming CO_2 and hydrogen and forming CO and water.

Effects of the presence and type of the catalyst were investigated at 700 °C temperature, air-free condition, with a S:B ratio of 3:1. The results are detailed in Fig. 4.

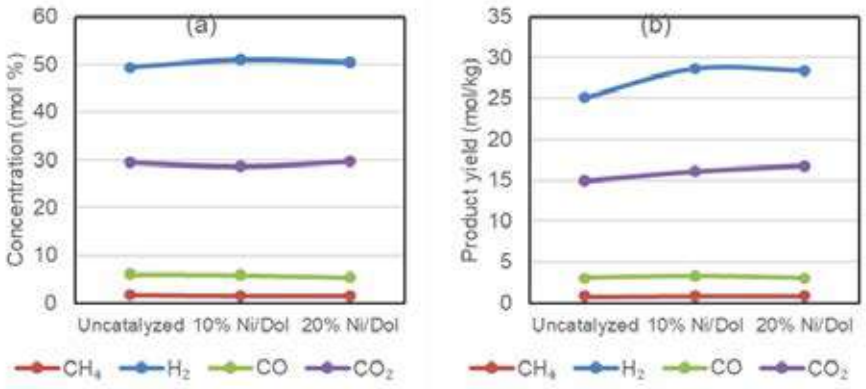


Fig. 4. Effect of catalyst on the steam reforming process (700 °C, air-free environment, S:B ratio 3:1)

The introduction of 10% Ni/Dolomite resulted in a 14% increase in hydrogen yield and a 3% rise in hydrogen concentration compared to the uncatalyzed condition. This was accompanied by an 11% increase in gas volume, indicating the efficacy of the catalyst. However, analysis of the yields obtained with 20% Ni/Dolomite catalyst revealed that increased nickel loading had a detrimental effect on hydrogen and CO_2 yields, attributed to nickel's catalysis of combustion reactions. Furthermore, catalyst utilization decreased nitrogen concentration while increasing gas volume.

V. Conclusions

The reforming of steam in an air-free environment resulted in a 24% increase in the hydrogen concentration. An increase in the reaction temperature from 600 to 700 °C led to a 3.3-fold increase in the hydrogen yield, while a further temperature increase to 800 °C had a slight negative effect. The use of 10% Ni/Dolomite was found to increase the hydrogen yield, while 20% Ni/Dolomite had some adverse effects due to nickel catalyzing the combustion reactions. Results presented in this study indicate that sugar beet pulp is a suitable candidate for hydrogen production either by conventional gasification or steam reforming of the biomass. The conditions for efficiently producing hydrogen from the sugar beet pulp were determined as steam reforming with a S:B ratio of 3:1, at 700 °C with 10% Ni/Dolomite catalyst.

Acknowledgements

This research was supported by the Scientific and Technological Research Council of Turkey (TÜBİTAK), project number 22AG034 – “Environmentally Compatible Sustainable Advanced Vehicle Technologies”.

References

Aho, A., Käldström, M., Kumar, N., Eränen, K., Hupa, M., Holmbom, B., Salmi, T., Fardim, P., & Murzin, D. Yu. (2013). Pyrolysis of beet pulp in a fluidized bed reactor. *Journal of Analytical and Applied Pyrolysis*, *104*, 426–432. https://doi.org/10.1016/j.jaap.2013.06.002

Ayas, N., & Karadeniz, S. (2017). Hydrogen from tobacco waste. *2017 2nd International Conference Sustainable and Renewable*

Energy Engineering (ICSREE), 78–82. https://doi.org/10.1109/ICSREE.2017.7951515

Babatabar, M. A., Manouchehri, M., Abbasi, H., & Tavasoli, A. (2023). Supercritical water Co-gasification of biomass and plastic wastes for hydrogen-rich gas production using Ni-Cu/AC-CaO catalyst. *Journal of the Energy Institute*, *108*, 101251. https://doi.org/10.1016/j.joei.2023.101251

Kiren, B., & Ayas, N. (2022). Nickel modified dolomite in the hydrogen generation from sodium borohydride hydrolysis. *International Journal of Hydrogen Energy*, *47*(45), 19702–19717. https://doi.org/10.1016/j.ijhydene.2021.11.159

Nicodème, T., Berchem, T., Jacquet, N., & Richel, A. (2018). Thermochemical conversion of sugar industry by-products to biofuels. *Renewable and Sustainable Energy Reviews*, *88*, 151–159. https://doi.org/10.1016/j.rser.2018.02.037

Rajaeifar, M. A., Sadeghzadeh Hemayati, S., Tabatabaei, M., Aghbashlo, M., & Mahmoudi, S. B. (2019). A review on beet sugar industry with a focus on implementation of waste-to-energy strategy for power supply. *Renewable and Sustainable Energy Reviews*, *103*, 423–442. https://doi.org/10.1016/j.rser.2018.12.056

Srinakruang, J., Sato, K., Vitidsant, T., & Fujimoto, K. (2006). Highly efficient sulfur and coking resistance catalysts for tar gasification with steam. *Fuel*, *85*(17–18), 2419–2426. https://doi.org/10.1016/j.fuel.2006.04.026

Yılgın, M., Deveci Duranay, N., & Pehlivan, D. (2010). Co-pyrolysis of lignite and sugar beet pulp. *Energy Conversion and Management*, *51*(5), 1060–1064. https://doi.org/10.1016/j.enconman.2009.12.010

Activated Carbon from Sugar Beet Pulp for CO_2 Capture

Fahriye Dönmez Dayi[1], Salahaldeen Aljafreh[1], Damla Dumlu [1] and Nezihe Ayas[1*]

[1] Department of Chemical Engineering, Faculty of Engineering, Eskisehir Technical University, Eskisehir 26555, Türkiye

* E-mail: nazcan@eskisehir.edu.tr

Abstract

Sugar beet pulp is a waste produced in significant amounts in Turkey. Utilizing sugar beet pulp as activated carbon would contribute to waste valorization and add value to sugar beet pulp. One of the uses of activated carbon is to purify hydrogen by removing gases such as CO_2 from the gas mixture produced by the gasification process. This study focuses on the synthesis of activated carbon from sugar beet pulp through the pyrolysis process and investigates the CO_2 adsorption capacity of activated carbon. Sugar beet pulp was activated by alkaline activation with KOH at 1:1 and 1:2 ratios before pyrolysis. The pyrolysis process was carried out at 700 °C with a heating rate of 10 °C/min and a holding time of 60 minutes. Activated carbons were characterized using X-ray diffractometry (XRD), and Fourier Transform Infrared Spectroscopy (FT-IR). The CO_2 adsorption capacity was determined in a fixed-bed column under 100 mL/min CO_2 gas flow at 20 and 35 °C at 1 atm, where the highest capacity was obtained for AC (1:2) at 20 °C as 164.59 mg/g.

Keywords: Activated carbon, CO_2 capacity, chemical activation, Sugar beet pulp

I. Introduction

Biomass is one of the most important sustainable sources for energy production. The gasification of biomass is a thermochemical process that converts solid biomass into valuable gases like methane, carbon dioxide, carbon monoxide, and hydrogen. Hydrogen gas as an energy carrier can be further used for fuel cells and energy applications, but they require a pure hydrogen gas with a purity of 99%. Therefore, the gas mixture produced by the gasification process needs to be purified and separated to be usable for energy applications and fuel cells (Mishra & Upadhyay, 2021).

Hydrogen purification methods can be physical or chemical, including adsorption, low-temperature separation, membrane separation, metal hydride separation, and catalysis. Adsorption is known to be one of the favorable methods between them, where adsorption is a surface process that leads to the transfer of a molecule from a fluid bulk to a solid surface. This can occur because of physical forces or chemical bonds. The solid surface is called an adsorbent and is usually made from carbon material. The adsorption properties of carbon materials are closely related to textual structures and surface chemistry. A great resource for making carbon materials is biomass. It is low in pollution, abundant, and renewable. The main elements of biomass are C, H, and O, which also contain a small amount of N and S. After the proper treatment, biomass can be converted into carbon materials with good adsorption performances. Activated carbon from biomass is one of the most common adsorbents for hydrogen gas purification. The biomass goes through a pyrolysis process. Pyrolysis is the most mature thermochemical conversion technology. Pyrolysis refers to a chemical process in which biomass is decomposed into solids (char), liquids (oil), and gases (syngas) at relatively high temperatures (Quan et al., 2023).

There are many factors affecting the produced char, including heating time, temperature, residence time, and feedstock. Besides that, carbon materials from biomass have limitations in chemical composition and pore structure, limiting their CO_2 adsorption capacity, making modification crucial for CO2 capture. Therefore, chemical activation was applied to obtain activated carbon with better absorption properties. Alkaline activation, involving potassium hydroxide, sodium hydroxide, and amino acids, aids in carbon dioxide adsorption by forming pores and introducing alkaline groups (Quan et al., 2023).

In this study, the activated carbon was synthesized from sugar beet pulp through the pyrolysis process and chemically activated with 50% KOH solution at different ratios. Sugar beet pulp is a source of waste raw material that will be used. The adsorption capacity of the produced activated carbon was determined using a fixed bed column with a height of 45 cm, and an inner diameter of 8 mm using a pure carbon dioxide gas for adsorption and nitrogen gas to remove the impurities and open the pores at 100 ^oC for 1 hour before the process.

II. Experimental Set-up and Procedure

In this study, sugar beet pulp was used as a raw material, and activated carbons were produced by the chemical activation method of biomass with KOH. Sugar beet pulp waste was obtained from Eskişehir Sugar Factory, and potassium hydroxide (KOH) and hydrochloric acid (HCl) were obtained from Sigma-Aldrich.

Synthesis of activated carbon: sugar beet pulp was dried in an oven at 105 °C until it reached a constant weight and was ground. After the grinding process, sieve analysis was performed, and the average size was determined to be 506 µm. The impregnation with a saturated potassium hydroxide solution was carried out at room temperature for 24 hours. The biomass: KOH ratio was equal to 1:1 and 1:2. Then, it was dried at 105 °C for 24 h, and the chemically activated sugar beet pulp was carbonized at 700 °C for 1 h at a heating rate of 10 °C/min under a nitrogen flow of 200 mL/min. After carbonization, it was kept in a 1 M HCl solution for 1 hour and washed with distilled water until pH=7. The final product was dried in an oven at 105°C overnight. Figure 1 shows the steps of activated carbon synthesis.

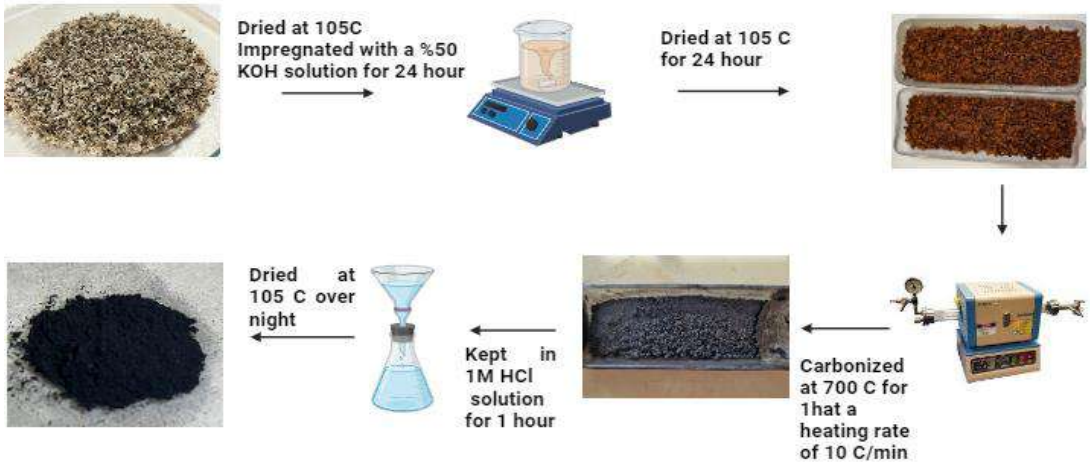


Fig. 1: Activated carbon synthesis steps.

III. Analysis

Characterization Techniques

The crystalline properties of activated carbons were examined with an XRD device (Rigaku Miniflex 600) operating at 40 kV voltage and 30 mA current. Cu-Kα radiation was used as the X-ray source. XRD analyses were performed with a scan angle of 15-85° at a scan angle of 0.02° and a scan speed of 4°/min.

The determination of functional groups of activated carbons was carried out with the FT-IR (Thermo Science Nicolet IS10) device. The analyses were carried out at 64 scanning speed and 4 cm^{-1} resolution, in the scanning range of 525 to 4000 cm^{-1}.

Carbon Dioxide Adsorption. Adsorption capacity tests were performed using a custom-designed fixed-bed stainless steel reactor system with a height of 45 cm, an inner diameter of 8 mm, and an outer diameter of 12 mm. The activated carbon sample was placed on the bed of the column and tightly capped. The device was connected to N_2 and CO_2 tubes. N_2 gas was used to remove the impurities and open the pores at 100 °C for 1 hour before the process. The reactor was then cooled to the CO_2 adsorption temperature. 99.9% purity CO_2 gas was used for adsorption capacity measurement and measurements were carried out for 90 minutes at 20 and 35°C. Desorption of the pores of the adsorbent was carried out with N_2 gas for 1 hour at 200 °C.

IV. Results and Discussions

Figure 2 demonstrates the FT-IR spectra of activated carbons. FTIR results show that the functional groups on the surface of activated carbons are similar. The bands in the range of 2360-2380 cm^{-1} are attributed to C-H stretching, which indicates the presence of the CH_2 –CO- group (Nagalakshmi et al., 2015). The peak at 2350 cm^{-1} and 1120 cm^{-1} can be attributed to the C–O stretching vibration. The bands around 3400-3500 cm^{-1} aise from –OH stretching in hydroxyl, carboxylic, and phenolic groups (Jahan and Feni, 2022).

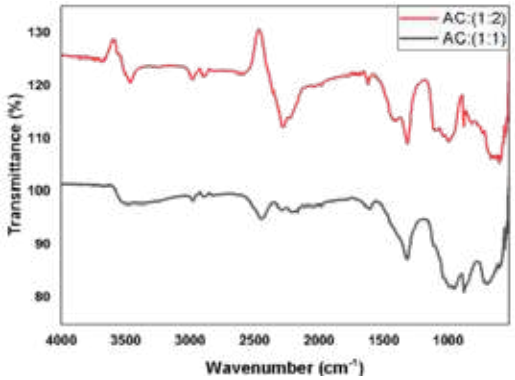


Fig. 2: FTIR spectra of activated carbons

The XRD analysis model of activated carbons in the range of 2θ=5°-85° is given in Figure 3. The XRD pattern of activated carbons exhibits distinct peaks at approximately 23° and 44° of the graphite crystallites of the carbon-based material, corresponding to the (002) and (100) planes, respectively. Broad diffraction peaks without a single significant sharp peak indicate the amorphous nature of activated carbon. However, the absence of extra peaks at AC (1:2) indicates the absence of other X-ray traceable compounds in the activated carbon sample (Kalyani and Anitha 2013). However, in the AC (1:1) sample, a diffraction peak is observed at approximately 27°, which is thought to be caused by the purification step.

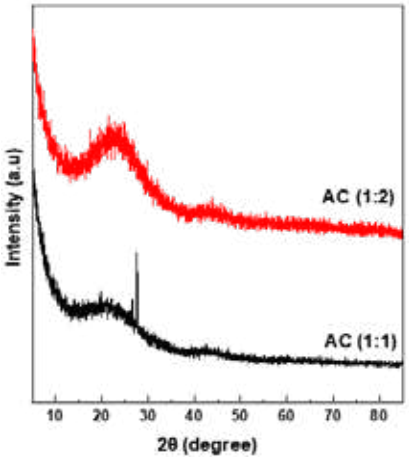


Fig. 3: XRD pattern of activated carbons

As shown in Figure 4, the adsorption capacity of CO_2 for AC (1:1) at 35 °C was 89.52 mg/g, and then at a lower temperature of 20 °C the capacity was increased to 141.32 mg/g. for AC (1:2) at 20 °C the adsorption capacity was 143.08 mg/g. Increasing the ratio of the alkaline will increase the adsorption capacity.

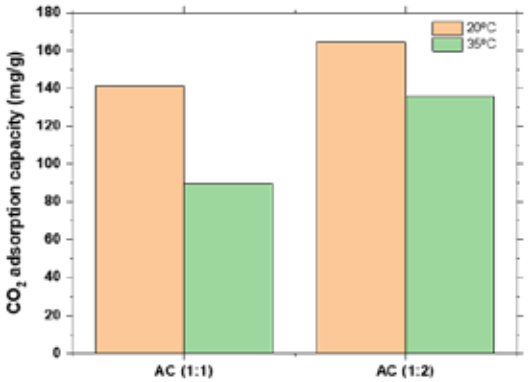


Fig. 4: Carbon dioxide adsorption capacities of activated carbons at 20 and 35 °C temperatures.

The adsorption capacity of CO_2 using different biomass sources for the synthesis of activated carbon was investigated in other studies. The results were found to be in the range of 30-100 mg/g. A study was done (Alhassan, 2018), using sugarcane bagasse; the obtained capacity was 48.5 mg/g at 1 bar and 25 °C. Another study done by (Sarwar, 2021), used corncob as a raw material for activated carbon, the obtained capacity was 149 mg/g at 1 bar and 25 °C. Compared with a study done by (Pu,

2021), the obtained capacity was 98.56 mg/g using the walnut shell as raw material, while (Al Mesfer, 2020) used the same raw material but at a lower temperature for the pyrolysis process, and the obtained capacity was 69,52 mg/g. The adsorption capacity of this study was higher than that of the obvious studies, as shown in Table 1.

Table 1. CO_2 adsorption capacity

Biomass	Activator	Impregnation ratio	Pyrolysis temperature (°C)	Adsorption capacity condition	CO_2 Adsorption Capacity (mg/g)
Sugar beet pulp	KOH	1:1	700	35°C, 90 min	89.52
				20°C, 90 min	141.32
		1:2		35°C, 90 min	135
				20°C, 90 min	164.59

V. Conclusions

In this work, the effect of activated carbon on CO_2 adsorption capacity was assessed after it was produced from sugar beet pulp using pyrolysis at 700 °C associated with KOH activation as a chemical treatment. The results showed that the CO_2 adsorption capacities of AC (1:2) had a better result, where at 20 and 35 °C the capacity measured as 164.59 and 135 mg/g, respectively. Further studies will include examining more parameters like, pyrolysis temperature, alkaline ratio, holding time, and heating rate, that will affect the activated CO_2 adsorption capacity. Additionally, a detailed micropore structure analysis and surface characterization of activated carbons will be carried out using the Brunauer-Emmett-Teller (BET) method.

Acknowledgment

This research was supported by the Scientific and Technological Research Council of Turkey (TÜBİTAK), project number 22AG034 – “Environmentally Compatible Sustainable Advanced Vehicle Technologies”.The authors would like to thank Kazım Taşkent Eskişehir Sugar Factory for providing the sugar beet pulp used in the study.

References

Al Mesfer, M. K., Synthesis and characterization of high-performance activated carbon from walnut shell biomass for CO2 capture. *Environmental Science and Pollution Research*, *27*(13), 15020-15028, (2020).

Jahan, M., & Feni, F., Environmentally Friendly Bifunctional Catalyst for ORR and OER from Coconut Shell Particles. Advances in Materials Physics and Chemistry, 12(5), 106-123, (2022).

Kalyani, P., Anitha, A., Refuse derived energy - tea derived boric acid activated carbon as an electrode material for electrochemical capacitors". Portugaliae Electrochimica Acta, 31(3), 165–174, (2013).

Mishra, S., & Upadhyay, R. K., Review on biomass gasification: Gasifiers, gasifying mediums, and operational parameters. Materials Science for Energy Technologies, 4, 329–340, (2021).

Nagalakshmi, T. V., Emmanuel, K. A., Suresh Babu, C., Chakrapani, C., & Divakar, P. P., Preparation of mesoporous activated carbon from jackfruit PPI-1 waste and development of different surface functional groups. Int. Lett. Chem. Phys. Astron, 54, 189-200, (2015).

Ogungbenro, A. E., Quang, D. V., Al-Ali, K. A., Vega, L. F., & Abu-Zahra, M. R., Synthesis and characterization of activated carbon from biomass date seeds for carbon dioxide adsorption. *Journal of Environmental Chemical Engineering*, *8*(5), 104257, (2020).

Pu, Q., Zou, J., Wang, J., Lu, S., Ning, P., Huang, L., & Wang, Q., Systematic study of dynamic CO2 adsorption on activated carbons derived from different biomass. *Journal of Alloys and Compounds*, *887*, 161406, (2021).

Quan, C., Zhou, Y., Wang, J., Wu, C., & Gao, N., Biomass-based carbon materials for CO2 capture: A review. Journal of CO2 Utilization, 68, 102373, (2023).

Sarwar, A., Ali, M., Khoja, A. H., Nawar, A., Waqas, A., Liaquat, R., ... & Asjid, M., Synthesis and characterization of biomass-derived surface-modified activated carbon for enhanced CO2 adsorption. *Journal of CO2 Utilization*, *46*, 101476, (2021).

Performance of nanometric Ti/TiN bilayer cathodic arc evaporated coating on 304SS as bipolar plate for PEMFC

[1*]Enis Furkan Uçar, [1]Erkut YILMAZ, [2]Özden Kisacik
[1]Turkish Energy Nuclear and Mineral Research Agency – Clean Energy Research Institute, Ankara Türkiye
[2] Turkish Energy Nuclear and Mineral Research Agency – Boron Research Institute, Ankara Türkiye

* E-mail: enisfurkan.ucar@tenmak.gov.tr

Abstract
Current research mainly focuses on surface properties, corrosion resistance, surface morphology and surface hydrophobicity of nanometric scale thinfilm titanium/titanium nitride (Ti/TiN) bilayer coating deposited on 304 stainless steel via cathodic arc evaporation (CAE) technique for using both proton exchange membrane fuel cell (PEMFC) and anion exchange membrane fuel cell (AEMFC) bipolar plate (BPP) application. The microstructure, crystal pahse, and hydrophobicity of coated BPPs is characterised by scanning electron microscopy (SEM), X-Ray diffraction and contact angle examinations. The corrosion resistance performance of coated BPPs is investigated by electrochemical corrosion test including potentiodynamic polarisation test at ambient temperature condition and PEMFC resembling corrosion media. Electrochemical test results reveal that as the coating pressure increase corrosion resistance of thinfilms slightly increase as well, this due less macro particle occurance. Micro ampere magnitude corrosion current values are applicable in the PEMFC technology. Hence Ti/TiN bilayer coatings investigated in this work has promising candidate as BPP material and is potentially suitable alternative to replace other types of BPPs such as graphite in PEMFC.

Keywords: PEM fuel cell, Bipolar plates, Cathodic Arc Evaporation, Corrosion resistance, Contact angle.

I. Introduction
PEMFC is the state-of-the-art technology that converts chemical energy into electricity from an electrochemical reaction between hydrogen and oxygen to serve as a power source in portable applications such as cars, as it offers high power output, fast startup and shutdown cycles, and low operating temperature without harmful byproducts [1,2]. Given the low power of a single PEM cell, it is imperative to connect the single cells in series using BPPs to increase the overall efficiency. BPPs, as one of the most important parts of a PEMFC stack, play a key role, such as transferring the electric current to the external circuit, separating the anode and cathode reactant gases, and connecting the single cells in series. Since the BPPs account for about 45% of the total cost of the stack, it is essential from an economic point of view to develop cost-effective and lightweight BPP materials. The BPP materials have to fulfil some requirements, e.g. high chemical stability, low corrosion rate and good electrical conductivity in the PEMFC environment. The first generation of BPPs was made of graphite due to its light weight, high electrical conductivity, excellent corrosion resistance and high chemical stability [3]. However, due to its inherent brittleness and poor machinability, the manufacturing cost of graphite BPPs with designed flow field channels is high. For the above reasons, new generation metallic BPPs have attracted much attention in recent years as they offer the following advantageshigh machinability and ease of manufacture, low weight, low production cost, high mechanical strength and desirable electrical and thermal conductivity, making them ideal alternatives to graphiteBPP [4]. So far, various metallic materials have been used as BPPs, such as titanium, aluminum, nickel and copper alloys and stainless steels. Among them, austenitic stainless steel has superior advantages such as low cost, high corrosion resistance and good electrical conductivity [5]. In the following research, regarding the high corrosion resistance of titanium and facile procedure of TiN deposition via cathodic arc evaporation technique, a nanometeric Ti/TiN multi-layer coating was deposited on 304SS. Different structural and compositional examinations were carried out on the Ti/TiN coated 304SS specimens.

II. Experimental Set-up and Procedure
2.1.BPP sample preparation:
A commercial AISI 304SS was used as substrate. The metal sheet was cut to 30x30x0.5mm prism specimens. After that step by step surface grinding procedure followed starting from 400# to 800# and 1200# grit papers. Finally polished by 0.5µm diamond polishing paste. The specimens were then ultrasonically cleaned in acetone, isopropyl alcohol and distilled water for five minutes respectively. After ultrasonic cleaning, specimens have dried by pressurised air. The specimens were attached to metallic wire net and placed right against the Titanium (Ti) target approximately 10 cm away from target seating. PVD coating procedure was conducted via a cathodic arc evaporation system with $4x10^{-4}$Pa base pressure for each coating procedure.

2.2. PVD process: Cathodic arc exaporation system (ONCEL Arc-PVD) and a titanium target (99.5% purity) disc with thickness of 20mm and diameter of 100mm were configure in target seat inside of chamber with radius and height of 600mm and 500mm respectively, to deposit Titanium and Titanium nitride films over the 304ss samples. Prior to vapor deposition a pre sputter cleaning process with DC bias voltage of -1000V was employed for 15min in order to remove surface contaminants and oxide layer of substrate. Overcome possible mismatch between 304SS and TiN thinfilms, Ti interlayer thinfilm coated for each substrate. Table 1 shows the operating parameters of coating procedure. Fig 1 shows the coating process.

Table 1. Coating parameters

	Base Pr (Pa)	Coating Pr (Pa)	Gas composition	Target substrate distance (cm)	Target applied power (W)	Substrate temperature (°C)	Substrate Bias (V)	Coating Time (min)
Ti Interlayer	$5{,}9x10^{-4}$	1	%100 Ar	10	1600W (80A 20V)	100	-150	5
A (TiN)	$5x10^{-4}$	0.5	%100 N_2	10	1600W (80A 20V)	100	-150	15
B (TiN)	$5{,}2x10^{-4}$	1	%100 N_2	10	1600W (80A 20V)	100	-150	15
C (TiN)	$4{,}9x10^{-4}$	1.5	%100 Ar	10	1600W (80A 20V)	100	-150	15



Fig. 1: Section of coating procedure.

III. Analysis

3.1. Surface Characterization: The surface wettability of the unocated substrate, Ti interlayer coated substrate and different coating pressure TiN specimens was studied by measuring the contact angle (σ) between the surface of specimen and 4 µl water droplet at ambient temperature, atmospheric pressure and relative humidity at about %44. Sessile drop method was used for static contact angle measurement of the droplets by constant camera recording of water droplet and angle calculating software with the help of captured pictures by camera The contact angles were acquired based on the measurement at three different locations on each specimen and the average values were obrtained with standart deviation of ±3°. Measurement set up shown in fig 2b.

3.2. Corrosion measurements: Potentiodynamic polarisation tests were carried out in three electrode cell configuration. Platinum wire as counter electrode, saturated calomel electrode (SCE) as reference electrode and Ti/TiN coated 30SS samles as working electrode. Cell composition can be seen in fig 2a. Prior to polarisatiin test, samples were cathodically polarized to -1V versusOCP for 10min to remove oxide layer and subsequently were stabilized at OCP for 30min to potentially reach steady state.Then, the potential was swept from -0.25V to 0.3V at $0.001Vs^{-1}$ scan rate. 0.5M H2SO4 with 2ppm HF solution at room temperature was used in order to simulate PEMFC inner media conditions. Measurement results analysed by palmsens software.

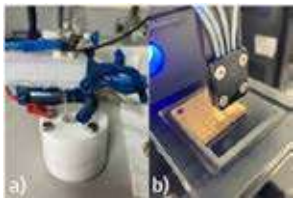


Fig. 2: a)Corrosion resistant measurement cell configuration b)Contact angle measurement setup.

3.4 Scanning Electron Microscopy

For thinfilm morphological properties SEM images have acquired. Macro particle size and macro particle amound over the film surface has determined by SEM imaging process. From 1000 times to 50000 times Different magnification SEM images acquired during the characterisation.

IV. Results and discussions

X-Ray diffraction pattern for the Ti interlayer and Ti/TiN bilayer coated 304SS is shown in Fig4 Due to low thickness of both Ti and TiN thin films peak designated to 304SS and Ti(011) peaks can be seen for Ti thinfilm and Ti/TiN thinfilm XRD spectra respectively.

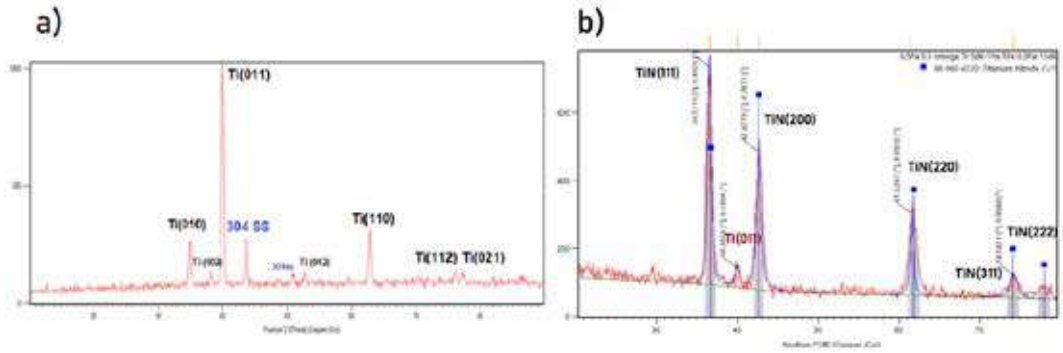


Fig. 4: X-Ray diffraction pattern for a) Ti interlayer and b) Ti/TiN bi layer thinfilms.

From Fig 5, Top SEM images shows that both macro particle size and amount decrese as the TiN coating N_2 pressure increases. This phenomenon most likely occurs due to aggressive increase in sputtering rate. The relationship between Mean particle size and particle amout changing with coating pressure is given in fig 6.

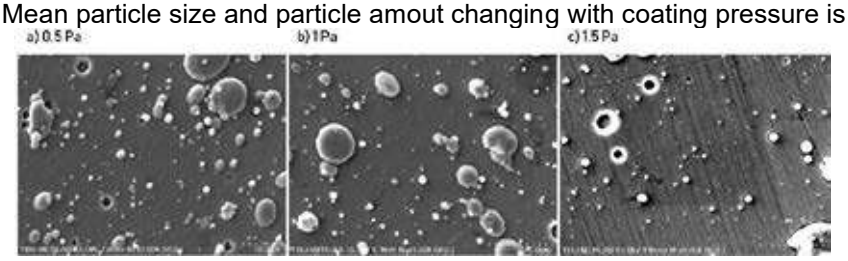


Fig. 5: Topographical SEM images of different TiN thinfilms in relation with coating pressure.

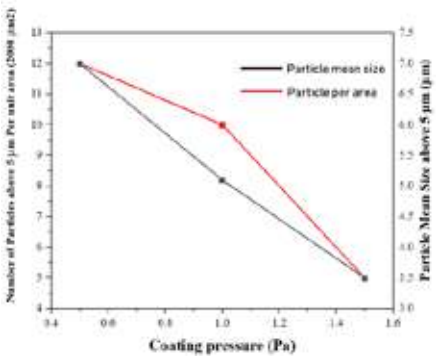


Fig. 6: relationship between Mean particle size and particle amout changing with coating pressure.

The performance of PEMFC is significantly influenced by wettability properties of its components. Hydrophobic behaviour for components such as GDL and BPPs has to be implemented in order to overcome flooding phenomenon. Figure 7 depict water contact angles dripping 4 µl water droplets for the 304SS, Ti interlayer and different coating N_2 pressure TiN thinfilms. All the coating configurations have enganced hydrophobicity when compared to uncoated 304SS, however, TiN thinfilm demonstrate better hydrophobicity than Ti interlayer, furthermore as the coating pressure increases hydrophobicity of TiN film increases as well which makes it more suitable for PEMFC usage.

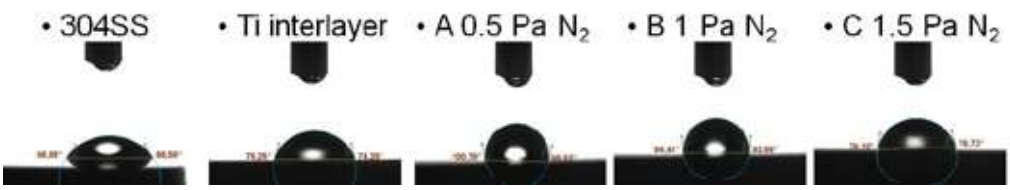


Fig. 7: Water contact angles images of the samples.

Corrosion behaviour of different N2 pressure coated TiN thinfilms is given in fig 8. Corrosion potential and corrosion current values are -0.159V and 2,36 µA, -0.191V and 2.30 µA, -0.168V and 1.317 µA for 0.5Pa TiN, 1 Pa TiN and 1.5Pa TiN thinfilms respectively.

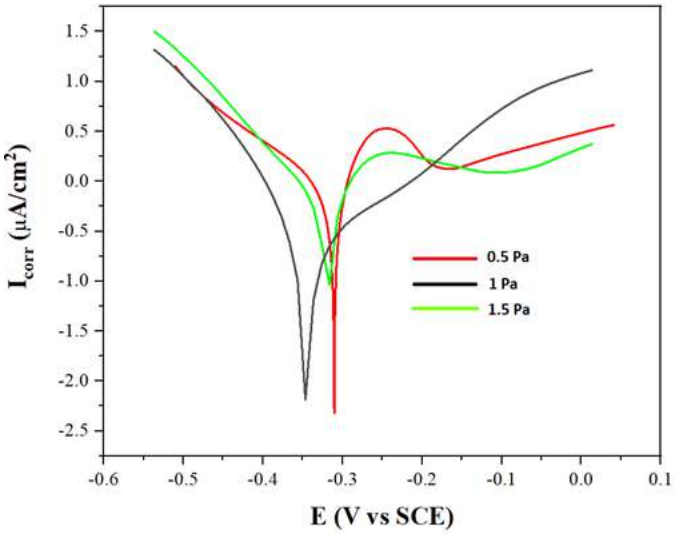


Fig. 8: Potentiodynamic polarisation behaviour of different N_2 coating pressure samples.

V. Conclusions

The findings from morphology of TiN thinfilms coated by different pressure N_2 with CAE reveals an increase in coating non-uniformity as an decrease in the N_2 flow rate. Corrosion current for all the tihnfilms are at the micro ampere levels however as the coating pressure increase, thinfilm macro particle occurance is decreases, therefore corrosion current decreases as the coating pressure increases.

References

[1] Y. Wang, S. Zhang, Z. Lu, L. Wang, W. Li, Corros. Sci. 142 (2018) 24
[2] F. Dundar, E. Dur, S. Mahabunphachai, M. Koç, J. Power Sources 195 (2010) 3546–3
[3] S. Shimpalee, V. Lilavivat, H. McCrabb, Y. Khunatorn, H.K. Lee, W.K. Lee, J. W. Weidner, Int. J. Hydrogen Energy 41 (2016) 13688–13
[4] W. Yoon, X. Huang, P. Fazzino, K.L. Reifsnider, M.A. Akkaoui, J. Power Sources 179 (2008) 265
[5] H. Rashtchi, K. Raeissi, M. Shamanian, Y. Acevedo Gomez, C. Lagergren, R. Wreland Lindstrom, € V. Rajaei, Fuel Cells 16 (2016) 784–

Analysis and assessment of a biomass-based cogeneration system with hydrogen-fueled gas turbine

Fatih Sorgulu[1*] and Ibrahim Dincer[2,1]
[1]Faculty of Mechanical Engineering, Yildiz Technical University, Besiktas, Istanbul, Türkiye
[2]Faculty of Engineering and Applied Science, Ontario Tech. University, Oshawa, Ontario, Canada

[*]e-mail: fatihs@yildiz.edu.tr

Abstract
In this study, an assessment of a commercially available hydrogen-fueled gas turbine which is newly developed and released on the market is performed. The hydrogen required for the gas turbine is produced by a hybrid sulfur-bromine cycle by providing heat with a biomass-based incineration unit. Electricity and heating requirements of the community are supplied by the cogeneration unit. The system is entirely analyzed in terms of energy and exergy. Parametric studies are conducted to assess system performances. The waste heat is minimized by integrating subsystems. A gas turbine which is up to 100% hydrogen capability with a power of 45 MW is considered. The overall energy and exergy efficiencies of the integrated system are obtained as 65.7% and 52.3%, respectively.

Keywords: Energy, Exergy, Hydrogen, Thermochemical cycle

I. Introduction

For a sustainable ecosystem, new fuels and novel systems must be integrated. Environmentally friendly integrated systems are needed to meet the increasing demand for energy due to population growth and changing lifestyles. Not only population but also environmental concerns increase. Many countries prepared their renewable energy and hydrogen-based roadmaps for a sustainable future. However, energy reliability and waste minimization should be provided by integrating energy storage subsystems. Integrated systems are more important than ever for sustainability in the energy, economic, and environmental impact. Numerous studies were conducted on hydrogen and natural gas blend, eventually, novel gas turbines and boilers were developed to run on 100% hydrogen. In this study, electricity and heating are provided to the community in an environmentally benign way. To reach higher efficiencies, subsystems are integrated by minimizing waste, and a clean renewable energy-based hydrogen energy system is aimed. Finally, a novel gas turbine with 100% hydrogen capability is analyzed.

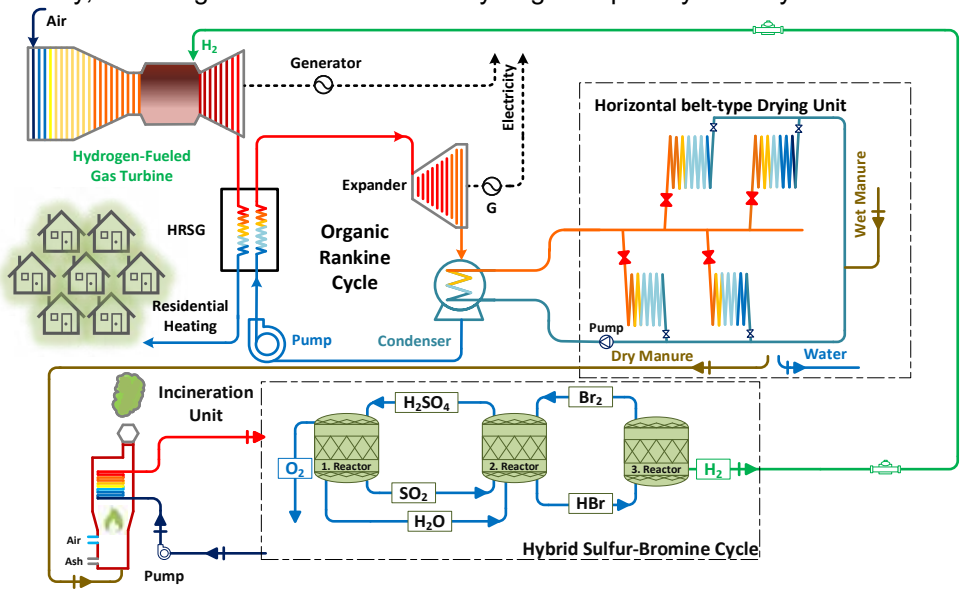


Fig. 1: Schematic illustration of the cogeneration system

II. System Description

As shown in Fig. 1, a hydrogen-fueled gas turbine, an organic Rankine cycle, a thermochemical cycle, a drying unit, and a biomass-based incineration unit are integrated for electricity and heating. Chicken manure is dried in a drying subsystem and supplied to the incineration unit. In order to produce hydrogen, heat is provided by the waste incinerator to the thermochemical cycle which is considered the hybrid sulfur-bromine cycle. GE Vernova 6B [1] gas turbine which is up to 100% hydrogen capability and with a capacity of 45 MW is considered for the cogeneration unit and integrated with the organic Rankine cycle. Hexamethyldisiloxane is used as a working fluid in the organic Rankine cycle.

III. Analysis and Assessment

The Aspen Plus software [2] is used for the three-step hybrid sulfur-bromine cycle which has a maximum temperature of 850 °C. Engineering Equation Solver (EES) [3] is employed for the calculations and parametric

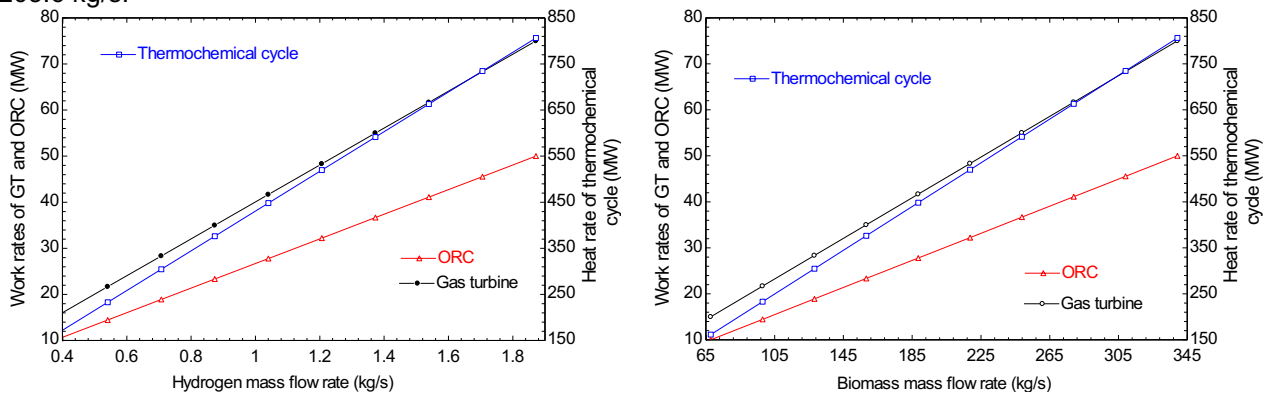
studies of the entire system. The overall energy and exergy efficiencies of the integrated system can be defined as follows:

$$\eta_{en,ov} = \frac{\dot{W}_{net} + \dot{Q}_H}{\dot{m}_{biom} \times LHV_{biom}} \text{ and } \eta_{ex,ov} = \frac{\dot{W}_{net} + \dot{E}x_{Q_H}}{\dot{m}_{biom} \times ex_{biom}} \quad (1)$$

Here, the waste heat of the organic Rankine cycle and hydrogen produced in the thermochemical cycle are utilized within the system. Thus, they are not considered in overall efficiencies. The net power provided by the cogeneration unit is the sum of the net power rates of the gas turbine and the organic Rankine cycle.

IV. Results and Discussion

The presently developed integrated system is analyzed and assessed in terms of Thermodynamics. As shown in Fig. 2, parametric studies are conducted to observe the effect of the changes in gas turbine and organic Rankine cycle work rates and thermochemical cycle heat rates as to various hydrogen and biomass mass flow rates. Here, the hydrogen requirement of the 45 MW hydrogen-fueled gas turbine is calculated as 1.123 kg/s. The wet manure mass flow rate supplied to the waste incinerator for the heat requirement of the thermochemical cycle is calculated as 203.6 kg/s.



(a) (b)

Fig. 2: Changes in work and heat rates as to (a) hydrogen and (b) biomass amount

V. Conclusions

The electricity and heating needs of the community are met with the novel gas turbine-based integrated system in an environmentally friendly manner. CO_2 emissions, due to natural gas usage, are removed by fueling gas turbines with 100% hydrogen. The energetic and exergetic efficiencies of the thermochemical cycle are calculated as 27.85 and 31.63%, respectively. The hydrogen required for the gas turbine with 45 MW output is calculated as 1.123 kg/s (daily 1.17M m^3). The overall energy and exergy efficiencies of the integrated system are found as 65.7% and 52.3%, respectively.

References

GE Vernova 6B Gas Turbine. Accessed at: https://www.gevernova.com/gas-power/products/gas-turbines/6b. [Accessed on: 20/04/2024].

ASPEN PLUS® User Guide. Accessed at: https://www.aspentech.com/en/products/engineering/aspen-plus. [Accessed on: 20/04/2024].

EES. Engineering Equation Solver Manual. Accessed at: www.fchart.com. [Accessed on: 20/04/2024].

Current Sharing and Voltage Regulation Based on Dynamic Consensus Algorithm in PV-Fuel Cell-Battery Sourced DC Microgrid

[1*]İlhami Poyraz, [1]M. Emin Asker
[1,2]Dicle University, Department of Electric Power and Energy System, Diyarbakır, 21280, Türkiye.

[1*]E-mail:ilhami.poyraz@dicle.edu.tr

Abstract

This study endeavors to achieve current sharing and voltage regulation within a distributed DC microgrid system. The system is modeled in the Matlab/Simulink environment and comprises a microgrid facility integrated with PV (photovoltaic system), fuel cell, and battery, interconnected with three parallel-connected buck-type DC-DC converters. The objective is to implement a dynamic consensus algorithm with low communication bandwidth to facilitate current sharing and voltage regulation.

Keywords: DC microgrid, dynamic consensus algorithm, fuel, current sharing

I.Introduction

In the realm of DC microgrids, achieving optimal current sharing and voltage regulation is crucial. Research has proposed innovative strategies to address these challenges. One approach involves a data-driven secondary control strategy that integrates the physical relationship between voltage and current, enhancing output quality and system robustness [1]. Another study introduces a decentralized demand response method with a DC boost converter to optimize droop coefficients, enhancing voltage stability and minimizing power loss [2]. Additionally, a hybrid control strategy for a hybrid energy storage system (HESS) in isolated DC microgrids has been developed, utilizing a rate limiter and prediction-based current control to improve power sharing and system performance [3]. These advancements showcase the ongoing efforts to enhance current sharing and voltage regulation in DC microgrid systems.

Increasing popularity of direct current (DC) microgrids compared to alternating current (AC) grid systems is attributed to their higher efficiency, reliability, and ease of integration with renewable sources. With the increasing utilization of renewable energy sources, DC microgrids are making energy generation, transmission, and distribution more efficient and flexible.

In systems where photovoltaic (PV) systems and fuel cells are used together in DC networks, they play a significant role in clean and renewable energy production. These systems generate electricity by utilizing natural sources such as sunlight or hydrogen. Photovoltaic systems convert sunlight directly into electricity by means of photovoltaic cells on solar panels, producing an electric current when exposed to sunlight. These systems are widely used, particularly in regions with abundant sunlight, in applications such as rooftop installations and commercial facilities.

On the other hand, fuel cells produce electricity through chemical reactions. By utilizing hydrogen and oxygen gases, they generate electricity while producing by-products such as water and heat. Fuel cells offer advantages such as high energy density and continuous energy supply. When these two technologies are used together in DC networks, they provide diversity in energy production and enhance energy security. Moreover, they can support continuous energy production even during different weather conditions and times when sunlight is not available. Thus, by increasing the sustainability and stability of energy systems, they contribute to reducing carbon emissions. Therefore, systems where photovoltaic systems and fuel cells are used together in DC networks can hold a significant position in the future of the energy sector. However, for these systems to operate effectively, critical issues such as current sharing among distributed generation units and voltage regulation need to be addressed.

II. Dynamic consensus algorithms

Dynamic consensus algorithms are a type of algorithm where multiple agents or devices interact to achieve a common goal or state. These algorithms are guided by a specific protocol or set of rules that enable agents to behave appropriately according to the goal or state.

Dynamic consensus algorithms used in DC microgrids are typically employed to manage system behaviors such as current sharing, voltage regulation, and frequency control. These algorithms can be used in a system where each component (e.g., photovoltaic systems, batteries, loads) has its own local control system, and these local control systems communicate with each other to optimize the system.

Dynamic consensus algorithms are commonly used in distributed systems where agents communicate with each other to achieve a common goal or state. These algorithms facilitate information exchange among agents to

coordinate their behaviors and reach the desired goal when the sum of the agents converges towards a specific goal or state.

The use of dynamic consensus algorithms in DC microgrids can enhance system efficiency, reduce energy imbalances, and ensure system stability. Given the distributed nature and complexity of interactive components, the use of these algorithms can assist in the more reliable and efficient operation of DC microgrids.

The effects of the dynamic consensus algorithm on current sharing and voltage regulation in PV-fuel cell-battery sourced DC microgrids have been thoroughly investigated. Data obtained from simulations indicate a significant improvement in system performance attributable to the algorithm, and its effects on system performance have been evaluated under various scenarios.

The data obtained from simulation studies using this algorithm demonstrate its capability to facilitate rapid and effective current sharing and voltage regulation among distributed generation units in DC microgrid systems. An illustrative example of a DC microgrid powered by photovoltaic (PV)-fuel cell-battery sources is presented Fig. 1.

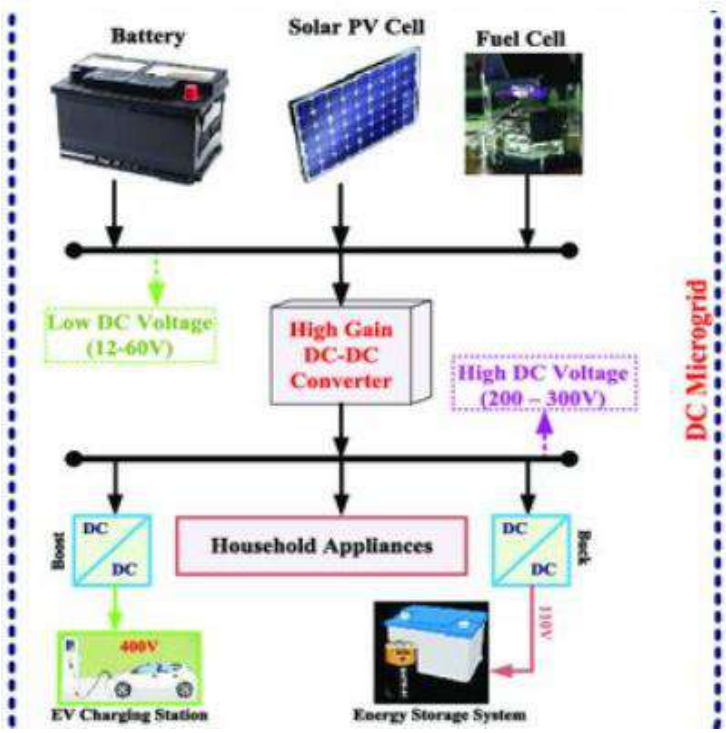


Fig. 1: DC microgrid powered by photovoltaic (PV)-fuel cell-battery sources

III.Conclusion

In this study, a distributed DC microgrid system was successfully modeled and simulated in the Matlab/Simulink environment. The system integrates a photovoltaic (PV) system, a fuel cell, and a battery, interconnected through three parallel-connected buck-type DC-DC converters. The primary objective was to achieve effective current sharing and voltage regulation using a dynamic consensus algorithm with low communication bandwidth. The simulation results demonstrated that the dynamic consensus algorithm effectively facilitated current sharing among the parallel converters while maintaining the desired voltage regulation across the microgrid. The low communication bandwidth requirement of the algorithm ensures minimal overhead and enhances the system's scalability and reliability.

References:

Yu, Yi, et al. "Distributed data-driven secondary regulation for the conflict between voltage recovery and accurate current sharing in DC microgrids." IEEE Transactions on Power Electronics (2023).

Vo-Van, Thanh., Wencong, Su. (2023). Improving Current Sharing and Voltage Regulation for DC Microgrids: A Decentralized Demand Response Approach. IEEE Transactions on Smart Grid, doi: 10.1109/TSG.2022.3222220

Arunkumar, Chirayarukil, Raveendran., Udaya, Bhasker, Manthati. (2023). Dynamic Power Sharing Assisted Hybrid Controller for PV Fed Isolated dc Microgrid. IEEE Systems Journal, doi: 10.1109/JSYST.2022.3195812

(2022). A Unified Distributed Secondary Controller using a Dynamic Consensus Algorithm in DC Microgrids. doi: 10.1109/isgtasia54193.2022.10003502

Vigneysh, Thangavel., Narayan, Krishnan., Natarajan, Prabaharan. (2023). DC Link Voltage Enhancement in DC Microgrid Using PV Based High Gain Converter with Cascaded Fuzzy Logic Controller. Energies, doi: 10.3390/en16093928

Enhanced Performance Prediction for Proton Exchange Membrane Fuel Cells Using Long-Short Time Memory Networks

[1]Masud Kabir and [1*]Sami Ekici
[1] Fırat University, Faculty of Technology, Department of Energy Systems Engineering, Elazığ, 23200, Türkiye

* E-mail: sekici@firat.eu.tr

Abstract
In this study, the Online System Identification (OSI) method has been tested for Proton Exchange Membrane Fuel Cells (PEMFCs) using a publicly available experimental dataset. The dataset contains two different load profiles: the first one utilized a ramp-up current profile to assess the general algorithm performance, while the second profile represented urban driving behavior through an urban dynamometer driving schedule, reflecting real conditions that may occur to a FC system in a vehicle. The dataset comprises the current profile of the PEMFC system, along with the recorded temperature variations resulting from the operation of both the current and the cooling fan, as well as the measured voltage values. The measured current and temperature values were utilized as inputs to the Long Short-Term Memory (LSTM) model, and the voltage values were predicted accordingly. The results demonstrated that the LSTM model successfully estimated PEMFC voltage in both scenarios. This study highlights the promising potential of OSI techniques and LSTM models in understanding and optimizing the performance of PEMFC systems under real-world conditions.

Keywords: Online system identification, proton exchange membrane fuel cells, LSTM networks, voltage estimation.

I. Introduction

Proton Exchange Membrane Fuel Cells (PEMFCs) have garnered significant attention as a promising clean energy technology with applications in power generation and transportation [1], [2] [3]. Accurately monitoring and predicting the performance of PEMFC systems is a critical challenge, as it directly impacts their stable and efficient operation. The combination of PEMFCs and auxiliary equipment is highly complex. In the operation of proton exchange membrane fuel cells, the real-time performance analysis and prediction of the electrolyte member conditions, fuel cell voltage, and current are of great significance for the stable and efficient operation of PEMFC [3]. Traditionally, the operation status of PEMFC is monitored by the water content of the electrolyte membrane [4]. The fuel cell voltage can be obtained by the polarization curve of the single cell. The current and stack output voltage of the entire system can be monitored. In the multi-parameter condition monitoring of proton exchange membrane fuel cells, these conditions are generally either estimated by experienced engineers based on physical models or predicted by relying on the electrochemical characteristics and external parameters of fuel cells. With the improvement of the performance requirements of proton exchange membrane fuel cells, the inherent limitations of conventional monitoring methods have emerged. The monitoring results are greatly affected by the influences of artificial expertise, experimental conditions, and manufacturing process parameters.

The present study investigates the use of an OSI method, specifically leveraging a LSTM model [5], to forecast the voltage output of a PEMFC system. A publicly available experimental dataset from a recent study that contained two distinct load profiles: a ramp-up current profile to assess the general algorithm performance, and an urban driving behavior profile that reflected real-world conditions a PEMFC system may encounter in a vehicle application were utitized [6]. The measured current and temperature values from the dataset were employed as inputs to the LSTM model, which was then tasked with predicting the corresponding voltage values.

The results demonstrate that the LSTM model successfully estimated the PEMFC voltage in both scenarios, highlighting the promising potential of OSI techniques and LSTM models in understanding and optimizing the performance of PEMFC systems under real-world conditions. This study contributes to the ongoing efforts to develop reliable and efficient PEMFC monitoring and control strategies, which are crucial for the widespread adoption of this clean energy technology.

II. Dataset and Procedure

This study is based on a publicly available PEMFC dataset obtained using a Horizon H-500 PEMFC setup [6]. The experimental setup involves an open-cathode type PEMFC, equipped with several features such as air cooling and self-humidification. The system is equipped with a variety of valves and sensors, and it is controlled using a National Instrument CompactRIO. This real-time controller is utilized to regulate the flow rates and temperatures of fluids within the system. During the experiment, the current, temperature, and voltage of the PEMFC stack are recorded every 100 ms. These data are used to update the model and facilitate monitoring of the experiment's progress. In the reference study [6], the health state of the installed PEMFC stack was assessed using polarization and power curves. Experimental polarization curves were obtained by applying fixed currents to the PEMFC and recording the corresponding output voltages. The PEMFC's voltage response was observed and recorded as the current level gradually increased. It's worth noting that in this study, the voltage required for polarization and power curve estimation was successfully predicted using the measured current and temperature, highlighting the effectiveness

of the proposed methods. The experimental setup utilized in the study to test the OSI method is depicted in Fig. 1. while, Tab. 1 provides the detailed specifications of the Horizon H-500 PEMFC [6].

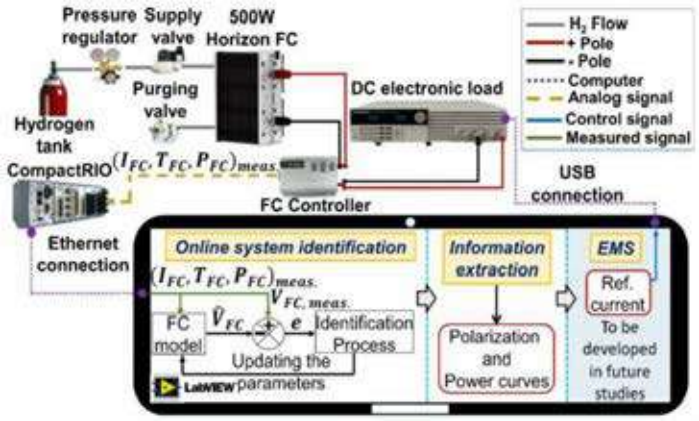


Fig. 1: Experimental Setup Utilized for OSI Method Testing.

Tab. 1: Specifications of the Horizon H-500 PEMFC.

PEMFC Technical Data	
Number of cells	*36*
Max current (shutdown)	*29 A*
Hydrogen pressure	*0.5-0.6 bar*
Cathode pressure	*1 bar*
Ambient temperature	*5 to 30 ºC*
Max stack temperature	*65 ºC*
Hydrogen purity	*99.999% dry H_2*
Size	*130 x 220 x 122 mm*
Cooling	*Air (integrated cooling fan)*

The utilized dataset comprises 11.751 experimental measurements for the first load profile and 6.231 for the second. The dataset was divided into 80% for training and the remaining 20% for testing. To achieve optimal performance, a grid search was performed during LSTM training. The grid search involved varying the following hyperparameters: hidden unit values ranged from 100 to 300, learning rate ranged from 0.0001 to 0.01, and epoch values ranged from 1000 to 2000. Through this search, the most suitable hyperparameters were determined to be 300 hidden units, a learning rate of 0.01, and 2000 epochs.

III. LSTM-based PEMFC Voltage Estimation

Due to the uncertainty of the multiplicative and partly understood physical-chemical-energy conversion methods for PEMFC stacks, the FC system performance cannot be measured directly [1], [7]. Hence, the obtained output performance, mainly including the current-voltage (I-V) and power curve, and state-of-the-art experimental methods remain the most commonly used PEMFC performance prediction methods. The existing studies on the PEMFC performance prediction models can be broadly divided into the following two categories [8]. Data-driven models are characterized by empirical methods that are built on experimental data measured in a particular working environment [7]. Compared to the understanding-based models, these models have stronger predictive abilities in the presence of random errors. The existing common data-driven methods include artificial neural networks (ANNs), support vector regression (SVM), random forest algorithms [9] and Kalman filters (KF) [10]. Nonetheless, there are shortcomings such as decreased prediction accuracy caused by local optima and overlearning. Despite the above-described problems, the existing studies have demonstrated a conventional advantage of LSTM, which is its strong learning ability when processing time series data. Thus, the LSTM might be an ideal alternative for the performance prediction model of PEMFC stacks.

In Fig. 2, the measured current and temperature values for the first load profile, along with the obtained PEMFC voltage prediction results, residual plot, and histogram, are depicted. Fig. 3 illustrates the test results for the second load profile. The Root Mean Squared Error (RMSE) for the first load profile is calculated as 0.3252, while for the second load profile, it is determined as 0.2566. Additionally, Fig. 4 presents regression curves for the test results of both loads. The correlation coefficient (R) is found to be 0.996 for the first load profile and 0.979 for the second load profile. These findings demonstrate the effectiveness of the proposed LSTM model and its robust alternative to traditional methods for online PEMFC parameter estimation.

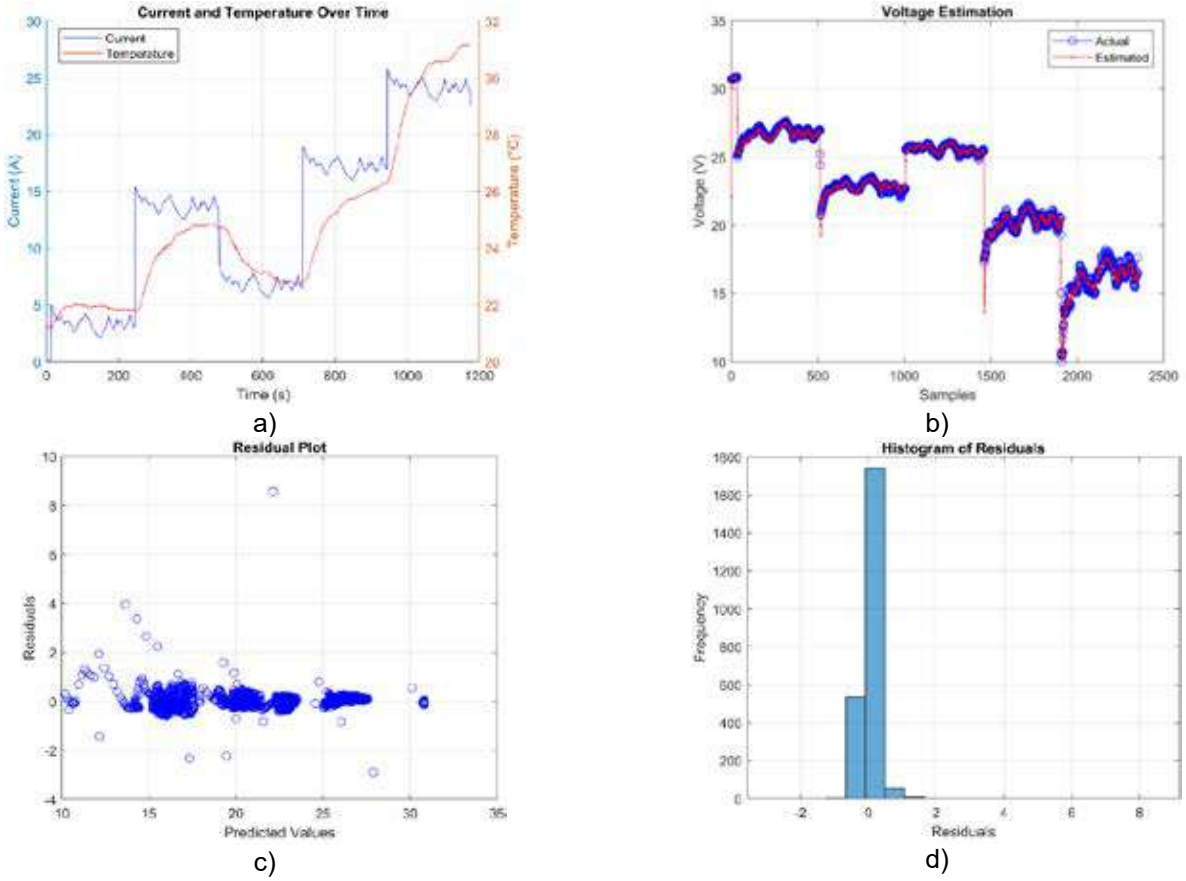


Fig. 2: LSTM-based PEMFC voltage estimation for the first load profile, a) PEMFC current and the measured temperature, b) voltage estimation by LSTM, c) residual plot for testing results d) histogram of residuals.

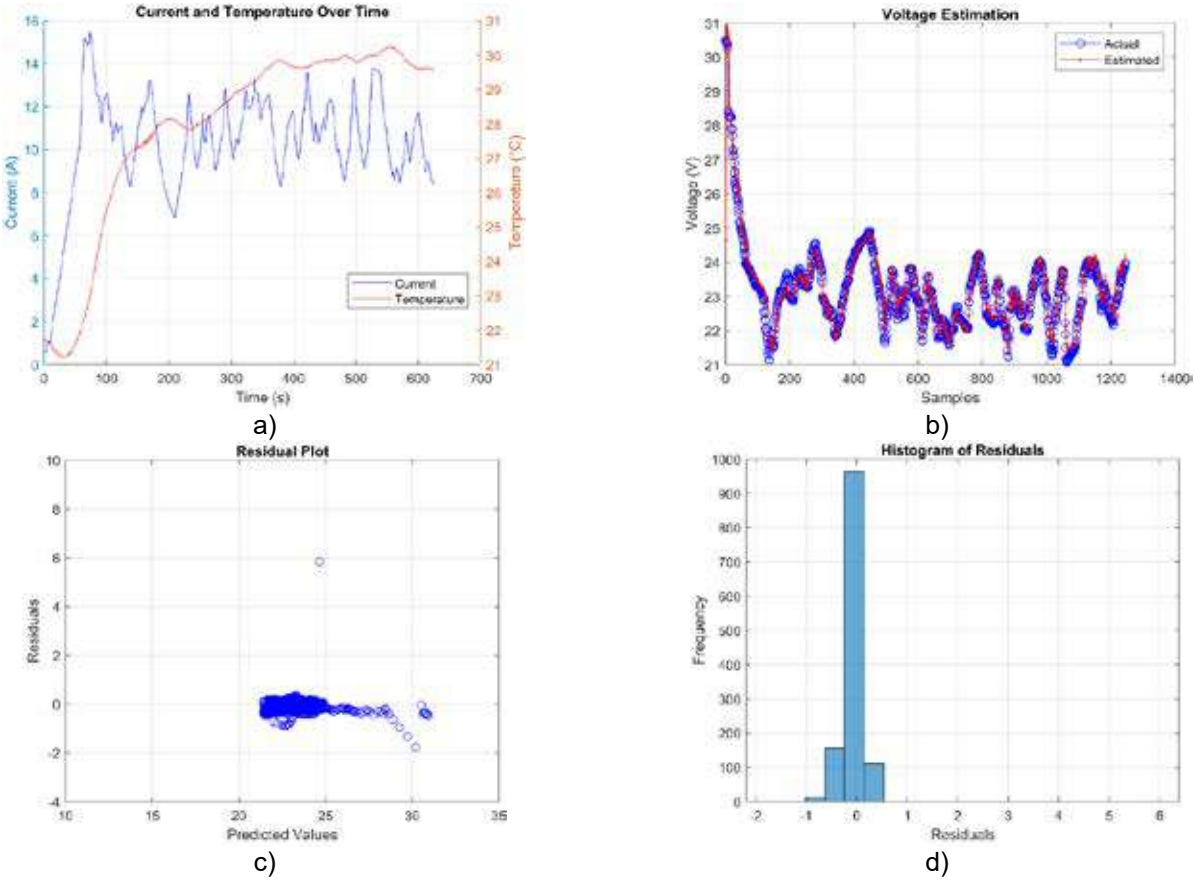


Fig. 3: LSTM-based PEMFC voltage estimation for the second load profile, a) PEMFC current and the measured temperature, b) voltage estimation by LSTM, c) residual plot for testing results d) histogram of residuals.

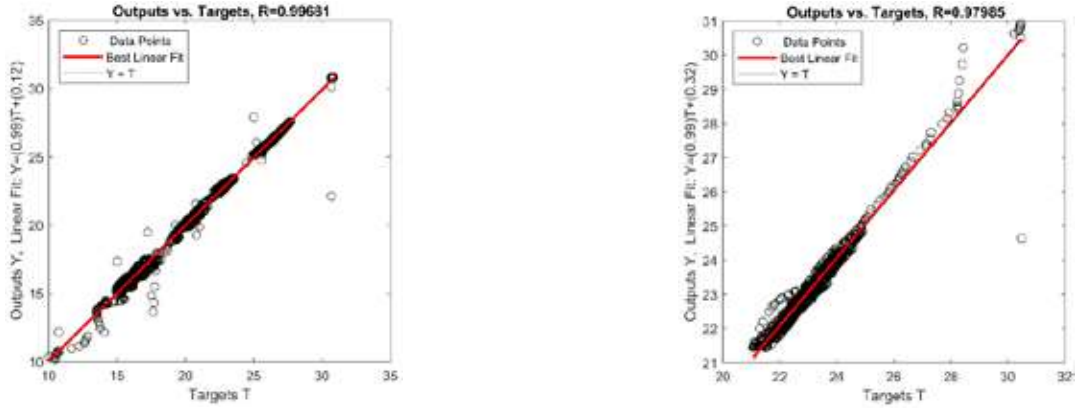


Fig. 4: Linear regression between the LSTM response and the target, a) first load profile, b) second load profile.

IV. Conclusions

In this study, we investigated the effectiveness of LSTM models for predicting the performance of PEMFC stacks. By utilizing measured current and temperature values, we trained LSTM models to predict PEMFC voltage with promising results. Our findings indicate that LSTM models offer a robust alternative to traditional methods for online PEMFC parameter estimation. Through grid search optimization, we identified optimal hyperparameters for the LSTM model, including 300 hidden units, a learning rate of 0.01, and 2000 epochs. These parameters yielded superior performance, as evidenced by the low Root Mean Squared Error (RMSE) values obtained for both load profiles. Moreover, regression analysis revealed strong correlations between predicted and measured values, with correlation coefficients of 0.996 for the first load profile and 0.979 for the second load profile. Overall, the results of this study underscore the potential of LSTM models in accurately predicting PEMFC performance. Future research could explore further enhancements to the LSTM architecture and investigate its application in real-world PEMFC systems.

References

Liang Y.F., Liang Q.C., Zhao J.F., Li M.J., Hu J.Y., Chen Y., Online identification of optimal efficiency of multi-stack fuel cells (MFCS), Energy Reports, 8, 979–89 (2022).

Fernandez A.M.I., Kandidayeni M., Boulon L., Chaoui H., An adaptive state machine based energy management strategy for a multi-stack fuel cell hybrid electric vehicle, IEEE Trans Veh Technol, 69, 220–34 (2020).

Yu P., Li M., Wang Y., Chen Z., Fuel cell hybrid electric vehicles: A review of topologies and energy management strategies, World Electr Veh J., 13 (2022).

Mitzel J., Gülzow E., Kabza A., Hunger J., Araya S.S., Piela P., et al. Identification of critical parameters for PEMFC stack performance characterization and control strategies for reliable and comparable stack benchmarking, Int J Hydrogen Energy, 41, 21415–26 (2016).

Wang C., Li Z., Outbib R., Dou M., Zhao D., A novel long short-term memory networks-based data-driven prognostic strategy for proton exchange membrane fuel cells, Int J Hydrogen Energy, 47,10395–408 (2022).

Kandidayeni M., Chaoui H., Boulon L., Kelouwani S., Trovao J.P.F., Online system identification of a fuel cell stack with guaranteed stability for energy management applications, IEEE Trans Energy Convers, 36, 2714–23 (2021).

Zhou S., Shearing P.R., Brett D.J.L., Jervis R., Machine learning as an online diagnostic tool for proton exchange membrane fuel cells, Curr Opin Electrochem, 31, 100867 (2022).

Gharibeh H.F., Yazdankhah A.S., Azizian M.R., Energy management of fuel cell electric vehicles based on working condition identification of energy storage systems, vehicle driving performance, and dynamic power factor, J Energy Storage, 31, 101760 (2020).

Su D., Zheng J., Ma J., Dong Z., Chen Z., Qin Y., Application of machine learning in fuel cell research, Energies, 16, (2023).

Kandidayeni M., Macias A., Boulon L., Trovão J.P.F.. Online modeling of a fuel cell system for an energy management strategy design, Energies.13, 1–17 (2020).

Evaluation of Hydrogen Energy Concept from Elementary School to University: Opinions of Energy Systems Engineers on Hydrogen Energy Concept

Eylem Kılıç
Van Yuzuncu Yil University, Faculty of Education, Department of Computer Education and Instructional Technology, Zeve Campus, Van, 65000, Türkiye

* E-mail:keylem@gmail.com

Abstract
The purpose of this study is not only to determine the opinions of energy systems engineers on hydrogen energy but also to evaluate the content of hydrogen energy, which is a renewable energy source, presented in primary, secondary, and university-level education programs. For this purpose, the content of science education programs at the primary and secondary levels has been examined. In addition, the curriculum of science education departments in universities has been examined, and scientific studies conducted in our country on renewable energy sources and hydrogen energy have been evaluated. A reflective journal form consisting of open-ended questions was applied to eight students graduating from the Energy Systems Engineering department of universities to determine their opinions on hydrogen energy. The data obtained were analyzed using the content analysis method. As a result of the research, it is observed that hydrogen energy is not adequately addressed in the primary and secondary education curricula, and in the science education department, there are elective courses related to renewable energy sources. The opinions of energy systems engineers on hydrogen energy will be presented in detail.

Keywords: Hydrogen energy, energy systems engineering, curriculum.

I. Introduction

The Ministry of Energy and Natural Resources of the Republic of Turkey aims to create a carbon-zero economy model by utilizing hydrogen through the "Turkey Hydrogen Technologies Strategy and Roadmap." Hydrogen, considering its contribution to sustainable energy, has been identified as one of the priority areas (ETKB, 2023). The word "hydrogen" comes from the combination of the Greek words "hydro" (water) and "genes" (generating). Hydrogen, first separated by Henry Cavendish in 1766, was later discovered to be usable as a fuel. This discovery was further advanced with William Robert Grove's contribution to the development of fuel cells in 1839. The hydrogen atom plays a role similar to the building blocks of life, the cell. Just as life began with the cell, the existence of the universe and the Earth also occurred with the emergence of the hydrogen element. Therefore, hydrogen is the most abundant and smallest element in the universe and on our planet. It is volatile, as it is about 14 times lighter than other gases in the atmosphere, and it is also harmless, colorless, and odorless. It is the fundamental energy source for other stars like the Sun (Özcan, 2008). As technology advances and research progresses, hydrogen energy with its high efficiency and low emission values has seen an expansion in its applications (Türk, 2022). Hydrogen energy is a chemical energy released in its molecules as a result of the dissociation of hydrogen in its pure form. Although hydrogen energy is not a natural energy, it becomes renewable when obtained from water and other infinite sources on Earth. However, this type of energy can be produced from both fossil fuels and renewable sources. Therefore, its renewable characteristic depends on the source of production. Green hydrogen obtained through electrolysis of water is a renewable energy source.

It is important for the priority and significance of hydrogen energy among sustainable energy sources to be understood and awareness to be increased by future generations. Therefore, it is important for this topic to be included in primary, secondary, and university levels of education. In this regard, the content related to renewable energy sources and hydrogen energy will be analyzed in the primary and secondary science education program (MEB, 2024). Additionally, it is crucial to evaluate the domain knowledge of science teacher candidates throughout their undergraduate education regarding this topic to provide education to students at this level. Furthermore, in vocational and technical Anatolian high schools, there are departments such as ship outfitting, plumbing technology, and air conditioning and renewable energy technology. The curricula of these departments will also be analyzed. Graduates from the Energy Systems Engineering department are appointed as teachers in these departments. With the increasing demand for the energy sector in our country, Energy Systems Engineering Departments were established through the Council of Ministers' decision published in the Official Gazette on November 13, 2009. Considering that energy systems engineers can also be appointed as teachers, it is crucial for them to create awareness of hydrogen energy in the basic education levels.

II. Method

In this study, the curriculum program related to hydrogen energy in primary education and relevant departments of universities was examined using the content analysis method. Additionally, reflective journals were written by eight energy systems engineering students who were continuing their pedagogical formation program at Van Yüzüncü Yıl University to determine their views on hydrogen energy, and the obtained responses were analyzed using the content analysis method.

III: Hydrojen energy in the curriculum

The science curriculum published by the Ministry of National Education in 2018 covers elementary school grades 3 to 8. In the science curriculum, there is no direct information about hydrogen energy. Instead, when questioning the concept of renewable energy, it can be seen that there is one achievement in the fifth grade, one achievement in the sixth grade, and four achievements in the eighth grade (Table 1). However, it is observed that only the achievement in the sixth grade is directly related to renewable energy (Çalımlı, 2021). Although Türk (2022) stated in their study that these achievements indirectly appear in grades three, four, and five, direct achievements related to energy are provided in the sixth grade.

Tab 1. Achievements related to renewable energy from the science curriculum

Grade Level	Unit Name	Domain Name	Achievement
5	*Humans and Environment*	*Living Things and Life*	*F.5.6.2.4. Discusses the benefits and harms of human-environment interaction using examples.*
6	*Matter and Heat*	*Nature of Matter*	*F.6.4.4.1. Classifies fuels as solid, liquid, and gas fuels and provides examples of commonly used fuels. It is stated that fossil fuels are limited and one of the non-renewable energy sources, and the importance of renewable energy sources is emphasized with examples.*
8	*Energy Transformations and Environmental Science*	*Living Things and Life*	*F.8.6.4.1. Endeavors to behave conservatively in the use of resources.*
8	*Energy Transformations and Environmental Science*	*Living Things and Life*	*F.8.6.4.2. Designs projects for the efficient use of resources.*
8	*Energy Transformations and Environmental Science*	*Living Things and Life*	*F.8.6.4.5. Identifies the problems that may be encountered in the future if resources are not used efficiently and presents solutions.*
8	*Electric Charges and Electrical Energy*	*Physical Events*	*F.8.7.3.4. Generates ideas about the advantages and disadvantages of power plants.*

In high school education, vocational high schools offer programs in Ship Equipment, Plumbing Technology, and HVAC and Renewable Energy Technology. When examining the framework program for renewable energy technologies, there is a course on renewable energy systems, and the second achievement of the course states, "Explains renewable energy sources, their types, and the advantages and disadvantages to the environment." There is no information specifically about hydrogen energy or other types of energy. When examining the framework program for Plumbing Technology and HVAC, no content related to renewable energy sources or hydrogen energy was found. In the framework program for Ship Equipment, no course or content was found.

IV. Hydrogen Energy in Education Faculty Science Education Teacher Training Program and Energy Systems Engineering Program at Universities

In the context of the new teacher training undergraduate programs published by the Higher Education Council (YÖK), when examining the science education teacher-training program in the Faculty of Education, the course on renewable energy sources is included as an elective course in the subject area. However, there is no specific course on hydrogen energy or other types of energy in the undergraduate program (YÖK, 2018). In the Energy Systems Engineering program, on the other hand, the course on hydrogen energy is seen as a technical elective course.

V. The Views of Energy Systems Engineers on Hydrogen Energy

Eight out of ten students continuing in the pedagogical formation program have participated in the study. Two of the energy systems engineers are female (25%) and six are male (75%). Among the participants, four are graduates from Şırnak, one from Yalova, one from Sinop, one from Tarsus, and another from Mehmet Akif Ersoy University. When asked if they had taken courses on hydrogen energy during their undergraduate studies, it is observed that all participants except one had taken such courses. Regarding sector experience, only one participant has more than 5 years of experience, while the other seven have between 2-4 years of experience. The participants were asked the question, 'What type of knowledge and skills did the content of the course provide you in terms of working on a hydrogen energy project?' The responses of the participants are provided in Table 2."

Tab 2. The Contributions of Taking a Hydrogen Course to Their Knowledge and Skills

Participants	Views
Participant 1	*It led me to research on fuel cells. And it was beneficial for me to continue my undergraduate thesis on fuel cells in a laboratory environment.*
Participant 2	*I gained some knowledge and experience but not in sufficient proportions.*

Participant 3	*Theoretical knowledge was adequate but lacking in practical application.*
Participant 4	*While hydrogen energy is a more powerful energy source compared to other petroleum derivatives, it is a disadvantaged source in terms of production and storage, despite being considered clean energy.*
Participant 5	*We did not participate in the project.*
Participant 6	*I learned about hydrogen fuel cells.*
Participant 7	*Energy generation through hydrogen cells.*

When participants were asked whether they found themselves sufficient to work on a project, **all except one** participant stated that they did not find themselves sufficient. Participants were asked the question, 'In your opinion, what role can hydrogen energy play in the energy sector in the future?' The opinions of the participants are provided in Table 3.

Tab 3. The Role of Hydrogen Energy in the Future Energy Sector

Participants	**Views**
Participant 1	*The non-renewable energy sources used worldwide have led to greenhouse gas emissions and acid rain over time, posing a significant threat to the habitats of living beings. While completely eliminating these effects may not be feasible, we can minimize them by solely relying on carbon-free energy sources. This would significantly improve the livability of the environment for the health and well-being of living organisms.*
Participant 2	*If we have the necessary investment and technology, we will have cheaper and safer energy usage, reducing dependency on external sources.*
Participant 4	*I am sure it will be a very important energy source once its disadvantages are eliminated; it's already too late.*
Participant 6	*Automobile and electricity production.*
Participant 7	*When used as fuel, hydrogen emits no gases into nature, making it a clean energy source. Additionally, the presence of hydrogen in nature is an advantage. However, efforts need to be made to reduce costs and make it a cheaper energy source.*

Participants were asked the question, 'What technological, economic, or political measures should be taken to promote the widespread adoption and increased use of this energy source?' The opinions of the participants are provided in Table 4.

Tab 4. Technological, economic, and political measures for the use of hydrogen energy

Participants	**Views**
Participant 1	*First and foremost, these should be popularized in education so that an informed society can emerge. Projects should be supported in vocational training, and projects should be popularized and implemented.*
Participant 2	*Good education should be provided on this matter, and experts in this field should be trained. Necessary areas and investments should be made, and developments should be made in the industrial sector.*
Participant 3	*More support should be provided for projects and initiatives related to hydrogen energy.*
Participant 4	*When we talk about politics, it ultimately comes down to money. The biggest obstacle in front of this resource is cost. I don't think this obstacle will remain if studies are conducted on this matter.*
Participant 6	*All countries need to make decisions for the freedom of use of this resource.*
Participant 7	*First and foremost, people need to be educated, and children should be provided with necessary education from a very young age. Priority should be given to education. Of course, this should be done by all countries worldwide. I'm sure if world leaders had used the money they spend on nuclear bombs, weapons, and wars for making the world cleaner and more livable, the world would be in a completely different state now.*

Participants were asked the question, 'What are your thoughts on the environmental sustainability impacts of the hydrogen economy?' The opinions of the participants are provided in Table 5.

Tab 5. The impacts of hydrogen energy on environmental sustainability

Participants	**Views**
Participant 1	*The damage caused to the environment by fuel-powered cars, with harmful emissions like carbon being at the forefront, is immeasurable. Cars powered by hydrogen energy, on the other hand, have a significant impact on a carbon-free life. Most importantly, they reduce external dependency and increase sustainability.*
Participant 2	*It will have a positive impact on the environment and reduce environmental pollution.*
Participant 3	*Despite being a clean energy source, it has not received sufficient attention and there hasn't been enough work done on sustainability*
Participant 4	*First and foremost, because it is clean energy, it is always sustainabl*
Participant 5	*It's clean energy and beneficial to the ecosystem.*
Participant 6	*I believe it is very beneficial in terms of sustainability, of course, provided that necessary safety measures are taken.*
Participant 7	*Certainly, due to its expensive nature, the contribution of hydrogen energy to the economy may be limited.*

Participants were asked the question, 'How do you evaluate the impacts of these new energy paradigms on society and the role of energy systems engineers?' The opinions of the participants are provided in Table 6.

Tab 6. Technological, economic, and political measures for the use of hydrogen energy

Participants	Views
Participant 1	*As an energy systems engineer, I am a supporter of renewable energy, and clean energy is desirable for everyone. Using renewable energy is an advantage for the health and economy of society.*
Participant 2	*It's unfortunate that this essential sector, which the country needs, is not receiving sufficient recognition and support.*
Participant 3	*I believe that the society lacks sufficient awareness on this issue.*
Participant 4	*Despite facing obstacles, as energy engineers, if we put our signatures under such resources, we can compete with other engineers and even surpass them. We must cut our own umbilical cord*
Participant 5	*I believe it's not being adequately promoted.*
Participant 6	*Energy systems engineers play a significant role in obtaining energy from various sources, especially in the widespread adoption and production of energy using hydrogen energy, after receiving the necessary detailed training.*
Participant 7	*I strongly believe that energy systems engineering is extremely crucial for our future. Especially with the depletion of fuels like petroleum and coal, people are being pushed towards renewable energy sources. Additionally, the increasing number of environmentally conscious individuals gives hope for renewable energy.*

Participants were asked the question, 'What do you think about the future of your department?' The opinions of the participants are provided in Table 7.

Tab 7. Their thoughts on the future of the department

Participants	Views
Participant 1	*The future is promising for our department. Turkey has a high energy potential, and I hope this will have a significant impact on our department.*
Participant 2	*Currently, it is not receiving the necessary attention. If this continues, I don't believe we will make progress. Without the necessary measures and authority, ordinary people rather than experts will end up doing the job, which will make it even more difficult.*
Participant 3	*I don't see any positive developments in my country.*
Participant 4	*Our department is truly valuable and deserves to be recognized, but it is being pushed into the background due to bureaucratic obstacles. As I mentioned earlier, we must cut our own umbilical cord.*
Participant 5	*I believe the country is not ready for this department.*
Participant 6	*Unfortunately, in Turkey, the field of energy systems engineering is not being given the opportunities it deserves, with very few appointments, and many engineers are working in different fields or trying to become teachers.*
Participant 7	*Although our department is not receiving sufficient attention in our country right now, I believe this will change in the future. Because the world will not accept being polluted by human hands any longer. Just like during the pandemic when people stayed indoors and nature began to cleanse itself...*

VI. Results and discussions

In this study, a content analysis of the concept of hydrogen energy has been conducted from primary education to relevant departments of universities. Additionally, the opinions of eight energy engineers regarding hydrogen energy have been included. When the curriculum is examined, it is observed that there is a direct attainment regarding renewable energy sources in the sixth grade. Therefore, it can be said that renewable energy is not sufficiently addressed in the curriculum up to the eighth grade. Looking at the high school curriculum, there is a course in the renewable energy technologies section, but no concept related to hydrogen technology was encountered. When it comes to university education, it is seen that there is an elective course on renewable energy in the science education teacher training department, and there is also a technical elective course on hydrogen energy in energy engineering. Energy engineers find hydrogen energy quite important for being a clean environment, but they often feel insufficient to work on a hydrogen energy project. Additionally, they believe that projects related to hydrogen energy need to be supported and that they do not receive sufficient attention, and there is not enough work done on sustainability. In conclusion, it is revealed that hydrogen energy is not included in the curriculum, and energy engineers, who are trained as experts in the field, do not consider themselves sufficient.

References

Çalımlı, A., “Fen Bilimleri Dersi Öğretim Programı Ve Ders Kitaplarında Yenilenebilir Enerji”, International Academic Social Resources Journal, (e-ISSN: 2636-7637), 6; pp:626-634,(2021).

YÖK. Yüksek Öğretim Kurulu Yeni Öğretmen Yetiştirme Lisans Programları, https://www.yok.gov.tr/kurumsal/idari-birimler/egitim-ogretim-dairesi/yeni-ogretmen-yetistirme-lisans-programlari, Erişim Tarihi: 02.04.2024

MEB. Millî Eğitim Bakanlığı Öğretim Programları İzleme ve Değerlendirme Sistemi, https://mufredat.meb.gov.tr/, Erişim Tarihi: 05.03.2024, (2024).

ETKB. Enerji ve Tabii Kaynaklar Bakanlığı Srtatejik Planı, https://sp.enerji.gov.tr/, Erişim Tarihi: 04.03.2024, (2024).

Özcan, B. Sürdürülebilir kalkınma ve hidrojen enerjisi. Humanities Sciences, 3(2), 152-160, (2008).

Türk, Ü. Ortaokul 8. Sinif öğrencilerinin yenilenebilir enerji kaynaklari konusunda modelleme yöntemi ile farkindalik oluşturulmasi, Master Thesis, Ordu University (2022).

Modeling and Simulation Photovoltaic-Electrolyzer-Fuel Cell in Microgrids

[1,2*]Musa Yılmaz, [1]Miroslav Penchev, [1]Alfredo A. Martinez-Morales, [1]Taehoon Lim, [1]Arun S.K. Raju
[1]College of Engineering - Center for Environmental Research and Technology (CE-CERT), University of California, Riverside, USA
[2]Batman University, Engineering Faculty, Electrical and Electronics Engineering, Batman, Türkiye.

[1]*E-mail:musay@ucr.edu

Abstract

Integration of PV systems with electrolyzers and fuel cells in microgrids is being investigated to increase grid reliability and sustainability. A reliable and efficient energy system has been established by converting solar energy into hydrogen through electrolysis and converting it back into electrical energy in fuel cells. While PV panels are used as the primary energy source, fuel cells serve as a backup source and meet changing demands. MATLAB/Simulink models have shown that this system maintains network stability and flexibility. Integration with energy storage systems such as lithium-ion batteries further improves microgrid performance and reliability.

Keywords: DC Microgrids, photovoltaic (PV) systems, electrolyzers, fuel cells, energy storage, grid reliability, sustainability.

I.Introduction

Sudden changes in weather conditions and load demands pose challenges in integrating renewable energy sources into electrical grids. As a solution to such problems, storing green hydrogen energy (GHE) using electrolyzers (EL) and fuel cells (FC) can be considered. Various power management control strategies have been employed to optimize, make efficient, reliable, and cost-effective the integration of renewable energy sources (RES) and FC/EL integrated power systems [1].

To enhance grid reliability by smoothing out electrical fluctuations in PV systems, the integration of a PEM electrolyzer with solar PV has been discussed. A transient thermal electrochemical model and a multi-software power control method were presented to demonstrate the electrolyzer's effectiveness in enhancing grid stability and flexibility [2].The application of microgrid designs, including both islanded and grid-connected systems using solar installations, is recommended for enhancing energy access and reliability. Simulink simulation is proposed as a valuable tool for analyzing PV system behavior, including power, voltage, and current levels in different operating conditions, providing insights for optimizing system performance[3].

The integration of a water electrolyzer and a PEMFC in a microgrid system shows promise in addressing real-time power imbalances. The experimental investigations conducted on the energy storage system in microgrids under various environmental conditions provide valuable insights into the system's performance and efficiency [4].

The hybrid power generation system, consisting of photovoltaic power generation devices, fuel cells, supercapacitors, electrolytic cells, hydrogen storage devices, and power regulation units, was designed and simulated to meet stable and continuous household electricity consumption. The combination of fuel cells and supercapacitors with photovoltaic devices ensures the stability and reliability of power supply in the hybrid power generation system, especially considering the fluctuations in sunshine intensity[5].

II.Photovoltaic Systems

Photovoltaic systems consist of various components such as solar modules, batteries, voltage conversion devices and transmission lines. These systems aim to efficiently utilize solar energy for electricity generation while incorporating features such as smart charging to extend battery life and increase energy storage capacity. Multiple photovoltaic power units with solar cell modules and inverters are interconnected via transmission lines to convert direct current into alternating current, facilitating efficient energy conversion and distribution. Photovoltaic systems in DC microgrid are given in Fig 1.

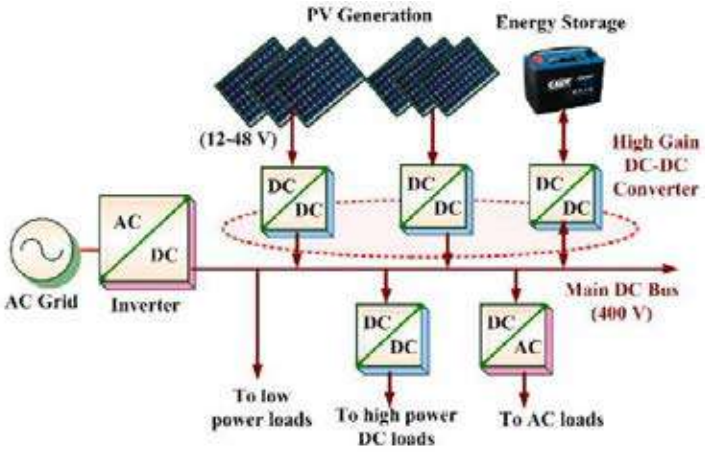


Fig. 1: Photovoltaic systems in DC microgrid[6]

III.Fuel cells/Electrolyzers systems

Fuel cells and electrolyzers play a crucial role in the integration of renewable energy sources into power systems, offering solutions for energy storage and conversion. Green hydrogen energy storage through electrolyzers and fuel cells is gaining global interest as a means to utilize surplus renewable energy efficiently. Electrolyzers split water into hydrogen and oxygen, contributing to the development of a green hydrogen economy across various sectors like chemical, materials, and transportation industries. Anion-exchange membrane (AEM) electrolyzers and fuel cells are emerging technologies that enable the transformation and utilization of renewable resources, providing cost-effective and efficient alternatives to conventional systems. Additionally, advancements in electrolyzer designs, such as reducing precious metal usage and enhancing cell durability, are essential for scalable deployment and sustainable hydrogen production. Overall, fuel cells and electrolyzers are pivotal components in achieving a zero-carbon economy and meeting the growing energy demands sustainably. Schematics of PEM devices: Electrolyzer and fuel cell are shown in Fig. 1.

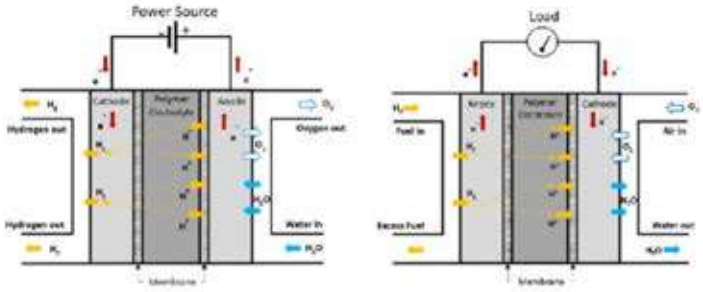


Fig.2 Schematics of PEM devices: Electrolyzer and fuel cell [7]

IV.Conclusion

This study investigates the integration of PV systems with electrolyzers and fuel cells in microgrids to enhance grid reliability and sustainability. MATLAB/Simulink simulations demonstrate that this hybrid energy system effectively maintains network stability and flexibility. Solar energy, converted into hydrogen via electrolysis, is stored and then converted back into electrical energy by fuel cells during high demand or low solar generation periods. The simulations reveal that fuel cells function reliably as a backup energy source, meeting varying energy demands. Integrating lithium-ion batteries further improves microgrid performance and reliability by balancing supply and demand and responding to sudden load changes. In conclusion, integrating PV systems with electrolyzers and fuel cells is an effective method to increase sustainability and reliability in microgrids. This hybrid system promotes efficient use of renewable energy and contributes to reducing the carbon footprint. Wider implementation of such systems holds significant potential for enhancing the flexibility and sustainability of energy grids in the future.

References

Hossain, Md Biplob, et al. "Advancement of fuel cells and electrolyzers technologies and their applications to renewable-rich power grids." Journal of Energy Storage 62 (2023): 106842.

Sai, Pushpitha, Vudata., Yifang, Wang., James, M., Fenton., Paul, Brooker. (2022). Transient Modeling and Optimization of a PEM Electrolyzer for Solar Photovoltaic Power Smoothing. Meeting abstracts, MA2022-01(39):1728-1728. doi: 10.1149/ma2022-01391728mtgabs

Munna, Kumar., Kanak, Bhengra., Jitendra, Kumar. (2021). Modeling and Simulation of Photovoltaic Solar Cell Microgrid. 181-189. doi: 10.1007/978-981-15-7994-3_16

Mircea, Raceanu., Nicu, Bizon., Adriana, Marinoiu., Mihai, Varlam. (2020). Design and Experimental Investigations of an Energy Storage System in Microgrids. 207-232. doi: 10.1007/978-3-030-23723-3_9

Xiaomin, Fang., Xiaolu, Li. (2023). Design and simulation of hybrid thermal energy storage control for photovoltaic fuel cells. Thermal Science, 27(2 Part A):1031-1039. doi: 10.2298/tsci2302031f.

Gupta, Nikita, et al. "Novel hybrid high gain converter: Combination of cuk and buck-boost structures with switched inductor for dc microgrid." *2020 2nd Global Power, Energy and Communication Conference (GPECOM)*. IEEE, 2020.

Alshehri, Feras, et al. "Modelling and evaluation of PEM hydrogen technologies for frequency ancillary services in future multi-energy sustainable power systems." *Heliyon* 5.4 (2019).

Assessing the Environmental Footprint of Catalysts in Photoelectrochemical Hydrogen Production Through Life Cycle Analysis

[1*]Muhammed Iberia Aydin, [2,3]Ibrahim Dincer
[1]Yildiz Technical University, Clean Energy Research Institute, Hydrogen Research Center, Istanbul, 34220, Türkiye
[2]Ontario Tech University, FEAS, Clean Energy Research Laboratory, Oshawa, Ontario, L1G 0C5, Canada

* E-mail: iberia.aydin@yildiz.edu.tr

Abstract
This study presents an analysis of the environmental impacts associated with the life cycle of catalysts and photoelectrochemical (PEC) hydrogen production. PEC technology, which utilizes solar energy to split water into hydrogen and oxygen, is widely studied for its potential to reduce reliance on fossil fuels and produce clean hydrogen. Despite its advantages, the sustainability of this technology heavily depends on the materials and processes used, particularly the catalysts that facilitate the water-splitting reaction. Steam methane reforming (SMR) had the highest global warming potential (GWP) at 7.2 kg CO_2 eq./kg H_2, while photoelectrochemical (PEC) and other methods such as Alkaline Electrolysis, High Temperature Electrolysis, Proton Exchange Membrane (PEM) Electrolysis, and Cu-Cl Cycle resulted significantly lower GWP values, approximately 0.57, 1.36, 1.30, 1.43, and 0.87 kg CO_2 eq./kg H_2 respectively. By identifying the most environmentally friendly catalysts and suggesting improvements in their design and production processes, this research aims to refine PEC technology to better align with global sustainability goals, enhancing the viability and ecological responsibility of hydrogen as a clean energy carrier.

Keywords: Photoelectrochemistry, photocatalysts, hydrogen production, clean energy

1. Introduction

Hydrogen technologies emerges as a promising candidate for sustainable development due to its potential to serve as a clean and versatile energy carrier (Acar and Dincer, 2019). Clean hydrogen can be obtained through several technologies such as electrolysis, thermochemical methods, biological methods, photocatalysis etc. Among these technologies, photoelectrochemical (PEC) systems have studied widely in the open literature. These systems utilize solar energy to split water into hydrogen and oxygen, offering a clean pathway to renewable hydrogen production that could significantly reduce the dependence on fossil fuels (Acar, et al. 2016). However, the environmental sustainability of this technology relies not only on its ability to produce clean energy but also on the materials and processes involved, particularly the catalysts that facilitate the water-splitting reaction.

PEC hydrogen production is an innovative method for utilizing solar energy to produce hydrogen. This process encompasses capturing solar light, separating and transferring photo-excited charge pairs, and conducting surface redox reactions (Aydin, et al., 2022). Various catalysts enhance these mechanisms, including metal oxides known for their efficiency in light absorption and charge separation, metal chalcogenides which provide stability and high efficiency, and innovative nanocomposites that improve light absorption and charge dynamics. Additionally, novel approaches such as integrating single atoms into catalyst structures, controlling structural defects, creating S-scheme heterojunctions, and using doped metal oxides (e.g., Fe–N-S-tridoped titanium oxide) have been studied to improve the photocatalytic activity and address challenges like efficiency and cost-effectiveness. Despite these advancements, ongoing research is crucial to further enhance the process's efficiency and reduce production costs.

Catalysts play a crucial role in enhancing the efficiency and viability of PEC systems (Dufour et al., 2012). However, the production, usage, and disposal of these catalysts may have substantial environmental impacts. Life Cycle Impact Analysis (LCIA) is required to comprehensively evaluate the sustainability of catalysts used in photoelectrochemical hydrogen production. This analysis provides a systematic approach to assessing the environmental impacts associated with all the stages of a catalyst's life cycle, from raw material extraction through manufacturing, use, and final disposal.

The objective of this study is to apply LCIA to investigate the environmental aspects of various catalysts used in PEC hydrogen production. By doing so, the research aims to identify not only the most environmentally friendly catalysts but also potential areas for improvement in catalyst design and production processes. This insight is essential for advancing PEC technology in a manner that aligns with global sustainability goals.

2. Methods

In this study, a Life Cycle Assessment (LCA) was performed according to the international standards for life cycle analysis (ISO 14040 and ISO 14044 (ISO, 2006)) to understand the environmental implications of photoelectrochemical hydrogen production, focusing on the use of various catalysts. Accordingly, the LCA consisted of four main phases: defining the goal and scope, conducting an inventory analysis, assessing environmental impacts, and interpreting results (Wolf et al., 2010). The study aimed to explore the environmental impacts throughout the lifecycle of hydrogen produced via photoelectrochemical methods, which involve innovative catalysts like metal oxides, metal chalcogenides, nanocomposites, and doped titanium oxide.

The inventory analysis was conducted using SimaPro 9 with the Ecoinvent 3 database, supplemented by targeted literature and laboratory studies when data gaps were encountered. Data obtained in this phase critically

assessed data sourced from literature using pedigree matrices to determine uncertainties. This process ensures a reliable database for the lifecycle stages of the catalysts used in hydrogen production as given in Figure 1. Scaling up of the PEC systems were studied from literature data or pilot projects to reflect realistic industrial deployment scenarios, emphasizing the materials required for manufacturing and the operational parameters of the catalysts.

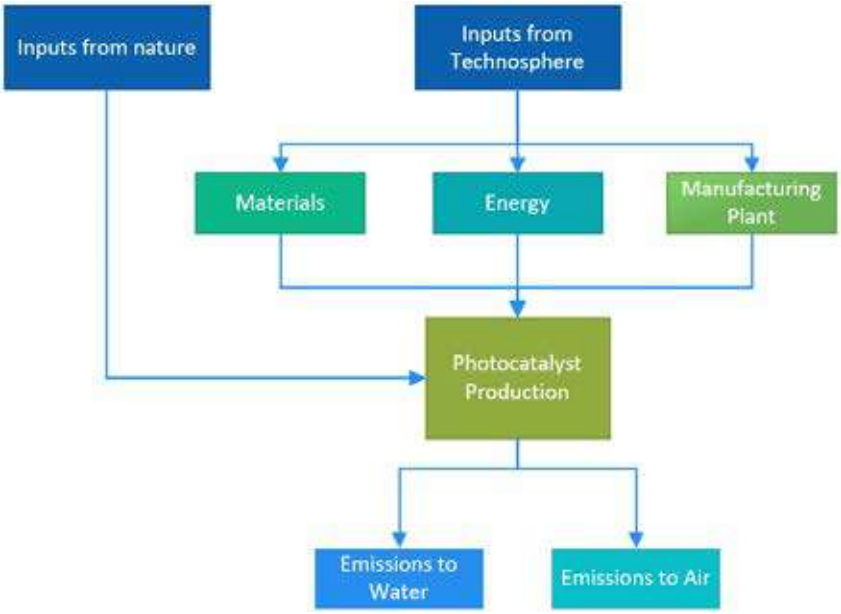


Fig. 1. Elementary flow of photocatalyst production

Impact assessment was carried out using the ReCiPe 2016 midpoint method to evaluate the environmental impacts associated with each stage of the hydrogen lifecycle. This included the production of catalysts, building the manufacturing plants and energy requirements for hydrogen generation. By highlighting the role of catalysts in minimizing environmental footprints, this study provides insights into the sustainable production of hydrogen. The results from this LCA are critical for understanding the full environmental potential and challenges of integrating advanced catalysts in hydrogen production systems.

3. Results and discussion

Global warming potential (GWP) results for various hydrogen production pathways are given in Figure 2. Accordingly, steam methane reforming (SMR) gave the highest GWP result with 7.2 kg CO_2 eq./kg H_2. PEC and other methods like Alkaline Electrolysis, High Temperature Electrolysis, Proton Exchange Membrane (PEM) Electrolysis, and Cu-Cl Cycle resulted in low GWP values, close to 0.57, 1.36, 1.30, 1.43 and 0.87, respectively. Unlike SMR, those technologies do not rely on fossil fuels as a feedstock to the process. Instead, the environmental burdens often come from the background processes such as manufacturing the required parts, synthesizing or mining the catalysts, the source of the energy etc.

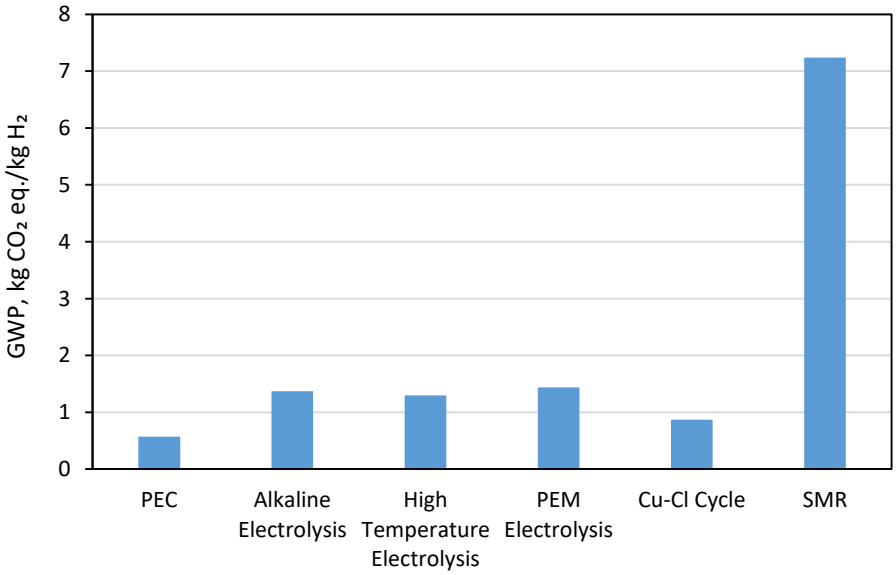


Fig. 2. Global warming potential results for various hydrogen production technologies

4. Conclusions

This study highlights the critical importance of catalysts in enhancing the efficiency and environmental sustainability of PEC hydrogen production systems. The research evaluated the environmental impacts of various catalysts throughout their lifecycle, from raw material extraction to manufacturing, use, and disposal. The results reveal that while PEC technology presents a lower global warming potential compared to conventional methods like steam methane reforming, significant environmental burdens are associated with the catalysts, particularly in their production and end-of-life stages. This finding emphasizes the need to refine catalyst materials and processes to better align with global sustainability goals. By advancing the design and manufacturing of these catalysts, the study aims to investigate the ecological footprint of PEC systems, thereby maximizing hydrogen's potential as a clean energy carrier in a sustainable future. The ongoing innovation and environmental evaluation are crucial for minimizing the impact while utilizing this technology.

References

Acar, C. and Dincer, I. 'Review and evaluation of hydrogen production options for better environment', Journal of Cleaner Production, 218, pp. 835–849. (2019)

Acar, C., Dincer, I. and Naterer, G.F. 'Review of photocatalytic water-splitting methods for sustainable hydrogen production', International Journal of Energy Research, 40(11), pp. 1449–1473. (2016)

Aydin, M.I., Selcuk, H. and Dincer, I. 'A photoelectrochemical reactor for ion separation and hydrogen production', Energy, 256, p. 124641. (2022)

Dufour, J. et al. 'Life cycle assessment of alternatives for hydrogen production from renewable and fossil sources', International Journal of Hydrogen Energy, 37(2), pp. 1173–1183. (2012)

ISO, ISO 14040:2006 -- Environmental management -- life cycle assessment -- Principles and Framework. ISO (2006).

Wolf, M.-A. et al. 'International Reference Life Cycle Data System (ILCD) Handbook-general guide for life cycle assessment-detailed guidance'. (2010)

Electroplated Copper-Based Electrodes: A Performance Investigation

[1]Zeynep Kuyumcu, [1]Hurmus Gursu, [1]Muhammed Iberia Aydin, [2,1]Ibrahim Dincer
[1]Yildiz Technical University, Clean Energy Technologies Institute, Istanbul, Esenler, Türkiye
[2]Ontario Tech University, Clean Energy Research Laboratory, Oshawa, Ontario, Canada

* E-mail: zeynep.kuyumcu@std.yildiz.edu.tr

Abstract
The increasing global energy demand, projected to reach 512.6 EJ by 2050. Depletion of non-renewable energy sources and their significant environmental impact, increasing the need for clean energy solutions like hydrogen. Hydrogen, which can be used in various applications including energy storage and vehicles, is seen as a viable clean energy source. Development of electrocatalysts for electrolysis is important for clean hydrogen generation. In this study, due to Copper (II) acetate was selected for electrodeposition to stainless steel because of their low costs and lack of studies in literature. Cu electrodes were synthesized with electrodeposition method in presence of different concentrations of copper acetate on 316L stainless steel. Copper acetate reduction (electrochemical reduction potential) and oxidation (electrochemical oxidation potential) at different pH values are also investigated. Synthesized electrodes were characterized by field emission scanning electron microscopy (FE-SEM) and X-Ray diffraction analysis (XRD). Due to gained information from characterizations and pH comparisions, Cu electrode activity in hydrogen evolution reaction (HER) are discussed for future use of Cu electrodes in hydrogen synthesis.

Keywords: Copper, electrodes, hydrogen evolution reaction, electrodeposition

1. Introduction

The energy consumption due to the increasing population will cause a major energy crisis in the close future. In 2019, the global energy demand reached 477.3 EJ and is expected to increase to 512.6 EJ by 2050 if the current trend continues (BP, 2023). In this scenario, greenhouse gas emissions are projected to be 985.9 Gt CO_2 eq. Until today, petroleum-based economy has managed to postpone enegry crisis by relying on non-renewable energy sources such as coals, fossil fuels and natural gases. However, non-renewable sources are gradually depleting, and more importantly, the environmental impacts caused by the use of fossil fuels are becoming a challenge (Dincer and Aydin, 2023). The damage these resources cause to nature can no longer be ignored. Hence, the nations of the globe have urged to take action, and net-zero goals have been set with Paris Agreement (Paris Agreement, 2015). Clean energy is the greatest need of the modern world to slow down the pace of the climate crisis and reach sustainable development goals.

Hydrogen is a strong candidate as a clean energy source. Hydrogen could be used in energy storage, vehicles, electric generation, feedstock etc. Unfortunately, global hydrogen still relies on fossil fuels. Today, more than 95% of hydrogen still produced using fossil-fueled pathways such as steam methane reforming and coal gasification (Dincer and Acar, 2014). Common methods of producing clean hydrogen include electrolysis (using renewable energy to split water into hydrogen and oxygen), thermochemical water splitting (using heat and chemical reactions), biological production (via microorganisms like algae and bacteria), and photoelectrochemical water splitting etc (Grimm et al., 2020). However, challenges such as high cost, infrastructure requirements, efficiency and scalability are the main concerns of the clean hydrogen production technologies.

Electrolysis is one of the oldest and most mature methods to produce clean hydrogen. In electrolysis method platinum (Pt) are widely preferable due to providing hydrogen and oxygen evolution reactions in an optimal rate (Vidales and Semai, 2023). Pt has higher stability and has higher costs than other candidates. Therefore, developing electrocatalysts that are low-cost, highly efficient, and stable is important for reducing investment and operational costs in electrolysis technologies. This study investigates the electrocatalytic properties of copper coatings on stainless steel. Among the copper solutions, copper (II) acetate was selected owing to low corrosion rate in presence of acetate ions (Kilinçeker and Galip, 2008).

2. Experimental and Analysis

This experiment involved in three electrode system which contains Ag/AgCl (in 3.0 M KCl), a graphite rod, 316L stainless steel (ss) as reference electrode, counter electrode and working electrode, respectively. Before electrodeposition, 316L ss electrodes were etched with HCl for 10 min, washed with ethanol for 15 min and with DI water 10 min to cleaning. Copper (II) acetate of different molarites (0.05 M, 0.1 M, 0.2 M) was prepared in water solution and used electrolyte for electroplating. Cyclic voltammetry was performed in +1 to -1.5V interval to understand oxidation and reduction peaks of copper ions. Chosen potentials were applied with chronoamperometry method for various times (2 min, 10 min, 20 min each). In this scope, deposition potential value, deposition time and concentration effects were studied for optimization. Acetic acid, and sodium acetate trihydrate was used as an additive chemical in optimizated concentration due to improve electrodeposition quality and hydrogen evolution reaction. All electrochemical experiments were runned in Gamry Reference 3000 as a potantiostat/galvanostat. Linear sweep voltammetry was used to analyze for hydrogen evolution mechanism on different copper based electrocatalyst prepared at different procedures. X-ray diffraction (XRD, Malvern PANalytical X'Pert PRO) was used to analyze crystal structrure of copper electrodeposition. The structural analysis of the copper-based material was performed by using field emission scanning electron microscopy (FE-SEM, Thermo Scientific).

3. Results and Discussion

FE-SEM images demonstrate to change in surface morphology for, a, b, c respectively (Figure 1). The size and variety of crystal structure on the electrode surface proportionally increase as the molarity of the solution. This can be related to the nucleation rate and mechanism integrated with concentration on stainless stell substrate.

a) Cu@0.05 b) Cu@0.1 c) Cu@0.2

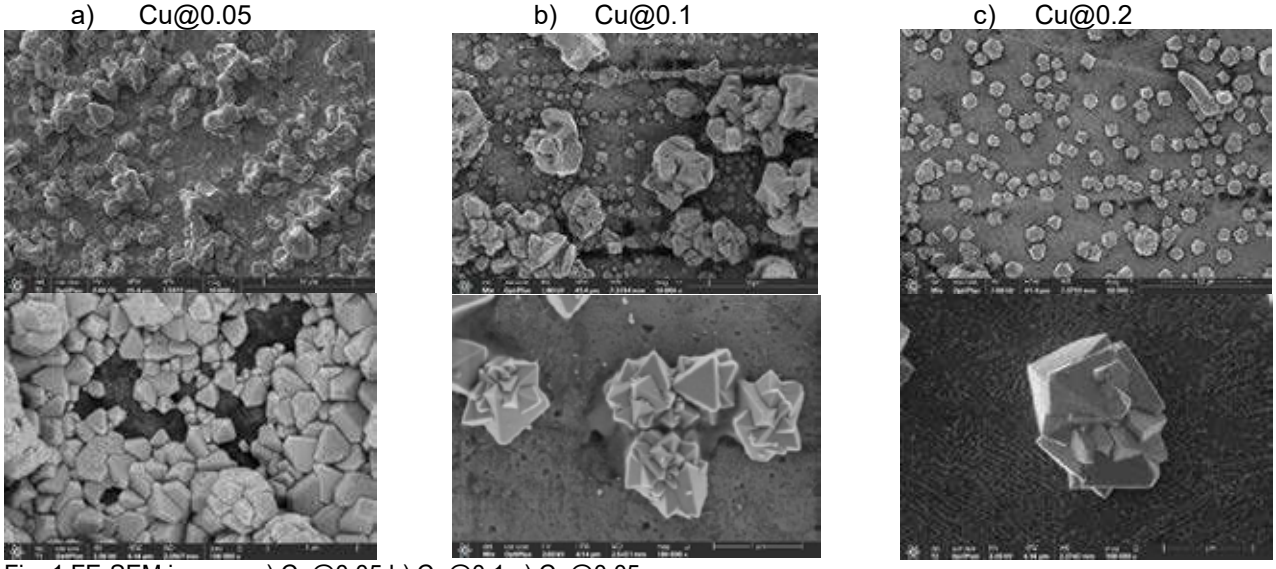


Fig. 1 FE-SEM images a) Cu@0.05 b) Cu@0.1 c) Cu@0.05

The experimental results show the potential of copper (II) acetate as a promising electrocatalyst in the electrolysis process for clean hydrogen production. Initially, the study evaluated the electrocatalytic efficiency of various copper acetate concentrations, with optimal performance observed at higher molarity. This was evidenced by linear sweep voltammetry (LSV) measurements. The copper electroplating on stainless steel showed superior durability and efficiency in hydrogen production compared to uncoated samples. These findings suggest that while copper acetate is a viable candidate for electrocatalyst production, the performance heavily depends on the concentration and pH.

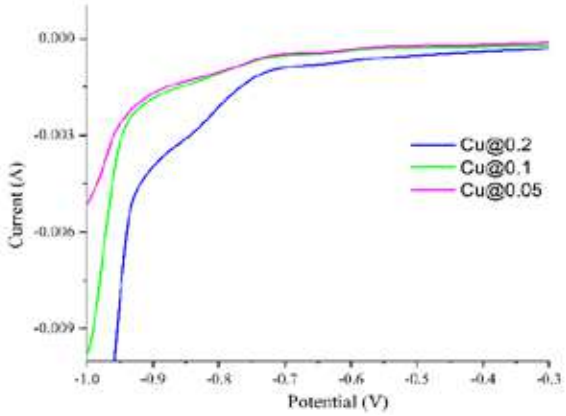


Fig.2 HER performance in 1M KOH

5. Conclusion

The results indicate that while copper electrochemical coating with copper acetate presents different electrolyte medium which is an alternative to more traditional catalysts like platinum, challenges such as scalability and long-term stability under operational conditions still need to be addressed. Future research should focus on these areas to addressing the stability and improve the practical applicability of copper acetate in industrial-scale hydrogen production systems.

References

BP. *Energy Outlook 2023 Edition*. (2023)

Dincer, I., Acar, C. Review and evaluation of hydrogen production methods for better sustainability. International Journal of Hydrogen Energy, *40*(34), 11094–11111. (2014)

Dincer, I., Aydin, M. I. New paradigms in sustainable energy systems with hydrogen. Energy Conversion and Management, *283*, 116950. (2023)

Grimm, A., de Jong, W. A., Kramer, G. J. Renewable hydrogen production: A techno-economic comparison of photoelectrochemical cells and photovoltaic-electrolysis. Int J. Hydrogen Energy, *45*(43), 22545–22555. (2020)

Paris Agreement. Paris agreement. In *Report of the Conference of the Parties to the United Nations Framework Convention on Climate Change (21st Session, 2015: Paris). Retrived December* (Vol. 4, p. 2017). HeinOnline. (2015)

Vidales, A. G., Semai, M. Platinum nanoparticles supported on nickel-molybdenum-oxide for efficient hydrogen production via acidic water electrolysis. Journal of Molecular Structure, *1290*, 135956. (2023)

Proton Exchange Membrane Water Electrolysis System: Steady-State Modeling and Assessment

[1*]Nurettin Sezer, [2]Sertac Bayhan
[1,2] Hamad Bin Khalifa University University, Qatar Environment and Energy Research Institute, Doha, Qatar

* E-mail: NSezer@hbku.edu.qa

Abstract
This study presents modelling and performance analysis of a Proton Exchange Membrane Water Electrolysis (PEMWE) system. The theoretical and actual cell potential of the system is determined based on the analysis of inherent cell potentials. The activation overpotential experienced a sudden surge at current densities less than 200 A/m^2. Ohmic overpotential increased linearly with the current density and varied from 0 to ~0.06 V when the current density is increased from 0 to 2.5 A/cm^2. Similarly, the concentration overpotential varied between 0 and ~0.05 V. According to these results, activation overpotential is the dominant polarization within the studied current density range. Due to the sluggish kinetics associated with the oxygen evolution reaction, significantly slower than the hydrogen evolution reaction, activation and concentration overpotential at the anode make more substantial contributions than those at the cathode to the overall overpotentials. Exergy and energy efficiency of the system is found to be 60.5% and 57.3%, respectively.
Keywords: Proton exchange membrane, electrolysis, hydrogen, cell polarization, exergy.

I. Introduction

Hydrogen has attracted growing research interest due to its exceptionally high energy per mass content and being a clean energy carrier, unlike the widely used hydrocarbon fuels. With the possibility of long-term energy storage and re-electrification, hydrogen promises to promote the effective utilization of renewable and sustainable energy resources. Clean hydrogen can be produced through a renewable-powered water electrolysis process. The proton exchange membrane water electrolysis (PEMWE) cell technology has been developed to offer high voltage efficiencies at high current densities. Besides, PEMWE cells are characterized by a fast system response to fluctuating renewable power, enabling operations at broader partial power load ranges while consistently delivering high-purity hydrogen with low ohmic losses. Activation and concentration overpotential along with ohmic overpotential should be investigated to analyze axtual electrochemical performance of PEMWE systems against theoretical. This study aims to perform electrochemical and thermodynamic performance assessment of a PEMWE system and provide insights into understanding the effect of inherent cell polarizations on its overall performance. The specific objectives of the study are listed as follows:

- To analyze inherent cell polarizations including activation, concentration, and ohmic overpotentials.
- To investigate overpotentials at varying current densities.
- To assess energy and exergy efficiency of the system.
- To investigate the effect of varying current density on cell voltage and efficiency.

II. Experimental Set-up and Procedure

In a PEMWE cell, the electrochemical half-cell reactions involve the anodic Oxygen Evolution Reaction (OER) and the cathodic Hydrogen Evolution Reaction (HER). The OER, HER, and the overall reaction are represented by:

$$2H_2O \rightarrow 4H^+ + O_2 + 4e^- \qquad E_a^0 = 1.229\ V \qquad (1)$$

$$2H^+ + 2e^- \rightarrow H_2 \qquad E_c^0 = 0.000\ V \qquad (2)$$

$$H_2O \rightarrow H_2 + \frac{1}{2}O_2 \qquad E_o^0 = 1.229\ V \qquad (3)$$

When direct current is applied to an electrolysis cell, the cell voltage increases above the thermodynamic reversible voltage due to several inherent cell overvoltage.

III. Analysis

The electrolysis cell voltage (V_{cell}) is expressed as the sum of the reversible voltage and overvoltage within the cell:

$$V_{cell} = E_r + V_{ohm} + V_{act} + V_{con} \qquad (4)$$

The open circuit voltage, E_r, also called the reversible cell voltage of an electrolyzer, is commonly determined using the Nernst equation:

$$E_r = 1.229 - 0.9 \times 10^{-3}(T - 298) + \frac{R \cdot T}{n \cdot F} l\,n\left(\frac{P_{H_2} \cdot P_{O_2}^{1/2}}{p_{H_2O}}\right) \qquad (5)$$

where T is the electrolysis cell temperature in K, R is the gas constant (8.315 J mol^{-1} K^{-1}), F is the Faraday's constant (96,485 $\mathrm{C/mol\ e^-}$ or $\mathrm{J/V\ mol\ e^-}$), $\mathrm{P_{H_2}}$ and $\mathrm{P_{O_2}}$ are the partial pressure of hydrogen and oxygen, respectively, and $\mathrm{p_{H_2O}}$ is the water pressure ($\mathrm{P_{H_2O}} = 1\ \mathrm{atm}$ for liquid water).

Ohmic overvoltage, V_{ohm}, pertains to the resistance of electrolyte material against the movement of protons. Minimizing ohmic overvoltage is of utmost importance. Manufacturing methods and processes play a substantial role in accomplishing this objective.

The conventional application of Ohm's law is as follows:

$$V_{ohm} = R \cdot I = \frac{\delta}{\sigma} I \quad (6)$$

In this equation, δ represents the thickness of the material, and σ represents the conductivity of the material. This equation is frequently used for membranes. For Nafion membranes, the membrane conductivity (σ) can be described as follows (Carmo et al., 2013; Falcão & Pinto, 2020; Han et al., 2015):

$$\sigma = (0.005139\lambda - 0.00326) \cdot exp\left[1268\left(\frac{1}{303} - \frac{1}{T}\right)\right] \quad (7)$$

where λ represents the water content of the membrane expressed as the $mol_{H_2O}/mol_{SO_3^-}$ ratio. This equation shows the correlation between the cell ohmic losses with temperature and humidity. Most literature used a humidification (λ) value between 14 and 22.

The activation overvoltage, V_{act}, refers to the energy loss in a reaction, which represents the amount of extra energy required to initiate the reaction. The Butler-Volmer equation is commonly used as the electrochemical model to describe the activation overpotential (Olivier et al., 2017):

$$V_{act} = V_{act,a} + V_{act,c} = \frac{R \cdot T_a}{\alpha_a F} arcsinh\left(\frac{I}{2i_{0,a}}\right) + \frac{R \cdot T_c}{\alpha_c F} arcsinh\left(\frac{I}{2i_{0,c}}\right) \quad (8)$$

In this equation, α_a and α_c represent the charge transfer coefficient at the anode and cathode, respectively, I represents the cell current density, while $i_{0,a}$ and $i_{0,c}$ denote the exchange current density at the anode and cathode, respectively. Exchange current densities serve as an indicator of the reactivity at the anode and cathode before an external potential is applied. Typically, high exchange current density implies that a lower potential is needed to initiate the reaction.

The concentration overvoltage, V_{con}, also known as mass transport overvoltage or diffusion overvoltage, is a result of mass transport losses at sufficiently high current densities that impede the access of reactant water to active catalyst sites due to the overpopulation of reacting molecules. Therefore, it slows down electrochemical reactions and reduces reaction efficiency. It can be estimated using the Nernst formula (Zhang et al., 2023):

$$V_{con} = V_{con,a} + V_{con,c} = \frac{R \cdot T_a}{4F} ln\left(\frac{C_{O_2,m}}{C_{O_2,m0}}\right) + \frac{R \cdot T_c}{2F} ln\left(\frac{C_{H_2,m}}{C_{H_2,m0}}\right) \quad (9)$$

where C represents the concentration, and C_O is the reference concentration of either oxygen or hydrogen at the interface of the membrane and electrode.

According to Faraday's law, the rate of hydrogen production (f_{H_2}) in an ideal electrolysis cell is directly proportional to the charge transfer flow, which is represented by the electric current (I_{cell}). Assuming a uniform current flowing through all electrolyzer cells in a stack, the hydrogen production rate in Nm^3/h can be expressed as follows (Wang et al., 2021):

$$f_{H_2} = \eta_f \frac{N_{cell} I_{cell}}{z \cdot F} \frac{22.41}{1000} 3600 \quad (10)$$

where η_f is the Faraday Efficiency, also known as current efficiency, N_{cell} is the number of cells constituting the electrolysis module, I_{cell} is the cell current in Amperes (A), z is the number of electrons transferred per mol of hydrogen (z =2), 22.41/1000 is the conversion factor from liters to moles for ideal gas at standard temperature and pressure, and 3600 is the conversion factor from seconds to hours. Faraday efficiency, also called voltaic efficiency, is calculated by the ratio of open circuit voltage to the cell voltage, represented by;

$$\eta_F = \frac{E_r}{V_{cell}} \quad (11)$$

Energy efficiency of the electrolyzer, $\eta_{en,electrolyzer}$, is calculated by;

$$\eta_{en,electrolyzer} = \frac{\dot{m}_{H_2} \cdot LHV_{H_2}}{\dot{W}_{electrolyzer}} \quad (12)$$

where $\dot{m}_{H_2}$ is the mass production rate of hydrogen, LHV_{H_2} is the lower heating value of hydrogen, and $\dot{W}_{electrolyzer}$ energy input rate of the electrolyzer. Exergy efficiency of the electrolyzer is calculated by the following formula,

$$\eta_{ex,electrolyzer} = \frac{\dot{m}_{H_2} \cdot ex_{H_2}}{\dot{W}_{electrolyzer}} \quad (13)$$

where ex_{H_2} is the sum of physical and chemical exergy of hydrogen; $ex_{H_2,ph}$ and $ex_{H_2,ch}$. Finally, the mass, energy, and exergy balance of the electrolyzer are;

$$\dot{m}_{H_2O} = \dot{m}_{H_2} + \dot{m}_{O_2} \quad (14)$$

$$\dot{m}_{H_2O} h_{H_2O} + \dot{W}_{electrolyzer} = \dot{m}_{H_2} h_{H_2} + \dot{m}_{O_2} h_{O_2} + \dot{Q}_{lost,electrolyzer} \quad (15)$$

$$\dot{m}_{H_2O} ex_{H_2O} + \dot{W}_{electrolyzer} = \dot{m}_{H_2} ex_{H_2} + \dot{m}_{O_2} ex_{O_2} + \dot{Q}_{lost,electrolyzer}\left(1 - \frac{T_0}{T_s}\right) + \dot{E}x_{dest,electrolyzer} \quad (16)$$

IV. Results and Discussions

The characteristics of the PEMWE are listed in Table 1. Figure 1 presents the polarization curves associated with the variations of the activation and concentration overpotentials at anode and cathode, ohmic overpotential across the cell, as well as the open circuit voltage and overall cell potential as a function of current density. The anode and cathode activation overpotential experienced a sudden surge at current densities below 200 A/m^2, followed by a continuous and steady increase with the increase of the current density. On the other hand, ohmic overpotential increased linearly with the current density and it varied from 0 to ~0.06 V when the current density is increased from 0 to 2.5 A/cm^2. Similarly, the concentration overpotential varied between 0 and ~0.05 V when the current density increased from 0 to 2.5 A/cm^2. These findings indicate that the activation overpotential is the dominant

polarization within the studied current density range of 0-2.5 A/cm^2. Due to the sluggish kinetics associated with the anodic oxygen evolution reaction, significantly slower than the cathodic hydrogen evolution reaction, activation overpotential and concentration overpotential at the anode make more substantial contributions than those at the cathode to the overall activation and concentration overpotentials. These findings are comparable to those previously reported in relevant literature (Liso et al., 2018).

Table 1. PEMWE subsystem operation parameters

Parameter	Value
Cell area (cm^2)	40
Cell current (A)	60
Cell potential (V)	1.655
Current density (A/cm^2)	1.5
Cell power density (kW/cm^2)	3.168
Energy efficiency (%)	57.26
Exergy efficiency (%)	60.49

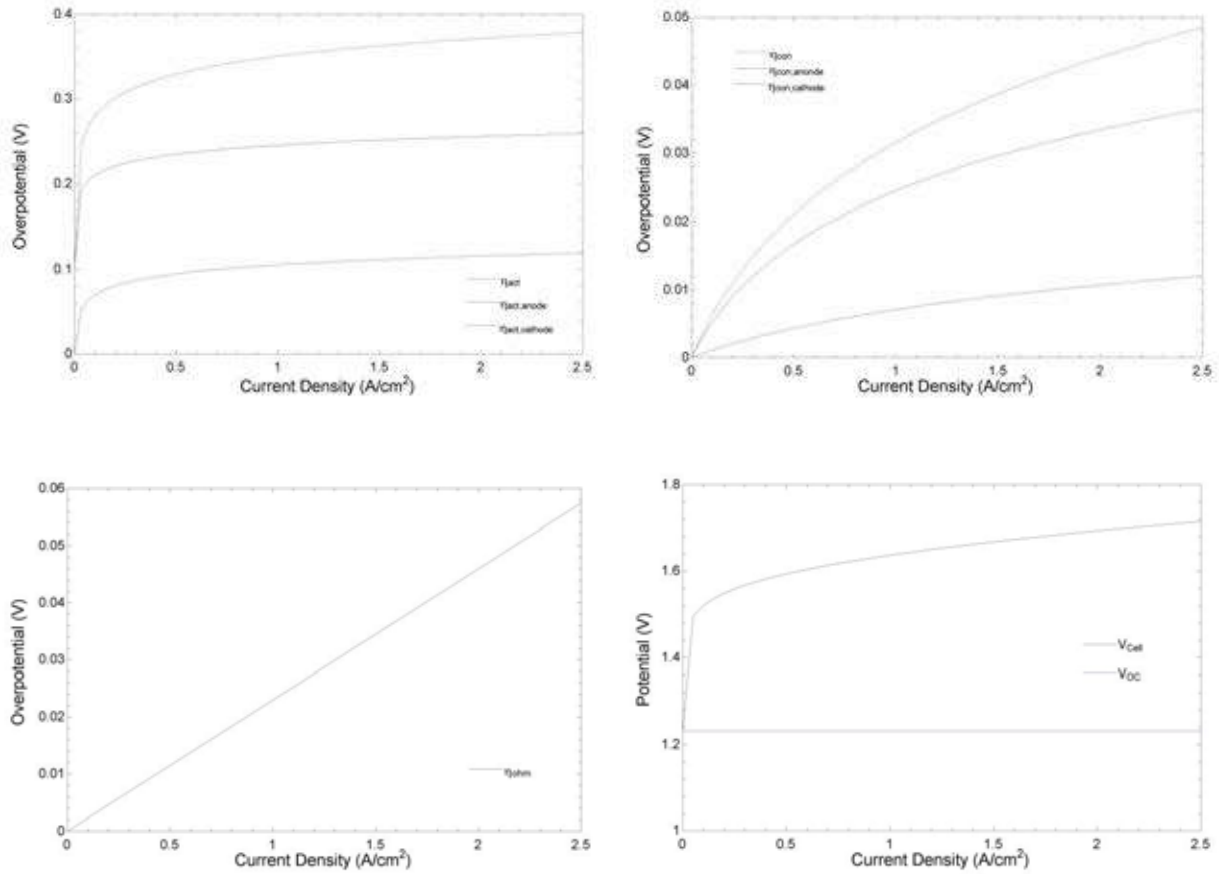


Fig. 1: Activation, concentration, and ohmic overpotential, and overall cell potential compared to open circuit voltage as a function of current density

Although the thermodynamic reversible cell potential, also called the open circuit voltage, for the electrolytic dissociation of water into gaseous hydrogen and oxygen to occur is 1.229 V, the inherent overpotentials increase the required cell potential. Figure 2 shows the increase in cell potential compared to the open circuit voltage which remains unchanged with the variation of current density. On the other hand, the energy and exergy efficiencies of the PEMWE cell decrease with current density as energy loss and exergy destruction rate of the cell increases due to the increased overpotentials (Figure 2).

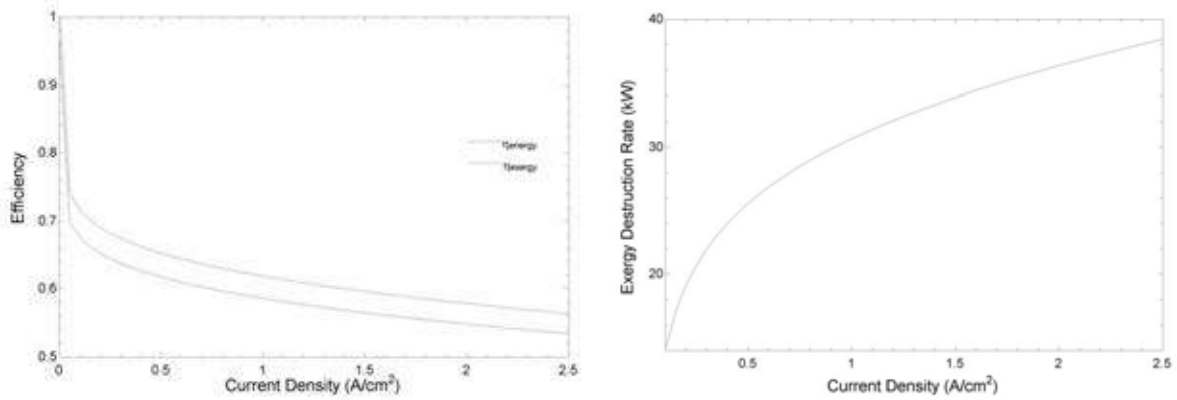


Fig. 2: Electrolyzer efficiency and exergy destruction rate at varying current densities

V. Conclusions

This study investigated the performance of a Proton Exchange Membrane Water Electrolysis (PEMWE) system. Inherent cell potentials are analyzed to indetify theoretical and actual cell potential of the system. According to results, activation overpotential is the dominant polarization within the studied current density range. Due to the sluggish kinetics associated with the oxygen evolution reaction, significantly slower than the hydrogen evolution reaction, activation and concentration overpotential at the anode make more substantial contributions than those at the cathode to the overall overpotentials. Exergy and energy efficiency of the system is found to be 60.5% and 57.3%, respectively.

Acknowledgements

This research was supported by ARG01-0428-230023, Qatar National Research Fund (a member of Qatar Foundation).

References

Carmo, M., Fritz, D. L., Mergel, J., & Stolten, D. (2013). A comprehensive review on PEM water electrolysis. In *International Journal of Hydrogen Energy* (Vol. 38, Issue 12, pp. 4901–4934). https://doi.org/10.1016/j.ijhydene.2013.01.151

Falcão, D. S., & Pinto, A. M. F. R. (2020). A review on PEM electrolyzer modelling: Guidelines for beginners. *Journal of Cleaner Production*, *261*, 121184. https://doi.org/10.1016/j.jclepro.2020.121184

Han, B., Steen, S. M., Mo, J., & Zhang, F.-Y. (2015). Electrochemical performance modeling of a proton exchange membrane electrolyzer cell for hydrogen energy. *International Journal of Hydrogen Energy*, *40*(22), 7006–7016. https://doi.org/10.1016/j.ijhydene.2015.03.164

Liso, V., Savoia, G., Araya, S. S., Cinti, G., & Kær, S. K. (2018). Modelling and Experimental Analysis of a Polymer Electrolyte Membrane Water Electrolysis Cell at Different Operating Temperatures. *Energies*, *11*(12), 3273. https://doi.org/10.3390/en11123273

Olivier, P., Bourasseau, C., & Bouamama, P. B. (2017). Low-temperature electrolysis system modelling: A review. In *Renewable and Sustainable Energy Reviews* (Vol. 78, pp. 280–300). Elsevier Ltd. https://doi.org/10.1016/j.rser.2017.03.099

Wang, S., Lu, A., & Zhong, C. J. (2021). Hydrogen production from water electrolysis: role of catalysts. In *Nano Convergence* (Vol. 8, Issue 1). Korea Nano Technology Research Society. https://doi.org/10.1186/s40580-021-00254-x

Zhang, F., Wang, B., Gong, Z., Zhang, X., Qin, Z., & Jiao, K. (2023). Development of photovoltaic-electrolyzer-fuel cell system for hydrogen production and power generation. *Energy*, *263*, 125566. https://doi.org/10.1016/j.energy.2022.125566

Second-Life Battery Utilization in PV Power Plants: Economic Analysis, Revenue Optimization, and Profit Increase

[1,2*]Feyza Turan, [1,3]Ali Rifat Boynuegri, [1]Ali Furkan Tetik, [1]Ozan Erdinc, [1]Yavuz Ates
[1]Yildiz Technical University, Faculty of Electric-Electronics, Department of Electrical Engineering, Davutpasa Campus, Istanbul, 34220, Türkiye
[2]Istanbul Topkapı University, Faculty, Department of Electrical Energy, Kazlicesme Campus, Istanbul, 3407, Türkiye
[3] Yildiz Technical University, Clean Energy Technologies Institute, Davutpasa Campus, Istanbul, 34220, Türkiye

* E-mail: feyza.turan@std.yildiz.edu.tr

Abstract
As the usage of battery systems continues to grow, it is expected that a significant number of second-life batteries (SLB) will enter the market in the coming years. This study encompasses the economic analysis of SLB utilization in photovoltaic (PV) power plants. Based on annual solar energy data, the annual revenue from grid energy sales with different SLB capacities for a 100 MW capacity PV system was calculated, and an optimization algorithm was modeled to maximize daily profits. Revenue increases were calculated based on SLB capacity values and their aging characteristics. Accordingly, utilizing a SLB with a capacity of 500 MWh resulted in a 17.9% higher profit compared to a system without a battery. Additionally, under optimal conditions, this system provides 92% of the maximum achievable profit.

Keywords: Second-Life Battery, Photovoltaic (PV) System, Battery Degradation

I. Introduction

Batteries play a pivotal role in contemporary energy systems, serving as indispensable components for various applications. As batteries reach the end of their original application lifespan, they still retain considerable potential for secondary use scenarios. Hence, evaluating batteries for second-life batteries (SLB) applications becomes imperative. The research by Kawala (2018) underscores the adverse environmental impact of battery production. By repurposing SLBs, not only can the demand for new batteries be partially met Lopez et al. (2014), but also a reduction in overall battery production can be achieved. The growing adoption of renewable energy systems underscores the significance of energy storage due to the intermittency of renewable energy sources. Herein lies the critical role of cost-effective battery solutions in fostering energy system sustainability and mitigating carbon emissions, crucial for attaining global emission reduction targets, as highlighted by the Council of Europe (2014) Particularly, European nations aspire to slash greenhouse gas emissions by 40%, necessitating efficient battery utilization and promotion of secondary use scenarios. Several studies have explored the potential of SLBs across diverse applications. Hegazy et al. (2015) designed and evaluated a hybrid photovoltaic (PV) /SLB system, offering a sustainable energy storage solution. Preusser et al. (2022) proposed a model utilizing SLBs from electric vehicles to enhance the profitability of public charging stations. Mandrile et al. (2023) examined SLB storage systems in electric ship propulsion, delineating current applications and future trends. Terkes et al. (2023) conducted a comprehensive review of the technical and financial uncertainties associated with SLBs in energy storage applications, evaluating factors influencing their performance.
In this study, an algorithm maximizing the annual revenue of a PV energy system was implemented by employing SLBs. The algorithm accounts for the variation in battery capacity due to aging, incorporating it into the calculations. Furthermore, it operates the decision-making mechanism based on dynamically changing energy sales prices and the energy output of the PV system. Annual profits obtained for different capacities were calculated, and the impact of capacity selection on operational revenues was examined.

II. Methodology

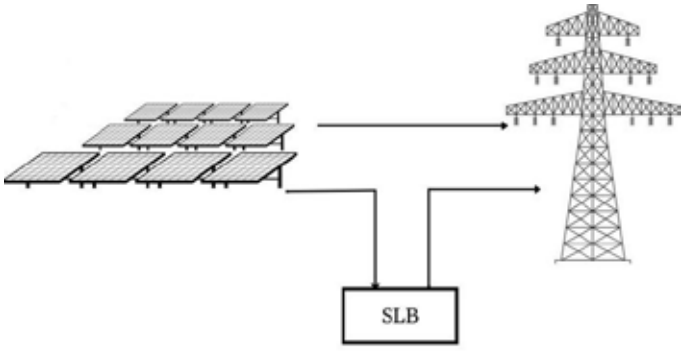


Fig. 1: System Definition

Utilizing a battery in conjunction with a PV system enables more effective management of the system. Battery usage provides flexibility in transferring energy to the grid. This flexibility allows for either supplying energy to the grid during peak pricing hours or maintaining reserve energy. Opting for a SLB instead of a new one yields both

economic and environmental advantages. In this study, a PV operating system is established as shown in Figure 1. The proposed model has been applied to the California region. In this model, the PV production was modeled to be 100 MW, and solar irradiance data were based on the California region.

The PV system can either directly sell energy to the grid or store it in batteries. This system utilizes an algorithm that maximizes the daily revenue from selling energy to the grid, taking into account battery costs and efficiencies. In doing so, the algorithm adapts to changes in battery capacity due to battery degradation.

Battery capacity degradation is caused by irreversible electrochemical side reactions and can be divided into calendar degradation and cycle degradation. Calendar degradation is related to time, temperature, and state of charge (SOC), while cycle degradation is caused by charge-discharge cycles. It is possible to measure the decrease in the capacity of the battery by the State of Health (SoH) value of the battery. The SoH of a battery indicates its overall health and is usually expressed as the ratio of the remaining capacity to the original capacity, as indicated below Ziyou et al. (2023):

$$\mathrm{SoH} = \frac{\mathrm{Q_{remain}}}{\mathrm{Q}} \tag{1}$$

To assess the SoH of a battery, the remaining capacity (Q_{remain}) must be calculated accurately. However, chemical degradations during battery use can complicate this calculation. In the literature, commonly used Arrhenius equations have been utilized for this purpose.

$$\mathrm{Q_{loss}} = \mathrm{A}.\,\mathrm{e}^{-\left(\frac{\mathrm{Ea+B.C_{rate}}}{\mathrm{R.T_{bat}}}\right)}.\,\mathrm{A_h}^{\mathrm{z}} \tag{2}$$

The coefficients in the Arrhenius equations have been adapted for the LiFePO4 battery used in this study, as shown in Eq. (3).

$$\mathrm{Q_{loss}} = 0.0032.\,\mathrm{e}^{-\left(\frac{15162-1516.\mathrm{C_{rate}}}{\mathrm{R.T_{bat}}}\right)}.\,\mathrm{A_h}^{0.824} \tag{3}$$

The objective function of the study is to maximize daily profit:

$$\mathrm{Profit} = \max \quad \sum_{t=0}^{N} \gamma(t).\left((P_{PV}(t) + P_{dis}(t) - P_{charge}(t)\right) \tag{4}$$

In Eqs. (4-10), $\gamma(t)$ signifies the price at which electricity is sold to the grid, $P_{PV}(t)$ denotes the power generated by the PV panel, $P_{dis}(t)$ represents the discharge power of the battery , $P_{charge}(t)$ indicates the charge power of the battery, $P_D(t)$ represents the power supplied to the grid, $\mathrm{P_{SBat}}$ is the SLB power, $\mathrm{SoC_{min}}$ indicates the minimum battery state of charge, $\mathrm{SoC_{max}}$ denotes the maximum battery SoC, and $\mathrm{SoH_{Sbat}(t)}$ represents the SoH of the SLB. The power balance can be written as follows;

$$P_{PV}(t) + P_{dis}(t) - P_{charge}(t) = P_D(t) \tag{5}$$

The constraint equations are provided in Eqs. (6-10), with the initial SoH value set at 80%.

$$\mathrm{SoC_{min}} \leq \mathrm{SoC(t)} \leq \mathrm{SoC_{max}} \tag{6}$$

$$\mathrm{P_{SBat}} \leq \mathrm{P_{PV}} \tag{7}$$

$$0 \leq \mathrm{P_{dis}(t)} \leq \mathrm{P_{SBat}} \tag{8}$$

$$0 \leq \mathrm{P_{charge}(t)} \leq (\mathrm{P_{PV}(t)}.\eta) \tag{9}$$

$$\text{-}\mathrm{P_{SBatlim}} \leq \mathrm{P_{SBat}(t)} \leq \mathrm{P_{SBatlim}} \tag{10}$$

These equations are used to increase the daily profit and thus the overall project revenue over its lifespan. The method to increase the profit from the daily energy sales of the PV system is by always being able to sell energy at the highest price. Therefore, during periods of low energy production or when the grid energy purchase price is low, if the battery is empty, it first charges the battery. Once the battery is charged and if energy production continues, it then supplies energy to the grid at the energy sale price for that hour. However, there are certain limitations to achieving this. When transferring energy from the battery to the grid, the battery is not fully discharged, as this increases the aging of the battery and leads to a shorter overall project lifespan. Therefore, the Depth of Discharge (DoD) value is limited to 0.8. Furthermore, to both extend the battery's lifespan and slow down the capacity degradation with each cycle, the battery charge-discharge rate (C_{rate}) is kept constant at 0.5. Additionally, since

battery aging varies with temperature, the battery temperature is assumed to be constant at 22 degrees Celsius. Moreover, the energy stored in the battery depends on its capacity, so using a larger battery can result in higher profits. In this study, the annual profit of the PV system has been calculated for battery-less systems and SLB systems with capacities of 250 MW and 500 MW.

III. Results and discussions

An optimization model based on the economic analysis of using secondary batteries in a PV plant has been proposed. The aim is to maximize daily profit. Additionally, the model has been tested in Matlab. The batteries used in this study have 80% SoH project initial values as batteries that are re-evaluated for another application after being used in one application. The initial production capacities of the compared batteries were taken as 250 and 500 MWh, respectively. Accordingly, when the batteries reached capacities of 200 and 400 MWh, they began to be utilized for the solar system as their second life. The profit obtained varies depending on the energy stored in the batteries. Batteries with different capacities yield different levels of revenue. Additionally, a battery undergoes some capacity loss after each use. Therefore, the amount of energy stored in each cycle gradually decreases over the project's lifetime. This demonstrates that the profit obtained is directly related to the SoH of the battery. Figure 2 illustrates the variation in SoH values of the two batteries used in this application over the operation of one year.

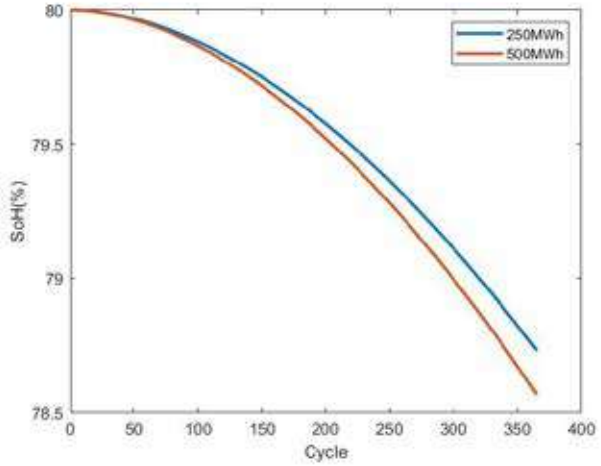


Fig. 2: SoH change of SLB's during Operation

According to the simulation conducted based on Equation 3, the battery with a larger capacity has experienced more degradation under the same conditions. In the calculations based on the new capacity values of the batteries for each cycle, the dynamic change in the energy sales price per hour has also been taken into account. The energy sales value has been obtained from actual data from California Grid status (2024). To maximize the profit from daily energy sales, decisions must be made regarding the direction of energy flow from the PV system to the grid and from the battery to the grid during specific time intervals. This decision depends on the energy price and the production values of the PV system. While the battery is charged during intervals when the PV system generates minimum revenue from energy sales, energy should be transferred from the battery to the grid during intervals with the highest energy prices. The algorithm for this study was developed in Matlab, and systems with no battery and systems with batteries of different capacity values were compared. Figure 3 presents the annual revenue values obtained from these systems.

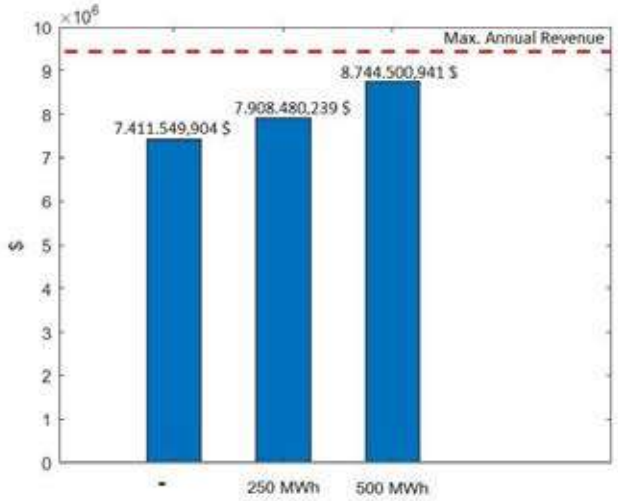


Fig. 3: Annual revenues based on battery capacities

The annual maximum revenue that can be achieved during the operation of a 100 MW PV system, as demonstrated in this study, amounts to $9,431,560. However, this value can only be realized if a battery large enough to store all of the PV system's energy production is utilized. The values pertaining to the study are presented in Table 1.

Tab.1: The parameter values

	System Without Battery	**250 MWh SLB System**	**500 MWh SLB System**
Initial SoH	**-**	%80	%80
Capacity value at the beginning of the second life project	**-**	200 MWh	400 MWh
Crate	**-**	0.5C	0.5C
DoD	**-**	%80	%80
Total Annual Revenue	7411549,904 $	7908480,239 $	8744500,941 $

When the battery with an initial capacity of 250 MWh is employed for the second life in this application, it yields an additional annual profit of $496,930.335 compared to the battery-less system. Conversely, employing a 500 MWh SLB yields $1,332,951.037 more profit than the battery-less system.

IV. Conclusions

This study implemented an algorithm to maximize annual profits of a PV system by integrating SLBs for grid energy transfer flexibility. Dynamic energy price variations and battery aging effects were considered. Results show higher profits with increased battery capacity: a 500 MWh battery led to a 17.9% increase compared to battery-less systems, while a 250 MWh battery resulted in a 6.7% rise. The utilization of a 500 MWh battery revealed that 92% of the maximum revenue achievable by operating this PV system with a sufficiently large battery was obtained. Integrating SLBs enhance operational revenues.

References

Amit K., “The spiraling environmental cost of our lithium battery addiction”, [Online]. Available: https://www.wired.com/story/lithium-batteries-environment-impact/

European Council,” The 2030 climate and energy framework”, [Online]. Available: https://www.consilium.europa.eu/en/policies/climate-change/

F. Mandrile, M. Pastorelli, S. Musumeci, I. A. Urkiri and A. Remirez, "Second Life Management From Battery Storage System of Electric Waterborne Transport Applications: Perspectives and Solutions," in *IEEE Access*, vol. 11, pp. 35122-35139, 2023, doi: 10.1109/ACCESS.2023.3265168.

‘’Grid Status’’ [Online]. Available: https://www.gridstatus.io/graph/lmp?iso=caiso&date=2024-01-01

K. Preusser, W. Wei and A. Schmeink, "Modelling Second-Life Batteries as the Energy Storage System for EV Charging Stations," *2022 IEEE International Conference on Communications, Control, and Computing Technologies for Smart Grids (SmartGridComm)*, Singapore, Singapore, 2022, pp. 199-205, doi: 10.1109/SmartGridComm52983.2022.9961054.

Lopez ´ Al, Ramírez-Díaz A, Castilla-Rodríguez I, Gurriar´ an J, Mendez-Perez JA. Wind farm energy surplus storage solution with second-life vehicle batteries in isolated grids. Energy Policy 2023;173:113373. https://doi.org/10.1016/j.enpol.2022.113373.

Musa Terkes, Alpaslan Demirci, ErdinGokalp,An evaluation of optimal sized second-life electric vehicle batteries improving technical, economic, and environmental effects of hybrid power systems,Energy Conversion and Management,Volume 291,2023,117272,ISSN 0196-8904,https://doi.org/10.1016/j.enconman.2023.117272.

O. Hegazy, M. A. Monem, P. Lataire and J. Van Mierlo, "Modeling and analysis of a hybrid PV/Second-Life battery topology based fast DC-charging systems for electric vehicles," *2015 17th European Conference on Power Electronics and Applications (EPE'15 ECCE-Europe)*, Geneva, Switzerland, 2015, pp. 1-11, doi: 10.1109/EPE.2015.7311727.

Ziyou Song, Shuo Feng, Lei Zhang, Zunyan Hu, Xiaosong Hu, Rui Yao,Economy analysis of second-life battery in wind power systems considering battery degradation in dynamic processes: Real case scenarios,Applied Energy,Volume 251,2019,113411, ISSN 0306-2619,https://doi.org/10.1016/j.apenergy.2019.113411.

Predicting the Remaining Useful Life of Lithium-Ion Batteries Using Machine Learning Algorithms

[1*]Cafer Budak
[1] Dicle University, The Faculty of Engineering, Electrical and Electronics Engineering, Sur/Kıtıbıl, Diyarbakır, 21000, Türkiye

* E-mail:cafer.budak@dicle.edu.tr

Abstract
This research investigates the application of machine learning algorithms to estimate the remaining useful life (RUL) of lithium-ion batteries. Utilizing data from the NASA Ames Prognostics Center, the Random Forest Regressor algorithm demonstrated high accuracy, achieving an R^2 value of 0.97 and an RMSE of 232. The analysis identified voltage load as the key predictor of battery life, and higher ambient temperatures were found to accelerate capacity degradation. These findings underscore the potential of machine learning in optimizing battery performance and reducing maintenance costs, ensuring efficient and cost-effective energy storage systems.

Keywords: Battery, Remaining Useful Life, Machine Learning, Random Forest, Energy Storage

I. Introduction

Renewable energy sources, such as solar and wind, are essential for reducing environmental issues caused by fossil fuels and achieving a sustainable energy future. However, their intermittent nature necessitates the use of energy storage systems to ensure a stable and reliable energy supply. Lithium-ion batteries, known for their high energy density and long lifespan, are commonly used in these systems. Over time, their performance degrades, making accurate predictions of their remaining useful life (RUL) critical for efficiency and reliability. Traditional methods often fall short in predicting battery RUL, but advancements in machine learning have significantly improved accuracy. Machine learning algorithms can process large datasets to make detailed and precise predictions. Various studies have employed different machine learning techniques for RUL prediction, highlighting the potential of these methods. Long et al. (2013) enhanced an autoregressive model with particle swarm optimization, while Chen et al. (2018) used a permutation entropy-based approach. Nuhic et al. (2013) applied data-driven methods, and Wang et al. (2019) used support vector regression with artificial bee colony optimization. Saha and Goebel (2008) utilized Bayesian techniques, and Liu et al. (2015) developed a framework for health indicator extraction. Wu et al. (2016) employed feedforward neural networks, and Shi and Chehade (2021) used LSTM networks for degradation analysis. Li et al. (2020) proposed an LSTM NN, and Liu et al. (2023) optimized it with an improved sparrow search algorithm. Youness and Aalah (2023) focused on explainable AI, while Li and Pelegri (2021) considered the entire charging and discharging process. Wang et al. (2023) devised a hybrid technique integrating statistical models and monitoring data patterns, and Ansari et al. (2022) combined RNN with particle swarm optimization. Wu and Lu (2023) introduced a method combining KPCA, ICEEMDAN, WOA, and ELM.
This study examined machine learning algorithms for predicting battery RUL and developed a model considering various performance factors. The Extra Tree Regressor algorithm's performance was highlighted, demonstrating the importance of machine learning in battery technology and energy storage systems.

II. Material and Method

Random Forest:

Random forest regression is a supervised machine learning algorithm that employs an ensemble of decision trees to predict continuous target variables. It utilizes the bagging method to create individual decision tree models by selecting random subsets of the training data. These smaller models are then combined to form the random forest model, which generates a single predicted value. This approach reduces variance and enhances accuracy by aggregating predictions from multiple decision trees (Li et al., 2012).

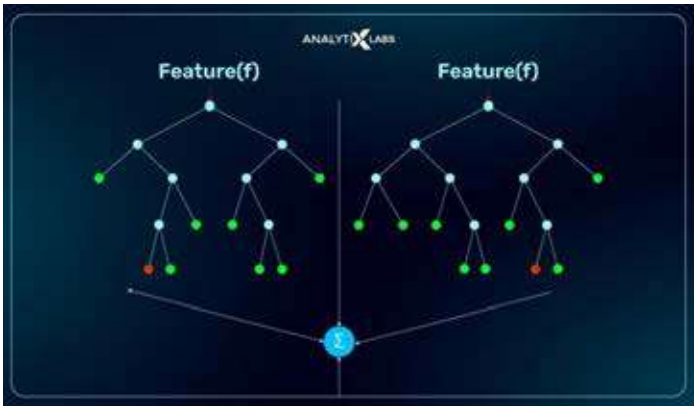


Fig. 1: Illustration of the general structure of the random forest model

When constructing the random forest regression model, variables representing potential features related to the results should be selected. The model size, number of trees, and depth are adjusted. After setting the parameters, the model is trained on the dataset.

Principle and Characteristics of Random Forest Operation:
Random forests are defined as a collection of decision trees, each generated using an independent and identically distributed random vector $\ominus_k$. Each tree builds a classifier $h(x,\ominus_k)$ by voting for the most popular class on input x. After k iterations, the final prediction is made by majority voting among the classifiers $\{h_1(x), h_2(x), \dots h_k(x)\}$:

$$H(x) = argmax \sum_{i=1}^{k} I(h_i(x) = Y)$$

In this equation (1), $H(x)$ represents the aggregated classification model, h_i is an individual decision tree, Y is the output class, and $I(.)$ is an indicator function. For each input variable, every tree in the forest casts a vote to determine the best classification outcome. This process is illustrated in Figure 1.

The margin function is defined as follows (Li et al., 2012):

$$mg\ (X,Y) = av_k I(h_k(X) = Y) - max_{\ j \neq Y} av_k I(h_k(X) = j)$$

Higher margin values indicate better classification accuracy and confidence.

Dataset:
The dataset from NASA Ames PCoE involved lithium-ion batteries subjected to various tests, including charging, discharging, and Electrochemical Impedance Spectroscopy at different temperatures. Experiments concluded when the batteries reached the end-of-life (EOL) criteria, defined as a 30% reduction in rated capacity (from 2 Ah to 1.4 Ah).

III. Analysis

The discharge parameters of a battery over time, displaying voltage, current, current load, and temperature measurements on the time axis. As the battery discharges, voltage decreases while current and temperature increase over time. The current load starts at a high value, remains constant for a while, and then rises again. These graphs provide information about the battery's performance by presenting various parameters related to the discharge process.
Figure 2 shows the capacity degradation of different batteries at different ambient temperatures. The capacity of the batteries decreases as the number of discharge cycles increases. Battery-29 has the highest capacity, while Battery-07 has the lowest. Battery-29 degrades faster than the other batteries, while Battery-07 degrades slower. The graph suggests a relationship between ambient temperature and battery capacity degradation, with higher ambient temperatures leading to faster degradation.

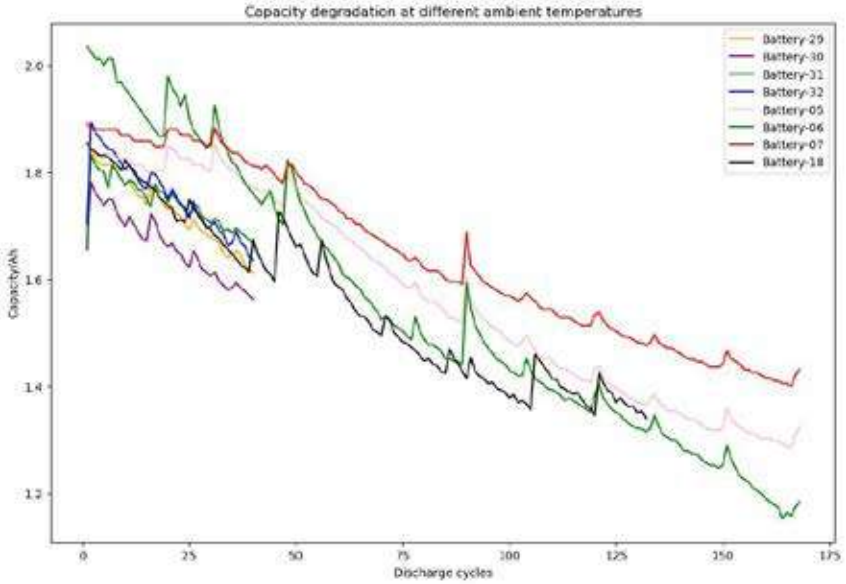


Fig. 2: Capacity degradation of different batteries at different ambient temperatures

Figure 3 compares the prediction results obtained with different machine learning methods and the proposed method.

Model	Adjusted R-Squared	R-Squared	RMSE	Time Taken
RandomForestRegressor	0.972413	0.972417	232.791	20.1087
BaggingRegressor	0.967671	0.967676	252.008	72.9651
XGBRegressor	0.964906	0.964911	262.563	7.14527

Fig. 3: Farklı makine öğrenmesi ve önerilen yöntem ile elde edilen tahmin sonuçlarının karşılaştırılması

The study uses RMSE (equation 3) and R^2 (equation 4) as primary performance metrics. RMSE measures the average magnitude of prediction errors, calculated as the square root of the mean squared differences between predicted and actual values, and is expressed in the same units as the predicted variable. R^2 assesses the model's ability to explain data variability, with values closer to 1 indicating a better fit and values near 0 indicating poor predictive power.

$$RMSE = \sqrt{\frac{\sum_{i=1}^{n}(y_i^{pre} - y_i^{exp})^2}{n}}$$

and

$$R^2 = \sqrt{\frac{\sum_{i=1}^{n}(y_i^{pre} - y_i^{exp})^2}{\sum_{i=1}^{n}(y_i^{exp} - \bar{y})^2}}$$

The importance ranking of features in Figure 4 shows that Voltage_load has the highest importance, while Current_measured has the lowest importance. This indicates that voltage load is the most critical factor in predicting battery performance. The values are listed below:

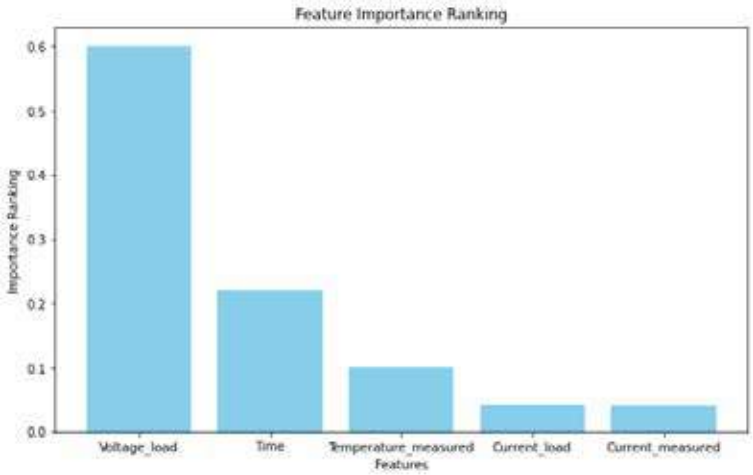


Fig. 4: Importance ranking of features in the dataset

IV. Results and discussions

This study applied machine learning algorithms to predict the remaining useful life (RUL) of lithium-ion batteries using data from the NASA Ames Prognostics Center of Excellence. The Random Forest Regressor algorithm outperformed other models, achieving an R^2 value of 0.97 and an RMSE of 232, demonstrating its high accuracy and low error rates. The analysis highlighted voltage load as the most critical factor in predicting battery performance, followed by time, measured temperature, load current, and measured current. Additionally, higher ambient temperatures were found to accelerate battery capacity degradation, emphasizing the importance of temperature control in battery management. Machine learning algorithms offer significant potential for optimizing battery technology and energy storage systems by improving performance and reducing maintenance costs. The Random Forest Regressor's success in accurately predicting battery life underscores its practical applicability in real-world scenarios. By ensuring timely battery replacements and minimizing unnecessary maintenance, these algorithms can enhance the efficiency and safety of energy storage systems. Future research should validate these findings with diverse datasets and explore the real-time performance of these algorithms in practical applications, broadening their impact on battery technology and energy storage solutions.

V. Conclusions

This study highlights the successful use of machine learning algorithms, particularly the Random Forest Regressor, in predicting the remaining useful life (RUL) of lithium-ion batteries. Voltage load and ambient temperature were identified as key factors affecting battery life. Applying these algorithms improves energy storage system reliability and efficiency, enabling timely battery replacements and reducing maintenance costs.

Acknowledgements
This research was not supported by any organization.

References

Long, B., Xian, W., Jiang, L., & Liu, Z. (2013). An improved autoregressive model by particle swarm optimization for prognostics of lithium-ion batteries. *Microelectronics Reliability*, *53*(6), 821-831.

Chen, L., Xu, L., & Zhou, Y. (2018). Novel approach for lithium-ion battery on-line remaining useful life prediction based on permutation entropy. *Energies*, *11*(4), 820.

Nuhic, A., Terzimehic, T., Soczka-Guth, T., Buchholz, M., & Dietmayer, K. (2013). Health diagnosis and remaining useful life prognostics of lithium-ion batteries using data-driven methods. *Journal of power sources*, *239*, 680-688.

Wang, Y., Ni, Y., Lu, S., Wang, J., & Zhang, X. (2019). Remaining useful life prediction of lithium-ion batteries using support vector regression optimized by artificial bee colony. *IEEE Transactions on Vehicular Technology*, *68*(10), 9543-9553.

Saha, B., & Goebel, K. (2008, March). Uncertainty management for diagnostics and prognostics of batteries using Bayesian techniques. In *2008 IEEE aerospace conference* (pp. 1-8). IEEE.

Liu, D., Zhou, J., Liao, H., Peng, Y., & Peng, X. (2015). A health indicator extraction and optimization framework for lithium-ion battery degradation modeling and prognostics. *IEEE Transactions on Systems, Man, and Cybernetics: Systems*, *45*(6), 915-928.

Wu, J., Zhang, C., & Chen, Z. (2016). An online method for lithium-ion battery remaining useful life estimation using importance sampling and neural networks. *Applied energy*, *173*, 134-140.

Shi, Z., & Chehade, A. (2021). A dual-LSTM framework combining change point detection and remaining useful life prediction. *Reliability Engineering & System Safety*, *205*, 107257.

Li, P., Zhang, Z., Xiong, Q., Ding, B., Hou, J., Luo, D., & Li, S. (2020). State-of-health estimation and remaining useful life prediction for the lithium-ion battery based on a variant long short-term memory neural network. *Journal of power sources*, *459*, 228069.

Liu, Y., Sun, J., Shang, Y., Zhang, X., Ren, S., & Wang, D. (2023). A novel remaining useful life prediction method for lithium-ion battery based on long short-term memory network optimized by improved sparrow search algorithm. *Journal of Energy Storage*, *61*, 106645.

Youness, G., & Aalah, A. (2023). An explainable artificial intelligence approach for remaining useful life prediction. Aerospace, 10(5), 474.

Li, C., & Pelegri, A. A. (2021). A Data-Driven Framework to Predict Lithium-Ion Battery Cell Imbalance for Real-Time Battery Management Systems. *Energies*, *14*(24), 8492.

Wang, M., Xiang, G., Cui, L., Zhang, Q., & Chen, J. (2023). Remaining useful life distribution prediction framework for lithium-ion battery fused prior knowledge and monitoring data. *Measurement Science and Technology*, *34*(12), 125108.

Ansari, S., Ayob, A., Lipu, M. H., Hussain, A., & Saad, M. H. M. (2022). Particle swarm optimized data-driven model for remaining useful life prediction of lithium-ion batteries by systematic sampling. *Journal of Energy Storage*, *56*, 106050.

Wu, W., & Lu, S. (2023). Remaining useful life prediction of lithium-ion batteries based on data preprocessing and improved ELM. *IEEE Transactions on Instrumentation and Measurement*.

A novel SOFC based multi-generation system with recompression sCO_2-BC, reheat tCO_2-RC, HDH unit and H_2 production

Gamze Soyturk, *Onder Kızılkan
Isparta University of Applied Sciences, Faculty of Technology, Department of Mechanical Engineering, 32200, Isparta, Türkiye

*E-mail: onderkizilkan@isparta.edu.tr

Abstract
This abstract introduces a novel Solid Oxide Fuel Cell (SOFC)-based multi-generation system engineered to address energy generation challenges while facilitating hydrogen (H_2) production. The system incorporates key components, including a recompression supercritical carbon dioxide Brayton Cycle (sCO_2-BC), a reheat transcritical carbon dioxide Rankine cycle (tCO_2-RC), a humidification and dehumidification (HDH) unit, and a hydrogen production subsystem. Integrating recompression, sCO2-BC optimizes energy recovery by harnessing waste heat, thereby bolstering the system's overall efficiency and power output. Complementing this, the reheat tCO_2-RC further enhances efficiency by utilizing waste heat from the sCO_2-BC to reheat the carbon dioxide working fluid, ensuring maximum energy utilization. Moreover, the inclusion of an HDH unit offers a novel approach to water management within the system. Additionally, this study presents parametric studies to examine the effects of some important parameters on system performance.

Keywords: SOFC, sCO_2-BC, HDH, tCO_2-RC, power generation, H_2 production

I. Introduction

The rising global energy demands, alongside escalating environmental concerns, have spurred a quest for innovative, efficient, and environmentally friendly energy conversion technologies. Integrating such technologies into energy conversion systems promises to optimize efficiency while simultaneously curbing adverse environmental impacts (Chitgar et al., 2019). Fuel cells emerge as a promising solution for energy conversion, given their capacity to meet safety standards, sustainability objectives, and environmental advantages. Among the various types of fuel cells, the Solid Oxide Fuel Cell (SOFC) stands out as an emerging technology suitable for both small and large-scale power plants (Gholamian and Zare, 2016). The high operating temperature range of SOFCs (600-1000 °C) enables waste heat utilization by other thermodynamic cycles, fostering the development of hybrid power systems that enhance overall performance (Zhong et al., 2021). There has been a noticeable surge in research attention towards SOFC-based integrated systems in recent years. One such study (Wang et al.,2021) proposed a trigeneration system, utilizing an SOFC as the topping cycle and a CO_2-based Rankine cycle with an LNG cold energy recovery system as the bottoming cycle. Parametric analyses were conducted to gauge the effects of crucial system parameters. In another study (Eveloy et al., 2016), a SOFC-assisted organic Rankine cycle (ORC) was suggested to enhance energy production rate and efficiency. Thermodynamic and economic analyses were carried out for six different working fluids, with toluene exhibiting the highest efficiency. Furthermore, a combined SOFC-based system was proposed for synchronous electricity and distilled water generation (Chitgar et al., 2019). This system integrated a Kalina cycle powered by waste heat from the SOFC alongside additional components such as a thermoelectric generator and a reverse osmosis desalination unit. Another investigation (Gholamian & Zare, 2016) delved into an integrated system comprising an Organic Rankine cycle and a Kalina cycle assisted by SOFC. Analyses were conducted regarding energy, exergy, and environmental impact, particularly focusing on carbon dioxide emissions. Additionally, research efforts have explored combined multi-generation systems for cooling and energy generation assisted by SOFC (Zhong et al., 2021). This system involved a supercritical CO_2 cycle for power generation and an ejector refrigeration cycle for cooling purposes. Another study (Alsarraf et al., 2022) proposed a SOFC-integrated multi-generation system with supercritical and transcritical CO_2 cycles, an ORC, and LNG as the heat sink. System performance was evaluated regarding energy and exergy, revealing a notable capture of carbon emissions and high SOFC efficiency. This study aims to design and develop a novel Solid Oxide Fuel Cell (SOFC) based multi-generation system that integrates various components, including recompression supercritical carbon dioxide Brayton cycle (sCO_2-BC), reheat transcritical carbon dioxide Rankine cycle (tCO_2-RC), a Humidification-Dehumidification (HDH) unit, and hydrogen (H_2) production.

II. System Description

Fig. 1 demonstrates the poly-generation system that utilizes an SOFC as the primary driving force. The proposed novel Solid Oxide Fuel Cell (SOFC)-based multi-generation system is designed to revolutionize energy generation, carbon emissions reduction, and hydrogen production. At its core, the system integrates advanced components to optimize efficiency, flexibility, and sustainability. The SOFC serves as the primary power generation technology, offering high efficiency and fuel flexibility. It operates by electrochemically converting fuel into electricity with minimal emissions. The Recompression sCO_2-BC enhances overall system efficiency by recovering waste heat from various components and increasing the power output of the cycle. This process involves compressing supercritical carbon dioxide to high pressures and recompression for further heat recovery. The Reheat tCO_2-RC complements the sCO_2-BC by utilizing waste heat from the latter to reheat the carbon dioxide working fluid. This reheating process optimizes thermal efficiency and enhances power generation capacity, contributing to overall system performance.

The HDH unit enables the direct conversion of carbon dioxide and water into hydrogen and carbon monoxide at high temperatures. This process utilizes the heat generated by the SOFC and other system components to drive the chemical reactions, facilitating hydrogen production. The integration of the HDH unit with the SOFC-based multi-generation system enables efficient and sustainable hydrogen production.

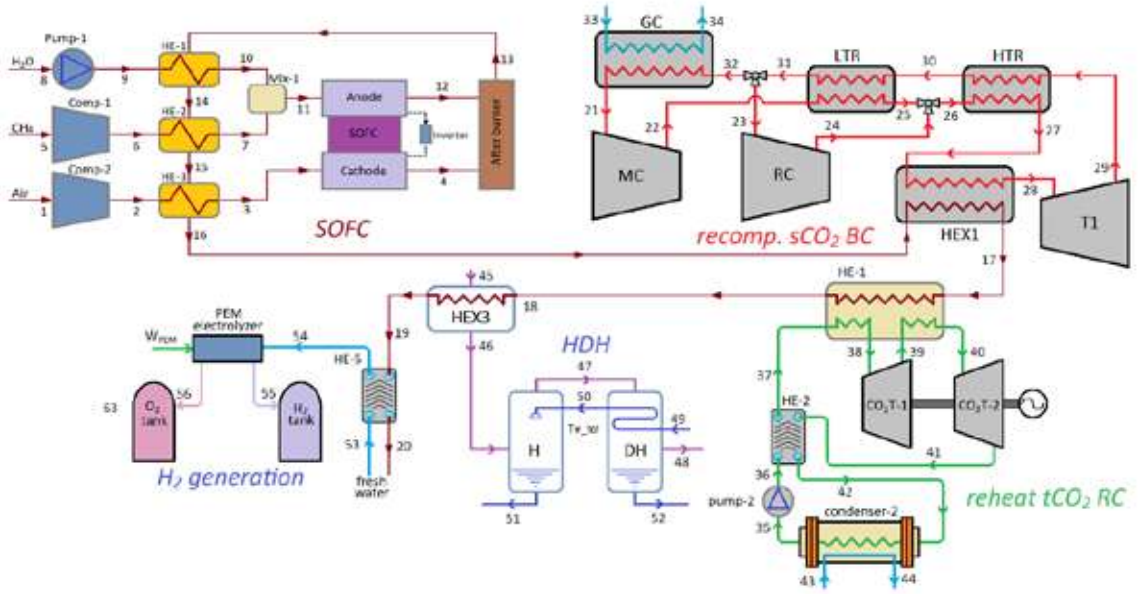


Fig. 1: Schematic representation of the SOFC-based poly-generation system

III. Analysis

This subchapter introduces a detailed definition of the thermodynamic methodology utilized in this paper. First and second law analyses are conducted using the EES (Engineering Equation Software) program for the system's performance evaluation. In this research, the thermodynamic analysis is made under the following assumptions using the design parameters.

- All devices operate under steady-state conditions.
- Change in kinetic and potential energies is negligible.
- The pressure losses and heat losses in the system are disregarded.
- Turbines and pumps are assumed to operate with isentropic efficiency.

For the thermodynamic assessment of the system, the mass, energy, and exergy conservation equations for the steady-state condition can be written as follows:

$$\sum \dot{m}_{in} = \sum \dot{m}_{out} \quad (1)$$

$$\dot{Q} - \dot{W} = \sum \dot{m}_{out} h_{out} - \sum \dot{m}_{in} h_{in} \quad (2)$$

where, $\dot{m}$ is the mass flow rate, $\dot{W}$ represents the power rate, $\dot{Q}$ indicates the heat transfer rate, and h is the specific enthalpy.

V. Results and discussions

The basic goal of this study is to investigate the performance of a novel SOFC-based multi-generation system incorporating recompression sCO_2-BC, reheat tCO_2-RC, an HDH unit, and H_2 production. A zero-dimensional analysis of the system designed for this purpose was performed using the EES software program. Fig. 2 shows the power generation/heat output in the hybrid system. The figure shows that the maximum power is at SOFC with 875.8 kW. This is followed by sCO_2 with 207.9 kW and tCO_2 with 154.7 kW. On the right side of the graph, the amounts of oxygen, hydrogen, and distilled water produced are seen. As seen in the figure, 15.8×10 kg/h distilled water, 10.8 kg/h O_2, and 1.4 kg/h H_2 were produced.

To ascertain the impact of crucial system parameters on performance, parametric studies were conducted by altering SOFC current density and operating temperature. Figure 3 illustrates the influence of current density on SOFC cell voltage and efficiency. It is evident from the graph that as the current density varies from 5000 to 10000 A/m^2, both the cell voltage and SOFC efficiency decrease. This decline occurs due to the heightened voltage losses accompanying increased current density, leading to a reduction in cell voltage. In Figure 3, the relationship between current density and net generated power of the SOFC, as well as the mass flow rate of fuel, is depicted. The graph illustrates that net power rises with increasing current density; nevertheless, beyond 8400 A/m^2, it begins to decline. This juncture can be identified as the optimal current density, where power generation peaks under the specified

conditions. On the right side of the graph, the mass flow rate of fuel is plotted against current density, revealing a linear increase in fuel rate as current density increases.

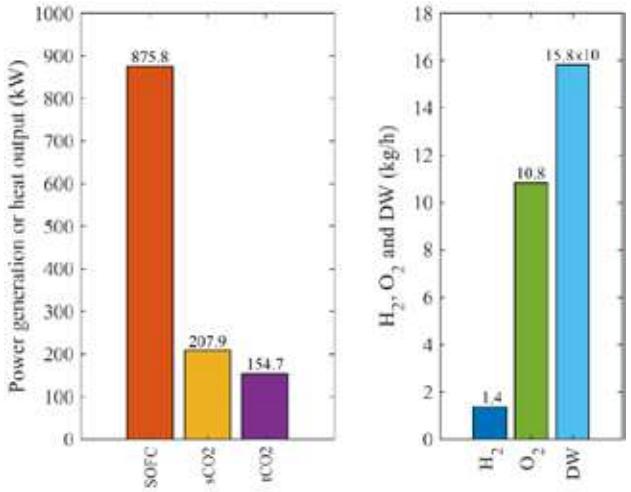


Fig. 2: Useful outputs of the SOFC-based poly-generation system

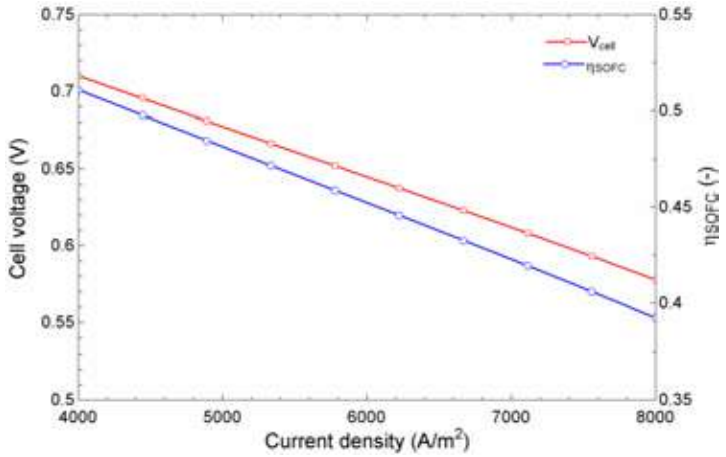


Fig. 3: Effect of current density on the cell voltage and SOFC efficiency

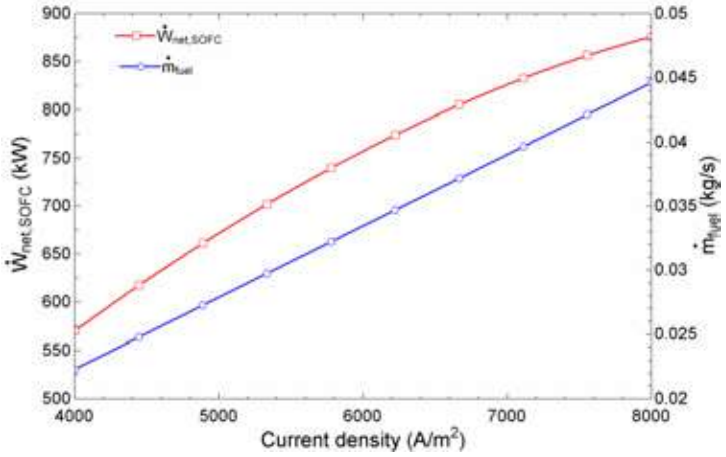


Fig. 4: Effect of current density on the SOFC net power and mass flow rate of the fuel

Fig. 5 shows the effect of SOFC operating temperature on net power production and energy efficiency. As seen in the figure, when the SOFC operating temperature is increased from 700℃ to 1000℃, SOFC net power decreases, and tCO_2 and sCO_2 net power increases slightly. Additionally, as seen in the figure, as the SOFC operating temperature increases, the efficiency obtained from the subsystems decreases. Fig. 6 shows the effect of SOFC operating temperature on H_2, O_2, and purified water production. As seen in the figure, as SOFC operating temperature increases, purified water production increases, and O_2 and H_2 production decreases.

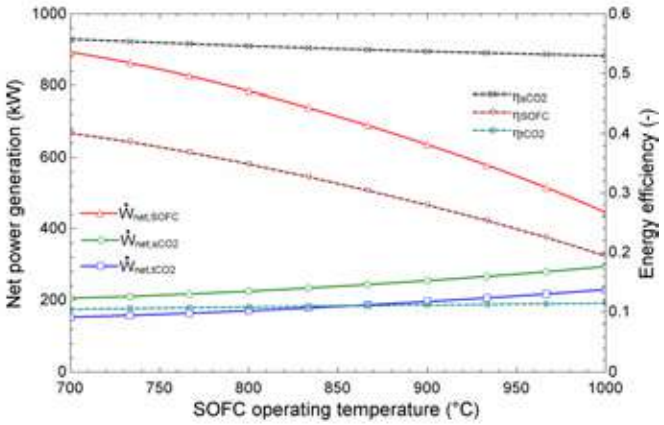


Fig. 5: Effect of SOFC operating temperature on the net power generation and energy efficiency

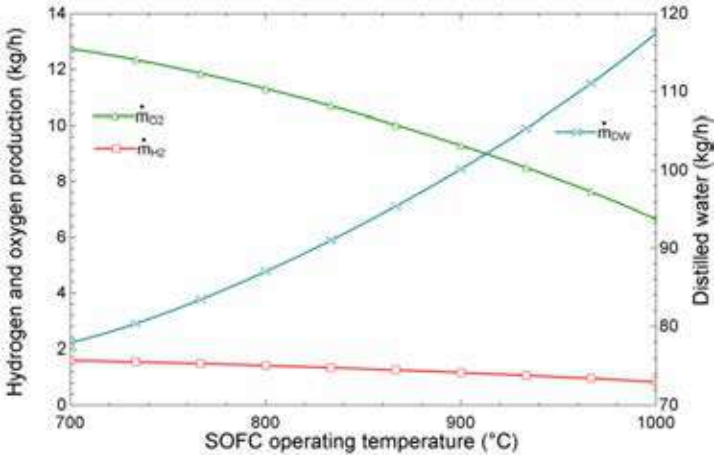


Fig. 6: Effect of SOFC operating temperature on the H_2, O_2, and distilled water production

V. Conclusions

The primary aim of this study is to design and develop a new SOFC-based multi-generation system that integrates various components, including recompression sCO_2-BC, reheat tCO_2-RC, an HDH unit, and H_2 generation. According to the results of the analysis, the net powers obtained from SOFC, sCO_2, and tCO_2 subsystems are 875.8 kW, 207.9 kW, and 154.7 kW, respectively. Additionally, the produced H_2, O_2, and purified water flow rates were calculated as 15.8×10 kg/h, 10.8 kg/h, and 1.4 kg/h, respectively. In the second stage of the study, parametric studies were conducted to examine the effects of some important variables on system performance. According to the parametric analysis results, as current density increases, cell voltage and SOFC efficiency decrease, and SOFC net power and fuel mass flow rate increase.

References

N. Chitgar, M. A. Emadi, A. Chitsaz, and M. A. Rosen, "Investigation of a novel multi-generation system driven by a SOFC for electricity and freshwater production," Energy Convers. Manag., vol. 196, pp. 296–310, (2019).

E. Gholamian and V. Zare, "A comparative thermodynamic investigation with environmental analysis of SOFC waste heat to power conversion employing Kalina and Organic Rankine Cycles," Energy Convers. Manag., vol. 117, pp. 150–161, (2016).

L. Zhong, E. Yao, H. Zou, and G. Xi, "Thermo-economic-environmental analysis of an innovative combined cooling and power system integrating Solid Oxide Fuel Cell, Supercritical CO_2 cycle, and ejector refrigeration cycle," Sustain. Energy Technol. Assessments, vol. 47, p. 101517, (2021).

H. Wang, Z. Yu, D. Wang, G. Li, and G. Xu, "Energy, exergetic and economic analysis and multi-objective optimization of atmospheric and pressurized SOFC based trigeneration systems," Energy Convers. Manag., vol. 239, p. 114183, (2021).

H. Wang, Z. Yu, D. Wang, G. Li, and G. Xu, "Energy, exergetic and economic analysis and multi-objective optimization of atmospheric and pressurized SOFC based trigeneration systems," Energy Convers. Manag., vol. 239, p. 114183, (2021).

V. Eveloy, W. Karunkeyoon, P. Rodgers, and A. Al Alili, "Energy, exergy and economic analysis of an integrated solid oxide fuel cell – gas turbine – organic Rankine power generation system," Int. J. Hydrogen Energy, vol. 41, no. 31, pp. 13843–13858, (2016).

J. Alsarraf, A. A. Alnaqi, and A. A. A. A. Al-Rashed, "Thermodynamic modeling and exergy investigation of a hydrogen-based integrated system consisting of SOFC and CO_2 capture option," Int. J. Hydrogen Energy, vol. 47, no. 62, (2022).

Thermal Performance of a Biogas-Fed Multi-generation Plant for Power, Cooling, and Hydrogen Generation with LNG Cold Energy Recovery

[1]Shoaib Khanmohammadi, [2]Gamze Soyturk, [2*]Onder Kizilkan
[1] Department of Mechanical Engineering, Kermanshah University of Technology, Kermanshah, Iran
[2] Isparta University of Applied Sciences, Technology Faculty, Department of Mechanical Engineering, Isparta/Türkiye

*E-mail: onderkizilkan@isparta.edu.tr

Abstract
This study examines the performance of a simulated poly-generation system through a parametric analysis, focusing on critical performance parameters' influence on system efficiency and outputs. The system integrates various subsystems, including a gas turbine unit, LNG turbine, sCO_2 and tCO_2 cycles, refrigeration cycle, and PEM electrolyzer for hydrogen production. Significant effects on net output power, energy efficiency, and output generation were observed by varying combustion chamber temperatures. Increasing combustion temperature led to improved system performance, enhancing energy efficiency and output generation. Evaluation of the system's second law performance highlighted the importance of combustion temperature in influencing exergy destruction rate and efficiency. These findings underscore the potential for enhancing poly-generation system performance through parameter adjustments, contributing to energy efficiency and sustainability advancements.

Keywords: Biogas, hydrogen, sCO_2 Brayton cycle, tCO_2 Rankine cycle, cooling

I. Introduction

Today, there are severe limitations in energy resources. The optimal use of available energy and optimizing energy systems are critical. On the other hand, using renewable energies and systems that produce diverse products can be beneficial in providing sustainable energy. Biomass energy converted to biogas can be a suitable source for gas turbines. Many studies have studied biomass fuels for biogas production and their use in gas turbines.

Zhang et al. (2019) studied a new system of cogeneration based on bio-energy to design and analyze a plant integrated with organic flash and carbon dioxide supercritical cycles. They applied energy, exergy, and exegeo-economic analyses and bi-objective and triple objective optimization on the proposed system. The results showed that the studied system has energy and exergy efficiency of 75.8% and 41.21%, with carbon dioxide emission of 0.518 t/kWh in its basic state. Moreover, the payback time was about 1.97 years with a net profit of 10.7 M$.

Hu et al. (2023) investigated a gas turbine and regasification of LNG for multi-generation purposes. Different subsystems were modeled in Matlab, and the suggested system was optimized. Calculations showed that with the change of pressure ratio between 6 and 18, the cooling could be decreased from 45 kW to 36 kW. It has also been reported that using artificial neural networks reduces the optimization time from 48 hours to 16 minutes.

Hai et al. (2024) investigated a multiple-production system using a gas turbine and hydrogen liquefaction process in another study. A Rankine cycle, a Rankine cycle with dual loop, an LNG regasification process, a PEM electrolyzer, and a Claud liquefaction cycle were used in this study. The result showed that recovery of LNG led to the consumed work in the liquefaction of about 7.96 kWh/kgH_2. Additionally, the optimization increased the total cost rate of about 10.98 $/h and an 18% improvement in hydrogen production.

Zhou et al. (2023) analyzed the use of biogas to set up a cogeneration system that generated electricity/cooling and recovered cold energy from liquefied natural gas. The integrated plant included an open Brayton cycle fed by biogas, a closed Bryton cycle, and an ejector-based refrigeration cycle employed to generate cooling. The optimization process applied to this system indicated that the energy and exergy efficiencies of 80.4% and 41.24% could be achieved. In the optimal state, the unit cost of the product was 10.07 $/GJ. As reported, the non-optimized plant's emission was 6091 kg/MWh, which, after optimization, reached 3913 kg/MWh of CO_2.

The application of geothermal energy, as well as the recovery of cold energy of LNG in a multiple production system of cooling, heating, electric power, and hydrogen, was carried out by Ebadollahi et al. (2019). The investigated system included different subsystems, each of which was added to the multiple production system to produce one of the products. The studied system obtained 1060 kW output power and 5.43 kg/h hydrogen generation. Thermal efficiency, exergy efficiency, and product unit cost were reported at 38.3%, 28.9%, and 347.9 $/GJ.

This study aims to comprehensively assess the thermal performance of a sophisticated multi-generation system fuelled by biogas, with a focus on power generation, cooling provision, and hydrogen production, while incorporating the recovery of cold energy from liquefied natural gas (LNG). The system under investigation integrates several key components, including a biogas power cycle, a recompression supercritical CO_2 Brayton cycle, a transcritical CO_2 Rankine cycle, an absorption refrigeration system, an LNG cold recovery cycle, and a hydrogen production unit. By examining the thermal dynamics and efficiency of each integrated component within the multi-generation system, this study aims to elucidate the overall effectiveness and potential of such a setup in harnessing energy resources and contributing to energy production paradigms.

II. System Layout and Performance Assessment

The proposed integrated poly-generation power system centers around a biogas cycle, as depicted in Figure 1. Comprising six subsystems, including a gas turbine cycle, a recompression sCO_2 Brayton cycle, a tCO_2 Rankine cycle, an LNG cycle for cold energy utilization, an absorption refrigeration cycle, and a hydrogen production unit, the framework is designed for multifaceted energy generation. Within the gas turbine cycle, the air is compressed by a compressor and directed to the combustion chamber, where it mixes with biogas—a blend of 60% methane (CH_4) and 40% carbon dioxide (CO_2)—for combustion (Safari and Dincer, 2019). The resulting high-temperature gas product, exiting the combustion chamber at 1246 °C, drives the gas turbine for power generation. The expanded gases then enter the recompression sCO_2 Brayton cycle, where they release energy to the compressed air after passing through a heat exchanger. Subsequently, CO_2 is compressed to a supercritical state, heated, and expanded in a turbine for power generation. In the tCO_2 power cycle, CO_2 undergoes compression, heating, and expansion processes facilitated by a pump, a CO_2 turbine, a condenser, an evaporator, and an internal heat exchanger. LNG is utilized to cool the CO2 stream to address condensation issues. Additionally, the cryogenic energy of LNG is harnessed through an LNG turbine before the LNG is directed to city pipelines for domestic use (Rejeb et al., 2022).

Exhaust gases heat the H_2O-LiBr solution in the generator, separating water vapor for refrigeration. The H_2O-LiBr absorption refrigeration cycle mirrors a vapor compression cycle. The H_2O-LiBr pair absorbs heat in the solution heat exchanger and then heats in the generator. Ammonia separation occurs, with a rectifier eliminating water content. Water vapor condenses in the condenser, expands via a valve, and extracts heat in the evaporator. It returns to the absorber, completing the cycle (Kizilkan et al., 2019). A PEM water electrolysis technique was chosen for hydrogen production for efficiency and environmental impact. Heated water enters the PEM unit, where electrolysis occurs, generating hydrogen and oxygen. Excess water is managed to regulate heat and maintain reactant concentration. Surplus power from the tCO_2 Rankine cycle supplies the electrical power needed (Soyturk et al., 2023).

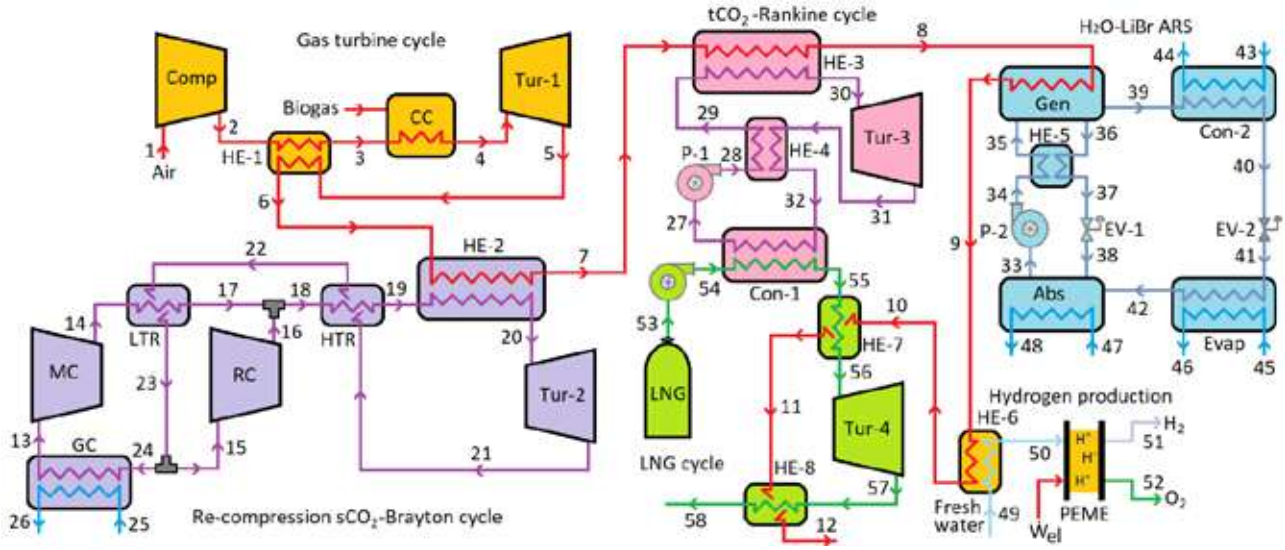


Fig. 1: Schematic depiction of the proposed system

The modeling process initiates with fundamental equations governing mass and energy conservation and then progresses to exergy analysis. The general mass balance, energy balance, and exergy balance equations for a steady-state control volume are expressed as (Cengel and Boles, 2015):

$$\sum \dot{m}_{i\ n} = \sum \dot{m}_{out} \tag{1}$$

$$\dot{Q} + \sum \dot{m}_{in} h_{in} = \dot{W} + \sum \dot{m}_{out} h_{out} \tag{2}$$

$$\dot{E}x_Q - \dot{E}x_W = \sum \dot{m}_{out} e_{out} - \sum \dot{m}_{in} e_{in} + T_0 \dot{S}_{gen} \tag{3}$$

In the above equations, ṁ denotes the mass flow rate, "in" and "out" stand for inlet and outlet points of the control volume, $\dot{Q}$ represents heat, $\dot{W}$ denotes work, h is the enthalpy, $\dot{E}x$ signifies the exergy rate, and $\dot{E}x_{dest}$ represents the rate of exergy destruction.

III. Result and Discussions

In this study, an analysis was conducted to evaluate the performance of a simulated system. Specifically, the study

focused on examining the general outputs of the modeled plant, including power generation and hydrogen production rates. According to the results of the analysis, the gas turbine unit emerges as the primary contributor to power generation, yielding a substantial output of 33233 kW. Additionally, the combined output from the LNG turbine, sCO_2, and tCO_2 cycles amounts to 6658.22 kW, while the refrigeration cycle generates 473.52 kW. Furthermore, the total net output power from the tCO_2 cycle is directed towards the PEM electrolyzer, resulting in a hydrogen production rate of 7.265 kg/h.

The exergy destruction rates were determined for various system components within the modeled system. The findings reveal that the combustion chamber exhibits the highest exergy destruction rate, accounting for 61% of the total exergy destruction rate, with a value of 27029 kW. Following closely, the GT compressor stands out as the second most significant contributor, with an exergy destruction rate of 3442 kW. Overall, the analysis underscores that the combustion chamber, GT compressor, and gas turbine collectively contribute to 75% of the total exergy destruction rate within the system.

A thorough exploration of system performance under varying parameters is essential for understanding its behavior. For this reason, the influence of critical performance parameters on system efficiency, exergy destruction rate, and outputs were investigated. Figure 2 illustrates how changes in combustion chamber temperature affect system performance as combustion chamber temperatures fluctuate from 900 °C to 1500°C. As the combustion chamber temperature rises, the net output power of all subsystems increases. Additionally, given the direct correlation between energy efficiency and total output power, elevating the combustion chamber temperature yields a notable enhancement in system energy efficiency.

Figure 3 further delineates shifts in the two primary outputs of the analyzed system. With rising combustion temperatures, both cooling generation and hydrogen production in the electrolyzer experience an uptick. Consequently, combustion temperature emerges as a pivotal parameter influencing outputs across all subsystems.

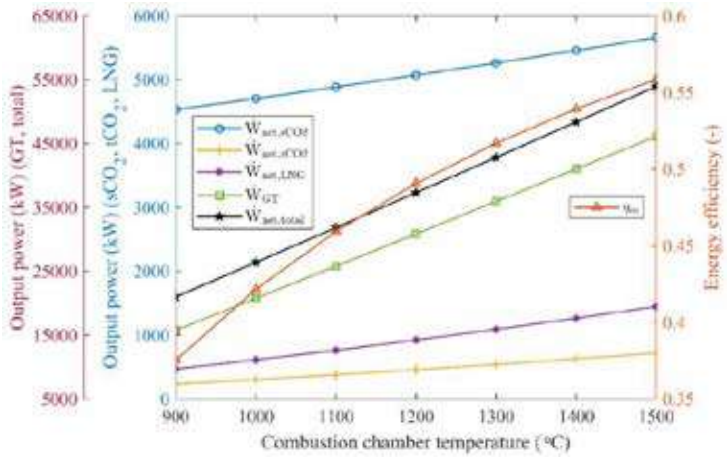


Fig. 2: Variation of power generation rates and efficiency with combustion chamber temperature

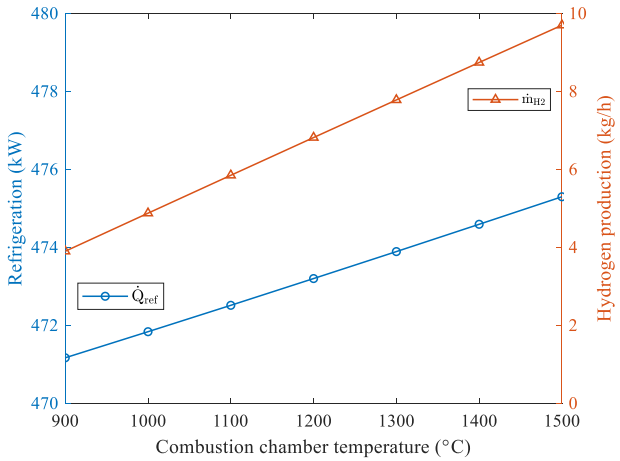


Fig. 3: Variation of cooling and hydrogen production rate with combustion chamber temperature

To assess the second law performance of the system, Figure 4 illustrates the exergy destruction rate and exergy efficiency. Elevating the combustion temperature from 900 °C to 1500 °C results in an increase in both the exergy destruction rate and efficiency. The heightened combustion temperature amplifies the exergy destruction rate owing to the highly reversible nature of the combustion chamber process. This increase stems from a widened difference between combustion air and gas product temperatures, leading to heightened entropy generation and exergy destruction rate. Furthermore, given the positive impact of enhanced combustion temperature on system output power, exergy efficiency also demonstrates improvement.

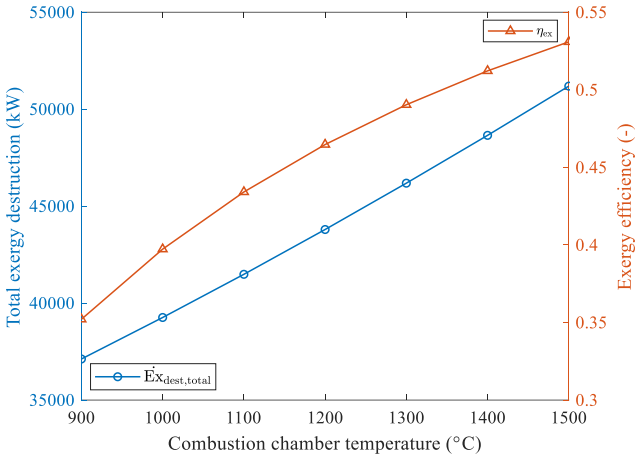


Fig. 4: Variation of total exergy destruction and exergy efficiency with combustion chamber temperature

V. Conclusions

This study evaluated the performance of a simulated system, focusing on its general outputs, such as power generation and hydrogen production rates. The gas turbine unit emerged as the primary power contributor, yielding 33233 kW. The combined output from other cycles totaled 6658.22 kW, with the refrigeration cycle generating 473.52 kW. The system's total net output power directed towards the PEM electrolyzer resulted in a 7.265 kg/h hydrogen production rate. Examination of exergy destruction rates highlighted the combustion chamber as the highest contributor, accounting for 61% of the total at 27029 kW. The GT compressor also exhibited a significant contribution at 3442 kW. Investigation into critical performance parameters, notably combustion chamber temperature, revealed notable improvements in system energy efficiency and output generation. These findings emphasize the significance of parameter adjustments in optimizing system performance, contributing to energy efficiency and sustainability advancements.

References

Cengel YA, Boles MA. Thermodynamics: an Engineering Approach. 2015. https://doi.org/10.1017/CBO9781107415324.004.

Ebadollahi M., Rostamzadeh H., Pedram M.Z, Ghaebi H., Amidpour M., Proposal and assessment of a new geothermal-based multi-generation system for cooling, heating, power, and hydrogen production, using LNG cold energy recovery, Renewable Energy, 135, 66-87, (2019)

Hai T., Alhaider M.M., Ghodratallah P., Singh P.K., Alhomayani F.M., Rajab H., Techno-economic-environmental study and artificial intelligence-assisted optimization of a multi-generation power plant based on a gas turbine cycle along with a hydrogen liquefaction unit, Applied Thermal Engineering, 237, 121660, (2024)

Hu Y., Badrawi S.I., Kumar J., Sabeh H.N., Alsenani T.R., Riaz F., Alkhalifah T., Alkhalaf S., Alturise F., Gas turbine-based system taking advantage of LNG regasification process for multi-generation purposes; Techno-economic-environmental analysis and machine learning optimization, Process Safety and Environmental Protection, 179, 10-26, (2023)

Kizilkan O., Khanmohammadi S., Saadat-Targhi M., Solar based CO2 power cycle employing thermoelectric generator and absorption refrigeration: Thermodynamic assessment and multi-objective optimization, Energy Conversion and Management, 200, 112072, (2019)

Rejeb O., Alirahmi S.M., Assareh E., Assad M.E.H., Jemni A., Bettayeb M., Ghenai C.,
Innovative integrated solar powered polygeneration system for green Hydrogen, Oxygen, electricity and heat production, Energy Conversion and Management, 269, 116073, (2022)

Safari F., Dincer I., Development and analysis of a novel biomass-based integrated system for multi-generation with hydrogen production, International Journal of Hydrogen Energy, 44(7), 3511-3526, (2019)

Soyturk G., Kizilkan O., Ezan M.A., Colpan C.O., PVT integrated hydrogen production with small-scale transcritical power cycle, Process Safety and Environmental Protection, 180, Pages 351-360, (2023)

Zhang X, Zeng R, Du T, He Y, Tian H, Mu K, Liu X., Li H., Conventional and energy level based exergoeconomic analysis of biomass and natural gas fired polygeneration system integrated with ground source heat pump and PEM electrolyzer, Energy Conversion and Management, 195, 313–327, (2009).

Zhou J., Ali M.A., Wais A.M.H., Almojil S.F., Almohana A.I., Alali A.F., Ali M.R., Sohail M., A novel modified biogas-driven electricity/cooling cogeneration system using open-and-closed Brayton cycle concepts: Environmental Analysis and Optimization, Ain Shams Engineering Journal, 14(12), 102230, (2023)

Empowering Fuel Cell Efficiency: Harnessing Machine Learning with DC/DC Boost Converter for Optimal Power Management

[1*]Ayse Kocalmis Bilhan
[1]Nevsehir Haci Bektas Veli University, Electrical Electronic Eng. Dept., Nevsehir, 50200, Türkiye

* E-mail: akbilhan@gmail.com

Abstract: This study focuses on the implementation of a machine learning algorithm-based maximum power point tracking (MPPT) controller for a PEMFC system. The performance of the proposed controller is evaluated under varying conditions in the MATLAB/Simulink environment to assess its efficacy. A Matlab model was first established that accurately captures the behavior of proton exchange membrane fuel cells. A dataset was then collected from fuel cells operating under different conditions, which was used to train machine learning algorithms. The results indicate that the suggested MPPT controller delivers accurate and rapid MPPT performance with reduced power fluctuations and higher production efficiency, demonstrating its potential to address the challenges associated with PEMFC systems.

Keywords: Fuel cells, mppt control, boost converter, machine learning, PEMCs

I. Introduction

FCs are electrochemical devices that convert chemical energy into electricity and offer advantages such as modularity, safety, low emissions, good transient response, and high scalability. In comparison to traditional energy sources, FCs reduce carbon dioxide emissions and have a wide range of applications in areas such as residential, portable, vehicular, space, and more. Fuel cells can be categorized in various ways depending on the type of electrolyte used within the fuel cell system. The classification of fuel cells can be based on their operating temperature, electrolyte, and other characteristics, such as Alkaline Fuel Cells (AFC), Direct Methanol Fuel Cells (DMFC), Phosphoric Acid Fuel Cells (PAFC), Molten Carbonate Fuel Cells (MCFC), Solid Oxide Fuel Cells (SOFC), and Proton Exchange Membrane Fuel Cells (PEMFC) (Acar and Dincer, 2020; Ozden and Tari, 2017) .

Typically, the voltage produced by a fuel cell is around 0.7V. In order to obtain a higher voltage, multiple cells can be arranged in series or parallel. In addition to increasing the voltage of the fuel cell by configuring the cells in series or parallel, recent research has also focused on modeling the DC/DC converters. To enhance the output voltage of a fuel cell (FC), a boost converter is the most fitting approach. DC-DC boost converters are employed to amplify the voltage obtained from FCs. To achieve a desired output voltage from a conventional DC-DC boost converter, a correct duty cycle must be selected. Many control methods have been used in the literature to improve the performance of FCs (Özdemir, 2021; Percin and Caliskan, 2023). Among these methods, machine learning methods have begun to increase their popularity day by day. Also, it is important to strike a balance between the voltage gain and the converter's efficiency to ensure optimal performance.

The present research gives an analyze of a MATLAB/Simulink-based Maximum Power Point Tracking (MPPT) control system for a PEMFC system, which utilizes an optimization algorithm based on machine learning. The primary objective of this method is to regulate the operating point of the system by tuning the duty cycle of the converter in response to varying conditions.

II. PEMFC

Proton Exchange Membrane (PEM) fuel cells employ a polymer membrane with proton-conductive properties as their electrolyte. The nomenclature PEM is an abbreviation for Polymer Electrolyte Membrane, while these cells are occasionally referred to as polymer membrane fuel cells or simply membrane fuel cells. In their initial stages of development during the 1960s, they were recognized as Solid Polymer Electrolyte (SPE) fuel cells. This particular technology has garnered substantial attention due to its numerous advantages, including high energy density, high energy efficiency, low operating noise, low cost, low operating temperature, short startup time, zero corrosion, use of solid electrolytes, and long lifespan, spanning from powering portable electronic devices such as cell phones to locomotives. The circuit diagram, the corresponding electrical circuit model, and voltage (V) versus current (I) relationship for the operation of a PEMFC are shown in Figure 1 (Nehrir and Wang, 2009).

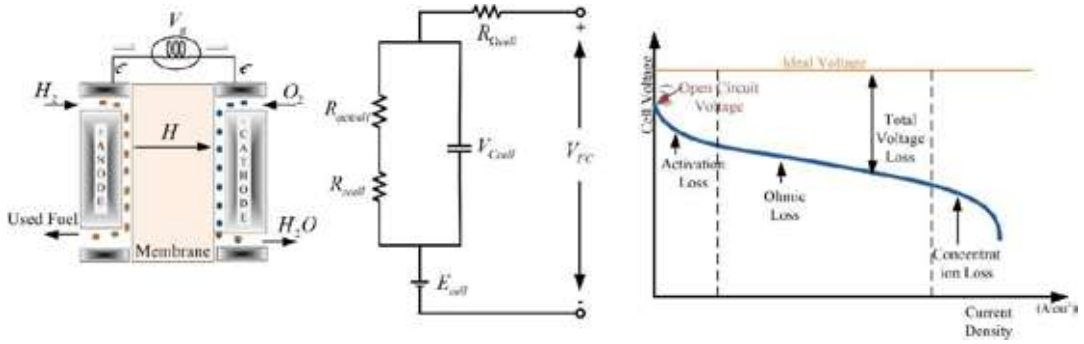


Figure 1. The circuit diagram, the corresponding electrical circuit model, and V-I relationship of PEMFC

In Fig. 1, $R_{\Omega cell}$ (ohmic resistance), R_{ccell} and $R_{actcell}$ are a function of FC temperature, and resistances of concentration and activation voltage components, respectively. The output voltage of a single cell can be calculated by using Eq. 1.

$$V_{FC} = E_{cell} - V_{actcell} - V_{\Omega cell} - V_{Ccell} \quad (1)$$

V_{FC} represents the output voltage value for a single cell, E_{cell} represents the open-circuit voltage of the FC, $V_{actcell}$ represents the voltage drop due to activation, V_{Ccell} represents the voltage drop due to density or mass, and $V_{\Omega cell}$ represents the voltage drop on the electrodes and membrane.

III.DC/DC Converter

Within the scope of this study, a DC-DC boost converter has been applied to generate a voltage output of superior stability for the load, involving the elevation of the input voltage to a more elevated and reliable level at the output. During a time interval of dT, the S (switch) is turned on and the D (diode) is turned off, while during a time interval of (1-d).T, the S (switch) is turned off and the D (diode) is turned on (Dandil et al., 2024; Kart et al., 2023; Refaat et al., 2024).

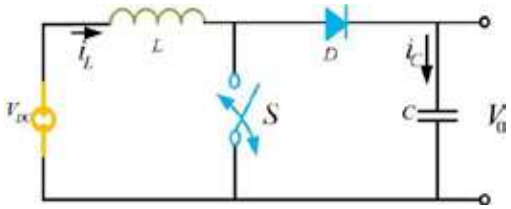


Figure 2. (a) DC/DC Boost Converter scheme

The duty cycle (d) of the boost converter can be calculated by using the voltage variation on the inductor Eq.4;

$$V_{DC} = \frac{V_0}{d-1} \quad (3)$$

IV. Results and Discussions

In order to reduce and partially eliminate the factors that cause poor performance, such as the low power value of the fuel cell stack, its transient characteristics, the slow dynamic response of the FC, and the charging and discharging control of the storage unit, a maximum power point tracking (MPPT) must be used and optimized. This ensures that the FC stack always delivers its maximum energy, even under varying operating conditions. In this study, the SVM method, which is commonly used in regression problems, and other classification methods were utilized to maximize the power output of the PEMFC system. The Classification Learner Toolbox in MATLAB offers a wide range of classifier types that are useful for solving classification problems (Gencer, 2024; Zhang et al., 2020).

In this study, the PEMFC power system consisting of a 1.5 kW PEM fuel cell feeding a resistive load through a DC-DC boost converter controlled using the ML MPPT controller is implemented using the MATLAB/Simulink environment. In this model, Machine Learning control is applied to the control system. The overall system scheme is shown in Fig. 3. The variable fuel flow rate is given in Fig. 4. The DC-DC Boost converter operates at 10kHz switching frequency, and an inductor value and a capacitor value are 10mH, and 100μF, respectively. The cell temperature is 338^0K. The FC output voltage (V_{fc}) is used as input of the MPPT classification algorithm. In order to regulate the output of the system under varying conditions of fuel flow, the MPPT control mechanism modulates the instant duty cycle value. The application of this value is achieved through the classification learning toolbox. After .15 sec, to evaluate the effectiveness of MPPT control, fuel flow is subjected to different changes. In order to evaluate the effectiveness of the MPPT control, it is important to note that the fuel cell's electrical output is directly influenced.

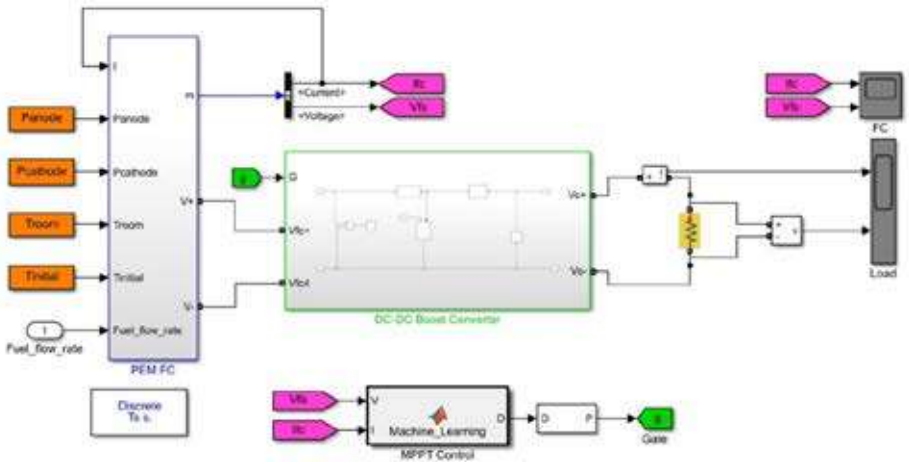


Figure 3. The model of a machine learning based MPPT controlled PEMFC

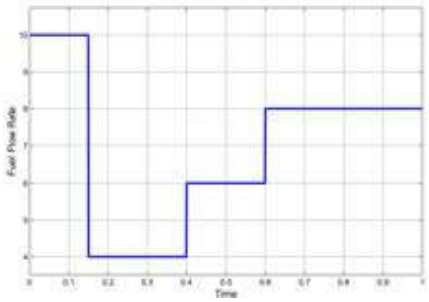
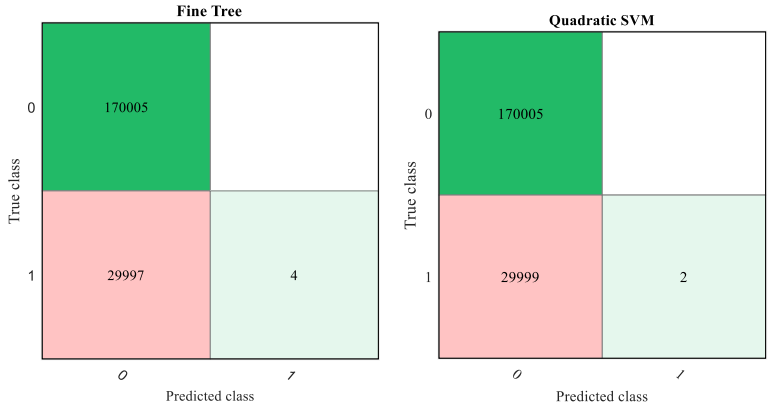


Figure 4. Fuel Cell Fuel flow rate

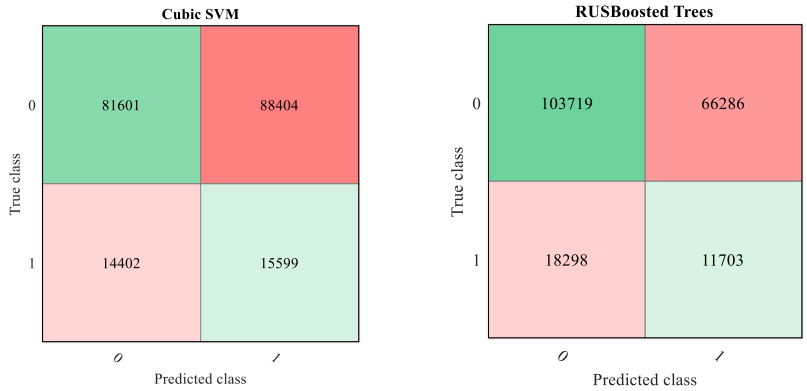
A comparison of Fine Tree, Quadratic SVM, Cubic SVM, Cubic KNN, Weighted KNN, Ensemble Boosted Trees, and Ensemble RUSBoosted Trees methods which are selected from the Classification Learning Toolbox in Matlab are given in Table I. The accuracy rates of Fine Trees, Quadratic SVM, Weighted KNN, and Ensemble Boosted Trees are 85%. These values of the proposed system indicate that the model is effective for MPPT control of fuel cell systems. In addition, while an accuracy of 57% was achieved with Ensemble RUSBoosted Trees, this rate dropped to 48.6% with Cubic SVM. The classification accuracy using Subspace Fine Tree, Quadratic SVM, Cubic SVM, RUSBoosted Trees for the system is given in Figure 5 (a), (b), (c), and (d), respectively. In Table I, TP, FP, FN, TPR, FPR, and ACC represent True Positive, False Positive, False Negative, True Negative, True Positive Rate, False Positive Rate, and Accuracy Rate, respectively.

Table I. Comparison of different methods

Classifiers	Accuracy(%)	TPR(%)	FPR(%)
Fine Tree	%85	100	<1
Quadratic SVM	%85	100	<1
Cubic SVM	%48.6	48	52
Cubic KNN	%83	97	3
Weighted KNN	%85	100	<1
Ensemble Boosted Trees	%85	100	<1
Ensemble RUSBoosted Trees	%57.7	61	39



(a) (b)



(c) (d)

Figure 5. Confusion matrix of (a) Fine Tree, (b) Quadratic SVM, (c) Cubic SVM, (d) RUSBoosted Trees

V.Conclusion

The global energy crisis and environmental issues have spurred a growing interest in clean and renewable energy sources, with fuel cells being a promising solution. As fuel cell power generation plays an increasingly pivotal role in the power system, addressing the challenges associated with this technology has become a pressing issue. This paper presents and models efficient power management in proton exchange membrane fuel cells using machine learning-based MPPT control and a DC/DC boost converter. . In order to train machine learning (ML) models for the proton exchange membrane fuel cell (PEMFC) system, a dataset was first collected. The collected dataset was then utilized as the foundation for training the ML models. Subsequently, the ML-based maximum power point tracking (MPPT) method was assessed for its ability to track the maximum power point (MPP) of the PEMFC system. This analysis was conducted under varying flow rate conditions to examine the efficiency and effectiveness of the proposed MPPT method. The highest load power and efficiency values were obtained using the Fine Trees, Quadratic SVM, Weighted KNN, and Ensemble Boosted Trees methods under these conditions.

References

Acar, C., Dincer, I., 2020. The potential role of hydrogen as a sustainable transportation fuel to combat global warming. International Journal of Hydrogen Energy, Hydrogen Energy Technologies for Mitigating Global Warming 45, 3396–3406. https://doi.org/10.1016/j.ijhydene.2018.10.149

Dandil, B., Acikgoz, H., Coteli, R., 2024. An effective MPPT control based on machine learning method for proton exchange membrane fuel cell systems. International Journal of Hydrogen Energy. https://doi.org/10.1016/j.ijhydene.2024.02.076

Gencer, A., 2024. Analysis of Fault Ride through the Improvement of PV Power Plant Based on Capacitive Bridge Fault Current Limiter Using Machine Learning. Electric Power Components and Systems 52, 1892–1905. https://doi.org/10.1080/15325008.2023.2298704

Kart, S., Demir, F., Kocaarslan, İ., Genc, N., 2023. Increasing PEM fuel cell performance via fuzzy-logic controlled cascaded DC-DC boost converter. International Journal of Hydrogen Energy. https://doi.org/10.1016/j.ijhydene.2023.05.130

Nehrir, M.H., Wang, C., 2009. Modeling and Control of Fuel Cells: Distributed Generation Applications | IEEE eBooks | IEEE Xplore. Wiley-IEEE Press.

Özdemir, M.T., 2021. Optimal parameter estimation of polymer electrolyte membrane fuel cells model with chaos embedded particle swarm optimization. International Journal of Hydrogen Energy, World Energy Strategies Congress and Exhibition 2019 (WESCE19) 46, 16465–16480. https://doi.org/10.1016/j.ijhydene.2020.12.203

Ozden, E., Tari, I., 2017. PEM fuel cell degradation effects on the performance of a stand-alone solar energy system - ScienceDirect. International Journal of Hydrogen Energy 42, 13217–13225.

Percin, H.B., Caliskan, A., 2023. Whale optimization algorithm based MPPT control of a fuel cell system. International Journal of Hydrogen Energy, The 6th International Hydrogen Technologies Congress (IHTEC-2022) 48, 23230–23241. https://doi.org/10.1016/j.ijhydene.2023.03.180

Refaat, A., Elbaz, A., Khalifa, A.-E., Mohamed Elsakka, M., Kalas, A., Hegazy Elfar, M., 2024. Performance evaluation of a novel self-tuning particle swarm optimization algorithm-based maximum power point tracker for porton exchange membrane fuel cells under different operating conditions. Energy Conversion and Management 301, 118014. https://doi.org/10.1016/j.enconman.2023.118014

Zhang, X., Han, P., Xu, L., Zhang, F., Wang, Y., Gao, L., 2020. Research on Bearing Fault Diagnosis of Wind Turbine Gearbox Based on 1DCNN-PSO-SVM. IEEE Access 8, 192248–192258. https://doi.org/10.1109/ACCESS.2020.3032719

Production of Black Phosphorus Doped Metal Chalcogenides Hybrid Materials and Their Use in Photocatalytic Hydrogen Production

[1*]Ecem Nur Demirel, [1]Bahadır Keskin, [2]Atıf Koca,
[1]Yıldız Technical University, Institute of Science, Inorganic Chemistry, Davutpaşa, Istanbul, 34220, Türkiye
[2]Marmara University, Faculty of Engineering, Chemical Engineering, Maltepe, Istanbul, 34854, Türkiye

* E-mail: ecemnurdemirel98@gmail.com

Abstract

Given the growing focus on clean and renewable energy sources amidst environmental concerns and the finite nature of fossil fuels, hydrogen (H_2) has emerged as a key contender for clean energy applications. One promising method for H_2 production involves photocatalytic water splitting, which offers a clean and cost-effective route. Various semiconductors, such as TiO_2, CdS, ZnS, MoS_2, among others, have been extensively explored for this purpose. However, their efficacy is often hindered by issues like charge recombination and inappropriate band gaps.

To address these limitations, researchers have been actively investigating modifications aimed at enhancing light harvesting and charge separation efficiency. This work provides a novel study of important photocatalysts utilized in photocatalytic H_2 production, along with elucidating recent advancements in their modification strategies. Notably, various photocatalyst heterostructures of black phosphorus doped metal chalcogenide hybrid materials are introduced, showcasing novel designs tailored to maximize H_2 production rates. These advancements signify promising strides toward realizing efficient and sustainable hydrogen production for clean energy applications.

Keywords: hydrogen production, water splitting, renewable energy

I. Introduction

In the 21st century, addressing the global energy challenge has become paramount, given the exponential rise in energy consumption. In 2008, energy demand soared to 15 TW, and projections suggest this figure could nearly double by 2050 due to population growth and increased production [1]. While clean and sustainable alternatives like solar, hydropower, geothermal, and wind energy exist, each faces its own set of limitations hindering widespread adoption.
Geothermal energy, while environmentally friendly, is costly to harness and limited in availability. Hydropower, though abundant, poses environmental concerns and requires substantial investment in dam construction. Wind energy, another promising source, suffers from intermittency issues as electricity generated is not easily stored [2].
Enter hydrogen (H_2), an environmentally friendly energy carrier garnering significant attention as a viable alternative to depleting fossil fuel reserves like petroleum and coal [3]. Photocatalytic water splitting, leveraging solar energy, emerges as an efficient method for H_2 production, utilizing the Earth's abundant solar resource and water. H2 holds promise as a clean energy source, derived from renewable resources and devoid of toxic emissions [4].
Semiconductors play a pivotal role in photocatalytic H_2 generation, with TiO_2 being a widely studied candidate due to its non-toxicity, stability, and affordability. However, TiO_2's wide band gap restricts light absorption to a fraction of the solar spectrum, limiting its efficiency. Moreover, its high recombination rate undermines photocatalytic activity, necessitating strategies such as semiconductor coupling to enhance performance [5].
Polymeric graphitic carbon nitride (g-C_3N_4), boasting a lower band gap of 2.7 eV, has emerged as a promising semiconductor for visible light-driven photocatalysis. Its chemical and thermal stability, coupled with cost-effective synthesis from readily available precursors, make it an attractive alternative [6], [7].
Achieving an internal quantum efficiency (IQE) of 100% in photocatalytic water splitting is the ultimate goal, requiring efficient migration of charge carriers to reaction sites to prevent recombination. However, challenges persist, with backward electron transfer limiting external quantum efficiency (EQE) to rarely exceed 50% [8].
Recently, great attention has been devoted to clean and renewable energy resources due to the environmental concerns and limitations of fossil fuel resources. Hydrogen (H_2) has been used widely as a source of clean energy in many applications. H_2 can be produced in a clean and cost-effective route, by photocatalytic water splitting. Several semiconductors including TiO_2, CdS, ZnS, MoS_2, etc. [9] have been used for photocatalytic water splitting. However, their limitations such as charge recombination and inappropriate band gap have persuaded researchers to apply modifications to them to increase their light harvesting and/or charge separation. This paper has reviewed important photocatalysts that are used in photocatalytic H_2 production and the recently applied modifications on them are explained. Several types of photocatalyst heterostructures are introduced and novel heterostructures for maximum H_2 production rate have been addressed [10].
The paper discusses the use of TiO_2-based photocatalysts for hydrogen production through photocatalytic water splitting. It highlights the limitations of TiO_2, such as charge recombination and inappropriate band gap, and the need for modifications to improve light harvesting and charge separation. The paper also introduces various types of photocatalyst heterostructures of black phosphorus doped metal chalcogenide hybrid materials and discusses

novel these heterostructures for maximum hydrogen production rate.

II. Experimental Set-up and Procedure

The photocatalytic Proton Coupled Electron Transfer (PCHER) method is a sophisticated mechanism that facilitates the photochemical decomposition of water under sunlight exposure (Wilson, 2020). In this process, a photocatalyst material absorbs sunlight and catalyses the separation of water molecules into oxygen and hydrogen gases. Among the effective materials for this method, hybrid structures of metal chalcogenides and black phosphorus have demonstrated high efficiency in hydrogen production.

To synthesize metal chalcogenides, a chemical vapour deposition technique is employed. This involves heating the materials in a tube furnace at 800°C for three hours under an Argon atmosphere. This high-temperature and controlled environment synthesis ensures the formation of the desired crystal structures. Specifically, in this study, various compositions of metal chalcogenides, such as $MoWS_2$, MoW_2S_2, and Mo_2WS_2, were created by mixing molybdenum disulfide (MoS_2) and tungsten disulfide (WS_2) in different ratios (1:1; 1:2; 2:1).

In addition to the metal chalcogenides, black phosphorus was synthesized using a hydrothermal method. This involves processing the material in an autoclave at 200°C for seven hours. The synthesized black phosphorus was then incorporated into the metal chalcogenide structures to examine their photocatalytic properties.

The photocatalytic hydrogen production performance of the synthesized materials MoS_2, WS_2, $MoWS_2$, MoW_2S_2, and Mo_2WS_2 were evaluated using a photocatalytic reactor system (Figure 1). During the tests, each sample was exposed to light for two hours. After this initial testing period, the system was stirred to ensure homogeneity and measurements were taken again to assess consistency and reproducibility.

By combining black phosphorus with these metal chalcogenides, the study aimed to enhance the photocatalytic efficiency and optimize hydrogen production rates. The detailed synthesis processes and testing methodologies highlight the systematic approach undertaken to develop and evaluate advanced photocatalysts for sustainable hydrogen generation.

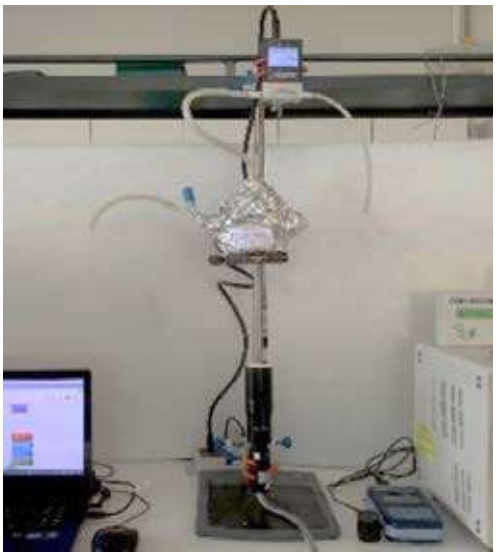


Fig. 1: Photocatalytic Reactor System

III. Analysis

In this section, the change of hydrogen production over time in PCHER performed under 1 sun light in the sacrificial electrolyte of 0.350 M Na_2S and 0.250 M Na_2SO_3 aqueous solution of different photocatalysts were given in Figure 2a-f. The graphs of PCHER hydrogen measurements show the impact of certain processes or variables on hydrogen levels.

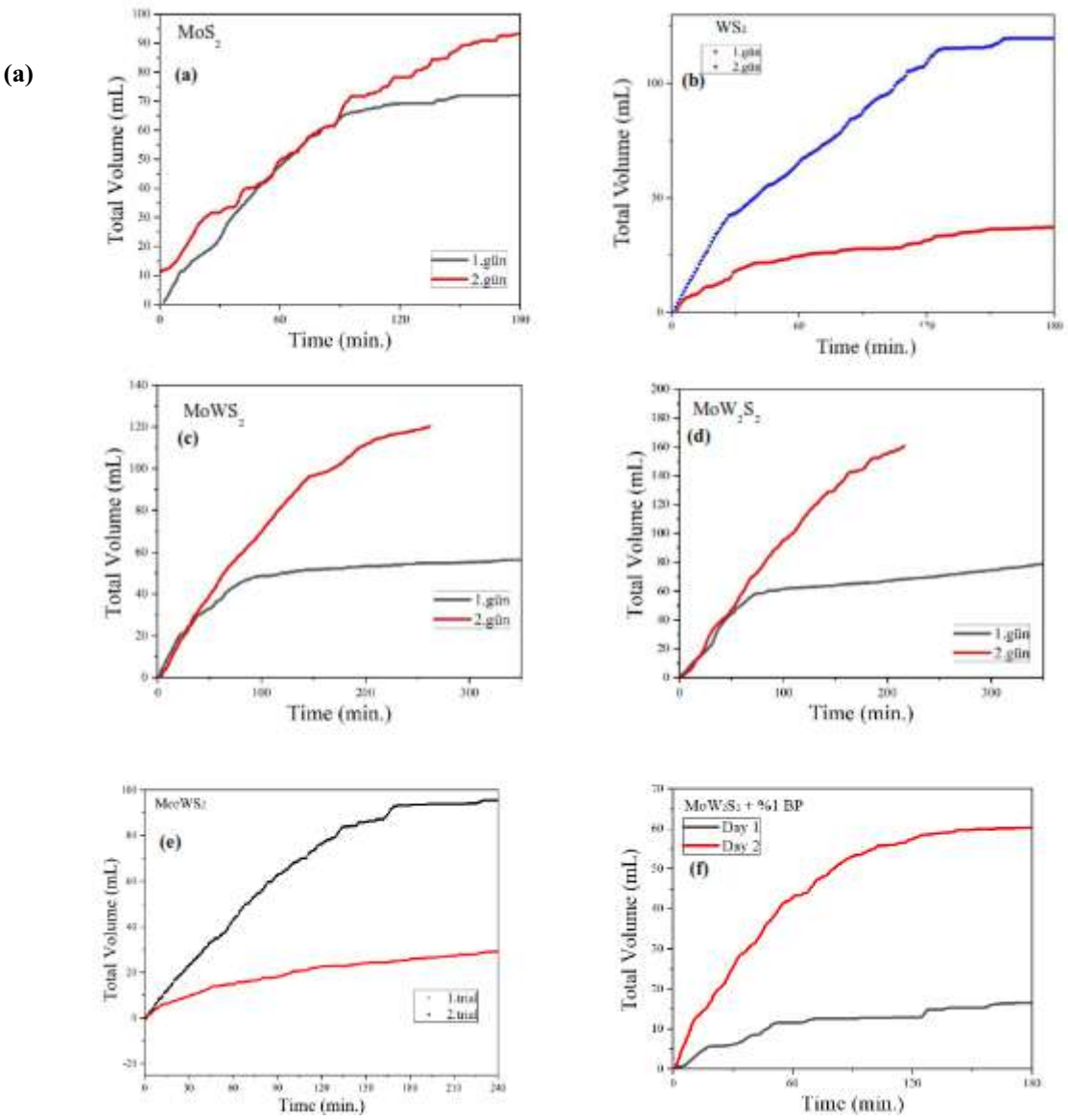


Fig. 2 Change of hydrogen production over time in PCHER performed under 1 sun light in the sacrificial electrolyte of 0.350 M Na_2S and 0.250 M Na_2SO_3 aqueous solution of MoS_2 **(a)**, WS_2 **(b)**, $MoWS_2$ **(c)**, MoW_2S_2 **(d)**, Mo_2WS_2 **(e)**, MoW_2S_2%1BP **(f)** photocatalysts

The crystal structures of WS_2, MoS_2 and WS_2/MoS_2 were examined by XRD analysis shown in Figure 3a-c. In Fig. 3c shows the XRD spectrum of WS_2 synthesized by the thermal sulfurization method. The intense XRD spectrum peak corresponding to the positions 2Θ = 14° and 40° shows the existence of the hexagonal structure of WS_2 (JCPDS-84-1398) Additionally, 2θ =14.4°, 28.9°, 33.3°, 34.2°, 39.6° and 49.9° peaks are (002), (004), (100), (110) respectively. (103) and (105) planes and corresponds to the hexagonal WS_2 phase Zhanga and Keerthana (2022). In Fig. 3b, the XRD spectrum of MoS_2 synthesized by the thermal sulfurization method is given. When the peaks in the XRD spectrum are compared with the literature, it is understood that they are compatible with the MoS_2 structure (JCPDS no. 37-1492). 2θ = 14.5°, 33.0°, 34.3°, 37.1°, 39.6°, 42.1°, 49.6°, 53.6°, 58.7°, 60.4 ° corresponds to (002), (100), (101), (102), (103), (104), (105), (106), (110) and (008) planes, respectively. Hexagonal MoS_2 formation occurs Miso (2016).

In Fig. 3c shows the XRD spectrum of the WS_2/MoS_2 composite prepared under the same synthesis conditions. According to Fig. 3a and Fig.3b compared to 3c, similar peaks detected in WS_2 and MoS_2 structures with slight shifts are also recorded in Fig 3c. The XRD spectrum in Figure 3c, 2θ = 14.3°, 28.8°, 33.3°, 34.2°, 37.0°, 41.7°, 49.7°, 53.4° and 60.3° positioned peaks were detected Nikpay (2021).

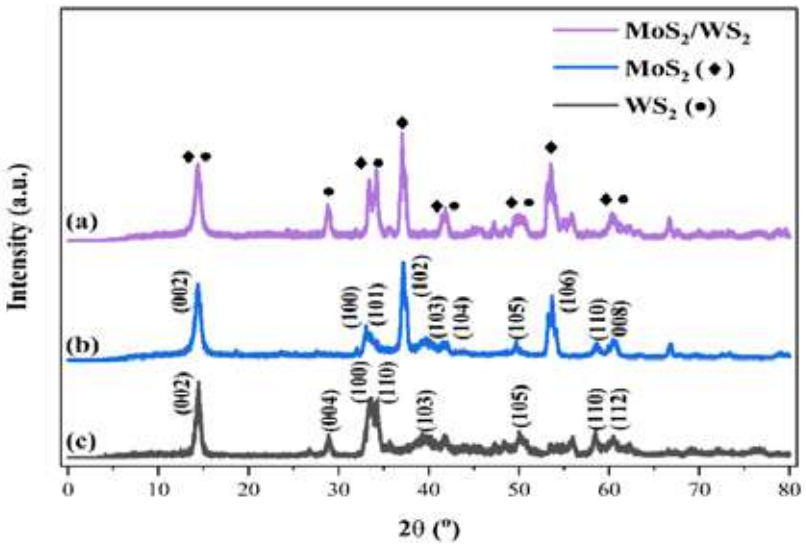


Fig. 3 XRD spectra of a) WS_2, b) MoS_2 and c) WS_2/MoS_2 composites

The Raman spectra of synthesized WS_2, MoS_2 and WS_2/MoS_2 samples are given in Figure 4a-c. Two characteristic and intense peaks, expressed as E_{2g} and A_{1g}, are observed for WS_2 and MoS_2 in Fig. 4a and 4b Lin (2021). In Fig. 4a, the E_{2g} and A_{1g} peaks of WS_2 are located at 348 and 421 cm^{-1}, respectively. For MoS_2, E_{2g} and A_{1g} peaks are located at positions 387 and 402 cm^{-1}, respectively in Fig. 4b. The E_{2g} and A_{1g} peaks of WS_2/MoS_2 composites are located similarly to the Raman spectra of WS_2 and MoS_2, the peaks of the peaks were detected at Raman shifts of 350 and 416 $cm^{-1,}$ respectively in Fig. 4c. As can be seen from the Raman spectra in Fig. 4, the existence of WS_2, MoS_2 and WS_2/MoS_2 structures is compatible with studies published in the literature. At the same time, the accuracy of the structures synthesized by the thermal sulfurization method was supported by XRD analysis.

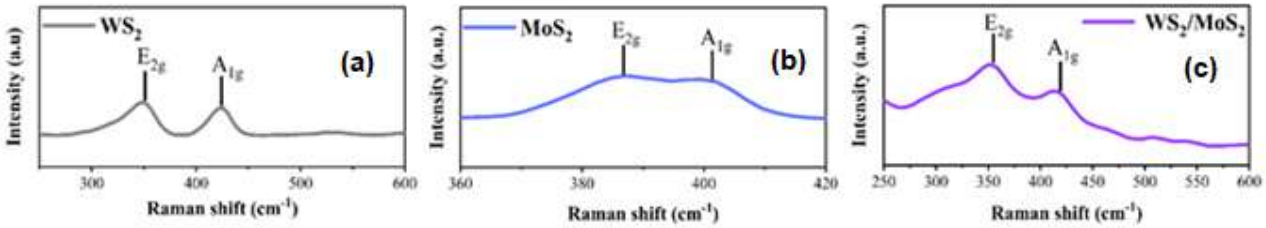


Figure 4. Raman spectra of a) WS_2, b) MoS_2 and c) WS_2/MoS_2 composites.

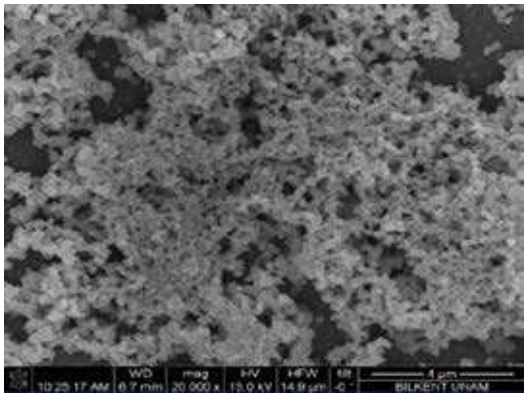


Figure 5. SEM image of WS_2/MoS_2 composite

SEM analysis was performed to investigate the morphology of the WS_2/MoS_2 composite in Figure 5. It shows the SEM image of the sample taken at x20,000 magnification scale. Accordingly SEM image of the composite in Fig. 5, it was seen that the sample consisted of spherical particles and the particles were clustered.

IV. Results and discussions

Figures 2 show the hydrogen production rates of PCHER analyses performed with MoS_2, WS_2, $MoWS_2$ (1:1), MoW_2S_2 (1:2), Mo_2WS_2 (2:1) structures. When these analyses were compared, the highest hydrogen production rate was achieved with the WS_2 structure for single metal chalcogenides. The maximum hydrogen production amount of the WS_2 structure was measured as 95.49 $mLh^{-1}g^{-1}$. Various compositions of metal chalcogenides, such as $MoWS_2$, MoW_2S_2, and Mo_2WS_2, were created by mixing molybdenum disulfide (MoS_2) and tungsten disulfide (WS_2)

in different ratios (1:1; 1:2; 2:1) were also tested in this PECHER system and the maximum hydrogen production amount of the Mo_2WS_2 (2:1) structure among them was measured as 110.85 $mLh^{-1}g^{-1}$. The synthesized black phosphorus incorporated into the metal chalcogenide structures was found not to enhance their photocatalytic properties as measured as 110.85 $mLh^{-1}g^{-1}$.

Table. 1: PCHER hydrogen production time variation in photocatalyst electrolytes of 1 sun, 0.350 M Na_2S and 0.250 M Na_2SO_3 aqueous solutions

Total H_2 volume (mL $h^{-1}g^{-1}$)		
Photocatalizer	**1 Hour**	**2 Hour**
MoS_2	49.54	78.22
WS_2	95.49	168.24
$MoWS_2$ (1:1)	46.85	82.08
MoW_2S_2 (1:2)	43.17	76.29
Mo_2WS_2 (2:1)	58.37	110.85
MoW_2S_2 %1 BP	42.97	57.56

V. Conclusions

The photocatalytic hydrogen production performance of the obtained metal chalcogen and black phosphorus hybrid materials was examined under various conditions and with different catalysts. Numerous experiments were conducted to determine the optimum conditions and enhance the efficiency of the catalysts, and the results were thoroughly evaluated.

In this study, the effectiveness of each catalyst under different experimental conditions was meticulously analysed. Experiments varied parameters such as light intensities, temperatures, pH levels, and different catalyst ratios, investigating their impacts on hydrogen production efficiency. Additionally, the long-term stability and reproducibility of the catalysts were tested.

The findings reveal that metal chalcogenides and black phosphorus hybrid materials possess high photocatalytic activity and significant potential in hydrogen production by effectively utilizing sunlight. Detailed analyses were conducted on how different ratios of metal chalcogenides and black phosphorus additives optimize hydrogen production rates. The role of the hybrid materials' crystal structures and surface properties in photocatalytic processes was also explored.

Results indicated that certain hybrid structures exhibited superior light absorption and charge transport capacities compared to others, leading to higher hydrogen production efficiency. This study's outcomes provide valuable insights for future research and applications aimed at environmentally sustainable clean energy sources.

Overall, the results demonstrate that metal chalcogenides and black phosphorus hybrid materials are promising candidates for photocatalytic hydrogen production. They can significantly contribute to sustainable energy production by efficiently utilizing sunlight. This study represents an important step towards future energy solutions and offers new perspectives for the development of clean and renewable energy sources.

Acknowledgements

This research was supported by Tübitak Scientific Research Projects Support Program (Tübitak Project no: 221M312)

References

International Energy Agency. (2008). World Energy Outlook 2008. IEA Publications.
Jones, R., & Pejovic, S. (2010). Renewable Energy Systems: Advances in Solar, Wind, Geothermal and Hydropower Technologies. Green Energy Solutions.
National Renewable Energy Laboratory. (2015). Hydrogen Production: Overview of Technology Options. NREL Publications.
Turner, J. A. (1999). "A Realizable Renewable Energy Future." Science, 285(5428), 687-689. DOI: 10.1126/science.285.5428.687
Fujishima, A., & Honda, K. (1972). "Electrochemical Photolysis of Water at a Semiconductor Electrode." Nature, 238, 37-38. DOI: 10.1038/238037a0
Wang, X., Chen, X., Thomas, A., Fu, X., & Antonietti, M. (2009). "Metal-Containing Carbon Nitride Compounds: A New Functional Organic–Metal Hybrid Material." Advanced Materials, 21(16), 1609-1612. DOI: 10.1002/adma.200801824
Dong, G., Zhang, L., & Qiu, J. (2014). "Active Sites and Mechanisms for Photocatalytic Hydrogen Evolution on C3N4-Based Potocatalysts." The Journal of Physical Chemistry C, 118(36), 21323-21330. DOI: 10.1021/jp5050008
Kudo, A., & Miseki, Y. (2009). "Heterogeneous Photocatalyst Materials for Water Splitting." Chemical Society Reviews, 38, 253-278. DOI: 10.1039/b800489g
Osterloh, F. E. (2008). "Inorganic Materials as Catalysts for Photochemical Splitting of Water." Chemistry of Materials, 20(1), 35-54. DOI: 10.1021/cm7024203
Wang, Q., & Domen, K. (2020). "Particulate Photocatalysts for Light-Driven Water Splitting: Mechanisms, Challenges, and Design Strategies." Chemical Reviews, 120(2), 919-985. DOI: 10.1021/acs.chemrev.9b00201

Green Hydrogen The Innovation of Green Energy to Detained The Carbon Emission

Syed Muhammad Ahmer Ali
University of Engineering & Technology Lahore Pakistan
Senior Process Engineer Ammonia Plant
ETI BAKIR GUBRE A.S
Mazıdağı, Mardin, Türkiye
Postal Code 47700

ahmer.ali@etigubre.com

Abstract
This paper focuses on the concept of green hydrogen, which means the generation of green hydrogen, usage and transportation of green hydrogen and converting it into useful products. The paper goes through the definitions and methods of green hydrogen production through different available electrolysis processes and technologies.

Green hydrogen is a valuable and sustainable alternative capable of diversifying the energy grid and reducing the dependency on fossil fuels, contributing to decarbonizing the global society Despite being widely applied on an industrial scale, hydrogen still faces major challenges, mainly due to the high cost incurred in its production, storage, transport, and the electricity required. Green hydrogen via electrolysis is an effective and efficient technology for capturing and storing renewable energy. It also helps to regulate the frequency and shifts loads.

Keywords: Green Hydrogen

I. Introduction

Green hydrogen can be produced by using clean electricity from surplus renewable energy sources, such as solar, wind power & hydropower to electrolyte water. Electrolysers use an electrochemical reaction to split water into its components

Contain a proton exchange membrane that uses a solid polymer electrolyte. When an electrical current is applied to its cell stack during water electrolysis, the water splits into hydrogen and oxygen. The hydrogen protons pass through the membrane to form H2 on the cathode side. The expected energy consumption per kg of Hydrogen 45- 50 Kwh.

Alkaline electrolysers

Contain water and a liquid electrolyte solution such as potassium hydroxide (KOH) or sodium hydroxide (NaOH). When current is applied to an alkaline cell tack, the hydroxide ions (OH-) move through the electrolyte solutions from the cathode to the anode of each cell. The hydrogen gas bubbles are generated at the cathode, and the oxygen gas is generated at the anode. The expected energy consumption per kg of Hydrogen is 50-55 Kwh.

of hydrogen and oxygen, emitting zero-carbon dioxide in the process. Green hydrogen currently makes up a small percentage of the overall hydrogen, because the production is expensive. Just as energy from wind power has reduced in price, green hydrogen will come down in price as it becomes more common.
Electrolysis is the technique used to produce hydrogen that consists of “breaking” the water molecules using an electric current in an electrolysers in order to extract the dihydrogen H2**.** The electricity must itself be carbon-free in ordar to consider this hydrogen as green or renewable.

PEM electrolysers

Solid oxide electrolysers

Solid oxide electrolysis cells (SOECs), are solid oxide fuel cells that run in regenerative mode. A SOEC uses a solid oxide, or ceramic, electrolyte. When current is applied, and water is fed into its cathode, the water converts into hydrogen gas and oxide ions. While the hydrogen gas is captured for purification, the oxide ions move to the anode and release electrons to an external circuit to become oxygen.According to the recent research of Haldor Topsoe It is most efficient electrolyser having 90-93 % stack efficiency. The expected energy consumption per kg of Hydrogen is 35- 40 kWh.

II. Experimental Set-up and Procedure

This research based the recent experiment and research of Haldor Topsoe, in which green hydrogen produced by the Solid oxide electrolysers. Solid oxide electrolysis cells (SOECs), are solid oxide fuel cells that run in regenerative mode. A SOEC uses a solid oxide, or ceramic, electrolyte. A dense ionic conductor consisting of ZrO2 doped with 8 mol-% Y2O3 (also known as YSZ, ytrium-stabilized zirconia). A water feed pump is available to feed the water in to the cell. The water was free from all impurities to prevent from degradation the material of stacks.230 A of current was provided for the electrolysis process. When current is applied, and water is fed into its cathode, the water converts into hydrogen gas and oxide ions. While the hydrogen gas is captured for purification, the oxide ions move to the anode and release electrons to an external circuit to become oxygen.A high temperature environment allowed the electrolyte to conducts the ions. The cell temperature is controlled by steam up to 700- 740 C°and cell pressure was 3.5 bar.A typical diagram of this experiment is under as;

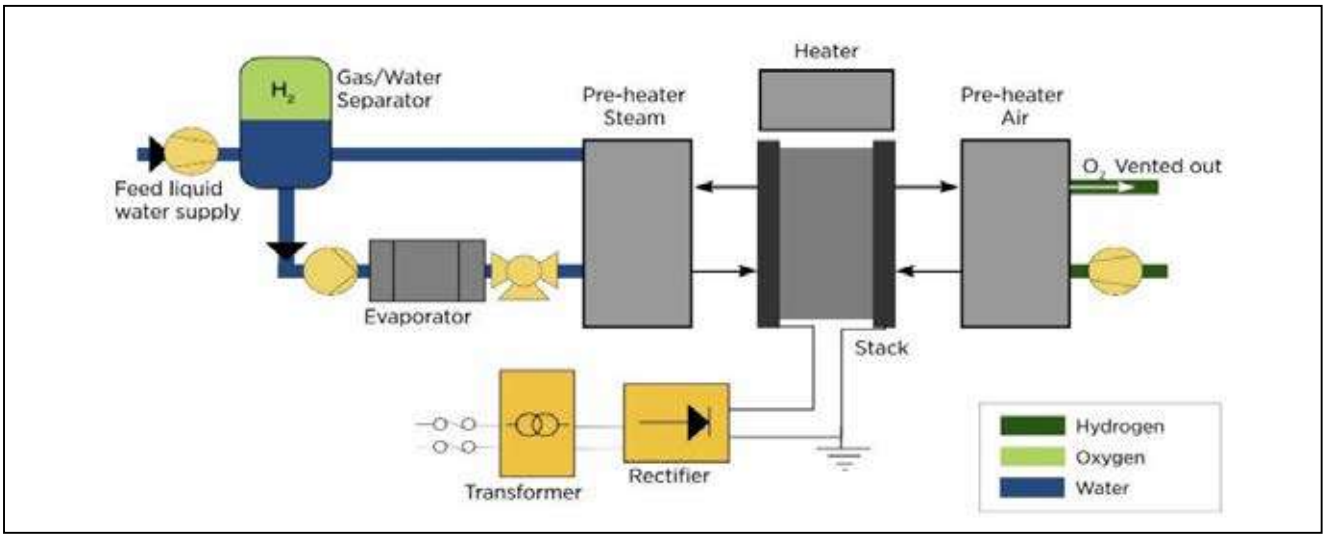


Fig. 1 Typical diagram of hydrogen unit.

III. Analysis

According to the experiment analysis following parameters were observed;
Test was carried out at 105% load and 80% load.
The cell temperature was in between 720 C° to 740 C° and electrolyser cell was operating at the pressue of 3.5 bar.
10 C° temperature was increase during the 1st 500 hours.
After 500 hours of operation no changed in temperature was made.
At the two occasions at t=1750h and t=2000h the temperature was changed at the load of 105% and 80% respectively.
For the smooth operaton and hydrogen production the current was provided up 230 A.
At the two occasions at t=1750h and t=2000h the current was changed at the load of 105% and 80% respectively.
Pressure remained consistently 3.5 bar during the test
The core electric power consumption noted for the production of 1 kg of hydrogen was 33.3kwh.
Working hours were more 2000.
Operating parameters remained same.
According to the trend current density was good.

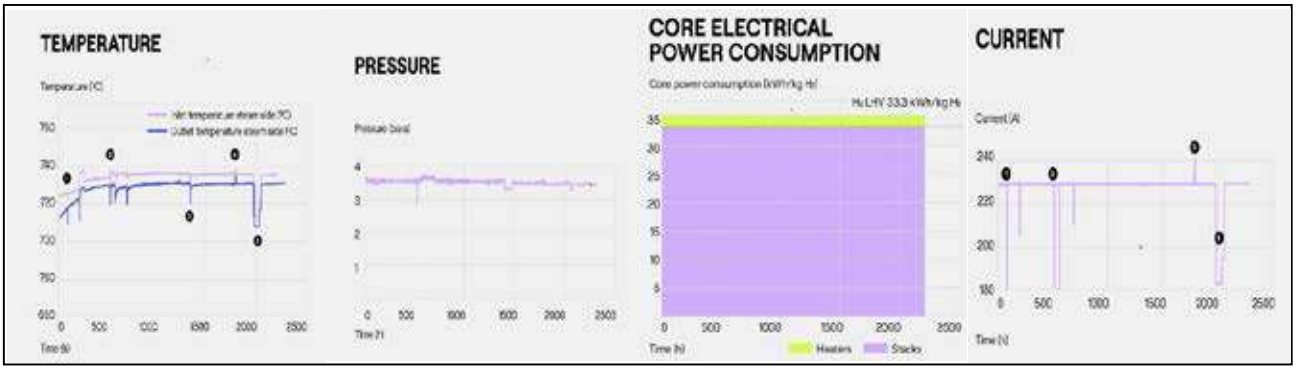


Fig. 2 Temperature, pressure, current and core Power consumption trends

IV. Results and discussions

In results, SOECs have shown high efficiency in green hydrogen production, with some experiments achieving efficiencies of over 90%. SOECs have demonstrated long-term stability, with some experiments running for over 2000, hours without significant degradation. SOECs can produce high-purity hydrogen (>99%), making them suitable for applications requiring high-quality hydrogen. SOECs can be scaled up to produce large quantities of green hydrogen, making them a promising technology for industrial applications.

SOECs can operate flexibly, allowing for variable hydrogen production rates and adaptability to changing energy demand.The production of green hydrogen through Solid Oxide Electrolysis Cells (SOECs) offers a promising solution for the transition to a low-carbon energy future. With its high efficiency, flexibility, and scalability, SOEC-based green hydrogen production has the potential to decarbonize various industries, from transportation to power generation. The integration of renewable energy sources and green hydrogen production can create a sustainable energy ecosystem, reducing greenhouse gas emissions and mitigating climate change.

However, challenges remain, including the need for further research and development to improve SOEC durability and reduce costs. Nevertheless, the benefits of green hydrogen production outweigh the challenges, and with continued innovation and investment, it can become a cornerstone of a sustainable energy future.
However, challenges remain, including the need for further research and development to improve SOEC durability and reduce costs. Nevertheless, the benefits of green hydrogen production outweigh the challenges, and with continued innovation and investment, it can become a cornerstone of a sustainable energy future.

As the world continues to grapple with the challenges of climate change and energy security, the production of green hydrogen through SOECs offers a beacon of hope for a cleaner, more sustainable future. With its potential to transform the energy landscape, green hydrogen is an opportunity that cannot be missed.

V. Conclusions

Green hydrogen production through Solid Oxide Electrolysis Cells (SOECs) offers a promising pathway for sustainable energy transition. In conclusion, SOEC-based green hydrogen production presents several advantages, including:

1. High efficiency: SOECs exhibit higher efficiency compared to traditional alkaline electrolysis, resulting in more hydrogen production per unit of electricity consumed.

2. Renewable energy integration: SOECs can effectively utilize renewable energy sources like solar and wind power, enabling a carbon-neutral hydrogen production process.

3. Low carbon footprint: By using renewable energy and avoiding fossil fuels, SOEC-based green hydrogen production significantly reduces greenhouse gas emissions.

4. Flexibility and scalability: SOECs can operate flexibly and be scaled up or down depending on energy demand, making them suitable for various applications.

5. Cost-effective: SOECs have the potential to reduce costs associated with hydrogen production, storage, and transportation.

However, further research and development are necessary to overcome challenges related to durability, materials, and system optimization.

Acknowledgements

I would like to acknowledge the contributions and support of my organization ETI BAKIR GUBRE A.S MAZIDAĞI MARDIN TÜRKIYE for their vision and commitment to sustainable energy solutions.

References

https://hydrogen.unido.org/acknowledgement
https://www.iea.org/reports/hydrogen-2156
https://www.irena.org/-/media/Files/IRENA/Agency/Publication/2020/Dec/IRENA_Green_hydrogen_cost_2020.pdf
https://www.topsoe.com/blog/breakthrough-in-green-hydrogen-topsoes-soec-demo-reveals-strong-results
https://www.unido.org/news/unido-irena-and-idos-publication-help-developing-countries-navigate-green-hydrogen-policy

Green hydrogen transportational challenges and innovative solutions to transport hydrogen

[1,2*] Zaheer Abbas
[1] NFC IET University, Engineering Faculty, Department of chemical Engineering, Multan, 60000, Pakistan
[2]ETİ Bakır, Mazıdağı, Mardin, Türkiye

* E-mail:zaheer.abbas@etigubre.com

Abstract
The main purpose to produce hydrogen is to store renewables energy in the chemical form so these can be later used or transport to other places. The transport of hydrogen is a challenge since hydrogen has low volumetric energy density, its transportation, storage, and final delivery to the point of use may represent a significant cost.There are several other approaches to hydrogen transport that are in various stages of development. Hydrogen can be converted into multiple carriers that have a higher energy density and higher transport capacity and can potentially be cheaper to transport over long distances. alternative routes to transport hydrogen by converting into other chemical compounds that are easy to handle and have several benefits over hydrogen transportation. There are several other approaches to hydrogen transport that are in various stages of development

Keywords: Hydrogen transportation, green vs grey hydrogen, innovative solutions to transport hydrogen, SOEC electrolyser.

I. Introduction

Hydrogen is one such promising environmentally friendly renewable energy carrier and it is the most abundant element in the universe. But hydrogen is not freely available on the earth. It is chemically combined with other elements and major amount is available in the form of water and fossil fuels. Solar and wind power sources are variable and intermittent they depend on weather conditions. Excess renewable energy produced during peak times can be used to create hydrogen through electrolysis This allows for seasonal energy storage where the surplus renewable energy produced during summer can be utilized to meet winter's higher demand.

Along with hydrogen production challenges transportation of hydrogen is also a difficult task. Hydrogen has low volumetric energy density, its transportation, storage, and final delivery to the point of use may represent a significant cost. To liquefy hydrogen, it must be cooled to cryogenic temperatures (−253°C /−423°F) through a liquefaction process. It takes energy to liquefy hydrogen liquefaction currently consumes more than 30% of the energy content of the hydrogen and is expensive.(U.S. Department of Energy (DOE)) The main drawback with liquid-based transportation of Hydrogen includes potential for the “boil-off” of Hydrogen from the container. Hydrogen can be converted into multiple carriers that have a higher energy density and higher transport capacity and can potentially be cheaper to transport over long distances.

Green hydrogen is not just a requirement as a source of energy but at the same time to decrease dependancy on fossil fuel and carbon emissions, green hydrogen for producton of chemicals like (ammonia, methanol) is far more important than to use hydrogen only as a source of energy. Almost 2% of global carbon dioxide (CO2) emissions come from the production of ammonia.(IEA 2021) In 2021, almost 180 million tons (Mt) of ammonia were produced globally which resulted in 450 Mt of direct CO2 emissions (ICEF 2022). The International Energy Agency’s Sustainable Development Scenario (SDS) envisions that ammonia demand for fertilizer in 2050 will total 230 Mt which will result in further more CO2 emissions.

II. Grey vs green hydrogen.

Energy consumption difference between green hydrogen and grey hydrogen is nearly.
3kwh /kg of hydrogen. As shown in a table below

Grey ammonia vs green ammonia

Product	Natural gas	Steam production	Electricity consumption	CO2 production	Water requirement	Net energy consumption
	Sm3/kg NH3	kg/kg NH3	Kwh / kg NH3	Kg/kg NH3	Kg/kg NH3	Kwh/kg NH3
Grey ammonia	0.892	2.15	0.665	1.55	1.34	7.30
Green ammonia		0.8	11.13		10.5	10.42

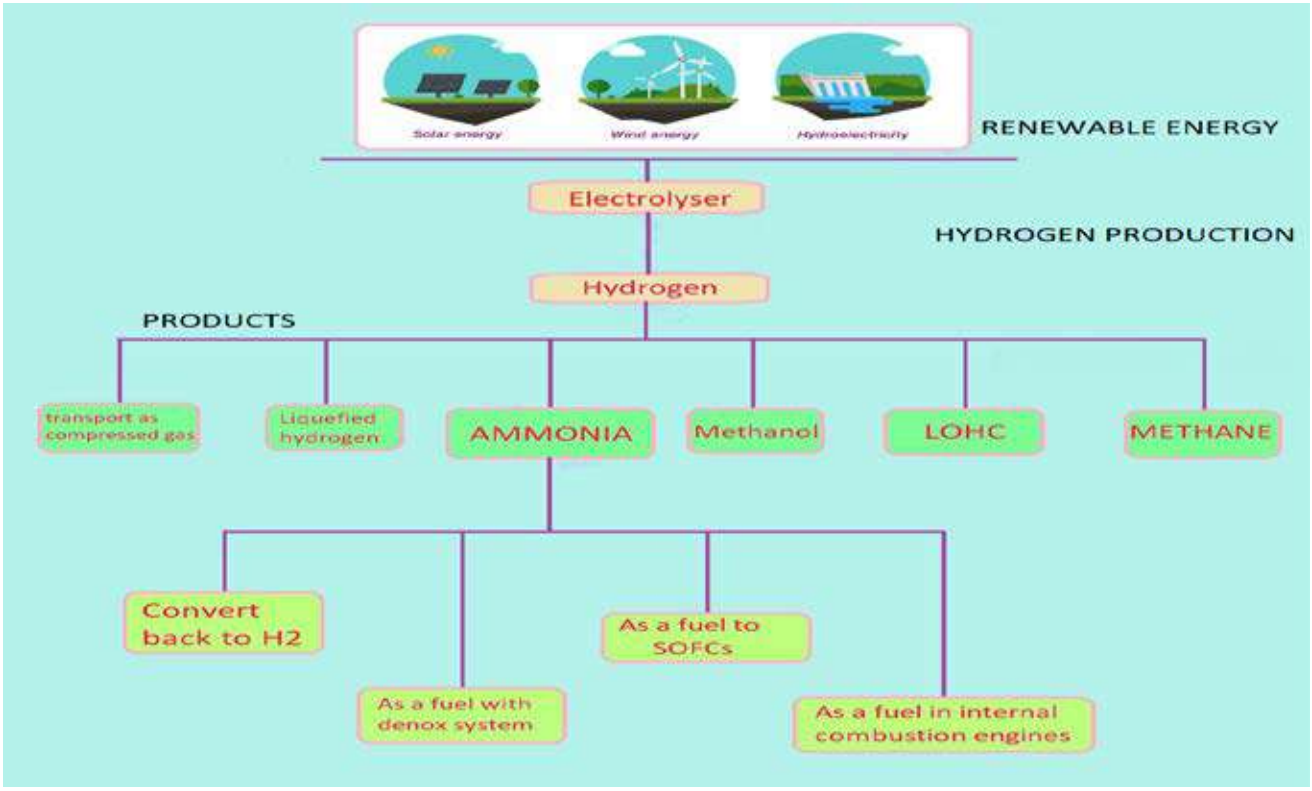
But the difference in production cost of green hydrogen is 3 times more than grey hydrogen. It is due to the difference in source of energy used to produce hydrogen. Hydrogen production through SMR via natural gas has the lower cost but this process has high carbon emission.

Green hydrogen					
utility	quantity	Energy in kw	Price /kw	price in tl	Price in usd
electricity	56 kw/kg of hydrogen	56	3 tl	168	5.16

GREY hydrogen						
Utility	Quantity	Calorific value kcal/sm3	Price/unit	Energy in kw	Total price in tl	Price in USD
Natural gas	5.0 sm3/kg of H2	8250	11.5 tl/sm3	47.94	57.5	1.76
electricity	1.67 kw/kg of H2		2.5 tl/ kw	1.67	5.01	0.156
Steam export	7.23 kg/kg of H2	5538		2.57 P	-7.71	-.23
total				43.7	54.8	1.68

III. Innovative solutions to transport hydrogen energy

Hydrogen can be converted into multiple carriers that have a higher energy density and higher transport capacity and can potentially be cheaper to transport over long distances. Following are the well known methods and products that can be produced by using green hydrogen.



a. Ammonia
b. Methanol
c. LOHC
d. Methane

Using ammonia as a carrier for hydrogen is probably the option with the most potential. When liquefied, ammonia contains 50% more hydrogen by volume than liquid hydrogen. And already have well developed storage and transportation infra structure.

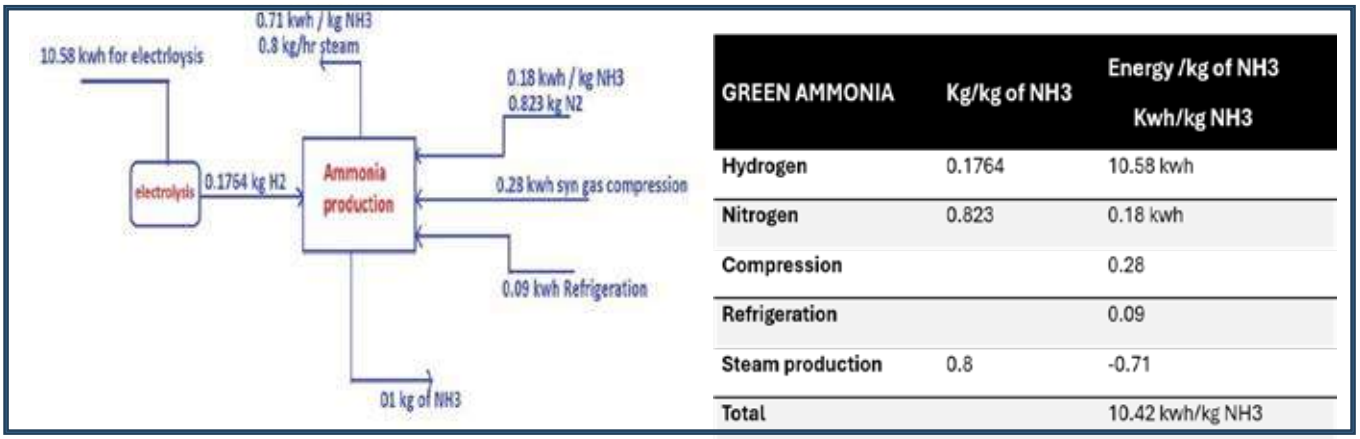
a. Ammonia

Ammonia has been used in various industries for a long time and there is a widespread infrastructure for ammonia synthesis. Also, ammonia can be stored in slightly refrigerated tanks at -33 °C or at ambient temperatures under a pressure of 8-10 bar. This makes storing and transporting ammonia relatively straightforward and affordable.

Integration of green hydrogen with grey ammonia production plant has several benefits.

- Green ammonia is produced by using hydrogen from water electrolysis and nitrogen from the air. These are then fed into the Haber process (also known as Haber-Bosch), all powered by sustainable electricity.
- To produce Ammonia as per equation given below.

  N2 + 3H2 ----> 2 NH3 -92KJ/mol
- 0.823 kg of N2 and 0.1764 kg of hydrogen is required to produce 01 kg of ammonia.



GREEN AMMONIA	Kg/kg of NH3	Energy /kg of NH3 Kwh/kg NH3
Hydrogen	0.1764	10.58 kwh
Nitrogen	0.823	0.18 kwh
Compression		0.28
Refrigeration		0.09
Steam production	0.8	-0.71
Total		10.42 kwh/kg NH3

Fig. 1. Energy requirement to produce ammonia with electrolysis.

A standard 5000 kw electrolyser stack has the capacity to deliver 1000 nm3/hr or 89 kg/hr of hydrogen at 30 bar pressure. If we use this hydrogen at existing ammonia plant,

- it will produce 12 ton/day of ammonia.
- It will reduce 20 ton/day of co2 emission.
- Existing ammonia plant can handle these changes without any visible change in energy consumption.
- No other CAPEX cost.
- No extra investment for storage.

Reaction of Ammonia production is exo thermic reaction so it will product nearly 12 ton of steam per day which will decrease the energy consumption

b. Methanol

Production of methanol with green hydrogen.Same size of electrolyser stack can be used to produce methanol.

CO2 + 3H2 ------> CH3OH + H20 -49 KJ/mol

- It will produce 11.5 ton/day of methanol.
- It will reduce 16 ton/day of co2 emission.
- At other green methanol plant CO2 is being captured by applying different technologies from flue gases. That is also energy consuming process.
- But at ammonia plant CO2 is a byproduct of ammonia production process with purity level up to 99 % so easily available to consume.

c. Methane

Methane can be produced by green hydrogen through methanation reaction. In this reaction CO or CO2 react with hydrogen to produce methane gas.

CO2 + 3H2 ------> CH4 + H20 -165 KJ/mol

Same electrolyser can be used to produce methane gas.
It will produce 8000 Nm3/day of methane gas.
As mentioned above CO2 is easily available at ammonia plant and all the above reactions except production of methanol are already being handled at ammonia plant.

d. LOHC.

LOHC is a liquid capable of absorbing and releasing hydrogen through a chemical reaction. This chemical reaction occurs under increased pressure and temperature with a catalyst present. Several agents can be used as a LOHC. A good example is dibenzyl toluene.

IV. Conclusions

Green hydrogen that can be produced from the electrolysis of water is an important key solution to tackle global decarbonization. Green hydrogen is fuel of future. But there is another side of the picture, which shows that world

also needs food. For food we need fertilizers. Nearly 500 tons of co2 is annually produced as a result of ammonia production which is used in fertilizers. To reduce fossil fuels dependency and decrease carbon emission, green hydrogen is more important for production of fertilizer than as an energy source. Because Hydrogen as a source of renewable energy can be replaced by wind, hydro, solar, nuclear and batteries. But production of ammonia , methanol and such other compound is not possible without hydrogen.

References

https://www.iea.org/news/new-iea-study-examines-the-future-of-the-ammonia-industry-amid-efforts-to-reach-net-zero-emissions

https://www.icef.go.jp/wp-content/uploads/2024/02/icef2022_roadmap_Low-Carbon_Ammonia.pdf

https://www.energy.gov/sites/default/files/2022-07/liquid-hydrogen-tech-workshop-report-2022.pdf

POSTERS

Syngas Desulfurization following Microwave Cycled Gas Bubbling on Coal and Biomass Pyrolysis

[1*]Yıldırım İsmail Tosun, [2]Fethullah Chichek,
[1*] ŞırnakUniversity, Department of Mining Engineering, Şırnak, Türkiye
[*]Corresponding author e-mail: yildirimismailtosun@gmail.com
[2] Azerbaijan Science Academy , Department of Radiation Problems, Baku, Azerbaijan

fcicek49@gmail.com

Abstract
In this study, the significant TG tests for desulfurization of gaseous extracts of gasified coal and wood tar mix have been made on salt and biochar carbon substrate as granules controlled with gasifier gas yield of coal and biomass char/tar feed in order to reach catalytic forming and desulfurization at 700 C providing heat transfer in microwave radiated cell to sequent column reactor. However, the results of filled bed poor iron slime yielded high heat transfer to coal and biomass char and tar. Due to the complex chemistry of coal, and porosity, heat conduction decreased in the microwave radiated salt cell system by granule size decrease. . This condition also gave tar gas high-heating conversion of 23% (in comparison without catalytic cracking to 7 %). The effect of condensing gas residence time in catalyst Fe_2O_3-rich pellet loading on tar processing to syngas cycled in the column unit studied at 700°C. The condensing gas to tars at residence of shorter 2-5 mins and 30 % porosity catalyst loading of 4%-8% volume fraction in the column were found appropriate to produce clean tars for syngas reforming with tar vapor content appropriate salt mixture of NaCl/KCl over biyochar substrate for industrial applications (less than 9 mg/m3 H_2S) in an downdraft biomass pyrolyzer without external heating.

Keywords Syngas desulfurization, microwave column, bubbling bed, Coal Tar, Biomass Tar”

I. Introduction

There are various objectives to make the necessary arrangements to increase the use of biomass and solar energy as the other device. Considering the known biomass area of the potential high forest fields in northern Anatolia and located in central and eastern Anatolia it is seen as having low to medium heat resources. As we have seen in our country there is a significant potential for biomass resources will be invested. The low heat waste will be great source for waste heat and in comparison the electricity production may reach on 60-70 % thermal performances by microwave co-combustion.

In conventional thermal processing, energy is transferred to the material through convection, conduction, and radiation of heat from the surfaces of the material. In contrast, microwave energy is delivered directly to materials through molecular interaction with the electromagnetic field. In conventional methods, energy is transferred due to thermal gradients, but microwave heating is the conversion transfer of electromagnetic energy to thermal energy through direct interaction of the incident radiation with the molecules of the target material.

Desulfurization with Microwave Radiation

Alkali salt of Na and salt components were reactive toward gaseous extracts and vapors of amorphous crystal structure of coal under certain temperature. The unsaturated substrate was chemisorbed onto the char carbon, with most sites covered by the substrate. In heterogeneous sulfur carbon faces on coal, carbonyl forms surface halides (NaCl/KCl) from which sulfur ions could be transferred to the chemisorbed substrate. Black carbon was active sorbents, which operated at lower temperatures and lower pressures of desulfurization of tar.

Molten Salts

The salt composition affects the desulfurization as seen in Figure 1. Hydrous form of vapor react at sorbent faces easly with with NaCl and KCl components in solid form.

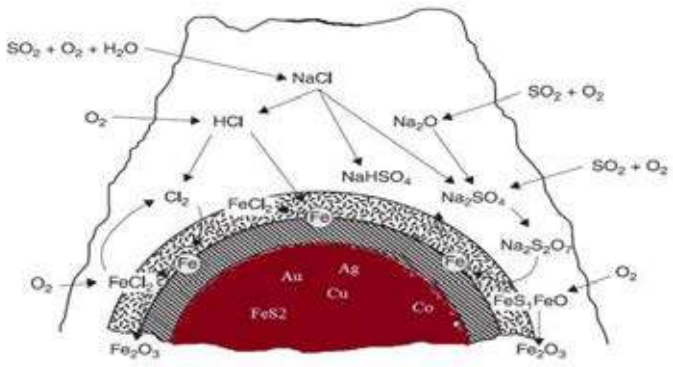


Fig. 1. Microwave radiated Bubbling Flow Desulphurization by semi molten solid salts granular sections

Under microwave radiation, alkali salts and Na and metal sulfide products are easily oxidized according to the following reaction. Depending on the pyrolysis temperatures and oxygen rateof coal H2S and SO_X gas can arise from coal above 200°C - 500°C in a short time, as shown in the chart below. Silicate content can only reach 200oC. The coal impurities and sulfur evove and react with Na and K salts of Cl and carbonates in semi solid form as given below:

$MeS + 3/2\ O_2 \rightarrow MeO + SO_2$ (M: Fe, Cu, Zn) (1)

$CuS + 3/2O_2 \rightarrow CuO + SO_2$ (2)

$ZnS + 3/2O_2 \rightarrow ZnO + SO_2$ (3)

$2FeS_2 + 11/2O_2 \rightarrow Fe_2O_3 + 4SO_2$ (4)

$H2S + NaCl/Na2CO3 \rightarrow Na2S + MeSO3 + SO_2$ (M: Fe, Cu, Zn) (5)

The ability for high extract yield of molten salts during biomass tar pyrolysis was investigated in this study. The thermo gravimetric analysis at bubbling bed reactor was recorded to study the thermal melting characteristics and bubbling affect of molten salt as the pyrolysis extracts. The NaCl-KCl-MgCl2 is appropriate for the preparation of H2-rich gas and the char with semi molten melts during hot gas passage and microporous form due to bubbling activation effect. NaCl-KCl-MgCl2 was efficient salt mixture for tar pyrolysis.

Materials and Methods

A type K thermocouple (wire diameter of 0.20 mm) was employed and the temperature was measured immediately after turning the power off. The variables studied were: incident microwave power, processing time and sample mass. For the microwave combustion tests, samples weighing about 15–20 g, were placed in fireclay combustion boats and heated. (Figure 2) and Desulphurization amount over salt/biochar substrate by TG apparatus used for gasifier and the gaseous extracts is shown from Figure 3.

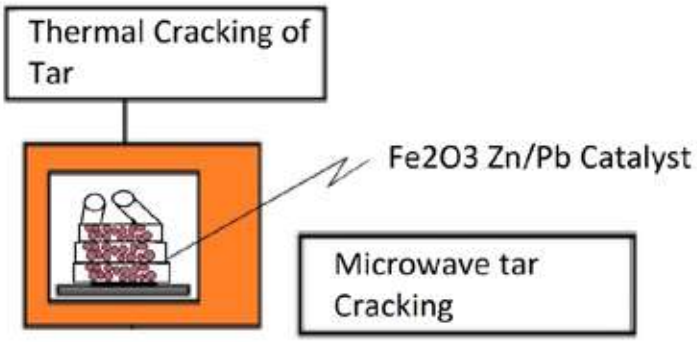


Fig. 2 Thermolysis Tar Cracking through Fe2O3 Zn/Pb catalyst.

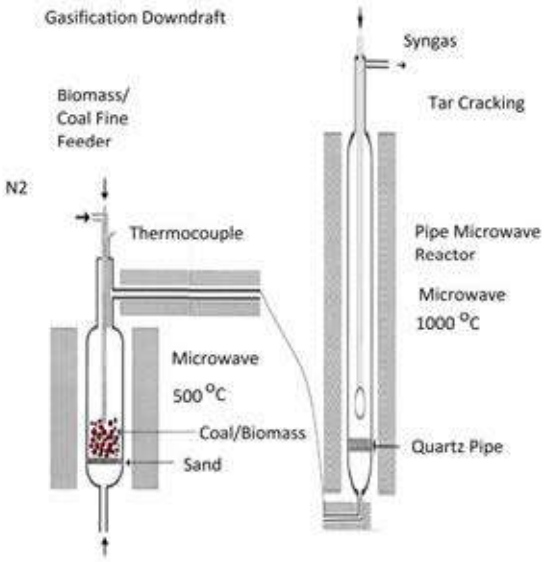


Fig. 3 Gasification and Thermolysis Tar Cracking through Fe2O3 Zn/Pb catalyst.

Gas Desulfurization Performance

There are excellent microwave heating conduction to gasified cracking of tar over hematite and Zn/Pb catalyst, which is used at higher temperature crackings even more than in high presurrized gasification. The exergy of microwave pyrolysis and thermolysis tar cracking is geatly depended on heat content of gasification and porosity of catalyst in the microwave pipe reaction bed in the reactor as illustrated in Figure 4 and this high exergy was

resulted at 30 minutes time as leads to lower power rates in the microwave syngas desulfurization.

Table 1. Summary of catalyst details for tar cracking. According to the saturation curves in column sorption shown in Fig 5, the response of the stage wiseback mixing model changes from a mixed flow condition managed at low pressure.



Fig 4. Desulphurization Column used in Tests

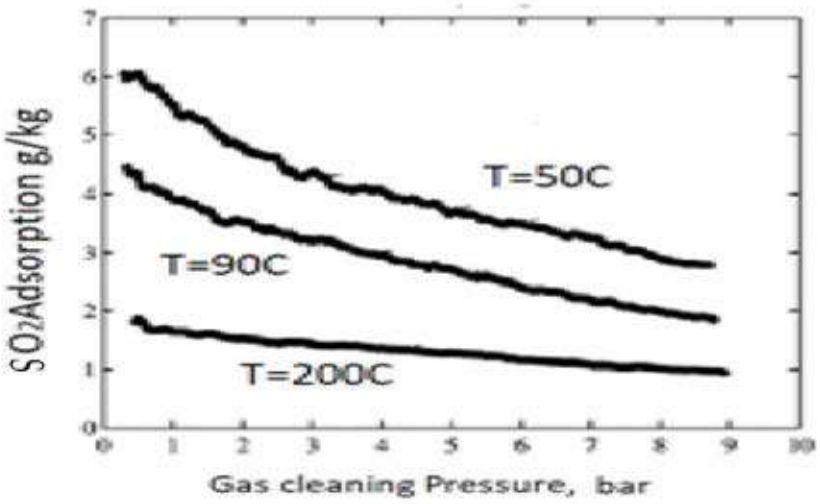


Fig 5. Desulfurization Saturation regarding column pressure

The porous solid salt column temperature produced from different combustion flue gas exit level or long duration of cooling of exhaust system. The temperatures at 250-300 °C were tested in three column series for adsorption SO_X as seen in Figure 5. Test results were determined as weight in TGA.

The column humidity produced from different combustion fuel and combustion temperature exit or fuel moisture content in the exhaust system. The steam amount in flue gas at exhaust chamber varied at 5-20% was tested in three column series for desulphurition SO_X as seen in Figure 3. Test results were determined as weight in TGA.

Results And Discussion

The kinetics of the cracking following pyrolysis and cracking temperature and partial pressure of volatile matter of biomass/ coal are also critical under microwave tar cracking. It can be seen that the solid content of tar oil increases significantly faster in the microwave cracking rates than in conventional control tests. More than 75% of the tar was removed within 10 minutes with microwave heated gasification of biomass/coal, while in conventional combustion the same degree of tar removal would require several hours.

M2CO3 +H2O(g) 2MOH+CO2(g) (11)
M2CO3+C M2O+2CO(g) (12)
H2(g)+CO2(g) CO(g)+H2O(g) (13)
M2CO3+H2(g)›2M(g)CO2(g)H2O(g) (13)
M2CO3›M2O+CO2(g) (13)

The influence of sulfates NaCl-KCl-MgCl2 and Na2SO4-K2SO4-MgSO4 on the pyrolysis process of biomass is shown in Eq. 7 and 8. It can be found that the pyrolysis process of biomass changes abnormally after the addition of sulfates. The char and methane were rapidly consumed from 300 °C and completely disappeared at about 450 °C. Almost all char derived from biomass tar pyrolysis was converted into CO2(g), and the reactions involved were mainly (15) and (16). As the temperature increased, sulfates went through a more complex conversion process with possible reactions (17) to (20).

M2SO4+2C ›M2S+2CO2(g) (16)
M2SO4+CH4 ›M2S+CO2(g)2H2O(g) (17)
M2S+3CO2(g) ›M2O+SO2(g)+3CO(g) (18)
M2O+H2O(g) ›2MOH (19)
M2SO4+H2(g) ›2MOH+ SO2(g) (15)
Li2S+M2SO4 ›M2S+Li2SO4

Conclusions

In modified pipe microwave reactor, where the average concentration of solids amounts to 10 - 50 g/m^3, i.e. the conditions for residence time are long enough for the thermal combustion of biomass waste and coal and extensive gas mixing with 60-70% N2 and air so enhancing biomass combustion and shutting air inlet in order to take the down draft gas, heat transfers to the microwave cracking section. It is necessary to create conditions of internal circulation without the transported coal and waste in modified pipe and downdraft gasified, 90-95% tar yield were observed at the end of combustion. Total heat values of biochars are of approximately 17.8 kJ/ kg for corn stalk and 16.2 kJ/ kg for

forest oak wood waste for tar cracking by microwave.
At 750C, the pyrolysis gas obtained from NaCl-KCl-MgCl2 contained 30,42 vol% H2 with the H2/CO ratio reaching 0,91. The carbonates demonstrated excellent improvement for the gas composition of biomass char pyrolysis products, with 22,7 vol% and 37,2 vol% syngas (H2/CO) collected from the Na_2CO3-K2CO3 and MgCl2 pyrolysis systems at 750 .C respectively. Semi-molten carbonates, the bio-oil and char prepared by biomass char pyrolysis also achieved better quality. The thermodynamic equilibrium resulted of the high extract gas formation of H2and CO from biomass and coal tar in molten salt composition of NaCl-KCl-MgCl2 during biomass tar pyrolysis. The sulfur reaction between MgCl2 and char tar char under high temperature 750C determined the high gas H2 yield and CO in pyrolysis gas products with the low consumption of salts and deterioating the biomass tar pyrolysis system.

References

D. Sutton, B. Kelleher, J.R.H. Ross,Review of literature on catalysts for biomass gasification, Fuel Process. Technol., 73 (2001), pp. 155-173

J.D. Adjaye, N.N. Bakhshi,Catalytic conversion of a biomass-derived oil to fuels and chemicals. 2. Chemical kinetics parameter estimation and model predictions, Biomass Bioenergy, 8 (1995), pp. 265-277

A.V. Bridgwater, Production of high grade fuels and chemicals from catalytic pyrolysis of biomass, Catal. Today, 29 (1996), pp. 285-295

J. Delgado, M.P. Aznar, J. Corella, Biomass gasification with steam in steam in fluidised bed: effectiveness of CaO, MgO, and CaO–MgO for hot raw gas cleaning, Ind. Eng. Chem. Res., 36 (1997), pp. 1535-1543

K. Raveendran, A. Ganesh, K.C. Khilar, Pyrolysis characteristics of biomass and biomass components, Fuel, 75 (1996), pp. 987-998

A. Demirbas, Hydrogen production from biomass by the gasification process, Energy Sources, 24 (2002), pp. 59-68

D. Wang, S. Czernik, D. Montane, M. Mann, E. Chornet, Biomass to hydrogen via fast pyrolysis and catalytic steam reforming of the pyrolysis oil or its fractions, Ind. Eng. Chem. Res., 36 (1997), pp. 1507-1518

J.D. Adjaye, N.N. Bakhshi, Catalytic conversion of a biomass-derived oil to fuels and chemicals. 2. Chemical kinetics parameter estimation and model predictions, Biomass Bioenergy, 8 (1995), pp. 265-277

P. Grange, E. Laurent, R. Maggi, A. Centeno, B. Delmon, Hydrotreatment of pyrolysis oils from biomass: reactivity of the various categories of oxygenated compounds and preliminary techno-economical study, Catal. Today, 29 (1996), pp. 297-301

M. Marquevich, S. Czernik, E. Chornet, D. Montane, Hydrogen from biomass: steam reforming of model compounds of fast-pyrolysis oils, Energy Fuels, 13 (1999), pp. 1160-1166

R.V. Pindoria, A. Megaritis, R.C. Messenbock, D.R. Dugwell, R. Kandiyoti, Comparison of the pyrolysis and gasification of biomass: effect of reacting gas atmosphere and pressure on eucalyptus wood, Fuel, 77 (1998), pp. 1247-1251

M. Stenseng, A. Jensen, K. Dam-Johansen, Investigation of biomass pyrolysis by TG analysis and differential scanning calorimetry, J. Anal. Appl. Pyrol., 58 (2001), pp. 765-780

V.R. Rustamov, K.M. Abdullayev, E.A. Samedov, Biomass conversion to liquid fuel by two-stage thermochemical cycle, Energy Conv. Manage., 39 (1998), pp. 869-875

Elliot. D.C. ,1987, ”Relation of Reaction Time and Temperature to Chemical Composition of Pyrolysis Oils”, ACS Symposion Series 376, Pyrolysis Oils from Biomass”. Edited by E.J. Soltes and T.A. Milne. Denver, CO. April 1987. .(1987)

Dayton D., 2002, A review of the literature on catalytic biomass tar destruction, National Renewable Energy Laboratory, Golden, Colorado, USA. .(2002)

Devi L., Ptasinski K.J., Janssen F.J.J., 2003, A review of the primary measures for tar in biomass gasification processes, Biomass Bioenergy 24, 125-140. .(2003)

Han J., Kim H., 2008, The reduction and control technology of tar during biomass/pyrolysis: an overview. Renewable and Sustainable Energy Reviews 12, 397-416.(2008)

A System Design for Co_2 Capture with Hydrogen and Methanol Production in a Cement Plant

[1*]Ibrahim Akgun and [2,1]Ibrahim Dincer
[1] Mechanical Engineering Department, Yildiz Technical University, Istanbul, 34349, Türkiye
[2] Clean Energy Research Laboratory, Ontario Tech. University, Oshawa, Ontario, L1G 0C5, Canada

*Corresponding author e-mail: iakgun@yildiz.edu.tr

Abstract
This research presents a novel and groundbreaking multigeneration system that has been specifically developed to tackle carbon dioxide emissions in cement production facilities. This system utilizes the calcium cycle to extract carbon dioxide from cement production processes, resulting in the production of methanol. The hydrogen gas used in the system is created through alkaline electrolysis and is supported by wind power. A portion of the hydrogen generated is utilized to react with carbon dioxide, producing methanol, while the remaining amount is stored in a storage tank. The system also produces electricity and hot water as valuable outputs. The design of the system incorporates other renewable resources, such as solar energy, to enhance the overall design. The system achieved a hydrogen production rate of 0.002063 kg/s and a methanol production rate of 0.04082 kg/s. Moreover, the system had an energy efficiency of 71.26% and an exergy efficiency of 60.42%, respectively.

Keywords: Cement, Hydrogen, Methanol, Exergy, Carbon Capture.

Introduction

Engineers and scientists strive to develop creative and groundbreaking solutions to address the pressing challenges of climate change and increasing global energy demands [1]. The cement industry is a substantial contributor to global CO_2 emissions, accounting for about 8% of the total [2]. In addition to its impact on global warming, this industry also poses a risk of terrestrial and marine ecotoxicity and abiotic depletion [3]. Although efforts have been made to incorporate geopolymers in concrete to enhance sustainability, conventional concrete is still more widely used [4]. The construction industry is predicted to fuel cement production growth, with estimates projecting an increase of 12-23% by 2050 [5]. In the production of cement, the majority of the CO_2 emissions are associated with the manufacturing of clinker. To create clinker, a combination of limestone, which serves as a calcium source, and other substances such as aluminium, silicon, and iron in the form of clay and sand is crushed and ground. This precalcined mixture is then heated to approximately 1450 ◦C in a rotary kiln and converted into calcium aluminate, calcium ferrite, and other compounds [6]. This mixture is referred to as clinker and is subsequently combined with gypsum to produce cement. The chemical reactions involved in this process can be summarized as follows: clay decomposition, dolomite decomposition, calcite decomposition, and alumina's reactions with various oxides. Both the breakdown of calcite and dolomite as well as the interaction of alumina with different oxides result in the formation of CO_2. Its production can also result from other chemical events like sintering. Numerous techniques have been developed to lower CO_2 emissions, such as the calcium looping method, which can extract up to 98% of the gas from flue gas streams. The carbonator and calciner, two fluidized beds, cooperate in this process to separate CO_2. CaO in the carbonator undergoes a reversible chemical reaction with CO_2 in the flue gas to form $CaCO_3$. The following is an explanation of this reversible chemical reaction: $CaO + \mathrm{CO}_2 \rightarrow CaCO_3$.

The main objective of this study is to meet the fundamental needs of a small residential community in Canakkale, Türkiye, by proposing an innovative multigeneration system that generates four beneficial outputs. Along with producing hot water and electricity, the system will also produce important energy carriers including hydrogen and methanol. The community's increased energy needs will be fulfilled by renewable resources, and the methanol will be manufactured using CO_2 gathered from a cement plant's calcium looping technology to improve sustainability. Comprehensive energy and exergy assessments are part of the study's analysis, which assesses how well the system operates in its designated environment.

Analysis

The proposed system is analysed thermodynamically to identify the mass flow rates, enthalpies, pressures, and temperatures of flows entering and exiting the system. The exergy destruction rate is determined to locate irreversible losses within each component of the system. The modelling is done using the EES software under specific assumptions, along with the balance equations written for mass, energy, entropy and exergy. The chemical reaction taking place in the methanol reactor is $\mathrm{CO}_2 + 3H_2 \rightarrow \mathrm{CH_3OH} + \mathrm{H_2O}$.

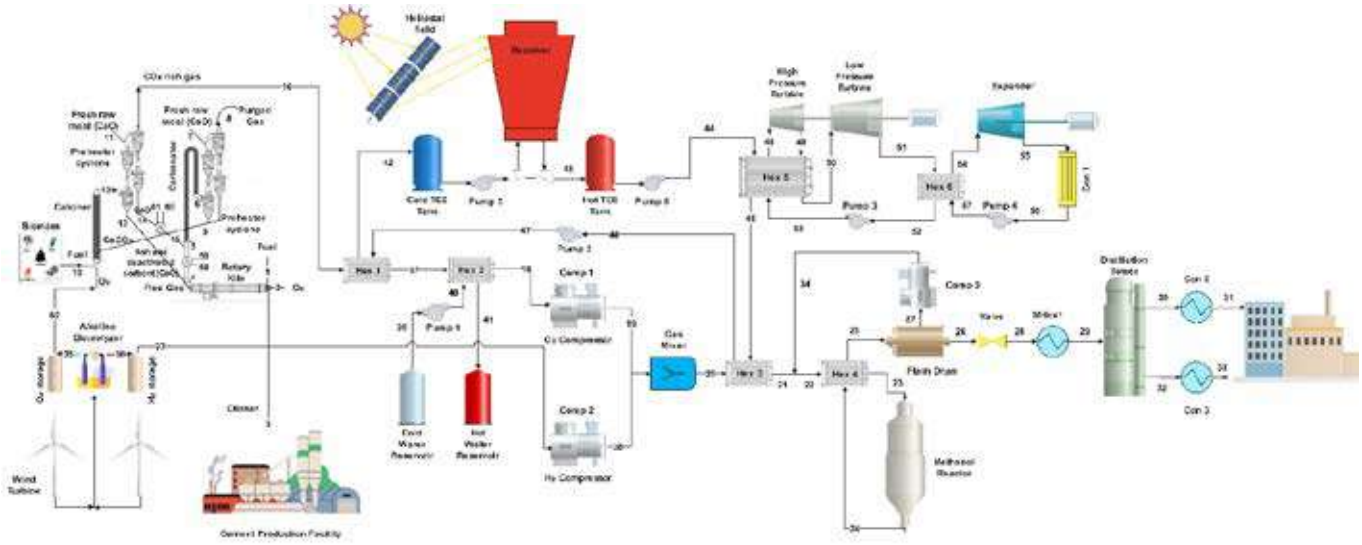


Fig. 1. Schematic view of the integrated system proposed for cement plants.

The overall energetic and exergetic efficiencies of the system are determined by

$$\eta_{en,ovr} = \frac{\dot{W}_{net}+\dot{Q}_{HW}+\dot{m}_{H3}LHV_{H3}+\dot{m}_{CH3OH}LHV_{CH3OH}}{\dot{m}_{CO2}h_{CO2}+ E_{WT}+\dot{Q}_{Solar}+\dot{Q}_{Fuel}}$$

$$\eta_{ex,ovr} = \frac{\dot{W}_{net}+\dot{Q}_{HW}\left(1-\frac{T_0}{T_S}\right)+\dot{m}_{H3}ex_{H3}+\dot{m}_{CH3OH}ex_{CH3OH}}{\dot{m}_{CO2}ex_{CO2}+ E_{WT}+\dot{E}x^{Q_{Solar}}+\dot{E}x^{Q_{Fuel}}}$$

where $\dot{W}_{net}$ is net power produced by the proposed system and is calculated as

$\dot{W}_{net} = \dot{W}_{HPT} + \dot{W}_{LPT} + \dot{W}_{Exp} - \dot{W}_{Pump1} - \dot{W}_{Pump2} - \dot{W}_{Pump3}. - \dot{W}_{Pump4}. - \dot{W}_{Pump5}. - \dot{W}_{Pump6}. - \dot{W}_{Comp1}. - \dot{W}_{Comp2}. - \dot{W}_{Comp3}.$

Results and Discussion

As a result, the High-Pressure Turbine (HPT) has a noteworthy exergy destruction of 2625 kW, whereas the Heat Exchanger 5 (HEX5) has the most exergy destruction of 5449 kW. The exergy destructions of the Pump4, Comp3, HEX1, and Comp2 subsystems are found to be 3.29, 4.05, 4.59, and 6.16 kW, respectively. Here it can be seen that HEX5 has the highest exergy destruction and Pump4 has the lowest exergy destruction.

A parametric study was conducted to evaluate the performance of the integrated system, taking into account the first and second laws of thermodynamics. The study examined the impact of varying the mass flow rate of carbon dioxide supplied to the integrated system and the effect of changing the ambient temperature on system performance. Fig. 2 show the effect of temperature on the system's energy and exergy efficiencies. As the temperature increases from 263 to 313 K, the energy efficiency improves from 66.42 to 72.86%, exergy efficiency increases from 56.75 to 61.62%.

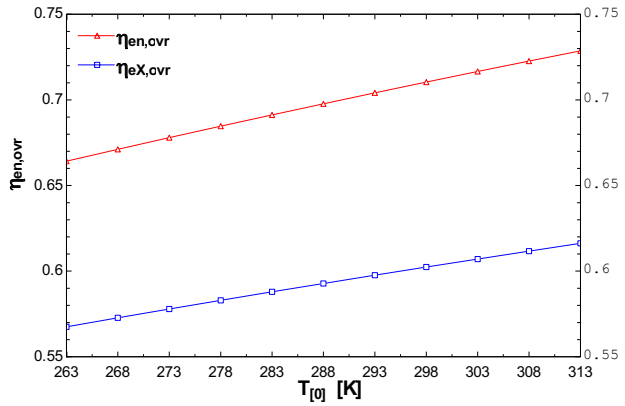


Fig 2. Variation of the ambient temperature with overall efficiencies.

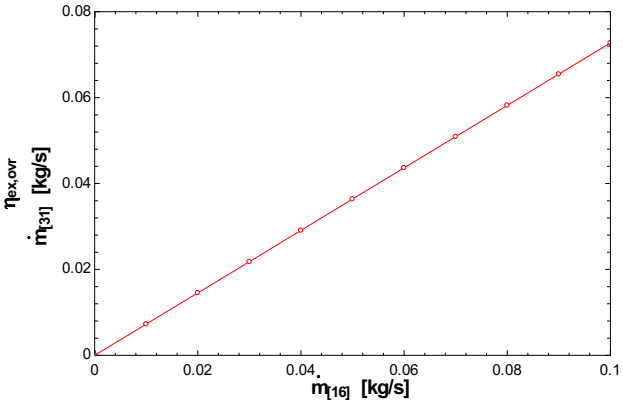


Fig 3. Exchange of supplied carbon dioxide with methanol

Figure 3 depicts the impact of varying carbon dioxide input on methanol production. As the carbon dioxide flow rate escalates from 0.01 kg/s to 0.1 kg/s, the corresponding methanol flow rate also ascends from 0.007273 kg/s to 0.07273 kg/s.

Conclusions

The following are the main conclusions drawn from the proposed integrated system for cement plants. Firstly, the net power produced, methanol flow rate, and hydrogen flow rate produced under specified conditions were 5528 kW, 0.04082 kg/s, and 0.002063 kg/s, respectively. Moreover, the produced hot water flow rate was calculated as 0.22296 kg/s. Secondly, the energy efficiency and exergy efficiency of the system were calculated to be 71.26% and 60.42%, respectively. These findings demonstrate the effectiveness of the proposed integrated system for cement plants in terms of power production and energy efficiency.

References

I. Dincer, A. Midilli, A. Hepbasli, and T. H. Karakoc, *Global Warming: Engineering Solutions*. Springer, 2009.

Bellona, “Climate action in the cement industry,” 2020. https://bellona.org/publication/factsheets-serie-1-climate-action-in-the-cement-industry.

C. Chen, G. Habert, Y. Bouzidi, and A. Jullien, “Environmental impact of cement production : detail of the different processes and cement plant variability evaluation,” *J. Clean. Prod.*, vol. 18, no. 5, pp. 478–485, 2010, doi: 10.1016/j.jclepro.2009.12.014.

R. Shanmuganathan *et al.*, “Utilisation of persistent chemical pollutant incorporating with nanoparticles to modify the properties of geopolymer and cement concrete,” *Environ. Res.*, vol. 219, no. December 2022, p. 114965, 2023, doi: 10.1016/j.envres.2022.114965.

International Energy Agency, “Technology Roadmap Low- Carbon Transition in the Cement Industry,” 2018. [Online]. Available: https://www.iea.org/reports/technology-roadmap-low-carbon-transition-in-the-cement-industry.

M. G. Plaza, S. Mart, and F. Rubiera, “Cement Industry : State of the Art and Expectations,” *Energies*, no. 1, 2020.

Biohydrogen and biomethane production using an integrated bioelectrochemical and anaerobic digestion reactor from poplar and cow manure wastes

[1*]A. Faruk Kılıcaslan, [1,2] A. Yagmur Goren, [1] Ibrahim Dincer and [3] Ali Khalvati
[1] Clean Energy Research Laboratory (CERL), FEAS, Ontario Tech. University, Oshawa, Ontario L1G 0C5, Canada
[2] Izmir Institute of Technology, Department of Environmental Engineering, Urla, Izmir 35430, Türkiye
[3] Viona Consulting INC., Agro-Environmental Innovation and Technology, Research and Development Company, Thornhill, Ontario L3T 0C6, Canada
* E-mail: ahmet.kilicaslan@ontariotechu.net

Abstract
The release of greenhouse gases from fossil fuels has brought about environmental concerns that have transformed industrial business planning and led to the development of state-of-the-art equipment for green bioenergy generation. Microbial electrolytic cells (MEC) have drawn much interest as a practical, innovative, and environmentally friendly method in this context. This study investigated the production of biohydrogen ($bioH_2$) from an energetic poplar and cow manure mixture in a membrane-less single-cell microbial electrolysis cell (MEC) and biomethane ($bioCH_4$) production in an anaerobic digestion cell. The MEC system was performed with 1.0 V. The highest $bioH_2$ production rate was measured as 1.797 mg/L, and it was obtained at the end of the first day. The maximum $bioCH_4$ production was obtained at the end of the first five days with 0.72 L.

Keywords: Microbial electrolysis, biohydrogen, biogas, energetic poplar leaves, organic sludge,

I. Introduction

Energy resources have an important effect on the development of civilizations. Because of their low cost, increased energy content, consistency, and advantages in storage, fossil fuels remain a vital energy source for nations with developed economies (Abbasi et al., 2022). However, the major obstacle to the sustainable growth of human society is the excessive use of non-renewable fossil fuels, which results in severe global energy shortages and biodiversity loss. Research into green, renewable energy sources that replace fossil fuels recently gained international traction (Deora et al., 2022). Specifically, there are a variety of sustainable and eco-friendly strategies that can be explored to address the global energy crisis. Hydrogen energy stands out among these renewable energy sources with its high energy density and carbon-free properties. While there are many environmentally friendly ways to produce hydrogen, biohydrogen production technologies, like dark and photo fermentation and microbial electrolysis cell processes, provide a more economical and sustainable alternative to methods that rely on fossil fuels (Goren et al., 2023). Historically, H_2 was produced by several photochemical, electrolytic, and thermochemical steps. Electrolysis is the process of dissolving water using electricity, whereas thermochemical techniques use pressure and heat to break molecular bonds. Using photolytic reactions, microorganisms emit H_2. Furthermore, fossil fuels serve as the basis material for thermochemical processes, whereas the more energy-intensive electrolytic and photolytic processes demand higher costs.

The many forms of wastewater, lignocellulosic biomass, and organic materials, which are inexpensive, readily available, and leftovers from other industries, can be used for the biological generation of H_2. The microbial electrolysis cell (MEC) is considered a practical and innovative technique in this area. MEC technology can process organic waste and produce gaseous energy simultaneously. Thus, the membrane-less MEC system was employed in this work to produce biohydrogen from a mixture of cow manure and poplar leaves. When the hydrogen production was finished in the MEC system, organic sludge was fed into an anaerobic digester to produce biomethane as well. In this process, $bioH_2$ and $bioCH_4$ were produced from a single organic mixture.

II. Experimental

All experimental runs were performed in the single-cell membrane-less MEC system and anerobic digestion cell, constructed using a glass material (Fig. 1). The aluminum plates are used as an anode and cathode electrodes. The membranes of the microbial electrolysis cell and anaerobic digester were 600 mL of cow manure, 4500 mL of acid-treated energetic poplar as a biomass source, and 225 mL of mineral oil. The copper wire connected to electrodes was used to link the MEC to the voltage delivered from an adjustable DC power supply. The $bioH_2$ gas and $bioCH_4$ were collected in an external cylindrical container, which includes an MQ-8 hydrogen sensor, and monitored during the experiments.

III. Analysis

To find the overall amount of biohydrogen created throughout each period, the cumulative biohydrogen production can be calculated as follows:

$$V_{H_{2,t}} = C_{H_{2,t}} \times V_{BG,t} + V_{HS} \times \left(C_{H_{2,t}} - C_{H_{2,t-1}}\right) \quad (1)$$

The variables $C_{H_{2,t}}$ and $C_{H_{2,t-1}}$ denote the H_2 concentrations measured at times t and t-1, and $V_{BG,t}$ and V_{HS} denote the reactor's headspace volume and the volume of biogas generated between times t and t-1, respectively. The cumulative H_2 production ($V_{H_{2,cum}}$) production was then computed as the total of the H_2 productions between each measurement ($V_{H_{2,cum}}$) throughout fermentation.

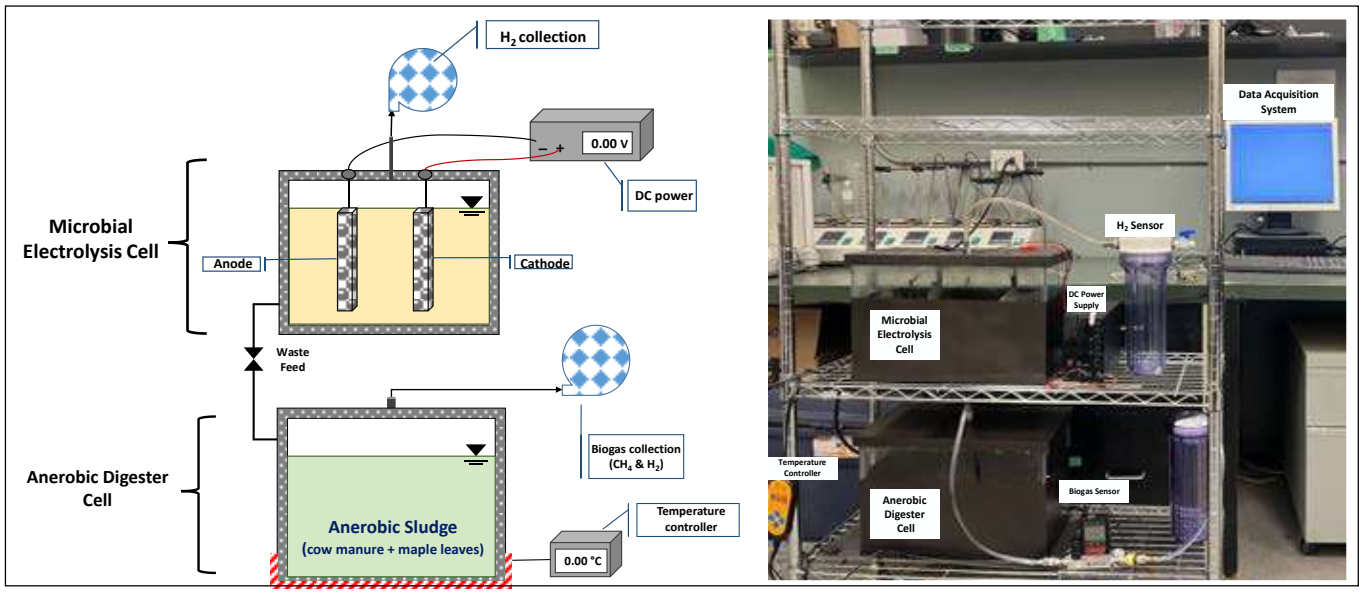


Fig. 1: Schematic diagram and experimental set-up for microbial electrolysis cell and anaerobic digester cell.

IV. Results and discussion

This study examined the effects of the days on hydrogen and methane production in MEC and anaerobic digestion systems, respectively. Hydrogen was produced in the MEC system, and methane was produced in the anaerobic digestion cell. The MEC system was worked under 1.0V applied voltages. This experiment was continued for 10 consecutive days, and daily hydrogen and methane production were measured. The highest hydrogen production was measured at the end of the first day at 1.797 mg/L. The hydrogen production rate kept decreasing continuously, and the lowest hydrogen production was measured at the end of the ten days at 0.071 mg/L. At the end of the ten days, organic sludge in the MEC system was carried to an anaerobic digestion cell with the help of the pump to the methane production process. The anaerobic digestion cell was heated from an external heater to obtain the optimum temperature for methane production. The methane production was changed for the first five days. The maximum methane production value was measured as 0.72 L. However, as expected, minimum methane production was measured at the end of the ten days with 0.482 L. The main reason for continuous drops in hydrogen and methane production is the decrease in the number of beneficial microorganisms daily.

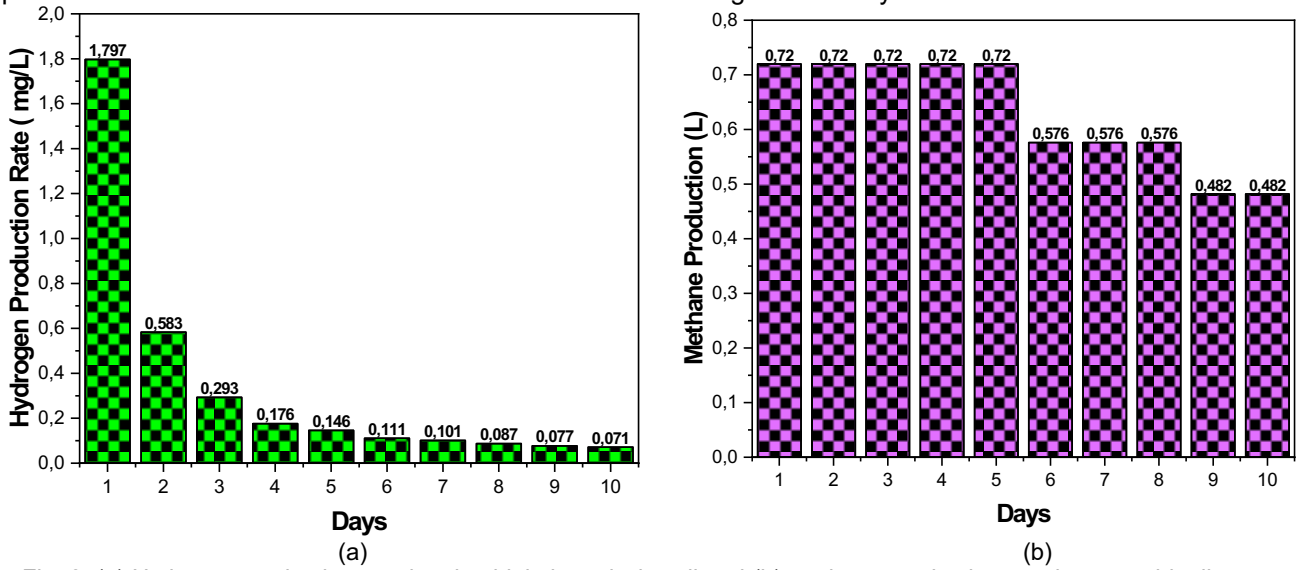


Fig. 2: (a) Hydrogen production rate in microbial electrolysis cell and (b) methane production rate in anaerobic digester cell.

V. Conclusions

In this paper, the membrane-less single-cell MEC and anaerobic digestion processes were performed for both sustainable bioH_2 production and bioCH_4 production. In the MEC system, aluminum electrodes are used, and 1.0 V is applied to the system. The maximum bioH_2 and bioCH_4 production was obtained at the end of the first day at 1.757 mg/L and 0.72 L, respectively. After the first day, gas production rates decreased because of the death of the microorganism. This study aims finally to ensure continuous bioH_2 and bioCH_4 production by feeding the system externally.

References

Abbasi KR, Shahbaz M, Zhang J, Irfan M, Alvarado R. 2022. Analyze the environmental sustainability factors of China: The role of fossil fuel energy and renewable energy. Renewable Energy 187:390–402.

Deora PS, Verma Y, Muhal RA, Goswami C, Singh T. 2022. Biofuels: An alternative to conventional fuel and energy source. Materials Today: Proceedings 48:1178–84.

Goren AY, Dincer I, Khalvati A. 2023. A Comprehensive Review on Environmental and Economic Impacts of Hydrogen Production from Traditional and Cleaner Resources. Journal of Environmental Chemical Engineering 111187.

Design of a Novel Solar-Based Sustainable Energy System with Energy Storage

[1]Ayse Sinem Meke, Ibrahim Dincer
CERL, FEAS, Ontario Tech. University, 2000 Simcoe St. North, Oshawa, ON L1G 0C5, Canada

* E-mails: Ayse.Meke@ontariotechu.ca

Abstract
This research explores a solar-driven energy infrastructure integrated with thermal energy storage to meet community sustainability needs by generating electricity, heat, fresh water, and hydrogen. Evaluation using thermodynamics laws emphasizes energy and exergy analyses. Two different case studies have been carried out. The CSP plant's ability to produce electricity is the only subject of the first case study. This case study's energy and energy efficiencies are 31.66% and 33.36%, respectively. The second case study looks at how the production of hydrogen and clean water can be combined with the heating and cooling systems that generate power. 29,018.10 kg of hydrogen and 369,013.52 m^3 of water are produced per day in this system. The energy and energy efficiencies reach 20.68% and 16.87%, respectively. Furthermore, an economic feasibility study shows LCOE of $0.13/kWh. The integrated energy system offers a path to developing greener communities in the long term by reducing carbon emissions.

Keywords: Solar energy, hydrogen, energy storage, energy, exergy, efficiency, energy storage, sustainability

I. Introduction

Global fossil fuel combustion, driving various sectors such as industry, transportation, and residential activities, significantly contributes to societal progress. However, this combustion process emits greenhouse gases, particularly carbon dioxide, leading to unprecedented atmospheric levels (Fávero, 2022). Such emissions have detrimental effects on the Earth's climate and ecosystems. To counteract these impacts, the exploration of alternative energy sources has become imperative (Caselles, 2021). Among these alternatives, solar energy emerges as a promising solution due to its versatility in applications ranging from transportation to clean fuel production and residential use (Cheng, 2022). Despite its promise, solar energy faces challenges related to intermittency, which can be addressed through effective storage solutions (İnada, 2022).

Renewable energy technologies, driven by the pursuit of sustainability, have seen significant advancements globally. Concentrated solar power (CSP) systems represent one such technology, offering a viable solution to diverse energy needs (Desai, 2015). This research aims to contribute to the understanding of renewable energy systems by evaluating the performance of CSP through two case studies involving concentrated solar power plants. By harnessing CSP technology, solar energy becomes a plentiful and sustainable resource, with these systems efficiently converting solar radiation into electrical power using cutting-edge technology.

This investigation, emphasizing CSP systems' superiority over conventional solar photovoltaic systems, particularly in ensuring consistent and dependable electricity supply, aligns with broader sustainable energy research efforts focusing on integrating solar energy into multigenerational industrial applications (Olabi, 2021).

The present study introduces a novel integrated energy system, distinguishing itself from existing literature through several key innovations. Firstly, it employs a unique design for subsystem integration. Secondly, it combines Rankine and Kalina cycles within a parabolic trough driven system. Additionally, the study considers two distinct operating modes: day and night. A comparative evaluation is conducted between single generation and multigeneration systems, serving as two separate case studies. Thermodynamic principles, encompassing both the first and second laws, are utilized to analyse these case studies. Unlike the first, the second case study incorporates heating and cooling loads, as well as hydrogen and clean water production. Energy and exergy analyses are employed to comparatively assess the two case studies.

II. System Description

The ongoing global pursuit of sustainable energy solutions has spurred remarkable innovations within the renewable energy sector. This study represents a significant contribution by focusing on the development and implementation of a multigenerational solar-powered sustainable energy system. The impetus behind this endeavour stems from the escalating need for both economically viable and environmentally friendly power generation solutions. At the heart of this research lies a sophisticated approach to harnessing thermal energy derived from solar fields and converting it into electricity. What sets this system apart is its adaptive nature, capable of operating in two distinct modes that dynamically adjust based on the availability of thermal energy resources.

In the first mode, the primary power generation subsystem utilizes water to generate superheated steam, driving a back pressure turbine to produce electricity. Simultaneously, a secondary subsystem employs a different working fluid and turbine configuration. However, when the thermal energy output from the primary subsystem exceeds a predetermined threshold, both subsystems collaborate, effectively utilizing excess heat from the primary system's exhaust steam. Conversely, when thermal energy falls below this threshold, priority shifts to the secondary subsystem for power generation, ensuring optimal efficiency and resource utilization at all times.

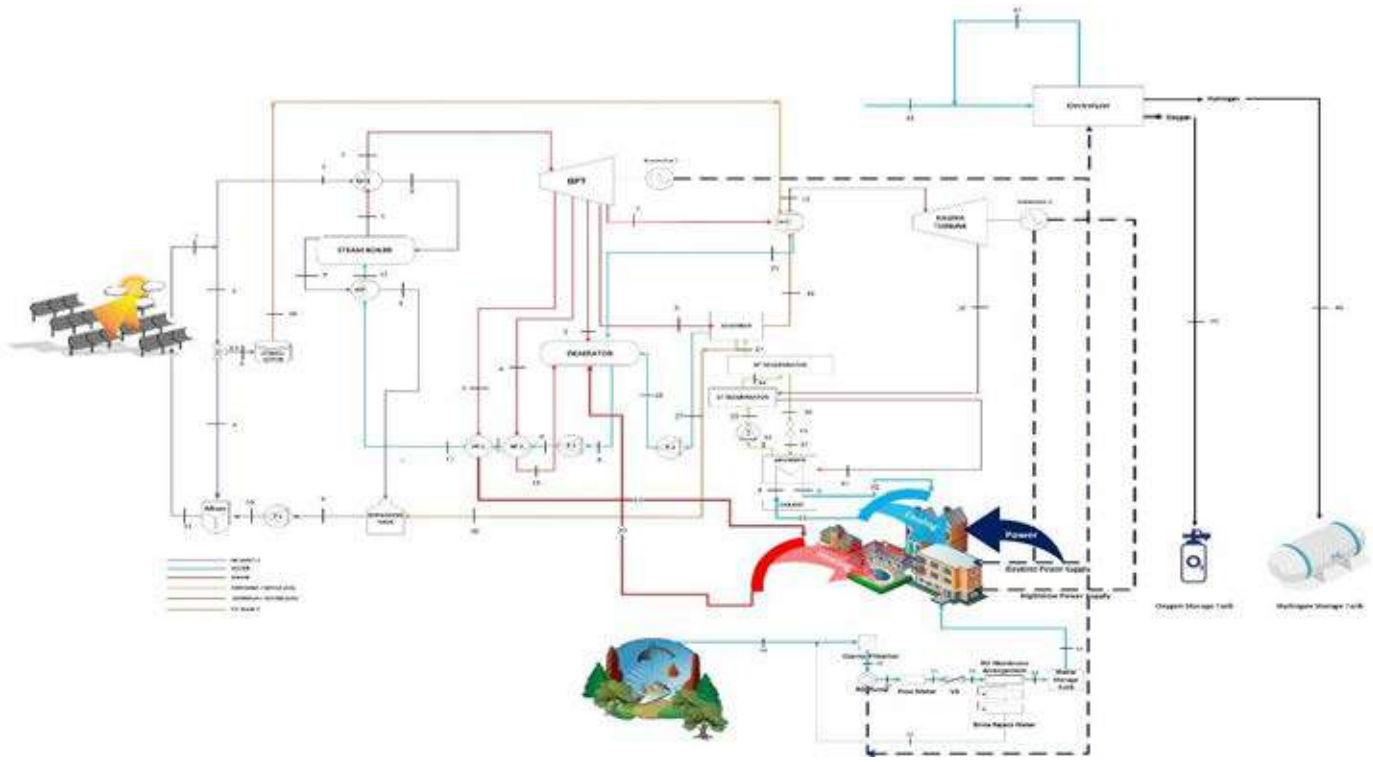


Fig. 1: Schematic Representation of the Process Diagram for Case Study 2

The efficacy and versatility of the designed multigenerational system are thoroughly examined through two comprehensive case studies. In Case Study 1, the focus lies solely on electricity production, tailored to meet the specific needs of the targeted community. Meanwhile, Case Study 2 (Fig. 1) encompasses a broader spectrum of energy requirements by integrating additional functionalities such as hydrogen production, heating, cooling, and desalination alongside electricity generation. This holistic approach underscores the system's capability to address diverse energy needs while promoting sustainability and resilience in the face of evolving energy landscapes.

In summary, the multigenerational solar-powered sustainable energy system represents a significant step forward in the quest for sustainable energy solutions. By combining cutting-edge technology with adaptive operational modes, this system not only offers a reliable source of electricity but also presents a comprehensive energy solution that can be tailored to meet the varying needs of different communities and regions.

III. Analysis

Analysis studies were carried out for both case studies, considering the first and second laws of thermodynamics. For the first case study, overall energy and exergy efficiency are calculated with equations 1 and 2 below.

$$\text{Energy Efficiency} = \frac{W_{net}}{Q_{in,HC}} \quad (1)$$

$$\text{Exergy Efficiency} = \frac{W_{net}}{Ex_{Q_{in,HC}}} \quad (2)$$

In the analysis made for Case Study 2, taking into account other useful outputs, the overall energy and exergy efficiencies are calculated from Equations 3 and 4 as:

$$\text{Energy Efficiency} = \frac{W_{net} + Q_{heating} + Q_{cooling} + m_{H_2} \times LHV_{H_2} + m_{fresh\ water} \times h_{fresh\ water}}{Q_{in,HC}} \quad (3)$$

$$\text{Exergy Efficiency} = \frac{W_{net} + Ex_{Q_{heating}} + Ex_{Q_{cooling}} + m_{H_2} \times ex_{H_2} + m_{fresh\ water} \times ex_{fresh\ water}}{Ex_{Q_{in,HC}}} \quad (4)$$

IV. Results and discussion

For case study 1, the system's excellent performance in utilizing solar energy to produce electricity is demonstrated by the achieved overall energy and exergy efficiencies of 31.66% and 33.36%, respectively. Considering the extra integration of heating and cooling systems, hydrogen, and clean water production case study 2's overall energy and energy efficiencies of 29% and 23% show a strong performance.

The changes in hydrogen production versus solar intensity for this study are given in Figure 2.

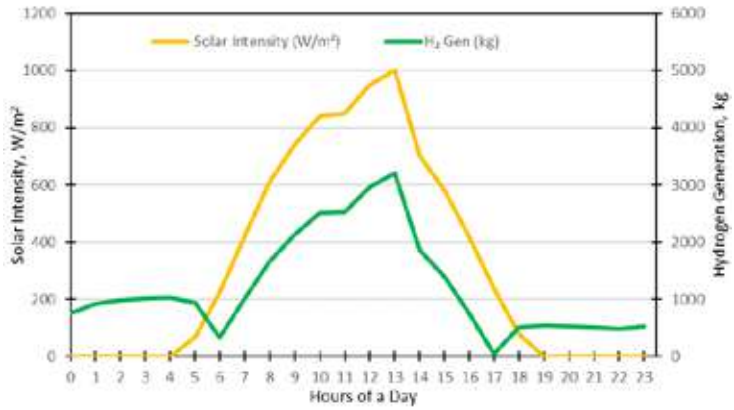
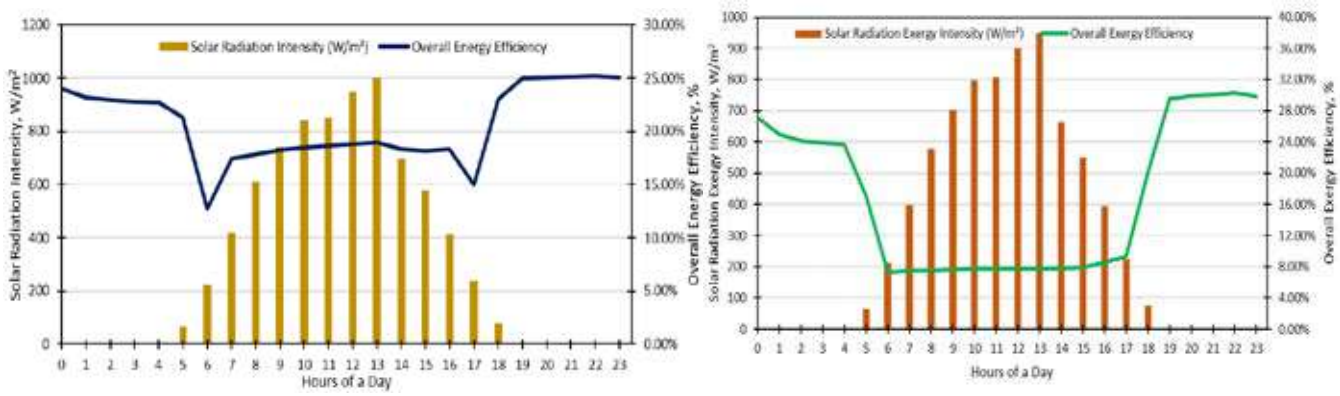


Fig. 2: The changes in hydrogen production versus solar intensity for case study 2

Hydrogen production exhibits a close correlation with solar irradiance. Peaks in hydrogen production align with periods of maximum solar energy availability. The system's exceptional efficacy in generating hydrogen from excess electricity underscores the potential of utilizing solar energy for the sustainable and environmentally friendly production of hydrogen fuel.



(a) (b)

Fig. 3: The overall energy (a) and exergy (b) efficiencies and energy of solar intensity for case study 2 according to hours of a day.

Figures 3a and 3b depict the energy and exergy efficiencies of Case Study 2's overall system. These visuals reveal how efficiency fluctuates with solar intensity, indicating the system's reliance on solar energy. During peak solar hours, efficiency is at its highest, showcasing the system's ability to convert solar energy into usable forms effectively. Conversely, efficiency drops during low solar intensity periods. This underscores solar energy's pivotal role in system performance, with efficiency decreasing at night.

V. Conclusions

In conclusion, the study demonstrates the effectiveness of the concentrated solar power system. Case Study 1 achieved high overall energy and energy efficiencies of 31.66% and 33.36%, respectively. In Case Study 2, although energy and exergy efficiencies were slightly lower at 20.68% and 16.87%, the system's integration of heating, cooling, hydrogen, and clean water production proved holistic. Daily production included 29,018.10 kg of hydrogen and 369,013.52 m^3 of clean water. Despite initial costs, the system offers significant long-term environmental and economic benefits for communities adopting sustainable energy solutions.

References

Caselles A, Sanz MT. The use of energies as a tool to stabilise climate and world population. International Journal of Global Warming 2021; 23:91–109.

Cheng P, Liu W, Ma J, Zhang L, Jia L. Solar-powered rail transportation in China: Potential, scenario, and case. Energy 2022; 245:123221.

Desai NB, Bandyopadhyay S. Optimization of concentrating solar thermal power plant based on parabolic trough collector. J Clean Prod 2015; 89:262–71.

Fávero LP, de Freitas Souza R, Belfiore P, Luppe MR, Severo M. Global relationship between economic growth and CO2 emissions across time: A multilevel approach. International Journal of Global Warming 2022; 26:38–63.

İnada AA, Arman S, Safaei B. A novel review on the efficiency of nanomaterials for solar energy storage systems. J Energy Storage 2022; 55:105661.

Olabi AG, Wilberforce T, Abdelkareem MA. Fuel cell application in the automotive industry and future perspective. Energy 2021; 214:118955.

Electric airplane energy storage and pem fuel cell island airport microgrid load frequency control

[1*]Cem Haydaroğlu
[1] Dicle University, Engineering Faculty, Department of Electrical and Electronics Engineering Department, Sur, Diyarbakır, 21280, Türkiye

* E-mail:cem.haydaroglu@dicle.edu.tr

Abstract
This study analyses the transformation in the energy sector and the effects of the transition to renewable energy sources on microgrid structures. Factors such as increasing energy demand, climate change concerns and decreasing fossil fuel reserves make the need for renewable energy even more important. In this study, a fuel cell Airport Microgrid (AMG) model is created in Matlab/Simulink and a controller is designed that continuously monitors the frequency deviations and adjusts the output power accordingly. This approach is considered as an important step for optimising control in microgrid structures and efficient use of renewable energy resources. Furthermore, the precise adjustment of the controller parameters using the ant colony optimisation algorithm is an innovative approach to improve the system performance.

Keywords: Hydrogen energy; PEM Fuel Cell; Ant optimisation algorithm; Electric aircraft; Airport microgrid

I. Introduction

Today, energy is essential for economic growth, but 71% of energy is supplied from fossil fuels (Arsad et al. 2022). Population growth and the rapid development of technology cause energy demand to increase rapidly. In addition, the use of fossil fuels causes climate change, greenhouse gas emissions, ecological and global problems. Especially in the next decade, energy consumption is expected to reach its peak. Therefore, the faster depletion of oil reserves, especially one of the fossil fuels, threatens the economy and energy security (Kilic 2024). Due to both environmental climate change and the depletion of fossil fuels, the transition to renewable energy sources has accelerated. Organisations such as the European Union have set targets to reduce carbon dioxide (CO2) emissions by 40% in the transition to clean energy sources (Hassan et al. 2024). In the light of these targets, a minimum 32% increase in renewable energy sources and a minimum 27% improvement in energy efficiency are foreseen today. In addition, deficiencies in electrical energy infrastructures need to be corrected to ensure energy security and stability of power systems. In addition, the aviation sector is responsible for about 3% of the total CO2 emissions to the environment. 24% of CO2 emissions to the environment come from fossil fuels used in road, air, sea and rail transport. All this situation has pushed the aviation sector to develop policies to decarbonise the aviation sector. renewable energy sources (RES) electric aircraft and hybrid electric aircraft (HEAC) have been tried to achieve the low-carbon target (Shayeghi, Davoudkhani, and Bizon 2024). For the transition to a decarbonised world economy, the capacity of operational water electrolysers is projected to reach 6000-3000 GW by 2050 (Kilic, Asker, and Haydaroglu 2024).

With the inclusion of renewable energy sources, electric vehicles, fuel cells and energy storage structures, the traditional grid structure has changed. With this change and development, the micro grid structure has come to the fore. Its biggest advantage is that it can operate independently from the grid. However, renewable energy sources such as wind turbines and solar energy change the amount of instantaneous power generation according to nature and weather conditions. In the event of an imbalance between the generated power and the load demand of the system, deviations in frequency occur and cause deterioration of power quality. In order to eliminate this situation, a load frequency control strategy is needed. In off-grid systems, it is necessary to limit frequency deviations with some predefined constraints to reduce the difference between the generated power and the demanded power. Many classical, smart and robust methods have been developed for load-frequency control in microgrids. In a microgrid consisting of thermal and hydroelectricity, frequency control was performed with a PI-based controller (Xu et al. 2018). General type-2 fuzzy logic sets and Modified Harmony Search Algorithm (MHSA) are used to update the proportional-integral (PI) controller for load frequency control in an islanded microgrid (Khooban et al. 2017). Load frequency control is performed using sliding mode control (SMC) in a microgrid consisting of DERs (Bagheri, Jabbari, and Mobayen 2021). Load frequency control in a microgrid using particle swarm optimisation algorithm (Safari, Babaei, and Farrokhifar 2021). Diesel generators are used as frequency regulators for load frequency control in microgrids, as well as having a negative impact on the environment by emitting pollutants to the environment. Therefore, the continuity and security of energy should be ensured by switching to environmentally friendly alternative technologies. Energy sustainability can be ensured by using environmentally friendly Hydrogen for the storage and transport of excess energy produced by renewable energy sources.

In this study, the Airport microgrid (AMG) model is created in Matlab/Simulink. A controller is designed to continuously monitor the frequency deviations and adjust the output power accordingly. There is no previous study using fuel cell and electrolyser in Airport microgrid network. In this system, ant colony optimisation algorithm is used

to fine tune the controller parameters.

II. Airport microgrid (AMG) model

Airport microgrid (AMG) model is given in Figure 1. This model is a microgrid consisting of diesel generator, wind turbine, solar energy, energy storage system, electric vehicle, fuel cell, electrolyser, terminal building and electric aircraft. The control of all the different parts of the AMG is controlled by the airport microgrid control centre (AMCC), which controls the various parts of the AMG under different operating conditions (Shayeghi, Davoudkhani, and Bizon 2024).

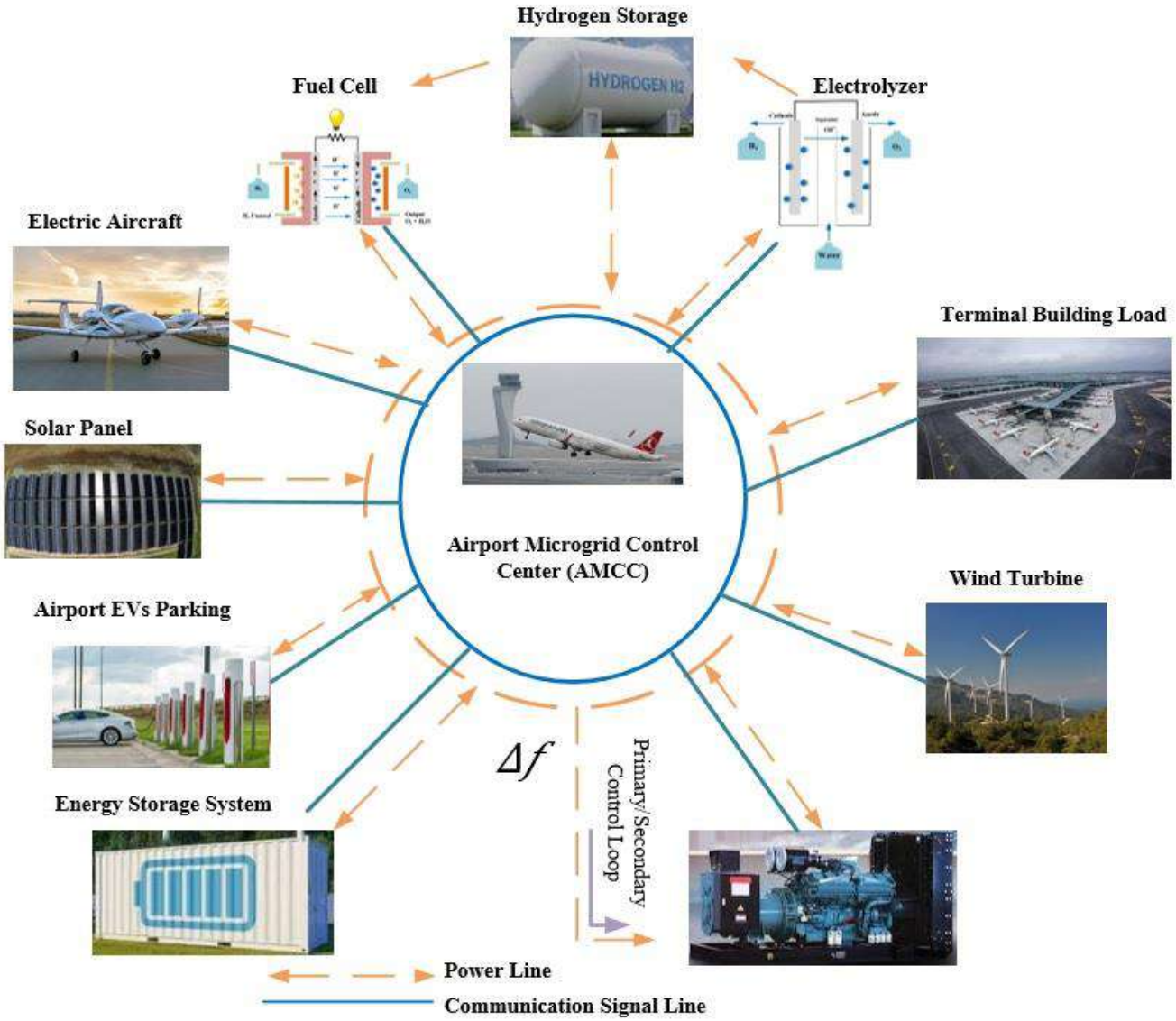


Fig. 1 Electric airplane energy storage and pem fuel cell island airport microgrid

III. Ant Colony Optimization (ACO) Algorithm

As shown in Figure 2, the Traditional Ant Colony Optimisation (ACO) algorithm uses the positive feedback mechanism of pheromones released by ants along the path to transfer information. This mechanism increases the flexibility of the algorithm and strengthens its capacity to identify superior solutions. Figure 2 illustrates the operation of the ACO algorithm. First, all parameters are initialised. Second, ants are randomly placed at different starting points and the next visit point is selected according to the 'path selection probability' principle while the forbidden list is updated. Then, the path segments travelled by the ants are recorded and the pheromone concentration of the path travelled by each ant is updated in real time. Finally, it is checked whether the current number of iterations has

reached the maximum. If not, the ants are relocated to repeat the process; if so, the optimal path is output (Qi 2024).



Fig. 2 Ant colony optimization algorithm

In this section, an airport microgrid system with PEM fuel cell and electrolyser bar is designed. The proposed controller design using ACO method is analysed and evaluated on the airport microgrid system. For this purpose, the ACO optimisation algorithm used in the determination of PID parameters is given in the literature as Integral Time-weighted Squared Error (ITSE), the functions are given in Equation 1.

$$ITSE = \int_0^\infty te^2(t)dt \quad (1)$$

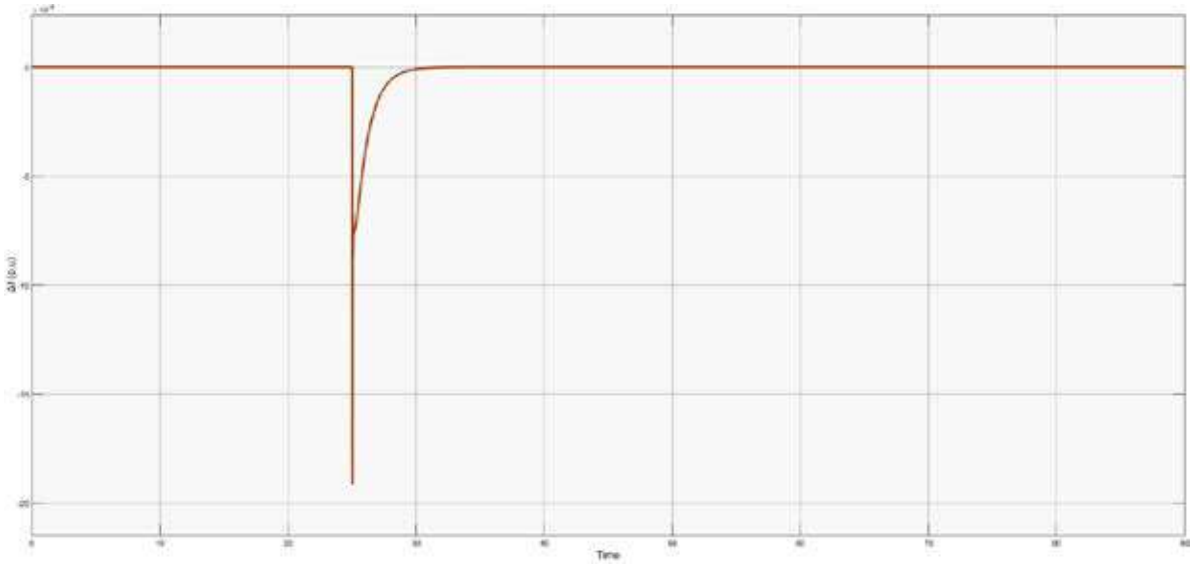


Fig. 3 Frequency response for airport microgrid

As seen in Figure 3, the frequency response of the system is shown when the load is included in the system. When this is analysed, it is seen that the frequency drops very quickly and stabilises very quickly. The smallest value of ITSE error value is calculated as Kp=19.15, Ki=14.48 and Kd=3.84 according to ACO optimisation algorithm.

IV. Conclusions

In this study, electrical network frequency control was performed in the airport microgrid network. PEM fuel cell and electrolyzier are used in the airport microgrid network. PID controller is preferred for load frequency control. ACO optimisation algorithm was used to determine the PID control parameters. In addition, the time to reach steady state, steady state error, damping ratio and ITSE cost value of the cost function is 0.17x10-4 . In future studies, different optimisation methods and different scenarios will be compared and new controller design will be made.

.

References

Arsad, A. Z. et al. 2022. “Hydrogen Energy Storage Integrated Hybrid Renewable Energy Systems: A Review Analysis for Future Research Directions.” International Journal of Hydrogen Energy 47(39): 17285–312. https://doi.org/10.1016/j.ijhydene.2022.03.208.

Bagheri, Amir, Ali Jabbari, and Saleh Mobayen. 2021. “An Intelligent ABC-Based Terminal Sliding Mode Controller for Load-Frequency Control of Islanded Micro-Grids.” Sustainable Cities and Society 64(March 2020): 102544. http://dx.doi.org/10.1016/j.scs.2020.102544.

Hassan, Qusay et al. 2024. “Green Hydrogen: A Pathway to a Sustainable Energy Future.” International Journal of Hydrogen Energy 50: 310–33. https://doi.org/10.1016/j.ijhydene.2023.08.321
.
Khooban, Mohammad Hassan, Taher Niknam, Frede Blaabjerg, and Tomislav Dragičević. 2017. “A New Load Frequency Control Strategy for Micro-Grids with Considering Electrical Vehicles.” Electric Power Systems Research 143: 585–98.

Kilic, Heybet. 2024. “Improving the Performance of Microgrid-Based Power-to-X Systems through Optimization of Renewable Hydrogen Generation.” International Journal of Hydrogen Energy (November 2023). https://doi.org/10.1016/j.ijhydene.2024.01.066.

Kilic, Heybet, M. Emin Asker, and Cem Haydaroglu. 2024. “Enhancing Power System Reliability: Hydrogen Fuel Cell-Integrated D-STATCOM for Voltage Sag Mitigation.” International Journal of Hydrogen Energy (March). https://doi.org/10.1016/j.ijhydene.2024.03.313.

Qi, Zhiqun. 2024. “Application of Improved Ant Colony Algorithm in Optimizing the Charging Path of Electric Vehicles.” World Electric Vehicle Journal 15(6): 230. https://www.mdpi.com/2032-6653/15/6/230.

Safari, Amin, Farshad Babaei, and Meisam Farrokhifar. 2021. “A Load Frequency Control Using a PSO-Based ANN for Micro-Grids in the Presence of Electric Vehicles.” International Journal of Ambient Energy 42(6): 688–700. https://doi.org/10.1080/01430750.2018.1563811.

Shayeghi, Hossein, Iraj Faraji Davoudkhani, and Nicu Bizon. 2024. “Robust Self-adaptive Fuzzy Controller for Load-frequency Control of Islanded Airport Microgrids Considering Electric Aircraft Energy Storage and Demand Response.” IET Renewable Power Generation. https://ietresearch.onlinelibrary.wiley.com/doi/10.1049/rpg2.12926.

Xu, Yanhe et al. 2018. “Load Frequency Control of a Novel Renewable Energy Integrated Micro-Grid Containing Pumped Hydropower Energy Storage.” IEEE Access 6: 29067–77.

Design and Simulation of a Novel Copper-Chlorine Thermochemical Cycle for Hydrogen Production

[1*] Sibel Uygun Batgi, and [2]Ibrahim Dincer
[1,2] Clean Energy Research Laboratory (CERL), FEAS, Ontario Tech University
2000 Simcoe Street North, Oshawa, Ontario, L1H 7K4, Canada

[*]Corresponding author e-mail: sibel.uygun@ontariotechu.ca

Abstract
Hydrogen is a clean energy source that does not contain carbon in its structure in today's world, most of the hydrogen is produced using fossil fuels. New technologies are being developed every day for clean hydrogen production. Thermochemical cycles are known as clean hydrogen production techniques. In this proposed study, a novel three-step copper-chlorine (Cu-Cl) thermochemical cycle that is entirely thermal is designed and simulated using Aspen Plus software. In the simulated system, the amount of Cu_2OCl_2 increased because of the increase in the flow rate of the amount of water used as a reactant, and the heat duty amount of the first heat exchanger also increased. As a result of 0.05 kmol/s $CuCl_2$ and 1 kmol/s H_2O reactant input into the system, the H_2 molar flow rate produced by the system was found to be 0.0245 kmol/s.

Keywords: Hydrogen production, Thermochemical cycles, Copper-chlorine cycle, Aspen Plus, Simulation

I. Introduction

Hydrogen is a carbon-free, clean energy source that will limit the consumption of fossil fuels to prevent global warming. Today, there are several hydrogen production techniques. Thermochemical cycles are one of the hydrogen production techniques. Today, it is known that there are more than 200 thermochemical cycles. Magnesium chloride, cadmium sulfate, iron chlorine, hybrid sulfur, and copper chlorine are some of them. While many thermochemical cycles require temperature of more than 800℃, the maximum temperature required for the Cu-Cl cycle is 550℃ Khalid et al. (2016). In these systems, where a series of reactions take place to split water, all chemical molecules are recovered in the cycle. There are several types of Cu-Cl cycles, and their configurations are presented in the literature Sutar et al. (2024). The Cu-Cl thermochemical cycle varies depending on the number of steps and the type of reaction occurring within the cycle. As the number of steps decreases, the temperature required for the cycle also increases. Many studies presented in the literature include an electrochemical step in addition to chemical reactions. Due to increasing electricity prices and the expense of the electrolysis equipment used, studies are being carried out to reduce or eliminate the electrical load brought on by the electrolysis step Farsi et al. (2020).

The main purpose of this study is to design a new system that works entirely with thermal energy by eliminating the electrolysis step. The proposed system is a three-step thermochemical cycle. System simulation is simulated and analyzed using Aspen Plus software, a chemical process simulation tool. This study investigated parameters such as the change in the amount of energy required for the system's equipment at varying molar flow rates of the reactants, as well as the change in the amount of product generated.

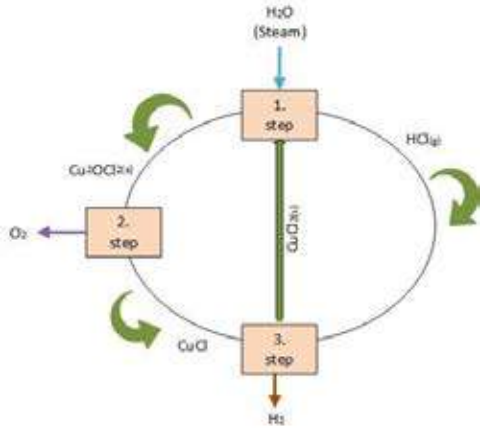


Fig. 1: Simplified demonstration of the proposed 3-step Cu-Cl cycle.

II. System Description

The designed system consists of three steps in the cycle. Each step requires heat addition. Fig. 1 shows the simplified demonstration of the proposed 3-step Cu-Cl cycle The Cu-Cl cycle begins with the hydrolysis of $CuCl_2$. Firstly, as a reactant, H_2O in the gas phase and $CuCl_2$ are supplied to the hydrolysis reactor in the system. This reaction takes place at 400℃. After the hydrolysis reaction is complete, $Cu_2OCl_{2(s)}$ and $HCl_{(g)}$ produce. The produced Cu_2OCl_2 is sent to the decomposition reactor. In the decomposition reactor, it decomposes at 530℃ to form CuCl and O_2. CuCl, which is formed from the decomposition reaction with the $HCl_{(g)}$ produced during the hydrolysis phase, reacts in the hydrogen production reactor at 500℃ and forms $CuCl_2$ and H_2. The cycle is completed in three steps. The $CuCl_2$ formed at the end of the reaction is fed back to the hydrolysis reactor and the cycle is started again. The

reactions taking place within the cycle are as follows:
Step 1: Hydrolysis step

$$2CuCl_{2(s)}+H_2O_{(g)}\rightarrow Cu_2OCl_{2(s)}+2HCl_{(g)} \quad (1)$$

Step 2: Decomposition step

$$T: Cu_2OCl_{2(s)}\rightarrow 1/2O_{2(g)}+2CuCl \quad (2)$$

Step 3: Hydrogen production step

$$2CuCl+2HCl_{(g)}\rightarrow 2CuCl_2+H_{2(g)} \quad (3)$$

III. Analysis

Aspen Plus simulations of the 3-step Cu-Cl cycle have been performed in this study. Aspen Plus predicts the behavior of process reactions and steps using standard engineering relationships, mass, and energy. Also, the Aspen Plus consist of several data bank in it. The Aspen plus database provides thermophysical and thermochemical properties for many elements and compounds. Fig. 2 shows the Aspen plus flowsheet of the 3-step Cu-Cl thermochemical cycle. The reactors used in the system simulation are RStoic reactors, while the selected method is the is the solid method in the Aspen Plus.

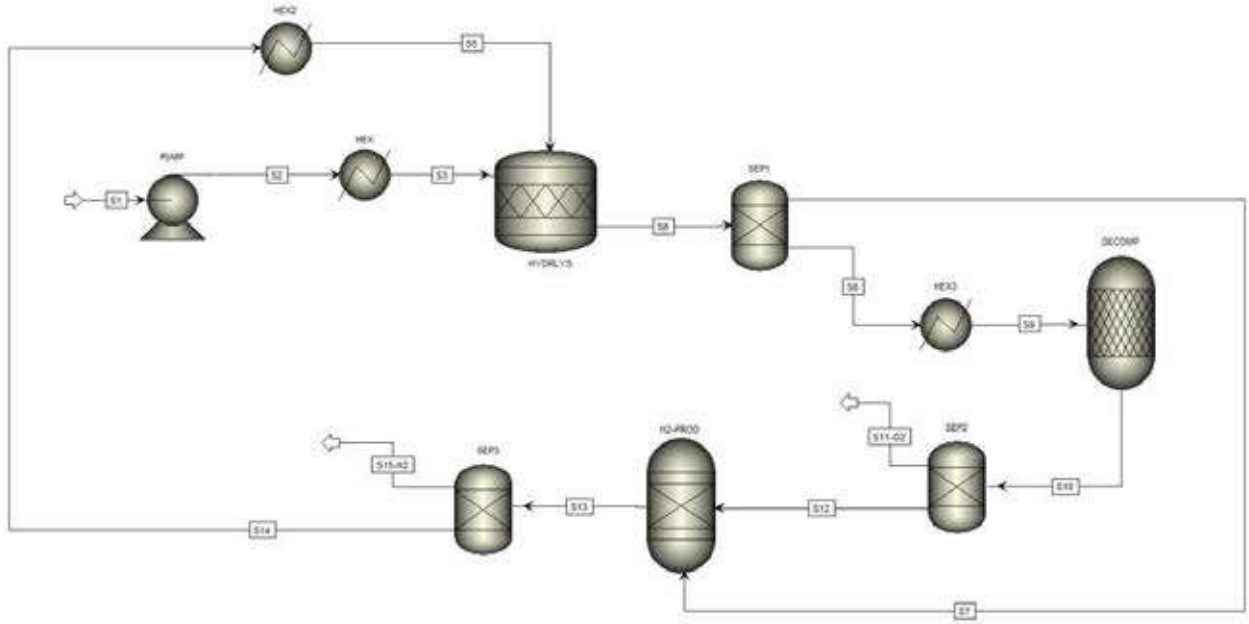


Fig. 2: Aspen plus flowsheet of the 3-step Cu-Cl thermochemical cycle.

IV. Results and discussion

After the system simulation using Aspen Plus, by increasing the molar flow rates of water fed to the hydrolysis reactor from 3000 kmol/h to 5000 kmol/h, the effect of the produced Cu_2OCl_2 molar flow rate and the heat duty of the first heat exchanger is analyzed by performing a parametric study. Fig. 3a shows that affect of H_2O mol flow rate on the produced Cu_2OCl_2 and heat duty of HEX1. Since the water flow rate has increased, the amount of required heat in HEX1 has also increased. By increasing the molar flow rates of $CuCl_2$ fed to the hydrolysis reactor from 100 kmol/h to 750 kmol/h, the effect of the produced H_2 molar flow rate and the thermal duty of the second heat exchanger is analyzed by performing a parametric study. Fig. 2 sows the the effect of $CuCl_2$ mol flow rate on the produced H_2 and heat duty of HEX2.

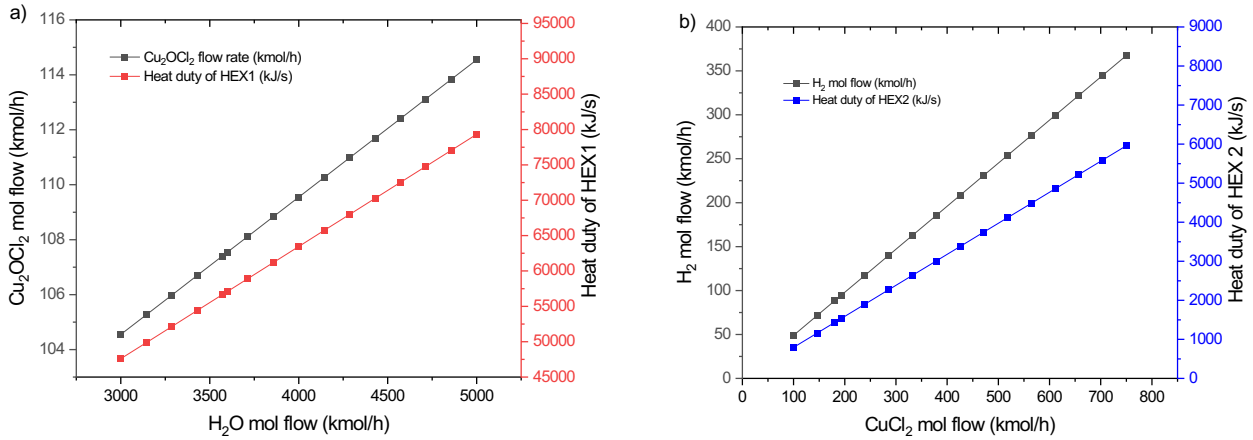


Fig. 3: a) the effect of H_2O mol flow rate on the produced Cu_2OCl_2 and heat duty of HEX1, b) the effect of $CuCl_2$ mol flow rate on the produced H_2 and heat duty of HEX2.

V. Conclusions

As a result of the parametric studies conducted, with the increasing mole flow rate of reactants, the amount of heat duty to be provided to the heaters used in the system also increases. For this reason, the optimum flow rate of the reactants should be determined. As a result of 0.05 kmol/s $CuCl_2$ and 1 kmol/s H_2O reactant input into the system, the H_2 molar flow rate produced by the system was found to be 0.0245 kmol/s.

References

Farsi, A., Dincer, I., & Naterer, G. F., Review and evaluation of clean hydrogen production by the copper–chlorine thermochemical cycle, International Journal of Cleaner Production, 276, 123833, (2020).

Khalid, F., Dincer, I., & Rosen, M. A., Analysis and assessment of an integrated hydrogen energy system, International Journal of Hydrogen Energy, 41(19), 7960–7967, (2016).

Sutar, S. V., Nirukhe, A. B., & Yadav, G. D., Hydrogen production using hybrid six-step copper-chlorine thermochemical cycle: Energy and exergy analyses, International Journal of Hydrogen Energy, 49, 1478–1489, (2024).

Design of an Integrated Multigenerational Energy System for Oleic Acid and Hydrogen Production

*G. Kubilay Karayel and Ibrahim Dincer
Clean Energy Research Laboratory, Faculty of Eng. and App. Science, Ontario Tech University, Ontario, Canada

*Corresponding author: gorkem.karayel@ontariotechu.net

Abstract
This study introduces a novel multigenerational integrated solar geothermal system designed to address various energy needs, including electricity generation, cooling, hot water production, oleic acid production, biomass production and hydrogen. Energy and exergy analysis are conducted to demonstrate the system's performance. A study employing parametric methods is undertaken to examine the impact of operating conditions and environmental parameters on the performance of the system. Results show that the multigeneration system achieves 72.6% efficiency, according to the energy analysis. However, exergy analysis provides valuable system performance insights that system has 36.6% exergetic efficiency. Exergy analysis shows that solar collectors destroy 75% of exergy, which is the main cause of system irreversibilities.

Keywords: Efficiency, energy, exergy, geothermal, multigeneration, solar energy

I. Introduction

There has been a growing focus on environmentally friendly and sustainable sources, such as renewable energy sources. Currently, there exists a diverse range of renewable energy sources that are still in the developmental phase, including solar and geothermal power. In recent times, there has been a growing interest among researchers in integrated multigeneration energy systems as a means to address concerns related to efficiency, cost, and environmental impact. Through the efficient utilization of renewable energy sources, it has the potential to economically rival fossil fuels or even entirely substitute them. Irreversibilities are inherent in all energy conversion processes, thereby imposing limitations on the efficiency of said processes. Hence, if the energy that is lost during conversion processes is effectively utilized, the efficiency of the system will be enhanced. Instead of relying solely on single generation plants, energy systems that aim to generate multiple sources, such as cogeneration, tri-generation, and multigeneration, are designed and implemented for this specific purpose.

The multigenerational integrated geothermalesolar system for the provision of electricity, cooling, space heating, hot water, and industrial heat was investigated by Al-Ali and Dincer (2014). The analysis of energy and exergy involves the comparison of efficiency among single-generation, cogeneration, trigeneration, and multigeneration systems. System performance is analyzed using parametric methods, which examine the impact of operating conditions and environmental parameters. The research revealed energy efficiencies of 16.4% and 78% for single-generation and multigeneration systems, respectively. Furthermore, the exergy efficiencies exhibit an increase to 26.2% and 36.6%. The solar collector system accounts for 75% of the exergy destruction. Mohammadi et al. (2023) conducted a study to enhance the efficiency of a geothermal-solar multigeneration system. The comprehensive system comprises a geothermal line, solar tower, steam Rankine cycle, two organic Rankine cycles, ejector refrigeration cycle, thermoelectric generator unit, and reverse osmosis subsystem. The energy-conversion system is responsible for the production of electricity, freshwater, and cooling components. According to the optimization process, the proposed system achieved an exergy efficiency of 25.4% and a product unit cost of 34.1 $/GJ. The results demonstrate a 48% and 43% enhancement compared to the initial case study. Based on empirical evidence, the range of freshwater production varies between 3.06 kg/s and 3.84 kg/s. The quantity of freshwater produced can range from 1,224 to 1,536 individuals, contingent upon the month.

This study introduces an innovative integrated system that merges solar and geothermal energies, with a specific emphasis on renewable energy sources. The main objectives of this research are to develop a conceptual framework for an innovative integrated system that integrates solar and geothermal energies. The proposed system is intended for applications that span multiple generations. An energy and exergy analysis will be performed to analyze the thermodynamics of the proposed integrated system. A comprehensive assessment of the system's performance will be conducted by considering its energy and exergy efficiencies. Furthermore, an empirical investigation will be undertaken to analyze the influence of different crucial variables on the overall performance.

II. System Description

Figure 1 illustrates the integrated multigeneration solar geothermal system. The integrated system in discussion generates six valuable outputs, namely cooling, electricity, hot water, hydrogen, oleic acid, and residual biomass. The comprehensive system comprises six primary cycles, specifically the geothermal solar cycle, Rankine cycle, organic Rankine cycle, absorption cooling, gasification of hydrogen, and oleic acid production process. The system generates renewable energy by harnessing heat from an injection well using geothermal water, ensuring a continuous supply of environmentally clean, green renewable energy.

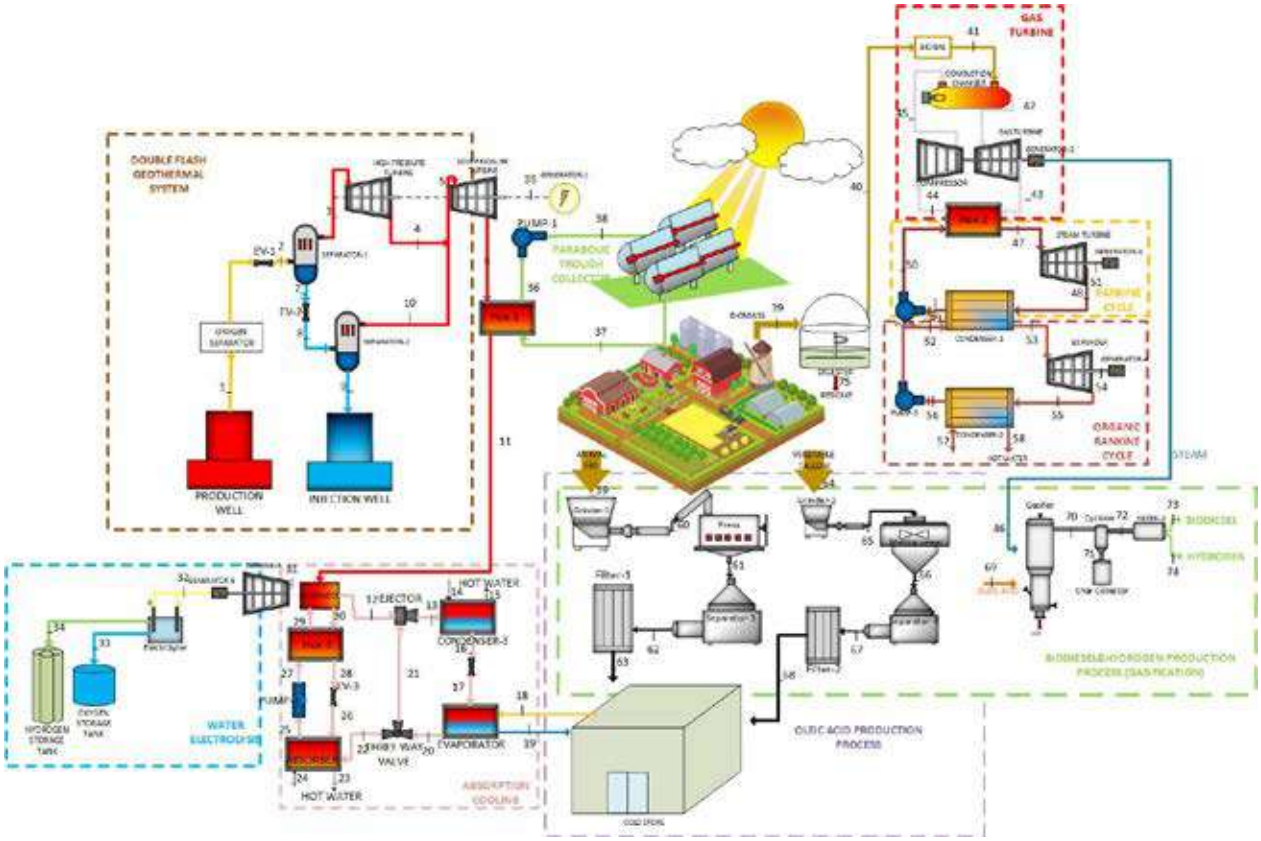


Fig.1. Illustration of proposed multigeneration system with state points.

III. System Analysis

The energy and exergy assessments for the proposed system were conducted using the EES software. In order to obtain more precise findings and ensure the appropriateness of the analytical process, it is necessary to make several assumptions. The assumptions should not have a significant impact on the results or the applicability of the system. Consequently, in order to determine energy and exergy, the source and environmental conditions are established. In order to implement the balancing equations, it is imperative to establish the performance of the components by considering their efficiencies, and consequently, the inefficiencies by considering the heat and pressure losses.

The electrolyte employed in alkaline electrolyzers, which can be regarded as the earliest method for water splitting via electrolysis and hydrogen production, exhibits deterministic properties. It is crucial to bear in mind. The predominant constituent of electrolytes is either potassium hydroxide (KOH) or sodium hydroxide (NaOH). The transportation of hydroxyl (OH_) ions at the anode and cathode electrodes of alkaline electrolyzers can be described as follows:

$2H_2O\ (l) \rightarrow O_2\ (g) + 4\ H^+\ (aq) + 4\ e^-$ (1)

$2H_2O\ (l) + 2\ e^- \rightarrow H_2\ (g) + 2\ OH^-\ (aq)$ (2)

Note that carboxylic acids and alkenes undergo reactions with oleic acid. Oleates, which are soaps, can be obtained by dissolving it in an aqueous base. Iodine acts as an additive within the double bond. The saturated derivative stearic acid is obtained through the process of hydrogenation of the double bond. The process of oxidation at the double bond exhibits a gradual rate in the presence of air and is commonly referred to as rancidification in food products and as drying in coatings. Olel alcohol is obtained by reducing the carboxylic acid group. The process of ozonolysis presents a significant pathway for the production of azelaic acid. The resulting substance is oleic acid.

$H_{17}C_8CH{=}CHC_7H_{14}CO_2H + 4"O" \rightarrow HO_2CC_7H_{14}CO_2H + H_{17}C_8CO_2H$ (3)

IV. Results and discussion

The energy and exergy efficiencies of the subsystems are illustrated in Figure 2. The Rankine cycle exhibits energy and exergy efficiencies of 21.14% and 18.07%, correspondingly. The Rankine, organic Rankine, gasification, and electrolyzer units are the primary system components that exhibit energy efficiencies of 21.14%, 25.84%, 37.42%, and 61.1%, respectively. Electrolysis is a process that exhibits the highest level of energy efficiency, attaining a value of 61.1%. The core subsystems, namely the Rankine, Organic Rankine, gasification, and electrolyzer, exhibit exergy efficiencies of 18.07%, 17.78%, 9.63%, and 63.2%, correspondingly. The exergy efficiency of the electrolysis process is notably high, with a recorded value of 63.2%. The electrolysis process demonstrates the most notable values in terms of energy and exergy efficiency.

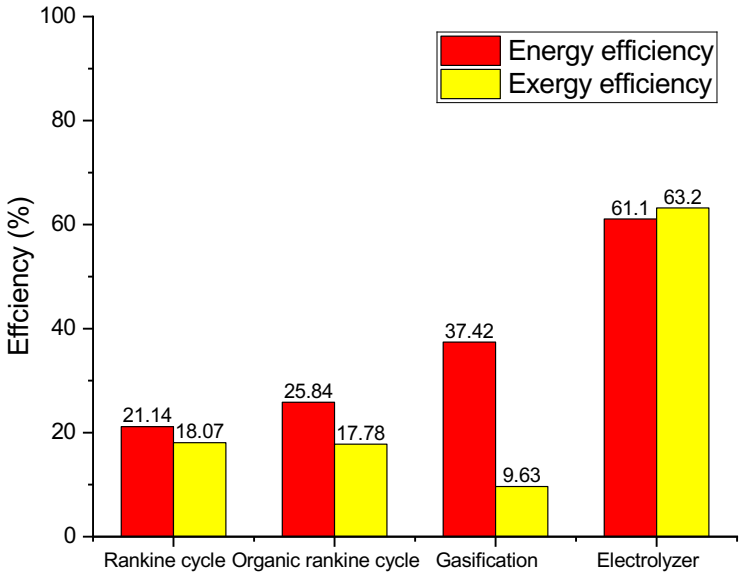


Fig.2: Efficiency of the processes in the system.

The results of the comparison are presented in Table 1. Both models demonstrate lower and higher concentrations of H_2 and CH_4, respectively, in comparison to the corresponding experimental data. The observed difference can be ascribed to the exclusion of in-bed olivine in the actual scenario where the modeling procedure was conducted. The neglect of the in-bed catalyst during the modeling procedure led to a reduced influence of the water-gas shift reaction, resulting in an increase in carbon monoxide (CO) levels in the simulated scenario compared to the real scenario. The suboptimal estimation of carbon dioxide (CO_2) levels can be ascribed to the alteration in the equilibrium of the water-gas shift reaction, which arises from the overestimation of CO. No change in the final output was observed when the in-bed catalyst effect was included in the kinetic model. In terms of LHV, yield, and cold gas efficiency, both models demonstrated a significant degree of concurrence with experimental data.

Table 1. Comparison of syngas composition and characteristics (850 °C, S/B = 0.25)

Parameter	Experimental Data (Pfeifer et al., 2004)	Aspen Plus Model
H_2 (%dry mole fraction)	41	32
CO (%dry mole fraction)	16	34
CO_2 (%dry mole fraction)	32	23
CH_4 (%dry mole fraction)	10	11
LHV (MJ/kg) $_{dry}$	14-15	14
Gas yield) (Nm^3/kg) $_{dry}$	0.84	1.39
Cold gas efficiency (%)	0.86-0.95	0.89

V. Conclusions

This paper presents the integration of solar and geothermal energy systems to create a new system for multigeneration purposes. The system under consideration is subsequently subjected to thermodynamic analysis, specifically focusing on energy and exergy analysis. It is then evaluated and assessed based on energy and exergy efficiencies. Multigeneration achieves 72.6% efficiency, according to the energy analysis. However, exergy analysis provides valuable system performance insights that system has 36.6% exergetic efficiency. Exergy analysis shows that solar collectors destroy 75% of exergy, which is the main cause of system irreversibilities. The study emphasizes the importance of exergy analysis and efficiency in accurately analyzing and representing system performance for the systems under consideration.

References

Al-Ali, M., & Dincer, I. (2014). Energetic and exergetic studies of a multigenerational solar–geothermal system. Applied Thermal Engineering, 71(1), 16-23.

Mohammadi, M., Mahmoudan, A., Nojedehi, P., Hoseinzadeh, S., Fathali, M., & Garcia, D. A. (2023). Thermo-economic assessment and optimization of a multigeneration system powered by geothermal and solar energy. Applied Thermal Engineering, 230, 120656.

Pfeifer, C., Rauch, R., & Hofbauer, H. (2004). In-bed catalytic tar reduction in a dual fluidized bed biomass steam gasifier. Industrial & engineering chemistry research, 43(7), 1634-1640.

Yapicioglu, A., & Dincer, I. (2023). A newly developed renewable energy driven multigeneration system with hot silica sand storage for power, hydrogen, freshwater and cooling production. Sustainable Energy Technologies and Assessments, 55, 102938.

Electrolytic Hydrogen Production with Coaxial Cylinder Electrolyzers: A CFD Study

Mohamed M. Ismail, and Ibrahim Dincer
Clean Energy Research Laboratory (CERL), Faculty of Engineering and Applied Science, Ontario Tech. University, 2000 Simcoe Street North, Oshawa, Ontario L1H 7K4, Canada

Corresponding author e-mail: Mohamed.Ismail4@ontariotechu.net

Abstract
This study investigates the optimization of hydrogen production in alkaline water electrolyzers (AWE) using a coaxial cylindrical design, through simulation analyses performed in the COMSOL Multiphysics. Key operational parameters, including electrode-separator gap sizes and current densities, were examined to assess their impact on system performance and hydrogen output. Results indicate that an optimal electrode-separator distance exists, balancing ohmic overpotential reduction with minimized gas bubble interference. The coaxial cylindrical design demonstrated superior thermal management capabilities, suggesting its potential for improving electrolyzer performance.

Keywords: CFD, Electrolysis, Hydrogen, Two Phase Flow.

1. Introduction

The ongoing global energy crisis, marked by falling fossil fuel supplies, increased demand, and escalating greenhouse gas emissions, has intensified the need for sustainable, effective, and environmentally friendly energy alternatives. This article explores sustainable hydrogen production as a crucial step toward a more sustainable energy future. Hydrogen stands out for its versatility and environmental benefits as an energy carrier, offering the potential to decarbonize sectors such as transport, industry, and electricity generation. The widespread adoption of hydrogen depends on the development of production methods that are efficient, cost-effective, and environmentally benign. Traditional hydrogen production methods, like gasification and pyrolysis, are carbon-producing and not considered environmentally sustainable. Conversely, water electrolysis, particularly when powered by renewable energy, represents a green approach to hydrogen production that aligns with environmental conservation goals. AWEs have the capability to produce hydrogen through electrolysis, presenting opportunities for greener energy solutions. This paper examines the computational fluid dynamics (CFD) analysis of alkaline water electrolysis using coaxial cylinder electrolyzers, utilizing COMSOL Multiphysics. It seeks to assess the performance and feasibility of this innovative design, which holds several potential benefits over conventional planar electrolysis systems. The coaxial cylinder design can enhance the performance of AWEs due to its increased electrode surface area, improved mass transfer, uniform electric field distribution, scalability, effective thermal management, and reduced ohmic losses [1]. These features could contribute to greater efficiency and reduced production costs, bringing sustainable hydrogen production within closer reach and increasing its viability as an energy source alternative to fossil fuels. However, the design also poses challenges, including complex manufacturing processes, material constraints, and maintenance issues, which need to be carefully balanced against its advantages. This paper presents CFD analyses of coaxial concentric cylinder AWEs to illustrate the potential benefits that this type of electrolyzer could offer.

2. Coaxial Cylinders AWE Model Description

This analysis focuses on studying the operational and performance dynamics of a cylindrical-shaped AWE that is 100 mm in length. The model comprises five coaxial cylinders, two cathodes, two separators, and a single dual polarization anode. Table 1 shows the input parameters used in the model. The design configuration involves a vertical upward flow by positioning the alkaline solution inlet at the bottom and the outlet at the top. A 1 mm thick separator is inserted between the two chambers where the gases are produced. The electrolyzer's compact design is intended to optimize the distribution of electric current within the electrolysis cell. Figure 1 illustrates the proposed 3D structure of the AWE. The cathodes are highlighted in red and are positioned to maximize hydrogen production efficiency. The anode, highlighted in blue, is located in the center and acts as the anode for the cathodes on both the inner and outer sides of the coaxial cylindrical model. This central positioning of the anode is crucial for facilitating a symmetric electrolytic reaction. All electrodes are 1mm thick. Separators, shown in yellow, are placed between the anode and each cathode to effectively partition the electrolytic space. The electrolyte volume is indicated in light grey. The model also incorporates an upward fluid flow along the z-axis, with the inlet at the bottom and the outlet at the top, ensuring a consistent and efficient path for the electrolyte flow through the system.

3. Modeling Details and Analysis

In the study, three modules from COMSOL Multiphysics were employed to construct a detailed model of the system for electrolytic hydrogen production. The “Hydroxide Exchange Water Electrolysis” model was utilized to simulate the electrochemical reactions involved in hydrogen production from water electrolysis. This model aids in understanding the reaction mechanisms and shows the polarization curves for the AWE. The second is the “Euler-Euler Two Phase Fluid Flow” model was selected for its capability to simulate the two-phase flow of the liquid electrolyte and the evolved gas bubbles [2]. This is essential for analyzing the interactions between evolved gas bubbles and the surrounding liquid electrolyte, which greatly impact the AWE performance. Furthermore, the “Heat Transfer in Solids and Liquids” model was incorporated to examine the system's thermal management. The generation and management of heat within the electrolyzer are critical for maintaining operational efficiency and

safety. Additionally, the “Thermochemical Multiphysics” interface was also used to link the heat generation from the electrolyzer module to the heat transfer module. The following governing equations are considered in accordance with the fundamentals of energy and mass conservation:

Conservation of mass:

$$\frac{\partial(\alpha\rho)}{\partial t} + \nabla\cdot(\alpha\rho\vec{\vartheta}) = 0 \quad (1)$$

Conservation of momentum:

$$\frac{\partial(\alpha\rho\vec{\vartheta})}{\partial t} + \nabla\cdot\left(\alpha\rho\vec{\vartheta}\vec{\vartheta}\right) = -\alpha\nabla P + \nabla\cdot(\alpha\bar{\bar{\tau}}) + F \quad (2)$$

Turbulent kinetic energy:

$$\frac{\partial(\rho k)}{\partial t} + \nabla\cdot\left(\rho k\vec{\vartheta}\right) = \nabla\cdot\left(\mu + \frac{\mu_t}{\sigma_k}\right)\nabla k + G_k - \rho\varepsilon \quad (3)$$

Dissipation:

$$\frac{\partial(\rho\varepsilon)}{\partial t} + \nabla\cdot\left(\rho\varepsilon\vec{\vartheta}\right) = \nabla\cdot\left(\mu + \frac{\mu_t}{\sigma_\varepsilon}\right)\nabla \varepsilon + C_{1\varepsilon}\frac{\varepsilon}{k}G_k - C_{2\varepsilon}\rho\frac{\varepsilon^2}{k} \quad (4)$$

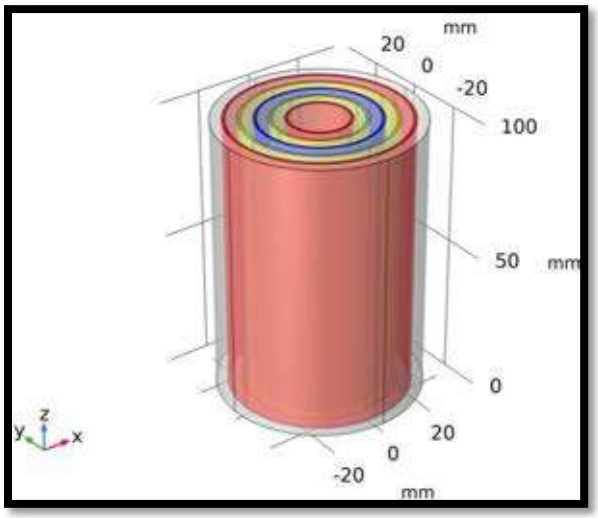


Figure 1 The coaxial cylinders AWE model geometry.

Within the Euler-Euler model, forces acting on dispersed gas bubbles in the electrolyte, including buoyancy forces, drag forces, and weight forces, were defined using the “Volume Forces” node [3]. These forces influence the movement and distribution of bubbles, which is important for accurately simulating the electrolysis process. The equivalent volume forces expression is presented as follows:

$$F_V = (\rho_l - \rho_g)gV + \frac{C_D\rho_l u^2 A}{2} - m_a a \quad (5)$$

Table 1 Model input parameters

Parameter	Value
Inlet Velocity [m/s]	0.01
Bubble Diameter [m]	5 x 10^{-5}
Operating Voltage [V]	2-32
Reference Pressure [Pa]	101,325
Inlet Temperature [C°]	25
KOH Concentration [mol/m³]	6000
Separator Porosity	0.5

4. Results and Discussion

In AWE, the distance between the electrode and the separator has a significant impact on the ohmic overpotential. When this distance is reduced, the amount of electrolyte between the electrode and separator decreases, leading to lower ohmic resistance and, therefore, a reduction in the electrolysis potential which makes the process more energy efficient. However, very small gaps between the electrode and separator can lead to an increase in the gas fraction during electrolysis. This increase can cause a rise in ohmic overpotential because gas bubbles act as insulators. Thus, there appears to be an optimal distance between the electrode and separator that allows for the

best performance of the electrolyzer cell. Figure 2 displays the results for different gap sizes. As shown in the figure, reducing the gap size tends to lower the electrolysis potential, indicating increased efficiency. However, there is a point at which further reducing the gap size does not improve efficiency due to the negative impact of increased gap bubbles.

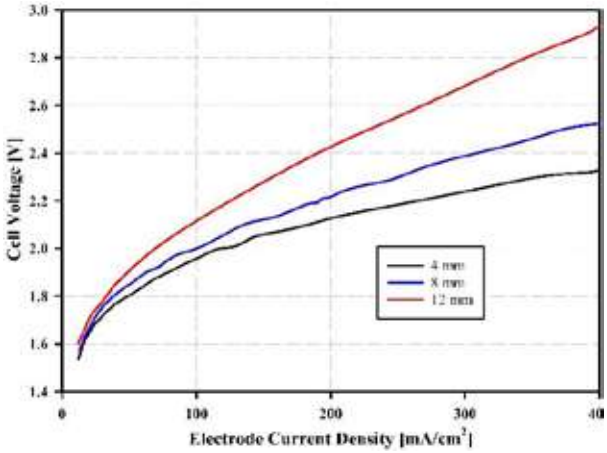


Figure 2 Polarization curves depicting for voltage vs electrode current density for different electrode-separator gaps (4 mm, 8 mm, and 12 mm).

Figure 3 displays the hydrogen volume fraction for a range of electrode current densities. It shows that hydrogen production increases with higher current densities. This increase aligns with electrochemical principles, which state that higher current densities speed up the reactions that produce hydrogen. However, increasing the current density not only boosts hydrogen production but also affects the AWE efficiency and operational costs. At higher current densities, electrodes dissipate more energy, leading to elevated temperatures. This can increase energy consumption and present heat management challenges. Thus, managing these aspects is crucial to optimizing hydrogen production and maintaining the efficiency of the system. The coaxial cylindrical shape of the AWE aids in managing these thermal challenges more effectively. Its design helps dissipate heat, allowing the system to operate efficiently even at higher current densities.

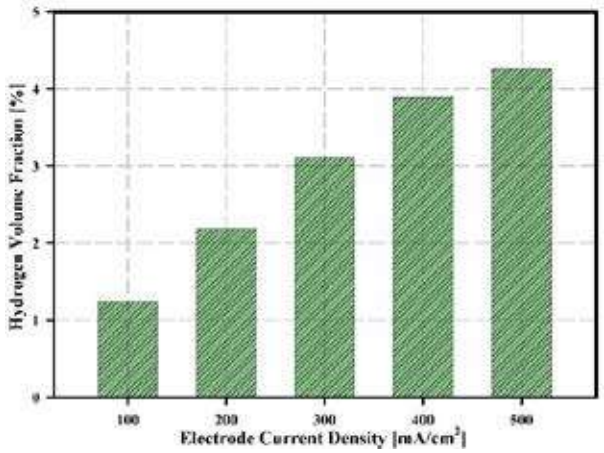


Figure 3 Hydrogen volume fraction vs electrode current density

5. Conclusion

This study investigated the factors influencing hydrogen production in AWEs with a coaxial cylindrical electrodes configuration. Our findings reveal that the electrode-separator gap size significantly affects the system's performance, with an optimal distance identified that minimizes ohmic overpotential. In conclusion, coaxial cylindrical electrodes AWEs is expected to offer optimized operation of AWEs in comparison to traditional AWEs configurations.

Nomenclature

A	cross-sectional area of the bubble [m^2]
a	acceleration of the bubble [m/s^2]
C	model constant
C_D	drag coefficient
F	interphase exchange force per unit volume [N/m^3]
G_k	generation of turbulent kinetic energy due to mean velocity gradients [W/m^3]
g	gravity acceleration [m/s^2]
K	turbulent kinetic energy per unit mass [m^2/s^2]
P	pressure [kPa]

t	time [seconds]
$\vec{\vartheta}$	velocity [m/s]
V	volume of the bubble [m^3]
Greek Letters	
α	volume fraction
ε	dissipation rate of turbulent kinetic energy [m^2/s^3]
μ	dynamic viscosity [kg/(m.s)]
μ_t	turbulent viscosity [kg/(m.s)]
ρ	density [kg/m^3]
σ_ε	turbulent dissipation rate constant
σ_k	turbulent kinetic energy constant
$\bar{\bar{\tau}}$	stress tensor [N/m^2]

References

K. Hu *et al.*, 'Comparative study of alkaline water electrolysis, proton exchange membrane water electrolysis and solid oxide electrolysis through multiphysics modeling', *Applied Energy*, vol. 312, p. 118788, Apr. 2022, doi: 10.1016/j.apenergy.2022.118788.

[D. Le Bideau *et al.*, 'Eulerian Two-Fluid Model of Alkaline Water Electrolysis for Hydrogen Production', *Energies*, vol. 13, no. 13, p. 3394, Jul. 2020, doi: 10.3390/en13133394.

H. Y. Wang and F. Dong, 'A method for bubble volume calculating in vertical two-phase flow', *J. Phys.: Conf. Ser.*, vol. 147, p. 012018, Feb. 2009, doi: 10.1088/1742-6596/147/1/012018.

Design and Analysis of a New Multigeneration System for a Hospital

[1*] Andre Bolt, [2] Ibrahim Dincer, [3] Martin Agelin- Chaab
[1]Clean Energy Research Laboratory (CERL), Faculty of Engineering and Applied Science, Ontario Tech. University, 2000 Simcoe Street North, Oshawa, Ontario L1H 7K4, Canada

*Corresponding author e-mail: Andre.Bolt@ontariotechu.ca

Abstract
The presented study illustrates the design and investigation of a new multigeneration system created specifically for a hospital located in Trelawny Jamaica. The multigeneration system utilizes solar-based electrolysis to produce oxygen for patients, while simultaneously producing hydrogen so that a portion of hydrogen produced can be used to synthesize natural gas. Furthermore, the proposed system will produce electrical power, hot water, and space cooling for its patients and staff. Most notably, the photovoltaic aspect of the system enables the system to produce hydrogen and oxygen at a production rate of 1.51e-3 kg/s and 2.41e-2 kg/s, respectively. Additionally, the system had a net electrical power output of 367 kW.

Keywords*:* Hydrogen, Methane, Oxygen, Solar Energy, Biomass Gasification

Introduction

As many developing countries strive toward industrialization and economic growth, they often use fossil fuels and other hydrocarbons as the mechanism to facilitate their growth and sustain their current society. Presently the majority of Jamaica's energy consumption is derived from non-renewable energy sources in the form of hydrocarbons. Most notably 64.8% of Jamaica's total energy demand is attributed to oil, and 23.7% is from natural gas [1]. Despite Jamaica primarily satisfying its energy demands through non-renewable resources, Jamaica is highly suited for renewable energy, and it has a substantial solar energy potential, given its geographic location.

Furthermore, Jamaica also has the potential to produce electricity and other useful outputs from sugar cane crops. Despite Jamaica's recent decline in its sugar production, sugar cane crops remain Jamaica's most lucrative crop. During the processing of sugar cane, a dry pulp waste product referred to as bagasse is produced. Several studies suggest sugarcane bagasse in Jamaica can be used for electricity production within a cogeneration system [2]. Through the implementation of this concept, the sustainability of sugar cane production can potentially be increased, and electricity can be generated. Parishes such as Trelawny would benefit greatly from electricity production through bagasse, given that the majority of Jamaica's sugar cane crops are grown here, and power outages occur more frequently within this region. These power outages can be considerably problematic in the healthcare sector within Jamaica. Furthermore, the implementation of this form of electricity production would have a substantial benefit from an economic perspective. This is likely attributed to 94% of Jamaica's electricity being produced from petroleum, the cost of electricity is therefore subjected to fluctuations in the oil market and currency exchange rates [3].

There have been six hospitals within Jamaica to integrate renewable energy within their infrastructure. The integration of renewable energy within Jamaican hospitals is expected to decrease Jamaica's hospital energy bill by approximately 22%. The ability for Jamaican hospitals' energy production to be separate from the grid, or self-reliant can have tremendous benefits not only from a sustainability perspective but it can also provide additional safety to patients in critical condition.

This short paper presents the design and analysis of a new multigeneration system designed to specifically meet the needs of a small hospital located within Trelawny Jamaica. The presented system utilizes a biomass gasification and a photovoltaic thermal (PVT) solar sub-system. The system will utilize the PVT sub-system to produce electrical power, all of which will be allocated toward hydrogen production through polymer electrolyte membrane (PEM) electrolysis. A portion of the hydrogen produced will be allocated toward natural gas production so that the existing systems that depend on natural gas within a small hospital can continuously operate. Furthermore, the oxygen produced from the process can also be provided to the patients in need. The thermal energy generated from the PVT system will be used to provide hot water to its occupants. The remainder of the system's useful output will be derived from biomass gasification through the waste material of processing sugar cane, referred to as bagasse. The thermal energy from the syngas produced will be used to provide the thermal energy input for an open Brayton cycle to produce electrical power for the small hospital. The remainder of the thermal energy carried by the fluid can be used to provide cooling, through the integration of the steam ejector cooling cycle. After the temperature of the fluid is adequately reduced, the CO_2 within the flue gas can be extracted and then reacted with hydrogen to synthesize natural gas/ methane.

Analysis

The presented multigeneration system is illustrated in Figure 1. The illustrated system can produce six useful outputs for its target demographic in Trelawny Jamaica.

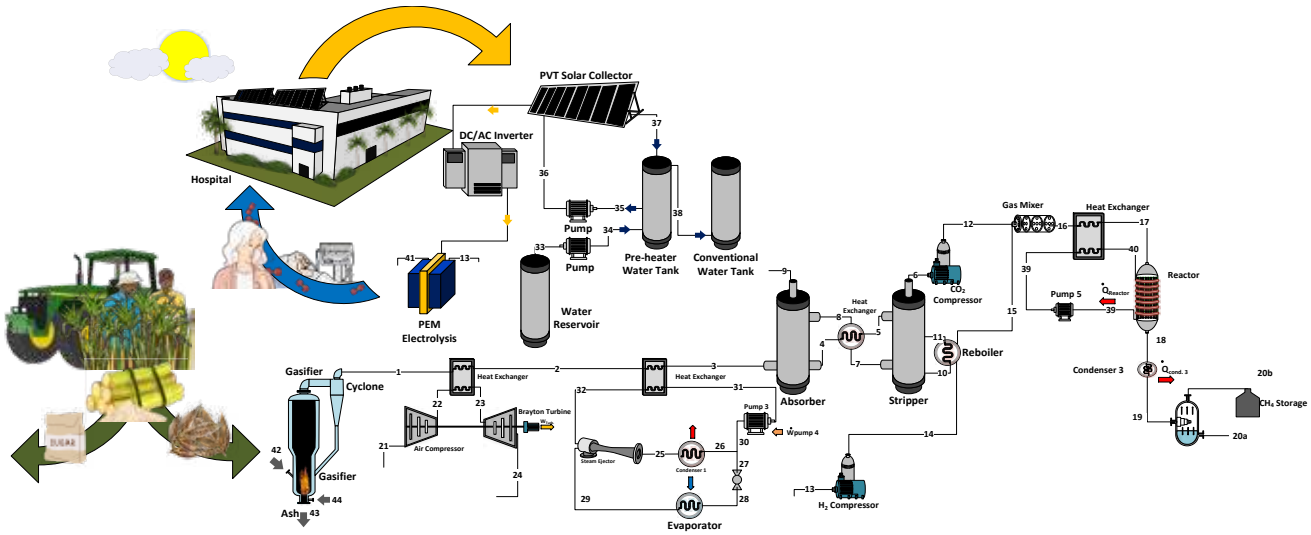


Fig. 1. The proposed multigeneration system

The useful outputs for the system include hydrogen, oxygen, natural gas, electrical power, space cooling, and hot water. The electrical power generated from the PVT system every month was modelled using the System Advisor Model (SAM) software, and the solar irradiation data from Trelawny. The solar irradiation data utilized will have a direct impact on the amount of electricity that can be produced, and therefore an impact on the amount of hydrogen, oxygen, and natural gas the system can produce.

The analysis takes into consideration the efficiency of the electrolysis process utilized, as a metric to calculate production rate at a steady state. The hydrogen production rate can be calculated as follows:

$$\dot{m}_{H_2} = \frac{(\eta_{El\,e.})(\dot{W}_{PVT})}{LHV_{H_2}} \quad (1)$$

Additionally, the electrolysis chemical reactions used to model hydrogen and oxygen production are presented as follows:

Anode: $H_2O \rightarrow 2H^+ + \frac{1}{2}O_2 + 2e^{-1}$ (2)

Cathode: $2H^+ + 2e^{-1} \rightarrow H_2$ (3)

Overall: $2H_2O \rightarrow H_2 + \frac{1}{2}O_2$ (4)

The electrolysis reaction can be used to calculate the amount of oxygen produced. Additionally, the Sabatier chemical reaction between the captured carbon dioxide and a portion of the generated hydrogen is presented as follows:

$$CO_2 + 4H_2 \rightarrow CH_4 + H_2O \quad \Delta H = -165\,\frac{kJ}{mol} \quad (5)$$

Results and Discussion

The performance of the overall system is largely dictated by the performance of the PVT sub-system. The amount of electrical power generated by the PVT sub-system will dictate the amount of hydrogen, oxygen, and natural gas produced. Figure 2 illustrates the generation rate of various gases, based on the peak daily average for the electrical power produced each month.

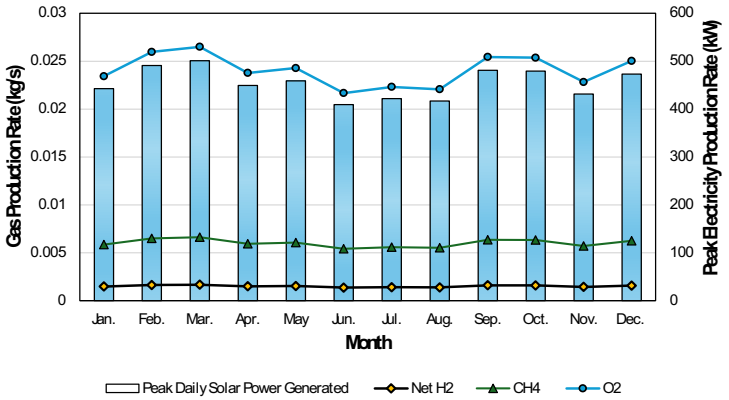


Fig. 2. Comparison between CH_4 and H_2 production rate with changing wind speed

As seen in Figure 2, the peak amount of electricity produced was 501.1 kW during March, whereas the smallest peak electricity production rate from the PVT system was 409.7 kW in June. This is attributed to the rainy season in Jamaica spanning from June to November, and that Trelawny Jamaica is a region which rains more frequently

on the island. The peak oxygen, net hydrogen, and methane production rates during March were 2.65e-2 kg/s, 1.67e-3 kg/s, and 6.62e-3 kg/s, respectively. Additionally, the other useful outputs generated by the system are summarized in Table 1.

Table 1. System Performance Parameters

Average Peak H_2 Generation Rate	1.51e-3 kg/s
Average Peak CH_4 Generation Rate	6.02e-3 kg/s
Average Peak O_2 Generation Rate	2.41e-2 kg/s
Hot Water Generation Rate	9.23e-3 kg/s
Net Power Output	367 kW
Cooling Load	73.25 kW

.

Conclusions

This short paper presented the design of a new and innovative multigeneration system capable of sustaining a small hospital located within Trelawny Jamaica. Most notably the system can produce various gases through PEM electrolysis and the Sabatier chemical reaction. The average peak oxygen production rate of 2.41e-2 kg/s has the benefit of helping patients who are connected to ventilators. Additionally, the system can produce a net hydrogen production rate of 1.51e-3 kg/s and is able to satisfy many other needs for the hospital such as space cooling, hot water, electricity, and natural gas.

References

[International Energy Agency, “Energy system of Jamaica.” [Online]. Available: https://www.iea.org/countries/jamaica

R. Contreras-Lisperguer, E. Batuecas, C. Mayo, R. Díaz, F. J. Pérez, and C. Springer, “Sustainability assessment of electricity cogeneration from sugarcane bagasse in Jamaica,” *J. Clean. Prod.*, vol. 200, no. 2018, pp. 390–401, 2018, doi: 10.1016/j.jclepro.2018.07.322.

National Renewable Energy Laboratory, “Energy Transition Initiative islands,” 2015.

An Integrated Plant for Urea and Ammonium Acetate Production Designed with Renewables

[1*]Zunayed Zakir Arnab, [1]Ibrahim Dincer
CERL, FEAS, Ontario Tech. University, 2000 Simcoe St. North, Oshawa, ON L1G 0C5, Canada

* E-mails: Zunayed.Arnab@ontariotechu.ca

Abstract
This investigates the synergistic potential of multigeneration systems in the simultaneous production of urea and ammonium acetate, pivotal compounds in various industrial and agricultural applications. The traditional approach to chemical production often operates within isolated systems, resulting in inefficiencies and environmental burdens. In contrast, multigeneration systems integrate diverse processes, harnessing waste and utilizing byproducts to enhance overall efficiency and sustainability. Also, this study demonstrates the feasibility and benefits of implementing a multigeneration approach for urea and ammonium acetate production. By integrating diverse processes such as solar energy, wind energy, biomass conversion, carbon capture, the system maximizes resource utilization and minimizes environmental impact. Furthermore, the use of advanced catalytic systems and process optimization techniques enhances conversion efficiency and product purity.

Keywords: Urea, Ammonium Acetate, solar energy, energy, exergy, sustainability, biowaste, wind energy

I. Introduction:

In the domain of chemical production, the imperative for sustainable and efficient methodologies is ever more pronounced. The global demand for essential compounds like urea and ammonium acetate continues to surge, driven by agricultural, industrial, and commercial sectors, necessitating innovation in traditional production processes (Tilman et al., 2011). Unfortunately, conventional methods often operate within isolated systems, leading to inefficiencies, resource depletion, and environmental degradation.

Against this backdrop, multigeneration systems emerge as a promising paradigm shift. These systems represent an integrated approach to chemical production, orchestrating diverse processes to maximize resource utilization and minimize environmental impact (Liao et al., 2017). By exploiting synergies between production pathways and valorizing waste streams and byproducts, multigeneration systems offer a route to sustainable and resilient chemical manufacturing.

This paper investigates the feasibility and benefits of implementing multigeneration systems for the concurrent production of urea and ammonium acetate. Through experimental analysis, theoretical modeling, and economic assessment, we aim to elucidate the potential advantages, challenges, and implications of this holistic approach. Our research seeks to contribute to the burgeoning knowledge on sustainable chemical production, with a focus on integrating multigeneration systems into mainstream industrial practices.

II. System Description and Analysis

In this intricate multigenerational system, the utilization of Concentrated Solar Power (CSP) technology marks a significant stride towards sustainable energy production. By harnessing solar radiation through CSP, the system maximizes the capture of sunlight, a virtually endless and renewable resource. The captured solar radiation is not merely converted into electricity directly. Instead, it undergoes a sophisticated process involving molten salt. This salt serves as a medium to absorb and store thermal energy efficiently. Through a controlled exchange of heat, the stored energy is then used to produce steam. This steam, in turn, drives turbines, a classical method in electricity generation, converting thermal energy into mechanical energy, and finally into electrical energy. Complementing the solar power generation, wind energy is also integrated into the system. The synergy between these renewable sources ensures a more consistent and reliable power supply. Furthermore, the generated electricity serves multiple purposes within the system. A portion is allocated to meet the energy demands of residential areas, contributing to sustainable living and reducing reliance on traditional power grids. Another fraction is directed towards an innovative process: hydrogen production using a Proton Exchange Membrane (PEM) electrolyzer. Hydrogen, known for its versatility and eco-friendliness, holds immense potential as a clean energy carrier. Simultaneously, another aspect of the system involves the production of essential chemicals. Pressure Swing Adsorption (PSA) technology is employed to extract Nitrogen, a crucial component for ammonia synthesis. Ammonia, in turn, plays a pivotal role in various industrial processes and is vital for agricultural applications. The system also tackles carbon emissions by capturing Carbon dioxide and Carbon monoxide from industrial smokestacks. This captured Carbon dioxide and Carbon monoxide serves as a raw material for chemical synthesis, contributing to a circular carbon economy. Through controlled reactions separately, both is transformed into valuable compounds, such as urea, acetic acid. Moreover, the system embraces a holistic approach by utilizing biowaste as a resource. Biomethane, a byproduct of biowaste processing, is harnessed alongside Carbon dioxide. These inputs undergo chemical transformations, yielding products like methanol, further enhancing the system's sustainability and resource efficiency (Oner., 2022). Thermodynamic equations were utilized to assess the power consumption of various components, thereby establishing the power consumption and production scenario for the multigeneration system. Extensive exergy and energy analyses were conducted to determine the comprehensive exergy and energy profiles.

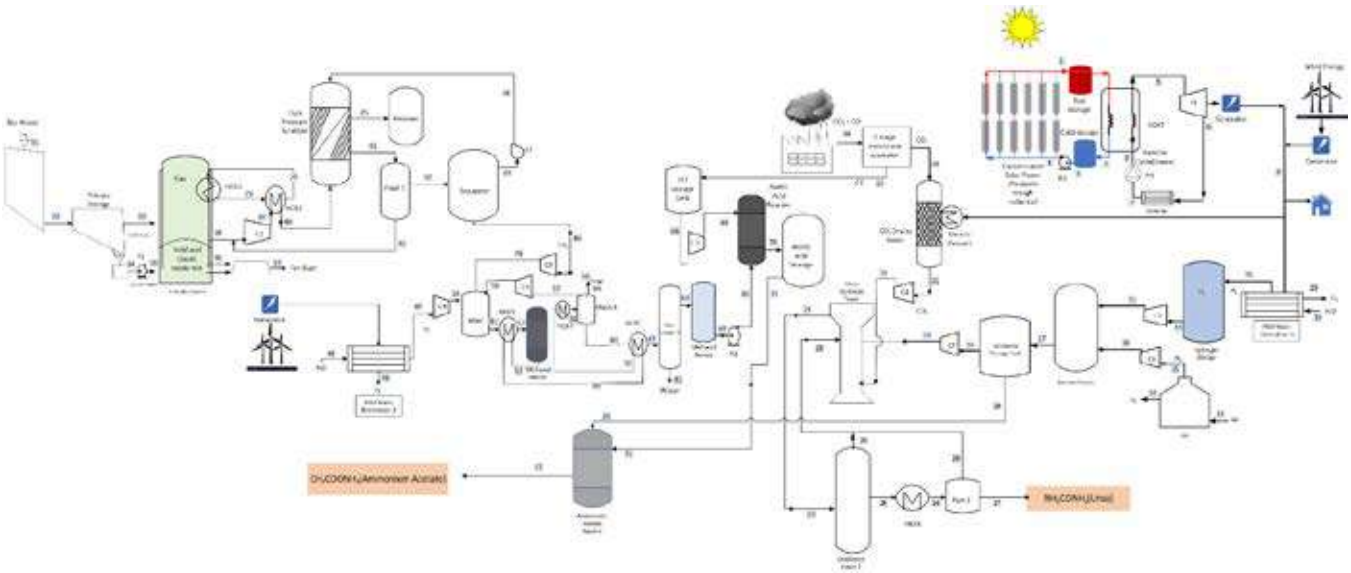


Fig. 1: A multigeneration system designed to produce Urea and Ammonium Acetate

III. Results and discussion

Based on the graph, the turbine produces power among all components, while on the other hand, the power is consumed by the pumps, compressors. Notably, Pump 3 stands out with a significant power consumption, attributed to its handling of molten salt. All the three compressors consume almost the same amount of power. Numerically explaining, Turbine 1 produces 31815 kW of energy, while pump 3 and pump 4 consumes 8248.5 kW and 3234 kW power respectively. To explain about the compressors power consumption, compressor 7, compressor 3, compressor 9 consumes 885.8 kW, 738.5 kW, 602.784kW respectively.

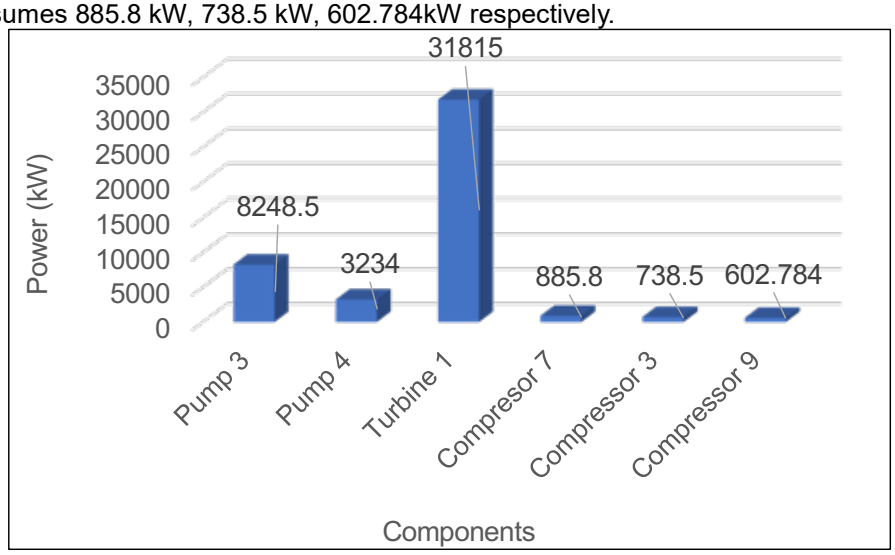


Fig.2: Power for several components of the multigeneration system

IV. Conclusions

In conclusion, this study has shed light on the synergistic potential of multigeneration systems for the simultaneous production of urea and ammonium acetate. By integrating diverse processes such as solar and wind energy utilization, biomass conversion, and carbon capture, multigeneration systems offer a promising pathway towards sustainable chemical production. Advanced catalytic systems and process optimization techniques further enhance efficiency and product purity. This research underscores the transformative potential of multigeneration systems in driving sustainable chemical production, paving the way for a more environmentally conscious and economically viable future.

References

Liao, W., Yu, Y., Lin, C., Ma, X., & Yang, X. Multigeneration systems for energy conversion: A review. Renewable and Sustainable Energy Reviews, 76, 588-603 (2017)

Oner O., Dincer I., Development and assessment of a hybrid biomass and wind energy-based system for cleaner production of methanol with electricity, heat and freshwater, Journal of Cleaner Production 367 (2022)

Tilman, D., Balzer, C., Hill, J., & Befort, B. L. Global food demand and the sustainable intensification of agriculture. Proceedings of the National Academy of Sciences, 108(50), 20260-20264. (2011)

Green Hydrogen Production System for a Village

Esra Gül Sendesen, Harun Koku, Inci Eroglu
Middle East Technical University, Faculty of Engineering, Chemical Engineering Department, 06800, Ankara, Türkiye

E-mail: esragulsendesen@gmail.com, ieroglu@metu.edu.tr

Abstract

This project aims to compile literature research and conduct calculations about the utilization of hydrogen in different ways. Hydrogen is produced using environmentally friendly methods, with a significant portion of the energy required for electrolysis being supplied by solar panels. A proton exchange membrane water electrolyzer does electrolysis, and solar panels supply the energy required for electrolysis. In addition, the PEM fuel cell is used to produce electricity from hydrogen produced in the electrolysis, and a heat pump is used to provide heat to houses and barns in this project. Produced hydrogen is designed using in a village in Van Turkey, comprising 50 houses, 50 transport vehicles, 1000 acres of planted land, and 20 barns, each 53 m². Three different scenarios are analyzed in this project. In the third scenario, which is the most comprehensive, the required hydrogen is 15.7 tons/year. The total capital investment cost is $2,700,000, and the operating cost is $179,400/year.

Keywords: Green hydrogen, solar energy, PEM fuel cell, PEM Water Electrolyzer, heat pump.

I. Introduction

There are various advantages to producing green hydrogen. Hydrogen can be stored in large quantities for a long time, and it has nearly three times the energy of fossil fuels. Green hydrogen can be easily produced when water and electricity are available for electrolysis. PEM water electrolyzer is chosen because hydrogen purity is high, and it is good for the environment since it is not corrosive. Here are the reactions that occur in a PEMWE,

Anode: $H_2O \rightarrow \frac{1}{2}O_2 + H^+ + 2e^-$

Cathode: $2H^+ + 2e^- \rightarrow H_2$

Green hydrogen is good for the environment and can be used for fuel, electricity, and heating. This project uses solar panels to provide electrical power during the daytime. Solar panels are a good source of clean energy, which is the project's motivation. Produced hydrogen can be used for several purposes. The first use of hydrogen is to produce electricity at night, which can be used in houses. Hydrogen is converted to electricity by using fuel cells. PEM fuel cell is chosen since it does not require high-temperature operation and reduces corrosion and leaking (Molaeimanesh and Torabi, 2022). Secondly, hydrogen is used as a fuel. Almost all vehicles depend highly on hydrocarbon fuels, and an average passenger car's annual carbon dioxide emissions are around 4.6 metric tons. Using hydrogen as a fuel can eliminate this problem since hydrogen is the only energy source that does not pollute. The third usage of hydrogen is heating. Heat pumps are used for this purpose. Heat pumps offer an energy-efficient alternative to furnaces. Moreover, since hydrogen is used for electricity, a heat pump is a good heating source because it is clean (Timmerman et al. 2014). The working principle of a heat pump is shown in Figure 1.

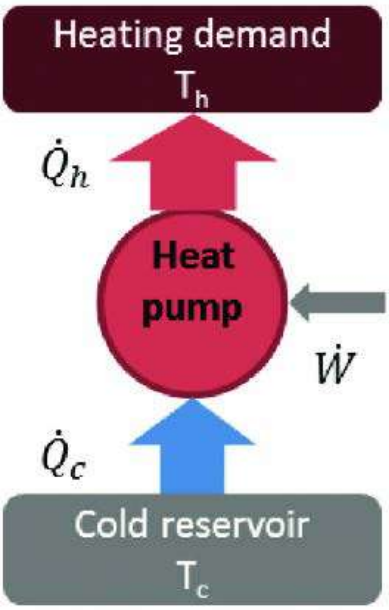


Fig.1: The working principle of a heat pump.

II. Method of Attack

Firstly, the project conducts an extensive literature review on hydrogen utilization, focusing on its applications in electricity generation, fuel production, and heating. It explores various environmentally friendly hydrogen production methods, emphasizing proton exchange membrane water electrolyzers. Information on solar panel usage to supply the required energy for electrolysis is gathered.

Based on the literature review findings, a comprehensive system is designed to encompass hydrogen production, storage, and utilization. Factors such as the number of houses, transport vehicles, planted land, and barns are considered to estimate the hydrogen requirements for each scenario accurately. Then, appropriate calculations are employed to determine the amount of hydrogen needed for each scenario. The total annual hydrogen consumption is calculated to provide electricity, fuel for vehicles, and heat to houses and barns. Aspen Plus software simulates the performance of the proton exchange membrane water electrolyzer, solar panels, pumps, air coolers, and heaters. The system specifications and parameters are inputted to obtain accurate power requirements for each component. The simulated values are ensured to align with the desired system capacities and operational parameters. As a design basis, green hydrogen is produced in a village in Van Turkey, comprising 50 houses, 50 transport vehicles, 1000 acres of planted land, and 20 barns, each 53 m².

Finally, a comprehensive cost analysis is conducted for the project. The costs associated with installing the PEM water electrolyzer, solar panels, PEM fuel cell, and other equipment used in the hydrogen production system are calculated. The total capital investment and annual operating costs are calculated, accounting for maintenance, labor, and other relevant expenses.

III. Analysis

Hydrogen is used as an electric fuel and heat source. How much hydrogen is needed is calculated while hydrogen is used as different sources. PEMFC is used to produce electricity from hydrogen. The reactions occur in the anode and the cathode are as follows:

Anode: $H_2 \rightarrow 2H^+ + 2e^-$

Cathode: $\frac{1}{2}O_2 + 2H^+ + 2e^- \rightarrow H_2O$

Overall: $\frac{1}{2}O_2 + H_2 \rightarrow H_2O$

The higher heating value of hydrogen is -286 $\frac{kJ}{mole}$. Eqn.1 is used to calculate electrical energy, and required hydrogen in a 55% efficient PEMFC using eqn.1,

$$W_{el} = -\Delta H \times \eta \quad \text{(Eqn.1)}$$

The heat loss of a regular house is calculated to estimate the hydrogen needed. Heat loss from convection is calculated using eqn. 2 for the walls, windows, floors, and roof. Heat loss from the windows, external walls, and the roof is due to convection. Heat loss from both conduction and convection occurs in the floors. Heat loss from convection is calculated using eqn. 2, and heat loss from conduction is calculated using eqn. 3.

$$Q = U \times A \times \Delta T \ (Eqn.2)$$

where Q is heat loss (W), U is overall heat transfer coefficient ($\frac{W}{m^2K}$), A is area (m^2), and ΔT is the temperature difference between outside and room (℃).

$$Q = -kA\frac{\Delta T}{\Delta x} \ (Eqn.3)$$

where k is thermal conductivity and Δx is thickness.

Since heat pumps are used for heating, eqn. 4 is used to find the required work for heat pumps.

$$\dot{W}_{s,net} = \dot{Q}_H \times \left(\frac{T_C - T_H}{T_H}\right) \ (Eqn.4)$$

IV. Results and Discussions

Three different scenarios for utilizing hydrogen are examined in this study. These scenarios are compared to see the minimum requirement of hydrogen in the village, the average requirement of hydrogen in the village, and the maximum requirement of hydrogen in the village. These three scenarios are compared in Table 1. Hydrogen is utilized for electricity and fuel in all scenarios. On the other hand, the heating of houses by hydrogen is done in the second and the third scenarios, and the heating of barns is done by hydrogen in the third scenario.

Table 1. Comparisons of Three Scenarios

Scenarios / Utilization	Scenario 1	Scenario 2	Scenario 3
Electricity	✓	✓	✓
Fuel	✓	✓	✓
Heating of houses		✓	✓
Heating of barns			✓
Total hydrogen need (tons/year)	12.6	15.5	15.7

The average house's electricity consumption is 1800 kWh/year. It is estimated that 4140.1 kg/year hydrogen is needed for the whole village's electricity supply at night. To fuel cars and tractors in all the operations of the tractors, from the preparation of the field before the planting to the harvest 8433.6 kg/year of hydrogen is used. To heat 50 houses 2913 kg/year of hydrogen is needed, and 3079.6 kg/year of hydrogen is required to heat 50 barns.

V. Conclusions

This project focuses on researching using hydrogen as a sustainable energy source in various applications. This study combines a literature review and calculations to assess hydrogen's feasibility and potential benefits. PEM electrolyzer powered by solar panels is used to generate hydrogen through electrolysis. The hydrogen produced is used in electricity, transportation fuel, and heating. The integration of PEM fuel cells allows electricity to be generated from the hydrogen produced during electrolysis, while heat pump systems provide heat to houses and barns. Necessary hydrogen in the most comprehensive scenario is 15.7 tons/year, while the total capital investment is estimated at US$2,700,000 with an operating cost of US$179,400/year.

References

Molaeimanesh G.R., Torabi, F., Fuel Cell Modeling and Simulation: From Microscale to Macroscale. Elsevier (2022).

Timmerman J., Vandevelde L., Van Eetvelde G. (2014). Towards low carbon business park energy systems: Classification of techno-economic energy models. *Energy*, *75*, 68–80 (2014).

Techno-Economic Analysis of Green Hydrogen Integration in Smart Grids: Pathways to Sustainable Energy Systems

[1]Muhammad Raza Zaffar, [2]Mohsin Raza Zaffar,[2*]Sulman Shahzad [3]Heybet Killic
[1] Project Management Unit, Multan Electric Power Company, 60600, Multan, Pakistan
[2] National Transmission & Despatch Company Limited, 60600, Multan, Pakistan
[3] Department of Electric Power and Energy Systems Dicle University 21280 Diyarbakır, Türkiye

* E-mail: salmanshahzad05@gmail.com

Abstract
The research does a thorough techno-economic analysis to evaluate the incorporation of green hydrogen into smart grids, emphasizing its ability to transform energy systems towards sustainability and resilience. We investigate the technical feasibility, economic viability, and environmental consequences of using green hydrogen for grid balancing and energy storage in a situation where renewable energy is dominant. This study intends to educate stakeholders, such as policymakers, investors, and energy industry professionals, about the strategic importance of green hydrogen in meeting global energy transition objectives.
Keywords: Techno-economic, green hydrogen, fuel, energy, renewable

I. Introduction

Hydrogen energy involves utilizing hydrogen gas (H2) as a fuel or energy transporter. Hydrogen is not naturally available in a useful form and needs to be extracted from chemicals that contain it, unlike other conventional fuels. Hydrogen is the most prevalent element in the universe. When utilized as a fuel, it combines with oxygen to create water and generates energy. The process can take place by combustion or more effectively in a fuel cell, resulting in the generation of electricity, heat, and water as secondary products (Squadrito et al., 2023). Hydrogen energy is crucial due to its capacity to function as a clean, sustainable, and adaptable energy transporter. It can be generated from different sources, stored, delivered, and converted into power or heat as required. Hydrogen's high energy density and lack of emissions during combustion make it a desirable substitute for fossil fuels, particularly in sectors where direct electrification is difficult, like heavy transport, industrial operations, and seasonal energy storage (Moradi & Groth, 2019). Renewable hydrogen is generated using renewable energy sources like wind, solar, and hydroelectric power, making the production process environmentally friendly. Renewable hydrogen is mostly produced through water electrolysis, a technique that separates water into hydrogen and oxygen using electricity supplied from renewable sources (Noussan et al., 2021). This technology differs from existing hydrogen production processes like steam methane reforming (SMR) that depend on fossil fuels and result in substantial carbon dioxide emissions. The environmental advantages of renewable hydrogen are significant (Wen & Aziz, 2024). Firstly, it provides a mechanism to reduce carbon emissions in sectors of the economy that are challenging to electrify, like heavy industries and long-distance transportation. Renewable hydrogen can improve the flexibility and resilience of the power system by serving as a storage medium for excess renewable energy, aiding in balancing supply and demand. Hydrogen fuel consumption only emits water vapor, making it a clean energy transporter that can greatly decrease air pollution and greenhouse gas emissions (Kopteva et al., 2021). This study article aims to evaluate the feasibility and effects of utilizing green hydrogen for grid balancing and storage to decrease dependence on fossil fuels for energy storage and grid stabilization.

II. Techno economic analysis

Pakistan has significant solar and wind energy potential and is targeting a shift to 80% renewable energy by 2030. This case study shows that it is technically feasible to utilize green hydrogen for grid balancing and storage in a renewable-heavy energy system.

Table 1 Initial investment costs

Item	Cost ($ per kW)	Capacity (MW)	Total Cost ($M)
Electrolyzer Facility	1,400	100	140
Storage and Pipeline Infrastructure	N/A	N/A	50
Total Initial Investment	N/A	N/A	190

Table 2 Annual operational costs

Cost Item	Cost Details	Total Cost ($M/year)
Electricity for Electrolysis	$0.05/kWh, 4,000 hours/year	20
Maintenance	2% of initial investment	3.8
Total Operational Costs		23.8

Table 3 Annual revenue streams

Revenue Source	Assumptions	Annual Revenue ($M)
Hydrogen Sales	$3/kg, 20 kg/MWh, 50% capacity factor	24

Grid Services	Providing grid balancing services	5
Total Revenue		29

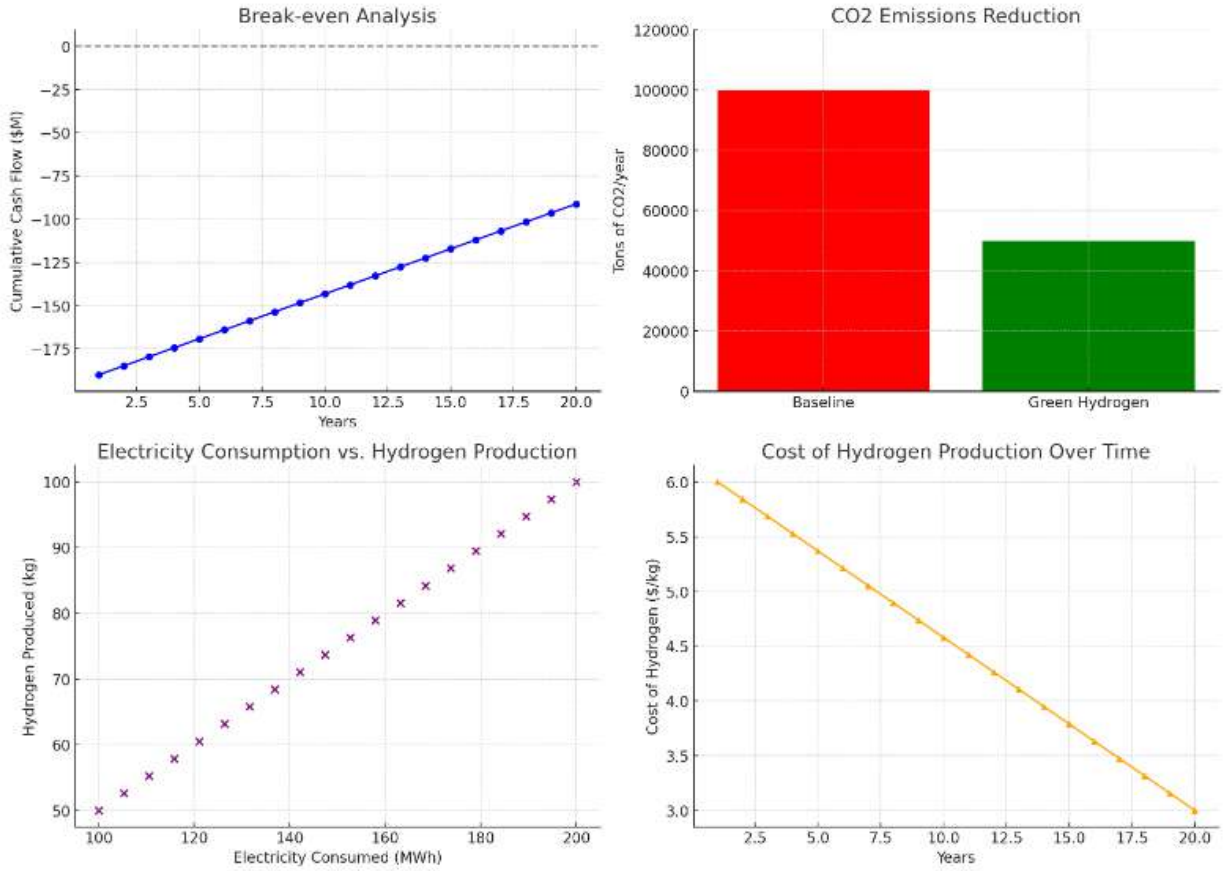


Fig.1: Graphical analysis

III. Discussion

The huge decrease in CO2 emissions, as seen in the CO2 Emissions Reduction graph, highlights the considerable environmental benefit of using green hydrogen technology. This reduction helps achieve global climate goals and also leads to a reduction in air pollution, which improves public health. The Electricity Consumption vs. Hydrogen Generation graph illustrates the efficiency of hydrogen generation, which is crucial for the scalability and sustainability of hydrogen as an energy carrier. The graph depicting the Cost of Hydrogen Production Over Time reveals the daunting economic obstacles. The high initial costs of hydrogen generation, which include expenses related to electrolyzer technology and infrastructure for storage and delivery, present a major obstacle to immediate general adoption. Anticipated cost decreases due to technology developments and higher production scales provide a positive economic picture for green hydrogen. The analysis emphasizes the crucial importance of policy and regulatory frameworks in promoting the green hydrogen economy. Offering incentives for renewable energy production, providing subsidies for hydrogen infrastructure, and implementing policies that support low-carbon technologies are crucial for mitigating the financial risks linked to early investments and operational expenses.

IV. Conclusions

Integrating green hydrogen into smart grids is a crucial opportunity to improve the sustainability and resilience of global energy systems. The techno-economic analysis shows that green hydrogen is a valuable part of renewable energy due to its long-term economic viability and large environmental advantages, despite the high initial investments needed. Strategic investments in technology development, infrastructure, and market formation are crucial to achieve this potential. Supportive legislative frameworks and international cooperation are essential for overcoming economic barriers and enabling the worldwide shift to a low-carbon energy system.

Acknowledgements

This research was supported by the Pakistan Science Foundation, Islamabad

References

Kopteva, A., Kalimullin, L., Tcvetkov, P., & Soares, A. (2021). Prospects and Obstacles for Green Hydrogen Production in Russia. Energies 2021, Vol. 14, Page 718, 14(3), 718. https://doi.org/10.3390/EN14030718

Moradi, R., & Groth, K. M. (2019). Hydrogen storage and delivery: Review of the state of the art technologies and risk and reliability analysis. International Journal of Hydrogen Energy, 44(23), 12254–12269. https://doi.org/10.1016/j.ijhydene.2019.03.041

Noussan, M., Raimondi, P. P., Scita, R., & Hafner, M. (2021). The role of green and blue hydrogen in the energy transition—a technological and geopolitical perspective. Sustainability (Switzerland), 13(1), 1–26. https://doi.org/10.3390/SU13010298
Squadrito, G., Maggio, G., & Nicita, A. (2023). The green hydrogen revolution. Renewable Energy, 216, 119041. https://doi.org/10.1016/J.RENENE.2023.119041
Wen, D., & Aziz, M. (2024). Perspective of staged hydrogen economy in Japan: A case study based on the data-driven method. Renewable and Sustainable Energy Reviews, 189. https://doi.org/10.1016/j.rser.2023.113907

Case Study of a Self-Powered Building Using Hydrogen as an Energy Carrier

[1]Mine Keleş, [1]Harun Koku, [1,*]İnci Eroğlu
[1] Middle East Technical University, Chemical Engineering Department, Ankara, 06800, Türkiye

e-mail: ieroglu@metu.edu.tr

Abstract

This research unveils the potential of hydrogen as a clean energy carrier for the Hydrogen Research Laboratory at METU's Chemical Engineering Department in Ankara, Turkey. The project's innovative approach is to harness clean solar energy with PV panels to meet the building's energy demand during the day, convert the surplus energy to hydrogen using a cutting-edge PEM electrolyzer, and utilize the stored hydrogen in the PEM fuel cell when solar energy is unavailable. It delves into three energy demand scenarios: average, peak summer, and peak winter, revealing the corresponding power demands and required hydrogen amounts of the building. Five storage options were meticulously evaluated for safety, feasibility, and economics, with the preferred choice of compressed gas at 30 bar & 25°C.

Keywords: Green hydrogen, solar energy, PEM electrolyzer, PEM fuel cell, compressed gas, metal hydride, self-powered building

I. Introduction

The core objective of this project is to underscore the pivotal role of renewable energy in meeting energy demand, championing renewable energy production and consumption, and zeroing in on its feasibility and advantages. In this vein, when solar energy is abundant, it can be harnessed directly, and any surplus will be converted into hydrogen and stored using electrolyzes for times when it is scarce. The stored hydrogen can be transformed into electrical energy as needed with the aid of fuel cells. The flowchart of Figure 1 vividly illustrates this symbiotic interaction. In this context, the utilization of solar energy during the daytime and the production and storage of hydrogen with solar energy for use at other times of the day are poised to play a pivotal role in meeting energy demands without emitting carbon-based gases, thereby significantly reducing the building's carbon footprint.

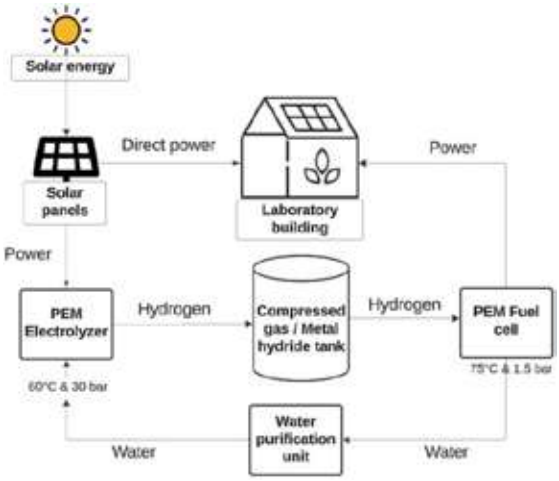


Fig. 1: Flowchart of the energy production and storage of hydrogen.

This project focused on the three scenarios below to determine the required energy and hydrogen demand and establish the system based on the most preferred one. Scenario 1 is based on average conditions for one year.

- Scenario 2 is based on summer peak demand when the air temperature is 40 °C.
- Scenario 3 is based on winter peak demand when the air temperature is -15 °C.

Furthermore, the research compared five alternate storage types regarding safety, economy, and feasibility. The five different storage types compared were as follows:

- Type 1 (MH) is a metal hydride tank at 10 bar & 25 °C with 0.82 m^3 volume.
- Type 2 (CG30-50) is a compressed gas tank at 30 bar & 25 °C with 0.05 m^3 volume.
- Type 3 (CG30-1000) is a compressed gas tank at 30 bar & 25 °C with 1 m^3 volume.

- Type 4 (CG300-20)is a compressed gas tank at 300 bar & 25 °C with 0.02 m^3 volume.
- Type 5 (CG700-50) is a compressed gas tank at 700 bar & 25 °C with 0.05 m^3 volume.

II. Methods

The two main energy demands for the laboratory building are the heating or cooling requirements ($Q_{heating/cooling}$) and the energy used by the appliances. Heat transfer with the surroundings can occur by conduction, convection, and radiation. To calculate heat that is transferred with conduction and convection, shown by $Q_{cond\&conv}$, the overall heat transfer coefficient (U) was used. Radiation can occur to or from terrestrial surroundings ($Q_{terrestrial}$), and solar radiation from the sun is transferred to the building (Q_{solar}). The required data and parameters were obtained from the literature, and cooling and heating duty were calculated. Then, the power consumed by the devices used in the laboratory and, in turn, the total energy demand of the building were determined.

Fuel cell types were investigated to supply this energy demand, and PEM fuel cells were selected.

One of the most eco-friendly methods of producing hydrogen fuel is water electrolysis, and PEM water electrolyzers are most appropriate for this project. The hydrogen demand determined the power and water the PEM electrolyzer requires.

In the proposed design, PV cells supply the energy for the PEM water electrolyzer. A market survey was conducted to decide the area and efficiency of a single PV cell, leading to the total number and area.

Finally, different storage types, from metal hydride and low to high-pressure compressed gas, are examined, and cost analysis is conducted.

III. Analysis

Energy consumption of electronic appliances:

The rating of the all-electronic appliances was determined, and the total power required was found to be 29.2 kW.

Energy consumption for heating and cooling duty:

Since the building is in Ankara, energy must be spent heating it in winter and cooling it in summer. The energy amounts are calculated using the equations below.

$$\dot{Q}_{cond\&conv} + \dot{Q}_{terrestrial} + \dot{Q}_{solar} + \dot{Q}_{heating/cooling} = 0 \quad (1)$$

$$U \cdot A \cdot \left(T_{\infty} - T_{building}\right) + \varepsilon \cdot \sigma \cdot A\left(T_{sky}^4 - T_{building}^4\right) + (\alpha_s \cdot A \cdot G_s) + \dot{Q}_{heating/cooling} = 0$$

Here, ε, σ and A are the emissivity, Boltzmann constant and area for radiation, respectively, whereas α is the absorption constant and G_s is the solar radiation flux. T_{sky} is the effective sky temperature, $T_{building}$ the building temperature, and T_{∞} the external air temperature. Radiation data for Ankara was obtained from (Çağlar et al., 2013).

PEM Fuel Cell Hydrogen Demand

A PEM fuel cell with an electrical efficiency based on HHV is used to supply power for the three scenarios. The usable energy for PEM fuel cells with 57% efficiency is 125.7 kJ/mol using Equation 2, based on a ΔG of 237.14 kJ/mol.

$$W_{usable} = \eta \times \Delta G \ (\mathrm{kj/mol}) \quad (2)$$

PEM Water Electrolyzer Energy Demand

For the PEM water electrolyzer:

$$W_{el.} = \frac{\Delta H_{H2O(l)}}{\eta} \quad (3)$$

Here η is the electrical efficiency, which is found in the literature to be 0.67 based on HHV (El-Shafie, 2023). A 67% efficient PEM electrolyzer needs 427 kJ of electrical energy to produce 1 mole H_2. The energy that 1 PV panel can produce can be calculated using Equation 5 (Markos & Sentian, 2016).

$$E\ (kW) = A \times r \times H \quad (4)$$

The PV cell chosen for this project has an area (A) of 2.59 m^2 and an efficiency (r) of 21.4 % (supplier data). The number of PV panels is calculated using Equation 6.

$$Number\ of\ PV\ Panels = \frac{Power\ \ demand\ of\ PEM\ \ electrolyzer}{Output\ power\ \ of\ 1\ PV\ cell} \quad (5)$$

IV. Results and Discussion

The results of Scenarios 1, 2, and 3 are summarized in Table 1. It was decided that the system should be set up according to the summer case because, in other cases, the amount of hydrogen produced during the daytime does not meet the required power demand at night. If the system is set according to the summer peak demand scenario, solar panels and electrolyzer work to produce 388 kW for 12 hours in the daytime. However, power is consumed instantaneously according to the average demand (40.3 kW), as illustrated in Figure 2.

Tab. 1: Results summary for three cases

	Average demand	**Summer peak**	**Winter peak**
Power demand of the building (kW)	40.4	111.6	48.0
H_2 demand of the PEM fuel cell (kg/h)	2.32	6.42	2.76
PEM electrolyzer power demand (kW)	137	378	163
Number of PV cells and area (m^2)	677 (1728 m^2)	967 (2504 m^2)	2550 (6604 m^2)

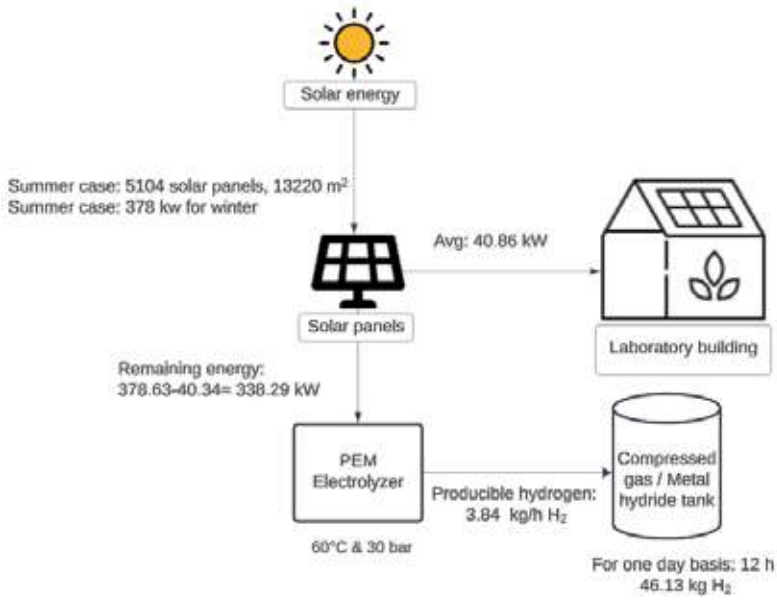


Fig. 2: Summer peak demand Scenario 1.

With 338 kW power, a total of 3.84 kg-H2 /h can be produced, and for 12 hours, 46.1 kg of hydrogen accumulates when solar energy is usable in the daytime. Otherwise, if the system is set according to the winter peak demand scenario, there is 122 kW remaining energy. With this, only 1.39 kg-H2 /h can be produced. Since this amount is less than the average case hydrogen demand (2.32 kg-H2 /h), it cannot be enough for nighttime uses.

Storage Types

The density values of each were calculated using the Peng-Robinson equation of state. Table 2 summarizes the results.

Tab. 2: Results of the five different storage types for the summer peak demand scenario based on 43.1 kg-H_2 (For the abbreviations of storage options, please see Introduction).

	MH	**CG30-50 (30 bar, 25°C)**	**CG30-1000 (30 bar, 25°C)**	**CG300-20 (300 bar, 25°C)**	**CG700-50 (700 bar, 25°C)**

Storage density(kg/m^3)	0.81	2.40	2.40	21.2	41.5
H_2 capacity (kg)	0.66	0.12	2.4	0.42	2.3
Number of tanks	70	385	20	110	21
Cost of one tank ($)	3,980	100	23,000	137	1,500
Total tank cost ($)	279,000	39,000	460,000	15,000	32,000

- Least cost: CG at 300 bar & 25 °C and 0.02 m^3
- Safest: MH at 10 bar & 25 °C and 0.82 m^3
- Most compact: CG at 30 bar & 25 °C and 1 m^3

It is sensible to choose CG at 30 bar & 25 °C and 1 m^3 as storage type because it is the safest and most compact type; moreover, there is no need to use a compressor after the PEM electrolyzer. This is why high-pressure storages are not chosen: A compressor is needed when high pressure is aimed for storage after the PEM electrolyzer. This causes extra costs, maintenance, and operation issues.

V. Conclusion

The project explores a solar-powered hydrogen system for METU Chemical Engineering's Hydrogen Research Lab. Three energy demand scenarios are analyzed: average, summer peak, and winter peak. Results show varying power demands: 40.4 kW, 112 kW, and 48.8 kW, respectively. PEM fuel cell produces hydrogen at rates of 2.32 kg/h, 6.42 kg/h, and 2.76 kg/h, with 0.53 electrical efficiency. PEM water electrolysis, powered by PV cells, meets demand with energy needs of 137 kW, 379 kW, and 163 kW. The most practical scenario is summer, ensuring 43.1 kg of stored hydrogen. Storage options were evaluated, and it is seen that Selecting CG storage at 30 bar & 25°C and 1 m^3 is logical due to its safety and compactness. Additionally, there's no requirement for a compressor following the PEM electrolyzer.

References

Çağlar A., Yamalı C., Baker DK., Kaftanoğlu, B. Türkiye'nin Ankara ilinde Yapılan Güneş Işınımı Ölçümleri. Isı Bilimi ve Tekniği Dergisi 33(2), 135-142, 2013.

El-Shafie, M. Hydrogen production by water electrolysis technologies: A Review. Results in Engineering. 20, 101426, (2023).

Markos, F. M., and J. Sentian. Potential of solar energy in Kota Kinabalu, Sabah: An estimate using a photovoltaic system model. Journal of Physics: Conference Series. Vol. 710. No. 1. IOP Publishing, (2016).

Design and Theoretical-Economic Analysis of Hydrogen Storage Power System: The Case of Dicle University

[1*]Faruk Barlaz, [1]Cem Haydaroğlu, [2]Yahya Akıl, [2]Heybet Kılıç
[1] Dicle University, Engineering Faculty, Department of Electrical and Electronics Engineering Department, Sur, Diyarbakır, 21280, Türkiye
[2] Dicle University, Department Electrical Power and Energy, Sur, Diyarbakır, 21280, Türkiye

* E-mail:faruk.barlaz@dicle.edu.tr

Abstract
This study was carried out with the aim of green hydrogen production with renewable energy sources within the campus area of Dicle University. This system analyses the hydrogen production system to be used for different purposes if needed with renewable energy sources components. The system includes photovoltaic panels (PV), wind turbines (WT), water electrolyser (AE), battery storage system (BSS), converter () and hydrogen storage tanks (HST). The aim of this study is to produce hydrogen, which is planned to be used for different purposes when needed for health and/or social facilities within the university, through renewable energy sources, accumulate it in storage tanks and provide it as input to different systems. This study simulates the amount of hydrogen needed with Homer Pro programme and makes an economic analysis of the amount of hydrogen to be obtained as a result of the electrolysis process with the remaining part of the energy produced from renewable energy sources.

Keywords: Hydrogen, Homerpro, Economic analysis

I. Introduction

Considering the dependence on energy in today's world and the rate of increase in population, renewable energy sources are seen as more reasonable and economical energy sources, considering the damages caused to health and ecosystem due to the fact that energy systems are limited, the accessible part is expensive and causes environmental and air pollution due to its use. Although their destructive effects on human health and the environment are more acceptable than traditional methods, the fact that they are more accessible and sustainable than fossil fuels in both micro and macroeconomic areas brings renewable energy resources to the forefront among OECD countries by Yıldırım, Uğur and Kaya, Muhammed (2021). The use of renewable energy sources in a system creates hybrid systems and provides positive results in many ways. The fact that the wind is not continuous and the sun's rays are only during the day or the weather is overcast limits the independent use of such systems, and when unfavourable conditions come together, problems such as insufficient capacity arise and cause the use of excessively large storage (BSS) capacities. In order to avoid these limitations and difficulties, the use of hybrid renewable energy systems (HRES) allows uninterrupted energy utilisation and prevents the use of excessively large storage systems. Storage systems consist of battery and inverter systems. These systems have different types and options in terms of hardware and features when considered in terms of economic dimensions by Das, B.K., M.S.H.K. Tushar, and R. Hassan (2021) - Engin, M. (2010).BSS are generally used to store electrical energy. However, there is also a growing interest in converting the excess energy produced by HRES into hydrogen and storing it in hydrogen tanks for energy storage.

Although it is abundant in nature, it is not pure. It is possible to obtain pure hydrogen by various methods by OĞLU, ÇiÇek Fethullah Abdulbaki; KIZI, AliYeva-ÇiÇek SamiRa Fahrettin (2022).Internationally, there is no agreed colour classification on the way hydrogen is produced. In 2019, after various discussions in the special session on hydrogen at the energy congress held in 2019, hydrogen gas produced with renewable energy systems was defined as green hydrogen in the classification that emerged after various discussions, and different colours were defined for other techniques and methods by A. Clerici and S. Furfari (2021).Renewable energy sources were used for the production of green hydrogen produced in the system under investigation and HOMER Pro software was used for the optimization of the hybrid system used. HOMER Pro is used to simulate various schemes of power plants developed by the National Renewable Energy Laboratory (NREL) of the United States of America and simulated to find the best optimised power plant configuration in terms of operating cost, net cost, gas emissions and economic comparisons of the system in the scheme, etc. by Linta Khalil etal (2021).

II. Experimental Set-up and Procedure

The design of the micro-grid established for hydrogen production to be used for different needs and purposes within the university campus has been realised. The temperature, solar and wind data for the installation were obtained from NASA data in HOMER Pro software. The hybrid energy system designed with HOMER Pro software was analysed. The HRES designed in the system consists of a combination of PV, WT, BSS, HST. Table 1 shows the unit costs of the renewable energy equipment used and Figure 1 shows the schematic representation.

Table 1. Unit cost values

Component	Capital ($)	Replacement (&)	O&M ($)	Fuel ($)	Salvage ($)	Total ($)
Generic 10 Kw	*$25,000.00*	*$79,701.84*	*$32,318.79*	*$0.00*	*($44,917.10)*	*$317,103.53*
Generic 1kWh Lead Acid	*$5,400.00*	*$2,022.38*	*$2,326.95*	*$0.00*	*($705.06)*	*$9,044.28*
Generic Electrolyzer	*$8,750.00*	*$3,712.40*	*$0.00*	*$0.00*	*($698.71)*	*$11,763.69*
Generic flat plate PV	*$20,010.09*	*$0.00*	*$1,034.72*	*$0.00*	*$0.00*	*$21,044.81*
Hydrogen Tank	*$1,000.00*	*$0.00*	*$0.00*	*$0.00*	*$0.00*	*$1,000.00*
Other	*$0.00*	*$0.00*	*$225,815.03*	*$0.00*	*$0.00*	*$225,815.03*
System Converter	*$2,417.12*	*$0.00*	*$0.00*	*$0.00*	*$0.00*	*$2,417.12*
System	*$287,577.20*	*$85,436.61*	*$261,495.50*	*$0.00*	*($46,320.86)*	*$588,188.45*

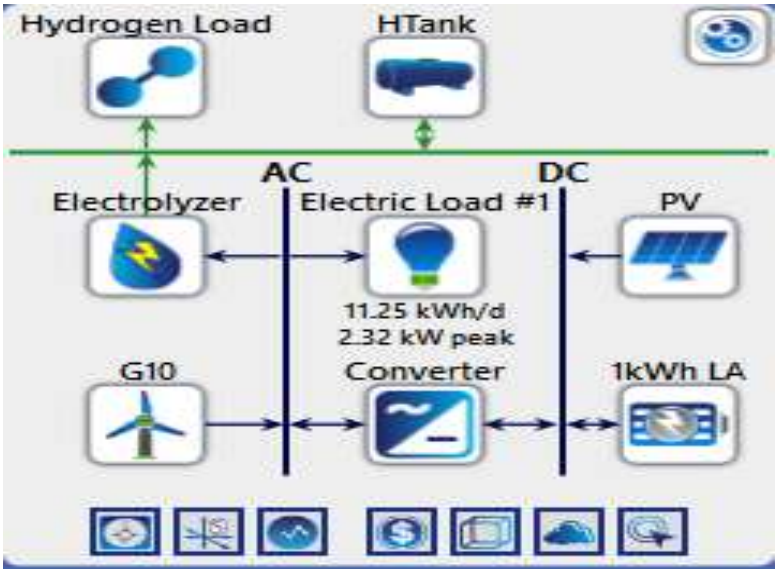


Fig 1. Hybrid renewable energy system configuration for electricity and hydrogen demands.

This is the specification of the components used in the hybrid renewable energy (HRES) system. A generic flat plate solar panel (PV) module, a generic 10KW wind turbine (WT), a generic 50 kWh lead-acid battery with a nominal voltage of 12V and a capacity of 83.4Ah and AE (0-7 kW) values are input for optimisation. The recommended configuration after optimisation is 8 kW PV panels, 5 kW wind turbine, 18 kWh battery storage system (BSS), 7 kW electrolyser (AE) and 400 kg hydrogen storage tank (HST) for solar electricity generation. A 5.95 kW converter is proposed to store electrical energy and meet the energy demand.

IV. Results and discussions

The HRES proposed by the system is designed to meet a daily energy production of 34.3 kWh and an energy demand with a peak value of 4,102 kW. The capital cost of the system is calculated as 287577 $, operating costs and maintenance costs are calculated as 261495 $. The Net Present Cost (NPC) of the system is 588188 $ and the Levelised Cost of Energy (COE) is 11.09 $/kWh. 18.6% of the energy requirement is met from PV panels and 67.528% from WT. Figure 2 shows the monthly energy production from each energy source on an annual basis.

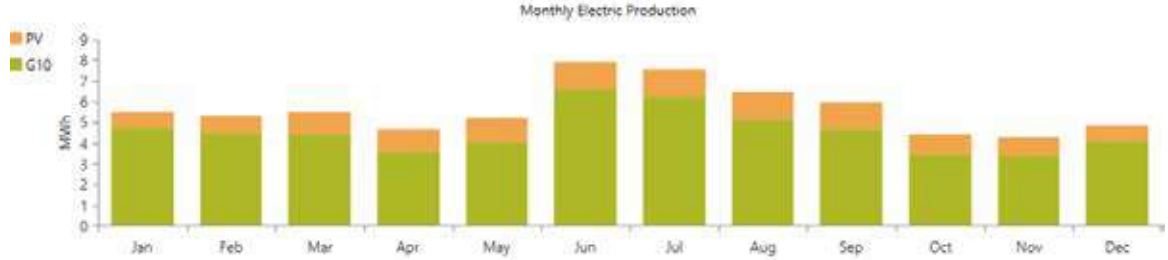


Fig 2. shows the production sources.

To meet the load demand, the excess energy produced from PV and WT energy sources is stored in batteries and then the excess energy is stored in an HST through an AE. Monthly hydrogen production in the system is shown in Figure 3. In summer months, there is an increase in hydrogen production as energy production is higher due to the prolonged sunshine hours and the intensity of the radiation.



Fig 3. Hydrogen produced by month

Some of the electricity generation is realised by PV panels. The power output graph of the PV panel is shown in Figure 4 and there is a noticeable increase in production especially in summer months. The gaps in the power output graph show that the generation is poor on cloudy days. The annual contribution of the PV panel to electricity generation is 12,532kWh/year. The power output graph for the wind turbine is given in Figure 5. Despite intermittent periods, the WT produced electricity almost continuously throughout the year, contributing a total of 12,532 kWh/year.

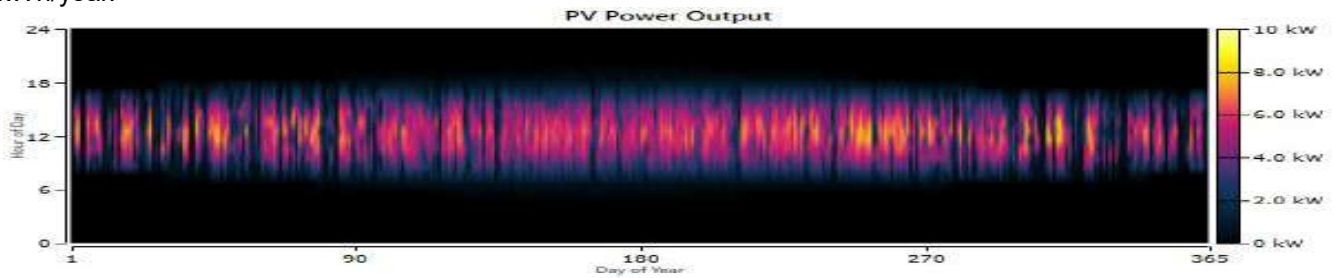


Fig4. PV panel power output graph

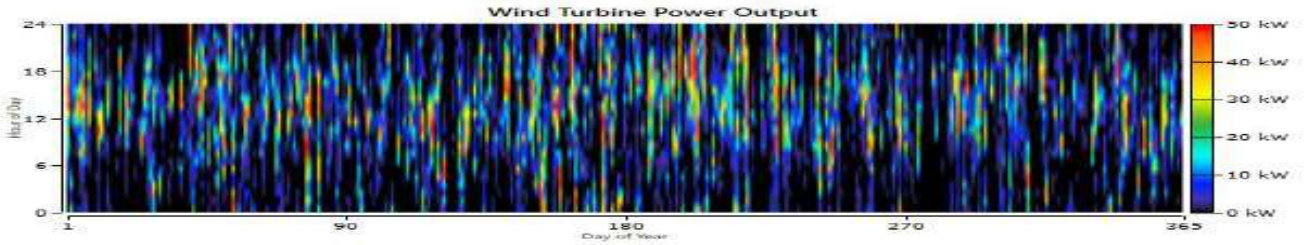


Fig 5. Power output graph of wind turbine

It is observed that the AE typically operates at full capacity and produces hydrogen, especially during daytime hours. The power output graph of the AE is shown in Figure 6. The excess energy generated by the microgrid is stored in the HST and a total of 28,387 kWh/year of energy input and 612 kg/year of hydrogen conversion is achieved during the 6,296 hours/year operation time of the AE. The stored hydrogen can be used in energy production to meet the demands as an input in different areas where it is needed.

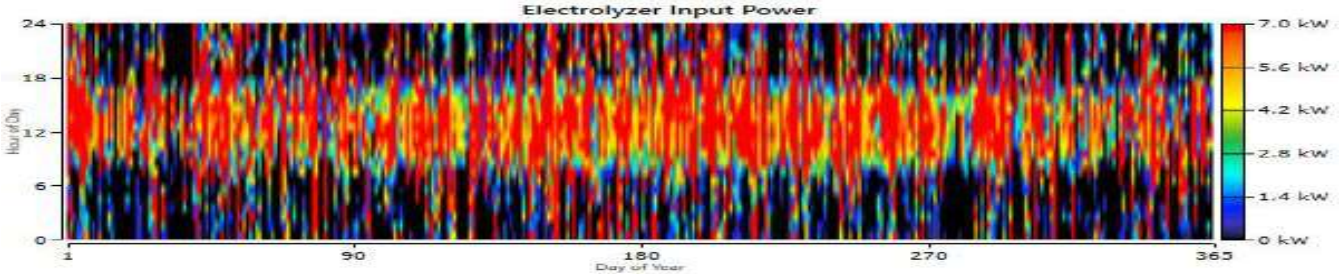


Figure 6. Electrolyser power output plot

V. Conclusions

For households or facilities located far from power transmission lines or city centres, on-site energy generation with HRES is a more environmentally friendly and cost-effective option. Since the energy produced by HRES is not stable, it must be stored. When the energy production is sufficient, hydrogen production is provided with the excess energy according to the moment of use in the settlement. As a result, it can be advantageous to store the excess energy as hydrogen. The designed system utilises PV and WT energy to generate power and directs the excess energy to the BSS and HST. The excess energy is efficiently stored through battery and hydrogen storage systems. Using a high capacity hydrogen storage tank to store excess energy during summer months can be more useful than having excessively high capacity batteries in the system. Hydrogen storage is done through an AE and the stored hydrogen can be used in different areas where it is needed. When needed, the stored hydrogen can be used to convert chemical energy into electricity through a fuel cell or for different areas.

References

Clerici and S. Furfari, "Challenges for green hydrogen development," 2021 AEIT International Annual Conference (AEIT), Milan, Italy, 2021, pp. 1-6, doi: 10.23919/AEIT53387.2021.9627053.

Das, B.K., M.S.H.K. Tushar, and R. Hassan, Techno-economic optimisation of stand-alone hybrid renewable energy systems for concurrently meeting electric and heating demand. Sustainable Cities and Society, 2021. 68: p. 102763.

Engin, M. (2010). Bornova İçin Güneş-Rüzgâr Hibrid Enerji Üretim Sistemi Tasarımı. Celal Bayar Üniversitesi Soma Meslek Yüksekokulu Teknik Bilimler Dergisi, 2(13), 11-20.

Linta Khalil, Kamran Liaquat Bhatti, M. Arslan Iqbal Awan, Mughees Riaz, Kiran Khalil, Nashitah Alwaz, Optimization and designing of hybrid power system using HOMER pro, Materials Today: Proceedings, Volume 47, Supplement, 2021, Pages S110-S115, ISSN 2214-7853, https://doi.org/10.1016/j.matpr.2020.06.054.

Çiçek, F. & Aliyeva Çiçek, S. (2022). Hidrojen gazinin üretim yöntemleri ve enerji kaynağı olarak avantaj ve dezavantajlari. Endless light in science 138-142.

S. M. Mariama, A. Scipioni, B. Davat and M. E. Ganaoui, "The Idea of Feeding a Rural Area in Comoros with a Micro-Grid System with Renewable Energy Source with Hydrogen Storages," 2018 6th International Renewable and Sustainable Energy Conference (IRSEC), Rabat, Morocco, 2018, pp. 1-5, doi: 10.1109/IRSEC.2018.8702853

Yıldırım, Uğur - Kaya, Muhammed. “Seçilmiş OECD Ülkelerinde Yenilenebilir Enerji Tüketiminin Makro Ekonomik Belirleyicileri”. Çankırı Karatekin Üniversitesi İktisadi ve İdari Bilimler Fakültesi Dergisi 11/1 (June 2021), 267-289. https://doi.org/10.18074/ckuiibfd.845859.

Determining the Hybrid Energy Potential of Türkiye's Blue Homeland in the Aegean Sea

[1*]Soner Çelikdemir, [2]Mahmut Temel Özdemir
[1] Bitlis Eren University, Adilcevaz Vocational School, Electric and Energy, Bitlis, 13000, Türkiye
[2] Firat University, Engineering Faculty, Electrical and Electronics Engineering, Elazig, 23000, Türkiye

* E-mail:celikdemirsoner@gmail.com

Abstract

The study aims to determine Turkey's offshore hybrid energy potential and green hydrogen production. For this purpose, the Aegean Sea within the Blue Homeland was analyzed. In addition to renewable energy potentials (REP), geopolitical importance, energy transmission lines, transportation routes, military and security areas, hydrocarbon potentials were also taken into consideration in determining the sample locations in this zone. Wind, solar and wave energy potentials of the identified locations were determined. It was then planned to produce green hydrogen from renewable energy potential. In this case, techno-economic analysis of the system was carried out, taking into account the transmission of the produced hydrogen to the mainland in different forms and with different transportation methods. As a result, 19,679 GWh of green energy will be produced in the zone. This energy will be obtained $400x10^3$ kg of green hydrogen through electrolysis. This green hydrogen will be transported to the mainland as compressed or liquefied hydrogen. The transportation cost of liquefied hydrogen is 0.584 M$/km, while the transportation cost of compressed hydrogen is 0.14 M$/km. In case of transportation by pipelines, the cost is 0.96 M$/km.

Keywords: Renewable energy potential, Green hydrogen energy, Blue homeland

I. Introduction

Today, the increase in population and technological tools continuously increases the demand for energy. This energy demand is usually met from fossil energy sources. However, this situation causes irreversible environmental impacts. When these negative effects are taken into account, renewable energy sources (RES) are important. Among the RES, wind, solar and wave energy are the main ones. These energy sources differ according to geographical and geological characteristics. Energy potentials are analyzed as offshore and onshore. In this study, the Aegean Sea, which is located within Turkey's blue homeland, is analyzed. The concept of 'continental shelf', which was officially defined with the 1958 Geneva Convention on the Law of the Sea, is expressed as the concept of Blue Homeland (Bahçe 2023). The visual of Türkiye's Blue Homeland continental shelf is given in blue color in Figure 1.

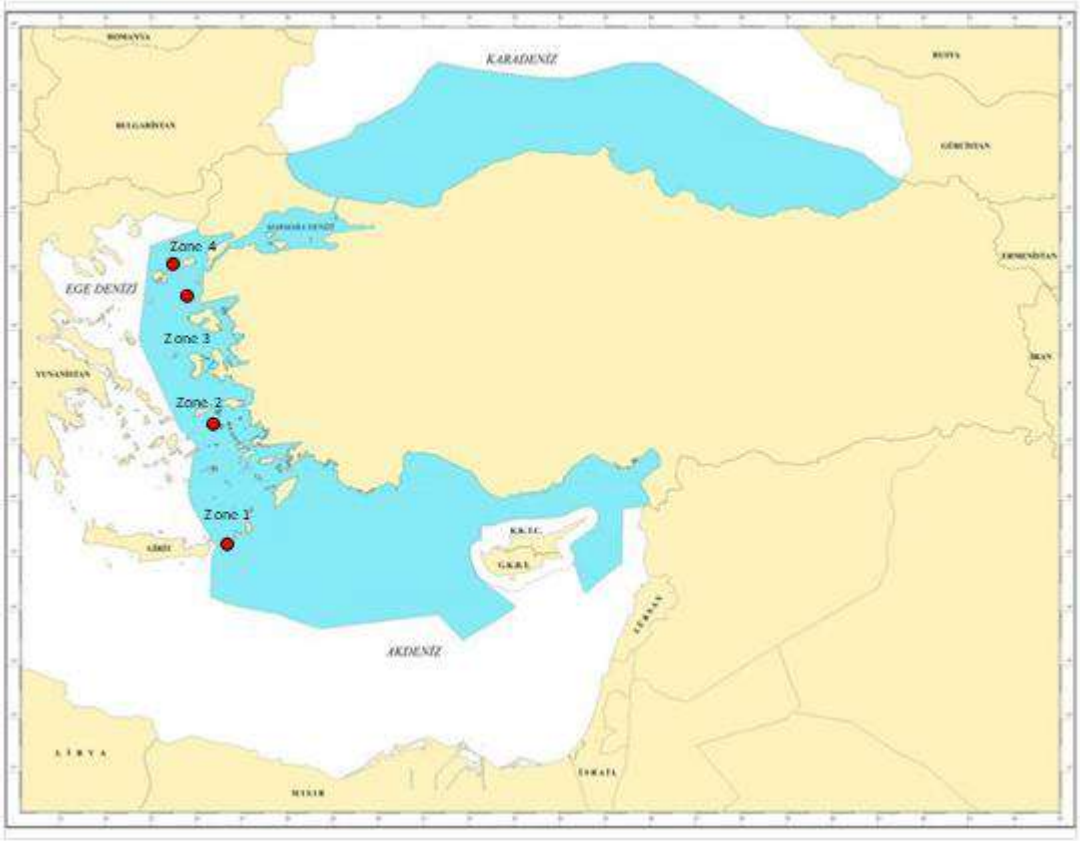


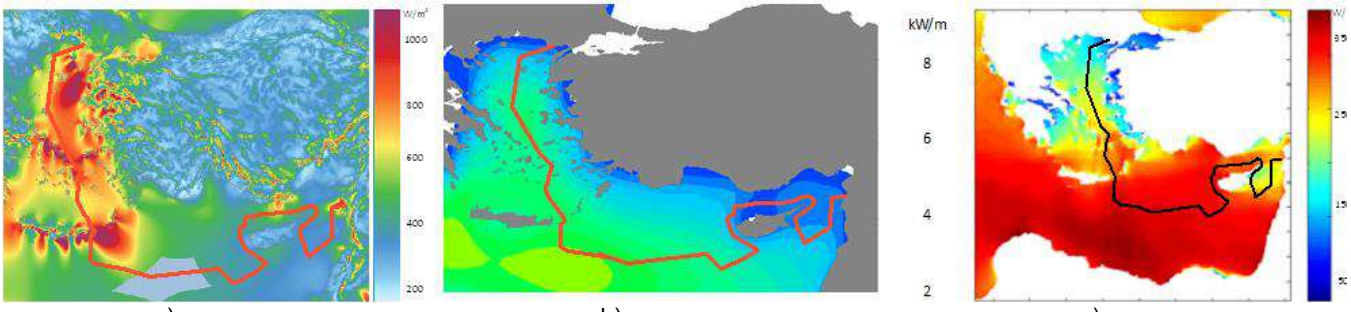
Fig.1: Türkiye's Blue Homeland Continental Shelf

In the literature, studies have been conducted to develop optimum energy cost solutions for different sites. In these studies, different hybrid solutions such as wind-solar, wind-wave, wind-solar-hydrogen have been discussed. Hybrid use of renewable energy sources can have many different purposes. It has been addressed by many researchers in recent years, especially focusing on hydrogen production systems. Today, there are different hydrogen production methods. The most common method is 'gray' hydrogen from natural gas, which produces significant carbon emissions. Less harmful than this method is 'blue' hydrogen. The production process is similar to gray hydrogen. The difference is that carbon capture and storage is utilized. Unlike these methods, the hydrogen produced by RESs is defined as 'green' hydrogen. The hydrogen obtained in such studies is referred to as green hydrogen (Gökçek and Kale 2018). Similarly, techno-economic analysis of hydrogen production from solar power plants has been carried out (Sellami and Loudiyi 2017). Wave power plants, another renewable energy source, are also considered for different zones (Oliveira-Pinto, Rosa-Santos, and Taveira-Pinto 2019; Ishaq and Dincer 2020).

Türkiye has a developing economy and its energy needs are constantly increasing. Turkey is going through a process to develop its own energy resources. The potential for offshore hybrid energy is therefore very important. In the study, sample locations are given first. Then, wind energy, solar energy and wave energy potential for 4 different zones were determined. Then, the energy that can be produced by RESs and the green hydrogen production situation are discussed. Finally, different transmission scenarios of the produced hydrogen to the mainland are analyzed.

II. System Description and Procedure

Turkey's solar energy potential has been calculated as 405 billion kWh/year and its economic potential as 380 billion kWh/year (Colak, Memisoglu, and Gercek 2020). As of 2021, the total installed capacity of solar power plants is 7.65 MW. Turkey's wind energy potential is calculated as 48000 MW. Turkey's gross wind energy potential in terrestrial areas is 400 billion kWh/year, technical wind energy potential is 120 billion kWh/year and economic wind energy potential is 50 billion kWh/year (Çelikdemir and Özdemir 2020). As of 2023, the total installed capacity of wind power plants is 10.25 MW. However, Turkey does not have any offshore WPPs installed. Turkey's wave energy potential is calculated as 10 TWh/year. However, there are no installed wave power plants in Turkey. Turkey's installed capacity reached 99.05 MW as of 2023. The ratios of the licensed installed power value according to energy sources are; 46.68% fossil-based energy sources, 31.83% hydroelectric power plants, 10.29% wind power plants, 7.62% solar power plants, 1.51% biomass and 1.67% geothermal energy sources. In the light of this information, it shows that Turkey's RESs are developing and open to further development. In addition, wind energy, solar energy and wave energy potential maps of the Eastern Mediterranean and Aegean Sea are given in Figure 2.



a) b) c)

Fig. 2: Blue Homeland energy potential a) Wind energy map b) Wave energy map c) Solar energy map

Within the Blue Homeland Continental Shelf Zone, 4 Zones with a square area of 3x3 km were identified. The rotor blades are directly effective in the conversion of wind energy into mechanical energy. The difference in kinetic energy when the wind touches and leaves the blades is equal to the amount of wind energy converted into kinetic energy. Kinetic energy equations are used to calculate this power. The amount of energy that can be obtained from a wind turbine is given in Equation 1.

$$E_e = \frac{\rho A}{2} v^3 \ t \tag{1}$$

Here; air density (kg/m^3), wind turbine swept area (m^2), wind speed at tower height (m/s) and t is the time (s). The coordinates and wind energy data for these Zones are given in Table 1.

Table 1. Coordinates and wind energy data for the Zones

Zone	Latitude	Longitude	Average wind speed (m/sn)	Power density (W/m2)
Zone 1	35.12103	26.60889	10.3	1123
Zone 2	37.53368	26.40838	9.51	910
Zone 3	39.82541	25.94696	9.53	914
Zone 4	40.18228	25.68191	9.25	939

The wind farms to be created by installing Generic 3.45 MW wind turbines proposed to be established in the zone will generate 11.629 GWh of energy annually. Solar energy, the source of many RESs, is the radiant energy

generated by the fusion process in the sun's core. The energy production structure of a solar panel also depends on external factors. Solar radiation, cell temperature and shading values are the main factors affecting the efficiency of solar modules. These factors should be taken into account when designing the system. The amount of energy to be obtained annually from a solar module is estimated using Equation 2.

$$E_e = A_{tp} \cdot A_v \cdot \eta_f \cdot P_R \cdot GHI \quad (2)$$

Here; E_e the annual electricity production of the solar module (kWh/yıl), A_{tp} the total area of the solar module (m^2), A_v the availability of the solar module, η_f the efficiency of the solar module, P_R the losses (temperature, shading, transmission, etc.) and the annual global horizontal radiation (kWh/m^2). The annual efficiency of solar modules varies regionally. However, the efficiency of offshore modules is higher than terrestrial modules. Solar energy data for the coordinates determined within the Blue Homeland Continental Shelf zone are given in Table 2.

Table 2. Solar energy data for Zones

Zone	DNI (kWh/m²)	GHI (kWh/m²)	DIF (kWh/m²)	GTI (kWh/m²)	Sıcaklık (C)
Zone 1	1882.1	1904.8	642.2	2108.5	19.4
Zone 2	1941.8	1827.6	618.0	2052.4	18.4
Zone 3	1774.6	1707.7	615.1	1931.6	16.8
Zone 4	1681.3	1660.6	620.7	1873.5	16.6

With the 1000 kWp solar panels proposed to be installed in the zone, a total of 5.704 GWh of energy will be generated annually. Wave energy is a source of energy generated by wind, seafloor movements, gravitational forces of the sun and moon, human activities and different mass movements on the water surface. In general, wave energy source is defined as the average wave power per unit of crest length. The wave energy source expression is given in Equation 3.

$$E_w = \frac{\rho g^2}{64\pi} \sum_{i=1}^{N} \sum_{j=1}^{M} H_S^2 \, T_E \, f_{i\,j} \quad (3)$$

Here; ρ seawater density (kg/m^3), g gravitational acceleration (m/s^2), H_s wave height (m), T_E energy period (s), $f_{i\,j}$ ise the frequency of wave formation and E_w is the wave energy. Accordingly, the average annual energy of the wave is denoted by $E_{i\,j}$ and given in Equation 4.

$$E_{i\,j} = \frac{\rho g^2}{64\pi} H_S^2 T_E h_{i\,j} \quad (4)$$

There are two important components that make up wave energy. These are wave height value and wave period value. These two components should be taken into consideration when analyzing the wave energy potential of a zone. Wave energy data for the coordinates determined within the Blue Homeland Continental Shelf zone are given in Table 3.

Table 3. Wave energy data for the Zones

Zone	Depth (m)	Average Wave Height (m)	Period (sn)	J (kW/m)	E (MWh/m)
Zone 1	919	1.11	4.7	8.9	77.964
Zone 2	52	1.12	4.6	9.3	81.468
Zone 3	26	1.05	4.6	8.95	78.402
Zone 4	150	1.03	4.5	8.9	77.964

With the 150 MW wave power plant to be established in the zone, 2.346 GWh of energy will be produced. Thus, the total amount of energy to be produced in 4 Zones will be 19.679 GWh of energy.

III. Hydrogen Production

Dinçer stated that the hydrogen era has begun (Dincer 2020). Hydrogen production has therefore emerged as an important engineering application. Although hydrogen is the most abundant and cleanest energy source, it is not readily available in nature as a chemical substance because it is mostly bound to other molecules. Therefore, it needs to be produced before it can be used. There are various methods in the literature to produce hydrogen. However, in order to be accepted as an alternative energy, it must have a renewable and sustainable-based process. In this context, water electrolysis is the only viable technology for large-scale 'green and clean' hydrogen production (Proost 2019). Water electrolysis is the process of separating water into hydrogen and oxygen by direct current. This technology has many advantages such as high efficiency and most importantly, it can be produced from renewable energy sources. This has revealed the necessity to investigate the hydrogen production from renewable energy sources in the Eastern Mediterranean region, which has a high renewable energy potential. This has been the most important motivation of this study.

There are many electrolysis technologies in the literature. In this study, the most advanced and widely used PEM electrolysis is taken as a reference. PEM has advantages such as high efficiency, life cycle, suitability for fluctuating electricity generation loads from renewable energy, hydrogen production at low pressure and direct

storage of the produced hydrogen without the need for compression. Thus, 19,679 GWh of the energy generated from RES can be used in hydrogen production. In this case, 39 kWh/kg for 100% efficiency, while the efficiency is around 70% under today's conditions. Considering this efficiency, energy consumption is 49 kWh/kg. According to this energy value, $400x10^3$ kg of hydrogen can be produced annually. In addition, different scenarios were considered for the transmission of the produced hydrogen to the mainland. These scenarios include pipelines, cargo ships and finally, if there are natural gas reserves, the produced hydrogen is mixed with natural gas and transported to the mainland. In this case, if the hydrogen produced is transported by cargo ships, there are two different methods. These are transportation as compressed or liquefied hydrogen. The cost of transporting liquefied hydrogen is 0.584 M$/km, while the cost of transporting compressed hydrogen is 0.14 M$/km. In the case of transportation by pipelines, the cost is 0.96 M$/km.

V. Conclusions

In this study, the RES potential for the Eastern Mediterranean and the Aegean Sea was examined and techno-economic analysis was carried out. For this purpose, the RES potentials of the determined regions were analyzed for wind, solar and wave energy sources. Since the regions are located between low pressure and high pressure air currents, it is seen that wind energy densities are high. When the latitude effect and daily insolation are taken into account as the main criteria in determining the solar energy potential, it is seen that the energy density of the regions is high. In addition to this situation, wave energy in the region was also added. As a result, 19,679 GWh of green energy will be produced in the region. This energy will produce $400x10^3$ kg of green hydrogen through electrolysis. This green hydrogen will be transported to the mainland as compressed or liquefied hydrogen. The transportation cost of liquefied hydrogen is 0.584 M$/km, while the transportation cost of compressed hydrogen is 0.14 M$/km. In case of transportation by pipelines, the cost is 0.96 M$/km.

References

Bahçe, Ahmet Furkan. 2023. “Türkiye’nin Doğu Akdeniz’de Mavi Vatan Politikasi.” *The Journal of Social Sciences* 63 (63): 481–509. https://doi.org/10.29228/SOBIDER.68570.

Çelikdemir, Soner, and Mahmut Temel Özdemir. 2020. “Adilcevaz Bölgesinde Rüzgar Enerji Potansiyelinin İncelenmesi.” *Bitlis Eren Üniversitesi Fen Bilimleri Dergisi* 9 (1): 204–14. https://doi.org/10.17798/bitlisfen.526670.

Colak, H. Ebru, Tugba Memisoglu, and Yasin Gercek. 2020. “Optimal Site Selection for Solar Photovoltaic (PV) Power Plants Using GIS and AHP: A Case Study of Malatya Province, Turkey.” *Renewable Energy*. https://doi.org/10.1016/j.renene.2019.12.078.

Dincer, Ibrahim. 2020. “Covid 19 Coronavirus: Closing Carbon Age, but Opening Hydrogen Age.” *International Journal of Energy Research* 44 (8): 6093–97. https://doi.org/10.1002/er.5569.

Gökçek, Murat, and Cihangir Kale. 2018. “Techno-Economical Evaluation of a Hydrogen Refuelling Station Powered by Wind-PV Hybrid Power System: A Case Study for İzmir-Çeşme.” *International Journal of Hydrogen Energy* 43 (23): 10615–25. https://doi.org/10.1016/j.ijhydene.2018.01.082.

Ishaq, H., and I. Dincer. 2020. “A Comparative Evaluation of OTEC, Solar and Wind Energy Based Systems for Clean Hydrogen Production.” *Journal of Cleaner Production* 246 (February): 118736. https://doi.org/10.1016/j.jclepro.2019.118736.

Oliveira-Pinto, Sara, Paulo Rosa-Santos, and Francisco Taveira-Pinto. 2019. “Electricity Supply to Offshore Oil and Gas Platforms from Renewable Ocean Wave Energy: Overview and Case Study Analysis.” *Energy Conversion and Management* 186 (April): 556–69. https://doi.org/10.1016/j.enconman.2019.02.050.

Proost, Joris. 2019. “State-of-the Art CAPEX Data for Water Electrolysers, and Their Impact on Renewable Hydrogen Price Settings.” *International Journal of Hydrogen Energy* 44 (9): 4406–13. https://doi.org/10.1016/j.ijhydene.2018.07.164.

Sellami, M.Hassen, and K. Loudiyi. 2017. “Electrolytes Behavior during Hydrogen Production by Solar Energy.” *Renewable and Sustainable Energy Reviews* 70 (April): 1331–35. https://doi.org/10.1016/j.rser.2016.12.034.

Strategic Importance of Hydrogen within the Scope of Türkiye's New Century Vision

Mehmet Firat Dogan
Marmara University, Faculty of Political Science, Political Science and Public Administration, Göztepe, Istanbul, 34722, Türkiye

* E-mail:mfiratdogan@hotmail.com

Abstract

Full independence of nation states begins with reducing foreign dependency on energy and increasing domestic production in the defense industry and technology. One of the biggest obstacles facing Türkiye within the framework of its new century goals is; Foreign dependency in energy and thus the current account deficit due to energy and strategic moves cannot be taken in order not to endanger energy security and international relations. Türkiye, which has been trying to become a power in its region and reduce its foreign dependency since the first days of the Republic, has a long way to go, even though it has tried to break its foreign dependency with the steps it has taken in the field of defense industry within the national and local framework in the last 20 years, and the natural gas exploration and oil extraction activities carried out. Here is the subject of this study; The aim is to examine hydrogen as an alternative energy source in reducing Türkiye's foreign dependency and to offer a way to the central government. It is aimed to reveal the energy potential by breaking the energy gap with hydrogen and combine it with new century strategies. In the general scope of our study, the contributions of hydrogen as an alternative energy source in reducing Türkiye's foreign dependency, getting one step closer to its domestic-national goals and becoming a regional power are explained. By applying the qualitative research method, local and international reports were used, a literature review was conducted and a vision plan was created. The data obtained were evaluated, the definition regarding the solution of Türkiye's energy problem was changed with the findings obtained, and the way out of the energy policy created by the Ministry of Energy was changed and additional articles were added.

Keywords: Hydrogen, Energy Policy, Turkiye

I. Introduction

The domestic and national Türkiye target that Türkiye has set within the scope of the new century perspective has gained great momentum after the first steps taken in 2004 and the FETO coup attempted to be carried out on July 15,2016. The main steps that a country must take towards becoming a global actor are reducing foreign dependency in energy, closing the current account deficit in the economy, and transitioning to domestic production in the defense industry and technology. Türkiye, which has been trying to become a power in its region since the day the Republic was first established. However, while it should have a greater say in the world with its deep-rooted history coming from the empire, the intense investments it has made in its people, the developments it has made after the industrial age, and the steps it has taken in the fields of defense industry and technology in the national and local framework, foreign dependency on energy has always been an obstacle. Although Türkiye has tried to break its dependence on foreign energy with natural gas exploration and oil extraction activities, it still has a long way to go with 74%. Within the framework of the hydrogen energy strategy and road map determined by Türkiye and the 2053 vision of the twelfth development plan, hydrogen energy was discussed within the framework of the European Union Green Consensus and only increasing the renewable energy potential was simply considered. However, although Türkiye's hydrogen potential is not found in any European Union country, the hydrogen sulphide deposits it has in the Black Sea require Türkiye to look at hydrogen energy from a very different perspective. How an issue is handled and defined at the beginning of the journey, the vision and road map to be established will vary depending on the starting path. The way Hydrogen Energy is handled will also affect the network structure, policy and outputs to be established. Therefore, in the new century of the Republic, the issue of Türkiye Hydrogen Technologies Strategy and Road Map in the perpective which is stated that our main goal will continue to be to raise our country above the level of contemporary civilizations within the framework of the 2053 vision (Türkiye,2023) and was prepared with the principle of creating a carbon zero economy model by using hydrogen in line with our Economic Development and 2053 net zero carbon emission targets stated in the Hydrogen Policy (Enerji,2023), should be changed.

Hydrogen technologies should be considered in order to close Türkiye's energy deficit, to address the current account deficit due to energy, and as a priority energy source in Türkiye's full independence and a new Hydrogen Strategy and Policy should be established by becoming aware of its own underground resource. One of Türkiye's views on energy resources is, of course, increasing clean energy resources due to the European Union Green Consensus but the main issue should be the energy deficit and the moves that Türkiye could not realize due to the energy deficit. The findings have shown that applying the same policy as other countries that do not have hydrogen resources is wrong and will prevent Türkiye from revealing its energy potential. Therefore, with the new hydrogen policy that will be established by urgently increasing Türkiye's research on hydrogen sulphide deposits in the Black Sea and by considering hydrogen as the main energy source, Türkiye will be able to achieve its new century goals with much more confident steps.

II. Basic Concepts and Theoretical Framework

In this part of the study, the concept definitions of hydrogen and hydrogen energy types will be given and how hydrogen can be obtained will be explained. Türkiye's Development Plan and Hydrogen Policy will be examined and attention will be drawn to their goals. Additionally, the benefits of obtaining hydrogen from HydrogenSulphide will be explained. In this context, it is thought that it will be important to discuss Türkiye's energy deficit in using hydrogen as the main energy source in this section in order to emphasize the importance of its mission in reducing foreign dependency. For an economy to develop and for this development to be long-term and sustainable; It depends on the ability to supply the required energy in sufficient quantities, at the least cost, in a reliable manner and with the methods that are most harmful to the environment (Şadan,2009). Developed countries focus their energy strategies on resource diversity, priority of local resources and low costs. Strategically, the first priority is to make the most of local resources in order to reduce foreign dependency on energy. Energy security is of strategic importance for countries to have a strong economic structure. When evaluated from Türkiye's perspective, high foreign dependency in energy is a significant risk that threatens energy security (Arslan, 2009).

Table 1. Change in Primary Energy Consumption

	Energy Consumption (1000 TOE)	Increase (%)	Increase (1000 TOE)
1970	18 872		
1980	31 973	69 %	13 102
1990	52 987	66 %	21 513
2000	80 500	52 %	27 513
2010	105 827	31 %	25 327
2017	145 305	37 %	39 478

With Table 1 showing the increase in primary energy resources in Türkiye, it is understood that the country's "energy dependency" has increased significantly(Önder,2019). Energy supply security is an important issue that affects the economic development and national security of countries. Therefore, every country must be able to provide energy from uninterrupted, reliable, cheap, clean and diversified sources. In recent years, Türkiye has not been able to produce policies that would reduce its foreign dependency by mobilizing its national resources in terms of energy. While energy, which has become more important in the global economy today, creates new and great opportunities for Türkiye's economy, on the other hand, it continues to be an increasingly costly input due to dependence on energy imports (Rusya, 2009). As explained in the Türkiye Hydrogen Technologies Strategy and Road Map of the Ministry of Energy and Natural Resources of T.R., gaining competence in hydrogen energy and technologies, which will play an important role in the 2053 net zero emission target in Türkiye, as well as advancing the existing knowledge to the commercialization process, is an important necessity for our country. is evaluated (Enerji,2023). In the report, it is stated that “The European Union aims to increase the share of hydrogen in Europe's energy consumption to 13-14% by 2050 in its long-term plans. In the Medium Term Program, it is stated that within the scope of green transformation policies, necessary steps will continue to be taken in all sectors to achieve our country's 2053 net zero emission targets[1]. Hydrogen technologies have begun to stand out as an important element in energy conversion. The report also underlined Türkiye's high foreign dependency by saying, "During the plan period, imports of energy raw materials, especially oil, natural gas and hard coal, continued to constitute more than 80 percent of the sector's imports. In Türkiye's long-term strategy, it is aimed to become a country that has ensured supply security and self-sufficiency with its domestic and renewable resources, it has also been stated that the main goal is to reduce energy import dependency to low levels.

The Black Sea has a great energy potential with a hydrogen capacity of 270 million tons. One of the most important resources that can be used in hydrogen production is hydrogen sulfide found at the bottom of the Black Sea (Gök,2022). Baykara et al. In their study, they saw hydrogen sulfide at the bottom of the Black Sea as a potential hydrogen source (Baykara, 2008). Midilli et al. They conducted a parametric study to estimate the hydrogen energy potential in the bottom waters of the Black Sea, depending on the H_2S concentration and water layer depth (Midilli, 2007). Petrov et al. They investigated the processes of H_2 and S production from H_2S found in the Black Sea bottom waters (Petrov, 2011). In their study, Şanlı and Mat suggested the direct use of Black Sea water containing H2S as fuel in a fuel cell. They argued that by using the fuel cell system, both electricity can be produced and the costs will be lower (Şanlı, 2015). Türkaslan in his study, designed a hydrogen production facility in a laboratory environment (Türkaslan, 2013). Stavros carried out the feasibility study and economic analysis of obtaining hydrogen from hydrogen sulphide at the bottom of the Black Sea (Stravroz, 2012). Karapekmez and Dinçer designed a system for the production of H_2 from H_2S gas (Karapekmez, 2021). Hydrogen production from hydrogen sulfide gas can be done by various developing methods (Türkaslan, 2013). Both the electrolysis of water and the electrolysis of hydrogen sulfide are endothermic reactions that require external energy. The amount of energy used in the electrolysis of water is approximately 3.235 times more than the amount of energy used in the electrolysis of hydrogen sulfide (Yılmaz, 2012). Figure 1 shows the distribution of hydrogen sulfide in the Black Sea. Midilli et al. they decomposed H_2S into H_2 and S in a PEM electrolyzer (Midilli, 2021). With the effect of decreasing energy resources and increasing energy costs, as well as environmental awareness, many countries have started to search for renewable and sustainable clean energy sources. Among these energy sources, hydrogen, which is abundant

in nature and environmentally friendly, has come to the fore. For Türkiye's energy supply security, it is necessary to diversify existing energy resources and especially focus on local energy resources. High dependence on foreign energy; It is among the main reasons for Türkiye's foreign trade and current account deficit problems. While Türkiye approaches energy security mainly from the perspective of taking advantage of its strategic location, other countries address the issue with different approaches such as sustainability, environmental impacts, diversification, and reducing dependency. Energy supply security can be achieved by reducing external dependency and increasing resource diversity. By providing this capability to the country through systematic and planned work, not only energy supply security can be ensured, but also sustainability can be achieved (Poyraz, 2014).

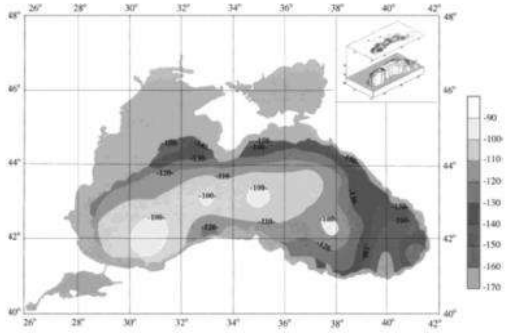


Fig1. Distribution of hydrogen sulfide in the Black Sea (Şeker, 2019)

III. Evaluation and New Hydrogen Policy

Starting the hydrogen policy from seeing hydrogen as just a side source of green energy and seeing it as the main issue will ensure supply security and entering a sustainable energy cycle in Türkiye. T.R. Ministry of Energy and Natural Resources, Türkiye's Hydrogen Technologies Strategy and Road Map and Türkiye's National Energy Plan and Twelfth Development Plan, as reviewed above, are missing hydrogen definition regarding the solution of Türkiye's energy issue and the way out of the energy policy created by the Ministry of Energy should be changed. It is wrong for Türkiye to implement the same policy as other countries that do not have a hydrogen source and to follow a similar hydrogen policy as the EU, and it will prevent Türkiye from revealing its energy potential.As stated in the Hydrogen Technologies Strategy and road map, the main issue of use of hydrogen energy for Türkiye should be energy security and reducing foreign dependency, not zero emission targets. Although the Road Map deals with hydrogen entirely from a clean energy perspective, the real importance of hydrogen for Türkiye comes from the fact that Türkiye has large hydrogen deposits that can meet almost all of its energy. Of course, we need to look forward within the framework of the clean energy vision in the developing world order, but the most important concept is Türkiye's energy security and use of its own national resources. In this context, Türkiye, the country with the world's largest hydrogen deposit, has a great potential within the framework of the new century vision.

Although the ministry plans have made a plan to develop more effective natural gas and zero emission technology, especially by using hydrogen together with natural gas, Türkiye's main vision plan should be on the development of fuel cells and the use of hydrogen directly as the main energy source. It is stated in the reports that a hydrogen road map integrated with the EU will be followed, However, Türkiye can make serious strategic moves independent of the EU due to the Black Sea hydrogen deposits it has. The report has repeatedly mentioned the value that hydrogen will add to our lives in order to achieve the 2053 net zero emission targets, but the main purpose of the use of hydrogen in our country should be included within the scope of energy diversity and energy security policies rather than green transformation policies. Hydrogen technology and fuel cells are energy production technologies that are considered not for zero emission purposes due to their high efficiency, but because they are high-efficiency technologies of the future.

Table 2. New Hydrogen Policy Additional Clauses

New Hydrogen Policy Additional Clauses
To change the way hydrogen is handled in the current Hydrogen Policy from the perspective of green hydrogen and zero-emission by-energy product and to treat it as a high-efficiency main energy source
Integrating the hydrogen issue into the country's future vision in the short term
Putting hydrogen policy at the center of general energy policy
To carry out an urgent project on the extraction of Hydrogen sulphide resources in the Black Sea
Moving on to R&D and P&D studies on the separation of hydrogen sulfide
Immediately commissioning local and national fuel cell production
Creating a University – Bureaucracy – Business partnership
To ensure that master's and doctoral students and academicians from the last 10 years are involved in the subject
To accelerate the work of hydrogen storage and distribution lines

The negative impact of wars and regional crises on every issue has been repeatedly mentioned in the development plan. Unfortunately, since the geography we are in is a geography where war has never ended for thousands of years, necessary precautions must be taken for energy independence. Türkiye must quickly grasp the

opportunities of its natural resources and future energy types, and realize that its hydrogen potential is much different than other countries. Although Türkiye's hydrogen potential is not available in any European Union country, the hydrogen sulphide deposits it has in the Black Sea require Türkiye to look at hydrogen energy from a very different perspective. In this context, in our study, within the framework of Türkiye's new century vision, the issue of looking at hydrogen has been removed from zero emission targets and addressed as reducing the energy deficit and ensuring energy security of Türkiye, which is a country with high-efficiency hydrogen technologies and Hydrogen sulphide deposits in the Black Sea, and the new Hydrogen Policy has been put forward.

V. Conclusions

In this study, attention is drawn to the potential of hydrogen energy, which is one of the energy models of the future, in Türkiye. In the 2023 hydrogen vision plan, it was concluded that hydrogen was under-evaluated and new hydrogen policies were proposed in order to draw the main issue correctly and determine the subsequent road map more effectively. In the new century strategy created within the framework of Türkiye's domestic and national goals, the importance of hydrogen sulfide deposits in the Black Sea was mentioned and this study was carried out to draw attention to the fact that hydrogen which is evaluated within the framework of 2053 zero emissions, has a much greater impact. In this context, Türkiye's perspective on the Hydrogen issue was changed in the study and the new hydrogen policy was prepared to guide the central government.

References

A. Karapekmez and İ. Dinçer, “Development of a multigenerational energy system for clean hydrogen generation,” Journal of Cleaner Production, vol. 299, 2021. doi:10.1016/j.jclepro.2021.126909

A. Midilli, M. Öztürk and İ. Dinçer, “Effective use of hydrogen sulfide and natural gas resources available in the Black Sea for hydrogen economy,” International Journal of Hydrogen Energy, vol. 46, pp. 10697-10707, 2021.

A. Midilli, M. Ay, A. Kale, and T. N. Veziroğlu, “A parametric investigation of hydrogen energy potential based on H2S in Black Sea deepwaters” International Journal of Hydrogen Energy, vol. 32, no. 1, pp. 117-124, 2007. doi:10.1016/j.ijhydene.2006.04.006

ARSLAN, V. (2009). “Enerji Kaynaklarında Güvenirlilik ve Kömürün Yeri”, TMMOB İzmir Kent Sempozyumu, 8-9-10 Ocak, ss.“215-228”

Baykara S. Z., H. E. Figen, A. Kale and T. N. Veziroğlu, “Hydrogen from hydrogen sulphide in Black Sea,” International Journal of Hydrogen Energy, vol. 32, no. 9, pp. 1246-1250, 2008. doi:10.1016/j.ijhydene.2006.07.021

Enerji ve Tabii Kaynaklar Bakanlığı, Türkiye Hidrojen Teknolojileri Stratejisi ve Yol Haritası, 2023

Gök K. and A. Sözen, “Design and Analysis of Hydrogen Production Combined System from Hydrogen Sulfide with Renewable Energy Source,” Gazi Journal of Engineering Sciences, vol. 8, no. 2, pp. 273-291, 2022.

K. Petrov, S. Z. Baykara, D. Ebrasu, M. Gulin, and T. N. Veziroğlu, “An assessment of electrolytic hydrogen production from H2S in Black Sea waters,” International Journal of Hydrogen Energy, vol. 36, pp. 8936-8942, 2011.

M. Stavros, “Feasibility study of hydrogen production and power in fuel cell reactors, from the H2S-rich Black Sea waters,” Master of Science (MSc) in Energy Systems, School of Science & Technology, International Hellenic University, Greece, 2012.

Önder Algedik, Cumhuriyet’in 100. Yılına Doğru Türkiye’nin Enerji Politikası: Sorunlar ve Çıkış Yolları Üzerine, Mülkiye İktisadi ve Sosyal Araştırmalar Merkezi Politika Metinler, 2019

Rusya Enerji Politikası ve Türkiye Perspektifi, SDE, Stratejik Düşünce Enstitüsü, 10.11.2009,

Sanlı A. and M. D. Mat, “Performance analysis of direct Black Sea hydrogen sulphide (in artificial sea water)/hydrogen peroxide fuel cellsi” International Journal of Hydrogen Energy, vol. 40, no. 35, pp. 6440-6448, 2015. doi:10.1016/j.ijhydene.2015.03.042

Şadan Çalışkan, Türkiye’nin Enerjide Dışa Bağımlılık Ve Enerji Arz Güvenliği Sorunu, Dumlupınar Üniversitesi, Sosyal Bilimler Dergisi Sayı:25, Aralık 2009

Türkaslan M., “Karadeniz Suyundan Hidrojen Üretimi,” Yüksek Lisans Tezi, Fen Bilimleri Enstitüsü, Gazi Üniversitesi, Ankara, Türkiye, 2013.

O. Yılmaz, “Deniz Suyundaki Hidrojen Sülfürün (H2s), Farklı Metal Elektrotlar Kullanılarak Elektro1Oksidasyonunun İncelenmesi,” Yüksek Lisans Tezi, Fen Bilimleri Enstitüsü, Gazi Üniversitesi, Ankara, 2012.

Poyraz Gürson ve arkadaşları, Yenilenebilir Enerji Politikaları ve Enerji Arz Güvenliği, International Conference on Eurosian Economies, 2014

S. Seker and N. Aydin, “Hydrogen production facility location selection for Black Sea using entropy based TOPSIS under IVPF environment,” International Journal of Hydrogen Energy, vol. 45, no. 32, pp. 15855-15868, 2019

Türkiye Cumhuriyeti Cumhurbaşkanlığı Strateji ve Bütçe Başkanlığı, On İkinci Kalkınma Planı, Karar no: 1396, 31.10.2023

A Recurrent Neural Network Model Predictive Control (RNN-MPC) Strategy for Efficient Energy Management in Hybrid Battery-Hydrogen Systems

Sulman Shahzad[1,2*] Heybet Killic[3]

[1]Department of Electrical Engineering, Islamia University of Bahawalpur, Bahawalpur 63100, Pakistan
[2] National Transmission & Despatch Company Limited, 60600, Multan, Pakistan
[3]Department of Electric Power and Energy Systems Dicle University 21280 Diyarbakır, Türkiye

* E-mail: salmanshahzad05@gmail.com

Abstract
This research suggests a novel method for controlling the energy in isolated DC microgrids by combining Model Predictive Control (MPC) with Recurrent Neural Networks (RNNs). The method deals with the sporadic nature of renewable energy sources by using the sequential data processing ability of RNNs to predict energy supply and demand patterns effectively. Our approach improves the grid's effectiveness and dependability by improving hybrid storage systems that consist of batteries and hydrogen storage units. The proposed system's performance is evaluated against traditional rule-based controls and earlier MPC implementations utilizing various forecasting models.
Keywords: Battery, hydrogen, neural network, predictive, renewable energy

I. Introduction

Isolated DC microgrids, especially those fueled by renewable sources like solar and wind, are essential for improving energy availability in distant and underserved areas. Yet, these energy sources are naturally sporadic, as their presence varies because of environmental factors. This intermittent nature presents substantial issues in maintaining a steady and dependable power supply, requiring strong energy management systems. Efficient management is crucial for ensuring power supply reliability and maximizing the performance and longevity of energy storage systems like batteries and hydrogen storage units (Garcia-Torres et al., 2021). Although renewable technology has advanced, the fluctuating nature of solar and wind energy can result in mismatches between energy supply and demand, which may lead to energy wastage or shortages. Without efficient predictive controls, surplus energy produced at peak times may surpass storage limits or be underutilized, while inadequate production during cloudy or low-wind periods might result in unfulfilled energy needs. Conventional energy management methods in microgrids typically rely on rule-based control systems that respond to changes instead of predicting them. Advanced technologies like Model Predictive Control (MPC) have been utilized to enhance energy output and consumption by employing predictive models to anticipate future needs and make proactive modifications. Model Predictive Control (MPC) uses forecasts of future conditions, limitations of the system, and operational goals to enhance control decisions within a certain timeframe (Fan et al., 2019). The success of Model Predictive Control (MPC) relies significantly on the precision of its forecasting models. Typical forecasting techniques used in Model Predictive Control (MPC) involve time-series analysis, numerical weather predictions, and simple machine learning models. These methods frequently face challenges due to the significant variability and non-linear characteristics of renewable energy data. Traditional approaches like as ARIMA and SVMs may struggle to capture intricate temporal patterns, particularly under changeable weather circumstances, resulting in subpar grid performance and heightened operational hazards (Liu et al., 2019). This research aims to investigate the combination of Recurrent Neural Networks (RNNs) with Model Predictive Control (MPC) for energy management in standalone DC microgrids with hybrid storage systems consisting of batteries and hydrogen storage units. RNNs are ideal for this task because they can handle sequences of data and effectively capture temporal relationships in extensive datasets. We plan to improve the accuracy of projecting energy demand and supply projections by utilizing the advanced deep learning features of RNNs (Prieto Cerón et al., 2022). This integration aims to enhance operational efficiency, increase power supply reliability, and prolong the lifespan of essential energy storage components to support sustainable and efficient microgrid operations.

II. Techno economic analysis

The self-sufficient DC microgrid in this work is designed to function autonomously without relying on a centralized power grid, mainly using renewable energy sources as depicted in figure 1. The system setup comprises the following primary components

Solar Panels: The electrical power output from photovoltaic (PV) systems can be expressed as

$$P_{PV}(t) = N_{parallel} * \eta_{converter} * mi\,n\left(N_{series} * P_{peak} * \frac{I(t)}{I_o}(1 - \frac{\beta}{100}(T(t) - T_0\right), P_m \quad (1)$$

Batteries: The state of charge equation can be reframed as follows

$$SOC(t) = SOC(t-\delta) + \delta\left(\frac{P_{charge}(t)}{\eta_{storage}} - P_{di\,scharge}(t) * \eta_{storage}\right) \quad (2)$$

Electrolysers and Hydrogen Tanks: This can be succinctly represented by

$$V_{H2}(t) = V_{H2}(t-\delta) + \delta * P_{H2}(t) \quad (3)$$

Fuel Cells: The power produced by fuel cells can be modeled as

$$P_{FC}(t) = \eta_{FC} * H_{usage}(t) \quad (4)$$

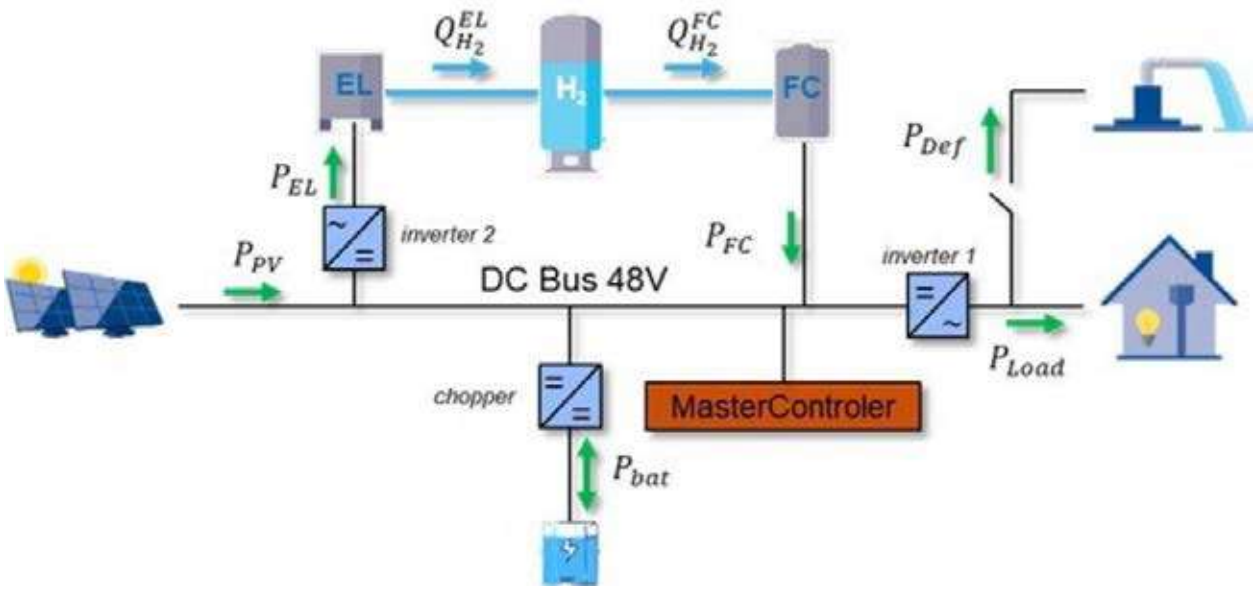


Fig.1: DC Microgrid

III. MPC Framework and RNN Architecture

Model Predictive Control (MPC) is used to optimize the microgrid's operation by forecasting future system states and adjusting current inputs to meet certain goals. At each time step t, the core function of MPC is to solve the optimization problem presented (Ma et al., 2020) .

$$\min_{u(t)} \sum_{k=0}^{H} L\big(x(t+k|t), u(t+k)\big) \quad (5)$$

The Recurrent Neural Network (RNN) used in this study is designed to forecast key variables such as future power demand, solar irradiance, and temperature. The RNN architecture includes:

Input Layer: Receives time-series data of past power usage, weather conditions (e.g., irradiance, temperature), and other relevant environmental or operational parameters.

Hidden Layers: Consist of LSTM (Long Short-Term Memory) units that can capture long-term dependencies in time-series data, crucial for accurate prediction in environments with high variability.

Output Layer: Provides predictions of future values for power production from PV panels and expected power consumption.

The RNN forecasts are used as predictions of future states and outputs in the MPC framework. This integration enables the MPC to predict future situations and proactively change control operations, thus improving the overall system performance. The RNN's predictive skills allow for more accurate and flexible control tactics, resulting in enhanced efficiency, cost reduction, and increased reliability of the microgrid.

IV. Results

Figure 1 shows the hydrogen volume stored in the tank throughout the year under three control strategies: Rule-Based Control (RBC), Model Predictive Control with Perfect Forecast (PF-MPC), and Recurrent Neural Network-based MPC (RNN-MPC). PF-MPC routinely demonstrates superior hydrogen storage capacity compared to RBC and RNN-MPC, indicating more efficient exploitation of hydrogen generation and storage capacities. RNN-MPC has superior performance than RBC but exhibits significantly reduced efficiency when compared to PF-MPC, emphasizing the efficacy of the forecasting model utilized in RNN-MPC. Figure 2 displays the state of charge (SOC) of batteries using a boxplot for each control approach. Comparing SOC in PF-MPC and RNN-MPC to RBC, the higher median and smaller interquartile range suggest a more stable and higher battery charge level. This indicates improved energy management and less frequent deep discharge, perhaps enhancing battery longevity. Figure 3 classifies energy losses into chemical, electrical, and availability losses for each control approach. MPC techniques (PF-MPC and RNN-MPC) show lower chemical and electrical losses compared to RBC, highlighting the advantages of predictive control in reducing inefficiencies in energy conversion and storage. Availability losses are marginally elevated for MPC techniques, possibly because of optimized charging cycles that target long-term energy availability rather than immediate loss mitigation. Figure 4 illustrates the monitoring of important components' aging, such as batteries, electrolysers, and fuel cells, by tracking their state of health (SOH) over the course of a year. The consistent State of Health (SOH) among all techniques indicates successful control of operational parameters affecting aging, such as cycling frequency and depth of discharge. The main objective function shows that the improved control techniques (PF-MPC and RNN-MPC) successfully distribute component consumption to prolong the operational lifespan of the system.

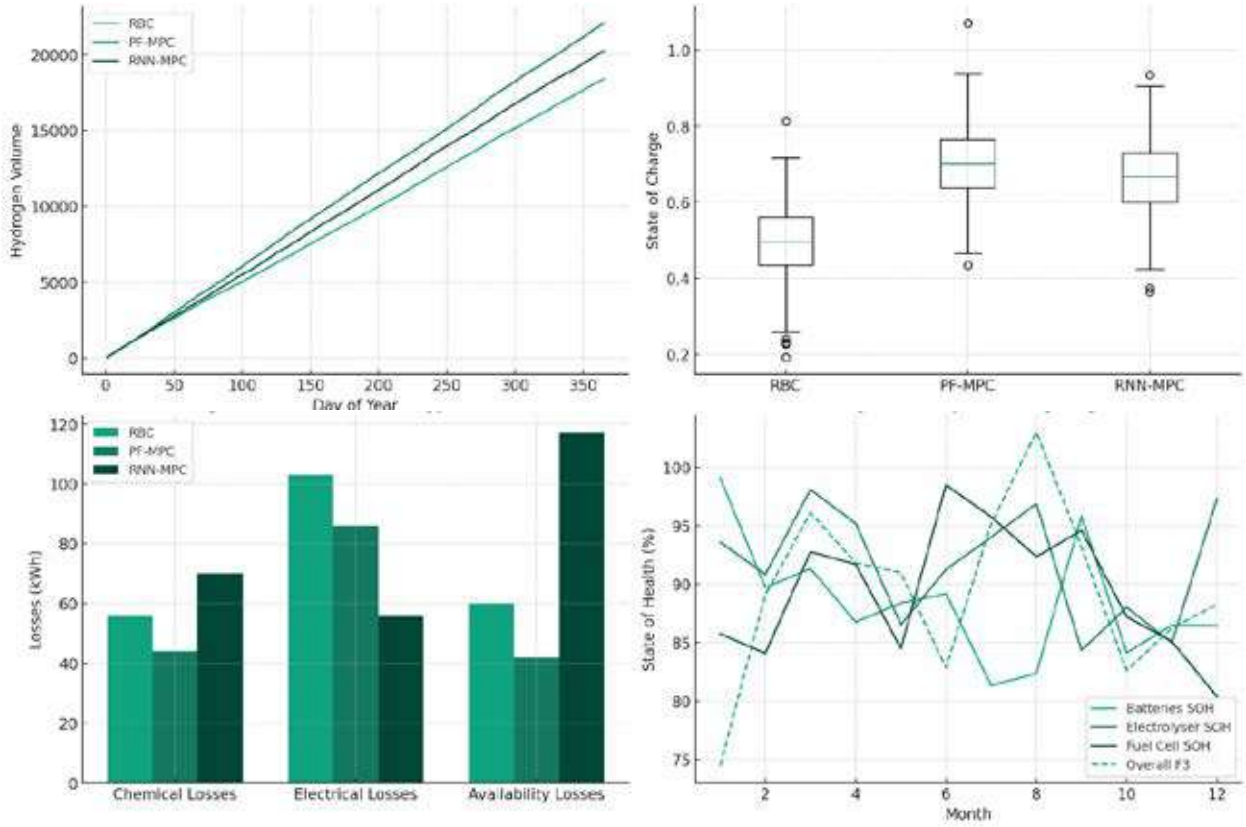


Fig.2: Graphs and results

V. Conclusions

Model Predictive Control (MPC), especially when combined with advanced forecasting models like RNN-MPC, greatly improves the efficiency and sustainability of microgrid operations. RNN-MPC may not always achieve the same level of performance as PF-MPC, but it offers a more practical solution for real-world scenarios when accurate predictions are not possible. The findings support the use of RNN-based MPC for successful and efficient microgrid control.

References

Fan, C., Wang, J., Gang, W., & Li, S. (2019). Assessment of deep recurrent neural network-based strategies for short-term building energy predictions. Applied Energy, 236, 700–710. https://doi.org/10.1016/J.APENERGY.2018.12.004

Garcia-Torres, F., Vazquez, S., Moreno-Garcia, I. M., Gil-De-castro, A., Roncero-Sanchez, P., & Moreno-Munoz, A. (2021). Microgrids Power Quality Enhancement Using Model Predictive Control. Electronics 2021, Vol. 10, Page 328, 10(3), 328. https://doi.org/10.3390/ELECTRONICS10030328

Liu, H., Chen, C., Lv, X., Wu, X., & Liu, M. (2019). Deterministic wind energy forecasting: A review of intelligent predictors and auxiliary methods. Energy Conversion and Management, 195, 328–345. https://doi.org/10.1016/J.ENCONMAN.2019.05.020

Ma, L., Zhang, X., Rao, Y., Fang, Z., Rao, Y., & Yang, J. (2020). A robust model predictive control for multi-microgrids frequency control. 2020 IEEE 4th Conference on Energy Internet and Energy System Integration: Connecting the Grids Towards a Low-Carbon High-Efficiency Energy System, EI2 2020, 1637–1641. https://doi.org/10.1109/EI250167.2020.9347210

Prieto Cerón, C. E., Normandia Lourenço, L. F., Solís-Chaves, J. S., & Sguarezi Filho, A. J. (2022). A Generalized Predictive Controller for a Wind Turbine Providing Frequency Support for a Microgrid. Energies, 15(7), 1–20. https://doi.org/10.3390/en15072562

Model-Free Predictive Control of a Hydrogen Energy Nano Grid System

[1,2*]Sulman Shahzad [3]Heybet Killic
[1]Department of Electrical Engineering, Islamia University of Bahawalpur, Bahawalpur 63100, Pakistan
[2] National Transmission & Despatch Company Limited, 60600, Multan, Pakistan
[3]Department of Electric Power and Energy Systems Dicle University 21280 Diyarbakır, Türkiye

* E-mail: salmanshahzad05@gmail.com

Abstract
Integrating hydrogen energy systems into micro grid designs shows potential for improving energy sustainability and efficiency. Managing the intricate and ever-changing relationships in these systems presents substantial control obstacles. This paper examines how Model-Free Predictive Control (MF-PC) can be used as a reliable method to enhance operational efficiency in hydrogen energy micro grids. We examine the conceptual framework, its implementation obstacles, and the possible effects on system performance and dependability.
Keywords: Hydrogen energy, fuel cell, nano grid, renewable energy, predictive control

I. Introduction

Hydrogen energy systems are becoming significant contributors to the renewable energy revolution as the global energy sector shifts towards sustainability. Hydrogen, with its high energy density and combustion that produces zero emissions, shows promise as a viable replacement to fossil fuels in different energy systems, such as microgrids (Shahzad et al., 2022). These small-scale grid systems, which can function apart from or in conjunction with conventional electricity grids, are gaining importance in remote and decentralized locations. Global energy consumption is expected to increase by almost 50% from 2018 to 2050, with renewable energy sources playing a significant role in fulfilling this rise in demand. Hydrogen is uniquely positioned among renewable energy sources because of its adaptability and compatibility with current energy infrastructure. Hydrogen is projected to make up to 18% of worldwide energy use by 2050, requiring a substantial increase in production to reach 70 million tons per year by then.

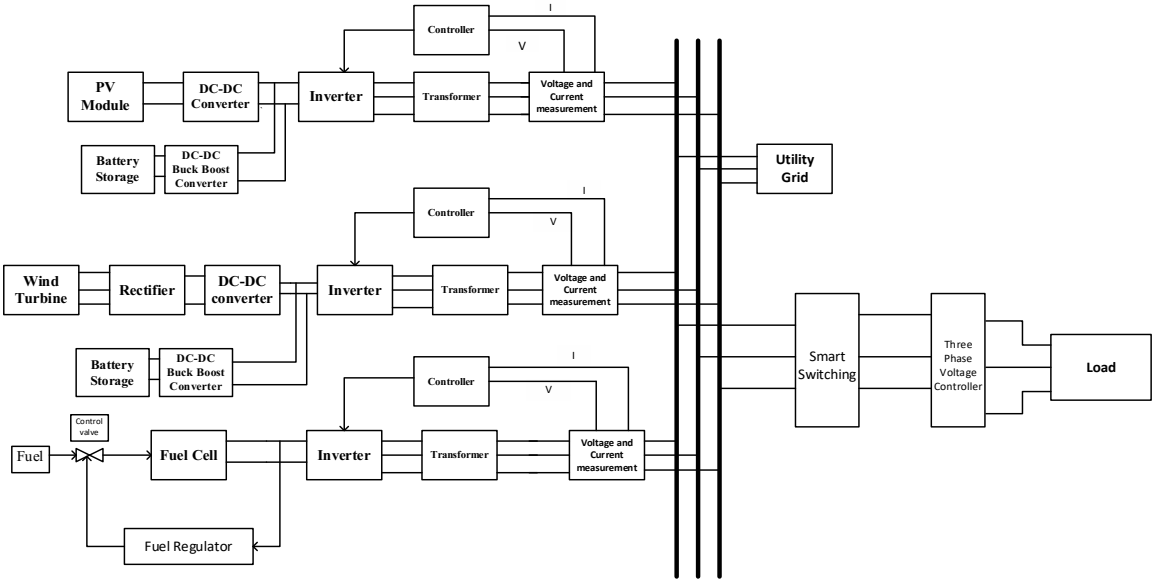


Fig.1: Nano grid system

Hydrogen energy can be generated from different renewable sources, mostly through electrolysis using solar or wind power. By 2020, around 4% of the world's hydrogen was generated from renewable energy sources. This percentage is projected to expand significantly due to the declining costs and growing use of renewable technology. The cost of solar PV modules has reduced by more than 80% since 2010, which has made solar-powered hydrogen manufacturing more practical (Azab, 2021). Nano grids are miniature versions of the conventional electricity grid that usually cater to specific locations like residential communities, tiny factories, or remote activities. Their purpose is to improve the local energy mix and strengthen energy security and reliability. By 2021, there are more than 2,000 nano grid installations globally, with an annual installation growth rate of over 10%. Incorporating hydrogen into nano grids requires producing and storing hydrogen, as well as converting it back to energy using fuel cells. The efficiency of these processes is crucial, with electrolyzers operating at roughly 60% efficiency and fuel cells reaching up to 60%, resulting in an overall round-trip efficiency of approximately 36% (A. Laib et al., 2020). Continual technological advancements are anticipated to greatly improve these efficiencies

II. Model-Free Predictive Control Strategy

Model-Free Predictive Control (MF-PC) is gaining recognition for its adaptability and resilience in managing intricate and ever-changing systems, such those seen in hydrogen energy micro grids. MF-PC removes the necessity for

intricate physical modeling of the system, which can be challenging and inaccurate because of the inherent fluctuation and uncertainty of renewable energy sources. Real-time system identification is a key element of MF-PC, utilizing methods like Recursive Least Squares (RLS) to estimate system characteristics dynamically. The RLS technique is ideal for systems with time-varying parameters or when initial parameter estimations are unavailable or imprecise. Research has demonstrated that RLS can dynamically estimate parameters efficiently for real-time use, decreasing model prediction error by up to 50% compared to fixed models. RLS algorithms can be tuned to run in microseconds on modern control technology, allowing for real-time applications in energy systems. MF-PC utilizes the specified model parameters to forecast upcoming system states and implement proactive control strategies. This method is very beneficial in energy systems with rapidly fluctuating demand and supply conditions. Integrating MF-PC in energy control systems can decrease system deviations by up to 30% during fluctuating load situations, improving system stability and reaction to disturbances (Kumar & Bae, 2022). Predictive models in MF-PC can attain forecast accuracies over 90% in stable situations, greatly improving decision-making. MF-PC's versatility stems from its capacity to integrate different operational objectives into a unified cost function that directs control action changes. The cost function may encompass elements like as energy efficiency, operational expenses, and system safety, customized to the unique requirements of the hydrogen nano grid. MF-PC can enhance energy efficiency by around 20% in comparison to conventional control methods by optimizing the cost function (O. Laib et al., 2019).

III. Results

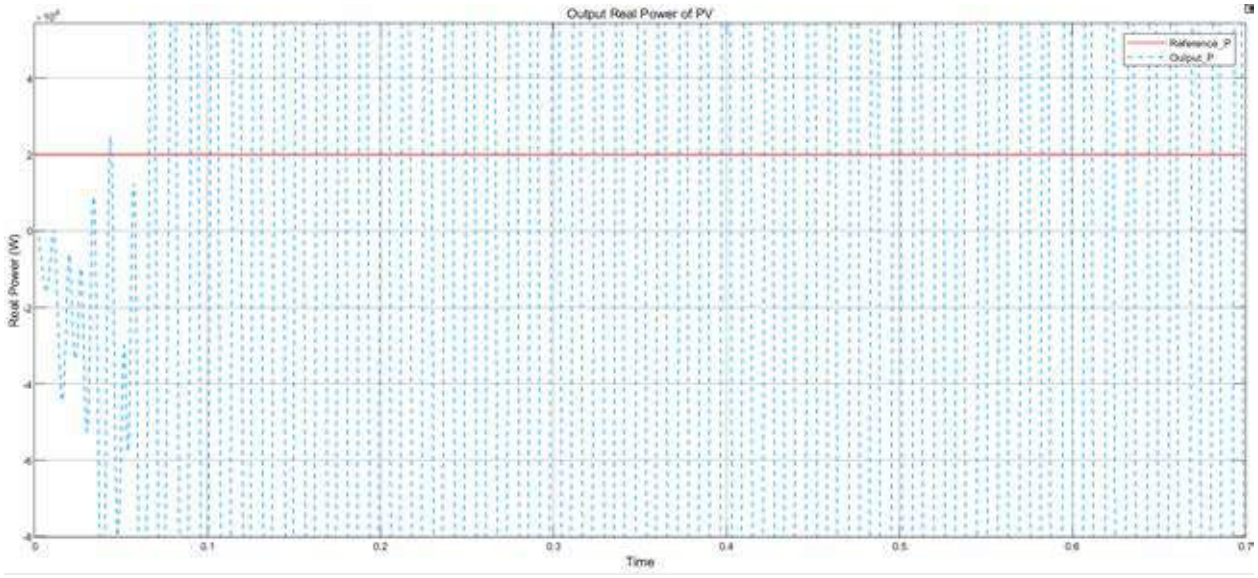


Fig.2: Active Power result using Conventional MPC

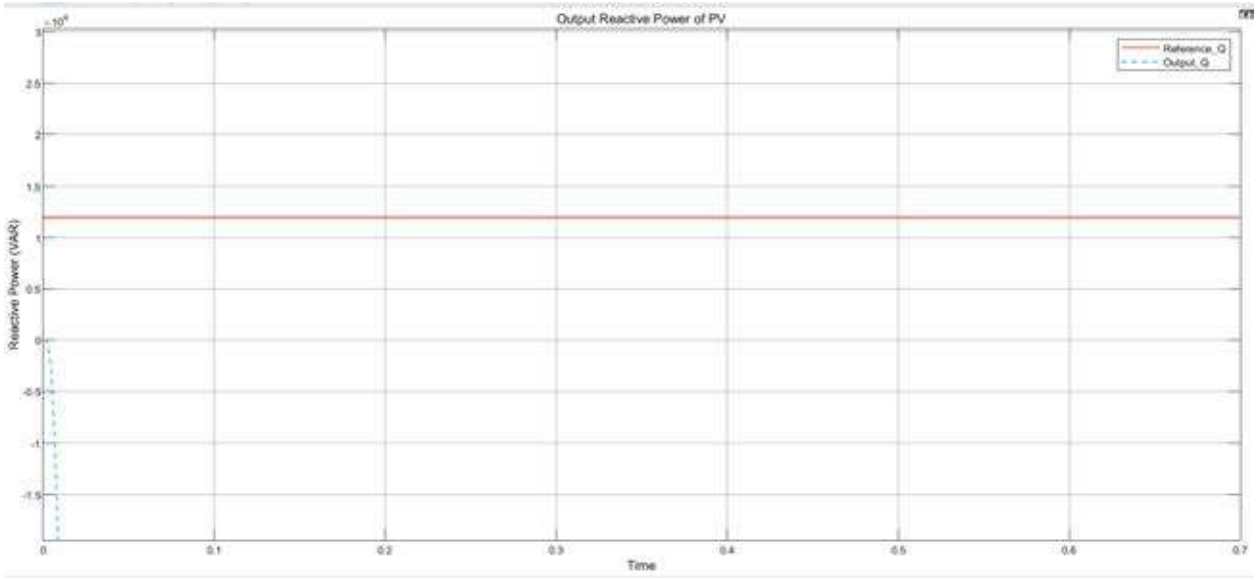


Fig.3: Reactive Power result using Conventional MPC

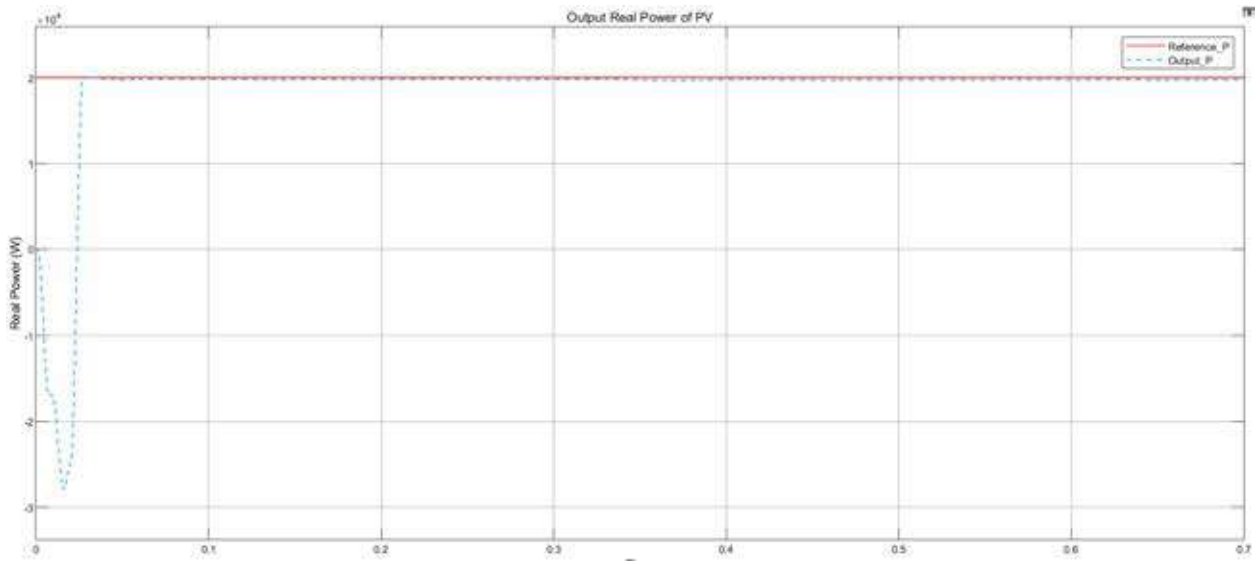


Fig.4: Active Power results using MF-MPC

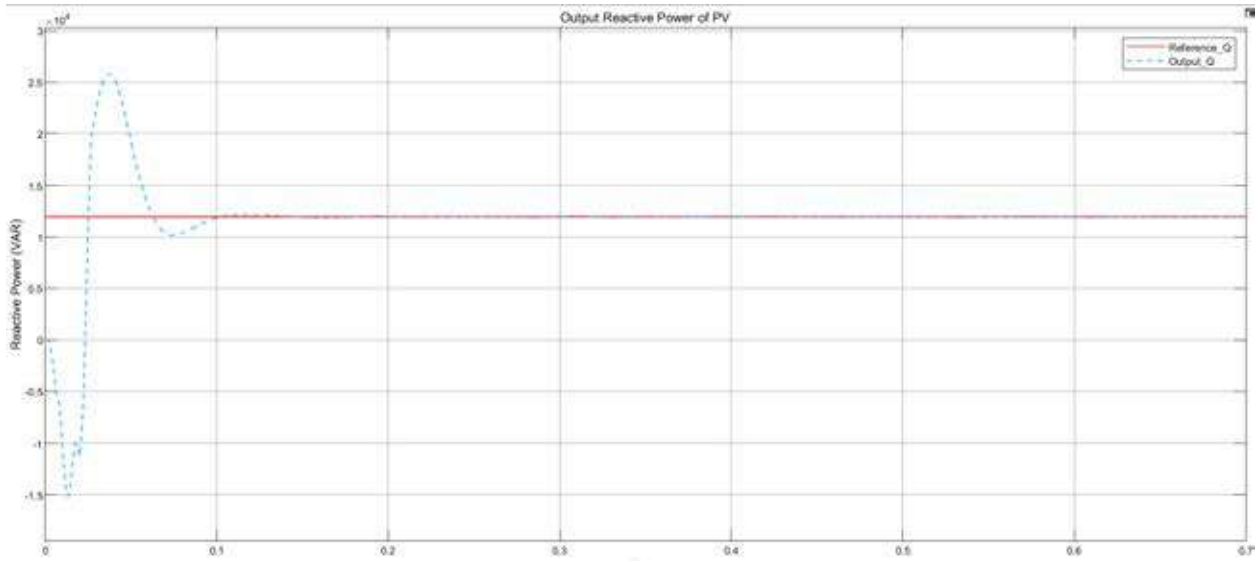


Fig.5: Reactive Power results using MF-MPC

IV. Conclusions

Model-Free Predictive Control provides a dynamic and economical method for handling the intricacies of hydrogen energy micro grids. Its ability to adjust instantly to changing system circumstances without requiring elaborate modeling makes it a vital asset in modern control systems, especially in the renewable energy sector where unpredictability is significant and operational efficiency is crucial.

References

Azab, M. (2021). A finite control set model predictive control scheme for single-phase grid-connected inverters. Renewable and Sustainable Energy Reviews, 135(July 2020), 110131. https://doi.org/10.1016/j.rser.2020.110131

Kumar, K., & Bae, S. (2022). Dynamic power management based on model predictive control for hybrid-energy-storage-based grid-connected microgrids. International Journal of Electrical Power & Energy Systems, 143, 108384. https://doi.org/10.1016/J.IJEPES.2022.108384

Laib, A., Krim, F., Talbi, B., & Sahli, A. (2020). A Predictive Control Scheme for Large-Scale Grid-Connected PV System Using High-Level NPC Inverter. Arabian Journal for Science and Engineering, 45(3), 1685–1701. https://doi.org/10.1007/S13369-019-04182-1/METRICS

Laib, O., Khadir, M. T., & Mihaylova, L. (2019). Toward efficient energy systems based on natural gas consumption prediction with LSTM Recurrent Neural Networks. Energy, 177, 530–542. https://doi.org/10.1016/J.ENERGY.2019.04.075

Shahzad, S., Abbasi, M. A., Chaudhry, M. A., & Hussain, M. M. (2022). Model Predictive Control Strategies in Microgrids: A Concise Revisit. IEEE Access. https://doi.org/10.1109/ACCESS.2022.3223298

Green Hydrogen: Innovations, Challenges, and Opportunities in a Low-Carbon World

[1,2*] Sulman Shahzad, [3]Heybet Killic
[1]Department of Electrical Engineering, Islamia University of Bahawalpur, Bahawalpur 63100, Pakistan
[2] National Transmission & Despatch Company Limited, 60600, Multan, Pakistan
[3]Department of Electric Power and Energy Systems Dicle University 21280 Diyarbakır, Türkiye

* E-mail: salmanshahzad05@gmail.com

Abstract
This research focuses on the technological, economic, and infrastructural obstacles involved in deploying green hydrogen solutions on a significant scale. The discussion includes breakthroughs in electrolyzer technology, cost reductions from economies of scale, and helpful government legislation. This article offers a thorough examination of the present condition, obstacles, and future potential of green hydrogen, providing useful perspectives on its significance in advancing worldwide sustainability and energy security objectives.
Keywords: Renewable energy, hydrogen, sustainability, electrolysis, zero carbon, energy storage

I. Introduction

The world population is expected to increase to around 9.7 billion people by 2050. Thus, there will be a corresponding rise in energy demand. The leading causes of this increase in energy demand, particularly in emerging nations, are the fast-paced urbanization and industrialization processes. Unfortunately, over 84% of the energy used worldwide is derived from fossil fuels, which are the mainstay of the current energy systems. Significant environmental problems, chief among them being climate change, have resulted from this dependence. The leading cause of carbon dioxide (CO2) emissions, a potent greenhouse gas that contributes to global warming, is the combustion of fossil fuels. The Intergovernmental Panel on Climate Change (IPCC) has frequently brought attention to the effects of these emissions, linking them to rising sea levels, extreme weather, and the extinction of wildlife. Additionally, the burning of fossil fuels produces air pollution, which is a significant health risk that causes respiratory illnesses and early death.

There is growing agreement on the necessity of switching to a low-carbon, more sustainable energy system considering these difficulties. Along with being environmental, this transformation is also economic, as nations look to guarantee their energy futures in the face of depleting fossil fuel supplies and unstable oil markets. Renewable energy is leading the charge in finding answers to these problems. Power can be produced without significantly harming the environment or depleting natural resources by using sources including biomass, solar, wind, hydro, and hydropower. Expanding governmental support, falling costs, and technology improvements are driving the growing adoption of renewable energy. The green hydrogen cycle is shown in Figure 1.

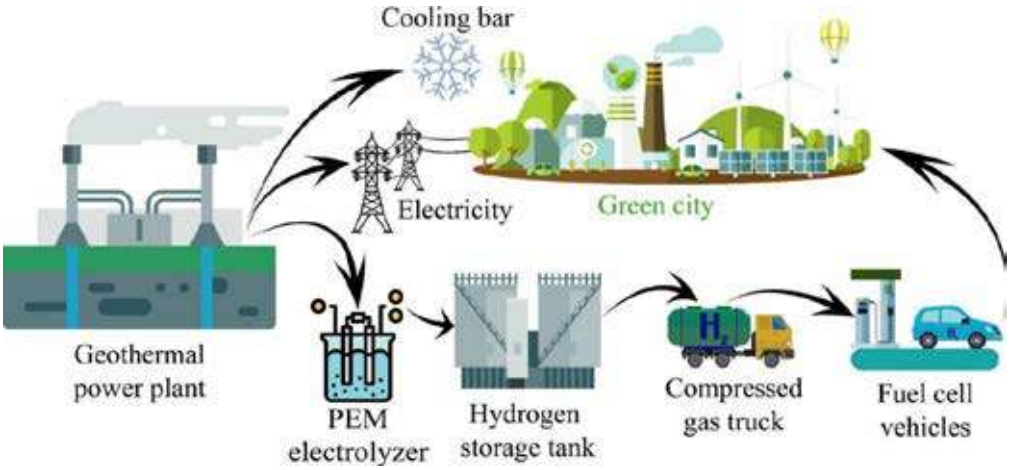


Fig. 1: Hydrogen Cycle

II. Challenges and Strategies

Establishing the infrastructure for a hydrogen economy requires significant upfront investments in production facilities, pipelines, fueling stations, and upgrading current systems. These investments' high capital requirements and extended payback period provide substantial obstacles, particularly during the initial phases of hydrogen economy growth. Hydrogen production facilities, particularly those intended for generating green hydrogen by electrolysis, demand substantial initial capital. Establishing an electrolysis plant typically costs between $500 and $1,400 per kilowatt capacity (Khani et al., 2020). Existing natural gas pipes are unsuitable for hydrogen transportation because of hydrogen embrittlement, a phenomenon in which hydrogen atoms penetrate the metal, leading to fracture. Constructing new pipelines explicitly designed for hydrogen or upgrading current pipelines with hydrogen-resistant materials is expensive. The cost of retrofitting a pipeline for hydrogen compatibility can range from $100,000 to $1 million per mile, depending on the pipeline size and the number of modifications needed (Kurtz

et al., 2018). Building hydrogen filling stations is considerably more costly than building traditional petrol stations, usually ranging from $1 million to $4 million per station. This covers expenses for compressors, storage tanks, and dispensers designed to manage high-pressure hydrogen. Large hydrogen storage systems, whether they use compressed, liquid, or solid-state hydrogen, need specialized containment systems to handle the high pressures and low temperatures necessary for practical storage. New materials resistant to hydrogen embrittlement could minimize pipeline retrofitting and lower maintenance expenses.

Creating hydrogen production and refueling facilities in modular and scalable forms can assist in controlling initial expenses by enabling infrastructure to expand by demand. Integrating hydrogen infrastructure with existing natural gas pipelines and energy systems can minimize early construction expenditures. For example, mixing hydrogen with natural gas up to approximately 15-20% can serve as a temporary solution that uses current infrastructure with little adjustments—promoting public-private partnerships to distribute the financial risk linked to infrastructure development (Wu et al., 2020). Governments can facilitate private investment by guarantees, subsidies, or by offering land and regulatory permissions. Governments can provide tax incentives, grants, or low-interest loans to support the establishment of hydrogen infrastructure. These incentives might mitigate the upfront expenses and expedite the implementation of essential amenities. Implementing definitive, enduring policies that promote the advancement of the hydrogen economy can offer the assurance investors require. Policies may involve long-term off-take agreements, set hydrogen prices, or required hydrogen quotas in specific sectors. Initiating pilot projects in places with the greatest need for hydrogen, such as industrial hubs or metropolitan areas with stringent emissions restrictions, might support the justification for more significant expenditures. Increasing infrastructure in response to growing demand can help mitigate financial risks. Initially targeting industries like heavy transport and industrial activities that stand to gain the most from hydrogen, such as trucks, buses, steel manufacture, and chemical processing, it can establish a solid demand base that can justify the initial infrastructure expenses.

It is crucial to transition hydrogen technologies from pilot projects to industrial scales for the hydrogen economy to develop and fulfill global energy needs. This problem involves expanding manufacturing methods, storage systems, and distribution networks, necessitating significant technological progress and financial investment. Electrolysis is not commonly performed on a large industrial scale currently. Pilot projects typically utilize electrolyzers with capacities that vary from a few kilowatts to a few megawatts. Industry predictions indicate that it is essential to increase the capacity of facilities to gigawatt levels to fulfill upcoming hydrogen needs. The European Union aims to deploy at least 40 gigawatts of renewable hydrogen electrolyzers by 2030 (Pan et al., 2020). SMR is scalable and currently the primary source of hydrogen; however, it depends on fossil fuels and carbon capture technology for sustainability.

Expanding green hydrogen production by steam methane reforming (SMR) depends on the extensive implementation and enhancement of carbon capture and storage (CCS) technologies. Hydrogen storage tanks are frequently utilized but are restricted in size by safety and material limitations. Liquid hydrogen storage is more compact but necessitates very low temperatures (-253°C), which makes it energy-demanding and challenging to expand (Xu et al., 2020). Metal hydrides and organic hydride technologies have the potential to provide safer and higher-density hydrogen storage. Scaling these technologies is difficult because of the expensive materials and the requirement for additional research on the kinetics and thermodynamics of hydrogen release and absorption. There are only a limited number of specialized hydrogen pipelines worldwide, mainly in areas with extensive industrial activity. Expanding this network to provide broader hydrogen distribution requires substantial investment.

III. Conclusions

Advancements in electrolysis technology and the use of renewable energy sources are driving the development of green hydrogen generation, which presents a viable method to reduce the impacts of climate change, improve energy security, and promote economic growth. The advancement of this technology encounters considerable obstacles such as the necessity for substantial capital investment in infrastructure, the demand for technological enhancements in efficiency and cost, and the establishment of supportive legislative frameworks. The full realization of green hydrogen's potential requires coordinated efforts from governments, businesses, and academia to tackle difficulties with new solutions, supportive policies, and collaborative projects.

References

Khani, H., El-Taweel, N. A., & Farag, H. E. Z. (2020). Supervisory Scheduling of Storage-Based Hydrogen Fueling Stations for Transportation Sector and Distributed Operating Reserve in Electricity Markets. IEEE Transactions on Industrial Informatics, 16(3), 1529–1538. https://doi.org/10.1109/TII.2019.2926779

Kurtz, J., Peters, M., Muratori, M., & Gearhart, C. (2018). Renewable Hydrogen-Economically Viable: Integration into the U.S. Transportation Sector. IEEE Electrification Magazine, 6(1), 8–18. https://doi.org/10.1109/MELE.2017.2784631

Pan, G., Gu, W., Lu, Y., Qiu, H., Lu, S., & Yao, S. (2020). Optimal Planning for Electricity-Hydrogen Integrated Energy System Considering Power to Hydrogen and Heat and Seasonal Storage. IEEE Transactions on Sustainable Energy, 11(4), 2662–2676. https://doi.org/10.1109/TSTE.2020.2970078

Wu, X., Li, H., Wang, X., & Zhao, W. (2020). Cooperative Operation for Wind Turbines and Hydrogen Fueling Stations With On-Site Hydrogen Production. IEEE Transactions on Sustainable Energy, 11(4), 2775–2789. https://doi.org/10.1109/TSTE.2020.2975609

Xu, D., Zhou, B., Wu, Q., Chung, C. Y., Li, C., Huang, S., & Chen, S. (2020). Integrated Modelling and Enhanced Utilization of Power-to-Ammonia for High Renewable Penetrated Multi-Energy Systems. IEEE Transactions on Power Systems, 35(6), 4769–4780. https://doi.org/10.1109/TPWRS.2020.2989533

Investigation of the Photocatalytic Activity of Pd(0) NPs-Decorated on Benzene Ring Doped Nanosheet g-C_3N4 (Pd@BD-g-C_3N_4) in the Hydrolysis Reaction of Ammonia Borane

[1]Halil İbrahim Önal, [2]*Feyyaz Durap
[1]Batman University, Energy Coordination Office, 72000-Batman, Türkiye
[2]Dicle University, Faculty of Science, Department of Chemistry 21280-Diyarbakır, Türkiye

* E-mail: fdurap@dicle.edu.tr

Abstract

The hydrogen economy, which is a sustainable and clean energy carrier that produces only water as a product when used in fuel cells, has high energy density, is non-toxic and produces zero emissions, is based on four concepts based on the production, storage, distribution and use of hydrogen[1]. Obtaining H_2 by photo/catalytic methods in the presence of a suitable catalyst from the hydrolysis of ammonia borane, which is widely used in solid hydrogen storage, is among the most studied topics[2]. It has been determined that systems made of nano-sized materials provide much better catalytic performances with their high surface areas and surface effective atomic numbers, and metal/metal oxide nanoclusters are used either in colloidal form or as decorated solid supports. In this study, Pd(0) nanoclusters at different weight ratios (1-3%) were decorated on the surface of semiconductor benzene-doped carbon nitride (BD-g-C_3N_4). The photocatalytic activity of the obtained nanocatalyst was examined in the hydrolysis of ammonia borane. It was determined that the Pd@BD-g-C_3N_4 nanocatalyst showed higher photocatalytic activity than BD-g-C_3N_4. The nanocatalyst with the highest photocatalytic activity was characterized by advanced analytical methods. Hydrolysis of hydrogen-rich AB (Eq.(1)) appears to be the most suitable route for portable hydrogen storage applications. Under ambient conditions, in the presence of a suitable catalyst, it can release 3 moles of H_2 for every mole of AB. In a typical experiment, 30.9 mg (1mmol) H_3NBH_3 was dissolved in 10 mL water, (corresponding to a maximum amount of 3 mmol=67 mL H_2 at 25.0 ± 0.1 °C)[3].

$$H_3N{\cdot}BH_3\ (aq) + 2H_2O\ (l) \xrightarrow{\text{Catalyst}} NH_4^+(aq) + BO_2^-(aq) + 3H_2(g)\ (1)$$

Method: BD-g-C_3N_4 was prepared from low-cost urea and m-trihydroxybenzene (phloroglucinol) by thermal polymerization method [4] and Pd@BD-g-C_3N_4 photocatalyst by wet impregnation-chemical reduction method[5].

Caracterization: The structure, composition and morphology of the nanocatalyst with the highest catalytic activity were characterized by FT-IR, UV-DR, XRD, SEM, TEM and XPS analyses. According to the analysis results obtained; i) the benzene ring was doped without damaging the crystal structure, ii) Pd@BD-g-C_3N_4 showed improved absorption in the visible range compared to BD-g-C_3N_4 due to the synergistic effect between Pd and BD-g-C_3N_4 and the surface plasmon resonance (SPR) effect of metallic nanoparticles. iii) Pd NPs were well dispersed on BD-g-C_3N_4, the particle size of Pd nanoparticles on the BD-g-C_3N_4 surface was in the range of 2.4-5.6 nm and the average diameter was determined as 3.9 nm.

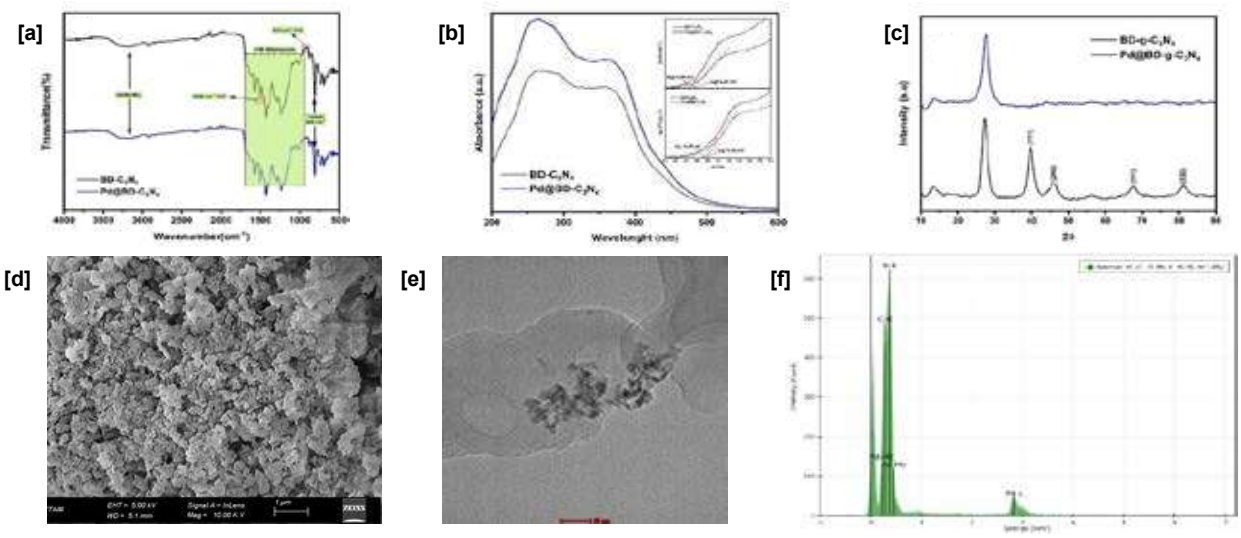


Fig.1: a) FT-IR b) UV-DR c) XRD d) SEM e) HR-TEM f) TEM-EDX analyzes of 2%Pd@BD-g-C_3N_4

Photocatalytic activity: it was determined that 2%Pd@BD-g-C_3N_4 nanocatalyst support material showed higher photocatalytic activity than BD-g-C_3N_4. The BD-g-C_3N_4 supported Palladium (0) nanoclusters were found to be highly active with a TOF of 1333 mol H_2/mol Pd.hour in the hydrolysis of ammonia-borane at 25±0.1 °C. Moreover the 2%Pd@BD-g-C_3N_4 nanocatalyst retained 66% of their initial catalytic activity in the hydrolysis of ammonia-borane in the fifth run.

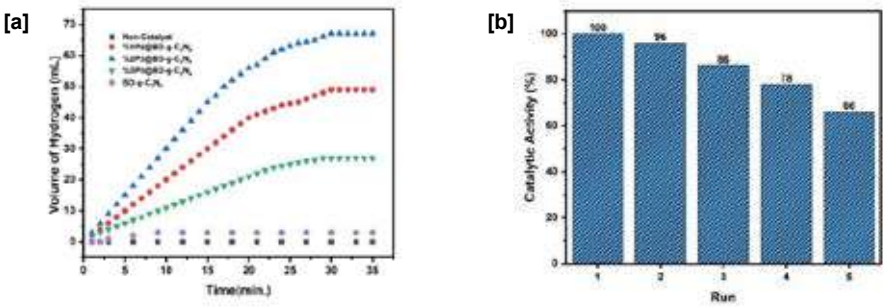


Figure 2. a) Graph of the volume of hydrogen produced from the hydrolysis of ammonia-borane by different nanocatalysts b) Reusability of %2Pd@BD- g-C_3N_4 in hydrolysis of ammonia-borane (in each run $H_3N.BH_3$;1 mmol) at 25.0 ± 0.1 °C.

Financial support and necessary facilities for this study were provided by Batman University Research Fund [BTÜBAP-2023-FED-10] and Dicle University.

Keywords: Hydrogen Energy, Photocatalysis, Palladium, BD-g-C_3N_4, Ammonia Borane

References

Rusman NAA, Dahari M. A review on the current progress of metal hydrides material for solid-state hydrogen storage applications. Int J Hydrogen Energy 2016, 41,12108-26.

Rand DAJ. A journey on the electrochemical road to sustainability. J Solid State Electrochem 2011, 15,1579-622

Durap, F., Zahmakıran, M., Özkar, S., Water soluble laurate-stabilized ruthenium (0) nanoclusters catalyst for hydrogen generation from the hydrolysis of ammonia-borane: High activity and long lifetime, international journal of hydrogen energy, 2009, 34(17), 7223-7230.

Yu, Y., Yan, W., Gao, W., Li, P., Wang, X., Wu, S., Song, W., Ding, K., “Aromatic ring substituted g-C_3N_4 for enhanced photocatalytic hydrogen evolution”, Journal of Materials Chemistry A, 2017, 5, 17199.

Önal, H. İ., Durap, F., Aydemir, M., Zahmakiran, M. (2024). Highly active Pd nanoparticles decorated on benzene-ring doped g-C_3N_4 as catalyst in methylene Blue degradation and Cr (VI) ions reduction. Applied Organometallic Chemistry, 38(5), e7442.

Power Flow Control for Renewable Energy Hydrogen based Dual Active Bridge used DC Microgrids

[1*]Heybet Kilic, [1]M. Emin Asker
[1]Dicle University, Department of Electric Power and Energy System, Diyarbakır, 21280, Türkiye

[1*]E-mail:heybet.kilic@dicle.edu.tr

Abstract

This study addresses the advantages and applications of using dual active bridge (DAB) technology to control power flow in DC microgrids using hydrogen from renewable energy sources. The dual active bridge consists of a bidirectional DC/AC H-bridge converter fed by a high-frequency converter, followed by a high-frequency (HF) transformer. It is thought that this technology will play an important role in applications such as charging electric vehicles. The dual active bridge system controls the bidirectional power flow between the grid and the battery by adjusting the phase shift between the gate control signals of the two bridges. This topology is recommended for applications where automatic bidirectional power flow, power density, reliability, efficiency and cost are key design considerations. In this study, a suitable DAB converter was designed for use in DC microgrids, and a day-ahead flow control was implemented using a MATLAB Simulink model based on a mathematical model. The results obtained using model predictive control are discussed.

Keywords: Dual Active Bridge, Renewable Energy, Hydrogen, Power Flow Control

I.Introduction

DC microgrids offer several advantages over their AC counterparts, including higher efficiency and lower costs [1]. Additionally, DC microgrids eliminate the need for complex reactive power regulation and frequency synchronization, leading to a simpler control system [2], [3]. These benefits make DC microgrids an attractive solution for a variety of applications, particularly in distributed energy systems and renewable energy integration.

Power flow control is crucial for efficient energy exchange and storage in renewable energy hydrogen-based double active bridge (DAB) DC microgrids. Research proposes innovative strategies like the dual-terminal direct power control scheme (DVF-DPC) with single-phase phase-shift control for DAB converters, enabling fast and precise power regulation under various operating conditions. Additionally, bidirectional DAB converters are designed to transfer power between energy storage systems and DC buses, facilitating power delivery to electrolyzers in green hydrogen production systems [4] [5]. To optimize power management and mitigate existing fluctuations, model predictive control (MPC) methods are proposed to coordinate electrolyzers and fuel cells in hydrogen-based DC microgrids and ensure a stable power supply from renewable sources [6]. These advancements highlight the potential for enhanced power flow control and system stability in renewable energy hydrogen-based DC microgrids.

The proposed control strategy effectively regulates the output voltage of a DC-DC dual active bridge converter in DC microgrid applications while ensuring the mean current in the high frequency transformer remains at zero, as demonstrated through simulations and experimental results. The controller design based on classical techniques proves to be successful in adapting to various voltage levels within the DC microgrid, highlighting the practical applicability and performance of the system in real-world scenarios[7].

Introduces the dual active bridge (DAB) converter as a crucial topology for isolated dc-dc converters in renewable energy systems, emphasizing its ground isolation benefits. It highlights the overview of control strategies and parameter design for the DAB converter, focusing on efficient power handling and voltage regulation for renewable energy sources like PV. The dual active bridge converter (DAB) is a significant topology for isolated dc-dc converters, providing essential features for renewable energy applications by enhancing safety and protection through ground isolation. Various control methods and parameter designs for the DAB power converter have been discussed, focusing on renewable energy sources like PV to ensure efficient power handling and voltage regulation[8].

In this study, a suitable DAB converter was designed for use in DC microgrids, and a day-ahead flow control was implemented using a MATLAB Simulink model based on a mathematical model.

II.Dual Active Bridge structure

The Dual Active Bridge (DAB) is a type of DC-DC converter known for its high efficiency and bi-directional power flow. This makes it ideal for applications like battery storage systems, electric vehicle charging, and renewable energy integration where power needs to flow in both directions. DAB achieves its efficiency through soft-switching techniques, resulting in a compact design due to its ability to operate at high frequencies. An additional benefit is galvanic isolation, which improves safety and reduces noise. These advantages make DAB a popular choice in various power electronics applications. Types of Hybrid Energy Storage Systems are given in Figure 1. The current change graph with the DAB converter switching signals used is given in Figure 2.

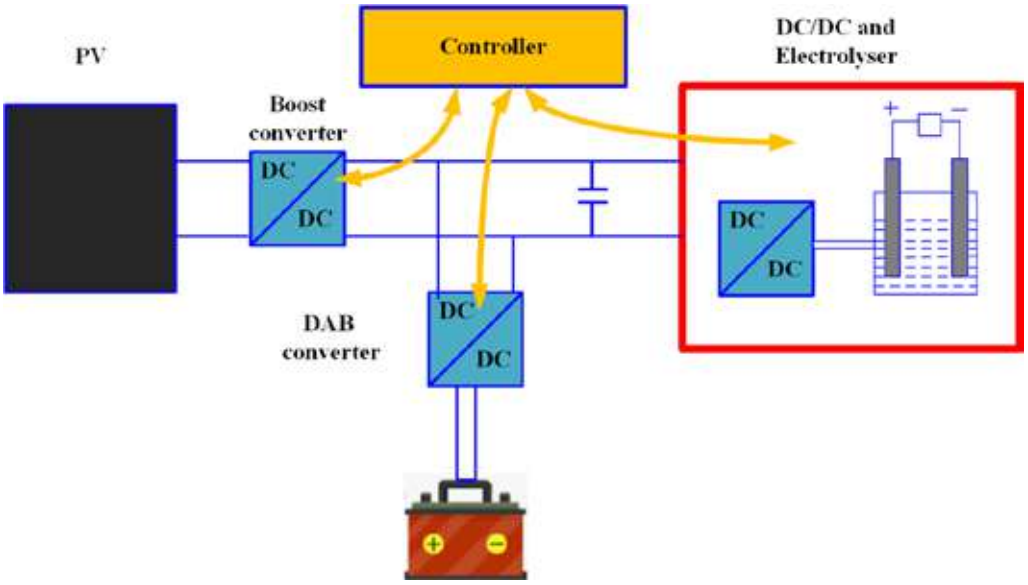


Fig.1: Types of Hybrid Energy Storage Systems

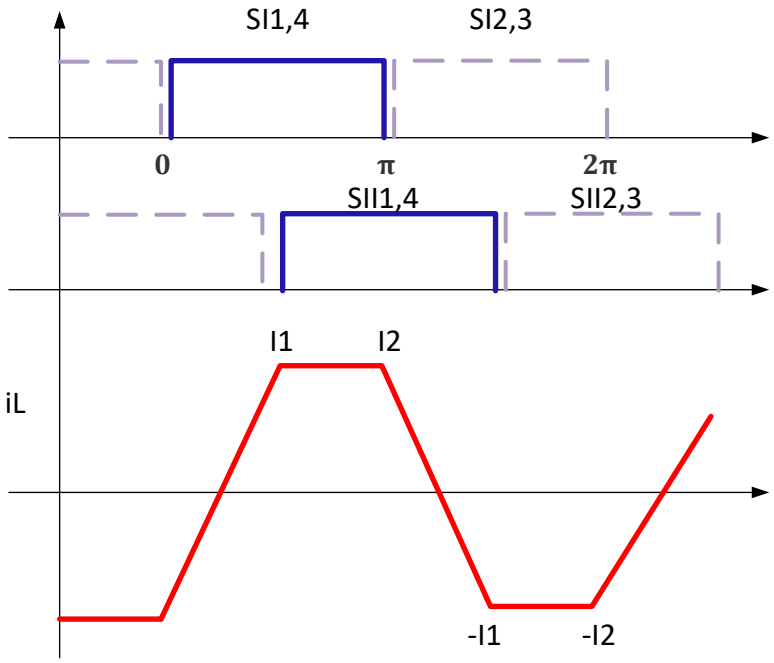


Fig.2: The DAB converter's switching signals and current waveform

III.Conclusion

This study explored the advantages and applications of using dual active bridge (DAB) technology to control power flow in DC microgrids powered by hydrogen from renewable energy sources. The designed DAB converter comprises a bidirectional DC/AC H-bridge converter fed by a high-frequency converter, followed by a high-frequency (HF) transformer. This technology is anticipated to play a crucial role in applications such as electric vehicle charging. The DAB system manages bidirectional power flow between the grid and battery by adjusting the phase shift between the gate control signals of the two bridges. This topology is recommended for applications prioritizing automatic bidirectional power flow, power density, reliability, efficiency, and cost.

A suitable DAB converter was designed for DC microgrids, and day-ahead flow control was implemented using a MATLAB Simulink model based on a mathematical model. The results obtained using model predictive control demonstrate the effectiveness of DAB technology in ensuring efficient power flow management in DC microgrids, highlighting its potential for future applications.

References

A. Radwan and Y. A.-R. I. Mohamed, “Assessment and mitigation of interaction dynamics in hybrid ac/dc distribution generation systems,” IEEE Transactions on Smart Grid, vol. 3, no. 3, pp. 1382–1393, 2012.

Z. Fan, B. Fan, and W. Liu, “Distributed control of dc microgrids for optimal coordination of conventional and renewable generators,” IEEE Transactions on Smart Grid, vol. 12, no. 6, pp. 4607–4615, 2021.

H. Tian and Y. Li, “Virtual resistor based second-order ripple sharing control for distributed bidirectional dc–dc converters in hybrid ac–dc microgrid,” IEEE Transactions on Power Electronics, vol. 36, no. 2, pp. 2258–2269, 2021.

Xiao, Zhongxiu, et al. "Dual-terminal voltage feedforward based direct power control scheme and stability analysis of dual active bridge converter in DC microgrid systems." IEEE Transactions on Power Electronics 38.4 (2022): 4475-4492.

Ganjavi, Amir, et al. "Design and Implementation of an SiC-Based 48 V-380 V Dual Active Bridge DC-DC Converter for Batteries Employed in Green Hydrogen Microgrids." *2022 IEEE 7th Southern Power Electronics Conference (SPEC)*. IEEE, 2022.

Zhang, Mengfan, and Qianwen Xu. "An MPC based power management method for renewable energy hydrogen based DC microgrids." 2023 IEEE applied power electronics conference and exposition (APEC). IEEE, 2023.

Esteban, Francisco Daniel, Federico Martín Serra, and Cristian Hernan De Angelo. "Control of a DC-DC dual active bridge converter in DC microgrids applications." *IEEE Latin America Transactions* 19.8 (2021): 1261-1269.

Panda, Anup Kumar, Nishit Tiwary, and N. Venkataramana Naik. "Overview of Control Strategies and Design of Isolated Bidirectional Dual Active Bridge Converter for Renewable Energy Systems." DC—DC Converters for Future Renewable Energy Systems (2022): 253-273.

Utilizing Battery-Super Capacitor Energy Storage for Hybrid Photovoltaic, Wind, and Fuel Cell Systems

[1]M. Emin Asker
[1]Dicle University, Department of Electric Power and Energy System, Diyarbakır, 21280, Türkiye.

[1] E-mail:measker@dicle.edu.tr

Abstract

Hybrid renewable energy systems (HRES) combine multiple energy sources to optimize energy production, enhance reliability, and ensure a stable energy supply. The integration of photovoltaic (PV), wind, and fuel cell systems is a promising approach due to their complementary characteristics. However, the intermittency and variability of these energy sources present significant challenges. At this point, energy storage systems (ESS) play a crucial role. Among various ESS technologies, the combination of batteries and supercapacitors offers an attractive solution due to their synergistic benefits. In this study, to examine the effects of hybrid energy storage on enhancing the performance of renewable energy systems, a hybrid energy system with a capacity of 60% PV, 25% wind, and 15% fuel cell was modeled and integrated with a system consisting of batteries and supercapacitors. Results regarding the impact of the hybrid storage system on PV and wind energy fluctuations were obtained and discussed.

Keywords: Hybrid energy storage systems, Fuel cell, photovoltaic, wind energy

I.Introduction

Renewable energy sources such as photovoltaic (PV), wind, and fuel cell systems have become increasingly popular due to their sustainability and ability to reduce carbon emissions. However, the intermittent nature of these sources poses challenges in providing a reliable power supply. Hybrid energy storage systems aim to address this issue by combining multiple storage technologies. This research explores the advantages of hybrid energy storage in enhancing the performance of renewable energy systems.

Hybrid systems that integrate different energy storage technologies such as batteries, supercapacitors, and flywheels can better manage the fluctuations in renewable energy production and demand. Understanding the potential of hybrid energy storage is crucial for optimizing the integration of renewable energy sources into the power grid, ultimately leading to a more sustainable and efficient energy future.

The transition to renewable energy sources is driven by the need to reduce carbon emissions and increase energy sustainability. While the integration of solar and wind energy systems provides clean power, their intermittent nature requires complementary systems for continuous energy production (Rahaf S. Ghanem et al.). These systems are supported by the integration of hybrid renewable sources and distributed generators into smart grid systems (Nelly Safitri et al., pp. 3202-3209). This comprehensive approach highlights the interaction between renewable energy and enabling technologies in shaping the future energy landscape.

Hybrid energy storage systems (HESS) optimize the performance and economics of renewable energy systems by integrating various energy storage technologies. Research shows that using batteries as primary storage and supercapacitors as supportive storage can improve power quality (I. Sulistiyowati et al.). Innovative optimization techniques and various storage configurations reveal the potential of hybrid energy storage systems in enhancing sustainability, reliability, and cost-effectiveness.

HESS store electricity generated from renewable sources. These systems typically consist of technologies such as batteries, supercapacitors, flywheels, and thermal storage units. By integrating multiple storage technologies, hybrid systems can optimize energy storage capacity and overall system performance while addressing the limitations of individual storage technologies. Hybrid energy storage systems play a critical role in improving the stability and efficiency of renewable energy systems (Alfred Rufer).

In this study, a hybrid energy system with 60% PV, 25% wind, and 15% fuel cell capacity was modeled and integrated with a system consisting of batteries and supercapacitors to examine the effects of hybrid energy storage on enhancing the performance of renewable energy systems. The impact of the hybrid storage system on PV and wind energy fluctuations was analyzed, and the results were discussed.

II.Hybrid Energy Storage Systems

HESS are configured using batteries and supercapacitors (SC) along with DC/DC converters and are classified as shown below (Figure 1). Active HESS is a structure obtained by using both a battery and a supercapacitor together with a DC/DC convert. Active HESS is designed to enhance the efficiency and flexibility of energy storage systems. This structure leverages the distinct characteristics of batteries and supercapacitors to provide advantages in energy storage and power management.

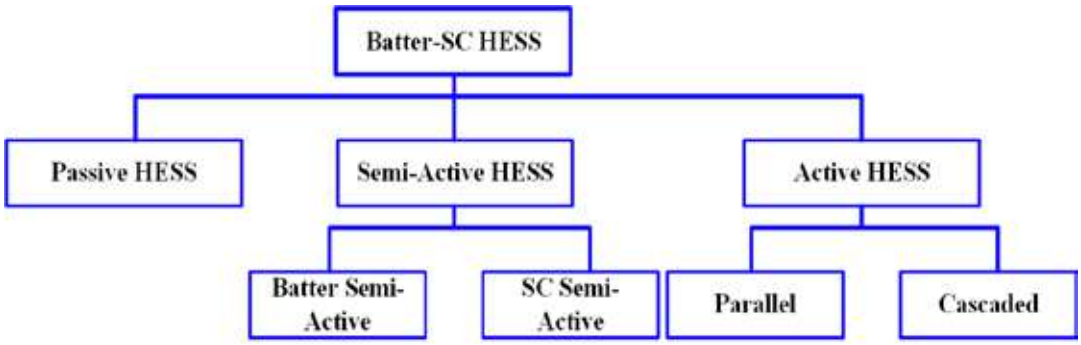


Fig. 1: Types of Hybrid Energy Storage Systems

III.The Integration of Energy Storage in PV, Wind, and Wind Energy Systems

The integration of energy storage in photovoltaic, wind, and fuel cell systems, as depicted in Fig. 2, offers various benefits and challenges. Energy storage systems store excess energy when it is produced, providing power during periods of low energy production and thus enhancing grid stability. In photovoltaic systems, this integration increases the self-consumption of generated electricity, improves energy independence, and reduces electricity costs. In wind energy systems, it provides backup power during periods of low wind activity, enhancing grid stability and increasing overall system efficiency. In fuel cell systems, it captures excess energy produced during low demand periods, ensuring a more stable electric grid and helping to reduce energy costs.

However, this integration also presents various challenges. There are economic and technical barriers such as high initial costs, limited storage capacity, and potential efficiency losses during energy conversion processes. Additionally, comprehensive system optimization and sophisticated control strategies are required to mitigate fluctuations in energy production in wind and photovoltaic systems. In fuel cell systems, appropriate sizing and integration of storage technologies are critical to maximizing system performance.

Despite these challenges, the integration of energy storage systems with renewable energy sources holds significant potential for a more sustainable, reliable, and cost-effective energy future. Overcoming these challenges through technological advancements and innovative solutions by researchers and industry professionals is essential to maximize the potential of hybrid energy storage systems (Ersan Kabalci).

IV.Simulation Results

Research findings indicate the significant potential of hybrid energy storage systems in enhancing the efficiency and reliability of renewable energy sources such as photovoltaic, wind, and fuel cells. The integration of multiple energy storage technologies allows for better management of energy fluctuations and mismatches, resulting in a more stable and consistent power supply. Analysis of key performance metrics, such as round-trip efficiency, response time, and cycle life, underscores the importance of optimizing the selection and combination of energy storage technologies to maximize overall system performance.

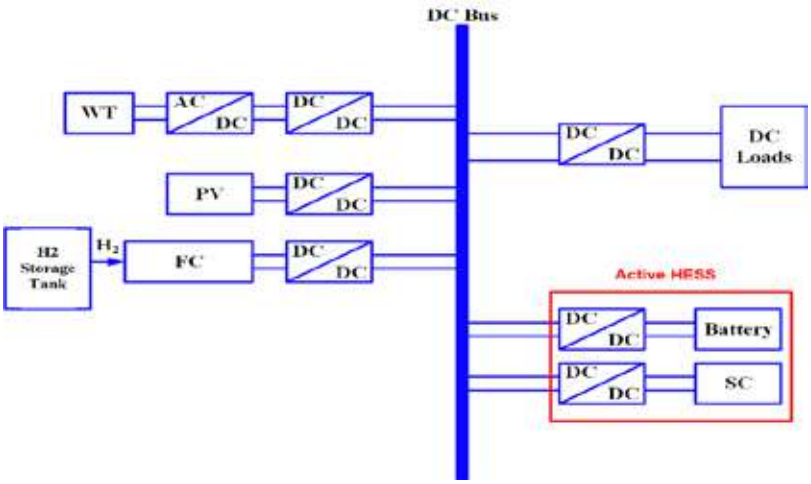


Fig. 2: Structure for renewable energy sources DC microgrid with active HESS

V.Conclusion

The integration of hybrid energy storage systems comprising batteries and supercapacitors has significantly enhanced the performance of PV, wind, and fuel cell systems. Energy storage systems have great potential to increase the effective utilization of renewable energy sources and ensure grid stability. Therefore, the implementation of technological advancements and innovative solutions is crucial for the future success of hybrid energy systems in terms of sustainability and efficiency.

References:

Rahaf S. Ghanem, Laura Nousch, M. Richter, "Modeling of a Grid-Independent Set-Up of a PV/SOFC Micro-CHP System Combined with a Seasonal Energy Storage for Residential Applications", 2022

Nelly Safitri, A. Yunus, F. Fauzi, Naziruddin Naziruddin, "Integrated arrangement of advanced power electronics through hybrid smart grid system", 2020, pp. 3202-3209

Otavio Lopes Alves Esteves, H. Gabbar, "Nuclear-Renewable Hybrid Energy System with Load Following for Fast Charging Stations", 2023

P. Sánchez-Palencia, S. Hamad, P. Palacios, R. Grau-Crespo, K. Butler, "Solar fuels by artificial photosynthesis: from inorganic to hybrid multifunctional materials", 2022

Umar Muhammad Kangiwa, Mohammed Gwani, Benjamin Joshua Wisdom, A. Yakubu, "Performance Investigation of Wind/Photovoltaic/Fuel cell Hybrid Energy System for Stand-alone Power Supply", 2024

Y. Belkhier, A. Oubelaid, "Novel design and adaptive coordinated energy management of hybrid fuel-cells/tidal/wind/PV array energy systems with battery storage for microgrids", 2024

I. Sulistiyowati, Jamaaluddin Jamaaluddin, I. Anshory, "Hybrid Energy Storage Performance Evaluation of Integrated Photovoltaic-Fuel Cell Systems", 2022

JING, Wenlong, et al. Battery-supercapacitor hybrid energy storage system in standalone DC microgrids: areview. *IET Renewable Power Generation*, 2017, 11.4: 461-469.

M. Singla, P. Nijhawan, A. Oberoi, "Cost–benefit comparison of fuel cell–based and battery-based renewable energy systems", 2021, pp. 1736-1755

Alfred Rufer, "Energy Storage", *CRC Press*, 2017-10-31

Ersan Kabalci, "Hybrid Renewable Energy Systems and Microgrids", *Academic Press*, 2020-11-21

Improving Power Quality in Microgrids with PEM Electrolyzer/Fuel Cell System

[1*]Heybet Kilic
[1] Dicle University, Department of Electric Power and Energy, Diyarbakır, 21280, Türkiye

* E-mail:heybet.kilic@dicle.edu.tr

Abstract
The fluctuating nature of renewable energy sources poses challenges for maintaining consistent power quality within microgrids. This paper explores the potential of a Proton Exchange Membrane (PEM) Electrolyzer/Fuel Cell system to improve the power quality in microgrids. The proposed system capitalizes on its dual functionality as an energy storage solution and a power generator to stabilize voltage and frequency variations. Through simulation studies, the effectiveness of the PEM system in enhancing grid stability and managing peak loads is demonstrated. The study analyzes how the PEM system responds under varying load demands and environmental conditions, offering insights into its practical application in real-world scenarios. The results indicate a promising capacity for PEM systems to significantly improve power quality, making them viable components in sustainable microgrid architectures.

Keywords: Microgrids, Power Quality, PEM Electrolyzer, Fuel Cell, Renewable Energy

I. Introduction

The transformation of energy systems through the integration of renewable energy sources is critical to achieving sustainable energy goals. Microgrids, which are small-scale power grids that can operate independently or in conjunction with the main electrical grid, play a pivotal role in this transformation. They provide resilience, enhance reliability, and facilitate the integration of renewable resources like solar and wind energy [1,2]. However, the inherent intermittency of these renewable sources poses significant challenges, particularly in terms of power quality issues such as voltage fluctuations, frequency instability, and harmonic distortions, which can adversely affect the operation and stability of both microgrids and the main grid [3,4].

To mitigate these challenges, advanced energy storage and conversion technologies are essential. Among these, Proton Exchange Membrane (PEM) systems, which include both electrolyzers and fuel cells, are increasingly recognized for their efficiency and flexibility [5,6]. PEM electrolyzers can store excess renewable energy by converting it into hydrogen, while PEM fuel cells can convert this stored hydrogen back into electricity on demand, providing a clean and responsive energy source that enhances grid stability [7,8].

The ability of PEM systems to provide rapid response solutions to balance supply and demand makes them particularly suitable for microgrid applications. They not only help in managing the variability of renewable energy but also in improving the power quality by providing ancillary services such as voltage control and frequency regulation [9]. Furthermore, these systems are conducive to the decentralization of energy resources, offering a scalable option for energy storage and generation across various contexts, from remote rural areas to urban settings.

This paper investigates the integration of PEM Electrolyzer/Fuel Cell systems within microgrids, focusing on their role in enhancing power quality. Through simulations, the study assesses the impact of these systems on the stability and reliability of microgrids, under different renewable integration scenarios and load conditions. The findings aim to demonstrate the effectiveness of PEM systems in maintaining high power quality in microgrids, supporting a more widespread adoption of renewable energy technologies.

II. Materials and Methods

This study investigates the impact of integrating a Proton Exchange Membrane (PEM) Electrolyzer/Fuel Cell system into a microgrid to enhance power quality, particularly focusing on voltage and frequency stability.

The core of the research methodology is based on dynamic simulations conducted using MATLAB/Simulink. This environment was chosen for its robustness in handling complex system dynamics and its extensive library of renewable energy conversion models. A model of the microgrid, including renewable energy sources (solar PV and wind turbines), load profiles, a PEM Electrolyzer, and a Fuel Cell system, was developed. Parameters such as solar irradiance, wind speed, and load demand were varied according to typical seasonal variations to assess the system's responsiveness and stability under different scenarios.

The PEM Electrolyzer model converts excess electrical energy into hydrogen by electrolyzing water. This hydrogen is then stored under pressure for subsequent use. The Fuel Cell model reconverts hydrogen back into electricity during peak load demands or when renewable generation is insufficient. The electrolyzer and fuel cell efficiency characteristics, along with their response times, were modeled based on data from existing literature [1,2] and manufacturer specifications.

An advanced control strategy was implemented to manage the operation of the integrated PEM system within the microgrid. The control logic was designed to optimize the energy flow, ensuring that the storage system charges

during periods of excess generation and discharges during demand peaks or insufficient generation. The control algorithm also included provisions for maintaining grid stability by regulating voltage and frequency to within predefined thresholds.

Data from the simulations and experimental setups were analyzed using statistical tools to evaluate the performance of the PEM system in improving the power quality of the microgrid. Performance metrics such as system efficiency, voltage deviation, and frequency variation were calculated and compared against the microgrid's operational requirements.

These methodologies provided a comprehensive understanding of how PEM Electrolyzer/Fuel Cell systems can be integrated and managed within a microgrid to improve power quality, offering insights into practical applications and scalability of this solution.

IV. Results and discussions

The integration of the PEM Electrolyzer/Fuel Cell system into the microgrid was analyzed through both simulation and experimental methods to assess its impact on improving power quality, particularly focusing on voltage stability and frequency regulation.

The simulation results demonstrated that the PEM Electrolyzer/Fuel Cell system significantly contributed to stabilizing the microgrid during periods of high renewable intermittency and varying load conditions. The system showed an overall efficiency of approximately 60% under optimal operational conditions, which is in line with efficiencies reported in related studies [1] Voltage stability was maintained within ±5% of the nominal voltage, and frequency variations were reduced by up to 50% compared to scenarios without the PEM system.

Table 1: Summary of System Performance Metrics

Metric	Without PEM System	With PEM System	Improvement
System Efficiency	55%	60%	+5%
Voltage Stability	±10%	±5%	+5%
Frequency Variation	±0.6 Hz	±0.3 Hz	50%
Response Time (sec)	N/A	< 5 sec	-

The use of the PEM system allowed for a higher penetration of renewable sources into the microgrid by providing a reliable means to balance the power supply during variable generation periods. This was evident from the reduced number of power quality incidents recorded in the microgrid, such as under-voltages and frequency drops, which often occur due to the stochastic nature of wind and solar inputs.

The results indicate that the PEM Electrolyzer/Fuel Cell system not only enhances the overall efficiency and stability of the microgrid but also facilitates a greater integration of renewable energy sources by acting as an effective buffer against the variability of these sources. Furthermore, the system's ability to quickly respond to power quality issues highlights its potential as a key technology in future smart grid applications, where dynamic response and flexibility are paramount.

The study also identifies areas for future research, particularly in scaling up the system for larger microgrid applications and exploring advanced control strategies to optimize the operational efficiency and life span of the PEM components.

V. Conclusions

This study investigated the potential of integrating a Proton Exchange Membrane (PEM) Electrolyzer/Fuel Cell system into a microgrid to address common power quality issues associated with the intermittent nature of renewable energy sources. The results clearly demonstrate that the PEM system significantly enhances the stability and reliability of microgrid operations, thereby supporting higher penetration of renewable energy.The simulation and experimental data revealed that the PEM system improves system efficiency by approximately 5%, maintains voltage stability within ±5% of the nominal value, and reduces frequency variation by up to 50%. These improvements are critical for ensuring the operational reliability of microgrids in real-world scenarios, where renewable energy sources are increasingly predominant.Moreover, the rapid response capability of the PEM system, typically under 5 seconds, underscores its suitability for dynamic power systems and its ability to mitigate abrupt fluctuations in power quality. This responsiveness not only aids in maintaining continuous power supply but also safeguards sensitive equipment and consumer appliances against potential damages caused by power instability.In conclusion, the PEM Electrolyzer/Fuel Cell system emerges as a robust solution for enhancing power quality in microgrids. It facilitates a smoother integration of renewable resources, offering a sustainable approach to managing the challenges posed by renewable energy variability. Future research should focus on optimizing the scalability

and economic viability of this technology, exploring innovative control strategies, and assessing long-term operational impacts to fully harness its benefits in larger-scale energy systems.The implications of this research are significant, suggesting that PEM systems could be instrumental in the global transition towards more sustainable and resilient energy infrastructures.

References

[1] Lasseter, R. H. (2002). "Microgrids." IEEE Power Engineering Society Winter Meeting, 1, 305-308.
[2] Hatziargyriou, N. et al. (2007). "Microgrids: An Overview of Ongoing Research, Development, and Demonstration Projects." IEEE Power & Energy Magazine, 5(4), 78-94.
[3] Katiraei, F., & Aguero, J. R. (2011). "Solar PV integration challenges." IEEE Power and Energy Magazine, 9(3), 62-71.
[4] Prodanovic, M., & Green, T. C. (2004). "High-quality power generation through distributed control of a power park microgrid." IEEE Transactions on Industrial Electronics, 53(5), 1471-1482.
[5] Chandorkar, M. C., Divan, D. M., & Adapa, R. (1993). "Control of parallel connected inverters in standalone AC supply systems." IEEE Transactions on Industry Applications, 29(1), 136-143.
[6] Zhang, L., Zhou, W., & Cai, H. (2011). "A review of the current status of the applications of fuel cells in microgrids." International Journal of Hydrogen Energy, 36(13), 7892-7902.
[7] Carmo, M., Fritz, D. L., Mergel, J., & Stolten, D. (2013). "A comprehensive review on PEM water electrolysis." International Journal of Hydrogen Energy, 38(12), 4901-4934.
[8] Wang, Y., Chen, K. S., Mishler, J., Cho, S. C., & Adroher, X. C. (2011). "A review of polymer electrolyte membrane fuel cells: Technology, applications, and needs on fundamental research." Applied Energy, 88(4), 981-1007.
[9] Thounthong, P., Rael, S., & Davat, B. (2009). "Energy management of fuel cell/battery/supercapacitor hybrid power sources for vehicle applications." Journal of Power Sources, 193(1), 376-385.

Evaluation of Hydrogen Transportation by Trucks in terms of Occupational Health and Safety: A Preliminary Hazard Analysis

Mehmet Tunç, Ramazan Solmaz
Bingöl University, Health Sciences Faculty, Occupational Health and Safety Department, 12000, Bingöl, Türkiye

E-mail: mtunc@bingol.edu.tr; rsolmaz@bingol.edu.tr; rsolmaz01@gmail.com

Abstract
One of the most important components of a sustainable hydrogen economy is hydrogen transportation and distribution. This can be done in a variety of ways. In practice, however, these systems bring with them significant risks that must be addressed if hydrogen is to be used safely. As in all other energy sectors, all aspects of the hydrogen system require improvements in occupational health and safety legislation. In this study, preventive measures in the transportation of hydrogen by trucks are provided as a representative example.

Keywords: Hydogen transportation, safety, hazard analysis, occupational health and safety

I. Introduction

Hydrogen is the simplest, cleanest and most abundant element in the universe. Although hydrogen gas is used in many different sectors, its most important use in our age is as an energy carrier, and the demand is increasing accordingly (IEA, 2019). For instance, in Europe, the overall demand for hydrogen is expected to surpass 45 million tons by the year 2050 (Berger, 2021). To benefit more from hydrogen, its transportation and distribution are also necessary, which are mostly being carried out by ships, trucks and pipelines. According to the International Energy Agency (IEA) (2019), transporting hydrogen by pipelines is the cheapest way for distances under 1500 km. But beyond that distance, shipping as ammonia or a liquid organic hydrogen carrier (LOHC) becomes cost-effective. Transporting hydrogen in liquid form reduces the volume and more hydrogen can be transported. In liquid form, it can be transported under high pressure and low temperature. Transporting hydrogen in liquid form reduces the volume and more hydrogen can be transported. It also makes the transportation process more efficient. In liquid form, it can be transported under high pressure and low temperature. Hydrogen gas can be transported under high pressure in special pressure tanks made of materials such as steel or carbon fiber composites. The Joint Research Centre (JRC) of the European Commission released HIAD 2.1 (latest version of The Hydrogen Incident and Accidents Database) in 2023. The data includes hydrogen-related accidents worldwide up to December 2023 (JRC, 2023). Based on this data, 12.8% (97 out of 755) of the accidents occurred during "hydrogen transport and distribution (HTD)".

Lowesmith and Hankinson (2013) discovered that the pipeline carrying a mixture of hydrogen and natural gas inflicted marginally less heat-related damage compared to the natural gas pipeline, despite operating at identical pressures. Thus, incorporating hydrogen seems to offer a moderately safer alternative under specific circumstances (Lowesmith and Hankinson, 2013). In a reported study (Stolecka, 2018), it is indicated that adding hydrogen to the natural gas network will further weaken the mechanical strength of steel and increase the probability of corrosion.

The transportation of hydrogen gas brings some hazards in terms of occupational health and safety. In order to make the hydrogen ecosystem more given, hazards and risks need to be identified through risk analyses, exposures and vulnerabilities need to be identified and solutions need to be proposed. However, the scientific studies on this topic were not sufficient. Therefore, in this study, the risks that may occur during hydrogen transportation as a representative example is analyzed and some recommendations were proposed.

II. Experimental Set-up and Procedure

According to the Hydrogen Safety Panel (HSP) (2020), the most critical section of a safety plan is identifying hazards and taking preventive/mitigative measures. In this study, preliminary hazard analysis (PreHA) method is selected to identify hazards arising from HTD.

This method assesses the impact (severity) and probability (likelihood) of an event to determine risk. Severity, including health, environmental, and economic effects, is evaluated to gauge the event's impact, and it is numbered from 1 (biggest impact) to 4 (lowest impact). Likelihood indicates how frequently the event may occur within a specific timeframe, and a letter is given from the most frequent one to the eliminated one (A, B, C, D and F respectively). Combining severity and likelihood reveals the overall risk level (MIL-STD-882E, 2012).

The paper analyzes 97 accidents associated with HTD, documented in JCR (2023), using the PreHA method. Finally, recommendations are provided for ensuring HTD safety, based on scientific studies.

III. Results and discussions

Hydrogen is transported and distributed via pipelines, ships, and trucks in various forms, including gas, liquid and combinations with substances like ammonia or liquid organic hydrogen carriers (IEA, 2019). In the mentioned document (JRC, 2023), the first accident recorded during HTD occurred in 1970, while the most recent accident was in 2023. While the year with the highest number of accidents was 2013, totaling nine incidents, there were some years where no accidents related to HTD were recorded at all.

When examining accidents related to HTD, it is observed that 71% of them involve hydrogen storage in the form of gas or gas mixture, 22% involve liquid, and the remaining 7% are unspecified (JRC, 2023).

Looking at the causes of 97 accidents, six main causes are identified. Sometimes one of these alone cause the accident (such as system design error), while other times it is observed that the accident occurs due to two or more causes (27 accidents). The cause of 16 out of 97 accidents is unknown as shown in Fig. 1.

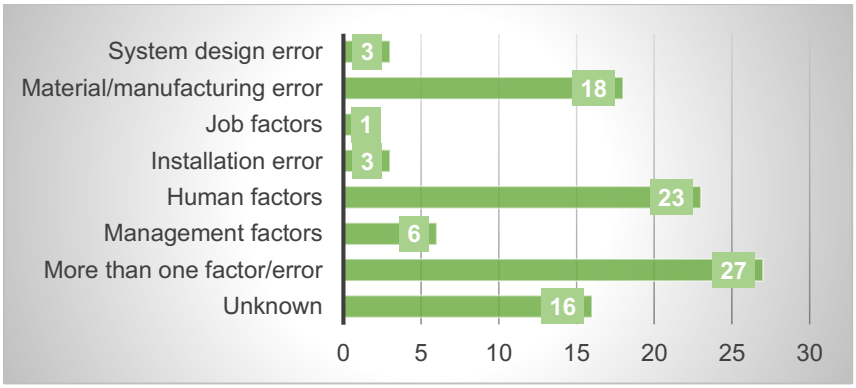


Fig. 1: Causes of 97 accidents in numbers (JRC, 2023)

Looking at the consequences of the accidents (JRC, 2023), it is observed that the most common outcome, occurring in 30 cases, is fire. In 28 cases, there was a hydrogen leak, but no ignition occurred. The number of accidents resulting in an explosion is 20. From the remaining accidents, 18 are classified as near misses, and 1 is classified as a false alarm (JRC, 2023).

Out of 97 accidents, 72 occurred during transportation by truck. It should be noted that several of these 72 accidents did not happen on the road but during the loading or unloading of hydrogen onto the truck. 16 accidents were related to pipeline distribution, accounting for 17% of the accidents. The transportation method of 4 accidents could not be determined from the information provided in the document. 2 accidents occurred during transportation by train, and 1 occurred during transportation by sea vessel. Additionally, 2 accidents, classified as "Other," occurred when individuals were transporting hydrogen cylinders with their personal vehicles for private use (JRC, 2023).

According to the 97 HTD accidents (JRC, 2023), hydrogen accidents were involved in four main HTD methods. Accidents in these transportation methods have six main causes (Fig. 1), according to JRC (2023), and they are also used in PreHA method in Table 1. However, when looking at the hazards associated with HTD by ship, truck, train, or pipeline, while there may be commonalities, the specific hazards can vary depending on the HTD method.

Trucks used for hydrogen transportation are vulnerable to similar risks as other heavy-duty vehicles, such as traffic accidents, rollovers, and collisions. These events can potentially cause hydrogen leaks or spills, which in turn pose fire or explosion hazards. While ensuring drivers receive adequate safety training and adhere to traffic regulations is crucial, it is equally important to follow proper maintenance and handling procedures to prevent accidents during refueling, maintenance, or repair of hydrogen trucks.

Gaseous hydrogen poses risks of leakage, leading to potential fire or explosion hazards due to its highly flammable nature. Liquid hydrogen is stored and transported at extremely low temperatures (-253°C). Exposure to higher temperatures can cause rapid vaporization, leading to a sudden increase in pressure within the storage tank. This pressure buildup may exceed the structural integrity of the containment system, resulting in a potential rupture or release of hydrogen gas.

Ammonia, is increasingly preferred for hydrogen transportation due to its higher energy density by volume compared to hydrogen. It is also easier to store, with the ability to be kept as a liquid at room temperature under moderate pressure or at sub-zero temperatures under atmospheric pressure. In case of a leakage, ammonia, a hazardous compound, can adversely affect the air, soil, and water quality, along with posing health risks to people living nearby (Flusberg, 2023).

Table 1. PreHA for hydrogen transportation by trucks

No	Transportation Method	Hazards	Causes	Effects	Risk Degree
1	Truck	Gaseous/ Liquid Hydrogen	According to JRC (2023) stats, there are six main causes: **1. Management factors** - Poor management/maintenance - Insufficient information to employees - Inadequate supervision - Long working hours, insufficient rest periods - Lack of communication - Lack of emergency plans - Work organization and management **2. Human factors** - Carelessness - Inadequate training - Competence - Fatigue and Stress - Use of Appropriate Personal Protective Equipment - Lack of motivation - Ability to make the right decision in emergency situations **3. Installation error** - Wrong placement - Wrong connections - Use of unsuitable materials in connections - Improper installation connections **4. Job factors** - Loading and Unloading Location Selection - Unsuitable tanker selection - Filling and unloading operations - Lack or misuse of safety equipment - Inadequate equipment **5. Material/manufacturing error** - Low quality material production, Poor material selection, etc. - Structural defects of tankers - Source errors - Inadequate protective materials (e.g. coatings) **6. System design error** - Inappropriate design - Use of inappropriate materials - Inadequate pressure and tightness tests - Emergency evacuation system problems - Fire prevention and extinguishing systems - Errors in the design of loading/unloading operations	Fire, Explosion, Frostbite, Asphyxiation, Hydrogen leakage	1B
2		Ammonia		Chemical exposure, Strong alkaline chemical respiration, Poisoning, Fire and explosion, Environmental pollution, Chemical burns	1B
3		Traffic		Traffic accident, Fire, explosion, Hydrogen leakage	1B
4		Roads		Traffic accident	1A
5		Untrained Driver		Traffic accident, Improper intervention in case of emergency etc.	1D
6		Lack of Signs on Truck		Traffic accidents, Improper emergency response etc.	2D

The transportation of hazardous materials, such as hydrogen, by trucks contributes to the overall traffic risks on roads. Increased truck traffic can lead to congestion, which may contribute to the likelihood of accidents or incidents, especially in urban or densely populated areas. The condition of roads, including factors such as potholes, sharp turns, and steep gradients, can affect the safety of transporting hazardous materials by trucks. Poor road conditions can increase the risk of accidents, or leaks, particularly for vehicles carrying sensitive cargo like hydrogen.

The lack of proper signage on trucks transporting hazardous substances like hydrogen can indeed pose significant hazards. It is of the utmost importance that hazardous materials are clearly identified by the use of placards and signage, in order to facilitate the rapid identification of the type of cargo being transported. In the absence of appropriate signage, emergency responders and other drivers may be unaware of the potential dangers associated with the truck's cargo. This lack of awareness can result in the implementation of inappropriate response measures in the event of an accident, thereby increasing the risk of injury, and property damage etc. These signs can also raise awareness in the public, enabling drivers to adjust their behavior accordingly, such as maintaining a safe distance and avoiding aggressive maneuvers.

IV. Conclusions

Trucks utilised for the transportation of hydrogen face a multitude of risks inherent to heavy-duty vehicles, including traffic accidents, rollovers, and collisions, which can lead to potentially hazardous hydrogen leaks, fires, or explosions. Both gaseous and liquid hydrogen present distinct risks, with gaseous hydrogen being highly flammable and prone to leakage, while liquid hydrogen's extreme cold temperatures pose challenges related to pressure management. Furthermore, the transportation of hazardous materials, such as hydrogen, increases the risk of traffic accidents on roads, particularly in congested urban areas. This risk is further compounded by the variable conditions of road infrastructure. In order to mitigate these hazards, it is imperative to implement rigorous safety protocols, ensure proper training for drivers, adhere to maintenance procedures, and comply with regulatory standards. Furthermore, it is of paramount importance to emphasise the significance of clearly identifying hazardous cargo through the use of appropriate signage. This not only assists emergency responders in their endeavours but also serves to enhance public awareness and promote road safety. Finally, it is of the utmost importance that during the transportation of hydrogen by trucks on roads, both national and international standards and regulations are adhered to. These encompass various aspects, including but not limited to, transportation, storage, and use of hydrogen.

Acknowledgements

The authors are greatly thankful to Bingöl University, Health Sciences Faculty, Occupational Health and Safety Department for supporting this study.

References

Berger R., 2021, Hydrogen transportation. The key to unlocking the clean hydrogen economy. Munique: Roland Berger GmbH, https://www.rolandberger.com/publications/publication_pdf/roland_berger_hydrogen_transport.pdf (Accessed: April 26, 2024)

Flusberg M. 2023, The challenges of hydrogen transport – and of using hydrogen for transport. https://www.linkedin.com/pulse/challenges-hydrogen-transport-using-martin-flusberg-vc4zf, (Accessed: (May 6, 2024

HSP (Hydrogen Safety Panel), 2020, Example safety plan for hydrogen and fuel cell projects, https://h2tools.org/sites/default/files/2020-10/Example_Hydrogen_Safety_Plan_September_2020.pdf, Accessed: April 26, 2024

JRC (Joint Research Centre), 2023, The hydrogen incident and accidents database 2.1 (HIAD 2.1), https://minerva.jrc.ec.europa.eu/en/shorturl/capri/hiadpt, (Accessed: 26.04.2024)

IEA (International Energy Agency), 2019, The Future of Hydrogen 203. International Energy Agency, Paris, pp 18, https://iea.blob.core.windows.net/assets/9e3a3493-b9a6-4b7d-b499-7ca48e357561/The_Future_of_Hydrogen.pdf, (Accessed April 26, 2024)

MIL-STD-882E, 2012, Department of defense standard practice system safety, MIL- STD-882e. Retrieved from http://everyspec.com/MIL-STD/MIL-STD-0800-0899/ MIL-STD-882E_41682/, (Accessed: October 31, 2022)

Lowesmith, B. J., & Hankinson, G., Large scale experiments to study fires following the rupture of high pressure pipelines conveying natural gas and natural gas/hydrogen mixtures, Process Saf Environ Prot, 91(1-2), 101-111, (2013)

Stolecka, K., Hazards of hydrogen transport in the existing natural gas pipeline network, J, Power Technol, 98 (4), 3292018, (2018)

Safety Risks in Solar-Hydrogen Energy System: Fine Kinney Risk Analysis

Mustafa Doğrubaş, Mehmet Tunç, İbrahim Yasin Erdoğan, Ramazan Solmaz
Bingöl University, Health Sciences Faculty, Occupational Health and Safety Department, 12000, Bingöl, Türkiye

E-mail: dogrubas@hotmail.com; ierdogan@bingol.edu.tr

Abstract

The demand for energy is increasing with technological advances and industrialisation. Due to the depletion of fossil fuel reserves and the increasing environmental impact, alternative energy sources have become more important in recent times. Hydrogen energy, produced from renewable energy sources, is of great importance in solving problems such as global warming and climate change. In addition, rising energy prices due to wars and global crises have led to intensive efforts to develop alternative energy sources and to achieve the best possible efficiency from existing systems. It is also necessary to take measures related to occupational health and safety in energy systems. This study examines a hybrid energy system supported by photovoltaic solar panels and hydrogen energy. The risk analysis of occupational health and safety issues in solar-hydrogen hybrid energy systems is carried out using the Fine-Kinney risk analysis method.

Keywords: Hydrogen production, solar energy, electrolysis, renewable energy, occupational health, occupational safety

I. Introduction

The increasing energy use and the need to switch to renewable energy sources instead of fossil fuels are crucial. Fossil fuels still make up a big chunk of our energy consumption, but they are running out fast and causing global warming, which harms all living things, including people. So, we need to limit their usage. We are building lots of renewable energy plants to meet the energy needs of industries and homes, and to mix up where our energy comes from. We are also figuring out how to make these plants work even better. Using a mix of alternative energy sources, like solar and hydrogen, can help us reach our energy goals.

Generating electricity using renewable energy sources and ultimately producing hydrogen is a milestone in finding solutions to future energy supply problems. Especially in countries with high annual sunshine duration, using solar energy to produce hydrogen through electrolysis is among the most important methods for preserving the natural environment.

Hydrogen, which is derived from fossil fuels, is a crucial fuel type in the transition to clean energy sources. The high utilization rate of fossil fuels results in significant greenhouse gas emissions. This occurs during the production of hydrogen. Developing hydrogen storage technology, increasing clean hydrogen production, and expanding the number of hydrogen-powered vehicles are important factors for accelerating the global energy transition. To transition to a hydrogen-based economy, we must improve the efficiency of energy production systems using fossil fuels, while also increasing hydrogen production through renewable energy sources. Furthermore, developing methods for hydrogen production using excess electrical energy from renewable sources is crucial. Storing this hydrogen by converting it into other energy types is also essential.

The solar-hydrogen system operates on the principle of several interacting components working together as an integrated system. In this system, electricity generated by solar panels is used to perform electrolysis of water, resulting in the production of hydrogen in a form known as green hydrogen. This hydrogen is then stored and converted back to electricity to meet energy demand. The system comprises photovoltaic (PV) panels, proton exchange membrane (PEM) electrolyzer, hydrogen storage tank, proton exchange membrane fuel cell (PEMFC), and power conditioning unit (PCU) (URL-1,2024).

The installation phase of solar energy systems comes with various risks related to occupational health and safety. These risks involve testing and certifying products, analyzing the land and solar energy potential, planning, overseeing installation, checking system efficiency, managing performance, and conducting periodic inspections. Moreover, despite the numerous advantages of producing hydrogen in this system, there are also risks to consider. Ensuring high purity in hydrogen production can be costly. Additionally, factors like the expense of fuel cells, challenges in storage and transportation, the possibility of leaks, and the risk of explosions and fires need to be taken into account.

Safety precautions are crucial when cleaning solar panels. Cleaning panels during production can expose workers or maintenance personnel to high currents and voltages. Therefore, the first step in the process is to disconnect the system from the mains and the electrical connections between the solar panels and the inverter. This ensures the safety of maintenance and repair personnel, allowing maintenance and inspection operations to be conducted

safely.

II. Experimental Set-up and Procedure

In this study, the Fine-Kinney risk analysis method is used to assess the risks in a solar-hydrogen hybrid energy system. Compared to other risk analysis methods, the risk scores that are higher in this method are more accurate and lower. Because in the Fine-Kinney method, the frequency of exposure to hazards plays a key role. The Fine-Kinney risk analysis method is a quantitative method based on equipment, work processes and machinery. In the method, calculations are made using the probability, exposure (frequency), and consequence (severity) of occurrence of the hazard when assessing the risks. In this method, the probability of occurrence of accidents/events, the frequency of occurrence, and the severity of the consequences are used to calculate risk scores (*R*).

R = Probability x Exposure x Consequence (1)

III. Results and discussions

Prior to commencing the study, it is essential to gain an understanding of the general principles underlying the photovoltaic method of electrical energy production. Solar panels are constructed by assembling numerous small photovoltaic cells, comprising silicon crystals. When exposed to sunlight, the surface of these crystals absorbs photons (Fig. 1). This process causes electrons within the crystal to move, generating electric current. The direct current (DC) generated is then converted to alternating current (AC) using an inverter device. This enables the energy to be made suitable for the grid voltage (sinusoidal), which is then offered to industrial facilities and subscribers for consumption. Depending on the type of system, charge controllers, batteries, and other elements may be used.

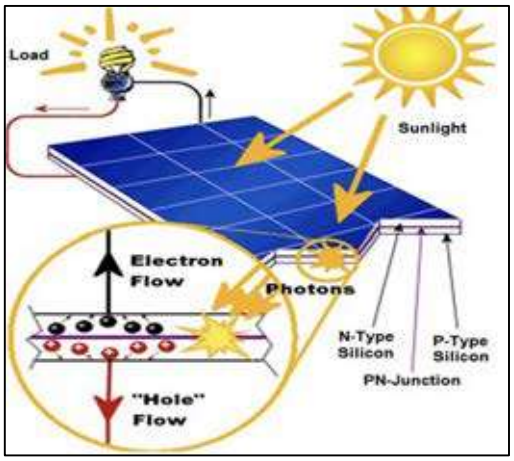


Fig. 1. Basic working principle of the solar cell (URL-2, 2024)

The efficiency of photovoltaic (solar cell) panels is determined by the material used in their production and the quality of this material. Silicon, a semiconductor material, is a preferred material for this purpose. Additionally, the average sunshine duration that a region receives throughout the year affects the efficiency of these systems. To increase the power output, a large number of panels can be used by connecting them in series or in parallel.

The high initial installation cost of solar power systems, the variability of sunshine duration, and the desire to obtain more energy from existing systems (solar power system) have led to the development of hybrid solar systems that utilize wind, hydrogen, and hydraulic resources to obtain more energy and provide uninterrupted energy flow.

Even today, hydrogen production is mostly realized using fossil fuels. However, due to global warming and the search for alternative energy sources, there is a tendency towards renewable energy sources. At this point, hydrogen, which boasts a number of advantages, stands out. It is more efficient than other fuel types and generates water as waste.

The direct current (DC) electrical energy required for the electrolysis method, which is the simplest method for hydrogen production, is obtained directly from solar panels. The electric current obtained is applied to the electrodes in the electrolysis cell to separate oxygen and hydrogen, which form the basic structure of water.

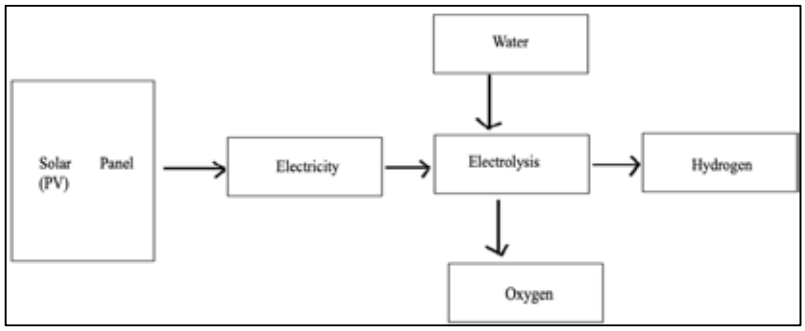


Fig. 2. Principle of hydrogen production from photovoltaic energy

As technology has advanced, numerous techniques have emerged for generating energy from hydrogen. Steam reforming is the most prevalent hydrogen production method, requiring temperatures between 700°C and 1100°C. In contrast, electrolysis of water can be conducted at temperatures between 50°C and 80°C. The primary difference between these two methods lies in the use of primary energy sources. For electrolysis, the primary energy source is electric current, whereas for steam reforming it is natural gas. One of the key objectives in the field of hydrogen production is to reduce the cost of electrolysis. Additionally, utilizing electrical energy generated from renewable sources in the electrolysis method is a crucial goal (Çiçek and Aliyeva-Ç, 2022). A solar hydrogen hybrid energy system production scheme is given in Fig. 3 (Yılmaz Ulu, 2010).

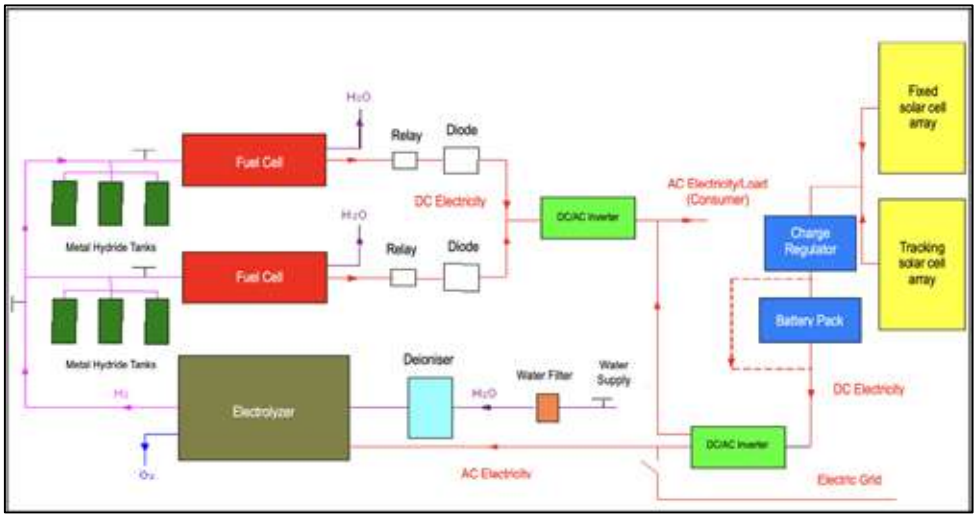


Fig. 3. Solar-Hydrogen Hybrid Energy System (Yılmaz Ulu, 2010)

A multitude of potential hazards exist throughout the entire process, beginning with the installation phase of solar energy systems and extending to the consumption phase. These hazards encompass a diverse range of areas, including chemical, physical, ergonomic, and electrical risks. Most of the risks associated with electricity generation, transmission, and distribution are also present in these systems. These risks vary significantly based on whether the system is connected to the grid or operates independently. Many potential hazards exist, such as those related to the transportation of batteries, panels, and construction materials, as well as incorrect electrical connections. In addition to general risks, there is a risk of falling associated with roof energy systems. Moreover, leaks during the transport, storage, or use of hydrogen in solar-hydrogen hybrid energy systems may pose environmental risks.

IV. Conclusions

There are always safety risks in power generation systems. These risks should be eliminated with a proactive approach by using an appropriate risk analysis method. Working at heights, occupational accidents during the installation phase or during maintenance and repair, leaks that may occur during the transport and storage of hydrogen, and the risk of explosion of the hydrogen tank are the high risks.

Solar-hydrogen system is one of the hydrogen production systems of the future. In parallel with the suitability of the method, it is necessary to carry out the necessary hazard risk analyses in terms of occupational health and safety related to the systems to be used, and to eliminate the safety and occupational accident hazards.

The risk analysis identified several high-risk factors, including falling from roof systems, inverter burning or explosion due to lack of a separator after solar panels, fire hazards, hydrogen tank explosion risk from leakage, and explosion risks from electrical faults in panels and transformers. To mitigate these risks, it's advised to use a

separator after solar panels and regularly inspect electrical connections and system faults by qualified individuals to prevent spark formation and fire. Roof systems should be avoided if possible, but if used, appropriate occupational health and safety precautions must be implemented.

Acknowledgements

The authors are greatly thankful to Bingöl University, Health Sciences Faculty, Occupational Health and Safety Department for supporting this study.

References

Çiçek F.A.O. and Aliyeva-Çiçek S.F.K (2022). Hidrojen gazının üretim yöntemleri ve enerji kaynağı olarak avantaj ve dezavantajları. Endless Light in Science, (3), 138-142

URL_1 https://yeserenerji.com/yesil-hidrojen-uretimi/ (Accessed: April 10, 2024)

URL_2 https://www.enerjipaketi.com/gunes-enerjisinden-elektrik-uretimi (Accessed April 14, 2024)

Yilmaz Ulu, E. (2010). Güneş-hidrojen hibrit enerji sisteminin deneysel ve teorik enerji, ekserji ve elektromanyetik analizi

The Energy Trilemma Approach to Assessment of Hydrogen Production Potential in Türkiye

[1*]Kadir Akgun, [1]Fatma Zehra Sukur, [1]Bestami Ozkaya
[1] Yıldız Technical University, Faculty of Civil Engineering, Department of Environmental Engineering, Institute of Science and Engineering, Istanbul, 34220, Türkiye

* E-mail: kadiirakgun@gmail.com

Abstract

The Energy Trilemma in international scale dates to the 1987 Brundtland report on sustainable development. The report elucidated the interconnectivity of three components, which later evolved into what is now recognized as the Energy Trilemma. The World Energy Trilemma Index (ETI) assesses three key dimensions of a country's energy system: energy security, energy equity, and environmental sustainability. Overcoming various challanges and increasing energy investments along the scientific research and infrastructure development in Turkiye has driven to the recent rise of its ETI.
This study tried investigating how does the adoption of hydrogen energy impact of Türkiye's ETI. Implementing hydrogen technologies has the potential to significantly impact on the ETI, offering environmental benefits, enhancing energy security, and presenting both economic implications and challenges and opportunities for integration.

Keywords: Sustainable, renewable, sources.

I. Introduction

The World Energy Trilemma Index (ETI) has been prepared annually since 2010 by the World Energy Council, with over 3,000 member organisations including governments, private and state corporations, academia, and civil society from nearly 100 countries and it presents a comparative ranking of 126 countries' energy systems. It provides an assessment of a country's energy system performance, reflecting balance and robustness in the three trilemma dimensions: Energy Security, Energy Equity, and Environmental Sustainability of Energy Systems, which are derived from sustainable development of 'energy, economy and environment' in Brundtland report published in 1987 and United Nations Framework Convention on Climate Change (UNFCCC) signed in 1992. (World Energy Council 2024) According to 2023 country rankings, Türkiye achieved an overall score of 64.6, which means it has a rank of 46 in the world. The country's balance grade is BBBd as shown in Figure 1 with scores 57.3 in energy security, 76.1 in energy equity and 68.2 in environmental sustainability. (ETI 2023) The country increases its energy security aspects by diversifiying energy sources and supply chains. New renewable energy investments and exploration of new domestic natural gas reserves are supported with developing new energy infrastructure, such as pipelines and terminals. Monitoring technological advances and pursuing localisation efforts through international and regional cooperation to increase energy import options and reduce dependence on a single source or route are also involved in rise of Türkiye's energy diversity. However, the highest portion of Türkiye's total CO_2 emissions originated from the energy sector, and it covers 85.2% of total emissions in 2021. (TUIK 2023)
Although Türkiye reduces its dependency on fossil fuels through implementing policies, accessibility and affordability of energy supply across the population and environmental sustainability on energy supply systems, there are development gaps in improving energy efficiency on the supply and demand sides, developing energy supply from other low-carbon sources for the progressively growth the share of renewable energy in the energy market and strengthening its macroeconomic stability and innovation capability. Thus, it is necessary to investigate the contribution of new energy technologies such as hydrogen energy to the countries' index and to identify the relation between hydrogen energy in the country strategies and country's rank of ETI.

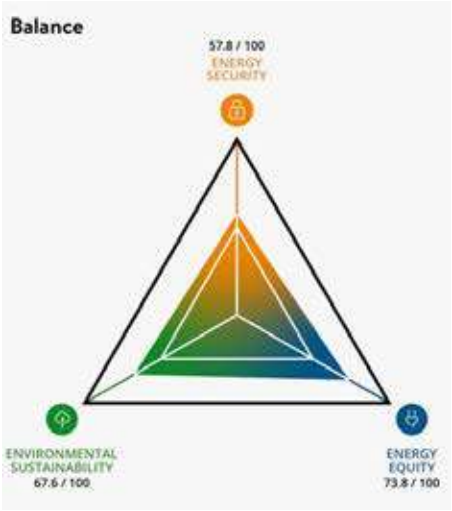


Fig. 1: Energy Trilemma Score of Türkiye in 2023 (ETI 2023)

II. Experimental Set-up and Procedure

The concept of energy security is focused on countrys' supply-side shocks, access to scarce resources, strategic reserves, energy efficiency, and exposure to commodity prices. Import independence, diversity of electricity generation and energy storage are used as key metrics by ETI in the frame of energy security to define how countrys respond prospect of demand-driven energy shocks, extreme weather events and beyond traditional oil and gas dependencies, new kinds of asymmetric threats such as data and technologies to both physical and digital infrastructures., critical minerals and metals.

To identify a variety of issues beyond access to affordable energy services, including measures related to education, health and safety, and equality, energy equity is described by the World Energy Council as accessibility and affordability of energy supply across the population and access to electricity, electricity prices and gasoline and diesel prices are used as key metrics of energy equity in ETI of countries. Energy equity includes also the financial and societal impacts of changes in cost, price, and value of energy services. Because it is hard to establish a world common index to monitor both impacts; electricity consumption in kWh per person per year is associated with income per day in $ to represent social impacts in the global energy equity measurement.

Environmental sustainability of ETI express how countrys response rising GHGs, manage and measure environmental concerns and take actions for emission reduction and prevention of emissions. In addition to the preference of renewable sources and avoidance of fossil fuels, the use of materials in energy sytems is a parameter of ETI as well for the demonstration of circularity. Final energy intensity, low carbon electiricity generation and CO_2 emissions per capita are the key metrics of this ETI division. (World Energy Council 2024)

In this study, by examining the methods of creating an effective hydrogen supply chain, utilising the country's renewable energy potentials to produce clean hydrogen, and implementation potentials of hydrogen applications in different sectors, it is identified its strengths and improvement areas within the Energy Trilemma Index parameters and with the targets in Turkiye's Hydrogen Technology Strategy and Roadmap.

III. Analysis

According to "Turkiye National Energy Plan" published by the Ministry of Energy and Natural Resources, final energy consumption of Turkiye is projected to increase from 105.5 Mtoe in 2020 to 148.5 Mtoe by 2035, and the share of the industrial sector, which has the highest share with 34.4%, is projected to increase to 38.7%, while the share of the residential and service sector, which is 40.1%, is projected to decrease to 34.9%.

The installed capacity of electricity production, which was 95.9 GW in 2020, is planned to increase to 189.7 GW in 2035, and the share of renewable energy sources in the installed capacity, which is 52.0%, is planned to reach 64.7% by 2035. In the plan, it is stated that to ensure emission reduction towards achieving the 2053 net zero emission targets, studies on mixing natural gas with hydrogen and synthetic methane will be carried out and the share of hydrogen in the gas mixture will be 3.5%. (MoEaNR 2022)

Turkiye aims to significantly increase its installed electrolyser capacity to support the production of hydrogen, with strategic investments and policy adjustments propelling its green hydrogen production to 3.4 million tons yearly by 2050. Türkiye's strategic investments and policy adjustments could propel its green hydrogen production to 3.4 million tons yearly by 2050. (MoEaNR 2023). However with an anticipated domestic demand for hydrogen at 1.9 million tons annually, potentially allowing Türkiye to export between 1.5 and 1.9 million tons yearly by 2050, indicating significant economic potential. (Hilali, Isiker ve Ulker 2023)

Tab. 1: Analysis of Hydrogen Technologies Roadmap in Turkiye with ETI

Roadmap		ETI
H_2 Production Technologies	Green H_2	
	Blue H_2	
	Turquise H_2	
H_2 Storage Technologies	Storage Cylinders	
	C based Absorbents	
	Borohydrides	
	Organic chemicals	
H_2 Distribution Technologies	Naturalgas Pipeline	
	Underground Storage Infrastucture	
	Pressurised and liquid H_2 transport vehicles	
H_2 Applications	Fuel Cells	
	Gas Turbines	
	Industry	

IV. Results and discussions

In summary, adopting the energy trilemma approach provides a holistic framework for evaluating Türkiye's potential in hydrogen production. This assessment considers factors such as renewable energy sources, policy effectiveness, economic feasibility, and sustainability. It highlights the need to tackle challenges, capitalize on opportunities, and develop robust policies to position Türkiye as a frontrunner in green hydrogen production.
The results indicate that Türkiye possesses substantial potential for green hydrogen production utilizing diverse renewable sources, positioning itself as a prospective leader in the international hydrogen market. With strategic investments and policy adaptations, Türkiye could feasibly scale its green hydrogen output to 3.4 million tons annually by 2050, offering considerable export opportunities by (Hilali, Isiker ve Ulker 2023)

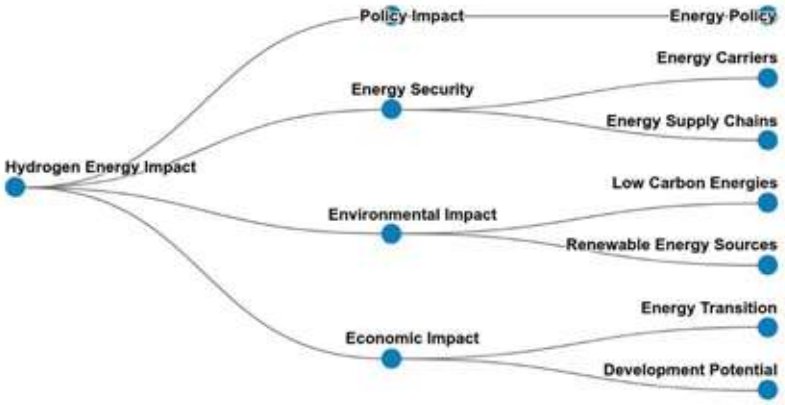


Fig. 2: Impact of Hydrogen Energy Applications

V. Conclusions

Hydrogen energy adoption can significantly improve Türkiye's Energy Trilemma Index by enhancing energy security, equity, and environmental sustainability. It diversifies the energy mix, reduces reliance on imports, and provides a stable supply. Hydrogen can improve energy access and create jobs, though high initial costs and technological challenges exist. Green hydrogen production offers substantial environmental benefits by reducing emissions, but its advantages depend on the production methods used. Economic growth and competitiveness can be driven by the hydrogen economy, requiring strategic investments and supportive policies. Integrating hydrogen into existing infrastructure and international cooperation are crucial for maximizing these benefits.

References

ETI. *Energy Trilemma Index.* 2023. www.trilemma.worldenergy.org (accessed March 31, 2024).

Hilali, I., Y. Isiker, and N. Ulker. “The hydrogen perspective for Türkiye, which is on the Asia-Europe energy transition route. Can Türkiye become hydrogen hub?” *International Journal of Hydrogen Energy*, 2023.

MoEaNR. *Turkiye National Energy Plan.* Ankara: Ministry of Energy and Natural Resources, 2022.

MoEaNR. *Türkiye Hydrogen Technologies Strategy and Roadmap.* Ankara: Republic of Türkiye Ministry of Energy and Natural Resources, 2023.

TUIK. *Turkish Greenhouse Gas Inventory 1990 - 2021.* Ankara: Turkish Statistical Institute, 2023.

World Energy Council. *World Energy Trilemma 2024: Evolving with Resillience and Justice.* London: World Energy Council, 2024.

Yilmaz, G., et al. “Hydrogen energy development in Turkey: Challanges and Opportunities.” *International Journal of Hyrdrogen Energy, Vol.52*, 02 01 2024: 1304-1311.

Smale-Scale Electricity Generation with Biohydrogen using PEM Fuel Cell

[1]Bugra Yilmaz, [2]Barbaros Durmus, [3*]Muhsin Tunay Gencoglu
[1] Fırat University, School of Civil Aviation, Department of Aviation Electrical Electronics, Elazığ, Türkiye
[2] Fırat University, Faculty of Engineering, Department of Environmental Engineering, Elazığ, Türkiye
[3] Fırat University, Faculty of Engineering, Department of Electrical and Electronics Engineering, Elazığ, Türkiye

* E-mail: mtgencoglu@firat.edu.tr

Abstract

Hydrogen energy is one of the clean fuels of the future. Hydrogen from renewable energy sources is considered green and environmentally friendly. Hydrogen gas production is also possible during wastewater treatment. This method reduces water pollution, producing hydrogen gas that can be used in fuel cells. In this study, hydrogen was produced by the anaerobic treatment method using domestic wastewater. In this process, microorganisms in the wastewater produced hydrogen, and hydrogen gas accumulated at the top of the reactor. Electricity was produced by feeding a 100 W Proton Exchange Membrane (PEM) Fuel Cell with stored hydrogen gas. Providing the resistive load with the electricity produced, the current-voltage data were recorded, and the polarization curve was obtained. This experimentally obtained curve was compared with that obtained from the 100 W PEM fuel cell model made in Matlab/Simulink.

Keywords: Hydrogen energy, PEM fuel cell, domestic wastewater, anaerobic treatment, Pleurotus ostreatusd

I. Introduction

There are various methods for hydrogen production, one of which is wastewater treatment. This method purifies wastewater from contaminants and is used for hydrogen gas production. With the development of the economy and living standards, water environment protection has become the consensus. Generally, nitrate, nitrite, and ammonium are the typical inorganic nitrogen pollution sources that seriously affect water quality. The biological method is widely applied in wastewater treatment to solve this dilemma (Wang, Qiao, and Zhou 2023). With the continuous development of the global economy and population growth, all types of domestic wastewater, industrial wastewater, medical wastewater, and so on are increasing. It is known that such wastewater types are rich in nitrogen (N) and phosphorus (P), which may cause eutrophication of water bodies and water pollution if they are directly discharged without treatment. With the gradual improvements in wastewater discharge requirements, effective N and P removal has become vital when upgrading wastewater treatment plants (You et al. 2023). With the advancement of urban and industrial, the intricacy of wastewater intensifies. Conventional remediation approaches might become inadequate. Contemporary methods, like membrane-associated procedures and ion exchange, are becoming more prevalent for N and P elimination.

Many treatment methods remove color and Chemical Oxygen Demand (COD) from industrial wastewater. One of them is anaerobic treatment, which is a biological method. Anaerobic treatment, with its most general definition, is converting organic materials into methane, hydrogen, and carbon dioxide by hydrolyzing and then acidifying by anaerobic microorganisms (Yang et al. 2023). Anaerobic treatment is the most sustainable and cost-effective technology for waste treatment and resource recovery in the form of biofuels, which not only minimizes the amount of waste but is also an efficient means of converting organic matter into clean energy (Yang et al. 2023). When fine-tuned, process parameters, including pH, temperature, and substrate levels, can amplify hydrogen and methane production. Furthermore, the combined digestion of diverse organic residues might present synergistic advantages. Less sludge is produced than aerobic treatment. At the end of the anaerobic treatment, about 98% of the COD turns into a gas mixture called biogas, which has a methane percentage of around 70%. Anaerobic digestion is primarily known for methane production. However, with modifications to typical operating conditions, it is possible to steer the process towards hydrogen production. Factors such as pH, temperature, and substrate type play a pivotal role. Hydrogenogenic bacteria thrive at slightly acidic pH values, and their activities can be maximized at thermophilic temperatures. The use of specific substrates can further promote hydrogen yield over methane. Integrating hydrogen production into anaerobic digestion systems could be valuable as we move towards a more sustainable energy future.

II. Hydrogen Production and Reactor

Since anaerobic treatment is a biological process, the most crucial share in purification belongs to microorganisms. Therefore, many different types of microorganisms play a role in anaerobic treatment. However, the primary function is performed by two groups of microorganisms. These are acid bacteria and methanogens that make up the vast majority of archaea. In Table 1, the main groups of microorganisms that are active in anaerobic systems are given.

Table 1. Main groups of anaerobic microorganisms

Microorganism	Function
Acid Bacteria	Butyric and propionic acid producers Acetic acid producers
Methane Bacteria	Acetic acid users Hydrogen users

The reactor used in this study is an upstream system with its primary operating feature. The reactor is made of fiberglass material. The entire prepared reactor has a volume of approximately 3.6 L and was manufactured in a cylindrical shape. There is a gas/solid/liquid separator before the sluice section, shown in Figure 1a. The schematic representation is in Figure 1b. As shown in Figure 1, oxygen entry into the reactor was prevented. Reactor inner and outer connection points are supported with silicone adhesive to ensure water-tightness. Many entry and exit points were created in the reactor. As a result of the liquid and air tests, the reactor was prepared for use. Reactor specifications are given in Table 2.

Table 2. Reactor features

Parameters	Value
Diameter	15 cm
Height	40 cm
Volume	3.6 L
Sample point	4 Pieces

Three control valves at different heights were used to take samples from various points in the reactor. There are direction changers for gas collection in the anaerobic reactor.



a) **b)**

Fig. 1. a) Up-flow sludge bed anaerobic reactor, b) Schematic representation of the reactor

An up-flow sludge bed anaerobic reactor was used in this study due to the advantages of rapid conversion in wastewater treatment with high COD load, allowing operation at low Hydraulic Retention Time (HRT), and not needing mixing. Feed to the reactor was given to the reactor from the bottom with a specially designed disperser to ensure homogeneity. The active anaerobic granules in the reaction zone convert organic materials into biogas. High-density granules are suspended in the sludge bed due to the superficial up-flow velocity and rising biogas bubbles. Granules reaching up with the gas enter the gas-solid separator. The granules are separated from the gas by striking the inclined wall and returning to the reactor. The biogas is collected in the gas collection system. Pleurotus fungi from the Pleurotaceae family, which are in the Basidiomycota branch, were used in the reactor. Many Pleurotus genera, such as Pleurotus ostreatus, are primary decomposers of oak trees and are found worldwide. Due to its adaptability to various climates and substrate materials, it is the most-produced fungi species worldwide after Agaricus Bisporus (Siwulski et al. 2020).

Using fungi in wastewater treatment has gained prominence recently (Mendoza-Tinoco et al. 2023). Particularly, species from the Pleurotus genus have shown proficiency in effectively decomposing lignocellulosic wastes. These fungi can decompose complex organic compounds into simpler molecules by producing extracellular enzymes. This plays a significant role in decomposing challenging compounds present in wastewater. Especially in degrading compounds like lignin, fungi can optimize wastewater treatment processes (Dias et al. 2010).

III. Modeling and Experimental Set-up

In this study, electricity was produced using hydrogen obtained from domestic wastewater and the H-100 PEM fuel cell manufactured by Horizon Company. Fuel cell, which is one of the alternative energy technologies, is an electrochemical device that directly converts the chemical energy of the fuel into electrical energy (Nalbant et al. 2019) (Soyturk et al. 2024). To model this 100 W PEM fuel cell, some parameters specified by the manufacturer and studies in the literature were examined (Özdemir 2021). Using the definition equations of the PEM fuel cell, its mathematical model was made in Matlab/Simulink, and these definitional equations are given below. Figure 2 shows

the experimental setup. During the experiments, the PEM fuel cell was connected to the rheostat, and the current and voltage were recorded instantly by multimeters by changing the resistance value.

$$V_{FC} = E_{Nernst} - V_{act} - V_{ohmic} - V_{con} \quad (6)$$

$$E_{Nernst} = 1.229 - \left(8.5 * 10^{-4} * (T - 298) + 4.308 * 10^{-5} * T * ln\left(P_{H_2} * (P_{O_2})^{1/2}\right)\right) \quad (7)$$

$$C_{O_2} = \frac{P_{O_2}}{5.08*10^6*exp(-498/T)} \quad (8)$$

$$V_{act} = \beta_1 + \beta_2 * T + \beta_3 * T * ln\left(\frac{P_{O_2}}{5.08*10^6*\exp(-498/T)}\right) * \beta_4 * T * \ln(I) \quad (9)$$

$$V_{ohmic} = I * (R_m + R_c) \quad (10)$$

$$R_m = \frac{\rho_m * l}{A} \quad (11)$$

$$\rho_m = \frac{181.6*\left[1+0.039*\left(I/A\right)+0.062*\left(T/303\right)^2*\left(I/A\right)^{2.5}\right]}{\left[\lambda-0.634-3*\left(I/A\right)\right]*\exp\left(4.18\left[\frac{T-303}{T}\right]\right)} \quad (12)$$

$$V_{con} = -B * ln\left(1 - \frac{I}{I_{lim}}\right) \quad (13)$$

$$B = \frac{R*T}{2*F} \quad (14)$$

Where, V_{FC}, cell voltage (V); E_{Nernst}, Nernst voltage (V); V_{act}, activation loss voltage (V); V_{ohmic}, ohmic loss voltage (V); V_{con}, concentration loss voltage (V); T, temperature (°K); P_{H2}, hydrogen partial pressure (atm); P_{O2}, oxygen partial pressure (atm); β, experience parameters; R_m, the impedance of proton exchange membrane (Ω); R_c, the equivalent contact resistance (Ω); ρ_m, the membrane specific resistivity (Ω.cm); I, the cell current (A); I_{lim}, the cell limit current (A); l is the thickness of proton exchange membrane (cm); A, the effective area of proton exchange membrane (cm^2); λ, the water content of proton exchange membrane; C_{O2}, oxygen concentrations (mol/cm^3); R the ideal gas constant (J/K.mol); F, Faraday constant (C).
All constants used in the equations are given in Table 3.

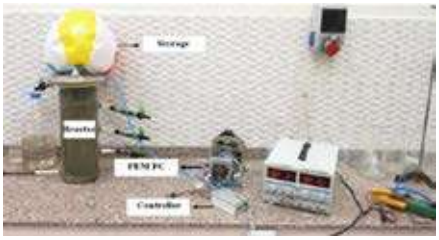


Fig. 2. The experimental set-up

IV. Results

In this study, both wastewater treatment and electrical results were obtained. Hydraulic Retention Time (HRT) lasts 24-36 hours in this system. For the preferred fungus, the pH value of the wastewater is ideally kept close to 6, and the pH value of the refined water is also approximately 6. The diameter of the balloon used to store hydrogen gas is 12 cm, and its volume is about 7250 cm^3. Gas production began within two weeks, and the balloon was almost filled at the end of 19 days. At the end of 28 days, the balloon was filled. Electricity production experiments were carried out with PEM starting from the 14th day when hydrogen gas was more abundant than methane and carbon dioxide. Table 3 shows the COD and turbidity values of wastewater and treated water. These values indicated that a good treatment was carried out.

Table 3. Wastewater and treated water COD and turbidity values

Parameters	Wastewater Value	Refined Value
COD (mg O_2/L)	≈1200	≈400
Turbidity (Nephelometric Turbidity Unit-NTU)	296	78

Figure 3 shows the simulation and experimental polarization curve, while Figure 4 shows the simulation and experimental power curve. The results obtained are similar to the graphics shared by the manufacturer. The difference between the simulation and experimental curves is that some parameters in the mathematical model for

the PEM fuel cell must be clearly known. In addition, not using the existing fuel cell for many years has gradually increased the value difference between the curves.

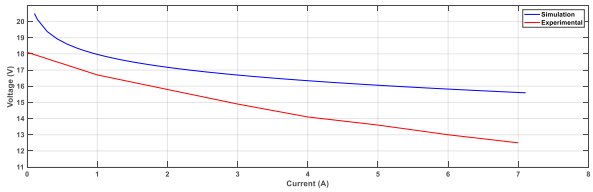


Fig. 3. Simulation and experimental polarization curves

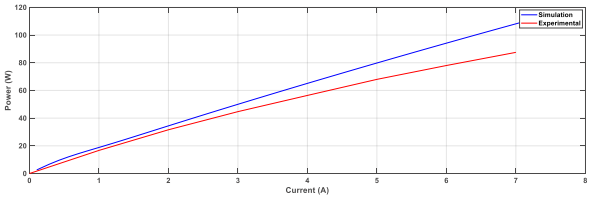


Fig. 4. Simulation and experimental power curves

V. Conclusions

Renewable energy sources and wastewater treatment are essential for a sustainable environment. Many methods to obtain hydrogen energy have become increasingly popular, especially in recent years. One of these methods is the treatment of wastewater. This method produces hydrogen gas using microorganisms, and wastewater pollution is reduced. This study showed that hydrogen produced by the fungus Pleurotus Ostreatus can be used as fuel for PEM fuel cells. Furthermore, wastewater is also treated with this method. Thus, water pollution is reduced, and clean energy is produced through the fuel cell. In the experimental system, polarization and power curves were obtained by feeding the variable resistance load with the generated electricity, and the curves were approximately compatible. The deformation of the PEM fuel cell membrane used in the study due to not being used for many years caused its performance to decrease. This resulted in the difference between the curves. Regarding wastewater treatment, the change in COD and turbidity values showed that good treatment was achieved. Future studies aim to produce hydrogen at different levels by different organisms, measure this production in quantity, and obtain electrical results for other loads.

References

Dias, Albino A., Gil S. Freitas, Guilhermina S. M. Marques, Ana Sampaio, Irene S. Fraga, Miguel A. M. Rodrigues, Dmitry V. Evtuguin, and Rui M. F. Bezerra. 2010. “Enzymatic Saccharification of Biologically Pre-Treated Wheat Straw with White-Rot Fungi.” *Bioresource Technology* 101(15):6045–50. doi: 10.1016/j.biortech.2010.02.110.

Mendoza-Tinoco T. P., V. Sánchez-Vázquez, M. del Carmen Fajardo-Ortiz, I. González, and R. Beristain-Cardoso, “How does a low-magnitude electric field influence anaerobic digestion in wastewater treatment? A review,” Chemosphere, vol. 325, no. March, 2023, doi: 10.1016/j.chemosphere.2023.138402.

Nalbant Yagmur, C. Ozgur Colpan, Yilser Devrim, Energy and exergy performance assessments of a high temperature-proton exchange membrane fuel cell based integrated cogeneration system, International Journal of Hydrogen Energy, Volume 45, Issue 5, 2020, Pages 3584-3594, ISSN 0360-3199. https://doi.org/10.1016/j.ijhydene.2019.01.252.

Özdemir, Mahmut. (2021). Optimal parameter estimation of polymer electrolyte membrane fuel cells model with chaos embedded particle swarm optimization. International Journal of Hydrogen Energy. 46. 10.1016/j.ijhydene.2020.12.203.

Siwulski, Marek, Anna Budka, Piotr Rzymski, Monika Gąsecka, Pavel Kalač, Sylwia Budzyńska, Zuzanna Magdziak, Przemysław Niedzielski, Patrycja Mleczek, and Mirosław Mleczek. 2020. “Worldwide Basket Survey of Multielemental Composition of White Button Mushroom Agaricus Bisporus.” *Chemosphere* 239. doi: 10.1016/j.chemosphere.2019.124718.

Soyturk Gamze, Onder Kizilkan, Mehmet Akif Ezan, C. Ozgur Colpan, Design, modeling, and analysis of a PV/T and PEM fuel cell based hybrid energy system for an off-grid house, International Journal of Hydrogen Energy Volume 67, 2024, Pages 1181-1193, ISSN 0360-3199, https://doi.org/10.1016/j.ijhydene.2023.11.291.

Wang, Chao, Sen Qiao, and Jiti Zhou. 2023. “Strategy of Nitrate Removal in Anaerobic Ammonia Oxidation-Dependent Processes.” *Chemosphere* 313(December 2022):137586. doi: 10.1016/j.chemosphere.2022.137586.

Yang, Shuyue, Zifu Li, Xuemei Wang, Shikun Cheng, and Lixin Zhu. 2023. “Research Progress of Enhanced Methane Production by Anaerobic Digestion of Blackwater.” *Journal of Water Process Engineering* 53(May):103719. doi: 10.1016/j.jwpe.2023.103719.

You, Junhao, Shilong Tang, Yongchen Zong, Hongtao Shan, Jun Wang, and Chunhui Fu. 2023. “Effects of Adding Different Ratios of Residual Sludge and Food Waste Co-Anaerobic Fermentation Liquid to AAO Wastewater Treatment Process.” *Journal of Water Process Engineering* 53(April):103735. doi: 10.1016/j.jwpe.2023.103735.

Integrated System Design that Produces Electricity with Solar, Wind, Hydrogen and Biomass Energy

[1]Bugra Yilmaz, [2*]Muhsin Tunay Gencoglu
[1] Fırat University, School of Civil Aviation, Department of Aviation Electrical Electronics, Elazığ, Türkiye
[2] Fırat University, Faculty of Engineering, Department of Electrical and Electronics Engineering, Elazığ, Türkiye

* E-mail: mtgencoglu@firat.edu.tr

Abstract

Since the industrial revolution, the use of fossil fuels in every field has been emitting greenhouse gases into the atmosphere. Consequently, we are facing a global climate crisis with increasing land and ocean temperatures. To reduce greenhouse gas emissions, the use of renewable energy sources such as solar and wind is considered an ideal solution. Rising temperatures and insufficient precipitation have led to the drying up of water resources in some regions, making access to drinking water impossible. Desalination systems can produce drinking water from saltwater, but the cost and energy requirements increase proportionally with water demand. For sustainable environmental management, not only renewable energy and clean water production but also wastewater management are of great importance. Discharging untreated domestic wastewater into nature can lead to long-term environmental problems. Considering these issues, it is evident that systems combining renewable energy and clean water production with wastewater treatment are necessary.

Keywords: Renewable energy, Green Hydrogen, Deionized water, Drinking water, Domestic wastewater treatment, Biohydrogen

I. Introduction

Humans have been using fire to produce heat and light for thousands of years. In the mining ages, many materials, from primitive kitchen utensils to hunting weapons, were made by melting metals. With the Industrial Revolution, fire was used in the development of more advanced systems. In this period, when there was no option other than fossil fuels for energy production, all steam-powered vehicles and factories were powered by coal or wood. Today, fossil fuels still dominate industry, energy, and transportation. Fossil fuels, indispensable and progressive carriers of human civilization for approximately 170 years, are now causing events that negatively change the planet's climate and whose consequences are visible. Greenhouse gases such as CO_2 and CH_4, which occur due to the use of fossil resources, prevent the sunlight reflected from the surface from passing from the atmosphere to space, causing surface temperatures to increase. Between 1880 and 2012, the global average land and ocean surface temperatures increased by 0.85 °C to 1.06 °C (IPCC 2013). The Intergovernmental Panel on Climate Change (IPCC) announced that the average temperature for the period 2013-2022 is approximately 1.14 °C higher than before the industrial revolution (WMO 2022). Copernicus Climate Change Service announced that 2022 will be the 2nd hottest year for Europe and the 5th year for the World, and also stated that the CO_2 concentration in the atmosphere increased by 2.1 ppm in 2022. In the same report, it was also stated that the last 8 years were the warmest 8-year period. Finally, July 2023 was recorded as the hottest month. It was stated that this month was 1.5°C above the global average temperature and exceeded July 2019, when the previous record temperature was measured, by 0.33°C (EUCCS 2022). With agreements such as the Paris Climate Agreement and the Kyoto Protocol, countries aim to prevent climate change before the point of no return by reducing CO_2 emissions. In particular, the IPCC plans to limit the temperature increase to 1.5 °C for 2050, with the goal of halving emissions by 2030 (WMO 2022). In the same statement, he stated that emissions should be reduced to zero by 2050 and that global temperature would reach equilibrium in the early 2070s (IPCC 2022). It has been emphasized that if these targets are not achieved, various environmental disasters will occur around the world. Ocean levels will rise, especially as a result of ice mass loss, and some coastal areas will be flooded. As the glaciers melt, natural life in the poles will be affected and animals will face the danger of extinction. At the same time, as a result of changes in ocean currents, storms will become more severe in some places and droughts will occur in some places. Events such as mixing of fresh water with ocean waters, rapid evaporation of drinking water resources due to rising temperatures, and rainfall irregularity/insufficiency are clear indicators that humanity will experience a serious clean water shortage (Barghash et al. 2022).

In order to reduce our carbon footprint, we can first bring the global temperature back into balance by reducing fossil fuel use or reducing it to zero. While solar and wind energy are leading clean energy sources, hydrogen has been increasing in popularity in recent years and is considered a suitable solution to the climate crisis with its greenhouse gas emission-free energy production (Qyyum et al. 2021). Since there is trace amounts of hydrogen gas in our atmosphere, it is of great importance to produce sufficient amounts of hydrogen to be used as fuel. There are many methods for hydrogen production (Abdin et al. 2015), and the produced hydrogen is symbolized in different colors according to the emission values that occur during production (Arcos and Santos 2023) (Nasser 2022) (Marouani et al. 2023). Gray hydrogen is produced by burning fossil fuels and causes CO_2 emissions into the atmosphere. Emission rates are also greatly reduced by carbon capture methods for blue hydrogen produced by burning fossil fuels. However, this method encounters the difficulties of carbon capture methods. Turquoise

hydrogen is produced from fossil fuels by the pyrolysis method, causing low emission values. Yellow hydrogen is produced by electrolysis of water through nuclear power plants and produces zero emissions. Finally, green hydrogen, which is considered the energy of the future, is produced by electrolysis of water using electricity produced by renewable energy sources and does not produce greenhouse gas emissions. Considering the current situation of our world and future predictions, using environmentally friendly energy sources instead of fossil fuels is not a choice but a necessity. Our country is facing a high risk of drought, according to data obtained from NASA's satellite images in 2021. Similarly, the World Wide Fund for Nature (WWF) and the World Resources Institute (WRI) also made statements warning our country about drought. In the research conducted by the General Directorate of Combating Desertification and Erosion and TÜBİTAK-BİLGEM in 2015, a desertification map was created and according to this map, it was shown that the center and west of Elazığ province were at high risk of desertification. Drought and desertification risks, the leading effects of which our country experiences, will lead to problems such as water scarcity and lack of access to clean drinking water in the coming years. Although there are different desalination methods that produce drinking water from lake or sea water, the Reverse Osmosis (RO) method, which is becoming increasingly common among them, is preferred due to its advantages such as high efficiency, low energy consumption and low maintenance need.

In addition to clean energy and drinking water production, wastewater management is also important for a sustainable environment. Leaving wastewater untreated to the soil or clean water resources causes environmental problems. To prevent this, treating wastewater with anaerobic fermentation offers a two-pronged solution. With the anaerobic fermentation method, in addition to biohydrogen production, the harmful effects of wastewater are largely eliminated. The treated water reaches a level that can be used for agricultural and landscape irrigation, and the remaining waste can be used for purposes such as fertilization. Irrigation of agricultural areas with purified water instead of drinking water would be a more suitable option in combating drought.

This study aims to design a system that will meet the electricity and clean water needs with solar, wind, hydrogen, and biomass energy. Hydrogen energy in the system will be produced in two ways: green hydrogen in the electrolyzer and biohydrogen in the wastewater treatment reactor. In the anaerobic fermentation process carried out with different microorganisms, wastewater treatment, and hydrogen production will be carried out.

II. Hybrid System Design

In this study, a PV system, wind turbines, and PEM fuel cells will be used to produce electricity, an electrolyzer and purification reactor will be used to produce hydrogen, and Reverse Osmosis device will produce clean water. Compared to distributed energy systems, a schematic representation of a self-sufficient integrated system that produces clean water and purifies wastewater is given in Figure 1. Auxiliary elements such as power switch, sensor, regulator, valve, and compressor are not shown in the figure. The relationship between the systems is given in Figure 2.

To determine the PV system, wind turbine, PEM fuel cell, and battery to be used, firstly, 2021 annual solar and wind energy data were obtained for the Elazığ province Fırat University, Department of Electrical and Electronics Engineering location (38.675 N, 39.187 E). Then, the power and energy values required by the loads must be determined. The power values and usage times of the domestic load group are given in Table 1.

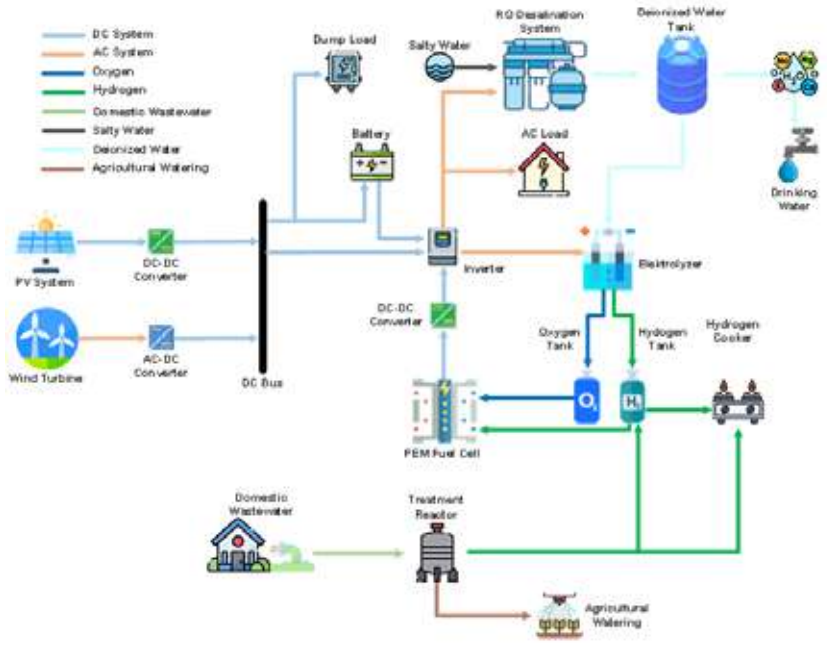


Fig. 1. Hybrid system schematic diagram

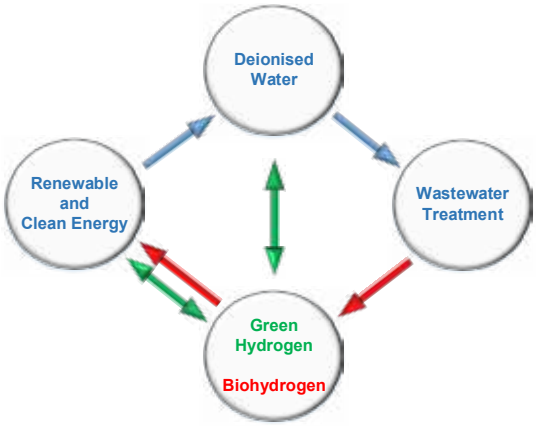


Fig. 2. Relationship between systems

Table 1. House Load Profile

Device Name	Power (W)	Usage Time (Hour/Day)	Energy (Wh/Day)
Air Conditioning	600	4*	2400
Refrigerator	100	5*	500
LCD TV	100	4*	400
Laptop	100	4*	400
Lighting	100	7	700
Kettle	1000	0.2*	200
Total	2000		4600

III. Energy Management

In the system, the electrolyzer, RO device, domestic loads, and devices in the structure of IMS are considered electrical loads. The total energy produced in the PV system and wind turbines ($E_{Produced}$) and the total energy consumed by the loads in the system ($E_{Consumed}$) will be monitored instantly in the LabVIEW environment with data received from current and voltage transducers. The PEM fuel cell and battery group will not be activated when production is high. To prolong the life of the battery group, the State of Charge (SoC) value will be selected as a minimum of 40%. The PEM fuel cell and battery group will be activated if the production is lower than the requested energy. However, depending on the condition of the battery group and hydrogen tanks and the size of the energy difference, priority will be given to the PEM fuel cell. If the energy produced by the PEM fuel cell (EPEM) along with the PV system and wind turbines meets the consumed energy, only the PEM fuel cell will feed the load; if it is low, the battery group will also be activated. If the net energy is negative and there is not enough hydrogen in the hydrogen tank, the battery group will continue to feed the loads until it drops below 40% SoC. With the management system to be created, it is planned to keep the number of cycles of the batteries as low as possible. However, suppose the PV system and wind turbines do not produce energy for meteorological reasons or in the event of a malfunction. The PEM fuel cell and the battery will be activated in that case.

The commissioning of the PEM fuel cell will be decided by looking at the data from the pressure sensor in the hydrogen tanks. If the pressure value drops below 4 bar, the fuel cell will be disabled. In this case, the requested energy will be met by allowing the SoC value of the battery group to drop below 40%. As long as the pressure value is higher than 4 bar, the SoC value will be kept at a minimum of 40%. When the produced energy is again more than the requested energy, the battery group will be charged. If more power is produced than the 3650 W power demanded by the entire system when the batteries and hydrogen tanks are full, the excess energy will be used to produce drinking water through distillation in the distiller connected to the DC bus and the total efficiency of the system will be increased. This device will be made using existing materials in the laboratory.

While the flow diagram of the SMS between the PV system, wind turbines, PEM fuel cell and battery is given in Figure 3a, the block diagram that is close to the LabVIEW-based measurement and control system is shown in Figure 3b. Parameters such as current, voltage, power, pressure, temperature and water level will be monitored instantly with the analog voltage signal produced by sensors and transducers, and when the specified conditions are met, the power switch, valves and pumps will be controlled with digital signals given from the management system.

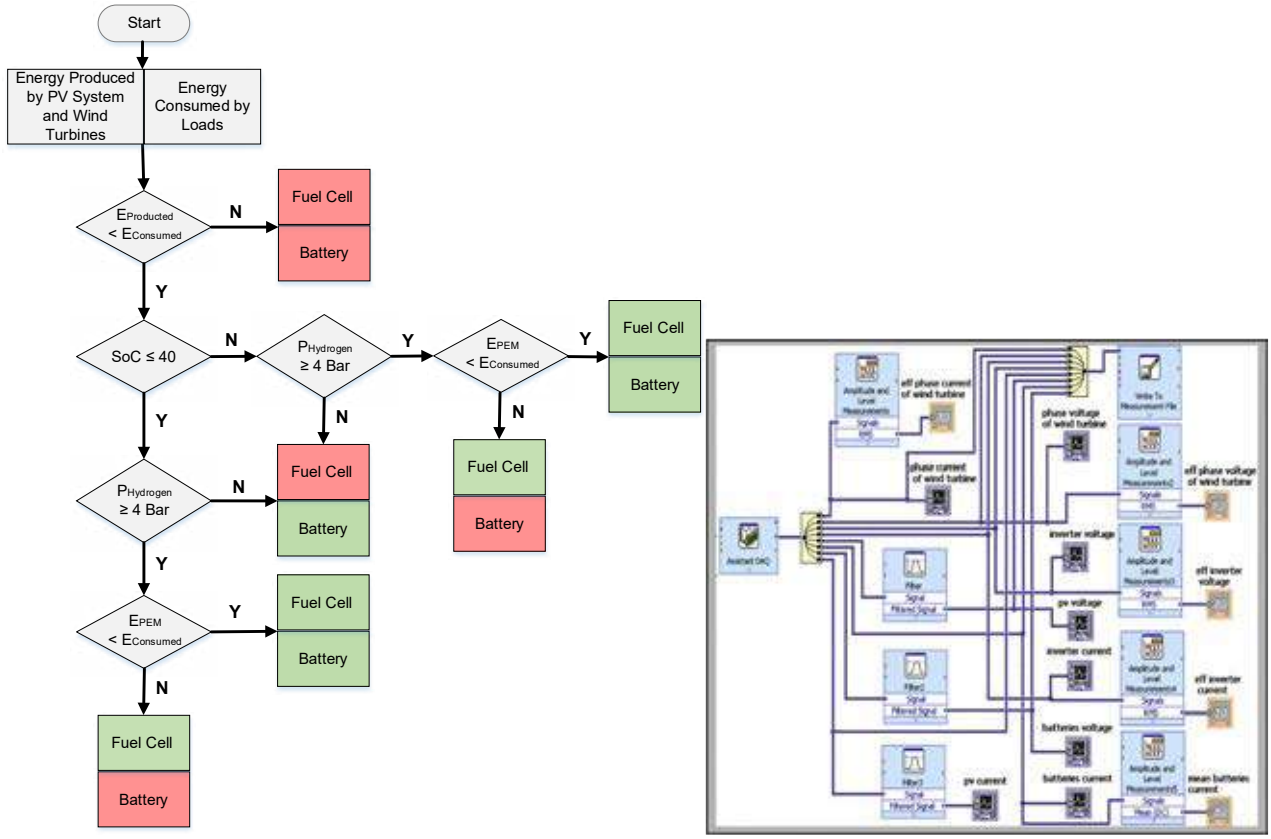


Fig. 3. a) EMS flowchart, **b)** LabVIEW block diagram

References

IPCC, "Summary for Policymakers," 2013. https://archive.ipcc.ch/pdf/assessment-report/ar5/wg1/WG1AR5_SPM_FINAL.pdf.

WMO, "Eight warmest years on record witness upsurge in climate change impacts," 2022. https://public.wmo.int/en/media/press-release/eight-warmest-years-record-witness-upsurge-climate-change-impacts#:~:text=Data from key monitoring stations,eight warmest years on record.

EUCCS, "2022 was a year of climate extremes, with record high temperatures and rising concentrations of greenhouse gases," 2023. https://climate.copernicus.eu/copernicus-2022-was-year-climate-extremes-record-high-temperatures-and-rising-concentrations.

IPCC, "The evidence is clear: the time for action is now. We can halve emissions by 2030," 2022. https://www.ipcc.ch/2022/04/04/ipcc-ar6-wgiii-pressrelease/.

H. Barghash, Z. AlRashdi, K. E. Okedu, and P. Desmond, "Life-Cycle Assessment Study for Bio-Hydrogen Gas Production from Sewage Treatment Plants Using Solar PVs," Energies, vol. 15, no. 21, pp. 1–17, 2022, doi: 10.3390/en15218056.

M. A. Qyyum et al., "Availability, versatility, and viability of feedstocks for hydrogen production: Product space perspective," Renew. Sustain. Energy Rev., vol. 145, no. February, p. 110843, 2021, doi: 10.1016/j.rser.2021.110843.

Z. Abdin, C. J. Webb, and E. M. A. Gray, "Solar hydrogen hybrid energy systems for off-grid electricity supply: A critical review," Renew. Sustain. Energy Rev., vol. 52, pp. 1791–1808, 2015, doi: 10.1016/j.rser.2015.08.011.

J. M. M. Arcos and D. M. F. Santos, "The Hydrogen Color Spectrum: Techno-Economic Analysis of the Available Technologies for Hydrogen Production," Gases, vol. 3, no. 1, pp. 25–46, 2023, doi: 10.3390/gases3010002.

M. Nasser, T. F. Megahed, S. Ookawara, and H. Hassan, "A review of water electrolysis–based systems for hydrogen production using hybrid/solar/wind energy systems," Environ. Sci. Pollut. Res., vol. 29, no. 58, pp. 86994–87018, 2022, doi: 10.1007/s11356-022-23323-y.

I. Marouani et al., "Integration of Renewable-Energy-Based Green Hydrogen into the Energy Future," Processes, vol. 11, no. 9, 2023, doi: 10.3390/pr11092685.

Main Sponsor

TENMAK
TURKISH ENERGY, NUCLEAR AND MINERAL RESEARCH AGENCY

Gold Sponsors

DICLE ELEKTRİK

ETİ BAKIR

HYDROGENIX

Other Sponsors

DİYARBAKIR

GAP

KARACADAĞ

AK-DAL

Anton Paar

otostore

MİTRAS ENERJİ
SOLAR TECHNOLOGY SOLUTIONS

Sustainable Production and Consumption Association
SPCA

SUNGATECH ENERGY

Solino

ünteks group

EKSİM enerji

TRL INSTRUMENTS

jiber

EFG

ORGANIZATION SECRETARIAT
BROS
Congress, Incentive and Events

Esentepe Mah. Sağlam Fikir Sok. Esen Palas Apt. A Blok No:2 D:9
Esentepe / Şişli - İstanbul / TURKEY
Tel: + 90 212 296 66 70 / **Fax:** + 90 212 296 66 71
hatice.cilek@brosgroup.net / www.brosgroup.net

ISBN: 978-605-70717-8-1